United States Department of Agriculture – Forest Service – Forest Products Lab and United States Endowment for Forestry and Communities
Research Agreement No. 21-00283

CRASH-TESTED BRIDGE RAILINGS AND TRANSITIONS FOR WOOD BRIDGES – PHASE IIB REPORT ON GLULAM BRIDGE POST AND AGT DEVELOPMENT

Submitted by

Aaron Lechtenberger, B.S.C.E.
Graduate Research Assistant

Ronald K. Faller, PhD., P.E.
MwRSF Director and Research Professor

Tewodros Y. Yosef, Ph.D.
Research Assistant Professor

Joshua S. Steelman, Ph.D., P.E.
Associate Professor

Cody S. Stolle, Ph.D.
Research Associate Professor

Robert W. Bielenberg, M.S.M.E.
Research Engineer

Scott K. Rosenbaugh, M.S.C.E.
Research Engineer

James P. Wacker, P.E.
Research Engineer,
U.S. Department of Agriculture,
Forest Service, Forest Products Laboratory

MIDWEST ROADSIDE SAFETY FACILITY
Nebraska Transportation Center
University of Nebraska-Lincoln

Main Office
Prem S. Paul Research Center at Whittier School
Room 130, 2200 Vine Street
Lincoln, Nebraska 68583-0853
(402)472-0965

Outdoor Test Site
4630 N.W. 36th Street
Lincoln, Nebraska 68524

Submitted to

United States Endowment for Forestry and Communities
10 S. Academy St Suite 101
Greenville, SC 29601-2632

United States Department of Agriculture – Forest Service
Forest Product Laboratory
One Gifford Pinchot Dr.
Madison, Wisconsin 53726

MwRSF Research Report No. TRP-03-494-25

July 28, 2025

TECHNICAL REPORT DOCUMENTATION PAGE

1. Report No. TRP-03-494-25	**2. Government Accession No.**	**3. Recipient's Catalog No.**
4. Title and Subtitle Crash-Tested Bridge Railings and Transitions for Wood Bridges – Phase IIb Report on Glulam Bridge Post and AGT Development		**5. Report Date** July 28, 2025 **6. Performing Organization Code**
7. Author(s) Lechtenberger, A.M., Faller, R.K., Yosef, T.Y., Steelman, J.S., Stolle, C.S., Bielenberg, R.W., Rosenbaugh, S.K., and Wacker, J.P.		**8. Performing Organization Report No.** TRP-03-494-25
9. Performing Organization Name and Address Midwest Roadside Safety Facility (MwRSF) Nebraska Transportation Center University of Nebraska-Lincoln Main Office: Prem S. Paul Research Center at Whittier School Room 130, 2200 Vine Street Lincoln, Nebraska 68583-0853 Outdoor Test Site: 4630 N.W. 36th Street Lincoln, Nebraska 68524		**10. Work Unit No.** **11. Contract** 21-00283 WBS #26-1113-0182-001
12. Sponsoring Agency Name and Address United States Endowment for Forestry and Communities 10 S. Academy St Suite 101 Greenville, SC 29601-2632 United States Department of Agriculture – Forest Service, Forest Product Laboratory One Gifford Pinchot Dr. Madison, Wisconsin 53726		**13. Type of Report and Period Covered** Final Report: 2022-2025 **14. Sponsoring Agency Code**

15. Supplementary Notes

Prepared in cooperation with U.S. Department of Transportation, Federal Highway Administration

16. Abstract

Limited research exists to develop bridge railing systems for high-service-level roadways that meet current vehicular impact safety standards. This study continued a multi-phase project aimed at developing, crash testing, and assessing a MASH Test Level 4 (TL-4)-compliant glued-laminated (glulam) timber bridge railing system with a curb, as well as a MASH TL-3 approach guardrail transition (AGT) system. A comprehensive literature review identified critical deck configurations and parameters, including deck thickness, cantilevered overhang dimensions, and panel geometry. Additionally, soil-interaction dynamics for AGT posts were examined through prior bogie impact testing. Cost-effective design strategies were proposed to minimize the exposure of timber deck elements to prolonged water accumulation beneath the asphalt wearing surface.

The AGT system design was based on an earlier crash-tested configuration. Dynamic impact testing of single, double, and triple AGT posts embedded in soil was conducted, yielding valuable insights into their impact behavior and performance. Data from these tests informed the calibration of BARRIER VII models, enabling the development of an optimized AGT system. Prototyping and iterative designing facilitated the creation of a reliable connection between the bridge railing and AGT systems. A critical impact point (CIP) investigation further identified locations most prone to failure under MASH TL-3 impact conditions for a final AGT system recommendation.

The study culminated in the design of four dynamic component tests to evaluate critical timber deck configurations and connections. Test no. TRTD-1, involving a 7,186-lb bogie impacting a surrogate post on a 5⅛-in. thick transverse Douglas Fir-Larch glulam deck, revealed premature tensile splitting of the deck due to insufficient restraint. This issue was addressed by introducing timber bolts through the scupper to enhance deck performance.

17. Key Words Glue-Laminated Timber, Glulam, Bridge Rail, Bridge Deck, Crashworthy, TL-4, Bogie Testing, Dynamic, MASH, BARRIER VII		**18. Distribution Statement** No restrictions. This document is available through the National Technical Information Service. 5285 Port Royal Road Springfield, VA 22161	
19. Security Classification (of this report) Unclassified	**20. Security Classification (of this page)** Unclassified	**21. No. of Pages** 576	**22. Price**

Form DOT F 1700.7 (8-72) Reproduction of completed page authorized

DISCLAIMER STATEMENT

This report was completed with funding from the U.S. Department of Agriculture – Forest Service – Forest Products Laboratory and U.S. Endowment for Forestry and Communities. The contents of this report reflect the views and opinions of the authors who are responsible for the facts and the accuracy of the data presented herein. The contents do not necessarily reflect the official views or policies of the U.S. Department of Agriculture. This report does not constitute a standard, specification, regulation, product endorsement, or an endorsement of manufacturers.

UNCERTAINTY OF MEASUREMENT STATEMENT

The Midwest Roadside Safety Facility (MwRSF) has determined the uncertainty of measurements for several parameters involved in standard full-scale crash testing and non-standard testing of roadside safety features. Information regarding the uncertainty of measurements for critical parameters is available upon request by the sponsor and the Federal Highway Administration.

A2LA ACCREDITATION

The tests reported herein are within the scope of MwRSF's A2LA Accreditation. MwRSF's accreditation documentation can be found in Appendix A.

ACKNOWLEDGEMENTS

The authors wish to acknowledge the U.S. Department of Agriculture - Forest Service - Forest Products Laboratory and U.S. Endowment for Forestry and Communities for sponsoring this project. Acknowledgement is also given to the following individuals who contributed to the completion of this research project.

Midwest Roadside Safety Facility
J.C. Holloway, M.S.C.E., Research Engineer & Assistant Director –Physical Testing Division
C.S. Stolle, Ph.D., Research Associate Professor
M. Asadollahi Pajouh, Ph.D., P.E., Research Assistant Professor
B.J. Perry, M.E.M.E., Research Engineer
A.E. Loken, Ph.D., Research Assistant Professor
A.T. Russell, B.S.B.A., Testing and Maintenance Technician II
E.W. Krier, B.S., Former Engineering Testing Technician II
D.S. Charroin, Engineering Testing Technician II
R.M. Novak, Engineering Testing Technician II
T.C. Donahoo, Engineering Testing Technician I
J.T. Jones, Engineering Testing Technician II
E.L. Urbank, Research Communication Specialist
Z.Z. Jabr, Engineering Technician
J.J. Oliver, Solidworks Drafting Coordinator
Undergraduate and Graduate Research Assistants

SI* (MODERN METRIC) CONVERSION FACTORS

APPROXIMATE CONVERSIONS TO SI UNITS

Symbol	When You Know	Multiply By	To Find	Symbol
		LENGTH		
in.	inches	25.4	millimeters	mm
ft	feet	0.305	meters	m
yd	yards	0.914	meters	m
mi	miles	1.61	kilometers	km
		AREA		
in^2	square inches	645.2	square millimeters	mm^2
ft^2	square feet	0.093	square meters	m^2
yd^2	square yard	0.836	square meters	m^2
ac	acres	0.405	hectares	ha
mi^2	square miles	2.59	square kilometers	km^2
		VOLUME		
fl oz	fluid ounces	29.57	milliliters	mL
gal	gallons	3.785	liters	L
ft^3	cubic feet	0.028	cubic meters	m^3
yd^3	cubic yards	0.765	cubic meters	m^3
		NOTE: volumes greater than 1,000 L shall be shown in m^3		
		MASS		
oz	ounces	28.35	grams	g
lb	pounds	0.454	kilograms	kg
T	short ton (2,000 lb)	0.907	megagrams (or “metric ton”)	Mg (or "t")
		TEMPERATURE (exact degrees)		
°F	Fahrenheit	5(F-32)/9 or (F-32)/1.8	Celsius	°C
		ILLUMINATION		
fc	foot-candles	10.76	lux	lx
fl	foot-Lamberts	3.426	candela per square meter	cd/m^2
		FORCE & PRESSURE or STRESS		
lbf	poundforce	4.45	newtons	N
lbf/in^2	poundforce per square inch	6.89	kilopascals	kPa

APPROXIMATE CONVERSIONS FROM SI UNITS

Symbol	When You Know	Multiply By	To Find	Symbol
		LENGTH		
mm	millimeters	0.039	inches	in.
m	meters	3.28	feet	ft
m	meters	1.09	yards	yd
km	kilometers	0.621	miles	mi
		AREA		
mm^2	square millimeters	0.0016	square inches	in^2
m^2	square meters	10.764	square feet	ft^2
m^2	square meters	1.195	square yard	yd^2
ha	hectares	2.47	acres	ac
km^2	square kilometers	0.386	square miles	mi^2
		VOLUME		
mL	milliliter	0.034	fluid ounces	fl oz
L	liters	0.264	gallons	gal
m^3	cubic meters	35.314	cubic feet	ft^3
m^3	cubic meters	1.307	cubic yards	yd^3
		MASS		
g	grams	0.035	ounces	oz
kg	kilograms	2.202	pounds	lb
Mg (or "t")	megagrams (or “metric ton”)	1.103	short ton (2,000 lb)	T
		TEMPERATURE (exact degrees)		
°C	Celsius	1.8C+32	Fahrenheit	°F
		ILLUMINATION		
lx	lux	0.0929	foot-candles	fc
cd/m^2	candela per square meter	0.2919	foot-Lamberts	fl
		FORCE & PRESSURE or STRESS		
N	newtons	0.225	poundforce	lbf
kPa	kilopascals	0.145	poundforce per square inch	lbf/in^2

*SI is the symbol for the International System of Units. Appropriate rounding should be made to comply with Section 4 of ASTM E380.

TABLE OF CONTENTS

LIST OF FIGURES

LIST OF TABLES

1 INTRODUCTION

1.1 Background

Aesthetic timber bridge railings are used across the U.S. to safely contain and redirect errant vehicles and prevent them from traveling off bridges. These timber railings, like all bridge railings, require successful completion of crash testing and evaluation programs to be approved for use. Over the span of 25 years, from 1988 to 2013, the development of bridge railing systems for timber deck bridges has been guided by a number of safety performance criteria. These criteria were outlined in the 1993 National Cooperative Highway Research Program (NCHRP) Report 350, *Recommended Procedures for the Safety Performance Evaluation of Highway Features* [1]; the 1989 American Association of State Highway and Transportation Officials (AASHTO) *Guide Specifications for Bridge Railings* [2]; the 2009 AASHTO *Manual for Assessing Safety Hardware* (MASH) [3]; and 2016 MASH [4]. The MASH criteria incorporated current vehicle profiles and characteristics to address changes in vehicular design and usage patterns. New roadside safety hardware categories for roadside safety were introduced, crash test documentation was standardized, impact conditions and safety performance evaluation criteria were updated, objective vehicle damage criteria were added, and refinements were made to the occupant risk limits.

Prior to the research reported herein, only three bridge railing systems had been developed for use on wood bridges using MASH impact safety standards, one of which had been crash tested. The only crash tested system to meet MASH impact safety criteria consisted of a Test Level 1 (TL-1) low-height, curb-type, glued-laminated (glulam) timber bridge railing system for transverse, nail-laminated timber decks [5-6]. For a later study, dynamic and static component testing was performed on the MASH TL-1 low-height glulam bridge railing when attached to both a transverse, nail-laminated timber deck and a transverse, glulam timber deck to establish adequacy for the use on a transverse glulam deck [7]. The other bridge railing system was developed to meet MASH Test Level 3 (TL-3) criteria and consisted of a steel W-beam rail and steel post bridge railing system [8]. Thus, a significant need existed to develop new and/or modify existing bridge railings for use on wood bridges under the MASH 2016 impact safety standards. With this need, it was also necessary to develop new, or adapt existing, approach guardrail transition systems to meet MASH impact safety standards and connect timber bridge railing systems to corrugated-beam guardrail systems located beyond the ends of the bridges. Barrier systems need to be subjected to full-scale vehicle crash testing and evaluation, or, depending on the specific requirements and conditions, static and/or dynamic component testing may be conducted as an alternative to full-scale crash testing when specific design changes are desired.

In collaboration with the United States Department of Agriculture – Forest Service – Forest Products Laboratory (USDA – FS – FPL), the US Endowment for Forestry and Communities, and the Midwest Roadside Safety Facility (MwRSF) of the University of Nebraska-Lincoln (UNL), initiated a multiphase project to: (1) identify timber bridge railing systems developed under earlier impact safety standards; (2) document bridge railings currently in use throughout the U.S.; (3) develop a comprehensive research plan to update selected bridge railing and approach guardrail transition systems; and (4) modify existing systems or develop new systems to meet current AASHTO MASH 2016 impact safety standards using the prioritized research plan as funding becomes available.

The first three goals of the research outlined above were accomplished in a Phase I effort [9-10]. During this phase, a survey was conducted which asked multiple state DOTs, companies, and agencies that work with timber bridge railings about their needs for timber bridge railings. From the survey responses, the most common need pertained to a MASH 2016 TL-4 glulam timber railing with a lower curb bridge railing system capable of attachment to transverse and longitudinal glulam decks as well as concrete decks. A TL-3 crashworthy approach guardrail transition system was also deemed necessary for the TL-4 timber bridge railing. Further discussion of these research results with methodologies and cited literature can be found in references [9-10].

Following the Phase I survey results, the Phase IIa efforts of the research program targeted the development of the highest priority bridge railing system, one glulam timber rail with curb bridge railing system designed to meet the MASH TL-4 impact safety criteria [10-11]. The development process relied upon the use of a two-dimensional (2-D) BARRIER VII finite element analysis (FEA) computer program to simulate vehicular impacts into roadside barriers to better understand impact performance and evaluate design variations [12-13]. An FEA bridge railing model was created to represent the NCHRP 350 TL-4 bridge railing system and subject it to simulated vehicle impacts at the conditions used in the physical full-scale vehicle crash tests. After close examination of BARRIER VII simulation results using multiple iterations for both crash tests, the FEA model was deemed to be sufficiently reliable to investigate and predict the impact performance of the bridge railing. Once validated, the BARRIER VII model was used with updated vehicle models and impact conditions to evaluate the bridge railing's structural capacity and safety performance under MASH impact conditions. The minimum railing height was increased to allow the system to meet the MASH 2016 TL-4 impact safety standards to mitigate concerns for vehicle override of the barrier while accounting for future roadway overlays on the bridge deck. The bridge railing components were resized to obtain the necessary railing height with the original deck wearing surface and a future overlay. Further, the connection between the timber railing and the bridge deck was designed to obtain a sufficiently strong connection using the BARRIER VII results. For a more in-depth understanding of the methodology, findings, and conclusions, see the thesis by Duren and the associated final research report [10-11]. The preliminary layout for the MASH TL-4 glulam timber railing with lower curb bridge railing system is shown in Figure 1.

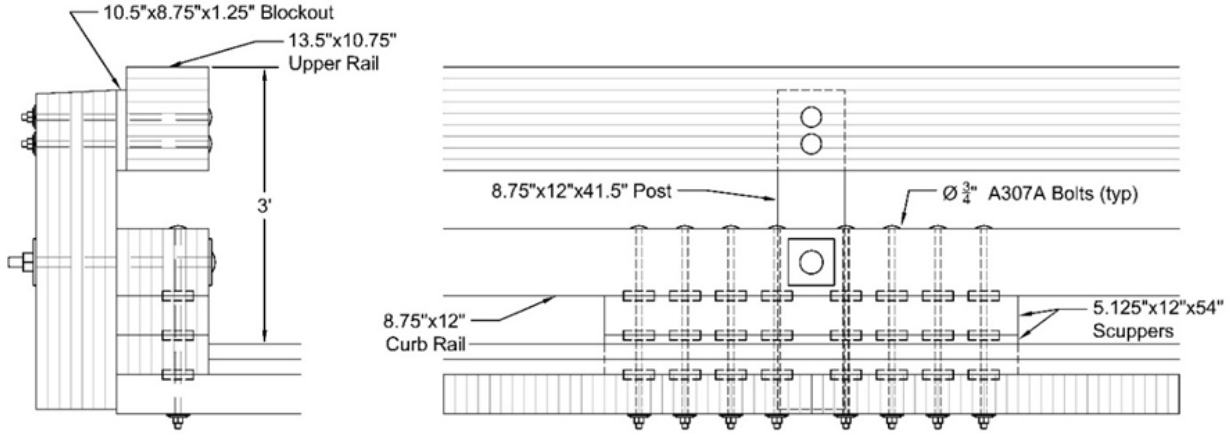

Figure 1. Preliminary Design of MASH TL-4 Glulam Timber Railing with Lower Curb, Phase IIa [10-11]

Although the Phase IIa effort resulted in a preliminary layout, the structural connections were not examined or designed. Only a limited investigation into the connections was performed using the American Wood Council National Design Standard (NDS) [14]. The Phase I effort outlined the need to develop an approach guardrail transition to connect the bridge railing to the adjacent guardrail system, but this effort had not been initiated.

1.2 Research Objective

The research objectives of this phase of the project included the continued development of a glulam timber rail with lower curb bridge railing to meet the MASH 2016 Test Level 4 (TL-4) safety performance criteria for use on both transverse and longitudinal glulam timber bridge decks, other desired deck types, and reinforced-concrete bridge decks. An approach guardrail transition (AGT) was also configured to connect W-beam guardrail systems to the glulam timber rail and lower curb bridge railing, and meet MASH TL-3 impact safety standards.

The bridge railing system was configured using glulam timber for all the wood components, such as the upper rail, lower curb rail, scuppers, spacer or offset blocks, and vertical support posts. The bridge railing system should be constructed and crash tested on a critical timber deck configuration in order to allow its use on alternative timber and reinforced concrete slab decks. A critical deck thickness and deck cantilever, or overhang, is to be determined. The research and development effort identified, through survey, literature review, and/or partner expertise, the practical ranges for glulam deck panel dimensions (i.e., widths, lengths, and thicknesses) as well as the ranges for deck cantilevers for transverse glulam timber decks. Alternative timber deck systems, such as innovations in stress-laminated, timber deck panels or beams, were considered for this study but not used. The development effort also considered common timber species for the structural components, such Southern Pine and Douglas Fir.

The development of the bridge railing and transition systems began with an initial condition in which the glulam timber deck included a 2-in. asphalt wearing surface. This surface thickness was intended to reflect the bridge deck condition at the time when the structure was first opened to traffic, with the railings installed in that configuration. In practice, many bridge decks will receive an additional asphalt overlay in the future, which can increase the total surface thickness by 2 in. To address this, the research and development effort considered a total surfacing thickness of 4 in. when determining the geometric and structural requirements of the railing system to meet the MASH 2016 TL-4 impact safety criteria and of the transition system to meet the MASH 2016 TL-3 criteria.

1.3 Research Approach

The research began with a focused effort to identify and consider various timber decks in use to determine the critical configuration. Discussions and collaboration with experienced partners were crucial in narrowing down the deck types suitable for the TL-4 bridge railing system. Detailed evaluation of timber deck characteristics, including typical dimensions, spans, and strengths, were gathered for the range of timber decks built across the US. Additionally, the study encompassed an exploration of the possible ranges for deck cantilevers on transverse glulam timber decks.

The design of all connections for the bridge railing was conducted following the literature review of timber bridge decks. A careful review of the Phase IIa BARRIER VII simulation results established the demands for the components. Review of lateral, longitudinal, and vertical vehicle impact loads from simulations and AASHTO LRFD Bridge Design Specifications (BDS) [15] were used to complete the connection designs. The vehicle impact loads applied to the bridge deck were the maximum impact loads the bridge railing connection capacities could transfer to the bridge deck and were used to evaluate its performance. The critical deck configurations for longitudinal and transverse decks were identified, recommendations were developed for dynamic component tests on transverse and longitudinal glulam timber decks, and 2-D and 3-D test plans were created for the bridge post connection to the critical deck configurations.

Excessive water on the bridge deck represents a significant risk to railing performance and long-term durability. Timber components exposed to repeated moisture infiltration are prone to strength loss, swelling, shifting, and other degradation that can compromise structural reliability. A literature review was performed to investigate methods for protecting wood against excess moisture, focusing on both deck elements and the railing–deck interface. Based on this review, cost-effective options were identified to reduce water exposure beneath the asphalt wearing surface and near the base of the bridge railing system. The lower components of the bridge post–scupper block system were found to be particularly vulnerable to moisture, prompting the need to design for elevated moisture content in those members. Accordingly, additional analysis was conducted on the timber scupper, incorporating reduced material properties for high-moisture conditions. The updated configuration was then re-evaluated using BARRIER VII simulation to assess performance under impact loads. These refinements were carried forward into the bridge railing system design, guiding further development of the critical transverse and longitudinal deck configurations and informing full-scale crash testing. The results were captured in updated 2-D drawings and 3-D models to reflect the optimized system layout and material durability considerations.

The development of an approach guardrail transition began with creating and calibrating a BARRIER VII model of a prior thrie-beam system. After the calibration effort, the barrier system development process continued with consideration of recent advancements to incorporate into the AGT system. A review was also conducted on the impact performance of wood posts embedded in soil with cross-sections larger than 6 in. x 8 in. The review identified research gaps that led to the need to conduct dynamic component testing on larger wood posts. Two-dimensional (2-D) and 3-D drawings were created for the necessary bogie tests. Three bogie tests were conducted, and the bogie testing results were evaluated and used to support the development of the new AGT.

Design concepts were brainstormed for the connection between the bridge railing and the thrie-beam AGT. The connection concepts were narrowed down through different limiting parameters for the bridge rail-to-AGT connection. Both half-post spacing and quarter-post spacing AGT concepts were configured and investigated through BARRIER VII computer simulation. The new AGT concepts included accommodation for a 2-in. thick wearing surface. The BARRIER VII effort simulated impacts with a MASH 2016 2270P pickup truck. Impacts with the small car were not performed in this effort as the pickup truck represented the higher impact loading. A critical impact point analysis was conducted on the proposed AGT systems to determine the impact locations for test designation nos. 3-20 using the 1100C small car sedan and 3-21 using the 2270P

pickup truck. This analysis provided the basis for a new AGT design, including 2-D plans of the system and its components.

Evaluation of the timber bridge railing continued through dynamic component testing. Although two post tests were planned on both transverse glulam and longitudinal glulam decks for a total of four tests, only one test is reported herein. The first dynamic component test was conducted to investigate the adequacy and performance of bridge post connection attached to a transverse, glulam timber bridge deck. The component test was extensively instrumented with string potentiometers and strain gauges on timber and steel components and accelerometers on the bogie vehicle. The test results were used to evaluate adequacy and effectiveness of the connection details. Based on the performance, changes were made to the bridge railing system for consideration in the future dynamic component tests and possibly for the full-scale vehicle crash testing program.

2 LITERATURE REVIEW

2.1 Introduction

The literature was reviewed for previous higher-performance bridge railings that were developed for timber bridge decks. Following this step, a review of prior NCHRP 350 and MASH approach guardrail transitions (AGTs) was performed to inform the design process for the new AGT system. The impact performance of 8-in. x 8-in. and larger timber guardrail posts embedded in soil was briefly investigated for the AGT design process as well. This investigation was followed by a review of timber deck types, sizes (i.e., widths, lengths, and thicknesses), and the mechanics for load distribution through them. Issues regarding the protection of timber decks from water runoff, the application of preservatives, and the mechanical properties of wood under impact loading emerged as significant focus areas over the course of railing development.

2.2 PL-2/TL-4 Bridge Railings for Timber Bridge Decks

2.2.1 GC-8000

Currently, four bridge railings for use on timber deck bridges have been developed and tested to the AASHTO PL-2/NCHRP-350 TL-4 impact conditions in the U.S. The Glulam Timber Rail with Curb Bridge Railing, also called GC-8000, was crash tested on a longitudinal timber bridge deck at MwRSF in 1993 [16]. The bridge railing was originally adapted from an AASHTO Performance Level 1 (PL-1) system crash tested by MwRSF and modified to meet the AASHTO PL-2 impact conditions [17-18].

The bridge deck was composed of 10¾-in. thick Douglas Fir-Larch glulam panels measuring 4 ft wide and 18 ft – 9 in. long. The post-to-deck panel connections included two ⅝-in. diameter, ASTM A722 steel transverse stressing rods spaced 22 in. apart. These rods passed through the exterior panels for a total length of 48 in. and were centered 3 in. below the top of the deck surface. The posts in this system were spaced at 6 ft – 3 in., so that the spacing would be consistent across multiple longitudinal deck panels. The system had an overall height of 35 in. and utilized a 2-in. asphalt wearing surface on top of the timber deck, which resulted in an effective height of 33 in. Photographs of the installed system are shown in Figure 2.

Figure 2. GC-8000 Timber Bridge Railing on Longitudinal Glulam Deck [16]

The only glulam component of the bridge railing system was the upper rail, which was 13½ in. tall x 6¾ in. wide and fabricated from combination 2 Douglas Fir-Larch glulam. The sawn lumber curb rails were nominally 6 in. tall x 12 in. wide. The sawn posts nominally measured 8 in. x 10 in. x 45¾ in. long. The sawn blockouts measured 4¾ in. wide x 7½ in. long x 13½ in. tall, and the scuppers nominally measured 8 in. tall x 12 in. wide x 4 ft long. All sawn components were Grade No. 1 Douglas Fir surfaced on all four sides and pressure-treated with creosote to a retention of 12 lb/ft^3. Splices used a single ⅝-in. thick x 13½-in. wide x 29-in. long steel plate placed in a groove cut through the middle of the upper rail. Four ASTM A307A 1¼-in. diameter bolts held the plate to the railing on either side, and four ASTM A307A ⅝-in. diameter bolts held the railing to the post. The upper railing was attached to the post at every other post location with two ASTM A307A ⅝-in. diameter bolts. The post was attached to the curb rail with one ASTM A307A 1¼-in. diameter bolt. The curb rail and scupper blocks were anchored to the deck with six ASTM A307A ¾-in. diameter vertical bolts with 4-in. diameter shear plates. These components are shown in Figure 3. The maximum dynamic deflection for this railing was 14.2 in., as determined from the pickup truck used in test no. FSCR-4.

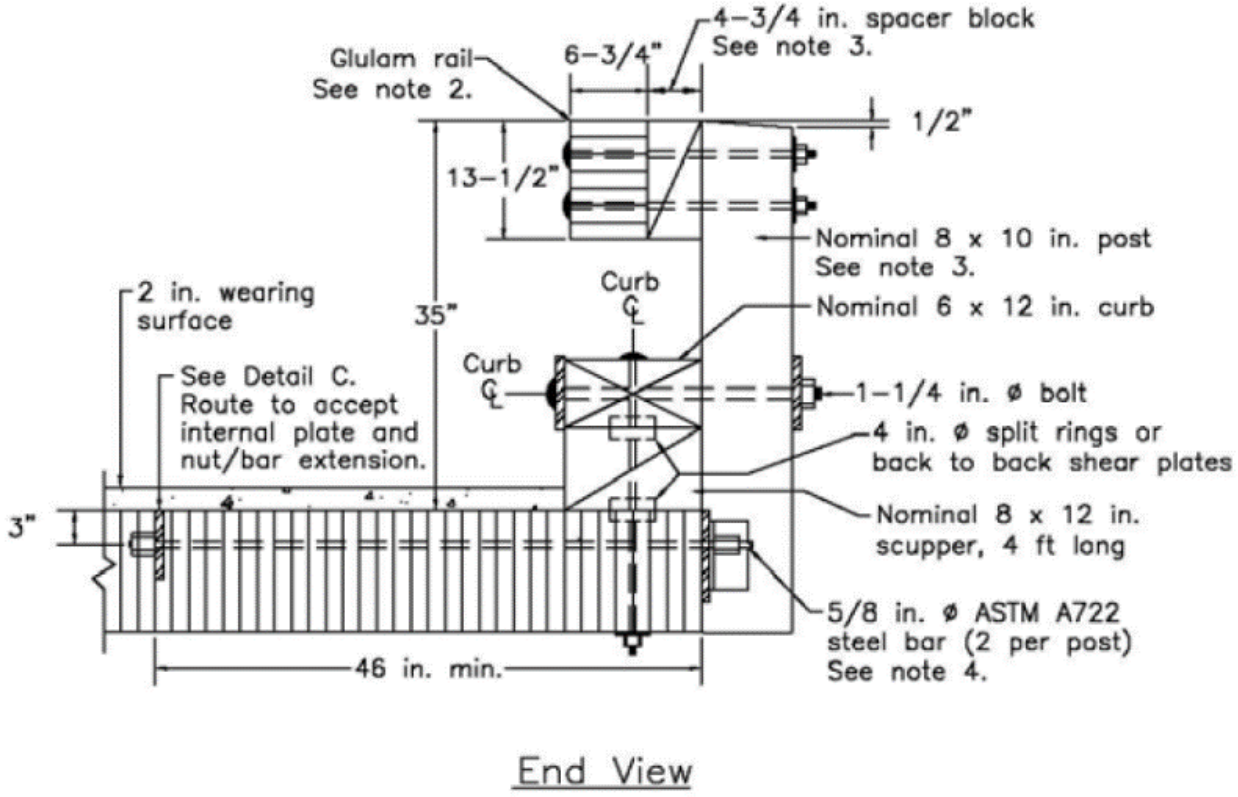

Figure 3. NCHRP 350 TL-4 Bridge Railing Cross-Section on Longitudinal Glulam Deck [16]

The bridge railing adequately resisted impact from an 18,000-lb single-unit-truck (SUT) traveling at 82.4 km/hr and at an angle of 16.8 degrees in crash test no. FSCR-1. Because this test condition also met NCHRP 350 TL-4 requirements (a 17,637-lb SUT travelling 80 km/hr and 15 degrees), the GC-8000 would be crashworthy for NCHRP 350 TL-4 with an additional pickup truck crash test. The test resulted in maximum dynamic and permanent set deflections of 6.5 in. and 1.2 in. respectively.

The bridge railing adequately resisted impact from a 4,508-lb pickup truck traveling at 57.5 mph and at an angle of 21.8 degrees in crash test no. FSCR-3. The test resulted in maximum dynamic and permanent set deflections of 6.1 in. and 0.4 in. respectively. These impact conditions were insufficient for TL-4 for NCHRP 350, so the test was rerun as test no. FSCR-4.

The bridge railing adequately resisted impact from a 4,601-lb pickup truck traveling at 61.4 mph and at an angle of 24.9 degrees in crash test no. FSCR-4. The test resulted in maximum dynamic and permanent set deflections of 14.2 in. and 2.1 in. respectively. The impact event led to rupture for one of the two transverse deck stressing rods at a post location, but this outcome was not a reason to consider the crash test a failure as the vehicle was safely captured and smoothly redirected.

2.2.2 TBC-8000

The Thrie-Beam and Channel Bridge Railing, also called TBC-8000, was crash tested on a longitudinal timber bridge deck at MwRSF in 1992 [19]. The Missouri combination steel railing system successfully met NCHRP 230 safety performance requirements [20] and was the concept behind introducing a steel bridge railing to test an alternate railing on a longitudinal timber bridge deck. A steel post and thrie-beam, similar to the Missouri system, were the primary components for redirecting vehicles for an AASHTO Performance Level 1 (PL-1) "steel" system [17-18]. The PL-1 AASHTO railing system, crash tested by MwRSF using a 5,600-lb vehicle at 44.2 mph and 19.1 degrees, successfully met impact requirements with a maximum dynamic deflection of 13.8 in. and a permanent maximum deflection of 8.1 in. [17]. To meet AASHTO PL-2 impact conditions, a C8x11.5 A36 steel channel was added to the top of the steel spacer blocks. A cross-section of the bridge railing is shown in Figure 4.

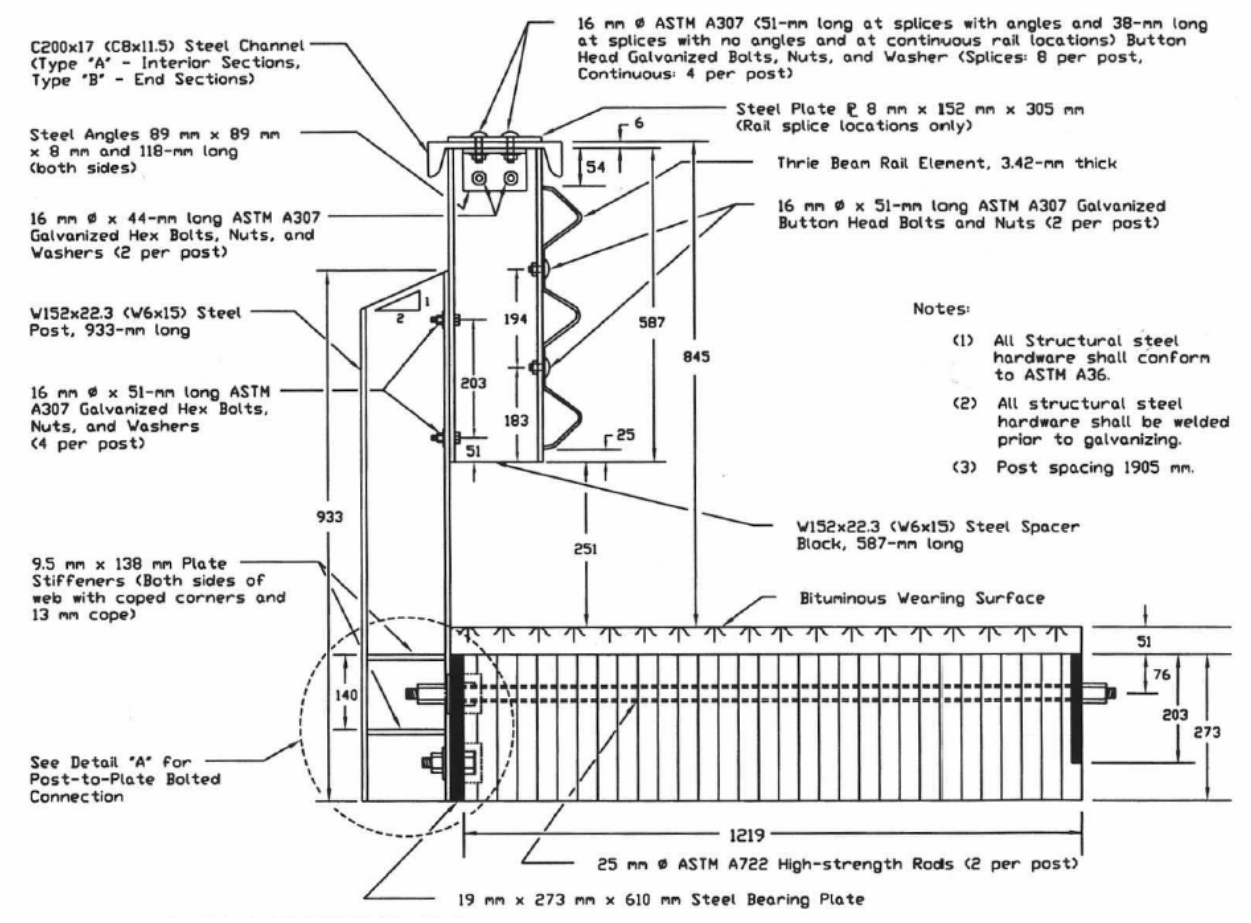

Figure 4. AASHTO PL-2 Bridge Railing Cross-Section on Longitudinal Glulam Deck [19]

The bridge deck was composed of 10¾-in. thick Douglas Fir-Larch glulam panels 4 ft wide and 18 ft – 9 in. long. The post-to-deck panel connections included two ⅝-in. diameter ASTM A722 steel stressing rods spaced 16 in. apart. These rods passed through the exterior panels for a total length of 48 in. and were centered 3 in. below the top of the deck surface. The posts in this system were spaced at 6 ft – 3 in. The system had an overall height of 35¼ in. and utilized a 2-in.

asphalt wearing surface on top of the timber deck, which resulted in an effective height of 33¼ in. The post and the blockout were both cut from W6x15 A36 steel sections. A photograph of the installed system is shown in Figure 5.

Figure 5. TBC-8000 Steel Bridge Railing on Longitudinal Timber Bridge Deck [19]

The bridge railing adequately resisted impact from an 18,001-lb SUT traveling at 51.2 mph and at an angle of 16.1 degrees in crash test no. FSTC-1. The test resulted in a maximum permanent set deflection of 8.19 in., which pertained to the thrie-beam railing. No damage was noted to the bridge deck as a result of the crash test into the bridge railing system.

2.2.3 Glulam Rail with Curb on Transverse Glulam Deck

In 1997, the third timber bridge railing was tested at MwRSF according to the NCHRP 350 TL-4 impact conditions when installed on a transverse glulam timber deck [21-25]. Two crash tests were conducted on this bridge railing, one test with the SUT and another test with the pickup truck. The bridge deck comprised 5⅛-in. thick Douglas Fir-Larch glulam panels measuring 4 ft wide and 13 ft long. The bridge posts were spaced on 8 ft centers, so that the posts would be centered at every other joint between panels. The bridge deck overhang was approximately 2 ft away from the centerline of the exterior girders. The bridge railing system had an overall top rail height of 35 in. above the deck panels and utilized a 2-in. thick concrete wearing surface on top of the timber deck, resulting in an effective top rail height of 33 in., similar to the GC-8000 bridge railing. Photographs of the installed system are shown in Figure 6.

Figure 6. NCHRP 350 TL-4 Glulam Timber Bridge Railing with Curb on Transverse Glulam Deck [25]

This system was completely fabricated with glulam components, with the upper rail segments and the posts using higher graded glulam as compared to the scupper blocks, curb rail segments, and blockouts. The upper rail's cross-section was 13½ in. tall x 8¾ in. wide, and the post dimensions were 8¾ in. x 10½ in. x 41½ in. long, both fabricated from Combination 48 Southern Yellow Pine glulam. The curb rail's cross-section was 6¾ in. tall x 12 in. deep, the blockout dimensions were 3⅛ in. thick x 8¾ in. wide x 10½ in. tall, and the scupper dimensions were 6¾ in. tall x 12 in. deep x 54 in. long. All three parts were fabricated from Combination 47 Southern Yellow Pine glulam. All components were pressure-treated with pentachlorophenol to a retention of 0.6 lb/ft3. The upper railing was attached to the post with two ASTM A307A ¾-in. diameter bolts. The posts were held to the curb rail with one ASTM A307A 1¼-in. diameter bolt. The curb rail and scupper blocks were anchored to the deck with six ASTM A307A ¾-in. diameter vertical bolts with 4-in. diameter split rings between timber layers. These components are shown in Figure 7.

During the third research and development program, the researchers reviewed and used the successful crash test results from the GC-8000 bridge railing system to revise the bridge railing configuration to avoid excessive damage to posts and blockouts. In test no. FSCR-1, it was observed that the 8000S SUT van body and frame structure leaned on the upper rail and extended over and below it on the back side, contacting and snagging on the top of several support posts and spacer blocks during the crash event. This behavior led the research team to place the upper rail higher than the top of the posts and spacer blocks in order to minimize vehicle snag and the associated damage to the timber elements.

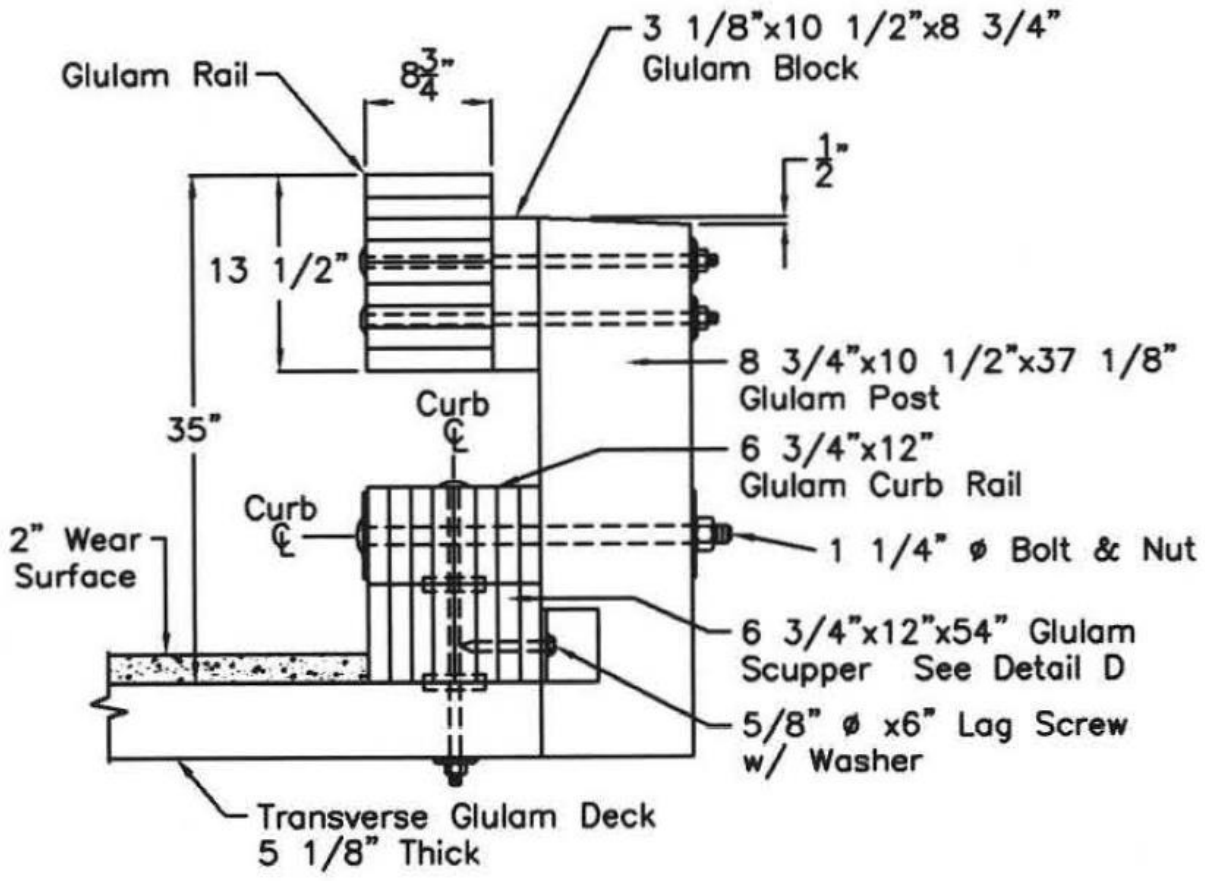

Figure 7. NCHRP 350 TL-4 Bridge Railing Cross-Section on Transverse Glulam Deck [20]

The bridge railing adequately resisted impact from a 17,637-lb SUT at 46.5 mph and at an angle of 16.0 degrees in crash test no. TRBR-1. The test resulted in maximum dynamic and permanent set deflections of 3.3 in. and 0.4 in. respectively. The vehicle obscured the railing from the overhead camera for much of the crash event, and greater dynamic deflections may have occurred but were not visible. No impact damage was noted to have occurred to the bridge deck during the crash test on the bridge railing; however, this damage would have been difficult to observe due to the placement of a 2-in. concrete wearing surface on top of the deck. A review of photographs revealed cracking in the concrete wearing surface at the interface to the concrete tarmac. The railing experienced gouging along the front face of the upper and curb railings as well as on top of the posts supporting the upper railing.

The bridge railing also adequately resisted impact from a 4,394-lb pickup truck traveling at 61.6 mph and at an angle of 27.4 degrees in crash test no. TRBR-2. The test resulted in maximum dynamic and permanent set deflections of 8.0 in. and 1.1 in. respectively. Most of the railing was visible to the overhead camera during the crash event, and the maximum deflection was not obscured. Again, no damage was noted to the bridge deck, and no photographs revealed any potential damage to the timber deck.

2.2.4 Steel Thrie-Beam Rail on Transverse Glulam Deck

In 1997, the fourth timber bridge railing was tested at MwRSF according to the NCHRP 350 TL-4 impact conditions when installed on a transverse glulam deck [21-25]. The previously developed TBC-8000 served as the basis for the development of the Steel Thrie-Beam on Transverse Glulam Deck. Two crash tests were conducted on this bridge railing, one test with the SUT and another test with the pickup truck. The bridge deck comprised 5⅛-in. thick Douglas Fir-Larch glulam panels measuring 4 ft wide and 13 ft long. The bridge posts were spaced on 8-ft centers, so that the posts would be centered at every other joint between panels. The deck panel overhang was approximately 2 ft away from the centerline of the exterior girders. The bridge railing system had an overall top rail height of 36 in. above the deck panels and utilized a 2-in. thick concrete wearing surface on top of the timber deck, resulting in an effective top rail height of 34 in. Photographs of the installed system are shown in Figure 8.

Figure 8. NCHRP 350 TL-4 Steel Thrie-Beam Bridge Railing on Transverse Glulam Deck [25]

This system was completely fabricated with steel components, using a 10-gauge thrie-beam rail as the primary railing component. An 8-in. wide x 3-in. tall x $^{3}/_{16}$-in. thick ASTM A500 Grade B HSS steel tube section was used for the top railing. The steel blockout and post were both ASTM A36 W6x15 steel sections. The blockout was $19^{3}/_{16}$ in. long, and the post was $37^{13}/_{16}$ in. long. The top rail was attached to the blockout using four ⅝-in. diameter bolts, which held it to two 3½-in. x 3½-in. x $^{5}/_{16}$-in. steel angles measuring 4⅝-in. long. These angles were bolted to the web of the blockout with two ⅝-in. diameter bolts. The thrie-beam rail was attached to the blockouts with two ⅝-in. diameter bolts, and the blockouts were attached to the posts with four ⅝-in. diameter bolts. Four stiffeners were welded in each post to increase local buckling resistance at the base. Two ¾-in. and two 1-in. diameter bolts were used to hold each post to two steel plate assemblies, one resting on the deck surface and the other attached beneath the bottom of the deck. Each steel plate assembly was 44 in. wide and 14 in. deep. Twelve ASTM A325 ⅞-in. diameter bolts held the steel plate assemblies to the transverse glulam deck panels. The farthest line of bolts holding the steel plate assemblies to the bridge deck was 12 in. centered away from the deck edge. The steel plate assemblies straddled two transverse glulam bridge deck panels. These components are shown in Figure 9.

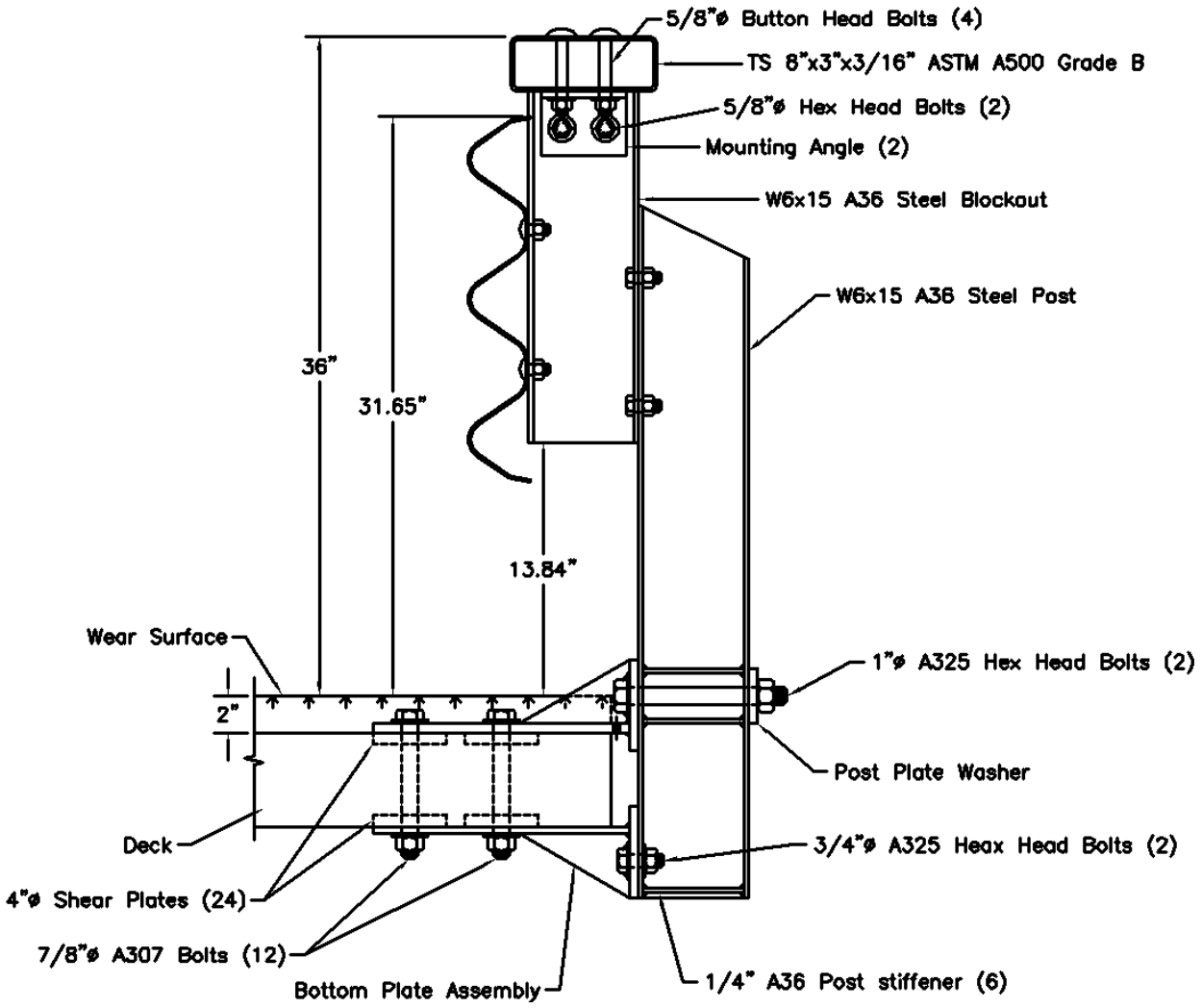

Figure 9. Steel Thrie-Beam Railing for NCHRP-350 TL-4 on Transverse Glulam Deck [25]

The bridge railing also adequately resisted impact from a 4,396-lb pickup truck traveling at 58.2 mph and at an angle of 25.5 degrees in crash test no. STTR-1. The test resulted in maximum dynamic and permanent set deflections of 5.4 in. and 4.6 in. respectively. No damage was noted on the timber bridge deck. Photographs showed cracking in the 2-in. concrete wearing surface above the steel assembly at some posts, and the concrete wearing surface was removed at some locations to examine damage to the steel assembly. No photographs showed the bridge deck following impact.

The bridge railing adequately resisted impact from a 17,785-lb SUT traveling at 47.5 mph and at an angle of 14.6 degrees in crash test no. STTR-2. The test resulted in a maximum permanent set deflection of 5.4 in. No maximum dynamic deflections were recorded. During the second test, the vehicle obscured the view of the top of the railing for an extended time period. No damage was noted to the timber deck.

2.2.5 Z B4-20 on Stress-Laminated Deck

The timber bridge railing designation Z B4-20 was developed in Norway in 2011 for use on stress-laminated timber decks [26]. The design conformed to the H2 containment class specified by EN1317 [27]. It was first simulated with LS-DYNA using impact conditions consisting of a 13,000-kg (28,660-lb) bus impacting the railing at a 20-degree angle and traveling 70 kph (43.5 mph) and a 900-kg (1,984-lb) small car impacting at a 20-degree angle and travelling at 100 kph (62 mph) [26]. Posts were spaced at 2 m (6.6 ft), which supported three railings (1.41 m, 0.74 m, and 0.47 m centered from the top of the bridge deck). The top of the system was 1.45 m (4.8 ft) above the bridge deck surface. The posts were secured to steel plates that were attached to the deck with two steel stressing rods, which penetrated 2 m (6.6 ft) into the deck and had a diameter of 20 mm (⅞ in.). The railings were composed of three steel pipe railings measuring 82.5 mm (3¼ in.) in diameter and made from low-strength steel with a 235 MPa (34 ksi) yield strength. These elements are shown in Figure 10.

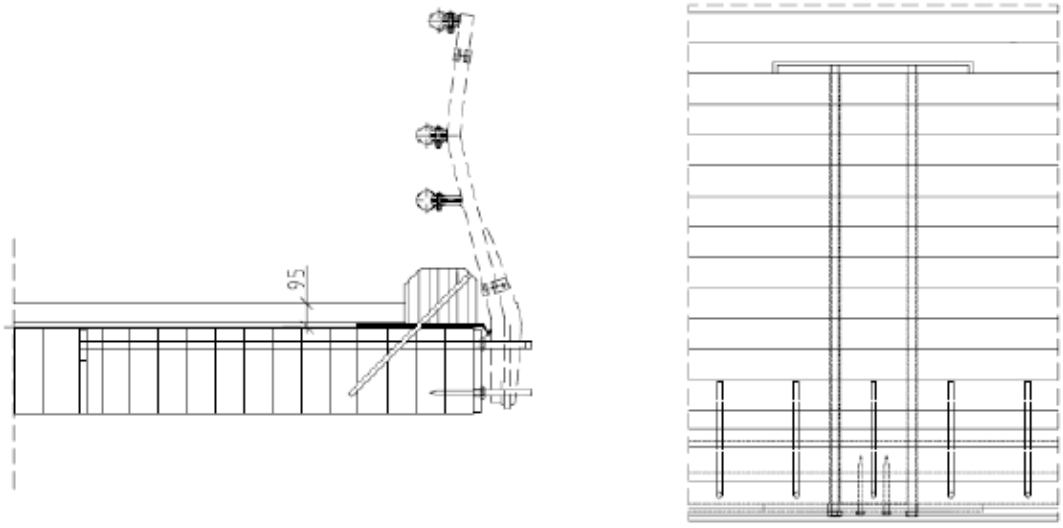

Figure 10. Bridge Railing Developed for Stress-Laminated Timber Decks in Norway: Cross-Section (left) and Plan View (right) [deck stressing rods not shown for clarity] [28]

The research and development effort for this railing utilized computer simulations instead of physical component testing. Furthermore, researchers investigated how the length of the rods used to anchor the posts to the bridge deck affected the deck rotation. Researchers found that longer stressing rods resulted in stiffer bridge decks and that a minimum stressing rod length of 1.6 m (63 in.) provided superior stress distribution and a reduction of the dynamic impact loads. Note that study details were not available in the railing development report. The stressing rods were spaced 240 mm (9.4 in.) from one another on a simulated bridge deck measuring 350 mm (13.8 in.) thick. The stressing rods were centered up to 57 mm (2¼ in.) from the top of the timber surface in the Norway bridge railing [28]. The simulated maximum dynamic deflections were not reported in the development effort, but additional documentation on the railing noted that dynamic deflections were intended to be 800 mm (31.5 in.) [29]. A photograph of the as-built railing system is shown in Figure 11.

Figure 11. Timber Bridge Railing for Stress-Laminated Deck Built by AB Varmförzinkning [30]

2.3 Approach Guardrail Transitions

2.3.1 Overview

Approach guardrail transitions (AGTs) are attached to the ends of bridge railings to provide structural continuity between the vehicle barrier systems on the bridge and along the approach roadway. These transitions prevent motorists from striking the bridge rail ends, which are often configured with rigid end buttresses. They also provide a gradual lateral stiffness transition between strong bridge railings and deformable guardrails to reduce risks for high deflections upstream from low deflection barriers, which may result in either vehicle snag or pocketing with excessive decelerations. These transition systems also need to perform in an acceptable manner by safely containing and smoothly redirecting errant vehicles without vehicle rollover.

AGTs incorporate posts that are embedded in soil, and the satisfactory performance of the posts placed in the soil is critical to their proper function. An appropriately-designed transition must consider a reasonable combination of post spacing, post type, post size, and embedment depth, which are gradually matched to the adjacent guardrail in advance of the transition. An AGT system is typically configured with thrie-beam or W-beam rail elements, both of which can be nested, but only W-beam rails have been stacked vertically. Nesting refers to two railings that overlap one another in the same "layer," and stacking refers to setting one railing above the other in elevation. AGT systems often use thrie-beam rails, while guardrail systems often use W-beam rails. For this common configuration, a transition piece is used to connect the W-beam guardrail to the thrie-beam AGT. These pieces were traditionally symmetric; however, more recently these segments have become asymmetric. Symmetric pieces maintain the same centerline between the thrie-beam and W-beam rails, and asymmetric transition sections maintain the same relative top elevation between barrier systems.

For the higher performance steel bridge rails that were developed and crash tested on timber decks, no details and crash-testing information are provided herein for the approach guardrail transitions connecting the steel bridge rails with the guardrail. These AGTs did not possess relevant background, such as a timber railing connection or timber posts of sizes of 8 in. x 8 in. or larger, which were deemed important to the new AGT design.

2.3.2 Thrie-Beam Transition to GC-8000

The GC-8000 bridge railing included an approach guardrail transition at the end of the bridge rail. The main upper transition rail was a 10-gauge thrie-beam rail measuring 12 ft – 6 in. long with a top rail height of 31 in. from the ground. The thrie-beam rail connected directly to a thrie-beam terminal connector, which was bolted to the bridge railing with five ⅞-in.-diameter bolts and an ASTM A36 ½-in. thick steel plate. The 10-gauge thrie-beam rail was also connected to a 12-gauge symmetric transition section, which connected to a 12-gauge W-beam guardrail system at a height of 27 in. The spacing between the last bridge railing post and the first AGT post was 4 ft – 1½ in., which shifted to quarter-post (18¾-in.) spacing between transition posts 1 through 5. The first two AGT posts were 8 in. wide x 8 in. deep x 6½ ft long with an embedment depth of 46 in. The gap between the end of the bridge deck and the edge of the first post was 8 in. AGT posts 3 through 7 were 8 in. wide x 8 in. deep x 6 ft long with an embedment depth of 40 in., although the spacing switched from quarter-post to half-post (3 ft – 1½ in.) spacing between posts 5 and 6. All posts were Grade No. 1 SYP treated with chromated copper arsenate (CCA).

The connection from the AGT to the bridge railing also included a taper in the lower timber curb railing under the thrie-beam rail and a reverse-tapered block underneath the upper timber railing. The transition is shown in Figure 12. The approach guardrail transition connected to the bridge railing with a steel plate embedded within a midplane kerf through the end of the upper bridge railing. This connection is detailed on several FPL plans for TL-4 timber bridge approach guardrail transitions [31-32].

Figure 12. AGT Developed for GC-8000 [16]

The thrie-beam transition to the GC-8000 was crash tested to NCHRP Report 230 Multiple Service Level 2 (MSL-2) standard impact conditions with a 4500S car in test no. FSCR-2 [33]. The transition adequately resisted impact from a 4,506-lb sedan traveling at 62.4 mph and at an angle of 24.8 degrees. The test resulted in maximum dynamic and permanent set deflections of 7.4 in. and 1.6 in., respectively. The lower tapered curb rail that transitioned to the lower curb bridge rail was significantly damaged. The bolts, which held the curb rail to the bridge deck, began to pull through the lower curb rail at the first bridge post. System CAD details are shown in Figures 13 and 14.

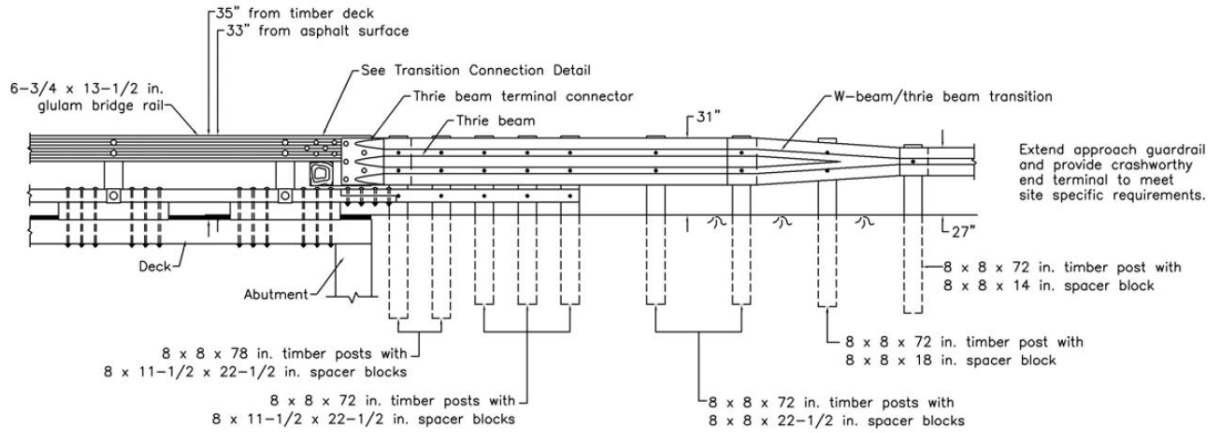

Figure 13. Front View of AGT Developed for GC-8000 [16]

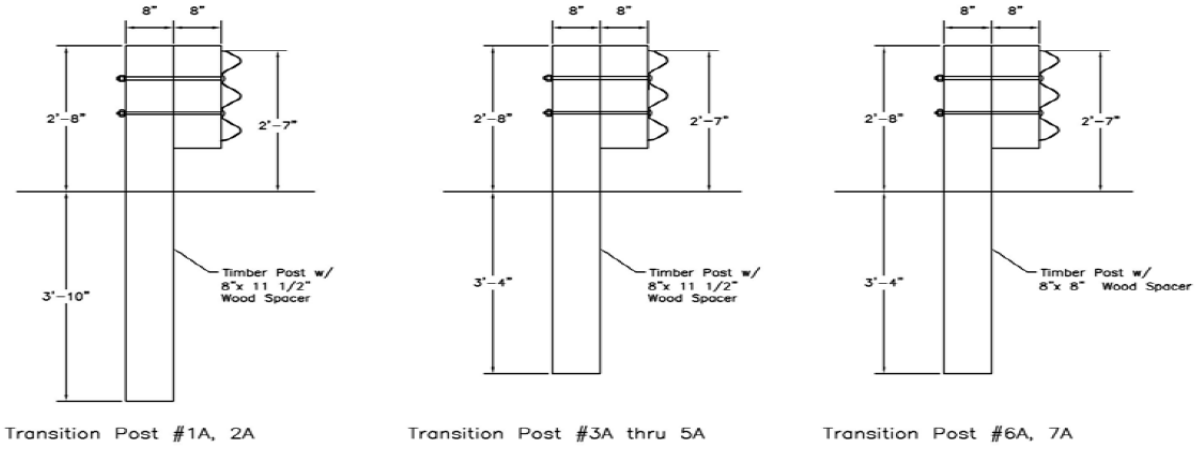

Figure 14. Cross-Section View of AGT Posts Closest to Bridge Railing [16]

2.3.3 Thrie-Beam Transition to Glulam Rail with Curb Bridge Railing

The 1997 AGT developed for the NCHRP 350 TL-4 Glulam Rail with Curb Bridge Railing was configured with an upper 10-gauge thrie-beam mounted at 31⅝ in. The lower curb rail was tapered off beneath the thrie-beam rail. Farther upstream, the thrie-beam rail transitioned to a 12-gauge W-beam guardrail system with a top mounting height of 27¾ in. [20]. These rail elements are shown in Figure 15. The spacing between the last bridge railing post and the first AGT post was 4 ft, which shifted to quarter-post (18¾-in.) spacing between AGT transition posts 1 through 7. The gap between the end of the bridge deck and the edge of the first post was 1 ft – 6 in. The first four AGT posts were 8 in. x 8 in. x 6½ ft with an embedment depth of 45.35 in., followed by three 6-ft long posts embedded 39.35 in. into the ground. Three additional 8-in. x 8-in. timber posts were located upstream from the half-post spacing using various embedment depths for the symmetric transition segment. All 8-in. x 8-in. posts were Grade No. 1D SYP treated with CCA.

After the transition element, a strong-post W-beam guardrail system was used for the roadside barrier. AGT CAD details are shown in Figures 16 and 17.

Figure 15. AGT Connecting to NCHRP 350 TL-4 Railing on Transverse Glulam Deck [25]

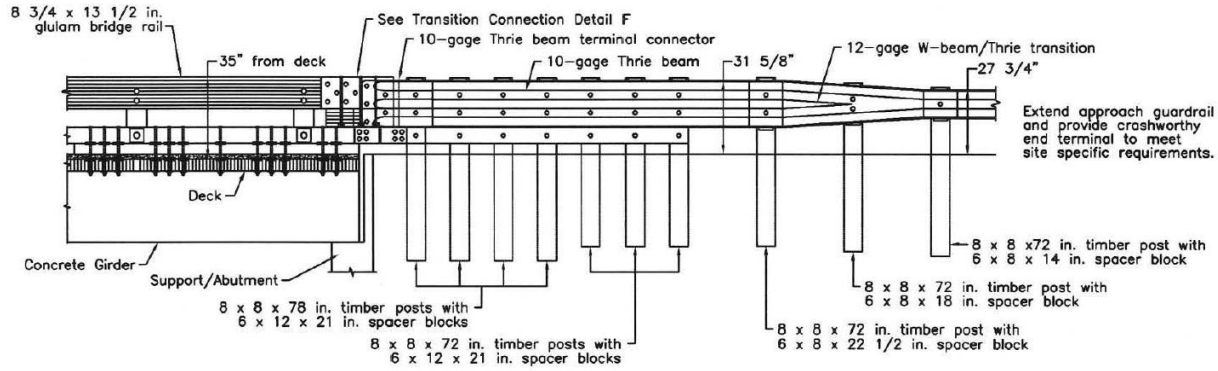

Figure 16. Front View of AGT Connected to NCHRP-350 TL-4 Railing on Transverse Glulam Deck and W-Beam Guardrail [25]

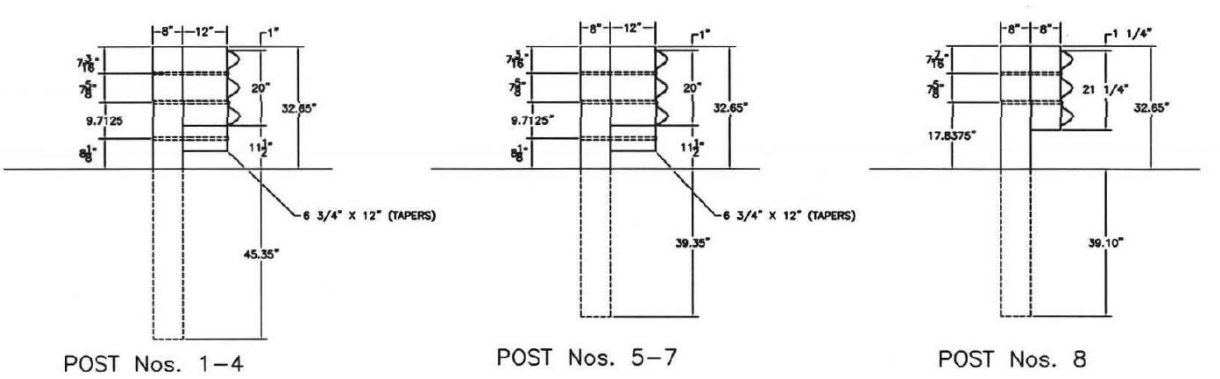

Figure 17. Cross-Section View of AGT Posts Closest to Bridge Railing [25]

The thrie-beam transition to the Glulam Rail with Curb was crash-tested to NCHRP 350 TL-4 impact safety standards. The transition adequately resisted impact from a 4,473-lb pickup truck traveling at 65.2 mph and at an angle of 26.4 degrees in crash test no. TRBR-3. The test resulted in maximum dynamic and permanent set deflections of 6.4 in. and 1.4 in. respectively. This impact did not seriously damage the timber curb rail transition. The primary damage was flattening of the thrie-beam rail and gouging of the upper glulam timber rail.

The transition also adequately resisted impact from a 17,644-lb SUT traveling at 51.3 mph and at an angle of 13.7 degrees in crash test no. TRBR-4. The test resulted in maximum dynamic and permanent set deflections of 4.9 in. and 1.9 in. respectively. Again, very little damage was observed to the tapered timber curb rail underneath the thrie-beam rail, which was flattened, and the end of the upper glulam rail was gouged.

2.3.4 Midwest Guardrail System Transition to Stiff Bridge Railing

In 2005, a new AGT system was crash tested, which was designed with a new upstream transition between the AGT and the guardrail following a previous failed crash test [34-35]. The upstream transition was designed with a new standard asymmetric guardrail piece, as shown in Figure 18. Three different posts were used for this AGT design: three W6x15 sections closest to the bridge rail with embedment depths between 54 to 55 in., seven W6x12 sections with a 58-in. embedment depth, and the remainder of the guardrail posts using W6x9 steel posts at a 40-in. embedment depth [35]. Half-post spacing was used for all posts, with three W6x9 posts spaced at half-post spacing before the fourth post was shifted to full-post (6 ft – 3 in.) spacing for the guardrail. The AGT configuration is shown in Figure 18.

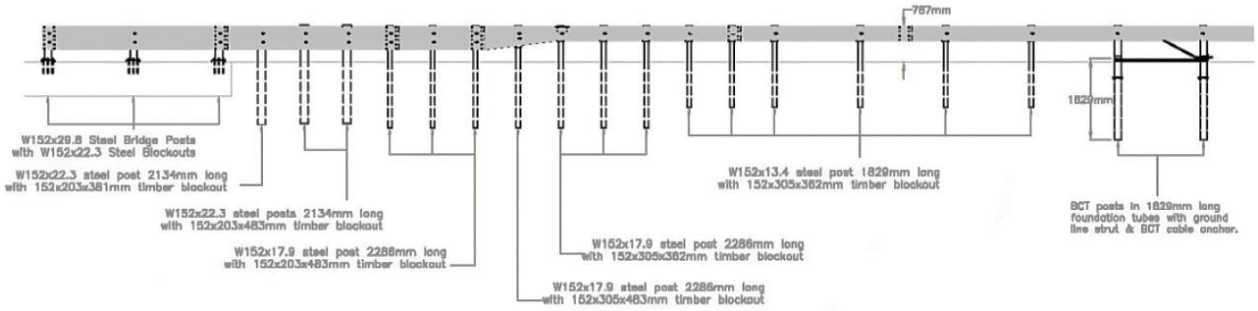

Figure 18. Front-View, Final Design of AGT Connection between MGS and Stiff Bridge Rail [35]

The transition adequately resisted impact from a 4,431-lb pickup truck traveling at 61.5 mph and at an angle of 24.9 degrees in crash test no. MWT-5. The test resulted in maximum dynamic and permanent set deflections of 23.8 in. and 14.8 in., respectively. Following this successful test, the transition also adequately resisted impact from a 1,992-lb small car traveling at 65.5 mph and at an angle of 20.4 degrees in crash test no. MWT-6. The test resulted in maximum dynamic and permanent set deflections of 12.1 in. and 9.7 in., respectively. A post-test photograph of crash test no. MWT-5 is shown in Figure 19.

Figure 19. Post-Test Photograph of Successful Crash-Test MWT-5 on Upstream Transition [35]

2.3.5 Standardized Midwest Guardrail System Transition to Stiff Bridge Railing

In 2010, additional modifications were made to the previous AGT design so that it utilized standard steel post sizes with only two sections versus three sections, and additional crash tests were conducted according to MASH 2009 safety performance criteria, which was the new crash testing standard. The two standard steel sizes in roadside construction are W6x15 and W6x9. The new AGT design changed the embedment depth, post spacing, and used only two posts sizes by eliminating the W6x12 posts. The AGT began (going upstream from the bridge) with three W6x15 posts at half-post spacing with a 55⅛-in. embedment depth, then four W6x9 posts at quarter-post spacing and a 40-in. embedment depth, and at the end four W6x9 posts at half-post spacing and a 40-in. embedment depth, all before connecting to the MGS [36]. CAD details for this design are shown in Figure 20.

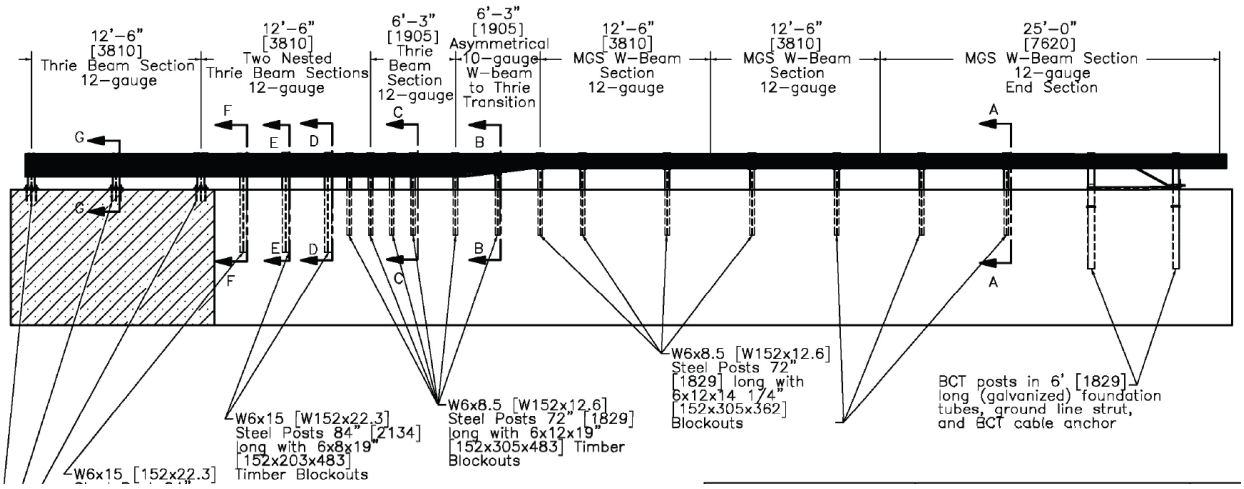

Figure 20. Elevation View of AGT Built with Two Standard Post Sizes [36]

Crash tests using MASH 2009-compliant vehicles, a 2270P pickup truck and a 1100C small car, were successfully conducted. The transition adequately resisted impact from a 5,158-lb pickup truck traveling at 61.2 mph and at an angle of 26.3 degrees in crash test no. MWTSP-2. The test resulted in maximum dynamic and permanent set deflections of 32.8 in. and 25.75 in., respectively. Following this successful test, the transition also adequately resisted impact from a 2,591-lb small car traveling at 61.0 mph and at an angle of 25.7 degrees in crash test no. MWTSP-3. The test resulted in maximum dynamic and permanent set deflections of 18.5 in. and 15.6 in., respectively. The small car test resulted in some tire snag on the posts, as shown in Figure 21, but this snag behavior did not result in a failed test because ride down accelerations and occupant impact velocities were not excessive.

Figure 21. MWTSP-3 Final Location of Small Car after Test with Wheel Snag [36]

2.3.6 Wood Post Alternative for Midwest Guardrail System Transition to Stiff Bridge Railing

As the above development effort concluded, research began investigating a timber post alternative for the W6x15 posts used in the steel post design [37]. Both W6x15 and W6x9 steel posts were used in the AGT design, however, a timber post equivalent was only needed for the W6x15 steel shapes as 6-in. x 8-in. timber posts have long been recognized as an equivalent to W6x9 steel posts. For this comparison, a total of twenty bogie tests on W6x15 steel posts and 8-in. x 8-in., 8-in. x 10-in., 10-in. x 10-in., and 6-in. x 10-in. timber posts, all embedded in soil, were conducted. The 8-in. x 8-in. timber posts were embedded at 54 in. into the soil, two in AASHTO Grade B material with moderate compaction and two with the same material with heavy compaction. One of these posts is shown in Figure 22. Four tests were also conducted on W6x15 steel posts placed in soil at both compaction levels.

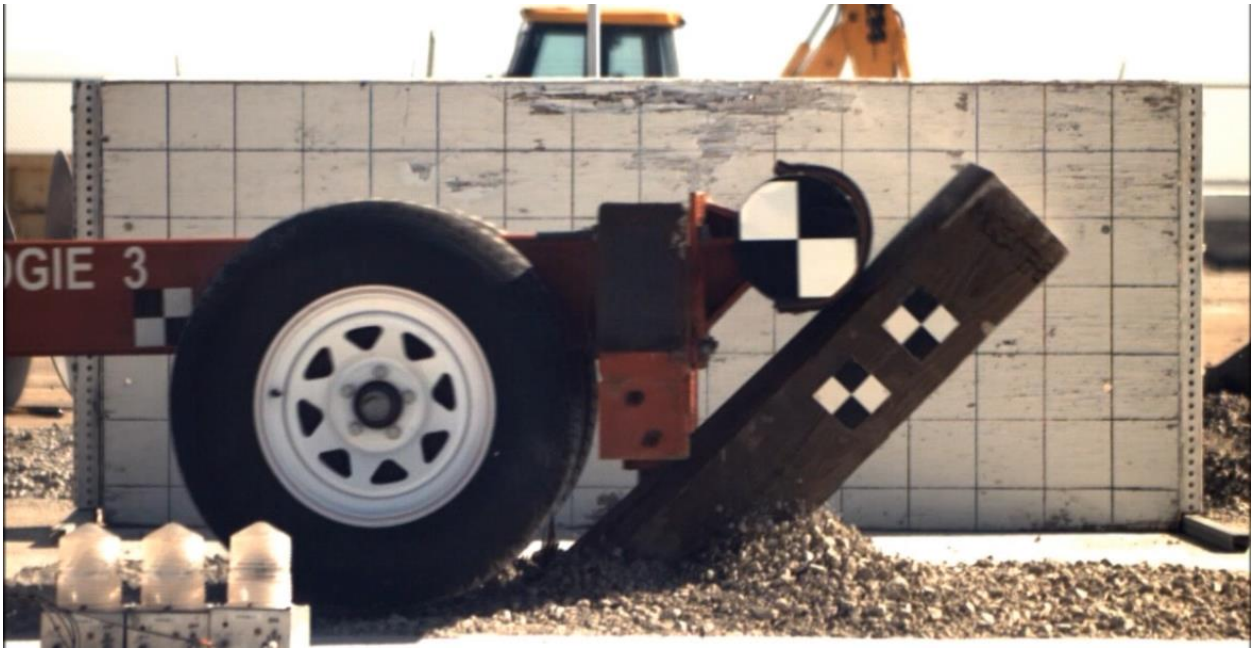

Figure 22. Bogie Test MGSATB-8 on 8-in. x 8-in. Post Embedded 54-in. into Heavily Compacted Soil

All 8-in. x 8-in. timber posts ruptured instead of rotating in the soil. Following this finding, eight tests were conducted on 8-in. x 10-in. timber posts, a single test on a 10-in. x 10-in. timber post, and three tests on 6-in. x 10-in. timber posts. The 8-in. x 10-in. post embedment was either 54 in. (three tests) or 48 in. (five tests); the 10-in. x 10-in. post embedment was 54 in.; and the 6-in. x 10-in. posts were embedded at 52 in. All posts were placed in heavily compacted soil. The 8-in. x 10-in. timber post was recommended as the equivalent post to the W6x15 steel section, largely because that size demonstrated post rotation in soil rather than post rupture. These posts absorbed more energy than the W6x15 posts, so the selection was conservative [37]. No crash tests were conducted to validate the performance of the AGT system using equivalent wood posts; only BARRIER VII simulations were performed to support the alternative post types in AGTs. Two AGT design variations were developed using alternative wood posts and are shown in Figures 23 and 24.

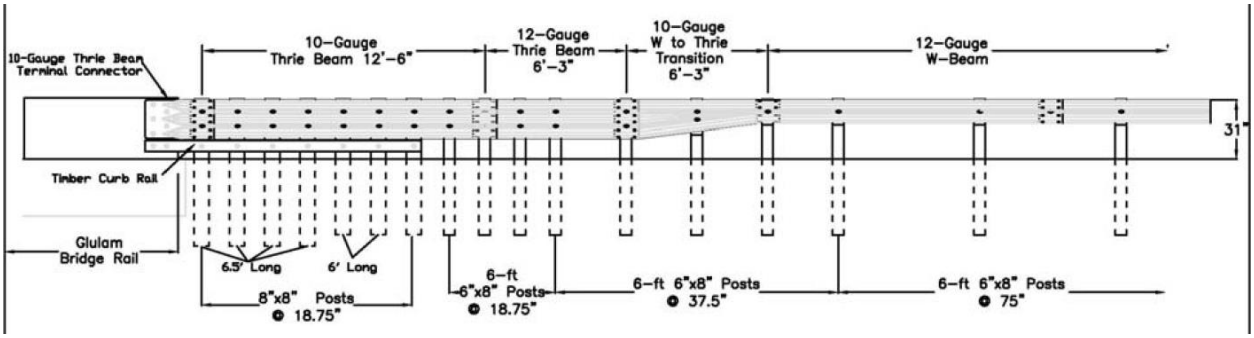

Figure 23. Proposed AGT Design Utilizing Quarter-Post Spacing [37]

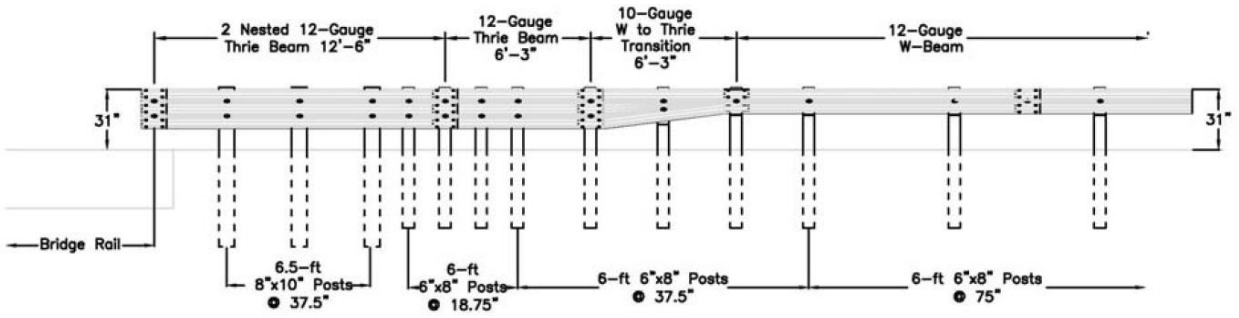

Figure 24. Proposed AGT Design Utilizing Half-Post Spacing [37]

The AGT system with wood-post equivalents replaced W6x9 steel posts with 6-in. x 8-in. timber posts at a 40-in. embedment depth and replaced W6x15 steel posts with 8-in. x 10-in. timber posts at a 48-in. embedment depth. In addition to the wood-post equivalent AGT, another system was configured with 8-in. x 8-in. timber posts at quarter post spacing, which was based on the satisfactory performance of the 1997 AGT [25], but utilizes a raised railing height of 31 in. and incorporated an upstream stiffness transition to prevent pocketing. Four 8-in. x 8-in. timber posts at quarter-post spacing would be installed with a 46-in. embedment depth, followed x three 8-in. x 8-in. timber posts at quarter post spacing and a 40-in. embedment depth. Four 6-in. x 8-in. timber posts at quarter post spacing and a 40-in. embedment depth compose the remainder of the AGT, shown in Figure 23.

2.3.7 Midwest Guardrail System Transition to Stiff Bridge Railing with 3-in. Overlay

MwRSF conducted further AGT research to investigate and develop a system that could accommodate a future 3-in. wearing surface and remain crashworthy [38]. The height of the guardrail is critical for allowing AGTs to redirect vehicles. Further, a future wearing surface can lower the effective height of the guardrail by increasing the height of vehicles relative to the guardrail elements. The thrie-beam terminal connector at the end of the bridge railing cannot easily be vertically adjusted years later for most systems.

MwRSF proposed an AGT design which vertically adjusted the initial height 3 in. upward using a symmetric transition section to maintain the 31-in. guardrail height, which positioned the thrie-beam rail at an overall height of 34 in. The symmetric transition segment does not exactly match between the 34-in. thrie-beam height and the 31-in. guardrail height, so the transition segment was shifted vertically ¾ in. upward to connect to the W-beam guardrail, as shown in Figures 25 and 26. When a 3-in. asphalt overlay is placed on the road, the symmetric transition piece can be removed and replaced with an asymmetric transition segment along with the W-beam guardrail being shifted up 3 in. to maintain a 31-in. rail height above the new overlay [38]. The shifted elevation of the guardrail and transition segment on a post is shown in Figure 27.

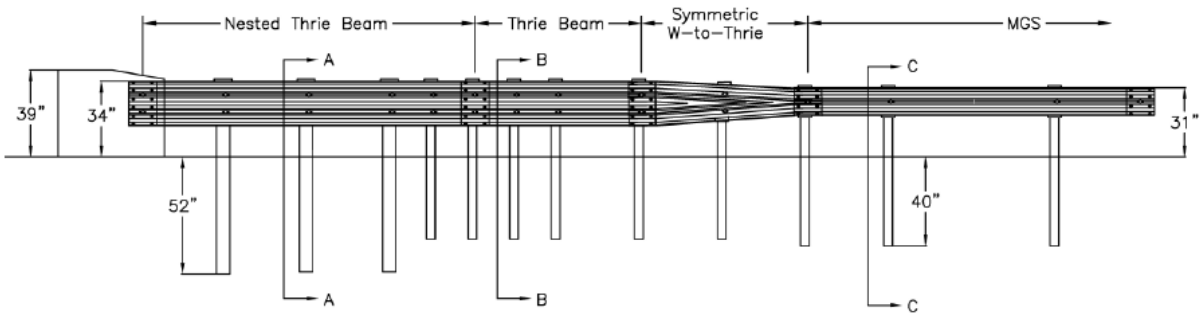

Figure 25. AGT System Configuration before Installation of 3-in. Wearing Surface [38]

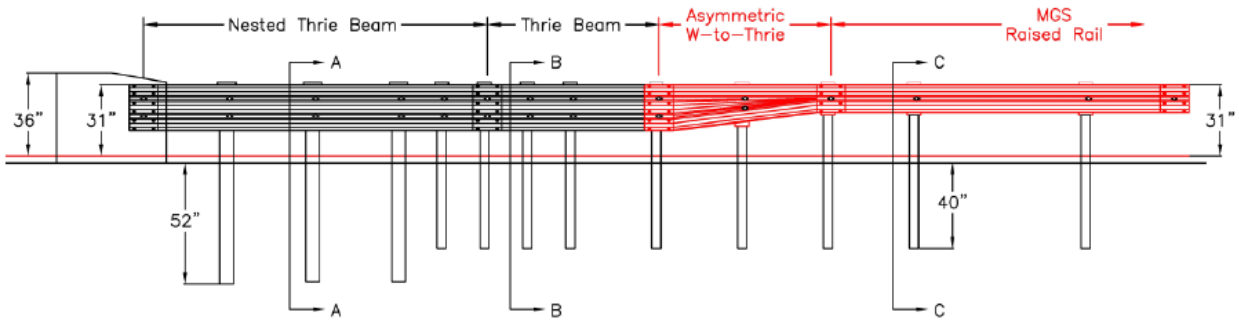

Figure 26. AGT System Configuration after Installation of 3-in. Wearing Surface [38]

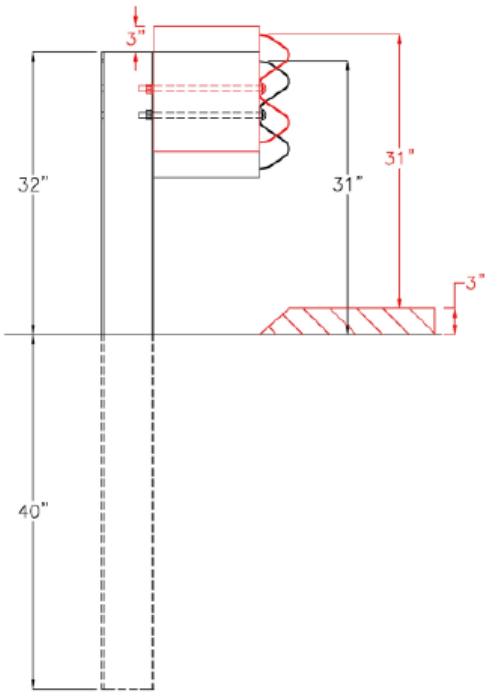

Figure 27. AGT System with Adjustable Height Post Cross-Section for Connecting Guardrail [38]

Crash testing with the MASH 2270P pickup truck and the 1100C small car were successfully conducted. The transition adequately resisted impact from a 5,024-lb pickup truck traveling at 62.2 mph and at an angle of 24.8 degrees in crash test no. 34AGT-1. The test resulted in maximum dynamic and permanent set deflections of 7.8 in. and 5.75 in., respectively. Following this successful test, the transition also adequately resisted impact from a 2,420-lb small car traveling at 62.1 mph and at an angle of 25.5 degrees in crash test no. 34AGT-2. The test resulted in maximum dynamic and permanent set deflections of 2.7 in. and 0.75 in., respectively.

2.3.8 Dynamic Component Testing of 8-in. x 8-in. Wood Posts and Larger

The development of a new AGT system to connect the timber bridge railing to the W-beam guardrail required additional research into post-soil interaction for wood posts measuring 8-in. x 8-in. and larger. Wood posts, due to their potential for rupture, need to rotate through soil to effectively maximize the energy absorbed during vehicle impacts. Dynamic component tests on 8-in. x 8-in. posts and larger placed in soil were less common, and several of these studies are discussed below.

The first study was conducted by the Southwest Research Institute (SwRI) to develop AGTs through dynamic component tests and full-scale vehicle crash tests [39]. The research effort examined 8-in. x 8-in., 10-in. x 10-in., and 12-in. x 12-in. wood posts and W6x15.5 steel posts, all struck by a swinging pendulum weighing 4,000 lb at 21 in. above the ground with a target speed of 20 fps. The set up for this test is shown in Figure 28. Twelve tests were conducted, two on 8-in. x 8-in., two on 10-in. x 10-in., and two on 12-in. x 12-in. wooden posts, two on W6x15.5 posts bent about the strong axis with soil paddles, two on W6x15.5 posts bent about the strong axis without soil paddles, and two on W6x15.5 posts bent about the weak axis. Neither the grade nor species of wood posts were provided in the SwRI study. The wood posts were embedded 36 in. into the ground (Strong Soil, Type S1), while the steel posts were embedded 44 in. into the ground (Strong Soil, Type S1).

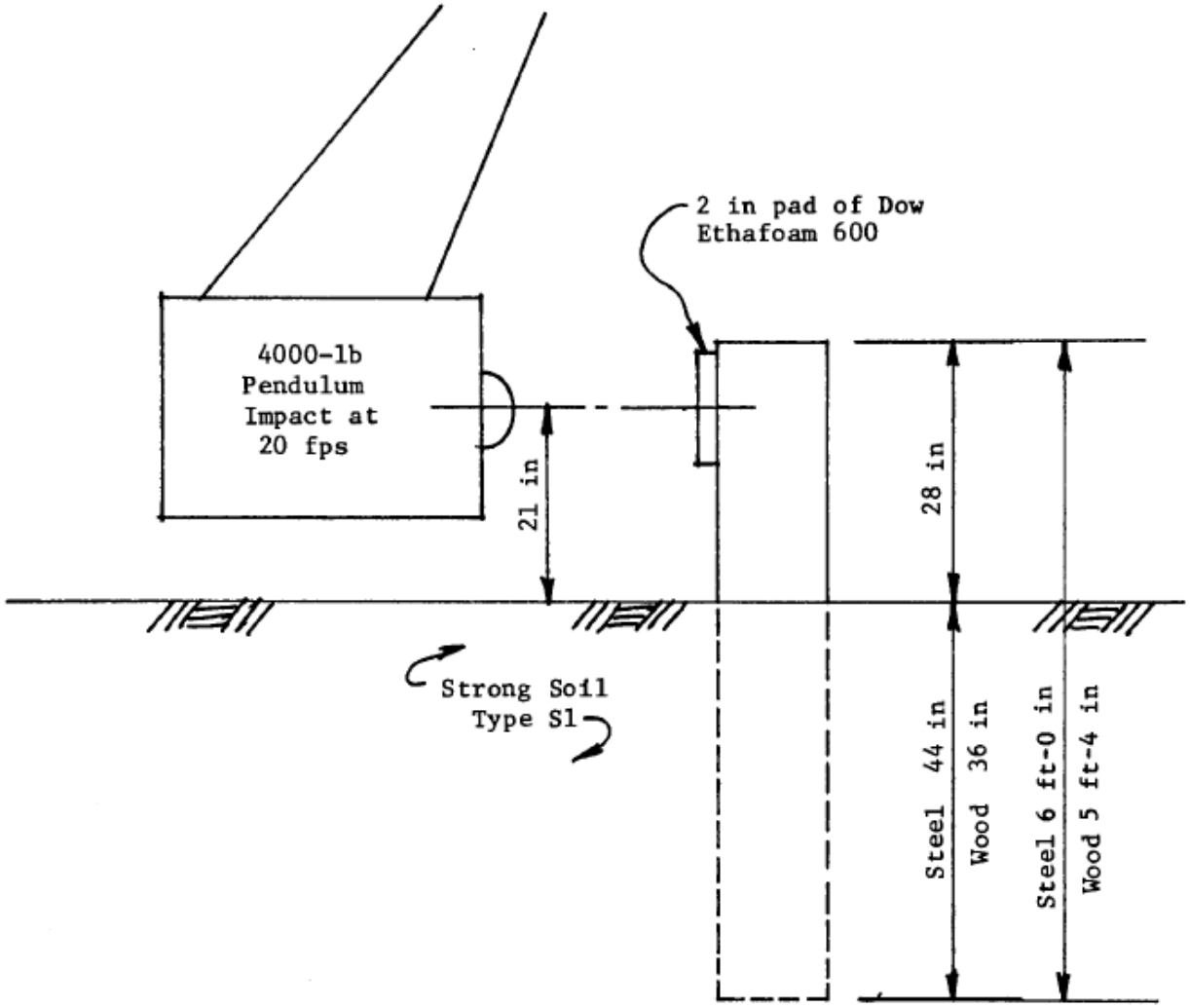

Figure 28. Diagram of Dynamic Component Test Setup by SwRI [39]

The results from the dynamic pendulum impact tests into wood posts are shown in Table 1. The designation “P#” in the table refers to the post shape size, so “P8” involves a test on an 8-in. x 8-in. post and so on. Test no. “2P10” lacks additional data as the post ruptured during the test. All other tests on wood posts resulted in rotation through soil.

Table 1. SwRI Study Dynamic Component Testing Results – Wood Posts [39]

Test No.	Maximum Force (k)	Time 1 (ms)	Distance 1 (in.)	Stiffness (k/in.)	Total Impulse (lb-s)	Time 2 (ms)	Distance 2 (in.)
1P12	20.7	32	7.32		2273.8	116	18.62
1P12-R	23.8	25	5.76		2271.2	98	15.67
Average	22.3		6.54	3.41			17.15
1P10	16.3	30	6.84		1544.2	100	18.12
2P10	16.4	26	6.00		-	-	-
Average	16.35		6.42	2.55			18.12
2P8	13.2	30	6.96		1287.3	103	19.75
1P8-R	11.6	34	7.92		1091.0	101	20.42
Average	12.4		7.44	1.67			20.07

The other study was conducted by MwRSF and was discussed in the summary of the AGT wood post alternative connecting MGS and a stiff bridge railing (Section 2.3.6) [37]. The results from the impact tests on 8-in. x 8-in., 8-in. x 10-in., 10-in. x 10-in., and 6-in. x 10-in. posts are shown in Table 2. Refer to Section 2.3.6 for an example of the test set up for that study.

Table 2. Wood-Post Dynamic Test Results, MGS Wood-Post Testing Series [37]

Test No.	Post Type	Embedment Depth (in.)	Impact Velocity (mph)	Peak Force (kips)	Average Force			Total Energy (kip-in.)	Failure Type
					@ 5 in. (kips)	@ 10 in. (kips)	@ 15 in. (kips)		
MGSATB-3	SYP 8x8	54	18.2	14.7	7.2	9.2*	NA	94.6	Fracture
MGSATB-4	SYP 8x8	54	18.7	25.4	7.3	10.6	11.9*	180.9	Fracture
MGSATB-7	SYP 8x8	54	21.4	17.3	10.9	7.5*	NA	73.0	Fracture
MGSATB-8	SYP 8x8	54	21.9	24.6	12.7	6.9*	NA	66.8	Fracture
MGSATB-9	SYP 8x10	54	19.9	15.7	7.5*	NA	NA	37.3	Fracture
MGSATB-10	SYP 10x10	54	20.5	36.7	25.6	28.2	NA	307.4	Rotation
MGSATB-11	SYP 8x10	54	20.6	30.9	21.6	25.1	NA	311.7	Rotation
MGSATB-12	SYP 8x10	54	19.4	25.6	18.1	20.8	NA	275.5	Rotation
MGSATB-13	SYP 8x10	48	20.2	19.1	13.7	14.6	15.1	298.8	Rotation
MGSATB-14	SYP 8x10	48	19.7	20.5	15.6	17.2	17.1	283.5	Rotation
MGSATB-15	SYP 8x10	48	21.0	31.5	20.0	24.5	20.8	324.5	Rotation
MGSATB-16	SYP 8x10	48	20.2	30.7	20.1	19.3*	NA	194.4	Fracture
MGSATB-17	SYP 8x10	48	19.6	32.1	23.4	24.7	NA	285.6	Rotation
MGSATB-18	SYP 6x10	52	21.0	21.8	14.7	17.7	18.4	352.2	Rotation
MGSATB-19	SYP 6x10	52	19.7	17.0	11.8	11.5*	NA	124.3	Fracture
MGSATB-20	SYP 6x10	52	24.5	13.9	5.5*	NA	NA	28.5	Fracture

* Fracture had already been initiated.

The Southwest Research Institute also conducted a study in 1971 to examine the rupture strength of wood posts [40]. Over 100 tests were conducted on Douglas Fir, Southern Pine, Red Oak, and Red Pine posts with sizes 4-in. x 4-in. through 8-in. x 8-in. A swinging pendulum was also used to strike the posts, which weighed 4,000 lb, as it represented the weight of a medium-sized passenger car. The test results for the 8-in. x 8-in. Southern Pine and Douglas Fir posts are summarized in Tables 3 and 4.

Table 3. SwRI Pendulum Test Results – 8-in. x 8-in. Southern Pine Posts [40]

Specimen	Width (in.)	Depth (in.)	Impact Velocity (fps)	Fracture Energy (kip-ft)	Peak Force (kips)	Average Force (kips)
A	7.88	8.38	19.9	11.7	22.0	11.6
B	8.25	8.38	29.8	17.3	24.3	9.4
C	8.06	8.12	29.4	13.9	25.9	11.8
D	8.06	8.50	27.6	6.3	29.4	7.3
E	8.00	8.12	27.6	12.1	25.2	10.9
F	8.12	8.38	29.6	12.4	28.4	10.5
G	7.94	8.31	29.2	9.9	28.0	9.2
H	8.12	8.25	27.6	10.9	25.4	9.9

Table 4. SwRI Pendulum Test Results – 8-in. x 8-in. Douglas Fir Posts [40]

Specimen	Width (in.)	Depth (in.)	Impact Velocity (fps)	Fracture Energy (kip-ft)	Peak Force (kips)	Average Force (kips)
A	7.60	8.00	15.0	7.52	22.1	9.8
B	7.60	7.88	14.7	6.70	16.9	6.9
C	7.75	8.00	14.9	7.45	21.5	9.5
D	7.60	7.88	14.7	6.18	17.5	7.2
E	7.60	7.88	15.0	6.86	20.9	9.2
F	7.60	7.75	14.8	8.00	23.0	10.5
G	7.75	7.75	14.8	8.23	22.1	10.6
H	7.60	7.88	14.9	7.07	19.0	8.9

2.4 W-Beam Guardrail System Background

2.4.1 Midwest Guardrail System with SYP 6-in. x 8-in. Grade No. 1 Posts

After MASH 2009 was published, additional full-scale vehicle crash testing was performed on the MGS using 6-in. x 8-in. Southern Yellow Pine (SYP) Grade 1 or better posts, which included the 2270P and 1100C vehicles impacting systems with at 31 in. and 32 in. rail height, respectively [43]. The successfully crash-tested system is shown in Figures 29 and 30. Note that the 32-in. top railing height was achieved with a 39-in. post embedment depth during the 1100C small car test where the top of the blockout matched the top of the post.

Figure 29. MGS Utilizing SYP Grade No. 1 Posts [43]

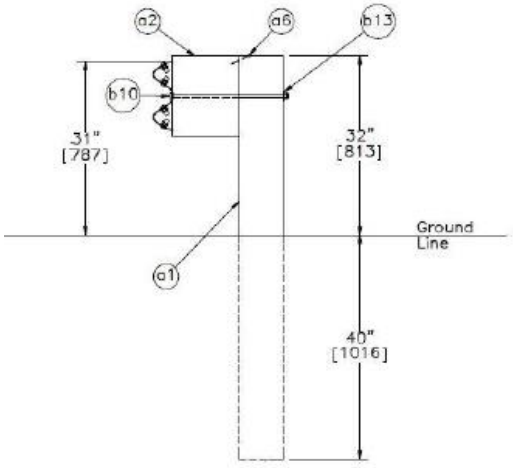

Figure 30. MGS Cross-Section of SYP Grade No. 1 Posts [43]

Crash testing under MASH 2009 was successfully conducted with the 270P pickup truck and 1100C car. The transition adequately resisted impact from a 5,029-lb pickup truck traveling at 62.2 mph and at an angle of 24.9 degrees in crash test no. MGSSYP-1. The test resulted in maximum dynamic and permanent set deflections of 40.0 in. and 30.25 in., respectively. Following this successful test, the transition also adequately resisted impact from a 2,442-lb small car traveling at 61.5 mph and at an angle of 25.3 degrees in crash test no. MGSSYP-2. The test resulted in maximum dynamic and permanent set deflections of 22.2 in. and 16.25 in., respectively.

2.4.2 Guardrail System using Raised Blockouts

The placement of future wearing surfaces will also raise the effective vehicle height relative to the top of the W-beam railing attached to the support posts. Texas A&M Transportation Institute (TTI) researchers investigated the efficacy of raising the blockouts on guardrail systems without raising or reinstalling the posts [44]. A new hole could be drilled into the posts above the old guardrail mounting hole to increase the guardrail height. TTI researchers conducted dynamic

component testing to investigate a rail height increase of 4 in. Two pendulum tests were conducted on 6-in. x 8-in. posts embedded 44 in. into the soil. The setup for these tests is shown in Figure 31.

Figure 31. Pendulum Testing Setup on Timber Guardrail Posts [44]

In both tests, a post 28 in. above grade had two ¾-in. diameter holes drilled in it, with one hole 3 in. from the top and the other 7 in. from the top. A ⅝-in. diameter bolt was inserted through the hole 3 in. from the top and fastened a surrogate W-beam guardrail and wooden blockout, which had a top mounting height of 32 in. above grade. A pendulum mass struck the W-beam guardrail 29.5 in. from the ground. The test configuration is shown in Figure 32. The post was embedded at 40 in., which was typical for MGS posts.

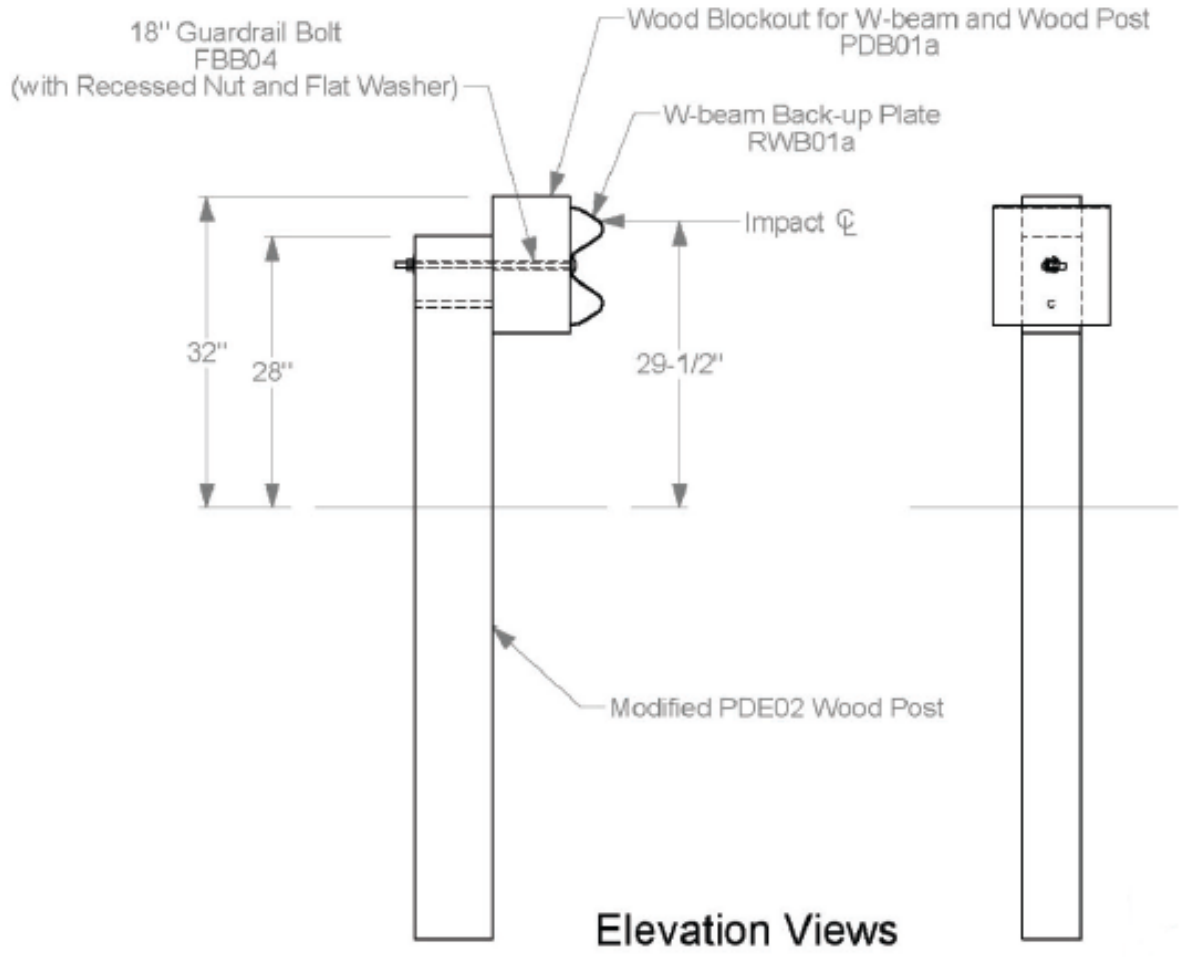

Figure 32. Test Configuration for Pendulum Impact Tests on Posts with Raised Timber Blockouts [44]

TTI's study found that increasing the top rail height by 4 in. did not adversely affect the timber posts in pendulum tests. In addition to these tests, an LS-DYNA computer simulation investigation was performed into whether the MGS could work as intended with a 4-in. overlay. Three different scenarios were evaluated using LS-DYNA: (1) MGS performance with a 4-in. overlay, (2) a 27¾-in. tall guardrail with a 4-in. deeper post embedment depth, and (3) a 27¾-in. tall guardrail with 4-in. overlay (maintaining system height). The first two simulations utilized MASH 2016 TL-3 impact conditions on the MGS (calibrated by both previous component tests and crash tests at MwRSF) using a 2270P vehicle. The final simulation used a NCHRP 350 2000P pickup truck vehicle model. All systems were found to provide satisfactory safety performance. Subsequent research has been conducted, along with a successful crash test, on steel-post guardrail systems with raised blockouts [45-46].

2.5 Deck Types

2.5.1 Introduction

The United States Forest Service's (USFS's) *Timber Bridges: Design, Construction, Inspection, and Maintenance* [47] offers an in-depth examination of the various types of timber bridge decks. These deck types may be either transverse or longitudinal, with transverse decks sitting on top of beams or stringers, and longitudinal decks supporting themselves on the abutments without connecting to additional super structure elements. Deck types include nail-laminated, glulam, spike-laminated, stress-laminated, and many others. This section will discuss the various deck types according to their fabrication and use.

2.5.2 Nail-Laminated Decks

The use of nails for assembling timber decks represents one of the most traditional methods in bridge construction. This technique involves aligning boards adjacently across their wide faces and securing them with multiple nails, as depicted in Figure 33. This method binds the smaller wooden pieces into a single, expansive, shallow beam structure. Typically, lumber dimensions for this application range from nominal 2 in. thick and 8- to 16-in. wide laminations [48], although current specifications from AASHTO *LRFD Bridge Design Specifications* require a nominal 6 in. as the minimum deck thickness for wood structures [15]. The construction process of transverse nail-laminated decks is depicted in Figure 34 for a nominally 6-in. deep deck constructed by MwRSF, illustrating how the individual boards are interconnected to form a cohesive decking system.

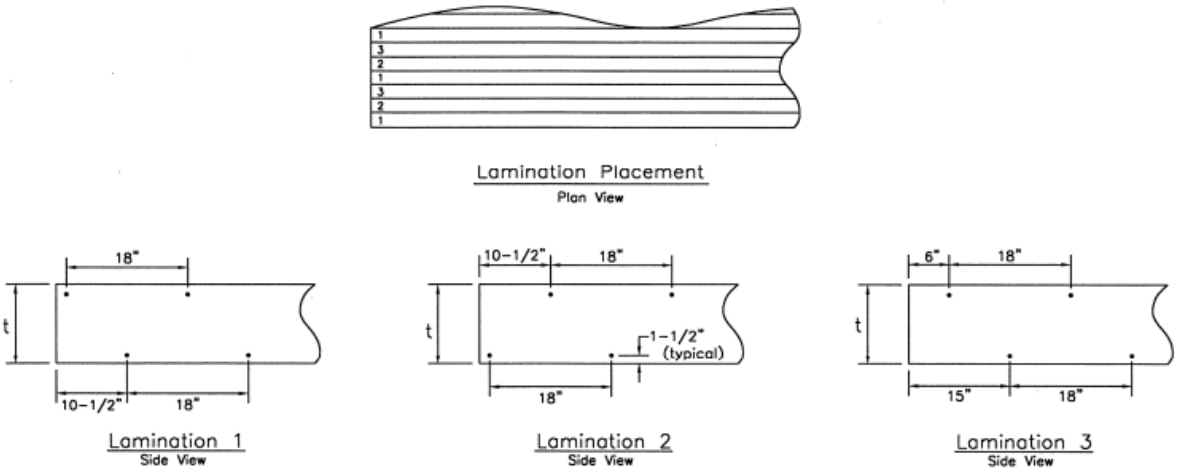

Figure 33. Nail-Laminated Lumber with Staggered Nailing Pattern [48]

Figure 34. Transverse Nail-Laminated Deck Construction [7]

An important component in the construction of longitudinal decks for timber bridges is the spreader beam, which distributes loads across the deck roadway width [50]. This assistance to load distribution is especially requisite for longitudinal nail-laminated decks because these decks struggle with load distribution. The nail-laminated design gained approval from AASHTO by idealizing the deck as a beam with a width equal to the vehicle tire width and deck depth [50]. The orientation of the boards can span either the length or the width of the bridge, as illustrated in Figure 35. It is important to note, however, that the schematic does not fully conform to AASHTO specifications. In particular, butt joints are not permitted, and each lamination must span continuously between abutments. Regardless of the board orientation, short deck spans are generally preferred to limit vertical deflections under traffic loads [47].

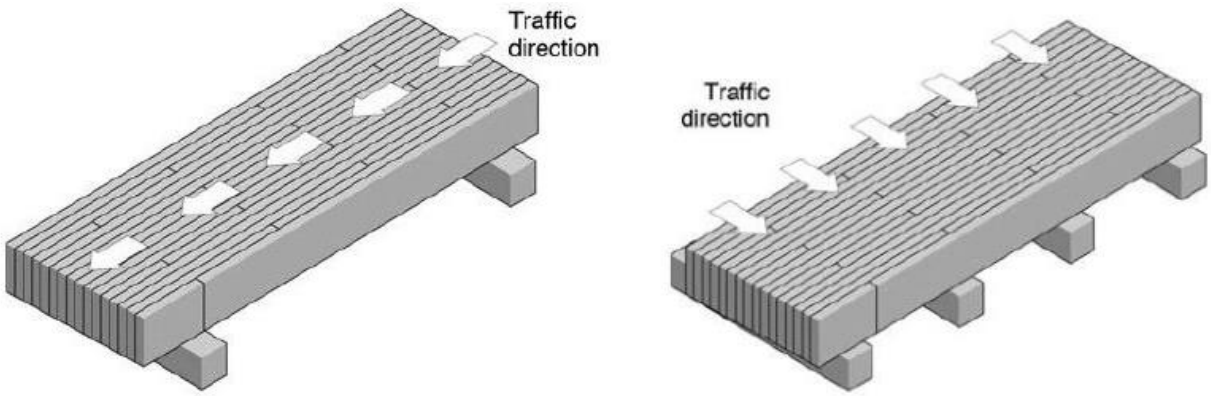

(a) (b)

Figure 35. Nail-Laminated Decks: (a) Longitudinal and (b) Transverse [51]

Nail-laminated decks have also been used with deck shear connectors and cast-in-place concrete to make a composite deck [51-52]. An example of this configuration is shown in Figure 36. A big advantage of the composite aspect is the rigidity of the concrete, promoting superior load distribution through the nail-laminated boards. In some cases, this deck has also been noted to perform well for up to eighty-four years with little maintenance [52].

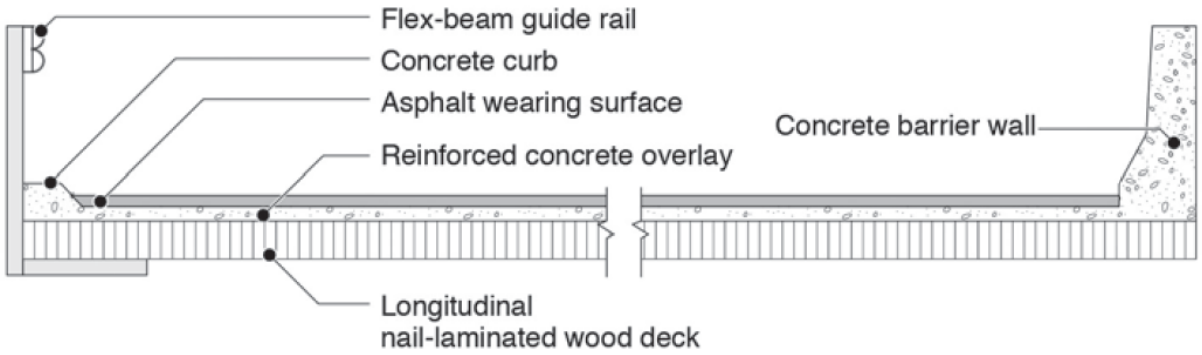

Figure 36. Cross-Section View of Timber-Concrete Composite Deck [51]

A notable advantage of nail-laminated decks is their low cost, owing to simple construction which does not require any specialized labor or machinery [6, 53]. The most specialized stage of construction is the pressure treatment of the wood, which is a cost borne by any timber bridge per AASHTO requirements [15]. This process made nail-laminated decks an attractive option compared to other timber bridge types, balancing traditional construction methods and the practical demands of bridge engineering.

Nail-laminated bridge decks rose to prominence in the 1920s, marking a significant trend in bridge construction. AASHTO (originally AASHO) had recently been founded, and new standards were being implemented across the U.S. for highway bridges. During the Great Depression, steel was expensive and wood was less costly, motivating the construction of highway bridge decks with timber and concrete with composite connections. The increased reliance on wood as a building material continued through World War II because steel continued to be expensive due to the war [52]. These decks demonstrated sufficient performance over that time frame so that thousands of nail-laminated decks would continue to be built into the 1960s [47, 50, 52].

While design guides in subsequent years continued to include references to nail-laminated decks [48, 52], changes in construction standards have led to restrictions. In Canada, the construction of longitudinal nail-laminated decks is now limited [51], and AASHTO *LRFD Bridge Design Specifications* has removed specifications for nail-laminated decks from Section 9: Decks and Deck Systems [15]. Despite these changes, many nail-laminated decks continue to demonstrate effective performance across various regions of the United States [52-54], using both longitudinal and transverse orientations [52, 55].

The adaptability of nail-laminated decks allows for construction in a range of thicknesses. While standard deck thicknesses typically align with standard dimension lumber widths – for example, dress lumber sizes of 2 in. x 6 in., 2 in. x 8 in., or 2 in. x 10 in. translating to deck thicknesses of 5½ in., 7¼ in., or 9¼ in. – custom dimensions can also be achieved by cutting larger sawn lumber boards to specific thicknesses. The actual size of the lumber used in these decks can vary, often leading to inconsistencies in the height of individual boards within the assembled deck. Such variations can result in some boards protruding more than others, and the natural curvature of wood beams may lead to further unevenness. This phenomenon results in uneven bearing on the superstructure, substructure, or spreader beams [50], as observed by construction crews at the MwRSF test site, illustrated in Figure 37.

Figure 37. Uneven Bearing of Nail-Laminated Decks on Supports [7]

The inherent variability in the dimensions of boards used in nail-laminated decks presents several challenges, particularly concerning load distribution and structural integrity. One significant issue arises at the point of load application – typically, a vehicle's tire. This localized stress tends to impact the first boards in contact, initiating a crushing effect around the nails. Consequently, this stress can lead to the gradual loosening or pulling out of nails, diminishing their ability to effectively transfer load from board to board – a process typically called delamination [51]. When the timber boards are not effectively shielded from water, this process becomes even more destructive, allowing the expansion and shrinkage of hydrophilic wood to further loosen nails and speed up the process of delamination [53]. This issue extends to composite nail-laminated decks which have not been properly designed to protect the timber from excess moisture [52]. Nail-laminated deck vulnerability to delamination is also a function of the deck's bending stiffness. The stiffness, oriented perpendicular to the wood boards, heavily depends on the frictional resistance offered by the nails' withdrawal capacity [56]. Point loads are less easily resisted because of nail-lamination's lower load distribution [57].

In response to these identified weaknesses, alternative deck types, such as spike-laminated and stress-laminated decks, have been developed [50]. While nail-laminated decks are likely no longer viable for meeting MASH 2016 TL-4 impact conditions, understanding their limitations and mechanics is crucial. This knowledge provides valuable insights into the challenges and functional considerations pertinent to other deck types, thereby informing the ongoing development of a MASH 2016 TL-4 bridge railing on multiple bridge deck types.

2.5.3 Glued-Laminated Decks

Glued-laminated timber (glulam) is a specialized construction material fabricated by bonding wooden boards using a waterproof structural adhesive. Following the adhesive bonding, these newly formed members undergo a pressure-treating process with preservatives, enhancing their durability and longevity [47]. Typically, glulam panels used in bridge decks are approximately 4 ft wide, although it is possible to increase the deck panel width to meet specific requirements [50]. A representative example of a typical loading condition for a glulam deck panel

is illustrated in Figure 38. It is important to note the designation of the bending axis in this context. Perpendicular to the bond line, this axis is identified as the y-y axis in Figure 38.

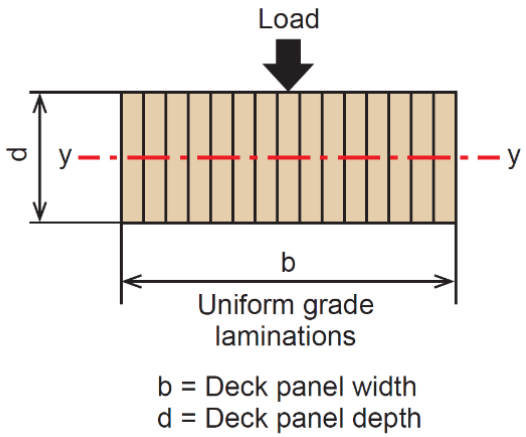

Figure 38. Glulam Deck Panel Loading Diagram [32]

In bridge construction, glulam deck panels distribute wheel loads through the panel with good lateral load distribution, and often employ a stiffener beam bolted underneath the panels to transfer the load from panel to panel [32]. Glued-laminated methods produce stiffer timber decks than nail-laminated and stress-laminated decks [56]. Correspondingly, glulam panels have the highest load distribution within the panel. The high load distribution is a function of the method of load transfer from lamination to lamination. In nail-laminated decks, the load must transfer through the nails to transfer into the next lamination, and through friction between laminations in stress-laminated decks (requiring that high stress be maintained). In glulam panels, the glued completely covers the area between two laminations, so that the whole area transfers load and the two laminations can act like a single rigid body.

In theory, glulam can be manufactured in any size. However, practical limitations arise due to the size constraints of pressure-treatment cylinders. This limitation is significant, because the AASHTO *LRFD Bridge Design Specifications* mandates preservative treatment for all permanent wooden members used in bridge construction, directly influencing the feasible dimensions of glulam deck panels [15]. Consequently, the fabrication process of glulam deck panels, involving both gluing and pressure-treating, necessitates their manufacture offsite. Once completed, these panels are transported to the bridge construction site for final installation. Maintenance requirements for glulam decks are relatively straightforward, primarily involving regular inspections and measures to protect the timber from water ingress.

The advent of glulam beam bridges can be traced back to the 1940s, a development largely facilitated by the introduction of fully water-resistant, phenol-resorcinol adhesives. These adhesives were a crucial innovation, enabling glulam structures to withstand exposure to water without compromising the adhesive's bond strength [47]. An exemplary instance of early glulam beam bridge construction is the Keystone Wye Bridge, constructed in 1968 in South Dakota. Originally, this bridge incorporated a concrete deck, but in 2022, it underwent a significant transformation with the replacement of its deck with a transverse glulam timber deck, complete with an asphalt overlay, as illustrated in Figure 39.

Figure 39. Keystone Wye Glulam Deck Panels [58]

The option of using glulam deck panels for the original construction of the Keystone Wye Bridge was not feasible at the time, as these panels were yet to be developed. It was not until the late 1960s that the Forest Products Laboratory pioneered the development of glulam deck panels [47]. Following this development, the usage of glulam deck panels in bridge construction began gaining traction in the 1970s [50]. These innovative deck panels offered versatility in their application, being suitable for laying across girders for transverse decks or across supports for longitudinal decks. The structural configurations and applications of these panels in both transverse and longitudinal deck orientations are further detailed in Figures 39 and 40.

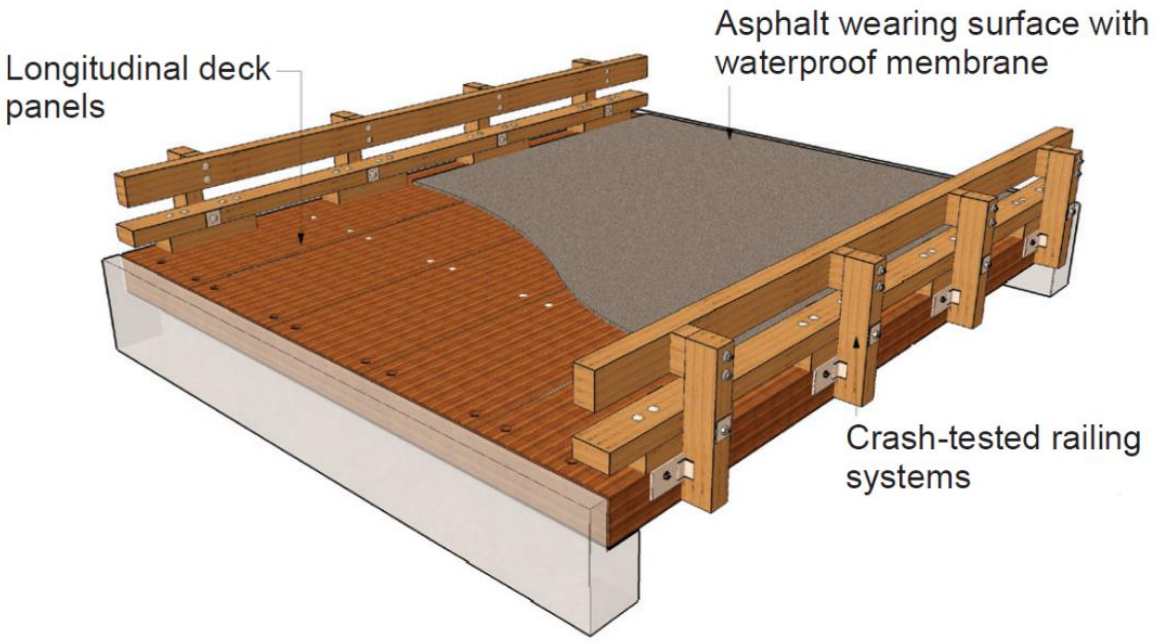

Figure 40. Longitudinal Deck Diagram [32]

The layout of glulam timber in bridge construction is strategically designed based on each member's specific location and function within the bridge's structure. The optimization of glulam encompasses both species selection and configuration, ensuring maximal structural efficiency and cost-effectiveness. For glulam girders, a common strategy involves using stronger species or higher-grade timber at the outer fibers – areas subjected to the greatest stress – while integrating a more economical, lower-grade species in the core. This approach balances strength requirements with material costs, optimizing the girder for its critical role in load bearing. In contrast, glulam panels, which form the bridge deck and directly bear vehicle loads, necessitate uniformity in species and grade throughout their construction [32]. This uniformity is crucial since vehicle loads can be applied at any location across the panel, demanding consistent strength and durability characteristics throughout.

The thickness of glulam panels can vary considerably, yet there are standard sizes that are commonly used. For western species, typical thicknesses range from 5⅛ in. to 12¼ in., whereas for southern pine species, the standard thicknesses span from 5 in. to 12 in. These dimensions play a significant role in determining the span capabilities of the decks. For instance, longitudinal deck spans can vary dramatically based on thickness, ranging from 11 ft – 2 in. for 8½ in. thick Southern Pine panels to 30 ft – 10 in. for 16 in. thick panels. Transverse decks, characterized by their overhang lengths, also demonstrate variation based on panel thickness – extending from 3 ft – 2 in. for 5 in. thick Southern Pine decks to 8 ft –10 in. for 8¾ in. thick Douglas Fir panels.

Maintenance inspections of glulam deck panels have found that they are prone to warping at the glulam panel ends, which can lead to cracking in the asphalt overlay. Such cracking is detrimental as it exposes the underlying wood to sitting water, accelerating the degradation process (an issue in common with nail-laminated deck) [59]. This warping behavior is typically associated with wood's natural expansion when its moisture content increases. The repeated cycles of expansion and contraction, driven by alternating wet and dry conditions, can gradually accumulate

damage within the timber. Cracks developing in the panel sections can expose areas of the timber that preservative treatments have not adequately penetrated. Consequently, all boards within a glulam panel become susceptible to water damage, rot, and insect infestation.

A significant factor contributing to this vulnerability is the manufacturing process of glulam. Since most glulam panels are pressure-treated after assembly, the preservative penetration is often less comprehensive than individual board treatments. The ends of bridges, where glulam panels are typically located, are particularly prone to various forms of damage. Contributing factors include the hydrophilic nature of the panel end grain [60], the accumulation of gravel and debris that trap moisture, limited airflow that would otherwise aid in moisture evaporation, and direct exposure to the ground.

Another challenge with longitudinal deck panels is their inability to transfer loads transversely between panels without mechanical connections. This limitation can lead to uneven load distribution, with some panels bearing disproportionate loads. Various techniques have been explored to facilitate transverse load transfer across the deck, thus avoiding concentrated loads that could weaken certain panels. Currently, the use of spreader beams is the prevalent method for achieving this load distribution, ensuring a more uniform stress profile across the deck structure [32, 50]. An example of this for longitudinal glulam bridge decks is shown in Figure 41.

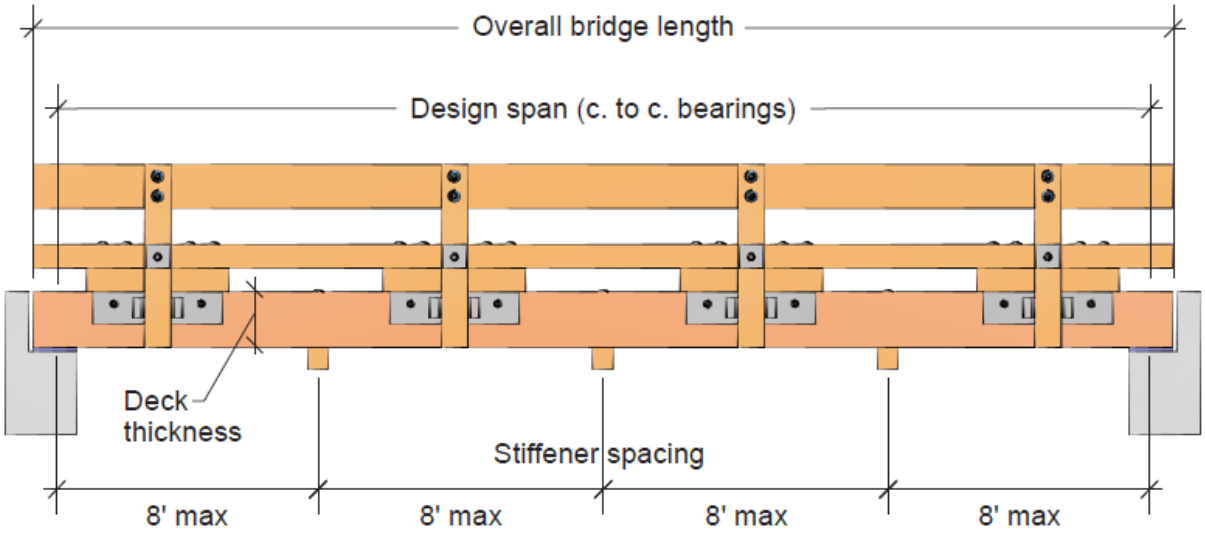

Figure 41. Elevation View of Longitudinal Glulam Bridge Deck with Railing and Spreader Beams [32]

2.5.4 Spike-Laminated Decks

Spike-laminated decks refer to a specific pre-fabrication method where long steel spikes are driven into lumber laminations to create partial-width deck panels. These panels are then transported to the bridge construction site for final assembly into a full-width bridge deck. The development of long-steel nail spikes represents a significant advancement in timber bridge deck design, emerging as a solution to the challenges posed by nail-laminated decks, such as uneven load bearing. This innovative design retains the basic principle of load distribution from board to

board utilized by nail-laminated decks, but furnishes large, 15.5-in. long ⅜-in.-diameter spikes for this purpose instead [50].

This deck construction method has also been called panelized, nail-laminated decks by the Timber Bridge Manual [47], nail-laminated by Torgerson Forest Products [61], and dowel-laminated by Wheeler Consolidated Inc, the construction firm which originated the design [50]. The Forest Products Laboratory's general technical report and the 9th edition of the AASHTO Bridge Design Specifications [15, 48] use the term "spike-laminated" to describe this deck type. Therefore, to maintain consistency with sources possessing the most authority among current bridge engineers, the term "spike-laminated" will be used throughout thus study to refer to decks constructed with steel spikes in prefabricated wooden panels.

In spike-laminated decks, the arrangement of spikes is critical. Spikes are typically placed in an alternating top-to-bottom pattern, spanning across four boards in a single "row." Each subsequent row features a different spike placement pattern, creating a staggered arrangement until the pattern replicates that of the first row. This spike placement is instrumental in ensuring effective load transfer across the panels or deck. The integration of ship-lap joints, supplemented by spikes for panel connection, further facilitates this load transfer, as illustrated in Figure 42.

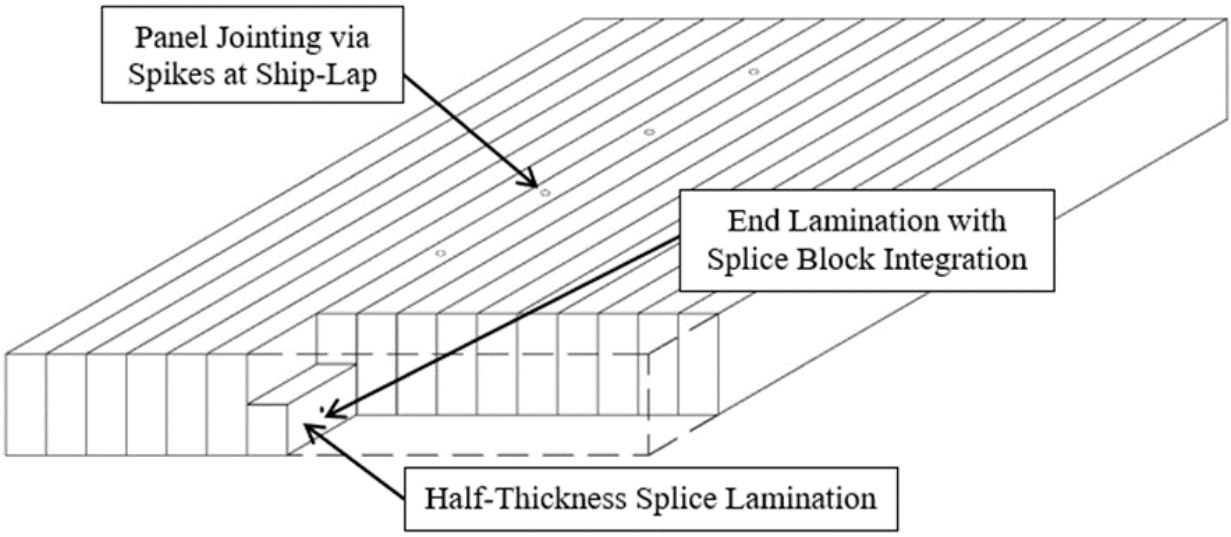

Figure 42. Example of Ship-Lap Joint

Typically spike-laminated deck thicknesses correspond to nominal dimension lumber widths, 6-in., 8-in., etc. For spike-laminated decks to achieve even load bearing on the foundation, the design requires only one side be surfaced after the whole panel has been assembled. The unsurfaced/uneven side, though irregular, is covered by a wearing surface, thereby circumventing the uneven load distribution commonly encountered in nail-laminated deck designs [50]. As a result of surfacing only one side of the lamination, spike-laminated decks' actual thickness relative to the nominal is not reduced as severely. Where a nail-laminated deck may have an actual thickness of 5½ in. for the 6-in. nominal deck, a spike-laminated deck will have an actual thickness of 5¾ in. The Minnesota Department of Transportation LRFD Bridge Design Manual for longitudinal spike-laminated bridges estimates that for spans 10 ft or less, nominally 10 in. decks are typical, and for spans 17 ft or less, nominally 12 in. decks are typical [62].

The construction of spike-laminated decks involves an offsite panel fabrication process, followed by transportation to the intended bridge site [50]. This process begins with the selection of lumber, typically 4 in. in width and depth, that meets the specific requirements of the bridge design. Subsequently, holes are drilled in each lumber member according to the design specifications to accommodate the spikes. Prior to assembly, the lumber undergoes a pressure-treatment process, which may include incising for deeper preservative penetration if necessary. Following this treatment, spikes are driven through the pre-drilled holes, as depicted in Figure 43. The final step in the panel fabrication is surfacing the bottom of the panel for a smooth bearing.

Figure 43. Spikes Being Driven Through Lumber for Spike-Laminated Deck Panel [63]

Upon completion, the panels are marked to indicate their specific placement within the bridge structure. They are then assembled on-site, utilizing shiplap joints to connect the panels securely. This construction method offers the flexibility to widen the bridge if needed by simply unbolting the panels (after removal of the initial wearing surface) and adding new panels to the structure. The assembly of these panels into a bridge deck is presented in Figure 44.

Figure 44. Assembly of Spike-Laminated Deck Panels into Bridge Deck [63]

AASHTO Bridge Design Specifications advises that spike-laminated deck applications be predominantly confined to secondary roads characterized by lower volumes of truck traffic. A potential vulnerability of these panels is the risk of delamination, particularly near edge-to-edge panel joints that are not interconnected [15]. Despite the improvements in mechanical load transfer offered by spike-laminated decks compared to their nail-laminated counterparts, they are not immune to the gradual weakening of this transfer over time [64]. The potential for delamination due to moisture content fluctuations and weak transverse stiffness, which adversely affect load distribution and sharing capabilities, remain issues for this deck type relative to glulam deck panels. Although it should also be noted that spike-laminated decks exhibit an added layer of redundancy in terms of water protection due to treating the timber member earlier on in the bridge panel process, maximizing the amount of surface area into which the preservative can penetrate [50].

However, it is noteworthy that Wheeler Consolidated, Inc. has undertaken full-scale testing of spike-laminated decks, conducted under the supervision of an independent testing firm. The results of these tests, which were presented to AASHTO and subsequently accepted, allowed Wheeler's spike-laminated decks to be designed using a deck distribution width equal to the tire width plus twice the deck thickness. In comparison, nail-laminated decks are typically designed with a distribution width equal to the tire width plus the deck thickness [65]. This difference reflects the improved mechanical load transfer capability of spike-laminated decks in addressing some of the inherent limitations of nail-laminated deck systems.

2.5.5 Stress-Laminated Decks

Stress-laminated decks represent a more advanced approach in timber bridge deck construction, where structural integrity is achieved through steel stressing rods. These rods vary in size, spacing, and pattern [48, 66], and their primary function is to exert pressure on the wooden boards, holding them together in tight contact. This pressure generates significant friction between the members, facilitating the transfer of loads across the deck through frictional forces. A crucial aspect of the design and maintenance of stress-laminated decks is the consistent maintenance of this friction to prevent slippage between boards, which is essential for load transfer [67-68].

The structural behavior of stress-laminated decks closely aligns with the theoretical model of an ideal orthotropic plate. A specific distribution mechanism is required to distribute the prestressing force effectively across the timber deck, as illustrated in Figure 45. This mechanism ensures that the stressing rod, particularly at the deck's edge, does not cause damage by pulling through the wood.

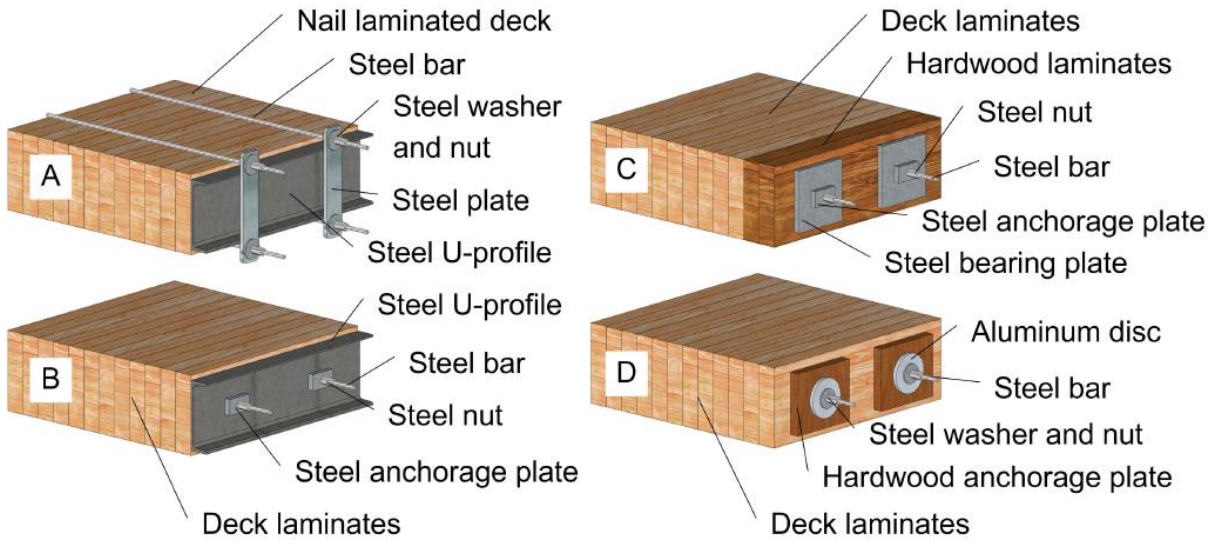

Figure 45. Stress-Laminated Deck Anchorage [68]

The thickness of stress-laminated bridge decks depends on the type of lumber used, which may consist of either sawn dimension lumber or prefabricated glulam members [48]. When sawn lumber is used, the deck thickness typically follows nominal dimensions (for example, 6 in. or 8 in.) and is planed to actual sizes during fabrication. Due to the limited availability of long sawn lumber, butt joints are often necessary [48]. These joints reduce structural continuity and can compromise deck integrity. Some designs, although not approved by AASHTO, have incorporated larger timber beams interspersed between the laminations. This creates a hybrid system that resembles a cast-in-place concrete deck supported by longitudinal girders. An example of such a configuration is shown in Figure 46. As an alternative, glulam members may be used for stress-laminated decks. In this case, the deck thickness is defined by the depth of the glulam members placed side by side. This method eliminates the need for butt joints for simple spans up to ~ 100 ft

but allows for longer (butt-jointed) continuous spans. For stress-laminated longitudinal decks designed to carry HL-93 loading, the minimum deck thickness typically begins at 12 in. [32, 48].

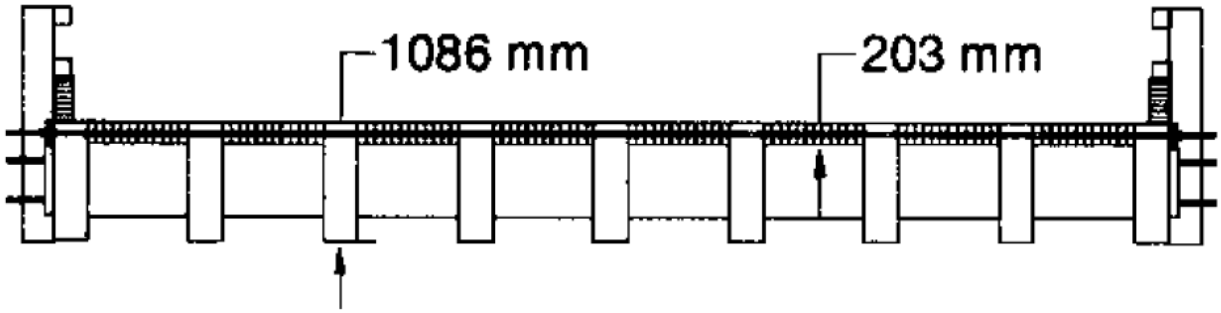

Figure 46. Cross-Section of Humphrey Stress-Laminated T-Beam Timber Bridge Deck [69]

The origin of the stress-laminated deck can be traced back to Canada, where it was initially conceptualized as a repair technique for nail-laminated decks. However, the method demonstrated such remarkable performance that it swiftly transitioned from a mere repair strategy to a foundational design approach [47]. The significance of this decking technique was further underscored in 1988 when the U.S. Congress enacted the Timber Bridge Initiative. This initiative aimed to establish a national program for constructing timber bridges, leveraging U.S. timber resources to enhance highway infrastructure. As a part of this initiative, several demonstration bridges featuring stress-laminated timber decks were constructed [69-71]. These bridges were subjected to extensive evaluation over subsequent years to assess their performance and viability.

Despite these efforts, the adoption of stress-laminated bridges in the U.S. remains limited. Kenneth Johnson from Wheeler Consolidated noted that, in light of Wheeler's funded research and knowledge of the deck performance, these decks were not expected to be very cost-effective relative to other timber bridge deck types [50]. While noting that one of the remarkable attributes of stress-laminated decks is their high strength capacity, deflection rather than strength often became the limiting factor in design and made the deck type less desirable for Wheeler to build relative to spike-laminated or glulam [50]. Other researchers have also noted that stress-laminated decks are typically less stiff than glulam deck panels [56].

In contrast to the US, the design has gained substantial traction in Nordic countries. There, stress-laminated decks are frequently integrated with transverse steel members, glulam trusses, and concrete abutments [64]. The stress-laminated deck spans are reduced by the transverse steel members (effectively curbing deflection). An illustration of this method, featuring a stress-laminated deck supported by steel cross beams, is presented in Figure 47.

Figure 47. Stress-Laminated Deck Built on Steel Cross-Beams [73]

Stress-laminated decks are also renowned for their exceptional dimensional stability. They exhibit high resistance to moisture-induced expansion and contraction, significantly mitigating the risk of cracking in bridge asphalt overlays [67]. This stability suggests that stress-laminated decks are less prone to differential expansion, which could otherwise lead to offsetting bridge railing posts. Although field investigations by bridge inspectors in the U.S. have revealed concerns regarding excessive moisture content in stress-laminated timber decks, this issue is often attributed to the absence of a waterproof layer over the deck [72]. Thus, it is important to note that the absence of dimensional shifts or differential expansion should not be misconstrued as an indication of reduced water protection requirements for these decks. Ensuring proper waterproofing remains critical to maintaining the longevity and structural integrity of stress-laminated timber bridges. Moisture protection concerns will be discussed in greater detail in the following section, but it should also be mentioned that these stress-laminated demonstration bridges were built prior to more recently published recommendations for moisture protection of the timber deck surface [32].

One of the primary challenges associated with stress-laminated decks lies in the maintenance of stress in the stressing rods, which was integral to the deck's load-transfer capacity. Post-construction, the rods must be restressed at several intervals over the following weeks and years. The need for re-stressing arises from the timber laminations compressing together and relieving the stress in the stressing rods [66]. Regular inspections are crucial to verify that the tension in the stressing rods remains adequate. If left unchecked the stressing rod tension will drop below acceptable thresholds, potentially compromising the deck's structural integrity [15]. Further concerns relate to the stiffness of stress-laminated decks, particularly in transverse orientation near the deck edges. Observations of mock-up stress-laminated bridge tests showed that serviceability loads allow interlaminar slip in these bridge decks, indicating a non-linear load-deflection relationship for typical loads [68].

2.5.6 Alternative Deck Types

2.5.6.1 Plank Decks

Among various timber bridge deck types, plank decks represent a notably common yet under-evaluated category [54]. Characterized by their simplicity, these decks consist of lumber boards laid flat on supports, which are typically fastened using nails or bolts [15]. While structurally straightforward, the AASHTO Bridge Design Specifications advise against using plank decks for roads subjected to heavy vehicle traffic. The Timber Bridge Manual also provides guidance for the design of these decks, and explicitly states that these decks should not be used with asphalt wearing surfaces and would not perform adequately with traffic railings, making this deck unsuitable for MASH TL-4 bridge railings [47].

Figure 48. Wooden Plank Bridge Deck [74]

2.5.6.2 Cross-Laminated-Timber Decks

Cross-Laminated-Timber (CLT) is an evolving method in timber lamination that is gaining prominence in construction. This technique involves the adhesive bonding of layers of boards at right angles to each other. This method resembles glulam timber but differs in the orientation of the laminations. An illustrative example of cross-laminated timber is depicted in Figure 49.

Originally popularized in European construction, CLT is now seeing increased adoption in North American building projects [49]. One notable application of CLT is in the construction of the Mistissini Bridge. However, it is important to highlight that the cross-laminated panels, in this instance, did not directly transfer vehicle loads from the superstructure to the substructure. Instead, they were placed atop glulam panels, which performed the load-bearing function [75]. Currently, the industry lacks specific design standards or guidelines for using CLT in bridge deck panels intended to carry vehicle loads. This gap in standardization and understanding is being addressed by ongoing research [76-77].

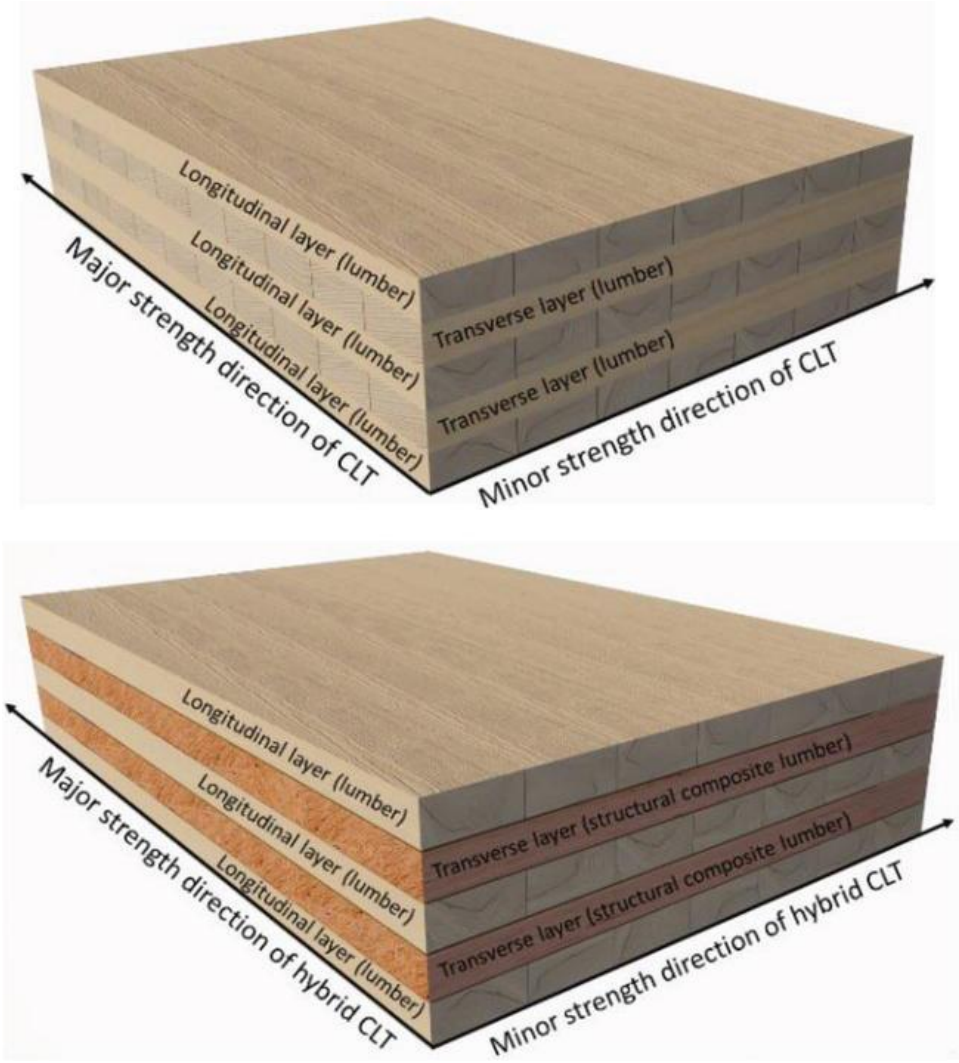

Figure 49. Cross-Laminated Timber [49]

2.5.6.3 Miscellaneous Techniques

In Switzerland, there is an emerging interest in utilizing glulam stress-laminated deck sections as a potential alternative to conventional pre-stressed concrete deck sections [78]. This innovative approach involves the design of a box girder superstructure that doubles as the bridge deck. This design aims to position it as a viable competitor to traditional concrete box girder bridges. However, the performance of this superstructure, particularly in real-world applications,

remains to be empirically validated. While specific design details of this glulam stress-laminated deck were not publicly disclosed, available images (as seen in Figure 50) indicate the design might incorporate elements of cross-laminated deck panels. This suggests a blend of stress-lamination and cross-lamination techniques in the construction of the deck.

Figure 50. Timber Glulam Box Girder [78]

Given the nascent stage of development for cross-laminated deck panels, particularly in bridge construction, it was prudent to await the establishment of standard practices and guidelines for these panels. Such standards will be instrumental in confirming whether the design can meet the impact safety and performance criteria set by the MASH 2016 TL-4 for bridge railings.

Bridge decking offered a wide range of possibilities for adhering wood into larger structural members, bringing unique properties and potential applications. Among these methods were cross-laminated panels, dowel-laminations using wood, laminated veneer lumber, parallel-strand lumber, laminated strand lumber, and various panel types, such as stapled, glued oriented strand board, screwed, dovetailed, and wood welded plates [57]. Despite this diversity, many of these timber fastening techniques have not been extensively explored in bridge deck construction, especially in bridges designed for vehicular traffic. Two noteworthy methods that merit discussion were oblique interlocked laminated decks and screw-laminated panels.

Oblique interlocked laminated timber decks functioned much like a stress-laminated timber bridge deck. Transverse steel rods were placed without prestressing in the deck fabricated from hexagonal timbers. Load was transferred by the timber's shear and bearing resistance and the rods prevented excessive transverse deformations. This potential deck design was investigated due to concerns about the ability of stress-laminated decks to maintain stress and transfer shear forces. Slip between stress-laminated deck laminations occur at low stress levels in the rods, which occur due to creep in the wood. Research reports showed that these decks lacked transverse stiffness

compared to the stress-laminated deck but succeeded in transferring shear forces without friction [79]. Testing of an oblique interlocked laminated timber deck is shown in Figure 51.

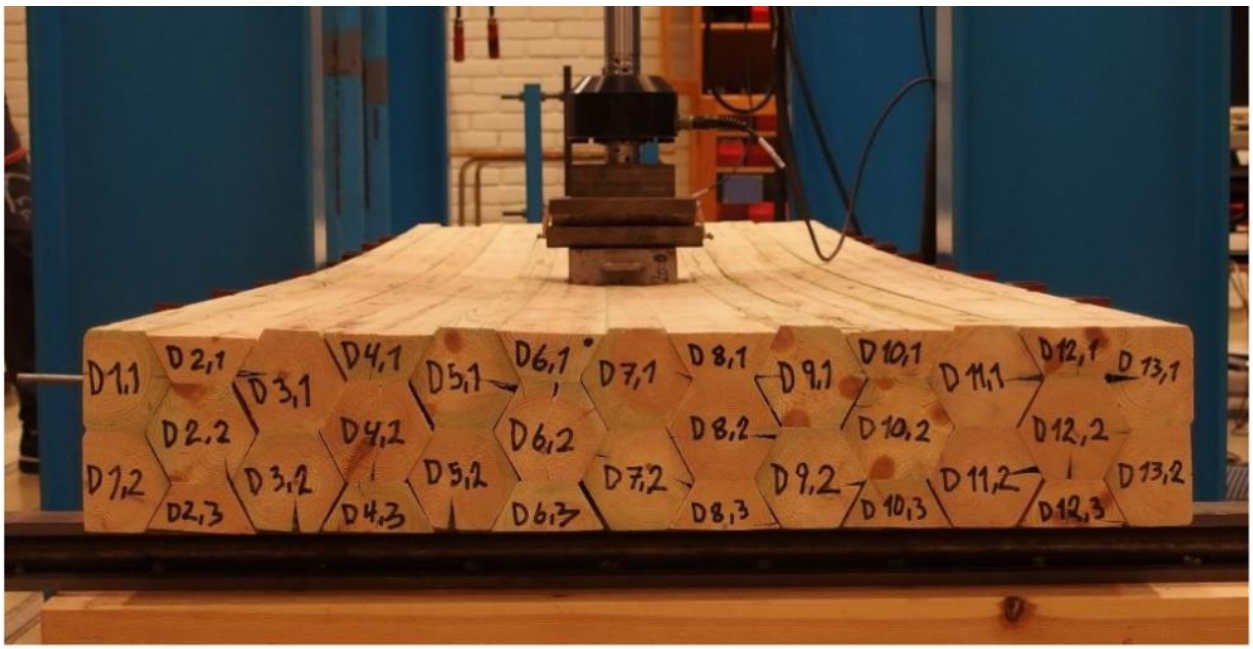

Figure 51. Testing of Oblique Interlocked Laminated Timber Deck [79]

Developed as an innovative alternative to traditional nail-laminated bridge decks, screwed-laminating was a technique which involved fastening the deck using screws set at 45° angles into adjacent boards. Comparative testing demonstrated that screw-laminated decks performed better than their nail-laminated counterparts. However, they have not shown comparable advantages when benchmarked against glulam or stress-laminated decks [56]. Spike-laminated decks were not examined for comparison, based on the published report.

The production of screw-laminated decks was limited, with no known manufacturers actively building these decks. This lack of commercial availability, coupled with their relative performance metrics, suggested that pursuing screw-laminated decks would not be a fruitful avenue for future development in bridge decking. Figure 52 shows a photo of a screw-laminated deck panel during testing to develop and compare performance against other timber deck types.

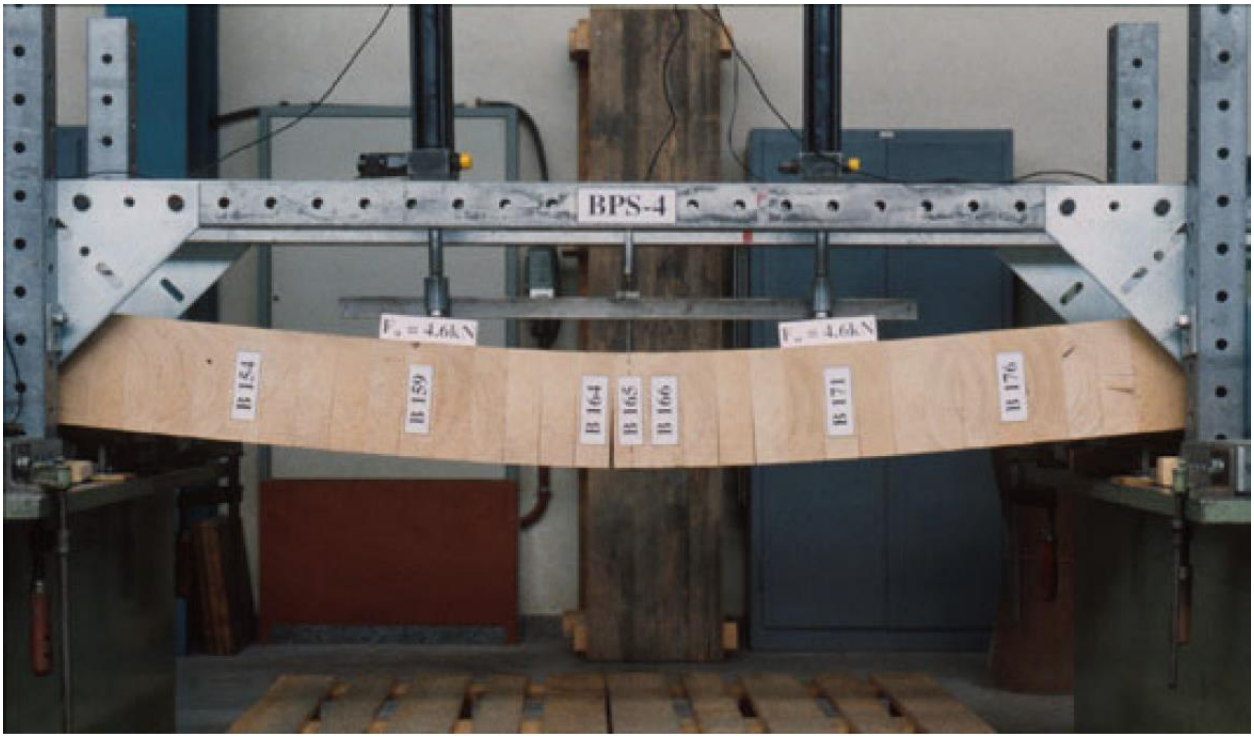

Figure 52. Screw-Laminated Deck Panel Under 4-Point Bending Test [56]

2.6 Timber Bridge Design with Moisture Mitigation Considerations

In the design of timber bridges, it is crucial to account for various service conditions to ensure their structural integrity over extended periods. A critical factor in this regard is the vulnerability of system components to high moisture content, known to reduce wood's structural strength [15]. Therefore, the design of bridge railings must incorporate strategies to withstand such wet-use conditions, and some review of bridge deck protection methods against moisture provides insight into the bridge deck vulnerability relative to the bridge railing. This review also investigated whether the wet-use factor should be applied to estimates of timber strength when impact load duration conditions were also present.

Protection of timber bridges from high moisture content was typically a serviceability concern, which included protection against rot, insect infestation, and other similar threats. Protection mechanisms against high water content were typically identical to the protection mechanism for the other serviceability concerns, and so some discussion of both was necessary. While using decay-resistant wood species could be used to alleviate serviceability concerns, such materials were often unavailable in the necessary quantities or specifications [3].

2.6.1 Timber Bridge Deck Waterproofing

When MwRSF built and tested TL-4 timber bridge railings on longitudinal and transverse glulam bridge decks, no material or design was used to protect the bridge deck surface beyond an asphalt or concrete wearing surface [16, 25]. This form of protection was noted to be insufficient for wood protection when wood shrinks or expands, which created cracks where water seeped into the wood deck surface and began deteriorating the wood [82]. To handle these issues, a three-layer

system was proposed to prevent water from reaching and sitting on the timber bridge deck surface: (1) an asphalt base course placed on the bridge deck; (2) a waterproof membrane; and (3) an asphalt base course placed over the waterproof membrane [82]. The referenced report describes the requirements for the membrane and asphalt specifications in greater detail. These recommendations continued to be included with the latest glulam timber bridge reports from the Forest Products Laboratory produced in 2019 [32]. The application of the two asphalt layers, waterproof layer, and relationship to the bridge railing are shown below in Figure 53.

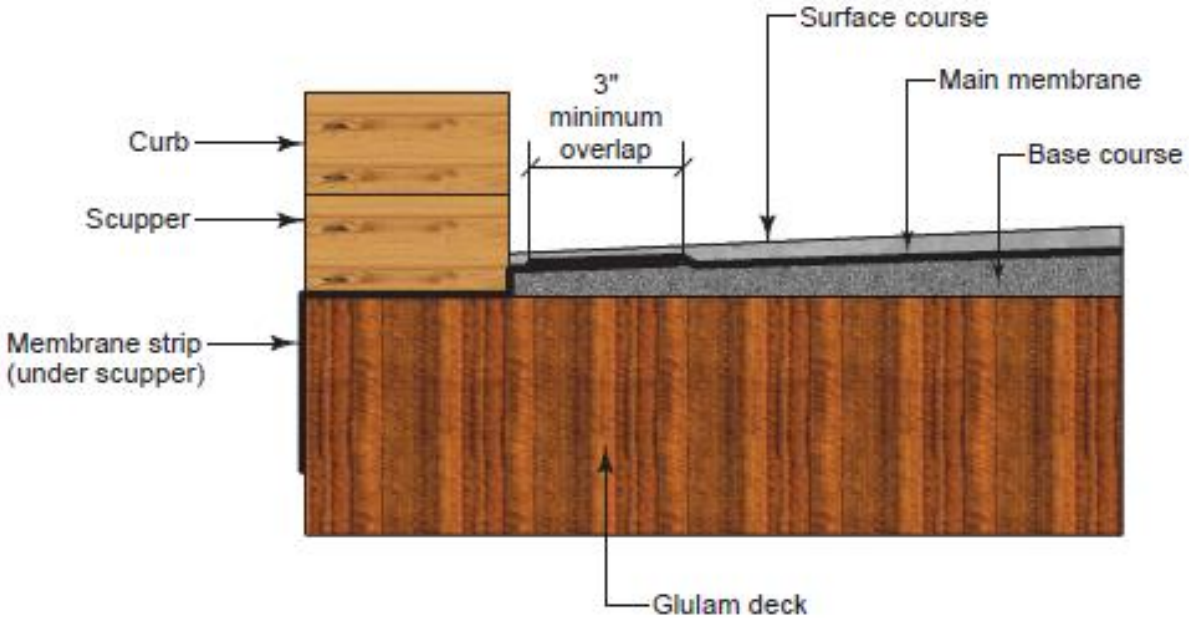

Figure 53. Diagram of Membrane Protecting Bridge Deck Surface, with Timber Railing [32]

In Minnesota, two demonstration bridges were constructed which utilized this method for protection of the bridge deck along with numerous other methods designed to protect the bridge deck and railing from water accumulation near vulnerable locations [83]. In addition to the asphalt wearing surface, a tack coating was applied to the top of both demonstration bridges, as shown in Figure 54. A tack coating is typically applied to increase the bonding connection either between different layers of asphalt or between asphalt and concrete so that fatigue cracking and other forms of damage to the asphalt wearing surface resulting from lack of bond to the ground surface do not occur [84]. Other methods of deck protection from water infiltration included the use of steel plates over the ends of the deck and flashing over the edges of the deck. Mechanical methods of deck and railing protection are discussed in greater detail in the following sections.

Figure 54. Tack Coat Applied to Timber Bridge Demonstration Bridge in Minnesota [83]

2.6.2 Consideration of Wet-Use Factor in Timber Bridge Railing Design

In Phase IIa of the project, the wet-use factor, a critical parameter in determining the strength of timber under varying moisture conditions, was initially set at 1.0. This decision was based on preliminary analyses indicating that the average moisture content throughout the year did not surpass 16% [11]. Additionally, the quick evaporation and lack of stagnant water around the upper and lower railings mitigated the risk of moisture-induced weakening because the water could not remain for extended periods. However, this approach drew concerns from FPL engineers. It was highlighted that during intense rainfall events, wood could temporarily absorb significant amounts of water, potentially leading to elevated moisture content levels that would not be reflected in the average. Such scenarios could temporarily weaken the timber's strength, posing a risk of railing failure post-storm, especially around the scuppers where water runoff would be concentrated. The flow of water around the scupper and sitting water on the deck suggested a high probability that this water would be adsorbed by the hydrophilic end grain of the scupper blocks.

The performance of wet timber under static loading vs impact loading was not initially considered to be affected by the moisture content in different ways, but A.J.M. Leijten discussed this relationship briefly when writing about the applicability of an instantaneous load factor for impact conditions [82]. Leijten mentions that timber is weakest under impact loading at 10%-15% moisture content (a dry moisture content for both glulam and sawn lumber), citing research by N.H. Kloot from the 1950s. Kloot's research suggested a complex relationship between timber

strength and moisture content under impact loads, differing from static loads, but his findings did not extend to providing a definitive method to describe this relationship [86].

These insights reinforced the initial decision to disregard the upper and lower railings from an analysis of performance with system components highly saturated with water. But this choice did not provide clarity regarding the resistance of the scupper in wet conditions and impact loading. Further investigation was conducted to describe the scupper compressive resistance perpendicular to the wood grain under impact loads and high moisture content. Three distinct research efforts were identified that investigated this question, focusing on wood compression properties under high-strain rates and varying moisture contents [87-89]. These studies included tests on both radial and tangential compression resistance, which are orientations perpendicular to the grain.

The findings of these studies all indicate a consistent trend: as moisture content in the timber increases, its resistance perpendicular to the grain decreases. Notably, experiments revealed that the resistance was at its lowest at the fiber saturation point. Intriguingly, at moisture contents reaching 200% – a level achievable due to the cellular structure of wood – an increase in resistance was observed. This phenomenon, however, might not directly indicate an enhancement in impact resistance. Instead, it could result from the water being unable to permeate further within the short timeframe of the impact, leading to a bursting of the cell walls. This bursting requires a greater initial force, which could be misconstrued as increased compressive resistance. This hypothesis was visually corroborated by Pierre et al. [88] through photographic evidence, shown in Figure 55.

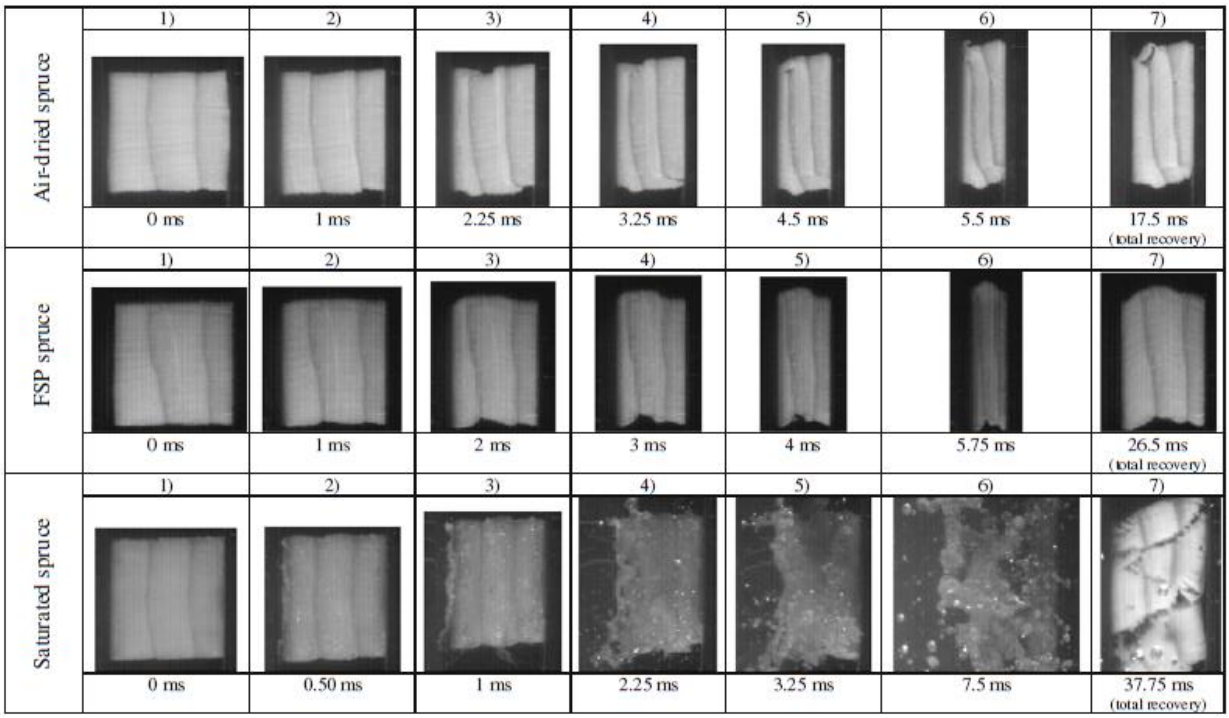

Figure 55. Results of Impact Compression Under Different Moisture Contents [88]

In the referenced experiments investigating timber compression properties under high-strain rates and varying moisture contents, the specimen sizes were notably small, with one set of

experiments using specimens measuring only ½ in. in each dimension. This disparity in size between the test specimens and actual scuppers used in bridges raises questions about the scalability of these effects from smaller to larger sizes. However, two key considerations suggest that size effects might not significantly alter the observed behaviors when scaled up.

Firstly, the American Society for Testing and Materials (ASTM) employs a standard specimen size of 2 in. x 2 in. x 30 in. for tests designed to measure standard compression stress perpendicular to the grain at various deformations [90]. Despite the relatively modest size of these standard specimens, the derived properties were considered to be applicable to 5-in. by 5-in. and larger structural timbers, as per typical engineering practices [91]. This indicated confidence in the representativeness of smaller specimen test results for larger timber components.

Secondly, the failure mechanism in the timber under compression perpendicular to the grain was predominantly characterized by the collapse of cellular walls [92-93]. This phenomenon was particularly relevant for glulam and was reflected in the NDS and ASTM definition for glulam design values perpendicular to the grain [14, 94]. When a lamination bears against an object, the resistance perpendicular to the grain of that lamination is the tabulated value because cell wall collapse (shown in Figure 56), signifying failure initiates in the cell walls of that particular lamination. This process is well-documented in existing literature [14, 93]. Essentially, the local capacity at the point of load application governs the overall capacity. Therefore, tests on smaller specimens are likely to be indicative of the behavior in larger timber components.

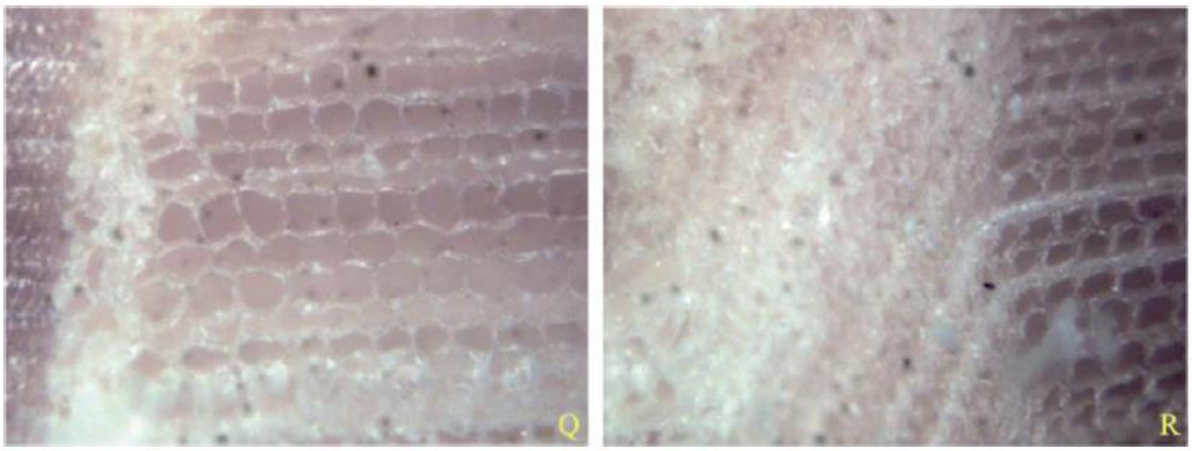

Figure 56. Cell Wall Collapse at Microscopic Level [93]

Consequently, based on these considerations, applying the wet-use factor to reduce the compressive resistance of the scuppers during high strain-rate impact loads is advisable. This application acknowledges the influence of moisture content on timber resistance. It ensures that the structural analysis and design of timber bridges, particularly the scupper elements, are effective under various environmental conditions.

2.6.3 Application of Preservatives in Timber Bridges

There are two general methods of improving the serviceability of timber, prevent water from obtaining access into the timber, and pressure-treating timber. Obstructing water access will

be discussed in the next section. Pressure treatment involves filling the wood with substances that are toxic to invasive organisms, effectively preventing them from consuming the wood. Historically, constructing bridges from naturally decay-resistant timber was feasible due to the availability of large, robust woods. As these strong, decay-resistant woods have become scarce in contemporary times, the industry has applied preservatives to less decay-resistant wood species to ensure similar durability and strength [47]. Some preservatives can serve a dual function: deterring wood-consuming or wood-inhabiting organisms by either making the wood toxic or unsuitable for habitation, primarily by preventing moisture penetration [95].

Wood preservation could be completed solely through various water-repellant coatings, but these options may be insufficient if excessive water is trapped into the wood by the coating. Oil-borne preservatives both poison the wood and offer water-repellency due to the co-working of the preservative and the oil solvent carrying the preservative [96]. AASHTO requires all structural timber members to be treated in oil-borne preservatives, because of water-repellency and reduced risk of check/splitting inherent to water-borne preservatives [15].

Water-borne preservatives are attractive for their compatibility with painting, but they present significant drawbacks. To apply these preservatives, the preservative is dissolved in water and then introduced into the wood under pressure. This process causes the wood to swell due to water absorption. As the wood dries and loses this absorbed water, it shrinks, which can lead to issues like checking, splitting, warping, or bending. Thus, the application of water-borne preservatives, despite its benefits, carries an inherent risk of wood deformation.

In water-borne preservatives suitable for treating glulam timber, the use of Ammoniacal Copper Zinc Arsenate (ACZA) is distinctly limited. ACZA is currently the only water-borne preservative approved for use in glulam timber, and its application is restricted to Coastal Douglas Fir among the various glulam species. This constraint presents a challenge for bridge builders who rely on Southern Yellow Pine or other types of glulam for their railing systems. Furthermore, ACZA and water-borne preservatives, in general, are known to be corrosive to steel hardware, complicating their use in construction [95].

The corrosion risk posed by water-borne preservatives to steel hardware used inside timber members is heightened compared to this hardware exposed to air. In solid wood, galvanized steel undergoes a different chemical reaction that accelerates corrosion, because the reaction inside wood does not produce insulating by-products obstructing the reaction [97]. The presence of copper in these preservatives further exacerbates this issue. The cupric ions, integral to the preservative's function of poisoning the wood, actively oxidize galvanized steel, leading to increased corrosion [97].

Available oil-borne preservatives for glulam timber, according to the American Wood Protection Association (AWPA), include Creosote (CR) formulations, Pentachlorophenol (PCP), Copper Naphthenate (CuN), 4,5-Dichloro-2-N-Octyl-4-Isothiazolin-3-One (DCOI), 3-Iodo-2-proponyl carbamate (IPBC), and Copper -8-quinolinolate (Cu8). Currently, IPBC and Cu8 have not received AWPA’s approval for use categories 4A or 4B, but they remain potential candidates for future sanctioning. Another noteworthy development is the advent of borates combined with a creosote coating, known as SBX-O, which, while approved for solid lumber, is yet to be authorized for glulam timber, presenting an area of future exploration.

In this array of preservatives, only Copper Naphthenate (CuN) and Copper-8-quinolinolate (Cu8) employ copper as their active biocidal component, effectively combating invasive organisms. Notably, the oil-based nature of these formulations plays a crucial role in minimizing the risk of corrosion, a significant consideration in maintaining the structural integrity of timber in construction [95]. However, out of all the options mentioned, only Creosote (CR), Pentachlorophenol (PCP), Copper Naphthenate (CuN), and 4,5-Dichloro-2-N-Octyl-4-Isothiazolin-3-One (DCOI) have currently obtained approval for use in bridge construction.

Coal-tar creosote, derived from the by-product of coal coking processes, stands as the most enduring wood preservative in industrial applications. It functions by imparting a water-repellent oily barrier and infusing wood with chemicals lethal to fungi, insects, and other invasive organisms [95]. Despite its efficacy, creosote poses significant health risks, being a recognized carcinogen [98]. These health concerns have prompted a shift within the timber bridge industry, with professionals increasingly avoiding coal-tar creosote due to the hazards it presents, particularly to those handling it [99].

Parallel to the decline in creosote usage, Pentachlorophenol (PCP), another widely-used oil-based wood preservative [100], faces its own challenges. Global cessation of PCP production has been driven by its detrimental environmental impacts [101]. While temporary means to access PCP for wood treatment might exist, its discontinuation globally necessitates that future preservative strategies for timber bridge railings exclude PCP [99].

The gradual discontinuation of traditional preservatives such as creosote and pentachlorophenol has narrowed the focus on alternative treatments for long-term use in glulam timber bridges. Currently, Oilborne Copper Naphthenate and 4,5-Dichloro-2-N-Octyl-4-Isothiazolin-3-One (DCOI) emerge as the primary choices for this application.

Copper naphthenate, in particular, has gained prominence as the most prevalent preservative treatment for highway bridges [99, 102-103]. Its formulation is available in both oil-borne and water-borne variants, with the industry demonstrating a strong preference for the oil-borne type. This preference is attributed to the oil-borne form's superior water repellency [102]. Comparative studies have indicated that oil-borne copper naphthenate is more effective than its water-borne counterpart, though this efficacy gap narrows at higher concentration levels [95].

DCOI represents a relatively new entrant in the wood preservative landscape, initially finding application in pole treatments and recently receiving approval for use in glulam timber. Conversations with DCOI suppliers have affirmed its availability for broader application in timber bridge construction.

2.6.4 Other Methods of Protection

Concerns over the damage caused by timber preservatives in the environment have motivated the development of timber protection methods that do not rely on them. These methods typically involve employing physical barriers to prevent rainwater from directly contacting the wood. Protection methods by design which precludes standing water near vulnerable components has also been explored in detail by Kropf [104] as well as by RISE more recently in Sweden [64].

2.6.4.1 Covered Timber Bridges

The use of covered bridges has been evaluated and subsequently deemed unsuitable for timber highway bridges. Protecting the bridge deck with a fully covered overhead structure is insufficient for a highway bridge because rain can still come onto the bridge deck from outside, high-speed vehicles, particularly large trucks such as semi-trucks, will propel a sheet of rainwater into the covered area [64]. This ingress of water is also coupled with limited airflow in covered structures and results in ineffective evaporation, leaving the wood exposed to prolonged periods of moisture. The issues with water mitigation only compound additional issues with using this concept for highway bridges, appropriate crash-tested bridge railings for these bridges would require additional design considerations for the walls/truss of the covered bridge, which cannot afford to be adversely affected lest the entire bridge collapse. An example of a covered bridge built in Middlebury, Vermont allowing two lanes of traffic and including a bridge railing and an approach guardrail transition is shown in Figure 57.

Figure 57. Pulp Mill Bridge Rd. in Middlebury, VT [105]

2.6.4.2 Flashing

A more common method of timber bridge protection from moisture by mechanical means involves the use of flashing, or metal plates designed to gather water and redirect it off the bridge deck. This method was used in two demonstration bridges built in Minnesota previously discussed [83]. Because the end grain of wood is very hydrophilic, flashing is ideally covering the edges of transverse bridge decks, as shown in Figure 58. There are two different plates used for the flashing in this figure, one of them covering the end grain (offset from the end grain by $^{1}/_{16}$ to ⅛ in. to avoid direct contact), while the other drained water away from the post hardware locations. There are different metals for this flashing material, and their quality as flashing material is based on their

propensity to corrode, which is a function of their active (anodic) vs passive (cathodic) properties (altogether forming a galvanic scale) in seawater [106].

Figure 58. Flashing on Transverse Timber Bridge Deck Edges, Covering Panel End Grain [83]

The other demonstration bridge built in Minnesota for this project used the TL-4 timber bridge railing crash tested by MwRSF on a longitudinal bridge deck [16]. On this bridge, the flashing, as shown in Figure 59, was located on both the bridge deck and the scuppers. Water flowing off the bridge flows to both sides of the bridge scupper, near the hydrophilic end grain which readily absorbs water. Flashing at this location protected the most vulnerable part of the scupper. However, it should be noted that the flashing was held in place by small nails – representing locations for water to make its way into the wood and cause damage. Unlike the previous method of flashing, the flashing here was not offset from the end grain of the wood, which may carry risks of trapping water against the end grain. Additionally, while the end grain was protected, the edges of the scupper were not. Water can still seep into the wood cells of the timber through the sides of the scuppers.

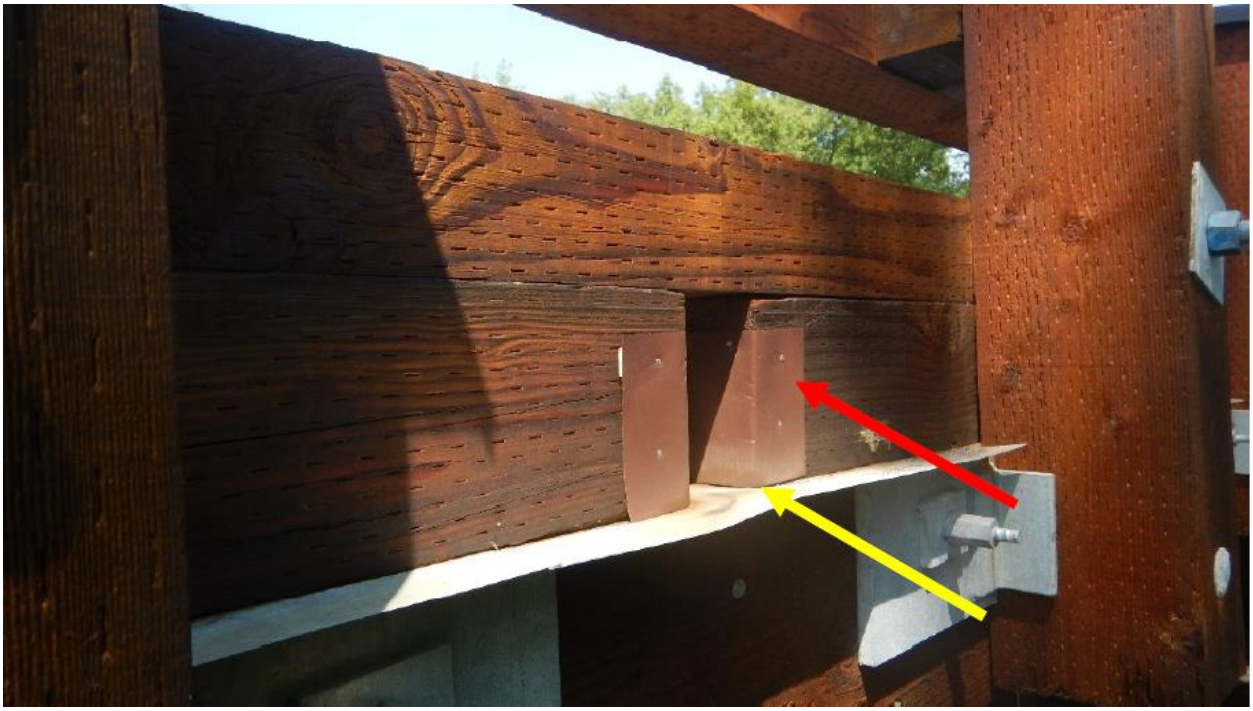

Figure 59. Flashing on Longitudinal Timber Bridge Deck Panels and Railing Scuppers. Top arrow: points to the flashing protecting the ends of the bridge scuppers. Bottom arrow: points to the flashing which carries water away from the bridge deck [83]

The last covering, very similar to flashing, applied to protect these bridges is a plastic cap over the top of the timber posts, as shown in Figure 60. Similar issues as previously noted were noted with this design. The nail that was used to hold the cap in place represented a risk for corrosion and a place for water to infiltrate and degrade the post.

Figure 60. Plastic Cap Covering Top of Post [83]

2.6.4.3 Heat and Chemical Treatments

Another method that was explored to enhance timber's durability in bridge construction involved the modification of wood surfaces to impede water absorption. Two prominent methods have emerged – heat treatment and chemical modification. Heat treatment of wood has demonstrated efficacy in altering its structure to resist water uptake. However, this benefit comes with a notable trade-off – the process weakens the wood's structural integrity [106]. This reduction in strength has been empirically validated through impact testing conducted in the Netherlands, where heat-treated wood exhibited diminished resilience under stress [108].

On the other hand, chemical treatments involve chemical reactions with the cellular walls of the wood, leading to the formation of a modified cellular structure. Unlike its untreated counterpart, the new cellular wall structure lacks the innate hydrophilicity [106]. The resulting wood possesses a substantial increase in dimensional stability over untreated counterparts, making it less prone to warping or swelling due to moisture fluctuations [109]. Comparisons with other treatment methods, however, have not been clearly established. In addition, the commercial application of this technology has faced hurdles, primarily due to the elevated costs of production [110]. Chemical treatments do not have the same level of widespread research and comparison in demonstrating efficacy compared to other wood preservation methods, especially wood preservatives. For example, its use as a treatment does not appear to be commercially available for commonly used species to build timber glulam bridges, nor were there any studies located which investigated its application to these species.

Although these treatments can bolster resistance to water, they may inadvertently escalate corrosion rates, surpassing even those observed in untreated wood [111]. This revelation poses significant implications for the long-term viability and maintenance of treated timber structures, especially when the wood is in close contact with metallic components or subjected to harsh environmental conditions. While in the future chemical treatment may become common, it has not been demonstrated to be a cost-effective measure which can reliably protect the timber bridges.

2.7 Summary and Conclusions

This literature review provided an examination of timber bridge railings, approach guardrail transitions and wooden posts used with them, and guardrail systems. Different bridge deck types used in bridge construction were reviewed, particularly emphasizing their mechanical response under impact loading conditions. The review examined construction methods, material properties, and suitability for different load-bearing scenarios. Serviceability limitations dealing with moisture content in the bridge members were investigated to evaluate design parameters for deck and railing components. Finally, the existing literature on dynamic testing of posts larger than 6 in. x 8 in. was reviewed. The key findings and conclusions are:

- Timber bridge railings and approach guardrail transitions have successfully handled NCHRP 350 TL-4 impact conditions and are properly the basis for design for MASH 2016 TL-4 and TL-3 impact conditions for bridge railings and AGTs respectively.

- Approach guardrail transitions (AGTs) have evolved since the most recent test of an appropriate MASH 2016 TL-3 transition, and will require updates to height, upstream transition, and compatibility with a wearing surface.

- Prior research into posts 8 in. x 8 in. and larger is not extensive, with limited research reports providing information on dynamic component and bogie tests on these posts in soil. Additional data was located on identifying the MOR of 8-in. x 8-in. posts.

- Nail-laminated timber decks are now considered outdated due to structural limitations. Limitations include uneven load distribution, susceptibility to delamination due to moisture changes, and a tendency for the nails to loosen under repeated stress cycles. The limitations have led to a decline in their use, particularly for roadside safety applications requiring adherence to updated impact safety standards like MASH 2016 TL-4.

- Glulam timber decks offer enhanced durability and structural efficiency. Adhesives make this method of lamination very stiff across laminated components, superior to any other method of lamination. Constraints include limitations to panel size down to the size of pressure-treatment cylinders, and load transfer beyond the glulam panel to other portions of the deck.

- Prefabricated spike-laminated panels, characterized by their use of steel spikes for load transfer, have been shown to provide superior load distribution and increased resistance to water damage over nail-laminated decks, overcoming the uneven bearing issues prevalent in nail-laminated decks.

- Stress-laminated decks exhibit high structural strength, utilizing steel rods to create frictional forces between timber boards. However, these decks face challenges in maintenance due to the need for periodic restressing, and cost considerations often constrain their implementation.

- Alternative deck types, including plank and cross-laminated timber (CLT), were evaluated for their potential in timber bridge construction. Plank decks, while simple, lack comprehensive design guidelines for modern load requirements, such as HL-93 loading. CLT, an emerging technology in timber lamination, shows promise but requires further empirical studies to establish its viability as a bridge decking material.

- Service conditions for timber bridge railings, such as wet-use scenarios and the selection of preservatives, were critically assessed. The study explored the implications of high moisture content on timber strength under impact loading and evaluated the efficacy of various preservative treatments in enhancing timber durability and longevity.

3 DEVELOPMENT OF A MASH TL-4 TIMBER BRIDGE RAILING SYSTEM

3.1 Overview

This project continued the work of a previous project, referred to here as "Phase IIa," involving the development of a MASH TL-4 glulam timber bridge railing. Phase IIa evaluated the needs of a MASH TL-4 timber bridge railing within BARRIER VII by modeling the glulam bridge railing and simulating impacts with MASH 2270P pickup truck and 10000S SUT vehicles [10-11]. The resulting design included several resized components and changes to the connection geometry from the original NCHRP Report 350 TL-4 timber bridge railing system [21-25, 121]. The glulam timber bridge railing connections were incomplete when Phase IIa concluded, which was the starting point for this project.

A design overview was provided in the Phase IIa study, which included the member sizes and changes from the NCHRP 350 configuration. Following this review, an overview of the BARRIER VII computer program has been provided for context to help others understand the logic and reasoning behind the BARRIER VII design input parameters used for the glulam timber bridge railing. These input parameters were reviewed and updated according to sponsor concerns about how effectively the timber bridge railing system handled excessive moisture within the bottom scupper and gutter-zone of deck superstructure underneath curb/scupper members. Following these updates, the connection design was completed, and an analysis of bridge deck capacity was conducted to determine the necessary dynamic component testing program to inform the critical deck parameters and determine the sufficiency of the timber bridge railing system's support posts.

3.2 Re-evaluation of Phase IIa Timber Bridge Railing Design

3.2.1 Phase IIa Final Design

The successful performance of the Glulam Rail with Curb on Transverse Glulam Timber Deck in 1997 [21-25, 121] served as the basis for design of the MASH 2016 TL-4 glulam timber bridge railing. The new railing design objectives included accommodation of a 2-in. wearing surface. For the revised design, the top railing height was increased beyond prior NCHRP 350 TL-4 guidelines to mitigate vehicle-to-barrier override risks. Thus, the railing height was set to 36 in. above the 2-in. asphalt overlay already on a 2-in. concrete wearing surface, marking a 5-in. height increase over the 1997 bridge railing. To accomplish the height increase while avoiding large gaps in the railing and increased vehicle snag on posts, the scupper block height was decreased from 6¾ in. to 5⅛ in., and another scupper block was added. The curb rail height was also increased from 6¾ in. to 8¾ in. The gap between the curb rail and the upper rail decreased by ½ in. from 8 in. to 7½ in., and the upper railing height did not change. Figures 61 and 62 illustrate how the configuration changed from the NCHRP-350 system by Fowler [21-25, 121] to the MASH 2016 system by Duren [10-11].

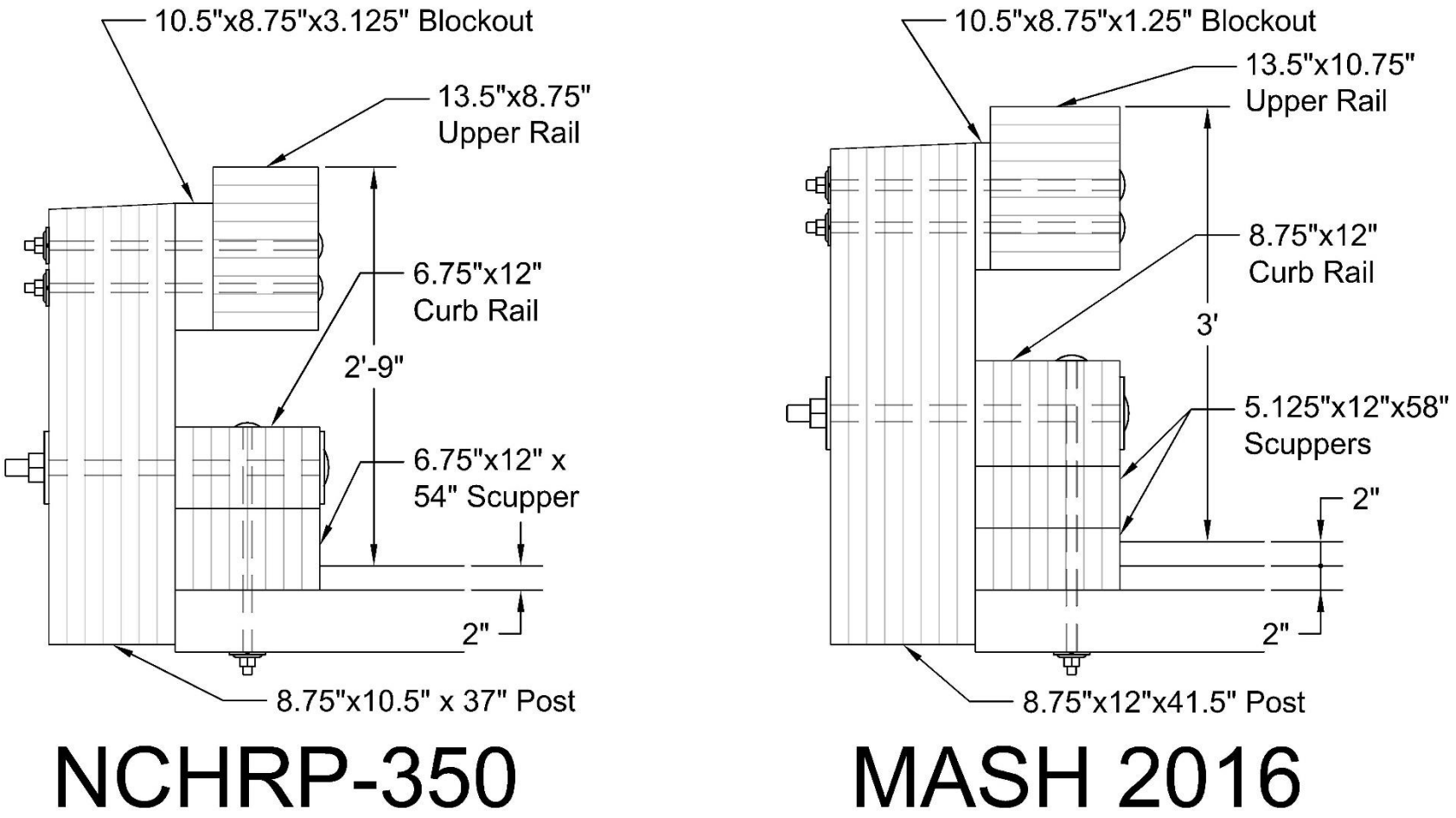

Figure 61. Cross-Sectional View of Phase IIa Design Changes from NCHRP-350 to MASH 2016

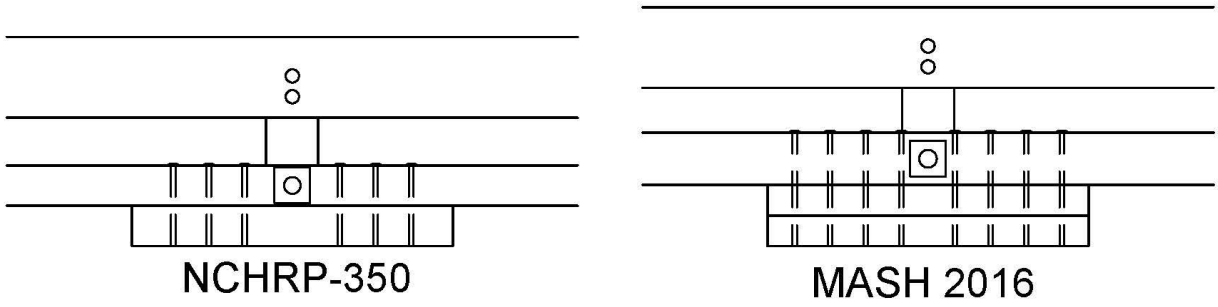

Figure 62. Elevation View of Phase IIa Design Changes from NCHRP-350 to MASH 2016

In addition to the curb rail and scupper block height increases, the width of the glulam upper rail was increased from 8¾ in. to 10¾ in. This change provided additional flexural resistance against excessive yielding that was observed in the BARRIER VII model analysis results [10-11]. The wider upper rail also allowed for a 2-in. reduction in the blockout width between the rail and the post. To further improve the flexural resistance of the curb rail connection, the number of bolts securing the curb rail to the bridge deck was increased from 6 to 8. The bolts were also repositioned 2 in. outward from the centerline of the curb rail and scupper blocks, toward the roadway. Although the bolt spacing was revised to accommodate these changes, the lengths of the scupper blocks remained unchanged. However, specific details related to these scupper block configurations were not provided in the final report by Duren et al. [11].

3.2.1.1 Overview of BARRIER VII Software

BARRIER VII [12-13], a two-dimensional (2D) vehicle-barrier simulation tool developed by Graham Powell at the University of California, Berkeley in 1973, has been essential in simulating full-scale vehicle crash tests into longitudinal barriers for nearly five decades. Since its inception, the software has been updated to accommodate smaller mesh sizes, enabling more detailed simulations of longitudinal barrier systems by increasing its computational capacity for larger element arrays, including beams, posts, and other components.

For impact loading on systems with deformable components, BARRIER VII models beam elements with an idealized bilinear, elastic, perfectly-plastic stress-strain response, allowing for both flexural and tensile loads. Strain hardening is included for scenarios where multiple members, each with different force versus deflection characteristics, are loaded in parallel. To simulate inelastic behavior, the tangent stiffness method is employed, while dynamic loads are integrated using midpoint constant acceleration numerical methods [12-13]. Additional parameters, such as cross-sectional area, length, and weight (included to account for inertial effects), are also required inputs to evaluate the beams' performance.

Post elements are modeled as springs with defined stiffness and yield moment to represent elastic-perfectly plastic behavior. The post parameters are shown in Figure 63. When a post reaches a defined shear or deflection failure threshold, BARRIER VII removes it from the system over prescribed time steps, redirecting loads to adjacent posts. The load-deflection curve for a post limited by deflection is shown in Figure 64, and Figure 65 shows the shear limit behavior. If no

failure occurs, the load-deflection curve will look like Figure 64, with deflection smaller than the deflection limit.

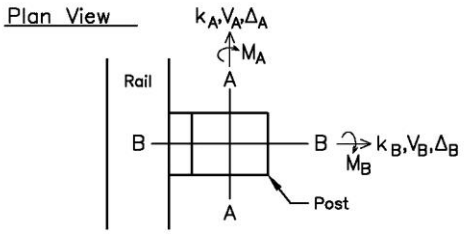

Figure 63. BARRIER VII Post Parameters [11]

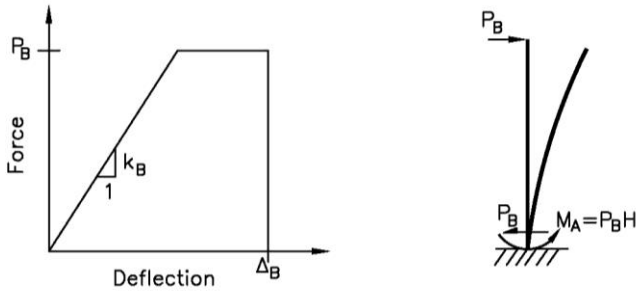

Figure 64. BARRIER VII Post Load-Deflection Curve when Limited by Deflection [11]

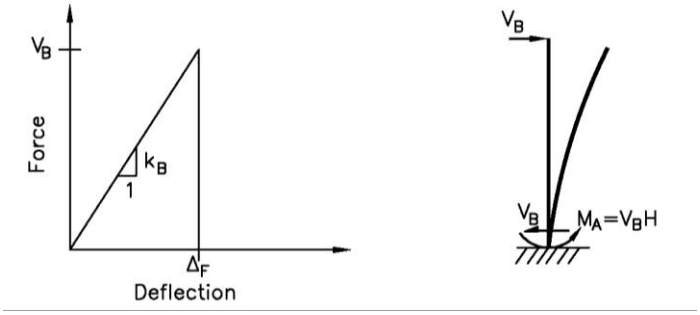

Figure 65. BARRIER VII Post Load-Deflection Curve when Limited by Shear [11]

In BARRIER VII simulations, vehicles are represented as deformable planar bodies, with prescribed shapes, masses, and rotational inertias. Vehicle deformation, including the crushing of metal and plastic components, is simulated using nonlinear springs with location-specific stiffness values that enable localized deformation. During crash events, these deformations reach predefined limits against the vehicle's frame and subsequently rebound as the vehicle disengages from the barrier. BARRIER VII captures this rebound behavior through the vehicle-specific parameters. Additionally, the vehicle model permits the user to designate contact points on the vehicle for interaction with each rail in a dual-rail system.

BARRIER VII vehicle models were initially based on standard vehicle configurations from 1989 AASHTO Guide Specifications and later modified according to NCHRP Report 350, with initial calibrations conducted by MwRSF using data from vehicle impacts into an instrumented wall at TTI in 1989 [113]. To align with MASH standards, a 2270P pickup model was developed, incorporating updated geometric and physical properties, thereby enhancing the model's applicability to current impact safety standards. A similar effort produced a foundational model for the updated 10000S vehicle, enabling enhanced analysis of semi-rigid barrier impacts [11]. Detailed finite element models, including respective input files, for the 2000P, 8000S, and 2270P vehicles and the 10000S vehicle are documented in Appendix A and Appendix C, respectively, of the original Phase IIa report [11].

3.2.1.2 Summary of BARRIER VII Model

The Phase IIa design utilized BARRIER VII simulations to evaluate the performance of the glulam timber bridge railing. Simulation results were compared against historical crash tests involving 2000P and 8000S vehicles, with additional predictions made for 2270P and 10000S impacts. This process allowed for critical evaluation of assumptions and modeling techniques, especially concerning the element properties and boundary conditions. The vehicles have been assumed to only contact the upper rail, because vehicles had been observed to "ride up" the bridge railing to some degree with their tires in previous crash tests. The resulting flexure on the post would reach the maximum faster, and deformation would start sooner as a result, leading to higher, more conservative deflections estimates in the model.

The MwRSF research effort to develop a MASH TL-4 bridge railing developed assumptions to map the BARRIER VII simulation assumptions to the bridge railing post configuration [10-11]. This model (shown in Figure 66), assumed that the deck was a fixed, rigid base for the BARRIER VII post rather than the curb rail. Each post connects the upper glulam and lower curb rails at specified nodes and heights, assuming rigidity between those nodes. The post's yield moment was conceptualized as a coupling between the vertical bolt tension and compression between the scupper and the bridge deck. As a consequence of this model formulation, connection components between the top of the bridge deck and the upper railing must remain linear-elastic for the glulam bridge post configuration to match the modelled BARRIER VII posts.

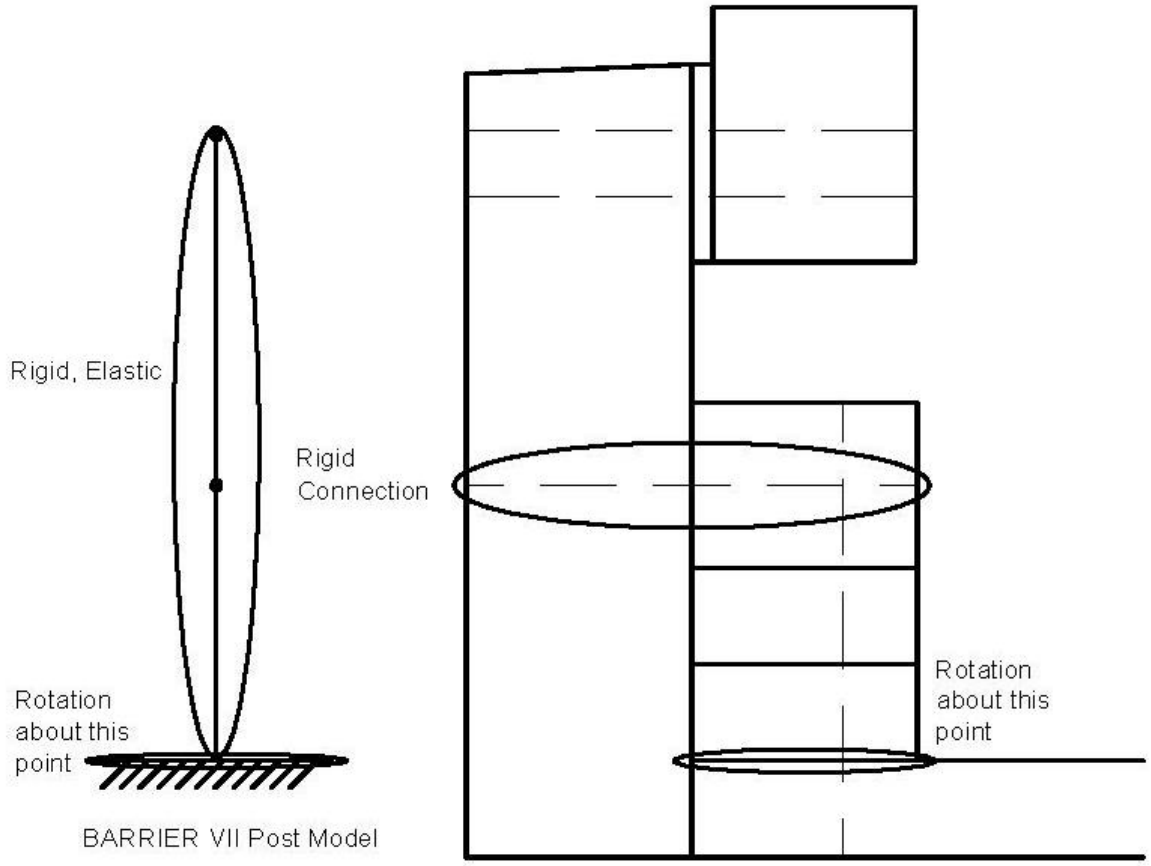

Figure 66. Phase IIa BARRIER VII Model

3.2.1.3 Post Yield Moment

The post's yield moment in BARRIER VII was represented by the couple formed from steel bolt tension and timber scupper block compression, resulting in a moment that resists applied rotation. In the Phase IIa research, timber and concrete were found to exhibit similar stress-strain characteristics [11], as shown in Figure 67. This similarity suggested that the analytical assumptions traditionally used for moment capacity in reinforced concrete beams could also be applied to the moment couple formed by the scupper and curb systems integral to TL-1 and TL-4 bridge railing designs. To approximate the compressive stress distribution in the scupper, the Whitney Stress Block Theory was employed, which positions a uniform compressive stress distribution across the compression zone at 85% of the material's compressive strength, offering a reliable approximation of observed non-linear stress distributions [11]. While the 85% factor is appropriate for concrete due to its parabolic stress distribution, there is no established equivalent for timber. Nevertheless, this reduction factor was retained for timber as a conservative estimate of compressive stress resistance perpendicular to the grain, pending further investigation.

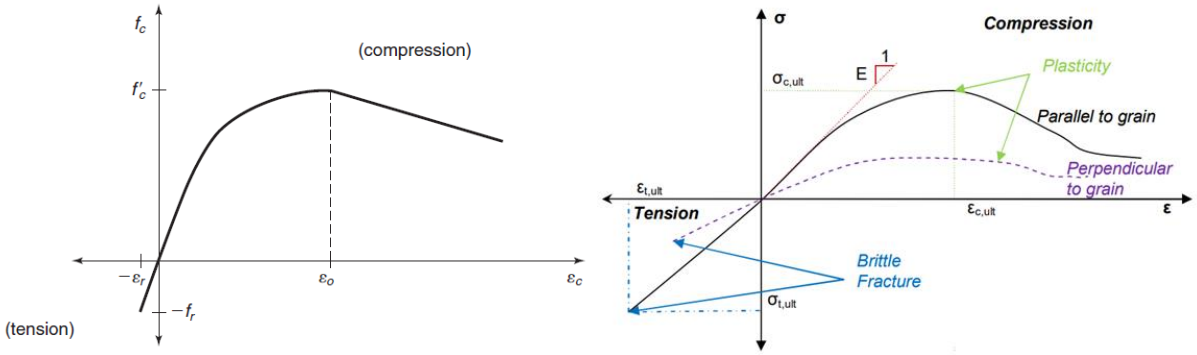

(a) (b)

Figure 67. Typical Stress-Strain Curve for: (a) Concrete [114] and (b) Timber [115]

As illustrated in Figure 68, key dimensions and factors include: d, the effective depth, or distance from the tension reinforcement to the extreme compressive fiber; c, the distance from the extreme compressive fiber to the neutral axis, representing the height of the compression zone; a, a proportion of c, indicating the depth of the equivalent rectangular stress block; β_1, a material-dependent factor that adjusts the stress block height based on material compressive strength; and f_c', the specified compressive strength of concrete (which will be taken as the compression strength of timber instead).

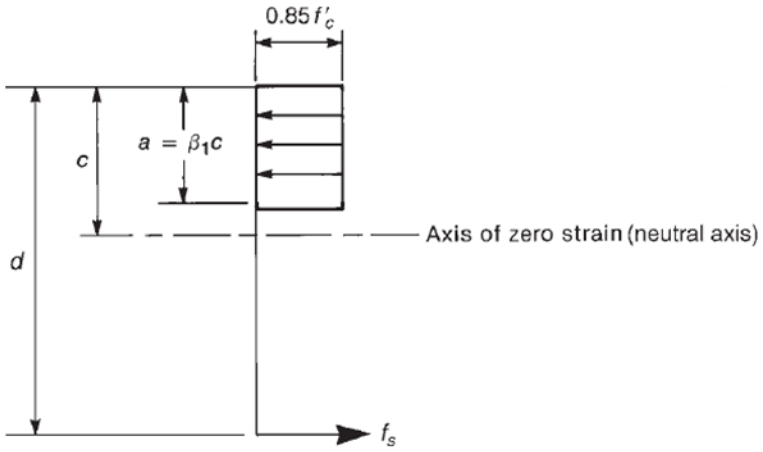

Figure 68. Whitney Stress Block [114]

For concrete with a compressive strength below or equal to 4,000 psi, a β_1 factor of 0.85 is used, simplifying the compression zone height to 85% of the neutral axis depth, following established concrete analysis practice under the Whitney Stress Block Theory. Since timber exhibits significantly lower compressive resistance perpendicular to the grain, the same β_1 value of 0.85 was conservatively applied here for consistency. Typical timber compression perpendicular to grain tests apply uniform loading across the specimen cross-section [90], thus the uniform stress distribution/magnitude may not correspond to the flexural stress distribution/magnitude in the

timber scupper and deck during the impact event. This discrepancy was noted because of the possibility of a more refined model which may be pursued in the future.

Given the potential underestimation of yield strength for ASTM A307A bolts at 45 ksi, as indicated by the National Design Specification (NDS) [116], the analysis instead adopted a bolt rupture strength of 60 ksi as more representative for f_y. By assuming that tensile (T) and compressive (C) forces are in equilibrium, Equations 1 through 5 are used to calculate the moment capacity.

$$C = T \quad \text{Eq. (1)}$$

$$0.85{F_{c\perp}}'ba = A_s f_y \quad \text{Eq. (2)}$$

$$a = \frac{A_s f_y}{0.85{F_{c\perp}}'b} \quad \text{Eq. (3)}$$

$$M_n = A_s f_y \left(d - \frac{a}{2}\right) \quad \text{Eq. (4)}$$

$$M_r = \varphi M_n, where\ \varphi = 1.0 \ \text{(for impact loading)} \quad \text{Eq. (5)}$$

where, ${F_{c\perp}}'$ is the compressive resistance of the timber perpendicular to grain, b is the scupper length, a is the equivalent stress block length, A_s is the area of the steel bolts used in the connection, f_y is the tensile strength of the bolts, M_n is the nominal moment capacity of the scupper and curb system, and d is the distance between the bolts and the extreme compressive fiber in the timber. An alternative model of the post yield moment was explored in Appendix B. Additional discussion of the compressive resistance perpendicular to grain can be found in Appendix E.

3.2.1.4 Post Stiffness

The quantification of post stiffness in bridge railing systems required an empirical approach. Direct analytical assessment, which would require detailed consideration of multiple components, like bolts, rails, and scupper blocks, is impractically complex given the marginal impact of post stiffness in BARRIER VII model. The post stiffness was derived from static component test data of bridge railing posts for a TL-1 curb bridge railing [5]. The resulting force-deflection relationship which best fit the data was determined to be trilinear, as shown in Figure 69 and Table 5 [10-11].

Table 5. TL-1 Post Load-Deflection Curve, Fitted from Data

Stiffness Estimate from Original West Virginia Rail Data [11]				
Deflection (in.)	Force (k)	Combined Stiffness (k/in.)	Post 1 (k/in.)	Post 2 (k/in.)
2.75	6.75	2.45	1.79	0.67
20	18.25	0.67	-	0.67

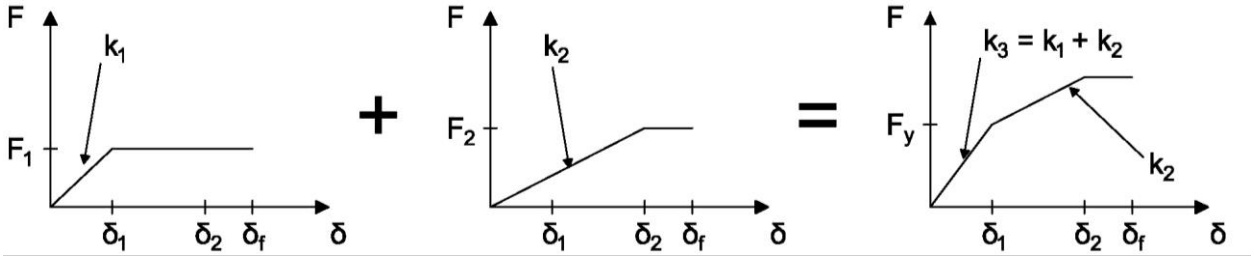

(a) (b) (c)

Figure 69. Bilinear Post 1 (a) and Bilinear Post 2 (b) with Linear Stiffness Used to Simulate Trilinear Post (c) Stiffness

A trilinear curve cannot be modeled for a single post within BARRIER VII. So, for BARRIER VII simulations, posts were modeled using overlapping entities with distinct stiffness characteristics to emulate trilinear stiffness behavior. This differentiation allows moments to bifurcate according to stiffness and deflection characteristics at yield. The force vs. deflection curve in Figure 69 illustrates this behavior, where F_1 and δ_1 denote the initial yielding force and corresponding deflection of the first post, respectively, with similar values for the subsequent post. The total yielding force, expressed as $F_1 + F_2$, corresponds to the moment per unit height, ensuring yield moments remain within the framework predicted by Equation 6:

$$M_{yield} = F_{yield}H = k_{post}\delta_{yield}H \qquad \text{Eq. (6)}$$

This empirical model captures the stiffness characteristics observed in testing of the TL-1 post configuration, but the load-deflection curve still required adjustment towards a TL-4 configuration. Adjustments were made to the post stiffness to account for variation in impact height, moment capacity, and the deck rotation. Without the vertical post, adjusting for these items envisions the TL-1 post system as being as tall as the TL-4 post system with steel bolts going all the way through 45 in. of timber railings, blocks, and bridge deck panels. The added vertical post made the TL-4 post system more rigid due to the lateral support behind the scupper blocks, but it was also more flexible due to the additional horizontal bolts used to hold the post configuration together.

The first adjustment dealt with the post heights, H, which affected the force, F, required to reach the yield moment, M_y, and the deflection, δ, corresponding to the angle of rotation at the bottom of the post. For equal rotation angles, θ, more deflection occurs in a taller system compared to a shorter system, as shown in Figure 70 and Equation 7. For an equal yield moment, a lower force occurs in a taller system compared to a shorter system, as shown in Figure 70 and Equation 8. The centroid of impact on the TL-1 system occurs at 18.375 in., and the centroid of impact on the TL-4 system occurs at 33.25 in. Subscripts "1" and "2" refer to the TL-1 and TL-4 systems, respectively. The results of adjusting the load-deflection deflections and forces in Table 5 for different heights is shown in Table 6.

$$\text{Tan}\,\theta = \frac{\delta_1}{H_1} = \frac{\delta_2}{H_2} \quad \rightarrow \quad \delta_2 = \delta_1 \frac{H_2}{H_1} \qquad \text{Eq. (7)}$$

$$M_y = F_1H_1 = F_2H_2 \quad \rightarrow \quad F_2 = F_1 \frac{H_1}{H_2} \qquad \text{Eq. (8)}$$

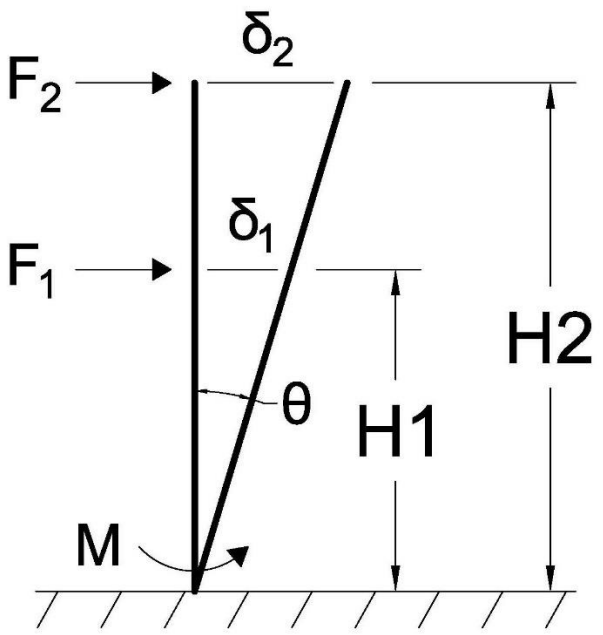

Figure 70. Force and Deflection Diagram for Height Adjustment

Table 6. TL-1 Post Load-Deflection Curve, TL-4 Post Height

Height Adjustment				
Deflection (in.)	Force (k)	Combined Stiffness (k/in.)	Post 1 (k/in.)	Post 2 (k/in.)
4.98	3.73	0.75	0.55	0.20
36.19	10.09	0.20	-	0.20

For the TL-4 system under development, the post moment capacity was expected to be higher than TL-1 Curb Rail system, so that it could handle higher impact demands. Hence, the force required to displace the post by 1 in. must increase proportionally to the ratio of the moment capacities. The relationship is shown in Equations 9 and 10. The flexural capacity of the TL-1 post, based on the estimate from the prior section, was 191.5 k-in., and the flexural capacity of the TL-4 post was 1,279.9 k-in. The results of adjusting the taller system based on the TL-1 curb rail system flexural capacity for the TL-4 post system is shown in Table 7.

$$F_1 H = M_{y_1} \; and \; F_2 H = M_{y_2} \quad \rightarrow \quad \frac{F_1}{M_{y_1}} = \frac{F_2}{M_{y_2}} \qquad \text{Eq. (9)}$$

$$\frac{F_1}{M_{y_1}} = \frac{F_2}{M_{y_2}} \quad \rightarrow \quad F_2 = F_1 \frac{M_{y_2}}{M_{y_1}} \qquad \text{Eq. (10)}$$

Table 7. TL-1 Post Load-Deflection Curve, TL-4 Post Height and Flexural Capacity

Moment Capacity Adjustment				
Deflection (in.)	Force (k)	Combined Stiffness (k/in.)	Post 1 (k/in.)	Post 2 (k/in.)
4.98	24.93	5.01	3.65	1.36
36.19	67.39	1.36	-	1.36

The deck was the last major factor differentiating the TL-1 curb rail posts from the TL-4 glulam upper and curb rail posts. The TL-1 curb railing static tests were conducted on a transverse nail-laminated timber bridge deck [5], while the TL-4 railing was being designed for use on a transverse glulam timber deck. The deck's flexural stiffness will modulate the degree to which the bridge post rotates and thus deflects; therefore, the rotational resistance of the deck will change the effective post stiffness. The deck's rotational stiffness was modeled as a Euler-Bernoulli cantilever beam, fixed to the girder with no rotation or displacement allowed.

The deck's rotational stiffness was characterized by three key parameters: moment of inertia (I); modulus of elasticity (E); and cantilever length (L), as shown in Equation 11. The cantilever length, L, was 50 in. for the transverse nail-laminated deck and 24 in. for the transverse glulam deck (from the centerline of the girder to the edge of the deck. The modulus of elasticity was 1500 ksi for SYP grade 1 lumber for the nail-laminated deck, and 1600 ksi for Combination 2 Douglas Fir-Larch glulam. The moment of inertia was calculated from an effective width centered on the post and the deck thickness, 5½ in. for the nail-laminated deck and 5⅛ in. for the glulam deck. The effective width had to be reduced for the nail laminated deck because the nails between wood boards had difficulty transferring load outwards (also noted in the literature review) and some discretion needed to be exercised to represent the moment of inertia contributing to stiffness. The width was estimated to be 72 in. (6 ft) for the nail-laminated deck and 96 in. (8 ft) for the glulam deck.

$$\theta = \frac{M_y L}{EI} \qquad \text{Eq. (11)}$$

Rigid assumptions are applied both to the post-deck connection and the post itself, isolating the effect of deck's rotational stiffness on the force-deflection behavior of the post from other deflection sources. Consequently, the post's deflection angle matches the rotational angle of the deck cantilever's end. Using small-angle approximations, this deflection angle can be correlated with the linear deflection along the scupper's height, as shown in Figure 71.

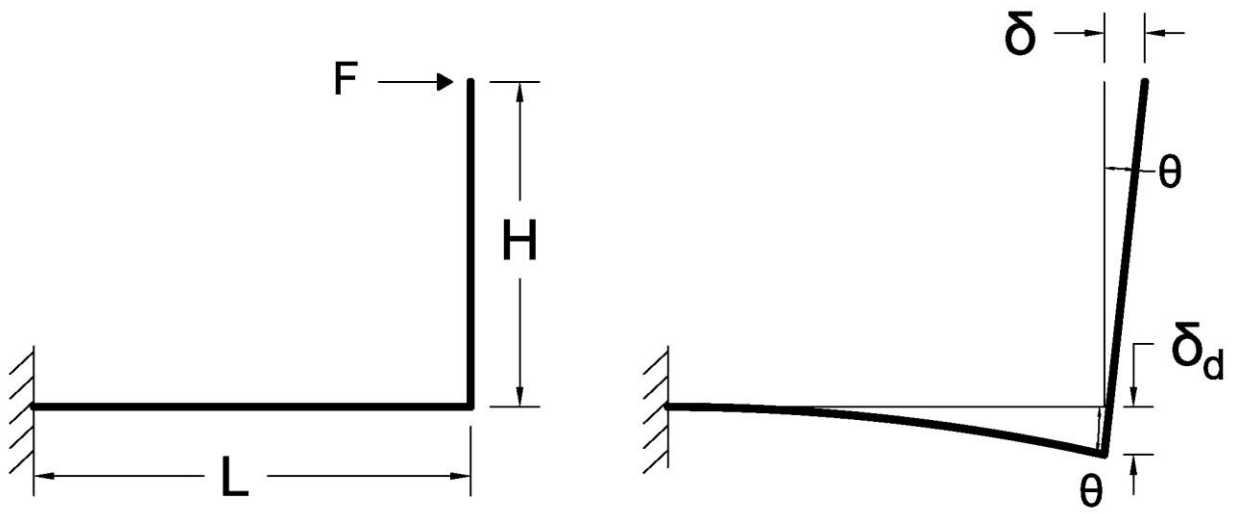

Figure 71. Timber Deck Overhang Deflection Diagram

The interaction of rotational stiffness with post deflection is laid out in Equations 12 through 14, where parameters characterizing the deck's rotational stiffness are applied to predict the ratio of post deflection on different decks. Based on the known deflections of a post on a nail-laminated deck, deflections for the same post on a glulam deck can be derived. Subscripts 1 and 2 denote the nail-laminated and glulam decks, respectively. The results of modifying the deck rotational stiffness for the deflections are shown in Table 8.

$$\text{Tan}\,\theta = \frac{\delta}{H} = \theta \qquad \text{Eq. (12)}$$

$$\delta = \frac{M_y HL}{EI} = \frac{FH^2L}{EI} \qquad \text{Eq. (13)}$$

$$\frac{\delta_1}{\frac{L_1}{E_1 I_1}} = \frac{\delta_2}{\frac{L_2}{E_2 I_2}} \quad \rightarrow \quad \delta_2 = \delta_1 \frac{L_2 E_1 I_1}{L_1 E_2 I_2} \qquad \text{Eq. (14)}$$

Further adjustments were made to force estimates [10-11] to describe the increased force required to cause identical deflection to a post on a glulam deck versus a nail-laminated deck. By equating the rotation angles produced by applied forces, the same framework that was previously established could compare the required forces for achieving equivalent deflections by varying stiffness properties, as expressed in Equation 15.

$$\theta_1 = \theta_2 \quad \rightarrow \quad \frac{F_1 HL_1}{E_1 I_1} = \frac{F_2 HL_2}{E_2 I_2} \quad \rightarrow \quad F_2 = F_1 \frac{L_1 E_2 I_2}{L_2 E_1 I_1} \qquad \text{Eq. (15)}$$

In Phase IIa, an adjustment to the deck rotational stiffness was applied to the deflections and forces for the calibrated system simulating crash test TRBR-1 and TRBR-2, but an adjustment to the forces was not applied to the MASH 2016 simulations for the 2270P and 10000S vehicle impacts. This oversight is shown by the shaded cells in Table 8, which resulted in an underestimation of the load-deflection behavior. The misrepresentation of the system's energy absorption capability at each post portrayed a lower-than-actual performance. Upon identifying this error, a recalibration of the critical impact point (CIP) investigation was deemed unnecessary

for further analysis, an enhanced post capacity to resist vehicle impacts would inherently improve the system's performance metrics.

Table 8. Surrogate TL-4 Post Load-Deflection Curve, as given from Phase IIa

Phase IIa System				
Deflection (in.)	Force (k)	Combined Stiffness (k/in.)	Post 1 (k/in.)	Post 2 (k/in.)
2.08	24.93	12.01	8.75	3.26
15.10	67.39	3.26	-	3.26

Another identified discrepancy involved the calculation of the yielding force within the report's published post force-deflection curves, shown in the shaded cells in Table 9. The yielding force shown for the final "capped" curve was inaccurately shown as 27.75 kips. This outcome was obtained by dividing the flexural capacity of an 8¾-in. x 10½-in. glulam post, 907.24 k-in., by the overall post configuration height, 33.25 in. This error presumably arose as an attempt to prevent forces higher than the post flexural capacity from being used in the model. But no independent force can be input as a variable for the BARRIER VII to cap the load-deflection curve. Instead, in BARRIER VII, the force creating the yield moment is the yielding force. The resulting yield force is based on the 1,279.9 k-in. divided by the impact height of 33.25 in. for 38.49 kips. The corresponding curve is shown in Table 10.

Table 9. Surrogate TL-4 Post Load-Deflection Curve, Phase IIa Report Yield Limit

Deck Rotational Stiffness Adjustment				
Deflection (in.)	Force (k)	Combined Stiffness (k/in.)	Post 1 (k/in.)	Post 2 (k/in.)
2.08	24.93	12.01	8.75	3.26
2.80	27.25	3.26	-	3.26
10.00	27.25	-	-	-

Table 10. Surrogate TL-4 Post Load-Deflection Curve, Phase IIa BARRIER VII Yield Limit

Deck Rotational Stiffness Adjustment				
Deflection (in.)	Force (k)	Combined Stiffness (k/in.)	Post 1 (k/in.)	Post 2 (k/in.)
2.08	24.93	12.01	8.75	3.26
6.24	38.49	3.26	-	3.26
10.00	38.49	-	-	-

The load-deflection curve with forces adjusted is shown in Table 11, and the load-deflection curve limited by the force causing yield moment on the post is shown in Table 12. The higher stiffness results in a load-deflection curve that is truncated by the yield moment of the post, so the post stiffness is bilinear instead of trilinear.

Table 11. Surrogate TL-4 Post Load-Deflection Curve, Forces Adjusted for Deck Rotational Stiffness

Deck Rotational Stiffness Adjustment				
Deflection (in.)	Force (k)	Combined Stiffness (k/in.)	Post 1 (k/in.)	Post 2 (k/in.)
2.08	59.76	28.79	20.97	7.82
15.10	161.56	7.82	-	7.82

Table 12. Surrogate TL-4 Post Load-Deflection Curve, Truncated by Yielding Force from Post Yield Moment

Cap Deflection for Final Estimate				
Deflection (in.)	Force (k)	Combined Stiffness (k/in.)	Post 1 (k/in.)	Post 2 (k/in.)
1.34	38.49	28.79	28.79	0.00
10.00	38.49	0.00	-	0.00

The impact of these miscalculations is visually demonstrated in Figure 72, which compares the initially reported final force-deflection curve, the force-deflection response as simulated by BARRIER VII, and a corrected force-deflection curve.

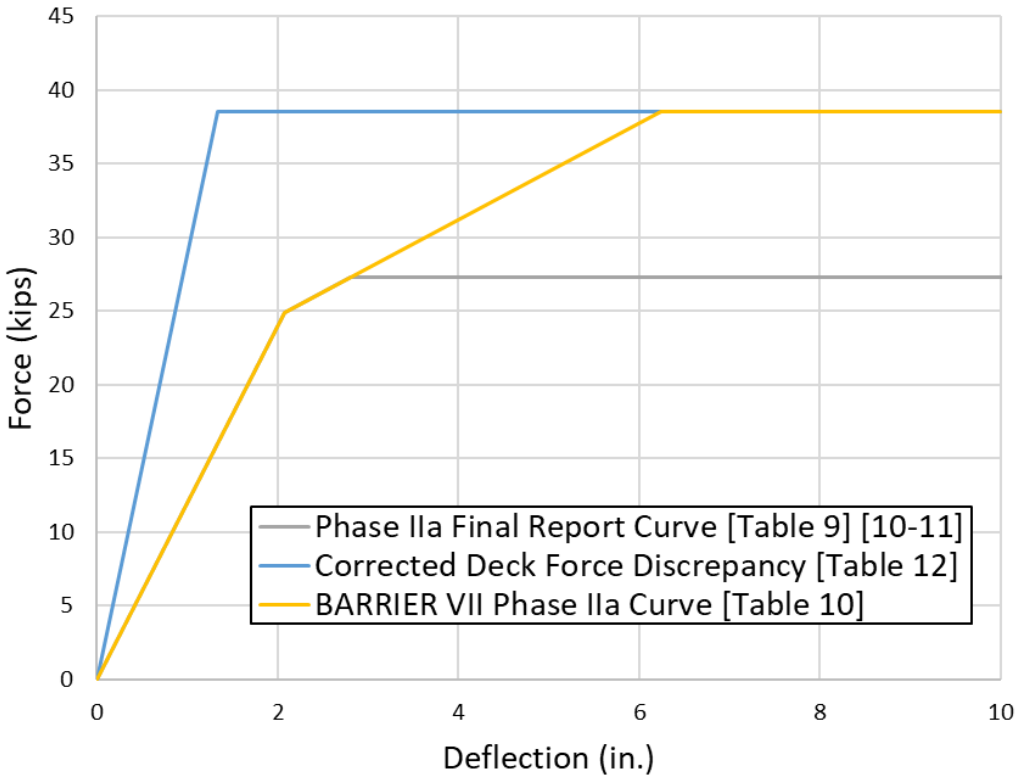

Figure 72. Surrogate TL-4 Post Load-Deflection Curves

3.2.2 Bridge Railing System – Design Updates

A review of the NDS bolt spacing requirements, previously unexamined in Phase IIa, revealed that the current bolt spacing did not meet the required specification [14]. The prescribed end distance from the center of the last bolt to the end of the scupper block or underlying deck panel was insufficient and needed lengthening from 54 in. to 58 in. to meet specified longitudinal load bolt spacing requirements. This adjustment led to modification of the post yield moment input parameter in BARRIER VII, as changing the scupper block length impacts the post-yield moment. The post-yield moment capacity was increased from 1,279.9 k-in. to 1,308.6 k-in., as calculated from Equations 1 through 5. Discussion of input variables can be found in Appendix E.

Bolt yield stresses given in materials certifications from previous component tests at MwRSF were examined, which showed bolt yield stress values of 50.4 ksi [7], 51.3 ksi [7], and 48.3 ksi [5]. The bolt strength was revised to utilize a lower estimate for ASTM A307A bolt suggested by NDS and others [14,117] so that the design was more conservative. The bolt diameter was increased from ¾ in. to ⅞ in. to address the reduced strength, producing a slight increase in the post yield moment, which increased from 1,308.6 kip-in to 1,327.7 kip-in. No further BARRIER VII calibration was necessary to demonstrate the performance of a stronger system configuration. The combined effects of these modifications on structural integrity and post stiffness are tabulated in Table 13 and illustrated in Figure 73.

Table 13. Surrogate TL-4 Post Load-Deflection Curve, Truncated by Updated Yielding Force from Post Yield Moment

Cap Deflection for Final Estimate				
Deflection (in.)	Force (k)	Combined Stiffness (k/in.)	Post 1 (k/in.)	Post 2 (k/in.)
1.34	39.93	29.86	29.86	0.00
10.00	39.93	0.00	-	0.00

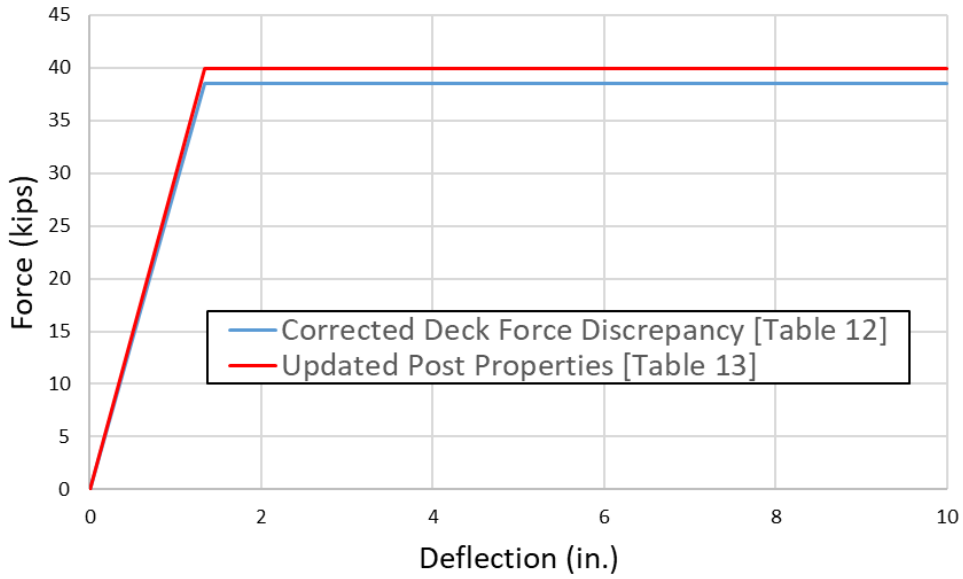

Figure 73. Adjusted Surrogate TL-4 Post Force-Deflection Curves for Flexural Capacity

3.2.3 Wet-Use Performance Analysis of Bridge Railing System

Given the high potential for frequent exposure to standing water in bridge scupper designs, a detailed assessment of the railing system's capacity under wet-use conditions was essential. This analysis incorporated a wet-use factor specific to the compressive resistance of glulam timber perpendicular to the grain, significantly influencing the compressive capacity of the scupper. Yield moments and post stiffnesses were recalculated to accurately reflect these conditions. If the post yield moment were calculated with 60 ksi bolt strength, as it was in Phase IIa, yet utilized ⅞-in. diameter bolts, the post yield moment would be 953.58 kip-in. By comparison, if 45 ksi bolt strength were used, a slightly higher post yield moment, 969.27 kip-in, was obtained. Obtaining a higher post yield moment from a lower bolt strength estimate indicated discrepancies within modeling assumptions. These discrepancies and their design implications are discussed in Appendix B. To enhance design robustness, the analysis proceeded with the more conservative, lower yield moment estimate, reinforcing system reliability amidst uncertainties inherent in wet-use conditions. The resulting force-deflection curve is shown in Table 14.

Table 14. Surrogate TL-4 Post Force-Deflection Curve, Updated Yield Force by New Yield Moment with High Moisture in Scupper

Cap Deflection for Final Estimate				
Deflection (in.)	Force (k)	Combined Stiffness (k/in.)	Post 1 (k/in.)	Post 2 (k/in.)
1.34	28.68	21.44	21.44	0.00
10.00	28.68	0.00	-	0.00

Further refinements to the stiffness assessment were made by standardizing the effective deck width used in the moment of inertia calculations. The effective deck width was an aspect lacking an objective basis for selecting 6 ft as opposed to 5 ft or 8 ft. If the glulam and nail-laminated deck had similar load distribution widths, this assumption conservatively estimated the post stiffness. Although this assumption removed an attempt to account for the difference in load distribution in a nail-laminated verses glulam deck, this assumption reduced the number of unknown assumptions used in the analysis and made the post stiffness estimate more conservative. This change modifies the deflections of the load-deflection curve by $b_{\text{glulam deck}}/b_{\text{nail laminated deck}}$, which is 8 ft/6 ft; and the forces of the load-deflection curve by $b_{\text{nail laminated deck}}/b_{\text{glulam deck}}$, which is 6 ft/8 ft. The load-deflection curve is tabulated in Table 15. Altogether, these changes were compiled into Figure 74, with "Wet-Use Equal Distr. Widths" showing the curve used for the wet-use CIP analysis.

Table 15. Surrogate TL-4 Post Force-Deflection Curve, Updated Yield Force by New Yield Moment with High Moisture in Scupper and Equalized Distribution Widths

Cap Deflection for Final Estimate				
Deflection (in.)	Force (k)	Combined Stiffness (k/in.)	Post 1 (k/in.)	Post 2 (k/in.)
2.38	28.68	12.06	12.06	0.00
10.00	28.68	0.00	-	0.00

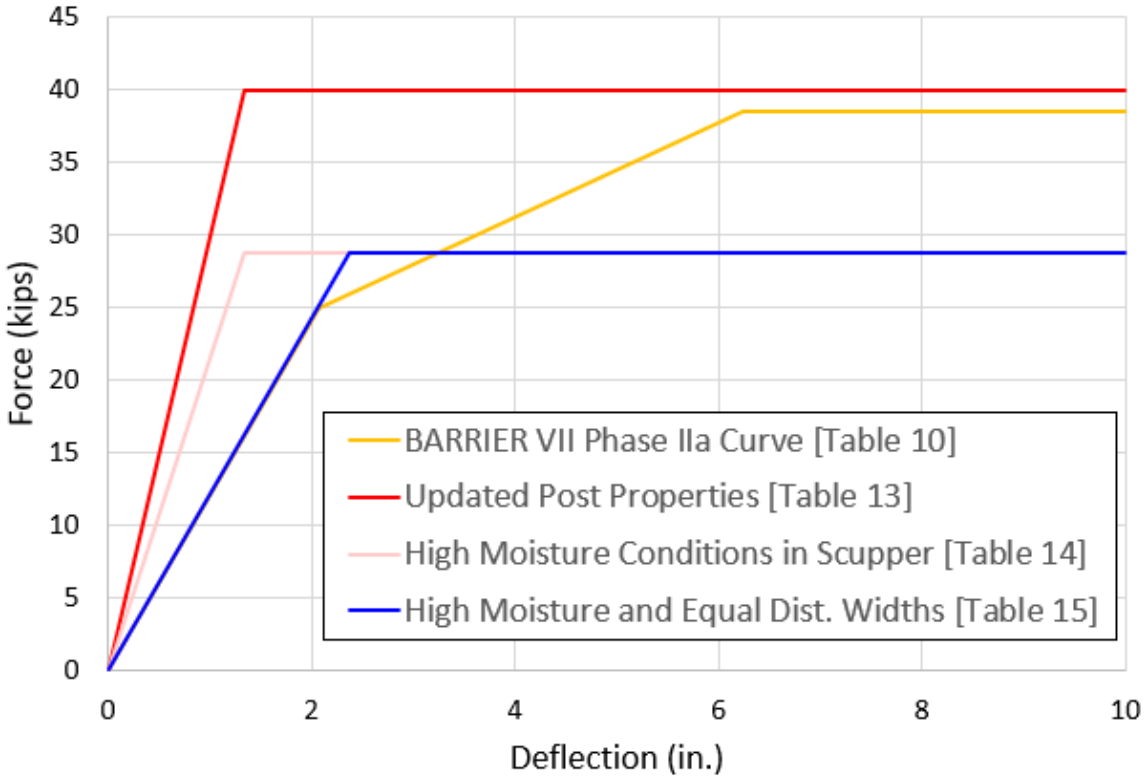

Figure 74. Adjusted Surrogate TL-4 Post Force-Deflection Curves for High Moisture and Equal Distribution Widths

The yellow BARRIER VII Phase IIa Curve represents the baseline model used at the conclusion of Phase IIa, prior to any adjustments for identified discrepancies. The red Updated Post Properties curve depicts Phase IIa results with discrepancies to stiffness resolved (the deck rotational stiffness is applied to both the deflections and the forces) and an updated post moment (modified with the relationship described by Equation 10). The pink High Moisture Conditions curve demonstrates Phase IIa with resolved discrepancies and adjustments for timber compression strength specific to wet-use conditions (Equation 10). Finally, the blue High Moisture Equal Dist. Widths curve combines all adjustments, including resolved discrepancies, standardized deck width distribution, and modified timber compression strength for High Moisture content in scupper (Equations 14 and 15).

In addition to the post stiffness, and post yield moment, the post weight was also updated. The original estimation of post weight did not include the scupper weight, which significantly increased the overall weight. The changes to the post stiffness, yield moment, and weight are highlighted in red in Table 16. The post yield moment over the B-axis, the stiffness in the A-axis direction, and both shear forces have been taken as the sum of the two-post configuration for this simulation; since, only a single post is modeled. The order of "B" and "A" axes are flipped for the yield moment, because the rotation about the "A" axis is what engages the "B" orientation shear and deflection limits, likewise for the "B" axis of rotation. Figure 75 shows the BARRIER VII model used to simulate the system given the need to adjust to a single-post set-up.

Table 16. Bridge Post Element Properties for BARRIER VII High-Moisture Conditions

Member Type	Member Size	Upper Rail Node Height (in.)	Curb Rail Node Height (in.)	Stiffness k_A & k_B (k/in.)	Weight (lb)	Nominal Yield Moment (k-in.)	Failure Shear Force (k)	Failure Deflection (in.)
Bridge Post	8¾"x10½" (glulam)	33.25	14.625	A-axis: 18.76 B-axis: 12.06	231.3	B-axis: 833.1 A-axis: 953.3	A-axis: 60.0 B-Axis 60.0	A-axis: 4.0 B-axis: 10.0

The BARRIER VII barrier model developed in Phase IIa was refined to investigate bridge railing systems under wet-use conditions, using a single-post model rather than a two-post configuration. This decision was informed by the observation that the yielding force threshold truncated the initial combined stiffness curve so that there was no second curve. For a conservative method, the lower stiffness curve derived from assuming equal deck distribution width was used to assess post stiffness under wet-use conditions. This model was used in a critical impact point (CIP) analysis. The analysis spanned a targeted range between posts 4 and 7, with impacts at 1-ft increments, and included a reduction in beam element lengths for enhanced precision at the locations of interest. Key performance metrics, such as maximum railing deflection, tensile force, and the count of yielded posts and rail elements, were assessed.

To optimize the investigation and prevent redundant analysis, the 10000S single-unit truck was identified as the critical vehicle for evaluating wet-use condition, as it generates the highest impact severity, 154.4 k-in. compared to 115.4 k-in. for the 2270P pickup truck. Comparative analyses from Phase IIa data also indicated that impacts involving the 2270P pickup truck resulted in less severe conditions for the bridge railing. Consequently, the wet-use evaluations were exclusively conducted with the 10000S SUT impacts. In contrast to previous CIP analyses, this analysis did not explicitly quantify lateral and longitudinal forces exerted by the vehicle on the railing, as these parameters indirectly reflect system performance. Instead, direct performance indicators, such as deflections, yielded members, and internal forces provided a more immediate measure of the railing's impact resilience.

Tables 17 and 18 present simulation results comparing railing performance in wet and dry conditions. Notably, maximum deflection increased from 8.05 in. to 9.18 in., with a corresponding shift in the deflection location. The maximum tensile force experienced by the railing also increased, from 76.26 kips to 84.93 kips, occurring 3 ft beyond post no. 6, consistent with previous CIP findings. Furthermore, the analysis recorded an increase in the number of yielded posts and upper rail elements. No post failures occurred due to shear or deflection limit being exceeded. The number of yielded upper rail elements increased from 13 to 17, with a consistent distribution across simulations. Meanwhile, the number of yielded curb rail elements remained unchanged across all simulations, each reflecting some degree of curb rail yielding. With respect to the vehicle trajectory, the differences between the simulations were negligible. Based on this assessment, the critical impact location was reaffirmed to be 3 ft downstream from post no. 6 or 5 ft downstream from post no. 7.

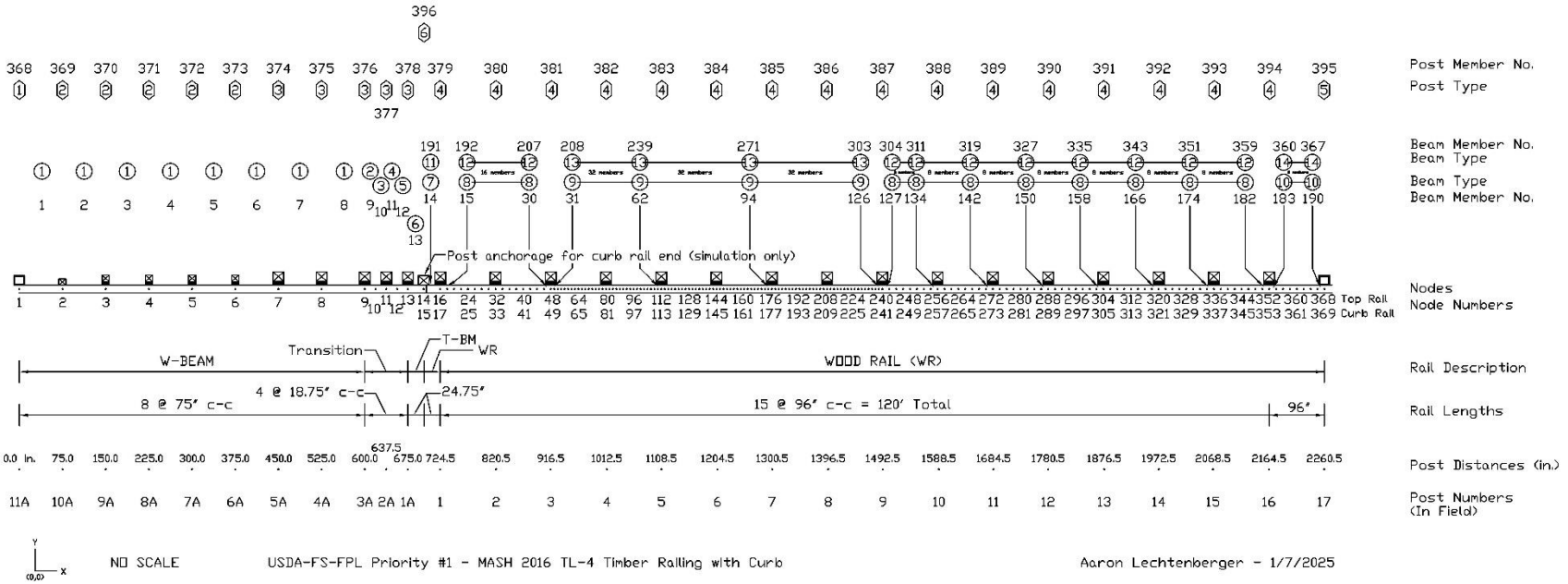

Figure 75. BARRIER VII Layout of System Under High-Moisture Conditions

Table 17. Critical Impact Point Investigation Comparison Metrics under Dry-Use and Wet-Use Conditions

Impact Location	Maximum Deflection Upper Rail Node (in.)		Maximum Upper Rail Element Tension (kip)		No. of Yielded Posts		No. of Upper Rail Elements Yielded		No. of Curb Rail Elements Yielded	
	Wet	Dry	Wet	Dry	Wet	Dry	Wet	Dry	Wet	Dry
Post 4	9.04	7.56	71.13	59.28	3	1	16	13	2	2
Post 4 + 1 ft	9.07	7.90	74.77	67.06	4	1	14	13	2	2
Post 4 + 2 ft	9.14	8.05	80.48	73.98	4	2	13	9	2	2
Post 4 + 3 ft	9.18	7.94	83.17	75.04	4	2	10	10	2	0
Post 4 + 4 ft	9.17	7.77	81.68	73.12	3	2	10	9	2	0
Post 4 + 5 ft	9.07	7.61	77.17	68.54	3	1	10	8	2	2
Post 4 + 6 ft	8.93	7.46	72.52	63.32	3	1	15	12	2	2
Post 4 + 7 ft	8.85	7.30	68.45	58.07	3	1	17	13	2	2
Post 5	8.96	7.54	71.46	59.49	3	1	15	12	2	2
Post 5 + 1 ft	9.07	7.89	75.77	67.61	4	1	14	13	2	2
Post 5 + 2 ft	9.13	8.05	81.58	74.83	4	2	13	9	2	2
Post 5 + 3 ft	9.18	7.92	84.29	75.58	4	2	10	10	2	0
Post 5 + 4 ft	9.11	7.76	82.28	73.75	3	2	10	9	2	0
Post 5 + 5 ft	9.07	7.61	78.19	69.09	3	1	10	8	2	2
Post 5 + 6 ft	8.92	7.47	73.45	64.07	3	1	15	13	2	2
Post 5 + 7 ft	8.84	7.30	69.64	58.53	3	1	16	13	2	2
Post 6	9.04	7.54	73.17	60.04	3	1	16	12	2	2
Post 6 + 1 ft	9.06	7.89	76.67	68.18	4	1	14	13	2	2
Post 6 + 2 ft	9.12	8.05	82.61	75.50	4	2	13	9	2	2
Post 6 + 3 ft	9.14	7.92	84.93	76.26	4	2	10	10	2	0
Post 6 + 4 ft	9.14	7.76	83.20	74.27	3	2	9	9	2	0
Post 6 + 5 ft	9.06	7.61	79.06	69.50	3	1	9	8	2	2
Post 6 + 6 ft	8.95	7.47	74.27	64.43	3	1	15	13	2	2
Post 6 + 7 ft	8.84	7.29	70.42	58.90	3	1	16	13	2	2
Post 7	8.99	7.54	73.44	60.51	3	1	14	13	2	2

Table 18. Vehicle Trajectory Comparison Between Wet and Dry CIP Investigation Results

Impact Location	Parallel Conditions				Exit Conditions					
	Time (s)		Speed (mph)		Time (s)		Speed (mph)		Angle (deg.)	
	Wet	Dry	Wet	Dry	Wet	Dry	Wet	Dry	Wet	Dry
Post 4	0.355	0.349	44.625	44.638	0.696	0.683	41.616	41.871	11.568	11.971
Post 4 + 1 ft	0.355	0.346	44.612	44.575	0.694	0.681	41.641	41.814	11.627	12.502
Post 4 + 2 ft	0.354	0.346	44.674	44.553	0.693	0.680	41.677	41.806	11.583	12.472
Post 4 + 3 ft	0.355	0.347	44.751	44.605	0.695	0.681	41.726	41.850	11.280	12.163
Post 4 + 4 ft	0.357	0.349	44.775	44.631	0.697	0.682	41.724	41.886	11.015	11.854
Post 4 + 5 ft	0.357	0.350	44.782	44.646	0.698	0.683	41.718	41.907	10.969	11.637
Post 4 + 6 ft	0.357	0.352	44.772	44.746	0.698	0.683	41.691	41.940	10.986	11.234
Post 4 + 7 ft	0.356	0.351	44.694	44.704	0.697	0.683	41.646	41.914	11.327	11.481
Post 5	0.355	0.349	44.648	44.642	0.696	0.683	41.622	41.874	11.515	11.957
Post 5 + 1 ft	0.354	0.346	44.615	44.580	0.694	0.681	41.642	41.819	11.631	12.481
Post 5 + 2 ft	0.354	0.346	44.675	44.553	0.693	0.680	41.678	41.807	11.583	12.478
Post 5 + 3 ft	0.355	0.347	44.740	44.606	0.695	0.681	41.725	41.851	11.308	12.162
Post 5 + 4 ft	0.357	0.349	44.780	44.636	0.697	0.682	41.726	41.887	10.992	11.847
Post 5 + 5 ft	0.357	0.350	44.780	44.681	0.698	0.682	41.719	41.908	10.979	11.625
Post 5 + 6 ft	0.357	0.352	44.775	44.745	0.698	0.683	41.694	41.941	10.984	11.252
Post 5 + 7 ft	0.356	0.351	44.694	44.704	0.697	0.683	41.646	41.915	11.323	11.482
Post 6	0.355	0.349	44.628	44.641	0.696	0.683	41.617	41.874	11.577	11.963
Post 6 + 1 ft	0.354	0.346	44.618	44.589	0.694	0.681	41.642	41.826	11.634	12.447
Post 6 + 2 ft	0.354	0.346	44.681	44.553	0.693	0.680	41.682	41.959	11.567	12.487
Post 6 + 3 ft	0.355	0.347	44.741	44.605	0.695	0.681	41.729	41.852	11.309	12.180
Post 6 + 4 ft	0.357	0.349	44.788	44.633	0.697	0.682	41.730	41.887	10.983	11.858
Post 6 + 5 ft	0.357	0.351	44.778	44.648	0.698	0.683	41.720	41.909	10.999	11.629
Post 6 + 6 ft	0.357	0.352	44.776	44.750	0.698	0.683	41.691	41.942	10.991	11.245
Post 6 + 7 ft	0.356	0.351	44.690	44.702	0.697	0.683	41.647	41.914	11.361	11.496
Post 7	0.355	0.349	44.644	44.643	0.696	0.682	41.625	41.874	11.548	11.951

3.3 Railing Connection Design

3.3.1 Design Cases Load Demand

In Phase IIa, the primary objective was to assess the bridge railing's capacity to withstand MASH 2016 impact conditions, as predicted by the BARRIER VII simulation. Given the satisfactory performance of the timber bridge railing system in BARRIER VII, the primary task following the Phase IIa research work was to determine the maximum loads transmitted through the system components. Since BARRIER VII does not account for vertical loads, additional analyses were required to confirm that the connections could withstand maximum load induced by vertical forces. Vertical load assessments followed AASHTO LRFD Bridge Design Specifications Chapter 13 Appendix A Section 4, which outlines design cases for analyzing bridge deck overhangs. No service load considerations were evaluated for this design.

Three loading scenarios for bridge deck overhangs are defined in the AASHTO guidelines [15]. Loads to deck overhangs come from bridge railings, so these cases were used to guide estimates of load demands to the bridge railing. Design Case 1 addresses lateral and longitudinal loads from vehicle impact and railing weight under Extreme Event Load Combination II. Longitudinal refers to the axial direction of the bridge railing, and lateral refers to the transverse direction of the bridge railing (off the bridge). BARRIER VII addresses these load directions, and demand estimates were found from analysis of program results. Design Case 2 addresses vertical vehicle impact loads and railing weight under Extreme Event Load Combination II. Vertical impact loads were calculated from preliminary MwRSF revisions to AASHTO Chapter 13 Table A13.2-1 based on MASH 2016 vehicle impact conditions [118]. Design Case 3 addresses the Strength I Load Combination limit state, but was not examined because transverse bridge deck designs typically avoid placing wheel loads on the overhang [32, 62]. In addition, longitudinal decks do not have an overhang.

Table 19. MASH Design Parameters for Bridge Railings [118]

Design Parameter	Railing Test Level 4
Minimum Barrier Height, H (in.)	36
Design lateral impact load, F_t (kips)	*Eqn. 16*
Design vertical impact load F_v (kips)	*Eqn. 17*
Design longitudinal impact load, F_l (kips)	*Eqn. 18*
Height of Lateral load application, H_e (in.)	*Eqn. 19*
Longitudinal Distribution of lateral and longitudinal loads, L_t or L_l (ft)	*Eqn. 20*
Longitudinal distribution over vertical loads, L_v (ft)	18

$$F_{t,TL-4} = \begin{cases} 2H - 4 \text{ kips} & 36 \text{ in.} \leq H \leq 42 \text{ in.} \\ 0.15H + 74 \text{ kips} & 42 \text{ in.} < H \end{cases} \quad \text{Eq. (16)}$$

$$F_{v,TL-4} = \begin{cases} 101 - 1.75H \text{ kips} & 36 \text{ in.} \leq H \leq 45 \text{ in.} \\ 32.7 - 0.23H \text{ kips} & 45 \text{ in.} < H \end{cases} \quad \text{Eq. (17)}$$

$$F_{l,TL-4} = \begin{cases} 0.867H - 9.6 \text{ kips} & 36 \text{ in.} \leq H \leq 42 \text{ in.} \\ 0.007H + 26.5 \text{ kips} & 42 \text{ in.} < H \end{cases} \quad \text{Eq. (18)}$$

$$H_{e,TL-4} = \begin{cases} 1.33H - 27 \text{ in.} & 36 \text{ in.} \leq H \leq 40 \text{ in.} \\ 0.15H + 24.3 \text{ in.} & 40 \text{ in.} < H \end{cases} \quad \text{Eq. (19)}$$

$$L_{t,TL-4} = \begin{cases} 4 \text{ ft} & 36 \text{ in.} \leq H < 39 \text{ in.} \\ 5 \text{ ft} & 39 \text{ in.} \leq H \leq 42 \text{ in.} \\ 0.09H + 1.2 \text{ ft} & 42 \text{ in.} < H \end{cases} \quad \text{Eq. (20)}$$

The lateral load demand for a height of 38 in. was 72 kips, while the Phase IIa CIP analysis found 82 kips from the SUT simulated crash test. In BARRIER VII, the lateral and longitudinal loads are distributed through the bridge railing using a stiffness matrix. When a post reaches its yield moment, it continues deflecting backward at the yielding load, limiting the maximum load on the post to the yield moment's force. In Phase IIa analyses of the dry system with the 10000S SUT, at least one post was always yielding. For a post yield moment of 1,327.8 k-in. (see section 3.2.2) and an impact height of 33.25 in., the maximum lateral load was 39.93 kips.

The longitudinal load demand was 23.35 kips for a height of 36 in., distributed over 4 ft. The exact transfer to a specific post versus axial transfer along the upper railing was unclear. BARRIER VII handled this question with its stiffness matrix, which included longitudinal stiffness in the posts and upper railing. The maximum longitudinal load was evaluated by checking the drop in upper railing axial loads across a post location to see how much is transferred to the post as opposed to the upper rail. The maximum drop in loads across a post location was found to be 20.02 kips for both the Phase IIa dry analysis and Phase IIb wet analysis.

The vertical load demand from Equation 17 was 38 kips for a height, H, of 38 in. The vertical load would be distributed over 18 ft according to Table 19. The resulting load on a single post was 16.9 kips, when posts are spaced at 8 ft. The railing weight was also included as a vertical load for Design Cases 1 and 2.

3.3.2 Load Demands to Connections

From the post, the load demands were distributed to the connections. There were six connections and components which required design: (1) the bolts holding the curb railing to the bridge deck (Jared Duren had already started designing these components in Phase IIa); (2) the bolts holding the upper railing to the vertical post; (3) the vertical post; (4) the horizontal bolt holding the post to the curb railing; (5) the upper rail splice; and (6) the curb rail splice. The locations of the connections are shown in Figure 76.

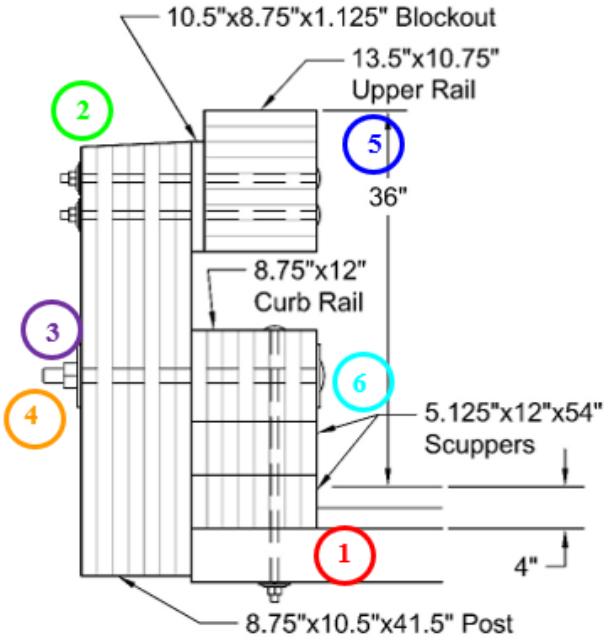

Figure 76. Phase IIa Post Configuration Connections to Design

3.3.2.1 Curb Railing to Bridge Deck

The curb rail to deck connection only experienced lateral and longitudinal loads, as Design Case 2 would not affect the vertical bolts. The maximum load at the top of the post was limited by the post yield moment, $M_{y\ post}$, calculated in section 3.2.1.3. The lateral load demand was 39.93 kips, while the longitudinal shear load of 20.02 kips was assumed to transfer directly to the post base like a cantilever loaded at the top. Both loads were applied at the midpoint of the upper rail, 33.25 in. above the deck. The lateral load compressed the post near the bottom, C_{post}, and tensioned horizontal bolt, $T_{h\ bolt}$, as shown in Figure 77. The lateral shear load at the post base was calculated by dividing the yield moment (1,327.8 k-in.) by the height to the horizontal bolt (14.625 in.), for 90.78 kips. The compression from the post was 50.85 kips, which reduced the lateral shear load to 39.93 kips at the deck level when added to the 90.78-kip lateral shear load. The lateral shear load remained 90.78 kips in the vertical bolts and scupper blocks above the deck.

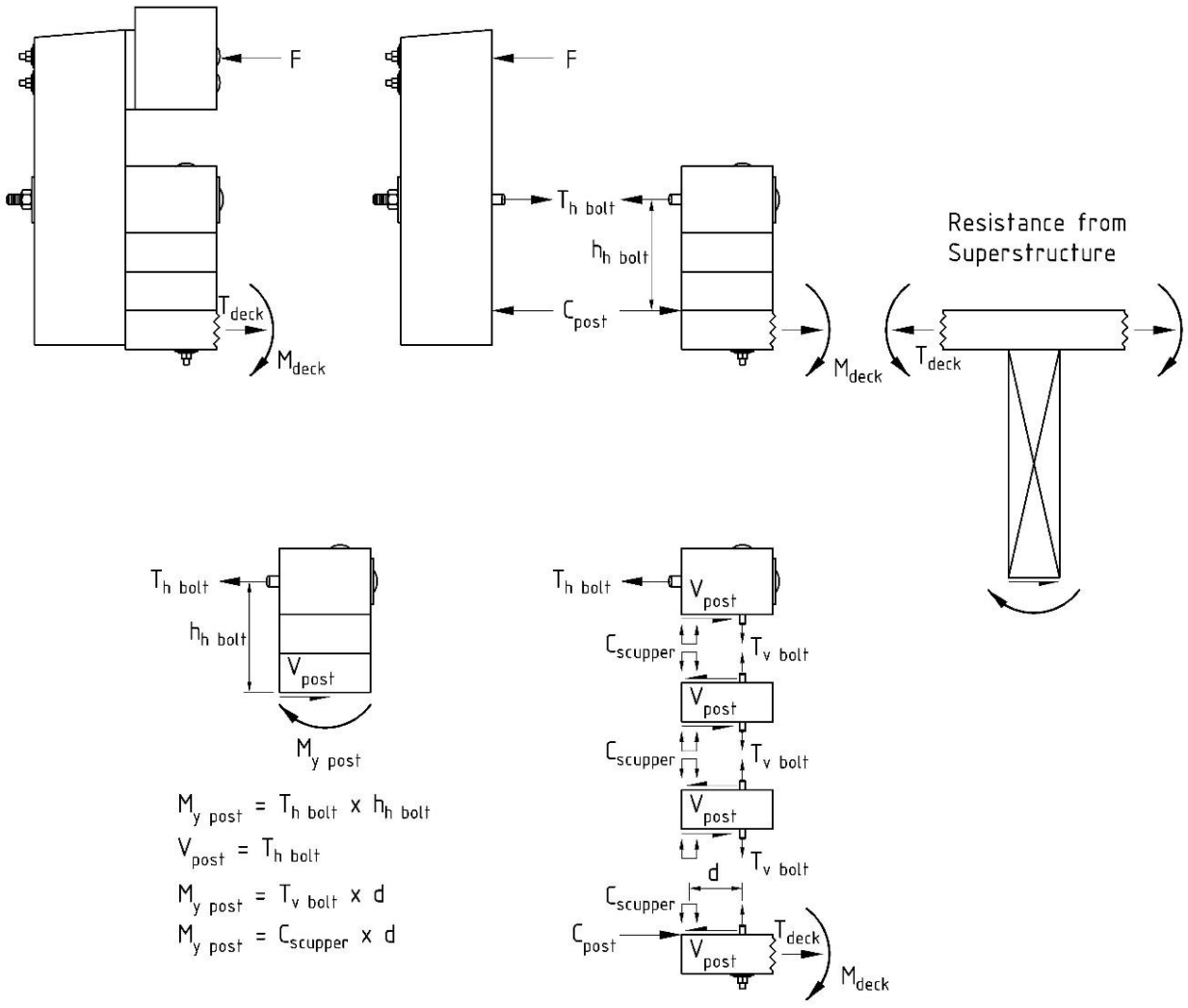

Figure 77. Post Configuration Loading Diagram

3.3.2.2 Upper Railing to Vertical Post

The lateral loads from Design Case 1 will not stress the bolts, but the longitudinal load will place the horizontal bolt in shear. The longitudinal load demand on this connection was 20.02 kips from the results from the BARRIER VII CIP analysis. The vertical load from Design Case 2 placed the bolt in shear (V_{bolt}), but due to the offset of the vertical load from the upper railing vertical support, tension also developed in the bolt (T_{bolt}). As shown in Figure 78, the vertical force was applied at the center of the upper railing.

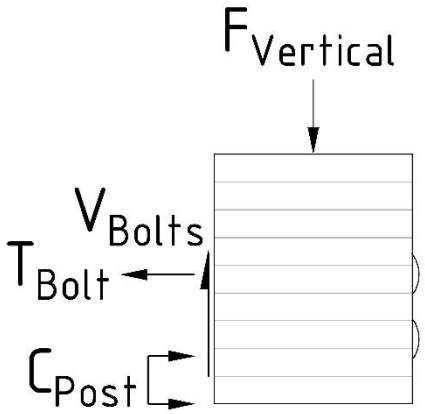

Figure 78. Free-Body-Diagram of Upper Railing Connection to Post Under Vertical Load

The tensile demand for the upper railing connection was calculated based on the moment demand, using an approach analogous to the post yield moment calculation. The moment demand was derived from the vertical design load and the assumed load centroid. The depth of compression was calculated from the moment demand, enabling the determination of the compressive and the tensile forces in the bolt.

The key variables include *a*, the depth in compression; f_c', the estimated timber perpendicular to grain compressive resistance; *b*, the width of the post; M_u, the calculated moment demand; and *d*, the depth from the bottom of the rail to the centerline of the bolt. Equations 21 through 24 were used for the analysis:

$$M_u = T_u\left(d - \frac{a}{2}\right) \quad \text{Eq. (21)}$$

$$T_u = C = 0.85 f_c' a b \quad \text{Eq. (22)}$$

$$a^2 - 2da + \frac{2M_u}{0.85 f_c' b} = 0 \quad \text{Eq. (23)}$$

$$a = \frac{2d - \sqrt{(-2d)^2 - 4(1)\left(\frac{2M_u}{0.85 f_c' b}\right)}}{2(1)} \quad \text{Eq. (24)}$$

The estimated perpendicular to grain compressive resistance for Douglas Fir-Larch, f_c', was 1,176 psi (see Appendix E for discussion of this estimate). The width of the post was 8.75 in. and the depth from the bottom of the railing to the uppermost supporting horizontal bolt was 7 in. The calculated moment demand, M_u, was 92.26 k-in., based on the vertical demand, 17.17 kips (design load and railing weight), and the distance from the vertical support to the load application point, 5.375 in. (half the width of the upper railing). The calculated compressive depth was 1.72 in., and the calculated tension in the bolt was 15.02 kips.

3.3.2.3 Vertical Post

Design Case 1 lateral and longitudinal loads placed the post in shear and flexure. Design Case 2 vertical loading did not place the post in significant shear or flexure, and the loads contributing to horizontal bolt shear, ~17-18 kips, were less severe than the longitudinal load, 20.02 kips. The BARRIER VII model distributed Design Case 1 loading via the railing stiffness matrix. The post's maximum longitudinal shear load occurred simultaneous to yielding. Therefore, combined lateral and longitudinal loads required analysis. These forces were resolved into a single shear load using the Pythagorean Theorem, illustrated in Figure 79.

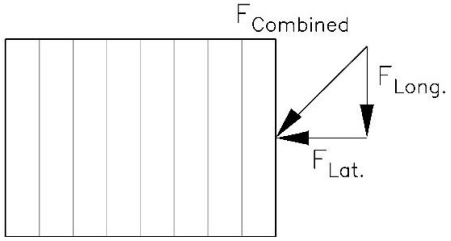

Figure 79. Post Design Case 1 Free-Body-Diagram Combined Shear

When the post experiences longitudinal load at the top, it rotates, as depicted in Figure 80. Adjacent posts were considered the primary resistance to this rotation. Each lag bolt, as drawn in Figure 80, resists rotation. However, it was not included in the model, because it was intended to prevent twist during assembly, not crash events.

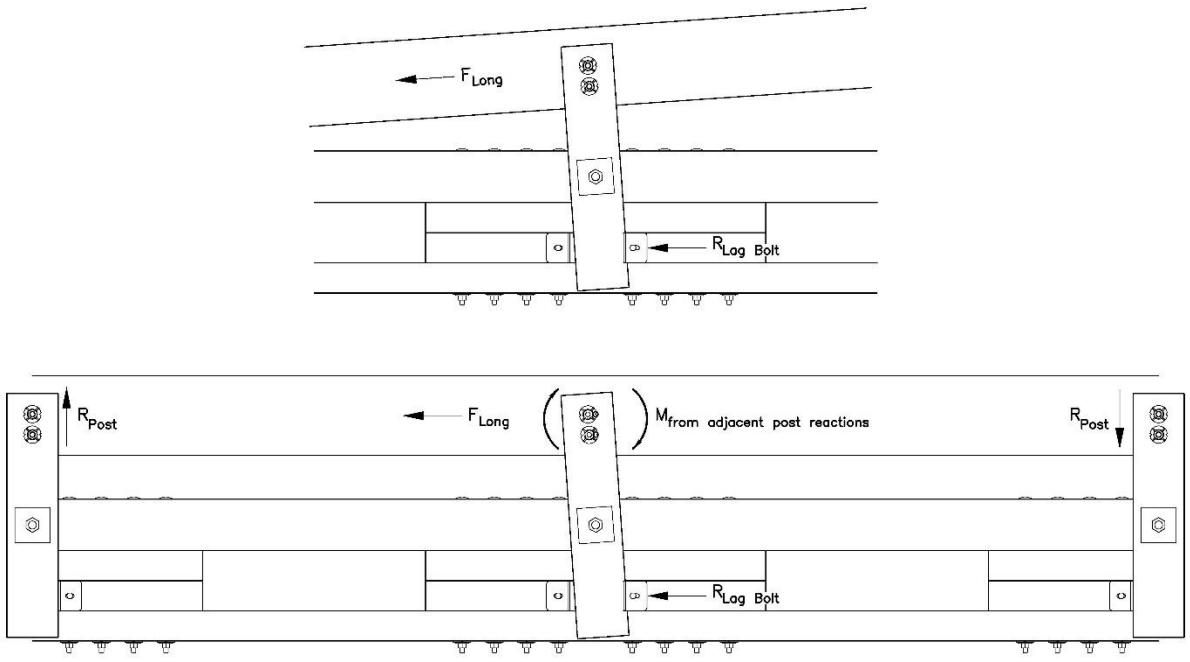

Figure 80. Resistance to Twist without Adjacent Posts (top) and Resistance to Twist with Adjacent Posts (bottom)

The horizontal bolt connecting the post to the curb rail was modeled as a pinned connection, as illustrated in Figure 81. The longitudinal shear load was modeled as linear between the upper rail and the curb rail. The flexural resistance provided by the adjacent posts connected to the upper rail was represented by an end moment at the upper rail connection.

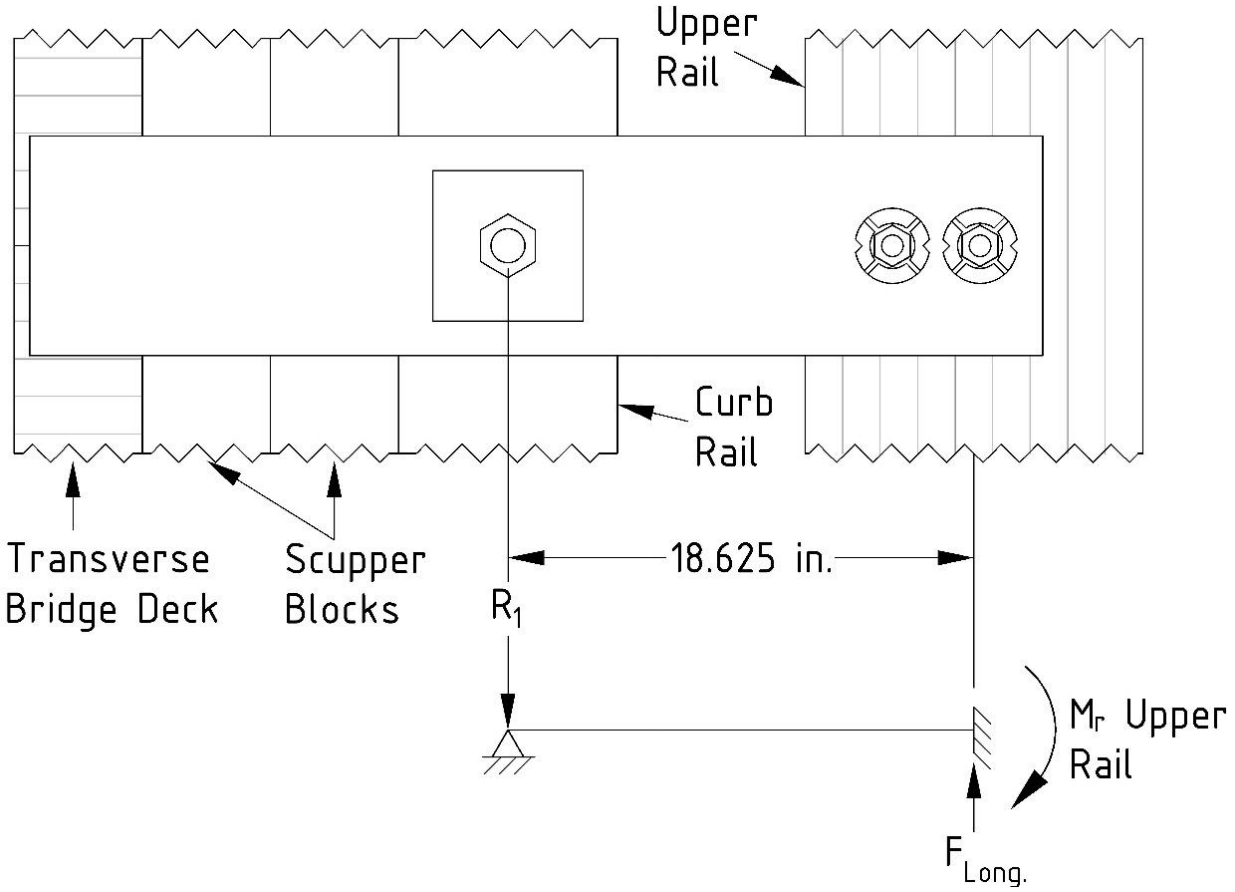

Figure 81. Free-Body-Diagram for Post Flexure from Longitudinal Loads

Lateral loads caused post flexure. Figure 82 illustrates the free-body diagram of the post, depicting the load application assumptions for the lateral load causing flexure. The support locations depicted in Figure 82 were chosen to align with BARRIER VII. Thus, ensuring that the load demands from BARRIER VII correspond to actual locations. The bottom of the post, where the compression resultant acts at the top of the deck, was represented by R_1, which corresponds to the location of B-shear in BARRIER VII (refer to Section 3.2.1.1). Although post compression occurs at the bottom of the post, BARRIER VII cannot model this behavior; hence, the need for some simplification of the analysis model. It was assumed that the compressive force can be represented by an equivalent force closer to the horizontal bolt of the curb rail. The variable w was the washer plate width. R_2 represented the top of the post in BARRIER VII, which was the center of the upper rail.

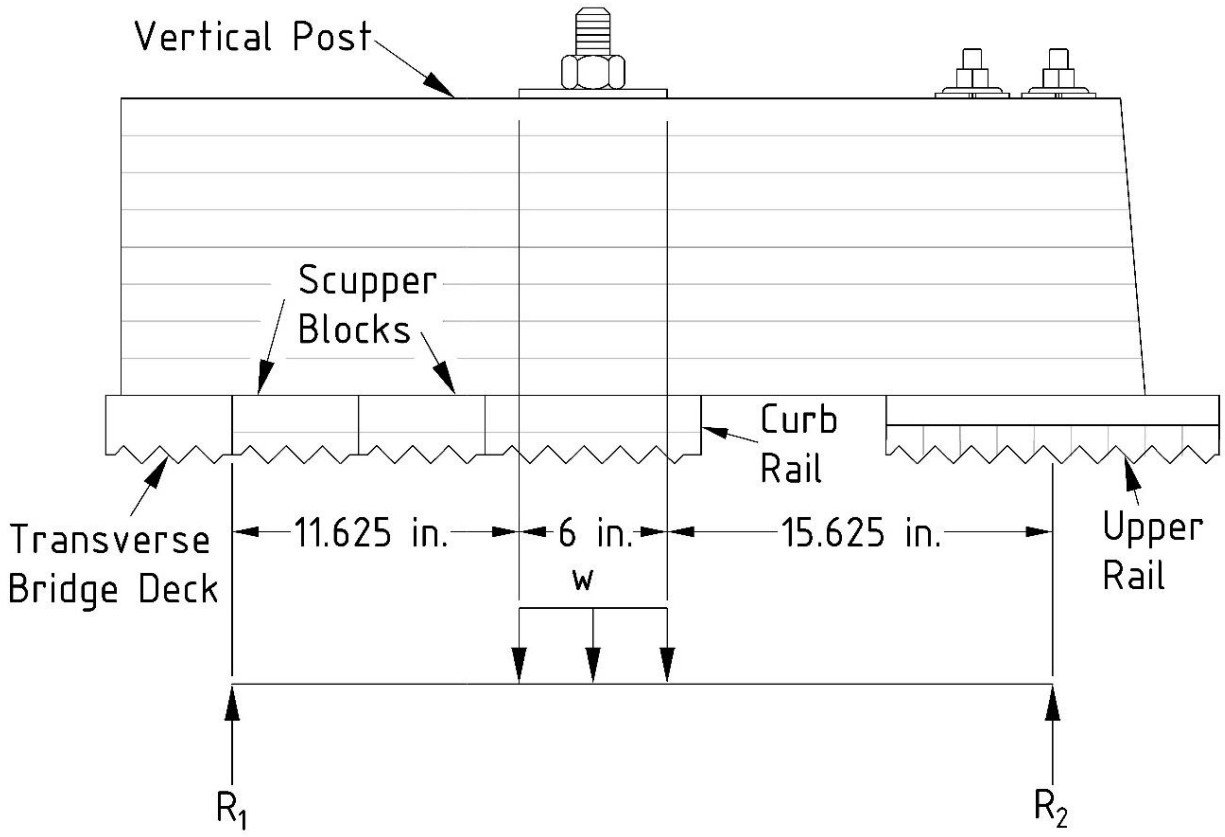

Figure 82. Free-Body-Diagram for Post Flexure from Lateral Loads

The shear and flexural loads were plotted for the length of the post because it was not clear where the load may exceed the capacity, due to the bolt hole and the combination of lateral and longitudinal loads. The shear longitudinal and lateral load demands on the post are shown in Figures 83 and 84, respectively. The combined shear demand is shown in Figure 85. The lateral load flexure and longitudinal load on the post are shown in Figures 86 and 87, respectively. For more detail and information on the equations used to develop the shear and flexural demand graphs, see Appendix H.

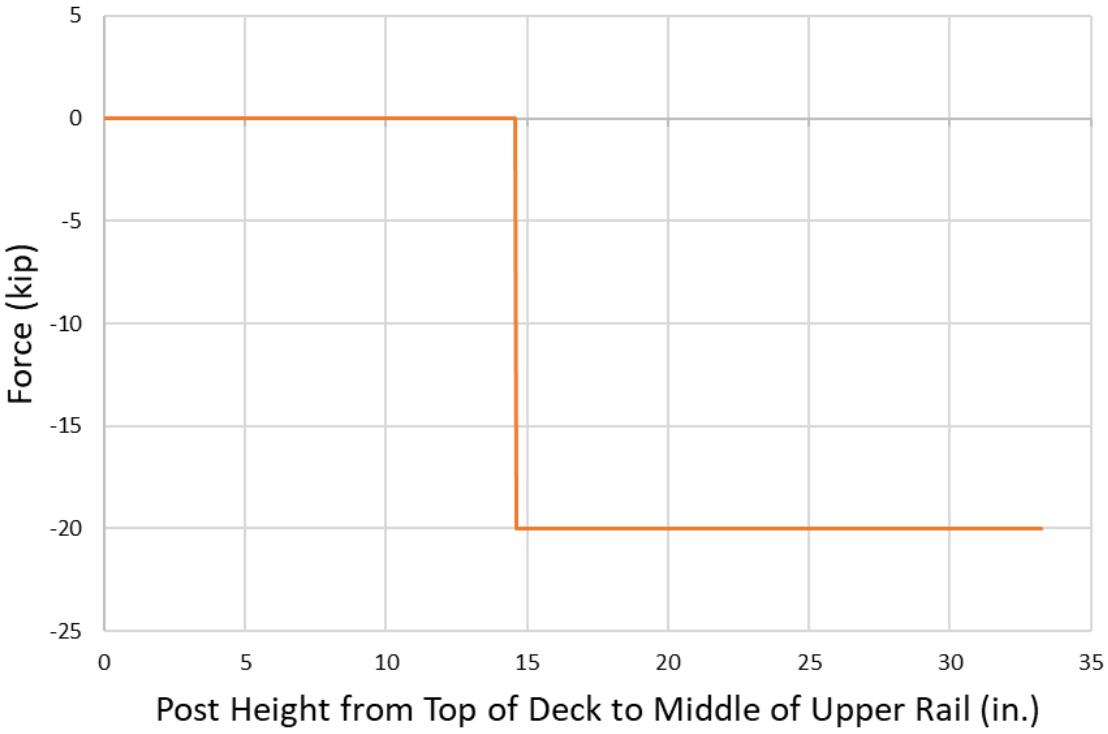

Figure 83. Longitudinal Shear Demand, Post Diagram

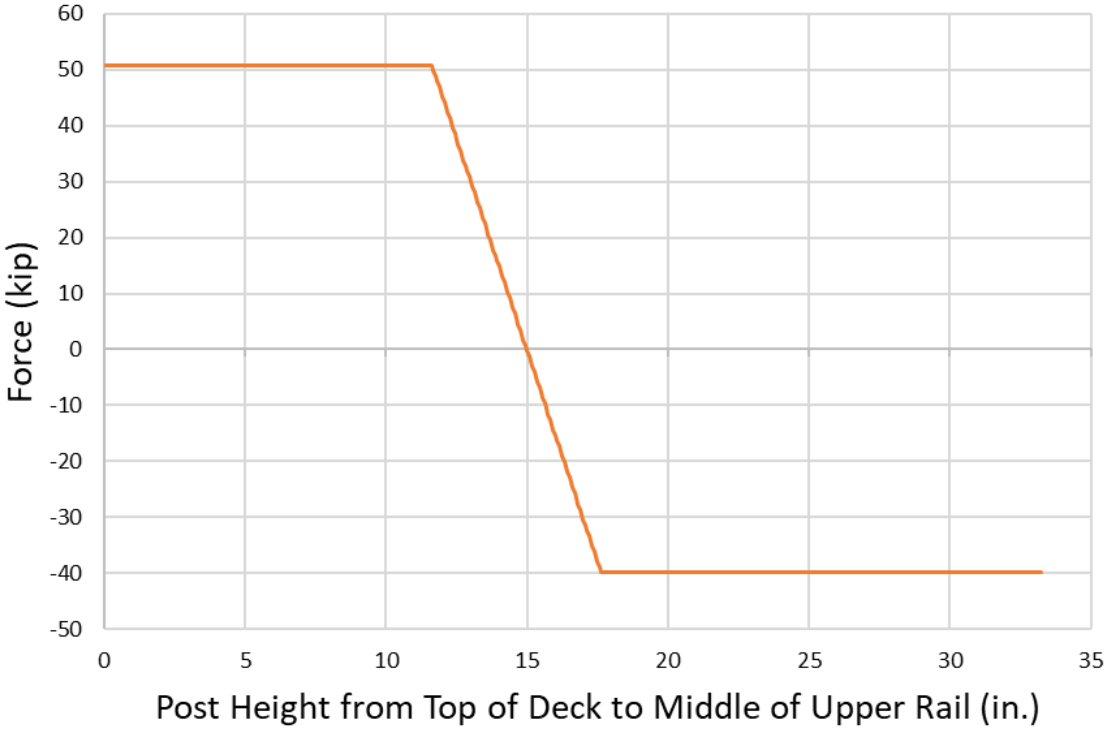

Figure 84. Lateral Shear Demand, Post Diagram

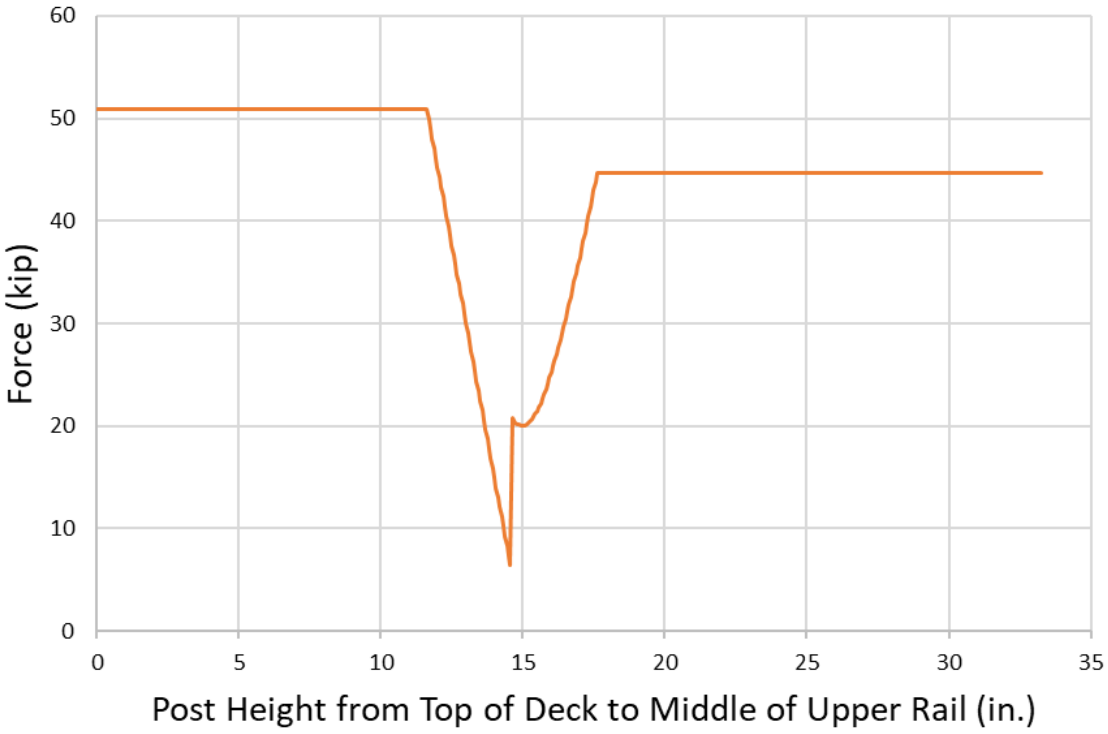

Figure 85. Combined Lateral and Longitudinal Shear Demand, Post Diagram

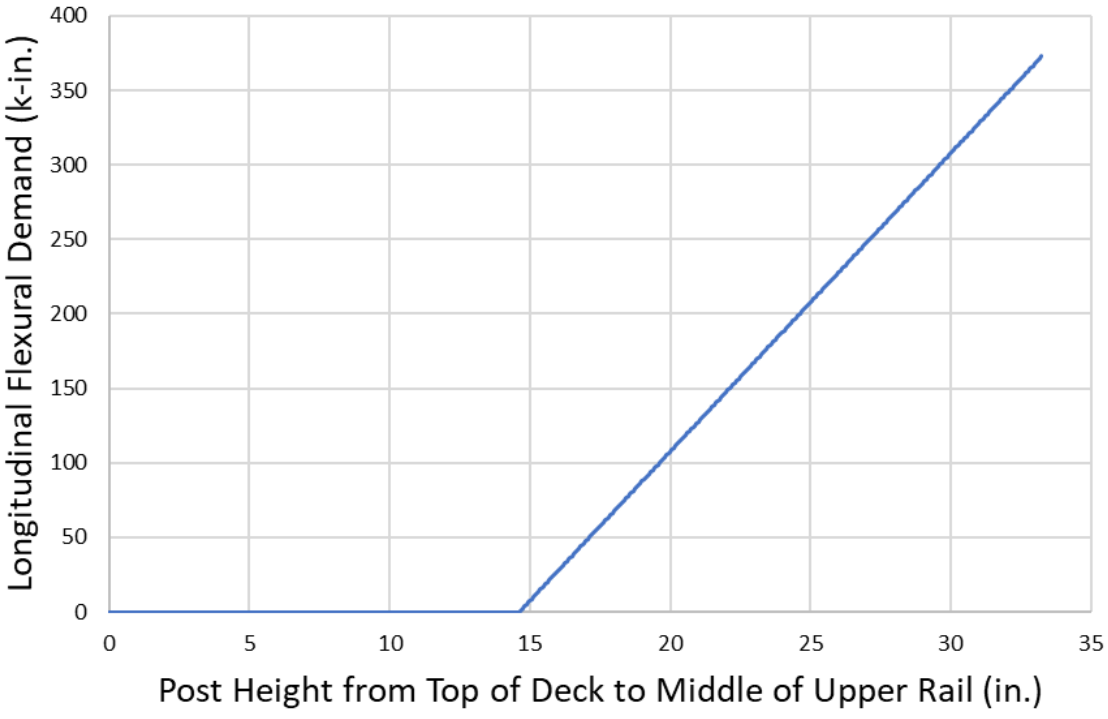

Figure 86. Longitudinal Flexural Demand, Post Diagram

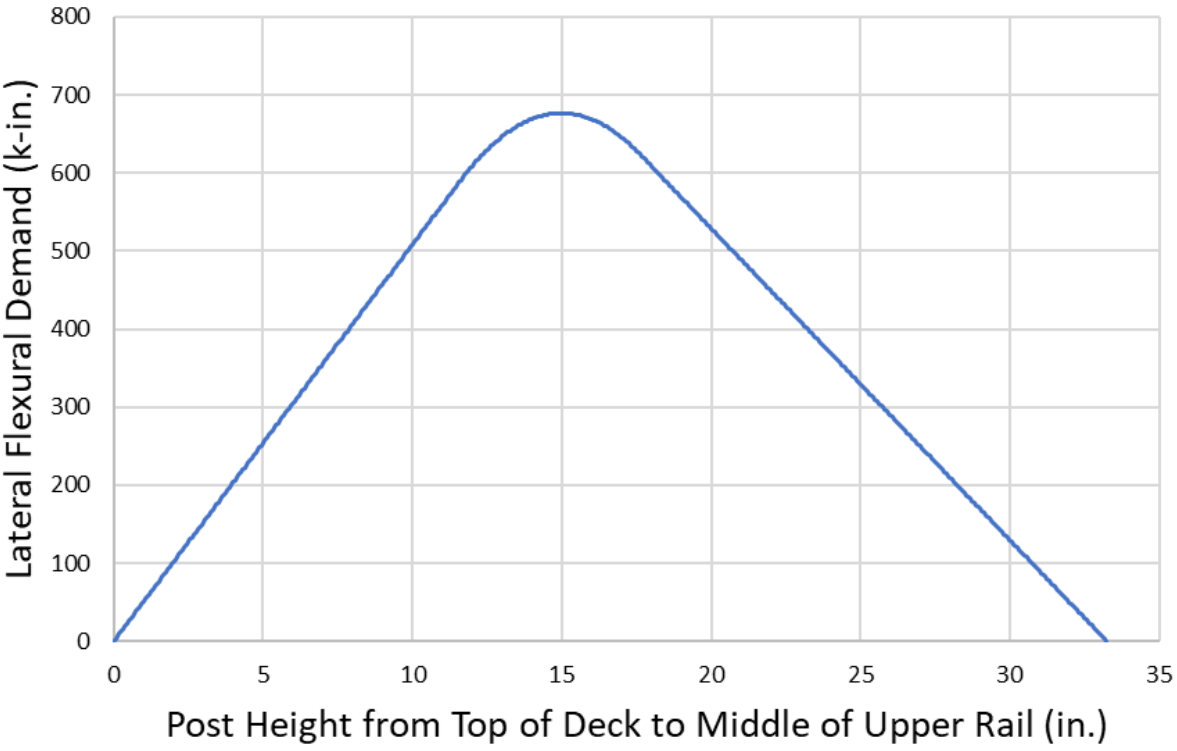

Figure 87. Lateral Flexural Demand, Post Diagram

3.3.2.4 Horizontal Bolt

Under Design Case 1, the horizontal bolt is under tension from the lateral load, and shear from the longitudinal load. Under Design Case 2, the design vertical loading resulted in shear of ~17-18 kips in the connection, which was less severe than the longitudinal loads in excess of 20 kips, from Design Case 1, so Design Case 2 was ignored for this connection. The horizontal bolt was expected to encounter combined tension and shear from Design Case 1.

The maximum load going through the post, according to analysis in section 3.3.2.1, was the load causing the yield moment. This load required the horizontal bolt to withstand 90.78 kips. Simultaneous to this load, the longitudinal shear load of 20.02 kips is also expected to be acting on the bolt.

3.3.2.5 Upper and Curb Railing Splices

The primary load demand of concern was the combined flexural and longitudinal loads on the extreme fibers of wood or splice plate edges. The longitudinal component of these loads was estimated from the BARRIER VII results of the wet-use CIP analysis for the SUT, as shown in Table 17. Flexural loads initially estimated from the BARRIER VII analysis were low and resulted in a lower load than the original 1997 design demand [121]. In addition, the analysis of the original design noted that the forces going through the splice were higher than expected [121]. Therefore, a higher load was estimated for the splice demand using the flexural capacity of the timber railing.

The tensile demand for the upper railing, T_u, was 188.38 kips, as determined from an upper railing flexural capacity of 1,568.6 kip-in. (see Phase IIa [10-11]) divided by the width of 10.75 in. and added to 84.93 kips. The tensile demand for the curb railing, T_u, was 83.71 kips, as determined from a curb railing flexural capacity of 938.59 kip-in. (see Phase IIa [10-11]) divided by a width of 12 in. and added to 10.98 kips (not shown in Table 17, obtained from wet-use CIP analysis of maximum curb rail tension). These demands applied to one side of the splice, as shown in Figure 88, with the other side handling an equal and opposite load. Detailed calculations and comparisons of the upper and curb rail splice demands are provided in Appendix J.

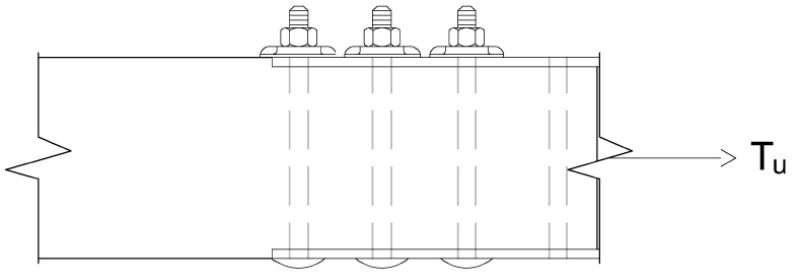

Figure 88. Upper Rail Splice Section with Tensile Demand

3.3.3 Curb Railing to Deck Design

Analysis and design of the vertical bolts holding the curb railing to the deck was initiated in Phase IIa. Two ASTM A307A ¾-in. diameter bolts were added to the six bolts used in the NCHRP-350 railing, and the bolt location was adjusted from 6 in. to 8 in. away from the deck edge to enhance the flexural capacity. Due to revisions in section 3.2.2, the bolt was enlarged, and the scupper block was lengthened. The shear capacity of the eight vertical bolts in the connection required evaluation. The lateral and longitudinal shear demands from section 3.3.2.1 were 90.78 and 20.02 kips, respectively.

3.3.3.1 Timber Shear Connectors

To enhance connection strength and improve load distribution, bolts in timber structures incorporate shear connectors. During consultation with Matt Smith, the president of Laminated Concepts Inc. (a company which builds timber bridges), concerns emerged regarding the approval of various timber shear connectors beyond those used in full-scale crash tests [119]. To provide bridge manufacturers with flexible design choices, the weakest shear connection was selected for dynamic component tests.

The NDS includes guidelines for three types of shear connectors for bolts: shear plates; split rings; and spike grids. While the NDS offers detailed guidelines and design values for shear plates and split rings, access to spike grid data was limited due to the unavailability of certain referenced sources. Historically, the Timber Engineering Company (TECO) produced spike grids, split rings, and shear plates, and published corresponding design values [120]. The NDS design values for split rings and shear plates are identical to those in TECO's design guide. Without a more recent reference for the spike-grid values, the estimates for spike grid design values were taken from TECO's design guide.

Table 20 summarizes shear connector design values for a ¾-in. diameter bolt. The values for ⅞ in. diameter bolts were identical to ¾-in. bolts for shear plates but were not tabulated for split rings (although ⅞-in. bolts could easily be used with split rings). The split rings and spike grids sizes would not change, but shear plates are modified to have larger holes for ⅞ in. bolts. Each shear connector possesses different strengths according to the utilized wood species. The tabulated strengths were sorted into three (TECO) or four (NDS) groups of timber species, based on similar densities. Across different wood species, shear plates were the weakest connectors, leading to their selection for standard use. Bridge construction specifications may include split rings or spike grids at the builder's discretion. In Table 20, groups A, B, and C correspond to timber species groups classified by their specific gravity, with the NDS extending group D designation to shear plates and split rings. TECO's design guide was limited to groups A, B, and C.

Table 20. Shear Connector Design Values

Shear Connector Type	Design Values for ¾-in. Diameter Bolt		
	Group A Load at 90° (lb)	Group B Load at 90° (lb)	Group C Load at 90° (lb)
4 in. Split Ring	4270	3660	3050
4 in. Shear Plate	3540	3040	2530
Spike Grid	3900	3500	3000

For shear plate connectors, NDS provides guidance on design for allowable limits, but not ultimate limits, based on ASD design. Ultimate limit loads, according to discussions from the development of the Glulam Rail with Curb on Transverse Glulam Deck, were 2 to 3 times greater than allowable limit loads [121]. Although 2.5 or 3 could be justified, the more conservative estimate was selected for design. Thus, the allowable shear plate capacities were doubled to estimate an ultimate load.

The longitudinal shear load demand was examined using the BARRIER VII results from Phase IIa and using Equation 17 for a 38-in. tall system height. The controlling maximum longitudinal load demand was 23.35 kips. The lateral load demand was 90.78 kips based on revised post yield moment of 1,327.7 k-in and a 14.625-in. lateral bolt (horizontal bolt) application height. The shear capacity of the bridge post configuration on transverse and longitudinal decks and the corresponding shear load demand under both transverse and longitudinal loading is shown in Table 21. For more information on how the shear capacities were determined, see Appendix F.

Table 21. Shear Plate Capacity on Timber Decks

Load Direction	Transverse Glulam Deck		Longitudinal Glulam Deck	
	Capacity (kip)	Demand (kip)	Capacity (kip)	Demand (kip)
Lateral Loading	77.82	90.78	77.82	90.78
Longitudinal Loading	41.47	23.35	44.91	23.35

The shear strength values in the lateral loading orientation were not sufficient and would require additional bolts. This analysis also did not consider any reduction for a deck with a high moisture content. With additional bolts, the connection would become stiffer and could transfer greater lateral loads into the shear connection, so that demand increased with capacity. The frictional resistance, previously ignored, was investigated to evaluate its impact on shear capacity as a way to address these concerns.

3.3.3.2 Friction

Reinforced concrete typically relies on concrete to assist with shear resistance (with steel stirrups as well), but an analogy cannot be easily made as the timber scupper blocks are not bonded to the timber bridge deck. However, each scupper block exerts a significant compressive force on the deck normal to the wood surface. This normal compressive force will develop a frictional resistance against lateral movement. The friction coefficient was based on the lowest coefficient for wood-on-wood interface, 0.3, from the wood handbook [60]. A lower estimate was justified due to the use of oil-borne preservative treatment which may reduce the friction that could develop between wood pieces. The full frictional resistance to the shear load was assumed to be employed before drawing on bolt shear resistance, because the compression from flexural resistance would always be present.

A frictional resistance of 64.94 kips develops from a compressive load of 216.48 kips, which was estimated to reduce the lateral load demand to 25.84 kips from 90.78 kips. The remaining shear load on the connectors, 25.84 kips, was significantly lower than the lateral loading shear capacity, 77.82 kips. Under high moisture conditions, the lateral loading shear capacity was reduced by 0.7, to 54.48 kips. The post yield moment, based around yielding the bolts, would maintain (because tension equals compression) 216 kips in compression, which obtains the same frictional resistance (keeping the 0.3 coefficient). But the shear load would be reduced from 90.78 kips to 65.19 kips because the yield moment would be lowered from 1,327.7 k-in. to 953.5 k-in. (see section 3.2.3). The wet-use scenario resulted in an even lower load of 0.25 kips going to the connection. Therefore, the existing design's shear capacity was considered to be sufficient.

3.3.4 Upper Rail to Post Design

The Glulam Rail with Curb on Transverse Glulam Deck secured the post to the upper rail with two ASTM A307A ¾-in. diameter bolts. The longitudinal shear load was 20.02 kips, the vertical shear load was 17.17 kips, and the tensile load was 15.02 kips, according to section 3.3.2.2. The shear capacity of the connecting bolts was evaluated using AASHTO Equation 6.13.2.7-2, without applying a higher strength reduction factor for impact loads on the hardware [2]. The tensile capacity of the bolt was evaluated first for combined loading effects, as outlined in AASHTO Section 6.13.2.11. Equation 6.13.2.11-1 was used if combined loads were not applicable, otherwise Equation 6.13.2.11-2 was used.

The shear load capacity of two ASTM A307A ⅞-in. diameter bolts were 24.35 kips, which exceeded the demand of both 17.17 kips and 20.02 kips. This analysis determined that a single ⅞-in. bolt has a combined load capacity of 15.56 kips, under combined shear and tensile loads. This capacity was sufficient to resist the estimated load demand of 15.02 kips.

3.3.4.1 NDS Connection Equations

The American Wood Council (AWC) National Design Standards (NDS) provide connection design yield limits to prevent yielding in the bolt-wood interface [122]. Depending on the connection configuration and the design of the connected wood members, the NDS identified four or six different yielding scenarios, illustrated in Figure 89.

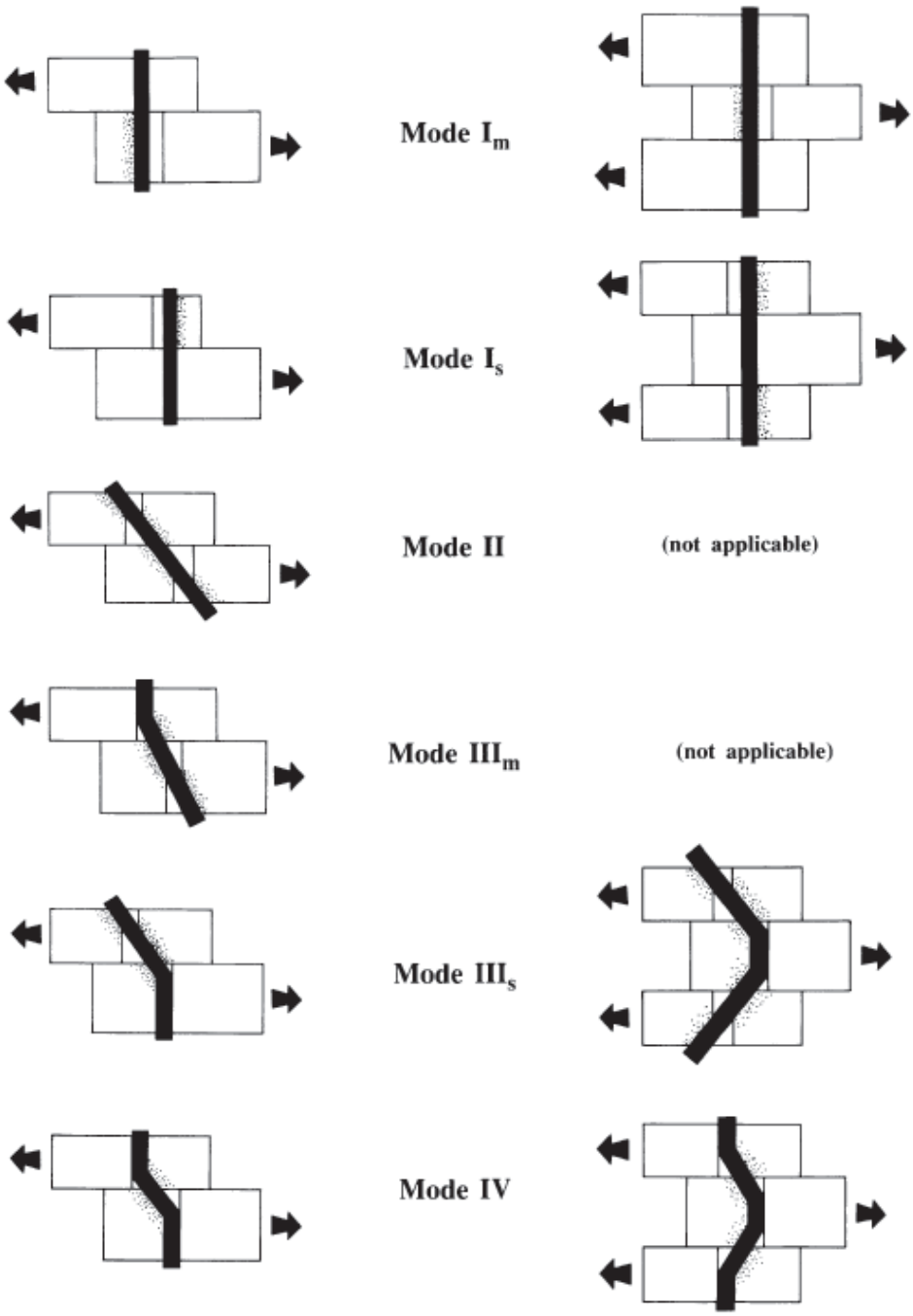

Figure 89. NDS Equations Connection Yield Modes [14]

The load on the connection came from either longitudinal loads (20.02 kips) or vertical loads (17.17 kips). However, the connection capacity calculated from these equations was dramatically lower than previously calculated connection capacities. Two ASTM A307A ⅞-in. diameter bolts in timber members with widths of 10¾ in. and 12 in. can resist 5.86 kips before yielding, which is markedly less than the bolt shear capacity of 24.35 kips. This calculated connection capacity per NDS yield limits meant substantial additional capacity was required, which was impractical and inconsistent with the observed performance of previous railing designs.

These equations were not used to design the Glulam Rail with Curb on Transverse Glulam Deck or GC-8000, and so no example for past usage on TL-4 timber railings was available. To get an idea of whether these equations would have successfully predicted the performance of the bolt's connections in those bridge railings, their capacity was calculated. Either crash-tested bridge railing connection only had a capacity of 4.43 kips. For comparison, the AASHTO Chapter 13 Table A13.2-1 guidelines for design forces on traffic railings for the TL-4 vertical design load was 18 kips, distributed over 18 ft [15]. This selection would place 8 kips on the railing, causing failure. The longitudinal load, 18 kips, over 3.5 ft, was even more critical.

A review of the NDS equations development indicates that they incorporate a reduction factor, which adjusts the connection capacity for duration of load, safety, and some connection-specific effects [117, 123-124]. The new NDS equations were based on tests which pressed bolts of different sizes into different species of wood blocks at different grain orientations [123-125]. The testing rate was 0.04 in./min. [125], which corresponded to a 5-minute yielding load [123]. Building on this information, the connection capacities were developed by the mechanics of either wood or bolts yielding. For instance, Mode I in Figure 89 calculated the load required for the bolt to uniformly yield all wood bearing on the bolt in compression for either of the connecting members. Other yield modes examine plastic yielding in the bolt with compressive yielding in the wood.

The reduction factor adjusted load duration in the connection strength equations from yielding over 5 minutes to yielding over 10 years [123]. The reduction factor was also designed to match the older values, which were developed through numerous tests of different connection configurations [117]. The older allowable capacities were based on a "proportional limit", which referred to the point at which slip in the joint was not accompanied by an increase in load, or when the load-displacement curve is no longer linear [117].

The newer study estimated the yielding load beyond the linear region of the load-displacement curve which the proportional limit characterizes [125]. The bearing stress of the wood was obtained by selecting "5% offset values". These values are derived from a plot of load and displacement (compression of steel dowel into the wood) bearing a linear elastic region, the slope of which is offset by 5% of the dowel diameter which is bearing into the wood along the displacement axis. The load which the offset slope selects from the as-tested load-displacement curve is divided over the bolt bearing area for the bearing stresses. An example of the 5% offset and the new selected load are shown in Figure 90. The yielding stresses were calculated and found to be close to the tabulated average stress values for glulam Douglas Fir, which NDS directs users to select. Therefore, removing the reduction factor would more closely approximate the connection yield capacity. The upper rail connection capacity for each loading orientation is shown in Table 22.

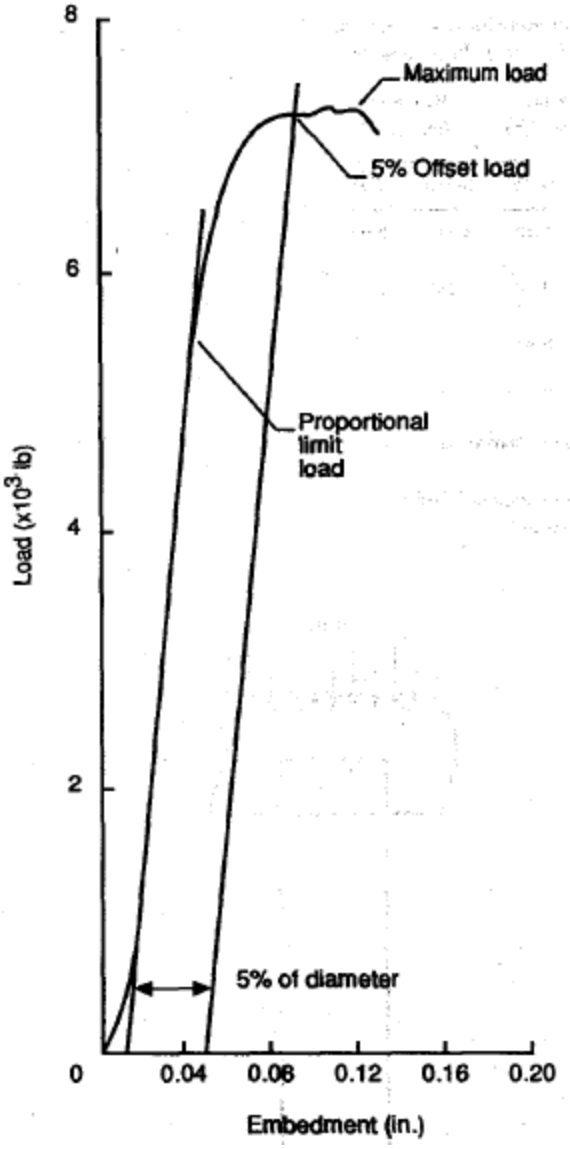

Figure 90. Typical Load-Displacement Curve for ¾-in. Diameter Bolt Bearing Capacity on Southern Pine Wood Block [125]

Table 22. Upper Rail to Post NDS Connection Equation Capacities vs. Demands

Vertical Loads (kips)		Longitudinal Loads (kips)	
Capacity	Demand	Capacity	Demand
21.74	17.17	21.74	23.35

As shown in Table 22, the longitudinal capacity did not exceed 23.35 kips. But the connection was not strengthened because it was judged to be unnecessary. First, the controlling yielding mode was Mode IV from Figure 89, which describes yielding of both the wood and the

bolt instead of rupture in the connection. A brief review of the literature has indicated that connections with a high length of bolt in the wood member relative to the bolt diameter display high ductility in their failure mode [123,126]. While vertical loads could push the railing down and allow vehicle rollover, the longitudinal loads would twist the connection but would remain attached until another failure such as splitting or bolt rupture broke the connection. Second, similar damage or failure has not been observed in past crash tests, so there was no additional evidence to support the need for a stronger connection here. Further details on the load demands and capacities for the upper railing-to-connection were provided in Appendix G.

3.3.5 Vertical Post Design

When both longitudinal and lateral loads act on the post, combined flexural effects need to be considered. The combined load demand has already been shown in Figure 85 in Section 3.3.2.3. While shear forces can be combined, flexural loads cannot be combined. To evaluate the combined stress state for the vertical post in flexure, similar load cases in AASHTO were reviewed. AASHTO Section 5.6.4.5 addresses biaxial flexure in concrete columns, and Section 6.8.2.3 covers biaxial flexure in steel members. Both sections recommend evaluating the sum of the ratios of load demand to capacity for each orientation. If the sum of these ratios is less than one, then the member is deemed appropriate. This method was used to evaluate post flexure.

The shear and flexural capacities were reduced for the hole in the post cross-section. Values for shear and flexural strength were derived from tabulated strength values and modified to estimate an actual resistance. Safety factors included in the calculation of tabulated design values, 10/13 for shear and flexural stress, were removed to obtain an average failure strength closer to tested specimens [127]. The strengths were adjusted from 5% to 50% estimates according to COV values from ASTM D2555 for Coastal Douglas Fir and a normal distribution [128]. The estimated average flexural strength was a little lower than tested MOR for Douglas Fir Specimens of similar sizes [129], providing some confidence for the calculated values.

The shear strength of glulam members must be reduced for cases which are not identical to the shear tests which produced the tabulated shear strengths [127]. The tabulated strengths were based on static loads, so the design code required reduction for impact loads. However, a shear strength reduction from static loading to impact loading would contradict the fact that wood members have a higher resistance under impact loading [14-15]. The reduction was ignored to obtain a more accurate strength estimate. The shear strength was 0.896 ksi, while the flexural strength was 5.879 ksi in the lateral direction and 6.473 ksi in the longitudinal direction. The shear and flexural capacities of the 8¾-in. x 10½-in. vertical post versus the shear and flexural demand are shown in Figures 91 and 92, respectively.

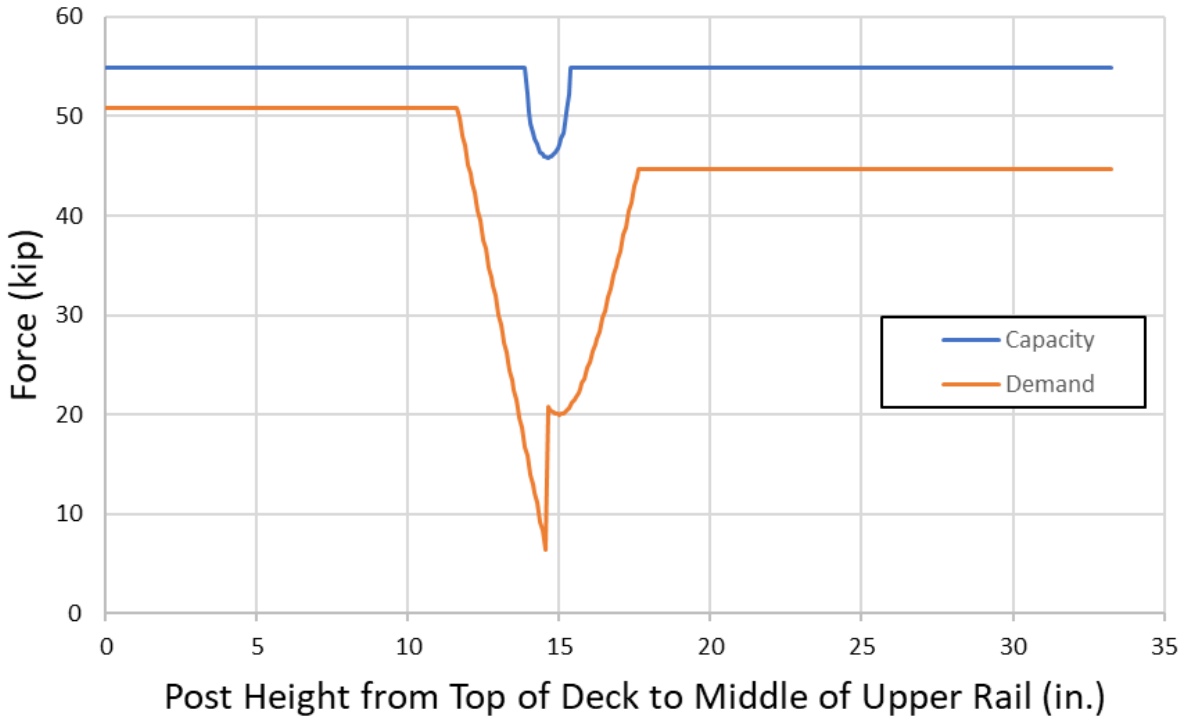

Figure 91. 10.5-in. x 8.75-in. Post Shear Capacity to Demand Comparison

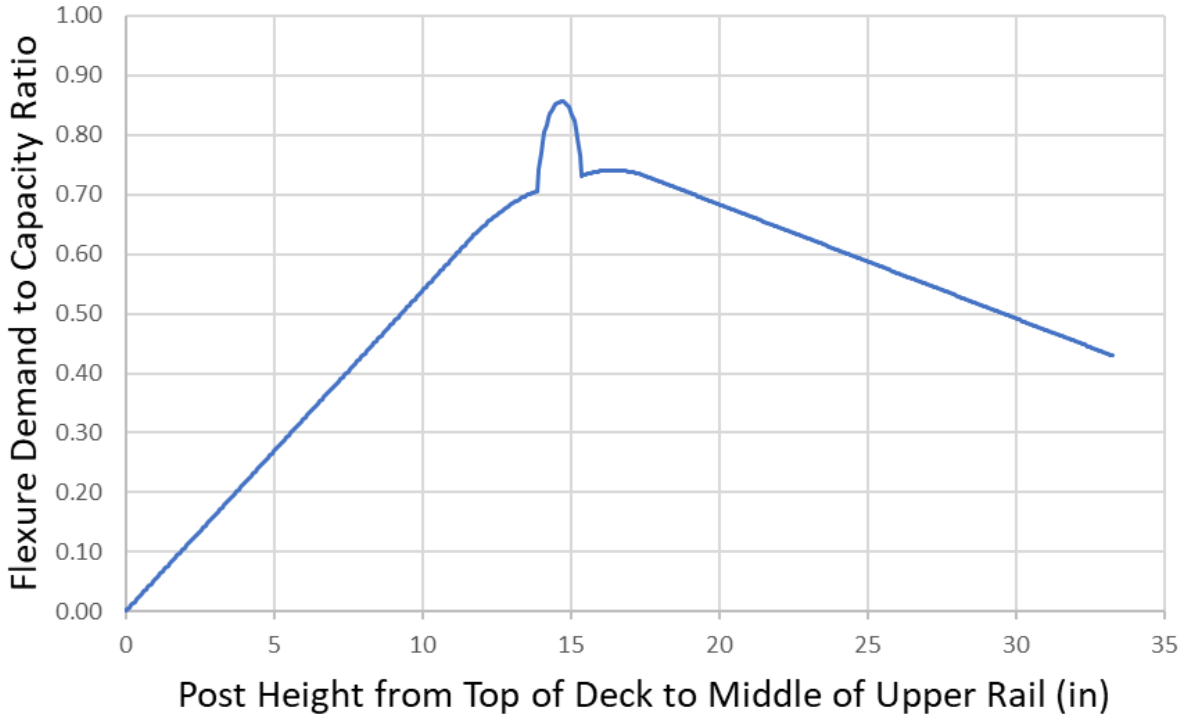

Figure 92. 10.5-in. x 8.75-in. Post Flexural Demand-Capacity Ratio Across Post Height

Although sufficient, the estimation methods were deemed to be overly aggressive for shear, because of the adjustment to an average strength from a 5% strength in addition to removal of the safety factor. So, it was decided to add another lamination, so that the post size increased from 8¾ in. x 10½ in. to 8¾ in. x 12 in.

3.3.6 Horizontal Bolt Design

An A307A 1¼-in. diameter bolt was used to connect the curb railing to the post that supports the upper railing in the Glulam Rail and Curb on Transverse Glulam Deck. This horizontal bolt must withstand larger shear and tensile forces during impact per MASH 2016 TL-4 crash conditions. A maximum tensile force of 90.78 kips was imparted to the horizontal bolt which loaded the bridge railing to deck connection. The maximum longitudinal shear load, 20.02 kips from the BARRIER VII analysis, was applied simultaneous to the maximum tensile load. The tensile and shear capacities of the 1¼-in. diameter ASTM A307A bolt, according to AASTHO 6.13.2.10.2-1 and AASHTO 6.13.7-1 were 44.77 kips and 24.85 kips, respectively. A combined loading check was irrelevant, because the tensile capacity was already insufficient.

To properly design a new bolt, either the bolt could be made larger to handle loads, or the bolt grade could be higher. A larger bolt would cause issues for the vertical post; since, a larger bolt would require more wood to be removed to make room for it, so a higher bolt grade was chosen. An ASTM A449 1⅜-in. diameter steel bolt was chosen to resist the shear and tensile loads. The increased size would not have been necessary if the reduction factors were not included, but it was considered unwise to neglect AASHTO requirements for connections to include strength reduction factors in extreme events. This bolt had a capacity of 94.80 kips, and in this case no combined check was necessary, because the shear demand to capacity ratio was low enough according to AASHTO 6.13.2.11 that shear could be ignored. The NDS bolt-wood equations estimated a 32.97-kip capacity, exceeding longitudinal shear loads. For more information on each of these limits, see Appendix H.

3.3.7 Upper and Curb Rail Splice Designs

The upper rail splice design utilized by the Glulam Rail and Curb on Transverse Glulam Deck satisfying NCHRP-350 TL-4 impact conditions had two ⅜-in. thick x 13½-in. tall x 28-in. long ASTM A36 steel plates. The upper railing splices were placed at post locations, and four ASTM A307A ¾-in. diameter bolts connected the splice plates to the posts. Four 1¼-in. diameter ASTM A307A steel bolts connected the upper railing to the splice plate on each side for a total of eight bolts. Notches were cut into the upper railing so that the splice plates sat flush on the front and rear faces of the railing, flush to the adjacent wood. The edges of the upper rail glulam beam were not coped. The splice design is shown in Figure 93.

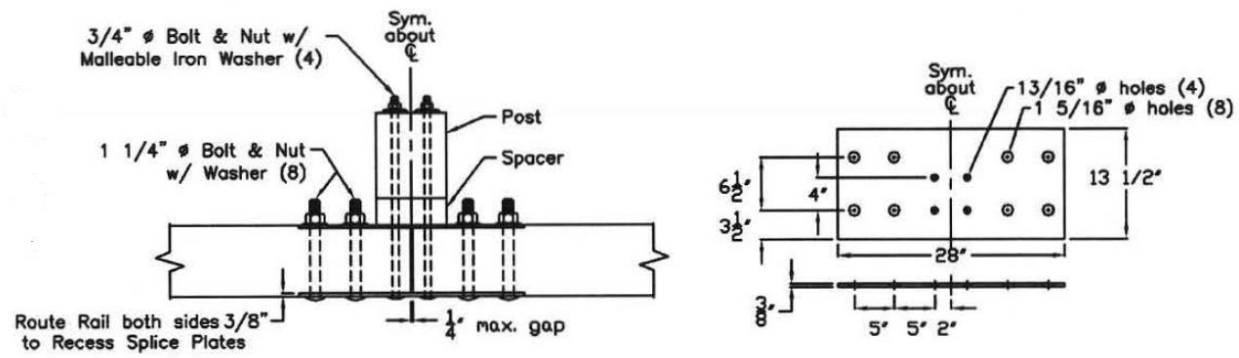

Figure 93. Upper Railing Splice for Glulam Rail and Curb on Transverse Glulam Deck [25]

The NCHRP-350 TL-4 system curb railing splice was formed with three ASTM A36 steel plates, one ⅜-in. thick x 6¾-in. tall x 12-in. wide plate was welded orthogonally between two ⅜-in. thick x 6¾-in. tall x 28-in. wide plates to form an "H" shape assembly. Six ASTM A307A ¾-in. diameter bolts were used to connect the curb rail to the splice on either side. Notches were also cut into the curb railing, so that the splice was fit without any steel protruding towards the roadway. The splices were placed between posts, because the post assembly with a large horizontal bolt made it very difficult to place splices at post locations. The corners of the curb rail were coped at the splice to make room for the splice assembly welds. The curb railing splice design is shown in Figure 94.

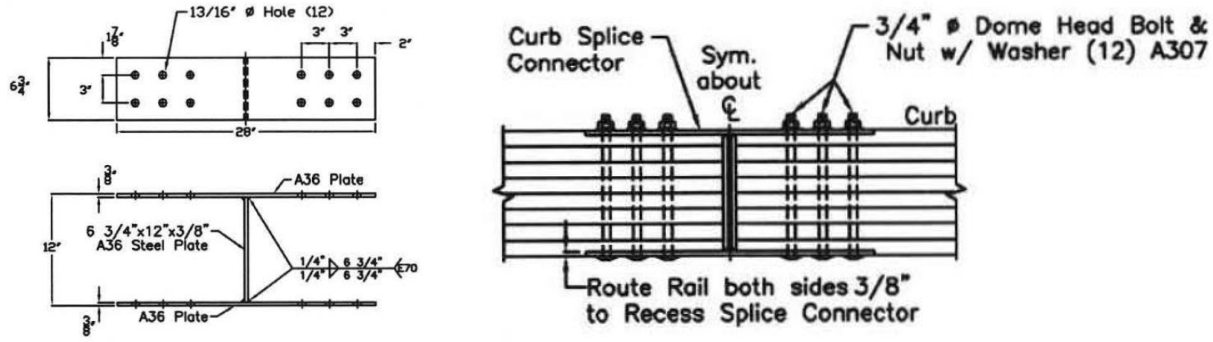

Figure 94. Curb Rail Splice Assembly for Glulam Rail and Curb on Transverse Glulam Deck [25]

Design Case 1 lateral loads on the splice were not examined because the railing would deflect at post locations to relieve some of the shear stress. In addition, the rupture capacity of the railing and splice plates against shear was well above 80 kips. Design Case 2 vertical loads were not examined, because the two ⅞-in. diameter bolts for non-splice locations in the upper rail-to-post connection were already found to be sufficient.

The capacity of the splice connection was the weakest of three load-bearing component limits: the steel plate; the steel bolts; and the timber beam. Each component was evaluated for its

strength and failure modes to ensure the integrity of the connection under load. The steel plate limits that were evaluated included yielding (AASHTO 6.8.2), rupture (AASHTO 6.8.2), and block shear failures (AASHTO 6.13.4). The steel bolt/plate limits that were evaluated included bolt bearing (AASHTO 6.13.2.9) and bolt shear rupture (AASHTO 6.13.2.7). The timber beam to bolt connection limit states that were evaluated included beam tensile rupture, row tear-out of bolts from beam, group tear-out of bolts from beam (NDS Appendices), and the connection equations discussed in section 3.3.4.1.

In addition to strength limit states, bolt spacing limits for steel and wood were also observed for AASHTO 6.13.2.6 and NDS 12.5, respectively. Wood bolt spacing requirements are not rigid. Therefore, user-based reduction factors were applied wherever requirements were not followed. The spacing requirements for both steel and wood are illustrated in Figure 95. Additional details and calculations for these railing capacities are also found in Appendix J.

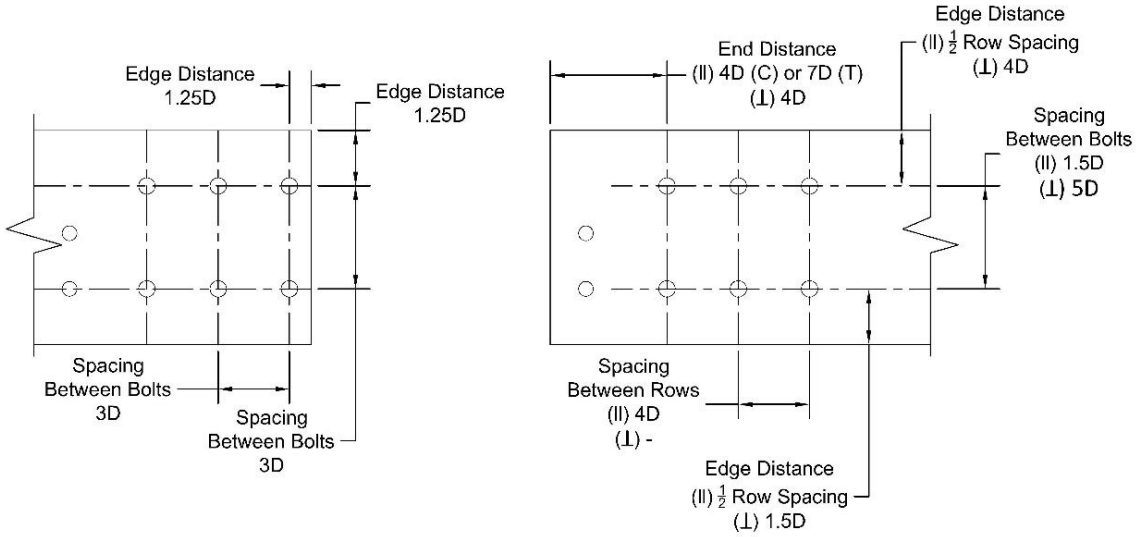

(a) Steel (b) Wood

Figure 95. Bolt Spacing Requirements for (a) Steel and (b) Wood

The upper rail splice design for the MASH 2016 TL-4 timber bridge railing reduced the size of the upper rail splice bolts from 1¼ in. diameter to 1 in. diameter and increased the number of bolts from four to six ASTM A307A bolts for one side of the splice, arranged according to Figure 96. These spacing requirements increased the length of the splice plates from 28 in. to 35 in. The curb rail splice design for the TL-4 timber bridge railing maintained six ASTM A307A ¾-in. diameter bolts, arranged according to Figure 97. The curb rail splice length remained 28 in., but the width increased from 6¾ in. to 8¾ in. to match the height of the curb railing.

The steel grade for the upper and lower splice plates were increased from ASTM A36 to ASTM A572 due to its ubiquity in construction. The upper rail and curb rail splice plates both maintained a ⅜ in. thickness. The critical limit for both the upper and curb rail splices was bolt shear rupture. A summary of the demand and capacities for each rail splice connection is shown below in Table 23.

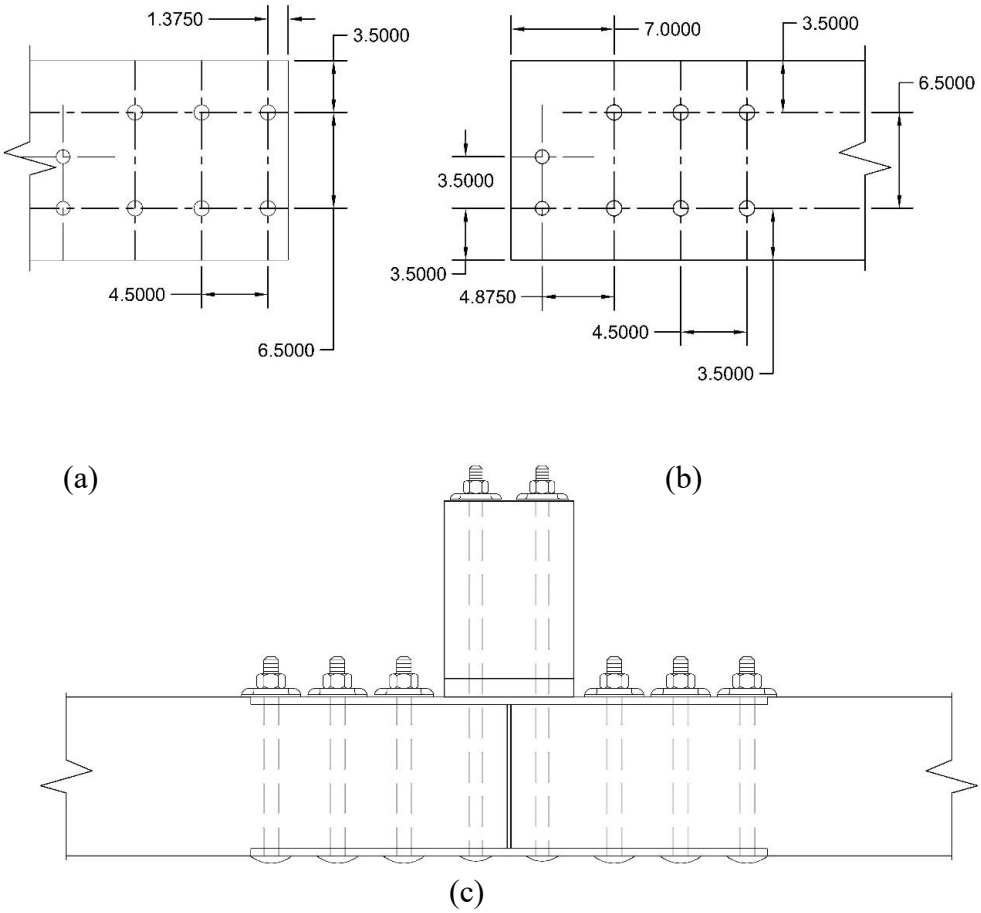

Figure 96. Upper Rail Connection Details: (a) Bolt Spacing Steel Splice Plate; (b) Bolt Spacing in Wood Rail; (c) Plan View of Connection

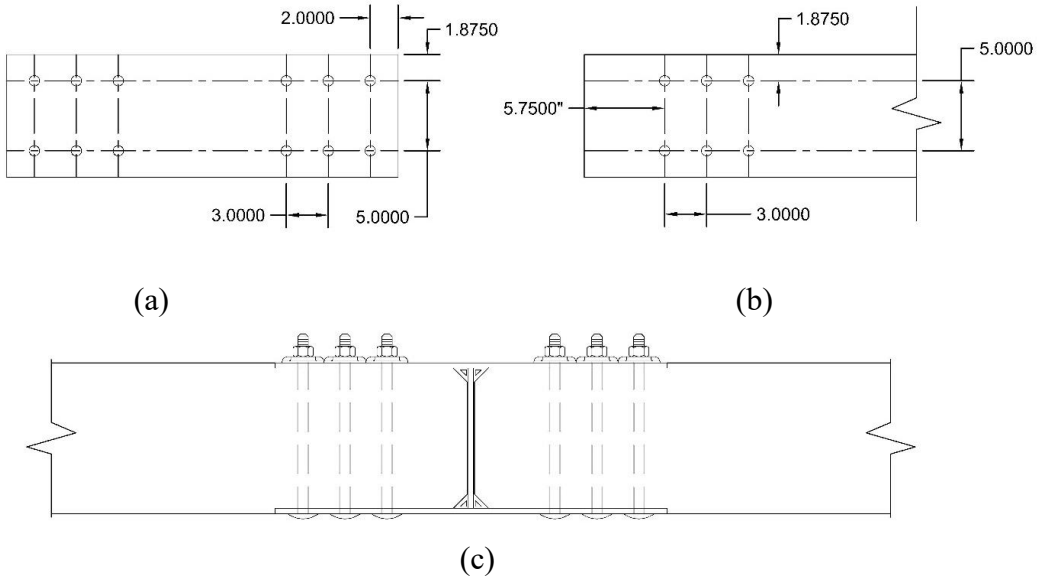

Figure 97. Lower Curb Rail Connection Details: (a) Bolt Spacing in Steel Plate; (b) Bolt Spacing in Wood Rail; (c) Plan View of Connection

Table 23. Upper and Curb Rail Splice Connection Limit Checks

Strength Limit	Upper Rail Splice (kips)	Curb Rail Splice (kips)
Load Demand	188.38	83.71
Splice Plate Yielding	240.47	155.86
Splice Plate Rupture	221.81	138.94
Block Shear Rupture	280.63	142.81
Bolt Bearing on Plate	280.80	210.60
Bolt Tear-out	485.55	374.40
Bolt Shear Rupture	*190.85	*107.35
Beam Row Tear-out	241.80	181.35
Beam Group Tear-out	229.65	184.89
NDS Wood-Bolt Limits	228.44	135.19

*Lowest

3.4 Critical Deck Configuration

3.4.1 Analysis of Resistance Mechanisms

The project objectives included identification of the critical timber bridge deck configuration to reduce the crash testing matrix. If testing was performed on the weakest, most critical deck with successful test results, then the bridge railing could be adapted to other less critical deck types without further crash testing. This goal required analysis of the deck capacities for multiple deck types. For this analysis, the impact loads imparted to the timber deck needed to be understood. Thus, an investigation was conducted to evaluate the flexural capacity of the deck for various assumptions. AASHTO Chapter 13 and its revisions [15,118] offers guidance for analyzing concrete decks, but nothing for timber decks. As a result, much of this analysis only included approximations.

Among deck categories, longitudinal and transverse decks have different mechanisms of resistance, which will require separate analysis for their adequacy. Longitudinal decks have wood grains oriented parallel to the bridge span, and transverse decks have wood grains oriented perpendicular to the bridge span. The longitudinal decks have historically required transverse reinforcing rods in the deck to strengthen the deck against lateral impact loads [16-17, 19]. Therefore, an analysis of the resistance mechanisms will be subdivided between transverse and longitudinal deck configurations.

In addition to the mechanism of resistance, the bridge deck type contributes to its load distribution away from each post location through the superstructure and to the substructure. The timber bridge deck types under evaluation were glued-laminated (glulam), spike-laminated, and stress-laminated. The common nail-laminated deck was not considered to possess sufficient stiffness or strength for TL-4 impact requirements. Other bridge deck types have not been developed (cross-laminated) or have not been used (screw-laminated), and evaluation was either impossible or had limited benefit to timber bridge builders. Plank decks are more widely used, but

their limited recommended use by AASHTO suggests that both plank and nail-laminated decks should not be used with TL-4 bridge railings.

Glulam and spike-laminated decks may be constructed in longitudinal or transverse orientations. However, stress-laminated decks should be built exclusively with boards in a longitudinal orientation, because the stressing rod ends create unnecessary maintenance issues when penetrating into the end abutments [51].

3.4.2 Longitudinal Deck

Longitudinal timber bridge decks are subjected to lateral, longitudinal, and vertical vehicle loads from Design Cases 1 and 2. Figure 98 shows these loads being applied to the longitudinal deck from the railing. The flexure transmitted to the deck from the lateral loads on the bridge post was also shown, representing the couple of scupper compression and vertical bolt tension from Figure 77. The vertical loads of Design Case 2, ~17-18 kips, were significantly lower than the applied compression and tension couple in the base of the scupper, 216 kips, which resisted the lateral load, F_{Lat}. Therefore, Design Case 2 was ignored.

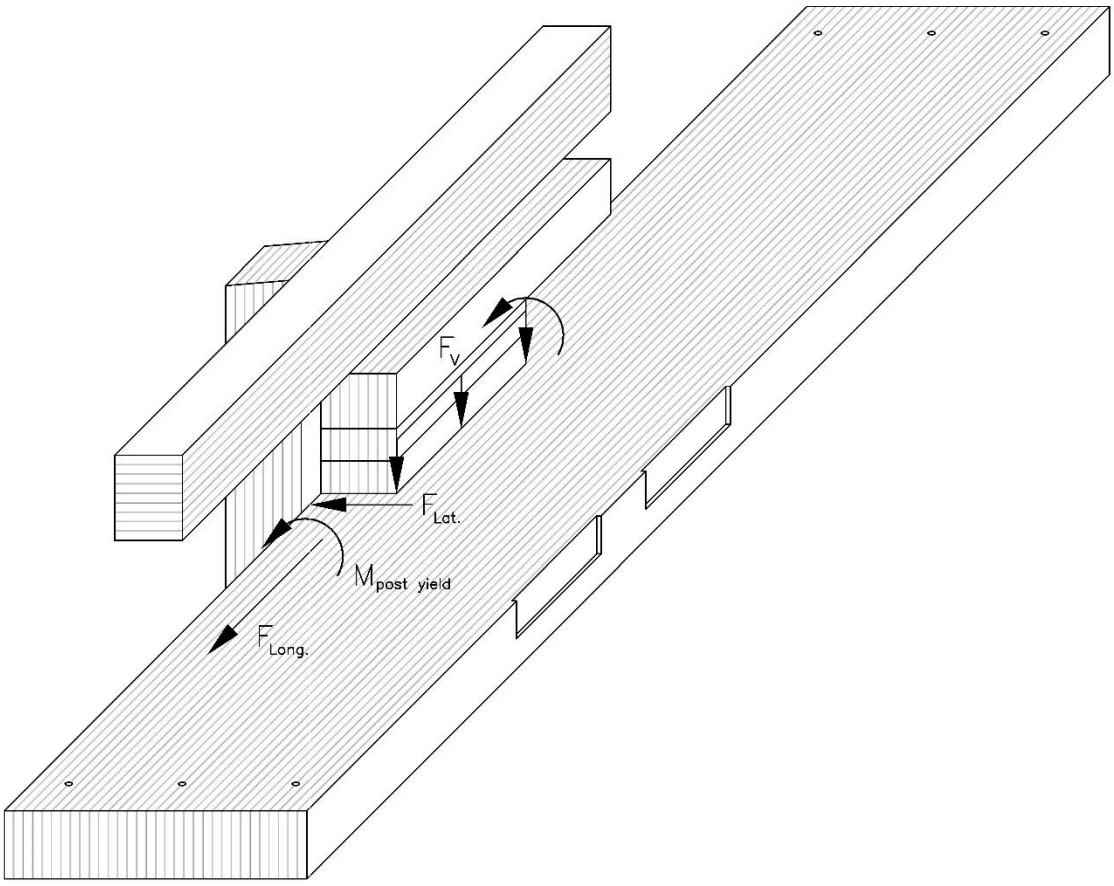

Figure 98. Longitudinal Deck External Force Diagram

The maximum longitudinal load from two post was 40 kips, per the maximum longitudinal load discussed in section 3.3.2.1 on one post. The longitudinal loads would be transferred parallel

to the wood grain of the longitudinal deck into six ASTM A307A ¾-in. diameter bolts anchored into the concrete support, three at each panel end. The factored shear rupture capacity, 53.7 kips, exceeded the demand. Wood-bolt yielding failure, described by NDS equations in section 3.3.4.1, roughly predicts a capacity of 51.4 kips utilizing highly conservative assumptions [130]. Therefore, the longitudinal loads apply any critical loads to the longitudinal deck panel.

Only lateral design impact loads, and the flexure created from them, remained for the design demand. As mentioned in the prior section, longitudinal decks rely on transverse steel rods to resist vehicle impact loads. When the GC-8000 was crash tested, the reinforcing rods consisted of two ASTM A722 ⅝-in. diameter rods placed at post locations every 6 ft – 3 in. along the deck. When the railing induced flexure into the deck by the tension and compression couple, the transverse steel rods would be in tension in the upper part of the deck, while the wood in the bottom part of the timber deck would be in compression.

The flexural resistance of the longitudinal deck was developed using a similar method to that provided in the Phase IIa report, which was based on using reinforced-concrete equations for determining timber post capacity for reinforced wood. The steel rods in the bridge deck provide tensile resistance, and the deck laminations (whether glulam, spike-laminated, or stress-laminated) provide compression resistance. Four parameters were used to describe the flexural resistance: the transverse deck rod capacity; the bridge deck lamination compressive resistance perpendicular to grain; the bridge deck thickness; and the longitudinal and vertical distribution of compressive stress near the bottom of the bridge deck. These parameters, except for the longitudinal compressive stress distribution, are shown in Figure 99.

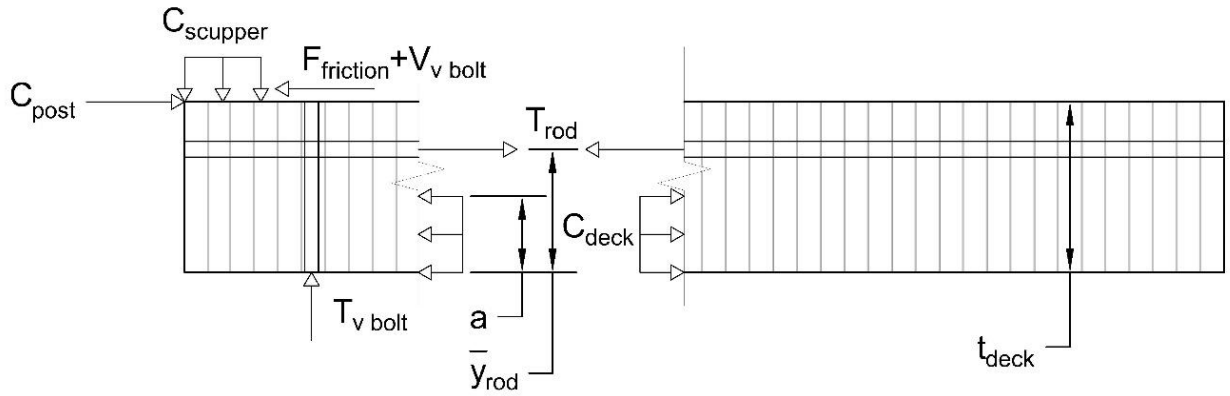

Figure 99. Longitudinal Deck Free-Body-Diagram of External and Internal Forces

The compression from the post scupper and the tension from the vertical bolt are shown in Figure 99, where together they form a moment couple which induces flexure into the longitudinal deck. The centroid of friction, post compression, and bolt shear (or shear plates) were all assumed to be at the top of deck and could summed up to the maximum load which BARRIER VII's post model would apply. These loads also contributed to flexure in the longitudinal deck. The weight of the railing and deck were excluded, because they were insignificant – roughly 700 lb for one post and only 1.4 k-in. to the increased moment at the bolt centerline as compared to 1327 k-in. from the post. Equation 25 represented the sum of moments in equilibrium, and Equation 26

represented the sum of lateral forces in equilibrium. These were used to solve for the tensile load demand and the compressive load demand.

$$\sum M = [M_{post\ yield} = \mathrm{f}(C_{scupper}, T_{bolt})] + (F_{friction} + V_{v\ bolt} - C_{post})(t_{deck} - \bar{y}_{rod}) + C_{deck}\left(\bar{y}_{rod} - \frac{a}{2}\right) + T_{rod}(0) = 0 \quad \text{Eq. (25)}$$

$$\sum F_x = -F_{friction} + C_{post} - V_{v\ bolt} + C_{deck} - T_{rod} = 0 \quad \text{Eq. (26)}$$

The compression within the longitudinal glulam deck, C_{deck}, was a function of the distribution of compression in the deck. The distribution of the compression zone involved the width of the compression region (going into the page) and height of compression, "a", which was also used to define the moment arm for the compression in Equation 26. The compressive stress also had to be defined for the compression region.

The width of compressive stress was approximated by assuming a large width that extended between midpoint locations of posts, 8 ft, as shown in Figure 100. A uniform (i.e. average) load distribution was selected over a triangular distribution to be consistent with how the compressive stress width was defined for the scupper.

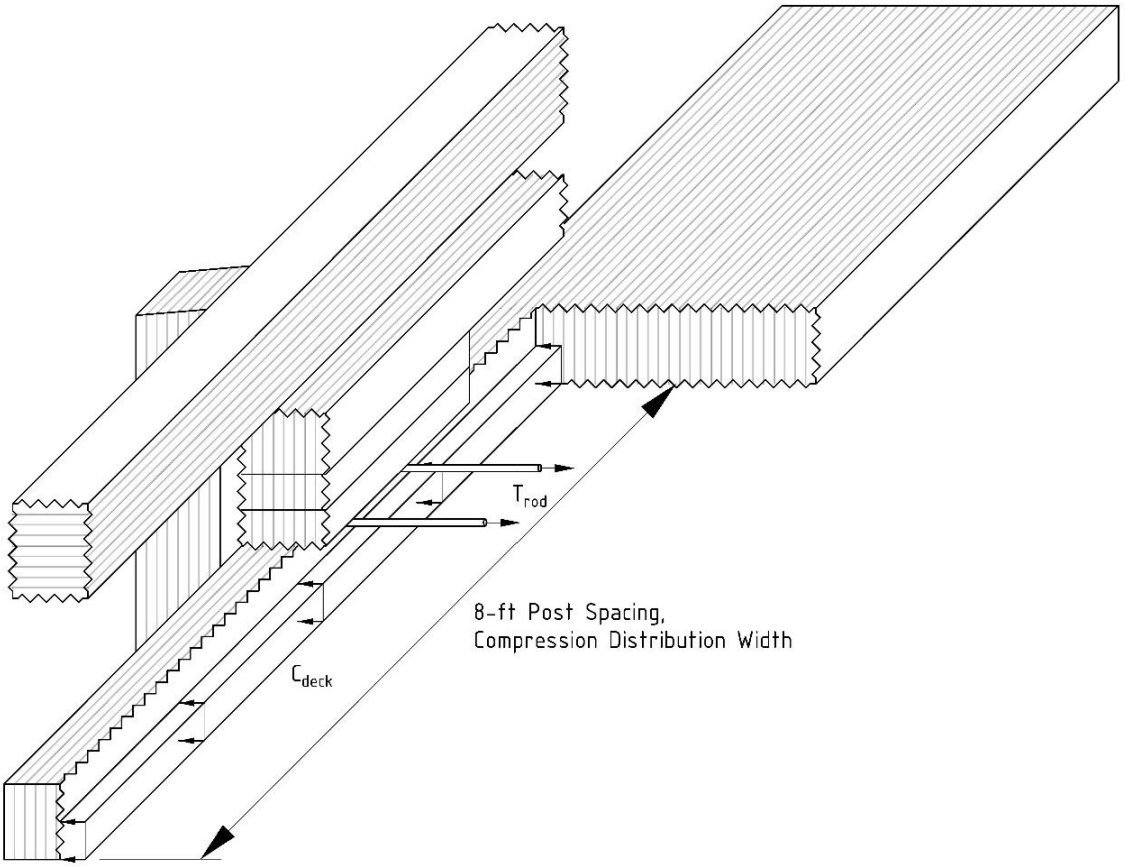

Figure 100. Longitudinal Deck Cutaway View

The compressive stress of the deck was approximated by a single value rather than a function. Tabulated values are based on the average compressive strength at 0.04 in. deformation [14], but higher deformations create higher compression strengths [92-93]. The compressive strength at 0.04 in. deformation was taken because it represented a stress estimate close to the compression perpendicular to grain yield limit, beyond which higher deformation did not result in significantly higher stresses [92-93, 131]. AASHTO's higher estimate for compression strength at 0.04-in. deformation was chosen to be consistent with how the scupper block compressive strength was defined for the post yield moment in section 3.2.1.3. AASHTO's Douglas Fir-Larch Combination 2 Glulam wood had a tabulated compressive strength of 0.56 ksi, and the factored strength was 1.176 ksi for Douglas Fir Larch [15].

The depth of compressive stress distribution was along the deck thickness. Three stress distributions were considered: uniform; triangular; and concrete (like reinforced-concrete equations for wood in the Phase IIa report), as shown in Figure 101. The uniform stress distribution was selected, because it was simpler, and the differences between stress distribution methods were not significant. The estimated tensile forces on the transverse deck rods was less conservative by ~2 to 5% using the uniform stress distribution as compared to the triangular and concrete distributions.

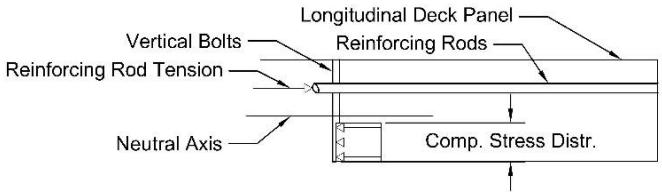

(a) Phase IIa Concrete Stress Distribution

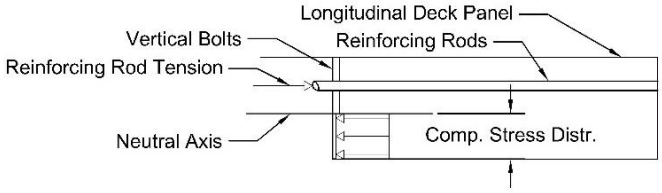

(b) Uniform Stress Distribution

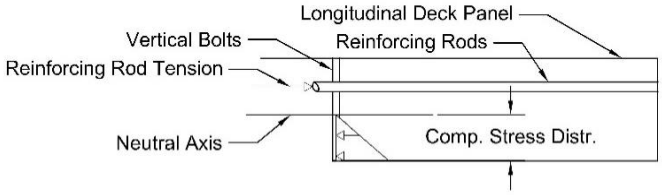

(c) Triangular Stress Distribution

Figure 101. Longitudinal Deck Stress Distributions Along Deck Thickness: (a) Phase IIa Concrete Stress Distribution; (b) Uniform Stress Distribution; and (c) Triangular Stress Distribution

Initial parameter values were 10¾ in. for the deck thickness, an applied moment of 1327.8 k-in. from the post (section 3.2.2), friction of 64.9 kips (section 3.3.3.2), post compression of 50.9 kips (section 3.3.2.1), and bolt shear of 25.8 kips (section 3.3.3.2). Equation 25 was solved by using a nonlinear solver to find the value of "a" at which the moments were equal to 0. Once "a" was obtained, the tensile demand on the rods was computed from Equation 26, 253 kips. For 12¼-in. thick glulam decks, the tensile demand decreased to 210 kips, demonstrating a significant reduction in rod demand based on the deck thickness.

ASTM A722 ⅝-in. diameter rods were previously used in the longitudinal glulam deck systems to meet NCHRP-350, but are no longer readily available. Williams Form Engineering does not offer them, and neither does Dywidag in their respective brochures [134-137]. Con-tech Systems, a company manufacturing ASTM A722 rods, no longer manufactures ¾-in. diameter rods [138] and likely not ⅝-in. diameter rods. Wheeler Consolidated Inc. raised concerns that the ⅝-in. diameter rods could only be purchased from Dywidag at a high cost [99]. The high cost was likely due to their specialized manufacture. Therefore, multiple options were explored and specified for the stressing rods so that timber bridge contractors had options for construction. Table 24 shows the longitudinal reinforcement specifications, rod diameters, and number of rods required to resist the impact loads for 10¾-in. thick Douglas Fir-Larch glulam decks. The ASTM A193 B7 specification includes 1-in. diameter rods even though they are slightly (5% to 10%) below strength. Southern Pine Glulam is typically denser than Douglas Fir, and transverse rods sufficient for Douglas Fir are also sufficient for Southern Pine.

Table 24. Longitudinal Deck Reinforcement Options for 10¾-in. thick deck

Specification	Tensile Strength (ksi)	Rod Diameter (in.)	Rod Net Area (in.)	Rupture Capacity (kip)	No. of Rods
ASTM A722 Grade 150	150	1	0.85	102.4	4
ASTM A354 BD	150	1	0.60	71.6	4
ASTM A615 Grade 97	115	1	0.76	70.4	4
ASTM A615 Grade 80	100	1	0.79	63.2	4
ASTM A193 B7	125	1	0.60	60.0	4

In addition to flexural failure modes, the longitudinal timber deck may be vulnerable to punching shear failure modes. The mechanics of this shear failure were initially investigated by examining similar punch-out shear failure modes in concrete. Punching shear capacity for concrete decks is estimated by multiplying shear strength by the shear failure area. The shear strength of the concrete deck is an estimated effective shear strength, and the distribution of load is assumed to be 45 degrees going into the deck from the compression area, as shown in Figure 102. "B" is the distance between the centerline of the bolts and the center of compression. "E" would be the distance between the center of compression and the edge of deck. "W_b" is the width of the scupper, and "h" is the deck thickness.

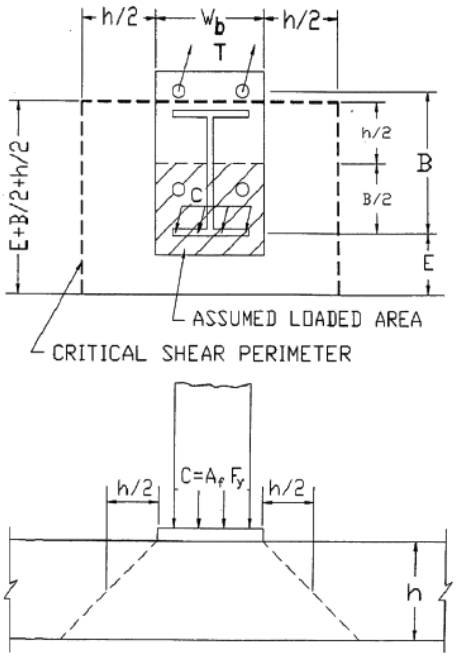

Figure 102. AASHTO Punching Shear Failure for Concrete Decks [15]

Adjusting parameters for concrete shear punchout for timber required some assumptions about how timber failure would occur. Timber is anisotropic, and shear failure along the longitudinal deck grain is more likely because of the weakened strength in that direction. The 45-degree failure line would reduce to 0-degrees. At the ends of the scupper, the failure plane would need to occur perpendicular to the wood grain. Wood typically does not fail perpendicular to grain because other failures occur first [132-133]. Shear parallel to grain was assumed to occur, but crack at a 45-degree angle between laminations, similar to concrete. This would reflect how when shear develops in an element, shear in the opposite direction develops to resist rotation, so the parallel to grain direction controls failure [134]. The punching shear area was calculated by Equation 27. The shear area was 663.6 in.^{2}. The tabulated shear strength was 0.265 ksi, which was adjusted for load duration, 2 for impact loads. The safety factor, 10/13, was removed to obtain an estimate closer to actual strength. The final shear strength was 0.689 ksi, and the punchout shear capacity was 457.2 kips.

$$A_{shear} = (W_b + 2E)h \qquad \text{Eq. (27)}$$

3.4.2.1 Critical Deck Type

Bridges constructed with glulam, spike-laminated, or stress-laminated decks have standard thicknesses based on typical wood member widths and thicknesses. The GC-8000 bridge railing was crash tested on a 10¾-in. thick longitudinal deck [16], which was taken as the baseline deck thickness for MASH 2016 TL-4.

Standard stress-laminated decks fabricated from glulam use a minimum thickness of 12 in. and therefore possess greater deck capacity as compared to glulam decks with a 10¾ in. thickness

[32]. Standard deck thicknesses and span lengths for Glulam decks are shown in Figure 103. The 12-in. thickness removed stress-laminated decks from consideration for the critical deck type, because the thickness played a significant role in increasing longitudinal deck capacity.

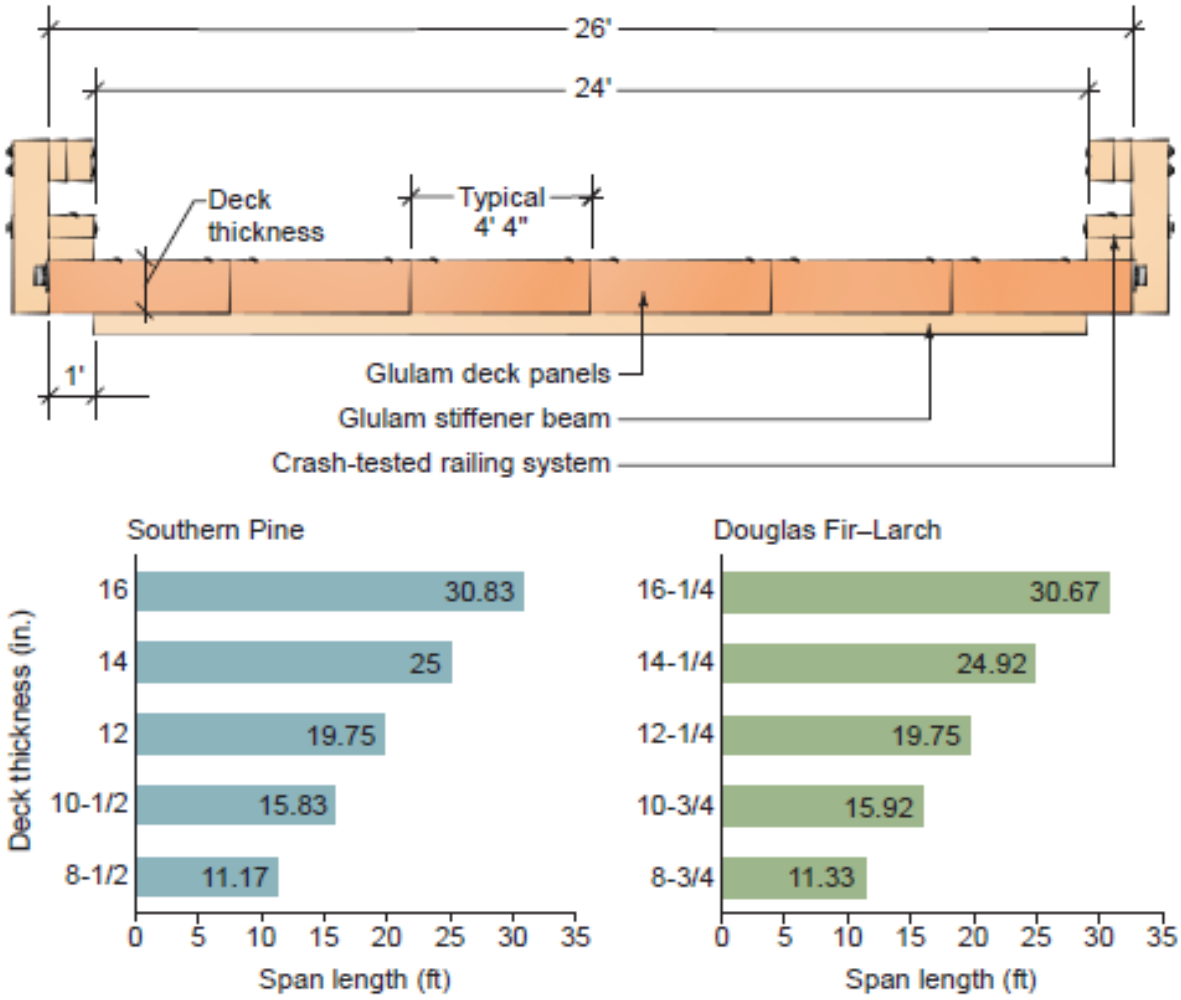

Figure 103. Longitudinal Glulam Deck Cross-Section (Top) and Span Charts for Multilane Bridges (Bottom) [32]

Stress-laminated decks may also utilize beams or girders, as shown in Figure 104, to reduce potential deck thickness. Stress-laminated decks utilizing beams may possess a minimum thickness of 5½ in. as compared to a glulam deck thickness of 10¾ in. The thinner stress-laminated deck superstructure designs were not considered for MASH 2016 TL-4, because of the dramatic difference between 5½ and 10¾-in. deck thicknesses and the critical role deck thickness played in longitudinal deck resistance to flexural loads.

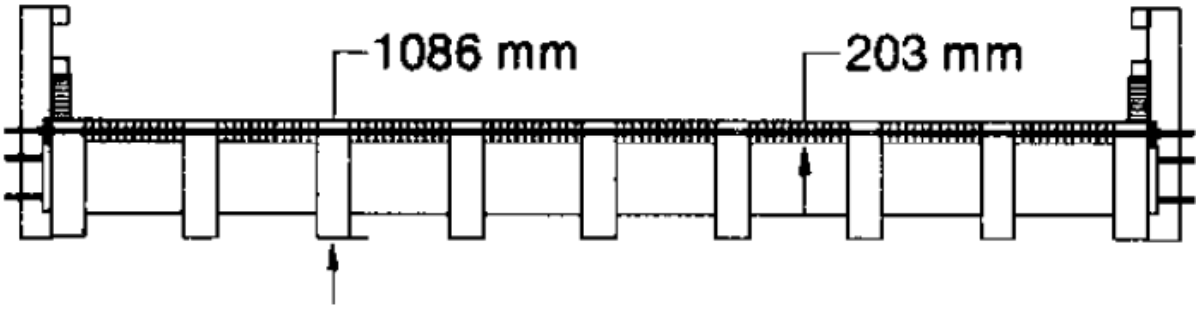

Figure 104. Cross-Section of Stress-Laminated Bridge Deck with Girders in Deck [69]

Standard member sizes for spike-laminated decks and stress-laminated decks built from sawn lumber are based on dressed, rough sawn, or full-sawn sizes. Dressed lumber is cut to the nominal size and left to dry before surfacing, which typically cuts off about ¼ in. from surfaced side, with actual dimensions about ½ in. less than the nominal dimensions. Rough sawn lumber has been cut to the specified size but not surfaced; these sizes are more variable and can be ⅛ in. larger or small than the nominal size. Full sawn lumber is surfaced to the same dimensions as the nominal size [15].

Spike-laminated bridges, as discussed in the literature review, are typically built from rough sawn lumber, but are closer to the nominal thickness of a deck than dressed lumber because only one side is surfaced. Thus, a nominally 12-in. thick deck would be 11¾ in. thick. Spike-laminated decks that were nominally 10 in. thick were also typically built for very short spans of 10 ft or so [62], which are typically found with low-volume roads for which TL-4 bridge railing is unnecessary. Once the deck thickness has been increased from 10 in. to 12 in., the flexural capacity of the deck increased substantially with thickness, making the spike-laminated deck more likely stronger than stress-laminated or longitudinal glulam decks on bridges which need TL-4 railings. The greater thickness-to-span ratio removed them from consideration for the critical deck type.

Stress-laminated decks built from sawn lumber with a lower thickness (10 in. nominal) were weaker than 10¾-in. thick glulam decks and could be considered a more critical deck type. The nominal thickness of 10 in. (9.75 in. actual for surfacing on only one side) increased the tensile demand to 298 kips and limited transverse rod options to only the strongest (ASTM A722). However, 10-in. thick nominal sawn stress-laminated decks were not selected, because few sawn stress-laminated bridges in the US were found over the course of the literature review (none aside from demonstration bridges), and the benefits of proving their strength were not clear for TL-4 bridge railings.

Although not discussed in the development of the GC-8000 bridge railing on longitudinal glulam decks, it was important to consider whether reinforcing rods need to be used with stress-laminated bridge decks. Earlier details for railings on stress-laminated bridges have not included reinforcement at post locations, trusting the existing prestressing rods to accomplish this task [80]. However, a more recently developed bridge railing in Norway for a stress-laminated deck (discussed earlier in this report) had included additional rods for the railing [26]. The current guidelines for stressing rod placement on decks using glulam beams is placing a rod at least every 4 ft [32], which falls short of the rod spacing currently estimated for 10¾-in. thick glulam decks:

4 rods within 4 ft – 10 in. Stressing rods may rupture during impact if no additional reinforcement is provided beyond requirements – especially given the existing stress in the rods. At least as many stressing rods are recommended within the post region as are typically provided for glulam deck.

3.4.3 Transverse Deck

Transverse decks need to handle lateral, longitudinal, and vertical vehicle impact loads from Design Cases 1 and 2. In addition to impact loads in each direction, the lateral load places a large flexural load onto the bridge deck as a result of the railing load distribution which manifests as a couple of tension and compression. All these load orientations are shown in Figure 105. Similar to the longitudinal deck, the vertical loads of Design Case 2 were significantly lower than the induced vertical forces which developed to resist lateral loads. Therefore, Design Case 2 was ignored.

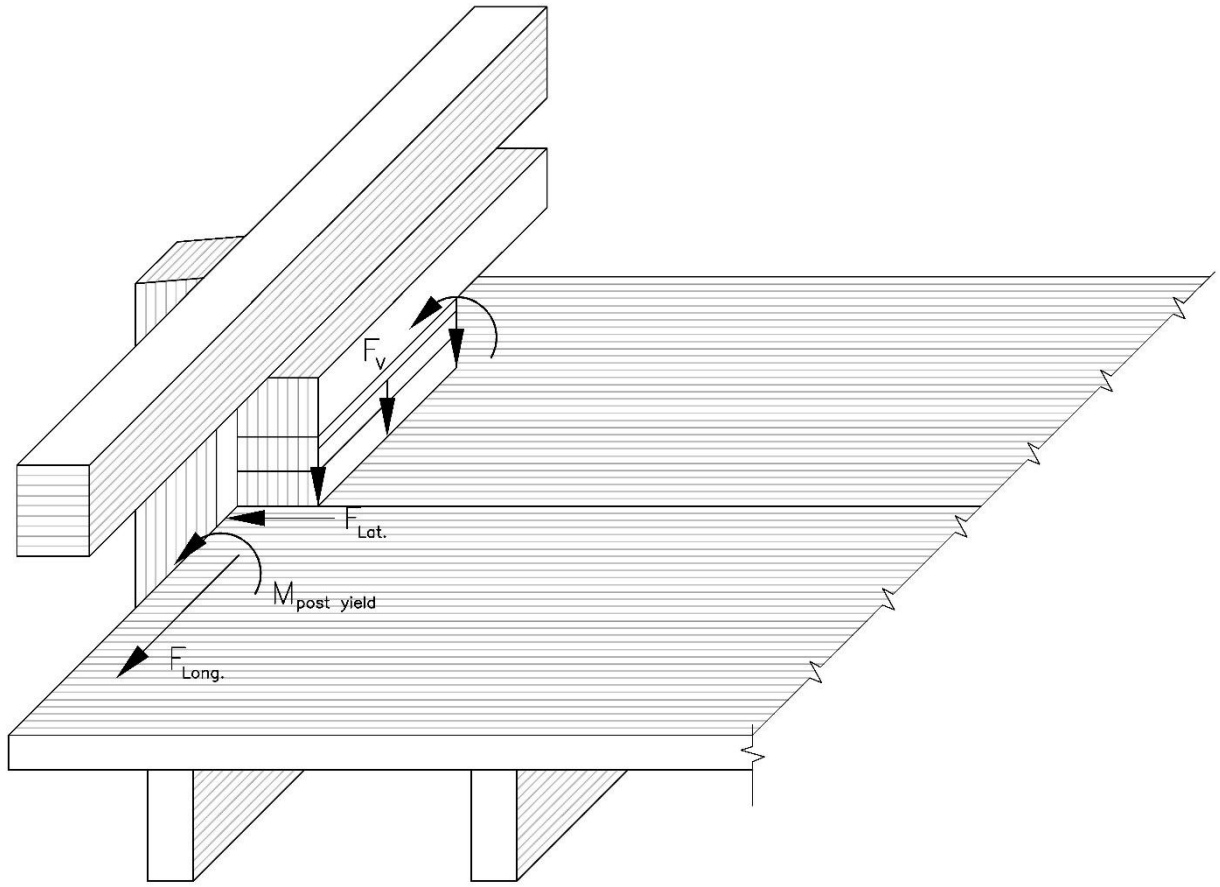

Figure 105. Transverse Deck External Force Diagram

For transverse decks, the deck overhang region was the primary area of concern, but no specific guidance existed for timber deck overhang design in AASHTO Chapter 13 [15]. As a result of a lack of specific guidance, previous crash testing experience at MwRSF and a basic knowledge of engineering mechanics served to outline the design methods and capacities.

The Glulam Rail and Curb on Transverse Glulam Deck successfully withstood NCHRP-350 TL-4 impact with a 5⅛-in. thick transverse timber deck with each post connected to two 4-ft wide deck panels. This bridge railing is shown in Figure 106. The transverse glulam timber deck panels functioned like a cantilever arm resisting flexure in the same orientation as the y-y tabulated bending strength. The two 4-ft wide panels to which each post was connected provided flexural resistance, which was characterized by timber flexural strength, distribution width, and thickness.

Figure 106. MwRSF NCHRP-350 TL-4 Tested Timber Bridge Railing [20]

The transverse deck thickness was straightforward to determine, and the flexural strength was determined by adjustments to the tabulated strength for end use. However, the width of distribution was difficult to determine. The width was limited by the panel width, but there were some questions about how much deck width beyond the scupper ends was involved, if any. A conservative estimate of distribution width limited the distribution width to the scupper, assuming shear failure initiates where the scupper block compresses the transverse deck. Without more information, and knowing that previous testing did not indicate failure, the width of the scupper block was selected as the distribution width for flexural loads in the deck.

The timber bridge flexural demand was 1,327.7 kip-in., with an additional 40 kips at the top of the bridge deck to escalate the extreme fiber tension. The 40 kips was assumed to cause an equal degree of compression at the bottom of the bridge deck with a centroid of rotation in the middle of the deck, so that the overall flexure is 1,430 kip-in.

The capacity of the timber deck was estimated as the section modulus multiplied by the flexural strength. The section modulus assumed that the width of the deck in flexure corresponded

to the length of the scupper, 58 in. For a 5⅛-in. thick deck panel (the thinnest available glulam panel), the section modulus would be 253.90 in.^{3}. The flexural strength of the deck was estimated from the tabulated values for Combination No. 2 Douglas Fir Glulam y-y bending flexural strength, 1.8 ksi. The tabulated strength was adjusted by removing the 10/13 safety factor, from 5% to 50% (1.33 from Phase IIa [10-11]), the volume factor (0.921), and the load duration factor (2 for impact loads). The final flexural strength was 5.731 ksi, and the flexural capacity was 1,455 kip-in., exceeding the 1,430 kip-in. demand.

The punching shear failure mode was investigated for the transverse glulam deck with the same parameters, which were used for the longitudinal glulam deck. Only the grain orientation was changed, which modified how the area in shear was calculated. The transverse deck grain orientation is parallel to the lateral direction and perpendicular to the longitudinal direction, and so the ends of the scupper were more likely to shear downwards while the shear failure plane along the back of the scupper extended at a 45-degree angle. These adjustments are shown in Equation 28.

$$A_{shear} = \left(W_b + 2\left(E + \frac{B}{2} + \frac{h}{2}\right)\right)h \qquad \text{Eq. (28)}$$

The shear demand was estimated from the tension in the eight vertical bolts holding the bridge railing to the deck, about 216 kips. The shear capacity of the bridge deck was estimated as described by Equation 28, which obtained a shear area of 374.1 in.^{2}. The shear strength of the bridge was also obtained from tabulated values and adjusted by removing the safety factor of 10/13 and using an impact load duration factor of 2. No shear reduction value was included for the same reasons discussed in section 3.3.5. The final shear strength was 0.689 ksi, and the shear capacity was 335.07 kips, exceeding the 216-kip demand. A 5% to 50% percentile adjustment to shear was not necessary, without the adjustment, the capacity would be 257.7 kips, still sufficient.

Longitudinal loads were not found to demonstrate a mode of failure for the transverse deck because the failure mode could not cause a failed crash test by itself. In combination with lateral loading, it did not make the failure mode more severe. If delamination were to occur due to longitudinal loading, the lateral loading would still utilize the full flexural resistance of the wood beneath the scupper. The shear punchout failure mode was also not made worse by delamination, because the failure plane still needed to shear away the transverse deck along the grain.

3.4.3.1 Critical Deck Type

The only two bridges for consideration for the critical deck type were glulam and spike-laminated bridges. As of the writing of this report, cross-laminated deck panels were under study, and it was not clear how existing lamination layups would perform, or which would be selected as the minimum tolerable configuration for timber bridges.

The minimum thickness for a glulam panel bridge deck is 5⅛ in. [31], which has already been tested in a full-scale crash test at MwRSF for NCHRP-350 TL-4 impact conditions [25]. The NCHRP-350 TL-4 bridge deck thickness was the starting point for MASH 2016 TL-4 deck thickness. The potential mass of wood in resistance is limited to two deck panels, but these decks

are rated to have a higher stiffness than any other deck type, so they were more likely to utilize more of the panel beyond the scupper length.

Spike-laminated decks were made from full-sawn lumber, so their thicknesses were estimated to be about ¼ in. less than the nominal, according to Wheeler's method of manufacture. This construction method ended up with an actual deck thickness of 5¾ in. for a 6-in. nominal deck. The difference was marginal for a 6-in. nominal deck, but much more significant for an 8-in. nominal deck, which was 7¾ in. rather than 6¾ in. The spike-laminated deck could hypothetically transfer flexural load beyond the limits of the scupper, but the stiffness of these decks was limited by the means used to transfer load. Both glulam and stress-laminated decks demonstrate continuous load transfer between laminations, but spike-laminated decks were limited to spike locations. Furthermore, spike-laminated decks were built with sawn lumber, which was significantly weaker than glulam lumber for the same species.

Although the spike-laminated deck was considered more critical for the transverse timber deck type of the same nominal thickness, it was nevertheless decided that glulam deck panels would be used for testing. This decision was due to two factors beyond the analysis discussed, (1) a glulam 5⅛-in. thick timber bridge deck from a previous project was already present at the test site and could be reused for dynamic component testing, and (2) Wheeler Consolidated Inc. was primarily responsible for building spike-laminated decks and testing one of their decks was felt to be a benefit specifically to them rather than to all timber bridge manufacturers.

3.5 Final Bridge Rail Configuration Recommendation

The completed MASH 2016 bridge rail design is shown in Figure 107, attached to the recommended decks. The recommended transverse glulam deck is 5⅛-in. thick, with the post sitting over the gap between two 4-ft wide panels. The recommended longitudinal glulam deck 10¾-in. thick deck utilizes four 1-in. diameter ASTM A193 Gr. B7 threaded rods.

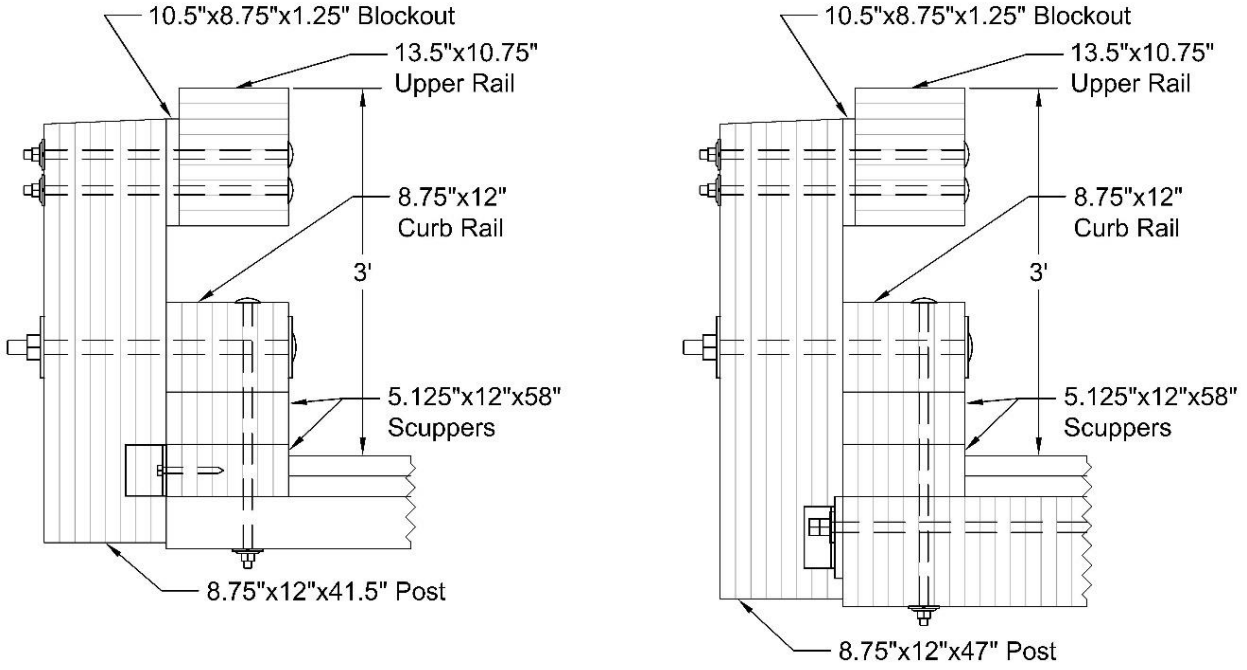

(a) (b)

Figure 107. (a) MASH 2016 Bridge Rail Design on Transverse Deck and (b) Longitudinal Deck

A dynamic component test plan for evaluating the bridge railing and deck configuration was developed for the two recommendations. The test plans are discussed in greater detail in section 5.1, and the first test was conducted and is evaluated through the remainder of chapter 5.

4 APPROACH GUARDRAIL TRANSITION DEVELOPMENT

4.1 Introduction

This research involved the development of an AGT system designed to satisfy the MASH 2016 TL-3 impact safety criteria, in conjunction with the design of a MASH 2016 TL-4 glulam timber bridge railing. In addition to meeting the impact performance requirements, the AGT was designed to accommodate a future 2-in.-thick wearing surface (similar to the bridge railing), connect to the MGS, include a properly stiffened upstream transition, mitigate excessive vehicle snagging or pocketing, and provide a continuous load path connecting both the upper and lower rails of the bridge railing to a single AGT structure.

To support the development of the AGT, a literature review was conducted focusing on AGT systems utilizing post cross sections larger than 6 in. x 8 in. (Section 2.3), along with a brief summary of the MGS system to which the AGT would be connected (Section 2.4). The review addressed key issues, such as upstream stiffness transition design, accommodation of future overlays or wearing surfaces, and conceptual AGT systems employing timber posts.

The design process commenced with the calibration of a BARRIER VII finite element model representing a previously crash-tested TL-4 AGT connected to a TL-4 timber bridge railing (Section 2.3.3). Calibration was intended to improve the accuracy of simulated impact conditions. Upon successful calibration, the design of the AGT-to-bridge railing connection was initiated. Multiple connection configurations were brainstormed and conceptually evaluated, considering the entire AGT system. Two candidate designs were selected for detailed study, and corresponding BARRIER VII models were developed to simulate their performance under TL-3 impact conditions.

In parallel with the simulations, bogie testing was performed to evaluate proposed post-in-soil configurations. These tests were particularly important for one concept that lacked detailed existing information. The results were used to update the finite element models. A critical impact point (CIP) analysis was also conducted to identify the most demanding impact locations.

4.2 BARRIER VII Model Calibration

In 1997, two full-scale crash tests, designated as TRBR-3 and TRBR-4, were conducted on an AGT system that connected an NCHRP Report 350 TL-4 glulam timber bridge railing to a strong-post W-beam guardrail system [25]. The AGT demonstrated successful performance in both tests and was selected as the reference system for developing an AGT capable of satisfying MASH TL-3 criteria while connecting the glulam timber railing to the MGS.

Prior to conducting the TRBR-3 and TRBR-4 crash tests, simulations of the AGT were performed using the BARRIER VII software. Following the tests, the simulation model was not updated to reflect the physical results. Therefore, in this study, the original BARRIER VII model was recalibrated to better represent the test outcomes and to serve as a more accurate platform for evaluating new AGT designs.

Calibration was performed by comparing key performance metrics from the crash tests with simulation outputs from BARRIER VII. These metrics included maximum dynamic railing

deflection, vehicle exit speed and time, and vehicle parallel speed and time. Because no post failures were observed during the physical tests, the simulation was required to reproduce this result.

To manage the number of variables within BARRIER VII, a structured calibration approach was adopted by grouping the parameters into five categories. The first group included adjustments to vehicle impact conditions, such as speed and angle. The second group focused on improving model precision by refining the mesh with a greater number of nodes and elements. The third group revised the material and geometric properties of the glulam bridge railing and its supporting posts, using data from the Phase IIa calibration effort. The fourth group updated the AGT post properties for both the 8-in. x 8-in. and 6-in. x 8-in. sections. The final group consisted of minor adjustments for fine-tuning and included discussion of parameters that did not improve model fidelity or were not representative of physical behavior.

4.2.1 Original Model Parameters

The baseline AGT model used for calibration was based on the configuration that performed successfully in crash tests TRBR-3 and TRBR-4. A geometric layout of the model is presented in Figure 108, which illustrates the types of beams and posts used in each segment of the system. Specific properties for each beam and post type are listed in Tables 25 and 26, respectively. This model was obtained from the MwRSF archives and executed using the BARRIER VII software. The model was verified to be complete and free of errors. Results from this initial simulation, prior to any calibration, are summarized in Table 27.

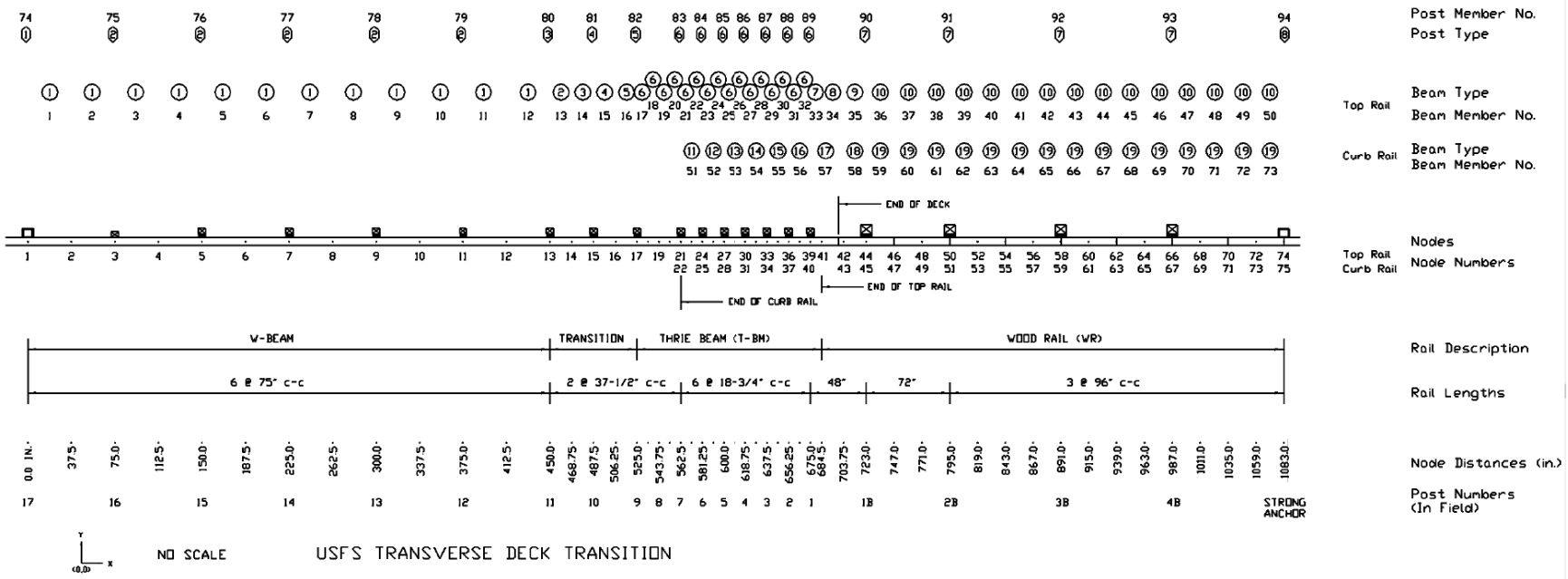

Figure 108. BARRIER VII Model Developed for Design of AGT Connection Glulam Timber Bridge Railing with Curb Rail and Strong W-Beam Guardrail [25]

This model was developed to resist longitudinal barrier crash conditions specified by NCHRP Report 350 TL-4. For Test 4-11, which corresponds to crash test TRBR-3, the required impact conditions involve a vehicle mass of 2,000 kg traveling at 100 kph and striking the barrier at a 25-degree angle. For Test 4-12, corresponding to TRBR-4, the vehicle mass must be 8,000 kg, with an impact speed of 80 kph and an impact angle of 15 degrees. Although these conditions represent the target values, minor deviations are permitted because achieving exact specifications during full-scale crash testing is often impractical due to time and cost constraints.

Table 25. BARRIER VII Model for 1997 Crash-Tested System Beam Properties

Beam No.	Moment of Inertia (in.^{4})	Area (in.^{2})	Length (in.)	Young's Modulus (ksi)	Weight (lb/ft)	Yield Force (k)	Yield Moment (k-in.)
1	2.31	1.99	37.5	30000	6.92	99.5	68.5
2	2.48	2.13	18.75	30000	7.40	106.2	73.8
3	2.84	2.40	18.75	30000	8.38	120.0	84.0
4	3.20	2.68	18.75	30000	9.35	134.0	94.0
5	3.58	2.96	18.75	30000	10.32	148.0	104.2
6	4.82	4.00	9.375	30000	13.95	200.0	140.0
7	4.82	4.00	9.5	30000	13.95	200.0	140.0
8	753.7	118.1	19.25	1400	41.0	67.9	1098.4
9	753.7	118.1	19.25	1400	41.0	67.3	1098.4
10	753.7	118.1	24.00	1400	41.0	67.9	1098.4
11	12.32	19.13	18.75	1500	6.63	6.38	50.0
12	49.36	30.38	18.75	1500	10.54	6.38	50.0
13	127.02	41.63	18.75	1500	14.44	6.38	50.0
14	260.36	52.88	18.75	1500	18.34	6.38	50.0
15	464.41	64.13	18.75	1500	22.25	6.38	50.0
16	754.23	75.38	18.75	1500	26.15	6.38	50.0
17	972.00	81.00	28.75	1500	28.1	46.6	50.0
18	972.00	81.00	19.25	1500	28.1	46.6	50.0
19	972.00	81.00	24.00	1500	28.1	46.6	50.0

Table 26. BARRIER VII Model for 1997 Crash-Tested System Post Properties

Post No.	Height of Node I (in.)	Height of Node j (in.)	k_A (k/in.)	k_B (k/in.)	W (lb)	M_B (k-in.)	M_A (k-in.)	Yield Accuracy Limit (%)	V_A (k)	V_B (k)	δ_A (in.)	δ_B (in.)
1	21	0	102.5	2.48	70.4	735	191.1	0.1	35	13.8	20	20
2	21	0	1.95	1.56	70.4	214.2	191.1	0.1	18.8	13.8	20	20
3	21	0	1.67	1.67	93.9	377.9	377.9	0.1	27.6	27.6	20.1	20.1
4	21	0	1.67	1.67	93.9	444.2	444.2	0.1	27.6	27.6	20.1	20.1
5	21	0	1.67	1.67	93.9	413.6	413.6	0.1	27.6	27.6	20.1	20.1
6	21	8.13	1.67	1.67	93.9	413.6	413.6	0.1	27.6	27.6	20.1	20.1
7	18	0.25	9.01	13.05	106.3	683.4	820.1	0.1	52.8	52.8	5.8	4.8
8	18	0.25	6338	13943	94.7	6820	1540	0.1	310	70	1	1

Overall, the target impact conditions produced higher dynamic deflections and longer exit times in both simulations compared to the crash tests. However, the simulated parallel time was shorter, and the simulated parallel velocity was greater than those recorded during the full-scale crash tests. A detailed comparison of the simulated results and actual crash test data for TRBR-3 and TRBR-4 is provided in Table 27. For Test TRBR-4, there was a significant discrepancy between the simulation and the crash test results in terms of vehicle exit speed and exit time. This difference occurred because, during the crash test, the rear portion of the truck leaned over the bridge railing and contributed to pulling the vehicle over the barrier. BARRIER VII lacks the capability to simulate vehicle rollover or significant leaning onto the barrier system. As a result, it was not possible to represent this behavior in the model, and the associated exit speed and exit time were excluded from the evaluation of model accuracy for TRBR-4.

Table 27. Comparison of Simulated Target Impact Conditions to TRBR-3 and TRBR-4

	Maximum Dynamic Deflection (in.)	Parallel Time (sec)	Parallel Velocity (mph)	Exit Time (sec)	Exit Velocity (mph)	Average Error
Test No. TRBR-3	6.42	0.243	45.36	0.553	44.18	
BARRIER VII Simulation	8.49	0.190	46.84	0.275	45.30	
% Error	32.24%	-21.81%	3.25%	-50.27%	2.54%	22.02%
Test No. TRBR-4	4.88	0.508	42.13	2.818	15.72	
BARRIER VII Simulation	8.20	0.324	43.40	0.594	42.13	
% Error	67.97%	-36.22%	3.02%	-	-	35.74%

4.2.2 TRBR-3 and -4 Impact Conditions

The calibrated BARRIER VII model was evaluated using the actual measured impact conditions from crash tests TRBR-3 and TRBR-4. For TRBR-3, the impact conditions included a vehicle mass of 2,029 kg, a speed of 104.9 kph, and an impact angle of 26.4 degrees. The corresponding vehicle weight was 4,473.2 lb, slightly higher than the nominal value of 4,410 lb. Additionally, the railing friction coefficient was increased from 0.3 to 0.45. For TRBR-4, the actual impact conditions included a vehicle mass of 8,003 kg, a speed of 82.5 kph, and an impact angle of 13.7 degrees. The corresponding vehicle weight was 17,643.6 lb, compared to the nominal 17,637 lb. The railing friction coefficient in this case was 0.64 instead of the default 0.3. No other input parameters were modified. Using these actual impact conditions, the model was simulated and compared to the full-scale crash test results. A detailed comparison of simulation outputs and measured data for both TRBR-3 and TRBR-4 is presented in Table 28.

Table 28. Comparison of Original Model with Actual Impact Conditions to TRBR-3 and TRBR-4

	Maximum Dynamic Deflection (in.)	Parallel Time (sec)	Parallel Velocity (mph)	Exit Time (sec)	Exit Velocity (mph)	Average Error
Test No. TRBR-3	6.42	0.243	45.36	0.553	44.18	
BARRIER VII Simulation	12.48	0.222	40.06	0.344	39.28	
% Error	94.54%	-8.64%	-11.68%	-37.79%	-11.10%	32.75%
Test No. TRBR-4	4.88	0.508	42.13	2.818	15.72	
BARRIER VII Simulation	8.06	0.370	40.61	-	-	
% Error	65.10%	-27.17%	-3.61%	-	-	31.96%

When the actual impact conditions were incorporated into the simulation, the average error for the pickup truck (TRBR-3) increased from 22.02% to 32.75%. This increase is primarily attributed to the higher impact speed and angle relative to the nominal conditions. In contrast, the average error for the single-unit truck (TRBR-4) decreased from 35.74% to 31.96%. The reduced error is likely due to the lower impact angle, which led to a less severe crash event. As a result, the original model's tendency to overpredict deflection, parallel velocity, and parallel speed was less pronounced in the case of the single-unit truck.

It is important to note that the evaluation of the TRBR-4 simulation excluded exit speed and exit time, because these results were significantly affected by physical behavior observed in the crash test that BARRIER VII cannot simulate. The truck body leaned over the bridge railing after impact and remained in contact, which prevented the vehicle from moving away cleanly. This behavior is outside the modeling capabilities of BARRIER VII, which does not support simulation of vehicle rollover or sustained interaction with the railing. Additionally, both simulations resulted in failure of a single post, a behavior that was not observed in either of the corresponding crash tests. This discrepancy suggests that while the model captures general trends in system response, further refinement may be needed to accurately reproduce localized structural behavior.

4.2.3 Expanded Node Array

Advancements in computer hardware and software capabilities have allowed for greater modeling precision within the BARRIER VII program compared to the version used during the original development of the AGT model. These improvements were implemented by researchers at MwRSF around the year 2000 and have enabled the use of significantly larger node and element arrays without compromising computational efficiency.

As a result, the updated BARRIER VII model includes a higher resolution mesh, allowing for more detailed representation of the system geometry. The original model was limited in terms of node and element count, containing 75 nodes and 94 members, which included 73 beam elements and 21 posts. This limitation also restricted the number of bridge rail posts that could be explicitly modeled, and it required the use of relatively large element sizes.

In contrast, the revised model employed a finer discretization strategy. By reducing element sizes and increasing the number of nodes, the updated model consisted of 598 nodes and 629 members, of which 596 were beam elements and 33 were posts. This enhanced resolution enabled a more detailed and accurate simulation of the system response to vehicular impact. The updated model layout is illustrated in Figure 109, and the comparison of simulation results to the crash test data is presented in Table 29.

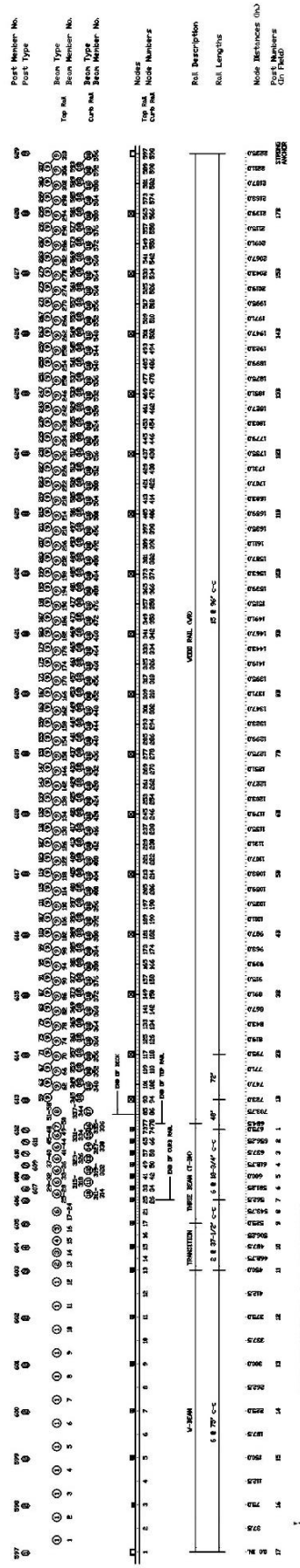

Figure 109. BARRIER VII Model of Expanded Nodes and Elements

The results from Table 29 show that the average error for the pickup truck was 30.83%, while the average error for the single-unit truck (SUT) was 27.13%. These values represent a slight decrease in error for both vehicle types compared to previous simulations. However, the simulation still resulted in a single post failure for both cases, which did not occur during the actual crash tests. To improve model accuracy, the density of the element array was first increased independently, prior to expanding the total number of nodes. This intermediate step yielded a modest improvement in the accuracy of the simulation. Following this, additional bridge posts were incorporated into the model to more accurately represent the actual number of bridge posts used in crash tests TRBR-3 and TRBR-4. The inclusion of these elements contributed to a more accurate representation of the physical system.

Table 29. Comparison of Expanded Node and Element Model with Crash Test Results

	Maximum Dynamic Deflection (in.)	Parallel Time (sec)	Parallel Velocity (mph)	Exit Time (sec)	Exit Velocity (mph)	Average Error
Test No. TRBR-3	6.42	0.243	45.36	0.553	44.18	
BARRIER VII Simulation	11.93	0.225	40.00	0.345	39.16	
% Error	85.94%	-7.41%	-11.82%	-37.61%	-11.36%	30.83%
Test No. TRBR-4	4.88	0.508	42.13	2.818	15.72	
BARRIER VII Simulation	7.43	0.377	40.71	-	-	
% Error	52.24%	-25.79%	-3.36%	-	-	27.13%

4.2.4 Bridge Railing and Post Properties

During Phase IIa of the research effort, a calibration study was conducted to develop a BARRIER VII model capable of replicating crash tests TRBR-1 and TRBR-2. As part of this effort, revised structural properties for bridge beams and posts were implemented in the model. However, an error occurred in this process: the wood species used for simulation was Douglas Fir-Larch rather than Southern Pine, which was the material used in the actual crash-tested bridge railing. This discrepancy most likely originated from the fact that the original BARRIER VII model used properties derived from Douglas Fir-Larch glulam. To correct this inconsistency, several key material properties were updated to reflect the characteristics of Southern Pine. These included the modulus of elasticity, unit weight, yield force, and yield moment. The original and revised beam input properties are summarized in Table 30.

Table 30. BARRIER VII Bridge Beam Input Properties, Original and New

Member	Model	Modulus of Elasticity, E (ksi)	Weight (lb/ft)	Yield Tension (kips)	Yield Moment (kip-in.)
8-9	Original	1400	41.0	69.9	1098.4
	New	1700	28.6	202.5	1160.0
10	Original	1500	6.63	6.38	50.0
	New	1400	4.9	8.3	43.7
11	Original	1500	10.54	6.38	50.0
	New	1400	7.7	64.8	110.3
12	Original	1500	14.44	6.38	50.0
	New	1400	10.6	88.8	207.1
13	Original	1500	18.34	6.38	50.0
	New	1400	13.5	112.8	334.2
14	Original	1500	22.25	6.38	50.0
	New	1400	16.4	136.8	491.5
15	Original	1500	26.15	6.38	50.0
	New	1400	19.2	160.8	679.1
16-17	Original	1500	28.1	46.6	50.0
	New	1400	20.7	95.4	749
18	Original	1500	28.1	46.6	50.0
	New	1400	20.7	143.1	749

In addition to the beam property updates, bridge post parameters were revised based on the Phase IIa calibration methodology. These updates included the post height, weight, stiffness, yield moment, shear strength, and failure deflection in both the longitudinal and lateral directions, labeled as the "A" and "B" axes, respectively. One additional correction was made after the Phase IIa work: the post weight was updated to include fasteners and other components that contribute to inertial resistance. This value was not initially included in the total post mass, which is important for simulating impact response. The updated post input values are shown in Table 31.

Table 31. BARRIER VII Bridge Post Input Properties, Original to New

BARRIER VII Input Property	Post 8		Post 9	
	Original	New	Original	New
Center of Upper Rail (in.)	18	28.25	18	28.25
Center of Curb Rail (in.)	0.25	10.125	0.25	10.125
"A" Axis Stiffness (k/in.)	9.01	30.01	-	-
"B" Axis Stiffness (k/in.)	13.05	22.44	-	-
Weight (lb)	106.3	170.1	-	-
"A" Axis Yield Moment (k-in.)	683.4	720.0	-	-
"B" Axis Yield Moment (k-in.)	820.1	833.1	-	-
"A" Axis Shear Failure (kip)	52.8	76.4	-	-
"B" Axis Shear Failure (kip)	52.8	94.9	-	-
"A" Axis Deflection Failure (in.)	5.8	4.0	-	-
"B" Axis Deflection Failure (in.)	4.8	10.0	-	-

4.2.4.1 Beam Yield Moment

The original AGT model used flexural and shear strength values based on NCHRP Report 350 tabulated average MOR values for Douglas Fir-Larch, specifically 6,800 psi for flexural strength and 960 psi for shear strength. These values are not appropriate for the present study because they are derived from ASTM D2555 average clear wood strength values, which are not adjusted for end-use conditions and apply to unseasoned coastal Douglas Fir [128]. Clear wood excludes knots, and unseasoned wood typically has lower strength than seasoned wood. Furthermore, these values are not applicable to glulam timber.

A more appropriate average MOR for glulam in this scenario can be derived from tabulated values that already account for grading rules, knot limitations, and other defects specific to each glulam combination. Both glulam and sawn lumber use the fifth-percentile values of strength distributions for design, so any average must be derived using a consistent adjustment methodology, as discussed during Phase IIa. The beam yield moment was calculated using the product of flexural strength and section modulus. Based on this approach, the upper rail yield moment for Southern Pine Combination 48 glulam was determined to be 1,160 kip-in. The curb rail yield moment, calculated from Combination 47 Southern Pine glulam, was 749 kip-in.

4.2.4.2 Beam Yield Force

The original beam tension capacities used in the model, such as the 67.9 kips assumed for some members, may have represented simplified mechanical assumptions or conservative limits for connector hardware. While these values provided a functional baseline, more detailed analysis of the mechanical connection limit states was performed in the current effort.

Updated yield forces were developed based on common failure mechanisms in glulam-to-steel connections. For the upper rail, row-tear-out of bolts from the wood was found to govern, with a capacity of 202.5 kips. For the curb rail, bolt shear was critical, with a capacity of 143.1 kips. These updated values are consistent with the nominal performance of bolted glulam connections and were applied in the BARRIER VII model to better approximate crash test behavior. In one specific case, Member 10 was limited to 8.3 kips, representing the nominal bolt shear capacity, as this member transfers axial force solely through a bolted connection.

4.2.4.3 Beam Modulus of Elasticity

The modulus of elasticity values used in the original model appear to be based on AASHTO LRFD Bridge Design Specifications from the 1990s, which included Combination 2 Douglas Fir-Larch glulam. These values assumed wet-use conditions unless specified otherwise. For example, the 1,400 ksi value for the upper rail suggests that a wet-use factor was applied, while the 1,500 ksi value used for the curb rail likely assumed dry-use conditions.

Given that the crash tests were conducted under dry conditions, the updated model adopted modulus values that reflect this environment. For the upper rail, 1,700 ksi was used, corresponding to Combination 48 Southern Pine glulam. For the curb rail, 1,400 ksi was applied, based on Combination 47 Southern Pine glulam. These selections align with dry-use assumptions, with moisture content below 16 percent and temperatures below 100 degrees Fahrenheit.

4.2.4.4 Beam Weight

The beam weights were updated to reflect an assumed average moisture content of 15%. Although the moisture content of the timber used in TRBR-3 and TRBR-4 was not explicitly recorded, the use of pressure treatment with pentachlorophenol and the presence of continuous airflow at the test site suggest that the wood was well-dried and unlikely to exceed typical air-dry moisture levels. Therefore, the updated weights are considered appropriate for this modeling effort.

4.2.4.5 Bridge Post Parameters

Several refinements were made to the post properties to improve consistency with the physical test configuration. The post height was adjusted to place the center of rotation at the top of the bridge deck rather than beneath the curb rail. Post weight was updated to include the scupper, and Phase IIa-based updates to stiffness, yield moment, and deflection capacities in both the longitudinal (A) and lateral (B) directions were retained.

Post shear strength was recalculated based on the mechanical performance of the bolted base connection rather than the material shear strength of the post. The base consists of six ¾-in. diameter bolts and split rings. The tabulated capacity of 3,660 lb per split ring in Southern Pine glulam (species group B) was adjusted using a group action factor of 1.0 for lateral loading and 0.8 for longitudinal loading. A geometry factor of 1.0 and a time-effect factor of 2.0 were also applied to better replicate the crash test behavior. Per recommendations from Forest Products Laboratory personnel, the allowable shear strength was converted to an estimated ultimate value by applying a multiplier of 2 [121]. The resulting total shear capacities were 87.8 kips for lateral loading and 70.7 kips for longitudinal loading.

4.2.4.6 Analysis Results

The analysis results for the updated model are summarized in Table 32. These results reflect the incorporation of revised beam and post properties based on glulam material specifications, connection mechanics, and dry-use assumptions. For TRBR-3, the average error across all metrics was 27.98%. For TRBR-4, the average error was 25.80%. These values are slightly higher than those obtained using only the updated node and element arrays, and a single post failed in both simulations, which did not occur in the physical crash tests. Nonetheless, the model still captured the key dynamic behaviors observed in the crash tests, and the results remain within an acceptable range for simulation-based calibration.

Table 32. Comparison of Updated Bridge Post and Railing Parameters with Crash Test Results

	Maximum Dynamic Deflection (in.)	Parallel Time (sec)	Parallel Velocity (mph)	Exit Time (sec)	Exit Velocity (mph)	Average Error
Test No. TRBR-3	6.42	0.243	45.36	0.553	44.18	
BARRIER VII Simulation	11.11	0.221	42.45	0.316	40.47	
% Error	73.16%	-9.05%	-6.42%	-42.86%	-8.41%	27.98%
Test No. TRBR-4	4.88	0.508	42.13	2.818	15.72	
BARRIER VII Simulation	7.18	0.365	41.22	-	-	
% Error	47.09%	-28.15%	-2.16%	-	-	25.80%

4.2.5 Revised AGT Post Properties

The AGT post parameters were one of the most important aspects of the calibration process. These parameters directly influence the structural behavior of the system and support all major design decisions for the new AGT. In particular, the relationship between the input values in BARRIER VII and physical properties, such as post spacing, embedment depth, wood species, and material grade is essential for producing realistic simulations that reflect crash test conditions.

Each AGT post in the model includes properties for height, axial and lateral stiffness, weight, yield moment about the major and minor axes, shear capacities in both directions, and deflection limits. These parameters affect how the posts respond under impact, including their resistance to bending and shear, as well as the extent of deformation.

The revised parameters were developed to better represent the expected behavior of glulam timber posts used in current AGT applications. These updates were guided by calibration data from

Phase IIa and reflect standard assumptions for modern glulam systems. The updated values also ensure compatibility with the structural characteristics of other components in the AGT system. A detailed comparison between the original 1997 post properties and the revised values is provided in Table 33.

Table 33. Summary of AGT Post Parameter Updates

Post	Model	k_A (k/in.)	k_B (k/in.)	W (lb)	M_A (k-in.)	M_B (k-in.)	V_A (k)	V_B (k)	δ_A (in.)	δ_B (in.)
1	1997	-	-	70.4	-	-	-	-	20.0	-
	Revised	-	-	47.6	-	-	-	-	5.0	-
2	1997	1.95	1.56	70.4	-	-	-	-	20.0	-
	Revised	11.3	4.2	47.6	-	-	-	-	4.0	-
3	1997	1.67	1.67	93.9	377.9	377.9	27.6	27.6	20.1	20.1
	Revised	11.3	11.3	57.2	377.4	407.8	47.6	47.6	5.0	10.0
4	1997	1.67	1.67	93.9	444.2	444.2	27.6	27.6	20.1	20.1
	Revised	11.3	11.3	61.4	351.7	380.1	47.6	47.6	5.0	10.0
5	1997	1.67	1.67	93.9	413.6	413.6	27.6	27.6	20.1	20.1
	Revised	11.3	11.3	70.9	310.9	336.0	47.6	47.6	5.0	10.0
6	1997	1.67	1.67	93.9	413.6	413.6	27.6	27.6	20.1	20.1
	Revised	11.3	11.3	86.4	307.0	331.8	47.6	47.6	5.0	10.0
7	1997	1.67	1.67	93.9	413.6	413.6	27.6	27.6	20.1	20.1
	Revised	11.3	11.3	91.9	413.0	446.3	47.6	47.6	5.0	10.0

4.2.5.1 Post Shear Limit

The origin of the post shear limit used in the original model could not be clearly identified, although it became evident during the calibration process that the assigned value was likely too low. In the simulation, this value led to premature post shear failure, which did not occur in either of the full-scale crash tests TRBR-3 or TRBR-4. Furthermore, shear failure has not been observed in any of the bogie tests on timber posts embedded in soil, where failure is consistently governed by flexural mechanisms [37, 39-40].

The tabulated shear strength for Southern Yellow Pine is consistent across all grades, including those classified as dense. A deeper review of the derivation of tabulated values revealed that a statistical adjustment factor of 1.3, based on a shift from the fifth percentile to the median using a coefficient of variation (COV) of 0.14, is typically used to approximate average behavior [60]. Additionally, design values commonly include a safety factor of 10/13, which corresponds

to an adjustment factor of approximately 1.3 when inverted [127]. For impact loading, a load duration factor of 2.0 may also be applied.

Despite applying these combined factors, the resulting shear strength estimate remained lower than the value used in the original model. Specifically, the adjusted value was approximately 23.8 kips, compared to the original model's 27.6 kips. This suggests that a strict interpretation of the adjustment process does not resolve the discrepancy observed between the simulated and tested behavior. Other considerations, including the distribution of shear force along the post, the distance to the point of rotation, and strength reduction factors applied under ASTM D245 (such as the 0.5 factor for strength ratio), further complicate a purely analytical derivation of shear capacity. However, detailed investigation of these factors was not feasible within the current project scope due to time constraints and the focus on other modeling priorities.

While the exact reason why shear does not govern failure remains uncertain, the consistent evidence from crash and bogie testing indicates that flexural behavior controls post response. Therefore, to better align the simulation with observed crash test behavior, the post shear limit in the BARRIER VII model was increased to 47.6 kips. This value was selected to prevent artificial shear failure in the model and allow the flexural limit states to govern, as they do in physical testing.

4.2.5.2 Post Yield Moment

The source of the post yield moment values used in the original AGT BARRIER VII model was not clearly documented. Rather than attempting to trace the origin of these values, this study adopted a previously established method for estimating AGT post yield strength that had been used in earlier BARRIER VII modeling efforts [37]. This approach involves estimating an average soil reaction force at a defined lateral deflection and embedment depth. Adjustments are then applied to account for different embedment depths, and the resulting average force is used to compute the yield moment based on the vertical distance from the base of the post to the midpoint of the rail.

The first step in this method is to identify the average soil force corresponding to a target lateral deflection. For post rotation about the transverse axis (designated as the A-axis, see Figure 63), a deflection of 10 in. was selected. This value reflects the fact that full-scale crash testing, particularly in TRBR-3, demonstrated post displacements exceeding 5 in. For post rotation about the longitudinal axis (the B-axis), which represents deformation parallel to the alignment of the AGT, a deflection of 5 in. was used to reflect the reduced movement in that direction.

Experimental data from previous bogie testing of AGT alternatives provided soil force measurements for both 8-in. x 8-in. and 8-in. x 10-in. timber posts. The data from 8-in. x 10-in. posts were used for estimating average soil force at 10 in. of deflection. These values are considered representative of the expected performance of 8-in. x 8-in. posts that did not fail prematurely. Data from 48-in. embedment depth tests were selected over those from 54-in. depths because the shorter depth more closely approximates the 45.35-in. embedment of AGT posts 1 through 4.

To adjust the soil force to the actual embedment depth of each post, Equation 29 was used.

$$F_s' = F_s \left(\frac{D_e'}{D_e}\right)^2 \quad \text{Eq. (29)}$$

In this equation, F_s' is the adjusted soil force at the target embedment depth, F_s is the measured soil force at reference embedment depth, D_e' is the actual embedment depth of the AGT post, and D_e is the reference depth of 48 in.

The soil's resistance to flexure does not change with the height at which the load is applied. However, a lower impact height produces a larger required force to generate the same moment. This relationship is illustrated in Figure 110, and described by Equation 30 for moment equilibrium. H_1 is the centerline height of the thrie-beam rail in the AGT and H1 is the centerline of the bogie impact head. The value F_1 represents the adjusted force required to height H_1 to achieve the same moment produced by F_2 at height H_2.

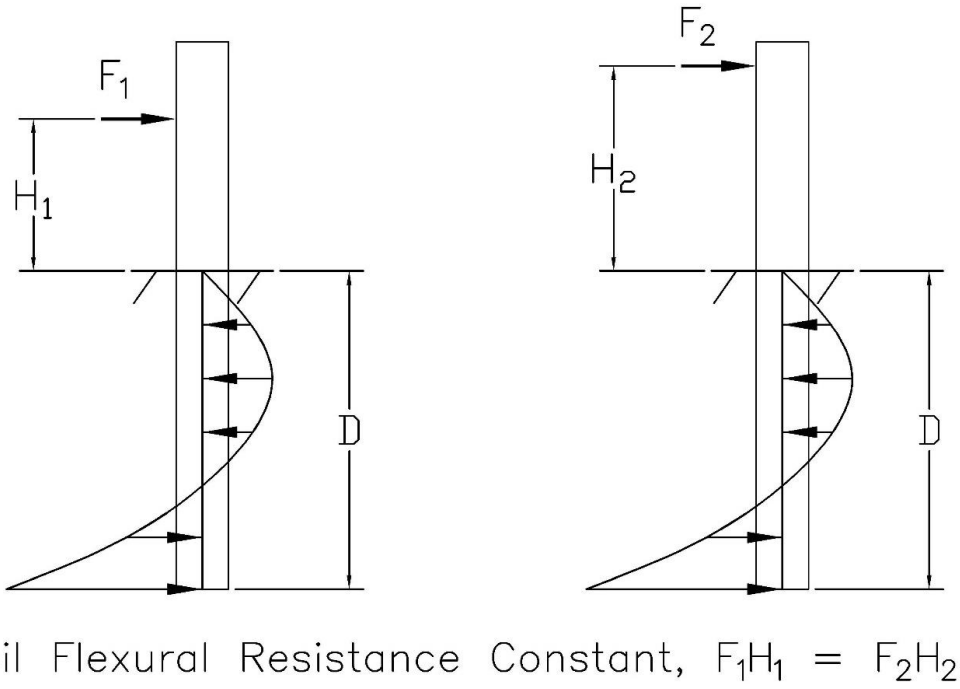

Figure 110. Post-Soil Load Distribution with Two Different Impact Heights

$$F_1 H_1 = F_2 H_2 \quad \text{Eq. (30)}$$

The soil flexural resistance is considered equivalent to the post yield moment and denoted as M_y, and is calculated by Equation 31.

$$FH = M_y \quad \text{Eq. (31)}$$

By combining Equations 29, 30, and 31, the yield moment can be expressed in terms of soil force and geometry in Equation 32.

$$\frac{H_1}{H_2} F_1 \left(\frac{D_e'}{D_e}\right)^2 H_2 = M_y \quad \text{Eq. (32)}$$

Using Equation 32, yield moments were calculated for each post. The bogie impact height H_2 was 24.875 in. The average soil force at 5 in. of deflection, denoted as F_{1B}, was 18.6 kips, and the average soil force at 10 in. of deflection, denoted as F_{1A}, was 20.1 kips. The resulting post yield moments are presented in Table 34.

Table 34. AGT Posts, Soil Forces, and Yield Moments

AGT Posts	Embedment Depth (in.)	F_{1B} (kips)	F_{1A} (kips)	M_{yB} (k-in.)	M_{yA} (k-in.)
1-4	45.35	19.08	20.61	413.0	446.3
5-7	39.35	14.36	15.52	310.9	336.0
8	39.10	14.18	15.32	307.0	331.8
9	41.85	16.25	17.56	351.7	380.1
10	43.35	17.43	18.84	377.4	407.8

4.2.5.3 Post Stiffness

The original post stiffness values in the BARRIER VII model were based on results from pendulum testing of 8-in. x 8-in. posts conducted by the Southwest Research Institute (SwRI) [39]. However, these stiffness values appeared significantly lower than those derived from bogie testing of similar posts carried out by MwRSF between 2007 and 2009 [37]. A comparison of stiffness values from these two test programs is presented in Figure 111.

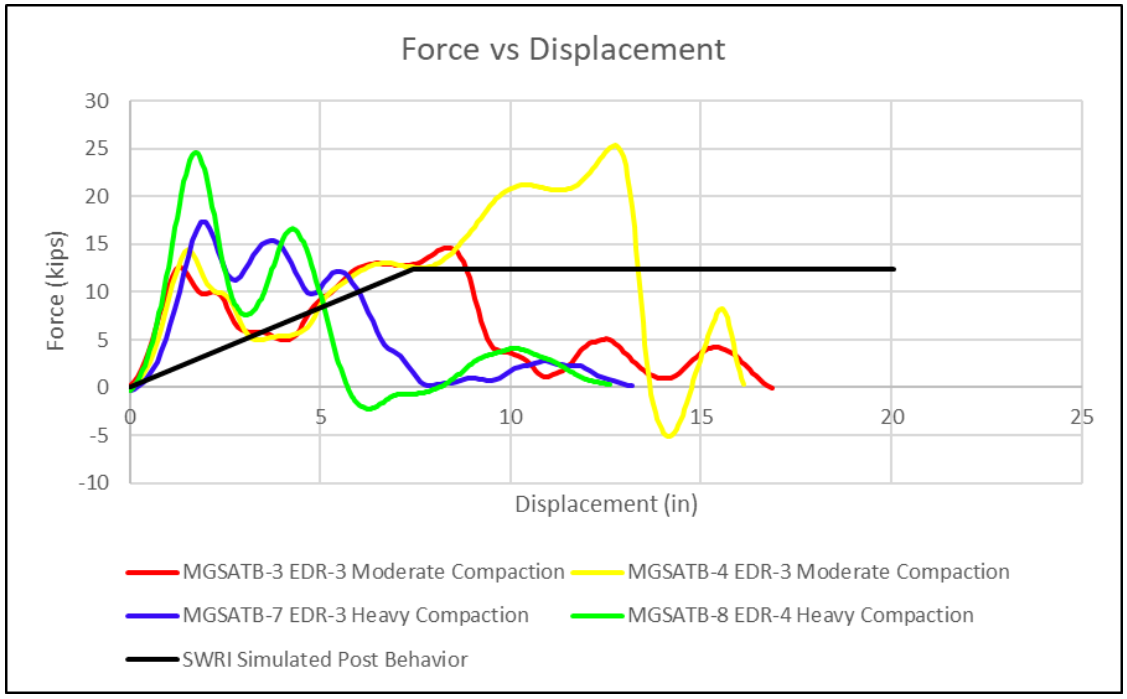

Figure 111. Load-Displacement Behavior of 8x8 Posts from Bogie Testing at MwRSF and Pendulum Testing at SwRI [37, 39]

The bogie test data suggested substantially higher stiffness than the SwRI pendulum test data, and the bogie tests more closely resemble the conditions experienced in full-scale vehicle crash tests. Furthermore, where the stiffness curve from the model aligned with bogie test results, it did so more closely for tests conducted in moderately compacted soil, rather than heavily compacted conditions. This suggests that the moderately compacted soil results may provide a more accurate representation of the crash test environment. In this context, the original stiffness value of 1.67 kips/in. is considered reasonable in principle.

However, when this stiffness value was used in multiple simulations, the results did not align well with observed deflections. Increasing the post weight in an attempt to simulate soil inertia also failed to reduce deflections. This modeling strategy was identified as problematic in prior commentary on BARRIER VII [13], which stated that increasing the mass of the barrier does not necessarily change overall performance in the expected manner.

Alternative explanations or adjustments within BARRIER VII to better capture post-soil inertia effects were not identified. Ultimately, the low stiffness value resulted in excessive deflection in the model before the posts were able to absorb meaningful amounts of energy, a behavior not observed in the crash tests. To better reflect actual post behavior, the initial stiffness was estimated based on the bogie tests conducted by MwRSF on 8-in. x 10-in. posts. The initial stiffness was defined as the first peak force divided by the corresponding displacement at that peak. This approach yielded an average stiffness of approximately 11.3 kips/in. Although this estimate does not explicitly account for post inertia, it provides a practical and empirically based means of capturing post resistance relative to deflection in BARRIER VII.

4.2.5.4 Post Weight

The post weight was recalculated based on the volume of the portion of the post above ground and an assumed moisture content of 15%. The calculation followed the weight estimation equation provided in the National Design Specification (NDS) for Wood Construction.

4.2.5.5 Post Deflection Limit

The post deflection limits were defined as 10 in. in the direction of impact and 5 in. in the upstream or downstream direction. These limits apply to posts that do not experience rupture. It is important to note that four bogie tests conducted by MwRSF on single 8-in. x 8-in. posts embedded in soil resulted in post rupture rather than full rotational displacement.

The bogie tests were conducted at an embedment depth of 54 in., compared to the 45.35-in. embedment used in TRBR-3 and TRBR-4. Additionally, the bogie test specimens were manufactured using Grade No. 1 lumber, while the crash-tested posts were made from higher-quality Grade No. 1D lumber. These differences likely contributed to the increased occurrence of rupture in the bogie tests. The shorter embedment and improved material properties used in the crash tests appear to favor rotation over rupture, which aligns with the observed post behavior during the full-scale tests.

4.2.5.6 Analysis Results

The simulation results for TRBR-3 and TRBR-4 using the fully updated AGT post parameters are summarized in Table 35. No post failures occurred in either simulation, indicating that the yield moments, shear limits, stiffness, and deflection constraints were consistent with physical behavior. For TRBR-3, representing the pickup truck test, the average error was 13.75%. This level of accuracy compares favorably with previous simulation efforts and reflects a reasonable match with test data, although it does not perform as well as an earlier calibration which achieved an error of 10.96%. The larger error in this case is primarily attributed to the exit time, which was approximately 50% shorter in the simulation than in the physical test.

Table 35. Comparison of Updated AGT Post Parameters with Crash Test Results

	Maximum Dynamic Deflection (in.)	Parallel Time (sec)	Parallel Velocity (mph)	Exit Time (sec)	Exit Velocity (mph)	Average Error
Test No. TRBR-3	6.42	0.243	45.36	0.553	44.18	
BARRIER VII Simulation	6.73	0.217	44.10	0.301	42.06	
% Error	4.89%	-10.70%	-2.78%	-45.57%	-4.80%	13.75%
Test No. TRBR-4	4.88	0.508	42.13	2.818	15.72	
BARRIER VII Simulation	2.53	0.378	42.71	-	-	
% Error	-48.14%	-25.59%	1.38%	-	-	25.04%

For TRBR-4, representing the single-unit truck test, the average error was 25.04 %. While this is a slight improvement over earlier simulations, the maximum dynamic deflection changed from being an overestimate to an underestimate. Overall, the updated AGT post parameters improved simulation fidelity and eliminated post failure, but certain kinematic features, particularly exit time, remain difficult to match precisely in BARRIER VII.

4.2.6 Final Model

Before proceeding with further analysis, the inconsistency in deflection errors between the single-unit truck (SUT) and pickup truck simulations required attention. The model underestimated deflection for the SUT and overestimated deflection for the pickup, which suggested a need to revisit the underlying parameters. The simulated system deflections were especially sensitive to post stiffness values, which had been estimated from bogie tests conducted in heavily compacted soil.

The soil in the 1997 crash tests was compacted using a pneumatic hand tamper. The same compaction method was also used in the post component tests. However, the component testing

reports distinguish between "moderate" and "heavy" compaction. Heavy compaction was achieved using a high-energy pneumatic tamper, while moderate compaction used the standard pneumatic tool. Since the 1997 crash test soil was also compacted with a pneumatic hand tamper and not a high-energy system, it is reasonable to conclude that the soil condition in the crash tests more closely resembled moderate compaction [25,37]. Soil compacted in this way exhibits a lower stiffness in post load–deflection behavior compared to heavily compacted soil.

Rather than developing an entirely new stiffness model, the approach here was to iteratively adjust the stiffness of the posts until the relative errors of the pickup and SUT simulations were approximately the same. This resulted in a post stiffness value of 5.4 kips/in. For the 6-in. x 8-in. posts evaluated on their 6-in. face, the stiffness was reverted to the original value in order to better reflect behavior in moderately compacted conditions.

The vehicle model was also updated. Both TRBR-3 and TRBR-4 showed tire marks on the lower curb rail, which indicated contact between the vehicle tires and the rail during impact. To replicate this interaction, contact was activated for the wheel nodes in the vehicle model by assigning a value of 1 to those nodes in the contact definition.

The results from the updated model are presented in Table 36. The pickup truck simulation (TRBR-3) showed an average error of 16.94%, while the SUT simulation (TRBR-4) showed an average error of 17.00%. These results represent the best balance that could be achieved, as further adjustments to parameters consistently improved the accuracy for one vehicle at the expense of the other. A more detailed investigation was not pursued in order to maintain time for other research objectives.

Although these error values are higher than those obtained in the Phase IIa bridge railing simulations, which yielded 10.96% for the pickup and 10.18% for the SUT, the results still offer useful insight. Specifically, the current model overpredicted deflections for the vehicle that exceeded the target impact conditions and underpredicted deflections for the vehicle that did not meet the target conditions. This pattern suggests that the model provides a conservative estimate for higher-severity impacts, offering a practical margin of safety that supports the robustness of the design.

Table 36. Comparison of Updated Vehicle Parameters with Crash Test Results

	Maximum Dynamic Deflection (in.)	Parallel Time (sec)	Parallel Velocity (mph)	Exit Time (sec)	Exit Velocity (mph)	Average Error
Test No. TRBR-3	6.42	0.243	45.36	0.553	44.18	
BARRIER VII Simulation	7.68	0.216	43.92	0.301	41.90	
% Error	19.66%	-11.11%	-3.19%	-45.57%	-5.16%	16.94%
Test No. TRBR-4	4.88	0.508	42.13	2.818	15.72	
BARRIER VII Simulation	3.74	0.370	42.29	-	-	
% Error	-23.45%	-27.17%	0.38%	-	-	17.00%

4.3 MASH 2016 TL-3 AGT and AGT Connection Design

The AGT was developed to meet the requirements of MASH 2016 TL-3. The design goals included successful redirection of both the 2270P pickup truck and the 1100C small car from critical impact trajectories, accommodation of a future 2-in. wearing surface, structural compatibility with the MGS, and the implementation of an upstream stiffness transition to improve system performance across the bridge approach.

Several of these goals were addressed in earlier studies, as described in Section 2.3.6. The present research effort was built on those findings and integrated them into a complete AGT system that satisfies the MASH 2016 criteria. Initial development focused on creating a structural connection between the glulam timber bridge and the AGT. Since key AGT characteristics such as system height directly influenced the required geometry and behavior of the connection, the connection design process also contributed to the broader AGT design.

A total of forty-nine AGT prototype configurations were developed. These prototypes were created in iterative batches of five to ten designs per cycle, with each iteration focusing on particular challenges such as post spacing, guardrail length, bolt layout, and taper geometry to reduce the potential for vehicle snagging. Each batch informed the development of subsequent designs, gradually improving performance and constructability.

The starting point for the AGT design was based on the Glulam Rail with Curb on Transverse Glulam Deck system [20], which had previously demonstrated acceptable performance under NCHRP-350 TL-4 impact conditions during crash test TRBR-3. The original connection design from this earlier system served as a reference for establishing comparable strength and stiffness characteristics. This initial connection concept is shown in Figure 112. Design parameters, structural limitations, and specific connection details are discussed in the following

chapters. A detailed comparison of the final two selected AGT systems is also provided. A complete record of the forty-nine developed AGT configurations can be found in Appendix A.

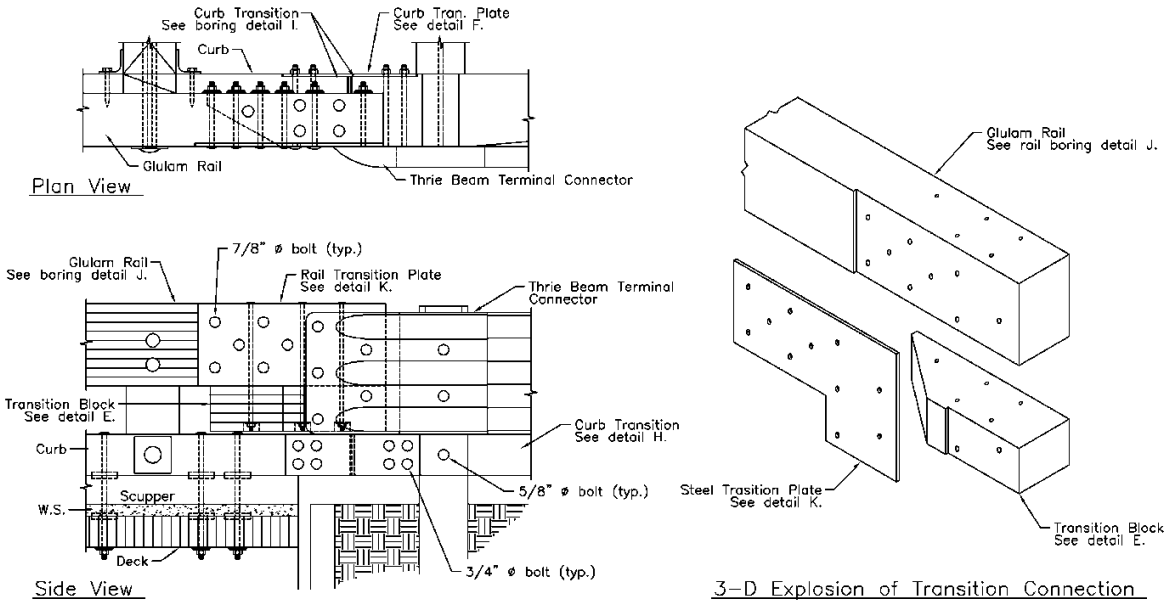

Figure 112. AGT to Bridge Railing Connection Developed for NCHRP-350 TL-4 System [20]

4.3.1 AGT Design Parameters

4.3.1.1 Components

The AGT connection to the glulam timber bridge railing was developed using standardized components typically employed in AGT systems throughout the United States. This approach was adopted to maximize constructability and minimize the need for custom fabrication. As a result, timber railing sections were not considered for the AGT portion.

Standardized W-beam and thrie-beam sections were used for the rail elements. These sections are commonly available in lengths of 312.5 in., 162.5 in., and 87.5 in., corresponding to installation lengths of 25 ft, 12.5 ft, and 6.25 ft, respectively. For timber posts, standard lengths are typically rounded to the nearest ½ ft. Tapered connections were constructed using simple glulam profiles to avoid complex geometries or fabrication techniques. Welded steel tapers were avoided in favor of easier-to-construct alternatives.

To further streamline the construction process, no welding was performed on the thrie-beam shoe. These components are typically galvanized, and welding would require special procedures or post-processing steps to maintain corrosion protection. A bolted connection was selected to preserve the galvanization and ensure compatibility with standard manufacturing practices.

4.3.1.2 Post Spacing

Post spacing is a critical factor in the strength and stiffness of any AGT system, as the posts serve as the primary load transfer points to the ground. In the previously tested Glulam Rail with Curb on Transverse Glulam Deck system, quarter-post spacing was used to achieve the necessary impact resistance. Additional details about this configuration are provided in Section 2.3.3. To enhance performance and accommodate geometric constraints, the spacing between the last two bridge posts in the system was reduced from 8 ft to 6 ft. The distance between the first bridge post and the last AGT post was further reduced to 4 ft. This configuration was made possible through the use of a specialized scupper design at the transition point between the bridge and AGT [19].

Since the NCHRP Report 350 system demonstrated the ability to resist MASH 2016 TL-3 impact severity, quarter-post spacing with 8-in. x 8-in. timber posts were considered a strong candidate for the current AGT design. However, the new design also required an upstream stiffness transition. Recommendations for such a transition were taken from a study of a timber post alternative to a stiff bridge railing AGT [37], as discussed in Section 2.3.6. That study recommended the use of 8-in. x 10-in. posts at half-post spacing, which was incorporated into design alternatives.

The minimum spacing between the nearest bridge post and the adjacent AGT post was limited by the physical constraints of the bridge structure. For example, the thickness of the concrete abutment backwall can be up to 2 ft [83, 140], which may overlap with the AGT post placement. Additionally, a 2-in. buffer is recommended between the edge of the timber deck and the start of the concrete backwall to prevent debris accumulation at the exposed end grain of the glulam girders.

If the spacing between the AGT and bridge posts were reduced to less than 6 ft, it would no longer be feasible to accommodate bridges with a 1-ft – 6-in. abutment backwall. In that case, the AGT post would be positioned directly adjacent to the concrete backwall, potentially interfering with any drainage features located at the bridge abutment.

Initially, the design used 6 ft of spacing between the final AGT post and the first bridge post in the quarter-post configuration. However, for ease of construction and compatibility with various abutment geometries, the spacing was increased to 8 ft in both the half-post and quarter-post systems. This allowed space for a 2-ft-thick abutment and maintained a 1-ft 6-in. clearance between the face of the timber post and the backwall. The increased clearance reduced the likelihood of interference with drainage systems or other infrastructure. To further reduce load demands, the quarter-post configuration was ultimately adjusted to use 7-ft spacing between the final AGT post and the first bridge post.

4.3.1.3 System Height Adjustment

The Glulam Rail with Curb on Transverse Glulam Deck had a height of 33 in. from the roadway surface to the top of the upper bridge railing. The connecting thrie-beam guardrail was positioned at a height of 31⅝ in, and this transitioned to a W-beam with a height of 27¾-in. The relatively small height difference between the upper glulam rail and the thrie-beam allowed for a direct connection between the two, with sufficient edge clearance for bolt placement. Specifically, the thrie-beam shoe bolts were located at least 3 in. from the edge of the glulam upper rail, ensuring

structural integrity. As shown in Figure 112, three bolts passed through the upper glulam railing, while two additional bolts were placed through the reverse taper section. The lower curb railing tapered away directly beneath the thrie-beam, so there was no overlap between the two components.

The original design did not account for a future wearing surface, and the transition between the thrie-beam and the W-beam was symmetric. In contrast, the MASH 2016-compliant systems specify a bridge railing height between 36 and 38 in. from the deck surface. Additionally, the crash-tested AGT system that included provisions for a future wearing surface used a height of 34 in. to the top of the thrie-beam [38]. In order to accommodate a 2-in. future wearing surface while maintaining compatibility with existing designs, this height differential had to be preserved.

A configuration with two vertically stacked W-beams was not used in this design. The required height transition from 38 in. to 32 in., consistent with MGS connection geometry, would not allow for proper bolt placement. Specifically, the upper W-beam shoe bolts would have to pass through the edge of the upper bridge rail, leaving insufficient edge distance for structural integrity. This constraint would allow only a single bolt to be installed with proper clearance, which was deemed inadequate.

Instead, a thrie-beam positioned at a height of 34 in. was selected. This rail element used a symmetric transition and was rotated slightly upward by ¾ in. to allow connection to the MGS at 31 in. When a 2-in. wearing surface is later added, this configuration allows for the removal of the thrie-beam to W-beam connection and the MGS section. New bolt holes would need to be drilled, and the W-beam would be remounted 3 in. higher to maintain system geometry and performance after resurfacing. This approach simplifies the long-term maintenance process and allows for future adaptation without requiring replacement of major structural elements.

The lower glulam curb railing was 8.75 in. tall and began 8.25 in. above the ground. It overlapped with the 20-in.-tall thrie-beam, which started 14 in. above the ground, creating a 3-in. vertical overlap. The thrie-beam railing was mounted flush with the face of both the upper and lower glulam railings. As the curb tapered away from the bridge face, the thrie-beam continued forward without occupying the same physical space. One of the thrie-beam end shoe bolts passed through the lower glulam bridge rail. To resolve this, a notch was cut into the curb to allow the bolt to pass through two steel plates instead of the wood member. Another bolt, located beneath the upper glulam railing, passed through the taper section. A notch was also cut in this location to avoid placing the bolt too close to the edge of the taper, which could compromise structural capacity.

4.3.1.4 Tapers

The AGT and timber bridge railing components were designed to terminate in a manner that would not pose a risk of wheel snag or pocketing. A taper allows a continuous railing element to come to an end gradually, thereby eliminating abrupt surfaces that could interfere with vehicle redirection. In the previous bridge railing to AGT design, two tapers were used. One was placed for potential reverse-direction impacts on the AGT thrie-beam, and the other was located at the end of the lower glulam curb railing. Both of these tapers were fabricated from glulam timber to match the existing rail components.

The new AGT connection required additional tapers at two locations: one for the upper glulam bridge railing and another for the AGT thrie-beam. These were necessary because the height difference between the upper glulam railing, which was 38 in., and the AGT thrie-beam, which was 34 in., was too large to avoid a snag risk without a transitional element. The taper could not extend downstream of the thrie-beam end shoe because doing so would reduce the strength of the upper glulam railing in a region where structural continuity was required for effective load transfer. Consequently, the taper was placed upstream and designed according to a standard 1 to 4 height-to-length ratio.

As with the Glulam Rail with Curb on Transverse Glulam Deck design, a reverse taper was also required for the end of the thrie-beam. This element was located directly beneath the upper glulam railing and rested on top of the lower curb rail. A built-up steel taper was initially considered for this connection, based on its use in earlier projects with similar requirements [149]. However, the design was not feasible in this case because a steel bolt located beneath the upper glulam rail would interfere with the fit of the steel taper. Steel components cannot easily be shaped to accommodate such obstructions.

A wooden reverse taper was used instead. Timber material allowed for precise cuts and can be shaped to fit tightly between the upper and lower railings. Even so, it was necessary to notch the reverse taper to allow space for the bolt beneath the upper glulam rail. Without this notch, the bolt hole could collect moisture, which would accelerate corrosion and reduce the longevity of the connection.

A taper was also required to bring the lower curb railing to an appropriate end. Due to the 3-in. vertical overlap between the lower glulam curb rail and the thrie-beam, alternative designs were considered in which the taper would be lowered beneath the thrie-beam to make room for the bottom bolt of the thrie-beam end shoe. This approach was ultimately rejected because lowering the taper would reduce the effectiveness of load transfer between the curb railing and its taper. The adopted solution involved cutting a notch in the edge of the lower glulam curb railing. This allowed the bolt to pass through the end shoe without requiring a hole to be drilled close to the edge of the wood member, where it would have been more vulnerable to splitting or structural weakening.

4.3.1.5 Connection Hardware

To connect all the glulam components, ASTM A307A bolts were used, and ASTM A572 steel was used for splice plates connecting the lower glulam railing with its taper and the upper glulam railing with the reverse taper. A single plate covering both the upper and lower railings, reverse taper, and lower glulam railing taper was considered, but rejected to avoid excessively heavy components as well as a highly convoluted steel plate. The bolts in the upper and lower glulam railing connections to their plates were evenly spaced into rows to allow for vertical bolts to pass through the entire assembly of the upper railing, reverse taper, and lower railing (29.75 in. total) to improve the stiffness of the connection.

4.3.2 Selected Design Concepts

The selected design concepts addressed the critical requirements related to component compatibility, system height transitions, taper geometry, and connection hardware. However, post spacing was not resolved by selecting a single configuration, since the trade-offs between spacing

and structural response had not been fully quantified. As a result, two designs were advanced for further evaluation. These included one with half-post spacing and one with quarter-post spacing. Figures 113 through 125 show the final configurations for each system.

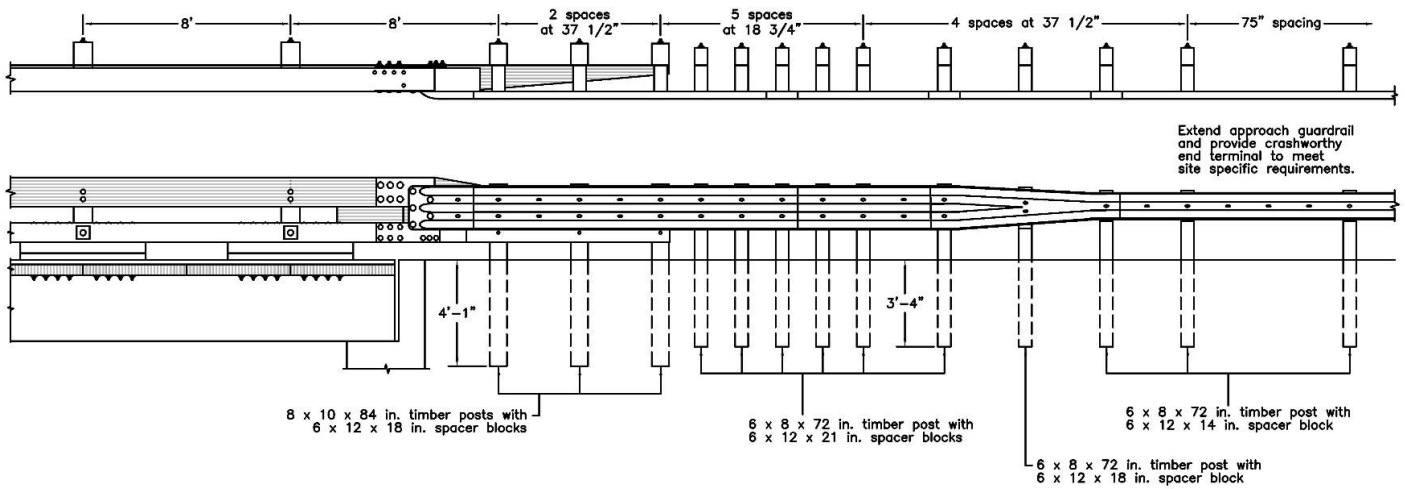

Figure 113. Half-Post MASH 2016 TL-3 AGT between TL-4 Bridge Rail and MGS

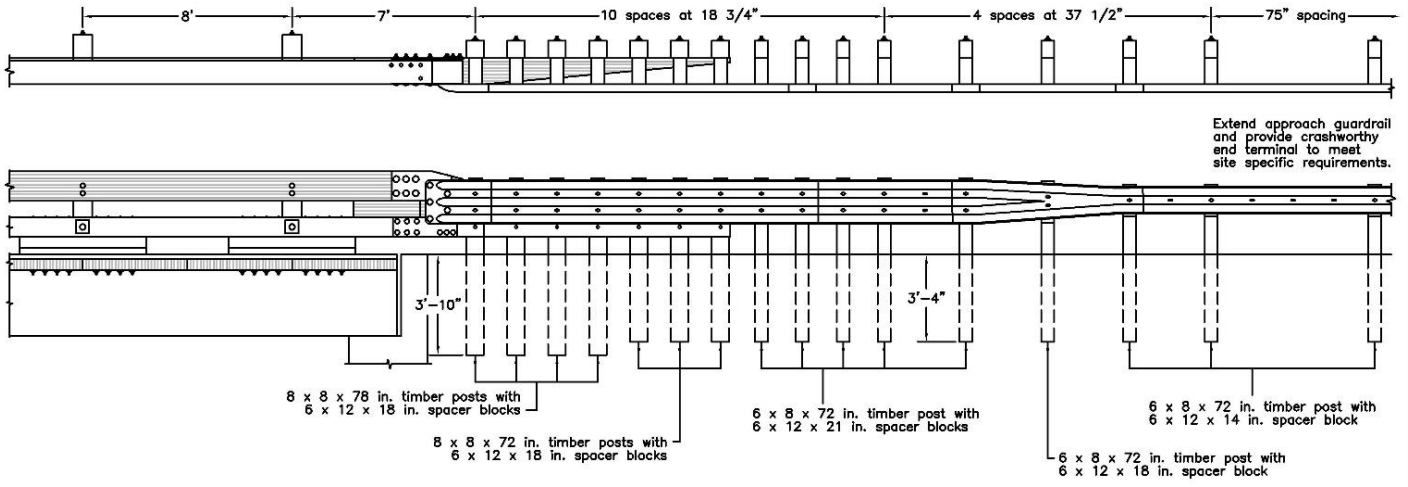

Figure 114. Quarter-Post MASH 2016 TL-3 AGT between TL-4 Bridge Rail and MGS

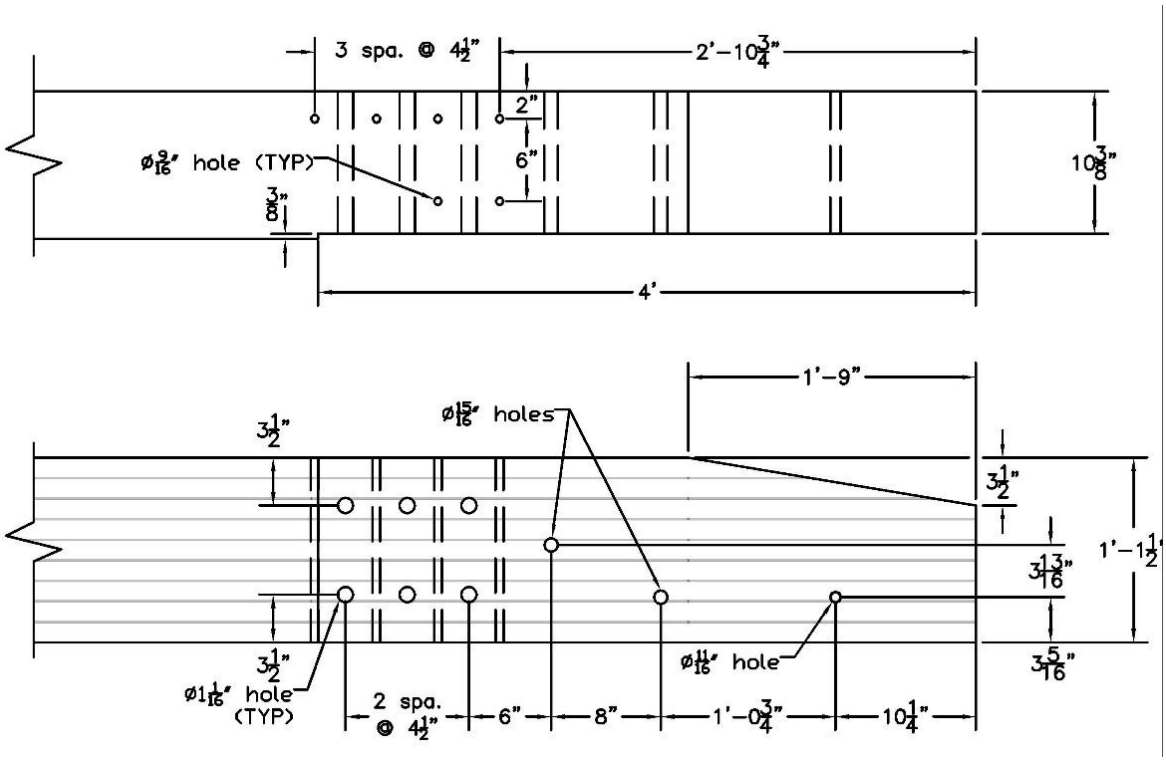

Figure 115. Cuts and Holes Needed in Upper Rail at End for Attachment to Half-Post System

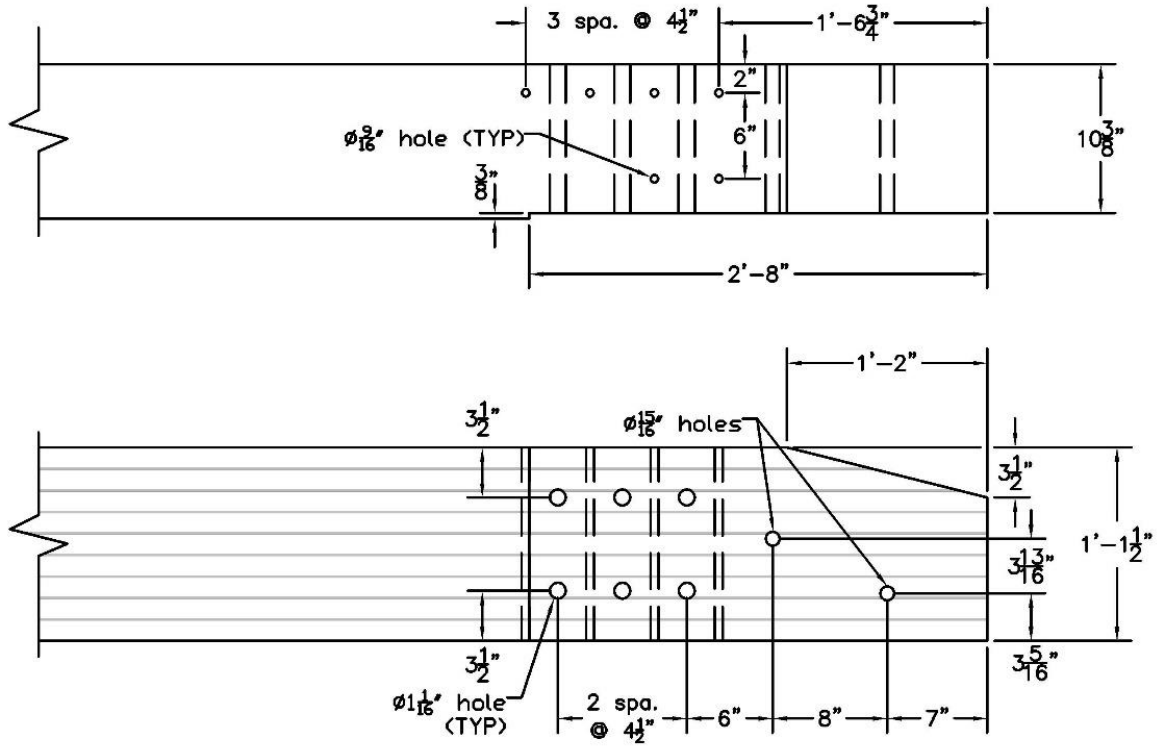

Figure 116. Cuts and Holes Needed in Upper Rail at End for Attachment to Quarter-Post System

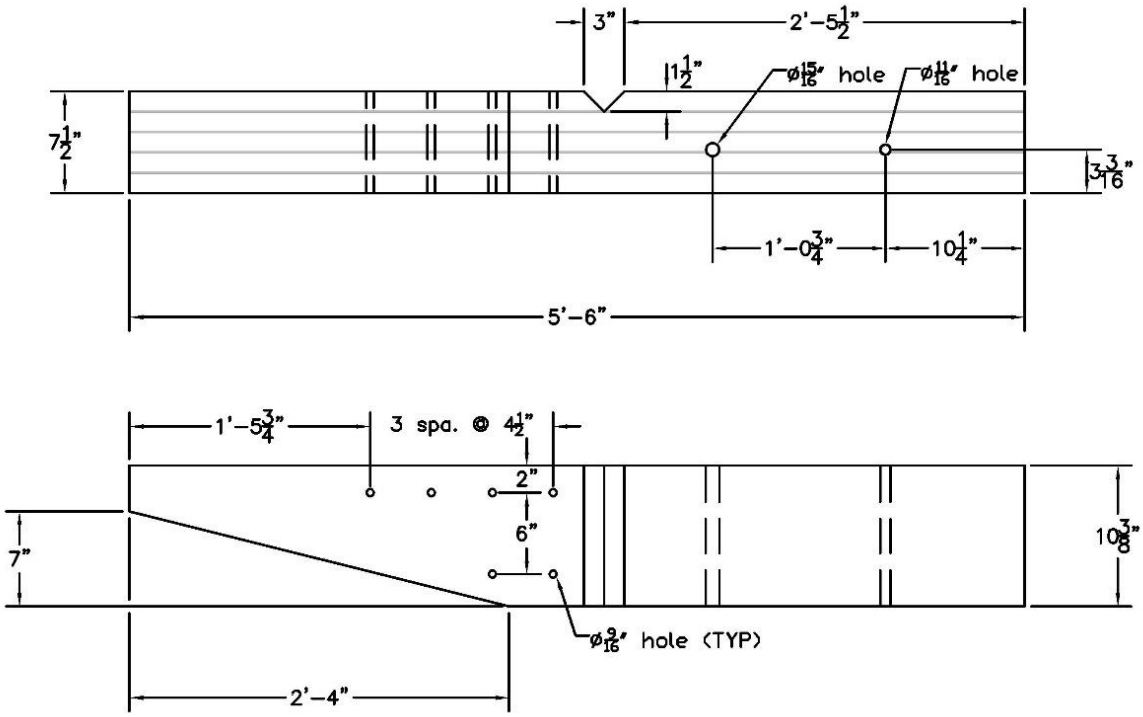

Figure 117. Reverse Taper Details for Half-Post System

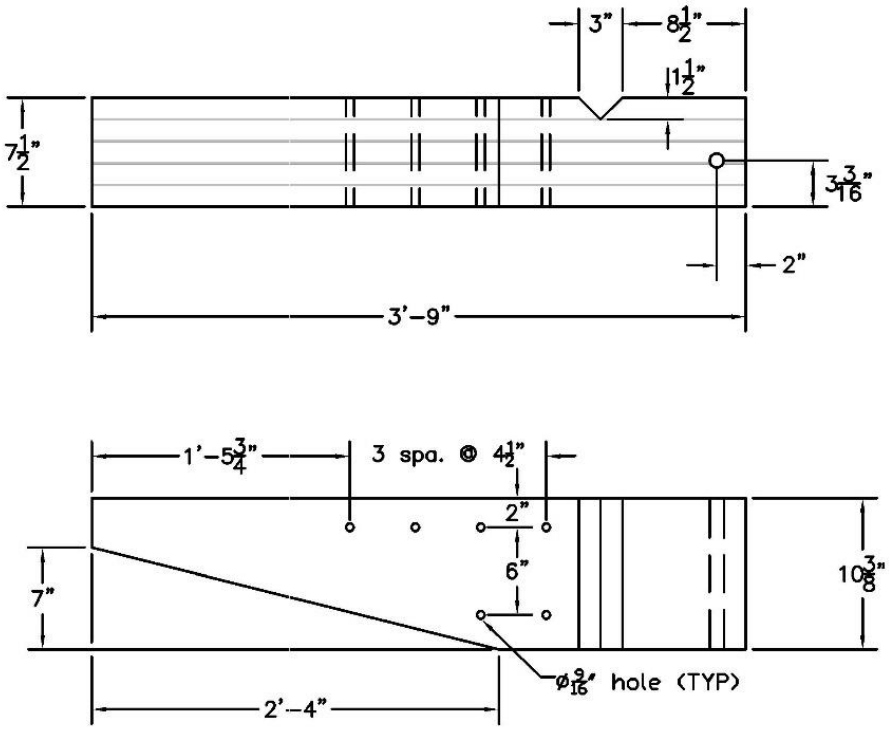

Figure 118. Reverse Taper Details for Quarter-Post System

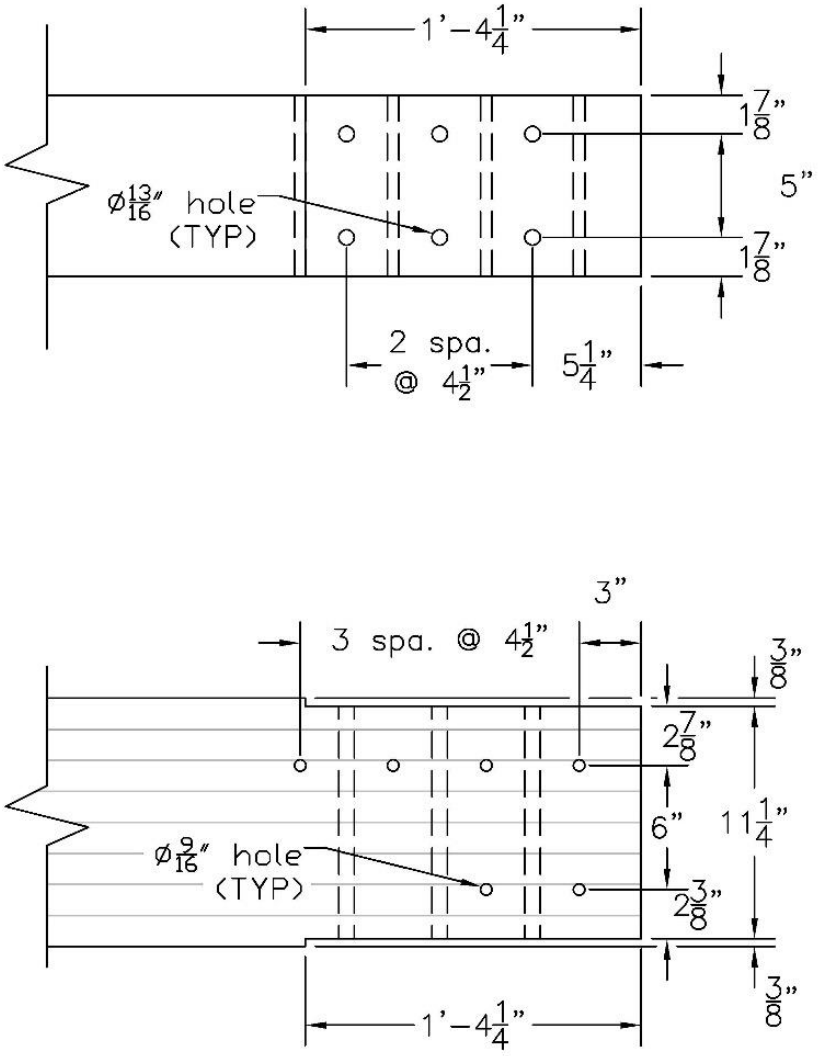

Figure 119. Cuts and Holes Needed at Curb Rail End for Both Systems

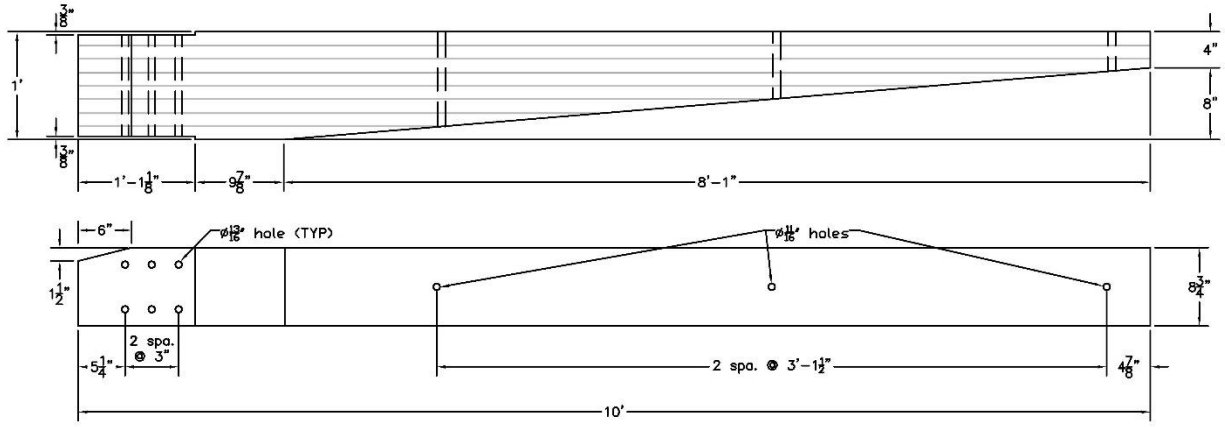

Figure 120. Curb Rail Taper Details for Half-Post System

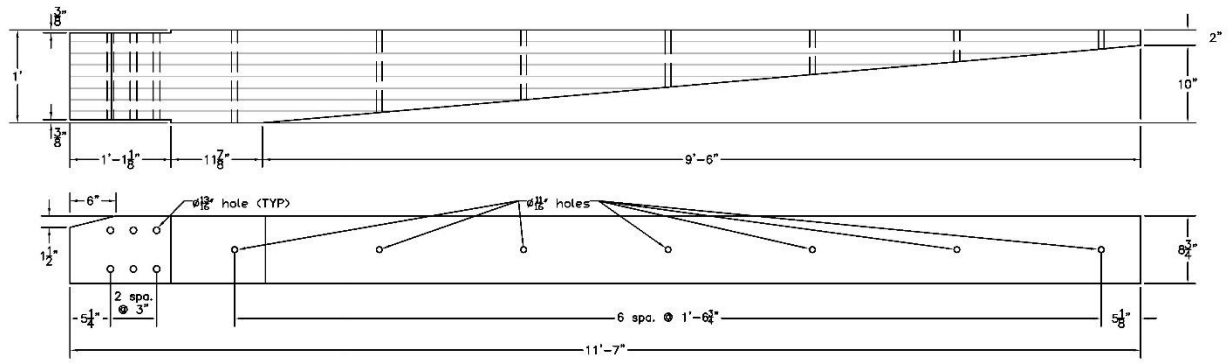

Figure 121. Curb Rail Taper Details for Quarter-Post System

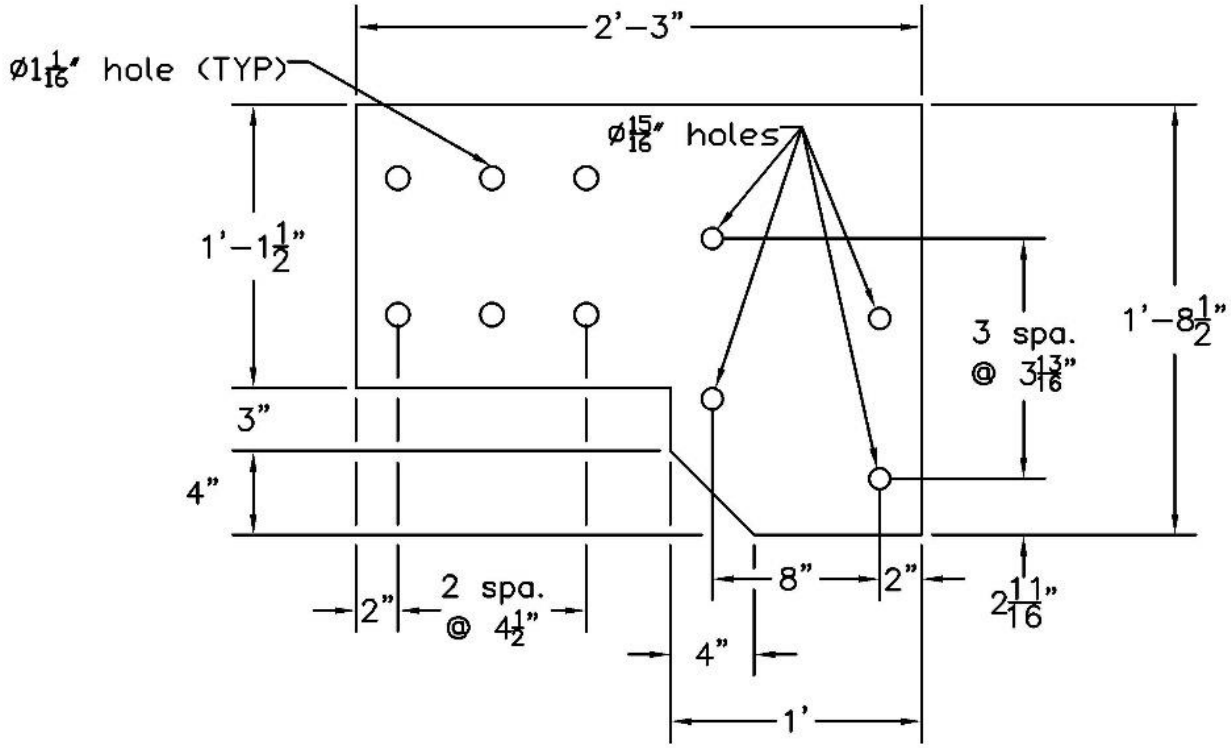

Figure 122. Upper Rail Plate Details for Half-Post System

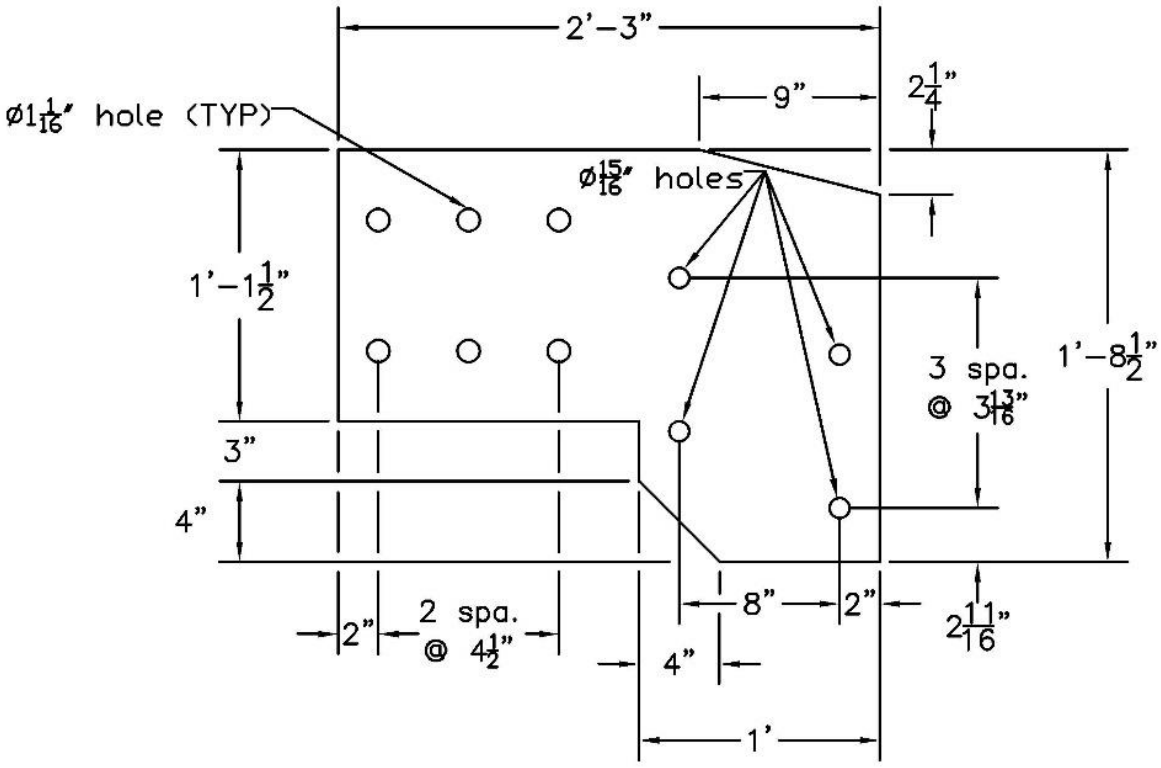

Figure 123. Upper Rail Plate Details for Quarter-Post System

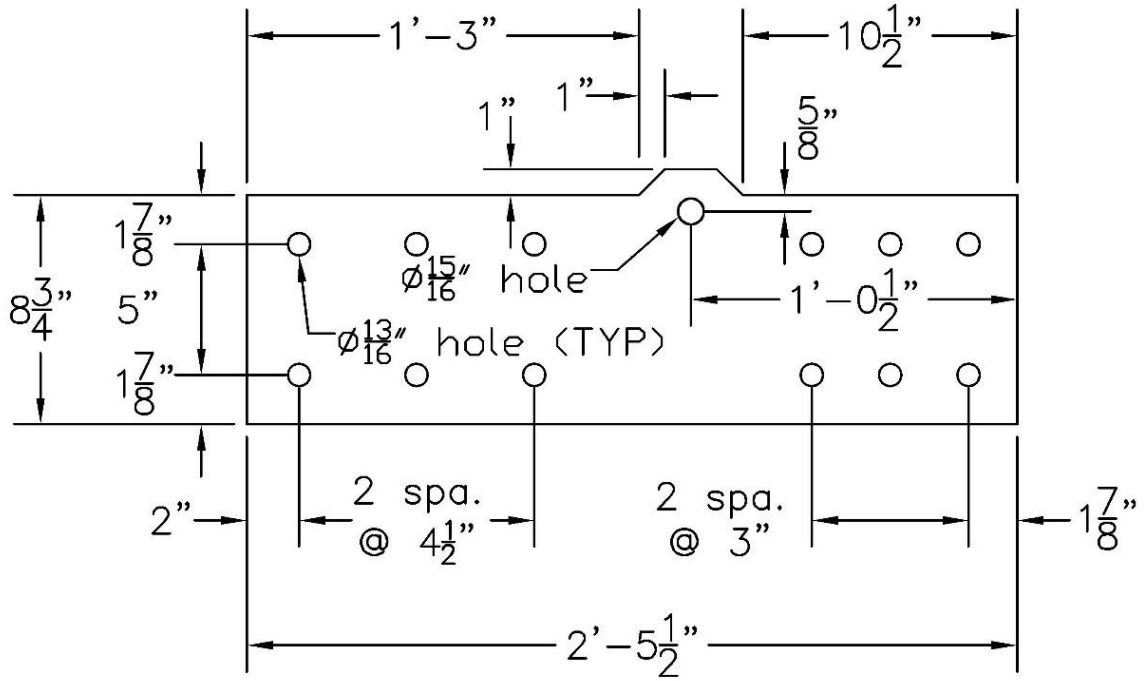

Figure 124. Curb Rail Plate Details for Both Systems

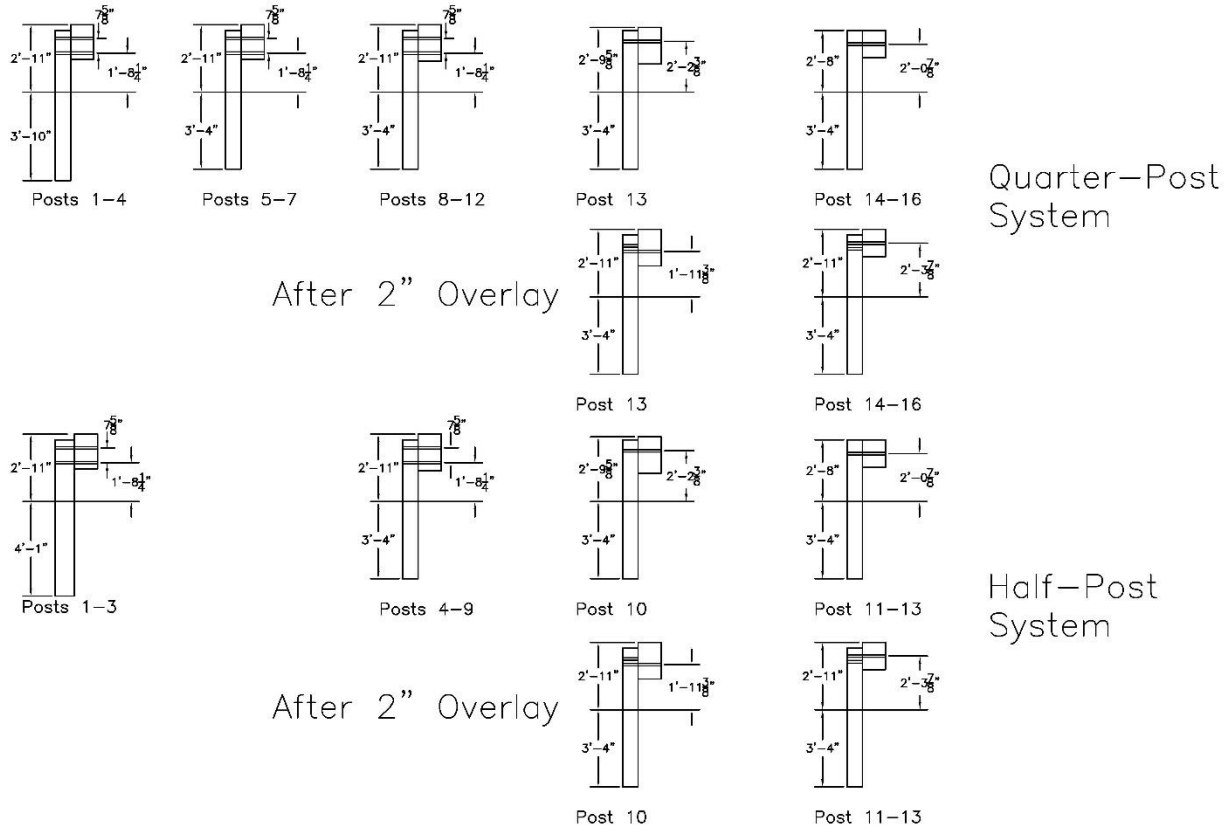

Figure 125. AGT Post Cross-sections for Both Systems

The half-post configuration, illustrated in Figure 113, includes the following components:

- Three 8-in. x 10-in. posts embedded 49 in. into the soil, placed at half-post spacing near the bridge.
- Five 6-in. x 8-in. posts with 40-in. embedment, placed at quarter-post spacing.
- Four additional 6-in. x 8-in. posts with 40-in. embedment at half-post spacing, leading to the connection with the MGS.

Originally, the half-post design included only four 8-in. x 10-in. posts. An additional 6-in. x 8-in. post was added to allow alignment with standard 12.5-ft thrie-beam segments and to facilitate a proper connection to the glulam bridge railing.

The quarter-post configuration, shown in Figure 114, uses:

- Four 8-in. x 8-in. posts embedded 46 in. into the soil, spaced at quarter-post intervals.
- Three more 8-in. x 8-in. posts with 40-in. embedment, also at quarter-post spacing.

- Four 6-in. x 8-in. posts with 40-in. embedment at quarter-post spacing.

- Four final 6-in. x 8-in. posts with 40-in. embedment at half-post spacing, completing the transition to the MGS.

Both systems use the same thrie-beam layout. A nested 12-gauge, 12.5-ft thrie-beam section is followed by a 12-gauge, 6.25-ft section, which then connects to a 10-gauge symmetric transition piece. In the configurations shown in Figures 113 and 114, the system is assumed to operate without an asphalt overlay. Under this condition, a symmetric thrie-beam to W-beam transition is used. All components are installed in the standard manner, except that the W-beam side of the transition is rotated upward by ¾ in. to accommodate height differences. Only the top bolt is installed at this stage.

If both top and bottom bolts are installed initially, the post would need to be removed and replaced when an overlay is added. This is because the new bolt holes would not maintain adequate edge distance from the original holes. After the overlay is placed, the symmetric transition is replaced with an asymmetric thrie-beam to W-beam transition. In that configuration, only the bottom bolt is installed. Figure 125 shows the hole locations for this post, which are spaced 3 in. apart. This same spacing is maintained for all MGS posts.

The plates connecting the upper rail and curb rail to the thrie-beam end shoe were based on the splices, to ensure that sufficient capacity was present in the bolts and plates. Six 1-in. diameter bolts 14 in. long hold the upper rail to its connection plate, and six ¾-in. diameter bolts 14 in. long will be used to hold the curb rail to its connection plate. An additional six ¾-in. diameter bolts 14-in. long will hold the curb rail taper to the curb rail connection plate. Two plates will be used for the upper rail as well, instead of one plate, as was used in the Glulam Rail with Curb on Transverse Glulam deck system. The bolt spacing in the curb rail was expanded from the curb rail from three in. to four and a half between bolts to fit vertical bolts through the connection.

Six ½-in. diameter bolts 32-in. long go through the upper rail, reverse taper, and curb rail to hold the reverse taper in place as well as provide additional stiffness to railing at the point of connection to the thrie-beam. This will also help transfer loads into both rails by ensuring less deflection of one railing without deflection of the other. The end shoe is held to the connection plates and the railings with five ⅞-in. diameter bolts, with only three going through railings, the remaining two go through the plates, and then empty space until going through the plate on the other side of the railing. For half-post spacing systems, an additional two ⅝-in. diameter bolts 14-in. long hold the end shoe to the upper railing and reverse taper.

4.4 Bogie Testing Program

4.4.1 Selecting Test Configuration

Two AGT configuration concepts were developed: one with half-post spacing and another with quarter-post spacing for the posts near the timber bridge railing. As discussed in Section 2.3.6, prior research investigated the performance of half-post configurations using bogie testing. However, this same research identified concerns with the 8-in. x 8-in. post size proposed for use in the quarter-post configuration. Specifically, these posts ruptured before developing sufficient

soil rotation when tested at a 54-in. embedment depth and did not dissipate energy equivalent to that of W6x15 steel posts.

Despite these findings, the same 8-in. x 8-in. post size and spacing performed well in the AGT tested as part of the TRBR-3 crash test. That system, designed for connection to a timber bridge railing, successfully redirected the vehicle, even though the impact severity exceeded the requirements for MASH 2016 TL-3. Before representing the quarter-post system in BARRIER VII simulations, additional bogie tests were designed to investigate this discrepancy.

The quarter-post AGT configuration included seven 8-in. x 8-in. posts positioned near the bridge. Four of these posts were embedded to a depth of 46 in., and the remaining three were embedded 40 in. These embedment depths are comparable to the AGT connected to the Glulam Rail with Curb on Transverse Glulam Deck but are shorter than the 54-in. depth evaluated in the previous research. Additionally, the bogie tests impacted individual posts, while the crash test applied loading to all posts simultaneously. This raised the hypothesis that the soil resistance was influenced by group effects, which could reduce the overall resistance when posts are closely spaced.

To examine this possibility, bogie impacts were conducted on one, two, and three posts in order to investigate whether group effects led to measurable changes in soil resistance. To avoid post rupture, the expected soil resistance based on 8-in. x 10-in. post data in heavily compacted soil at 54-in and 48-in. embedment was adjusted using Equation 29. The 8-in. x 8-in. post capacity, referred to as modulus of rupture (MOR), was estimated from the peak force prior to failure. This approach aligns with ASTM procedures, where MOR is based on peak force observed in static testing of structural-size lumber [139]. Pendulum testing by Southwest Research Institute (SwRI) on 8-in. x 8-in. Southern Yellow Pine (SYP) posts in rigid sleeves provided peak force data, which was used to estimate MOR [40]. The results are summarized in Table 37.

Table 37. SWRI 8x8 SYP Post Pendulum Rupture Tests

SWRI 8x8 SYP Fracture Tests			
Peak Force (k)	Section Modulus (in.^{3})	Height (in.)	MOR (ksi)
22.0	92.2	24	5.73
24.3	96.6	24	6.04
25.9	88.6	24	7.02
29.4	97.1	24	7.27
25.2	87.9	24	6.88
28.4	95.0	24	7.17
28.0	91.4	24	7.35
25.4	92.1	24	6.62
		Average MOR	6.76

The grade of the SYP posts used in the SwRI study was not reported, making it difficult to directly apply the results for post selection. For comparison, results from similar tests conducted by MwRSF using Grade 1 SYP posts are shown in Table 38.

Table 38. MWRSF 8x8 SYP Grade 1 Post Bogie Tests

MWRSF 8x8 SYP Grade 1 Post Bogie Tests						
Test	Source	Force (k)	Section Modulus (in.^{3})	Height (in.)	MOR (ksi)	
MGSATB-3	EDR-3	14.66	85.33	36.875	6.33	
	EDR-4	14.47	85.33	36.875	6.25	
					Test Average	6.29
MGSATB-4	EDR-3	25.37	85.33	36.875	10.96	
	EDR-4	23.31	85.33	36.875	10.07	
					Test Average	10.52
MGSATB-7	EDR-3	12.18	85.33	28.875	4.12	
	EDR-4	10.40	85.33	28.875	3.52	
					Test Average	3.82
MGSATB-8	EDR-4	16.61	85.33	32.875	6.40	
						6.40
					Average MOR	6.76

The MOR values calculated from peak forces were nearly identical in both the SwRI and MwRSF tests. These were taken to represent typical Grade 1 SYP performance. However, only four posts were tested by MwRSF, and the variation was high. Furthermore, the ASD estimate for

MOR in Grade 1 SYP posts is 4.67 ksi, which remains lower than the test average even after factoring in safety, duration, and statistical adjustments. To evaluate whether post failure should have occurred, the applied stress was estimated using a modified form of Equation 32, now referred to as Equation 33:

$$f_{cr} = F_1 \left(\frac{D_e'}{D_e}\right)^2 \frac{H_1}{H_2} H_2 \frac{1}{S} \qquad \text{Eq. (33)}$$

where F_1 is the average soil force at 10 in. of deflection, D_e is the original embedment (54 or 48 in.), D_e' is the adjusted embedment depth, H_1 is the bogie impact height (24.875 in.), H_2 is the thrie-beam centerline height (24 in.), S is the post section modulus (85.33 in.^{3} for an 8×8 post). The estimated applied stresses from 8×10 posts for embedment depths ranging from 54 to 40 in. are shown in Table 39.

Table 39. Post Applied Stress from 40 in. Embed. to 54 in. Embed.

Soil Resistance	Applied Stress (ksi) at 10-in. Deflection				
	54-in. Embed.	49-in. Embed.	46-in. Embed.	43-in. Embed.	40-in. Embed.
8x10 Post at 54-in.	6.69	5.51	4.85	4.24	3.67
8x10 Post at 48-in.	7.47	6.15	5.42	4.74	4.10

By comparing the applied stress values from Table 39 with the estimated modulus of rupture (MOR), the analysis suggests that an 8-in. x 8-in. post should not have failed at 54 in. of embedment. However, the observed rupture in previous tests indicates that the analytical prediction may not accurately reflect post performance. As a result, the allowable stress design (ASD) estimate was considered more reliable for post capacity assessment.

Further examination of the differences between measured soil resistance at 54-in. embedment and calculated resistance values adjusted to different embedment depths revealed discrepancies. The accuracy of resistance predictions decreased as the adjustment diverged from the original test conditions. This trend suggests that large adjustments in embedment depth introduce significant uncertainty in estimated resistance. For example, resistance calculated for 46-in. embedment more closely matched measured resistance at 48 in. than predictions for larger differences in depth.

These observations informed the decision to select an embedment depth that was close to previously tested values. A 43-in. embedment was chosen because it falls between 46 in. and 40 in., providing a balance that improves the accuracy of estimated soil resistance. Although the predicted applied stress at this depth still approaches the conservative lower-bound MOR, this embedment depth allows for a reasonable and representative test configuration. The selected test setup was considered sufficient to evaluate whether post group effects contribute to changes in soil resistance, and whether such effects are relevant to the AGT system performance.

4.4.2 Test Plan

Three bogie tests were planned to evaluate whether post spacing influences the soil resistance of 8-in. x 8-in. posts embedded at a depth of 43 in. and arranged at quarter-post spacing. The test sequence included a single-post impact, a two-post impact, and a three-post impact. These configurations were designed to assess potential group effects and their influence on soil resistance, particularly in closely spaced post arrangements.

The impact height was set at 24 in. to represent the centerline of the thrie-beam that the posts would support in the AGT configuration. A minimum deflection of 10 in. was targeted for each test to capture soil force behavior at that displacement level. This data would also serve as essential input for the BARRIER VII simulation models being developed for the AGT system using quarter-post spacing with 8-in. x 8-in. posts.

A bogie vehicle with an approximate weight of 7,000 lb was selected for the tests. This weight was intended to ensure sufficient energy to achieve the target deflection while also preventing the bogie from climbing or riding up the front face of the posts. The impact speed was set at 20 mph to remain consistent with previously conducted dynamic component tests. Three-dimensional test plans and CAD drawings were developed for each configuration. These drawings specified the impact height, bogie mass and velocity, post material and geometry, and embedment depth. Figures 126 through 129 present these test details.

Test No.	Part No.	Post Type	Bogie No.	Impact Height in.	Impact Speed mph	Embeded Post Depth (Y) in.
TRAGT-1	a1	8"x8"x78" Wood Post	2	24	20	43

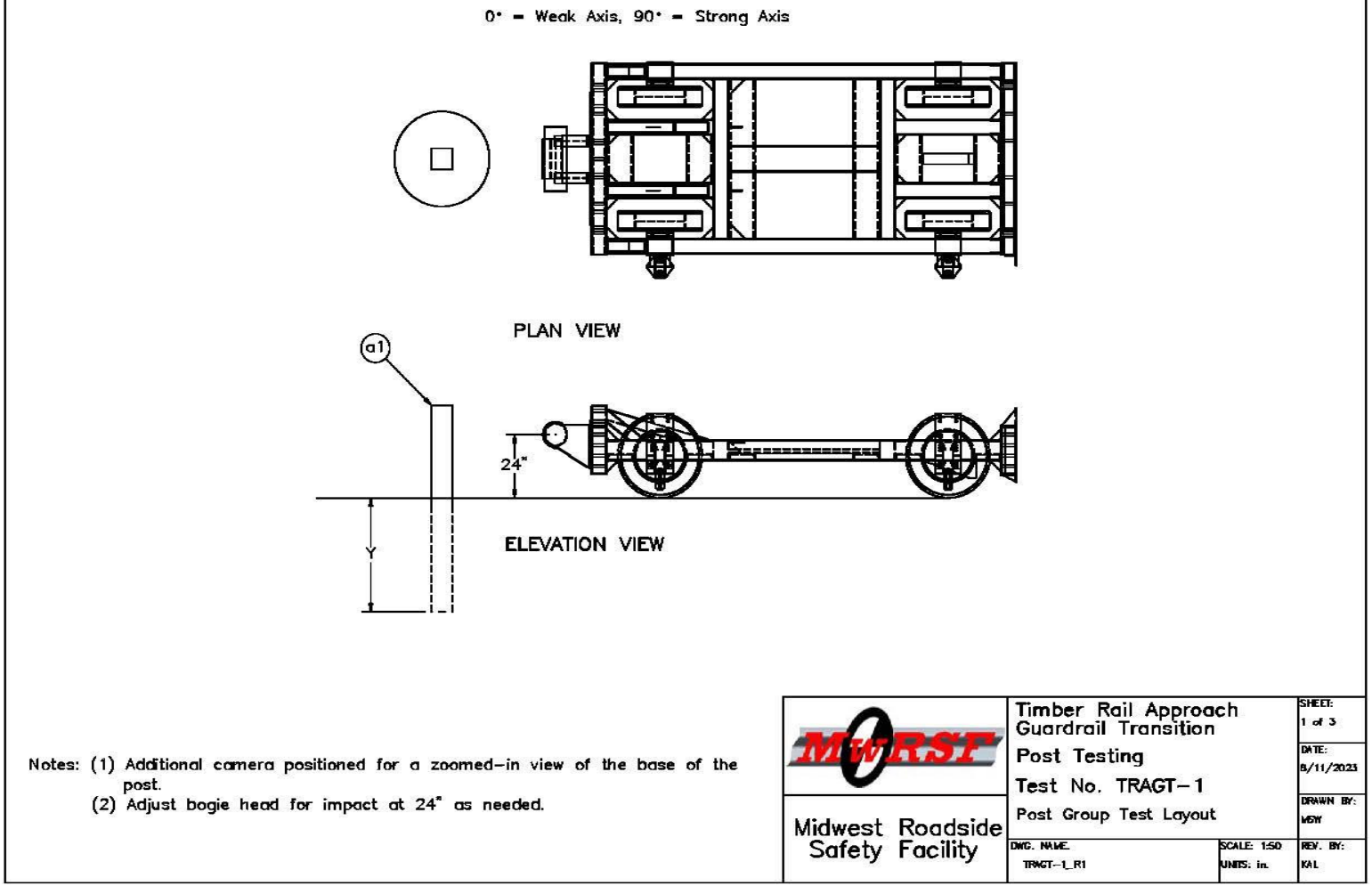

Figure 126. Test Layout, Impact on Single Post, Test No. TRAGT-1

Test No.	Part No.	Post Type	Bogie No.	Impact Height in.	Impact Speed mph	Embeded Post Depth (Y) in.
TRAGT-2	a1	8"x8"x78" Wood Post	2	24	20	43

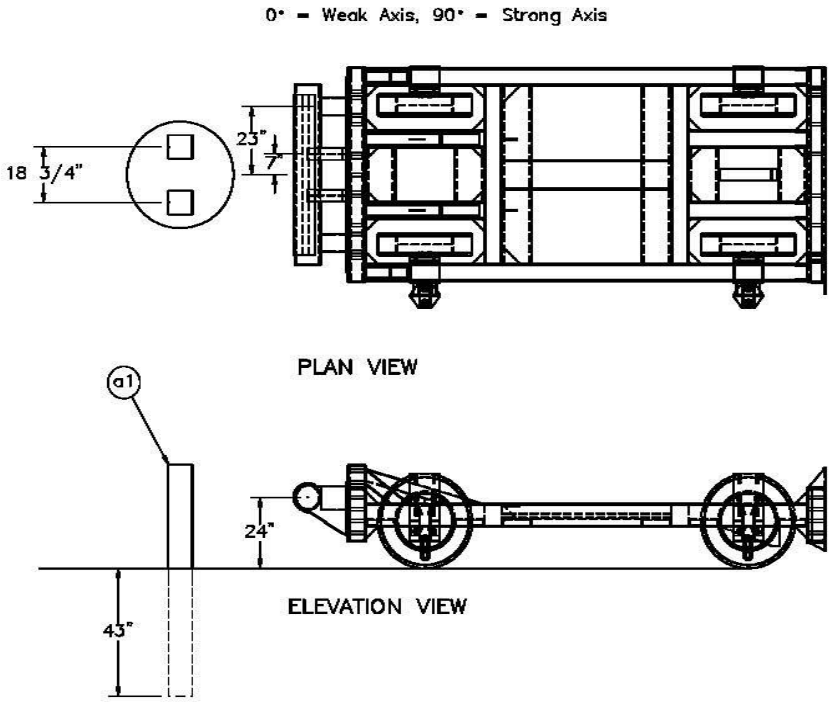

Notes: (1) Additional camera positioned for a zoomed-in view of the base of the post.
(2) Adjust bogie head for impact at 24" as needed.

Midwest Roadside Safety Facility	Timber Rail Approach Guardrail Transition Post Testing Test No. TRAGT-2 Post Group Test Layout	SHEET: 1 of 3 DATE: 2/14/24 DRAWN BY: MSW/MM
	DWG. NAME: TRAGT-2_R2 SCALE: 1:50 UNITS: in.	REV. BY: KAL

Figure 127. Test Layout, Impact on Single Post, Test No. TRAGT-2

Test No.	Part No.	Post Type	Bogie No.	Impact Height in.	Impact Speed mph	Embeded Post Depth (Y) in.
TRAGT-3	a1	8"x8"x78" Wood Post	2	24	20	43

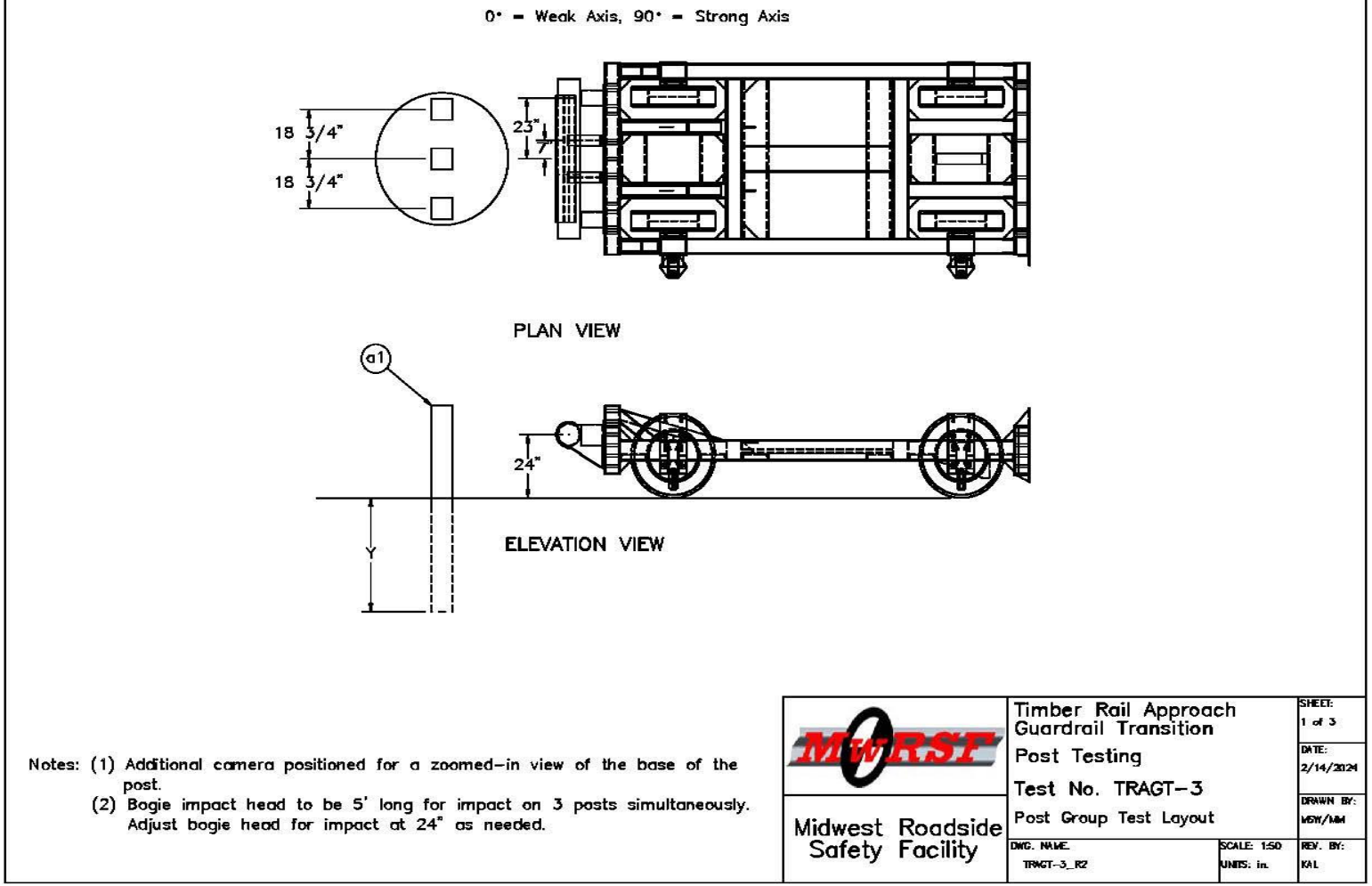

Figure 128. Test Layout, Impact on Single Post, Test No. TRAGT-3

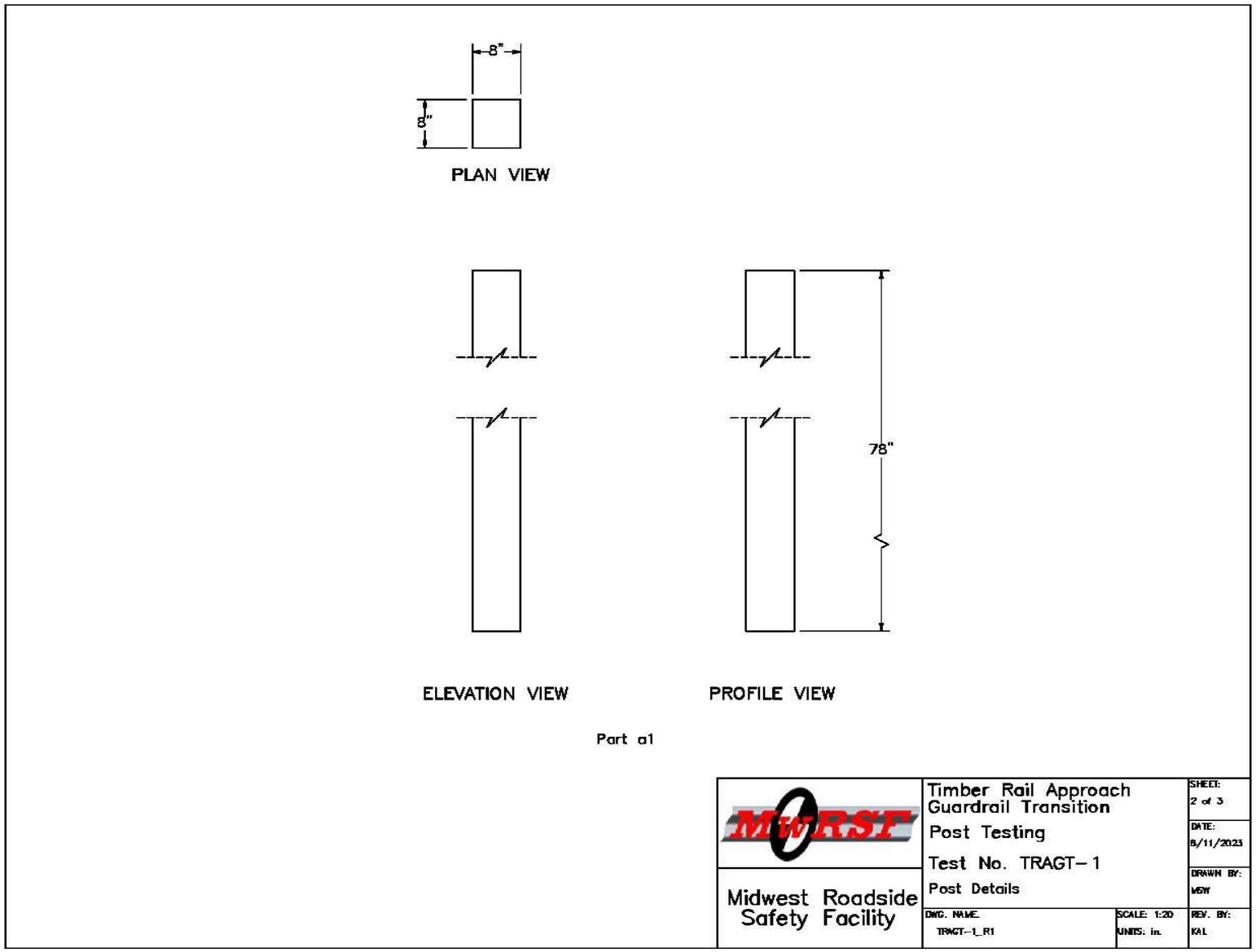

Figure 129. Post Dimensions, Test Nos. TRAGT-1, TRAGT-2, and TRAGT-3

The design assumed posts with actual cross-sectional dimensions of 8 in. x 8 in., consistent with earlier test programs [37]. In practice, however, posts that are surfaced on all four sides (S4S) are typically reduced to 7.5 in. x 7.5 in. To maintain the full 8-in. nominal dimensions, rough-sawn lumber was specified. This type of lumber is cut to size while still wet and is not surfaced, which allows it to retain its larger dimensions upon drying. A brief review of Department of Transportation specifications from several states indicated that surfaced four-sided posts are permitted [141-143], although rough-sawn lumber was more commonly specified, partly because S4S material tends to be more expensive. The review also showed that Grade No. 1 timber is the minimum required for most states, while Nebraska requires select structural grade [144]. Furthermore, Southern Yellow Pine (SYP) was found to be the typical species available for guardrail posts, whereas Douglas Fir was not commonly available [145-146].

Ten rough-sawn SYP posts were procured for the bogie test series and were labeled numerically from 1 to 10. Prior to testing, a secondary visual inspection was conducted to exclude any posts with knots or other defects located within the critical flexural region. Post selection for each test was based on knot size and location, as well as visible ring density. Post no. 1 was selected for the single-post impact test. Posts nos. 7 and 8 were selected for the two-post test. Posts no. 3, no. 4, and no. 5 were selected for the three-post test. The detailed inspection records for all ten posts are included in Appendix L.

4.4.3 Test Facility and Setup

Physical testing was conducted at the MWRSF outdoor testing facility, which is located at the Lincoln Air Park on the northwest side of the Lincoln Municipal Airport. The facility is approximately 5 miles (8 km) northwest from the University of Nebraska-Lincoln's city campus.

4.4.4 Equipment and Instrumentation

Equipment and instrumentation utilized to collect and record data during the component bogie tests included a bogie vehicle, accelerometers, retroreflective optic speed trap, high-speed and standard-speed digital video, and digital still cameras.

4.4.4.1 Accelerometers

Two accelerometers measuring acceleration in longitudinal (direction of bogie movement), lateral, and vertical directions were fastened to the bogie vehicle near its center of gravity, as shown in Figure 130. Only longitudinal acceleration is reported due to minimal impact of other acceleration directions.

Both accelerometers, called SLICE-1 and SLICE-2, were manufactured by Diversified Technical Systems, Inc. of Seal Beach California. Triaxial acceleration and angular sensor modules were mounted inside the bodies of custom-built SLICE 6DX event data recorders equipped with 7GB of non-volatile flash memory and recorded data at 10,000 Hz to the onboard microprocessor. The accelerometers had a range of ±500g's in each of the three directions (longitudinal, lateral, and vertical) and a 1,650 Hz (CFC 1000) anti-aliasing filter. The SLICE MICRO Triax ARS had a range of 1,500 degrees/sec in each of three directions (roll, pitch, and yaw). The raw angular rate measurements were downloaded, converted to the proper Euler angles for analysis, and plotted. The "SLICEWare" computer software program and a customized

Microsoft Excel worksheet were used to analyze and plot both the accelerometer and angular rate sensor data.

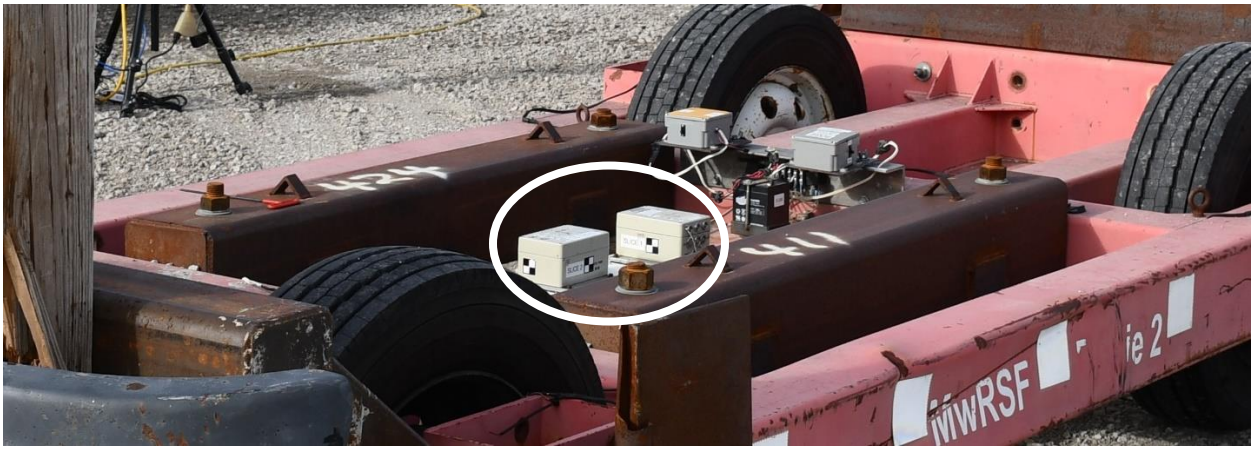

Figure 130. Accelerometers on Bogie Vehicle, SLICE-1 on Left and SLICE-2 on Right

4.4.4.2 Bogie Vehicle

A rigid-frame bogie was used to impact each post, or all posts simultaneously with an extended impact tube. The first test was conducted with a different impact head than the next two tests because the first bogie test did not require an extended impact head. The first bogie head was fabricated with an 8-in diameter x ½ in. thick standard steel pipe, while the second bogie head was fabricated with an 8⅝-in. diameter x ½-in. thick x 60½-in. long steel tube, which is shown in Figure 131. Both bogie heads utilize a neoprene pad wrapped around the tube to reduce local damage to the post and mitigate some of the initial impulse magnitude. The center of the bogie head, which was the impact height, was set 24 in. from the ground for all three tests. The weight of the bogie for test no. TRAGT-1 was 6,854 lb, and the weight of the bogie for test nos. TRAGT-2 and -3 was 7,188 lb.

Figure 131. Bogie Impact Head, Test Nos. TRAGT-2 and TRAGT-3

The bogie tires were directed with a railing guide, which went between two steel tubes extending from the bogie over and down at the front tire and at the back tire, shown in Figure 132. The railing guide came to a stop before impact so that neither bogie vehicle tire covered the guide. A pickup truck pulled the bogie with a steel cable at a 2:1 mechanical advantage. The wire pulling the bogie detached prior to impact, and a radio-controlled brake system installed on the bogie was used to stop the bogie after impact to bring the bogie safely to a stop after the test.

Figure 132. Bogie Railing Guide System, Ends Prior to Impact with Post

4.4.4.3 Retroreflective Optic Speed Trap

A retroreflective optic speed trap was used to determine the speed of the bogie before impact for test nos. TRAGT-1, -2, and -3. In all tests, three retroreflective targets, spaced at approximately 18-in. intervals, were applied to the side of the bogie vehicle, as shown in Figure 133. When the emitted beam of light was reflected by the targets and returned to the Emitter/Receiver, a signal was sent to the data acquisition computer, recording at 10,000 Hz, as well as the external LED box activating the LED flashes. The speed was then calculated using the spacing between the retroreflective targets and the time between the signals. LED light and high-speed digital video analysis are used as a backup if vehicle speeds cannot be determined from the electronic data.

Figure 133. Five Retroreflective Optic Traps on Side of Bogie Vehicle

4.4.4.4 Digital Photography

A single AOS high-speed camera was used for the first bogie test, and two AOS high-speed cameras were used for the following two tests. One GoPro digital video camera was used to record the first test, test no. TRAGT-1, and three GoPro digital video cameras were used to record the following two tests, test nos. TRAGT-2 and -3. A single Panasonic digital camera was used to document TRAGT-1, and two cameras were used to document test nos. TRAGT-2 and -3. The AOS high-speed camera had a frame rate of 500 frames per second, the GoPro video cameras had a frame rate of 240 frames per second, and the Panasonic digital video cameras had a frame rate of 120 frames per second. The cameras were placed laterally from the post, with views perpendicular to direction of bogie movement, as shown in Figure 134. A digital still camera was also used to document pre and post-test conditions for all tests.

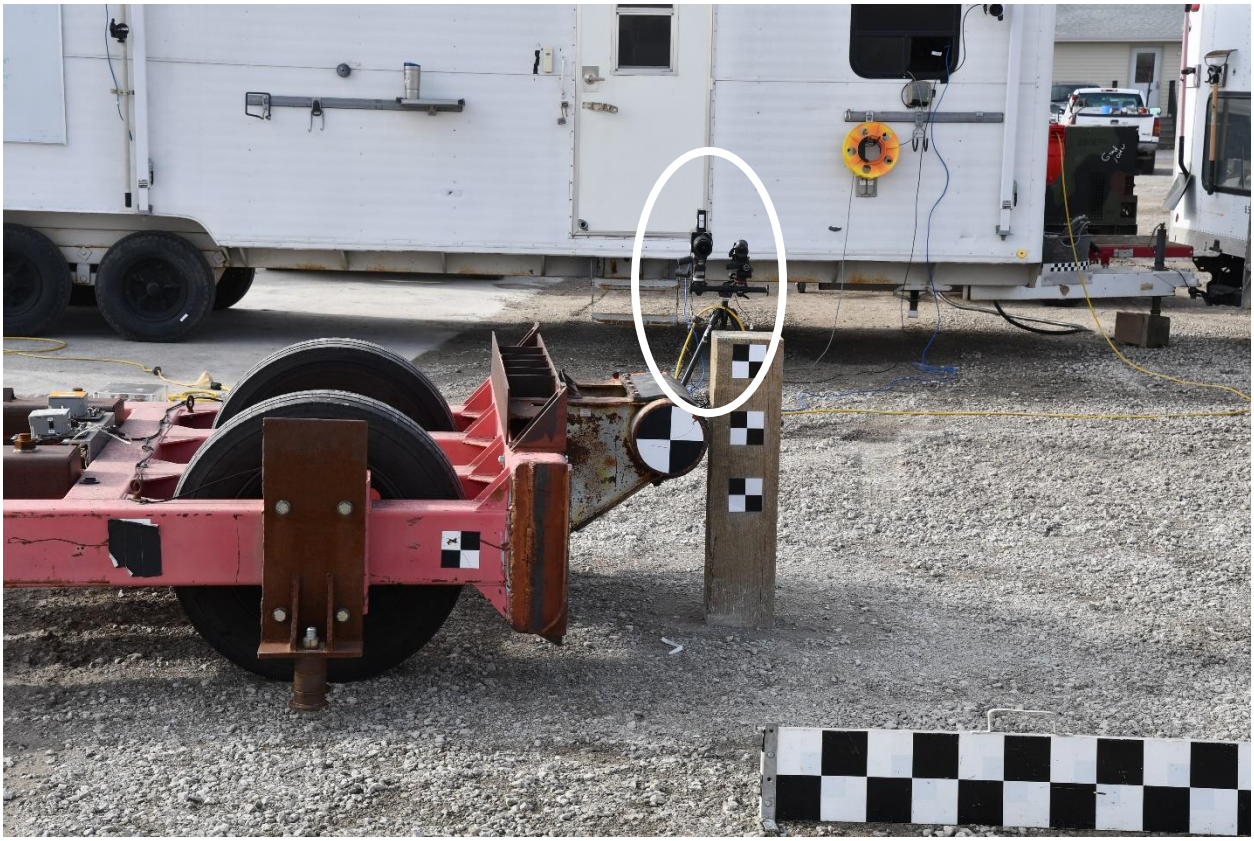

Figure 134. AOS High-Speed Camera

4.4.5 End of Test Determination

The end of the tests occurred when the bogie head was no longer in contact with the post. Contact was lost during post rupture, and there have been no major sources of error found in the data due to using this end of test determination. Sources of error such as bogie vibration are a function of the testing limitations, not when the range of testing is considered complete.

4.4.6 Data Processing

The electronic accelerometer data obtained in dynamic testing was filtered using the SAE Class 60 Butterworth filter conforming to the SAE J211/1 specification [147]. The pertinent acceleration signal was extracted from the bulk of the data signals. The processed acceleration data was then multiplied by the mass of the bogie to get the impact force using Newton's Second Law. Next, the acceleration trace was integrated to find the change in velocity versus time. Initial velocity of the bogie, calculated from the retroreflective optic speed trap data, was then used to determine the bogie's velocity and the calculated velocity trace was integrated to find the bogie's displacement. This displacement is also the displacement of the post. Combining the previous results, a force versus deflection curve was plotted for each test. Finally, integration of the force versus deflection curve provided the energy versus deflection curve for each test.

The information desired from these bogie tests are the differences in the load-displacement curves between a single post, two-post, and three-post systems at the impact height. This information will inform the design team about the possible benefits of using 8x8 posts at closer spacing compared to 8x10 at more distance spacing. Significant variation in the wood strength is a function of wood's high variability, even for wood cut from the same tree – because of knots and grain orientation. Weak points in the wood fail at lower loads, forming cracks which may prevent load distribution through the entire section, and when this occurs the timber member is left resisting the same loads through reduced section.

Although the acceleration data was applied to the impact height, the data came from the c.g. of the bogie. Error was added to the data since the bogie was not perfectly rigid and sustained vibration. The bogie may have also rotated during impact, causing differences in accelerations between the bogie center of mass and the impact head. While these issues may affect the data, the data was valid. Filtering procedures were applied to the data to smooth out vibrations and rotation of the bogie during the test was minor. One useful aspect of using accelerometer data was that it includes influences of the post inertia on the resistive force. This was important as the mass of the post would affect barrier performance as well as test results.

4.5 Testing Results and Discussion

Three dynamic component tests were conducted on three different post configurations. Each setup was impacted by a bogie vehicle weighing either 6,854 or 7,188 lb, traveling at approximately 20 mph. The impact height was 24 in., corresponding to the centerline of the thrie-beam. The variation in bogie weight was due to the use of different impact head configurations; longer impact heads were required for the two-post and three-post tests, which resulted in additional mass.

For each test, data from onboard accelerometers was used to generate force-time and energy-time curves, as well as force-deflection and energy-deflection curves. All three tests resulted in post rupture. A discussion of possible causes for these failures is presented in the following section. Moisture content was measured for some posts before testing, but not all posts were rechecked on the test day.

4.5.1 Test No. TRAGT-1 (One Post)

Test no. TRAGT-1 was conducted on a single 8-in. x 8-in. Southern Yellow Pine (SYP) Grade 1 timber post. The embedment depth for this test was 45.875 in., slightly deeper than the planned 43 in. The bogie used for this test weighed 6,854 lb and was fitted with an impact head designed for a single-post configuration. The actual impact speed was measured at 19.54 mph.

Two accelerometer slices, SLICE-1 and SLICE-2, recorded peak forces of 29.0 kips and 38.6 kips, occurring at 0.0094 seconds and 0.0124 seconds respectively. Neither peak coincided with the initial inertial spike, indicating that these forces are representative of structural response rather than dynamic artifacts.

The post failed due to rupture approximately 44 in. from the top of the post, which corresponds to about 9 in. below the ground line. The displacement at the time of rupture was between 3.22 in. and 4.23 in. Using data from SLICE-1 and SLICE-2, force versus displacement and energy versus displacement curves were generated and are presented in Figures 135 and 136, respectively.

By the time data collection ended at 0.1 seconds, SLICE-1 had recorded 148.2 kip-in. of absorbed energy, while SLICE-2 recorded 127.7 kip-in. The modulus of rupture (MOR) was calculated using the average of the peak forces and was determined to be 13.08 ksi. The soil moisture content measured near the post at the time of testing was 4.67%. Sequential photographs of the impact event and a photograph of the impact aftermath are shown in Figure 137.

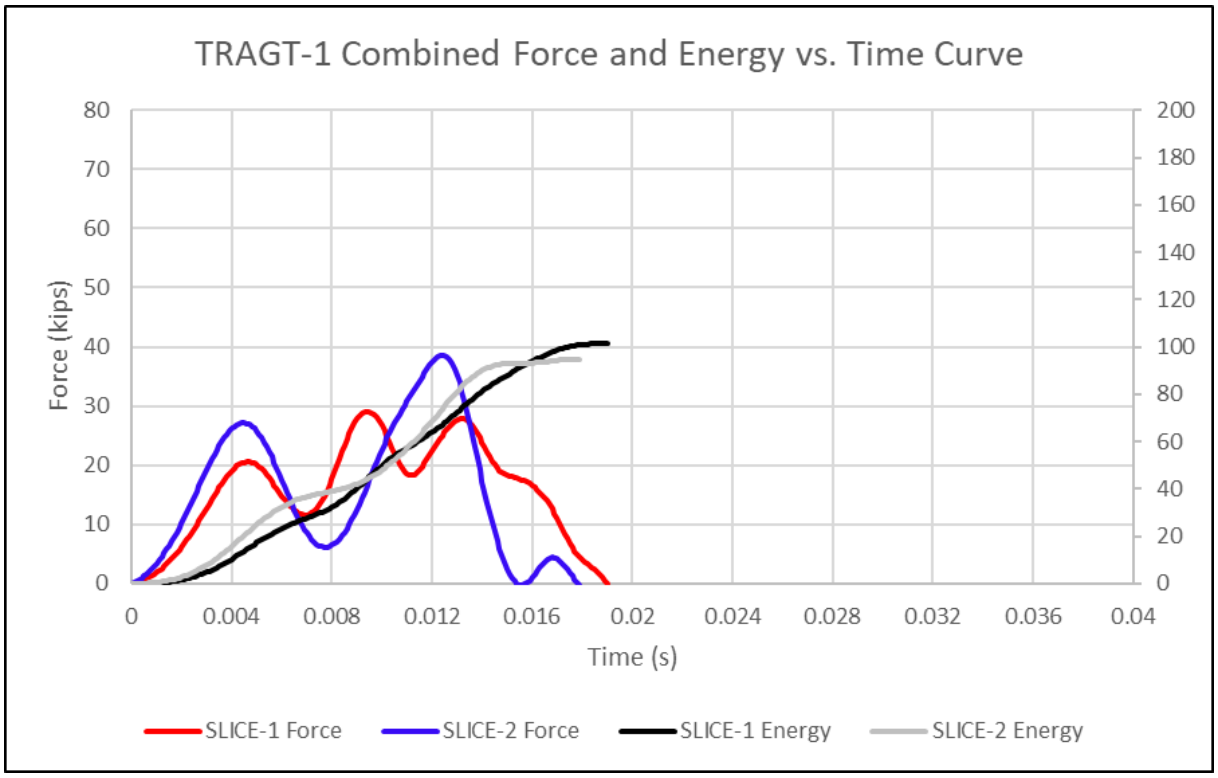

Figure 135. Combined Force and Energy vs. Time Curve, Test No. TRAGT-1

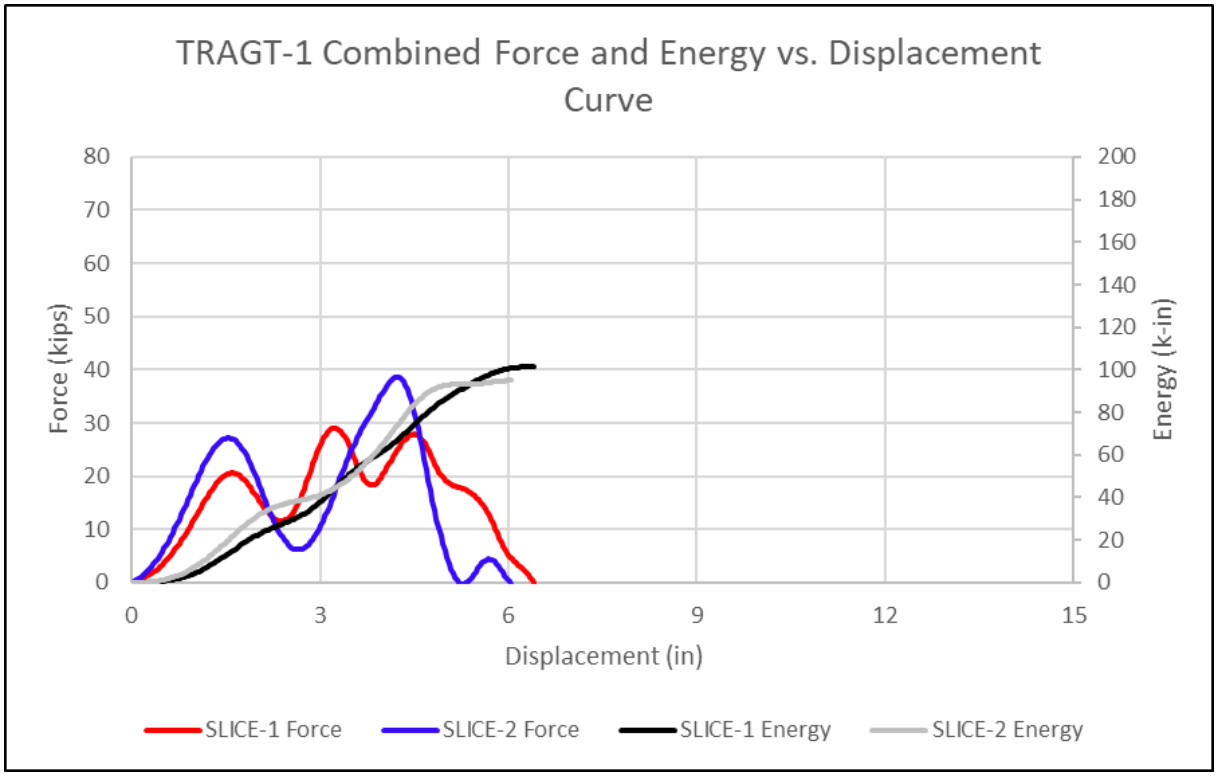

Figure 136. Combined Force and Energy vs. Displacement Curve, Test No. TRAGT-1


Impact


0.020 sec


0.040 sec


0.060 sec


0.080 sec


0.100 sec

Figure 137. High-Speed Camera Time-Sequential, Post-Impact Photographs, Test No. TRAGT-1

4.5.2 Test No. TRAGT-2 (Two Posts)

Test no. TRAGT-2 was conducted on two 8-in. x 8-in. Southern Yellow Pine (SYP) Grade 1 timber posts. Both posts were embedded 43 in. into the ground, consistent with the selected test configuration. For this test, the bogie vehicle weighed 7,188 lb and was equipped with a longer impact head to accommodate the two-post configuration. The actual speed at impact was 20.03 mph.

The maximum forces recorded by SLICE-1 and SLICE-2 were 36.7 kips and 44.7 kips, occurring at 0.0044 seconds and 0.0046 seconds, respectively. Both peak forces occurred within the initial inertial spike, making it difficult to determine whether these values fully reflect the structural response of the posts.

The posts ruptured approximately 41 in. from the top, or 6 in. below the ground surface. For SLICE-2, it was not possible to determine the force at which rupture occurred, since the subsequent force peak was significantly lower and appeared after rupture had already taken place, as inferred from SLICE-1. For SLICE-1, rupture occurred at a displacement of approximately 3.10 in.

Force versus displacement and energy versus displacement curves were generated using data from both accelerometer slices and are shown in Figures 138 and 139, respectively. By the end of data collection at 0.0858 seconds, SLICE-1 had recorded 176.1 kip-in. of absorbed energy, while SLICE-2 had recorded 173.4 kip-in. The modulus of rupture could only be calculated using SLICE-1, which was the only sensor that recorded a peak force outside the inertial spike. This peak was 17.90 kips, corresponding to a modulus of rupture of 6.29 ksi. The soil moisture content near the test location was measured at 3.93 %. Sequential photographs of the impact event and a photograph of the aftermath are shown in Figure 140.

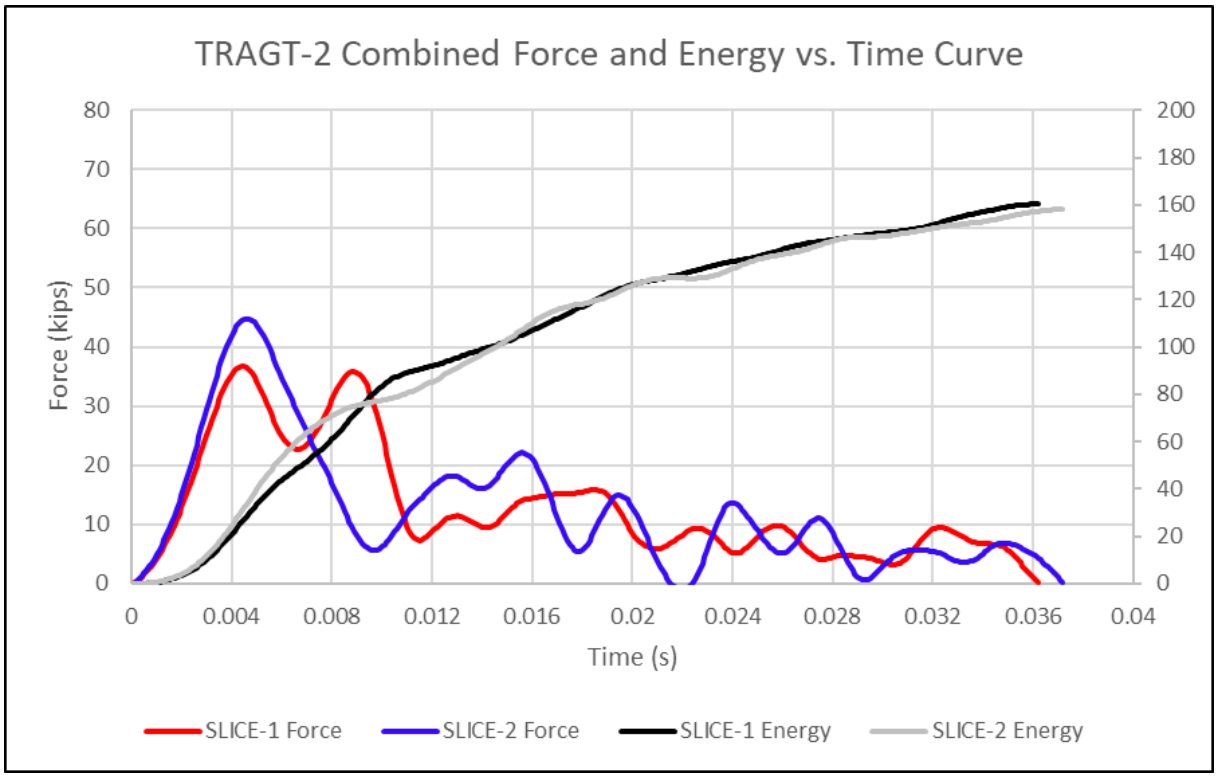

Figure 138. Combined Force and Energy vs. Time Curve, Test No. TRAGT-2

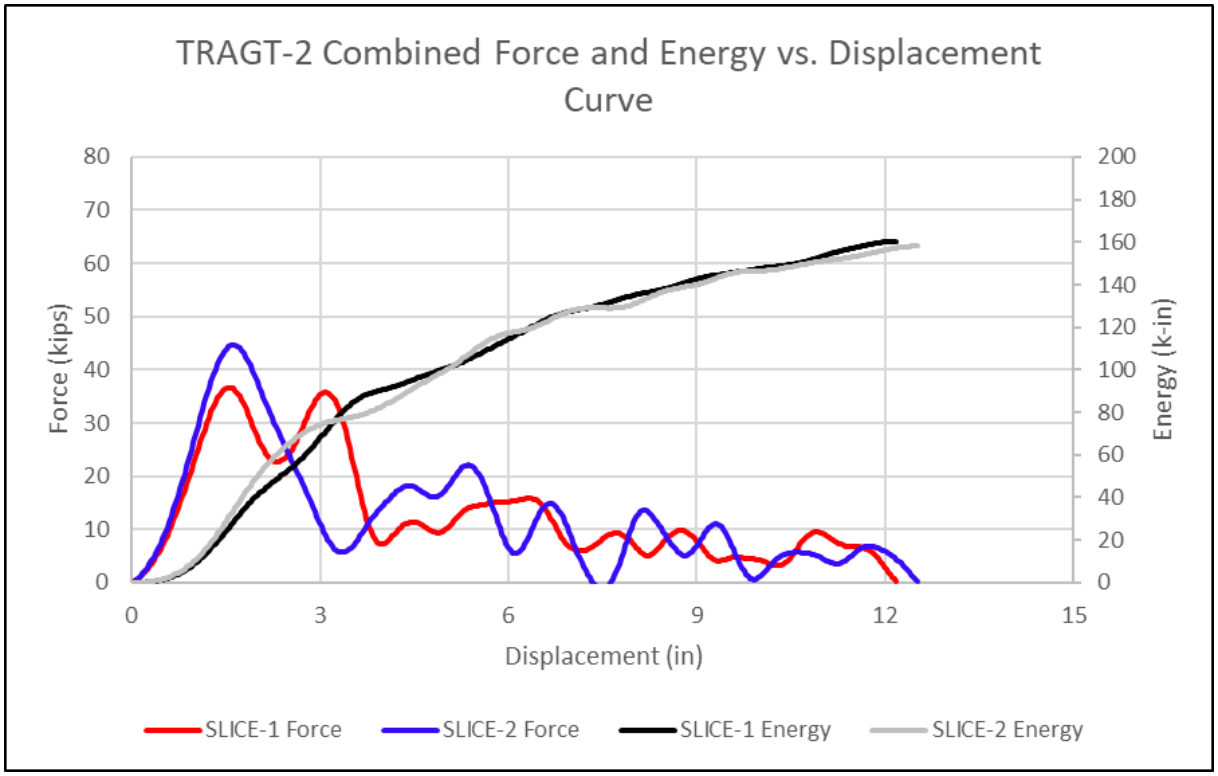

Figure 139. Combined Force and Energy vs. Displacement Curve, Test No. TRAGT-2


Impact


0.020 sec


0.040 sec

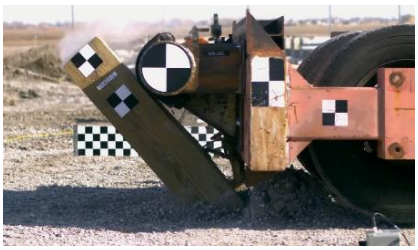
0.060 sec


0.080 sec


0.100 sec

Figure 140. High-Speed Camera Time-Sequential, Post-Impact Photographs, Test No. TRAGT-2

4.5.3 Test No. TRAGT-3 (Three Posts)

Test no. TRAGT-3 was conducted on three 8-in. x 8-in. Southern Yellow Pine (SYP) Grade 1 timber posts. All three posts were embedded 43 in. into the soil, consistent with the previous test setups. The bogie vehicle used for this test weighed 7,186 lb and was equipped with a longer impact head appropriate for a multi-post configuration. The actual impact speed was recorded as 19.74 mph.

Post rupture behavior was captured using an AOS digital high-speed camera. Post no. 4 appeared to rupture immediately upon impact, while the remaining two posts failed approximately 0.01 seconds after impact. The maximum force recorded by SLICE-1 was 67.0 kips at 0.0087 seconds, and SLICE-2 recorded a peak of 63.9 kips at 0.0048 seconds. The peak from SLICE-2 occurred within the inertial spike, while the SLICE-1 peak was recorded outside of it. The rupture occurred approximately 39.17 in. from the top of the posts, which corresponds to 4.17 in. below the ground surface. The failure was associated with a displacement of 2.97 in.

Force versus displacement and energy versus displacement curves were generated from SLICE-1 and SLICE-2 data and are shown in Figures 141 and 142, respectively. At the end of data collection, which concluded at 0.07 seconds, SLICE-1 recorded an absorbed energy of 190.6 kip-in. and SLICE-2 recorded 185.7 kip-in. The SLICE-2 force-displacement curve exhibited a secondary rise in force following the initial peak. This secondary “bump,” with a value of 55.8 kips, was interpreted as a secondary peak adjacent to the inertial spike. This value was averaged with the second peak from SLICE-1 to estimate the modulus of rupture. Based on this approach, the calculated MOR was 6.76 ksi. The measured soil moisture content at the time of testing was 3.91%. Sequential photographs of the impact event and a photograph of the aftermath are presented in Figure 143.

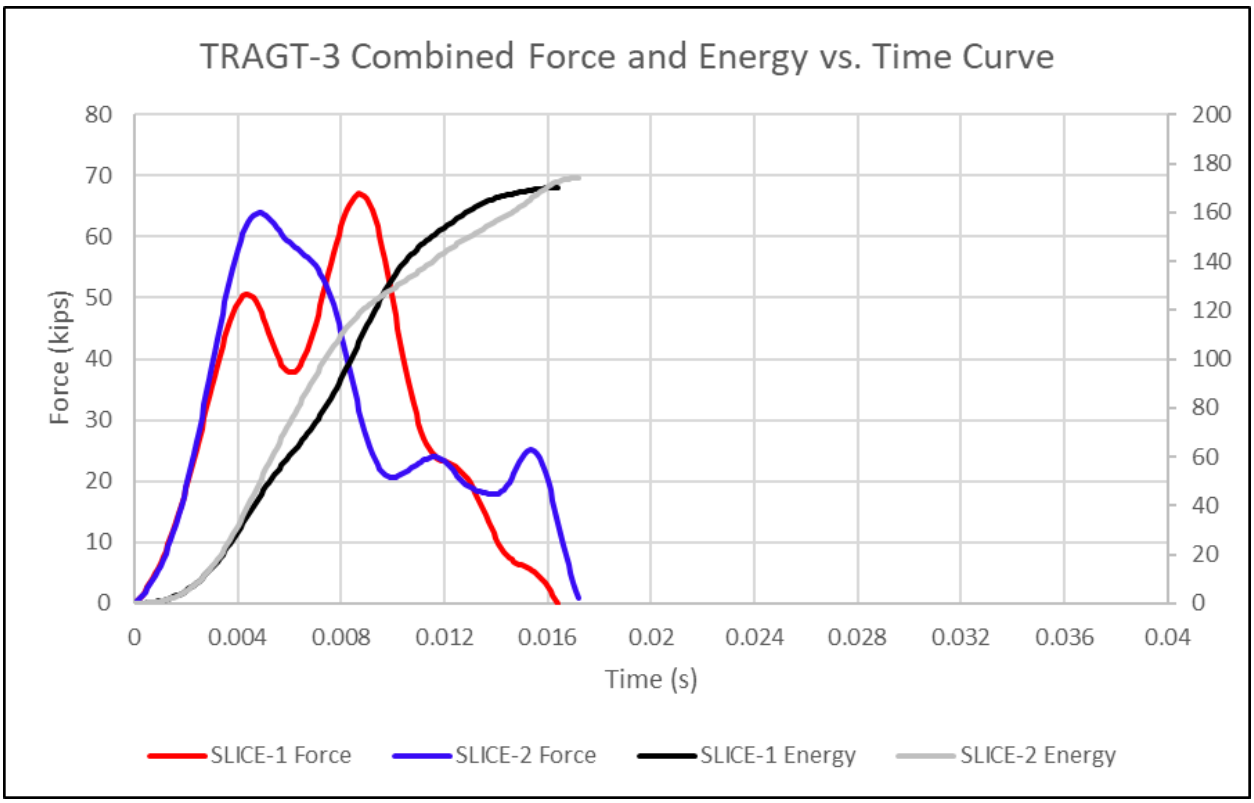

Figure 141. Combined Force and Energy vs. Time Curve, Test No. TRAGT-3

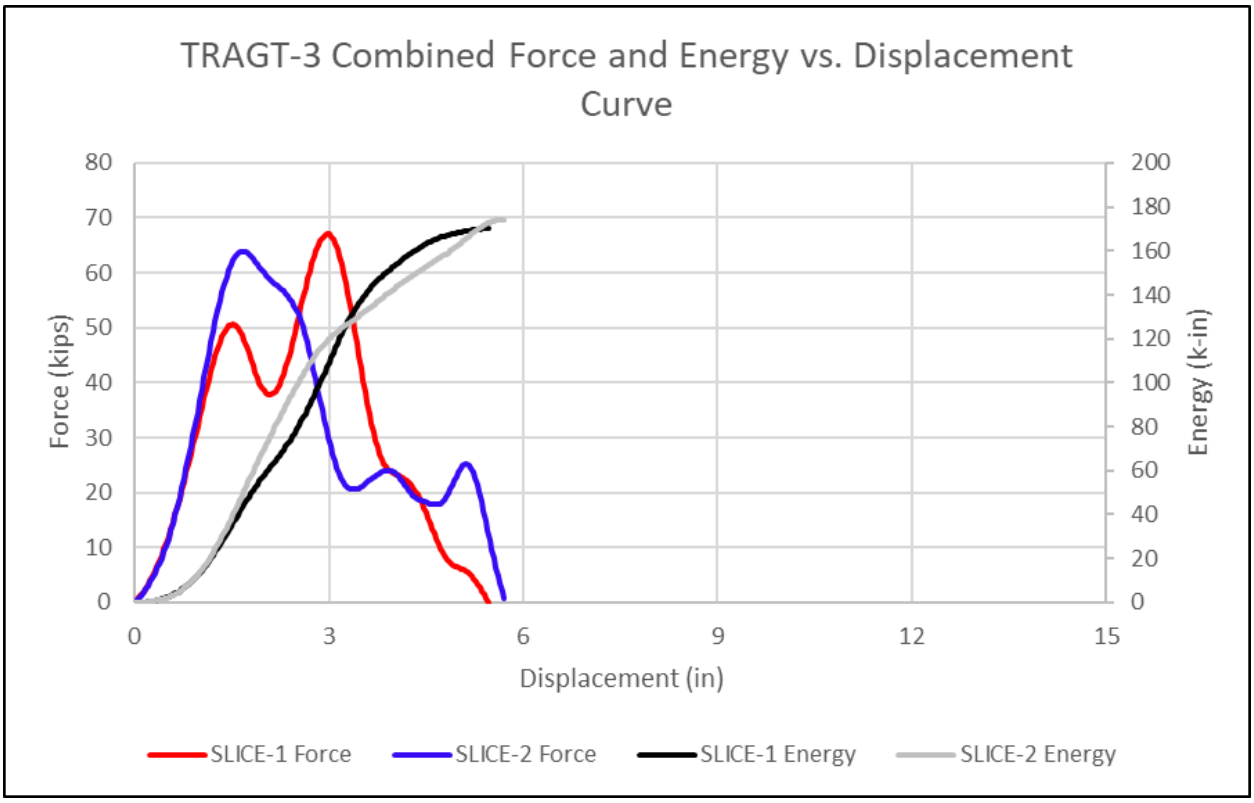

Figure 142. Combined Force and Energy vs. Displacement Curve, Test No. TRAGT-3


Impact


0.020 sec


0.040 sec


0.060 sec


0.080 sec


0.100 sec

Figure 143. High-Speed Camera Time-Sequential, Post-Impact Photographs, Test No. TRAGT-3

4.5.4 Discussion of Results

Post rupture was not anticipated in these tests, although the allowable stress design (ASD) estimates for the modulus of rupture (MOR) were relatively close to the values observed. The MOR values obtained from earlier tests by SwRI and MwRSF remained within a plausible range. While estimating the precise location of rupture below the soil line is difficult, even assuming rupture at the ground surface results in MOR values that exceed the estimated applied soil stress on the posts.

In particular, the first test yielded an MOR of 10.7 ksi, which was more than double the estimated applied stress of 4.74 ksi. This estimate was based on a peak force near 38 kips, a distance from the ground to the centroid of rotation of 24 in., and a post section modulus of 85.33 in^3. For the second and third tests, the calculated MOR values ranged from 5.06 to 5.91 ksi.

One major source of variability is the soil, which remains a significant unknown factor. Although testing was performed in December and February, ambient temperatures in the days preceding the tests remained consistently above freezing. Furthermore, worksite equipment used during preparation introduced localized heating near the posts. These factors may have weakened the soil, resulting in a lower resistance than originally anticipated.

An additional variable under consideration was the method of soil compaction used in the 1997 crash test of the AGT system. While no direct compaction method was listed for that test, a related test conducted at the same time and on the same transverse glulam deck referenced the use of a pneumatic hand tamper. In later reports [37], a distinction was made between moderate- and high-energy pneumatic tampers. Because this distinction was not specified in the earlier report, it is reasonable to infer that a moderate compaction method may have been used, which would result in a lower soil stiffness compared to that of heavily compacted soils.

Another contributing factor was the difference in timber grade between the tested bogie posts and those used in the crash-tested AGT. The bogie test specimens were SYP Grade 1, whereas the AGT system used SYP Grade No. 1D. The “1D” designation refers to dense Grade 1 lumber, which generally exhibits higher bending strength. While AASHTO does not provide separate values for dense grades, the NDS does. According to NDS, dense SYP is defined as material having six or more growth rings/in. with at least one-third summerwood, or four rings/in. with at least one-half summerwood [148 The tabulated bending strength of Grade 1 SYP is 1.35 ksi, whereas for Grade 1D SYP, it is 1.55 ksi [14-15].

Although the difference in timber grade from the 1997 crash tests was not recognized until after the present bogie tests, the use of denser material would likely not have altered the outcome of the first or subsequent tests. The bogie impact and soil yield capacity significantly exceeded the post significantly, as seen from the post capacity in test TRAGT-1. However, this difference may explain some of the variation between test results and expectations.

In the absence of a single definitive explanation for the rupture behavior, the bogie testing still provided valuable insight into design limitations. The 8-in. x 8-in. posts may remain viable for AGT applications, provided their use accounts for the limitations observed in bogie testing. The posts used in this study were Grade 1 SYP, while the crash-tested AGT system used Grade 1D, which is stronger and more consistent with the performance seen in the first test. The first post

ruptured at approximately 5 in. of deflection. If denser posts were used together in an AGT configuration, it is possible that system deflections would remain below this failure threshold.

Based on these observations, the allowable deflection for 8-in. x 8-in. posts at quarter-post spacing was limited to 5 in. The post yield moment used in BARRIER VII modeling was therefore set equal to the rupture capacity of the posts, thereby ensuring that the model reflects the observed failure mode while incorporating a conservative design threshold.

4.6 MASH 2016 AGT Design

4.6.1 Design Summary

The new AGT was designed to meet the MASH 2016 TL-3 impact conditions. These conditions involve impact from both 1100C and 2270P vehicle types, each traveling at 62 mph and striking the system at a 25-degree angle. Two AGT configurations were developed and evaluated: a half-post spacing system utilizing 8-in. x 10-in. posts near the bridge railing, and a quarter-post spacing system utilizing 8-in. x 8-in. posts near the bridge railing.

Both systems were designed to accommodate a future 2-in. asphalt overlay, as described in Section 4.3.1.3. Each system incorporated an upstream transition segment consistent with the transition design developed in prior studies [36], with modifications for timber post equivalents [37]. Both configurations were connected to the Midwest Guardrail System (MGS).

The BARRIER VII finite element modeling program was used to simulate TL-3 crash conditions for both vehicle types and AGT configurations. Evaluation criteria for performance included system deflection, pocketing potential, and internal force magnitudes throughout the railing system, as part of a Critical Impact Point (CIP) investigation.

In the initial design of the quarter-post system, an 8-ft spacing was used between the first AGT post and the adjacent bridge post. This spacing was later reduced to 7 ft to mitigate failure risk in the first AGT post. Without this adjustment, the failure of one post increased the spacing to 9 ft – 6¾ in. and resulted in end shoe force demands approaching the known rupture capacity of the thrie-beam end connection.

4.6.2 Half-Post Spacing BARRIER VII Model

The half-post spacing configuration refers to the placement of stiffer AGT posts near the bridge railing at half of the standard post spacing. The first 8-in. x 10-in. AGT post was positioned 8 ft away from the last bridge post, followed by two additional 8-in. x 10-in. AGT posts at half-post spacing. All 8-in. x 10-in. posts were embedded 49 in. into the ground and extended 35 in. above the ground, resulting in a total post length of 7 ft. These posts supported a 25-ft section of nested 12-gauge thrie-beam.

Following this segment were five 6-in. x 8-in. posts placed at quarter-post spacing. These posts were embedded 40 in. and extended 32 in. above grade, giving them a total length of 6 ft. They supported both the 25-ft nested 12-gauge thrie-beam and a 12.5-ft segment of 12-gauge thrie-beam. This segment was followed by four additional 6-in. x 8-in. posts at half-post spacing, embedded 40 in. and extending 32 in. above ground. These final posts supported a 12.5-ft segment

of 12-gauge thrie-beam, a 12.5-ft transition segment from thrie-beam to W-beam, and the W-beam of the MGS system. This final portion provided the structural connection between the AGT and MGS. The complete BARRIER VII model for this configuration is presented in Figure 144.

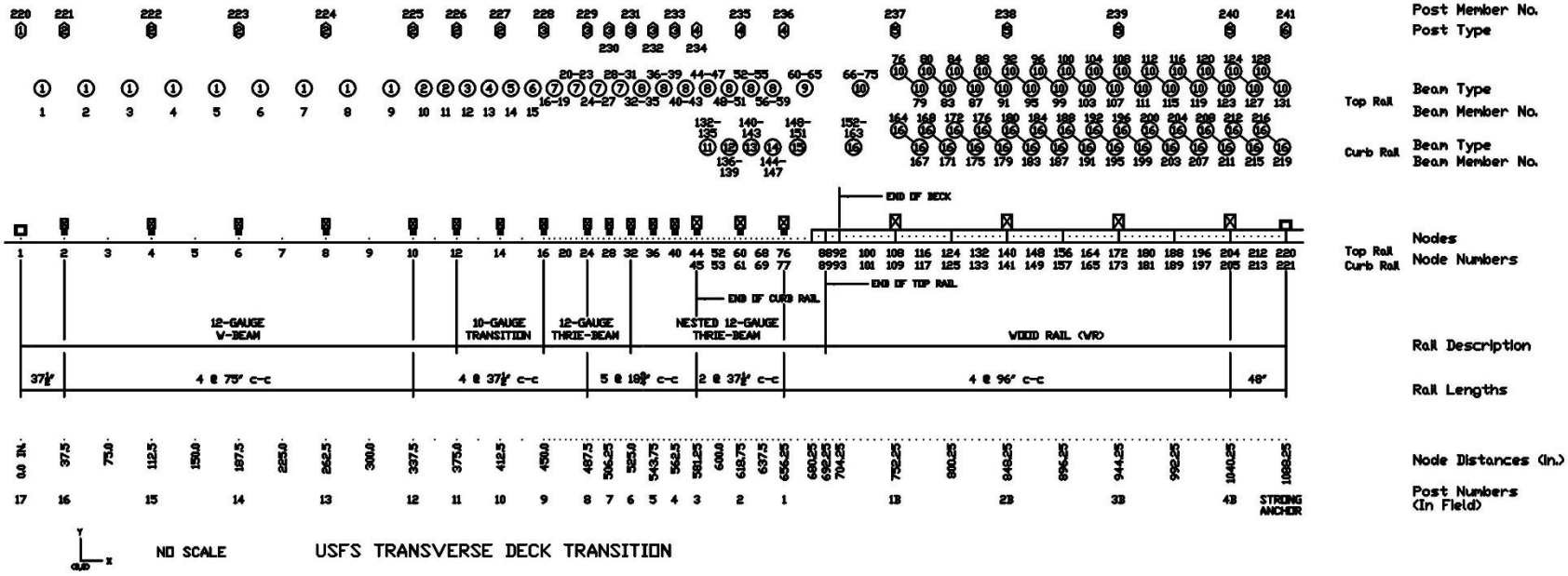

Figure 144. Half-Post BARRIER VII Model

4.6.2.1 Node Spacing

The BARRIER VII model used two nodes between posts up until the start of the upstream stiffness transition, which were spaced 37½ in. or 18¾ in. apart. To support the CIP analysis, the region from the beginning of the upstream stiffness transition to the first bridge post was modeled with higher spatial resolution. Finer element lengths in this area were used to accurately capture local deflections and identify critical locations for vehicle pocketing. From the W-beam to thrie-beam transition point to the final AGT post, the model utilized beam elements with lengths of 4.6875 in. In general, quarter-post spaced segments were modeled with four elements between posts, and half-post spaced segments with sixteen elements between posts. Beyond the last AGT post, beam elements were 6 in. long, which resulted in sixteen elements across the 8-ft bridge post span.

4.6.2.2 Post Parameters

Six post elements were defined in the BARRIER VII model to represent different regions of the AGT system. These included two end posts located at the upstream and downstream ends of the system, one bridge post, one 8-in. x 10-in. AGT post, and two 6-in. x 8-in. AGT post types.

The end post properties were based on the calibrated post parameters previously shown in Table 26. Adjustments were made to node height, weight, shear capacity, and deflection limits to reflect the updated system configuration. The node height increased to 24.875 in. for the upstream end and 33.25 in. for the downstream end to reflect taller system geometry. The upstream end post weight and shear capacity were updated to match the other 6-in. x 8-in. posts, with values of 32.67 lb and 35.7 kips, respectively. These values were calculated using the same procedures described in Section 4.2.5.4 for post weight and in Section 4.2.5.1 for shear capacity. Additionally, the upstream post's maximum allowable lateral deflection was reduced from 20 in. to 5 in. to reflect limited deformation when the post is encased in a metal sleeve. All post parameters are provided in Tables 40 and 41.

Table 40. Post Properties for Half-Post AGT BARRIER VII Model

B7 Post No.	Height of Node I (in.)	Height of Node j (in.)	k_A (k/in.)	k_B (k/in.)	W (lb)	M_B (k-in.)	M_A (k-in.)
1	24.875	0	102.5	2.48	32.67	735	191.1
2	24.875	0	2.4	4.2	32.67	224	256
3	24	0	2.4	4.2	32.67	224	256
4	24	12.625	7.2	11.3	59.56	481	458
5	33.25	14.625	18.76	29.86	239.37	833	1327.7
6	33.25	14.625	6338	13943	94.7	6820	1540

Table 41. Post Properties for Half-Post AGT BARRIER VII Model, Cont.

B7 Post No.	Yield Accuracy Limit (%)	V_A (k)	V_B (k)	δ_A (in.)	δ_B (in.)	Post Description
1	0.1	35.7	35.7	5.0	5.0	End Post
2	0.1	35.7	35.7	5.0	20.0	6x8 Wood Post
3	0.1	35.7	35.7	5.0	20.0	6x8 Wood Post
4	0.1	59.5	59.5	6.0	15.0	8x10 Wood Post
5	0.1	93.8	103.7	4.0	10.0	Bridge Post
6	0.1	310	70	1.0	1.0	End Post

The bridge post parameters were drawn from the Phase IIa calibration effort and were further modified as described in 3.2.2. These properties were not originally tabulated for BARRIER VII because additional changes were applied to reflect behavior under elevated moisture conditions, as presented in Table 16. Specifically, three attributes were updated: the stiffness in the "B" direction, the yield moment about the "A" axis, and the shear capacity.

The "B" direction stiffness was revised to 29.86 kips/in., based on the values in Table 13, which account for different load distribution widths. This change was introduced to ensure the AGT system approaching the bridge railing exhibits increased potential for pocketing, consistent with prior test observations. The yield moment about the "A" axis was adjusted to 1,327.7 kip-in., and the post shear capacity was increased based on the values presented in Table 21 and the methodology described in Section 3.3.3.1. Complete bridge post values are shown alongside end post data in Table 42.

Table 42. Bridge Post Element Properties for BARRIER VII

Member Type	Member Size	Upper Rail Node Height (in.)	Curb Rail Node Height (in.)	Stiffness k_A & k_B (k/in.)	Weight (lb)	Nominal Yield Moment (k-in.)	Failure Shear Force (k)	Failure Deflection (in.)
Bridge Post	8¾"x12" (glulam)	33.25	14.625	A-axis: 18.76 B-axis: 29.86	239.37	B-axis: 833.1 A-axis: 1327.7	A-axis: 93.8 B-Axis 103.7	A-axis: 4.0 B-axis: 10.0

The 8-in. x 10-in. post parameters defined in the BARRIER VII model included node heights, stiffness values in lateral and longitudinal directions, post weight, yield moment, shear capacity, and deflection limits. Node heights were assigned based on the vertical centers of the thrie-beam and curb rail taper.

Lateral stiffness was obtained from bogie test load-deflection curves, where the 8-in. face exhibited a stiffness of 11.3 kips/in. [37]. Initially, the longitudinal stiffness was estimated using the same approach, but the BARRIER VII model produced excessive axial loads. This behavior indicated that the soil stiffness contribution in the longitudinal direction was overestimated. In this orientation, the post is expected to rupture rather than rotate, meaning soil resistance does not play a significant role. Additionally, the stiffness over the 10-in. face is smaller than the stiffness over the 8-in. face due to differences in moment of inertia. Therefore, the longitudinal stiffness was adjusted using the ratio of longitudinal to lateral moments of inertia (0.64), multiplied by the lateral stiffness, resulting in a longitudinal stiffness of 7.2 kips/in. Post weight was calculated based on the exposed portion above ground and estimated as 59.56 lb.

The yield moment for the 8-in. face was determined using an average soil yield force of 17.67 kips at 15 in. of deflection, derived from bogie testing on 8-in. x 10-in. posts with 48-in. embedment. Using Equation 32, and applying a bogie impact height (H_1) of 24.875 in, system impact height (H_2) of 24 in., a bogie embedment depth (D_e) of 48 in., and a system embedment depth (D_e') of 49 in., the resulting yield moment was 458 kip-in. For the 10-in. face, the average soil yield force was 25.6 kips based on bogie testing of 10-in. x 10-in. posts at 5 in. deflection and 54-in. embedment. Using the same equation with an adjusted embedment depth of 49 in., the yield moment was calculated as 481 kip-in. The shear capacity was determined using the method in Section 4.2.5.1 and resulted in a limiting shear of 59.5 kips. The deflection limits were set at 6 in. for bending over the 10-in. face and 15 in. for bending over the 8-in. face. These post parameters were shown in Tables 40 and 41.

The 6-in. x 8-in. post parameters also included node height, stiffness, weight, yield moment, shear capacity, and deflection limits. Node heights were chosen based on the centerlines of the thrie-beam and curb rail taper. Lateral stiffness was taken from bogie test data on 6-in. x 8-in. posts used in research on MGS performance over wire-faced MSE walls [150], and was set at 4.2 kips/in. on the 6-in. face. Longitudinal stiffness was derived from the ratio of longitudinal to lateral moment of inertia (0.56), multiplied by the lateral stiffness. This resulted in a longitudinal stiffness of 2.4 kips/ in. Post weight was estimated by calculating the portion above ground, resulting in a value of 32.67 lb.

The yield moment over the 6-in. face was calculated from an average soil yield force of 10.28 kips at 20 in. deflection from tests on 6-in. x 8-in. posts embedded 40 in. With H_1 equal to 24.875 in. and H_2 equal to 24 in., Equation 32 yielded a moment of 256 kip-in. For the 8-in. face, the estimated soil force exceeded the rupture threshold. As a result, the rupture limit was taken as the controlling yield moment. This was calculated based on a modulus of rupture (MOR) value of 4.67 ksi for the section modulus of the 6-in. x 8-in. post, giving a limiting moment of 224 kip-in. The shear capacity was again developed using the method from Section 4.2.5.1 and set at 35.7 kips. The deflection limits were established at 5 in. for bending over the 8-in. face and 20 in. for the 6-in. face. All post values were included in Tables 40 and 41.

4.6.2.3 Beam Parameters

Seventeen different beam element types were defined within the BARRIER VII model to represent the various structural components of the AGT system. The model included one element for the 12-gauge W-beam and two elements for the nested 12-gauge W-beam. Four elements were defined to represent the 10-gauge W-beam to thrie-beam transition. One element was created for

the 12-gauge thrie-beam, and two elements were created for the nested 12-gauge thrie-beam. One element was used for the upper glulam railing, five elements for the lower glulam taper, and one element for the lower glulam rail.

The material properties for the W-beam and thrie-beam sections are well-established and available in multiple prior AGT BARRIER VII models [16, 25, 36-37]. The parameters used in this study were adopted directly from those examples without modification, except for the beam element lengths, which were adjusted to suit the refined mesh and modeling strategy.

The glulam railing components were drawn from BARRIER VII models developed by Mike Fowler and Jared Duren [10, 25]. The upper and lower glulam railing properties were based on Jared Duren's model, with revisions providing detailed definitions for the AGT transition region. The upper and curb railing axial capacities were reduced to the splice limit defined in Table 23.

The lower curb rail taper was divided into five individual elements with gradually increasing section properties. This stepped configuration allowed the model to more accurately capture the gradual stiffness transition in the lower railing. The curb rail taper is fastened to the AGT posts using a single ⅝-in. diameter ASTM A307A bolt at each post. This bolt constrained the axial force capacity of each taper element to the bolt's shear capacity, which was calculated to be 6.3 kips. For all beam elements in the taper, the flexural strength from Phase IIa was scaled based on the average geometric properties of the corresponding section. All beam element parameters are listed in Table 43.

Table 43. Half-Post BARRIER VII Model Beam Parameters

B7 Beam No.	Beam Element Description	Moment of Inertia (in.^{4})	Area (in.^{2})	Length (in.)	Young's Modulus (ksi)	Weight (lb/ft)	Yield Force (k)	Yield Moment (k-in.)
1	12-Gauge W-Beam	2.29	1.99	18.75	30000	6.92	99.5	68.5
2		2.29	1.99	9.375	30000	6.92	99.5	68.5
3	10-Gauge W-Beam to Thrie-Beam Transition	2.48	2.13	18.75	30000	7.40	106.2	73.8
4		2.84	2.40	18.75	30000	8.38	120.0	84.0
5		3.20	2.68	18.75	30000	9.35	134.0	94.0
6		3.58	2.96	18.75	30000	10.32	148.0	104.2
7	12-Gauge Thrie-Beam	3.76	3.10	4.6875	30000	10.81	155.0	109.5
8	Nested 12-Gauge Thrie-Beam	7.52	6.20	4.6875	30000	21.62	310	219
9		7.52	6.20	6	30000	21.62	310	219
10	Glulam Upper Rail	1397.6	145.1	6	1600	34.5	190.9	1568.6
11	Tapered Curb Rail	78.5	41.6	4.6875	1500	9.9	6.3	137.2
12		180.0	54.9	4.6875	1500	13.1	6.3	238.5
13		344.4	68.1	4.6875	1500	16.2	6.3	367.6
14		587.1	81.4	4.6875	1500	19.4	6.3	524.6
15		978.6	96.5	6	1500	23.0	6.3	737.5
16	Glulam Curb Rail	1260.0	105.0	6	1500	25.0	107.4	872.8

4.6.3 Quarter-Post Spacing BARRIER VII Model

The quarter-post spacing system configuration is named for the reduced spacing of stiffened posts near the bridge railing. The first 8-in. x 8-in. AGT post was spaced 8 ft from the adjacent bridge post. This was followed by six additional 8-in. x 8-in. AGT posts at quarter-post spacing. Of these, the first four were embedded 46 in. into the ground and extended 32 in. above grade, giving a total post length of 6.5 ft. The next three were embedded 40 in. into the ground and also extended 32 in. above grade, for a total length of 6 ft. These seven posts supported a 25-ft nested 12-gauge thrie-beam segment of the AGT.

Following this segment, four 6-in. x 8-in. posts were installed at quarter-post spacing, embedded 40 in. into the ground and extending 32 in. above grade. These posts supported the 25-ft nested 12-gauge thrie beam and an additional 12.5-ft 12-gauge thrie-beam segment. The final section consisted of four 6-in. x 8-in. posts at half-post spacing, also embedded 40 in. and extending 32 in. above grade. These supported a 12.5-ft 12-gauge thrie beam, the 12.5-ft transition between the thrie-beam and W-beam, and the W-beam segment of the MGS. This portion completed the AGT connection to the MGS. The BARRIER VII model for the quarter-post spacing configuration is shown in. Figure 145.

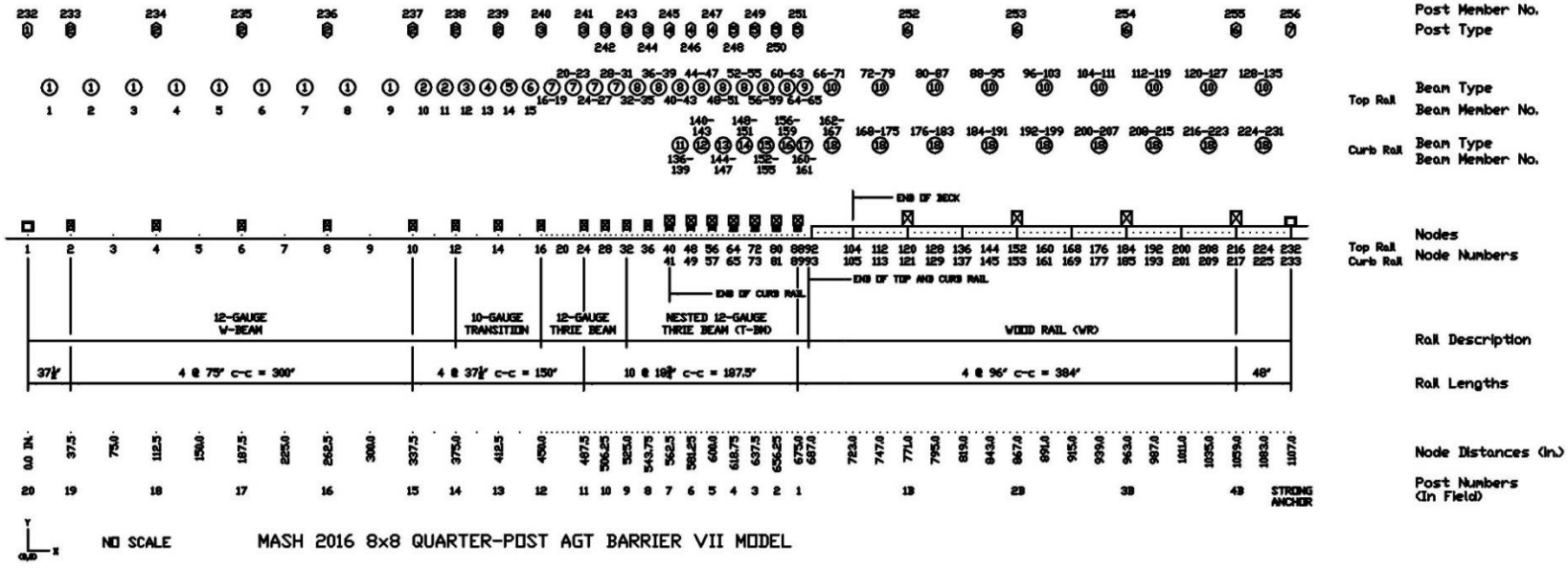

Figure 145. Quarter-Post BARRIER VII Model

4.6.3.1 Node Spacing

The CIP analysis required increased resolution between the beginning of the upstream stiffness transition and the first bridge post. This refinement helped identify localized behavior and possible pocketing points.

Within this zone, the BARRIER VII model included two nodes between each post until the upstream stiffness transition began. The transition zone was defined as the location where the W-beam to thrie-beam transition element connected to the first thrie-beam segment. From this point to the last AGT post, the model used element lengths of 4.6875 in. Posts with quarter-post spacing were represented with four beam elements between each post, and posts with half-post spacing were represented with sixteen elements between them. After the last AGT post, beam element lengths were increased to 6 in., resulting in sixteen total elements between the 8-ft-spaced bridge posts.

4.6.3.2 Post Parameters

Seven different post elements were defined in the BARRIER VII model for the quarter-post configuration. These included two end posts representing the upstream and downstream boundaries of the system, one bridge post, two 8-in. x 8-in. AGT posts, and two 6-in. x 8-in. posts. The parameters for all posts, except the two 8-in. x 8-in. AGT posts, were reused from the half-post spacing BARRIER VII model.

The 8-in. x 8-in. post parameters included node heights, stiffness values in both directions, post weight, yield moment, limiting shear capacity, and limiting deflection. Node heights were selected to match the vertical centers of the thrie-beam and the curb rail taper. The stiffness in both lateral and longitudinal directions was based on load-deflection curves from prior bogie testing on these posts, which reported a stiffness of 11.3 kips per in. on the 8-in. face [37]. Although post rupture was the dominant failure mode in the tests, the stiffness values used in the model were consistent with those obtained experimentally. The post weight was estimated by calculating the portion of the post located above ground, resulting in a value of 43.56 lb.

Since rupture was observed in bogie testing, the post yield moment was capped at the rupture moment corresponding to a deflection of 5 in. The post grade was increased from standard Grade 1 southern yellow pine (SYP) to dense Grade 1D SYP. This change increased the tabulated bending strength from 1.35 ksi to 1.55 ksi. After applying appropriate adjustments for load duration, safety factor, and the conversion from the 5^{th} percentile to 50^{th} percentile values, the average modulus of rupture (MOR) was estimated at 5.36 ksi. Based on the section modulus of the 8-in. x 8-in. post, the yield moment was calculated to be 457 kip-in.

The limiting deflection was set at 5 in. for both orientations of the post. This deflection limit was associated with a total energy absorption of 79 kip-in. Although the MOR adjustment increases the predicted moment capacity, the associated energy value remains a conservative estimate, as bogie test results showed energy absorption values ranging from 56.7 to 101.6 kip-in. for lower-grade posts. The shear capacity of the posts was estimated using the method described in Section 4.2.5.1 and was set at 47.6 kips. All post parameters are summarized in Tables 44 and 45.

Table 44. Post Properties for Quarter-Post AGT BARRIER VII Model

B7 Post No.	Height of Node I (in.)	Height of Node j (in.)	k_A (k/in.)	k_B (k/in.)	W (lb)	M_B (k-in.)	M_A (k-in.)
1	24.875	0	102.5	2.48	32.67	735	191.1
2	24.875	0	2.4	4.2	32.67	224	256
3	24	0	2.4	4.2	32.67	224	256
4	24	12.625	11.3	11.3	43.56	457	457
5	24	12.625	11.3	11.3	43.56	457	457
6	33.25	14.625	18.76	29.86	239.37	833	1327.7
7	33.25	14.625	6338	13943	94.7	6820	1540

Table 45. Post Properties for Quarter-Post AGT BARRIER VII Model, Cont.

B7 Post No.	Yield Accuracy Limit (%)	V_A (k)	V_B (k)	δ_A (in.)	δ_B (in.)	Post Description
1	0.1	35.7	35.7	5.0	20.0	End Post
2	0.1	35.7	35.7	5.0	20.0	6x8 Wood Post
3	0.1	35.7	35.7	5.0	20.0	6x8 Wood Post
4	0.1	47.6	47.6	5.0	5.0	8x8 Wood Post
5	0.1	47.6	47.6	5.0	5.0	8x8 Wood Post
6	0.1	93.8	103.7	4.0	10.0	Bridge Post
7	0.1	310	70	1.0	1.0	End Post

4.6.3.3 Beam Parameters

Eighteen different beam element types were defined in the BARRIER VII model for the quarter-post spacing system. Two elements were created for the 12-gauge W-beam. Four elements were defined for the 10-gauge W-beam to thrie-beam transition. One element was used to represent the 12-gauge thrie-beam, and two elements were assigned to the nested 12-gauge thrie-beam. One element was used for the upper glulam railing, six elements for the lower glulam taper, and two elements for the lower glulam rail.

The glulam railing components were based on previously developed BARRIER VII models by Mike Fowler and Jared Duren [10, 25]. The upper and lower glulam railings were adapted from Jared Duren's model. The upper and curb railing axial capacities were reduced to the splice limit defined in Table 23. The lower curb rail taper was divided into six separate elements. Each of these

elements represented a gradual increase in sectional properties, allowing the model to capture the progressive stiffness change along the taper.

The lower curb taper is connected to the AGT posts using a single ⅝-in. diameter ASTM A307A bolt at each post. This connection constrains the axial capacity of each taper element to the shear capacity of the bolt, which was calculated to be 6.3 kips. The flexural strengths for each beam element were derived by multiplying the baseline properties established in Phase IIa by the average cross-sectional properties of each segment. The curb rail axial capacity was reduced to account for the presence of two 1-in. diameter bolt holes, which decreased the effective cross-sectional area of the curb rail. Although not consistent with the half-post system, the forces in the curb rail did not exceed 100 kips, so the inconsistent limits did not present any issues. The material and geometric parameters for each of these beam elements are provided in Table 46.

Table 46. Quarter-Post BARRIER VII Model Beam Parameters

B7 Beam No.	Beam Element Description	Moment of Inertia (in.^{4})	Area (in.^{2})	Length (in.)	Young's Modulus (ksi)	Weight (lb/ft)	Yield Force (k)	Yield Moment (k-in.)
1	12-Gauge W-Beam	2.29	1.99	37.5	30000	6.92	99.5	68.5
2		2.29	1.99	18.75	30000	6.92	99.5	68.5
3	10-Gauge W-Beam to Thrie-Beam Transition	2.48	2.13	18.75	30000	7.40	106.2	73.8
4		2.84	2.40	18.75	30000	8.38	120.0	84.0
5		3.20	2.68	18.75	30000	9.35	134.0	94.0
6		3.58	2.96	4.6875	30000	10.32	148.0	104.2
7	12-Gauge Thrie-Beam	3.76	3.10	4.6875	30000	10.81	155	109.5
8	Nested 12-Gauge Thrie-Beam	7.52	6.20	4.6875	30000	21.62	310	219
9		7.52	6.20	4.75	30000	21.62	310	219
10	Glulam Upper Rail	1397.6	145.1	6.00	1600	34.5	190.9	1568.6
11	Tapered Curb Rail	16.6	24.8	4.6875	1500	5.9	6.3	48.7
12		66.4	39.4	4.6875	1500	9.4	6.3	122.7
13		171.0	54.0	4.6875	1500	12.8	6.3	230.5
14		350.5	68.5	4.6875	1500	16.3	6.3	371.9
15		625.2	83.1	4.6875	1500	19.8	6.3	547.0
16		1015.3	97.7	4.6875	1500	23.3	6.3	755.8
17	Glulam Curb Rail	1260.0	105.0	4.75	1500	25.0	107.4	872.8
18		1260.0	105.0	6.00	1500	25.0	107.4	872.8

4.7 CIP Investigation

4.7.1 Evaluation Metrics

The CIP investigation was conducted to identify locations within the AGT and bridge railing system that exhibited high lateral deflections, significant pocketing, or risk of wheel snag. Simulations were carried out using BARRIER VII for two vehicle types: the 2270P pickup truck and the 1100C small car. For both the half-post and quarter-post configurations, impacts were simulated at successive nodes beginning at the upstream end of the upstream stiffness transition and continuing to the first bridge post. Maximum deformation locations, points of peak internal force, the onset of pocketing, and wheel snag events were analyzed to recommend a single impact point for full-scale crash testing.

To efficiently process multiple simulations, Python scripts were developed and executed using Google Colab. Each script followed a consistent sequence: it began with a BARRIER VII input file, created a copy, modified the impact location based on a specified list, ran BARRIER VII using the new input, and extracted relevant output files. Scripts for the pickup truck simulation on the half-post system are provided in Appendix M. These scripts were modified as needed to run the small car simulations and to analyze the quarter-post system.

Four parameters were collected from each simulation: maximum lateral deformation of the railing, maximum force in a railing member, pocketing angle, and the occurrence of wheel snag. For each, the node or member responsible was recorded. In the quarter-post configuration, post failure for the 8-in. x 8-in. AGT posts was also manually verified by reviewing the simulation output.

For the quarter-post system, the output files were reviewed independent of the python code to check for 8-in. x 8-in. post failure. Altogether, the information gathered provided insight into where risks of pocketing and wheel snag were highest, as well as locations of high stress in the system.

In previous research on transitions between MGS and stiff bridge railings, pocketing was defined as a sudden and localized reduction in deflection that creates a sharp bend in the railing system. This condition can produce large longitudinal forces on the vehicle, potentially resulting in excessive deceleration or even rollover, as observed in crash test MWT-2. That study defined the critical pocketing angle as 23 degrees. Any pocketing angle equal to or below this value was considered acceptable for redirecting the vehicle. An overhead diagram showing the geometry of pocketing is provided in Figure 146. Pocketing angles were calculated by taking the inverse tangent of the difference in deflection between a node and the average deflection of the preceding three, five, or nine nodes. This method was used consistently across simulations to identify sharp local changes in the guardrail profile and to determine critical deformation zones.

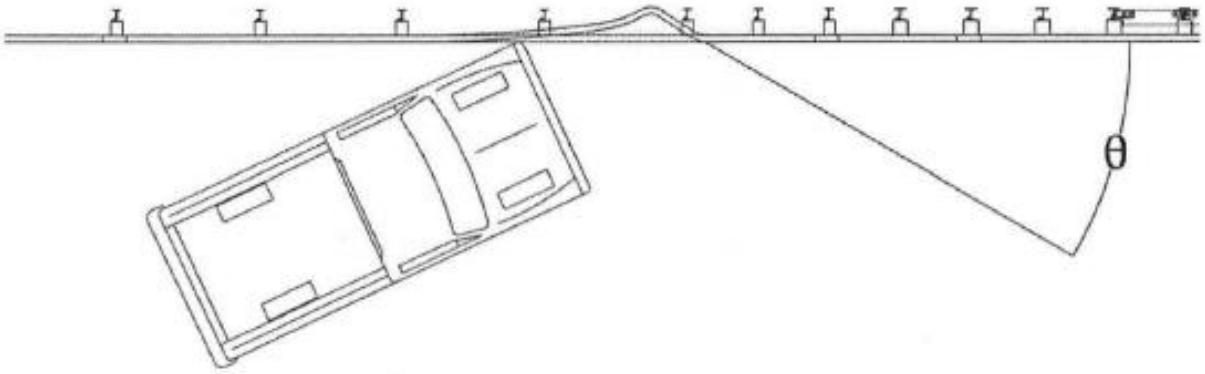

Figure 146. Critical Pocketing Angle [35]

Wheel snag was defined as the point where the vehicle wheel made contact with a post. This was measured in inches and is illustrated in Figure 147. Although the vertical deflection of the railing at the post location, denoted as "dy," can be obtained directly from BARRIER VII output, estimating the actual overlap between the vehicle wheel and the post required additional parameters that are not included in BARRIER VII. These include the post embedment depth, impact height, wheel width, and blockout depth.

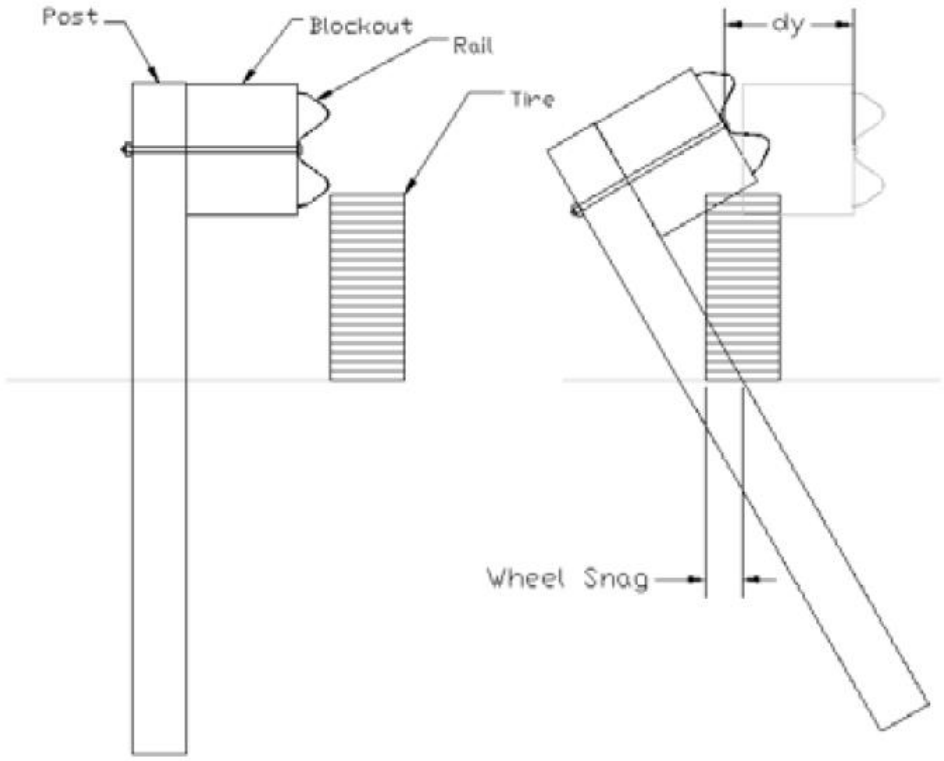

Figure 147. Wheel Snag Diagram [112]

For the simulations, the post embedment depth (D_e) and the impact height (H_{impact}) were 40 in. and 24 in. respectively. These were necessary to define the angle of backward rotation of the post. Wheel snag beyond the curb railing taper was not a concern because the curb rail would physically block the wheel from making contact with posts in that region. The half-post and quarter-post systems utilized the same post embedment depth and impact height for the AGT posts which were not protected by the curb railing.

The blockout depth (d_{block}) was 12 in. and was needed for estimation of the distance from the edge of the wheel to the post. Half of the wheel width (b_{wheel}) based on 2270P pickup truck tires, which typically measure about 265 mm in width, according to prior analysis of crash-tested systems [38, 149]. This adjustment was necessary because BARRIER VII reports the center location of the wheel rather than the outer edge, and the objective was to determine the precise location where initial contact (snag) could occur. Equation 34 defines how wheel snag was calculated:

$$snag = y_{wheel} - d_{block} + b_{wheel} - dy_{railing}\left(\frac{\frac{2}{3}D_e}{\frac{2}{3}D_e + H_{impact}}\right) \qquad \text{Eq. (34)}$$

4.7.2 Half-Post System Pickup Truck

The first CIP analysis was conducted on the half-post system using a MASH 2016 2270P pickup truck. Maximum lateral deflections were observed in the upstream portions of the system, where structural stiffness was lower. As impact simulations progressed along the AGT, deflections initially decreased but began to rise again when the pickup truck impacted between the third and second AGT posts from the bridge railing. This rise in deflection reached a maximum of 11.5 in. at node 88, corresponding to the transition between the steel thrie-beam and the glulam timber upper rail. This occurred when the impact was simulated at node 68, located halfway between the first and second AGT posts.

The maximum internal forces experienced by railing members initially decreased from the 80-kip range to the 60-kip range throughout the 12-gauge thrie-beam section. Forces remained relatively consistent until an increase was observed between the second AGT post and the midspan between the first bridge post and the first AGT post. The highest force across all simulations was 87.3 kips and occurred in member 60. This member is part of the nested AGT thrie-beam located adjacent to the end shoe, which is connected to the glulam upper rail using five ⅝-in. diameter bolts.

The maximum pocketing angle observed was 14.6 degrees, occurring during simulated impact at node 68. This pocketing event extended to node 80, which corresponds to the interface between the end of the thrie-beam and the beginning of the bridge railing. An additional significant pocketing event was identified farther upstream, resulting from impact on node 28 and concluding at node 34. This pocket had a maximum angle of 13.9 degrees and occurred within the upstream transition zone where quarter-spaced 6-in. x 8-in. posts were used. Wheel snag events on the curb rail taper began with impact at node 28 and extended to impact at node 32. The overlap between the vehicle wheel and post during these events ranged from 1.4 to 3.9 in. Maximum deflections and member forces from the CIP simulations are summarized in Table 47. All pocketing and wheel snag results up to the curb rail taper are presented in Table 48.

Table 47. Half-Post System Pickup Truck CIP Results Deflections and Forces

Impact Node	Impact Location (in.)	Max Deflection (in.)	Node of Max Deflection	Location of Max Deflection (in.)	Max Force (kips)	Max Force Member
16	450	14.9	31	521.7	76.9	28
18	459.375	14.4	32	526.3	77.8	28
20	468.75	12.8	35	540.1	68.8	28
22	478.125	12.6	37	549.4	69.5	36
24	487.5	11.7	38	553.9	68.9	36
26	496.875	11.2	39	558.5	66.9	36
28	506.25	10.6	42	572.4	63.8	36
30	515.625	10.0	46	586.5	63.4	41
32	525	10.1	50	595.8	63.9	44
34	534.375	9.9	52	600.4	65.4	44
36	543.75	9.7	54	605.0	63.7	44
38	553.125	9.5	62	623.8	63.0	44
40	562.5	9.8	66	633.2	64.0	52
42	571.875	9.8	68	637.9	64.3	52
44	581.25	9.7	70	642.5	65.9	52
48	590.625	9.6	72	647.1	65.4	52
52	600	9.9	80	668.5	62.1	52
56	609.375	10.1	86	686.5	64.9	60
60	618.75	10.6	86	686.5	71.4	60
64	628.125	11.3	88	692.5	81.9	60
68	637.5	11.5	88	692.5	87.3	60
72	646.875	11.3	88	692.5	89.3	62
76	656.25	11.0	88	692.5	86.2	62
80	668.25	10.0	88	692.4	69.8	60
84	680.25	9.1	88	692.4	59.8	60
88	692.25	8.0	88	692.4	53.3	60
92	704.25	6.4	88	692.3	40.2	76
96	716.25	5.5	116	776.3	30.4	76
100	728.25	5.4	120	788.3	31.2	76
104	740.25	5.5	122	794.3	30.2	76
108	752.25	5.2	126	806.3	27.6	76

Table 48. Half-Post System Pickup Truck CIP Results Pocketing and Wheel Snag

Node	Impact Location (in.)	Maximum 3-Node Pocket (deg.)	Maximum 3-Node Pocket Node	Front Tire Snag	Snagged Post
16	450	12.1	19	3.6	2nd 6x8
18	459.375	12.4	26	4.4	2nd 6x8
20	468.75	12.0	30	3.8	2nd 6x8
22	478.125	13.2	30	3.9	1st 6x8
24	487.5	13.3	30	3.8	1st 6x8
26	496.875	13.8	34	3.5	1st 6x8
28	506.25	13.9	34	3.2	3rd 8x10
30	515.625	12.5	35	2.9	3rd 8x10
32	525	11.8	38	1.4	3rd 8x10
34	534.375	11.2	42	-	-
36	543.75	11.5	42	-	-
38	553.125	11.7	48	-	-
40	562.5	11.6	48	-	-
42	571.875	10.3	50	-	-
44	581.25	9.6	54	-	-
48	590.625	10.6	64	-	-
52	600	9.8	64	-	-
56	609.375	8.3	68	-	-
60	618.75	11.2	80	-	-
64	628.125	14.3	80	-	-
68	637.5	14.6	80	-	-
72	646.875	14.0	82	-	-
76	656.25	12.8	84	-	-
80	668.25	10.6	86	-	-
84	680.25	9.4	84	-	-
88	692.25	8.3	84	-	-
92	704.25	6.5	84	-	-
96	716.25	4.0	84	-	-
100	728.25	2.3	108	-	-
104	740.25	2.3	108	-	-
108	752.25	2.1	108	-	-

4.7.3 Half-Post System Small Car

The second CIP analysis was conducted on the half-post system using a MASH 2016 1100S small car. Maximum lateral deflections were observed in the upstream portions of the system, where structural stiffness was lower. As impact simulations progressed along the AGT, deflections initially decreased but began to increase again when the small car impacted between the first and second AGT posts from the bridge railing. This increase reached a maximum deflection of 6.7 in. at node 88, corresponding to the transition between the steel thrie-beam and the glulam timber upper rail. This occurred when the impact was simulated at node 76, which is aligned with the first AGT post.

The maximum force across all simulations was recorded during impact at node 68. This force was 51.1 kips and occurred in member 61. Member 61 is part of the nested AGT thrie-beam adjacent to the end shoe, which is connected to the glulam upper rail with five ⅝-in. diameter bolts.

The maximum pocketing angle observed was 10.5 degrees, resulting from simulated impact on node 24, which corresponds to the centerline of the fifth 6-in. x 8-in. AGT post following the 8-in. x 10-in. posts. This pocket concluded at node 30, located within the quarter-post spaced region of 6-in. x 8-in. AGT posts. A smaller pocketing event initiated from impact at node 68 and reached a pocketing angle of 9.8 degrees. It concluded at node 80, which is located at the critical junction of the upper glulam rail and the thrie-beam shoe. Wheel snag events on the curb rail taper began with impact at node 32 and continued until impact at node 36. The overlap between the vehicle wheel and post during these events ranged from 3.4 to 5.2 in. Maximum deflections and member forces from the CIP simulations are provided in Table 49. All pocketing and wheel snag results up to the curb rail taper are presented in Table 50.

Table 49. Half-Post System Small Car CIP Results Deflections and Forces

Node	Impact Location (in.)	Max Deflection (in.)	Node of Max Deflection	Location of Max Deflection (in.)	Max Force (k)	Max Force Member
16	450	9.4	27	502	50.5	24
18	459.375	8.4	29	511	45.1	24
20	468.75	7.9	31	521	43.7	28
22	478.125	7.3	32	525	44.9	28
24	487.5	6.7	35	539	40.0	32
26	496.875	6.2	37	549	38.3	32
28	506.25	5.7	38	553	37.3	36
30	515.625	5.2	40	563	34.0	36
32	525	5.2	42	572	31.7	41
34	534.375	5.1	46	586	33.9	44
36	543.75	5.2	50	595	34.4	44
38	553.125	5.2	52	600	34.0	44
40	562.5	4.8	54	605	27.7	45
42	571.875	4.7	64	628	25.8	47
44	581.25	5.0	66	633	30.3	52
48	590.625	5.2	68	638	33.1	52
52	600	5.1	70	642	28.5	53
56	609.375	4.9	80	668	25.6	55
60	618.75	5.3	82	674	30.5	60
64	628.125	5.9	86	686	41.0	61
68	637.5	6.5	88	692	51.1	61
72	646.875	6.3	88	692	50.7	62
76	656.25	6.7	88	692	48.5	62
80	668.25	6.1	88	692	40.5	61
84	680.25	5.3	88	692	30.0	61
88	692.25	4.1	88	692	20.3	61
92	704.25	3.1	98	722	13.3	62
96	716.25	2.5	110	758	10.3	76
100	728.25	2.3	116	776	10.5	76
104	740.25	2.0	120	788	10.2	76
108	752.25	1.8	124	800	9.6	76

Table 50. Half-Post System Small Car CIP Results Pocketing and Wheel Snag

Node	Impact Location (in.)	Maximum 3-Node Pocket (deg.)	Maximum 3-Node Pocket Node	Front Tire Snag	Snagged Post
16	450	10.1	20	5.9	4th 6x8
18	459.375	9.3	26	6.7	3rd 6x8
20	468.75	9.5	26	6.5	3rd 6x8
22	478.125	10.2	30	6.6	2nd 6x8
24	487.5	10.5	30	6.3	2nd 6x8
26	496.875	9.0	31	5.3	1st 6x8
28	506.25	8.0	35	5.6	1st 6x8
30	515.625	7.7	36	4.8	1st 6x8
32	525	7.0	38	5.2	3rd 8x10
34	534.375	6.2	40	4.7	3rd 8x10
36	543.75	6.7	42	3.4	3rd 8x10
38	553.125	6.7	46	-	-
40	562.5	5.8	50	-	-
42	571.875	5.8	52	-	-
44	581.25	5.8	56	-	-
48	590.625	5.9	64	-	-
52	600	5.5	66	-	-
56	609.375	4.8	68	-	-
60	618.75	5.7	80	-	-
64	628.125	8.8	80	-	-
68	637.5	9.8	80	-	-
72	646.875	9.2	82	-	-
76	656.25	8.3	84	-	-
80	668.25	7.0	84	-	-
84	680.25	5.9	84	-	-
88	692.25	4.5	84	-	-
92	704.25	2.8	84	-	-
96	716.25	1.8	82	-	-
100	728.25	1.3	82	-	-
104	740.25	0.9	86	-	-
108	752.25	0.9	108	-	-

4.7.4 Quarter-Post System Pickup Truck

The third CIP analysis was conducted on the quarter-post system using a MASH 2016 2270P pickup truck. Maximum deflections were observed in the upstream portions of the system, where structural stiffness was lower. As the simulated impact location progressed downstream, deflections initially decreased until the second 8-in. x 8-in. AGT post. Beyond this point, deflections began to increase again and reached their maximum value downstream. A maximum deflection of 6.5 in. occurred at node 92, where the end shoe is located. This resulted from impact at node 76, positioned between the second and third AGT posts adjacent to the bridge section.

The maximum forces in the simulations exceeded 80 kips when the pickup truck impacted the end of the W-beam to thrie-beam transition. These forces steadily decreased for impacts further downstream until the simulations reached the 46-in. embedded 8-in. x 8-in. AGT posts. The maximum force recorded across all simulations was 103.8 kips, resulting from an impact at node 76. This location is midway between the second and third AGT posts adjacent to the bridge section. The maximum force occurred in member 64, which is part of the thrie-beam shoe. In earlier model, an 8-ft spacing was used between the last AGT post and the first bridge post, which resulted in a max force of 113 kips. This was dangerously close to the tested limits of the thrie-beam end shoe [151], and so the spacing was reduced to 7-ft to help mitigate the risk of rupture.

The maximum pocketing angle observed was 13.2 degrees and resulted from simulated impact at node 26. This location is approximately 4 in. downstream from the center of the 6-ft 3-in. section of 12-gauge thrie-beam. The pocketing event concluded at node 34, near the start of the nested 12-gauge thrie-beam section. A second pocketing event initiated from impact at node 80 and reached a pocketing angle of 9.1 degrees. This pocket concluded at node 92, where the thrie-beam end shoe is located. Wheel snag on the curb rail taper began with impact at node 24 and continued through node 26. The amount of overlap between the vehicle wheel and post was 9.2 to 9.6 in. at this location, with similar overlap observed further upstream. Maximum deflections and member forces from the CIP simulations are summarized in Table 51. All pocketing and wheel snag results up to the curb rail taper are presented in Table 52.

Table 51. Quarter-Post System Pickup Truck CIP Results Deflections and Forces

Node	Impact Location (in.)	Max Deflection (in.)	Node of Max Deflection	Location of Max Deflection (in.)	Max Force (k)	Max Force Member
16	450	14.4	31	521.8	81.0	28
18	459.375	13.3	32	526.4	84.8	33
20	468.75	12.3	34	535.5	71.7	28
22	478.125	11.7	37	549.5	70.4	36
24	487.5	11.1	39	558.7	69.1	36
26	496.875	10.9	40	563.3	69.0	36
28	506.25	10.3	44	572.6	65.6	36
30	515.625	9.2	46	577.1	58.9	36
32	525	8.2	50	586.4	54.1	36
34	534.375	6.4	52	590.9	49.8	40
36	543.75	5.5	54	595.5	45.9	44
38	553.125	4.8	58	604.8	41.6	44
40	562.5	4.5	62	614.2	36.5	48
44	571.875	4.2	66	623.5	32.1	48
48	581.25	4.0	70	632.9	29.5	52
52	590.625	4.2	76	647.0	30.3	52
56	600	4.3	82	661.0	31.6	56
60	609.375	4.7	84	665.7	35.9	56
64	618.75	5.1	92	687.1	46.9	64
68	628.125	5.7	92	687.1	67.0	64
72	637.5	6.3	92	687.1	92.4	64
76	646.875	6.5	92	687.0	103.8	64
80	656.25	5.5	92	687.0	91.2	65
84	665.625	5.1	100	711.0	81.1	65
88	675	4.9	106	729.1	66.8	64
92	687	4.7	110	741.1	42.9	64
96	699	4.6	112	747.1	36.3	64
100	711	4.7	120	771.1	35.7	65
104	723	5.1	124	783.1	38.3	64
108	735	5.1	126	789.1	37.5	78
112	747	5.1	130	801.1	37.0	78
116	759	5.1	134	813.1	34.3	78

Table 52. Quarter-Post System Pickup Truck CIP Results Pocketing and Wheel Snag

Node	Impact Location (in.)	Maximum 3-Node Pocket (deg.)	Maximum 3-Node Pocket Node	Front Tire Snag (in.)	Snagged Post
16	450	12.0	19	9.8	2nd 6x8
18	459.375	11.4	26	9.7	1st 6x8
20	468.75	12.1	30	9.8	1st 6x8
22	478.125	12.5	30	9.4	7th 8x8
24	487.5	13.1	30	9.6	7th 8x8
26	496.875	13.2	34	9.2	7th 8x8
28	506.25	12.8	35	-	-
30	515.625	11.6	35	-	-
32	525	10.6	38	-	-
34	534.375	8.8	44	-	-
36	543.75	7.9	44	-	-
38	553.125	7.2	50	-	-
40	562.5	6.9	52	-	-
44	571.875	6.0	58	-	-
48	581.25	5.7	60	-	-
52	590.625	5.6	66	-	-
56	600	5.2	68	-	-
60	609.375	5.6	76	-	-
64	618.75	5.6	78	-	-
68	628.125	6.0	84	-	-
72	637.5	7.7	92	-	-
76	646.875	8.9	92	-	-
80	656.25	9.1	92	-	-
84	665.625	8.8	92	-	-
88	675	7.7	92	-	-
92	687	4.0	92	-	-
96	699	2.9	92	-	-
100	711	2.4	94	-	-
104	723	2.4	96	-	-
108	735	2.3	118	-	-
112	747	2.3	120	-	-
116	759	2.2	120	-	-

4.7.5 Quarter-Post System Small Car

The fourth CIP analysis was conducted on the quarter-post system with a MASH 2016 1100S small car. Maximum deflections were observed from simulated impacts on the upstream portion of the system, where the system exhibited lower stiffness. As impacts were simulated further downstream along the AGT, deflections generally decreased, except during impacts on the 46-in. embedded AGT posts, where maximum deflection began to increase again. The largest deflection in this region was 3.5 in. at node 92, resulting from impact at node 76, located between the second and third 8-in. x 8-in. AGT posts adjacent to the bridge section.

Maximum forces during the small car simulations never exceeded 50 kips. The maximum force was 49.3 kips and occurred in member 24, part of the 12-gauge thrie-beam, due to impact on node 16. Further downstream, the forces experienced a second, smaller peak that peak with the deflection.

The highest pocketing angle observed was 10.1 degrees, resulting from a simulated impact at node 24, corresponding to the second 6-in. x 8-in. post considered in the simulation, moving downstream. This pocket concluded at node 20, located midway between the fourth and fifth 6-in. x 8-in. AGT posts from the beginning of the CIP analysis. Another pocket formed as a result of impact at node 76, reaching a pocketing angle of 5.6 degrees. This pocket concluded at node 92, where the thrie-beam end shoe was located.

The wheel snag on the curb rail taper occurred between impact at nodes 28 and 30, and resulted in 3.6 to 4 in. of overlap. Greater overlaps of 6 to 7 in. were observed in the upstream portions. Maximum deflection and force values from the CIP results are shown in Table 53. All results from pocketing and wheel snag up to the curb rail taper are shown in Table 54.

Table 53. Quarter-Post System Small Car CIP Results Deflections and Forces

Node	Impact Location (in.)	Max Deflection (in.)	Node of Max Deflection	Location of Max Deflection (in.)	Max Force (k)	Max Force Member
16	450	9.3	27	502.2	49.3	24
18	459.375	8.5	29	511.5	46.5	28
20	468.75	7.8	31	520.8	44.5	28
22	478.125	6.8	32	525.3	42.6	28
24	487.5	6.0	35	539.3	40.6	28
26	496.875	5.2	36	544.0	36.0	32
28	506.25	4.5	38	553.3	26.8	36
30	515.625	3.8	39	557.9	20.8	40
32	525	3.2	44	572.0	17.4	40
34	534.375	2.7	46	576.6	15.7	40
36	543.75	2.5	52	590.7	14.9	40
38	553.125	2.2	58	604.8	14.6	44
40	562.5	2.1	58	604.8	13.5	44
44	571.875	1.9	62	614.1	13.3	48
48	581.25	1.9	68	628.2	12.4	48
52	590.625	1.8	74	642.2	12.4	52
56	600	1.8	76	646.9	11.7	52
60	609.375	2.0	84	665.7	12.6	56
64	618.75	2.3	86	670.4	13.2	56
68	628.125	2.6	90	681.0	16.0	64
72	637.5	3.2	92	687.0	30.6	64
76	646.875	3.5	92	687.0	45.2	64
80	656.25	3.0	92	687.0	37.2	64
84	665.625	2.4	92	687.0	25.8	64
88	675	2.1	104	723.0	17.0	64
92	687	2.1	110	741.0	14.5	64
96	699	2.1	114	753.0	13.2	64
100	711	2.2	118	765.0	12.6	64
104	723	2.2	122	777.0	12.3	64
108	735	2.1	126	789.0	12.2	78
112	747	1.9	128	795.0	12.0	78
116	759	1.8	132	807.0	11.4	78

Table 54. Quarter-Post System Small Car CIP Results Pocketing and Wheel Snag

Node	Impact Location (in.)	Maximum 3-Node Pocket (deg.)	Maximum 3-Node Pocket Node	Front Tire Snag (in.)	Snagged Post
16	450	10.1	20	5.9	3rd 6x8
18	459.375	9.6	26	6.8	2nd 6x8
20	468.75	9.5	26	6.4	2nd 6x8
22	478.125	9.7	30	5.5	2nd 6x8
24	487.5	9.7	30	5.6	1st 6x8
26	496.875	8.3	31	4.6	1st 6x8
28	506.25	6.0	32	4.0	7th 8x8
30	515.625	5.3	35	3.6	7th 8x8
32	525	4.2	38	-	-
34	534.375	3.6	42	-	-
36	543.75	3.3	44	-	-
38	553.125	3.1	50	-	-
40	562.5	2.8	52	-	-
44	571.875	2.6	58	-	-
48	581.25	2.3	60	-	-
52	590.625	2.2	66	-	-
56	600	2.0	68	-	-
60	609.375	2.1	76	-	-
64	618.75	2.2	78	-	-
68	628.125	2.7	84	-	-
72	637.5	3.4	90	-	-
76	646.875	5.6	92	-	-
80	656.25	5.1	92	-	-
84	665.625	3.8	92	-	-
88	675	2.2	92	-	-
92	687	1.7	92	-	-
96	699	1.3	90	-	-
100	711	1.2	90	-	-
104	723	1.2	92	-	-
108	735	1.0	94	-	-
112	747	0.9	100	-	-
116	759	0.9	120	-	-

4.7.6 Analysis of Results

The results of the CIP analyses for both the half-post and the quarter-post systems were broadly within reason and did not suggest immediate concerns with either model. Deflections remained consistently below 10 in. in the stiffened portion of the quarter-post system. However, the half-post system showed higher deflections of up to 11.5 in. at the downstream transition. A higher deflection from the BARRIER VII model was anticipated since the program assumes that all vehicle energy is absorbed by deflecting the railing system. In actual crashes, some of the pickup truck's energy is dissipated vertically, either by vehicle rotation or loss of ground contact by the wheels. The simulation results compared well with the measured 8.4-in. deflection from crash test TRBR-3, which had a higher impact energy. Given the tendency of BARRIER VII to overestimate deflections, this agreement was considered acceptable.

Pocketing was below the 23-degree critical limit in all simulations. The worst-case pocketing scenario occurred in the half-post system during pickup truck impact between the two AGT posts nearest the bridge railing. The pocket ended just before the start of the timber bridge railing, indicating that the stiffness change between the thrie-beam and the upper glulam rail may be contributing to this localized behavior. Upstream impacts showed less severe pocketing, with angles peaking just below 14 degrees.

Wheel snag was more severe in the quarter-post system than in the half-post configuration, approaching 10 in. compared to 6 in. This result is logical given that the 8-in. x 8-in. posts in the quarter-post system introduce a sharper stiffness increase relative to the 8-in. x 10-in. posts in the half-post system. This also aligns with the observed greater deflections in the half-post model.

In general, the half-post system exhibited more flexibility, resulting in greater deformation and larger pocketing values. The quarter-post system, being stiffer, reduced deflection and pocketing but introduced higher internal forces in the railing and increased the risk of wheel snag in the upstream region. Since snagging at the curb rail taper, post rupture, and high forces through the thrie-beam end shoe all represent serious risks, the quarter-post system poses the more critical design challenge. The higher deflections seen in the half-post system occur in sections where the curb taper protects against wheel snag, and the pocketing remains well below the threshold that would indicate a design flaw.

4.8 Conclusions

Two systems were developed to connect the timber bridge railing design to MGS, incorporating both a 2-in. wearing surface and an upstream stiffness transition. These systems were designated as the half-post and quarter-post configurations. Modeling constraints for the quarter-post system were informed by bogie tests conducted on 8-in. x 8-in. Grade 1 Southern Yellow Pine posts embedded in soil.

Four CIP simulations were conducted, two for the 1100S small car and two for the 2270P pickup truck. Both systems demonstrated acceptable performance metrics. However, the quarter-post system exhibited more critical design issues. These included greater wheel snag, higher potential for post rupture, and increased internal forces in the thrie-beam end shoe. Consequently, while both systems performed adequately in the simulation framework, the quarter-post system presents a higher risk of failure in full-scale crash testing.

5 DYNAMIC COMPONENT TEST OF BRIDGE POST PROTOTYPE

5.1 Component Testing Program

The objective of this study was to develop a timber bridge railing to meet MASH 2016 TL-4 vehicle impact conditions and for use on different timber bridge deck types, as discussed in Chapter 3. The design identified two critical deck configurations, a 5⅛-in. transverse glulam timber deck and a 10¾-in. longitudinal glulam timber deck with four 1-in. diameter ASTM A193 grade B7 steel rods. A successful deck configuration test would permit all larger or stronger decks of that type to be used with the bridge railing. Dynamic component bogie testing was conducted to evaluate the applicability of design assumptions, investigate structural behavior and load distribution, observe failure patterns, determine if design modifications were necessary, and develop a more refined configuration.

A dynamic component bogie test involves using a surrogate vehicle propelled into a bridge railing assembly to create an impact event. The bogie vehicle can range from approximately 2,000 lb to 7,000 lb. The bogie vehicle is guided via a track and pulled with a steel cable to obtain the desired speed and kinetic energy. By simulating the anticipated maximum energy from an oblique vehicle impact into a longitudinal barrier, the lateral strength of the bridge post can be isolated and evaluated without the use of a full-scale vehicle crash test.

Four dynamic component tests were planned, two tests on the transverse deck and two tests on the longitudinal deck. The first test would be test no. TRTD-1 for Timber Railing on Transverse Deck, while the second test would be test no. TRTD-2. The third test would be test no. TRLD-1 for Timber Railing on Longitudinal Deck, and the fourth test would be test no. TRLD-2. The two tests on a specific bridge deck type would use ⅞-in. diameter vertical bolts for the first test, or ¾-in. diameter vertical bolts for the second test, configured to connect the lower rail, both scuppers, and deck together. This investigation was planned to determine whether ⅞-in. diameter bolts were necessary and to confirm the strength of the deck. Initially, the decks were not expected to rupture at an average load of 40 kips over 10 in. of railing displacement. If the bridge post configuration could absorb close to an average of 40 kips over a deflection of 10 in., as measured by bogie accelerometers, then the system was expected to be sufficiently strong for a full-scale crash test.

For this testing program, 3-D test plans and CAD details were developed for the individual post assemblies that would be subjected to lateral impact loading when installed on the two different deck types. If the testing program revealed any design challenges within any of the initial planned tests, then the research team would revise the configuration and testing program to address the challenges. This research report only includes the results from the first of four planned tests, which involved an impact event with a post attached to a 5⅛-in. thick transverse glulam timber bridge deck.

5.2 Test No. TRTD-1 Test Configuration

The short bridge section for test no. TRTD-1 reused a bridge section which had already been constructed for use in testing a TL-1 bridge railing on a 5⅛-in. thick transverse glulam Douglas Fir-Larch combination 2 [7]. The deck panels were rearranged so that the test occurred on timber deck panel ends that had not been previously loaded. The test plans are shown in Figures 148 through 169.

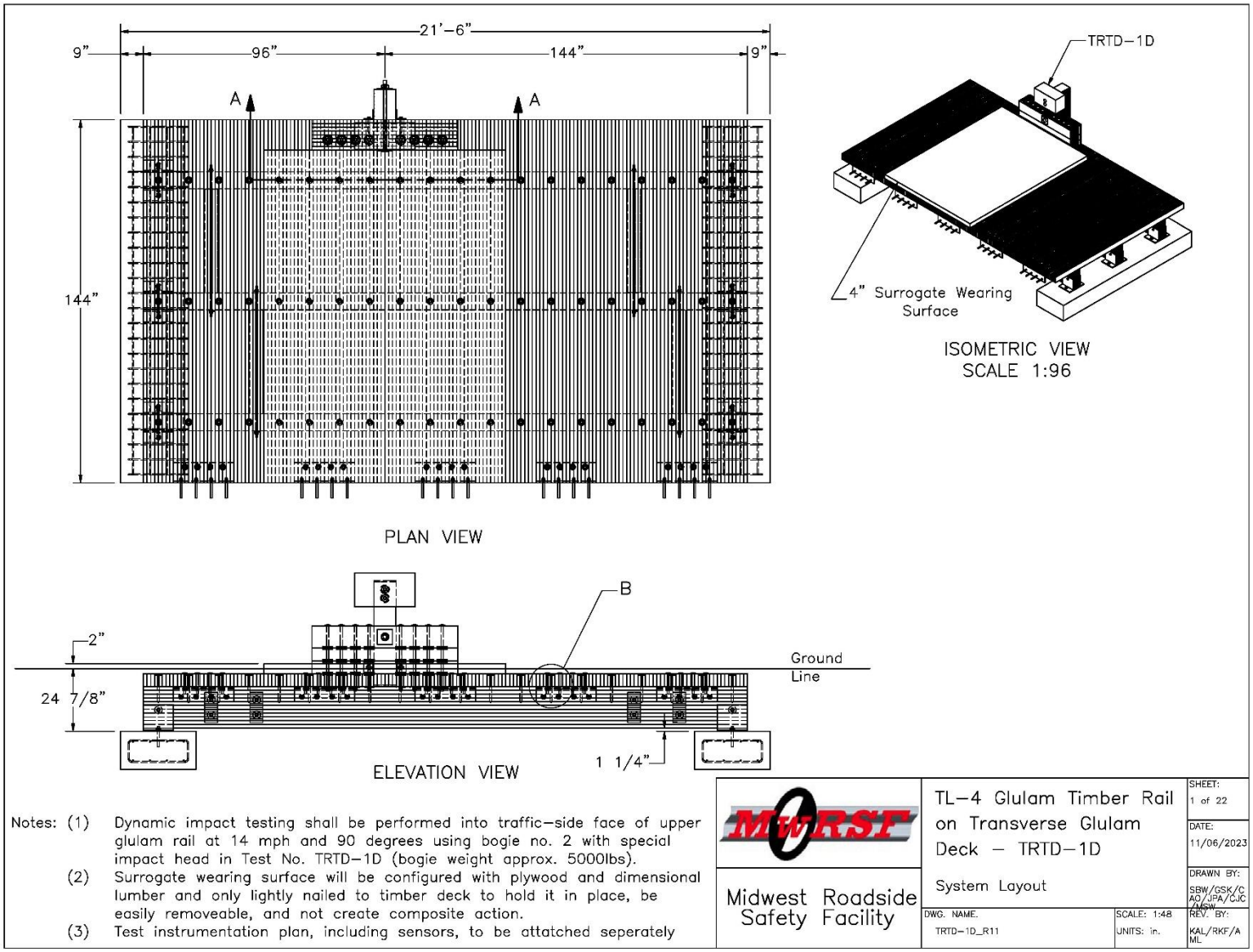

Figure 148. System Layout, Test No. TRTD-1

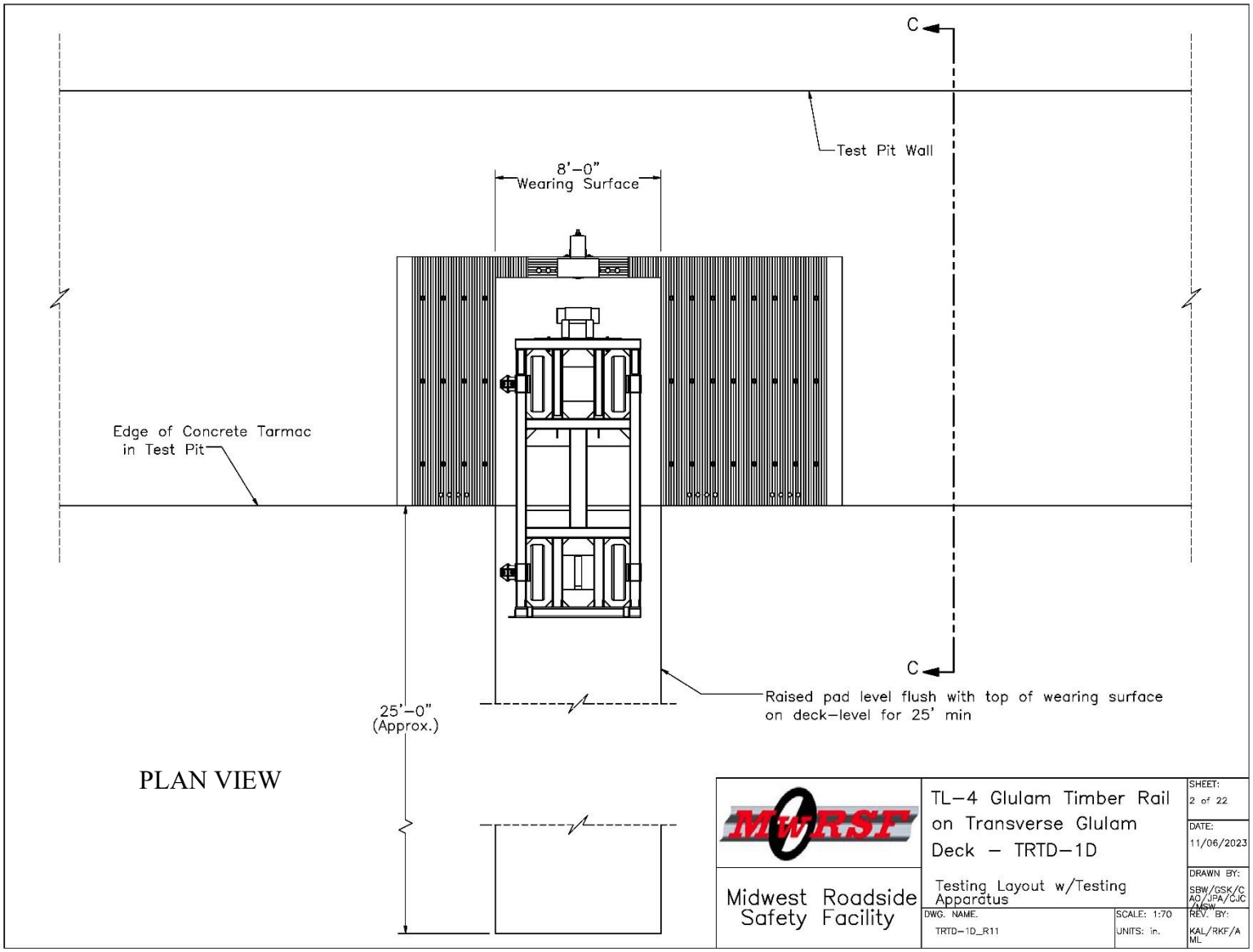

Figure 149. Layout with Bogie, Test No. TRTD-1

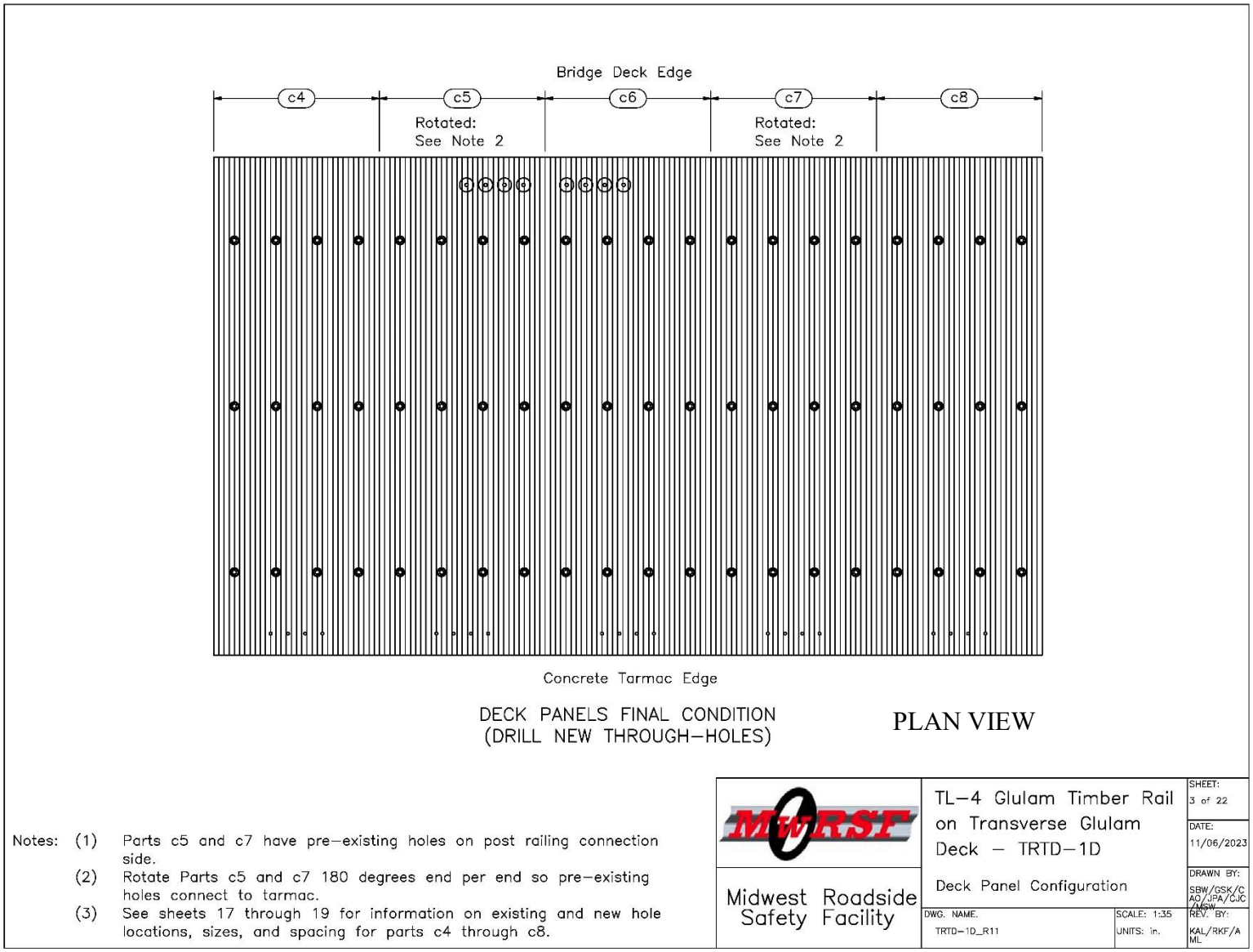

Figure 150. Deck Panel Configuration, Test No. TRTD-1

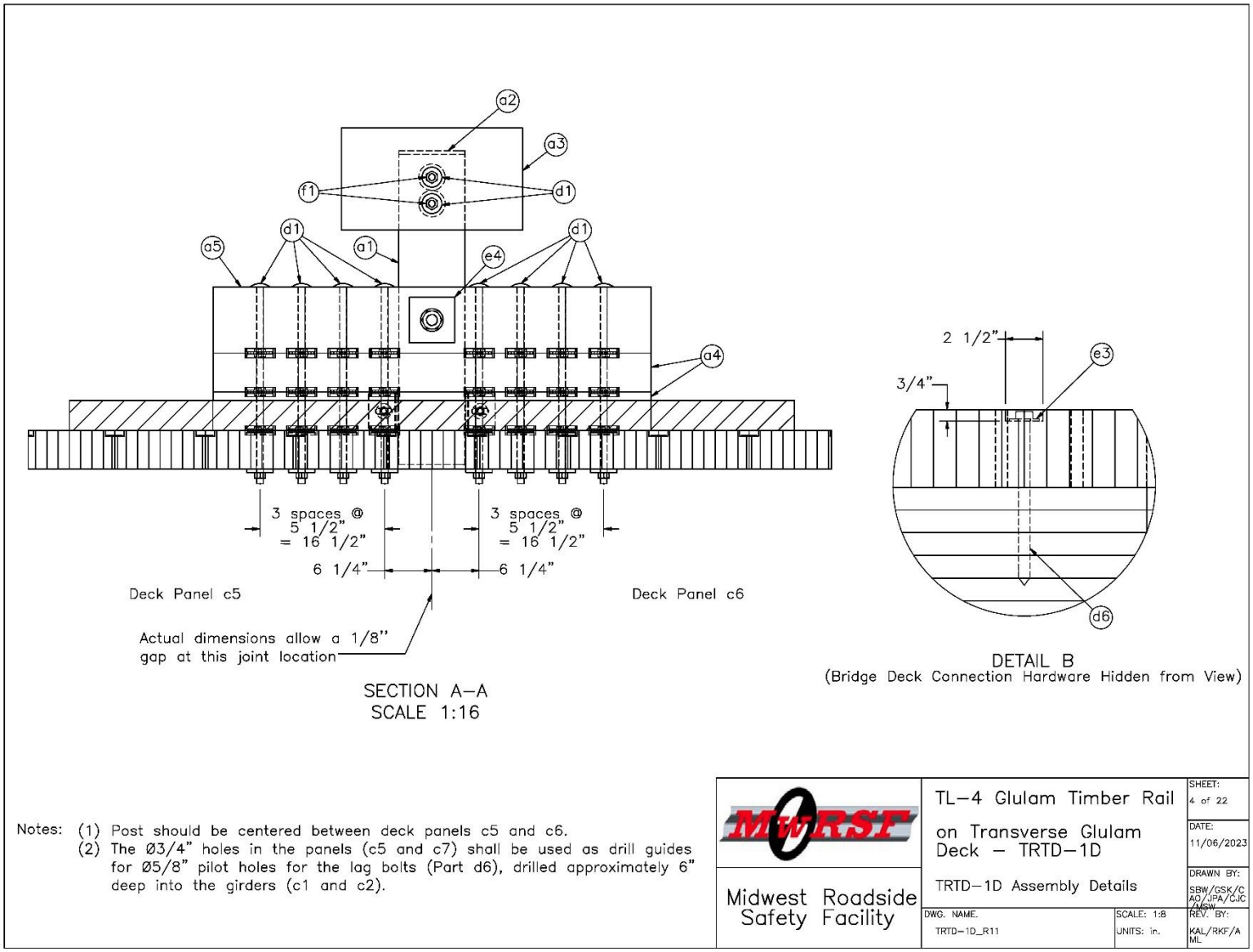

Figure 151. Post and Deck Assembly Details, Test No. TRTD-1

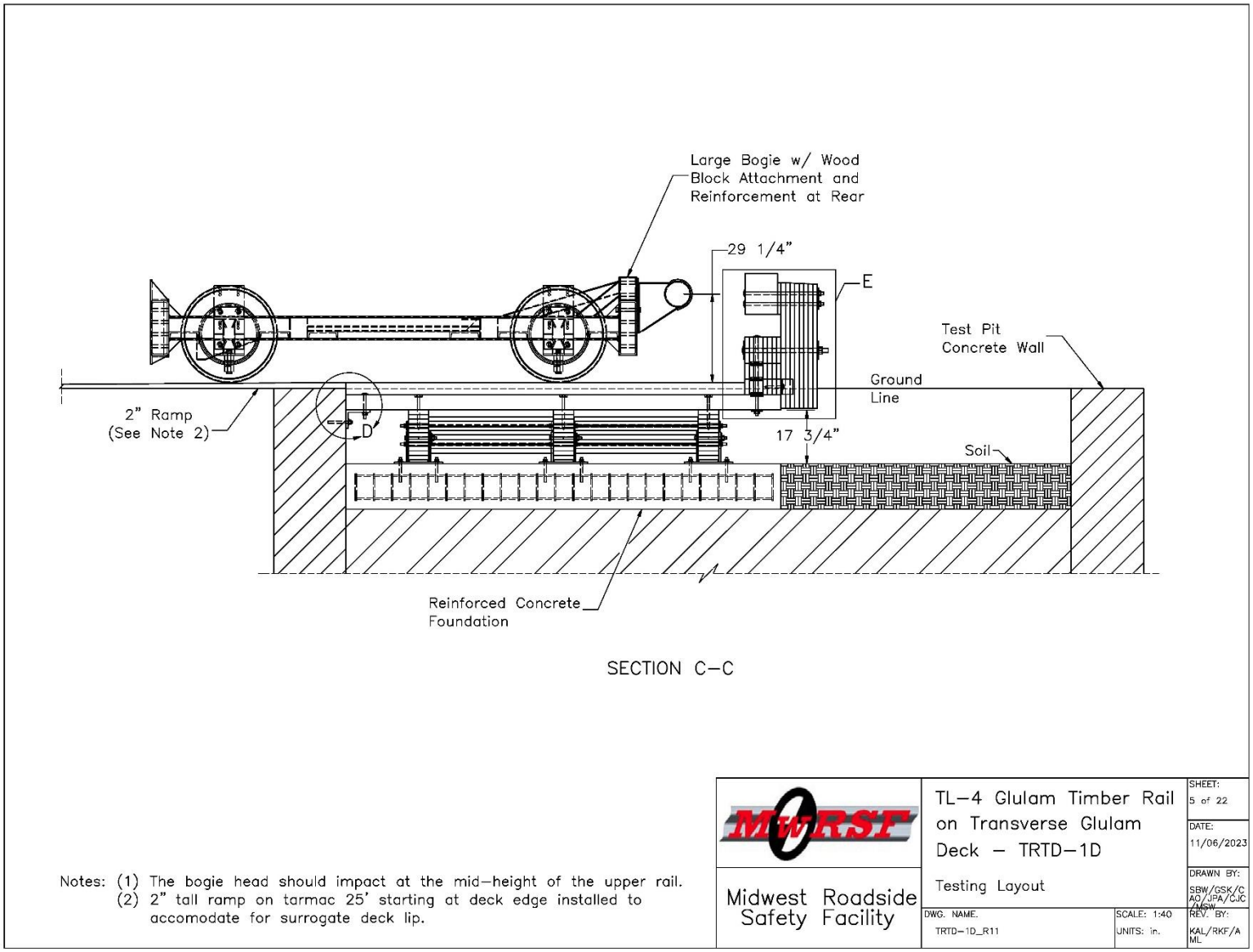

Figure 152. Layout, Elevation View, Test No. TRTD-1

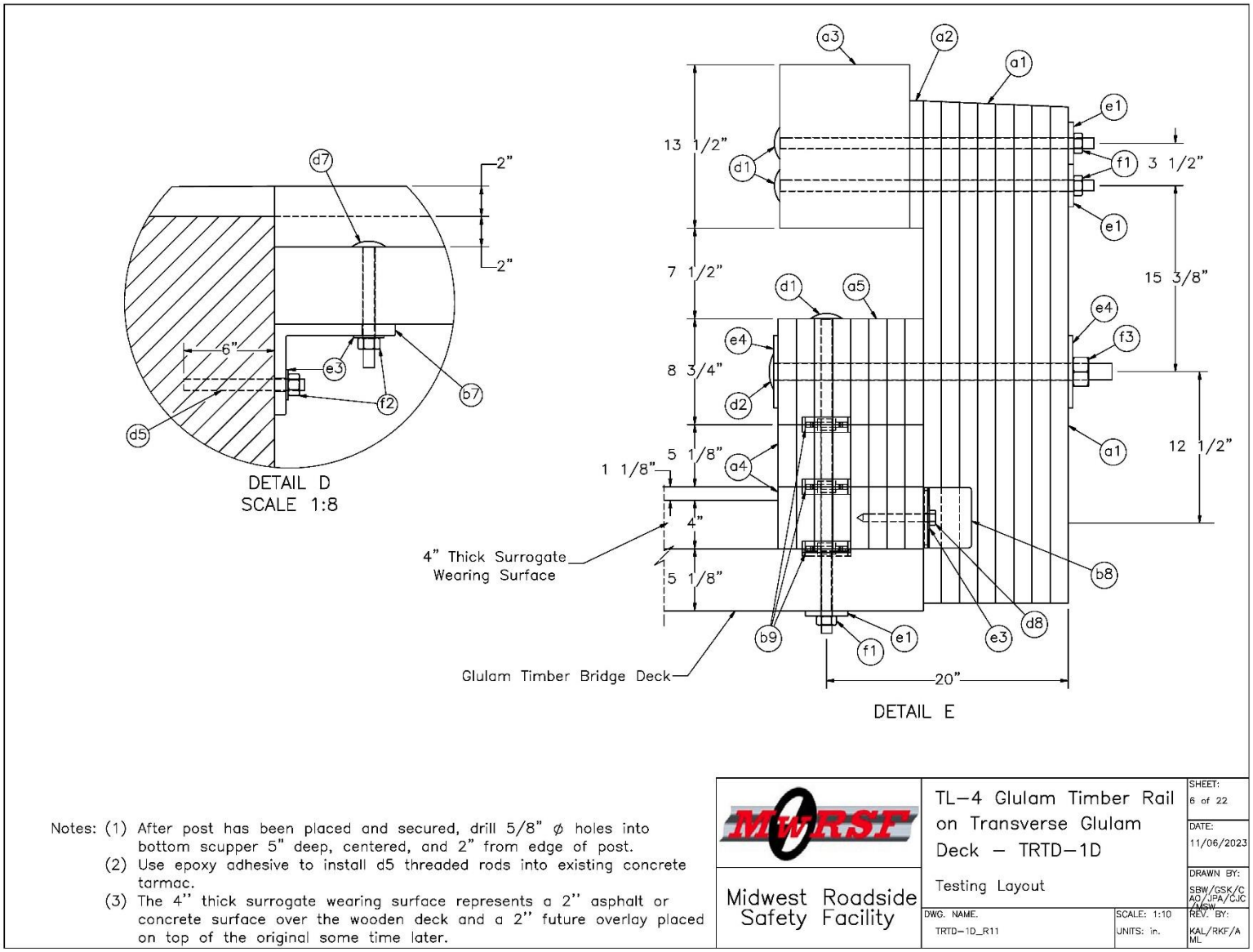

Figure 153. Post and Deck Assembly Details, Section View, Test No. TRTD-1

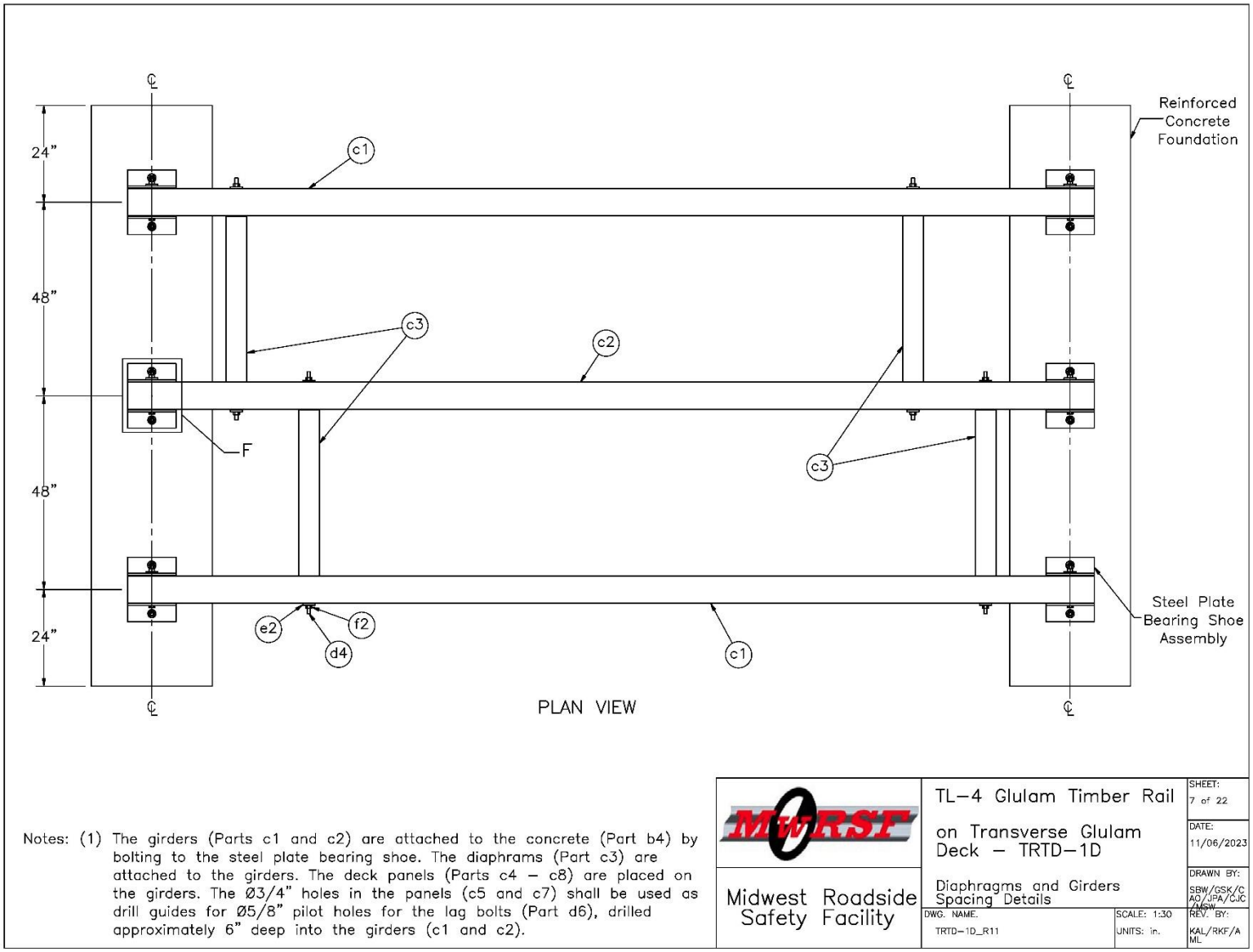

Figure 154. Diaphragm and Girder Spacing Details, Test No. TRTD-1

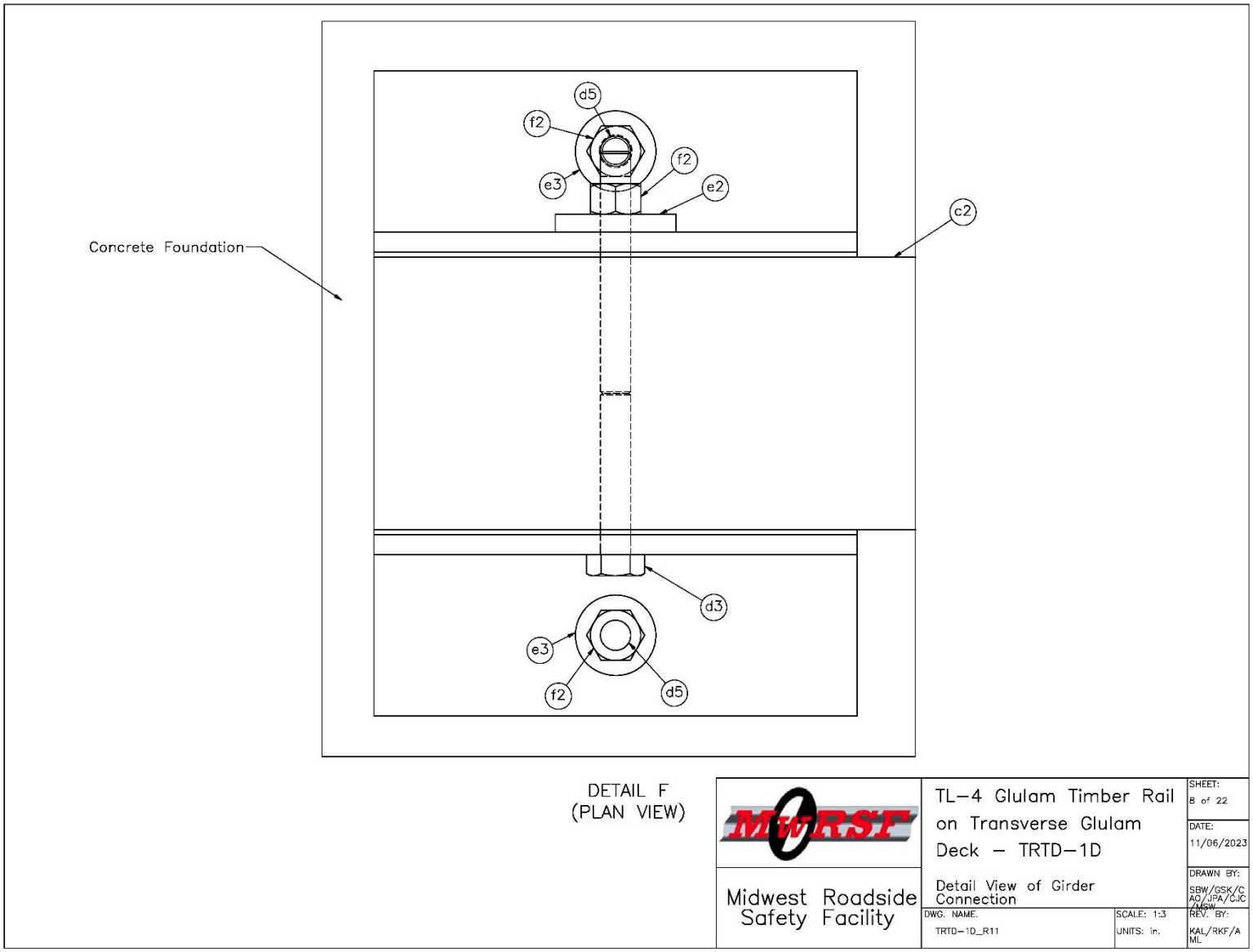

Figure 155. Girder Connection Details, Test No. TRTD-1

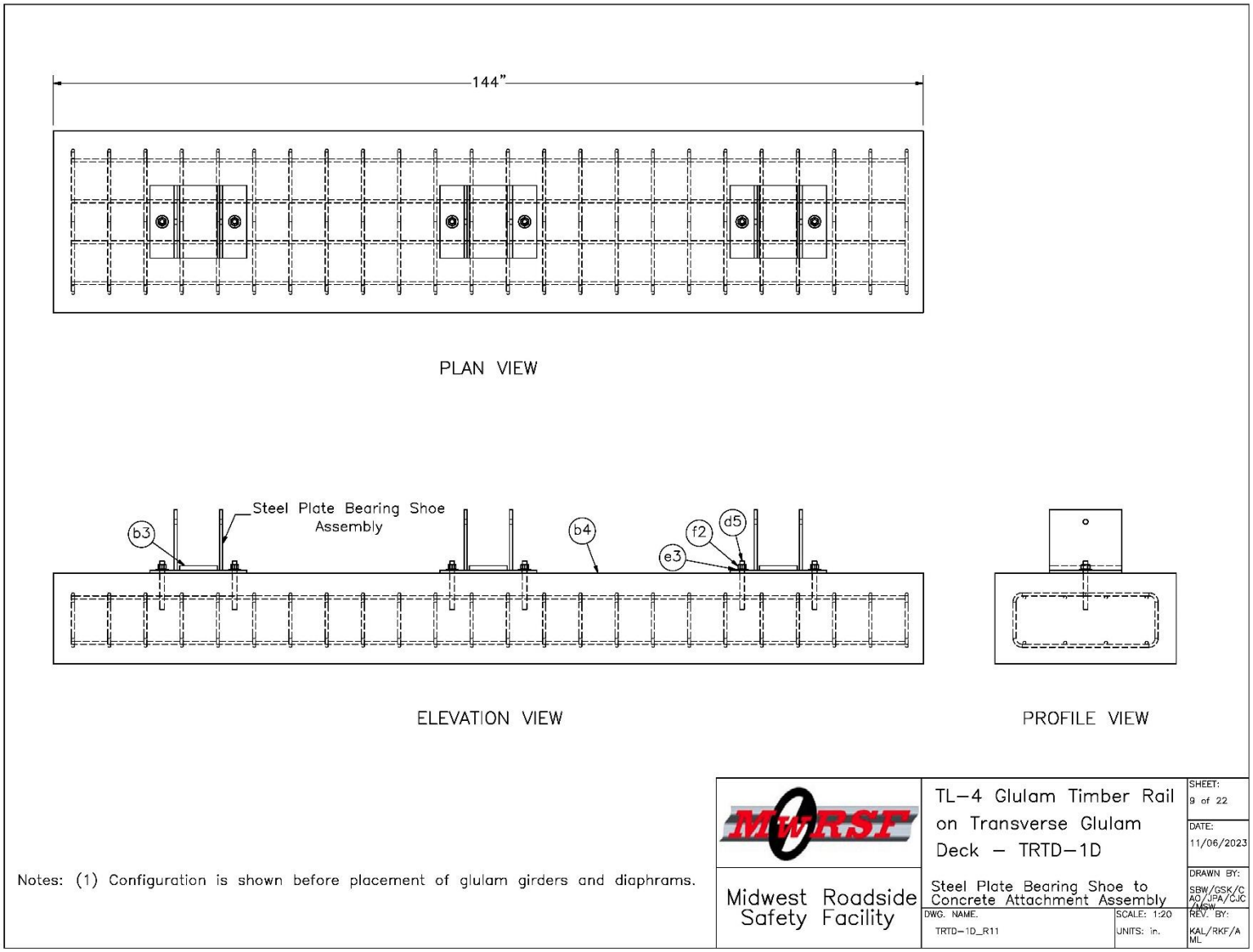

Figure 156. Concrete and Bearing Assembly Details, Test No. TRTD-1

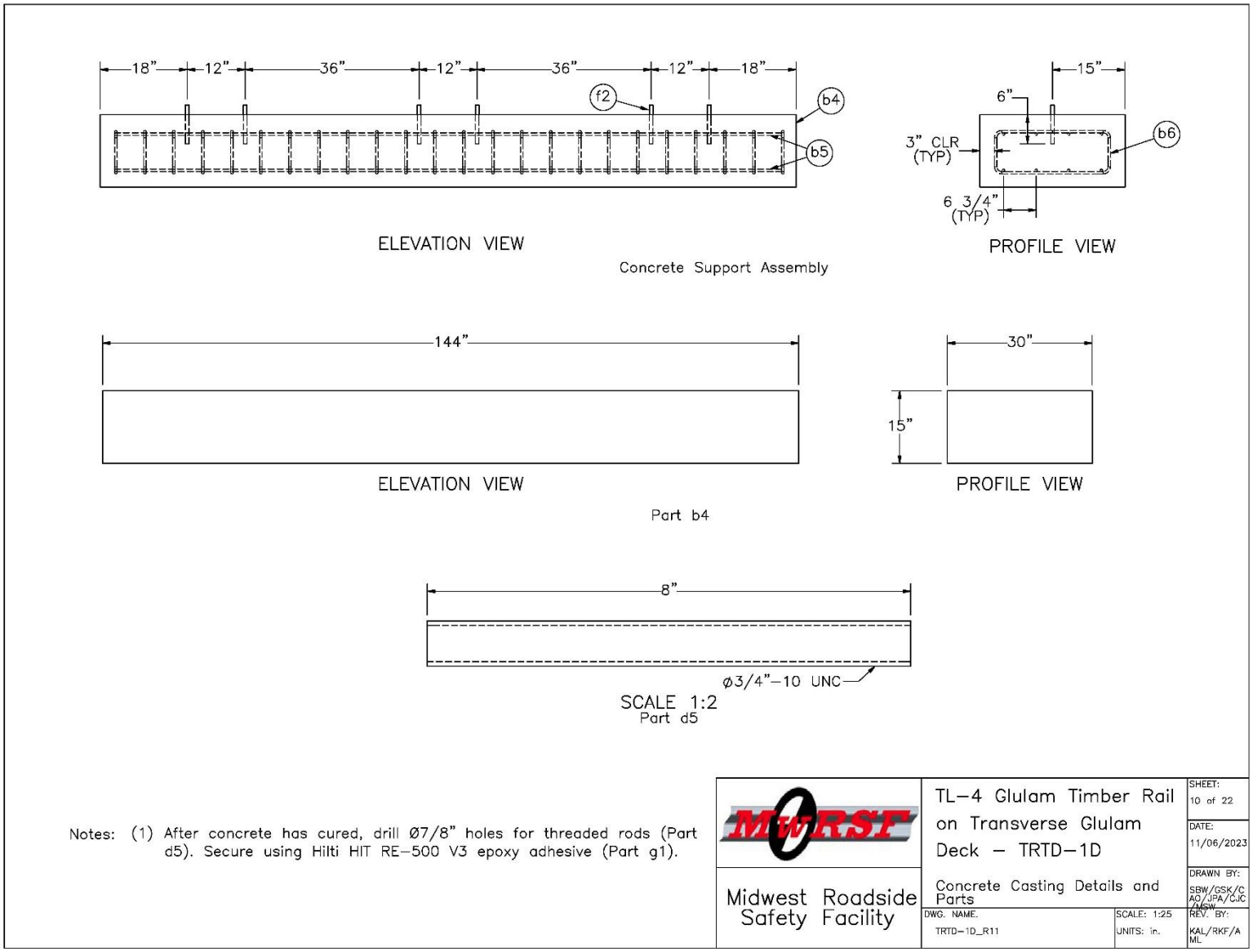

Figure 157. Concrete Casting and Embedded Rod Details, Test No. TRTD-1

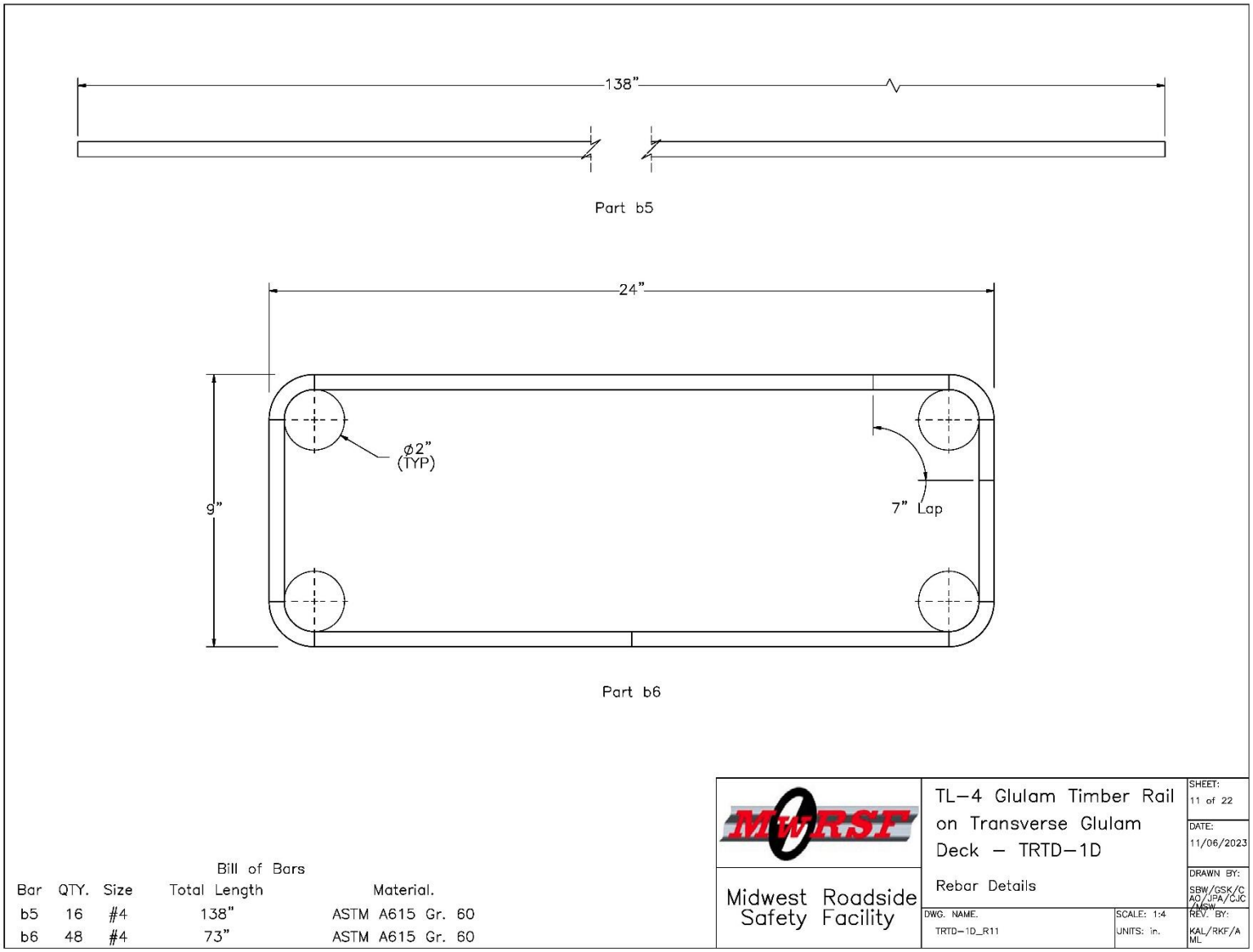

Figure 158. Rebar Details, Test No. TRTD-1

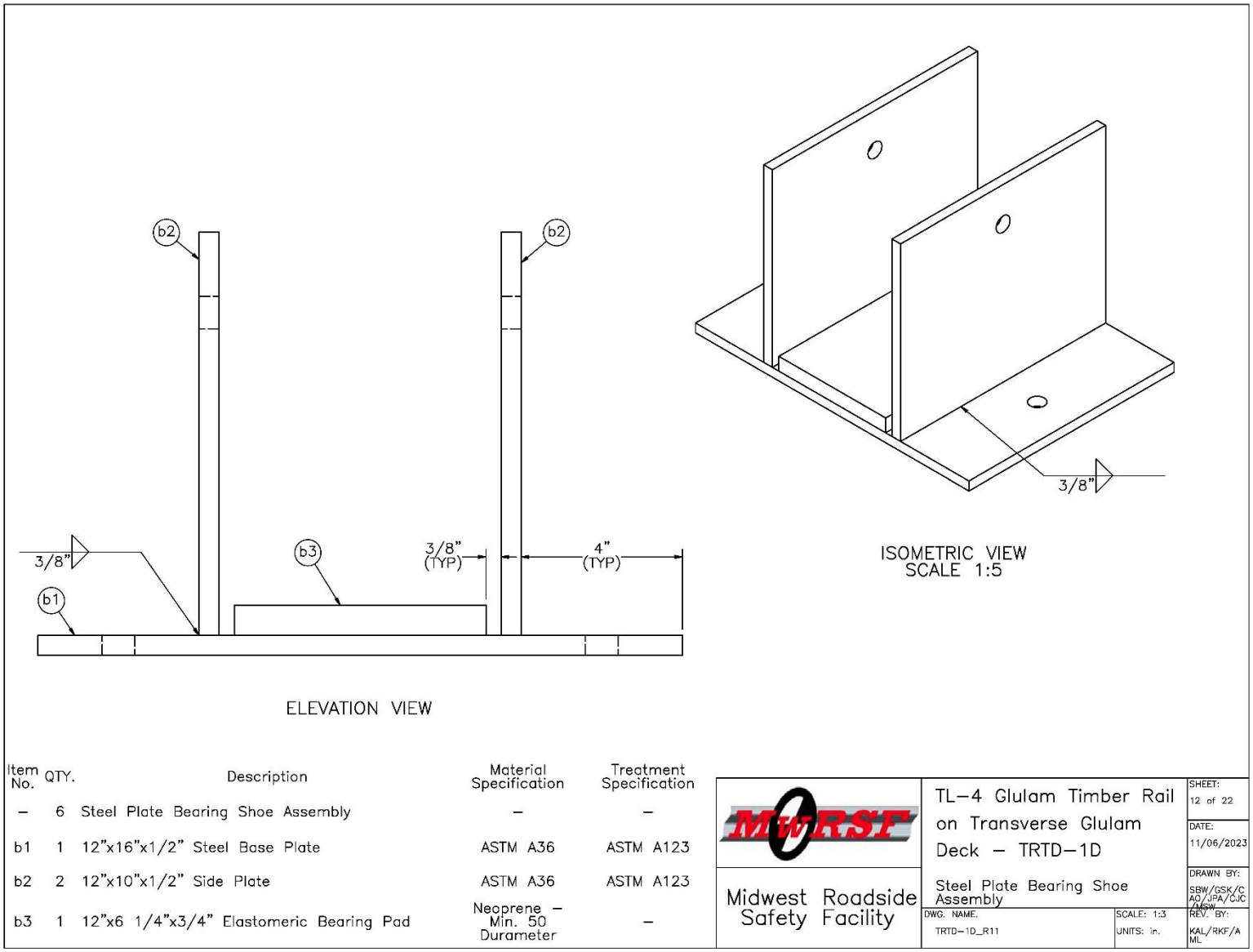

Item No.	QTY.	Description	Material Specification	Treatment Specification
–	6	Steel Plate Bearing Shoe Assembly	–	–
b1	1	12"x16"x1/2" Steel Base Plate	ASTM A36	ASTM A123
b2	2	12"x10"x1/2" Side Plate	ASTM A36	ASTM A123
b3	1	12"x6 1/4"x3/4" Elastomeric Bearing Pad	Neoprene – Min. 50 Durameter	–

Midwest Roadside Safety Facility

TL–4 Glulam Timber Rail on Transverse Glulam Deck – TRTD–1D

Steel Plate Bearing Shoe Assembly

SHEET: 12 of 22
DATE: 11/06/2023
DRAWN BY: SBW/GSK/CAO/JPA/CJC/AGW
REV. BY: KAL/RKF/AML
DWG. NAME. TRTD–1D_R11
SCALE: 1:3
UNITS: in.

Figure 159. Steel Plate Bearing Assembly Details, Test No. TRTD-1

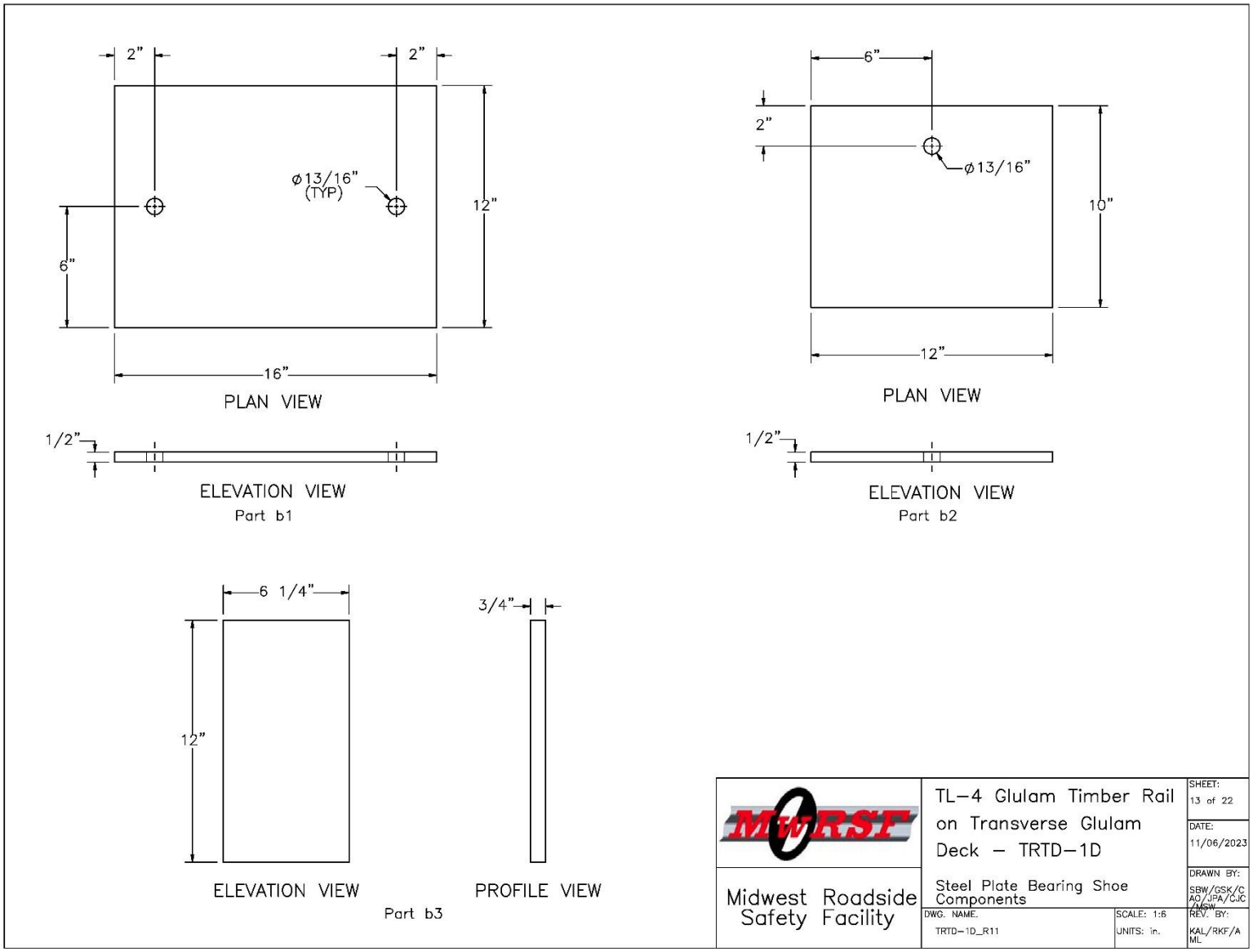

Figure 160. Steel Plate Bearing Assembly Component Details, Test No. TRTD-1

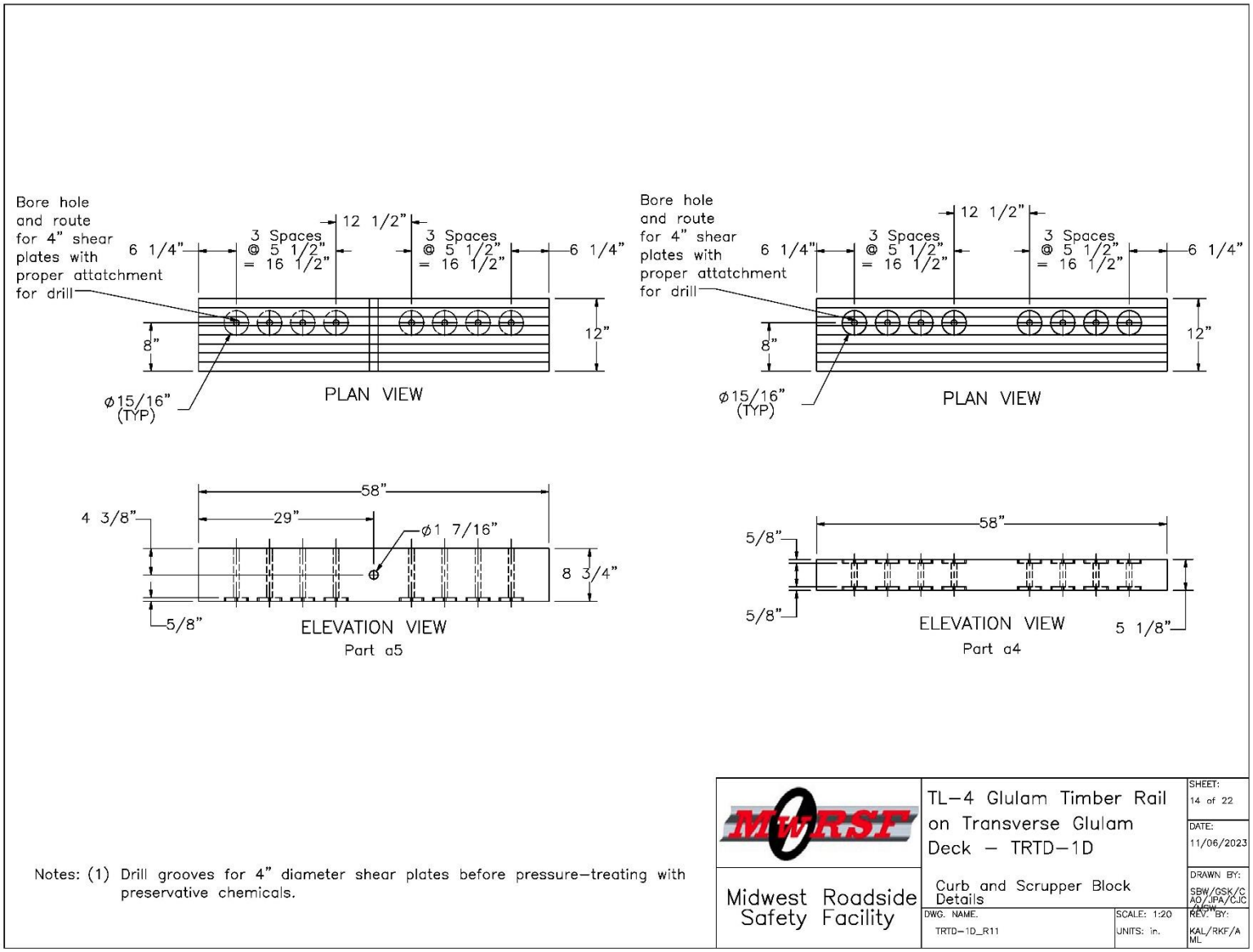

Figure 161. Scupper and Curb Rail Details, Test No. TRTD-1

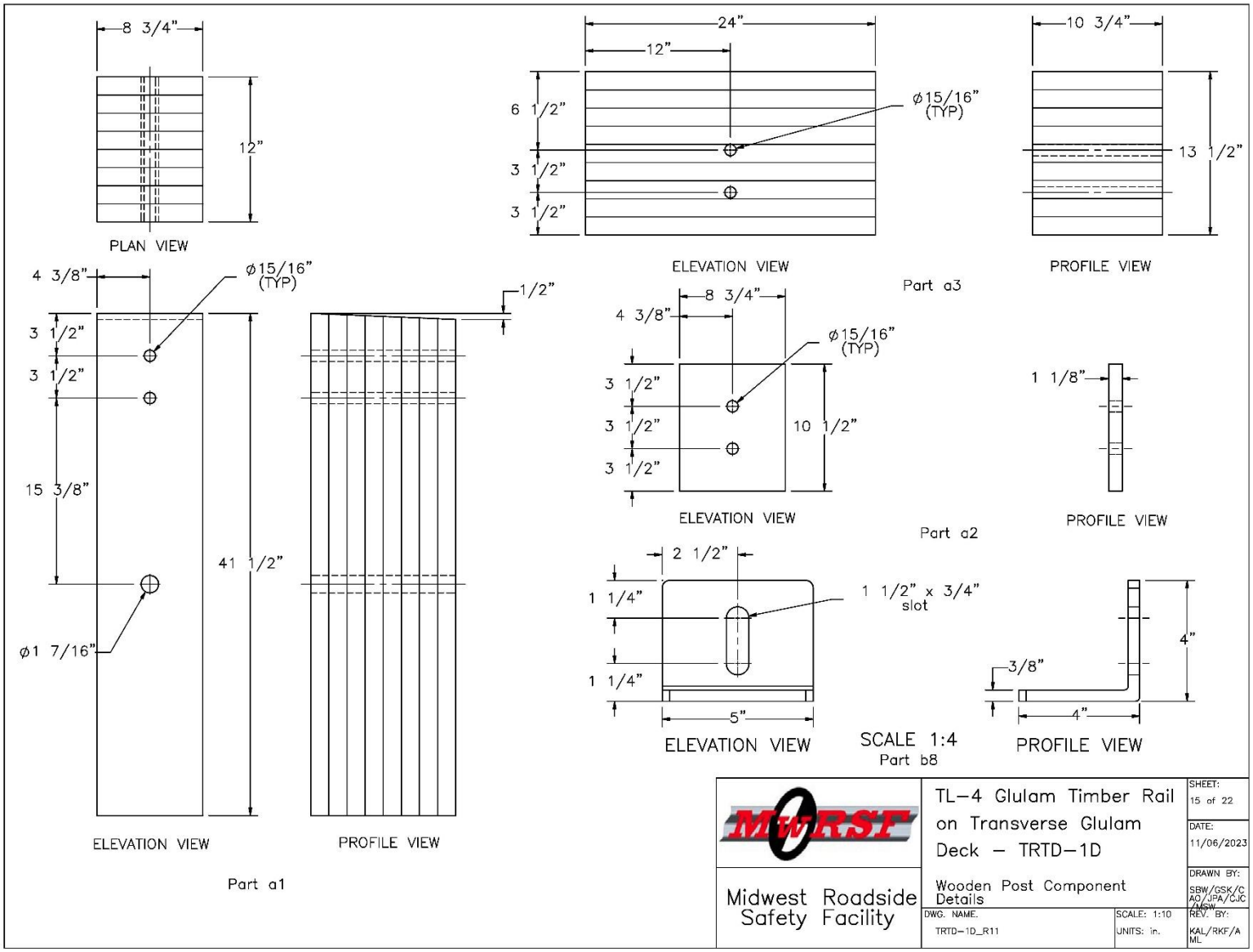

Figure 162. Vertical Post, Upper Rail, Blockout, and Angle Guide Details, Test No. TRTD-1

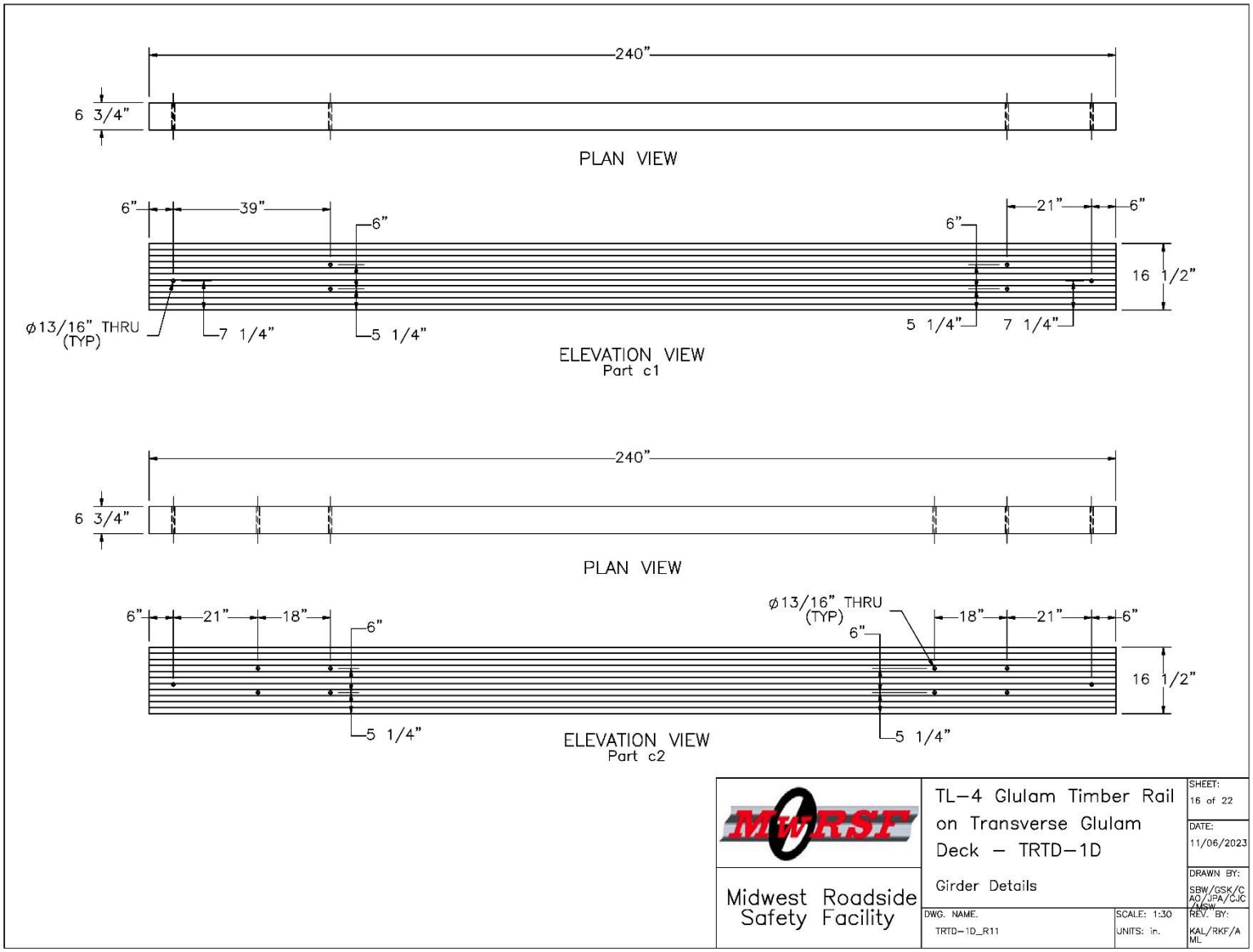

Figure 163. Girder Details, Test No. TRTD-1

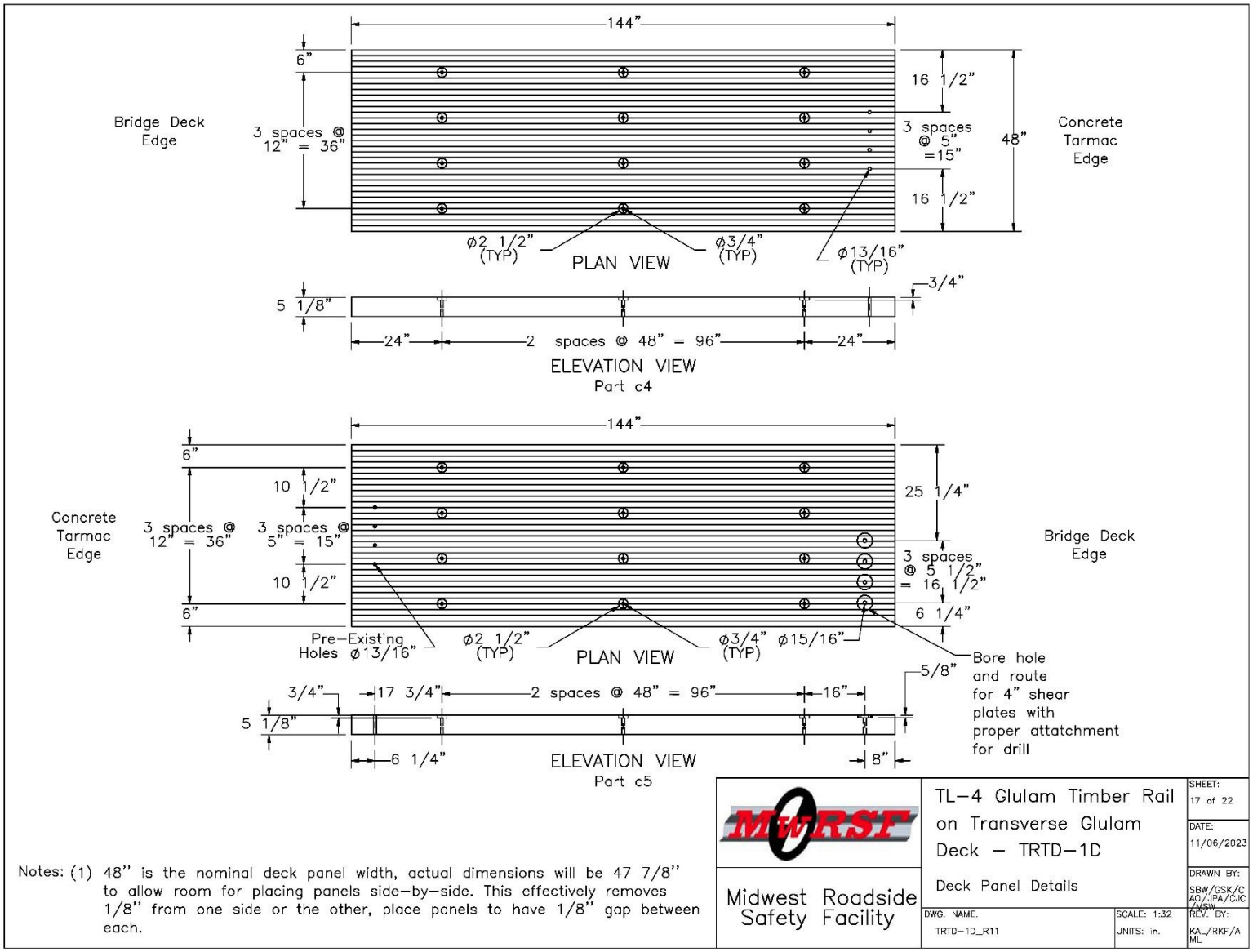

Figure 164. Deck Panel Details, Page 1, Test No. TRTD-1

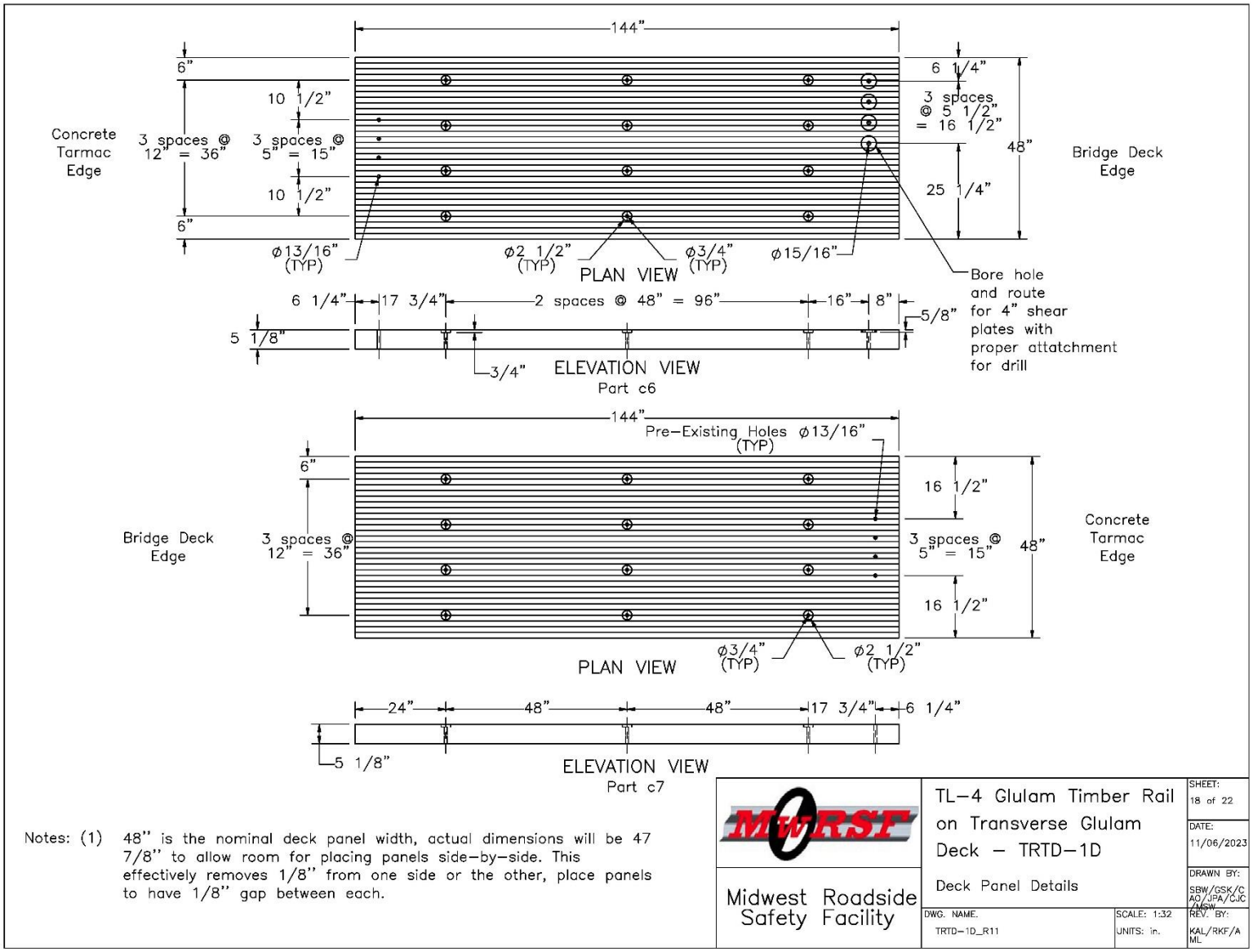

Figure 165. Deck Panel Details, Page 2, Test No. TRTD-1

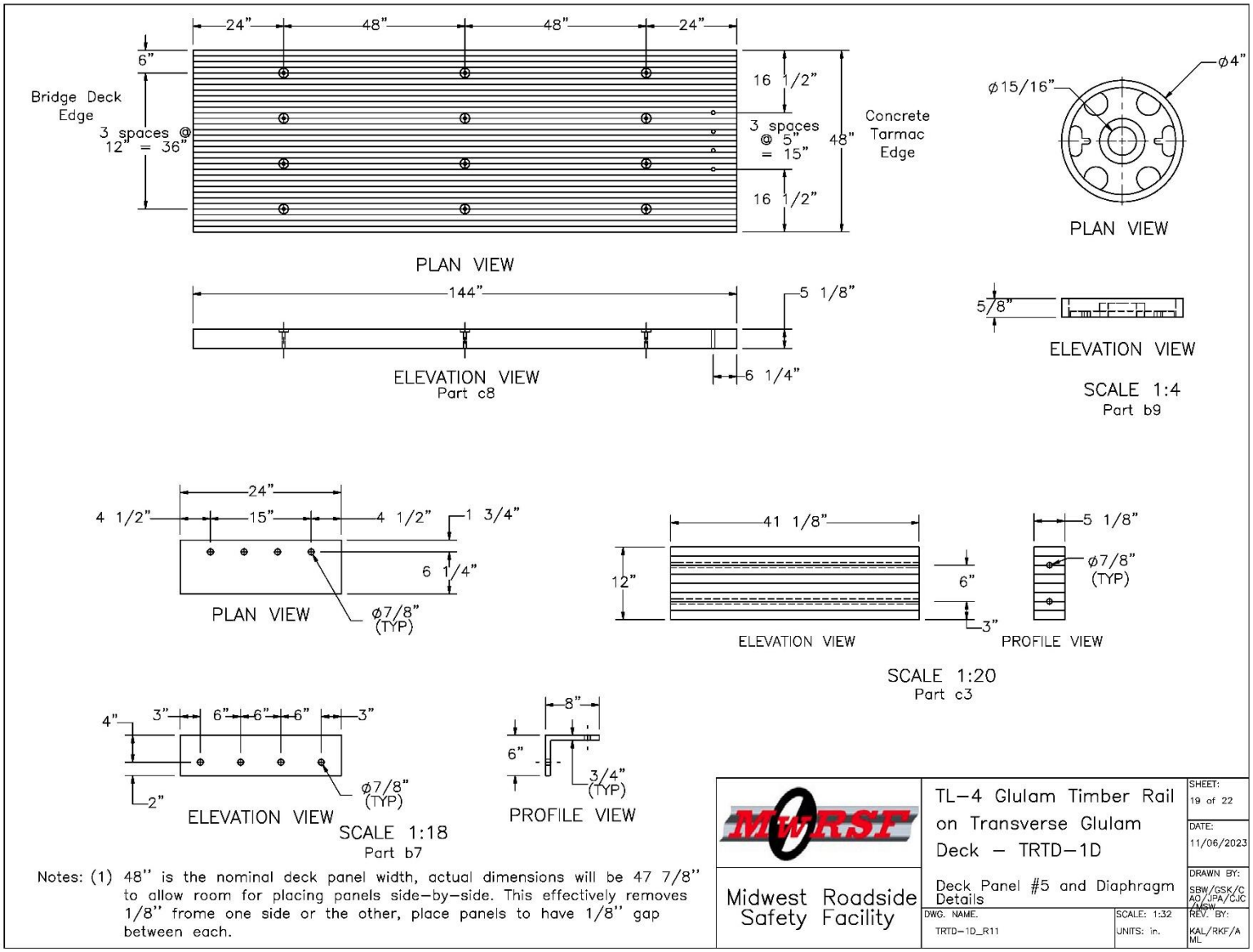

Figure 166. Deck Panel, Tarmac Angle Restraint, Diaphragm, and Shear Plate Details, Test No. TRTD-1

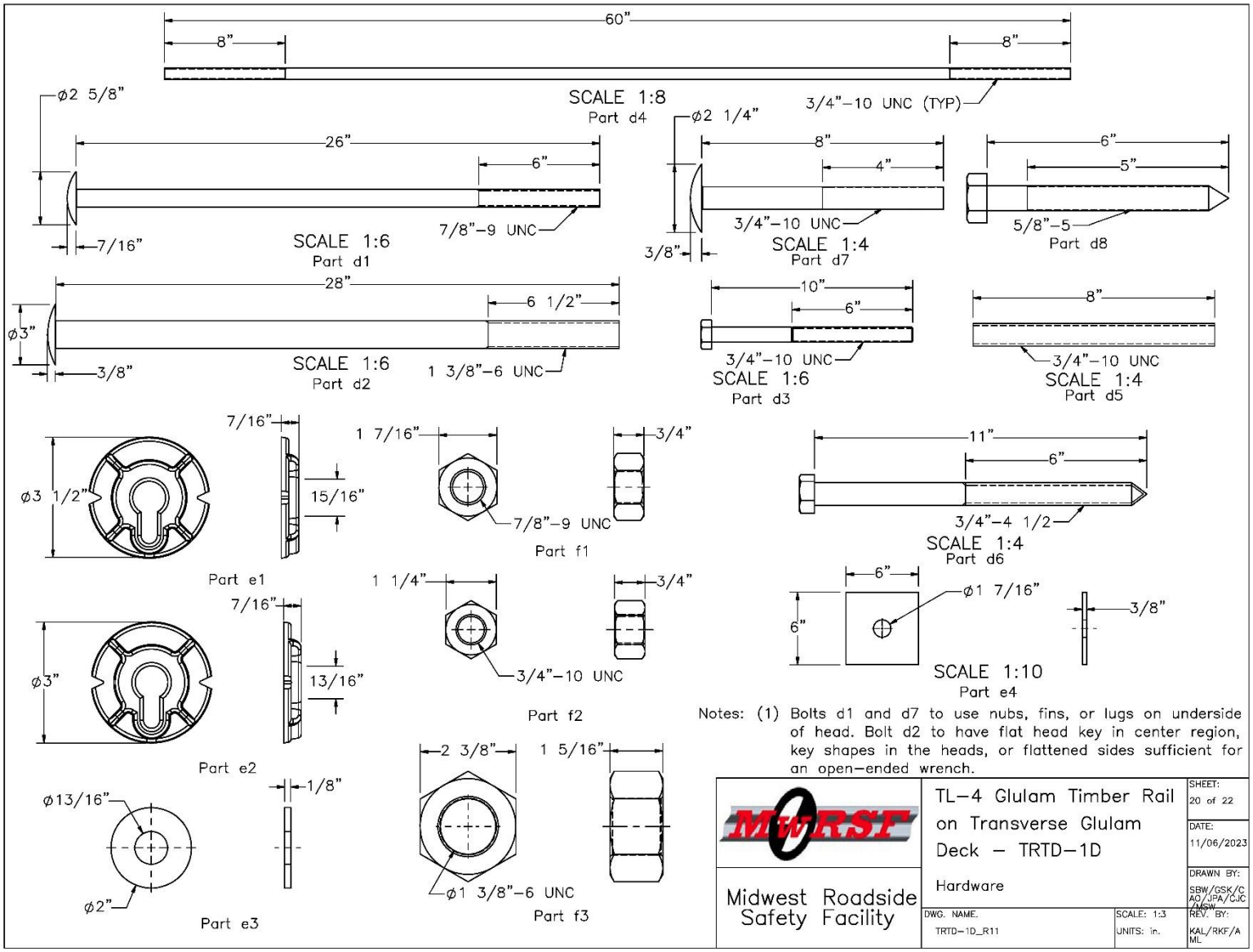

Figure 167. Connection Hardware Details, Test No. TRTD-1

Item No.	QTY.	Description	Material Specification	Treatment Specification	Hardware Guide
–	1	4" Thick Surrogate Wearing Surface	–	–	
a1	1	41 1/2"x12"x8 3/4" Glulam Post	Comb. 48 (SP) or Comb. 2 (Western Species)	Copper Naphthenate – 0.06 lbs/cu. ft Retention, AWPA Category 4A (UC4A)	–
a2	1	1 1/8"x10 1/2"x8 3/4" Glulam Blockout	Comb. 48 (SP) or Comb. 2 (Western Species)	Copper Naphthenate – 0.06 lbs/cu. ft Retention, AWPA Category 4A (UC4A)	–
a3	1	24"x13 1/2"x10 3/4" Glulam Upper Rail	Comb. 48 (SP) or Comb. 2 (Western Species)	Copper Naphthenate – 0.06 lbs/cu. ft Retention, AWPA Category 4A (UC4A)	–
a4	2	58"x12"x5 1/8" Glulam Scupper Block	Comb. 48 (SP) or Comb. 2 (Western Species)	Copper Naphthenate – 0.06 lbs/cu. ft Retention, AWPA Category 4A (UC4A)	–
a5	1	96"x12"x8 3/4" Glulam Curb Rail	Comb. 48 (SP) or Comb. 2 (Western Species)	Copper Naphthenate – 0.04 lbs/cu. ft Retention, AWPA Category 4A (UC4A)	–
b1	6	12"x16"x1/2" Steel Base Plate (Existing Material)	ASTM A36	ASTM A123	–
b2	12	12"x10"x1/2" Side Plate (Existing Material)	ASTM A36	ASTM A123	–
b3	6	12"x6 1/4"x3/4" Elastomeric Bearing Pad (Existing Material)	Neoprene – Min. 50 Durameter	–	–
b4	2	15"x30"x12' Concrete Support (Existing Material)	Min f'c = 4,000 psi NE mix 47 BD	–	–
b5	16	#4 Rebar, 138" Long (Existing Material)	ASTM A615 Gr. 60	Epoxy Coated (ASTM A775 or A934)	–
b6	48	#4 Rebar, 73" Unbent Length (Existing Material)	ASTM A615 Gr. 60	Epoxy Coated (ASTM A775 or A934)	–
b7	5	8"x 6", 3/4" Thick 24" Long Steel Angle	ASTM A36	ASTM A123	–
b8	2	4"x4", 3/8" Thick, 5" Long Steel Angle	ASTM A36	ASTM A123	–
b9	48	7/8"x4"x5/8" Shear Plate	ASTM A47 Grade 32510 or ASTM D5933	Hot-Dip	12407
c1	2	16 1/2"x6 3/4"x20' Long Outside Glulam Girder (Existing Material)	24F-V4 Douglas Fir	Pentachorophenal in Heavy Oil 0.6 lbs/cu. ft Retention	–
c2	1	16 1/2"x6 3/4"x20' Long Glulam Girder (Existing Material)	24F-V4 Douglas Fir	Pentachorophenal in Heavy Oil 0.6 lbs/cu. ft Retention	–
c3	4	12"x5 1/8"x41 1/8" Long Glulam Diaphragm (Existing Material)	Comb. No. 2 Douglas Fir	Pentachorophenal in Heavy Oil 0.6 lbs/cu. ft Retention	–

Notes: (1) Timber rails, posts, scuppers, and blockouts shall be treated with Copper Naphthenate (CuN) or 4,5-Dichloro-2-N-Octyl-4-Isothiazolin-3-One (DCOI) in heavy oil to a minimum retention of 0.075 lbs/cu. ft. or 0.20 lbs/cu. ft. respectively in accordance with AWPA Standard U1 to the requirements. Use category 4C (UC4C).
(2) Wood shall be cut, drilled, and completely fabricated prior to treatment with preservative. Drain excess chemicals and dry all treated wood at the place of manufacture.
(3) All field cuts, bore holes, and damages shall be treated with material acceptable to the engineer prior to installation.

Midwest Roadside Safety Facility

TL-4 Glulam Timber Rail on Transverse Glulam Deck – TRTD-1D

Bill of Materials

SHEET: 21 of 22
DATE: 11/06/2023
DRAWN BY: SBW/GSK/CAO/JPA/CJC/AGW
REV. BY: KAL/RKF/AML
DWG. NAME. TRTD-1D_R11
SCALE: None
UNITS: in.

Figure 168. Bill of Materials, Page 1, Test No. TRTD-1

Item No.	QTY.	Description	Material Specification	Treatment Specification	Hardware Guide
c4	1	5 1/8"x4'x12' Long Glulam Deck Panel #1 (Existing Material)	Comb. No. 2 Douglas Fir	Pentachorophenal in Heavy Oil 0.6 lbs/cu. ft Retention	–
c5	1	5 1/8"x4'x12' Long Glulam Deck Panel #2 (Existing Material)	Comb. No. 2 Douglas Fir	Pentachorophenal in Heavy Oil 0.6 lbs/cu. ft Retention	–
c6	1	5 1/8"x4'x12' Long Glulam Deck Panel #3 (Existing Material)	Comb. No. 2 Douglas Fir	Pentachorophenal in Heavy Oil 0.6 lbs/cu. ft Retention	–
c7	1	5 1/8"x4'x12' Long Glulam Deck Panel #4 (Existing Material)	Comb. No. 2 Douglas Fir	Pentachorophenal in Heavy Oil 0.6 lbs/cu. ft Retention	–
c8	1	5 1/8"x4'x12' Long Glulam Deck Panel #5 (Existing Material)	Comb. No. 2 Douglas Fir	Pentachorophenal in Heavy Oil 0.6 lbs/cu. ft Retention	–
d1	10	7/8"–9 UNC x 26" Timber Bolt w/ Nubs	ASTM A307A	ASTM A123	FBB08
d2	1	1 3/8"–6 UNC x 28" Timber Bolt w/o Nubs	ASTM A449	ASTM A123	FBB08
d3	6	3/4"–10 UNC x 10" Hex Bolt (Existing Material)	ASTM A307A	ASTM A123	FBX20a
d4	8	3/4"–10 UNC x 8" on a 60" Long Tie Rod (Existing Material)	ASTM A307A or F1554 Gr. 36 or SAE J429 Gr. 2	ASTM A123	FRR28a
d5	32	3/4"–10 UNC x 8" Threaded Rod (20 new, 12 existing)	ASTM A193 Gr. B7 or SAE J429 Gr. 5	ASTM A123	FRR20a
d6	60	3/4"–4 1/2 x 11" Lag Bolt (Existing Material)	ASTM A307A	ASTM A123	FBL20
d7	20	3/4"–10 UNC x 8" Timber Bolt w/ Nubs	ASTM A307A	ASTM A123	FBB08
d8	2	5/8"–5 x 6" Lag Bolt	ASTM A307A	ASTM A123	FBL16
e1	10	7/8" Dia. Malleable Iron Washer	ASTM F47	ASTM A123	–
e2	22	3/4" Dia. Malleable Iron Washer (Existing Material)	ASTM A47	ASTM A123	–
e3	114	3/4" Flat Washer (42 new, 72 existing)	ASTM F844	ASTM A123 or A153 or F2329	FWC20a
e4	2	6"x6"x3/8" Steel Plate Washer	ASTM A36	ASTM A123	–
f1	10	7/8"–9 UNC Dia. Heavy Hex Nut	ASTM A563A	ASTM A123	FNX22b
f2	74	3/4"–10 UNC Dia. Heavy Hex Nut (40 new,34 existing)	ASTM A563A	ASTM A123	FNX20b
f3	1	1 3/8"–6 UNC Dia. Heavy Hex Nut	ASTM A563A	ASTM A123 or A153 or F2329	
g1	–	Epoxy Adhesive (Existing Material)	Hilti HIT RE–500 V3 or equivalent with min. bond strength 1,670 psi	–	–

Midwest Roadside Safety Facility

TL–4 Glulam Timber Rail on Transverse Glulam Deck – TRTD–1D

Bill of Materials

SHEET: 22 of 22
DATE: 11/06/2023
DRAWN BY: SBW/GSK/CAO/JPA/CJC/AGW
REV. BY: KAL/RKF/AML
DWG. NAME: TRTD–1D_R11
SCALE: 1:96
UNITS: in.

Figure 169. Bill of Materials, Page 2, Test No. TRTD-1

5.3 TRTD-1 Construction

5.3.1 Substructure

The prior construction of the two abutments is shown in Figures 170 through 172. Two 144-in. x 15-in. x 30-in. reinforced concrete surrogate bridge supports were constructed to form the substructure. Details for the substructure in the test plans were shown in Figures 154 through 158. Four longitudinal no. 4 bars reinforced the top and bottom of the concrete blocks. Stirrups, also no. 4, were spaced at 6-in. centers and enclosed the longitudinal rebar. Six ¾-in. diameter ASTM A193 grade B7 steel rods were drilled and grouted 6 in. into the concrete blocks to anchor the steel bearing assemblies for the superstructure.

Figure 170. Forms for Test No. TRTD-1 Substructure, Test No. TRTD-1

Figure 171. Forms for Substructure with Rebar Cage, Test No. TRTD-1

Figure 172. Fully Cast Substructure and Steel Bearing Assemblies, Test No. TRTD-1

5.3.2 Superstructure

The bridge superstructure was constructed from glulam girders and glulam deck panels. Test plan details for the superstructure assembly are shown in Figures 148 through 155. Details for the superstructure components are shown in Figures 159 and 160, as well as Figures 163 through 166. Three 24F-V4 Douglas Fir-Larch glulam 16.5-in. tall x 6.75-in. wide x 20-ft long girders were placed within steel plate bearing assemblies. The base of the assembly was a 12-in. x 16-in. x ½-in. thick steel plate with two 12-in. x 10-in. x ½-in. thick side plates welded to the top of the base plate. A 12-in. x 6¼-in. x ¾-in. thick elastomeric bearing pad was horizontally placed between the vertical side plates. A single ¾-in. diameter ASTM A307A bolt held one girder end and the side plates of one assembly together. Four 12-in. x 5⅛-in. x 41⅛-in. long diaphragms were spaced between the three girders, each with two holes running through the length of the diaphragm for the placement of two ¾-in. diameter ASTM A193 grade B7 steel threaded rods. Five 5⅛-in. x 48-in. x 144-in. long deck panels formed the bridge deck and were held to the girder with twelve lag bolts per panel, which penetrated through the panels and were anchor into the underlying girders. The deck panels and girders are shown in Figures 173 through 175.

Figure 173. Shipped Glulam Superstructure Components, Test No. TRTD-1

Figure 174. Glulam Girders with Diaphragms Bolted to Supports, Test No. TRTD-1

Figure 175. Superstructure Girders with Deck Panels on Top, Test No. TRTD-1

5.3.3 Surrogate Bridge Railing

Details for the bridge railing post assembly in the test plans are shown in Figures 151 and 153. Details on the components of the bridge assembly are shown in Figures 161 and 162. The upper rail segment was 13½-in. tall x 10¾-in. wide x 2-ft long and was held to the vertical post with two ⅞-in. diameter ASTM A307A steel bolts. The vertical 12-in. deep x 8¾-in. wide x 41½-in. long post was held to the 8¾-in. tall x 12-in. wide x 58-in. long curb rail by a single, 1⅜-in. diameter ASTM A449 steel timber bolt. The bolt used two 6-in. x 6-in. x ⅜-in. thick ASTM A36 steel plates with holes for the washers. Underneath the curb rail were two 5⅛-in. tall x 12-in. wide x 58-in. long scuppers. The curb rail and scuppers were held to the deck by eight ⅞-in. diameter ASTM A307A steel bolts. All timber railing material was fabricated from Douglas Fir-Larch Combination No. 2 glulam. Combinations No. 1 and No. 2 Douglas Fir-Larch glulam have identical tabulated perpendicular to grain compressive design values. Hence, Combination No. 1, which was originally intended as the material grade for the curb rail and scuppers, would also be acceptable for those pieces. Photographs of the completed bridge post assembly are shown in Figures 176 and 177.

Figure 176. Side View of Assembled Bridge Post and Impact Bogie Vehicle, Test No. TRTD-1

Figure 177. Completed Bridge Post on Bridge Deck, Test No. TRTD-1

5.4 Transverse Deck Testing Equipment and Instrumentation

5.4.1 Overview

The first test involved a post system installed on a transverse glulam deck using ⅞-in. diameter ASTM A307A steel bolts to hold the curb rail to the scuppers and deck. Construction and testing proceeded more rapidly by using the existing bridge deck system.

5.4.2 Bogie Vehicle

A rigid-frame bogie was used to impact the bridge post and deck configuration. The impact head was bolted to the bogie vehicle, creating a rigid attachment with an impact height of 29¼ in. for test no. TRTD-1. The bogie head was fabricated with an 8⅝-in. diameter x ½-in. thick x 60½-in. long steel tube with a neoprene pad wrapped around the tube to reduce local damage to the post and mitigate some of the initial impulse magnitude. The bogie vehicle weighed 7,188 lb and is shown in Figure 178.

Figure 178. Bogie Vehicle

5.4.3 Accelerometers

Two triaxial accelerometer systems, measuring accelerations in the longitudinal (direction of bogie movement), lateral, and vertical directions, were fastened to the rigid frame bogie vehicle near its center of gravity. However, only longitudinal accelerations were reported herein due to minimal accelerations in the other two directions.

Both accelerometer systems, called SLICE-1 and SLICE-2, were manufactured by Diversified Technical Systems, Inc. of Seal Beach California. Triaxial acceleration and angular sensor modules were mounted inside the bodies of custom-built SLICE 6DX event data recorders equipped with 7GB of non-volatile flash memory and recorded data at 10,000 Hz to the onboard microprocessor. The accelerometers had a range of ±500g's in each of the three directions (longitudinal, lateral, and vertical) and were equipped with a 1,650 Hz (CFC 1000) anti-aliasing filter. The SLICE MICRO Triax ARS had a range of 1,500 degrees/sec in each of three directions (roll, pitch, and yaw). The raw angular rate measurements were downloaded, converted to the proper Euler angles for analysis, and plotted. The "SLICEWare" computer software program and a customized Microsoft Excel worksheet were used to analyze and plot both the accelerometer and angular rate sensor data. The accelerometers on the bogie are shown in Figure 179.

Figure 179. Accelerometer and Rate Transducer Systems on Bogie Vehicle

5.4.4 Retroreflective Optic Speed Trap

A retroreflective optic speed trap was used to determine the speed of the bogie vehicle before impact. Retroreflective targets, spaced at approximately 18-in. intervals, were applied to the side of the bogie vehicle. When the emitted beam of light was reflected by the targets and returned to the Emitter/Receiver, a signal was sent to the data acquisition computer, recording at 10,000 Hz, as well as the external LED box activating the LED flashes. The speed was then calculated using the spacing between the retroreflective targets and the time between the signals. LED light and high-speed digital video analysis are used as a backup if vehicle speeds cannot be determined from the electronic data. The retroreflective optic tape on the side of the bogie is shown in Figure 180.

Figure 180. Retroreflective Optic Tape on Side of Bogie Vehicle

5.4.5 Digital Photography

Three AOS high-speed cameras were used for test no. TRTD-1. Two of these cameras captured the impact from cross-sectional side views, with one facing north and the other facing south. The third camera was mounted overhead, looking down on the post. In addition, six digital video cameras, either GoPro or Panasonic, were positioned to capture the impact event from multiple angles. Two cameras were placed behind the post, one on the north side and one on the south side. Two more cameras were set up adjacent to the high-speed cameras to supplement the side views. One camera recorded an overhead view, and another was positioned beneath the post to capture an upward view. The AOS high-speed cameras recorded at 500 frames per second, the GoPro cameras at 240 frames per second, and the Panasonic cameras at 120 frames per second. All cameras were placed laterally relative to the post, with views perpendicular to the direction of bogie travel. A digital still camera was also used to document the pre-test and post-test conditions for all tests.

5.4.6 Surface Strain Gauges

LFLAB-10-11 strain gauges from Tokyo Measurement Laboratories and intended for wood and gypsum materials were used to obtain transverse strains from the top of the glulam timber deck. These gauges had a resistance of 120 Ohm, and were roughly 10 mm x 3.1 mm. The gauges were adhered to the deck with CN-E adhesive with an operable range of -30 to 120 degrees

Celsius. Preliminary trials adhering the strain gauges to other wood surfaces found that oil-based, preservative-treatments on timber surfaces did not allow adherence using a strain gauge adhesive provided by TML. Sanding the wood surface was found to be neither practical nor effective. A precoating of Devon 5-minute epoxy, as recommended by TML's technical engineer, was applied to the deck surface. This precoating was found to successfully create a bonding surface for the strain gauges that would hold the gauges more firmly to the wood specimens.

The maximum transverse deck strain locations were assumed to occur near the edge of the outer girder or near the vertical bolts. The strain gauge locations for test no. TRTD-1 are shown in Figure 181, and a deck surface strain gauge is shown in Figure 182.

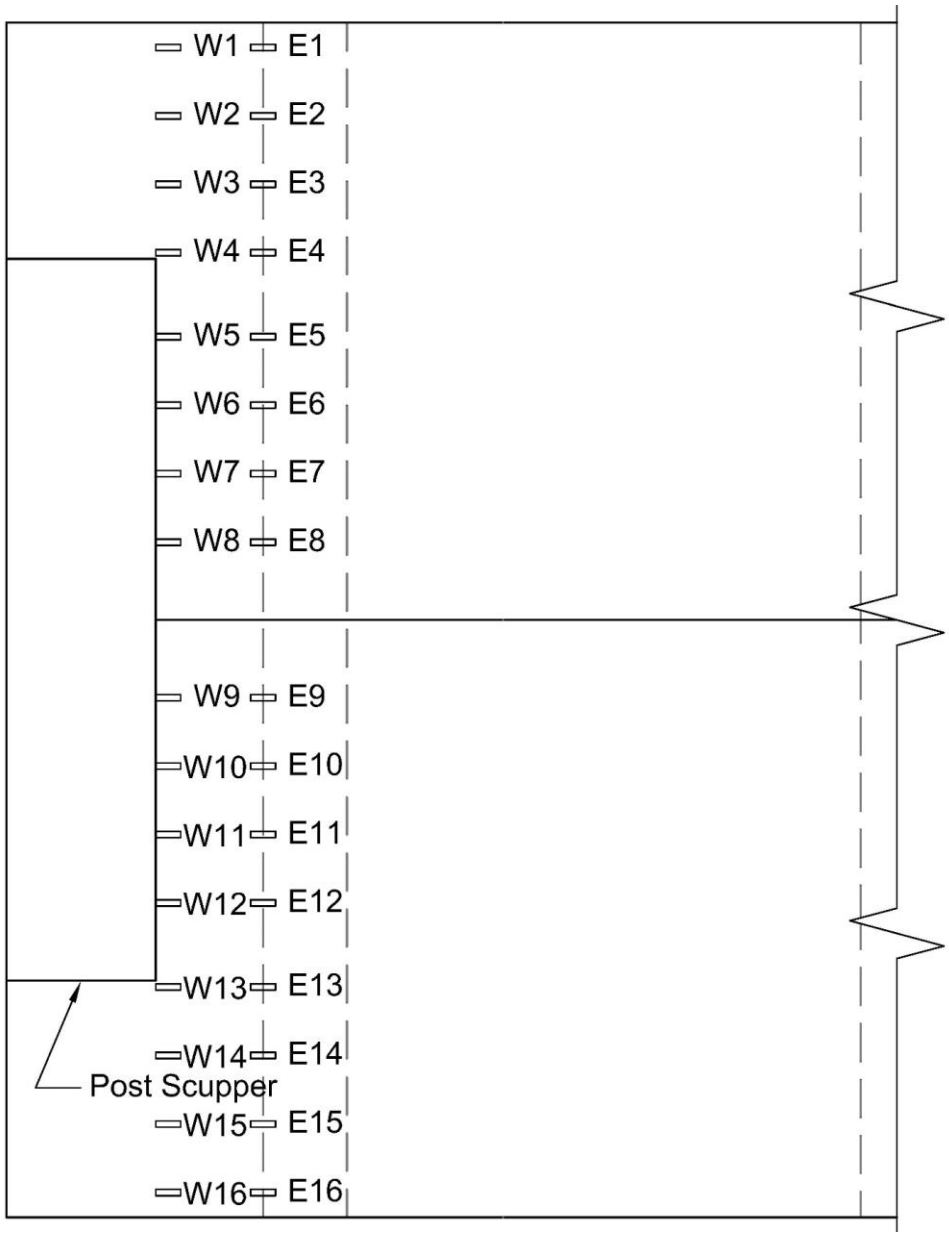

Figure 181. TRTD-1 Deck Surface Strain Gauge Locations (dashed lines denote girder edges)

Figure 182. Deck Surface Strain Gauges

5.4.7 Bolt Axial Strain Gauges

BTM-6C two-wire and three-wire strain gauges, developed by Tokyo Measurement Labs and marketed in the United States by Texas Measurement Labs, were used to obtain axial strain readings from the horizontal and vertical timber bolts. The two-wire gauges were remaining gauges from timber bridge railing tests that were conducted in 1997, while the three-wire gauges were newly ordered for use in the dynamic component testing reported herein. Both gauges operated with 120±0.5 ohms resistance and a temperature range of -10 to 80 degrees Celsius. The 1997 gauges used a gauge factor of 2.1, while the 2023 gauges used a gauge factor of 2.14. Both types of gauges required that a small 2-mm hole be drilled into either bolt end. Once the hole has reached the necessary depth where the full axial load would be developed, an adhesive was prepared and injected into the hole with a syringe. The gauge was placed in the hole immediately afterwards, and the adhesive was cured with the gauge in the bolt. Figure 183 shows the location of all eight vertical bolts with axial strain gauges. The horizontal bolt with its axial strain gauge is shown as d2 for the traffic side face of the system. Figure 184 shows all the vertical bolts with strain gauges, and Figure 185 zooms into two of the two-wire gauges within the instrumented vertical bolts.

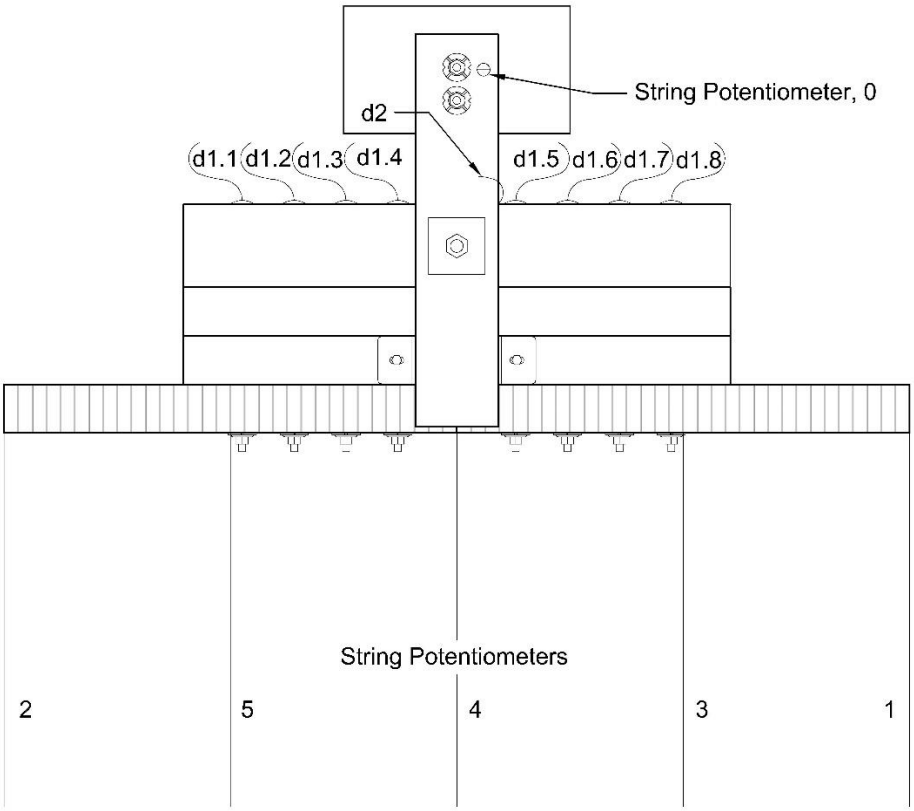

Figure 183. String Potentiometer and Bolt Axial Gauge Locations on Bridge Post System, String Potentiometers Numbered 0 to 5

Figure 184. Vertical Bolt Axial Strain Gauges and All String Potentiometers

Figure 185. Bolt Axial Strain Gauges on Bolts d1.1 (right) and d1.2 (left) in test no. TRTD-1

5.4.8 String Potentiometers

Five string potentiometers were used to measure the vertical displacements of the deck, and one was used to measure the lateral displacement of the post. String potentiometers function by measuring the axial movement of a retractable string that extends from and retracts into a housing unit containing the sensor. The strings were attached to the bridge deck and the post using small screws. Figure 186 shows the string potentiometers, which were mounted on heavy wood beams to prevent the sensor housings from lifting during the test. A steel post was also used to secure the housing of the lateral string potentiometer. Among the six string potentiometers, one was capable of measuring displacements up to 20 in. and was used for lateral displacement (string potentiometer 0 from Figure 183). The two potentiometers installed at the exterior edges of the deck panels (2 and 1 from Figure 183) had measurement capacities of up to 5 in., while the three interior potentiometers (5, 4, and 3 from Figure 183) could measure up to 10 in.

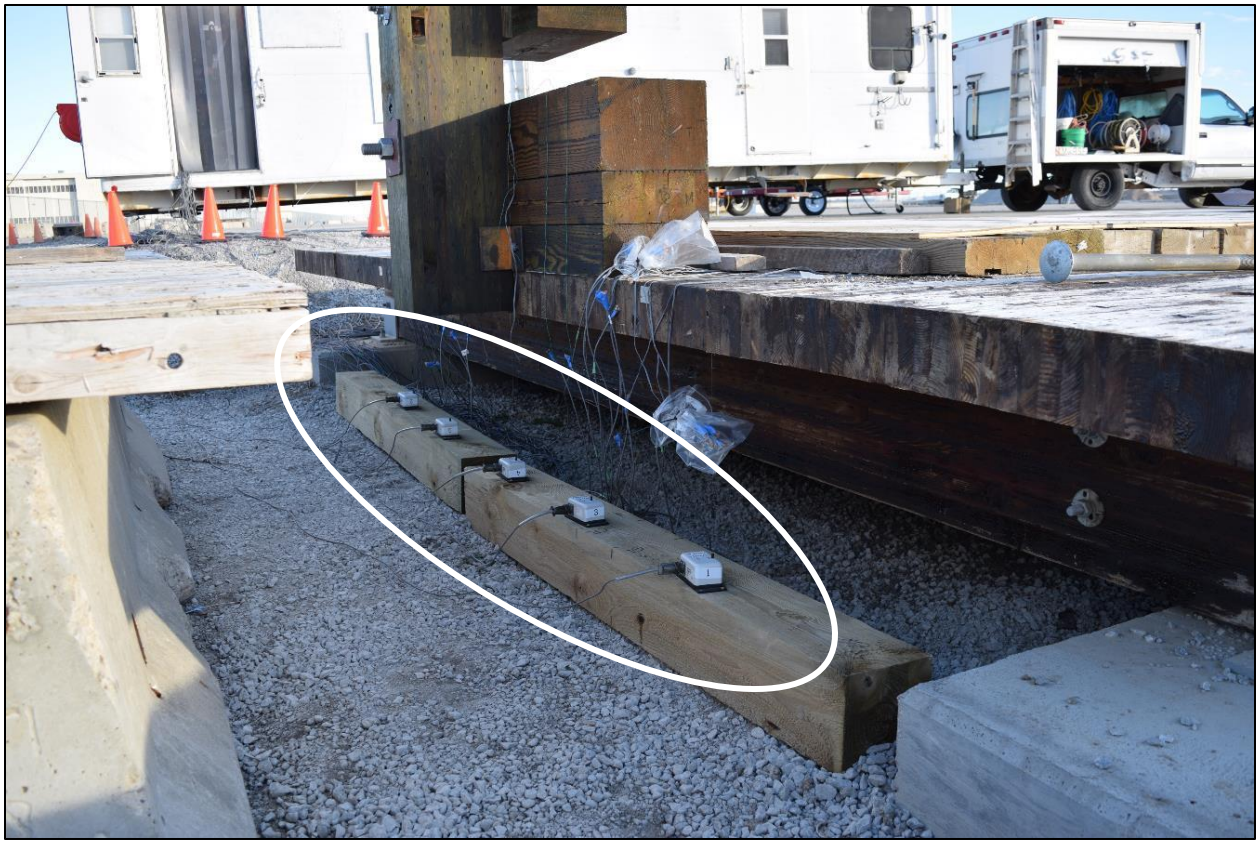

Figure 186. Test No. TRTD-1 String Potentiometers Measuring Deck Deflection

5.4.9 Pressure Film

Fujifilm Prescale Low Pressure Surface Pressure Mapping Sensor Film, marketed by Sensor Products Inc., is used for measuring the pressure experienced by two flat surfaces. The sensor film, called "pressure film" for the remainder of this report, makes use of two films to create a reaction between them to produce a "dye" to designate under pressure the degree of surface pressure. Figure 187 shows how a section of this film is red following an applied pressure, while the remainder of the film is white where no or limited pressure has been applied. The low-pressure film type estimates pressures in the range of 350 to 1,400 psi, which was selected for Douglas Fir-Larch glulam perpendicular to grain strength under applied load conditions, 1,176 psi. The operating temperature range for this film is 20 to 35 degrees Celsius, and the humidity range is 35% to 80% relative humidity. Additionally, product specialists have noted that this film is not intended for shear applications as film damage may become an issue.

Figure 187. Pressure Film Between Back of Vertical Post and Back of Transverse Glulam Deck or Scupper Blocks, After Test No. TRTD-1

5.5 Dynamic Component Test No. TRTD-1 Results

5.5.1 Overview

Test no. TRTD-1 was conducted on February 9, 2024, using a 7,186-lb bogie to impact a timber bridge post mounted on a 5⅛-in. thick transverse glulam deck. The bogie head struck the middle of the upper rail segment, which was 33.25 in. above the top of the deck and 29.25 in. above the top of two 2-in. thick wearing surfaces. The bogie was traveling 11.99 mph, close to the target speed of 12 mph, which impacted the post system at a 90-degree angle. The impact event rotated the post system and bridge deck, causing the top of the post to deflect backward and downward. Cracks developed in the scupper blocks and curb rail, which ultimately ruptured and allowed large displacements at low loads. The vertical post, upper rail block, and a portion of the curb rail ultimately broke away from the remaining post system when the 1⅜-in. diameter horizontal bolt ripped out of the curb rail that was anchored to the deck by vertical bolts.

The progressive failure of the system began at 0.026 seconds after impact, indicated by vertical splits in the bottom scupper. At 0.030 seconds, vertical cracks were visible in the curb rail. At the crack locations, the vertical bolt heads began to pull into the wood. The cracks propagated through the curb rail and split it into a smaller and larger segment, with the small segment held down by the vertical bolts and the large segment rotating with the horizontal bolt, vertical post, and upper rail. After 0.056 seconds a second horizontal crack initiated in the small segment. At 0.098 seconds, the horizontal bolt began to pull out of the small segment. At 0.1072 seconds, the post was no longer providing any resistance to the head of the bogie vehicle. The bogie vehicle stopped when the lower body hit the vertical bolts. Sequential photographs are shown in 188 and 189, along with damage photographs after the event.


Impact


0.020 sec


0.040 sec


0.060 sec


0.080 sec


0.108 sec

Figure 188. Left-End, High-Speed Video Time-Sequential Photographs and Post Impact Photographs, Test No. TRTD-1


Impact


0.020 sec


0.040 sec


0.060 sec


0.080 sec


0.108 sec

Figure 189. Right End High-Speed Video Time-Sequential Photographs and Post-Impact Photographs, Test No. TRTD-1

5.5.2 System Damage

5.5.2.1 Curb Railing

Figure 190 shows the curb rail before impact. Figure 191 shows the splintered portion of curb rail connected to the vertical bolts. Figure 192 shows the portion of curb rail which broke away with the vertical post and upper rail segment.

Figure 190. Curb Rail Prior to Impact

Figure 191. Damaged Curb Rail Attached to Bolts Following Impact

Figure 192. Damaged Curb Rail Attached to Bolts Following Impact

5.5.2.2 Scupper Blocks

For this test, left and right were understood from the perspective of the bogie facing the post. The bogie was facing west, to the right was the north, and to the left was the south. Figure 193 shows the scupper blocks before the test was conducted. Figure 194 shows the cross-section of the scupper blocks after the component test. Figure 195 shows the top of the higher scupper block (left) and the top of the lower scupper block (right). Figure 196 shows the bottom of the higher scupper block (left) and the bottom of the lower scupper block (right). Figure 197 shows a before- and after-test image of the post configuration from a similar angle.

Figure 193. Scupper Ends Prior to Impact on Left End and Right End

Figure 194. Scupper Ends After Impact on Left End and Right End

Figure 195. Top of Upper Scupper (left) and Top of Lower Scupper (right)

Figure 196. Bottom of Upper Scupper (left) and Bottom of Lower Scupper (right)

Figure 197. Post Before Test (left) and Post After Test (right)

5.5.3 Force vs. Displacement and Energy vs. Displacement Responses

The accelerometers from the bogie provided load vs. displacement and energy vs. displacement curves consistent with MwRSF procedures for analysis. The timing of wood splitting that was identified from high-speed video footage (sequential shots show each camera angle in Figures 188 and 189) was plotted to the load versus displacement curve as a series of lines in Figure 198. The scupper split occurred when the force dropped in SLICE-2, while SLICE-1 continued to increase before reaching its maximum value. There appears to be some level of "noise" between 0.025 and 0.055, where the maximum and minimum accelerations are opposed or mismatched; the two accelerometers aligned in high and low readings after this region.

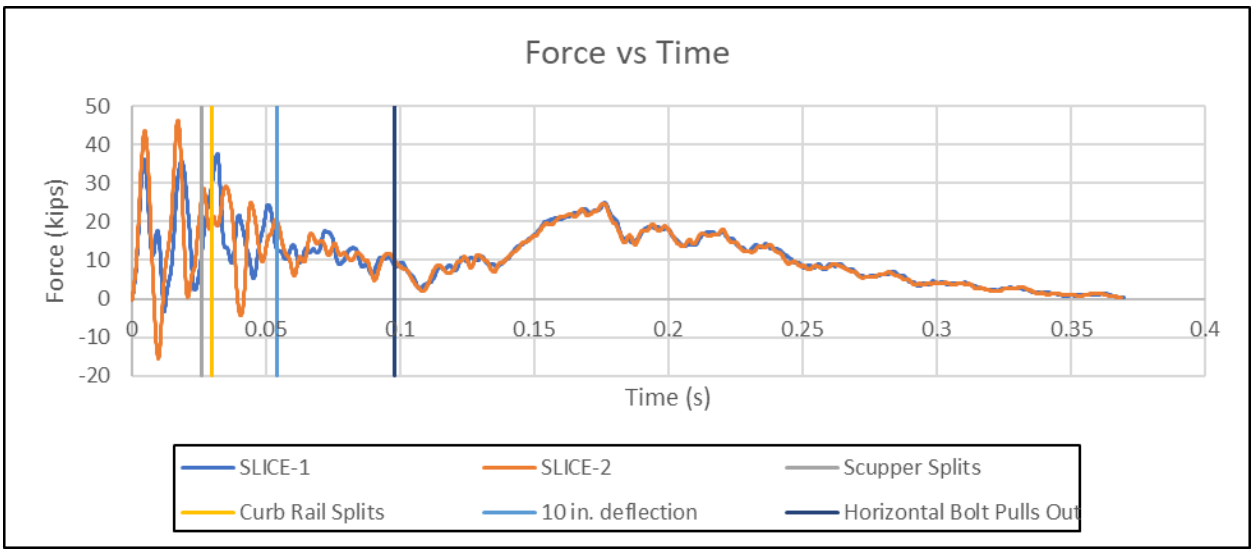

Figure 198. Test No. TRTD-1 Force vs. Time

The force versus displacement curve from the accelerometers is plotted in Figure 199. The average force through 5 in. of deflection was 16.1 kips, and the average force through 10 in. of deflection was 17.025 kips. The peak force for SLICE-1, 37.7 kips, occurred at 6.26 in. of deflection. The peak force for SLICE-2, 46.4 kips, occurs at 3.48 in. of deflection.

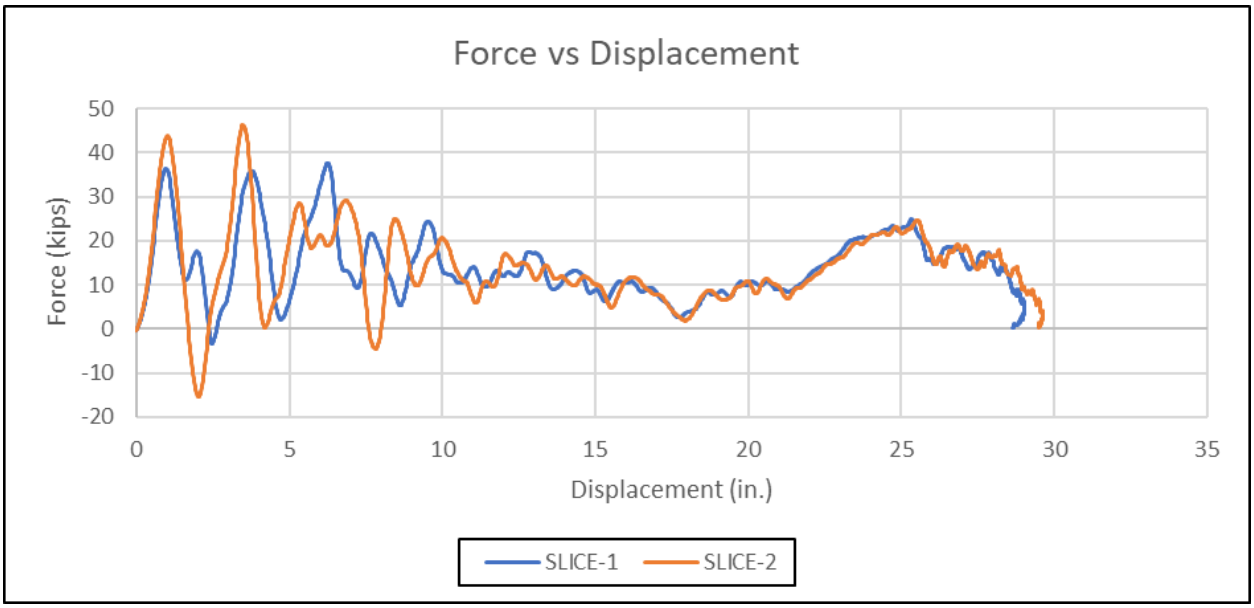

Figure 199. Test No. TRTD-1 Force vs. Displacement

The energy versus deflection behavior of the post is shown in Figure 200. The energy versus deflection curve did not display any region of oscillating peaks and valleys between the accelerometers. At 10 in. of deflection, the absorbed energy was about 172.6 k-in. and 167.9 k-in. for SLICE-1 and -2, respectively.

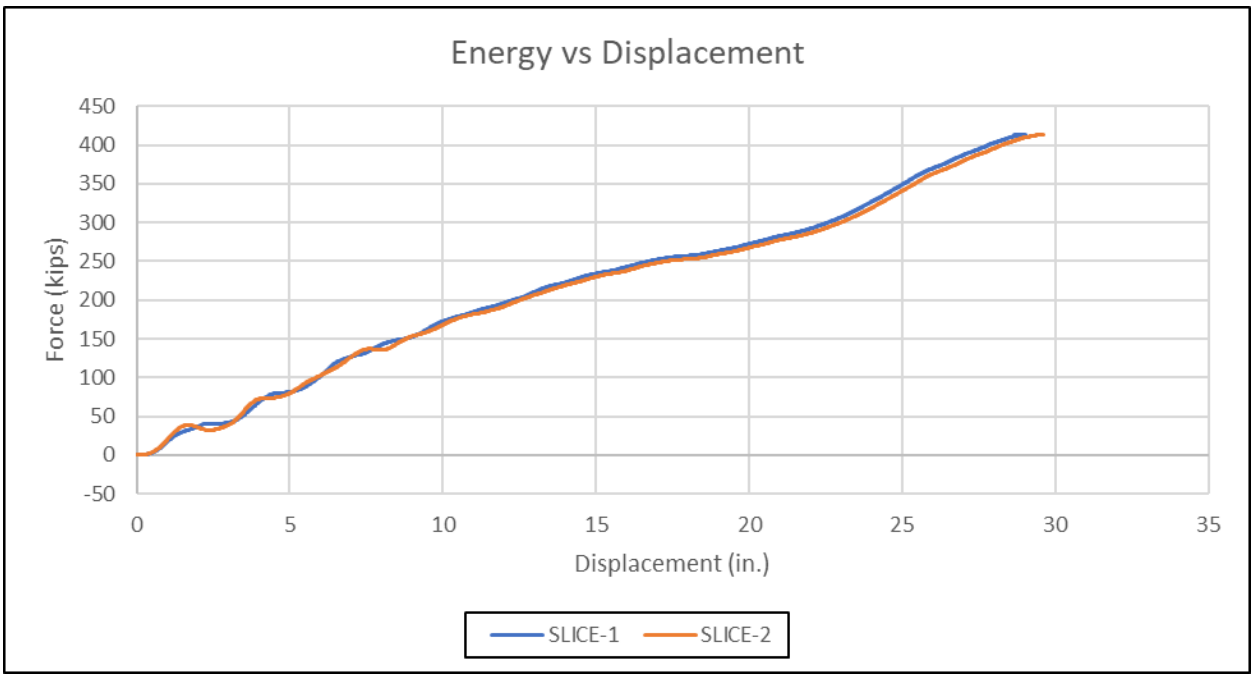

Figure 200. Test No. TRTD-1 Energy vs. Displacement

5.5.4 Bolt Axial Strain Gauges

The TML bolt axial strain gauges provided strain results at 10,000 Hz, which was filtered through functions available in LS-PrePost, a program available for LS-DYNA finite element analysis. CFC-60, the same filter used to filter the accelerometer data, also obtained at 10,000 Hz, was used to filter the raw strain gauge data. The time of impact was estimated by examining when the first curve begins to diverge from steady readings. The deck surface strain gauges and string potentiometers were also checked for the beginning of impact, because all these instruments were recorded on the same DAQ and shared the same clock. The axial strain gauge for bolt d2 first indicated impact, at 8.8778 seconds from when the DAQ started recording data. The filtered results of bolt axial strain gauge data over time are shown in Figure 201.

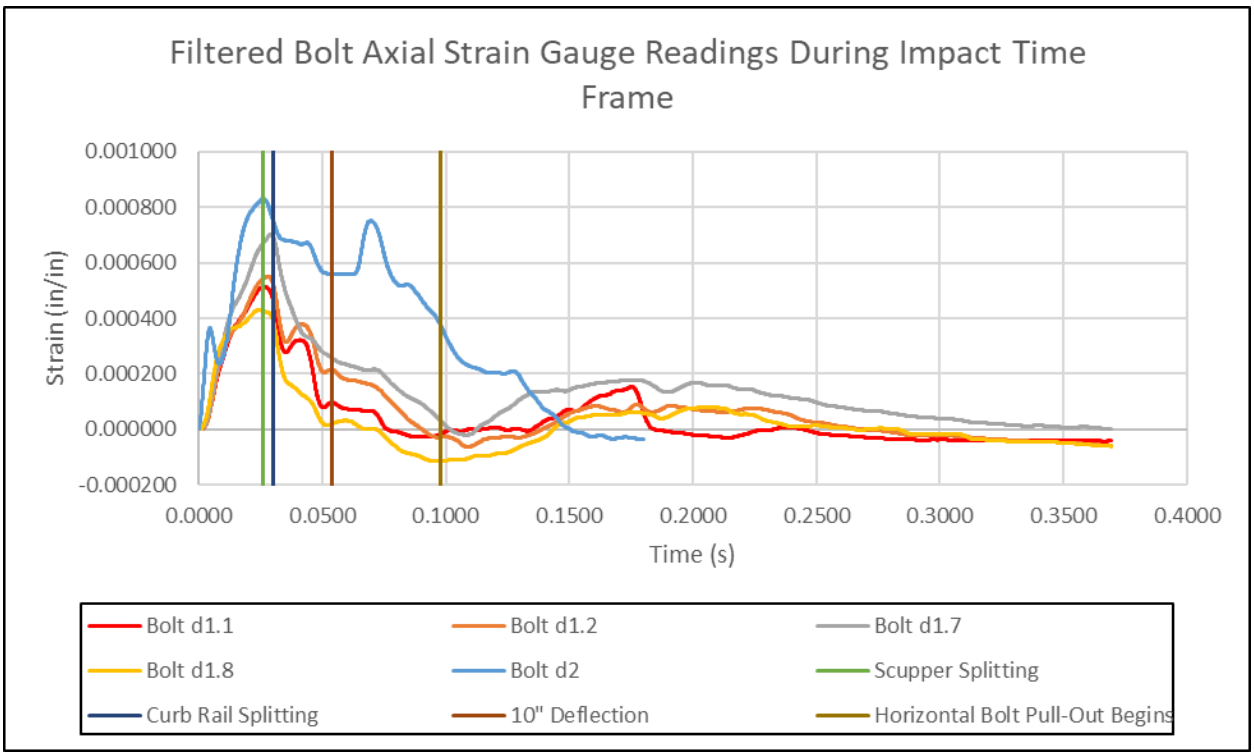

Figure 201. Test No. TRTD-1 Bolt Axial Strain Gauge Strain vs. Time

Bolt d1.3 is not shown, although data was collected for it, because the data displayed extreme non-linear drift before and after the impact event. Only the two exterior bolts on both sides of the post provided data for analysis. Bolt d2 was cut off at 0.1802 seconds as the wire was cut during the test. The time stamps for scupper and curb rail splitting, 10-in. of deflection, and the horizontal bolt pull-out are included with this graph as reference points for the bolt force at specific events. Strain was measured in the horizontal bolt while the vertical bolt strain was near zero, and the horizontal bolt strain spiked a second time after the curb rail had split.

If the strain readings were below the yield strain, then the bolt forces were estimated by assuming linear-elastic behavior. The yield strain for the vertical ASTM A307A bolts was estimated to be 0.00166 based on young's modulus for steel of 29,000 ksi and a yield stress of 48.1 ksi. The yield strain for the horizontal ASTM A449 bolt was 0.00295 from a yield (proof) stress of 85.5 ksi (based on received specifications). Neither the vertical bolt maximum strain values, 0.00043 to 0.000702, nor the horizontal bolt maximum strain value, 0.000831, exceeded their respective yield strains. Hence, the maximum forces in the bolts could be estimated, 8.94 kips to 12.23 kips for the vertical bolts and 35.77 kips for the horizontal bolt.

5.5.5 Deck Surface Strain Gauges

Two glulam timber deck panels were instrumented with 32 strain gauges, 12 of these gauges failed at various stages of data collection. Figure 202 shows the strain gauge locations for gauges which survived. Gaps between numbered gauges represent failed gauge locations. Gauges failed for various reasons: the lead wires broke; the shunt calibration failed (the circuit couldn't connect); or post-test data was unreasonable.

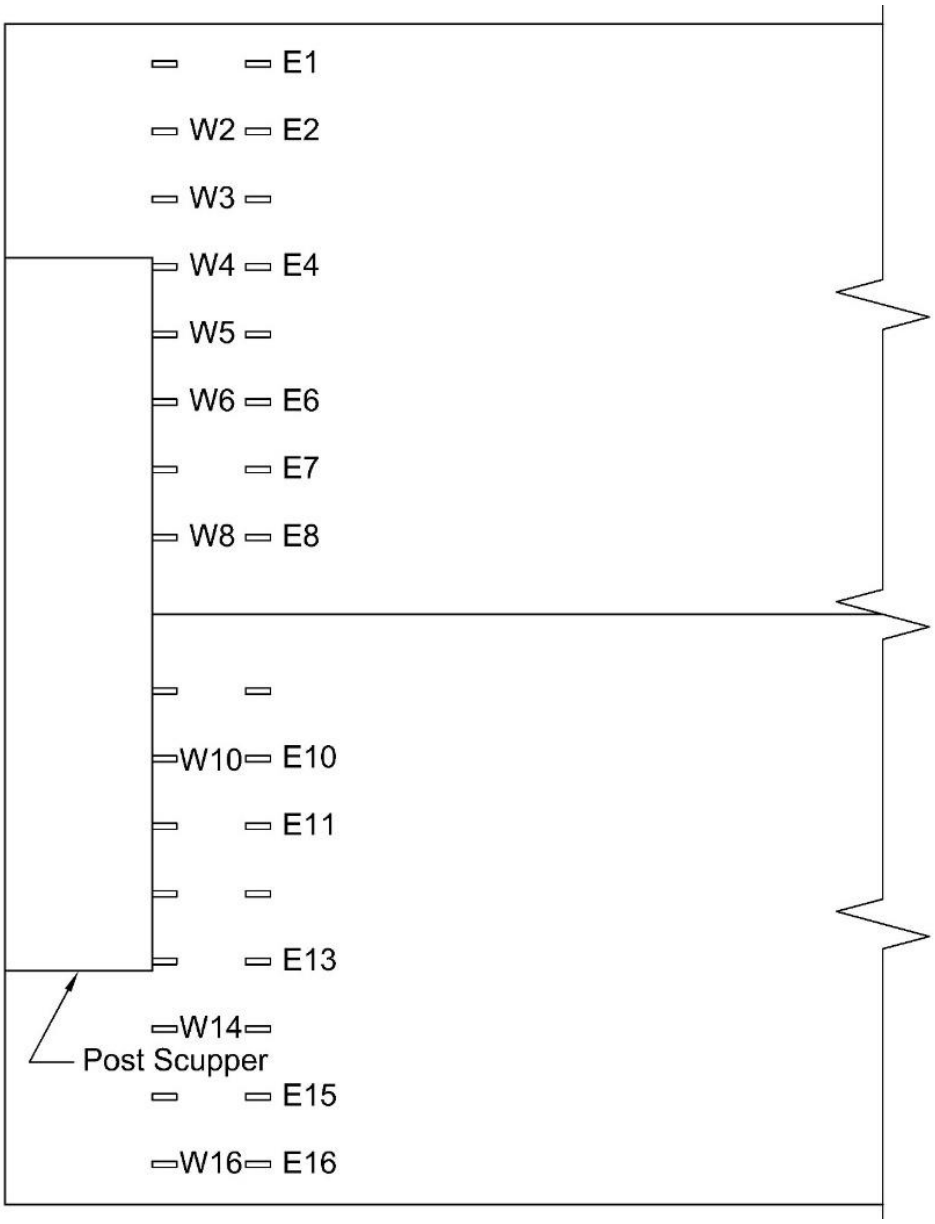

Figure 202. Deck Surface Strain Gauge Locations

The deck surface gauges were installed to observe strain/stress distribution at the timber deck surface during impact along or close to critical flexural locations. Critical flexural locations were identified before the test as the bolt line and the outer edge of the girder. The strain vs. time readings for all gauges is shown in Figure 203. The dashed lines represent the gauges closest to the edge of the exterior girder underneath the bridge deck, while the solid lines represent gauges which were before the scupper. Preliminary trials conducted before the full-scale component test revealed inconsistencies in strain measurements under laboratory conditions. As a result, the recorded strain data should be interpreted with caution. The peak stress observed in the gauges occurred immediately before the onset of scupper splitting. However, the cause of the significantly higher strain values recorded by gauges E7 and E10, relative to the others, remains unclear.

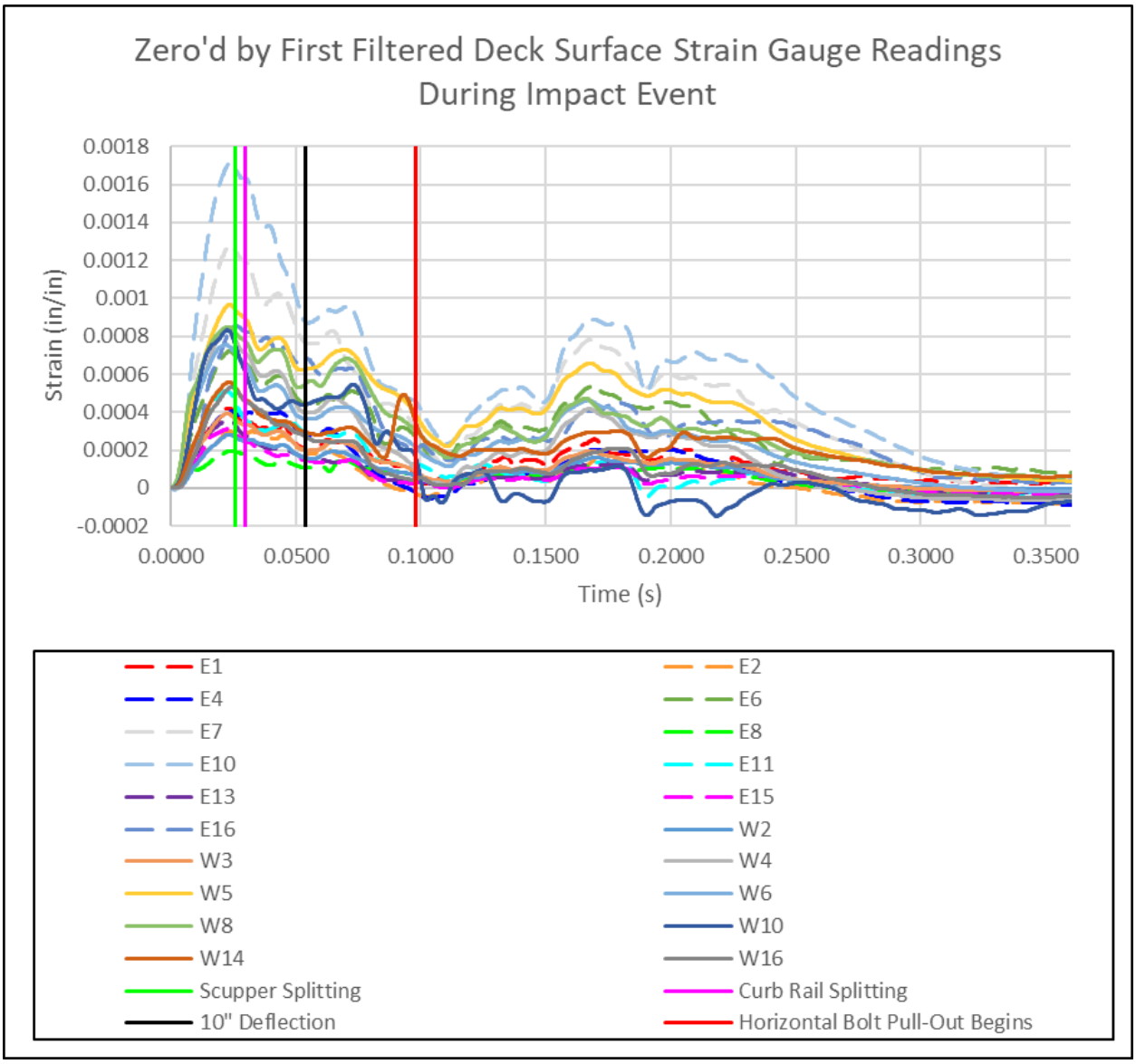

Figure 203. Strain vs. Time Curve for Deck Surface Strain Gauges

The strain gauge readings were plotted as bar graphs at 0.026 seconds, 0.030 seconds, and 0.054 seconds in Figures 204, 205, and 206, respectively. By plotting the strain gauge measurements as bar graphs at specific points in time, the change in strain magnitude at gauge locations could be viewed over time. Each strain gauge location was represented by two bars to show the difference in the deck strain before scupper and at the outer edge of the girder. Locations where the strain gauge did not survive were included as "empty" bars to show where data was lost. Gauges located near the girder edge consistently recorded higher peak strain values compared to those positioned directly behind the scupper block. However, these girder-edge gauges also exhibited greater variability, whereas the gauges behind the scupper showed more uniform strain responses.

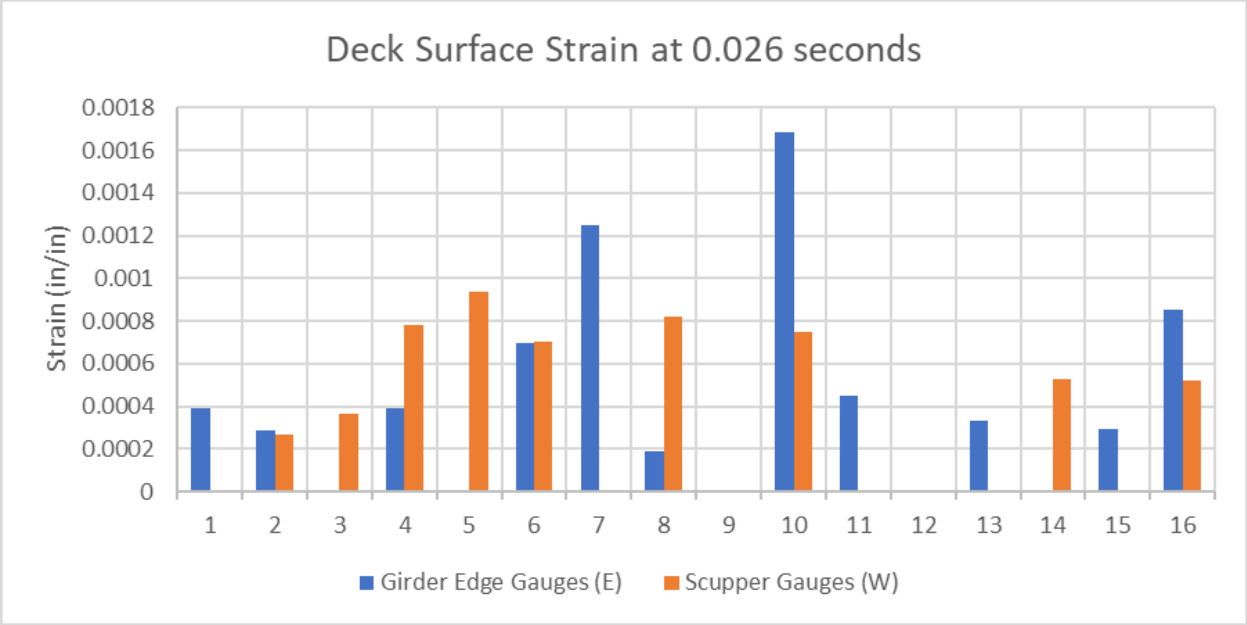

Figure 204. Deck Strain Gauges Across Both Deck Panels at 0.026 Seconds After Impact

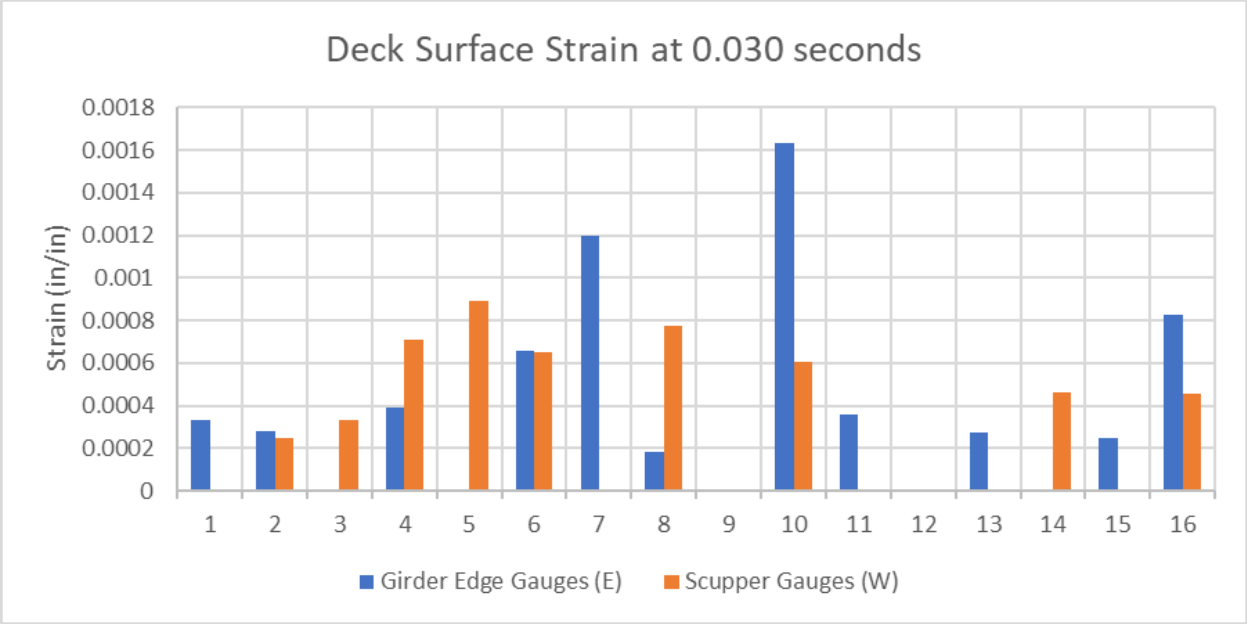

Figure 205. Deck Strain Gauges Across Both Deck Panels at 0.030 Seconds After Impact

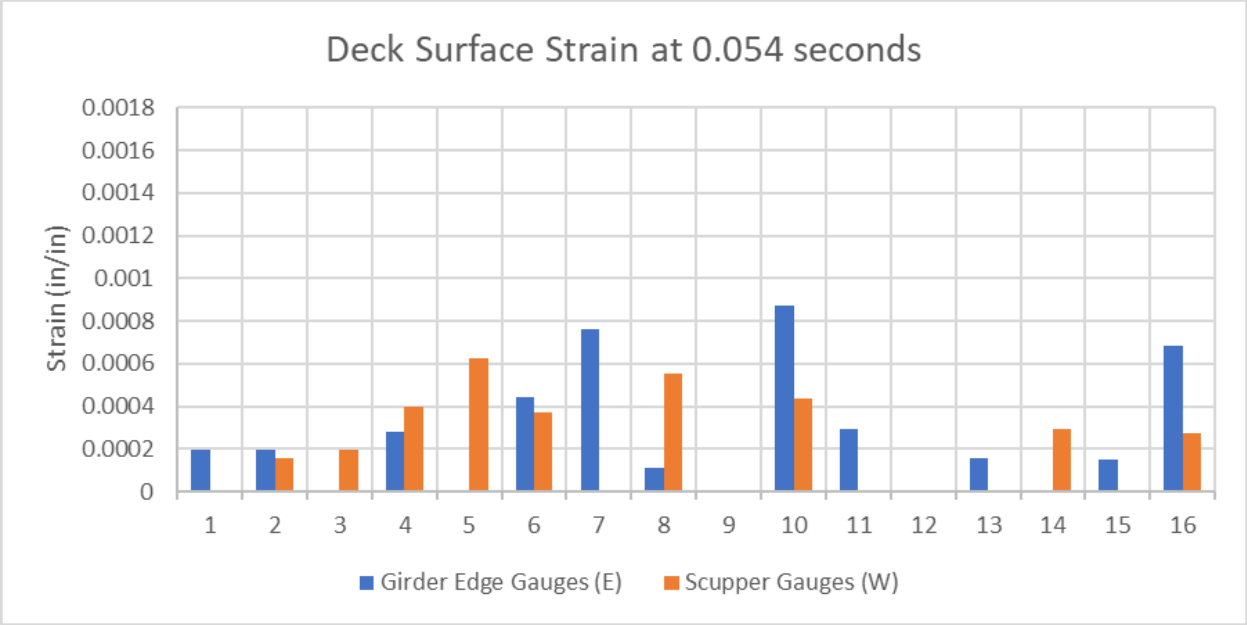

Figure 206. Deck Strain Gauges Across Both Deck Panels at 0.054 Seconds After Impact

5.5.6 String Potentiometers

One string potentiometer was used to measure the lateral deflection of the upper rail, while five others recorded the vertical deflection along the outer edge of the bridge deck. The estimated impact time used for the bolt and deck surface strain gauges also applied to all string potentiometer measurements because all values were passed through the same data acquisition system with the same frequency. The lateral string potentiometer data were compared with the displacements obtained by integrating the bogie-mounted accelerometer data, as shown in Figure 207, since both sensors measured the same quantity. This comparison revealed an offset between the two measurements, indicating that the string potentiometer recorded deflection with a delay. A detailed review of the high-speed video footage showed that the string became slack during the impact, which likely caused the delayed response in the string potentiometer reading.

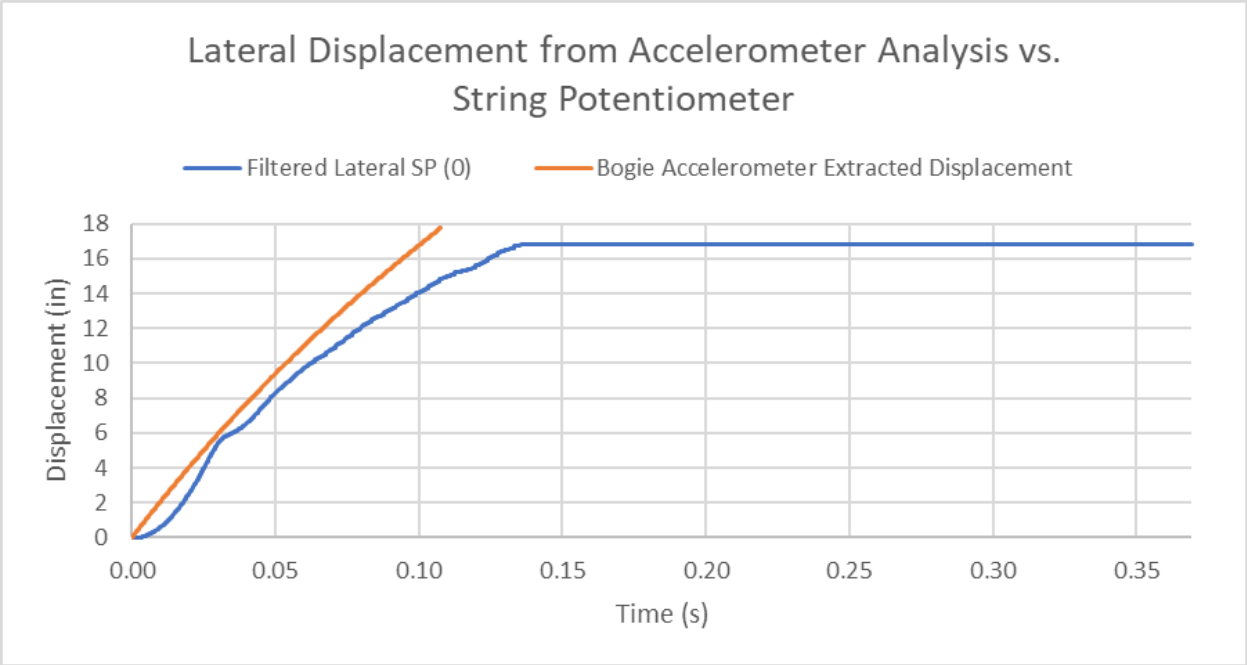

Figure 207. Test No. TRTD-1 Bogie Accelerometer vs. String Potentiometer Lateral Post Deflections

The maximum vertical deformation was measured at the outer edge of both deck panels beneath the center of the post. A strain vs. time graph of each vertical string potentiometer is shown in Figure 208. The vertical displacement readings for the deck were delayed relative to deck strain readings. This was consistent with the delay in the lateral deflections with respect to the bogie accelerometer. In contrast to the delayed deflection readings, the vertical displacements decreased toward zero faster than the deck strain readings by comparing the timing of the horizontal bolt pull-out from Figure 203.

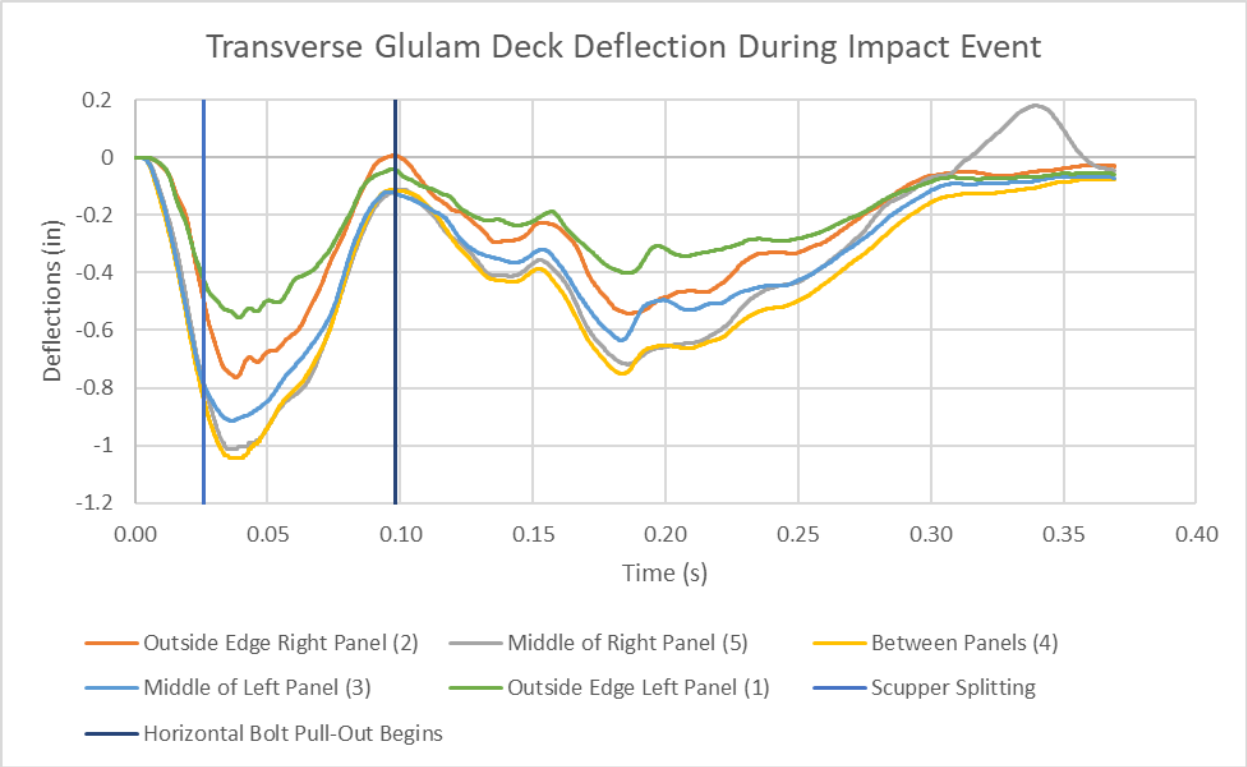

Figure 208. Test No. TRTD-1 Strain vs. Time Graph for Deck Deflections from String Potentiometers

Some cracks were observed at the edge of the deck panels near the edge of the scupper, shown in Figures 209 and 210. Although these cracks appear to be minor, they are noted because they may reflect flexure in the deck panel orthogonal to the direction of grain.

Figure 209. South Deck Panel Laminations Before (left) and After (right) Test

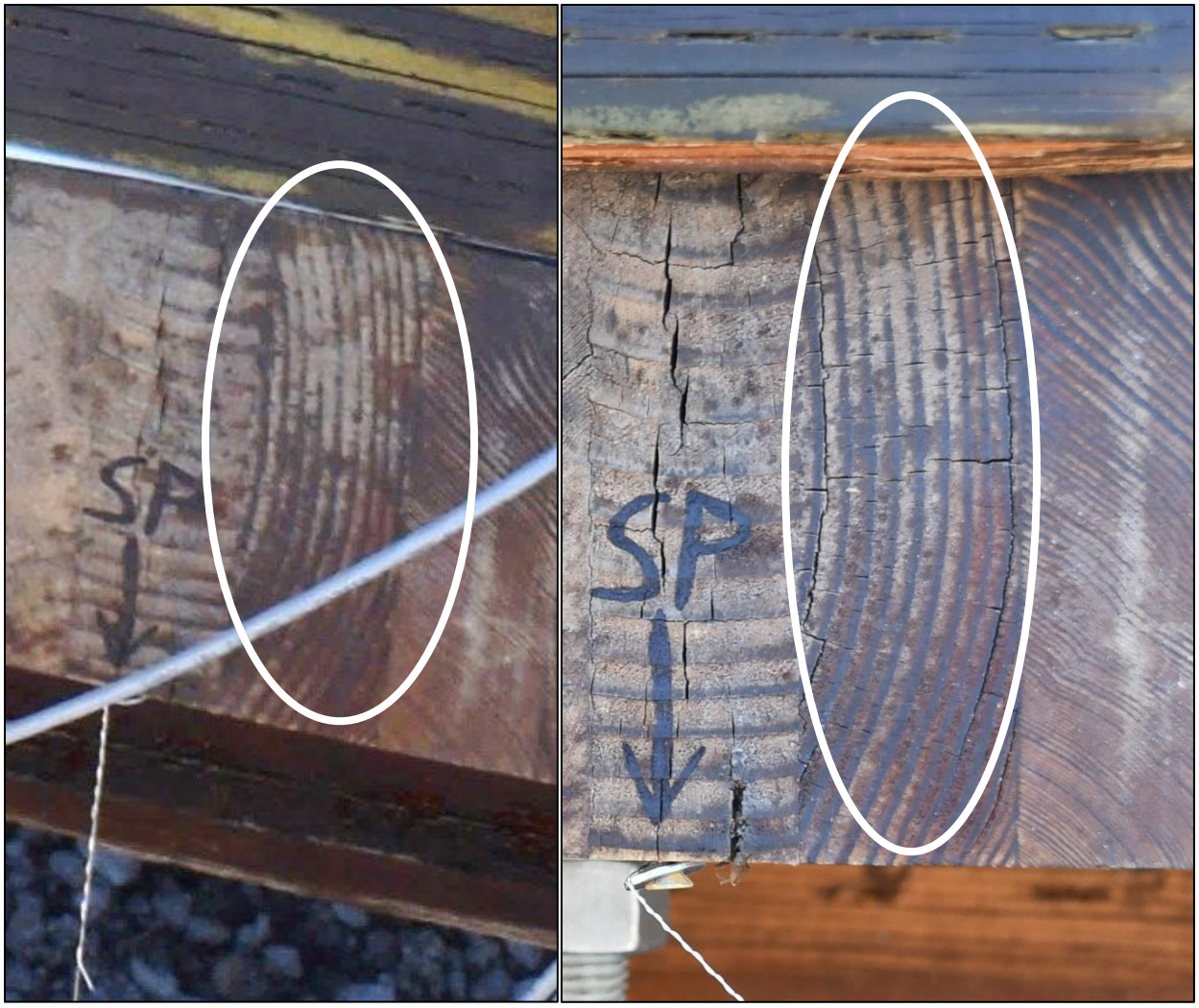

Figure 210. End Laminations of Left Deck Panel Before (left) and After (right) Component Testing

5.5.7 Deck and Post Compression

The pressure film underneath the scupper after impact is shown in Figure 211. The pressure film between the vertical timber post and the bridge railing assembly is shown in Figure 212 (it fell off after the test). The area in compression at the bottom of the scupper was estimated to be the full scupper length (58 in.) by 1.25 in.

Figure 211. Pressure Film Underneath Bottom Scupper after Test No. TRTD-1

Figure 212. Pressure Film Between Post and Scupper/Deck after Test No. TRTD-1

5.6 Discussion of Results

5.6.1 Post Load-Deflection Response

The post assembly was originally designed to resist an average load of 40 kips over 10 in. of deflection. However, accelerometer data estimated the average force to be only 17.03 kips over the same deflection range, which is less than half of the target design load. The average force was calculated by dividing the total energy by the corresponding displacement, whereas the energy was obtained by integrating the force vs. displacement curve. The bogie accelerometer's force vs. deflection response, along with the target design load, is presented in Figure 213.

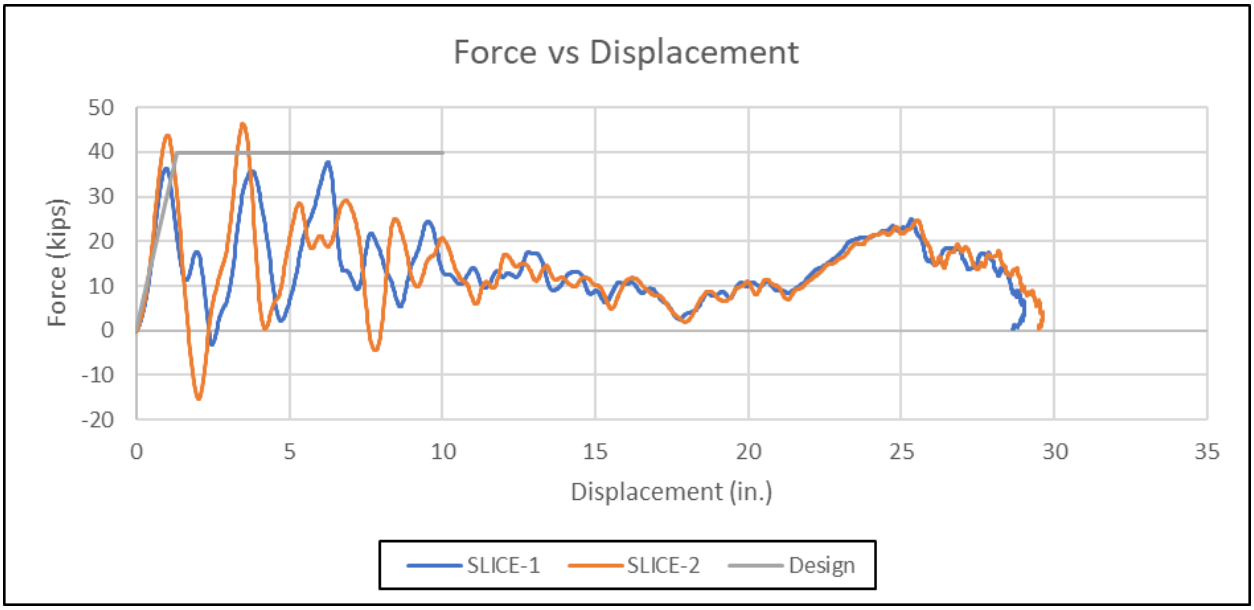

Figure 213. Force vs. Displacement with Design Load, Test No. TRTD-1

The maximum force in the horizontal bolt was ~35 kips. This load seemed to validate the load distribution discussed in section 3.3.2.1, because the bolt strain readings matched bolt load estimates using the observed bogie load at the top of the post. An average load of 17 kips at the top of the post would have produced a load of 38.6 kips in the horizontal bolt. The slight reduction in the measured load with respect to the estimated load was expected given the assumption of a moment arm of 14.625 in., when the centroid of compression in the post was known to extend lower and thereby reduce the load in the horizontal bolt.

The yield moment of the whole post configuration on the transverse deck was calculated using both the vertical bolts and the horizontal bolt. At 0.026 seconds, the total estimated load in the vertical bolts, 37.49 kips, was doubled to obtain the total vertical load which could be expected from all the bolts, 74.98 kips. Doubling the exterior bolts was necessary, because no bolt readings were available for the interior bolts. The vertical bolt load predicted a compressive width, 1.29 in., very similar to the estimated 1.25 in. observed from the pressure film – indicating that the approximated total vertical bolt load was close to the actual load. The distance from the bolt centerline to the deck edge is 8 in., and the compression region is about 1.25 in. wide from the deck edge, so the total distance between tension and compression is 7.375 in. The vertical bolt

flexural resistance is about 553 kip-in. The horizontal bolt at the same time has a load of 35.76 kips, and is 14.625 in. from the top of the deck; giving a flexural resistance of 523 kip-in.

Contrary to what would be expected, the vertical bolt yield moment was higher than the horizontal bolt yield moment. The difference was noted but was not considered a cause for alarm, because there were many uncertainties in estimating the moment arm. The scupper blocks, curb rail, vertical post, and transverse bridge deck are all in motion before the first cracks start in the scupper block, and so the moment arm location and magnitude change with the post geometry. A difference of 1 in. in the moment arm would increase the horizontal yield moment over the vertical bolt yield moment.

5.6.2 Cause of System Failure

One priority of the research effort following the impact test was to mitigate the failure and lower-than-expected lateral resistance prior to the next test. As such, a failure analysis was necessary before conducting additional tests. The observed cracks seemed to reduce the lateral resistance provided by the system. Figure 214 shows the cracks in the scupper which appear to start first. The cracks in the scupper appeared to be either tensile from high compression or shear. The shear strength of wood parallel to grain was much higher than the tensile strength perpendicular to grain, so cracks were likely to be tensile [60]. Since this would also be resisted by the bolts, only tensile stresses seemed to be positioned to generate these cracks in their position. The tensile strength of wood perpendicular to grain is not tabulated by NDS, because this property is very weak. NDS requires this orientation of wood to always be reinforced if loaded. As a result, some additional study had to be conducted on the tensile strength perpendicular to grain.

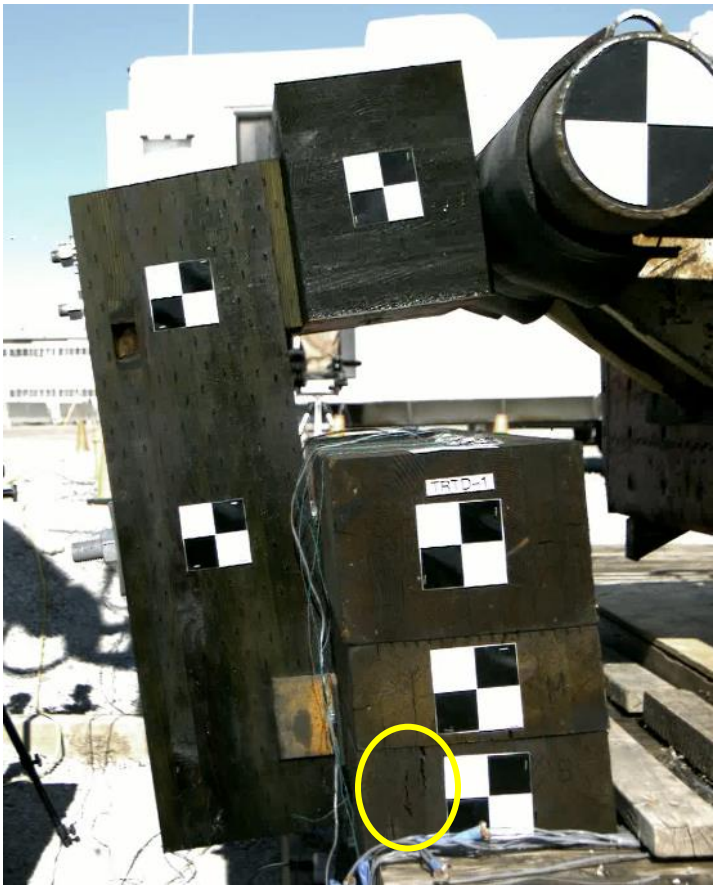

Figure 214. Test No. TRTD-1 Tensile Cracks in Scupper at 0.0260 Seconds after Impact

First, the loading demand which caused the tensile stress was not directly applied, as compression and shear forces acted on the scupper at the crack location. For tensile splitting, the compressive and shear stress tractions produced tensile stress. Mohr's circle was used to approximate a combined stress state from applied shear and compressive stresses.

The analysis was based on the wood scupper blocks having the same general properties in the radial and tangential directions. Although typically applied to isotropic materials, a 2D Mohr's Circle was approximated for the plane anisotropic material, where the wood strengths are the same in the radial and tangential orientations. This analysis also assumed that there was no cracking in the timber sections prior to loading, and that the material behavior was linear-elastic up to the point of cracking. Wood is a complex material, which reflects a composite rather than a continuum.

Finally, the compressive and shear stresses were uniformly distributed through the longitudinal orientation of the scupper blocks. Compressive and shear stresses, as shown in Figure 215, were used for Mohr's circle to determine the principal stresses.

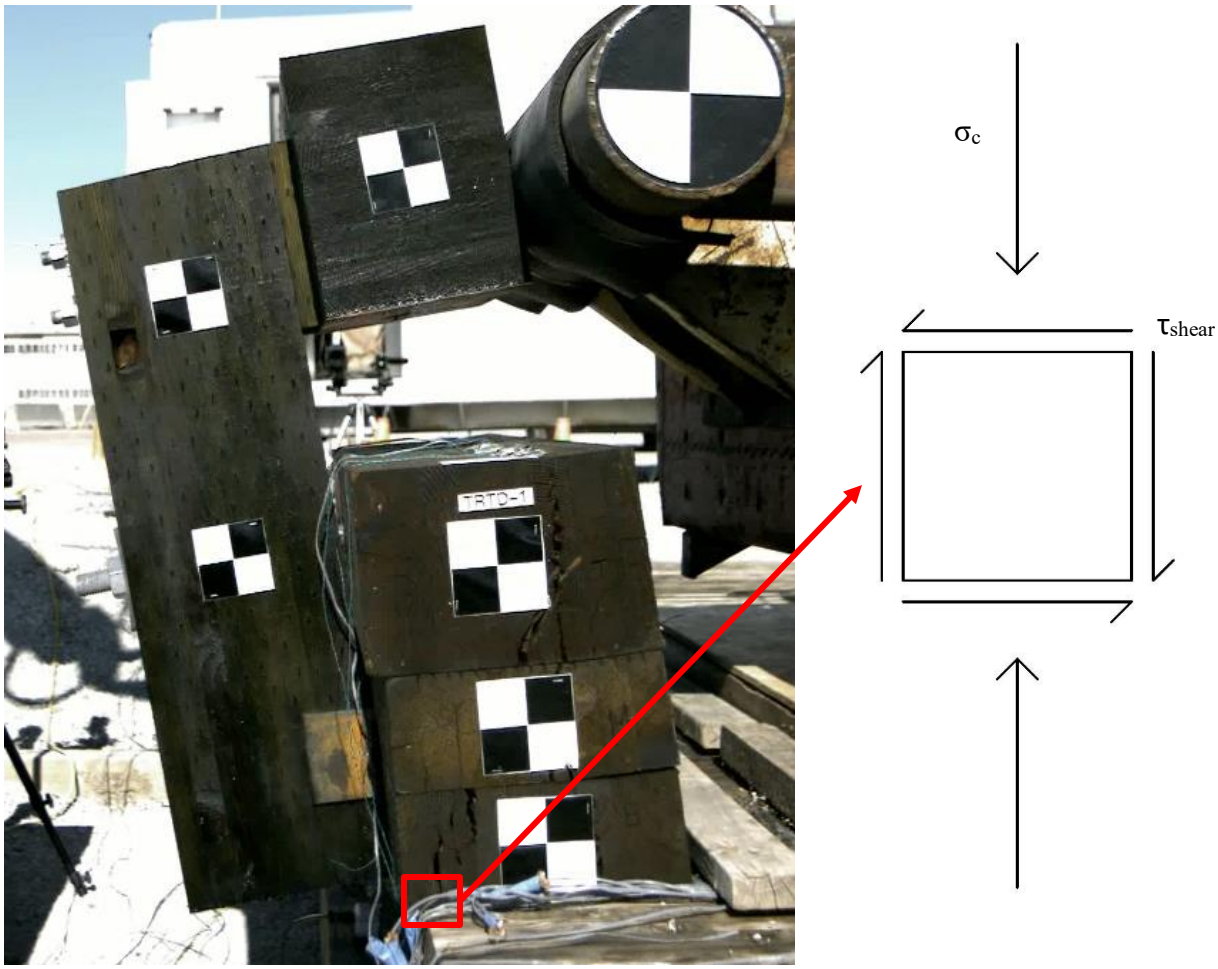

Figure 215. Stress Block of External Stresses to Evaluate Principal Stresses

The compression was assumed to be equal to the tension in the vertical bolts because tension (T) and compression (C) both develop as a moment couple to resist rotation. The compression was divided over the area observed in the pressure film to obtain compressive stress. From strain gauge data available for instrumented horizontal and vertical bolts, the tension was about 77 kips when the scupper blocks began to split. The compressive area (A_c) was based on 58 in. length and a 1¼ in. width.

The shear stress was assumed to be friction from the horizontal bolt but developed in the compression region and limited to the friction coefficient (μ) which ranged between 0.3 to 0.5 for wood-to-wood surfaces [60]. Both friction and the bolt shear capacity (V) resisted the lateral load imparted through the horizontal bolt. The frictional area was equal to the area in compression. Equations 35 through 41 defined the relationships between applied tractions to the scupper block and the elements of 2D Mohr's Circle. Equations 42 through 45 defined the principal stresses perpendicular to grain according to 2D Mohr's Circle.

$$C = T \qquad \text{Eq. (35)}$$

$$V = \mu C \qquad \text{Eq. (36)}$$

$$A_c = A_s \quad \text{Eq. (37)}$$

$$\sigma_c = \frac{C}{A_c} \quad \text{Eq. (38)}$$

$$\tau_s = \frac{V}{A_s} \quad \text{Eq. (39)}$$

$$\sigma_y = -\sigma_c \quad \text{Eq. (40)}$$

$$\sigma_x = 0 \quad \text{Eq. (41)}$$

$$R = \sqrt{\left(\frac{\sigma_x - \sigma_y}{2}\right)^2 + {\tau_s}^2} \quad \text{Eq. (42)}$$

$$\sigma_{avg} = \frac{\sigma_x + \sigma_y}{2} \quad \text{Eq. (43)}$$

$$\sigma_{p(tensile)} = \sigma_{avg} - R \quad \text{Eq. (44)}$$

$$\sigma_{p(compression)} = \sigma_{avg} + R \quad \text{Eq. (45)}$$

The variation in the friction coefficient gave a principal tensile stress between 88 and 220 psi. The principal compression stress was between 1,150 and 1,282 psi. Stress diagrams for these two scenarios are shown in Figures 216 and 217. The principal stress directions aligned with a compressive strut that would be expected to form. In addition, the principal compressive stress was close to the design estimate of 1,176 psi.

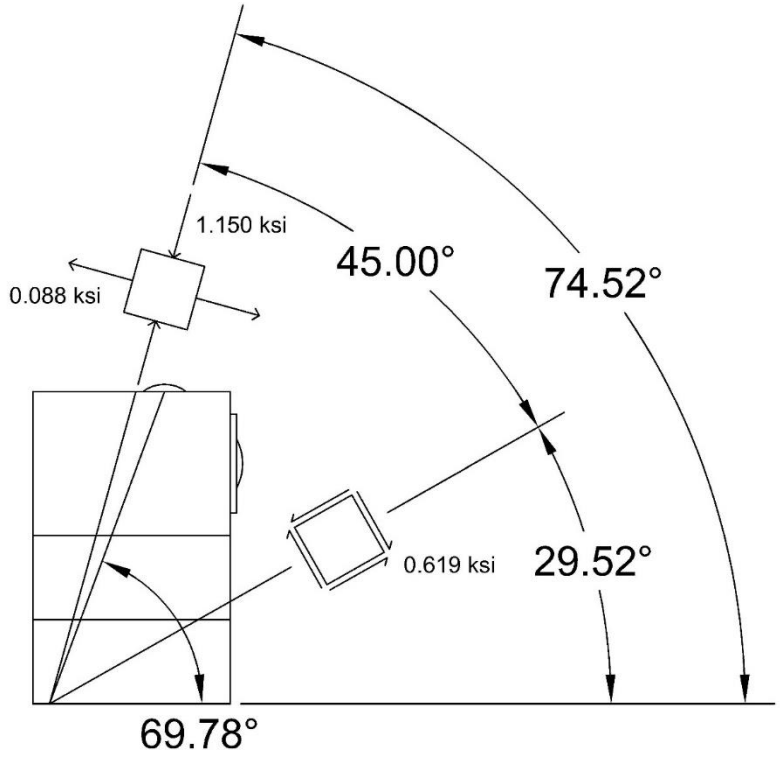

Figure 216. Mohr's Circle of Stresses in Scupper at Compression Block Assuming Low Friction Coefficient

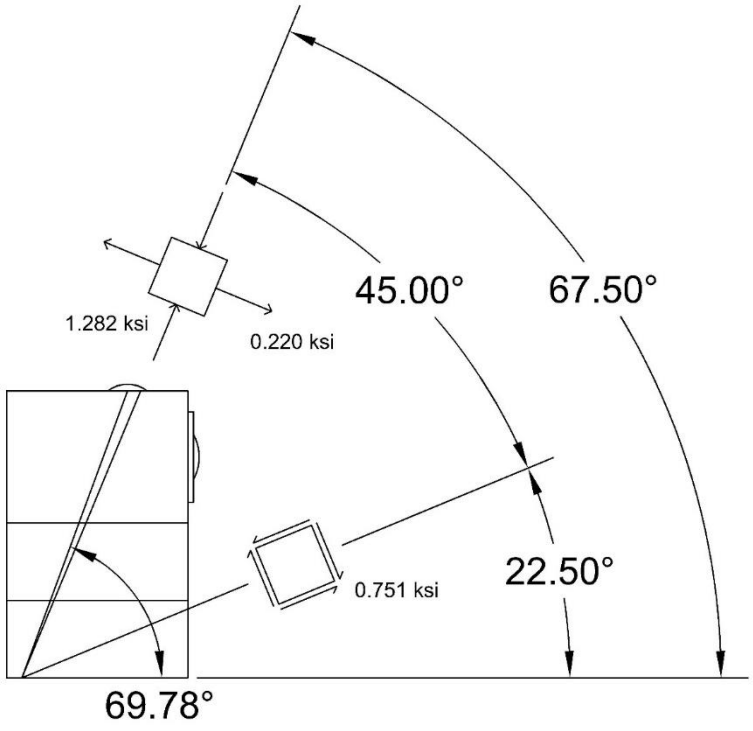

Figure 217. Mohr's Circle of Stresses in Scupper at Compression Block Assuming High Friction Coefficient

An additional literature review was performed to determine whether the calculated principal tensile stress perpendicular to grain could have developed cracking. Timber strength perpendicular to grain is not tabulated for design. However, the procedures in ASTM D143 carefully outline how this strength property should be tested with 2-in. x 2-in. x 2½-in. specimens [90]. ASTM D2555 allows estimates of the tensile strength perpendicular to grain by taking a third of the shear strength [128]. The corresponding specimen size for this method utilizes cross-sectional dimensions of 1-in. x 2-in. block at midsection, corresponding to ASTM D143 [90]. These sources was used to estimate a strength of 340 psi for Douglas Fir, given the specimen size.

Size effects commonly reduce timber strength, and the given strength value was given for a significantly smaller specimen than as-tested the scupper block. J.D. Barrett examined the influence of the size effect of Douglas Fir on the tensile strength perpendicular to grain by collecting test data on the perpendicular to grain strength calculated from many different specimens [152]. The largest specimen that was tested, a 10¾-in. x 10¾-in. x 34-in. block, was also fabricated glulam, and the average tension strength perpendicular to grain was found to be 100 psi. In addition to the other sizes discussed in the study, the calculated tensile perpendicular to grain stress between 88 and 220 psi appeared to be a reasonable estimate of the tension rupture perpendicular to grain failure stress in the scupper block.

Putting together all the available data, the system was only able to achieve a maximum resistance at the top of the post of about 17 kips over 10 in. of deflection because the scupper block began to split. The splitting reduced the magnitude of the scupper compression and vertical bolt tension which resisted the applied flexure put into the curb rail, scupper block, and bridge deck panel connection from the horizontal bolt. The scupper block splits reduce the flexural resistance, but the curb rail split fully removed the vertical post and upper railing from the system. The curb rail split around the same time because it is a component in the vertical bolt and scupper block and curb rail compression and developed the same tensile splitting force perpendicular to grain.

5.6.3 Design Modifications

Design modifications were investigated to mitigate tensile perpendicular to grain splitting of the curb rail and scupper blocks. For this purpose, the maximum compressive load would be used to estimate a maximum tensile splitting stress, along with the shear load. By designing against this stress, splitting could be prevented in the scupper blocks and curb rail. The maximum compressive load which could be placed on the scupper was 216 kips, which corresponded to a compressive stress of 1.87 ksi for a distribution width of 2 in. The tensile strength perpendicular to grain would range from 155 and 386 psi for 0.3 and 0.5 friction coefficients, respectively.

Potential techniques for reducing tensile splitting include (1) lengthening the scuppers, (2) placing lag screws across the crack region, (3) orienting the grain against tensile splits, (4) using a single scupper block instead of two blocks, and (5) placing bolts across the tensile split in the scupper blocks.

5.6.3.1 Lengthening Scupper

The first option can only accommodate a 10-in. increased scupper block length before interfering with the curb rail splice plate. It would reduce the compressive stress and shear stress by a ratio of 58 to 68 (the two different scupper block lengths). From this reduction, the principal

tensile stress range would decrease from 155 and 386 psi to 132 and 330 psi, a range still significantly higher than the stress which likely caused the scupper blocks to split, 88 to 220 psi. Lengthening the scupper would also increase the size effect reduction on the strength, so failures at lower strengths could be expected. This method of increasing strength, by itself, was deemed insufficient.

5.6.3.2 Lag Screws

The second option placed lag screws through the crack region. Lag screw sizes range from ¼ in. diameter to 1¼ in. diameter, each with their own capacity and corresponding number of needed screws. These options are shown in Table 55. The lag screw steel grade was ASTM A307A. Higher steel grades were possible but did not improve the connection strength because the connection strength is typically controlled by the threads and wood density. The capacities in lb per in. of thread were taken from NDS Table 12.2A. The lag bolt capacity was found from NDS Table 11.3.1, which defines the factors necessary for inclusion. Moisture and temperature factors were assumed to be 1.0. The end grain factor and the toenail factors were not applied, and the load duration factor was 2 (although these are lag screws, they were not used as a connection). The length of the threads on the bolts are 2/3 of the total length, 10 in. This estimate comes from Builders Stainless, an online distributor of stainless-steel fasteners – compared to threaded lengths estimates by Portland Bolt & Manufacturing Co. they are less conservative.

Table 55. Lag Screw Capacity and Number of Each Required

Lag Screw Diameter (in.)	½	⅝	¾	⅞	1	1⅛	1¼
Capacity (lb/in. threads)	378	447	513	576	636	695	752
Ultimate Capacity (kip)	10.08	11.92	13.68	15.36	16.96	18.53	20.05
No. Lag Screws	6 to 12	4 to 10	4 to 8	4 to 8	4 to 8	4 to 6	4 to 6

To obtain an estimate closer to an ultimate value instead of an allowable value, the allowable estimated were doubled. The allowable values were reduced by a factor of 5 from estimated average values [14]. Neither commentary in NDS, nor the original document [153], identified the time over which the specimens were loaded or whether safety factors or 5% estimates were included with the NDS estimates. In addition, the tested screw diameters used to develop the tabulated values were smaller than the lag screw diameters which would be used to strengthen the curb rail and scupper blocks. Rather than calculate the effect of these factors on the strength, a simpler adjustment from NDS allowable values to an ultimate value was utilized. The ultimate load was approximated from the allowable values by applying a factor of two, similar to how the shear plate and split ring allowable values were adjusted to an ultimate capacity [121].

The required number of lag screws was determined by calculating the number needed to exceed the estimated tensile load demand. The load demand was estimated from the tensile stress and the tensile area and adjusting the direction of tensile force to be parallel to the deck surface. From a tensile stress of 155 to 368 psi, a 58-in. long x 5⅛-in. tall scupper block and a principal angle of 15.48 to 22.50 degrees, the tensile load causing splitting ranged between 44 to 106 kips. The corresponding number of lag screws was a multiple of two so that the bolts could be evenly distributed across the scupper block.

5.6.3.3 Different Grain Orientation

By adjusting the orientation of the grain, it was thought that the scupper block may not need to engage the strength perpendicular to grain. If the splitting tensile load worked parallel to the grain, then there may be no cracks causing strength reduction and failure. Designing and building a different grain orientation in the scupper block would likely present higher costs for the manufacture of scupper blocks, while allowing not addressing potential new issues in the alternative orientation. Secondary issues from a weaker orientation in other directions could be resolved with additional steel hardware. This alternative design would not be possible for the curb railing.

5.6.3.4 Single Scupper Block

Another considered option to reduce cracking was doubling the tensile area, which could be completed with a single scupper. Glulam lamination widths are, 10¾ in. and 10½ in. for western and southern pine glulam varieties, respectively, which are conveniently close to the width of combining two scuppers, 10¼ in. However, a single scupper block may encounter issues with a greater reduction to the tensile strength from the size effect.

5.6.3.5 Bolts

Bolts placed through the 12-in. wide scupper block would also restrain tensile splits perpendicular to grain. Like the lag screws, this method would use a timber bolt to prevent snagging on the bolt head on the traffic-side face of the scupper block. The estimated tensile demand would be identical to the demand calculated for the lag bolts, 44 to 106 kips. The bolt capacity was based on 45 ksi yield strength. The required number of bolts (varying for different friction coefficients) for multiple bolt sizes was shown in Table 56.

Table 56. Bolt Capacity and Number of Fasteners Required per Scupper

Bolt Diameter (in.)	½-in.	⅝-in.	¾-in.	⅞-in.	1-in.
Bolt Capacity (kips)	8.84	13.81	19.88	27.06	35.34
No. of Bolts	6 to 14	4 to 8	4 to 6	2 to 4	2 to 4

5.6.3.6 Selected Modification

Bolts were selected to provide increased strength to the scupper blocks and curb rail to mitigate against tensile splitting for the next dynamic component test no. TRTD-2. A longer scupper block could have been provided but was deemed unnecessary. Lag screws were considered

inferior as the bolts prevent cracking across the whole scupper block width. The lag screw has concerns regarding effective length or loss of strength resulting from splitting at the wrong location. Bolts were also significantly easier and less costly than redesigning the scupper block grain orientation. The placement of bolts also did not risk having further loss of strength from an exacerbated size effect of a single scupper block, which could not have restrained curb rail splitting.

Four ⅝-in. diameter ASTM A307A steel bolts were selected for the scupper blocks, while two ⅝-in. diameter ASTM A307A steel bolts for selected for the curb railing. Although the number of bolts was on the lower end for that size, there were a couple opportunities to later modify the post system for the planned tests on a longitudinal deck if the bolts were insufficient to restrain cracking. It was economical to investigate whether the lower limit was sufficient to prevent cracking. In addition, the timber deck panels were treated with oil-based preservatives, so the developed friction was expected to be lower than the upper limit of a 0.5 coefficient. If the bolt strength estimates for ASTM A307A steel bolts were above 45 ksi, the bolts could also withstand higher load. Therefore, this design modification was deemed to be reasonable.

In addition to the horizontal bolts placed through the timber members, another design modification included $^{3}/_{16}$-in. thick x 20-in. long x 4-in. wide ASTM A36 steel plates installed underneath each row of four vertical bolts. During the test, splitting in the curb rail seemed to be exacerbated by the concentrated stress of the vertical bolt heads. Steel plates would better distribute the compressive load out from the bolt heads so that the curb rail is less likely to crack at that location. To assist with load transfer from the horizontal bolt to the vertical bolts, the ASTM A36 steel washer plate on the front curb rail was also expanded from 6 in. x 6 in. to 21 in. x 8 in. The two additional horizontal bolts in the curb rail would go through the expanded steel plate near the ends, preventing the ends from flaring up and presenting a snag risk in the crash testing program. The ends of the steel plate extended beyond the innermost vertical bolts to better transfer the post loading to the lower curb rail, scupper blocks, and deck. All proposed modifications for the next dynamic component bogie test are shown in Figure 218.

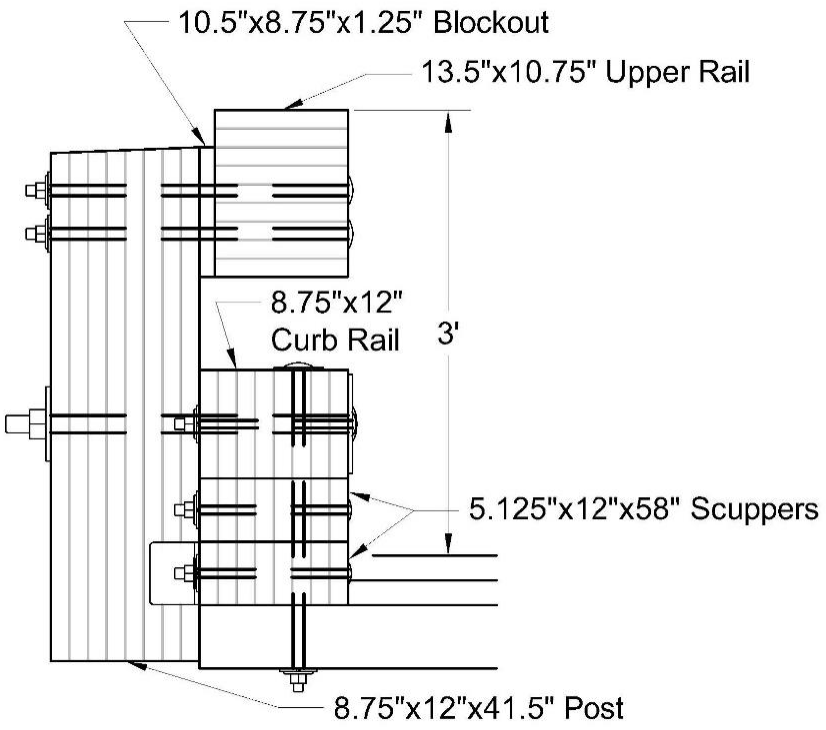

End View

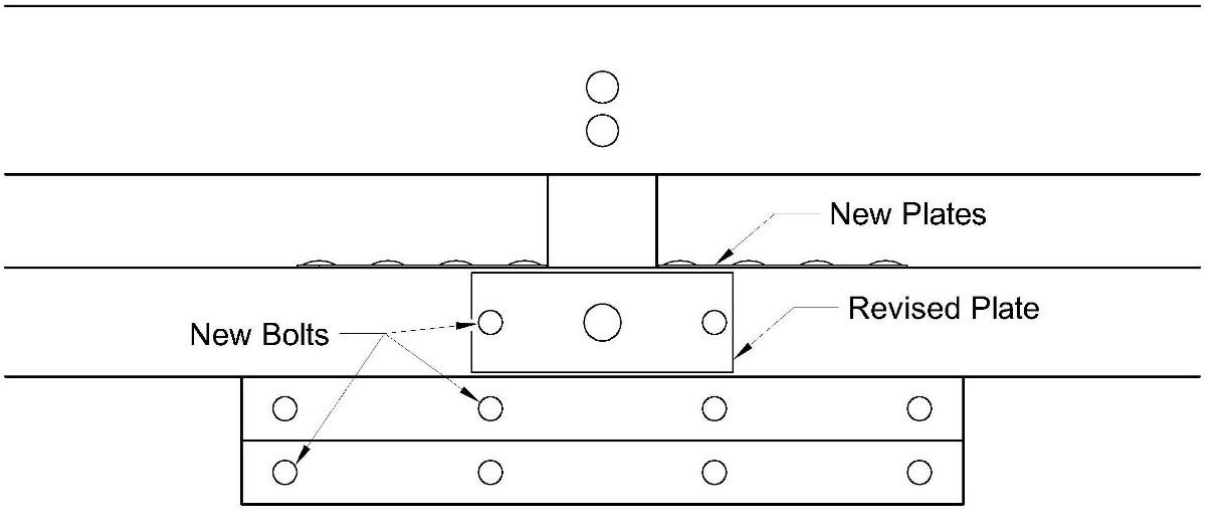

Front View

Figure 218. System Modifications for Test No. TRTD-2

6 SUMMARY, RECOMMENDATIONS, AND FUTURE RESEARCH

6.1 Summary

This project completed the initial development of a MASH 2016 TL-4 Glulam Timber Bridge Railing, which could utilize all glulam components, accommodate an initial 2-in. concrete overlay and a future 2-in. wearing surface, and perform acceptably under high moisture conditions. The development effort included a literature review of timber bridge railings, timber bridge decks, and timber bridge railing moisture mitigation.

The BARRIER VII computer simulation effort, previously conducted in Phase IIa of this project, was revisited to address prior calculations with revisions and consider moisture mitigation for select design components. Following these revisions, the bridge railing connections were sized to resist updated demands, which were estimated from the BARRIER VII simulations and updated MASH 2016 design loads for AASHTO Chapter 13 Design Case 1 and Design Case 2. The connections that were used in the Glulam Rail with Curb on Transverse Glulam Deck system were compared to the demand and, if insufficient, strengthened. The bolts connecting the upper rail to the vertical post increased from ¾ in. to ⅞ in. diameter, the horizontal bolt in the middle of the post increase from 1¼ in. to 1⅜ in. diameter with an updated steel grade from A307A to A449, the vertical bolts were increased in size and number from six ¾-in. diameter bolts to eight ⅞-in. diameter bolts. The vertical post size was also increased from 10½ in. x 8¾ in. to 12 in. x 8¾ in.

The research team also identified two critical deck configurations for dynamic component testing. The dynamic component testing would inform researchers of the critical bridge deck configuration, so that a full-scale crash test could be conducted on the most critical design. Two deck types, a longitudinal glulam deck and transverse glulam deck, were targeted for investigation in dynamic component testing. The critical transverse deck utilized glulam panels measuring 5⅛ in. thick. The critical longitudinal deck utilized glulam panels measuring 10¾ in. thick, with four 1-in. diameter ASTM A193 grade B7 steel threaded rods transversely placed through the outer deck panel.

The project initiated the development of a MASH 2016 TL-3 AGT for the bridge railing, which was required as no crashworthy transition currently existed. The new AGT was designed to accommodate a future 2-in. wearing surface and an upstream stiffness transition. A literature review was conducted on MASH AGT systems which were developed after the Glulam Rail with Curb on Transverse Glulam Deck system. The 1997 system had been modeled in BARRIER VII to predict the railing performance prior to crash testing. This BARRIER VII model was calibrated to more closely match the crash tests from test nos. TRBR-3 and TRBR-4 by adjusting component parameters. The calibrated design gave guidance on how post and beam parameters can more accurately simulate railing performance in response to vehicle impact.

After the calibration effort was completed, the connection design between the timber bridge railing and the AGT occurred. Several AGT options were brainstormed and developed, and two were selected for simulation in BARRIER VII. Both systems had similar upstream transition sections, but different downstream stiffness transitions near the bridge railing. The “quarter-post spacing system” utilized 8-in. x 8-in. timber posts installed at 1-ft 6¾-in. centers near the bridge rail end; and the “half-post spacing system” utilized 8-in. x 10-in. posts at 3-ft 1½-in. centers near the bridge end. The final connection between the bridge railing and AGT used an 8-ft spacing

between the first bridge post and the first AGT post for the half-post system and a 7-ft allowable spacing between the first bridge post and first AGT post for the quarter-post system.

Three bogie tests were conducted on 8-in. x 8-in. timber posts embedded in soil to investigate whether multiple quarter-spaced posts reduced the soil resistance. Due to premature post rupture, post group effects on soil resistance could not be adequately studied with the limited testing program. However, the test results demonstrated the limits of the 8-in. x 8-in. timber posts for the quarter post system, and the 8-in. x 8-in. BARRIER VII model was revised to account for a stiffer post, which absorbed less energy. In addition, the post grade was increased from Grade 1 SYP to Grade 1D SYP. The two systems were modelled in BARRIER VII, and two critical impact point analyses were conducted with pickup truck and small car vehicle impacts. The half-post system demonstrated greater flexibility and reduced wheel snag risk, while the quarter-post system reduced deflections but demonstrated higher wheel snag risk. The quarter-post system was selected as the more critical design due to a higher probability of failure due to post rupture, thrie-beam end shoe damage, and wheel snag risk.

Four dynamic component tests were planned to evaluate the bridge post system, two on the critical transverse glulam deck configuration (TRTD) and two on the longitudinal glulam deck configuration (TRLD). Tests began with the transverse deck, because the bridge superstructure was available on-site. Test no. TRTD-1 and TRLD-1 used ⅞-in. diameter vertical bolts, and test no. TRTD-2 and TRLD-2 used ¾-in. diameter vertical bolts. Only one dynamic component bogie test, test no. TRTD-1, was conducted and evaluated for this report. The average load at the impact height was less than half of what was expected, and the curb rail and scupper blocks cracked and split. Similar to the accelerometer data, the connections did not reach their respective limits. The timber deck strain gauges did not show the predicted stress distribution. Because of uncertainty surrounding the deck gauges and the lack of clear signs of deck damage, the primary design issue was the bridge railing components. Analysis of stress distribution, assuming a uniform stress distribution through the scuppers, provided a rough estimate of excess tension stress perpendicular to grain. Various methods of strengthening the timber components were explored, and the design modification settled on adding transverse steel bolts. Four ASTM A307A steel bolts were proposed in each scupper and two bolts in the curb rail for the next dynamic component test. In addition, plates were placed underneath the vertical bolt heads, and a larger front plate was used on the curb rail to improve load distribution.

6.2 Future Component and Full-Scale Crash Test Plans

Additional dynamic component testing must still be completed for this project. Four dynamic component tests were planned but only one test, test no. TRTD-1, was completed and reported herein. Three additional tests, TRTD-2, TRLD-1, and TRLD-2, are planned and underway. The testing plans that were initially developed for the longitudinal deck did not include the modifications developed following test no. TRTD-1 because the modifications had not yet been proven. Plans for test no. TRTD-2 are shown in Figures 219 through 242, and plans for test no. TRLD-1 are shown in Figures 243 through 266. Plans for test no. TRLD-2 are not shown, because they are identical to test no. TRLD-1, with the exception of the vertical bolts being ¾ in. diameter instead of ⅞ in. diameter. TRLD-2 was later cancelled, and the reasons for this decision will be discussed in the subsequent report. Dynamic Component Test TRTD-3, shown in Appendix N, was developed in place of TRLD-2. Full-scale crash test plans for bridge railing and AGT system are shown in Appendix O. Most materials required for TRTD-3 have already been

acquired, and some materials for the full-scale bridge railing crash test have been purchased with funds from Crash-Tested Bridge Railings and Transitions for Wood Bridges Complementary to FS025 (Project No. 25-01024).

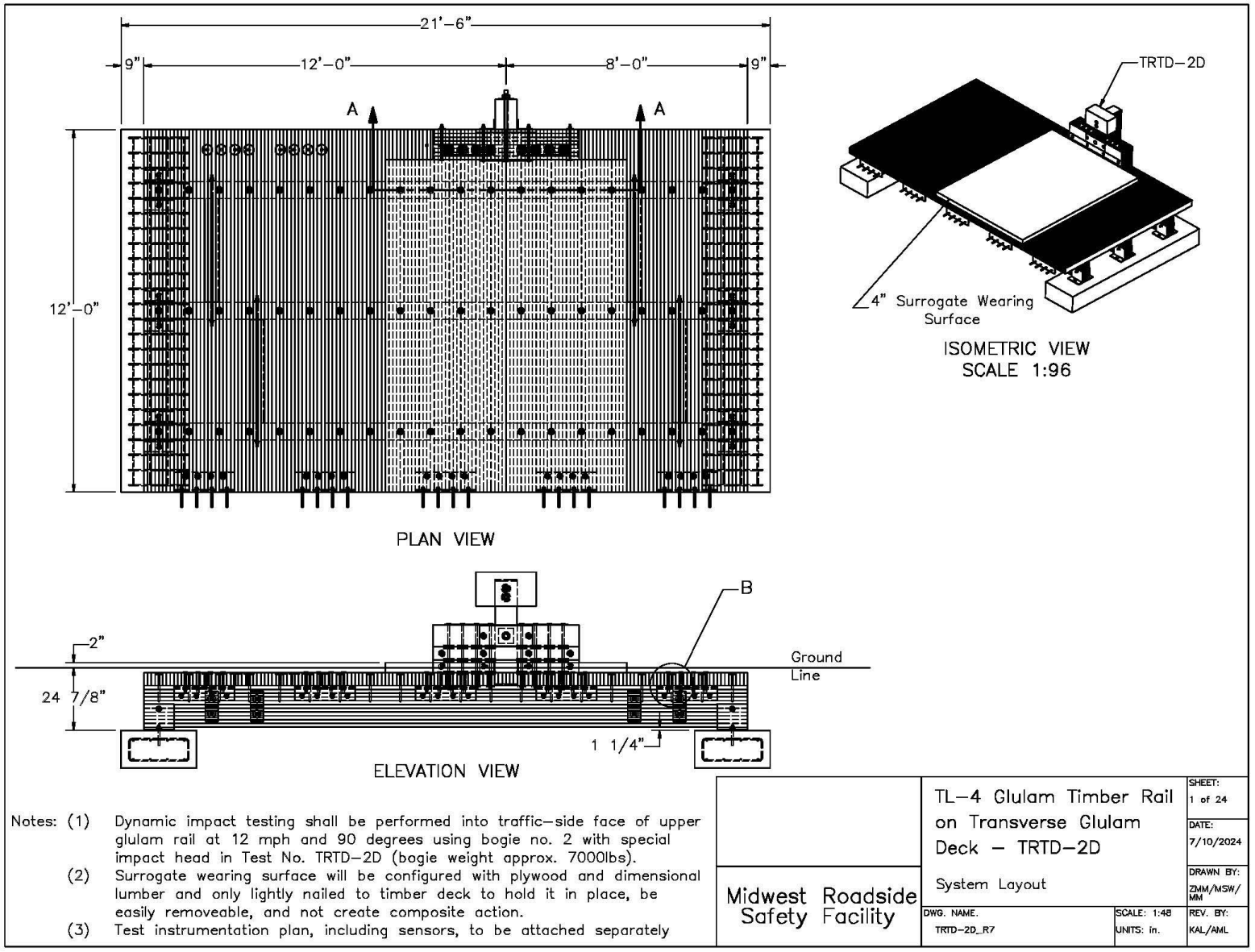

Figure 219. System Layout, Test No. TRTD-2

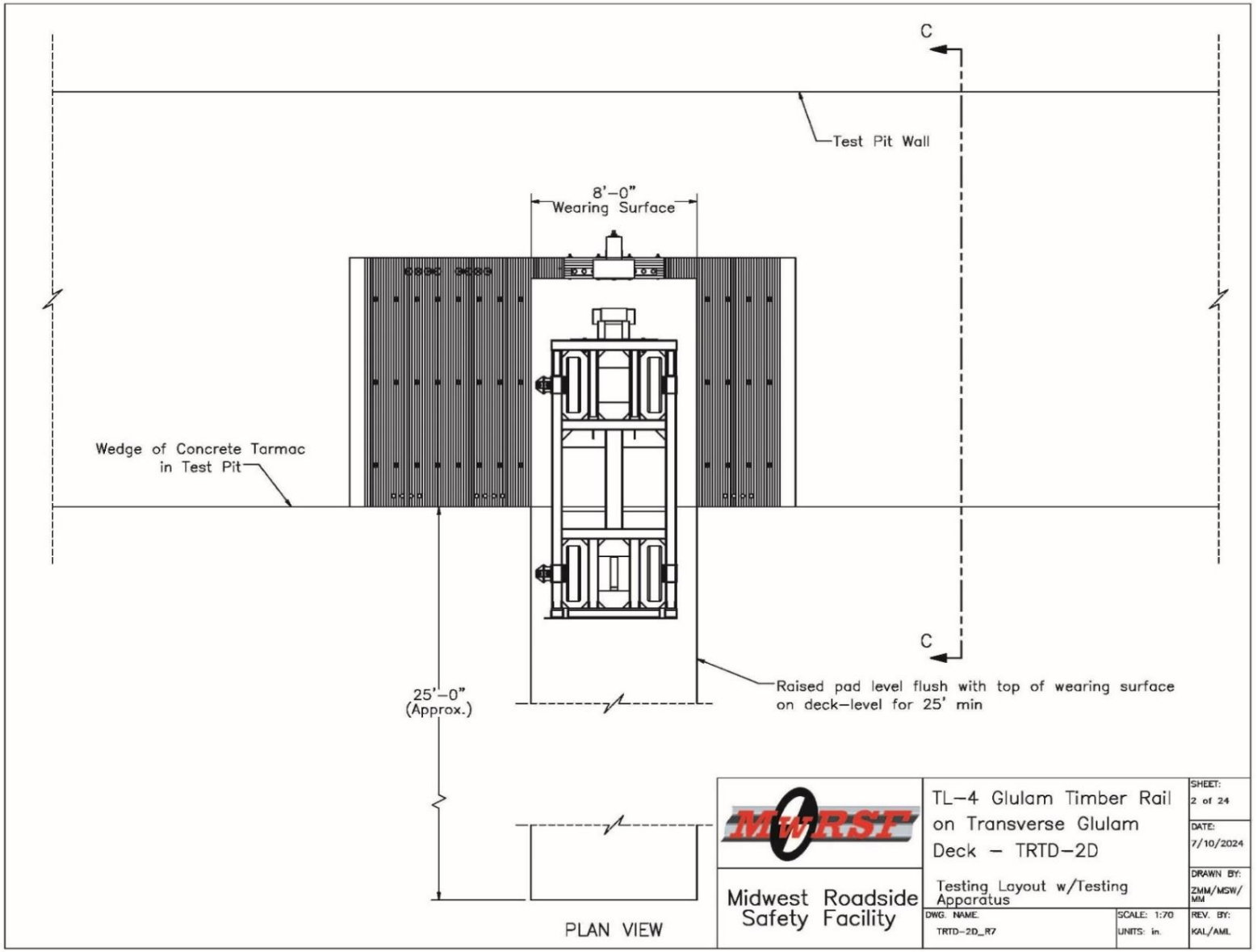

Figure 220. Test Layout with Bogie, Test No. TRTD-2

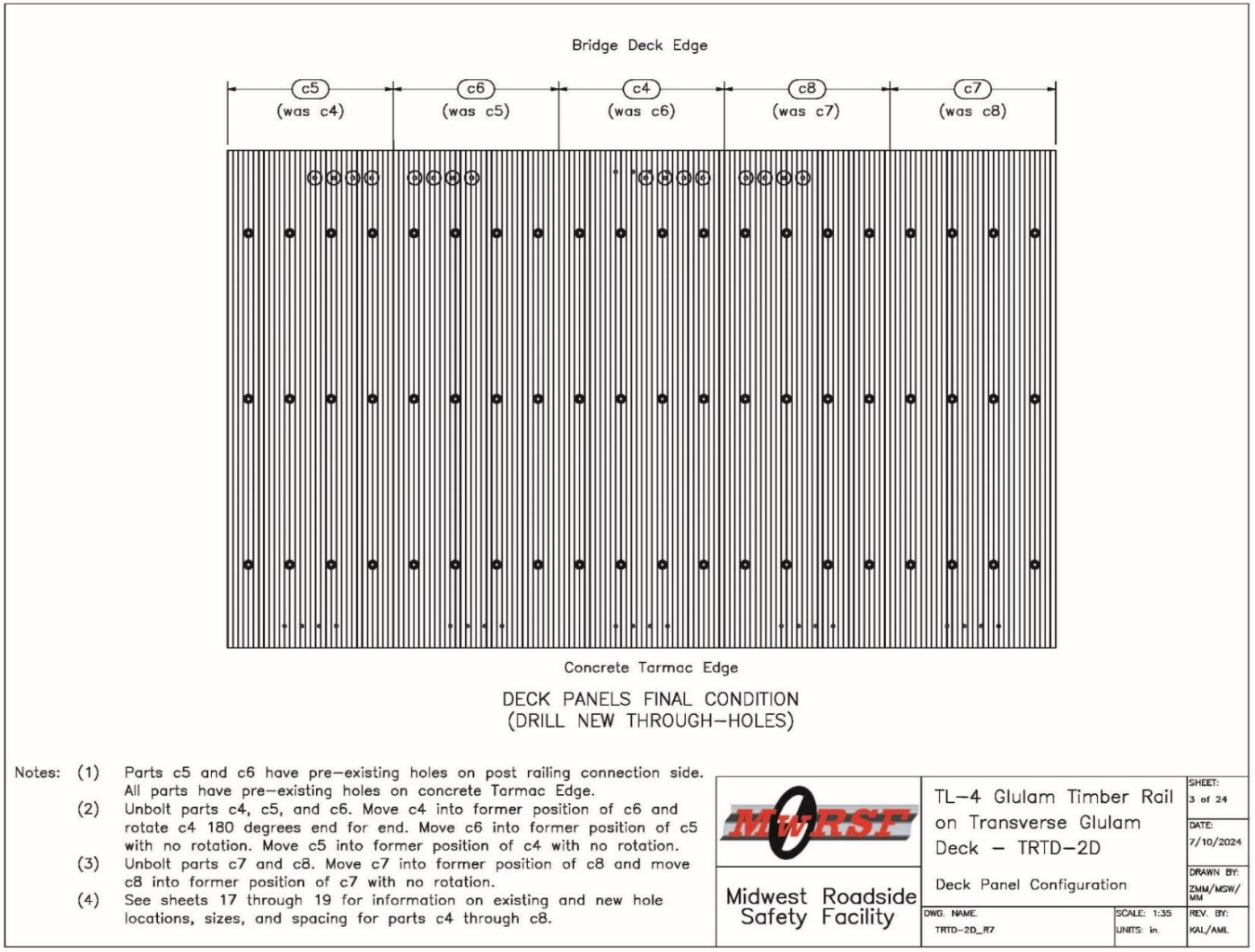

Figure 221. Deck Panel Configuration, Test No. TRTD-2

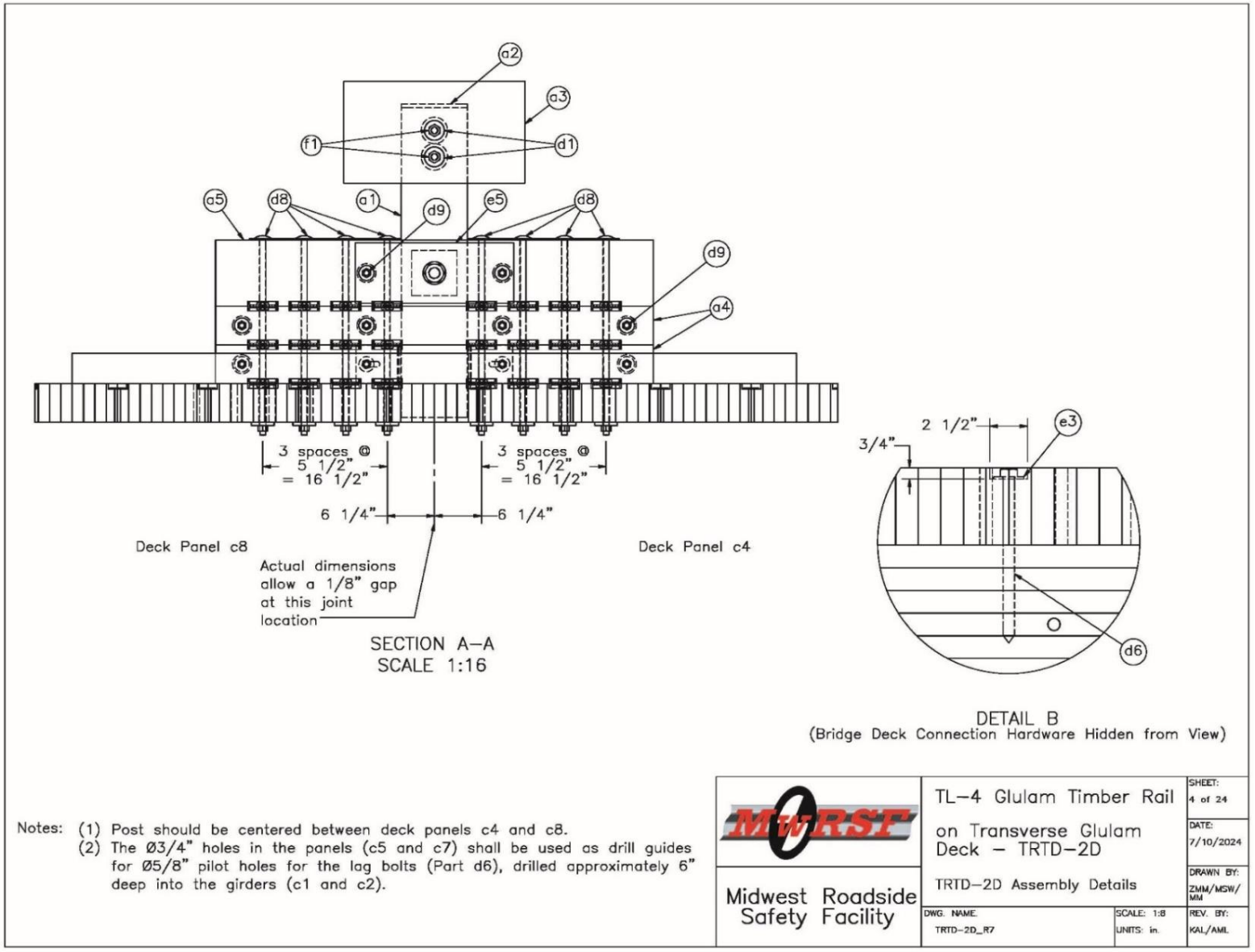

Figure 222. Post and Deck Assembly Details, Test No. TRTD-2

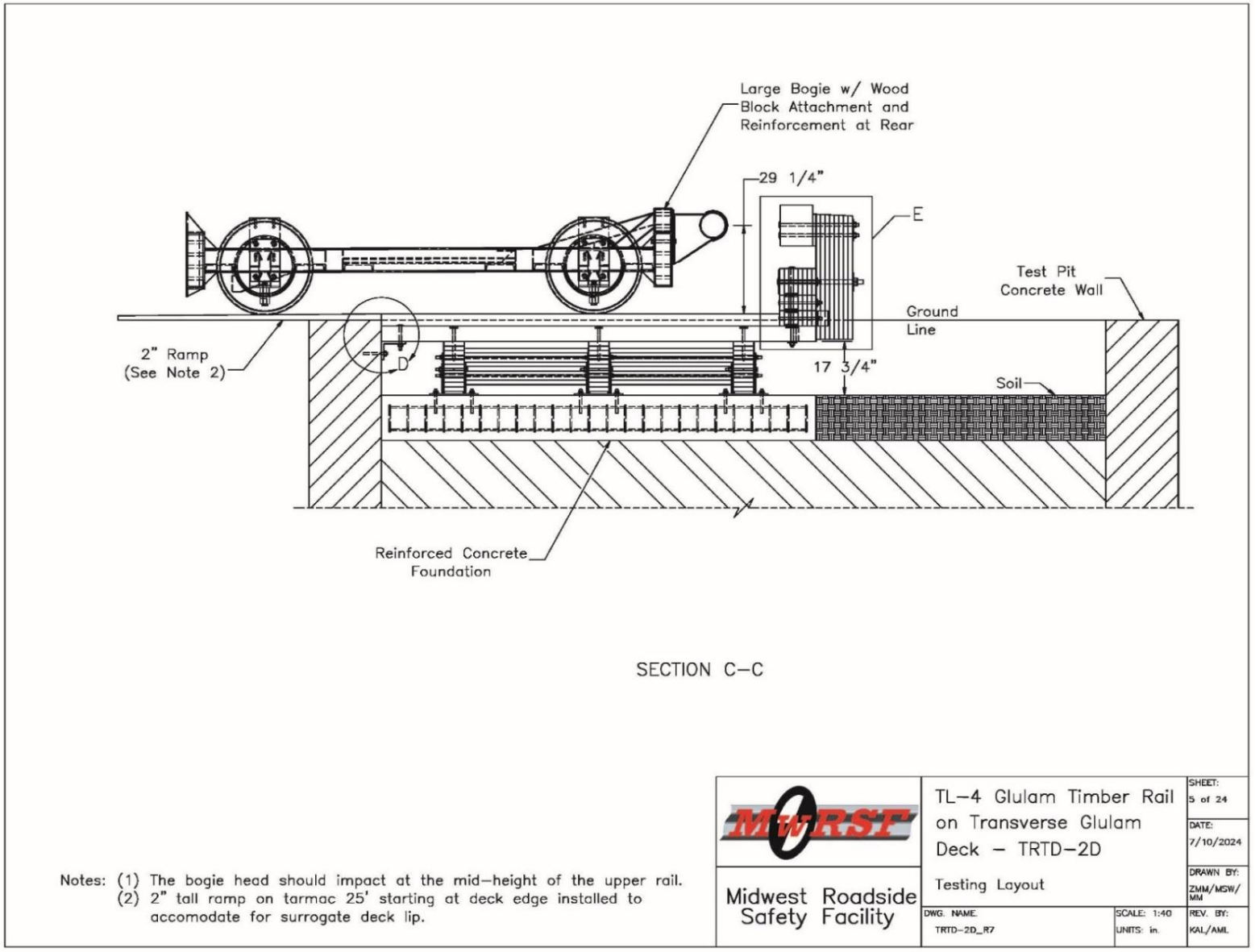

Figure 223. Layout, Elevation View, Test No. TRTD-2

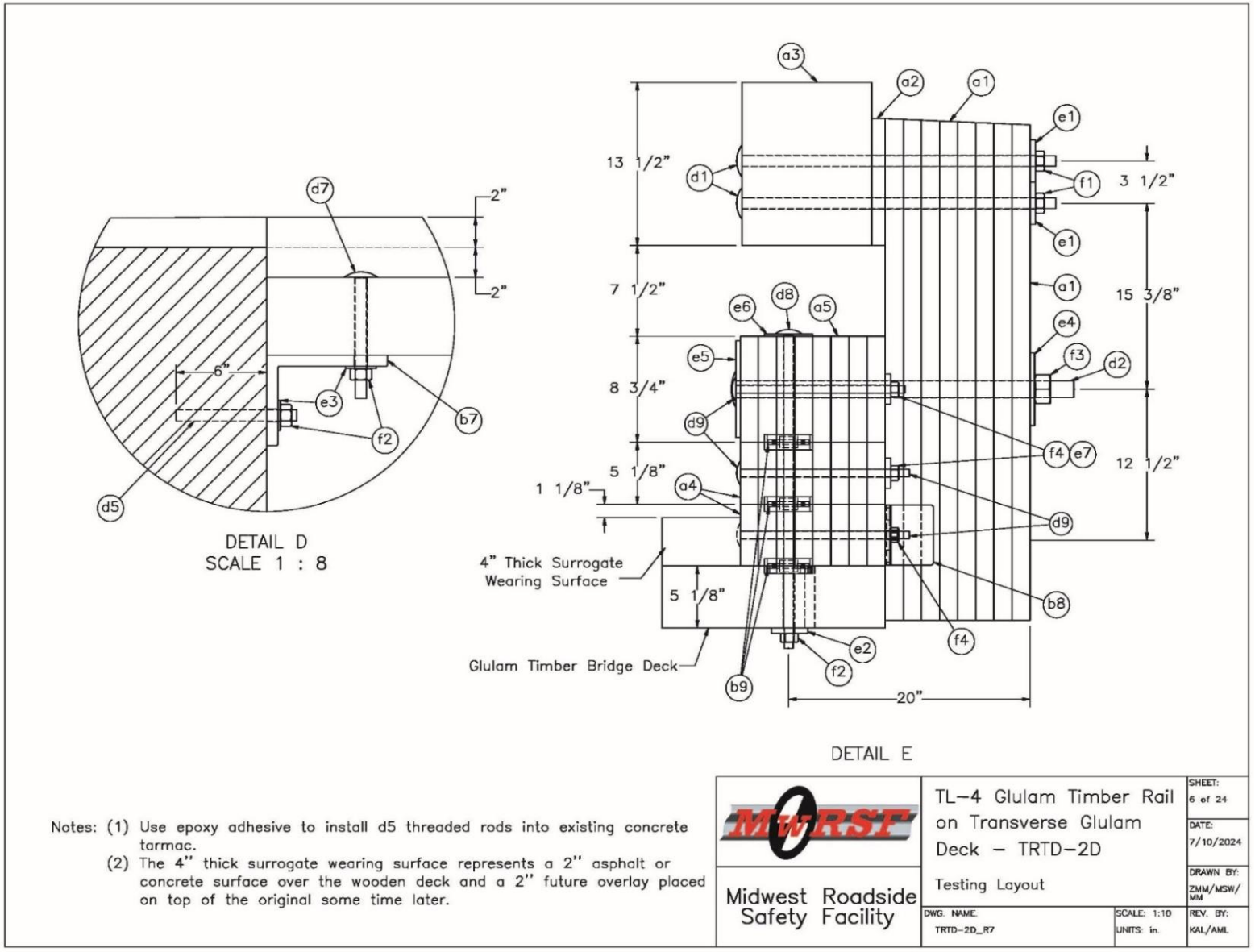

Figure 224. Post and Deck Assembly Details, Section View, Test No. TRTD-2

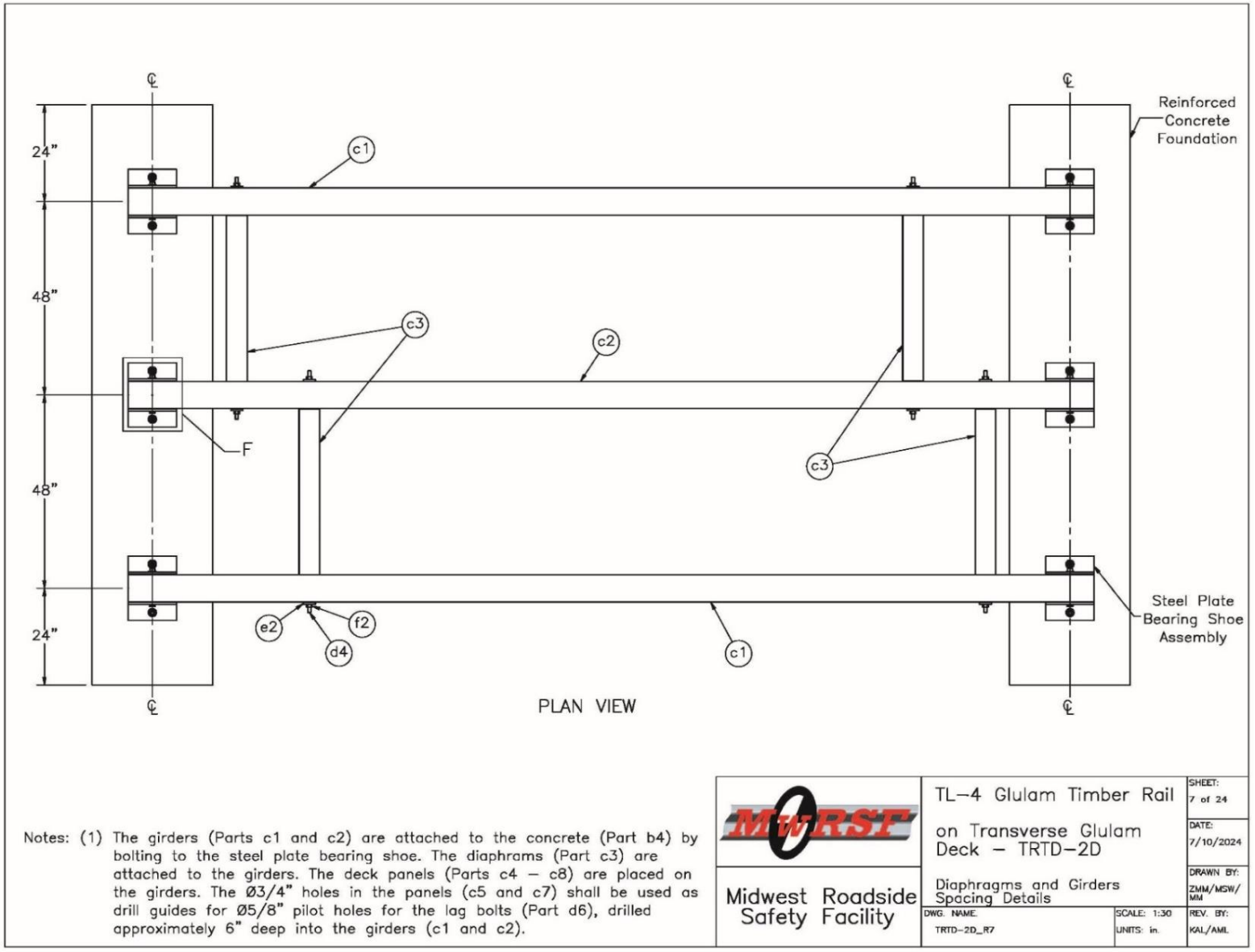

Figure 225. Diaphragm and Girder Spacing Details, Test No. TRTD-2

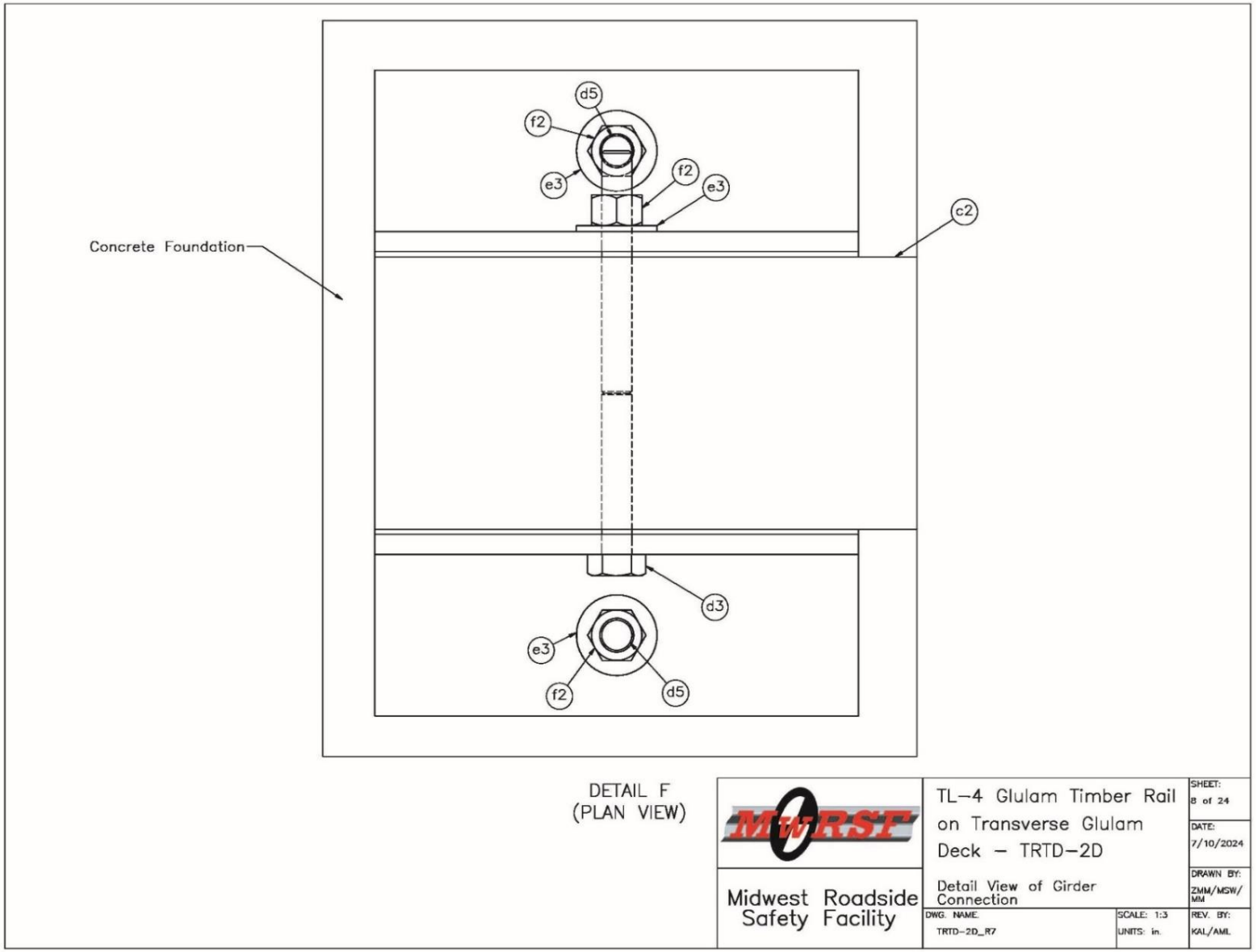

Figure 226. Girder Connection Details, Test No. TRTD-2

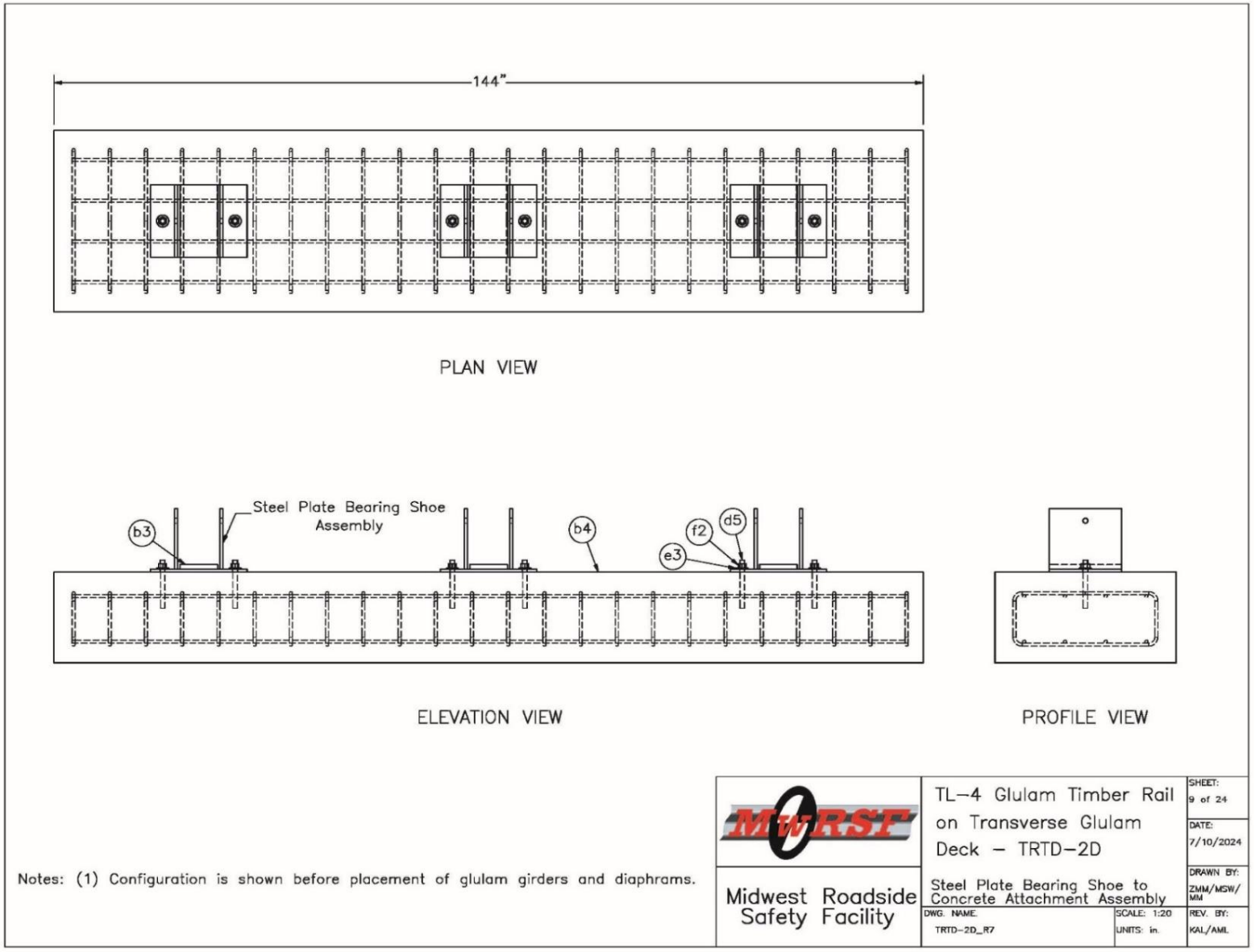

Figure 227. Concrete and Bearing Assembly Details, Test No. TRTD-2

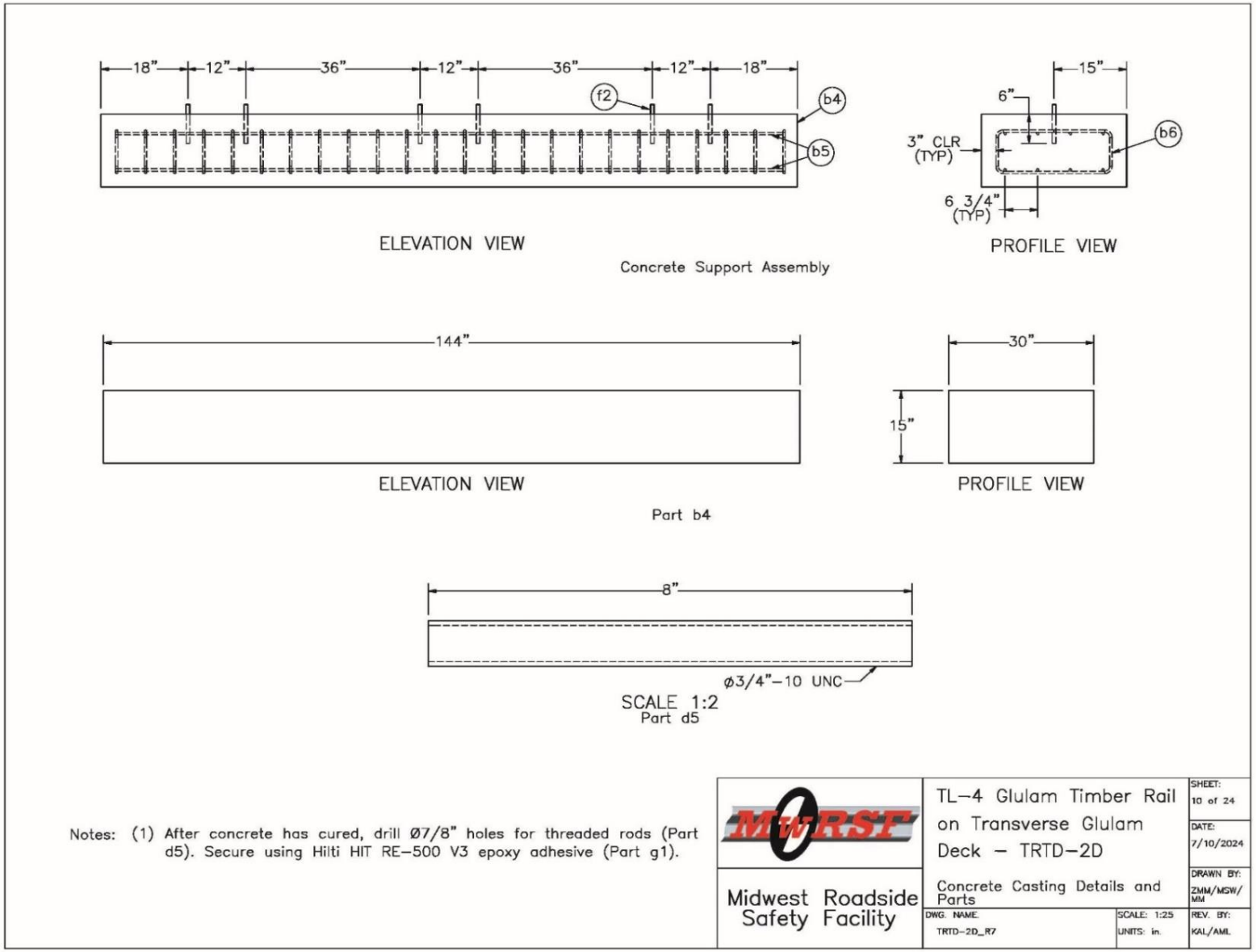

Figure 228. Concrete Casting and Embedded Rod Details, Test No. TRTD-2

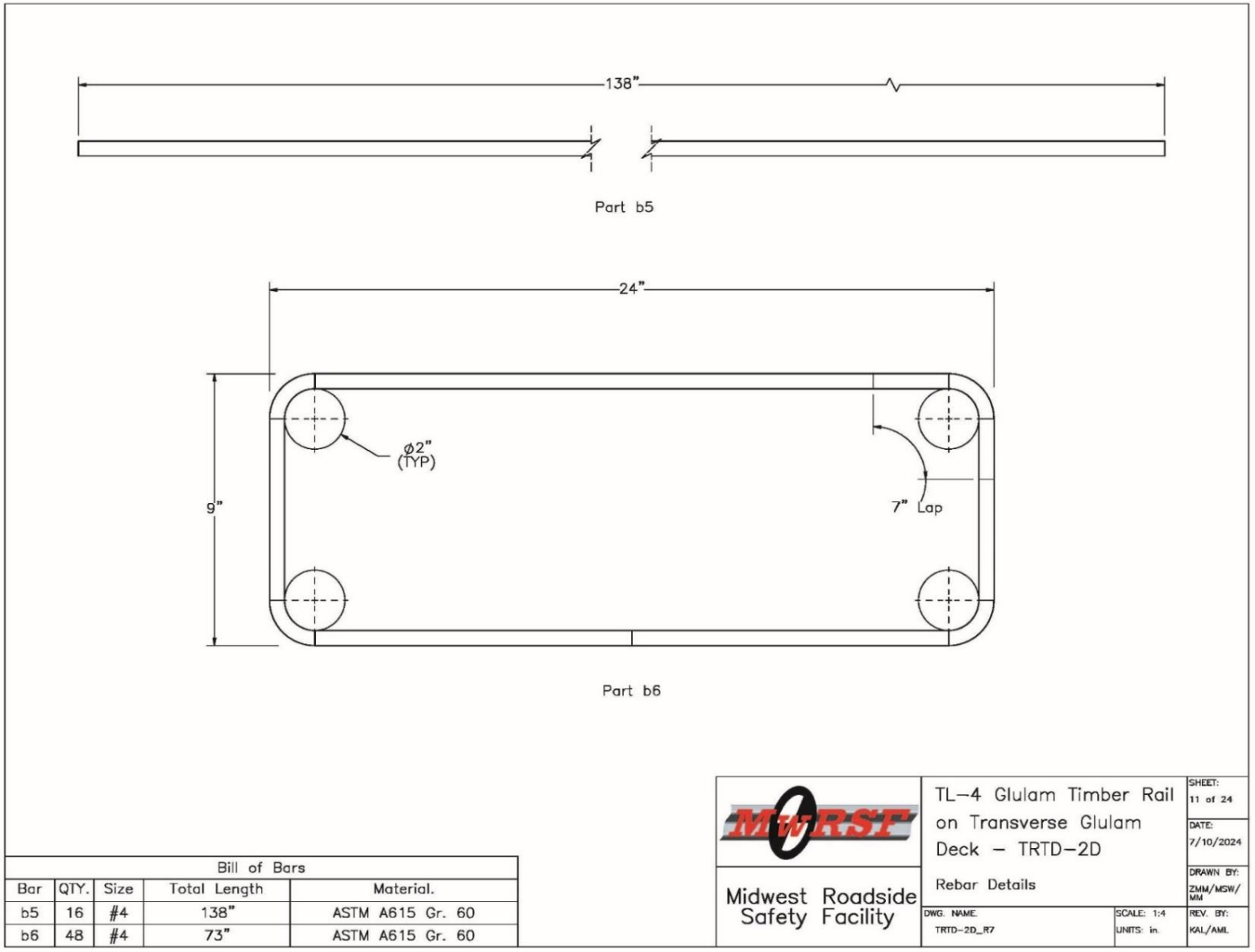

Figure 229. Rebar Details, Test No. TRTD-2

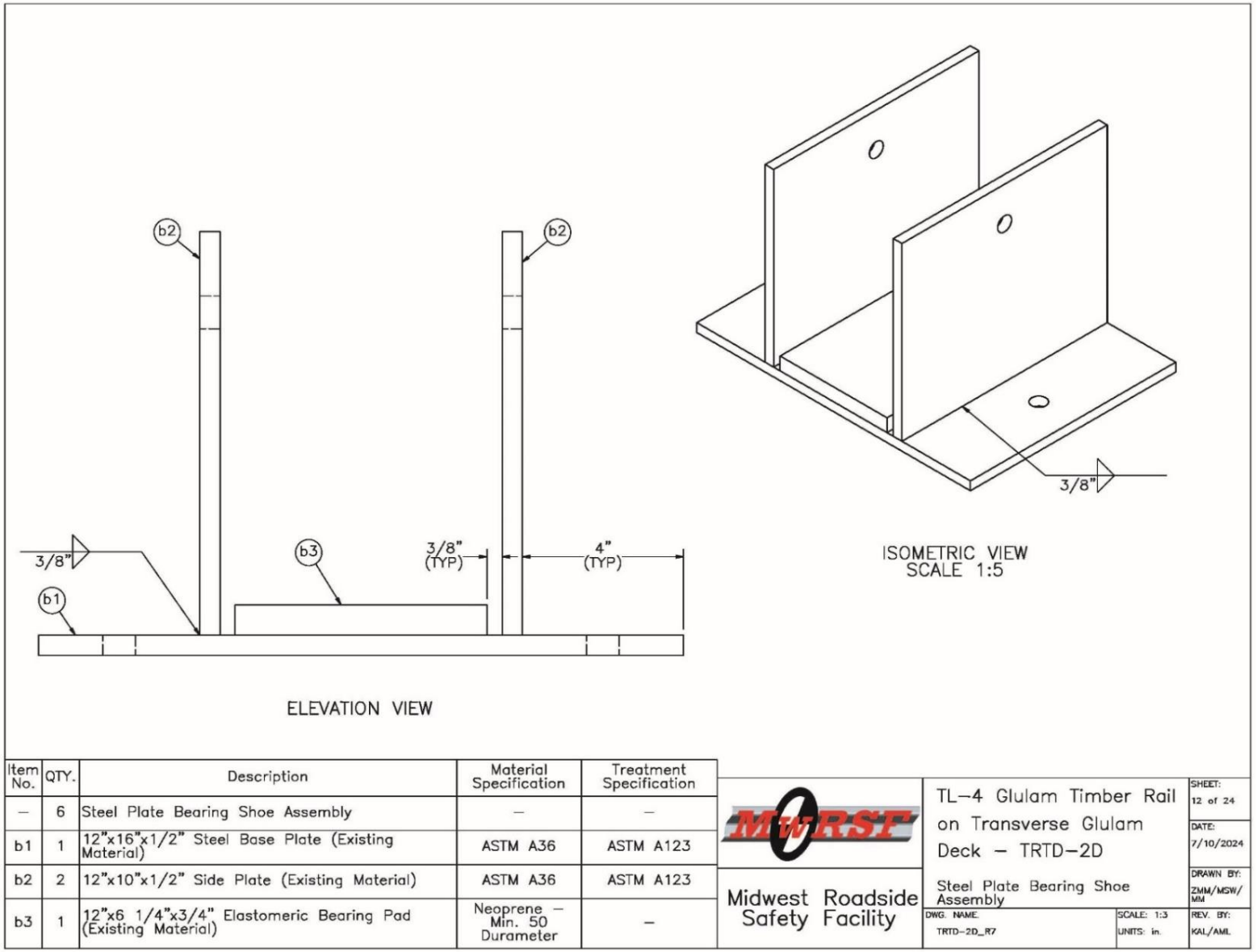

Item No.	QTY.	Description	Material Specification	Treatment Specification
–	6	Steel Plate Bearing Shoe Assembly	–	–
b1	1	12"x16"x1/2" Steel Base Plate (Existing Material)	ASTM A36	ASTM A123
b2	2	12"x10"x1/2" Side Plate (Existing Material)	ASTM A36	ASTM A123
b3	1	12"x6 1/4"x3/4" Elastomeric Bearing Pad (Existing Material)	Neoprene – Min. 50 Durameter	–

Midwest Roadside Safety Facility

TL–4 Glulam Timber Rail on Transverse Glulam Deck – TRTD–2D

Steel Plate Bearing Shoe Assembly

DWG. NAME: TRTD–2D_R7 | SCALE: 1:3 | UNITS: in.

SHEET: 12 of 24 | DATE: 7/10/2024 | DRAWN BY: ZMM/MSW/MM | REV. BY: KAL/AML

Figure 230. Steel Plate Bearing Assembly Details, Test No. TRTD-2

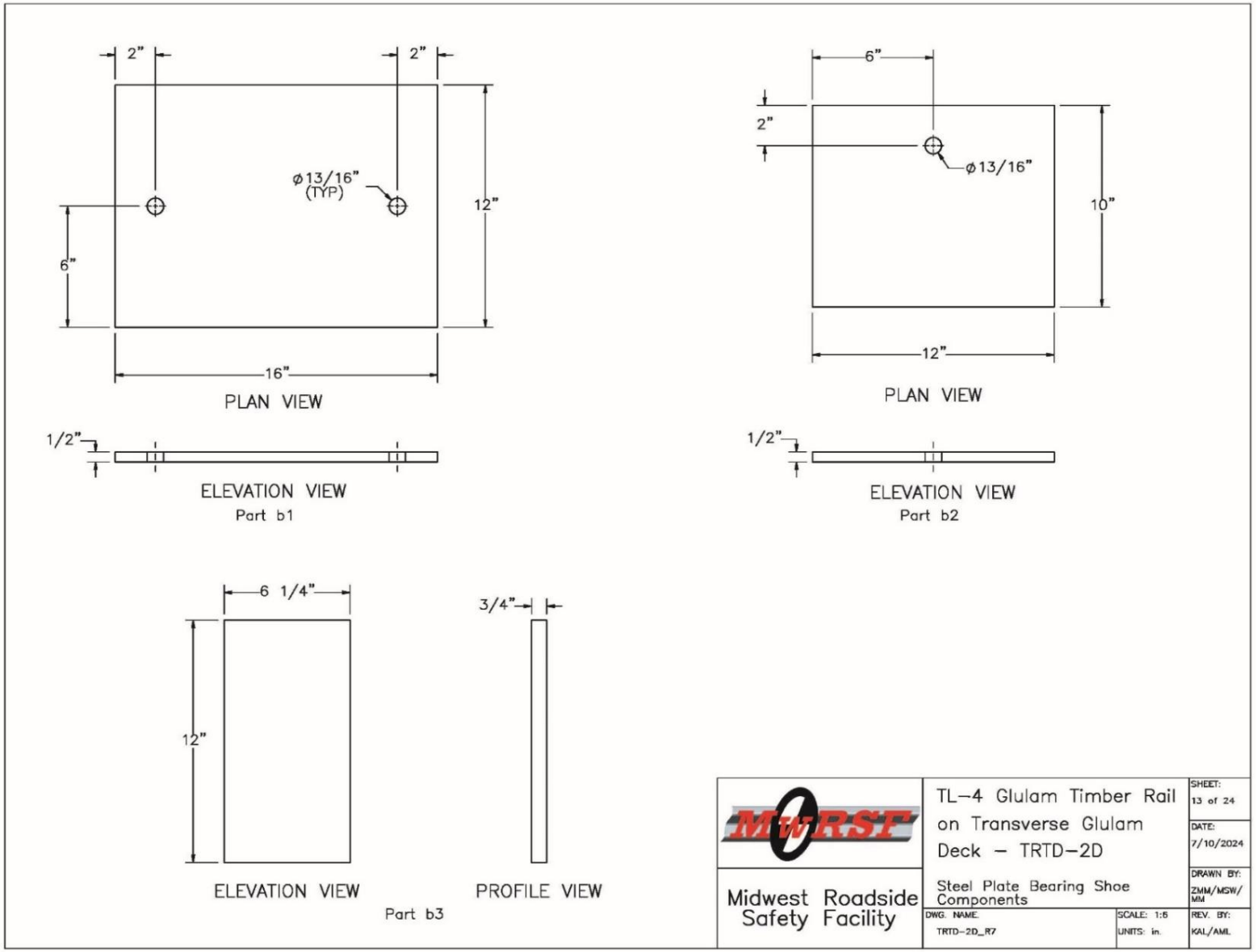

Figure 231. Steel Plate Bearing Assembly Component Details, Test No. TRTD-2

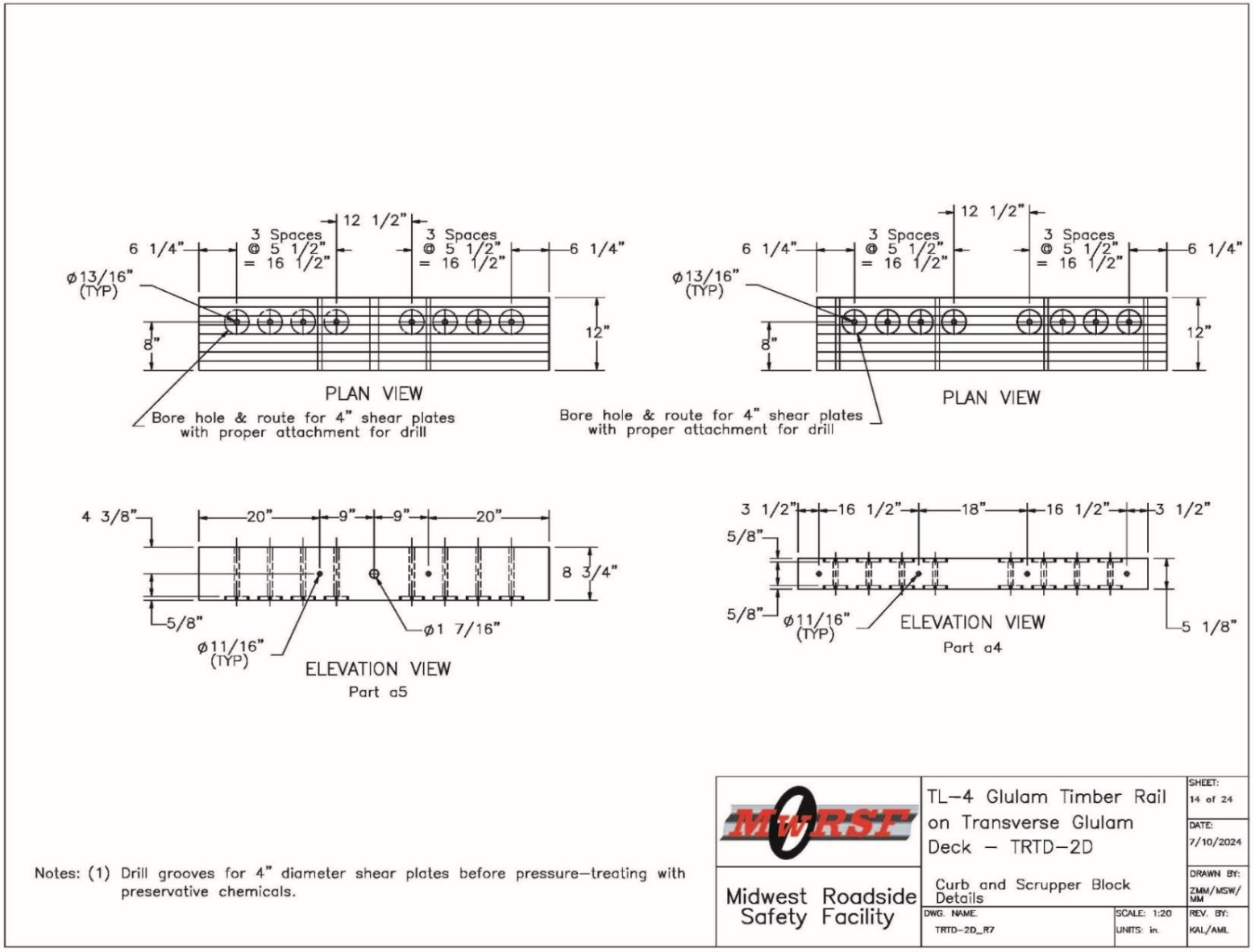

Figure 232. Scupper and Curb Rail Details, Test No. TRTD-2

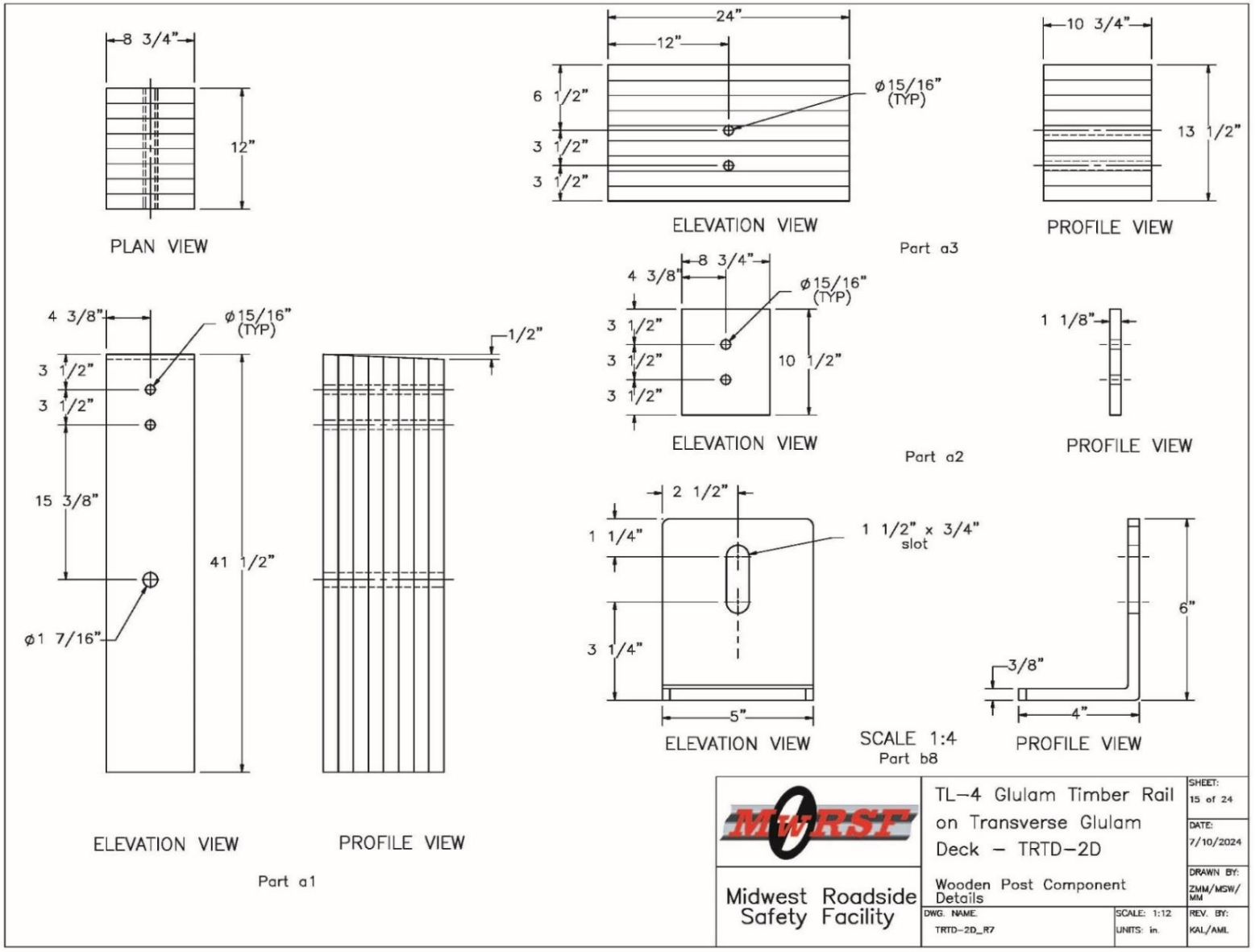

Figure 233. Vertical Post, Upper Rail, Blockout, and Angle Guide Details, Test No. TRTD-2

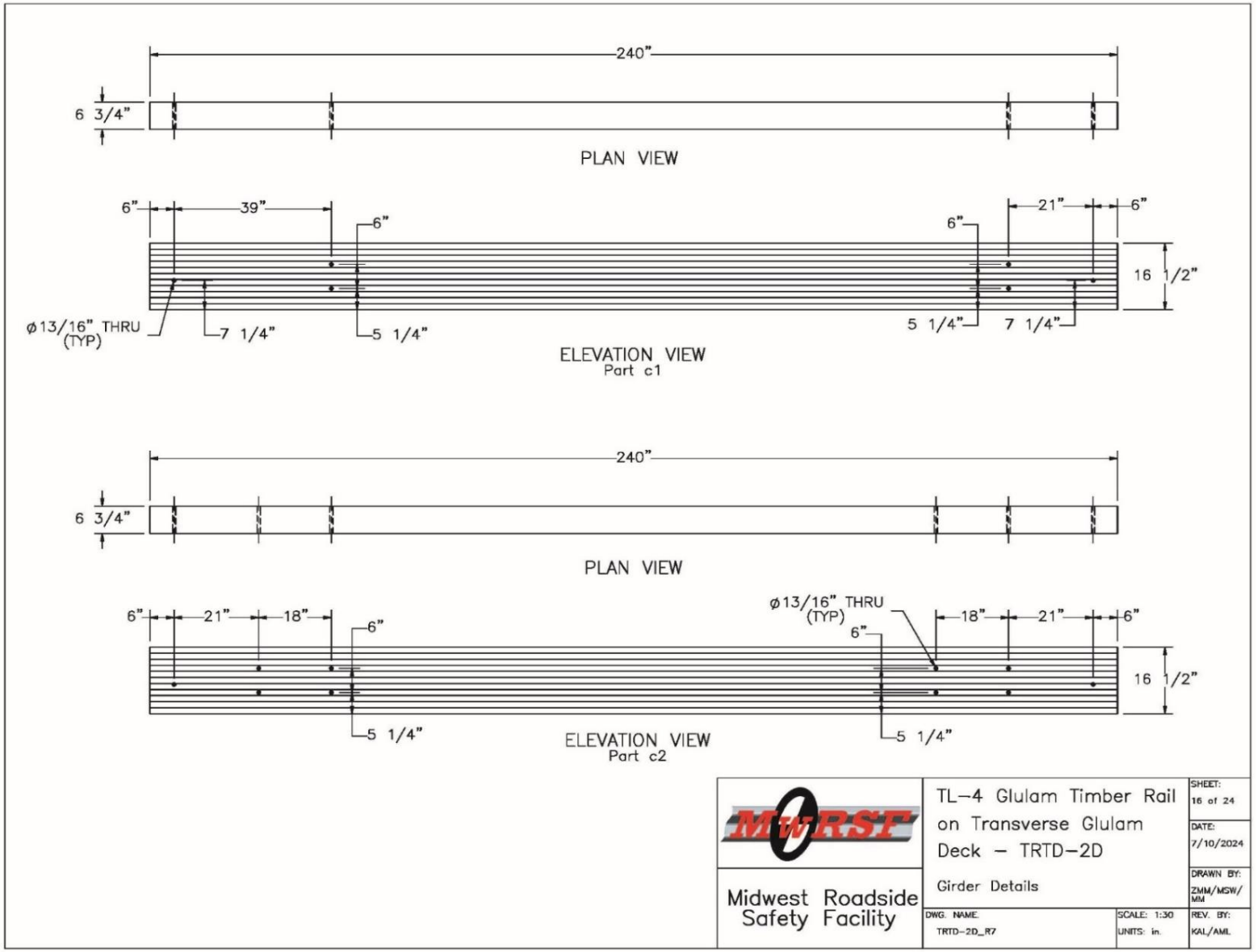

Figure 234. Girder Details, Test No. TRTD-2

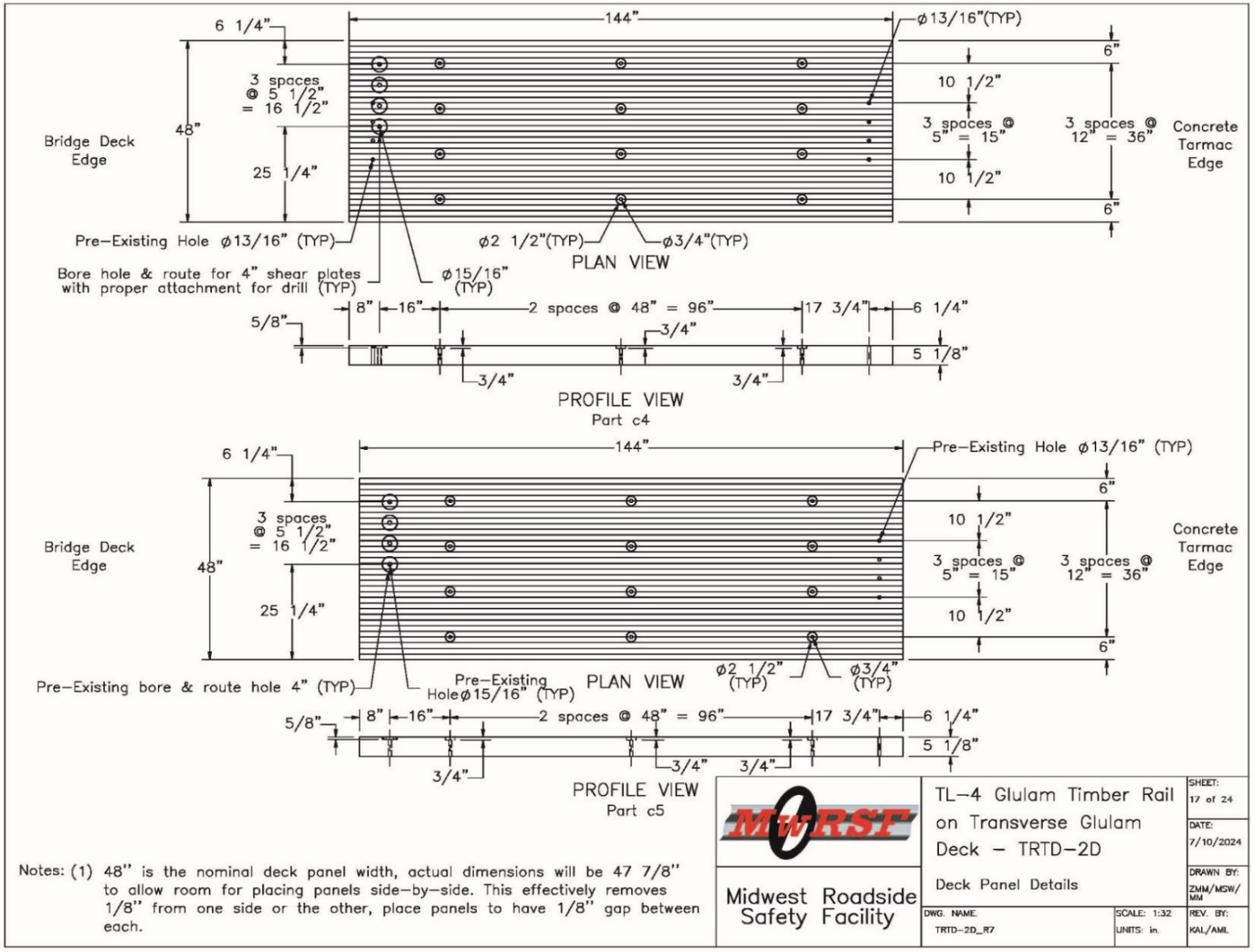

Figure 235. Deck Panel Details, Page 1, Test No. TRTD-2

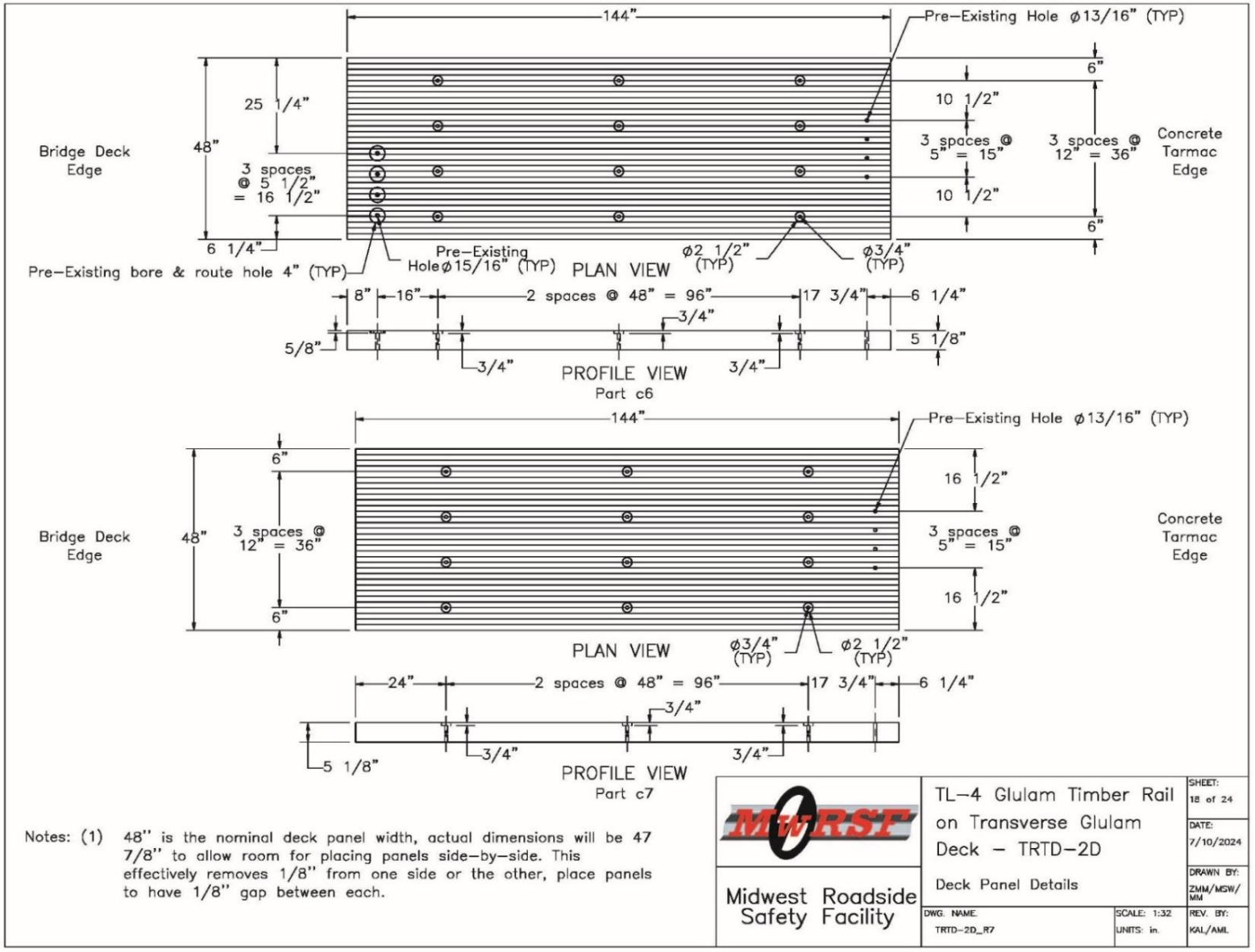

Figure 236. Deck Panel Details, Page 2, Test No. TRTD-2

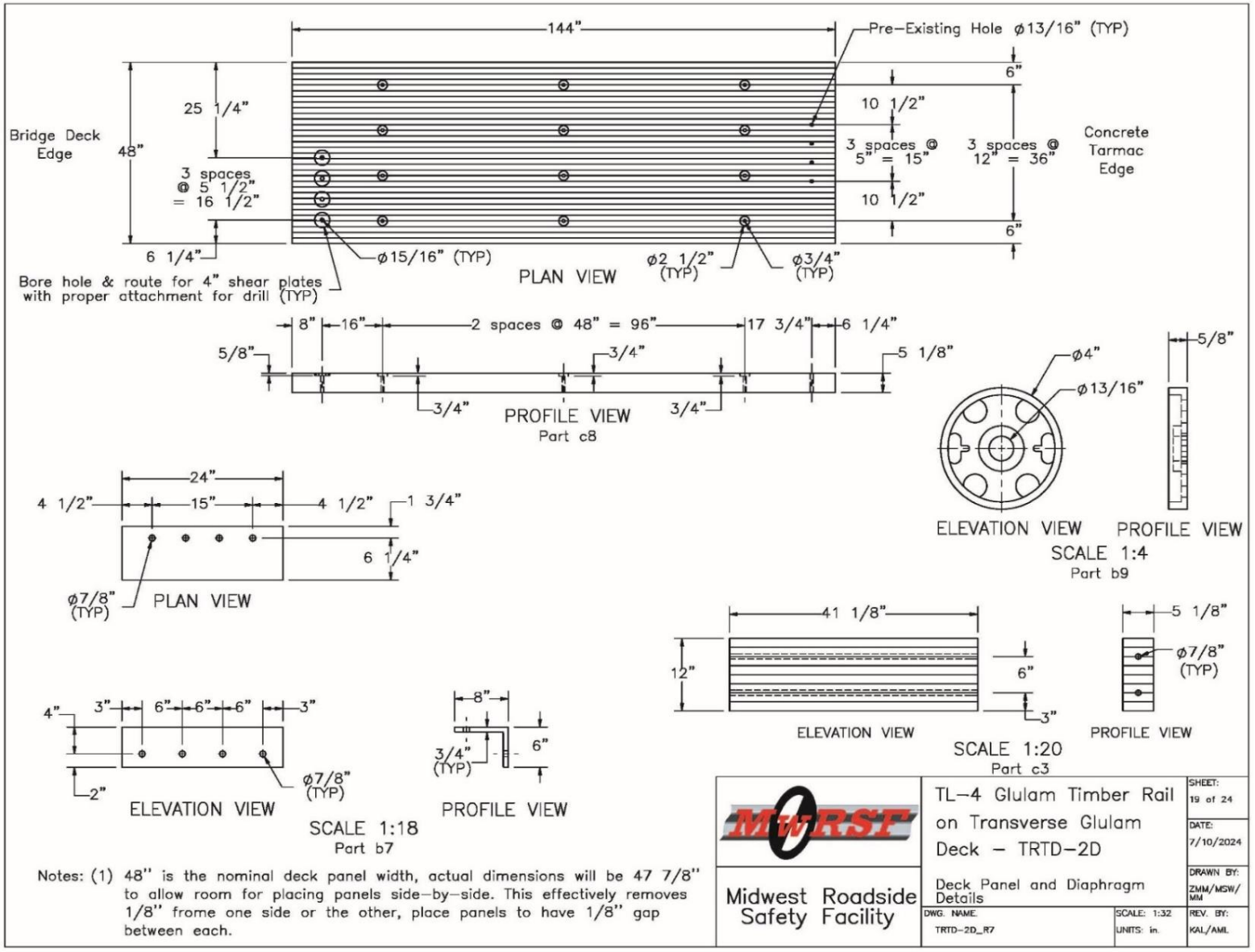

Figure 237. Deck Panel, Tarmac Angle Restraint, Diaphragm, and Shear Plate Details, Test No. TRTD-2

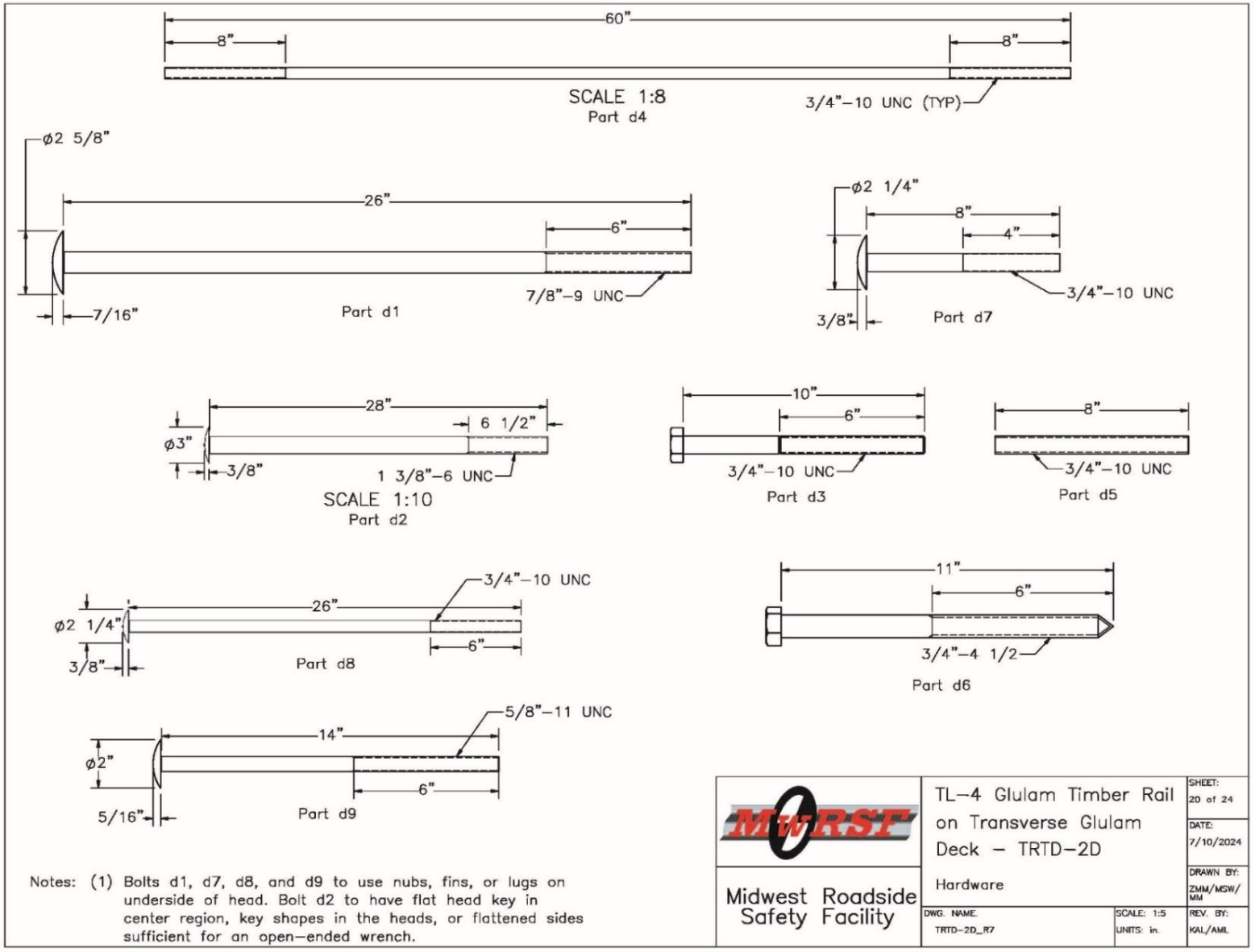

Figure 238. Connection Hardware Details, Page 1, Test No. TRTD-2

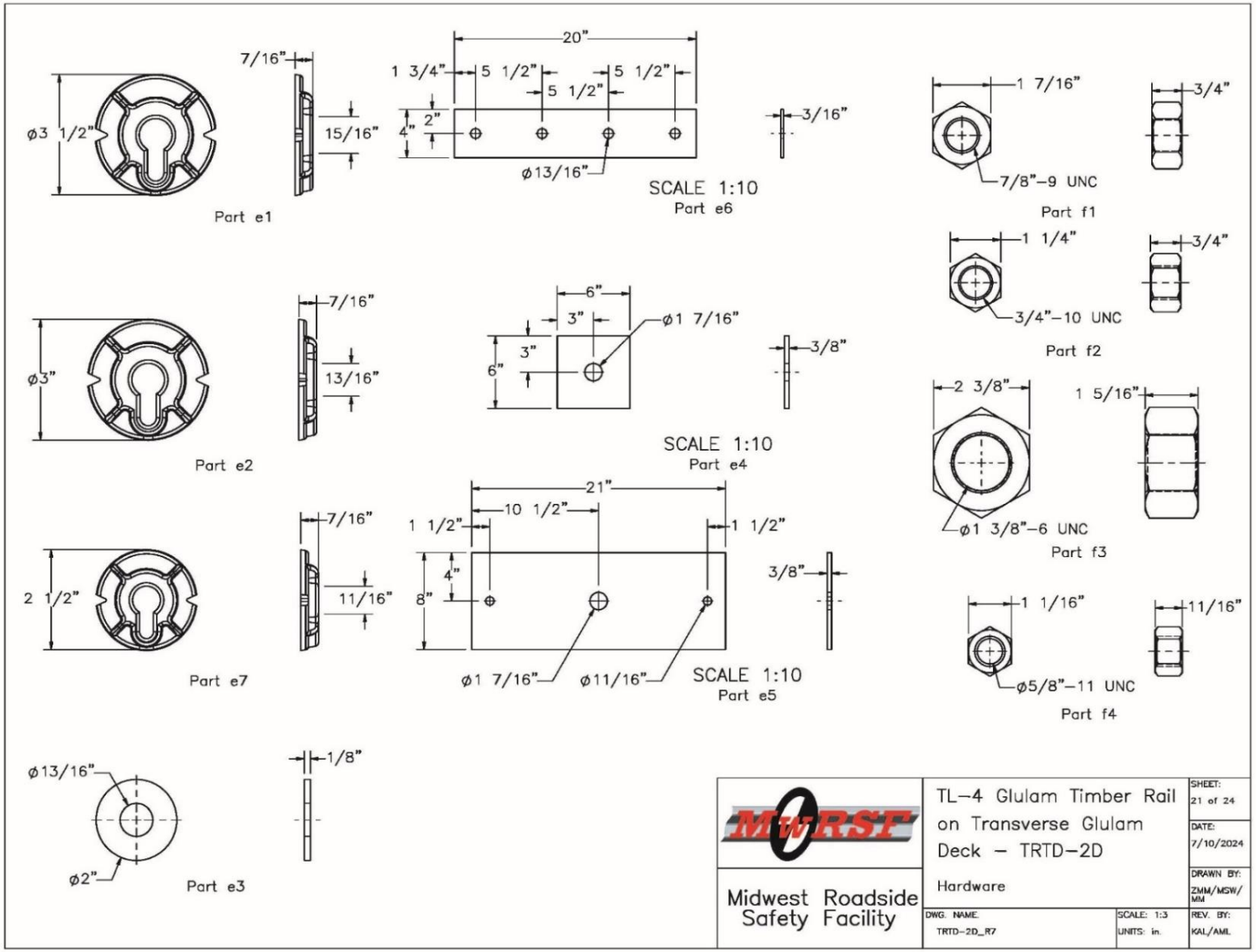

Figure 239. Connection Hardware Details, Page 2, Test No. TRTD-2

Item No.	QTY.	Description	Material Specification	Treatment Specification	Hardware Guide
–	1	4" Thick Surrogate Wearing Surface	–	–	–
a1	1	41 1/2"x12"x8 3/4" Glulam Post	Comb. 48 (SP) or Comb. 2 (Western Species)	See Notes 1–3	–
a2	1	1 1/8"x10 1/2"x8 3/4" Glulam Blockout	Comb. 48 (SP) or Comb. 2 (Western Species)	See Notes 1–3	–
a3	1	24"x13 1/2"x10 3/4" Glulam Upper Rail	Comb. 48 (SP) or Comb. 2 (Western Species)	See Notes 1–3	–
a4	2	58"x12"x5 1/8" Glulam Scupper Block	Comb. 48 (SP) or Comb. 2 (Western Species)	See Notes 1–3	–
a5	1	96"x12"x8 3/4" Glulam Curb Rail	Comb. 48 (SP) or Comb. 2 (Western Species)	See Notes 1–3	–
b1	6	12"x16"x1/2" Steel Base Plate (Existing Material)	ASTM A36	ASTM A123	–
b2	12	12"x10"x1/2" Side Plate (Existing Material)	ASTM A36	ASTM A123	–
b3	6	12"x6 1/4"x3/4" Elastomeric Bearing Pad (Existing Material)	Neoprene – Min. 50 Durameter	–	–
b4	2	15"x30"x12' Concrete Support (Existing Material)	Min f'c = 4,000 psi NE mix 47 BD	–	–
b5	16	#4 Rebar, 138" Long (Existing Material)	ASTM A615 Gr. 60	Epoxy Coated (ASTM A775 or A934)	–
b6	48	#4 Rebar, 73" Unbent Length (Existing Material)	ASTM A615 Gr. 60	Epoxy Coated (ASTM A775 or A934)	–
b7	5	8"x 6", 3/4" Thick 24" Long Steel Angle	ASTM A36	ASTM A123	–
b8	2	6"x4", 3/8" Thick, 5" Long Steel Angle	ASTM A36	ASTM A123	–
b9	48	3/4"x4"x5/8" Shear Plate	ASTM A47 Grade 32510 or ASTM D5933	Hot–Dip	12405

Notes: (1) Timber rails, posts, scuppers, and blockouts shall be treated with Copper Naphthenate (CuN) or 4,5–Dichloro–2–N–Octyl–4–Isothiazolin–3–One (DCOI) in heavy oil to a minimum retention of 0.075 lbs/cu. ft. or 0.20 lbs/cu. ft. respectively in accordance with AWPA Standard U1 to the requirements. Use category 4B (UC4B).
(2) Wood shall be cut, drilled, and completely fabricated prior to treatment with preservative. Drain excess chemicals and dry all treated wood at the place of manufacture.
(3) All field cuts, bore holes, and damages shall be treated with material acceptable to the engineer prior to installation.

MwRSF
Midwest Roadside Safety Facility

TL–4 Glulam Timber Rail on Transverse Glulam Deck – TRTD–2D
Bill of Materials

SHEET: 22 of 24
DATE: 7/10/2024
DRAWN BY: ZMM/MSW/MM
REV. BY: KAL/AML
DWG. NAME: TRTD–2D_R7
SCALE: None
UNITS: in.

Figure 240. Bill of Materials, Page 1, Test No. TRTD-2

Item No.	QTY.	Description	Material Specification	Treatment Specification	Hardware Guide
c1	2	16 1/2"x6 3/4"x20' Long Outside Glulam Girder (Existing Material)	24F–V4 Douglas Fir	Pentachorophenal in Heavy Oil 0.6 lbs/cu. ft Retention	–
c2	1	16 1/2"x6 3/4"x20' Long Glulam Girder (Existing Material)	24F–V4 Douglas Fir	Pentachorophenal in Heavy Oil 0.6 lbs/cu. ft Retention	–
c3	4	12"x5 1/8"x41 1/8" Long Glulam Diaphragm (Existing Material)	Comb. No. 2 Douglas Fir	Pentachorophenal in Heavy Oil 0.6 lbs/cu. ft Retention	–
c4	1	5 1/8"x4'x12' Long Glulam Deck Panel (Existing Material)	Comb. No. 2 Douglas Fir	Pentachorophenal in Heavy Oil 0.6 lbs/cu. ft Retention	–
c5	1	5 1/8"x4'x12' Long Glulam Deck Panel #2 (Existing Material)	Comb. No. 2 Douglas Fir	Pentachorophenal in Heavy Oil 0.6 lbs/cu. ft Retention	–
c6	1	5 1/8"x4'x12' Long Glulam Deck Panel (Existing Material)	Comb. No. 2 Douglas Fir	Pentachorophenal in Heavy Oil 0.6 lbs/cu. ft Retention	–
c7	1	5 1/8"x4'x12' Long Glulam Deck Panel (Existing Material)	Comb. No. 2 Douglas Fir	Pentachorophenal in Heavy Oil 0.6 lbs/cu. ft Retention	–
c8	1	5 1/8"x4'x12' Long Glulam Deck Panel (Existing Material)	Comb. No. 2 Douglas Fir	Pentachorophenal in Heavy Oil 0.6 lbs/cu. ft Retention	–
d1	2	7/8"–9 UNC x 26" Timber Bolt w/ Nubs	ASTM A307A	ASTM A123	–
d2	1	1 3/8"–6 UNC x 28" Timber Bolt w/o Nubs	ASTM A449	ASTM A123	–
d3	6	3/4"–10 UNC x 10" Hex Bolt (Existing Material)	ASTM A307A	ASTM A123	FBX20a
d4	8	3/4"–10 UNC x 8" on a 60" Long Tie Rod (Existing Material)	ASTM A307A or F1554 Gr. 36 or SAE J429 Gr. 2	ASTM A123	FRR28a
d5	32	3/4"–10 UNC x 8" Threaded Rod (Existing Material)	ASTM A193 Gr. B7 or SAE J429 Gr. 5	ASTM A123	FRR20a
d6	60	3/4"–4 1/2 x 11" Lag Bolt (Existing Material)	ASTM A307A	ASTM A123	FBL20
d7	20	3/4"–10 UNC x 8" Timber Bolt w/ Nubs (Existing Material)	ASTM A307A	ASTM A123	FBB08
d8	8	3/4"–10 UNC x 26" Timber Bolt w/ Nubs	ASTM A307A	ASTM A123	FBB08
d9	10	5/8"–11 UNC x 14" Timber Bolt w/ Nubs	ASTM A307A	ASTM A123	FBB08

Midwest Roadside Safety Facility

TL–4 Glulam Timber Rail on Transverse Glulam Deck – TRTD–2D

Bill of Materials

SHEET: 23 of 24
DATE: 7/10/2024
DRAWN BY: ZMM/MSW/MM
REV. BY: KAL/AML
DWG. NAME: TRTD–2D_R7
SCALE: 1:96
UNITS: in.

Figure 241. Bill of Materials, Page 2, Test No. TRTD-2

Item No.	QTY.	Description	Material Specification	Treatment Specification	Hardware Guide
e1	2	7/8" Dia. Malleable Iron Washer	ASTM A47	ASTM A123	–
e2	24	3/4" Dia. Malleable Iron Washer (8 new, 16 existing)	ASTM A47	ASTM A123	–
e3	118	3/4" Flat Washer (Existing Material)	ASTM F844	ASTM A123 or A153 or F2329	FWC20a
e4	1	6"x6"x3/8" Steel Plate Washer	ASTM A36	ASTM A123	–
e5	1	8"x21"x3/8" Steel Plate Washer	ASTM A36	ASTM A123	–
e6	2	4"x20"x3/16" Steel Plate Washer	ASTM A36	ASTM A123	–
e7	8	5/8" Dia. Malleable Iron Washer	ASTM A47	ASTM A123	–
f1	2	7/8"–9 UNC Dia. Heavy Hex Nut	ASTM A563A	ASTM A123	FNX22b
f2	82	3/4"–10 UNC Dia. Heavy Hex Nut (8 new, 74 existing)	ASTM A563A	ASTM A123	FNX20b
f3	1	1 3/8"–6 UNC Dia. Heavy Hex Nut	ASTM A563A	ASTM A123 or A153 or F2329	–
f4	10	5/8"–11 UNC Dia. Heavy Hex Nut	ASTM A563A	ASTM A123	FNX16b
g1	–	Epoxy Adhesive (Existing Material)	Hilti HIT RE–500 V3 or equivalent with min. bond strength 1,670 psi	–	–

Midwest Roadside Safety Facility

TL–4 Glulam Timber Rail on Transverse Glulam Deck – TRTD–2D

Bill of Materials

SHEET: 24 of 24
DATE: 7/10/2024
DRAWN BY: ZMM/MSW/MM
REV. BY: KAL/AML
DWG. NAME: TRTD–2D_R7
SCALE: None
UNITS: in.

Figure 242. Bill of Materials, Page 3, Test No. TRTD-2

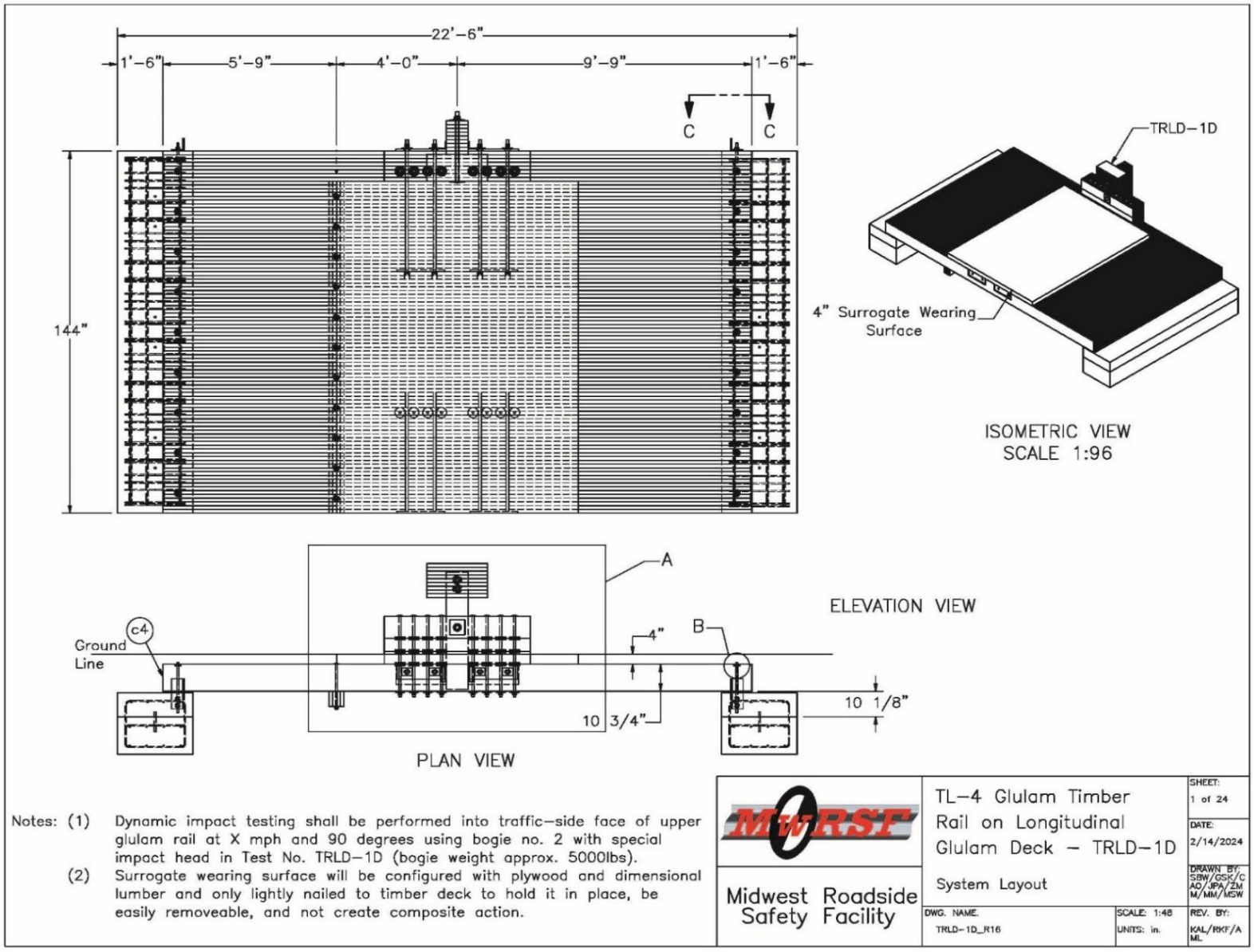

Figure 243. System Layout, Test No. TRLD-1

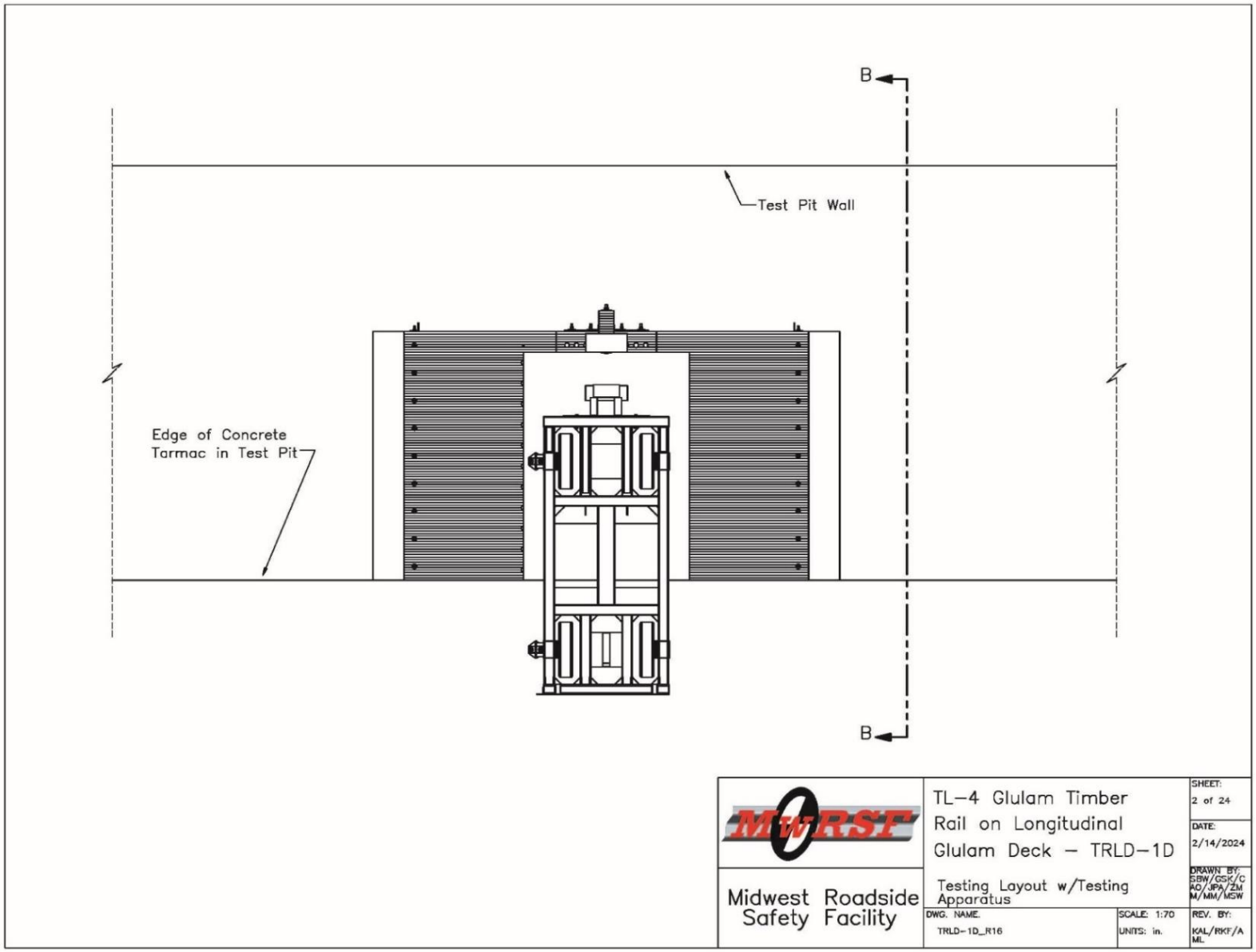

Figure 244. Layout with Bogie, Test No. TRLD-1

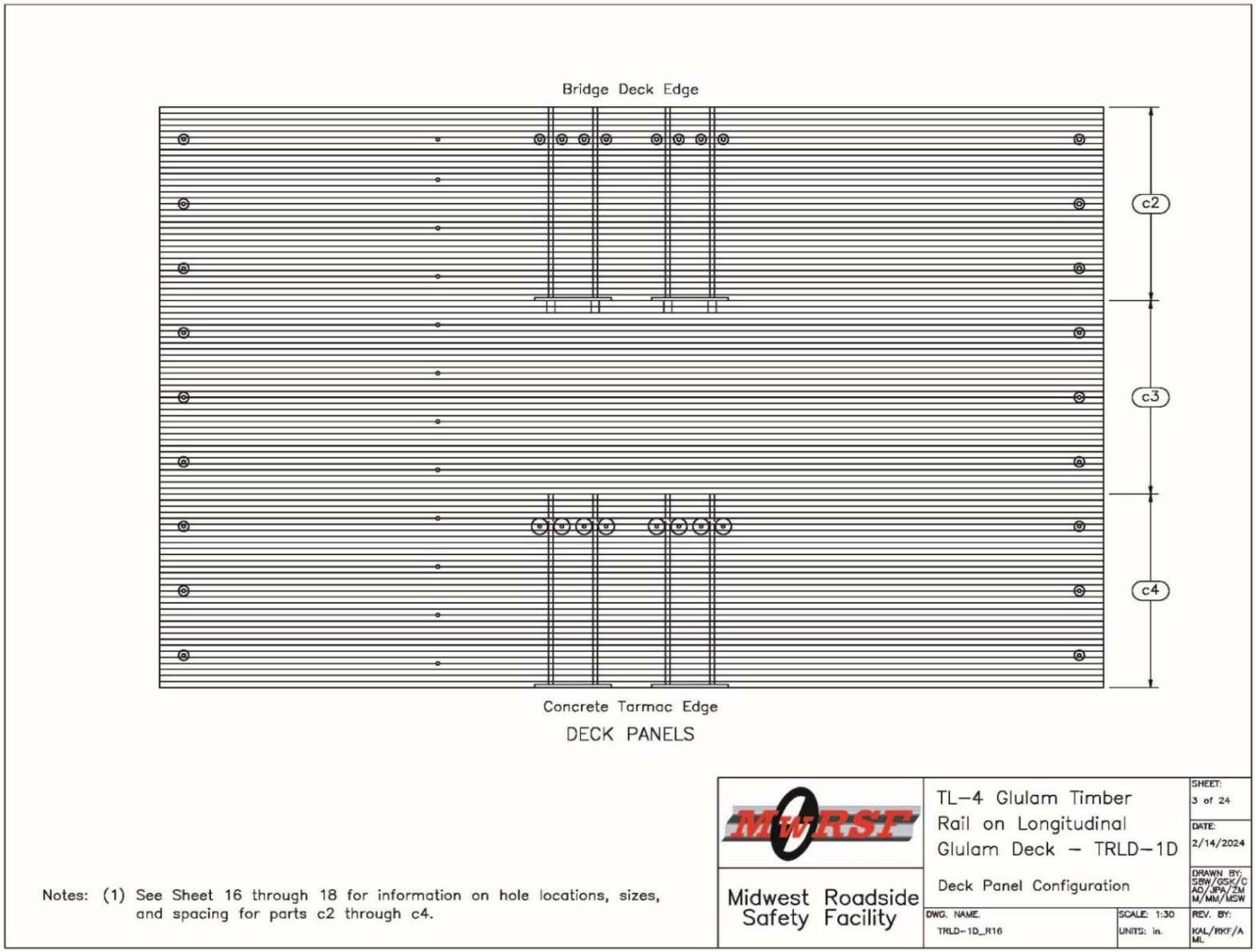

Figure 245. Deck Panel Configuration, Test No. TRLD-1

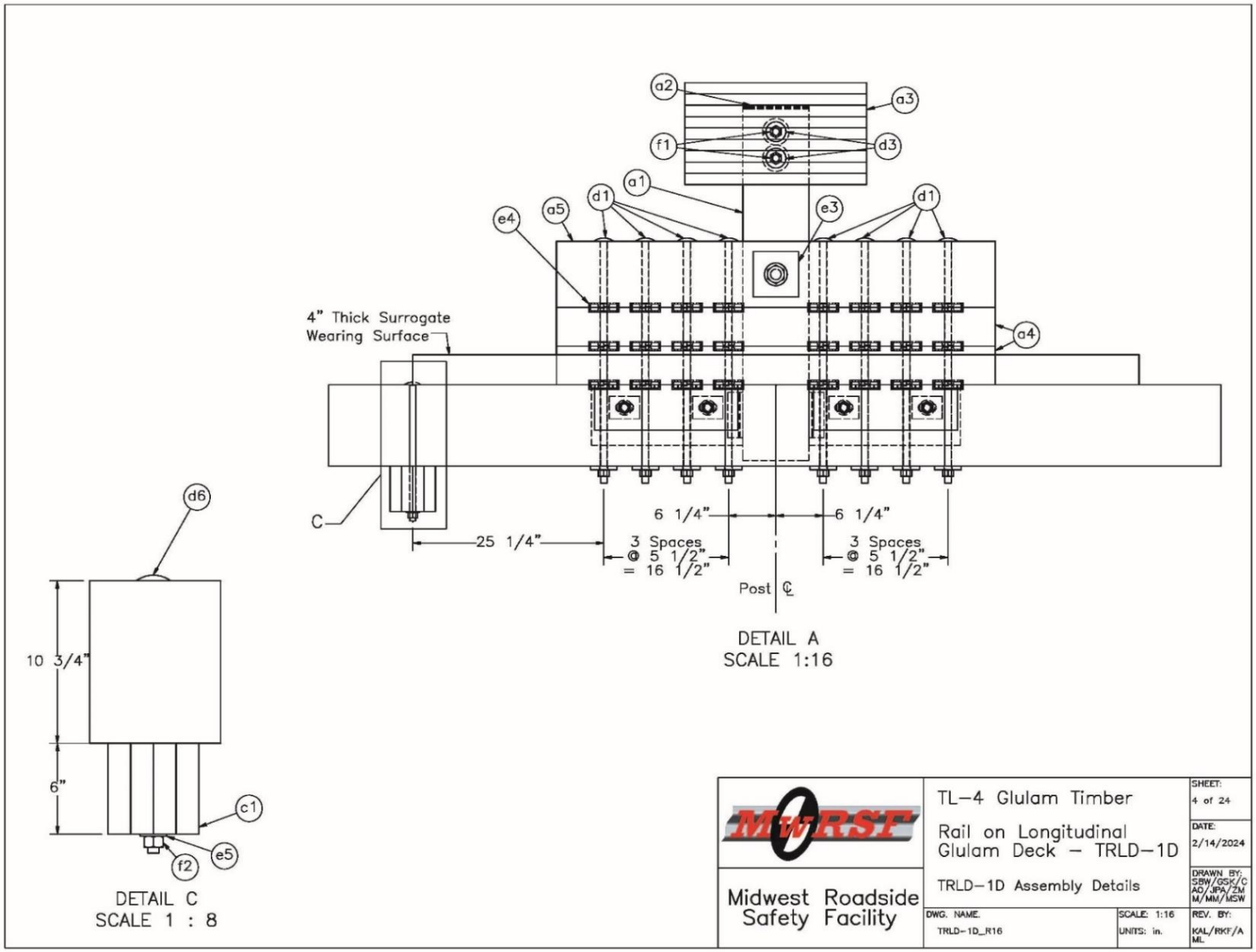

Figure 246. Post and Deck Assembly Details, Test No. TRLD-1

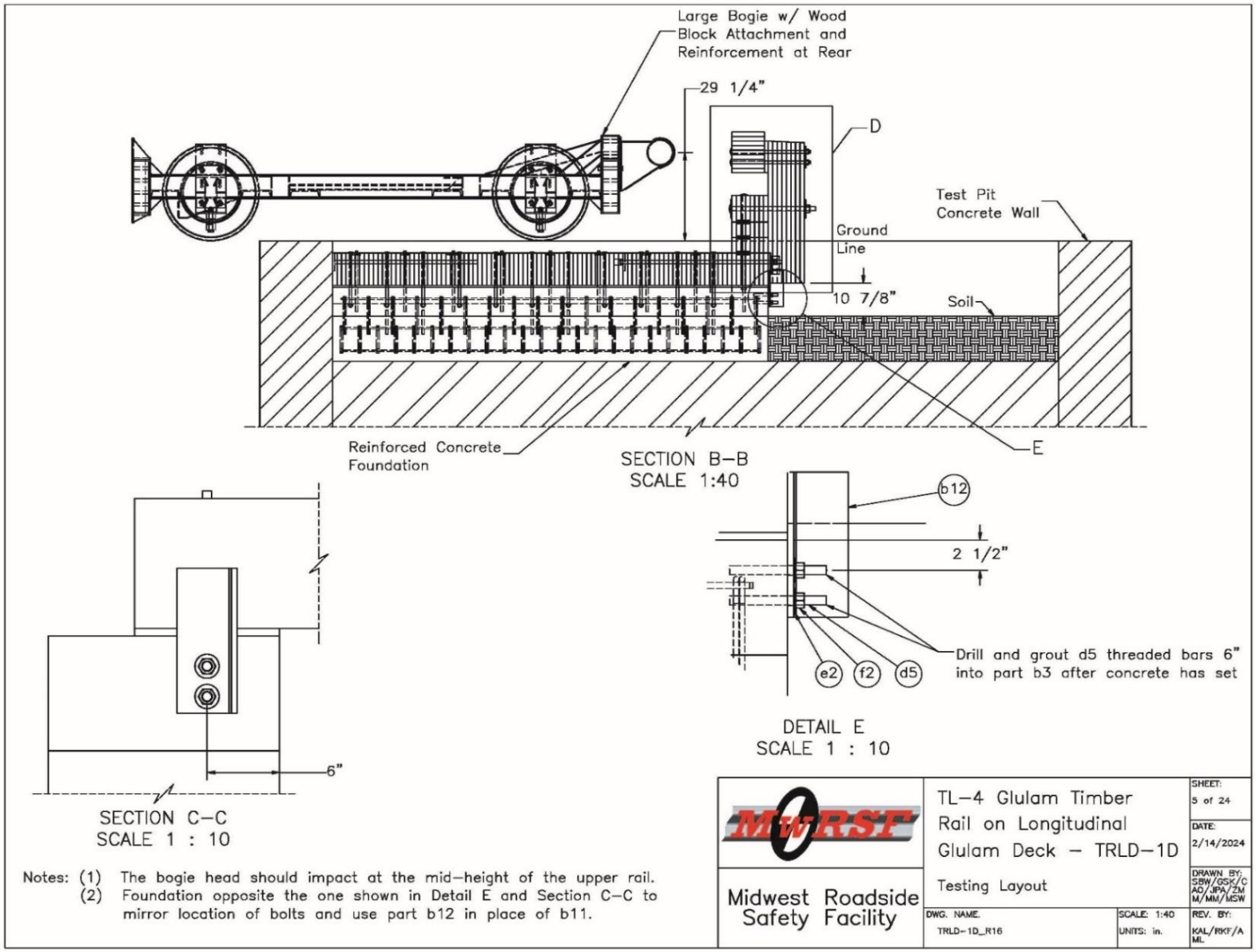

Figure 247. Layout, Elevation View, Test No. TRLD-1

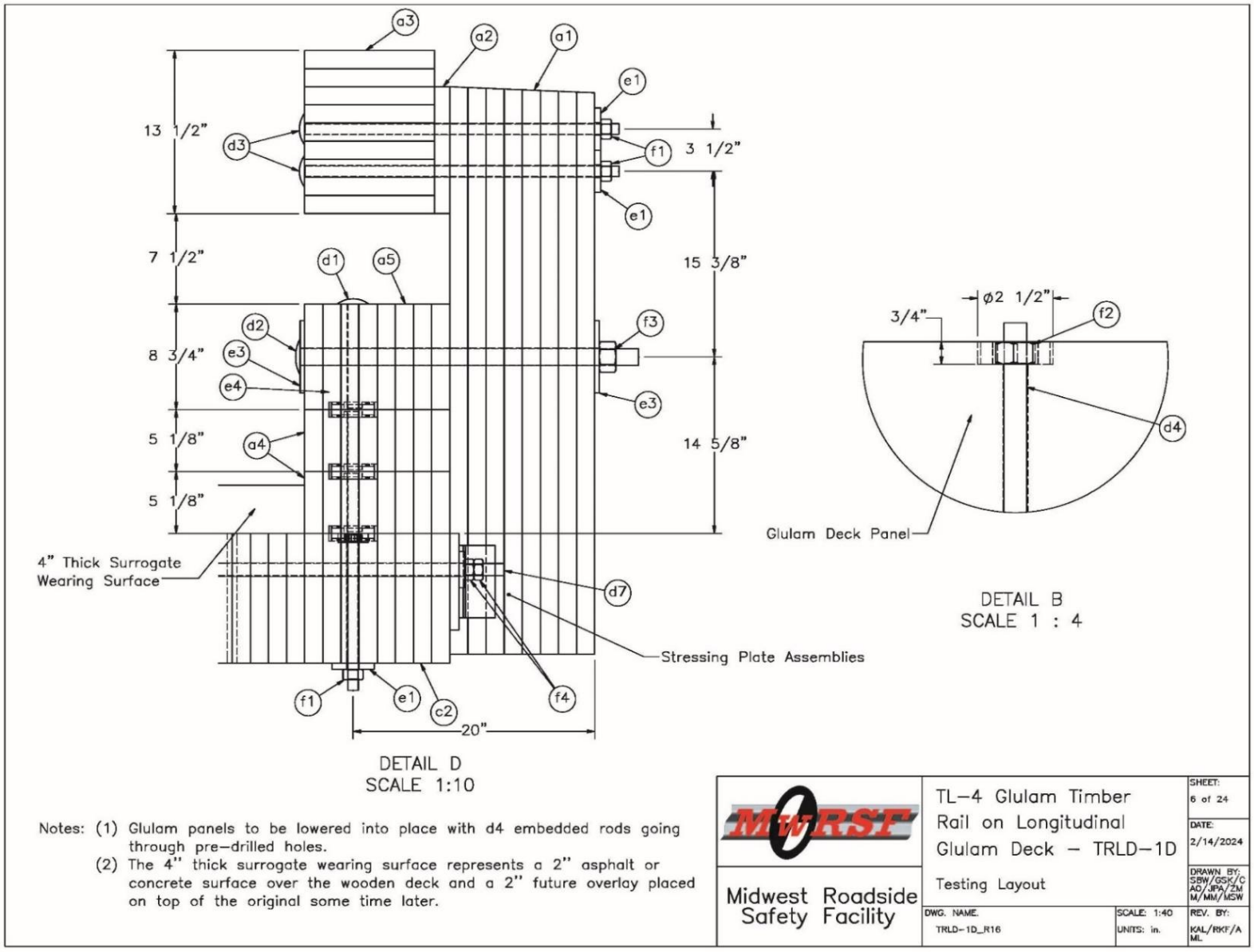

Figure 248. Post and Deck Assembly Details, Section View, Test No. TRLD-1

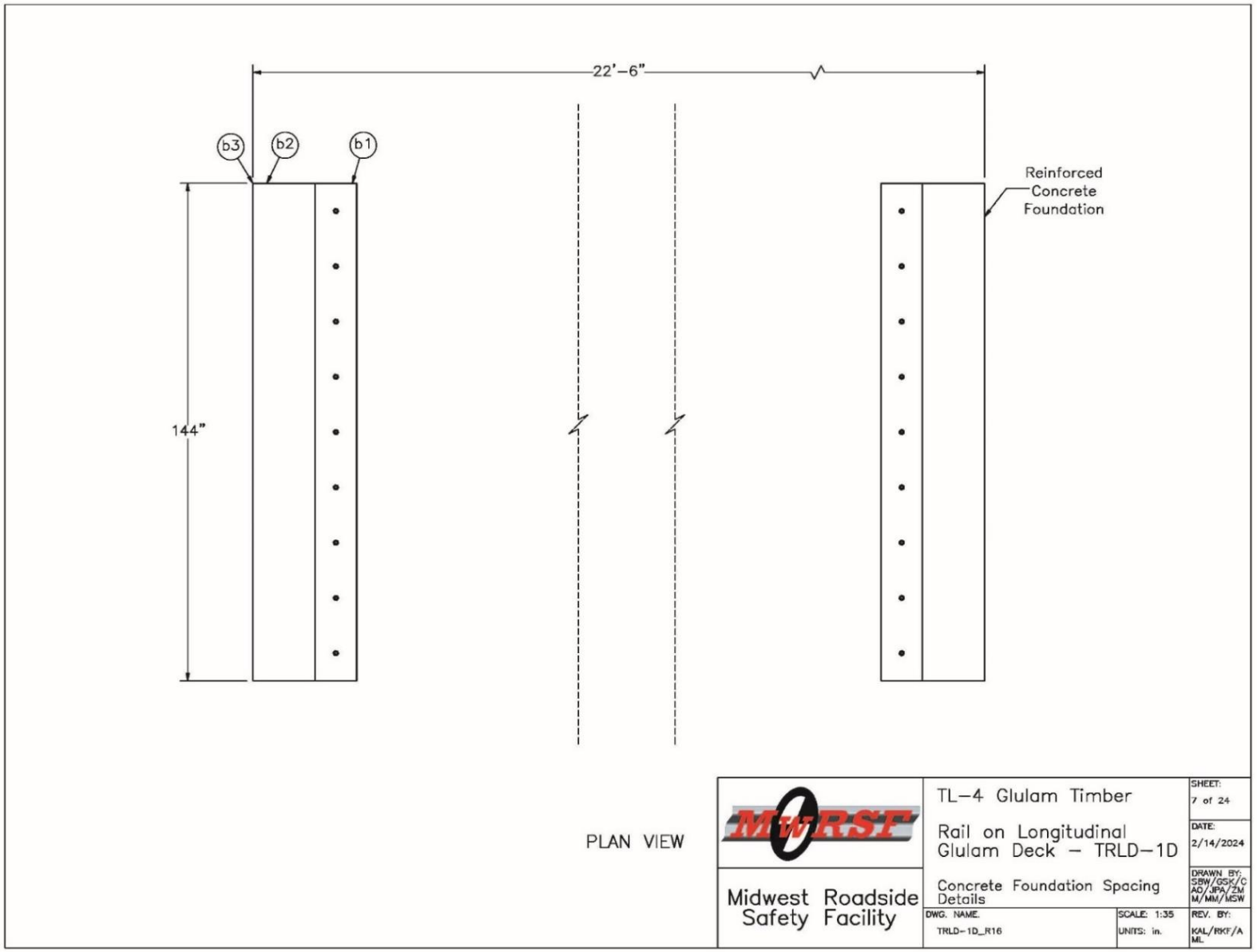

Figure 249. Foundation Layout, Test No. TRLD-1

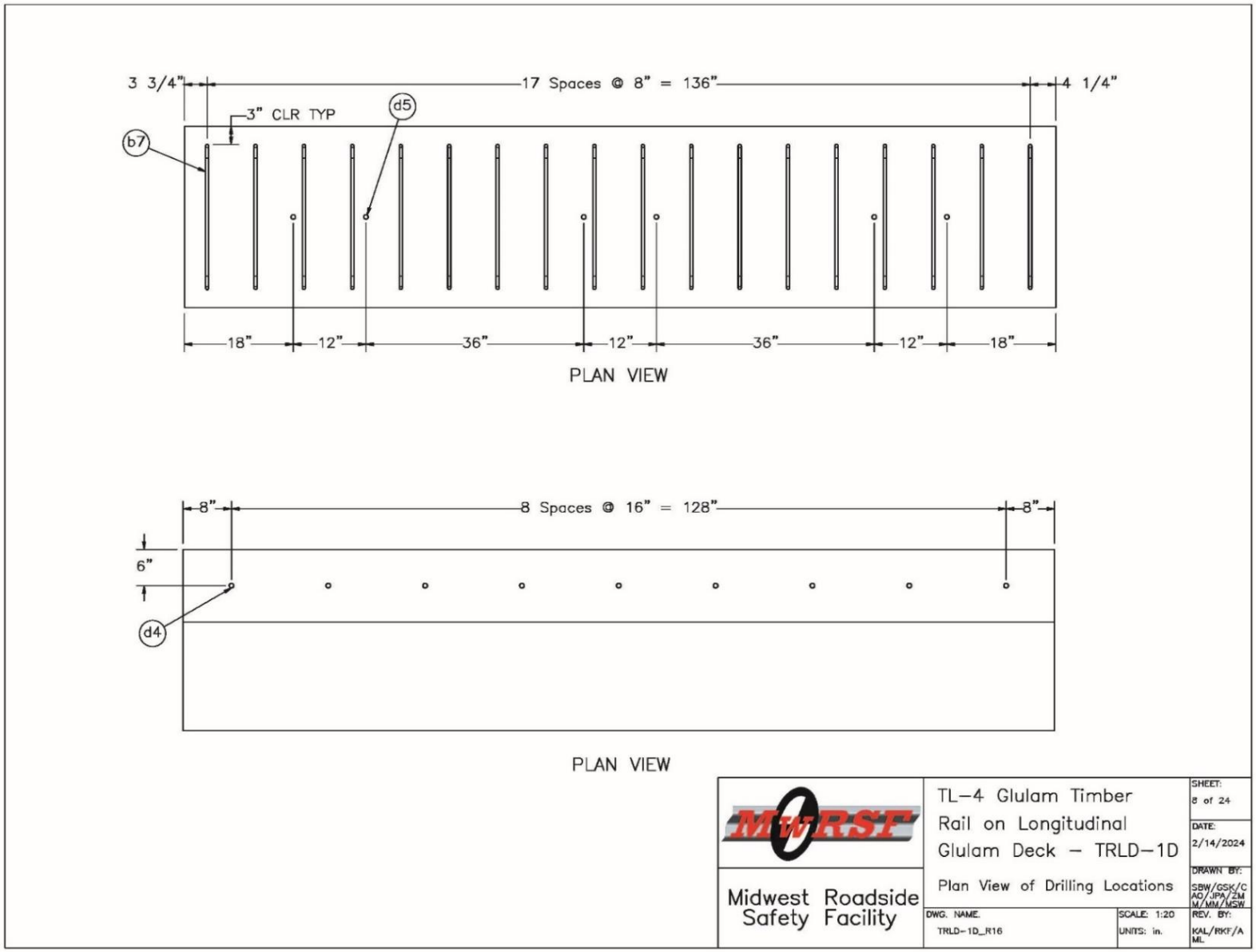

Figure 250. Layout of Existing Rebar and Embedded Rods in Foundation, Test No. TRLD-1

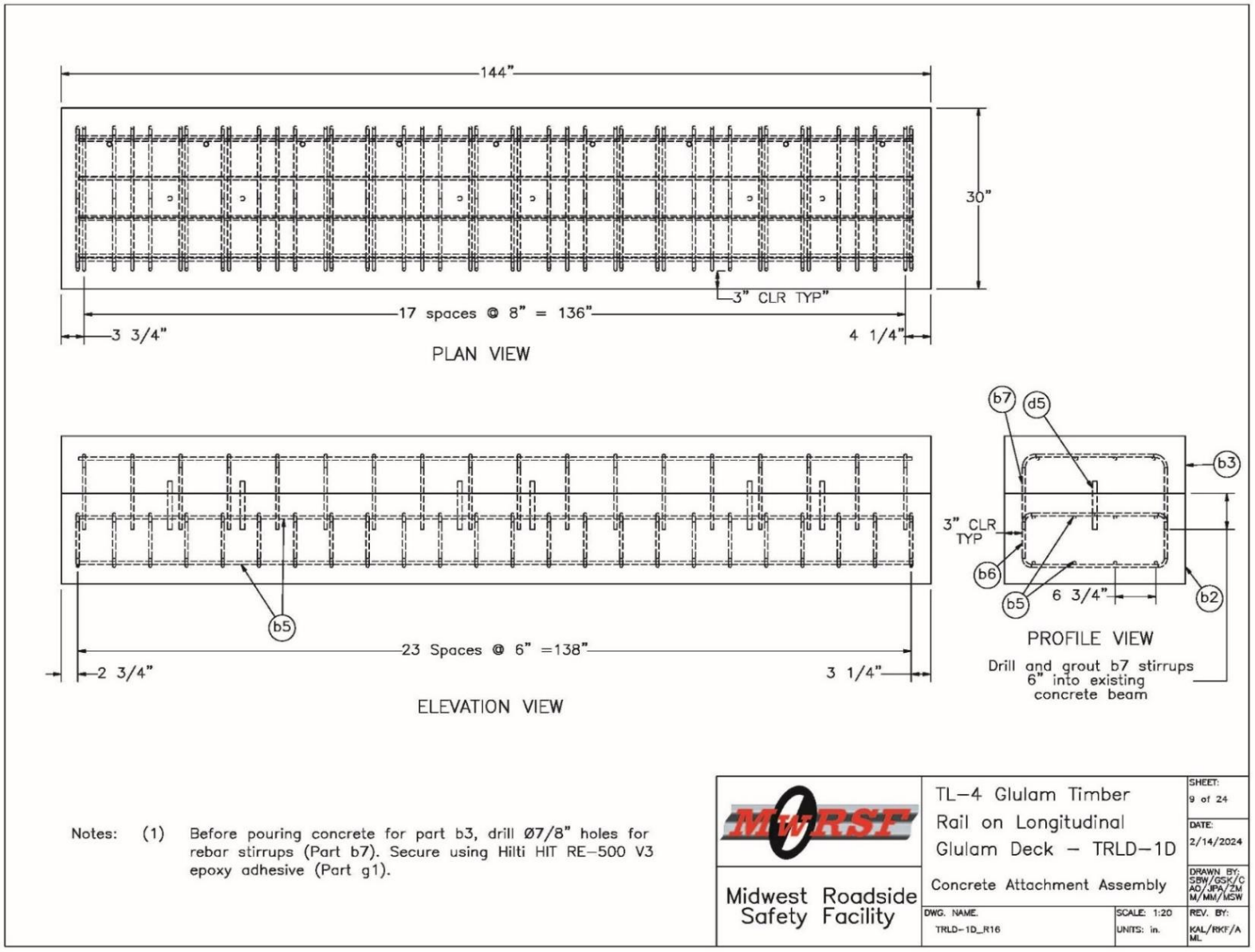

Figure 251. Rebar Layout, Test No. TRLD-1

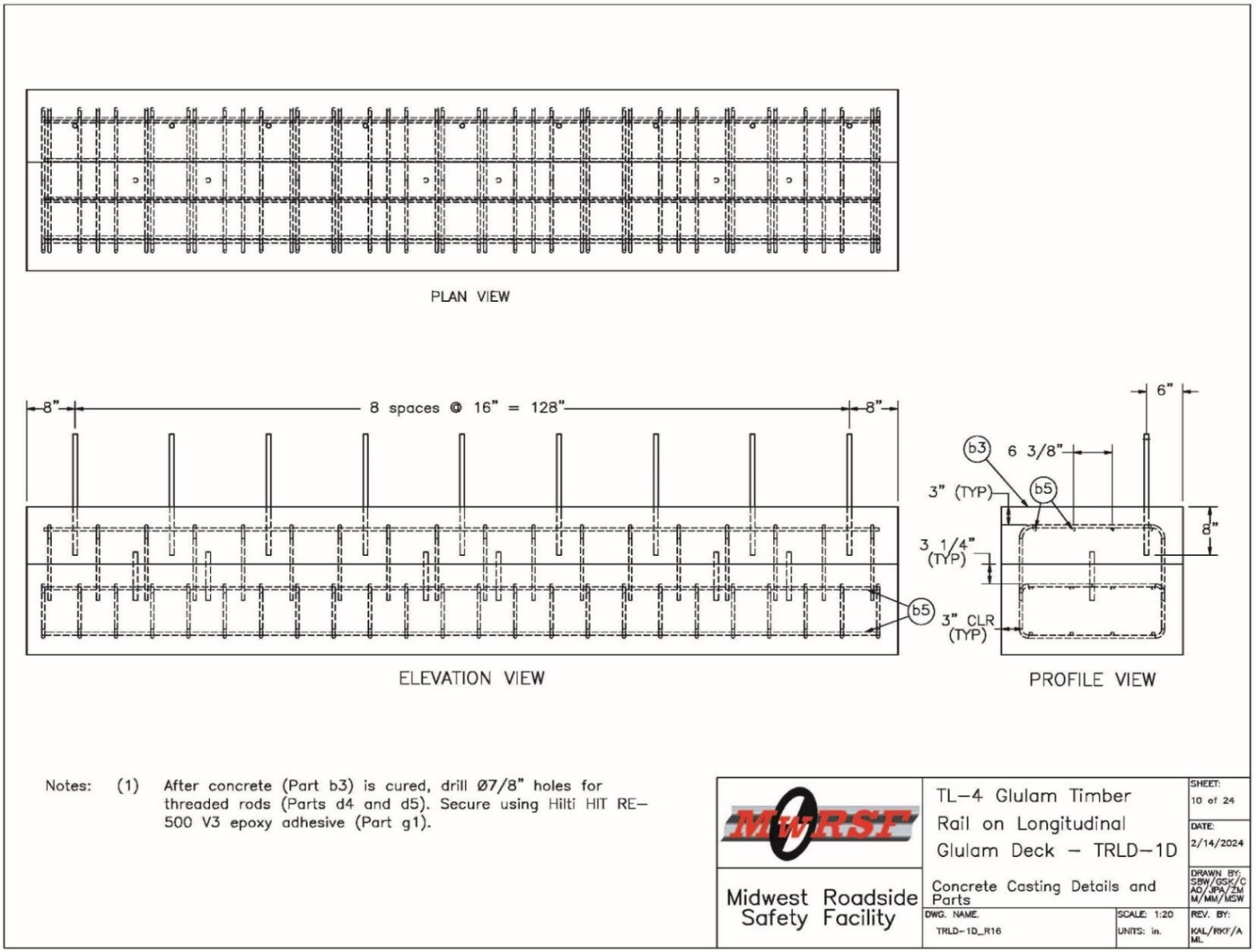

Figure 252. Rebar Layout with Embedded Rods, Test No. TRLD-1

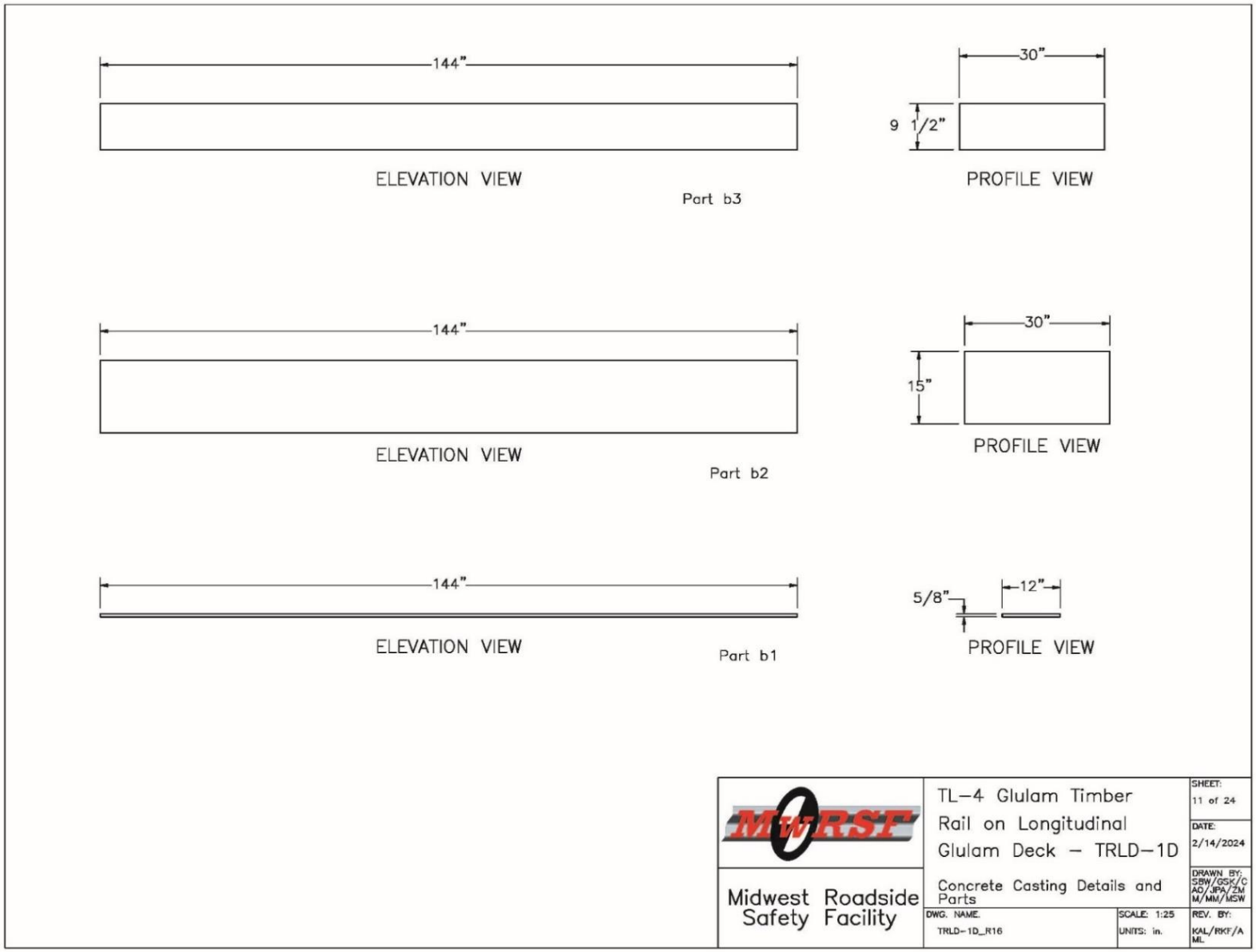

Figure 253. Concrete Details, Test No. TRLD-1

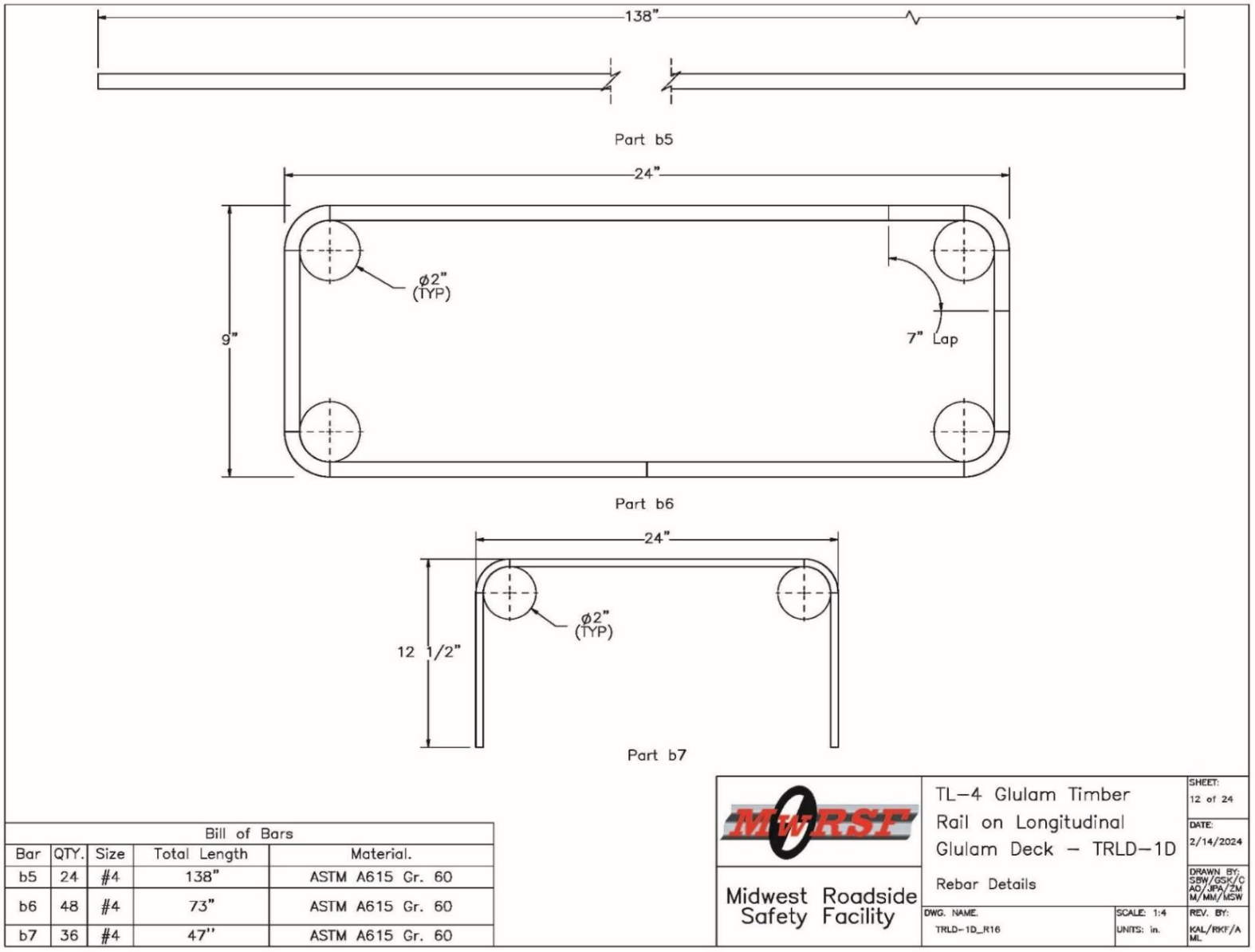

Bill of Bars				
Bar	QTY.	Size	Total Length	Material.
b5	24	#4	138"	ASTM A615 Gr. 60
b6	48	#4	73"	ASTM A615 Gr. 60
b7	36	#4	47''	ASTM A615 Gr. 60

Midwest Roadside Safety Facility

TL-4 Glulam Timber Rail on Longitudinal Glulam Deck – TRLD-1D

Rebar Details

SHEET: 12 of 24
DATE: 2/14/2024
DRAWN BY: SBW/GSK/CAO/JPA/ZMM/MM/MSW
REV. BY: KAL/RKF/AML
DWG. NAME. TRLD-1D_R16
SCALE: 1:4
UNITS: in.

Figure 254. Rebar Details, Test No. TRLD-1

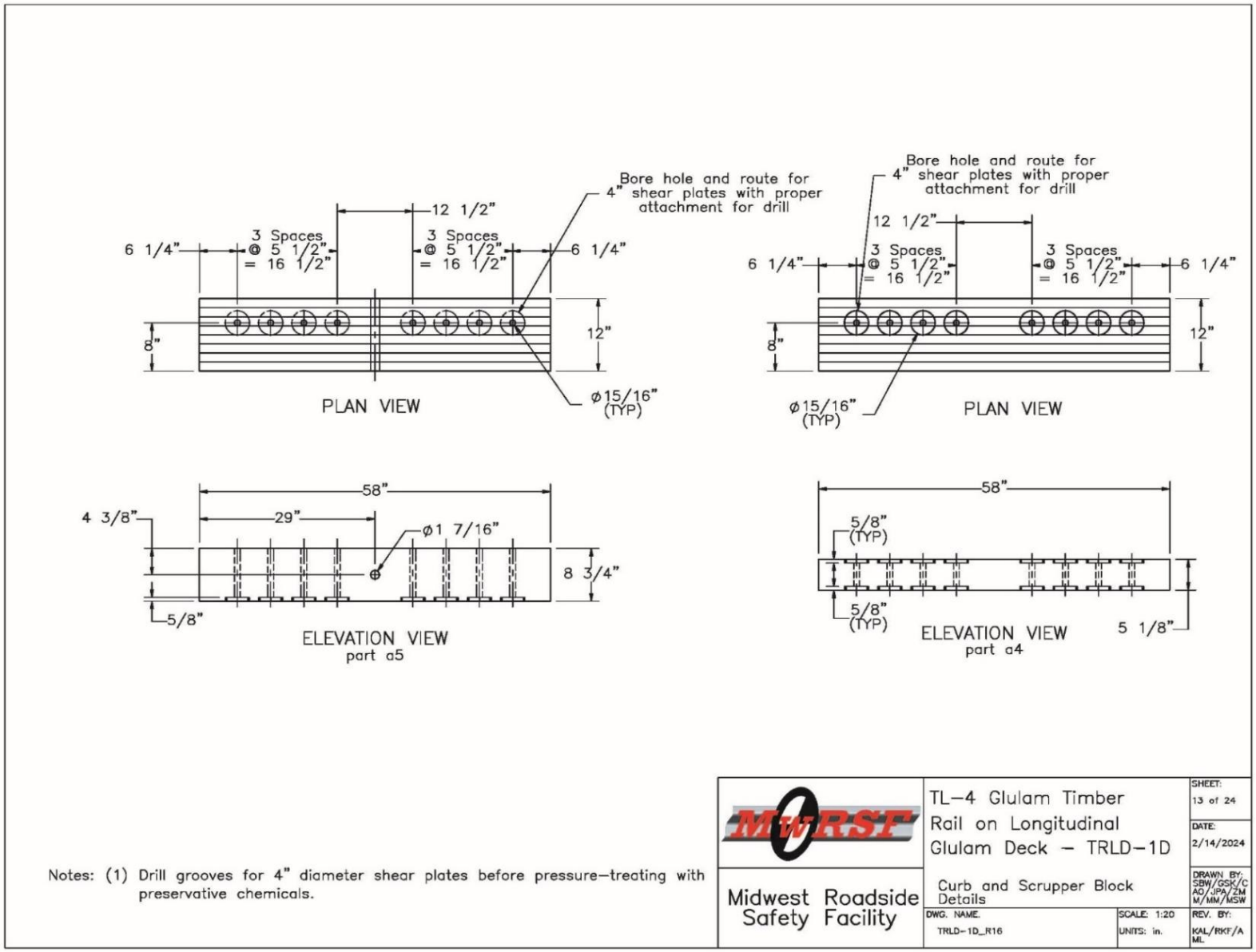

Figure 255. Scupper and Curb Rail Details, Test No. TRLD-1

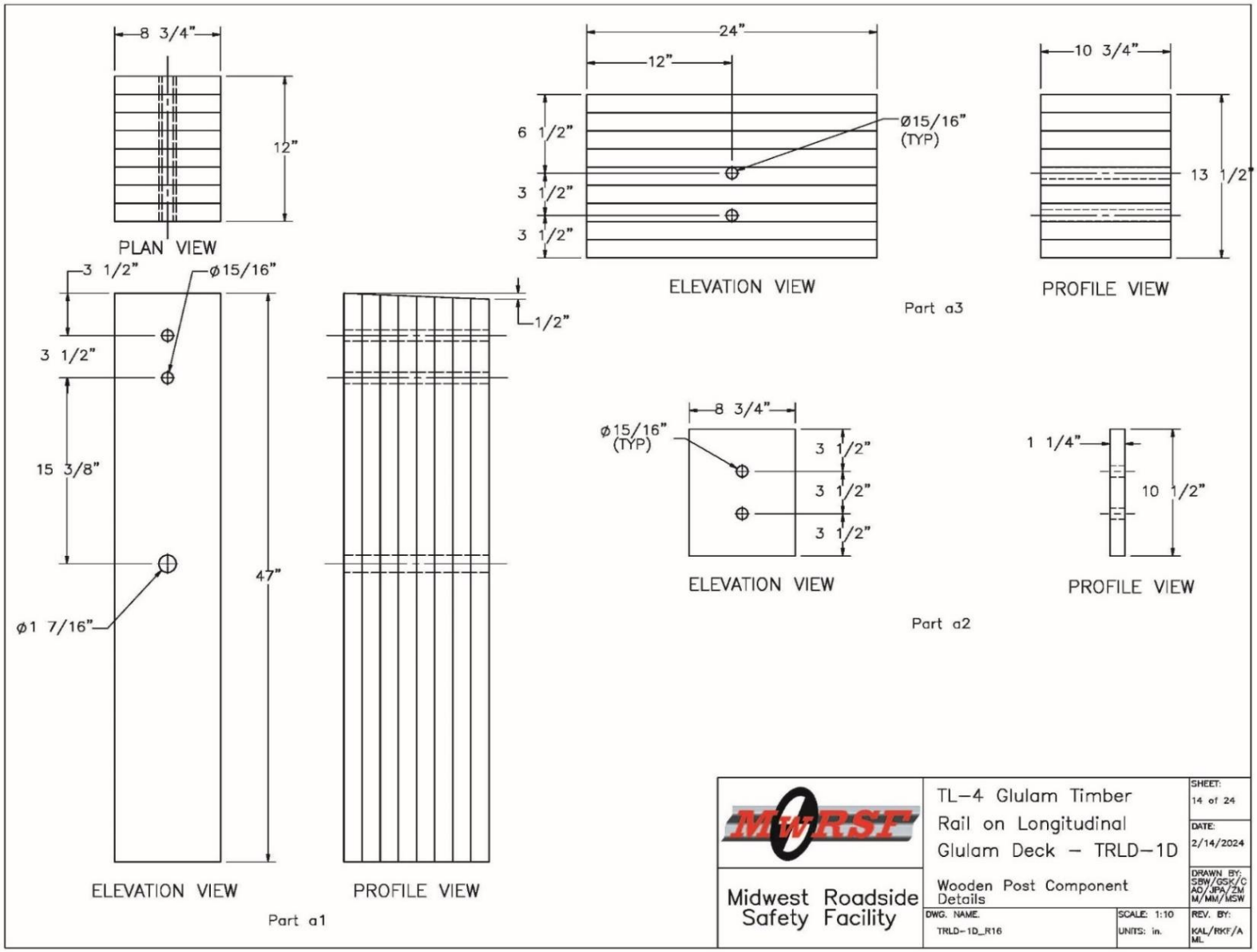

Figure 256. Vertical Post, Upper Rail, Blockout, and Angle Guide Details, Test No. TRLD-1

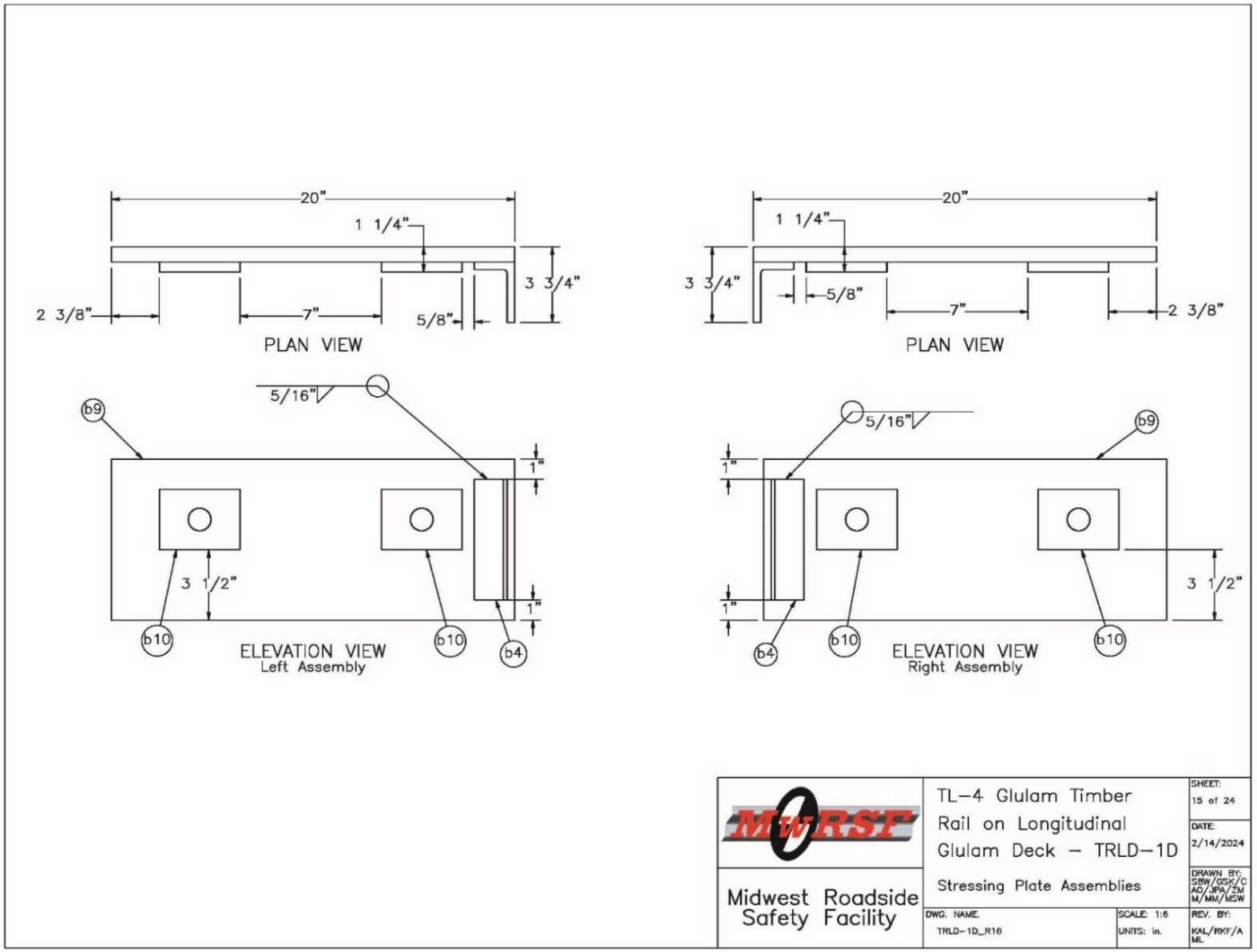

Figure 257. Stressing Plate Assembly Details, Test No. TRLD-1

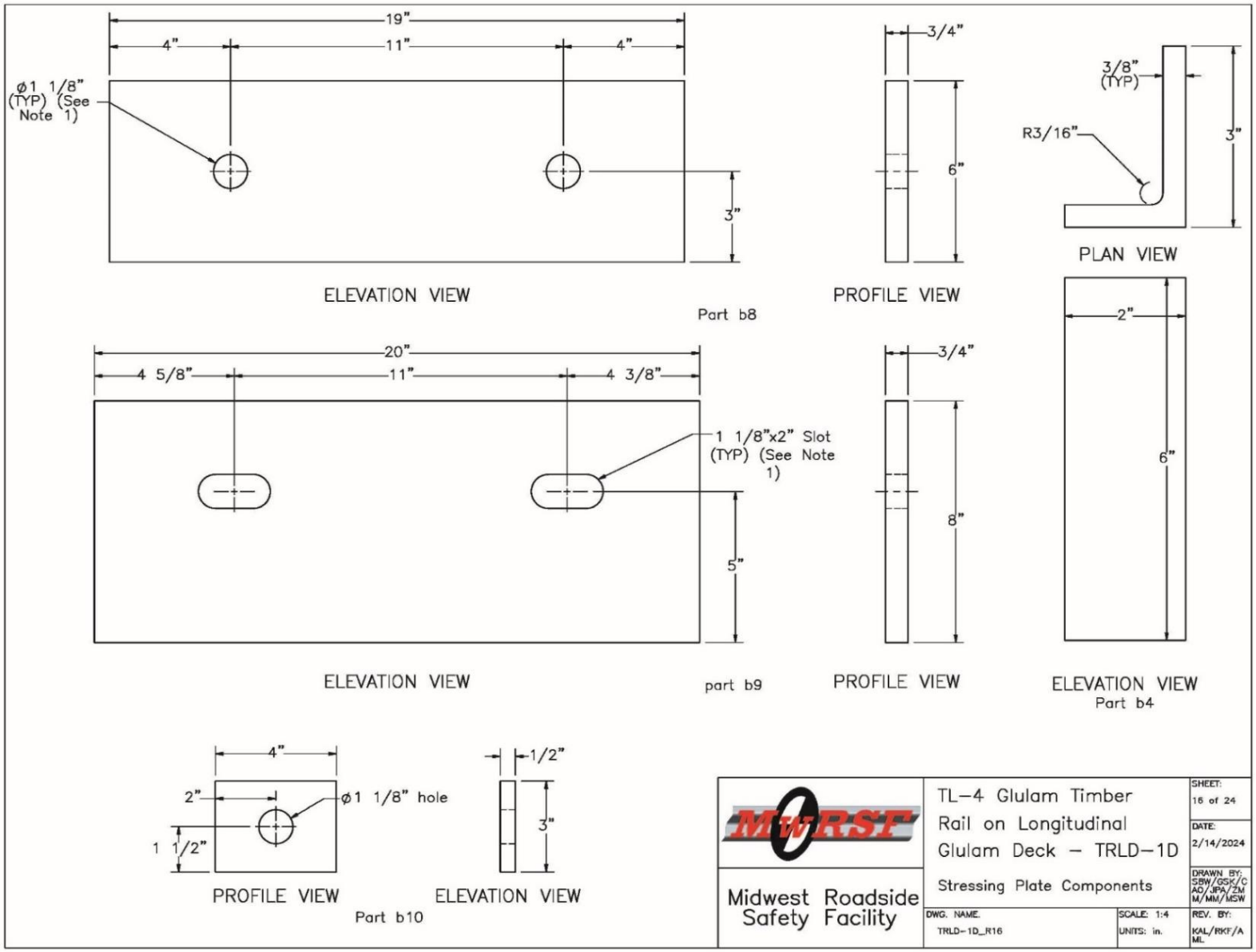

Figure 258. Stressing Plate Assembly Component Details, Test No. TRLD-1

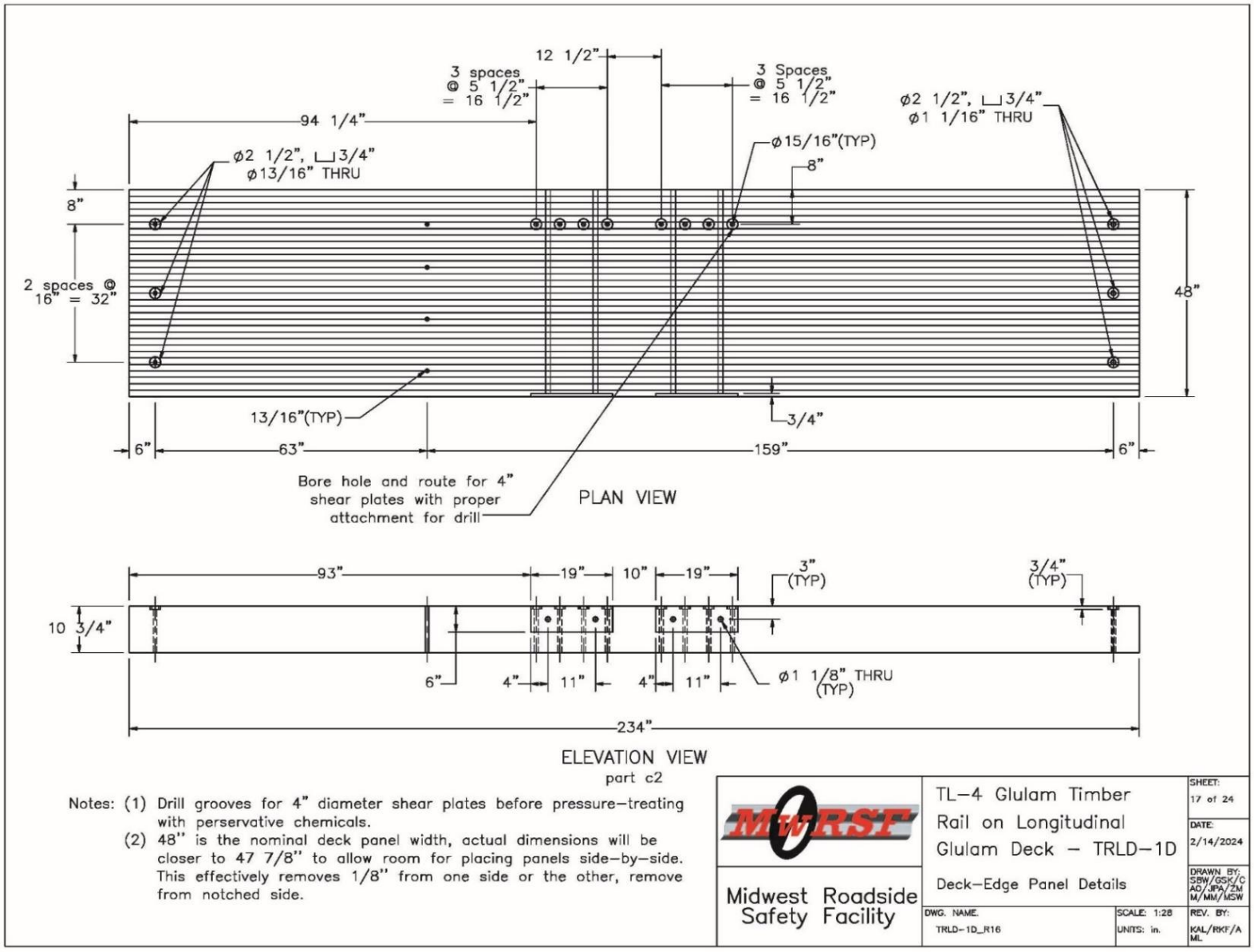

Figure 259. Deck Panel 1 Details, Test No. TRLD-1

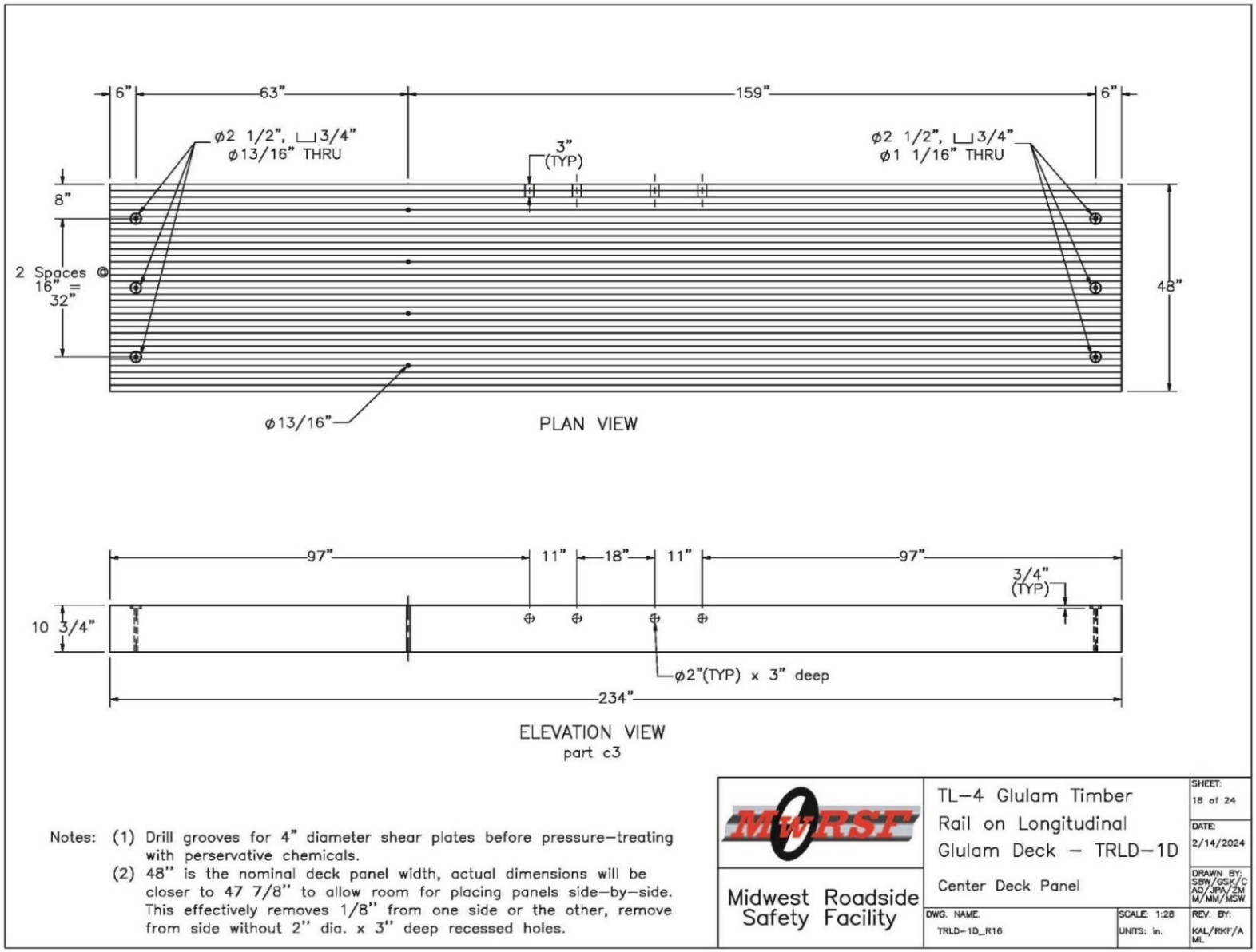

Figure 260. Deck Panel 2 Details, Test No. TRLD-1

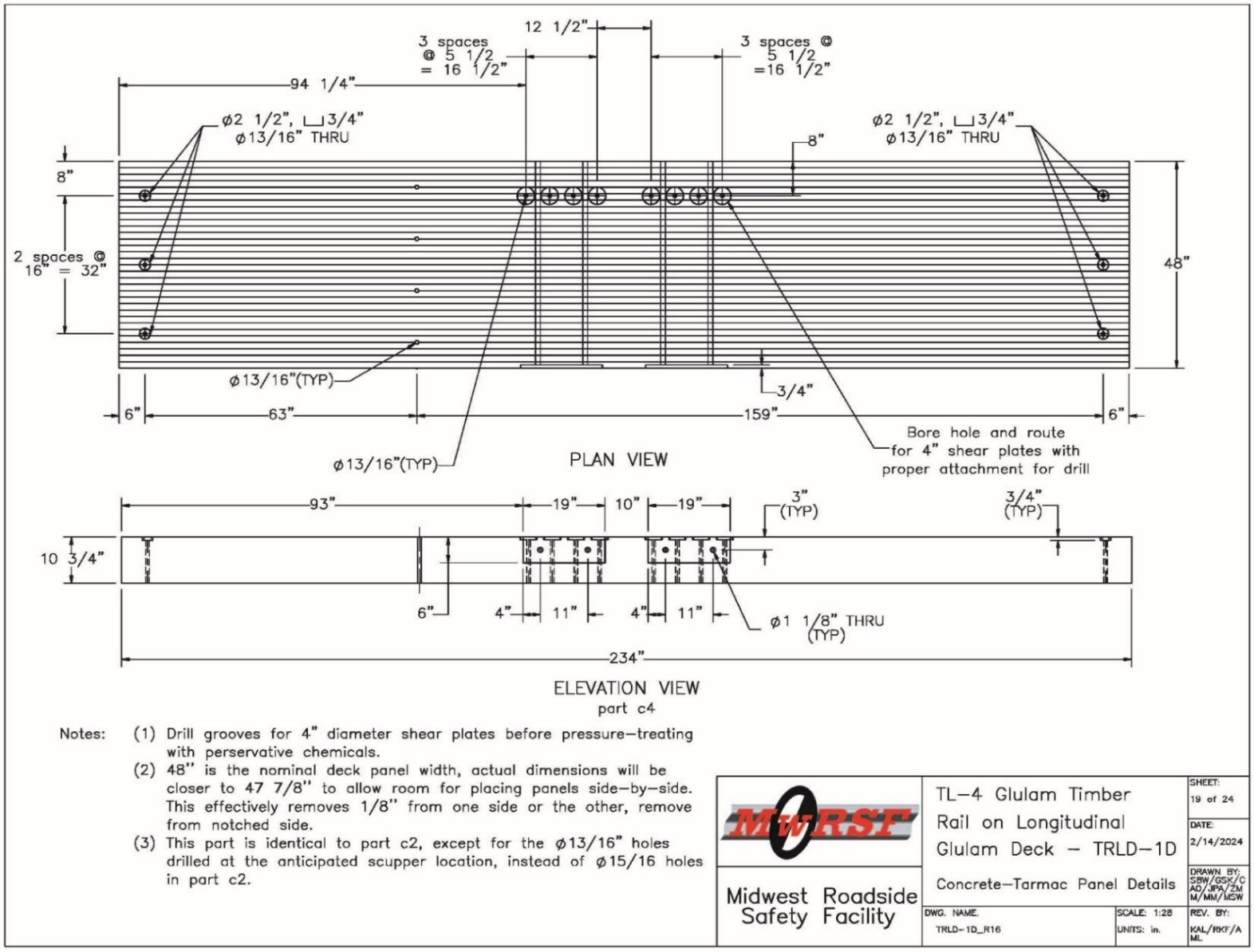

Figure 261. Deck Panel 1 Details, Test No. TRLD-1

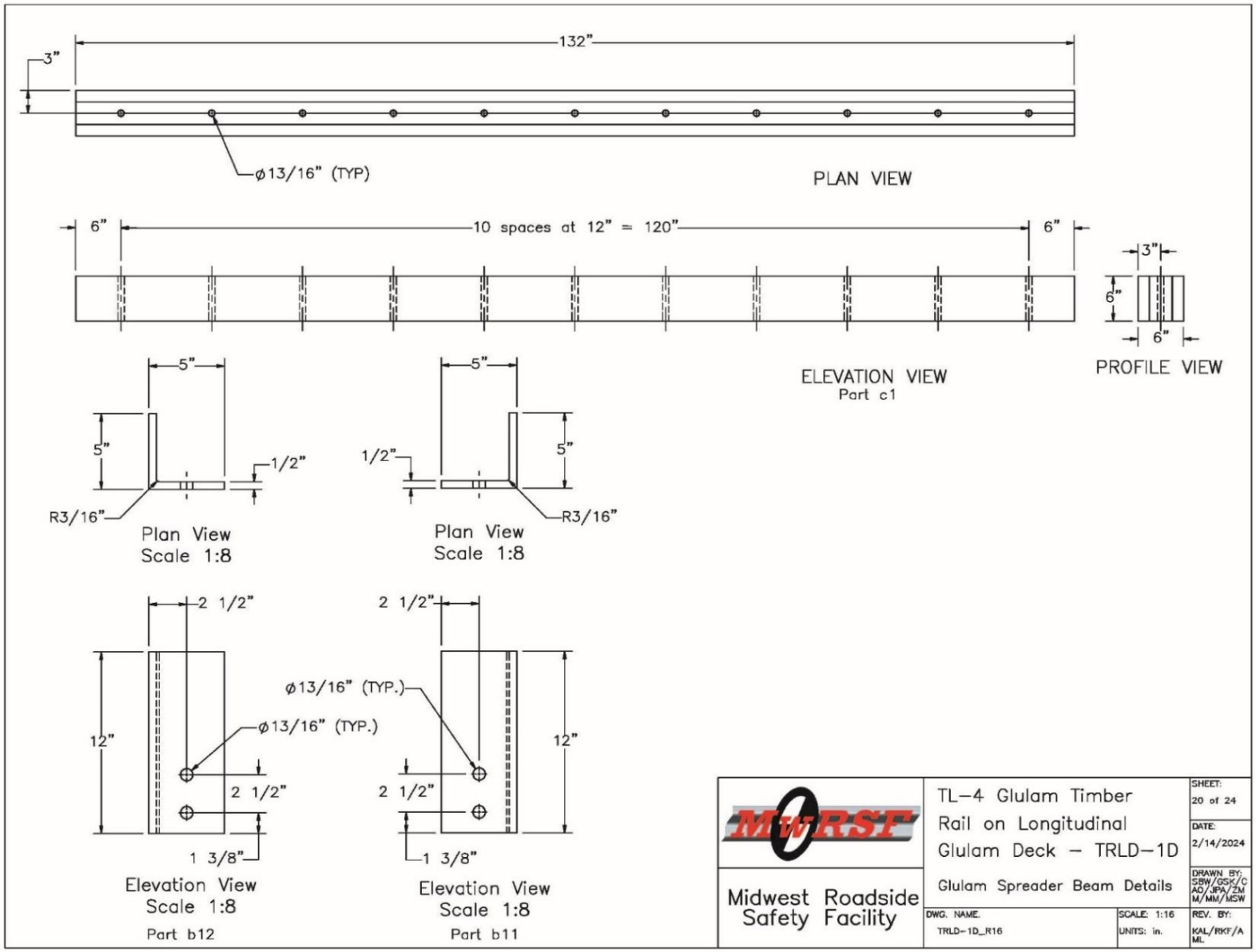

Figure 262. Spreader Beam and Deck Panel Edge Hardware Details, Test No. TRLD-1

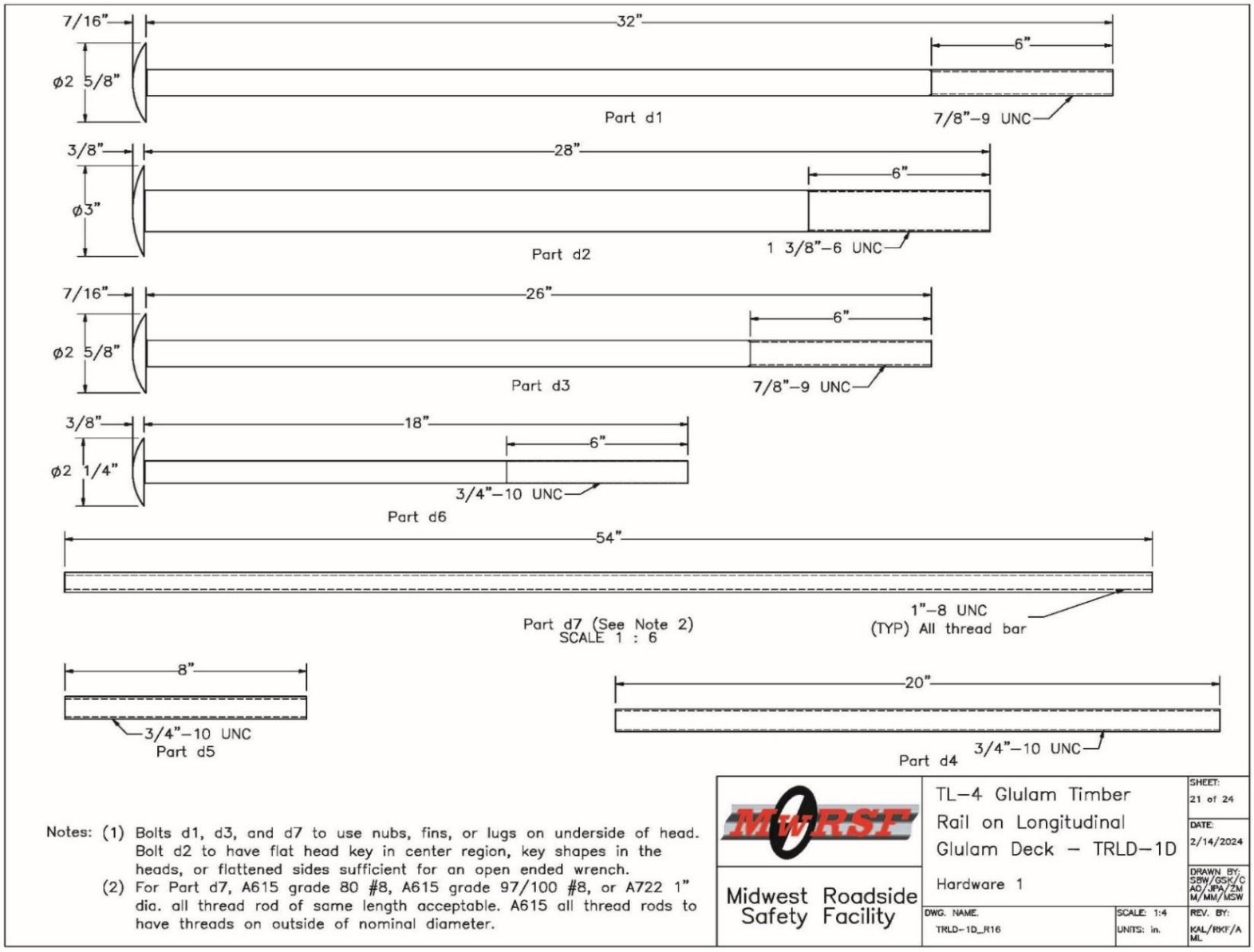

Figure 263. Bolt and Rod Hardware Details, Test No. TRLD-1

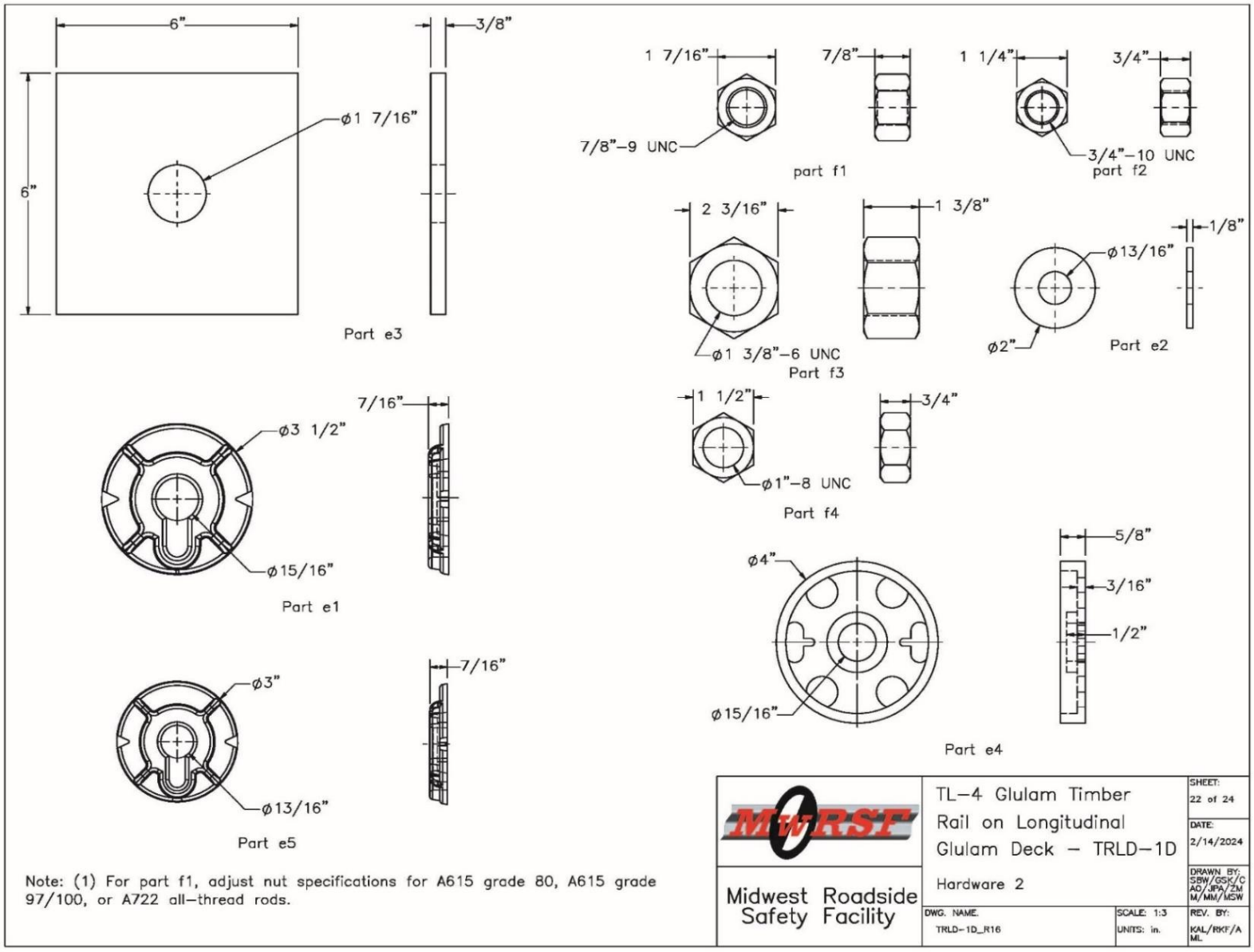

Figure 264. Washer and Nut Connection Hardware Details, Test No. TRLD-1

Item No.	QTY.	Description	Material Specification	Treatment Specification	Hardware Guide
–	1	4" Thick Surrogate Wearing Surface	–	–	
a1	1	47"x12"x8 3/4" Glulam Post	Comb. 48 (SP) or Comb. 2 (Western Species)	See Notes 1–3	–
a2	1	1 1/4"x10 1/2"x8 3/4" Blockout	Comb. 48 (SP) or Comb. 2 (Western Species)	See Notes 1–3	–
a3	1	24"x13 1/2"x10 3/4" Glulam Upper Rail	Comb. 48 (SP) or Comb. 2 (Western Species)	See Notes 1–3	–
a4	2	58"x12"x5 1/8" Glulam Scupper Block	Comb. 48 (SP) or Comb. 2 (Western Species)	See Notes 1–3	–
a5	1	58"x12"x8 3/4" Glulam Curb Rail	Comb. 48 (SP) or Comb. 2 (Western Species)	See Notes 1–3	–
b1	2	1'x12'x5/8" Elastomeric Bearing Pad	Neoprene – Min. 50 Durameter	–	–
b2	2	15"x30"x12' Concrete Support (Existing Material)	Min f'c = 4,000 psi NE mix 47 BD	–	–
b3	2	12'x30"x9 1/2" Concrete Cap	Min f'c = 4,000 psi NE mix 47 BD	–	–
b4	2	3"x2"x3/8" Thick, 6" Long Steel Angle	ASTM A36	ASTM A123	–
b5	24	#4 Rebar, 138" Long (8 new, 16 existing)	ASTM A615 Gr. 60	Epoxy Coated (ASTM A775 or A934)	–
b6	48	#4 Rebar, 73" Unbent Length (Existing Material)	ASTM A615 Gr. 60	Epoxy Coated (ASTM A775 or A934)	–
b7	36	#4 Rebar, 47'' Unbent Length	ASTM A615 Gr. 60	Epoxy Coated (ASTM A775 or A934)	–
b8	2	19"x6"x3/4" Steel Stressing Plates	ASTM A36	ASTM A123	–
b9	2	20"x8"x3/4" Steel Stressing Plate	ASTM A36	ASTM A123	–
b10	4	3"x4"x1/2" Steel Anchor Plate	ASTM A36	ASTM A123	–
b11	1	5"x5"x1/2" Thick, 12" Long Steel Angle	ASTM A36	ASTM A123	–
b12	1	5"x5"x1/2" Thick, 12" Long Steel Angle	ASTM A36	ASTM A123	–

Notes:
(1) Timber rails, posts, scuppers, and blockouts shall be treated with Copper Naphthenate (CuN) or 4,5–Dichloro–2–N–Octyl–4–Isothiazolin–3–One(DCOI), in heavy oil to a minimum retention of 0.075 lbs /cu. ft. or 0.20 lbs/cu. ft. respectively in accordance with AWPA Standard U1 to the requirements. Use category 4C (UC4C).
(2) Wood shall be cut, drilled, and completely fabricated prior to treatment with preservative. Drain excess chemicals and dry all treated wood at the place of manufacture.
(3) All field cuts, bore holes, and damages shall be treated with material acceptable to the engineer prior to installation.

Midwest Roadside Safety Facility

TL–4 Glulam Timber Rail on Longitudinal Glulam Deck – TRLD–1D

Bill of Materials

SHEET: 23 of 24
DATE: 2/14/2024
DRAWN BY: SBW/GSK/CAO/JPA/ZMM/MM/MSW
REV. BY: KAL/RKF/AML
DWG. NAME. TRLD-1D_R16
SCALE: None
UNITS: in.

Figure 265. Bill of Materials, Page 1, Test No. TRLD-1

Item No.	QTY.	Description	Material Specification	Treatment Specification	Hardware Guide
c1	1	6"x6"x11' Glulam Spreader Beam	Comb. 48 (SP) or Comb. 2 (Western Species)	See Notes 1–3	–
c2	2	19.5'x4'x10 3/4" Long Glulam Edge Panel	Comb. 48 (SP) or Comb. 2 (Western Species)	See Notes 1–3	–
c3	1	19.5'x4'x10 3/4" Long Glulam Center Panel	Comb. 48 (SP) or Comb. 2 (Western Species)	See Notes 1–3	–
c4	2	19.5'x4'x10 3/4" Long Glulam Edge Panel	Comb. 48 (SP) or Comb. 2 (Western Species)	See Notes 1–3	–
d1	8	7/8"–9 UNC x 32" Timber Bolt w/ Nubs	ASTM A307A	ASTM A123	FBB08
d2	1	1 3/8"–6 UNC x 28" Timber Bolt w/o Nubs	ASTM A449	ASTM A123	FBB08
d3	2	7/8"–9 UNC x 26" Timber Bolt w/ Nubs	ASTM A307A	ASTM A123	FBB08
d4	18	3/4"–10 UNC x 20" Threaded Rod	ASTM A193 Gr. B7 or SAE J429 Gr.5	ASTM A123	FRR20a
d5	16	3/4"–10 UNC x 8" Threaded Rod (4 new, 12 existing)	ASTM A193 Gr. B7 or SAE J429 Gr. 5	ASTM A123	FRR20a
d6	11	3/4"–10 UNC x 18" Timber Bolt w/Nubs	ASTM A307A	ASTM A123	FBB08
d7	4	1"–8 UNC x 54" Long All Thread Stressing Rod	ASTM A193 Gr. B7 or SAE J429 Gr.5	ASTM A123	FRR24a
e1	10	7/8" Dia. Malleable Iron Washer	ASTM A47	ASTM A123	–
e2	4	3/4" Flat Washer	ASTM F844	ASTM A123 or A153 or F2329	FWC20a
e3	2	6"x6"x3/8" Steel Plate Washer	ASTM A36	ASTM A123	–
e4	48	4" Dia, 5/8" Thick Shear Plate	ASTM A47 Grade 32510	Hot–Dip	12405
e5	11	3/4" Dia. Malleable Iron Washer	ASTM A47	ASTM A123	–
f1	10	7/8"–9 UNC Heavy Hex Nut	ASTM A563A	ASTM A123	FNX22b
f2	31	3/4"–10 UNC Heavy Hex Nut	ASTM A563A	ASTM A123	FNX20b
f3	1	1 3/8"–6 UNC Heavy Hex Nut	ASTM A563A	ASTM A123 or A153 or F2329	–
f4	16	1"–8 UNC Heavy Hex Nut	ASTM A563A	ASTM A123	FNX24b
g1	–	Epoxy Adhesive	Hilti HIT RE–500 V3 or equivalent with min. bond strength 1670 psi	–	–

Midwest Roadside Safety Facility

TL–4 Glulam Timber Rail on Longitudinal Glulam Deck – TRLD–1D

Bill of Materials

SHEET: 24 of 24
DATE: 2/14/2024
DRAWN BY: SBW/GSK/CAO/JPA/ZM/MM/MSW
REV. BY: KAL/RKF/AML
DWG. NAME. TRLD-1D_R16
SCALE: 1:96
UNITS: in.

Figure 266. Bill of Materials, Page 2, Test No. TRLD-1

6.3 Future Research

Future development of timber bridge railings may benefit from improved modeling techniques, particularly because tensile splitting of the scupper blocks and curb rail was not explicitly considered. BARRIER VII does not capture the complex load distribution within the post configuration due to its limitation as a two-dimensional analysis tool. Although the connection design was relatively conservative, it has been challenging to determine the ultimate capacity for loading scenarios that were not included in physical testing. This limitation has remained a concern throughout the design process. Several simplifying assumptions were made in the design due to the time required for more detailed investigation. A comprehensive wood material model in LS-DYNA that can simulate crack initiation, crack propagation, wood splitting, and eventual component failure may serve as a useful tool for validating design performance with reduced reliance on full-scale testing. Another possible approach is to use Peridynamic modeling to evaluate whether and how cracks may develop and propagate in critical components.

In addition to developing new methods of analysis, future research has also targeted multiple additional timber bridge railings and approach guardrail transitions according to the priorities developed in TRP-03-429-20-R1 [9].

7 REFERENCES

1. Ross, H.E., Sicking, D.L., Zimmer, R.A., and Michie, J.D., *Recommended Procedures for the Safety Performance Evaluation of Highway Features*, National Cooperative Highway Research Program (NCHRP) Report 350, Transportation Research Board, Washington, D.C., 1993.

2. *Guide Specifications for Bridge Railings*, American Association of State Highway and Transportation Officials (AASHTO), Washington, D.C., 1989.

3. *Manual for Assessing Safety Hardware (MASH)*, American Association of State Highway and Transportation Officials (AASHTO), Washington, D.C., 2009.

4. *Manual for Assessing Safety Hardware (MASH), Second Edition*, American Association of State Highway and Transportation Officials (AASHTO), Washington, D.C., 2016.

5. Rosenbaugh, S.K., Benner, C.D., Faller, R.K., Bielenberg, R.W., Reid, J.D., and Sicking, D.L., *Development of a TL-1 Timber, Curb-Type, Bridge Railing for Use on Transverse, Nail-Laminated, Timber Bridges*, Final Report to the West Virginia Department of Transportation, Transportation Research Report No. TRP-03-211-09, Project No.: WV-09-2007-B1, Sponsor Agency Code: SPR-3(017) Supplement #53, Midwest Roadside Safety Facility, University of Nebraska-Lincoln, May 6, 2009.

6. Mongiardini, M, Rosenbaugh, S.K., Faller, R.K., Reid, J.D., Bielenberg, R.W., and Sicking, D.L., *Design and Testing of Two Bridge Railings for Transverse, Nail-Laminated, Timber Deck Bridges*, Paper No. 11-2936, Transportation Research Record No. 2262, Journal of the Transportation Research Board, TRB AFB20 Committee on Roadside Safety Design, Transportation Research Board, Washington D.C., January 2011.

7. Masterson, R.W., Faller R.K., Rosenbaugh, S.K., Bielenberg, R.W., Steelman, J.S., Duren, J.T., and Yosef, T.Y., *Adaptation and Development of a MASH TL-1 Low-Height, Glulam Timber Bridge Railing for Use on Transverse Glulam Decks*, Report No. TRP-03-467-23-R1, Midwest Roadside Safety Facility, University of Nebraska-Lincoln, Lincoln, Nebraska, September 8, 2023.

8. Williams, W.F., *W-Beam Bridge Rail for Temporary Timber Deck Bridge Installations*, Memorandum, TM-405160-40, Texas A&M Transportation Institute, College Station, TX. August 2013.

9. Duren, J.T., and Faller, R.K., *Crash-Tested Bridge Railings and Transitions for Wood Bridges – Phase I*, Final Report to the United States Department of Agriculture-Forest Service-Forest Products Laboratory, Transportation Report No. TRP-03-429-20-R1, Midwest Roadside Safety Facility, University of Nebraska-Lincoln, Lincoln, Nebraska, July 2020.

10. Duren, J.T., *Prioritization of Research on Bridge Railings for Use on Timber Deck Bridges and Development of Two Glulam Bridge Railing Systems*, Thesis, University of Nebraska – Lincoln, July 2021.

11. Duren, J.T., Faller, R.K., Yosef, T.Y., Bielenberg. R.W., Rosenbaugh, S.K., and Steelman, J.S., *Crash-Tested Bridge Railings and Transitions for Wood Bridges*, Report No. TRP-03-465-23, Midwest Roadside Safety Facility, University of Nebraska-Lincoln, Lincoln, Nebraska, March 20, 2023.

12. Powell, G.H., *Computer Evaluation of Automobile Barrier Systems*, Report No. FHWA-RD-73-73, FHWA, August 1970.

13. Powell, G.H., *BARRIER VII: A Computer Program for Evaluation of Automobile Barrier Systems*, Report No. FHWA-RD-73-51, FHWA, U.S. Department of Transportation, April 1973.

14. *National Design Specification Supplement*, 2018 Edition, Third Electronic Version, NASI/AWC NDS-2018, American Wood Council, April 2019.

15. *AASHTO LRFD Bridge Design Specifications, 9th Edition*, American Association of State Highway and Transportation Officials (AASHTO), Washington, D.C., 2020.

16. Hitz, R.A., Polivka, K.A., Faller, R.K., Ritter, M.A., Rosson, B.T., and Holloway, J.C., *Development of the GC-8000 Bridge Railing and Transition*, Report No. TRP-03-161-06, Midwest Roadside Safety Facility, University of Nebraska-Lincoln, Lincoln, Nebraska, May 2, 2006.

17. Faller, R.K., Ritter, M.A., Holloway, J.C., Pfeifer, B.G., and Rosson, B.T., *Performance Level 1 Bridge Railings for Timber Decks*, Transportation Research Record 1419, TRB, National Research Council, Washington D.C., October 1993, pp.21-34.

18. Ritter, M.A., Faller, R.K., Holloway, J.C., Pfeifer, B.G., and Rosson, B.T., *Development and Testing of Bridge Railings for Longitudinal Timber Decks by Full-Scale Crash Testing*, Draft Report to the U.S. Department of Agriculture, Forest Service, Forest Products Laboratory, Transportation Research Report No. TRP-03-29-94, Civil Engineering Department, University of Nebraska-Lincoln, August 1992.

19. Polivka, K.A., Faller, R.K., Ritter, M.A., and Rosson, B.T., *Development of the TBC-8000 Bridge Railing*, Draft Report to the U.S. Department of Agriculture, Forest Service, Forest Service, Forest Products Laboratory, Report No. TRP-03-30-93, Midwest Roadside Safety Facility, Civil Engineering Department, University of Nebraska-Lincoln, September 5, 2000.

20. Mak, K.K., and Campise, W.L., *Testing and Evaluation of Missouri Thrie-Beam Bridge Rail System and Transition*, Final Report to the Missouri Highway and Transportation Department, Final Report No. 87-4, Texas Transportation Institute, Texas A&M University, College Station, Texas, May 1988.

21. Faller, R.K., and Rosson, B.T., *Crashworthy Barriers for Timber Bridges*, 18th Annual Structural Conference – Engineered Wood Systems, Sponsored by the University of Nebraska-Lincoln and the American Society of Civil Engineers Nebraska Section, Kiewit Conference Center, Omaha, Nebraska, October 2, 1998.

22. Ritter, M.A., Faller, R.K., and Duwadi, S.R., *Crashworthy Railing for Timber Bridges*, Proceedings of the 1999 Pacific Timber Engineering Conference (PTEC), Rotorua, New Zealand, March 14-18, 1999, New Zealand Forest Research Institute, Forest Service Research Bulletin No. 212, Volume 3: 325-332.

23. Faller, R.K., Rosson, B.T., Ritter, M.A., and Duwadi, S.R., *Railing Systems for use of Timber Deck Bridges*, Transportation Research Record No. 1656, Journal of the Transportation Research Board, Transportation Research Board, Washington, D.C., July 1999, 110-119.

24. Faller, R.K., Ritter, M.A., Rosson, B.T., Fowler, M.D., and Duwadi, S.R., *Two Test Level 4 Bridge Railing and Transition Systems for Transverse Timber Deck Bridges*, Paper No. 5B0110, Transportation Research Record No. 1696, Journal of the Transportation Research Board Volume 1, Fifth International Bridge Engineering Conference, Tampa, Florida, April 3-5, 2000, Transportation Research Board, Washington, D.C., 334-351.

25. Polivka, K.A., Faller R.K., Ritter, M.A., Rosson, B.T., Fowler, M.D., and Keller, E.A., *Two Test Level 4 Bridge Railing and Transition Systems for Transverse Glue-Laminated Timber Decks*, Report No. TRP-03-71-01, Midwest Roadside Safety Facility, University of Nebraska-Lincoln, Lincoln, Nebraska, January 30, 2002.

26. Lund, B.A., and Pezzucchi, M.S., *Development of a New Barrier System for Stress Laminated Road Bridge Decks*, Conference Proceedings International Conference on Timber Bridges, September 2010.

27. *European Standard EN 1317-2:1998 – Road restraint systems – Part 2: Performance classes, impact test acceptance criteria and test methods for safety*, CEN European Committee for Standardization, Brussels, Belgium, June 2006.

28. *Träbroräcke Z B4-20*, AB Varmförzinkning, Norwegian Public Roads Administration, Available: https://www.vegvesen.no/fag/teknologi/vegutstyr/rekkverk/zb4-20-h2-2m/, July 22, 2024.

29. *Road restraint systems - Part 5: Product requirements and evaluation of conformity for vehicle restraint systems*, Certification 0402-CPR-SC0266-11, Issue 6, RISE Research Institutes of Sweden AB, February 12, 2020.

30. *Products Roadside Protection Z Tubeprofile B4*, AB Varmförzinkning, Available: https://www.varmforzinkning.se/en/roadside-protection/z-tubular-profiles/z-tubeprofile-b4/, July 23, 2024.

31. Forest Product Laboratory, *Plans for Crash-Tested Wood Bridge Railings for Concrete Decks*, General Technical Report No. FPL-GTR-108, United State Department of Agriculture – Forest Service – Forest Products Laboratory and Federal Highway Administration, August 1998.

32. Wacker, J.P., and Smith, M.W., *Standard Plans for Glued-Laminated Timber Bridge Superstructures: Longitudinal Glulam Decks, Stress-Laminated Glulam Decks, Glulam Stringer Bridges, and Transverse Glulam Decks*, General Technical Report No. FPL-GTR-260, United States Department of Agriculture – Forest Service – Forest Products Laboratory and Federal Highway Administration, November 2019.

33. Michie, J.D., *Recommended Procedures for the Safety Performance Evaluation of Highway Appurtenances*, National Cooperative Highway Research Program (NCHRP) Report No. 230, Transportation Research Board, Washington, D.C., March 1981.

34. Polivka, K.A., Faller, R.K., Sicking, D.L., Reid, J.D., Rohde, J.R., and Holloway, J.C., *Crash Testing of Missouri's W-Beam to Thrie-Beam Transition Element*, Report No. TRP-03-94-00, Midwest Roadside Safety Facility, University of Nebraska-Lincoln, Lincoln, Nebraska, September 12, 2000.

35. Eller, C.M., Polivka, K.A., Faller, R.K., Sicking, D.L., Rohde, J.R., Reid, J.D., Bielenberg, R.W., and Allison, E.M., *Development of the Midwest Guardrail System (MGS) W-Beam to Thrie Beam Transition Element*, Report No. TRP-03-167-07, Midwest Roadside Safety Facility, University of Nebraska-Lincoln, Lincoln, Nebraska, November 26, 2007.

36. Rosenbaugh, S.K., Lechtenberg, K.A., Faller, R.K., Sicking, D.L., Bielenberg, R.W., and Reid, J.D., *Development of the MGS Approach Guardrail Transition Using Standardized Steel Posts*, Report No. TRP-03-210-10, Midwest Roadside Safety Facility, University of Nebraska-Lincoln, Lincoln, Nebraska, December 21, 2010.

37. Rosenbaugh, S.K., Schrum, K.D., Faller, R.K., Lechtenberg, K.A., Sicking, D.L., and Reid, J.D., *Development of Alternative Wood-Post MGS Approach Guardrail Transition*, Report No. TRP-03-243-11, Midwest Roadside Safety Facility, University of Nebraska-Lincoln, Lincoln, Nebraska, November 28, 2011.

38. Rosenbaugh, S.K., Fallet, W.G., Faller, R.K., Bielenberg, R.W., and Schmidt, J.D., *34-in. Tall Thrie Beam Transition to Concrete Buttress*, Report No. TRP-03-367-19-R1, Midwest Roadside Safety Facility, University of Nebraska-Lincoln, Lincoln, Nebraska, July 2, 2019.

39. Bronstad, M.E., Calcote, L.R., Ray, M.H., and Mayer, J.B., *Guardrail-Bridge Rail Transition Designs Volume 1, Research Report*, Report No. FHWA/RD-86/178, Southwest Research Institute, San Antonio, Texas, April 1988.

40. Michie, J.D., Gatchell, C.J., and Duke, T.J., *Dynamic Evaluation of Timber Posts for Highway Guardrails*, Highway Research Report 343, Highway Research Board, Washington, D.C., January 1971

41. Stroughton, R.L., Stocker, J.R., and Nordlin, E.F., *Dynamic Tests of Metal Beam Guardrail*, Transportation Research Record 556, Transportation Research Board, National Research Council, Washington, D.C., 1975.

42. Polivka, K.A., Faller, R.K., Sicking, D.L., Reid, J.D., Rohde, J.R., Holloway, J.C., Bielenberg, R.W., and Kuipers, B.D., *Development of the Midwest Guardrail System (MGS) for Standard and Reduced Post Spacing and in Combination with Curbs*, Report No. TRP-03-139-04, Midwest Roadside Safety Facility, University of Nebraska-Lincoln, Lincoln, Nebraska, September 1, 2004.

43. Gutierrez, D.A., Lechtenberg, K.A., Bielenberg, R.W., Faller, R.K., Reid, J.D., and Sicking, D.L., *Midwest Guardrail System (MGS) with Southern Yellow Pine Posts*, Report No. TRP-03-272-13, Midwest Roadside Safety Facility, University of Nebraska-Lincoln, Lincoln, Nebraska, September 4, 2013.

44. Dobrovolny, C.S., Schulz, N., and Mohanakrishnan, A., *Evaluation of the Crashworthiness Alternative of Raising Wood Blockouts on Wood Post*, Report No. FHWA/TX 12-602371-00001, Texas Transportation Institute, Texas A&M University, College Station, Texas, 2015.

45. Menges, W.L., Kuhn, D.L., and Dobrovolny, C.S., *Pendulum Testing on Composite Blockouts Raised on Steel Posts*, Test Report No. TM No. 605311, Texas Transportation Institute, Texas A&M University, College Station, Texas, 2017.

46. Dobrovolny, C.S., Menges, W.L., and Kuhn, D.L., *MASH Test 3-11 of 28-Inch W-Beam Guardrail System with 8-Inch Composite Blockouts Raised 4 Inches on Steel Posts*, Test Report No. 608421-1, Texas Transportation Institute, Texas A&M University, College Station, Texas, 2017.

47. Ritter, M.A., *Timber Bridges: Design, Construction, Inspection, and Maintenance*. United States Department of Agriculture-Forest Service. Washington, D.C., 1990.

48. Wacker, J.P., and Smith, M.W., *Standard Plans for Timber Bridge Superstructures*, General Technical Report No. FPL-GTR-125, United States Department of Agriculture – Forest Service – Forest Products Laboratory and Federal Highway Administration, October 1996.

49. IntechOpen, Lumber-Based Mass Timber Products in Construction, Available: https://www.intechopen.com/chapters/66693, April 18, 2023.

50. Johnson, K.A. *Timber Bridge Decks: Comparison of Types, and Evolution of Design*, Wheeler Consolidated, Inc., St. Louis Park, Minnesota, April 2002.

51. Moses, D., Alexander, M., McAlister, K., Mesa, K., Lehan, A., Brown S., and Dulay, G., *Ontario Wood Bridge Reference Guide*. Canadian Wood Council.

52. Wackers, J.P., Dias, A.M.P.G., and Hosteng, T.K., *100-year performance of timber-concrete composite bridges in the United States*, Journal of Bridge Engineering, Volume 25, Number 3, January 2020.

53. Zhu, W., Li, L., Gong, M., Chui, Y., and Zhou, J., *On-Site Monitoring of the Moisture Content of Bridge Decks Made of Nail-Laminated Timbers*, Journal of Structural Engineering, Volume 147, Number 7, May 2021.

54. Wacker, J.P., and Brashaw, B.K., *Comparative Durability of Timber Bridges in the USA*, In: The international research group on wood protection, Section 2, Test methodology and assessment: Paper prepared for the IRG48 Scientific Conference on Wood Protection, Ghent, Belgium, June 4-8, 2017.

55. Brashaw, B., *Development and Integration of Advanced Timber Bridge Inspection Techniques for NBIS*. Minnesota Department of Transportation.

56. Widmann, R., *Screw-Laminated Timber Deck Plates*, Swiss Federal Institute for Materials Testing and Research EMPA. International Association for Bridge and Structural Engineers (IABSE) Symposium Report. 2001.

57. Buck, D., Wang, X., Hagman, O., Gustafsson, A., *Comparison of Different Assembling Techniques Regarding Cost, Durability, and Ecology – A Survey of Multi-layer Wooden Panel Assembly Load-Bearing Construction Elements*, BioResources, Volume 10, Number 4, October 2015.

58. South Dakota Department of Transportation. Keystone Wye Bridge - U.S. Highway 16 and 16A, Available: https://dot.sd.gov/keystonewyebridge-pcn-04fu, May 3, 2023.

59. Sprinkel, M.M., *Glulam Timber Deck Bridges*, Virginia Highway & Transportation Research Council, November 1978.

60. Forest Product Laboratory, *Wood Handbook: Wood as an Engineering Material*, General Technical Report No. FPL-GTR-282, United State Department of Agriculture – Forest Service – Forest Products Laboratory and Federal Highway Administration, March 2021.

61. Torgerson Forest Products. Previous Successes, Available: https://torgersonforest.com/previous-successes/, May 3, 2023.

62. *LRFD Bridge Design Manual*, Minnesota Department of Transportation Bridge Office, Oakdale, MN, 2022.

63. Wheeler Consolidated. Highway Bridges: Panel-Lam Plant Fabrication, Available: http://www.wheeler-con.com/highway-bridges/panel-lam-timber-vehicle-bridges/panel-lam-plant-fabrication/, September 21, 2023.

64. Pousette, A., Malo, K.A., Thelandersson, S., Fortino, S., Salokangas, L., and Wacker, J.P., *Durable Timber Bridges Final Report and Guidelines*, RISE Research Institutes of Sweden, 2017.

65. *AASHTO Standard Specifications for Highway Bridges, 17th Edition*, American Association of State Highway and Transportation Officials (AASHTO), Washington, D.C., 2002.

66. Ekevad, M., Jacobsson, P., and Forsberg, G., *Slip between Glue-Laminated Beams in Stress-Laminated Timber Bridges: Finite-Element Model and Full-Scale Destructive Test*, Journal of Bridge Engineering, Volume 16, Number 2, March 2011.

67. Crocetti, R., Ekholm, K., and Kliger, R., *Stress-laminated-timber decks: state of the art and design based on Swedish practice*, European Journal of Wood Products, Volume 74, September 2015.

68. Ekholm, K., *Performance of Stress-Laminated-Timber Bridge Decks*, Thesis for Degree of Doctor of Philosophy Department of Civil and Environmental Engineering Chalmers University of Technology, 2013.

69. Forest Product Laboratory, *Field Performance of Timber Bridges: 21. Humphrey Stress-Laminated T-Beam Bridge*, Research Paper No. FPL-RP-597, United States Department of Agriculture – Forest Service – Forest Products Laboratory and Federal Highway Administration, June 2001.

70. Forest Product Laboratory, *Field Performance of Timber Bridges: 17. Ciphers Stress-Laminated Deck Bridge*, Research Paper No. FPL-RP-572, United State Department of Agriculture – Forest Service – Forest Products Laboratory and Federal Highway Administration, October 1998.

71. Forest Product Laboratory, *Field Performance of Timber Bridges: 20. Gray Stress-Laminated Deck Bridge*, Research Paper No. FPL-RP-592, United State Department of Agriculture – Forest Service – Forest Products Laboratory and Federal Highway Administration, January 2001.

72. Dahlberg, J.M., and Wacker, J.P., *Field Evaluation of Stress-Laminated Hardwood Timber Bridges with Extended Service Life*, Conference Proceedings World Conference on Timber Engineering, August 2021.

73. Dyken, T., and Burkart, H., *New Concepts for Timber Bridge Decks with Cross Beams: Stress Laminated Decks and Interlocked Laminated Decks*, Conference Proceedings International Conference on Timber Bridges, May 2022.

74. Mackey, L., Bridge Deck options for 15'x35' vehicle bridge, eng-tips.com, Available: https://www.eng-tips.com/viewthread.cfm?qid=455463, July 7, 2019.

75. Lefebrve, D., and Richard, G., *Design and construction of a 160-Metre-Long Bridge in Mistissini*, Quebec, Internationales Holzbau-Forum, 2014.

76. Kode, A., van de Lindt, J.W., and Amini, M.O., *Investigation of Cross Timber Bridge Decks as a Sustainable Solution for Repair of Deficient Rural Wood Bridges*, Mountain-Plains Consortium 21-437, Colorado State University, May 2021.

77. Phares, B., and Dahlberg, J., Laboratory Investigation of Cross-Laminated (CLT) Decks for Bridge Applications, Iowa State University, Available: https://intrans.iastate.edu/research/in-progress/laboratory-investigation-of-cross-laminated-clt-decks-for-bridge-applications/, September 21, 2023.

78. Zöllig, S., *Infrastructure made of wood – opportunities for decarbonization of the public sector*, Conference Proceedings International Conference on Timber Bridges, May 2022.

79. Burkart, H., and Dyken T., *Oblique Interlocked Laminated Timber Deck*, Norwegian Public Road Administration, Report 420, September 2018.

80. Forest Product Laboratory, *Plans for Crash-Tested Bridge Railings for Longitudinal Wood Decks*, General Technical Report No. FPL-GTR-87, United States Department of Agriculture – Forest Service – Forest Products Laboratory and Federal Highway Administration, September 1995.

81. Forest Product Laboratory, *Plans for Crash-Tested Bridge Railings for Longitudinal Wood Decks on Low-Volume Roads*, General Technical Report No. FPL-GTR-107, United States Department of Agriculture – Forest Service – Forest Products Laboratory and Federal Highway Administration, August 1998.

82. Weyers, R.E., Loferski, J.R., Dolan, J.D., Haramis, J.E., Howard, J.H., and Hislop, L., *Guidelines for Design, Installation, and Maintenance of a Waterproof Wearing Surface for Timber Bridges*, General Technical Report No. FPL-GTR-123, United States Department of Agriculture – Forest Service – Forest Products Laboratory and Federal Highway Administration, January 2001.

83. Brawshaw, B., Wacker, J., Fosnacht, D., Aro, N., Young, M., and Vatalaro, R., *Development of Cost-Competitive Timber Bridge Designs for Long-Term Performance*, Final Report, Natural Resources Institute, University of Minnesota-Duluth, Duluth, Minnesota, June 2020.

84. *Tack Coat Best Practices*, U.S. Department of Transportation – Federal Highway Administration – Office of Asset Management, Pavements, and Construction, FHWA-HIF-16-017, April 2016.

85. Leijten, A.J.M., and Jansson, B., *Load Duration Factors for Instantaneous Loads*, CIB-W18/36-9-1, International Council for Research and Innovation in Building and Construction, August 2003.

86. Kloot, N.H., *The Effect of Moisture Content on the Impact Strength of Wood*, Australian Journal of Applied Science, Volume 5, No. 2, 1954.

87. Widehammar, S., *Stress-Strain Relationship for Spruce Wood: Influence of Strain Rate, Moisture Content and Loading Direction*, Journal of Experimental Mechanics, Volume 44, No. 1, February 2004.

88. Pierre, F., Almeida, G., Huber, F., Jacquin, P., and Perré, P., *An original impact device for biomass characterization: results obtained for spruce and poplar at different moisture contents*, Journal of Wood Science and Technology, Volume 47, 2013.

89. Renaud, M., Rueff, M., and Rocaboy, A.C., *Mechanical behavior of saturated wood under compression: part 1. behavior of wood at high rates of strain*, Journal of Wood Science and Technology, Volume 30, 1996.

90. *ASTM Standard D143-22 Standard Test Methods for Small Clear Specimens of Timber*, Revised 2022, ASTM International, West Conshohocken, Pennsylania.

91. *ASTM Standard D245-22 Establish Structural Grades and Related Allowable Properties for Visually Graded Lumber*, Revised 2022, ASTM International, West Conshohocken, Pennsylania.

92. Tabarsa, T., and Chui, Y.H., *Stress-Strain Response of Wood Under Radial Compression. Part I. Test Method and Influences of Cellular Properties*, Journal of Wood and Fiber Science, Volume 32, No. 2, April 2000.

93. Huang, C., Gong, M., Chui, Y., and Chan, F., *Mechanical behavior of wood compressed in radial direction-part I. New method of determining the yield stress of wood on the stress-strain curve*, Journal of Bioresources and Bioproducts, Volume 5, July 2020.

94. *ASTM Standard D3737-18(2023)e1 Standard Practice for Establishing Allowable Properties for Structural Glued Laminated Timber (Glulam)*, Revised 2023, ASTM International, West Conshohocken, Pennsylania.

95. Lebow, S., Ross, R., Zelinka, S., and Clausen, C., *Evaluation of Wood Species and Preservatives for WisDOT Sign Posts*, Wisconsin Department of Transportation, October 2013.

96. Khademibami, L., and Bobadilha, G.S., *Recent Developments Studies on Wood Protection Research in Academia: A Review*, Frontiers in Forests and Global Change, Volume 5, March 2022.

97. Zelinka, S.L., *Chapter 23: Corrosion of Metals in Wood Products*, Developments in Corrosion Protection, InTech, 2014.

98. IARC Monographs on the Evaluation of Carcinogenic Risks to Humans, *Chemical Agents and Related Occupations: Volume 100F A Review of Human Carcinogens*, International Agency for Research on Cancer, Lyon, France, 2012.

99. Conversation with David Clemens, Director Engineered Product Sales, Wheeler Consolidated, Eden Prairie, Minnesota, December 13th, 2022.

100. Brient, J.A., Manning, M.J., and Freeman, M.H., *Copper naphthenate – protecting America's infrastructure for over 100 years and its potential for expanded use in Canada and Europe*, Journal of Wood Material Science and Engineering, Volume 15, No. 6, November 2020.

101. Erickson, B.E., *The end of pentachlorophenol is near: US EPA proposes to ban all uses of wood preservative citing health risks to workers*, Chemical and Engineering News, March 9th, 2021.

102. Conversation with Brett Franks, Quality & Continuous Improvement Management, Bell Lumber and Pole, Saint Paul, Minnesota, December 18th, 2022.

103. Conversation with Bill Abbott, President, Copper Care Wood Preservatives Inc., Columbus, Nebraska, December 13th, 2022.

104. Kropf, F.W., *Durability and Detail Design – The Result of 15 Years of Systematic Improvements*, National Conference on Wood Transportation Structures, Madison, WI, October 1996.

105. 420 Pulp Mill Bridge Rd, Google Earth, Available: https://www.google.com/maps/@44.0247545,-73.1780611,3a,18.3y,112.26h,88.45t/data=!3m7!1e1!3m5!1s1Ht8SLjD8PkWZokQZ-jIUQ!2e0!6shttps:%2F%2Fstreetviewpixels-pa.googleapis.com%2Fv1%2Fthumbnail%3Fpanoid%3D1Ht8SLjD8PkWZokQZ-jIUQ%26cb_client%3Dmaps_sv.share%26w%3D900%26h%3D600%26yaw%3D112.26000871231953%26pitch%3D1.5494988761389692%26thumbfov%3D90!7i16384!8i8192?authuser=0&coh=205410&entry=ttu, July 30, 2024.

106. *Dissimilar Metals*, Department of Defense, Standard Practice, MIL-STD-889C, July 7, 1976.

107. Teng, T., Arip, M.N.M., Sudesh, K., Nemoikina, A., Jalaludin, Z., Ng. E., and Lee, H., *Conventional Technology and Nanotechnology in Wood Preservative: A Review*, Journal of Bioresources, Volume 13, No. 4, September 2018.

108. Leijten, A.J.M., Commonwealth Scientific and Industrial Research Organization, *Impact Strength of Modified Wood Species*, 9th International Conference on Durability of Building Materials, Paper No. 125, 2002.

109. Giridhar, B.N., Pandey, K.K., Prasad, B.E., Bisht, S.S., and Vagdevi, H.M., *Dimensional Stabilization of Wood by Chemical Modification Using Isopropenyl Acetate*, Journal Ciencia y Tecnologia, Volume 19, No. 1, 2017.

110. Mantanis, G.I., *Chemical Modification of Wood by Acetylation or Furfurylation: A Review of the Present Scaled-up Technologies*, Journal of Bioresources, Volume 12, No. 2, April 2017.

111. Tjeerdsma, B.F., Kattenbroek, B., and Jorissen, A., *Acetylated wood in exterior and heavy load-bearing constructions: building of two timber traffic bridges of acetylated Radiata pine*, 3rd European Conference on Wood Modification, Cardiff, UK, October 2007.

112. Hascall, J.A., Faller, R.K., Reid, J.D., and Sicking, D.L., *Investigating the Use of Small-Diameter Softwood as Guardrail Posts (Dynamic Test Results)*, Report No. TRP-03-179-07, Midwest Roadside Safety Facility, University of Nebraska-Lincoln, Lincoln, Nebraska, March 28, 2007.

113. Beason, W.L., Hirsch, T.J., and Campise, W.L., *Measurement of Heavy Vehicle Impact Forces and Inertia Properties*, Report No. FHWA-RD-89-120, Submitted to the Office of Safety and Traffic Operations R&D, Federal Highway Administration, Texas Transportation Institute, Texas A&M University, May 1989.

114. Wight, J.K., and MacGregor, J.G., *Reinforced Concrete Mechanics and Design*, Sixth Edition, Pearson Education, Upper Saddle River, New Jersey, 2012.

115. Hopkins, D.J., *The Fire Performance of Engineered Timber Products and Systems*, Dissertation, Loughborough University, June 2011.

116. Breyer, D.E., Fridley, K.J., Cobeen, K.E., and Pollock, D.G., *Design of Wood Structures – ASD/LRFD*, Sixth Edition, McGraw-Hill, New York, New York, 2007.

117. Trayer, G.W., *The Bearing Strength of Wood Under Bolts*, Technical Bulletin No. 332, Washington, DC, U.S. Department of Agriculture, Forest Service, Forest Products Laboratory, 1932.

118. Steelman, J.S., *MASH Railing Load Requirement for Bridge Deck Overhang, Interim Report*, Midwest Roadside Safety Facility, University of Nebraska-Lincoln, January 6, 2021, In Progress.

119. Conversation with Matt Smith, President, Laminated Concepts Inc., New York, New York, January 5th, 2023.

120. Timber Engineering Company, *Design Manual for TECO Timber Connector Construction*, Washington, DC, Timber Engineering Company, 1962.

121. Fowler, M.D., *Design and Testing of a Test Level 4 Bridge Railing for Transverse Glulam Timber Deck Bridges*, Masters Thesis, Department of Civil and Environmental Engineering, University of Nebraska-Lincoln, Lincoln, Nebraska, 1997.

122. Johansen, K.W., *Theory of Timber Connections*, International Association for Bridge and Structural Engineering, Volume 9, 1949.

123. McLain, T.E., Soltis, L.A., Pollock Jr., D.A., and Wilkinson, T.L., *LRFD For Engineered Wood Structures – Connection Behavioral Equations*, Journal of Structural Engineering, Volume 119, Issue 10, October 1, 1993.

124. Soltis, L.A., and Wilkinson, T.L., *United States Adaptation of European Yield Model to Large-Diameter Dowel Fastener Specification*, Proceedings of International Timber Engineering Conference, Volume 3, 1991.

125. Wilkinson, T.L., *Bolted Connection Allowable Loads Based on the European Yield Model*, Madison, WI, U.S. Department of Agriculture, Forest Service, Forest Products Laboratory, 1991.

126. Karim, A.R.A., Quenneville, P., Sa'don, N.M., and Ingham, J.M., *Assessing the Bolted Connection Strength of New Zealand Hardwood*, Proceedings of New Zealand Society for Earthquake Engineering, Paper 41, 2010.

127. Yeh, B., Williamson, T.G., and O'Halloran, M.R., *Shear Strength of Structural Glued Laminated Timber Based on Full-Size Flexure Tests*, Proceedings of Pacific Engineering Conference, Rotorua, New Zealand, March 1999.

128. *ASTM Standard D2555-17a Establishing Clear Wood Strength Values*, Revised 2017, ASTM International, West Conshohocken, Pennsylania.

129. Hernandez, R., Moody, R.C., Falk, R.H., *Fiber Stress Values for Design of Glulam Timber Utility Structures*, Research Paper No. FPL-RP-532, United States Department of Agriculture – Forest Service – Forest Products Laboratory, August 1995.

130. *General Dowel Equations for Calculating Lateral Connection Values with Appendix A*, Technical Report 12, American Wood Council, Leesburg, Virginia, 2015.

131. Bendtsen, B.A., and Galligan, W.L., *Mean and Tolerance Limit Stresses and Stress Modeling for Compression Perpendicular to Grain in Hardwood and Softwood Species*, Research Paper No. FPL-337, United States Department of Agriculture – Forest Service – Forest Products Laboratory and Federal Highway Administration, August 1979.

132. Green, D.W., *Wood: Strength and Stiffness*, Encyclopedia of Materials: Science and Technology, Second Edition, USDA Forest Service, 2001.

133. Muthumala, C.K., Silva, S.D., Arunakumara, K.K.I.U., and Alwis, P.L.A.G., *Assessment of the Shear Failure Modes of Softwood and Hardwood Timber under Different Wood Joints*, Journal of Failure Analysis and Prevention, Volume 23, May 22, 2023.

134. Breyer, D.E., Fridley, K.J., Cobeen, K.E., and Pollock, D.G., *Design of Wood Structures – ASD/LRFD*, Sixth Edition, McGraw-Hill, New York, New York, 2007.

135. Williams Form Engineering Corporation, 150 ksi All-Thread-Bar, Available: https://www.williamsform.com/threaded-bar/150-ksi-all-thread-bar/, November 17, 2023.

136. Dywidag, Post-Tensioning Systems Multistrand Systems Bar Systems Repair and Strengthening, Brochure, April 20, 2020.

137. Dywidag, Geotechnical Product Range, Brochure, September 27, 2022.

138. Conversation with Horst Aschenbroich, President, Con-Tech Systems Ltd., Delta, Canada, April 28th, 2023.

139. *ASTM Standard D198-22a Standard Test Methods of Static Tests of Lumber in Structural Sizes,* Revised 2022, ASTM International, West Conshohocken, Pennsylania.

140. Abutments-Stub Bridge Cell Library, Illinois Department of Transportation (IDOT), Available: https://idot.illinois.gov/content/dam/soi/en/web/idot/documents/doing-business/specialty-lists/highways/bridges/cell-libraries/bridge/abutments-stub.pdf, July 30, 2024.

141. *Standard Specifications for Highway Construction*, Nebraska Department of Transportation (NDOT), Lincoln, NE, 2017.

142. *Standard Specifications for Highway and Bridge Construction*, Iowa Department of Transportation (IOWADOT), Ames, IA, 2023.

143. *Standard Specifications for Road and Bridge Construction*, Arizona Department of Transportation, Phoenix, AZ, 2021.

144. *Standard Specifications for Roads and Structures*, North Carolina Department of Transportation (NCDOT), Raleigh, NC, 2024.

145. *2023 Product Catalog*, American Timber and Steel, Norwalk, OH, 2023.

146. FLW International. Guard rail, Available: https://www.flwinternational.com/guard-rail.html, April 23, 2024.

147. Society of Automotive Engineers (SAE), Instrumentation for Impact Test – Part 1 – Electronic Instrumentation, SAE J211/1 MAR95, New York City, New York, July 2007.

148. Southern Pine Council, *A Guide to Southern Pine Lumber Export Grades*, Borchure, 2002.

149. Rasmussen, J.D., Rosenbaugh, S.K., Faller, R.K., Alvarado, R., Mauricio, R., Bielenberg, R.W., and Steelman, J.S., *Development of a MASH TL-3 Approach Guardrail Transition to a MASH TL-4 Steel Bridge Rail*, Report No. TRP-03-411-20, Midwest Roadside Safety Facility, University of Nebraska-Lincoln, Lincoln, Nebraska, December 2020.

150. Homan, D.M., Thiele, J.C., Faller, R.K., Rosenbaugh, S.K., Rohde, J.R., Arens, S.W., Lechtenberg, K.A., Sicking, D.L., and Reid, J.D., *Investigation and Dynamic Testing of Wood and Steel Posts for MGS on a Wire-Faced MSE Wall*, Report No. TRP-03-231-11, Midwest Roadside Safety Facility, University of Nebraska-Lincoln, Lincoln, Nebraska, February 2012.

151. Stolle, C.S., Schroder, B.D., Ammon, T.J., Holloway, J.C., Faller, R.K., and Rilett, L.R., Testing and Evaluation of Soil Foundation and End Anchorage Designs, Report No. TRP-03-353-17, Midwest Roadside Safety Facility, University of Nebraska-Lincoln, Lincoln, Nebraska, December 15, 2017.

152. Barrett, J.D., *Effect of Size on Tension Perpendicular-to-Grain Strength of Douglas-Fir*, Journal of Wood and Fiber Science, Volume 6, No. 2, 1974.

153. Fairchild, I.J., *Holding Power of Wood Screws*, Technologic Papers of the Bureau of Standards, No. 319, Department of Commerce, Washington, D.C., July 17, 1926.

8 APPENDICES

Appendix A. A2LA Accreditation Documents

Accredited Laboratory

A2LA has accredited

MIDWEST ROADSIDE SAFETY FACILITY (MwRSF)

Lincoln, NE

for technical competence in the field of

Mechanical Testing

This laboratory is accredited in accordance with the recognized International Standard ISO/IEC 17025:2017 *General requirements for the competence of testing and calibration laboratories*. This accreditation demonstrates technical competence for a defined scope and the operation of a laboratory quality management system (*refer to joint ISO-ILAC-IAF Communiqué dated April 2017*).

Presented this 1st day of December 2021.

Vice President, Accreditation Services
For the Accreditation Council
Certificate Number 2937.01
Valid to November 30, 2023

For the tests to which this accreditation applies, please refer to the laboratory's Mechanical Scope of Accreditation.

Figure A-1. Midwest Roadside Safety Facility A2LA Accreditation Certificate No. 2937.01

SCOPE OF ACCREDITATION TO ISO/IEC 17025:2017

MIDWEST ROADSIDE SAFETY FACILITY (MwRSF)[1]
University of Nebraska-Lincoln
4630 NW 36th Street
Lincoln, NE 68524
Ms. Karla Lechtenberg Phone: 402 472 9070

MECHANICAL

Valid To: November 30, 2023 Certificate Number: 2937.01

In recognition of the successful completion of the A2LA evaluation process, accreditation is granted to this laboratory to perform the following tests:

Tests	Test Methods[2]
Full-Scale Vehicle Crash Tests of Highway Safety Features	NCHRP Report 350; MASH; EN 1317
Full-Scale Vehicle Crash Tests of Perimeter Protection Systems and Access Control Devices	ASTM F2656; SD-STD-02.01 Revision A
Bogie Dynamic Tests of Highway Safety Features	Non-Standard Test Method: Dynamic Testing of Steel Post and Rigid Foundation; Non-Standard Test Method: Dynamic Testing of Post in Soil; Non-Standard Test Method: Dynamic Testing of Spacer Blocks
Crushable Nose Bogie Testing for Breakaway Supports	Non-Standard Test Method: Dynamic Testing of Breakaway Supports; AASHTO Breakaway Poles and Supports; NCHRP Report 350

On the following types of products, materials, and/or structures:
Metal, Wood, Concrete and Plastic Structures, Components of Structures, Fasteners, and Roadway Pavements.

[1] Administrative office located at: 2200 Vine Street, 130 Whittier Building, Lincoln, NE 68583-0853.

[2] This laboratory performs field testing activities for these tests.

(A2LA Cert. No. 2937.01) 12/01/2021 Page 1 of 1

5202 Presidents Court, Suite 220 | Frederick, MD 21703-8515 | Phone: 301 644 3248 | Fax: 240 454 9449 | www.A2LA.org

Figure A-2. Midwest Roadside Safety Facility Scope of Accreditation to ISO/IEC 17025

Accredited Laboratory

A2LA has accredited

MIDWEST ROADSIDE SAFETY FACILITY (MwRSF)

Lincoln, NE

for technical competence in the field of

Mechanical Testing

This laboratory is accredited in accordance with the recognized International Standard ISO/IEC 17025:2017 *General requirements for the competence of testing and calibration laboratories*. This accreditation demonstrates technical competence for a defined scope and the operation of a laboratory quality management system (*refer to joint ISO-ILAC-IAF Communiqué dated April 2017*).

Presented this 27th day of June 2024.

Mr. Trace McInturff, Vice President, Accreditation Services
For the Accreditation Council
Certificate Number 2937.01
Valid to November 30, 2025

For the tests to which this accreditation applies, please refer to the laboratory's Mechanical Scope of Accreditation.

Figure A-3. Midwest Roadside Safety Facility A2LA Accreditation Certificate No. 2937.01

SCOPE OF ACCREDITATION TO ISO/IEC 17025:2017

MIDWEST ROADSIDE SAFETY FACILITY (MwRSF)[1]
University of Nebraska-Lincoln
4630 NW 36th Street
Lincoln, NE 68524
Ms. Karla Lechtenberg Phone: 402 472 9070

MECHANICAL

Valid To: November 30, 2025 Certificate Number: 2937.01

In recognition of the successful completion of the A2LA evaluation process, accreditation is granted to this laboratory to perform the following tests:

Tests	Test Methods
Full-Scale Vehicle Crash Tests of Highway Safety Features	NCHRP Report 350; MASH; EN 1317
Full-Scale Vehicle Crash Tests of Perimeter Protection Systems and Access Control Devices	ASTM F2656; SD-STD-02.01 Revision A
Bogie Dynamic Tests of Highway Safety Features	Non-Standard Test Method: Dynamic Testing of Steel Post and Rigid Foundation; Non-Standard Test Method: Dynamic Testing of Post in Soil; Non-Standard Test Method: Dynamic Testing of Spacer Blocks
Crushable Nose Bogie Testing for Breakaway Supports	Non-Standard Test Method: Dynamic Testing of Breakaway Supports; AASHTO Breakaway Poles and Supports; NCHRP Report 350

On the following types of products, materials, and/or structures:
Metal, Wood, Concrete and Plastic Structures, Components of Structures, Fasteners, and Roadway Pavements.

[1] Administrative office located at: 2200 Vine Street, 130 Whittier Building, Lincoln, NE 68583-0853.

(A2LA Cert. No. 2937.01) 06/27/2024 Page 1 of 1

5202 Presidents Court, Suite 220 | Frederick, MD 21703-8515 | Phone: 301 644 3248 | Fax: 240 454 9449 | www.A2LA.org

Figure A-4. Midwest Roadside Safety Facility Scope of Accreditation to ISO/IEC 17025

Appendix B. Material Certifications

Table B-1. Bill of Materials, Test No. TRTD-1

Item No.	Description	Material Specification	Reference
a1	41½-in. Long x 12-in. x 8¾-in. Glulam Post	Comb. 48 (SP) or Comb. 2 (Western)	Order#221047-C38A
a2	10½-in. x 8¾-in. x 1⅛-in. Thick Glulam Blockout	Comb. 48 (SP) or Comb. 2 (Western)	Order#221047-C38A
a3	24-in. Long x 13½-in. x 10¾-in. Glulam Upper Rail	Comb. 48 (SP) or Comb. 2 (Western)	Order#221047-C38A
a4	58-in. Long x 5⅛-in. x 12-in. Glulam Scupper Block	Comb. 48 (SP) or Comb. 2 (Western)	Order#221047-C38A
a5	58-in. Long x 8¾-in. x 12-in. Glulam Curb Rail	Comb. 48 (SP) or Comb. 2 (Western)	Order#221047-C38A
b1	12-in. x 16-in. x ½-in. Thick Steel Base Plate	ASTM A36	H#A1A281
b2	12-in. x 10-in. x ½-in. Thick Side Plate	ASTM A36	H#A1A281
b3	12-in. x 6¼-in. x ¾-in. Elastomeric Bearing Pad	Neoprene – Min. 50 Durameter	L#1237403
b4	15-in. x 30-in. x 12-ft Concrete Support	Min. f'c = 4000 psi NE mix 47 BD	Ticket#1275082
b5	138-in. Long #4 Rebar	ASTM A615 Gr. 60	H#3600014740
b6	73-in. Long Unbent Length #4 Rebar	ASTM A615 Gr. 60	H#3600014740
b7	8-in. x 6-in. x ¾-in. Thick 24-in. Long Steel Angle	ASTM A36	H#6-19750 H#6-21565 H#6-21566
b8	4-in. x 4-in. x ⅜-in. Thick 5-in. Long Steel Angle	ASTM A36	H#63231163/02
b9	⅞-in. Shear Plate	ASTM A47 Gr. 32510 or ASTM D5933	P#12407
c1	16½-in. x 6¾-in. x 20-ft Long Exterior Glulam Girder	24F-V4 Douglas Fir	PO#Q3021
c2	16½-in. x 6¾-in. x 20-ft Long Interior Glulam Girder	24F-V4 Douglas Fir	PO#Q3021
c3	12-in. x 5⅛-in. x 41⅛-in. Long Glulam Diaphragm	Comb. 48 (SP) or Comb. 2 (Western)	PO#Q3021
c4	5⅛-in. x 48-in. x 12-ft Long Glulam Deck Panel #1	Comb. 48 (SP) or Comb. 2 (Western)	PO#Q3021
c5	5⅛-in. x 48-in. x 12-ft Long Glulam Deck Panel #2	Comb. 48 (SP) or Comb. 2 (Western)	PO#Q3021
c6	5⅛-in. x 48-in. x 12-ft Long Glulam Deck Panel #3	Comb. 48 (SP) or Comb. 2 (Western)	PO#Q3021
c7	5⅛-in. x 48-in. x 12-ft Long Glulam Deck Panel #4	Comb. 48 (SP) or Comb. 2 (Western)	PO#Q3021
c8	5⅛-in. x 48-in. x 12-ft Long Glulam Deck Panel #5	Comb. 48 (SP) or Comb. 2 (Western)	PO#Q3021

Table B-2. Bill of Materials, Test No. TRTD-1, Cont.

Item No.	Description	Material Specification	Reference
d1	⅞-in. Dia. 9 UNC 26-in. Long Timber Bolt w/ Nubs	ASTM A307A	H#1201036150
d2	1⅜-in. Dia. 6 UNC 28-in. Long Timber Bolt w/o Nubs	ASTM A449	H#5394485
d3	¾-in. Dia. 10 UNC 10-in. Long Hex Bolt	ASTM A307A	P#91975
d4	¾-in. Dia. 10 UNC 60-in. Long Threaded Rod	ASTM A307A or F1554 Gr. 36 or SAE J429 Gr. 2	H#1202027708
d5	¾-in. Dia. 10 UNC 8-in. Long Threaded Rod	ASTM A193 Gr. B7 or SAE J429 Gr. 5	H#10768680
d6	¾-in. Dia. 10 UNC 11-in. Long Lag Bolt	ASTM A307A	P#22492
d7	¾-in. Dia. 10 UNC 8-in. Long Timber Bolt w/ Nubs	ASTM A307A	H#1201037998
d8	⅝-in. Dia. 11 UNC 6-in. Long Lag Bolt	ASTM A307A	P#22352
e1	⅞-in. Dia. Malleable Iron Washer	ASTM A47	PB#164896
e2	¾-in. Dia. Malleable Iron Washer	ASTM A47	H#2019112802
e3	¾-in. Dia. Flat Washer	ASTM F844	P#1133186
e4	6-in. x 6-in. x ⅜-in. Steel Plate Washer	ASTM A36	H#23027702
f1	⅞-in. Dia. Heavy Hex Nut	ASTM A563A	P#36716
f2	¾-in. Dia. Heavy Hex Nut	ASTM A563A	P#36718
f3	1⅜-in. Dia. Heavy Hex Nut	ASTM A563A	H#1-01746
g1	Epoxy Adhesive	Min. Bond Strength = 1,670 psi	Hilti COC

APA

Certificate of Conformance

THE UNDERSIGNED MANUFACTURER HEREBY CERTIFIES that the structural wood products identified below and marked with a collective mark of **APA – The Engineered Wood Association (APA)** were manufactured in accordance with the specifications indicated below.

☑ ANSI A190.1 Standard for Structural Glued Laminated Timber

Job Name: TRTD-TRLD

Job Location: MWRSF Proving Grounds

Customer's Order No.: 221047-C38A Date: 10-6-2023 Mfgr's Order No.: 604595

Distributor: WESTERN WOOD STRUCTURES

Order Description:

Signature: Title: Quality Control

Company: Zip-O-Laminators, LLC

Address: 2701 W. 1st Ave
PO Box 2130
Eugene OR 97402

Date: 10-6-2023

IT IS HEREBY CERTIFIED that the structural glued laminated timber production of the above-named manufacturer which carries a collective mark of *APA* is subject to regular audit by *APA – The Engineered Wood Association,* such audit consisting of the inspection of the manufacturing process, with sampling to verify the quality of glulam construction and the adequacy of glue bond.

by
Steve Zylkowski
Director, Quality Services

REPRESENTING THE ENGINEERED WOOD INDUSTRY

7011 South 19th Street • Tacoma, Washington 98466-5333 • Phone: (253) 565-6600 • Fax: (253) 565-7265 • www.apawood.org

EWS Cert Conformance.pdf

Figure B-1. Glulam Timber Railing Components, Test No. TRTD-1 (Item Nos. a1-a5)

SSAB

1770 Bill Sharp Boulevard, Muscatine, IA 52761-9412, US

Test Certificate

WARNING: This product can expose you to chemicals including nickel and nickel compounds, which are known to the State of California to cause cancer. For more information go to www.P65Warnings.ca.gov.

Form TC1: Revision 4: Date 6 Feb 2019

Customer:
STEEL & PIPE SUPPLY
P.O. BOX 1688

MANHATTAN
KS 66502

Customer P.O.No.: 4500358483 | **Mill Order No.** 41-628789-01 | **Shipping Manifest:** MT427225

Product Description: ASTM A36(19)/A709(18)36/ASME SA36(19)
AASHTO M270(20)36, 0.80-1.20 MN

Ship Date: 19 Feb 21 | **Cert No:** 061886005
Cert Date: 19 Feb 21 | (Page 1 of 1)

Size: 0.500 X 96.00 X 240.0 (IN)

Tested Pieces: / **Tensiles:** / **Charpy Impact Tests**

Heat Id	Piece Id	Tested Thickness	Tst Loc	YS (KSI)	UTS (KSI)	%RA	Elong % 2in	Elong % 8in	Tst Dir	Hardness	Abs. Energy(FTLB) 1	2	3	Avg	% Shear 1	2	3	Avg	Tst Tmp	Tst Dir	Tst Siz (mm)	BDWTT Tmp %Shr
A1A281	B58	0.310 (DISCRT)	L	50	68		37		T													
A1A281	B59	0.497 (DISCRT)	L	46	67		37		T													

Chemical Analysis

Heat Id	C	Mn	P	S	Si	Tot Al	Cu	Ni	Cr	Mo	Cb	V	Ti	B	N	IIW	ORGN
A1A281	.16	.84	.009	.002	.04	.030	.33	.11	.14	.02	.001	.003	.006	.0001	.0073	.36	USA

KILLED STEEL
MERCURY IS NOT A METALLURGICAL COMPONENT OF THE STEEL AND NO MERCURY WAS INTENTIONALLY ADDED DURING THE MANUFACTURE OF THIS PRODUCT.
CEV (IIW) = C + MN/6 + (CR+MO+V)/5 + (NI+CU)/15
MTR EN 10204:2004 INSPECTION CERTIFICATE 3.1 COMPLIANT
100% MELTED, POURED, AND ROLLED IN THE USA
PRODUCTS SHIPPED:
A1A281 B56 PCS: 6, LBS: 19602

IPI Cust Part #: 721696240

WE HEREBY CERTIFY THAT THIS MATERIAL WAS TESTED IN ACCORDANCE WITH, AND MEETS THE REQUIREMENTS OF, THE APPROPRIATE SPECIFICATION

Brian Wales
SENIOR METALLURGIST - PRODUCT

Figure B-2. ASTM A36 Bearing Assembly Base Plate, ASTM A36 Bearing Assembly Side Plate, Test No. TRTD-1 (Item Nos. b1 and b2)

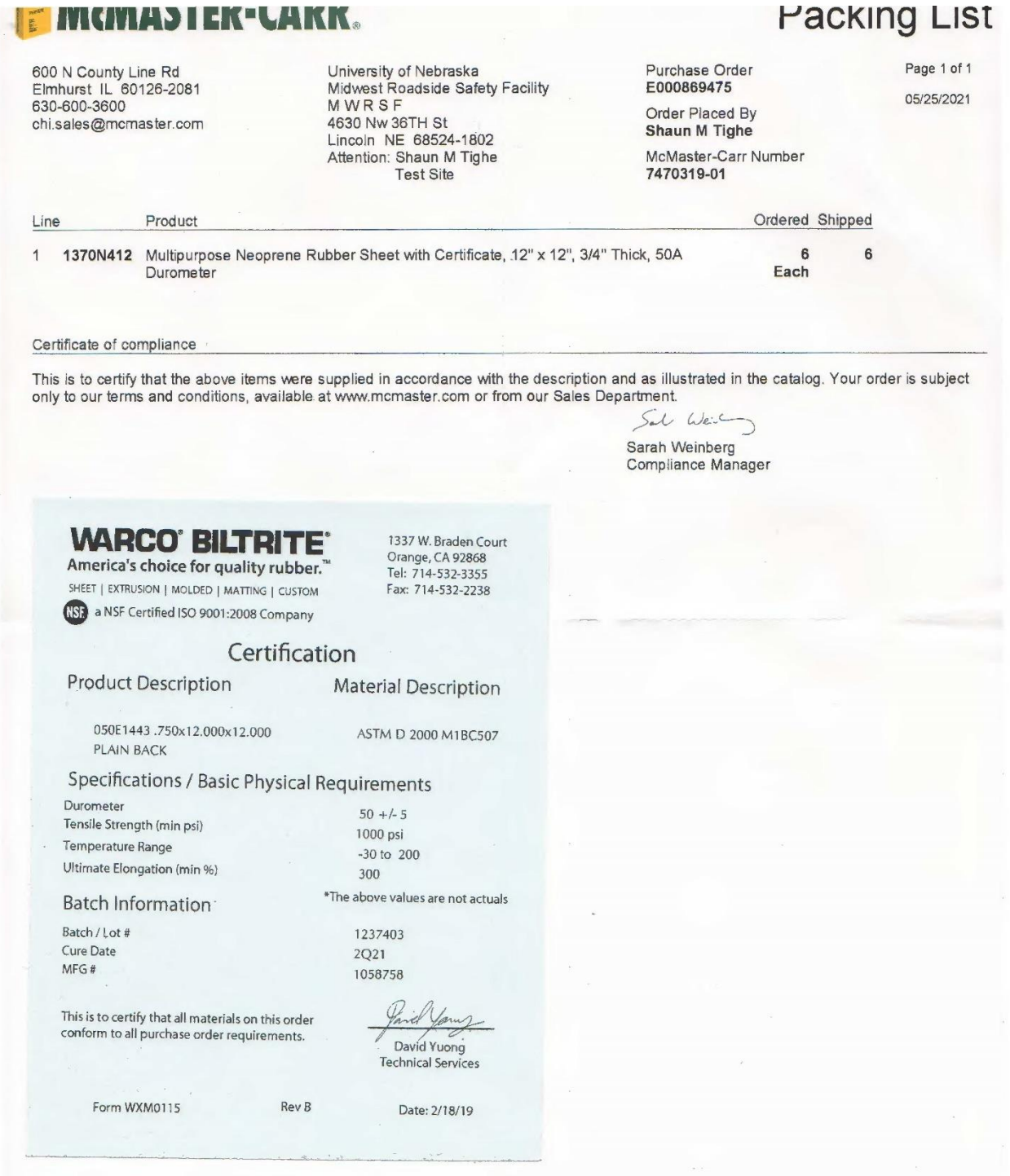

MCMASTER-CARR®

Packing List

600 N County Line Rd
Elmhurst IL 60126-2081
630-600-3600
chi.sales@mcmaster.com

University of Nebraska
Midwest Roadside Safety Facility
M W R S F
4630 Nw 36TH St
Lincoln NE 68524-1802
Attention: Shaun M Tighe
Test Site

Purchase Order
E000869475
Order Placed By
Shaun M Tighe
McMaster-Carr Number
7470319-01

Page 1 of 1
05/25/2021

Line		Product	Ordered	Shipped
1	**1370N412**	Multipurpose Neoprene Rubber Sheet with Certificate, 12" x 12", 3/4" Thick, 50A Durometer	**6 Each**	**6**

Certificate of compliance

This is to certify that the above items were supplied in accordance with the description and as illustrated in the catalog. Your order is subject only to our terms and conditions, available at www.mcmaster.com or from our Sales Department.

Sarah Weinberg
Compliance Manager

WARCO® BILTRITE®
America's choice for quality rubber.™
SHEET | EXTRUSION | MOLDED | MATTING | CUSTOM
NSF a NSF Certified ISO 9001:2008 Company

1337 W. Braden Court
Orange, CA 92868
Tel: 714-532-3355
Fax: 714-532-2238

Certification

Product Description	Material Description
050E1443 .750x12.000x12.000 PLAIN BACK	ASTM D 2000 M1BC507

Specifications / Basic Physical Requirements

Durometer	50 +/- 5
Tensile Strength (min psi)	1000 psi
Temperature Range	-30 to 200
Ultimate Elongation (min %)	300

*The above values are not actuals

Batch Information

Batch / Lot #	1237403
Cure Date	2Q21
MFG #	1058758

This is to certify that all materials on this order conform to all purchase order requirements.

David Yuong
Technical Services

Form WXM0115 Rev B Date: 2/18/19

Figure B-3. Elastomeric Bearing Pad, Test No. TRTD-1 (Item No. b3)

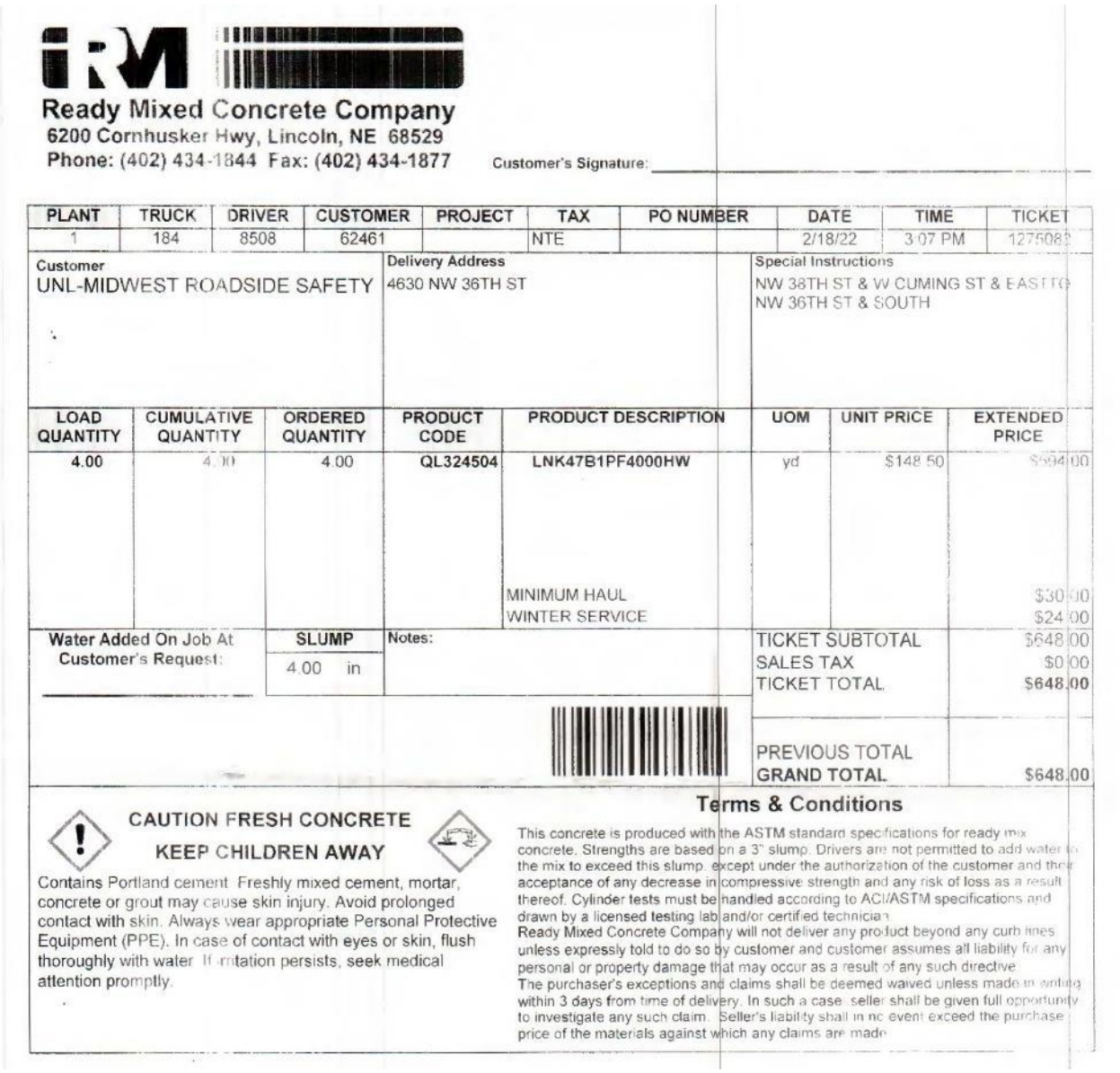

Ready Mixed Concrete Company
6200 Cornhusker Hwy, Lincoln, NE 68529
Phone: (402) 434-1844 Fax: (402) 434-1877

Customer's Signature: _____

PLANT	TRUCK	DRIVER	CUSTOMER	PROJECT	TAX	PO NUMBER	DATE	TIME	TICKET
1	184	8508	62461		NTE		2/18/22	3:07 PM	1275082

Customer	Delivery Address	Special Instructions
UNL-MIDWEST ROADSIDE SAFETY	4630 NW 36TH ST	NW 38TH ST & W CUMING ST & EAST TO NW 36TH ST & SOUTH

LOAD QUANTITY	CUMULATIVE QUANTITY	ORDERED QUANTITY	PRODUCT CODE	PRODUCT DESCRIPTION	UOM	UNIT PRICE	EXTENDED PRICE
4.00	4.00	4.00	QL324504	LNK47B1PF4000HW	yd	$148.50	$594.00
				MINIMUM HAUL			$30.00
				WINTER SERVICE			$24.00

Water Added On Job At Customer's Request:	SLUMP	Notes:		
	4.00 in		TICKET SUBTOTAL	$648.00
			SALES TAX	$0.00
			TICKET TOTAL	$648.00
			PREVIOUS TOTAL	
			GRAND TOTAL	$648.00

CAUTION FRESH CONCRETE
KEEP CHILDREN AWAY

Contains Portland cement. Freshly mixed cement, mortar, concrete or grout may cause skin injury. Avoid prolonged contact with skin. Always wear appropriate Personal Protective Equipment (PPE). In case of contact with eyes or skin, flush thoroughly with water. If irritation persists, seek medical attention promptly.

Terms & Conditions

This concrete is produced with the ASTM standard specifications for ready mix concrete. Strengths are based on a 3" slump. Drivers are not permitted to add water to the mix to exceed this slump, except under the authorization of the customer and their acceptance of any decrease in compressive strength and any risk of loss as a result thereof. Cylinder tests must be handled according to ACI/ASTM specifications and drawn by a licensed testing lab and/or certified technician.
Ready Mixed Concrete Company will not deliver any product beyond any curb lines unless expressly told to do so by customer and customer assumes all liability for any personal or property damage that may occur as a result of any such directive.
The purchaser's exceptions and claims shall be deemed waived unless made in writing within 3 days from time of delivery. In such a case, seller shall be given full opportunity to investigate any such claim. Seller's liability shall in no event exceed the purchase price of the materials against which any claims are made.

Figure B-4. Concrete for 12-ft x 30-in. x 15-in. Supports, Test No. TRTD-1 (Item No. b4)

NUCOR®

Mill Certification

09/02/2020

MTR#:458890-2
Lot #:360001474020
ONE NUCOR WAY
BOURBONNAIS, IL 60914 US
815 937-3131
Fax: 815 939-5599

Sold To: SIMCOTE INC
1645 RED ROCK RD
ST PAUL, MN 55119 US

Ship To: SIMCOTE INC
1645 RED ROCK RD
ST PAUL, MN 55119 US

Customer PO	MN-3748	Sales Order #	36013225 - 1.31
Product Group	Rebar	Product #	2110206
Grade	A615 Gr 60/AASHTO M31	Lot #	360001474020
Size	#4	Heat #	3600014740
BOL #	BOL-567414	Load #	458890
Description	Rebar #4/13mm A615 Gr 60/AASHTO M31 60' 0" [720"] 6001-10000 lbs	Customer Part #	
Production Date	08/12/2020	Qty Shipped LBS	22725
Product Country Of Origin	United States	Qty Shipped EA	567
Original Item Description		Original Item Number	

I hereby certify that the material described herein has been manufactured in accordance with the specifications and standards listed above and that it satisfies those requirements.

Melt Country of Origin : United States — Melting Date: 08/07/2020

C (%)	Mn (%)	P (%)	S (%)	Si (%)	Ni (%)	Cr (%)	Mo (%)	Cu (%)	V (%)	Nb (%)
0.34	0.90	0.015	0.043	0.198	0.18	0.23	0.06	0.40	0.012	0.002

Other Test Results

Yield (PSI) : 66100 — Tensile (PSI) : 99200 — Average Deformation Height (IN) : 0.036

Elongation in 8" (%) : 14.5 — Bend Test : Pass — Weight Percent Variance (%) : -4.00

Comments:

All manufacturing processes of the steel materials in this product, including melting, have occurred within the United States. Products produced are weld free. Mercury, in any form, has not been used in the production or testing of this material.

Zachary Sprintz, Chief Metallurgist

Page 1 of 1

Figure B-5. ASTM A615 Gr. 60 No. 4 Rebar for Concrete Supports, Test No. TRTD-1 (Item Nos. b5 and b6)

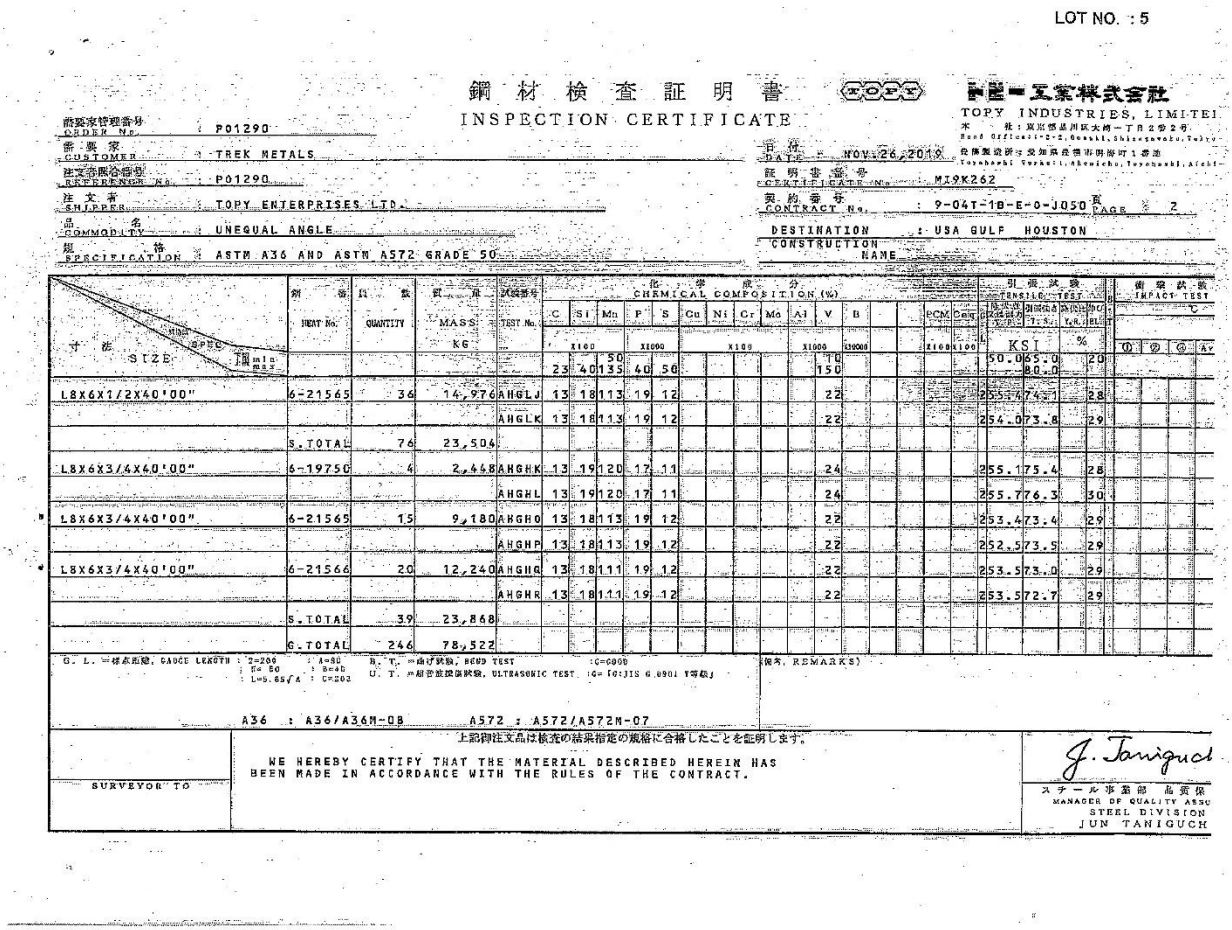

LOT NO. : 5

鋼 材 検 査 証 明 書

INSPECTION CERTIFICATE

東京一工業株式会社
TOPY INDUSTRIES, LIMITED

注文番号 ORDER No. : P01290
需要家 CUSTOMER : TREK METALS
注文者照合番号 REFERENCE No. : P01290
注文者 SHIPPER : TOPY ENTERPRISES LTD.
品名 COMMODITY : UNEQUAL ANGLE
規格 SPECIFICATION : ASTM A36 AND ASTM A572 GRADE 50

日付 DATE : NOV.26,2019
証明書番号 CERTIFICATE No. : MI9K262
契約番号 CONTRACT No. : 9-04T-1B-E-0-J050 頁 PAGE 2
DESTINATION : USA GULF HOUSTON
CONSTRUCTION NAME

寸法 SIZE	材質 SPEC	材番 HEAT No.	本数 QUANTITY	重量 MASS KG	試験番号 TEST No.	化学成分 CHEMICAL COMPOSITION (%) C	Si	Mn	P	S	Cu	Ni	Cr	Mo	Al	V	B	PCM	Ceq	引張試験 TENSILE TEST 降伏点 Y.P. KSI	引張強さ T.S. KSI	伸び El. %	衝撃試験 IMPACT TEST 温度 ℃	①	②	③	Av
						X100			X1000				X100			X1000	X10000	X100	X100								
						23	40	50 135	40	50						70 150					50.0	65.0 80.0	20					
L8X6X1/2X40'00"		6-21565	36	14,976	AHGLJ	13	18	113	19	12						22					255.4	74.1	28					
					AHGLK	13	18	113	19	12						22					254.0	73.8	29					
		S.TOTAL	76	23,504																							
L8X6X3/4X40'00"		6-19750	4	2,448	AHGHK	13	19	120	17	11						24					255.1	75.4	28					
					AHGHL	13	19	120	17	11						24					255.7	76.3	30					
L8X6X3/4X40'00"		6-21565	15	9,180	AHGHO	13	18	113	19	12						22					253.4	73.4	29					
					AHGHP	13	18	113	19	12						22					252.5	73.5	29					
L8X6X3/4X40'00"		6-21566	20	12,240	AHGHQ	13	18	111	19	12						22					253.5	73.0	29					
					AHGHR	13	18	111	19	12						22					253.5	72.7	29					
		S.TOTAL	39	23,868																							
		G.TOTAL	246	78,522																							

G. L. ＝標点距離, GAUGE LENGTH : 2=200 ; 4=80 ; L=5.65√A : C=203
B. T. ＝曲げ試験, BEND TEST : C=G090
U. T. ＝超音波探傷試験, ULTRASONIC TEST. : G=(G:JIS G 0901 Y等級)

備考, REMARKS)

A36 : A36/A36M-08 A572 : A572/A572M-07

上記注文品は検査の結果指定の規格に合格したことを証明します。

WE HEREBY CERTIFY THAT THE MATERIAL DESCRIBED HEREIN HAS BEEN MADE IN ACCORDANCE WITH THE RULES OF THE CONTRACT.

SURVEYOR TO

J. Taniguch

スチール事業部 品質保
MANAGER OF QUALITY ASSU
STEEL DIVISION
JUN TANIGUCH

Figure B-6. ASTM A572 Gr. 50 Angle Anchors for Trasnverse Glulam Timber Deck Panels, Test No. TRTD-1 (Item No. b7)

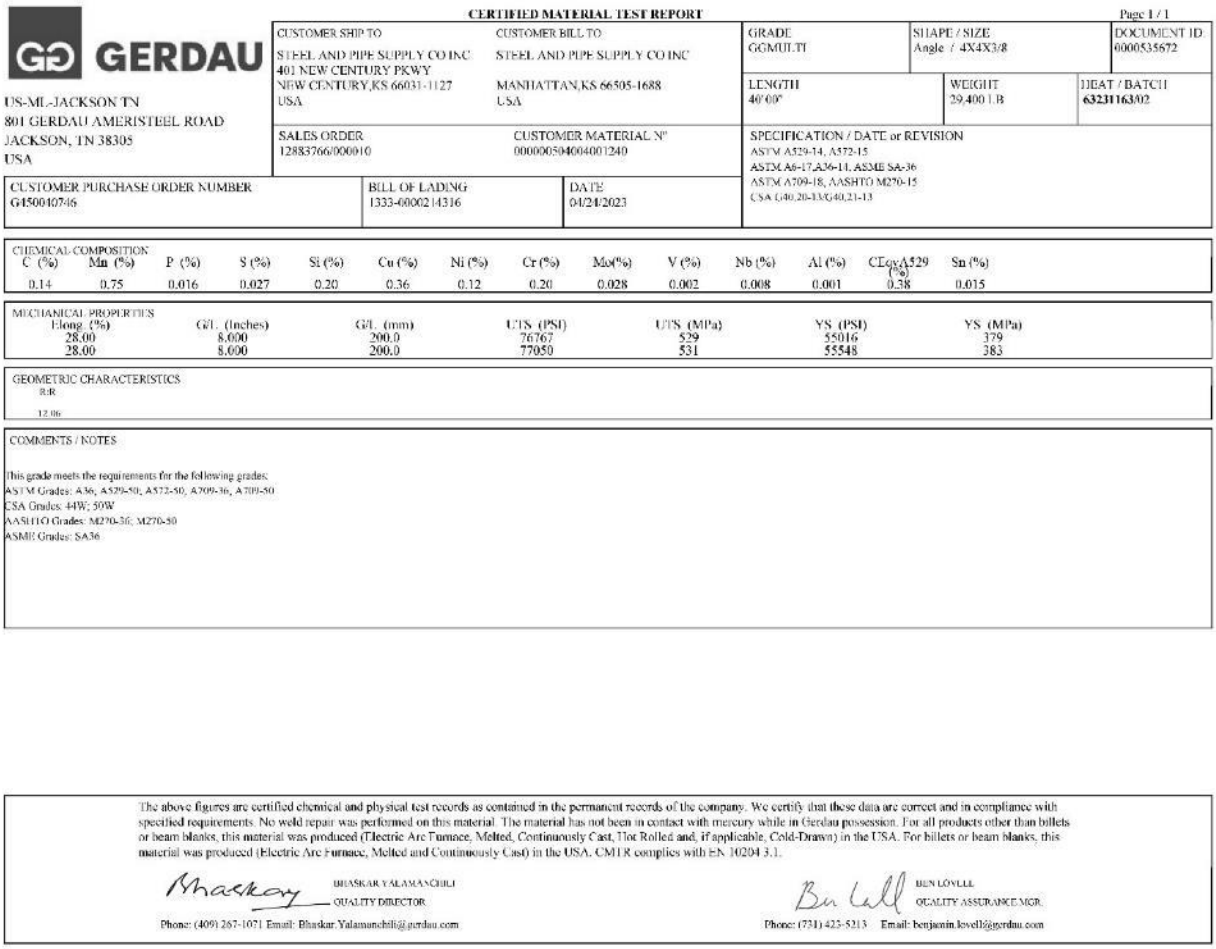

CERTIFIED MATERIAL TEST REPORT Page 1 / 1

GERDAU

US-ML-JACKSON TN
801 GERDAU AMERISTEEL ROAD
JACKSON, TN 38305
USA

CUSTOMER SHIP TO
STEEL AND PIPE SUPPLY CO INC
401 NEW CENTURY PKWY
NEW CENTURY,KS 66031-1127
USA

CUSTOMER BILL TO
STEEL AND PIPE SUPPLY CO INC
MANHATTAN,KS 66505-1688
USA

GRADE	SHAPE / SIZE	DOCUMENT ID
GGMULTI	Angle / 4X4X3/8	0000535672

LENGTH	WEIGHT	HEAT / BATCH
40'0.0"	29,400 LB	6323116300

SALES ORDER: 12883766/000010
CUSTOMER MATERIAL N°: 000000504004001240

SPECIFICATION / DATE or REVISION
ASTM A529-14, A572-15
ASTM A6-17,A36-11, ASME SA-36
ASTM A709-18, AASHTO M270-15
CSA G40.20-13/G40.21-13

CUSTOMER PURCHASE ORDER NUMBER: G4500410746
BILL OF LADING: 1333-60002 14316
DATE: 04/24/2023

CHEMICAL COMPOSITION

C (%)	Mn (%)	P (%)	S (%)	Si (%)	Cu (%)	Ni (%)	Cr (%)	Mo(%)	V (%)	Nb (%)	Al (%)	CEqvA529 (%)	Sn (%)
0.14	0.75	0.016	0.027	0.20	0.36	0.12	0.20	0.028	0.002	0.008	0.001	0.38	0.015

MECHANICAL PROPERTIES

Elong. (%)	G/L (Inches)	G/L (mm)	UTS (PSI)	UTS (MPa)	YS (PSI)	YS (MPa)
28.00	8.000	200.0	76767	529	55016	379
28.00	8.000	200.0	77050	531	55548	383

GEOMETRIC CHARACTERISTICS
R/R
12.06

COMMENTS / NOTES

This grade meets the requirements for the following grades:
ASTM Grades: A36, A529-50, A572-50, A709-36, A709-50
CSA Grades: 44W, 50W
AASHTO Grades: M270-36, M270-50
ASME Grades: SA36

The above figures are certified chemical and physical test records as contained in the permanent records of the company. We certify that these data are correct and in compliance with specified requirements. No weld repair was performed on this material. The material has not been in contact with mercury while in Gerdau possession. For all products other than billets or beam blanks, this material was produced (Electric Arc Furnace, Melted, Continuously Cast, Hot Rolled and, if applicable, Cold-Drawn) in the USA. For billets or beam blanks, this material was produced (Electric Arc Furnace, Melted and Continuously Cast) in the USA. CMTR complies with EN 10204 3.1.

BHASKAR YALAMANCHILI
QUALITY DIRECTOR
Phone: (409) 267-1071 Email: Bhaskar.Yalamanchili@gerdau.com

BEN LOVELL
QUALITY ASSURANCE MGR.
Phone: (731) 423-5213 Email: benjamin.lovell2@gerdau.com

Figure B-7. ASTM A572 Gr. 50 Angle Support for Glulam Timber Vertical Post, Test No. TRTD-1 (Item No. b8)

University of Nebraska System

Purchase Order		
Purchase Order Date	PO/Reference No.	Revision No.
Oct 9, 2023	**E001143261**	**0**

SAP Vendor #	191233
Supplier Name	PORTLAND BOLT & MFG CO INC
Address	3441 NW GUAM ST PORTLAND, Oregon 97210 United States
Contact Person / Telephone	
Contact	See Customer Contact Information below
Email	
Phone	

Supplier Instructions:

Send an order confirmation via email to Customer Name indicated below, to include expected shipping date and purchase order number. To assure prompt payment the purchase order number must appear on all packages, invoices, and related documents. Packing slips must accompany all shipments. This purchase order is governed by the Standard Terms of Purchase at http://www.nebraska.edu/offices-policies/business-finance/procurement/terms-of-purchase, unless an agreement referenced in the item description is effective between the vendor and the Board of Regents of the University of Nebraska, in which case such agreement shall govern.

Billing Information	Customer Contact Information	Delivery Information
Tax Exempt #05-8905401 University of Nebraska-Lincoln Accounting Dept invoices@nebraska.edu PO Box 880623 Lincoln, NE 68588-0623 United States	Customer Name Shaun M Tighe Telephone +1 402-472-0071 Email STIGHE2@UNL.EDU **Delivery Information** Preferred Delivery Date Shipping Method Standard Carrier-Standard Delivery	**Mark & Ship Packages as shown below:** Attn: Shaun M Tighe University of Nebraska MIDWEST ROADSIDE SAFETY FACILITY Unloading Point Test Site 4630 NW 36 ST LINCOLN, NE 68524 United States

Additional Information

Quote Number	*no value*
Pricing Code	

Line No.	Product Description	Catalog No.	Size / Packaging	Unit Price	Quantity	Ext. Price
1 of 1	4" Shear Plate, (7/8" bolt diam.) hot-dip galvanized. Part# 12407	Part#12407	1/EA	6.50 USD	50 EA	325.00 USD

ADDITIONAL INFO

Price	6.50
Catalog No.	Part#12407
Item Notes (included on PO)	Specification: ASTM A47 Grade 32510, ASTM D5933

Shipping, Handling and Tax charges are calculated and charged by each supplier. Total **325.00 USD**

Figure B-8. ASTM A47 Shear Plates for ⅞-in. Diameter Bolts, Test No. TRTD-1 (Item No. b9)

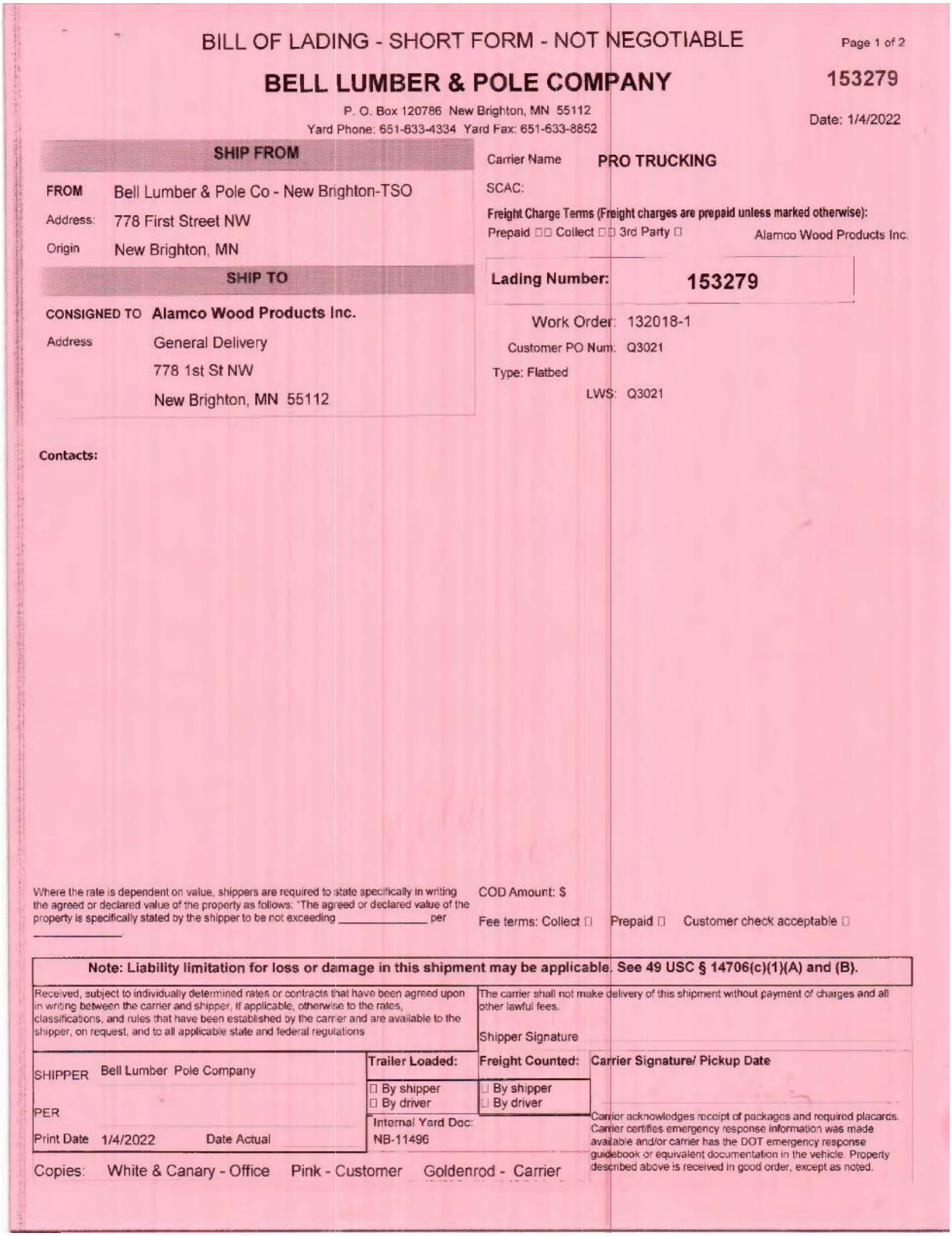

BILL OF LADING - SHORT FORM - NOT NEGOTIABLE

Page 1 of 2

BELL LUMBER & POLE COMPANY

153279

P. O. Box 120786 New Brighton, MN 55112
Yard Phone: 651-633-4334 Yard Fax: 651-633-8852

Date: 1/4/2022

SHIP FROM

FROM Bell Lumber & Pole Co - New Brighton-TSO
Address: 778 First Street NW
Origin New Brighton, MN

Carrier Name **PRO TRUCKING**
SCAC:
Freight Charge Terms (Freight charges are prepaid unless marked otherwise):
Prepaid ☐☐ Collect ☐☐ 3rd Party ☐ Alamco Wood Products Inc.

SHIP TO

CONSIGNED TO **Alamco Wood Products Inc.**
Address General Delivery
778 1st St NW
New Brighton, MN 55112

Lading Number: 153279

Work Order: 132018-1
Customer PO Num: Q3021
Type: Flatbed
LWS: Q3021

Contacts:

Where the rate is dependent on value, shippers are required to state specifically in writing the agreed or declared value of the property as follows: "The agreed or declared value of the property is specifically stated by the shipper to be not exceeding _____ per _____

COD Amount: $
Fee terms: Collect ☐ Prepaid ☐ Customer check acceptable ☐

Note: Liability limitation for loss or damage in this shipment may be applicable. See 49 USC § 14706(c)(1)(A) and (B).

Received, subject to individually determined rates or contracts that have been agreed upon in writing between the carrier and shipper, if applicable, otherwise to the rates, classifications, and rules that have been established by the carrier and are available to the shipper, on request, and to all applicable state and federal regulations

The carrier shall not make delivery of this shipment without payment of charges and all other lawful fees.

Shipper Signature

SHIPPER Bell Lumber Pole Company

PER

Print Date 1/4/2022 Date Actual

Trailer Loaded:
☐ By shipper
☐ By driver

Freight Counted:
☐ By shipper
☐ By driver

Internal Yard Doc:
NB-11496

Carrier Signature/ Pickup Date

Carrier acknowledges receipt of packages and required placards. Carrier certifies emergency response information was made available and/or carrier has the DOT emergency response guidebook or equivalent documentation in the vehicle. Property described above is received in good order, except as noted.

Copies: White & Canary - Office Pink - Customer Goldenrod - Carrier

Figure B-9. Transverse Glulam Timber Deck Panels, Girders, and Diaphragms, Test No. TRTD-1 (Item Nos. c1 through c8)

Portland Bolt & MANUFACTURING COMPANY
800-547-6758 | www.portlandbolt.com

FOR	MIDWEST ROADSIDE SAFETY FACIL
PB INVOICE	164700
CUSTOMER PO	EE001115367
EST. SHIP DATE	8/31/2023

Certificate of Conformance

We certify that the following items were manufactured and tested in accordance with the chemical, mechanical, dimensional and thread fit requirements of the specifications referenced.

7/8" X 26" DOMESTIC HOT-DIP GALVANIZED ASTM A307 GRADE A TIMBER BOLT WITH 6" THREAD

HEAT	1201036150	BASE STEEL	A36	DIAMETER	7/8	SOURCE	NUCOR STEEL

C	MN	P	S	SI	NI	CR	MO	CU	V
0.120	0.670	0.017	0.045	0.180	0.090	0.190	0.020	0.270	0.002

TN	YIELD	SLENG	RA	ELONG	CE	HR
65,300 PSI	48,100	8 "	47.00 %	28.00 %	0	73 HRB

1-3/8" X 28" DOMESTIC HOT-DIP GALVANIZED ASTM A449 TIMBER BOLT WITH 6" THREAD

HEAT	5394485	SOURCE	KREHER STEEL CO LLC

C	MN	P	S	SI	NI	CR	MO	CU	V
0.420	0.910	0.019	0.032	0.240	0.090	1.010	0.200	0.190	0.005

TN	PROOF	HR
143,640 LBF	85,460	241 HBN

lot#21105

3/4" X 8" DOMESTIC HOT-DIP GALVANIZED ASTM A307 GRADE A TIMBER BOLT WITH 4" THREAD

HEAT	1201037998	SOURCE	NUCOR STEEL

C	MN	P	S	SI	NI	CR	MO	CU	V
0.120	0.630	0.012	0.027	0.170	0.080	0.140	0.020	0.310	0.002

TN	RA	YIELD	ELONG	SLENG
65,300 PSI	62.00 %	46,800	30.00 %	8 "

3/4" X 26" DOMESTIC HOT-DIP GALVANIZED ASTM A307 GRADE A TIMBER BOLT WITH 6" THREAD

HEAT	1202044144	SOURCE	NUCOR STEEL

C	MN	P	S	SI	NI	CR	MO	CU	V
0.140	0.680	0.016	0.040	0.220	0.090	0.160	0.020	0.270	0.002

TN	RA	YIELD	ELONG	SLENG
67,500 PSI	50.00 %	46,900	30.00 %	8 "

Products

- ASTM A307 GRADE A ALL THREAD ROD

Figure B-10. 26-in. Long ⅞-in. Dia. ASTM A307A Timber Bolts, 28-in. Long 1⅜-in. Dia. ASTM A449 Timber Bolt, and 8-in. Long ¾-in. Dia. ASTM A307A Timber Bolts, Test No. TRTD-1 (Item Nos. d1, d2, and d7)

FASTENAL®

Fastenal Company
P.O Box 1286
WINONA, MN 55987-1286

The store serving you is
3201 N. 23rd Street STE 1

LINCOLN, NE 68521
Phone #: (402)476-7900
Fax #: 402/476-7958

Packing Slip

Date	Reference No.	Page
7/1/21	NELIN400587	1

DUE DATE: 07/31/2021

Cust. No. NELIN3402
Cust. P.O. E000867825
Job No. MIDWEST ROADSIDE SAFETY FACIL

Sold To
UNL / UNMC E-SHOP / PUNCHOUT
UNIVERSITY OF NEBRASKA
1700 Y ST
LINCOLN, NE 68588-0646

Ship To
Picked up at Fastenal Store

Contract No:
2018.000208

This Order and Document are subject to the "Terms of Purchase" posted on www.fastenal.com.

Line No.	Quantity Ordered	Quantity Shipped	Quantity Backorder	Description	Control No.	Part No.	Price / Hundred	Amount
1	6	6	0	3/4-10x9-1/2 A307A G	120306283	91975	693.1600	41.59 G
2	12	12	0	B7 Std 3/4-10x8Galv	935935-1	0186717	867.7400	104.13 G
3	60	60	0	3/4x11GalvHex Lag	line50358	22492	1,071.1300	642.68 G
4	80	80	0	3/4 USS F/W GALV	210220089	1133186	78.2600	62.61 G
5	42	42	0	HVY HX GALV 3/4-10	180198094	36716	97.1800	40.82 G

Received By

Comments
Deliver To:MIDWEST ROADSIDE SAFETY FACILITY Contact: UNL

Tax Exemption
Government
NE

Subtotal	891.83
Shipping & Handling	0.00
State Tax	0.00
County Tax	0.00
City Tax	0.00
TOTAL USD	891.83

If you re-package or re-sell this product, you are required to maintain
Reasonable collection and attorneys fees will be assessed to all accounts placed for collection
No materials accepted for return without our permission.
X indicates part is a hazardous material
** indicates part was sold at a promotional or special discount price*

An electronic invoice will be available within two days.
All discrepancies must be reported within 10 days.

0

Thank You !

FORM - IN13

Figure B-11. 10-in Long ¾-in. Dia. ASTM A307A Hex Bolts, 11-in. Long ¾-in. Dia. Lag Bolts, ⅞-in. Heavy Hex Nuts, Test No. TRTD-1 (Item Nos. d3, d6, and f1)

Portland Bolt & MANUFACTURING COMPANY
Phone: 800-547-6758 | Fax: 503-227-4634
3441 NW Guam Street, Portland, OR 97210
Web: www.portlandbolt.com | Email: sales@portlandbolt.com

CERTIFICATE OF CONFORMANCE

For: MIDWEST ROADSIDE SAFETY FACIL
PB Invoice#: 142080
Cust PO#: MGTD
Date: 5/27/2021
Shipped: 5/28/2021

We certify that the following items were manufactured and tested in accordance with the chemical, mechanical, dimensional and thread fit requirements of the specifications referenced.

Description: 3/4 X 60 GALV ASTM A307A ROD

Heat#: 1202027708 **Base Steel:** A36 **Diam:** 3/4

Source: NUCOR STEEL **Proof Load:** 0

C :	.130	**Mn:**	.680	**P :**	.011	**Hardness:**	0
S :	.039	**Si:**	.150	**Ni:**	.080	**Tensile:**	67,600 PSI
Cr:	.110	**Mo:**	.020	**Cu:**	.240	**Yield:**	50,400 PSI
Pb:	.000	**V :**	.002	**Cb:**	.000	**Sample Length:**	8 INCH
N :	.000			**CE:**	.2637	**Charpy:**	

RA: 46.00%
Elon: 29.00%
CVN Temp:

Other:
ALL ITEMS MELTED & MANUFACTURED IN THE USA

By: _____
Certification Department Quality Assurance
Dane McKinnon

Figure B-12. 5-ft Long ¾-in. Dia. ASTM A307A Threaded Rods, Test No. TRTD-1 (Item No. d4)

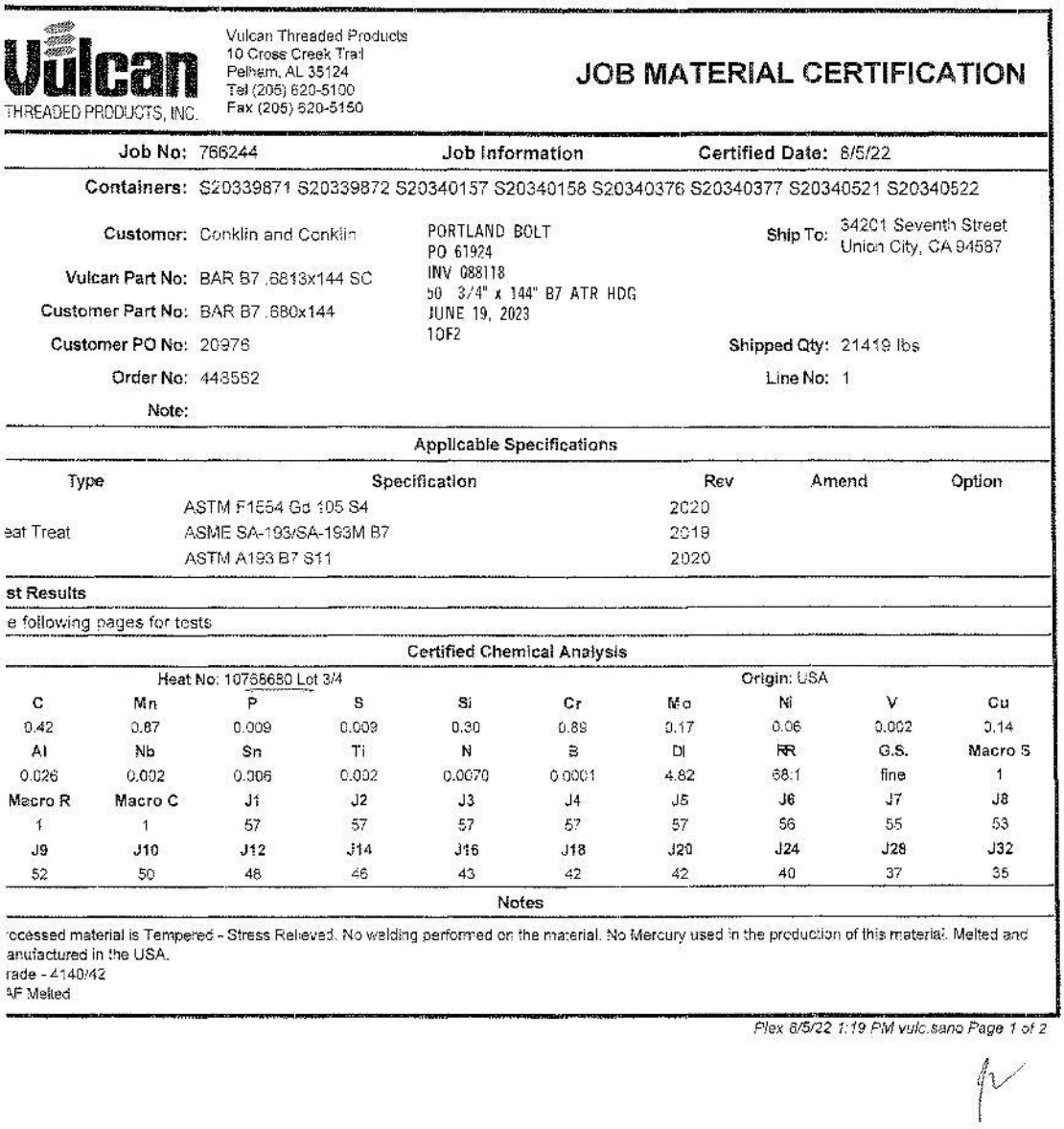

Vulcan
THREADED PRODUCTS, INC.

Vulcan Threaded Products
10 Cross Creek Trail
Pelham, AL 35124
Tel (205) 620-5100
Fax (205) 620-5150

JOB MATERIAL CERTIFICATION

Job No: 766244 **Job Information** **Certified Date:** 8/5/22

Containers: S20339871 S20339872 S20340157 S20340158 S20340376 S20340377 S20340521 S20340522

Customer: Conklin and Conklin
PORTLAND BOLT
PO 61924
INV 088118
50 3/4" x 144" B7 ATR HDG
JUNE 19, 2023
1OF2

Ship To: 34201 Seventh Street
Union City, CA 94587

Vulcan Part No: BAR B7 .6813x144 SC
Customer Part No: BAR B7 .680x144
Customer PO No: 20976
Order No: 448552
Note:

Shipped Qty: 21419 lbs
Line No: 1

Applicable Specifications

Type	Specification	Rev	Amend	Option
	ASTM F1554 Gd 105 S4	2020		
eat Treat	ASME SA-193/SA-193M B7	2019		
	ASTM A193 B7 S11	2020		

st Results

e following pages for tests

Certified Chemical Analysis

Heat No: 10786680 Lot 3/4 Origin: USA

C	Mn	P	S	Si	Cr	Mo	Ni	V	Cu
0.42	0.87	0.009	0.009	0.30	0.89	0.17	0.06	0.002	0.14
Al	Nb	Sn	Ti	N	B	DI	RR	G.S.	Macro S
0.026	0.002	0.006	0.002	0.0070	0.0001	4.82	66.1	fine	1
Macro R	Macro C	J1	J2	J3	J4	J5	J6	J7	J8
1	1	57	57	57	57	57	56	55	53
J9	J10	J12	J14	J16	J18	J20	J24	J28	J32
52	50	48	46	43	42	42	40	37	35

Notes

ocessed material is Tempered - Stress Relieved. No welding performed on the material. No Mercury used in the production of this material. Melted and anufactured in the USA.
rade - 4140/42
AF Melted

Plex 8/5/22 1:19 PM vulc.sano Page 1 of 2

Figure B-13. ASTM 193 Gr. B7 8-in. Long ¾-in. Dia. Threaded Rods, Test No. TRTD-1 (Part No. d5)

FASTENAL®

Fastenal Company
P.O Box 1286
WINONA, MN 55987-1286

The store serving you is
3201 N 23rd St
Unit 1
LINCOLN, NE 68521
Phone #: (402)476-7900
Fax #: 402/476-7958

Packing Slip

Date	Reference No	Page
7/26/23	NELIN446475	1

Discount Due Date 2% 10 8/4/2023
Final Due Date NET30 8/24/2023
Contract No:
2018.000208

Cust. No. NELIN2067
Cust. P.O. TRTD
Job No.

Sold To
UNL TRANSPORTATION/Midwest Roadside Safe
1931 NORTH ANTELOPE VALLEY PKWY
LINCOLN, NE 68588
402-472-7937; 402-472-8660(Fax)

Ship To
Picked up at Fastenal Store

This Order and Document are subject to the "Terms of Purchase" posted on www.fastenal.com.

Line No.	Quantity Ordered	Quantity Shipped	Quantity Backorder	Description	Control No.	Part No.	Price / Hundred	Amount
1	5	5	0	5/8x6GalvHex Lag	170126372	22352	319.4900	15.97 E
2	50	50	0	3/4 USS F/W GALV	170129716	1133186	110.0800	55.04 E
3	15	15	0	HVY HX GALV 7/8-9	120504912	36718	153.9400	23.09 E
4	50	50	0	HVY HX GALV 3/4-10	210306584	36716	104.0600	52.03 E

Received By

Comments
Contact: Shaun Tighe

If you re-package or re-sell this product, you are required to maintain integrity of Country of Origin to the consumer of this product.

Reasonable collection and attorneys fees will be assessed to all accounts placed for collection
No materials accepted for return without our permission.

X indicates part is a hazardous material

" indicates part was sold at a promotional or special discount price

FORM - IN13

Tax Exemption
Exempt
NE

Subtotal	146.13
Shipping & Handling	0.00
State Tax	0.00
County Tax	0.00
City Tax	0.00
TOTAL USD	146.13

An invoice will be mailed in approximately five days.
All discrepancies must be reported within 10 days. "D"

Thank You !

Figure B-14. 6-in. Long ⅝-in. Dia. Lag Screw, Flat ¾-in. Dia. Washer, ¾-in. Dia. Heavy Hex Nut, Test No. TRTD-1 (Item Nos. d8, e3, and f2)

Portland Bolt
& MANUFACTURING COMPANY
800-547-6758 | www.portlandbolt.com

ORDER # 164896
DATE 7/21/2023
PAGE 1 of 1

sales@portlandbolt.com Phone: 800.547.6758 | Fax: 503.227.4634
www.portlandbolt.com 3441 NW Guam St. Portland OR, 97210

SALESPERSON Steven Wallenstein
DIRECT PHONE 800.598.4204
EMAIL steven@portlandbolt.com

SOLD TO
MIDWEST ROADSIDE SAFETY FACIL
WHITTIER SCHOOL ROOM 130L
2200 VINE ST
LINCOLN, NE, 68583-0853
Phone: 402.472.0965 | Fax: 402.472.2022

SHIP TO
MIDWEST ROADSIDE SAFETY FACIL
4630 NW 36TH STREET
LINCOLN, NE, 68524

ATTN Shaun <stighe2@unl.edu>
CUSTOMER PO E001117299
COMMENT SHIP WITH S/O#164801
SHIP DATE 7/24/2023
SHIP VIA UPS Ground

LINE	QTY. ORDERED	DESCRIPTION
1	15	7/8" import hot-dip galvanized malleable iron washer
2	5	1-3/8" import hot-dip galvanized ASTM A563 Grade A heavy hex nut

Figure B-15. ⅞-in. Dia. Bolt Malleable Iron Washers, Test No. TRTD-1 (Item No. e1)

INV#:MB19-137

CERTIFIED MATERIAL TEST REPORT

Factory: SHENG DA-LI MACHINERY FACTORY
Item: ROUND WASHER
Customer: BBI
Quantity Shipped:72CTNS.
Sampling Plan per: 32510 MALLEABLE IRON
Size & Description: 3/4"

Date: 2019-12-12
Lot No: 9100963-02
Finish:HDG.
BBI/PO:B19100963
Part No: P39086
Heat No: 2019112802

Material Test Results

材 质 报 告

Chemical Analysis (%) 化学成分									
C	Si	Mn	P	S					
2.55	1.52	0.51	0.053	0.053					

Mechanical Properties Test Results

机 械 性 能 报 告

	Standard Requirements 要求	Test Results 检验结果
Tensile Strength (Mpa) 抗拉强度	345	363
Yield Strength (Mpa) 屈服强度	224	253
Elongation (%) 延伸率	10	14.1

All tests are in accordance with the methods prescribed in the applicable ASTM specification. We certify that this data is a true representation of information provided by the material supplier and our testing laboratory.

REMARK: 1.The report is issued according to ISO16228 F3.1 (EN10204 3.1).
2.Test Facility: M

王国钊

(Signature of Q.A. Lab Mgr.)

Figure B-16. ¾-in. Dia. Bolt Malleable Iron Washers, Test No. TRTD-1 (Item No. e2)

STEEL AND PIPE SUPPLY
SPS Coil Processing Tulsa
5275 Bird Creek Ave.
Port of Catoosa, OK 74015

METALLURGICAL TEST REPORT

PAGE 1 of 1
DATE 04/07/2023
TIME 07:43:33

SOLD TO

SHIP TO
13716
Kansas City Warehouse
401 New Century Parkway
New Century KS 66031-1127

Order	Material No.	Description	Quantity	Weight	Customer Part	Customer PO	Ship Date
40401413-0010	701272120	3/8 72 X 120 A36 STP MIL PLT	11	10,111.200			04/06/2023

Chemical Analysis

Heat No. 23027702 Vendor BIG RIVER STEEL LLC DOMESTIC Mill BIG RIVER STEEL LLC **Melted and Manufactured in the USA**
Produced from Coil

Carbon	Manganese	Phosphorus	Sulphur	Silicon	Nickel	Chromium	Molybdenum	Boron	Copper	Aluminum	Titanium	Vanadium	Columbium	Nitrogen	Tin
0.1900	0.8400	0.0090	0.0010	0.0400	0.0400	0.0400	0.0120	0.0002	0.0900	0.0320	0.0010	0.0040	0.0010	0.0082	0.0045

Mechanical / Physical Properties

Mill Coil No. 23027702-03

Tensile (PSI)	Yield (PSI)	% Elong (2 in)	Rckwl	Grain	Charpy	Charpy Dr	Charpy Sz	Temperature	Olsen
72600.000	48200.000	36.00			0	NA			
71200.000	48100.000	35.50			0	NA			
71600.000	47800.000	33.00			0	NA			
67300.000	44400.000	32.00			0	NA			

Batch 1001258659 11 EA 10,111.200 LB
Batch 1001258665 11 EA 10,111.200 LB
Batch 1001258681 11 EA 10,111.200 LB
Batch 1001258686 5 EA 4,595 LB
Batch 1001258673 11 EA 10,111.200 LB

THE CHEMICAL, PHYSICAL, OR MECHANICAL TESTS REPORTED ABOVE ACCURATELY REFLECT INFORMATION AS CONTAINED IN THE RECORDS OF THE CORPORATION.
The material is in compliance with EN 10204 Section 4.1 Inspection Certificate Type 3.1
This test report shall not be reproduced, except in full, without the written approval of Steel & Pipe Supply Company, Inc.

Figure B-17. 6-in. x 6-in. x ⅜-in. Thick Steel Plate Washer, Test No. TRTD-1 (Item No. e4)

Certified Material Test Report to ISO16228 F3.1 (EN 10204-2004 3.1)
FOR ASTM A563-15,GRADE A HEAVY HEX NUTS

FACTORY: NINGBO HAIXIN HARDWARE CO.,LTD. DATE: APR.19.2021
ADDRESS: XIJINGTANG LUOTUO NINGBO ZHEJIANG 315205 COUNTRY OF ORIGIN: CHINA
CHINA MFG LOT NUMBER: 5170870011
CUSTOMER: BRIGHTON-BEST INTERNATIONAL (TAIWAN) INC PO NUMBER: U82918
QNTY: 1,440MPCS PART NO: 324340
MANUFACTURER DATE: 2021/1/26

SAMPLE SIZE : ACC. TO ASME B18. 18. 1 - 11
SIZE:1.3/8-6+0.027(HDG)
FINISH:HOT DIP GAL PER ASTM A153-09/ASTM F2329-13

STEEL PROPERTIES TEST FACILITY: S
STEEL GRADE: 45# HEAT NUMBER: 1-01746

CHEMISTRY SPEC:	C %*100	Mn%*100	P %*1000	S %*1000
	0.55max	0.30min	0.12max	0.15max
TEST:				
	0.46	0.59	0.013	0.001

DIMENSIONAL INSPECTIONS SPECIFICATION: ASME /ANSI B18.2.2-2015 TEST FACILITY: M

CHARACTERISTICS	TEST METHOD	SPECIFIED	ACTUAL RESULT	ACC.	REJ.
WIDTH A/F	2.119"-2.188"		2.131"-2.164"	32	0
WIDTH A/C	2.416"-2.526"		2.428"-2.471"	32	0
THREAD	ASME B1.1-03	2B	PASSED	8	0
HEIGHT	1.310"-1.378"		1.329"-1.356"	32	0
MARK			PASSED	100	0
HDG THICKNESS	ASTM A153-09/ASTM F2329-13 min:43um		59UM-71UM	20	0

MECHANICAL PROPERTIES: SPECIFICATION: ASTM A563-15 GR-A TEST FACILITY: M

CHARACTERISTICS	TEST METHOD	SPECIFIED	ACTUAL RESULT	ACC.	REJ.
HARDNESS :	ASTM E18-12	Min B68-C32 Max	HRB85-87	5	0
PROOF LOAD:	ASTM F606-11	MIN75000 PSI	75000 PSI	5	0

ALL TESTS IN ACCORDANCE WITH THE METHODS PRESCRIBED IN THE APPLICABLE ASTM OR SAE SPECIFICATION. WE CERTIFY THAT THIS DATA IS A TRUE REPRESENTATION OF INFORMATION PROVIDED BY THE MATERIAL SUPPLIER AND OUR TESTING LABORATORY.
Maker's ISO# ISO9001-0068481

(SIGNATURE OF QA/LAB MGR.)
(NAME OF MANUFACTURER)

Figure B-18. ASTM A563 Gr. A 1⅜-in. Dia. Heavy Hex Nut, Test No. TRTD-1 (Item No. f3)

Date: 12/13/2016

Subject: Certificate of Conformance

Product: HIT RE-500 V3 Adhesive

To Whom it May Concern:

This is to certify that the HIT-RE 500 V3 is a high-strength, slow cure two-part epoxy adhesive contained in two cartridges separating the resin from the hardener.

Additionally, this certifies that the product has been seismically and cracked concrete qualified as represented in ICC-ES report ESR- 3814.

Sincerely,

Hilti, Inc.

5400 South 122 East Avenue

Tulsa, Oklahoma 74146

800-879-8000

800-879-7000 fax

US-Sales@hilti.com

Figure B-19. Hilti CoC Epoxy Adhesive, Test No. TRTD-1 (Item No. g1)

Appendix C. Accelerometer Data Plots

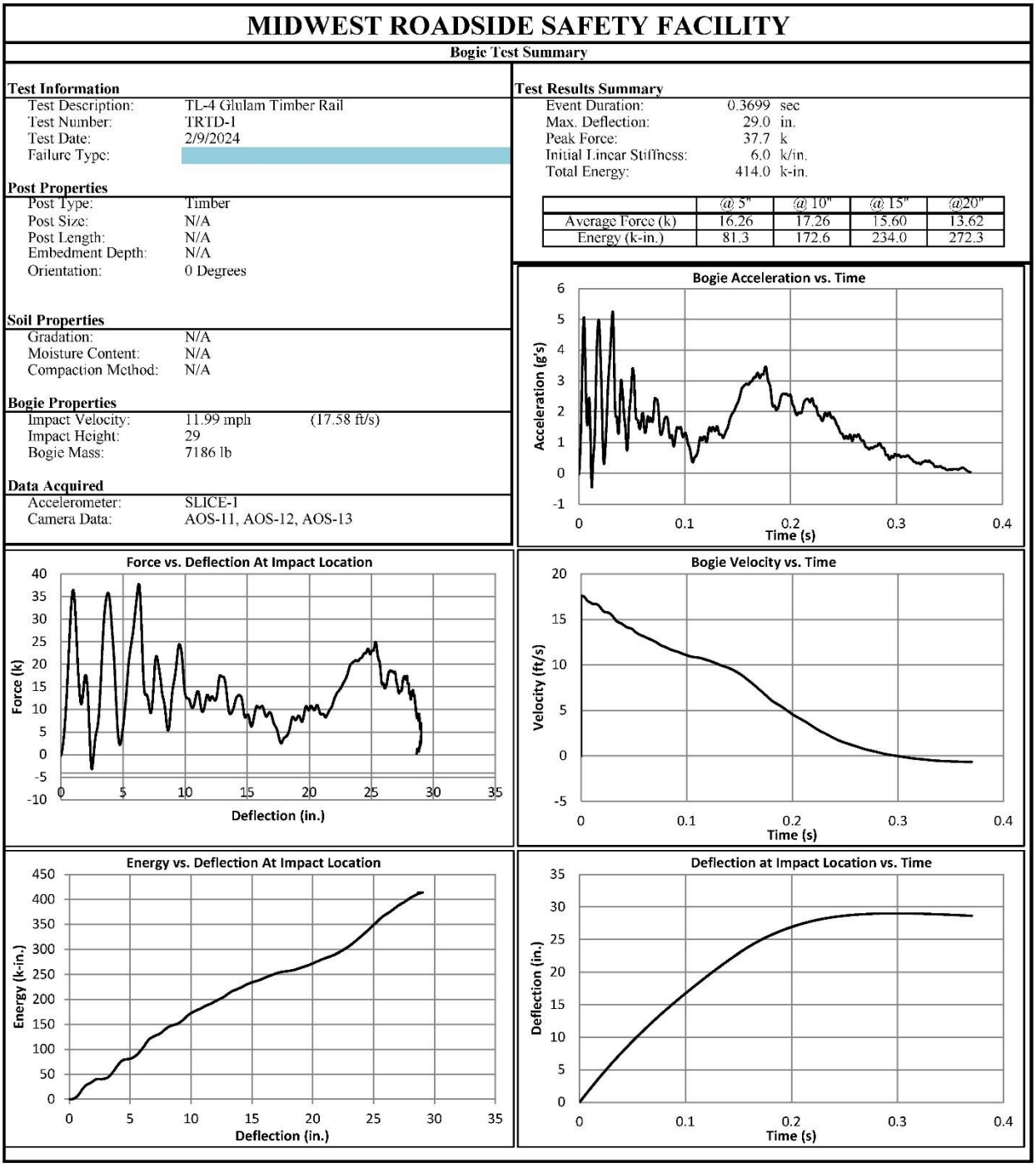

Figure C-1. SLICE-1 Summary Page, Test No. TRTD-1

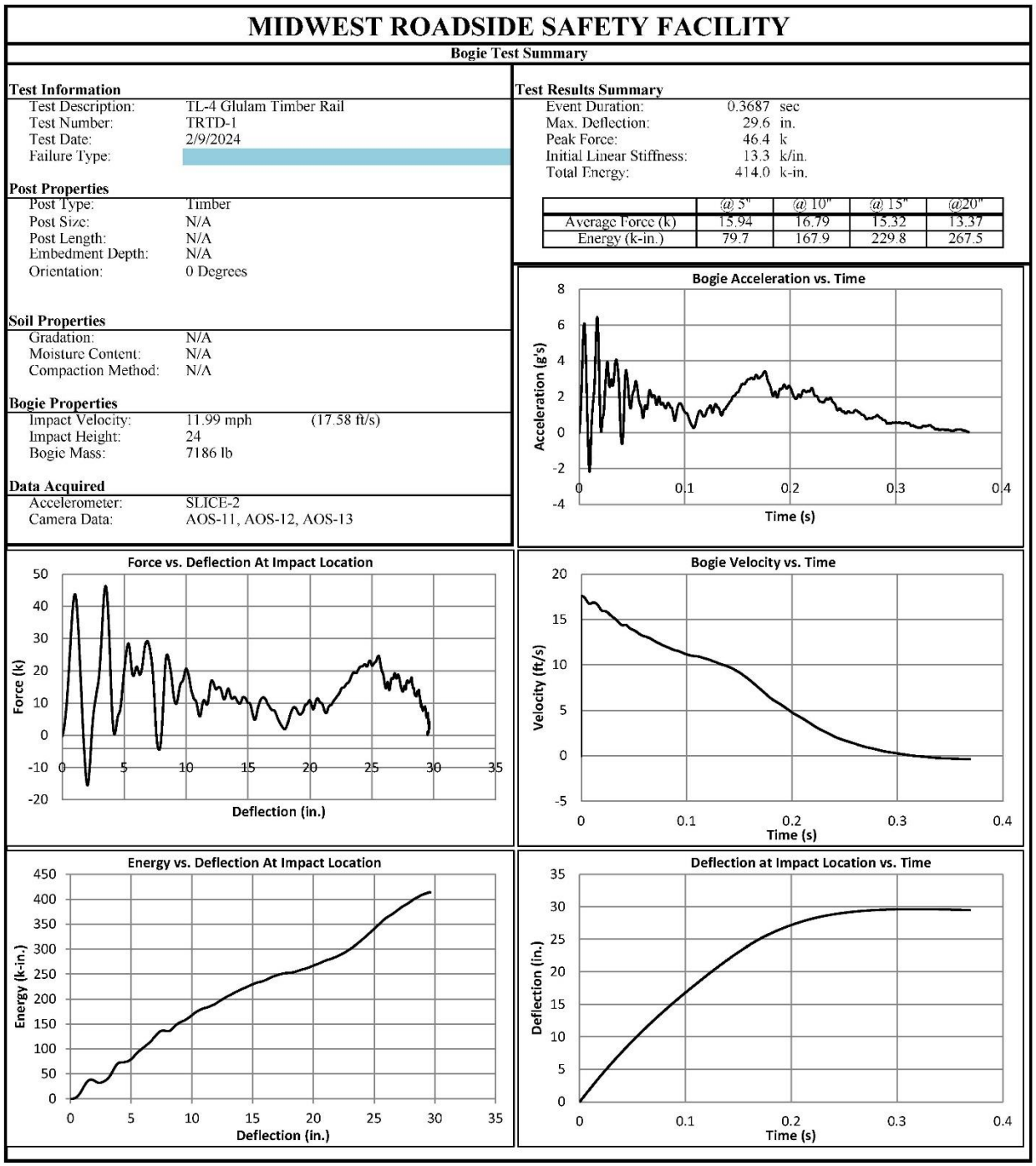

Figure C-2. SLICE-2 Summary Page, Test No. TRTD-1

Appendix D. Alternative Post Yield Moment Model

The reinforced timber equations from section 3.2.1.3 were approximations of the post to deck connection. An alternative method was explored for describing post to deck connection because there were some discrepancies with the predictions with came from the reinforced timber model. The first discrepancy came from the horizontal bolt axial strain readings of test TRBR-1 in 1997. The research report for crash test TRBR-1 included a summary of the instrumented horizontal bolt strain gauges, shown in Figure D-1.

Hardware Type	Gauge No.	Gauge Location	Maximum μ Strain[1] (mm/mm)	Maximum Load[2] (kN)	Maximum Stress[3,4] (MPa)	Comments
Strain Gauge	1	Post Bolt No. 3	486	62.02	99.2	Bolt attaching curb rail to post
	2	Post Bolt No. 4	806	102.65	164.2	Bolt attaching curb rail to post
	3	Post Bolt No. 5	1,043	126.98	203.1	Bolt attaching curb rail to post
	4	Post Bolt No. 6	1,036	125.99	201.5	Bolt attaching curb rail to post
	5	Post Bolt No. 7	806	128.12	204.9	Bolt attaching curb rail to post
	6	Post Bolt No. 8	551	68.74	110.0	Bolt attaching curb rail to post
	7	Top Rail Plate No. 1	NA	NA	NA	Traffic-side face at post no. 6
	8	Top Rail Plate No. 1	657	NA	136.0	Back-side face at post no. 6
	9	Curb Rail Plate No. 1	212	NA	43.9	Back-side face at midspan between post nos. 5 and 6
	10	Wood Rail	NA	NA	NA	Back-side face at midspan between post nos. 5 and 6
String Potentiometer	Gauge No.	Gauge Location	Relative Maximum Deck to Girder Displacement (mm)		Comments	
	1	String Pot No. 1	0.094		Midspan girder no. 1 (outer girder)	
	2	String Pot No. 2	0.538		¾-point girder no. 1 (outer girder)	
	3	String Pot No. 3	0.224		⅞-point girder no. 1 (outer girder)	
	4	String Pot No. 4	1.049		Joint between girder no. 1 and 2 (outer girder)	
	5	String Pot No. 5	0.300		¼-point girder no. 2 (outer girder)	

[1] - All strain values are shown as the absolute value only.
[2] - All load values calculated using calibration factor obtained from individual load test data.
[3] - For bolts, elastic stress values are shown as the absolute value only and calculated by dividing the load by the tensile stress area equal to 625.16 mm² (0.969 in²). Minimum yield stress for the bolts is 248 MPa (36 ksi).
[4] - For plates, elastic stress values are shown as the absolute value only and calculated by multiplying the strain by the modulus of elasticity equal to 207,000 MPa (30,000 ksi). Minimum yield stress for the plates is 248 MPa (36 ksi).
NA - Not available or not applicable.

Figure D-1. Summary of Strain Gauge Readings from TRBR-1

Although, the table above shows the same strain for bolts at post nos. 4 and 7, this is believed to be an error because the data through the rest of the row is properly proportionate between force and stress. Converting to imperial units, 1 kN = 0.2248 kip, the maximum loads on the horizontal bolts were:

Table D-1. Maximum Bolt Forces in Kips

Strain Gauge Location	Maximum Load (kip)
Post 3 Bolt	13.94
Post 4 Bolt	23.08
Post 5 Bolt	28.55
Post 6 Bolt	28.32
Post 7 Bolt	28.80
Post 8 Bolt	15.45

The model which has been developed through Phase IIa and is in use for evaluating the railing for MASH TL-4 Impact conditions was initially calibrated against the performance of the NCHRP-350 system tests TRBR-1 and TRBR-2 to validate the accuracy of the new model. If the NCHRP-350 railing design parameters are put into the model developed with yielding at the base of the scupper and reinforced timber equations used to describe the moment capacity, then the force in the horizontal bolt could be predicted. If the six vertical ¾ in. diameter bolt stresses were 60 ksi, then the force in the horizontal bolt would be 71 kips once the post begins to yield, far above the maximum of 28 kips observed from the instrumented horizontal bolt strain gauges. The following equations demonstrate how this force was obtained:

$$P_{h\ bolt} = \frac{M_n}{h_{center\ of\ h\ bolt\ to\ top\ of\ deck}} = \frac{A_s f_y \left(d - \frac{a}{2}\right)}{h}$$

$$A_s = {d_b}^2 \frac{\pi}{4} = 2.651\ in^2$$

$$a = \frac{A_s f_y}{0.85 F_{cp} b} = \frac{(2.651\ in^2)(60\ ksi)}{0.85(560\ psi * 2.1)(54\ in)} = 2.946\ in$$

$$P_{h\ bolt} = \frac{(2.651\ in^2)(60\ ksi)\left(6\ in - \frac{2.946\ in}{2}\right)}{10.125\ in} = 71\ kips$$

A review of simulations from Phase IIa CIP analysis with the SUT shows several locations where different posts are yielding. The BARRIER VII software reduces the yield moment by roughly 10% to conservatively estimate railing performance, but this would only reduce the horizontal bolt yielding load to 64 kips, which is still considerably higher than 28 kips.

Since the horizontal bolt transfers the load to the vertical bolts, it was not possible for the vertical bolts to be yielding. Rather than vertical bolt yielding, the potential for compression underneath the bolt head was investigated. Dynamic component tests have been conducted on TL-1 posts by MwRSF in an earlier project [7]. The TL-1 post utilized vertical bolts but did not include any vertical post or horizontal bolt. In dynamic tests, the bolt head can be seen in Figure D-2 pulling through the top of the wood railing, representing a different failure mode.

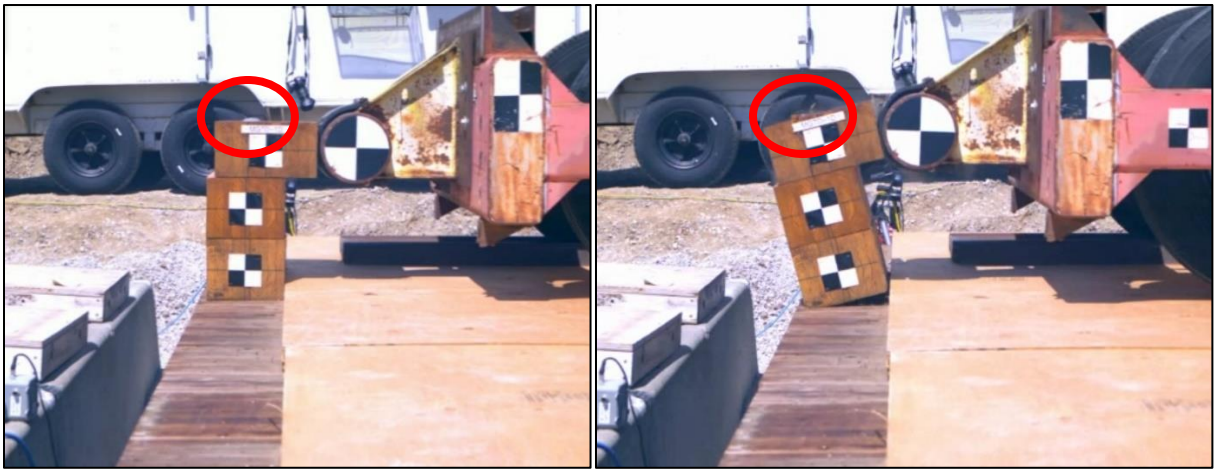

Figure D-2. Left, Post at Start of Impact with Domed Bolt Heads Visible; Right, Domed Bolt Heads No Longer Visible [7]

The vertical bolts were noted to start pulling through the top of the scupper in static tests on TL-1 curb rail posts as well, according to existing photographs of prior MwRSF static testing, shown in Figure D-3.

Figure D-3. From top right to bottom left: Test Nos. WVS-1, WVS-2, WVS-3, WVS-4, WVS-5, MGTD-1S, MGTR-1S, MGTR-1SB, MGTR-1D

To develop the tensile load in the timber bolt, the timber bolt head must push against the wood directly underneath it. In the orientation shown above, the timber strength is in compression perpendicular to grain. If this property is lower than the steel yielding, then the steel won't yield due to tensile forces. The following equation shows this comparison:

$$T_{bolt} = min\left(A_s f_y, A_c F'_{c\perp}\right)$$

Combination 47 Southern Pine glulam wood was used for the railings in Figure D-3, which has a tabulated strength of 740 psi. AASHTO adjusts tabulated values by a factor of 2.1 to adjust ASD to LRFD, which was consistent throughout the research project. The temperature factor was not applied because temperature was less than 100 degrees Fahrenheit. The moisture factor was not applied for this estimate because the moisture content on site for the conducted tests was unlikely to be greater than 16% within the glulam members. After applying these factors, the compressive design value was 1,554 psi. The area of steel under the head of a 2.25 in. diameter bolt head which has a 0.75 in. diameter shank is 3.53 in. The compressive force under the bolt head was 5.5 kips, about a fourth of the yielding load (~22 kips for 50.5-ksi steel).

The alternative bolt force estimate was utilized with the reinforced timber equations to predict the horizontal bolt load, which came out as 18.8 kips. This model underpredicted the load significantly and would likely have resulted in BARRIER VII simulations which were less well calibrated to TRBR-1 and -2. Since the geometric properties were reliable, the possibility of an underprediction of the compressive load was investigated.

The tabulated values for glulam timber compression perpendicular to grain are described by ASTM D3737. The values are based on an empirical equation relating the specific gravity of a wood species to its compressive design value perpendicular to grain. The data for the compressive resistance of wood was gathered at 0.04-in. deformation. The specific gravity was reduced according to whether the wood grain was dense, close, medium, or coarse. Then those values were reduced for the worst-case scenario of load bearing direction to angle of growth rings, and increased according to the seasoning factor, which adjusts green specimen strength to dry specimen strength.

The effect of the angle of grain on compressive resistance was based on unpublished research, which concluded that compressive stress perpendicular to grain decreases under different growth ring orientations. The magnitude of the decrease was different for different orientations and species as well. The growth ring angles orientations in test MGTD-1D are shown in Figure D-4, demonstrating that all orientations are present in the glulam scupper blocks.

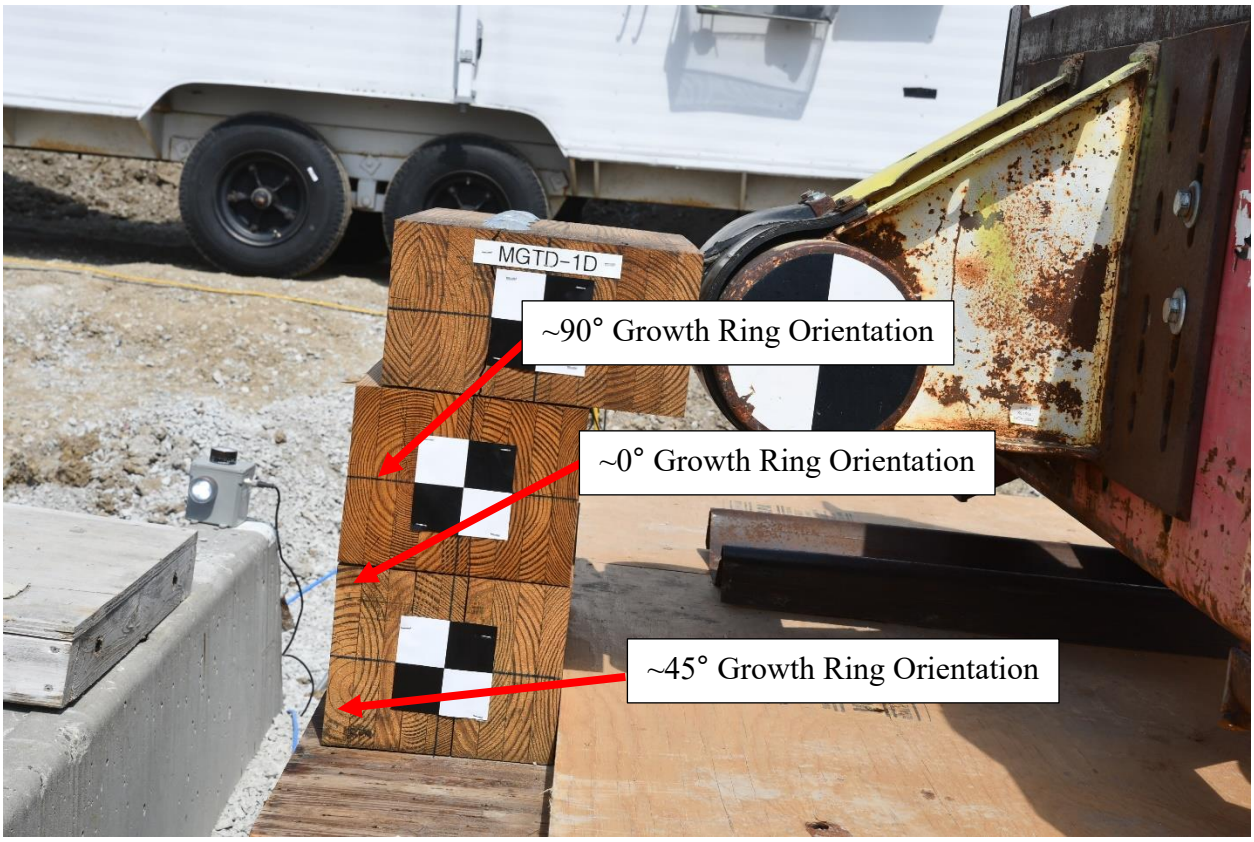

Figure D-4. Growth Ring Orientation in Dynamic Component Test

While the load duration factor applies to timber in compression perpendicular to grain, NDS does not include this factor in calculation of the design value. This was because the primary concern for most uses of timber in compression perpendicular to grain was serviceability rather than strength. The tabulated values reflect the stress under 10-minute loads.

The 0.04-in. deformation limit selected for the design value would suggest greater resistance when deformation increases. However, an increase to the resistance for 0.06-in. or 0.1-in. deformation would not linear because the relationship between stress and strain is nonlinear after cell walls begin to collapse [93], which likely begins prior to 0.04-in. deformation [131]. Nevertheless, some localized compression was considered as a possible method of increasing the force in the bolt. The grain directly underneath the bolt head might locally increase stress when a smaller area is in compression as shown in Figure D-5, which can be accounted for by the bearing area factor.

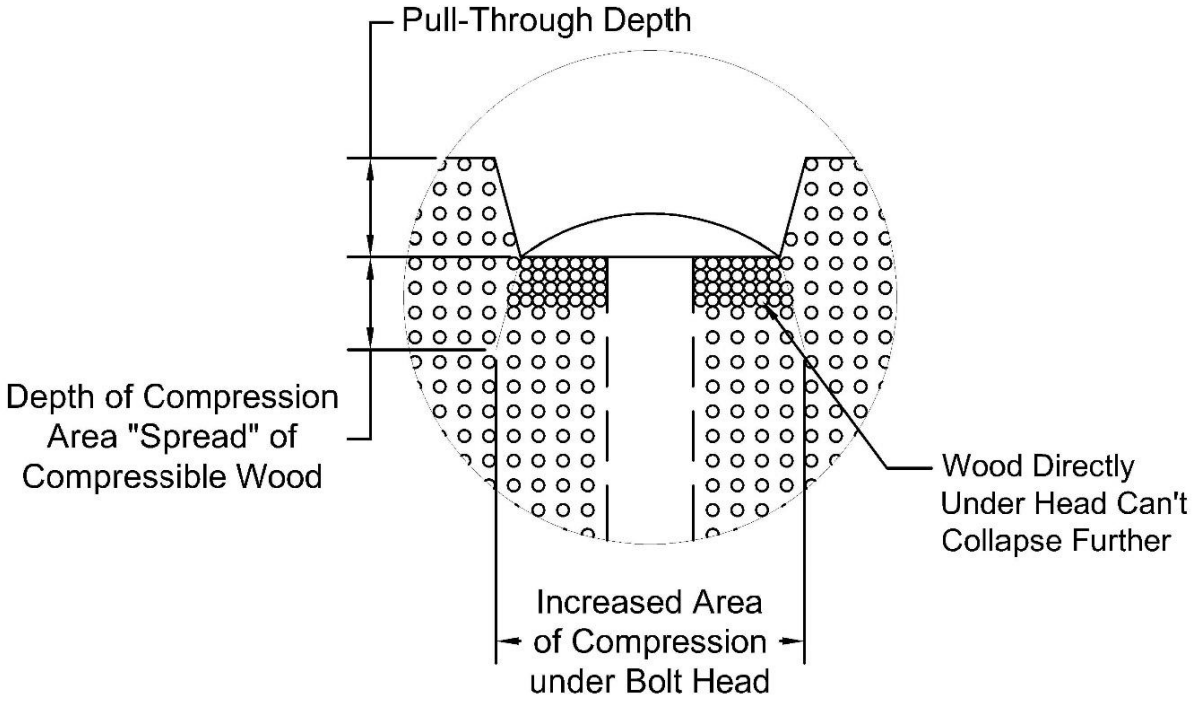

Figure D-5. Bolt Head Pull-Through Model

Utilizing the bearing area factor, the calculated force in a ¾-in. diameter bolt was 8.1 kips. For all 6 bolts, and utilizing the bearing area factor for the compression into the deck as well, the estimated moment from the bolts was 275 kip-in. For a 10.125-in. height from the horizontal bolt to the top of the deck, the load was 27.2 kips. This load was much closer to the measured 28.8 kips from TRBR-1.

However, modeling yield moment in BARRIER VII results in the failure of multiple posts and severe deflections, over 13 in., which were not observed in full-scale crash testing. The model, which was developed in Phase IIa and presented in chapter 3, better approximated the overall system behavior and was more useful for designing the system for full-scale crash testing, despite its limitations. Therefore, the model based around localized failure of timber under the bolt heads was not developed further. However, the model nevertheless pointed towards local failure patterns which helped the research team design modifications to strengthen the timber components of the post following TRTD-1 and create better load distribution.

Appendix E. Post Yield Moment

The yield moment equations presented in Section 3.2.1.3 rely on selected input variables, summarized as follows. The steel bolt stress, F_y, was taken as 45 or 60 ksi. The total steel bolt area, A_s, was calculated using eight ¾-in. diameter bolts (3.534 in.^{2}) and eight ⅞-in. diameter bolts (4.811 in.^{2}). Thread reduction was not applied to these areas. The scupper width, b, was either 54 or 58 in., and the distance from the edge of compression zone to the vertical bolt centerline, d, was 8 in. The design value for compression perpendicular to grain for glulam combination 2 Douglas Fir-Larch was 560 psi.

To convert allowable stress design (ASD) values to load and resistance factor design (LRFD), the compression perpendicular to grain design value, F_{cp}, was adjusted using a format conversion factor. Based on AASHTO guidance, this factor is defined as $C_{KF} = 2.1/\varphi$, where φ is the strength reduction factor. For simplification, the strength reduction factor was omitted and a multiplier of 2.1 was applied directly. Additional modification factors for moisture content, load duration, temperature, and bearing area were considered. All factors were set to 1.0, with the exception of the moisture content factor, which was reduced to 0.53 to reflect high-moisture conditions. The resulting compressive resistance perpendicular to grain used for design was 1.176 ksi. No further adjustments were made in the primary design approach.

A more detailed estimate of the compressive resistance was also investigated. This approach considered the effects of time-dependent impact loading, increased resistance due to localized deformation, bearing area effects, and growth ring orientation. Test data from green Douglas Fir specimens reported compressive stresses perpendicular to grain of 700 psi at 0.04-in. deflection and 864 psi at 0.1-in. deflection [131]. Although resistance would increase with further deformation, the precise extent of deformation across the bearing surface was unknown. These two values were therefore treated as bounding cases, as higher-strain data were not available. Existing research indicated that increases in perpendicular-to-grain compressive resistance diminish after reaching a yield-like stress plateau [92-93].

The influence of growth ring orientation was considered by applying a reduction factor of 1/1.67. This adjustment was based on the most conservative estimate available [94]. Because glulam members can contain any growth ring orientation relative to the loaded surface, the maximum reduction was considered applicable throughout the design.

The bearing area factor was not included in the Phase IIa analysis. Although not explicitly addressed, this omission may be due to the large bearing width of 54 or 58 in. compared to the relatively short bearing length of 6 in. Commentary in older NDS guidance suggested that compression perpendicular to grain across the full length of a beam tends to decrease rather than increase. However, component tests of TL-1 curb rail posts indicated that only localized areas of the glulam block, between 1 and 2 in., were under compression [5, 7]. This observation suggests that bearing area effects could be relevant under localized loading.

Among the omitted factors, the time effect factor was the most critical. Design values in the NDS are based on a 10-minute load duration. For a one-second impact load, the resistance could be increased by a factor of 1.25 [14]. A seasoning factor of 1.5 for sawn timber was applied instead of the 1.9 factor for glulam because the source data were based on sawn lumber. This approach is consistent with the development of glulam design values, which are derived from regression models based on sawn lumber data.

Temperature effects were not applied, since strength reduction for wood generally occurs only when temperatures exceed 100 degrees Fahrenheit. These conditions are uncommon for extended periods across most of the United States. Based on the combination of factors applied to the initial compressive stress values, the estimated range of compressive resistance perpendicular to grain was approximately 0.933 to 1.333 ksi.

Given the uncertainty associated with the more detailed estimates, and the relatively small potential benefit, the original value of 1.176 ksi was retained. Applying the 1.25 time effect factor increased the resistance to a level that was considered unreasonably high. Therefore, the simplified method was adopted as the preferred basis for design.

Appendix F. Shear Connector Design

This appendix goes into greater detail on the assumptions used to produce the shear connector capacities given in Table 21. These capacities were obtained by taking reference design values and modifying them according to their intended end use. This approach was required because the reference design values published by NDS are based on physical test data. Alternative methods of estimating the shear connector strength by analytical means were unlikely to be successful and would have required an unnecessary time investment for the project.

Reference design values were obtained from NDS Table 13.2B "Shear Plate Connector Unit Reference Design Values". For the scupper, the number of faces of member with connectors on same bolt is 1 because the load is only moving in one direction with respect to the support at any given place rather than the shear plates restraining a piece of wood on both sides with two supports. The net thickness of the member is greater than 1¾ in. Lateral forces on the scupper place loads perpendicular to the wood grain, longitudinal loads on the scupper place loads parallel to the wood grain. The lower reference design value was taken when two load-to-grain orientations were present. Douglas Fir-Larch was a Group B species because the specific gravity is 0.50 (NDS Supplement Table 5B). This value, P, is 3040 lb for lateral loads on both decks and longitudinal loads on a transverse deck, and 4360 lb for longitudinal loads on a longitudinal deck.

According to NDS Table 11.3.1, these values shall be modified (according to ASD design) by a load duration factor, C_D, moisture factor, C_m, temperature factor, C_t, group action factor, C_g, geometry factor, C_Δ, penetration depth factor, C_d, and metal side plate factor, C_{st}. The load duration factor of 1.6 for impact loads was utilized, because NDS appendix B.1.2 (e) prohibited a factor of 2 for connections under impact loads. The moisture factor was 1.0 for dry use analysis and 0.7 for wet-use analysis. The temperature factor was 1.0, according to Phase IIa analysis. The group action factor was determined according to NDS 11.3.6: $C_g = \left[\frac{m(1-m^{2n})}{n[(1+R_{EA}m^n)(1+m)-1+m^{2n}]}\right]$.

n = the number of fasteners in a row

R_{EA} = lesser of $\frac{E_s A_s}{E_m A_m}$ or $\frac{E_m A_m}{E_s A_s}$

E_m = modulus of elasticity of main member, psi

E_s = modulus of elasticity of side member, psi

A_m = gross cross-sectional area of main member, in.^{2}

A_s = gross cross-sectional area of side member, in.^{2}

m = $u - \sqrt{u^2 - 1}$

u = $1 + \gamma \frac{s}{2}\left[\frac{1}{E_m A_m} + \frac{1}{E_s A_s}\right]$

s = center to center spacing between adjacent fasteners in a row, in.

γ = load/slip modulus for a connection, lb/in., 500,000 lb/in. for 4 in. split ring or shear plate connectors

Under lateral loading, each bolt was considered its own row, and under longitudinal loading, all eight bolts were considered a single row.

Table F-1. Group Action Factor for Lateral Loading on Transverse Deck

Group-Action Factor	
No. Fasteners in Row	1
$E_{Curb\ Rail}$	1500000
E_{Deck}	1600000
CX-Area of Deck	246.00
CX-Area of Scupper	276.75
R_{EA}	0.89
γ	500000
Bolt Spacing	5.5
u	1.01
m	0.890
C_g	1.00

Table F-2. Group Action Factor for Longitudinal Loading on Transverse Deck

Group-Action Factor	
No. Fasteners in Row	8
$E_{Curb\ Rail}$	1500000
E_{Deck}	1600000
CX-Area of Deck	738.00
CX-Area of Scupper	61.50
R_{EA}	0.08
γ	500000
Bolt Spacing	5.5
u	1.02
m	0.840
C_g	0.71

Table F-3. Group Action Factor for Lateral Loading on Longitudinal Deck

Group-Action Factor	
No. Fasteners in Row	1
$E_{Curb\ Rail}$	1500000
E_{Deck}	1600000
CX-Area of Deck	1032.00
CX-Area of Scupper	276.75
R_{EA}	0.27
γ	500000
Bolt Spacing	5.5
u	1.00
m	0.915
C_g	1.00

Table F-4. Group Action Factor for Longitudinal Loading on Longitudinal Deck

Group-Action Factor	
No. Fasteners in Row	8
$E_{Curb\ Rail}$	1500000
E_{Deck}	1600000
CX-Area of Deck	516.00
CX-Area of Scupper	61.50
R_{EA}	0.12
γ	500000
Bolt Spacing	5.5
u	1.02
m	0.838
C_g	0.72

The geometry factor, C_Δ, was determined according to spacing limitations, which are summarized in NDS Table 13.3. Spacing limitations from the table include edge distance, end distance, and spacing. The design must satisfy the minimal spacing limitations and utilize reductions for spacings insufficiently large to fully develop the connection strength. The edge distance is measured orthogonally to the grain from the center of the shear connector to the nearest edge. The edge distance limits are broken into loaded and unloaded limits. The loaded edge is the edge from which the load is attempting to tear the connector out, and the unloaded edge is opposite the loaded edge. The end distance is measured parallel to the grain from the end of the wood piece to the center of the nearest shear connector. The spacing between shear connectors can be measured orthogonal or parallel to the load, but the orthogonal orientation has the same minimum spacing as the parallel orientation while the parallel orientation has additional requirements to fully develop the connection strength.

When the design distance was between the minimum (Min.) and the fully developed strength (Full), linear interpolation was used to locate the geometry factor (C_Δ) per NDS 13.3.2. The end distance in the longitudinal deck was not recorded because the shear connector was never closest to the end of the longitudinal panel, the connector nearest to the end of the panel would always be the anchor bolts. The calculated geometry factors for longitudinal loads to the shear connection are shown for both longitudinal and transverse decks in Table F-5, the same is shown for lateral loading in Table F-6.

Table F-5. Geometry Factor for Transverse and Longitudinal Decks under Longitudinal Loads

Spacing Parameter	Transverse Deck				Longitudinal Deck			
	Design	Min.	Full	C_Δ	Design	Min.	Full	C_Δ
Loaded Edge Distance	6.25	2.5	3.75	1	-	-	-	-
Unloaded Edge Distance	6.25	2.5	3.75	1	-	-	-	-
End Distance	8	3.5	7	1	-	-	-	-
Spacing Parallel to Grain	-	-	-	-	5.5	5	9	0.56
Spacing Perpendicular to Grain	5.5	5	6	0.75	-	-	-	-
Geometry Factor				0.75				0.56

Table F-6. Geometry Factor for Transverse and Longitudinal Decks under Lateral Loads

Spacing Parameter	Transverse Deck				Longitudinal Deck			
	Design	Min.	Full	C_Δ	Design	Min.	Full	C_Δ
Loaded Edge Distance	-	-	-	-	8	2.5	3.75	1
Unloaded Edge Distance	-	-	-	-	40	2.5	3.75	1
End Distance	8	3.5	7	1	-	-	-	-
Spacing Parallel to Grain	-	-	-	-	5.5	5	5	1
Spacing Perpendicular to Grain	5.5	5	5	1	-	-	-	-
Geometry Factor:				1				1

The scupper was not evaluated for spacing limitations because it could not exert lateral or longitudinal resistance and could move with the bolts (aside from frictional resistance). The transverse and longitudinal bridge decks provided resistance which the spacing limitations are concerned with. In addition, it was not clear whether spacing limitations could be applied to the

longitudinal deck, because the original testing regimen which formed the basis for the values in Table 13.3 did not include test set-ups similar to the posts on bridge decks. The reductions to deck capacity were conservative and did not sufficient to cause issues with design. Therefore, it was unnecessary to evaluate whether the shear connector spacing requirements on the longitudinal deck were accurate estimates of the capacity for this project.

The penetration depth factor adjusts for use of shear plates or split rings with lag screws, because bolts are being used, this will not apply. The metal side plate factor adjusts shear plates to higher strength when metal side plates are used, this is not being used and will not be a factor. ASD was selected over LRFD due to concerns with how the ASD to LRFD format adjustment is applied to the original tabulated strengths.

Adjusting the tabulated design values by the discussed parameters obtained allowable capacities, not ultimate capacities. This was discussed in section 3.3.3.1. A factor of 2 was used to adjust allowable capacities to ultimate capacities. The shear capacities for transverse decks under lateral and longitudinal loads and longitudinal decks under lateral and longitudinal loads are shown in Table F-7 through Table F-10, respectively.

Table F-7. Shear Plate Capacity on Transverse Deck under Lateral Loads

Reference Design Value	3040	lb
Moisture Factor	1	
Temperature Factor	1	
Group Action Factor	1.00	
Geometry Factor	1	
Penetration Depth Factor	1	
Load Duration Factor	1.6	
Allowable Capacity, Single Shear Plate	4.86	kips
Allowable Capacity, All Shear Plates	38.91	kips
Ultimate Capacity, All Shear Plates	77.82	kips

Table F-8. Shear Plate Capacity on Transverse Deck under Longitudinal Loads

Reference Design Value	3040	lb
Moisture Factor	1	
Temperature Factor	1	
Group Action Factor	0.71	
Geometry Factor	0.75	
Penetration Depth Factor	1	
Load Duration Factor	1.6	
Allowable Capacity, Single Shear Plate	2.59	kips
Allowable Capacity, All Shear Plates	20.74	kips
Ultimate Capacity, All Shear Plates	41.47	kips

Table F-9. Shear Plate Capacity on Longitudinal Deck under Lateral Loads

Reference Design Value	3040	lb
Moisture Factor	1	
Temperature Factor	1	
Group Action Factor	1.00	
Geometry Factor	1	
Penetration Depth Factor	1	
Load Duration Factor	1.6	
Allowable Capacity, Single Shear Plate	4.86	kips
Allowable Capacity, All Shear Plates	38.91	kips
Ultimate Capacity, All Shear Plates	77.82	kips

Table F-10. Shear Plate Capacity on Longitudinal Deck under Longitudinal Loads

Reference Design Value	4360	lb
Moisture Factor	1	
Temperature Factor	1	
Group Action Factor	0.72	
Geometry Factor	0.5625	
Penetration Depth Factor	1	
Load Duration Factor	1.6	
Allowable Capacity, Single Shear Plate	2.81	kips
Allowable Capacity, All Shear Plates	22.46	kips
Ultimate Capacity, All Shear Plates	44.91	kips

Appendix G. Upper Rail Bolts Design

The connection of the upper rail to the post must handle induced tension from the offset vertical design loads, and shear from the longitudinal or vertical design loads. The tensile load on the upper connection bolt is detailed below. Then the steel bolt shear rupture, tensile rupture, and the bolt-wood yielding failure modes from NDS were examined.

The unit weight of Douglas Fir-Larch glulam is given by NDS, 0.238 lb/in.^{2}/ft at 15% moisture content. For a 10¾ in. x 13½ in. beam over 8 ft (the post spacing) the weight is 276 lb. The impact design load of 38 kips over 18 ft works out to 16.89 kips from 8 ft of the distributed load acting on a single post, which gave a total of 17.17 kips for Design Case 2. The centroid of vertical forces applied at the upper railing glulam beam midspan, half of 10.75 in. from the support, 5.375 in. This offset of load from support developed a moment of 92.26 kip-in. at the face of the connection to the blockout. The width in compression was described by

$$a = \frac{2d - \sqrt{(-2d)^2 - 4(1)\left(\frac{2M_u}{0.85f_c'b}\right)}}{2(1)}$$

Where "d" was the distance from the bottom of the blockout to the centerline of the upper bolt, 7 in. "b" was the width of the blockout, 8.75 in. "f_c'" was the factored compression perpendicular to grain design value, 1.176 ksi (see Appendix E).

$$a = \frac{2(7\ in) - \sqrt{\left(2(7\ in)\right)^2 - 4\left(\frac{2(92.26\ kip-in)}{0.85(1.176\ ksi)(8.75\ in)}\right)}}{2} = 1.72\ inches$$

The compression was described by equations (1) and (2) from section 3.2.1.3, 0.85f_c'ab, which was 15.02 kips. The compression equals the bolt tension, hence the bolt tension was also 15.02 kips. The unfactored shear capacity of a single bolt was described by AASHTO equation 6.13.2.7-2, $R_n = 0.45A_bF_{ub}N_s$, where A_b is the nominal area of the bolt, F_{ub} is the ultimate strength of the bolt (60ksi for A307A steel), and N_s is the number of shear planes. The vertical load, 17.17 kips, and the tensile load, 15.02 kips, apply on the connection at the same time, and so the bolt capacity to resist both needs to be examined. AASHTO Section 6.13.2.11 describes whether a combined check is necessary, and is shown below.

$$\frac{P_u}{R_n} = \frac{(17.17\ kips)/2}{0.45(0.601\ in^2)(60\ ksi)1} = \frac{8.585\ kips}{16.24\ kips} = 0.53 > 0.33$$

Therefore, combined loads into the upper bolt will need to be considered. Combined action of tension and shear is given by AASHTO 6.13.2.11-2:

$$T_n = 0.76A_bF_{ub}\sqrt{1 - \left(\frac{P_u}{\varphi_s R_n}\right)^2}$$

Where T_n is multiplied by the strength reduction factor $\varphi_t = 0.8$ for A307A bolts in tension according to AASHTO 6.5.4.2. The shear strength reduction factor, φ_s, for A307A bolts in shear is 0.75.

$$T_r = \varphi_t T_n = (0.8)0.76(0.601\ in^2)(60\ \text{ksi})\sqrt{1-\left(\frac{(8.585\ kips)}{(0.75)0.45(0.601\ in^2)(60\ ksi)1}\right)^2}$$
$$= 15.56\ kips$$

The factored bolt capacity of 15.56 kips under combined loads exceeds the tensile demand, 15.02 kips.

The connection must also be sufficient to resist the maximum shear. The shear from the design impact vertical load and dead load is 17.17 kips, and the shear from the design impact longitudinal load is 23.35 kips (see section 3.3.2.2). The longitudinal loads will govern analysis.

$$\varphi_s R_n = (0.75)0.45(1.203\ in^2)(60\ ksi)1 = 24.35\ kips$$

The factored shear capacity, 24.35 kips, exceeds the ultimate shear demand, 23.35 kips.

Following the bolt tensile rupture check with combined loads and the shear rupture check were the wood-bolt yielding checks. Figure 89 shows each failure mode, which is described by the following equations:

Mode I_m, yielding of only wood in main member

$$Z = \frac{Dl_m F_{em}}{R_d}$$

Mode I_s, yielding of only wood in side member

$$Z = \frac{Dl_s F_{es}}{R_d}$$

Mode II, yielding of wood in main and side members with no bolt yielding

$$Z = \frac{k_1 Dl_s F_{es}}{R_d}$$

Mode III_m, yielding of wood in main member and bolt

$$Z = \frac{k_2 Dl_m F_{em}}{(1+2R_e)R_d}$$

Mode III_s, yielding of wood in side member and bolt

$$Z = \frac{k_3 D l_s F_{em}}{(2 + R_e) R_d}$$

Mode IV, yielding of wood in main and side members as well as the bolt

$$Z = \frac{D^2}{R_d} \sqrt{\frac{2 F_{em} F_{yb}}{3(1 + R_e)}}$$

The variable "D" represents the diameter of the bolt. For the upper rail connection to the post, this will be ⅞ in. The variables "l_m" and "l_s" represent the length of the bolt in the main and side members respectively. The main member will be the upper railing, for a length of 10.75 in., and the side member will be the post, for a length of 12 in. The variables "F_{em}" "F_{es}" represent the dowel bearing strength of the wood, tabulated in NDS Table 12.3.3 according to bolt diameter, specific gravity of wood, and orientation of bolt with respect to the direction of the wood grain. Larger bolts than 1 in. diameter can use equation given at bottom of table to predict strength.

Because the loads can be applied in multiple different directions, the dowel-bearing strength of the wood will be different for vertical loads compared to longitudinal loads. Because the direction of the grain in the upper rail is different from the direction of grain in the post, there will also be differences between the upper rail dowel bearing strength and the lower rail dowel bearing strength. These differences are illustrated in Figure G-1.

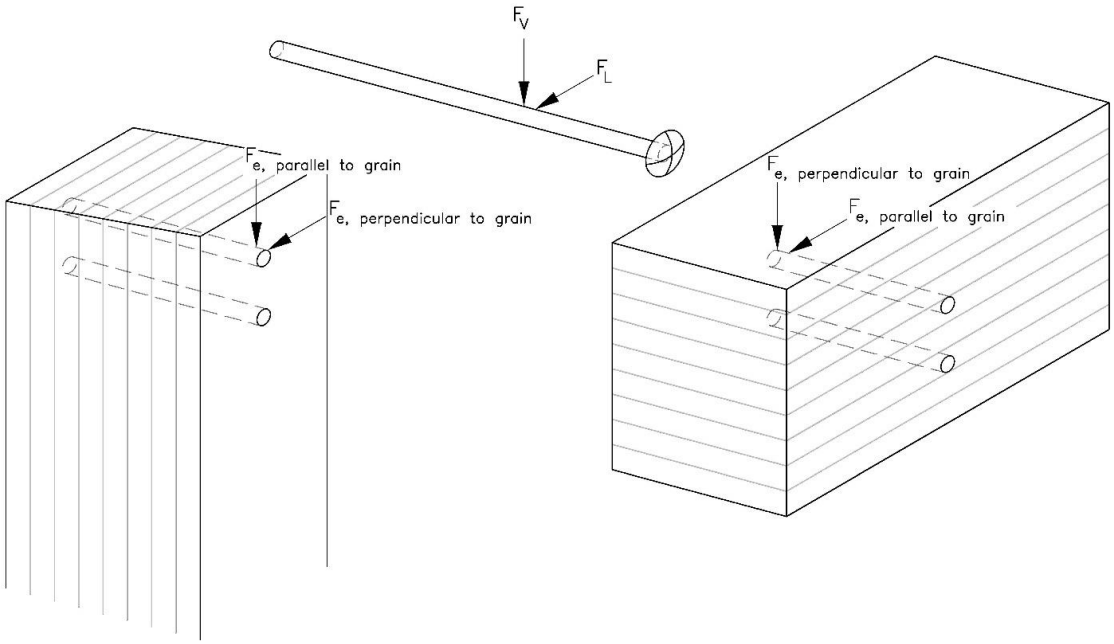

Figure G-1. Dowel Bearing Strength Orientation

Under vertical loads, the dowel bearing strength of the main member is 5600 psi and the dowel bearing strength of the side member is 2400 psi. Under longitudinal loads the dowel bearing strength of the main member is 2400 psi and the dowel bearing strength of the side member is

5600 psi. The variable "R_d" represents the reduction factor, discussion of why this will be removed/ given a value of 1 can be found in section 3.3.4.1. The variable "k_1" is a conglomeration of values, used to simplify the equation, and is calculated by the following equation,

$$k_1 = \frac{\sqrt{R_e + 2{R_e}^2\left(1 + R_t + {R_t}^2\right) + {R_t}^2{R_e}^3} - R_e(1 + R_t)}{(1 + R_e)}$$

The variable "R_e" represents the ratio of the dowel bearing stress in the main member to the dowel bearing stress in the side member, F_{em}/F_{es}. The variable "R_t" represents the ratio of the length of dowel in the main member to the length of dowel in the side member, l_m/l_s. The variable "F_{yb}" represents the bolt yielding stress and can be assumed to be 45 ksi for A307A bolts.

The variable "k_2" is also a conglomeration of values used to simplify the equation, and it is calculated by the following equation,

$$k_2 = -1 + \sqrt{2(1 + R_e) + \frac{2F_{yb}(1 + 2R_e)D^2}{3F_{em}{l_m}^2}}$$

The variable "k_3" is also a conglomeration of values used to simplify the equation, and it is calculated by the following equation,

$$k_3 = -1 + \sqrt{\frac{2(1 + R_e)}{R_e} + \frac{2F_{yb}(2 + R_e)D^2}{3F_{em}{l_s}^2}}$$

Once the yielding failure mode strength have been calculated, these values will be unfactored values, requiring modification for load duration, moisture, temperature, group, geometry, end grain, diaphragm, and toe-nail. The temperature, end grain, diaphragm, and toe-nail factors will not apply to this case and can be ignored.

The load duration factor selected was 2, despite limits from NDS on the connection capacity. Part of the reason for this was that the failure mode was ductile rather than brittle, due to the long length of bolt in either wood member relative to its diameter. Other tests conducted on timber connection configurations have found that this ratio produces a more ductile failure []

The geometry factor will reduce the strength of the connection where bolts are too close to one another. Figure 12G from NDS will be examined to determine applicability of spacing requirements. Bolt rows are always parallel to the load direction, the edge distance is always perpendicular to the load direction, and the end distance is always parallel to the load direction. End distance requirements were not considered applicable because there were no ends near post locations. At splice locations the bolts develop their shear resistance through the steel splice plate rather than the wooden beam.

Fastener (bolt) spacing requirements applied to the upper rail for vertical loads. Row spacing requirements applied to the vertical post for longitudinal loads. Both members were loaded parallel to grain for their case, which must satisfy 1.5D (1.3125 in.). The spacing distance is 3.5

in. between bolts and is sufficient for both scenarios. Edge distance requirements applied to the upper rail for longitudinal loads, and to the post for the vertical loads. The edge distances in the upper rail, 3.5 and 6.5 in., were greater than the required 1.5D (1.3125 in.) and 4D (3.5 in.), respectively, for ⅞-in. diameter bolts. The edge distances in the post, 4.375 in., also exceeded 1.5D and 4D.

The moisture factor in Phase IIa of this research effort was considered to not be applicable because of the high degree of exposure of the upper rail to wind (and therefore evaporation). The addition of the moisture factor to estimates of system strength in BARRIER VII only apply to the bottom of the post. The upper railing to vertical post connection will continue to be considered a dry use scenario.

The group action factor was calculated as described in Appendix F in for the longitudinal loads in Table G-1 and for the vertical loads in Table G-2 below.

Table G-1. Group Action Factor for Longitudinal Loads

Group-Action Factor	
No. Fasteners in Row	1
$E_{Upper\ Rail}$	1600000
E_{Post}	1600000
CX-Area of Upper Rail	145.13
CX-Area of Post	105.00
R_{EA}	0.72
γ	147327.8
Bolt Spacing	3.5
u	1.00
m	0.930
C_g	1.00

Table G-2. Group Action Factor for Vertical Loads

Group-Action Factor	
No. Fasteners in Row	2
$E_{Upper\ Rail}$	1600000
E_{Post}	1600000
CX-Area of Upper Rail	145.13
CX-Area of Post	105.00
R_{EA}	0.72
γ	147327.76
Bolt Spacing	3.5
u	1.00
m	0.930
C_g	1.00

Calculating the unfactored yield strength, and multiplying it by the applicable factors, gives the calculated strength of the connection below for the longitudinal loads in Table G-3, and the vertical loads in Table G-4.

Table G-3. Yielding Modes Strength for Longitudinal Loads

Unfactored Yielding Failure Modes Design Strength (kips)		Factored Design Strength (kips/bolt)	Total Strength (kips)
I_m	22.575	45.15	90.30
I_s	58.800	117.60	235.20
II	16.681	33.36	66.72
III_m	8.937	17.87	35.75
III_s	16.738	33.48	66.95
IV	5.435	10.87	21.74

Table G-4. Yield Modes Strength for Vertical Loads

Unfactored Yielding Failure Modes Design Strength (kips)		Factored Design Strength (kips/bolt)	Total Strength (kips)
I_m	52.675	105.35	210.70
I_s	25.200	50.40	100.80
II	15.500	31.00	62.00
III_m	15.065	30.13	60.26
III_s	9.857	19.71	39.43
IV	5.435	10.87	21.74

Appendix H. Vertical Post Design

The vertical post was under shear and flexural demand from applied lateral and longitudinal loads. The shear demand from lateral loads changed across the length of the vertical post, and so either a critical location needed could be defined or multiple locations needed to be checked simultaneously. Multiple locations could readily be checked simultaneously using a graph and plotting demand and capacity with respect to the length of the post, so this option was chosen to examine whether the vertical post was sufficient.

According to the models discussed and shown in Section 3.3.2.3, the equation used to determine the lateral shear demands was as follows:

$$V_{u_{lat}}(x) = if\left(and\left(x > d_1 - \frac{l_w}{2}, x < d_1 + \frac{l_w}{2}\right), F_{comp} - \left(\frac{T_u}{l_w}\right)(x - (d_1 - l_w)), if\left(x > d_1, -F_{Lat}, F_{comp}\right)\right)$$

The variable "l_w" represents the length of the washer, which was 6 in., the variable "F_{comp}" represents the compression at the deck level, which was 50.85 kips (see section 3.3.2.1), and the variable "T_u" represents the tension in the bolt connecting the post to the curb railing, 90.78 kips (see section 3.3.2.1). The tension in the bolt is a function of the yield moment divided by the distance from the centerline of the bolt to the top of deck, 14.625 in.

This equation checked to see if the location in question was between the ends of the washer plate. If the location was within the washer plate, then the check was true and the compression is linearly transitioned from 50.85 kips to 39.93 kips across the width of the washer plate, which was 6 in. Otherwise, another check examined if the location of the load was above or below the horizontal bolt. If the location was above the horizontal bolt, then a constant shear load of 39.93 kips was assumed. Locations below the horizontal bolt assumed a shear load of 50.85 kips.

The equation used to determine the longitudinal shear demand was as follows:

$$V_{u_{long}}(x) = if(x < d_1, 0, -20.02\ kips)$$

This equation checked to see whether the load was above or below the horizontal bolt location. If the load was above the horizontal bolt location, then a constant shear load of 20.02 kips was assumed. Otherwise, the longitudinal shear load below the horizontal bolt location was assumed to be 0. This assumed that the lag bolt and angle used in the design to provide stability was not present. It is possible for higher shear loads to develop from longitudinal loads with the lag bolts and angles, but some degree of displacement needs to occur before the connection can be loaded due to slots in the angle. In order to encounter significant longitudinal shear load increase by loading the lag bolt and angle, the upper railing would also need to flex over its x-x axis to allow the post to turn. This scenario was seen as unlikely, and the applied loads were sufficient to examine the post capacity with little to no movement.

Both shear loads, V_{ulat} and V_{ulong}, were combined via Pythagorean Theorem:

$$V_u(x) = \sqrt{{V_{u_{Lat}}}^2 + {V_{u_{Long}}}^2}$$

The flexural demand from lateral loads was described by the following equation:

$$M_{u_{lat}}(x) = if\left(and\left(x > d_1 - \frac{l_w}{2}, x < d_1 + \frac{l_w}{2}\right), F_{comp}x - \frac{1}{2}\left(\frac{T_u}{l_w}\right)\left(x - \left(d_1 - \frac{l_w}{2}\right)\right)^2, if\left(x < d_1, F_{comp}x, F_{Lat}(L_{Total} - x)\right)\right)$$

The equation for lateral flexural demand was similar to lateral shear demand. If the location was within the limits of the washer plate, then the demand was estimated by one equation. If the location was above the horizontal bolt, then the distance from the centerline of the horizontal bolt was multiplied by the lateral demand at the top of the post. If the location was below the horizontal bolt, then the compression at the bottom of the post was multiplied by its distance from the centroid. The only new variable introduced by this equation was "L_{Total}", which represented the total length of the post between the centroid of the applied load at the post and the centroid of applied compression at the bottom.

The flexural demand from longitudinal loads was described by the following equation:

$$M_{u_{long}}(x) = if\left(x < d_1, 0, -20.02(x - d_1)\right)$$

The equation for longitudinal flexural demand was also similar to the longitudinal shear demand. If the location was below the centroid of the horizontal bolt, no flexural demand applied. If the location was above the centroid of the horizontal bolt, the flexural demand was obtained by multiplying the shear by its distance from the centroid of the horizontal bolt, for a maximum longitudinal flexural demand at the upper rail connection.

The shear and flexural capacities of the post were calculated according to a changing section at the bolt location across the post length. The change in the section was determined as a width, "r", that reduced the nominal post width, 8¾ in.

$$r(x) = if\left(and(x > d_1 - r_h, x < d_1 + r_h), 2\sqrt{{r_h}^2 - (x - d_1)^2}, 0\right)$$

The variable "r_h" represented the bolt hole radius, 0.71875 in., "d_1" was identical to the previously given definition, 14.625 in. Like the lateral shear and flexure equations, this equation determined whether a reduction applied by whether the location "x" was within range of the bolt hole. No reduction was applied for "x" outside the bolt hole, and the equation of a circle in terms of "r", "x", and "y" ($r^2 = x^2 + y^2$) was used to determine the width of the hole in the center of the vertical post section with "y" being the unknown variable calculated at each point "x". The reduction was implemented into the area of the vertical post section by the following equations:

$$b(x) = b_0 - r(x)$$

$$A(x) = db(x)$$

The post width, "b", was the width at location x, while "b_0" was the nominal post width, 8.75 in. The net shear area was represented by "A" at location x, and "d" was the post depth, 12 in.

According to the changing section, the lateral section modulus was calculated as follows:

$$S_{lat}(x) = \frac{d^2 b(x)}{6}$$

The variables "d" and "b" were the same width and depth as those used to calculate the net shear area.

The longitudinal section modulus was calculated as follows:

$$S_{long}(x) = \frac{d\left({b_0}^3 - r(x)^3\right)}{12}\frac{2}{b_0}$$

The variables in this case were consistent with those used for the net shear area. This equation calculated the section modulus from the moment of inertia because the depth of the section remained the same while the interior was hollowed out for the bolt.

The shear capacity, φV_n, was determined by multiplying the net shear area by the factored shear strength, F_v', and then reducing it by two-thirds, consistent with standard practice for rectangular members subjected to flexure. The factored shear strength was calculated as the product of the nominal, tabulated shear strength (265 psi, from NDS Supplement Table 5B) and appropriate end-use factors, along with additional adjustments to reflect average strength under impact loading. Both the moisture and temperature factors were taken as 1.0. A shear reduction factor, C_{vr}, of 0.72 was applied. The load duration factor was 2.0. To convert allowable design values to average strength estimates, a factor of 1.3 was applied. This factor reflects an average-to-design ratio for shear strength assuming a coefficient of variation (COV) of 0.14. The adjusted shear strength reflects a transition from the 5th percentile value to a 50th percentile (average) estimate. With all applicable end-use factors included, the factored shear strength was calculated to be 0.896 ksi.

The lateral flexural capacity of the post, φM_n, was calculated by multiplying the factored bending strength, F_b', by the section modulus, S(x). This was repeated for the longitudinal loading orientation. The lateral bending strength was based on bending about the x-x axis of the post, for which the tabulated design value is 1.7 ksi for combination 2 Douglas Fir-Larch from NDS Supplement Table 5B. The moisture, C_M, and temperature factor, C_t, were both 1.0. The beam stability factor, C_L, was 1.0 based on NDS section 3.3.3.1, where the depth to breadth ratio is less than 2. The volume factor is based on $C_V = \left(\left(\frac{21}{L}\right)\left(\frac{12}{d}\right)\left(\frac{5.125}{b}\right)\right)^{1/x}$ where L is the length of the glulam member in ft (3 ft-11 in.), d is the depth of the glulam (12 in.), b is the width of the glulam (8.75 in.), and x is a power factor (5 for Southern Pine species, 10 for Douglas Fir-Larch or other

species); this was 1.12. NDS section 5.3.5 states that the lesser of the beam stability factor and the volume factor be used for flexural strength estimates, hence the beam stability factor was used. The flat use, C_{fu}, curvature, C_c, and stress interaction, C_I, factors did not apply in this scenario. The load duration factor, C_D, was 2 for impact load duration. The flexural strength was increased by a factor of 1.3 to remove the safety factor used for developing tabulated values. The resulting lateral factored bending strength was 4.42 ksi.

The longitudinal bending strength was based on bending about the y-y axis of the post, for which the tabulated design value is 1.8 ksi for combination 2 Douglas Fir-Larch from NDS Supplement Table 5B. The moisture, C_M, and temperature factor, C_t, were both 1.0. The beam stability factor, C_L, and volume factor, C_V, were identical for the longitudinal strength. The longitudinal strength utilized the flat use factor, C_{fu}, 1.04 for 8.75-in.-wide laminations. The curvature, C_c, and stress interaction, C_I, factors did not apply in this scenario. The load duration factor, C_D, was 2 for impact load duration. The flexural strength was increased by a factor of 1.3 to remove the safety factor used for developing tabulated values. The resulting longitudinal factored bending strength is 4.867 ksi.

Appendix I. Horizontal Bolt Design

The horizontal bolt connecting the post to the curb railing was designed to resist tensile and shear loads. The connection was also examined for bolt-wood yield limit states as well.

The tensile capacity of the bolt, like the bolts connecting the upper rail to the post, was described by AASHTO 6.13.2.10.2-1:

$$T_n = 0.76 A_b F_{ub}$$

The bolt area was "A_b", the bolt ultimate tensile strength was "F_{ub}", and the bolt tensile capacity was "T_n". The tensile capacity was reduced by the strength reduction factor $\varphi_t = 0.8$.

The bolt tensile demand, 90.78 kips (see section 3.3.2.4), exceeded the capacity of the 1¼ in. diameter bolt specified for the previous NCHRP-350 design (44.77 kips). As a result, a larger and stronger bolt was selected. Table I-1 show the two options considered for timber headed bolts.

Table I-1. Timber Bolt Size and Specification Meeting Tensile Demand

Specification	Ultimate Strength (ksi)	Diameter Req'd (in.)	Capacity (kip)
A307A	60	1.875	100.73
A449	105	1.375	94.80

Combined effects of tensile and shear loads were also checked. The shear demand came from the longitudinal loads, 20.02 kips (see section 3.3.2.4). The bolt shear capacity was calculated in the same manner as the upper rail bolts:

$$R_n = 0.45 A_b F_{ub} N_s = 0.45(1.485\ in^2)(105)(1) = 70.16$$

The ratio of the shear demand, 20.02 kips, to the nominal shear capacity was:

$$\frac{P_u}{R_n} = \frac{20.02\ kips}{70.16\ kips} = 0.29 < 0.33$$

Therefore, no combined check for tension and shear was necessary.

Spacing limitations for the curb rail bolt to post connection were examined. These limitations were strictly edge distance because the end of the vertical post or the curb rail was too far away from the horizontal bolt in either case. In addition, no bolt spacing check was necessary for one bolt. The vertical post and the curb rail have the same width, and so the parallel to grain edge distance and loaded edge distance were the only metrics which needed to be checked. The parallel to grain edge distance, 1.5D (2.0625 in.), was satisfied by 4.375 in. on either side of the bolt. But the loaded edge distance, 4D (5.5 in.) was violated for longitudinal loads in the vertical post. This geometry was also an issue for the TL-4 NCHRP-350 design (5 in.), which did not note severe damage in the vertical post at the horizontal bolt location. Given the successful performance of the system in the past to loads exceeding the TL-4 NCHRP-350 IS, and the increase to post strength, failure was not anticipated to occur from bolt pull-out at a post location.

The bolt-wood yielding failure modes from NDS were examined and the parameters were similar to the upper rail to post connection. However, the following differences applied: the group factor was not used because there was one bolt, the yield strength was 81 ksi according to Portland Steel Bolt's website on A449 bolts, consistent with ASTM A449-14(2020), and the dowel bearing strength parallel to grain was calculated by

$$F_{e,parallel} = 11200G$$

And the dowel bearing strength perpendicular to grain was calculated by

$$F_{e,perpendicular} = \frac{6100G^{1.45}}{D^{0.5}}$$

These equations were given by NDS at the bottom of Table 12.3.3 for bolts larger than 1-in. diameter. The wood-bolt yielding results for the longitudinal loads are shown in Table I-2, and the wood-bolt yielding capacities for the vertical loads are shown in Table I-3.

Table I-2. Yielding Modes Strength for Longitudinal Loads

Unfactored Yielding Failure Modes Design Strength (kips)		Strength (kips)
I_m	31.35	62.70
I_s	92.40	184.80
II	24.52	49.04
III_m	15.28	30.55
III_s	26.28	52.56
IV	16.55	33.10

Table I-3. Yield Modes Strength for Vertical Loads

Unfactored Yielding Failure Modes Design Strength (kips)		Strength (kips)
I_m	92.40	184.80
I_s	31.35	62.70
II	24.52	49.04
III_m	26.28	52.56
III_s	15.28	30.55
IV	16.55	33.10

The maximum longitudinal shear demand was 23.35 kips according to section 3.3.2.4. The maximum vertical shear demand was 17.25 kips, obtained by adding 0.08 kips of weight to the calculated vertical load on the upper railing in section 3.3.2.2. Based on the calculated bolt yield capacity and demand, no wood-bolt yielding was expected.

Appendix J. Upper and Curb Rail Splice Design

The upper rail and the curb rail splice limits have been named in section 3.3.6, along with the method for calculating load demand. Here will be covered the calculations of the load demand and the connection capacity.

By combining the flexure of the upper rail elements divided by the upper rail width (10.75 in.) with half the tension at that location (divided between the two plates), the maximum force going through a plate is obtained. The calculated demand by this method of analysis, 154.03 kips, came from impact at 3 ft downstream from post 6 in an upper rail element between posts 7 and 8 at t = 0.16s. This is also the time of the maximum tensile force (76.26 kips) but not the location (which was on a member element further upstream also between posts 7 and 8). 154.03 kips was felt to be too low an estimate for reasons already discussed in section 3.3.6. Therefore, the flexural demand from BARRIER VII was changed to be the flexural capacity of the railing.

Additionally, the wet-use analysis resulted in higher tensile forces going through the railing due to the weakened posts. The maximum tension is 84.93 kips and 11.85 kips in the upper (from Table 17) and curb rails, respectively. The calculated upper railing capacity is 1568.6 k-in and curb railing capacity 869.3 k-in (calculations shown in Phase IIa's final report Appendix B). For the upper railing width of 10.75 in., the maximum demand would now be 188.38 kips. For the curb railing width of 12 in., the maximum demand would now be 78.37 kips.

Three block shear failures are shown in Figure J-1 below, with the jagged lines representing the failure. Block shear failure was evaluated according to AASHTO 6.13.4 in which the block shear failure capacity is described by

$$R_r = \varphi_{bs} R_p (0.58 F_u A_{vn} + U_{bs} F_u A_{tn}) \leq \varphi_{bs} R_p \left(0.58 F_y A_{vg} + U_{bs} F_u A_{tn}\right)$$

In which φ_{bs} is the strength reduction factor for connections in block shear failure, 0.80. R_p is a reduction factor for holes which are punched, the assumption is that the holes in the plates will be drilled, hence 1.0 for this case. F_u is the ultimate strength of the steel, A36 steel will be used for an ultimate strength of 58 ksi. F_y is the yield strength of the steel and will be 36 ksi for the splice plate. A_{vn} is the net area in shear, A_{vg} is the gross area in shear, and A_{tn} is the net area in tension. Each of these is shown in Table J-1. U_{bs} is the reduction factor for uniform vs non-uniform tensile stress, which will be uniform in this case, hence 1.0.

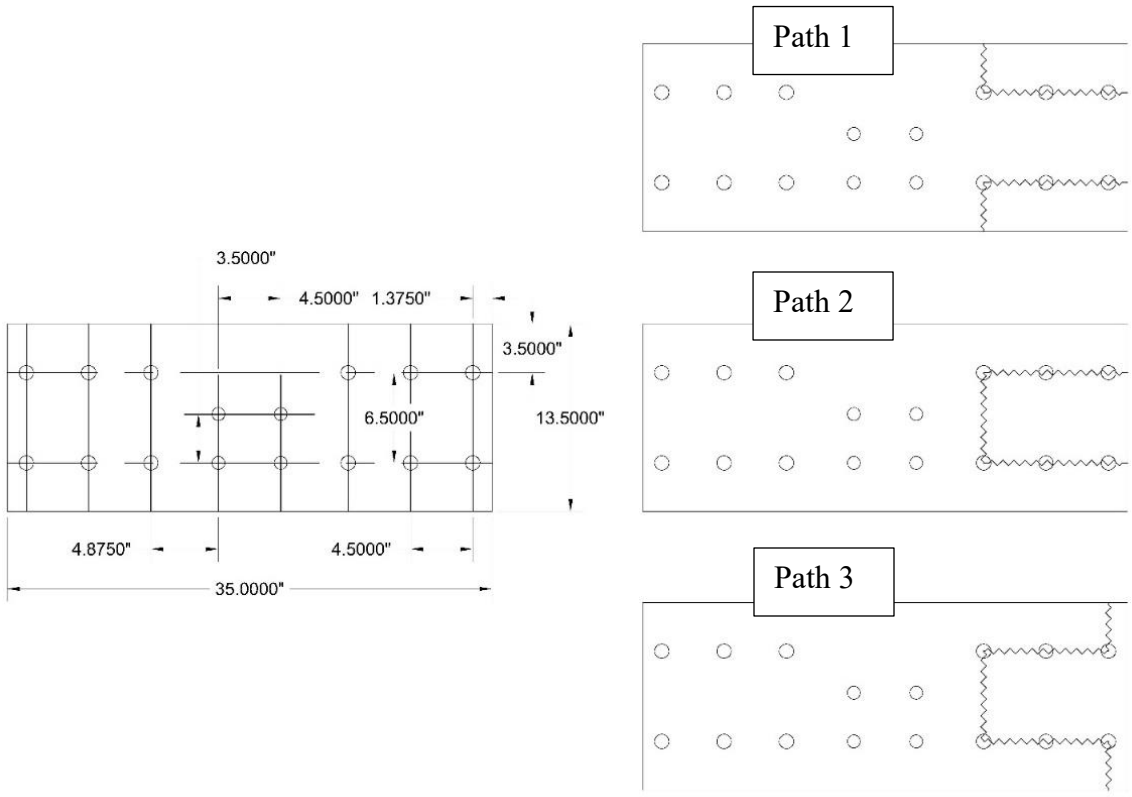

Figure J-1. Upper Rail Splice Block Shear Failure Paths

Table J-1. Upper Rail Block Shear Areas

Block Shear Areas			
	Path 1	Path 2	Path 3
A_{gt} (in.²)	3.50	3.25	6.75
A_{nt} (in.²)	2.97	2.72	5.69
A_{gv} (in.²)	10.38	10.38	9.00
A_{nv} (in.²)	7.72	6.88	6.88

The block shear capacity for each failure path is: 311.05 kips for path 1, 299.45 kips for path 2, and 414.24 kips for path 3. The controlling failure is path 2, 299.45 kips.

Table J-2. Curb Rail Block Shear Areas

Block Shear Areas			
	Path 1	Path 2	Path 3
A_{gt} (in.²)	2.50	4.38	1.88
A_{nt} (in.²)	2.09	3.56	1.47
A_{gv} (in.²)	5.00	3.00	5.00
A_{nv} (in.²)	3.78	2.19	3.78

The block shear capacity for each failure path is: 180.67 kips for path 1, 215.41 kips for path 2, and 151.67 kips for path 3. The controlling failure is path 3, 151.67 kips.

The splice plate yield strength, according to AASHTO 6.8.2.1 for general cases, is:

$$P_r = \varphi_y P_{ny} = \varphi_y F_y A_g$$

Where φ_y is 0.95 according to AASHTO 6.5.4.2, F_y is the yield strength (36 ksi), and A_g is the gross section in tension. The resulting yield strength is 230.85 kips for a ½ in. thick steel plate 13½ in. tall. The rupture strength of the splice plate is described by the same section in AASHTO as the yield strength, and is:

$$P_r = \varphi_u P_{nu} = \varphi_u F_u A_n R_p U$$

Where φ_u is 0.80 according to AASHTO 6.5.4.2, F_u is the ultimate strength (58 ksi), A_n is the net section of the splice plate, R_p is the same reduction factor as described above for punched holes (1.0 for this case), and U is the reduction factor for shear lag (1.0, because the tensile for can safely be assumed to transmit evenly across the section). The calculated rupture strength is 263.90 kips.

The bearing strength of the plate is its capacity to resist the bolts pulling through the metal splice plate until the bolts pull through the plate to a point where one of the bolts pulls free. AASHTO 6.13.2.9 describes this failure, when the distance between bolts or the end is greater or equal to 2d (where d is the nominal diameter of the bolt). The nominal capacity is:

$$R_n = 2.4dtF_u$$

Where t is the thickness of the plate (½ in.), and F_u is the ultimate strength. The applied strength reduction factor, φ_{bb}, is 0.8 for bolts bearing on material according to AASHTO 6.5.4.2. For 6 – 1 in. diameter bolts, the bearing strength of the splice plate is 334.08 kips.

The bolt shear strength of the splice is described by AASHTO 6.13.2.7:

$$R_n = 0.45A_b F_{ub} N_s$$

Where A_b is the area of the bolt(s), F_{ub} is the ultimate strength of the bolts (60 ksi for A307A bolts), and N_s is the number of shear planes which will be 2 due to the distribution of the presence of two splice plates. The applied strength reduction factor, φ_s, is 0.75 for A307A bolts in shear according to AASHTO 6.5.4.2. The capacity of all the steel hardware in the upper rail and curb rail splices is shown in Table J-3.

Table J-3. Steel Hardware Capacities

Failure Mode	Yielding	Rupture	Block Shear	Bearing	Bolt Shear
Upper Rail Capacity (kips)	230.85	263.90	299.45	334.08	190.85
Curb Rail Capacity (kips	149.63	165.30	151.67	250.56	107.35

NDS Appendix E describes various wood failure mechanisms which need to be examined: net section tensile failure, row tear-out failure, and group tear-out failure. Net tensile failure is the wood cross-section pulling apart. Row tear-out failure involves the bolts tearing through the wood with wood shear failure occurring on both sides of the bolts tearing through. Group tear-out failure involves shear failure along the bolts with tensile failure in the wood section between bolts. See Appendix Figure J-2 for each of these failures mapped unto the end of the beam.

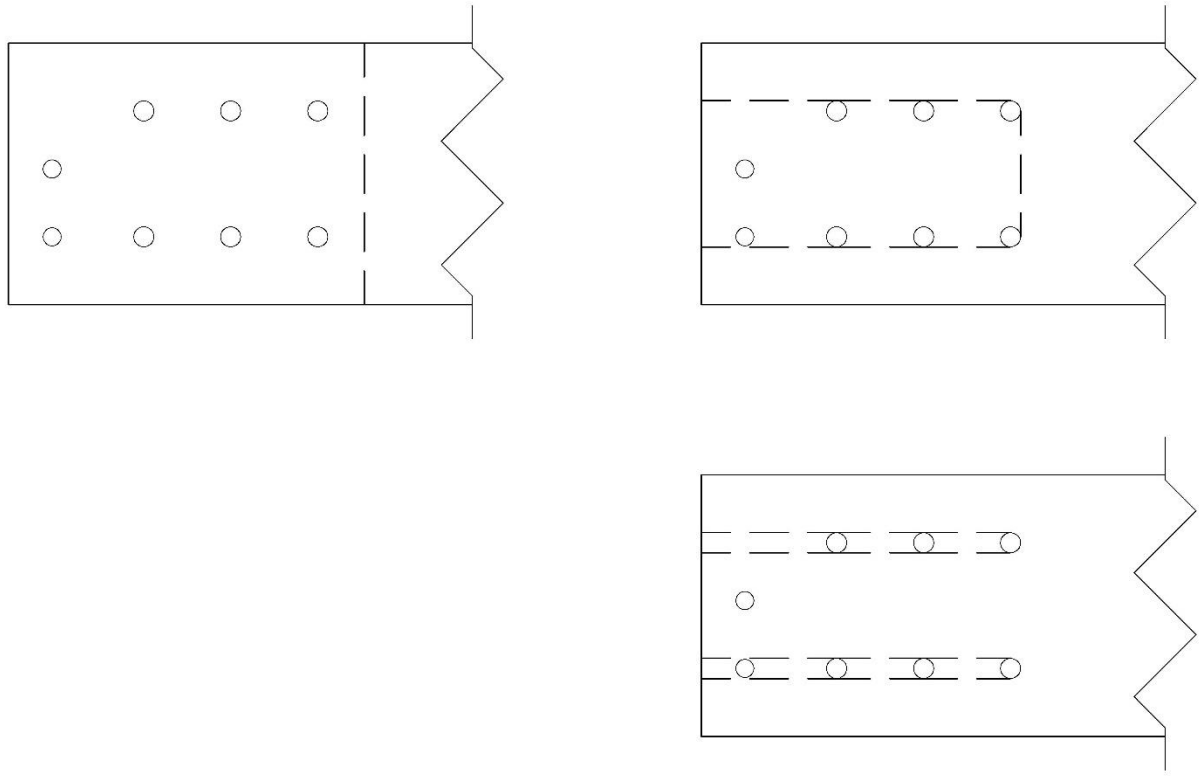

Figure J-2. From top right to bottom left: Net Tensile Failure, Row Tear-out Failure, Group Tear-out Failure.

The tensile strength parallel to grain is 1250 psi for combination 2 Douglas Fir-Larch according to NDS Supplement Table 5B. The factored tensile strength can be represented by the equation:

$$F_t' = F_t C_M C_t \varphi \lambda$$

C_M is the moisture content factor applicable for wet wood. Because of the height of the railing from the ground and the airflow allowing evaporation of water, the moisture content factor was concluded to not reduce the strength in this scenario – so it will be 1.0. C_t is the temperature factor, which will also not apply in this case because the temperature across every US state is on average less than 100 degrees Fahrenheit, with exceptions for regions in some states. This will be 1.0 as a result. The format adjustment factor from ASD to LRFD is 2.70 and the strength resistance factor is 0.80. The time effect factor will be limited to 1.0, because the design is checking connection strength. The factored shear strength is 2700 psi or 2.7 ksi.

The shear strength is 230 psi for combination 2 Douglas Fir-Larch when loaded about the Y-Y axis according to NDS Supplement Table 5B. The Y-Y axis describes a vehicle load impacting the railing laterally, which best represents the loading scenario. Other shear strength values are higher, and so this estimate is conservative in any case. The factored shear strength can be represented by the equation:

$$F_v' = C_M C_t C_{vr} K_F \varphi \lambda$$

The shear reduction factor is applied to shear strength use scenarios which are different from testing which produced the values. These scenarios include any kind of impact loading, and so the reduction must be applied. It will be 0.72. The format adjustment factor from ASD to LRFD is 2.88 and the strength resistance factor is 0.75. The time effect factor will be limited to 1.0, because the design is checking connection strength. The factored shear strength is 358 psi or 0.358 ksi.

The net tensile section for the upper rail is 145.13 square in. (13.5 in. x 10.75 in.), and 105 square in. for the curb rail (8.75 in. x 12 in.).

The row tear-out section is strictly shear, A_{shear}. The minimum distance between a bolt and the location the bolt no longer transfers load from the wooden beam into the steel splice is the critical distance, $l_{critical}$. This value, based on Figure 96, is 5.5 in. for the upper rail and 3 in. based on Figure 97 for the curb rail. The width of the beam is reduced by the splice plate, b_{beam}. For ½ in. thick plates the width is 9¾ in. for a 10¾ in.-width upper rail and 11 in. for a 12 in.-width curb rail. The capacity for a single bolt is doubled to account for shear on both sides of the bolt. The shear area is $A_{wood_{shear}} = 2n_{bolts}l_{critical}b_{beam}$, for 526.5 square in. for the upper rail splice and 396 square in. for the curb rail splice.

The group tear-out section is a combination of shear and tension, A_{shear} and $A_{tensile}$. The shear area is calculated in the same manner, except only the exterior edge of the exterior bolts will contribute. The shear area will be 263.25 square in. for the upper rail and 198 square in. for the curb rail. The area in tension, $A_{tensile}$, is the product of the width of the beam, b_{beam}, and the spacing between rows of bolts, s_{bolts}. This spacing is 6.5 in. for the upper rail according to Figure 96 for the upper rail and 5 in. for the curb rail according to Figure 97. The area in tension for the upper rail is therefore 63.375 in. and 48.75 in. for the curb rail.

Table J-4. Timber Beam Connection Capacities

Member	Net Tensile (kips)	Row Tear-Out (kips)	Group Tear-Out (kips)
Upper Rail	391.84	188.49	237.39
Curb Rail	283.50	141.65	195.19

Appendix K. AGT Design Alternatives

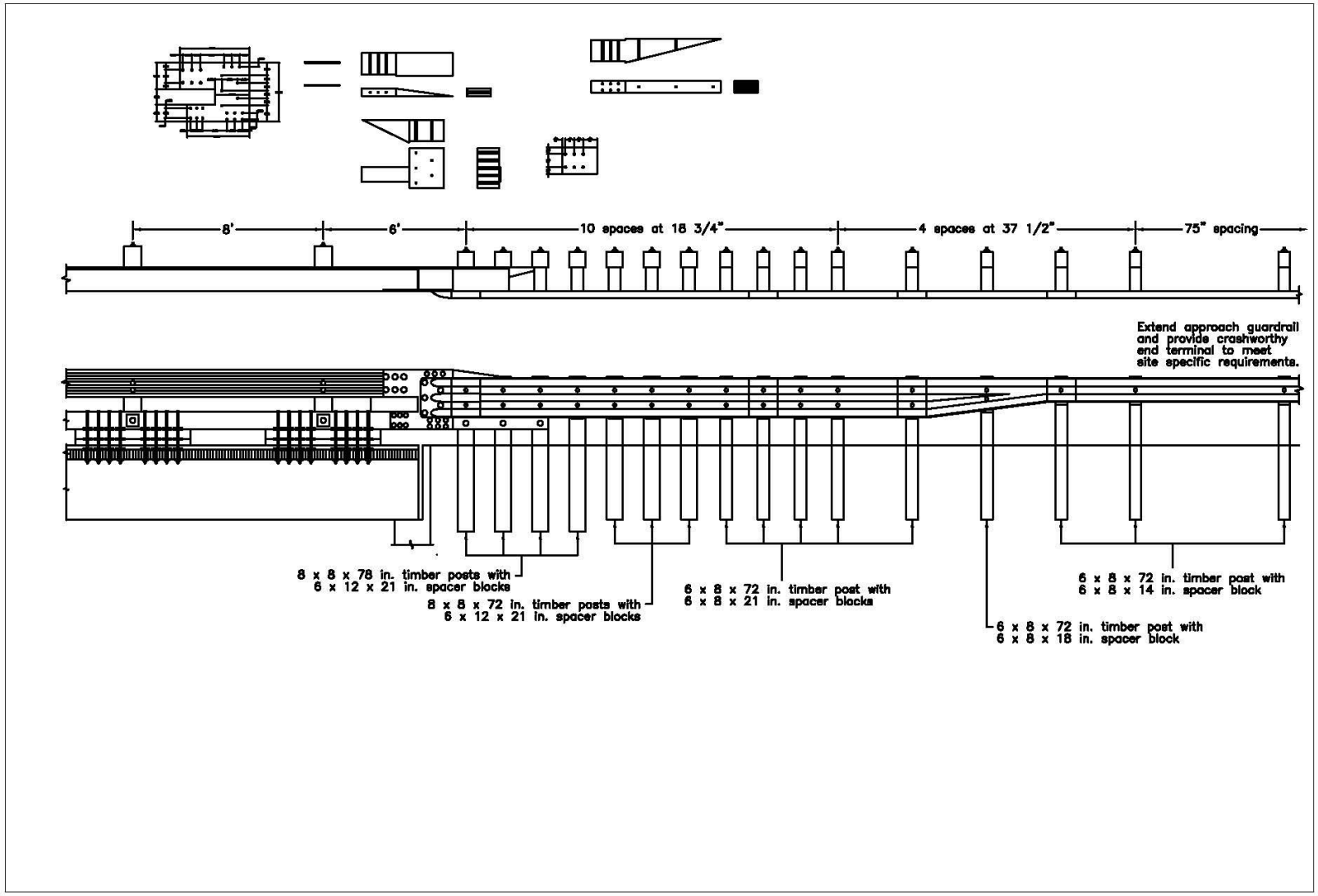

Figure K-1. Option 1.1 – Quarter-Post Spacing, 6-ft Gap, U-Plate, Removed Blockouts, Wood Reverse Taper, Thin Curb Taper

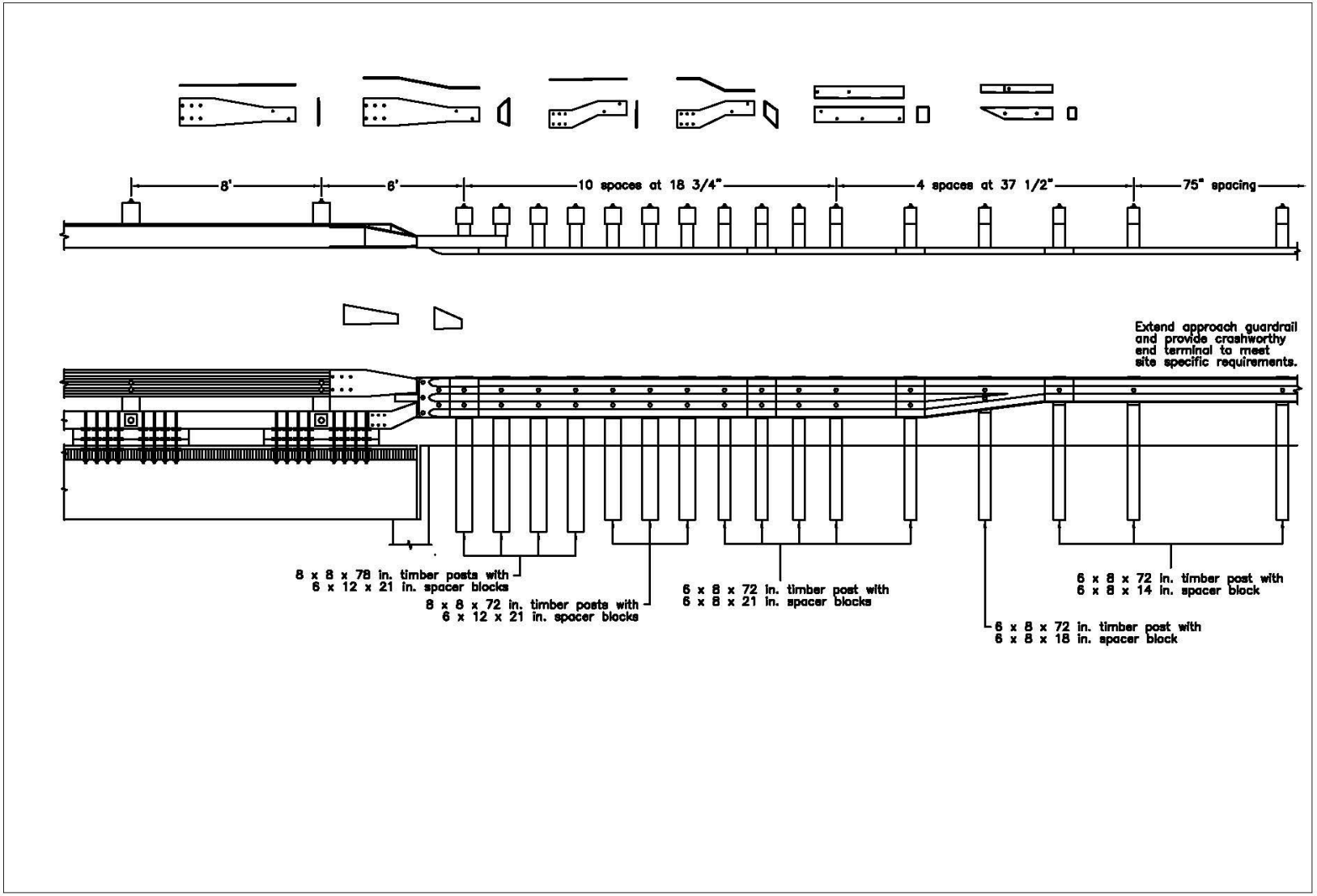

Figure K-2. Option 1.2 – Quarter-Post Spacing, 6-ft Gap, Steel Components, Partial Removal of Blockouts, Steel Reverse Taper, No Curb Taper

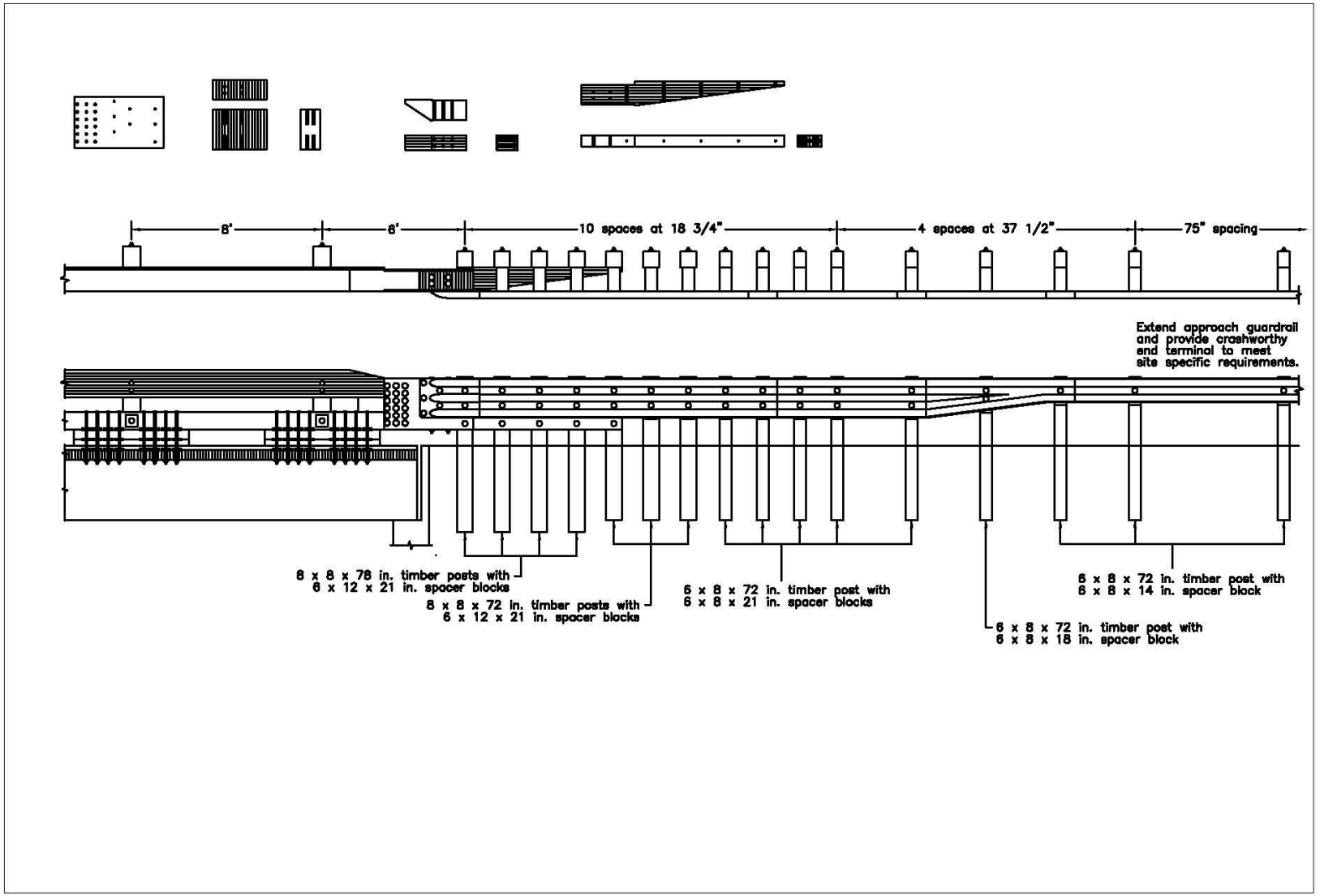

Figure K-3. Option 1.3 – Quarter-Post Spacing, 6-ft Gap, Plate, Separated Block, Removed Blockouts, Wood Reverse Taper, Thin Curb Taper

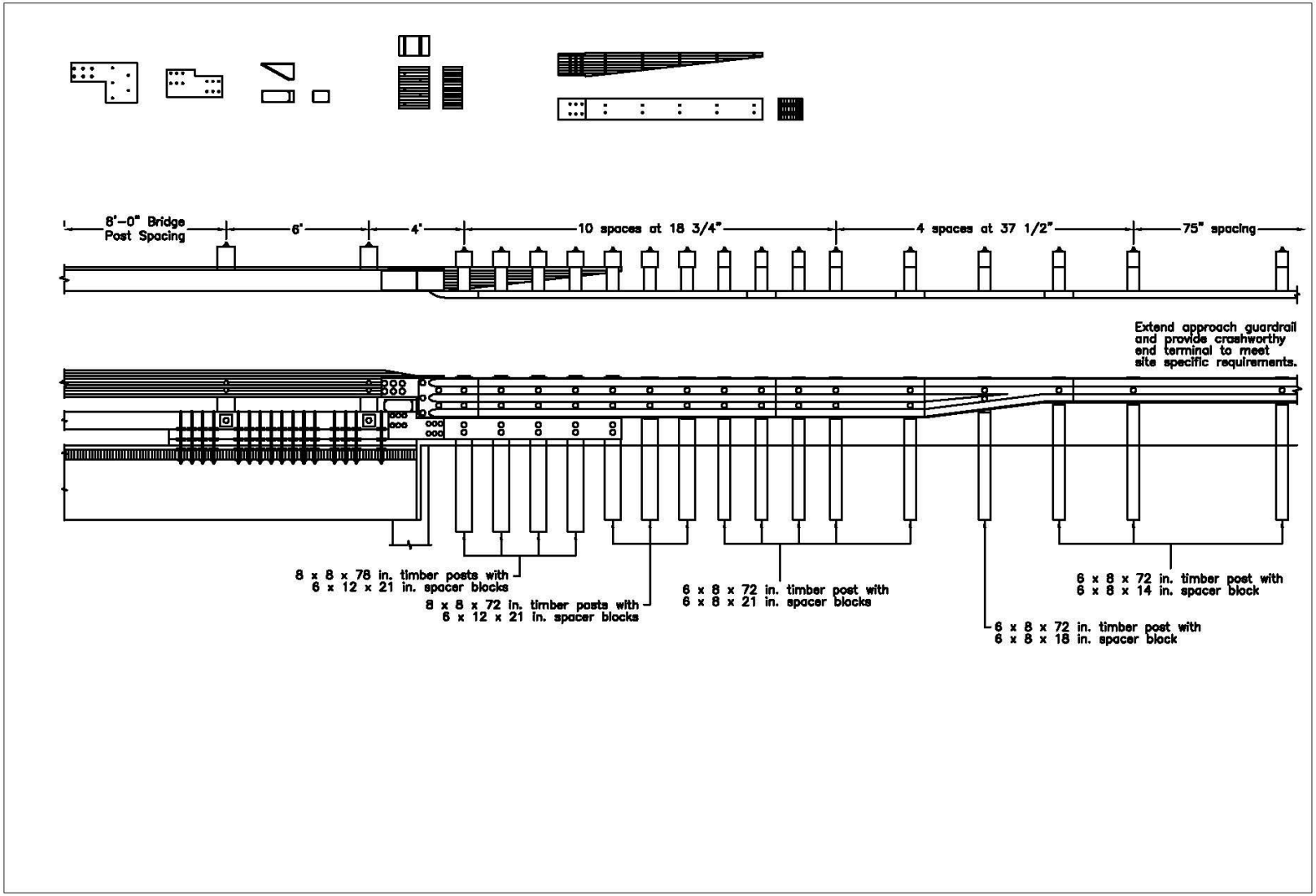

Figure K-4. Option 1.4 – Quarter-Post Spacing, 4-ft and 6-ft Gaps, L-Plate, Separated Block, Steel Reverse Taper, Thick Curb Taper

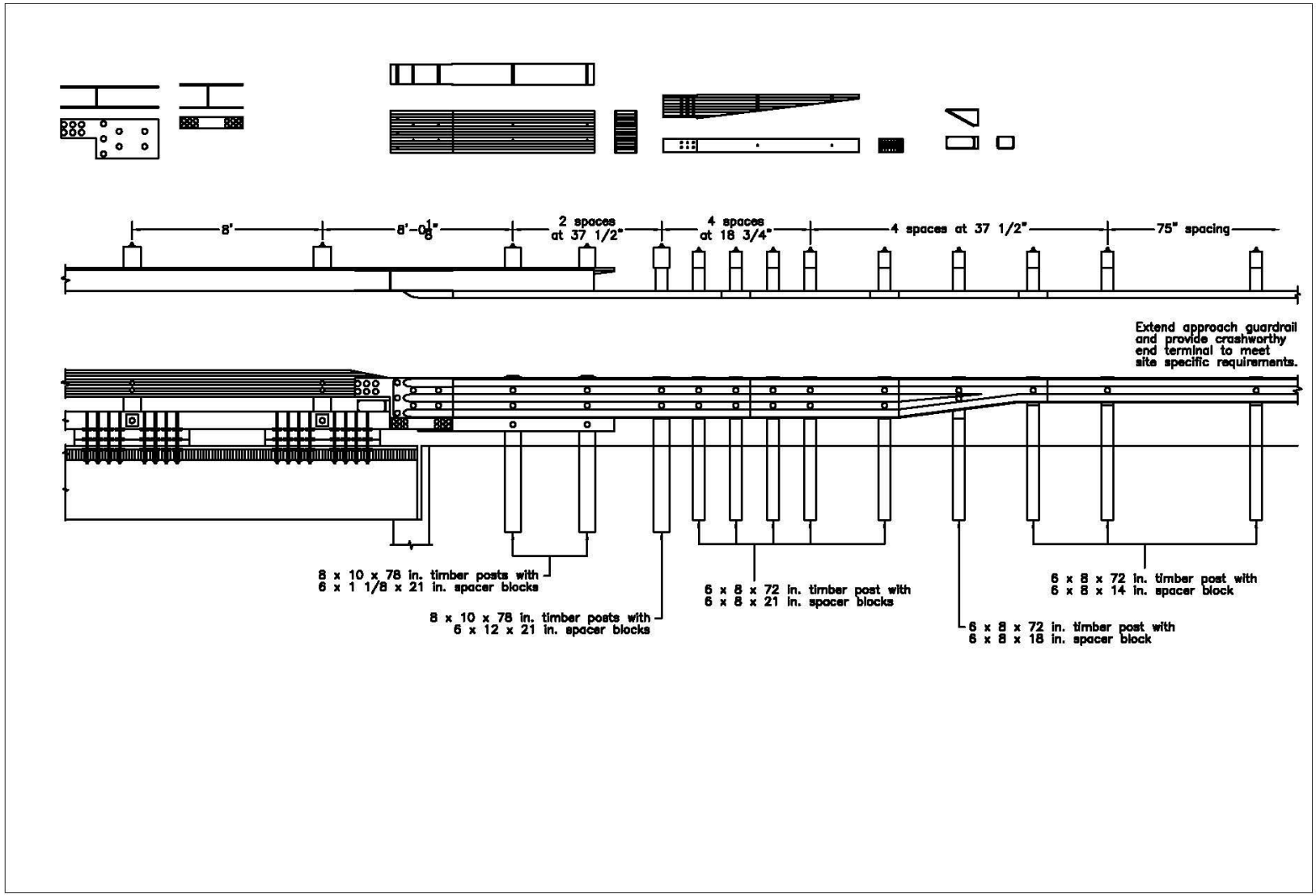

Figure K-5. Option 1.5 – Half-Post Spacing, 8-ft Gap, L-Plate, Separated Block, Removed Blockouts, Steel Reverse Taper, Thin Curb Taper

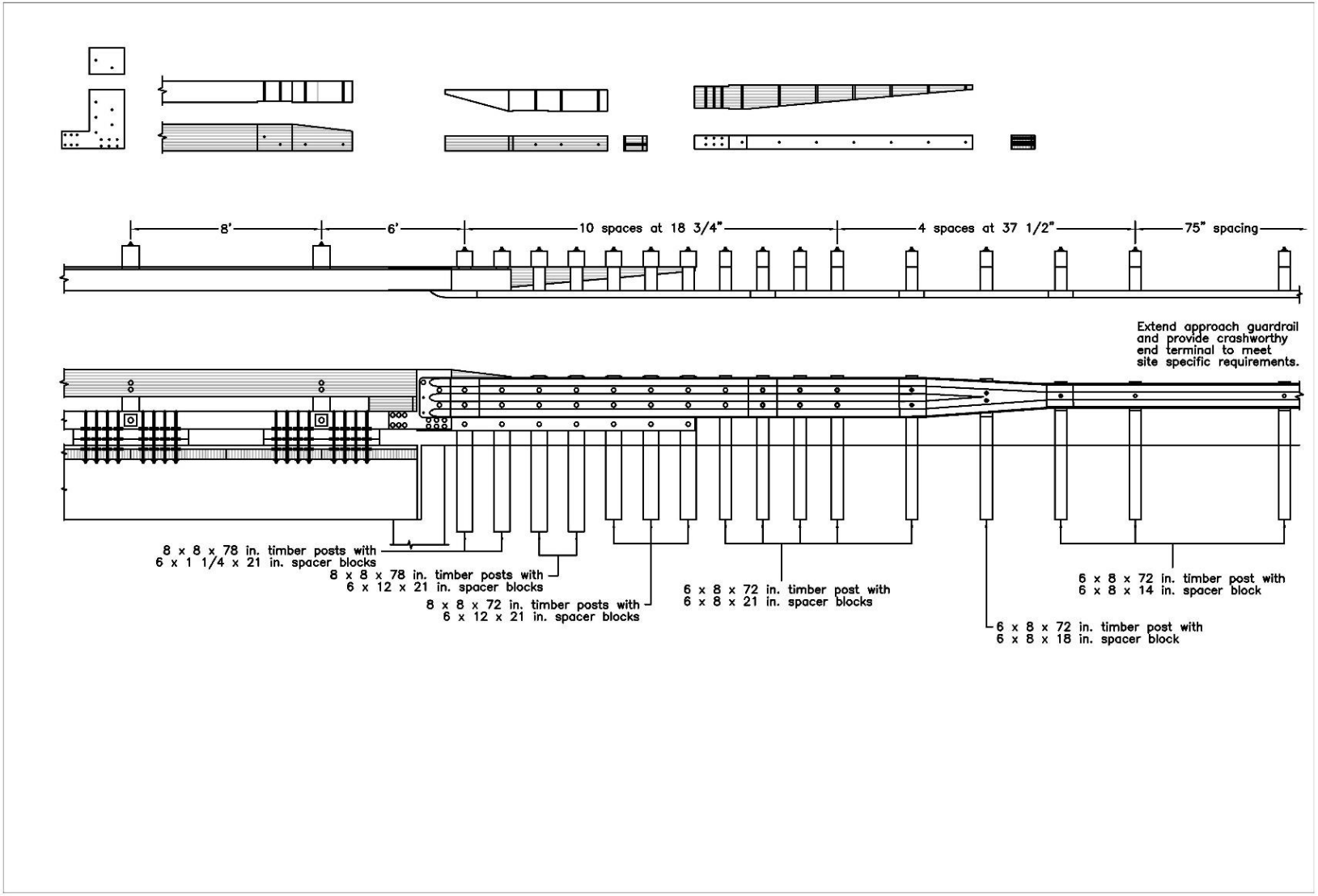

Figure K-6. Option 2.1 – Quarter-Post Spacing, 6-ft Gap, Lower L-Plate, Removed Blockouts, Wood Reverse Taper, Thin Curb Taper

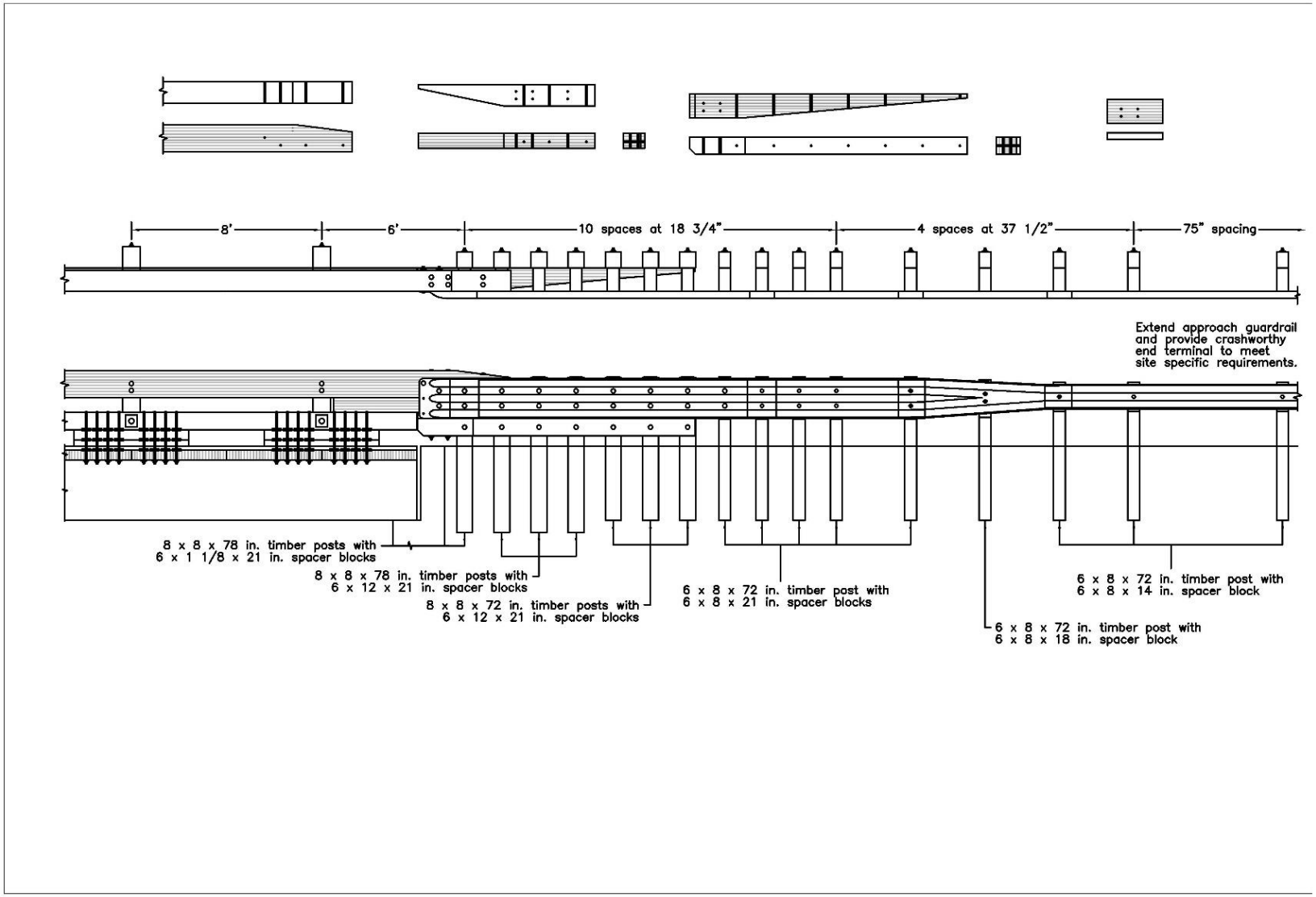

Figure K-7. Option 2.2 – Quarter-Post Spacing, No Plate, Missing Bolts, Removed Blockouts, Wood Reverse Taper, Separated Stepped Curb Taper

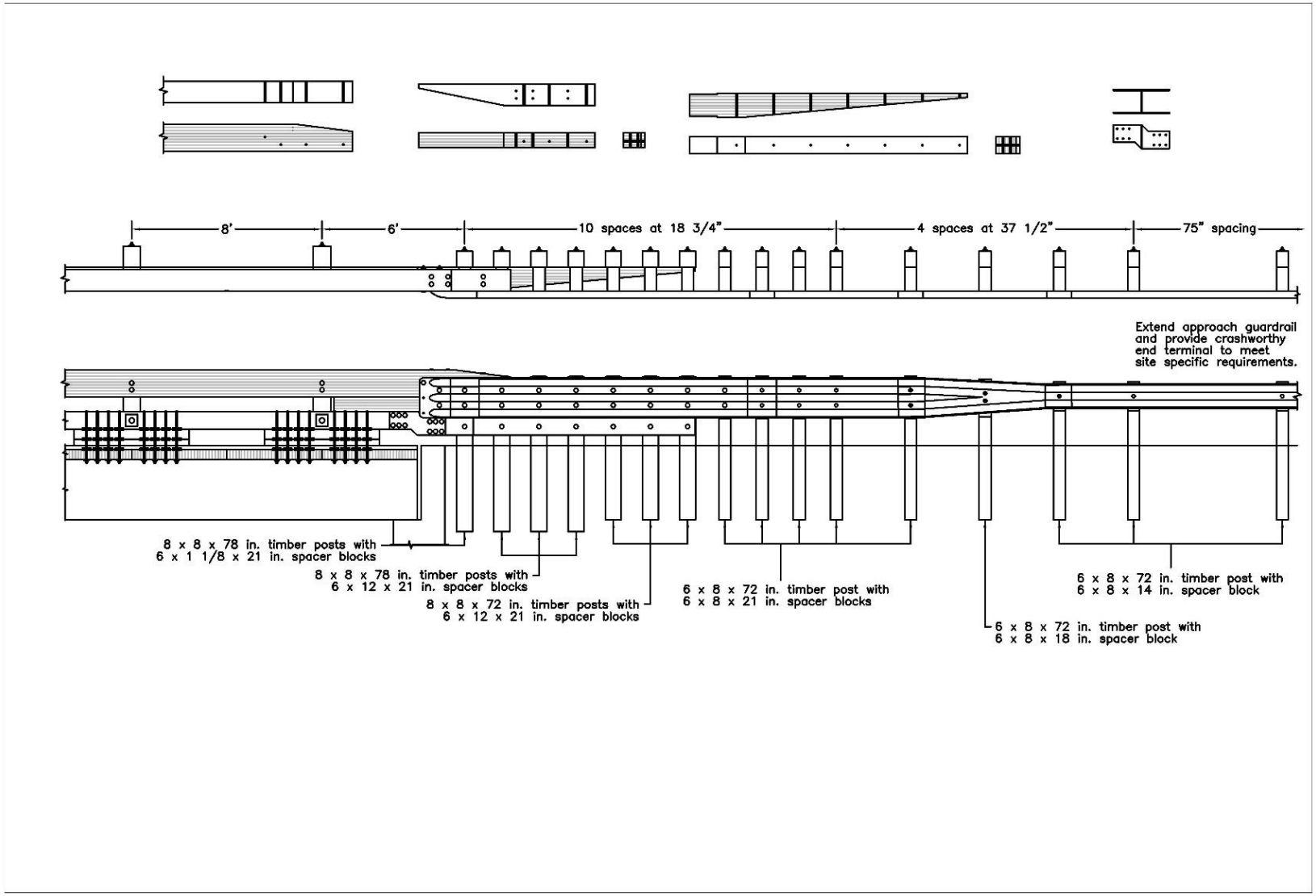

Figure K-8. Option 2.3 – Quarter-Post Spacing, 6-ft Gap, No Plate, Missing Bolts, Removed Blockouts, Wood Reverse Taper, Stepped Curb Taper

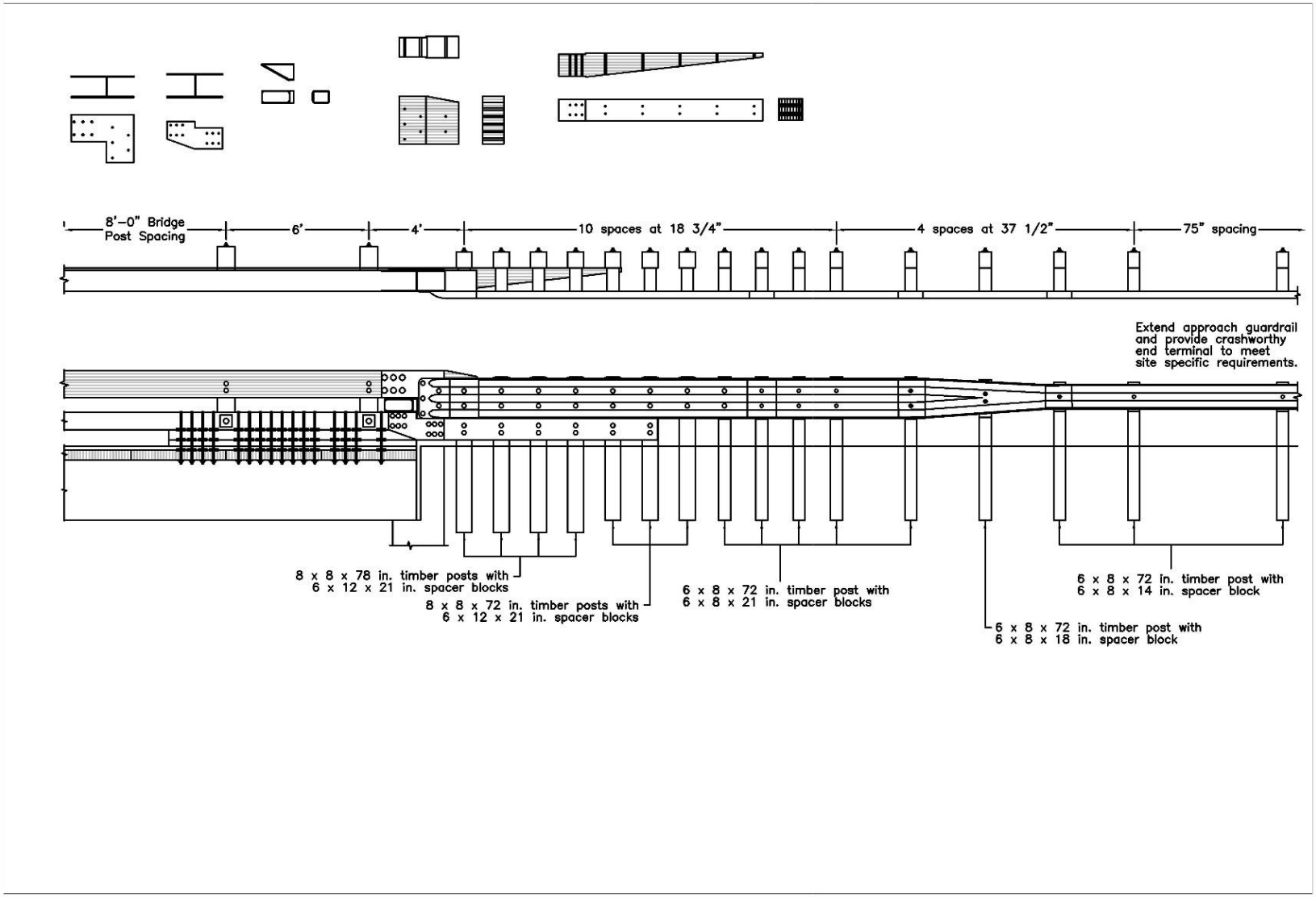

Figure K-9. Option 2.4 – Quarter-Post Spacing, 6-ft Gap, L-Plate, Separated Block, Removed Blockout, Steel Reverse Taper, Thick Stepped Curb Taper

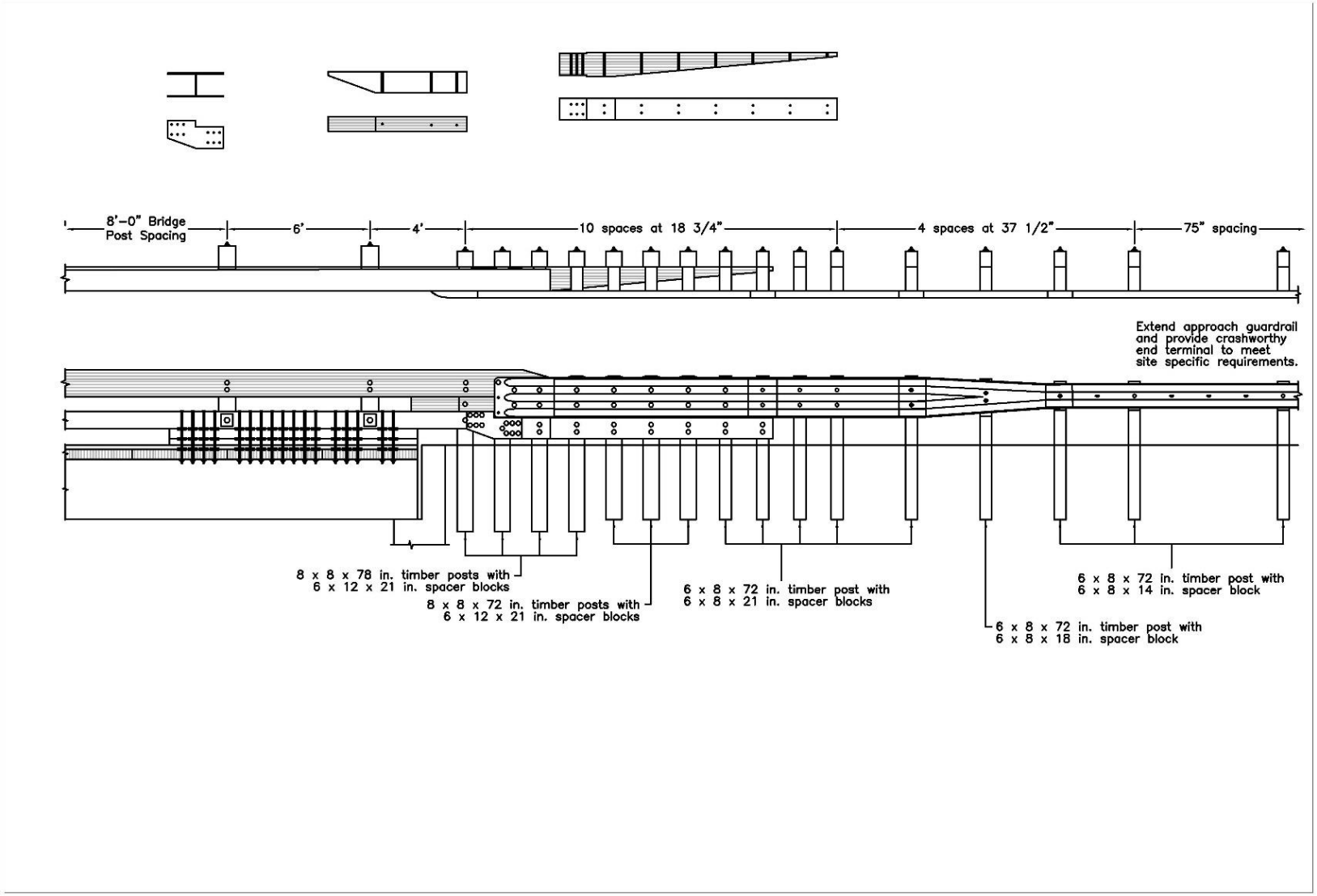

Figure K-10. Option 2.5 – Quarter-Post Spacing, 4-ft and 6-ft Gaps, No Plate, Missing Bolts, Removed Blockouts, Wood Reverse Taper, Stepped Thick Curb Taper

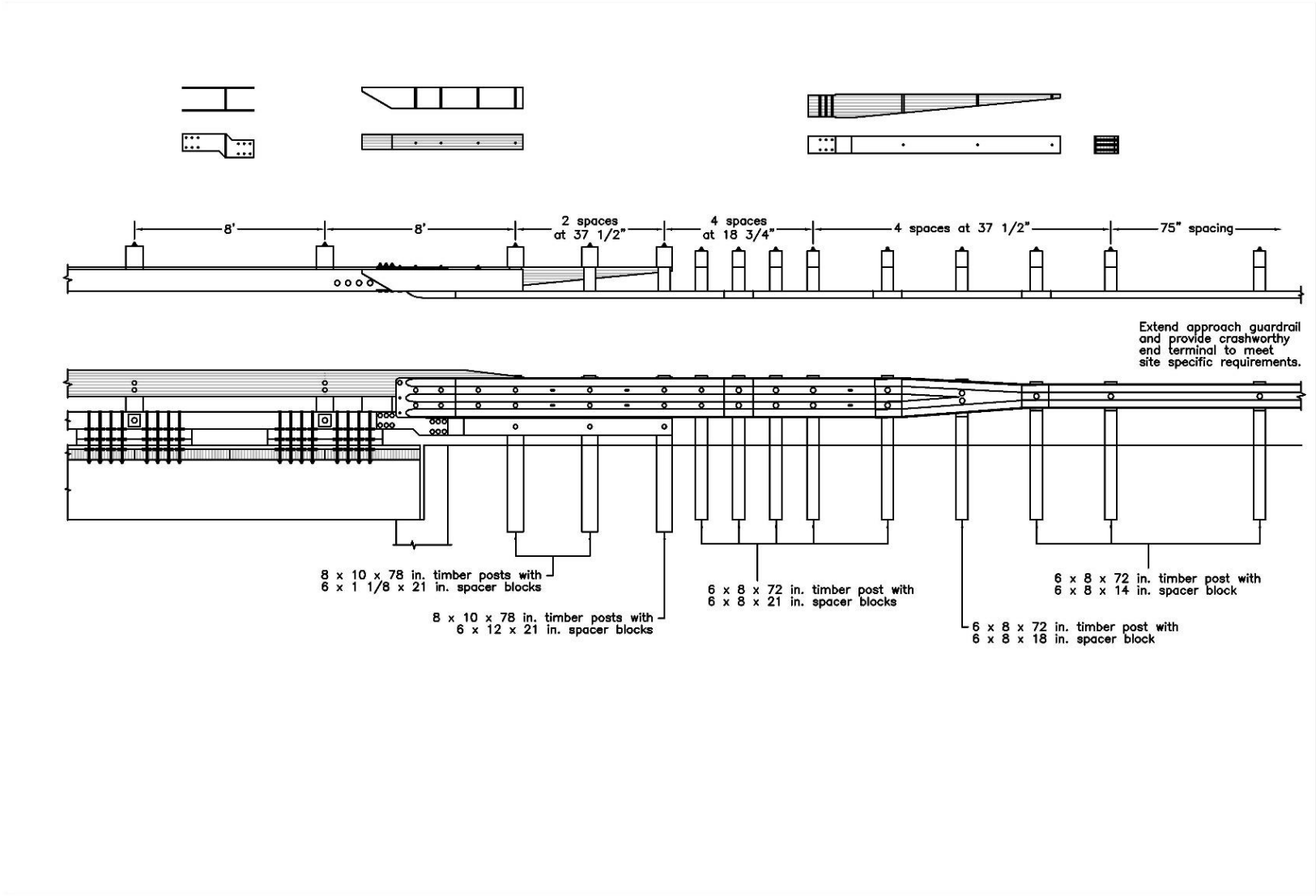

Figure K-11. Option 2.6 – Half-Post Spacing, 8-ft Gap, No Plate, Missing Bolts, Removed Blockout, Wood Reverse Taper, Stepped Curb Taper

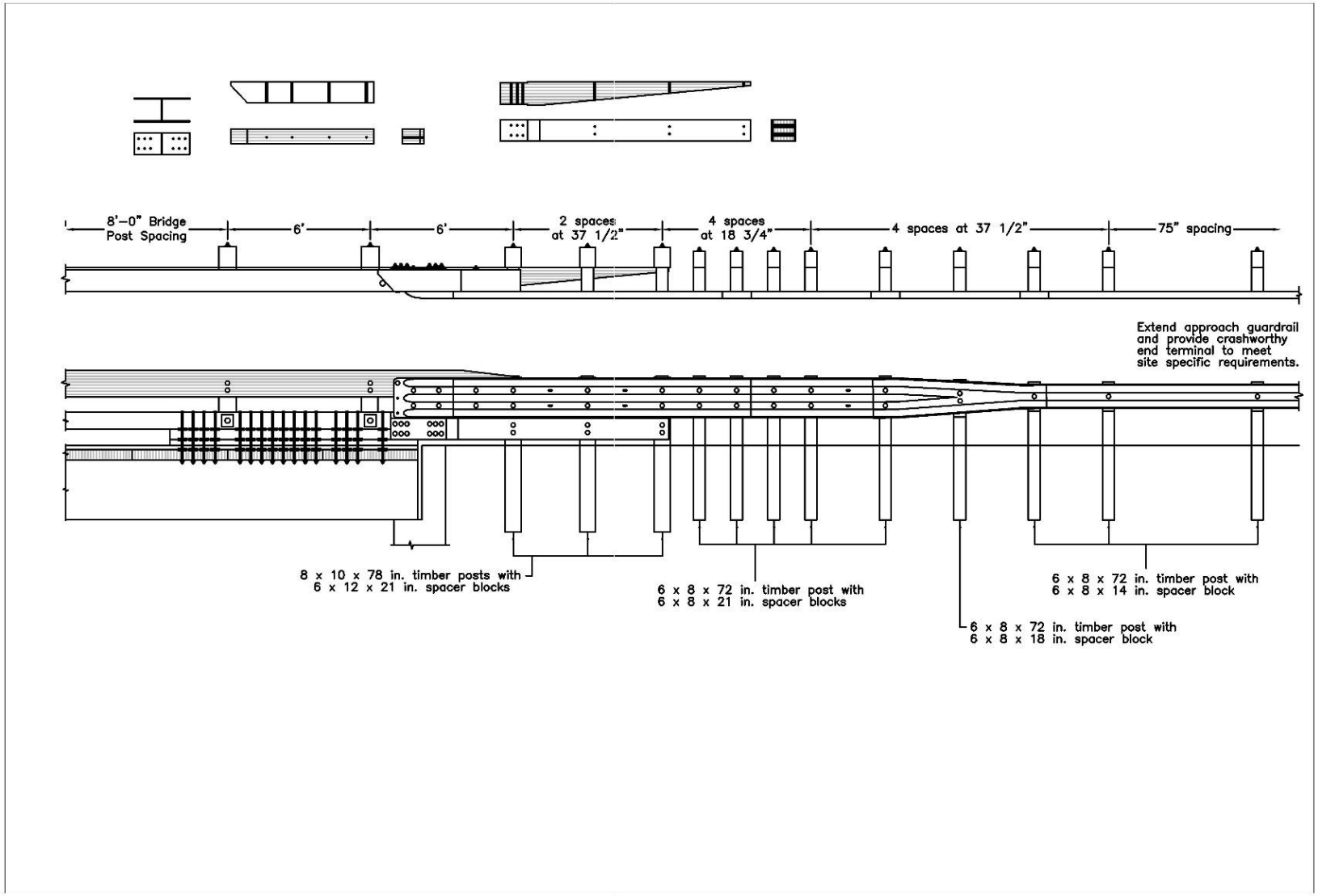

Figure K-12. Option 2.7 – Half-Post Spacing, 6-ft Gap, Removed Blockout, Wood Reverse Taper, Stepped Thick Curb Taper

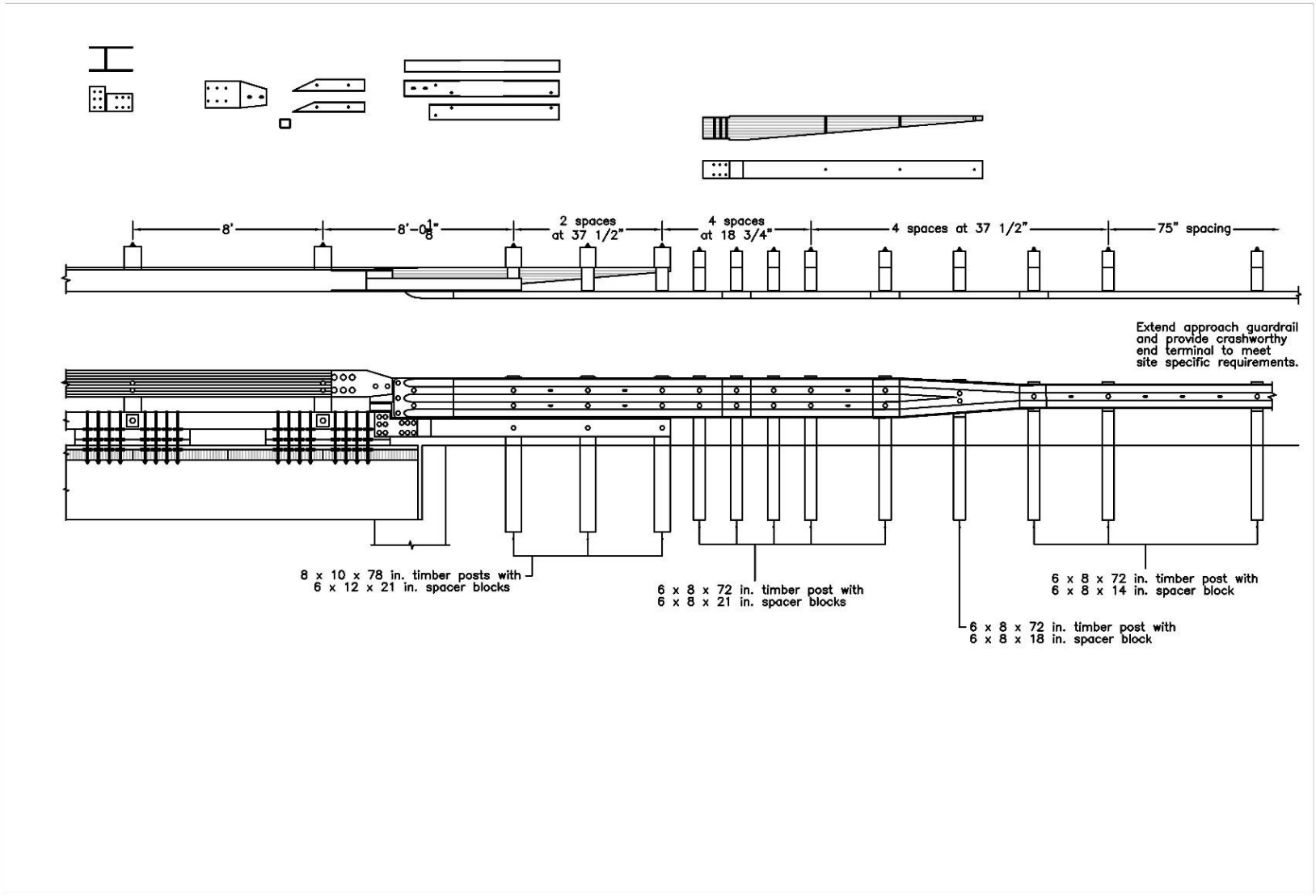

Figure K-13. Option 2.8 – Half-Post Spacing, 8-ft Gap, Steel Components, Partially Removed Blockout, Steel Reverse Taper, Stepped Thick Curb Taper

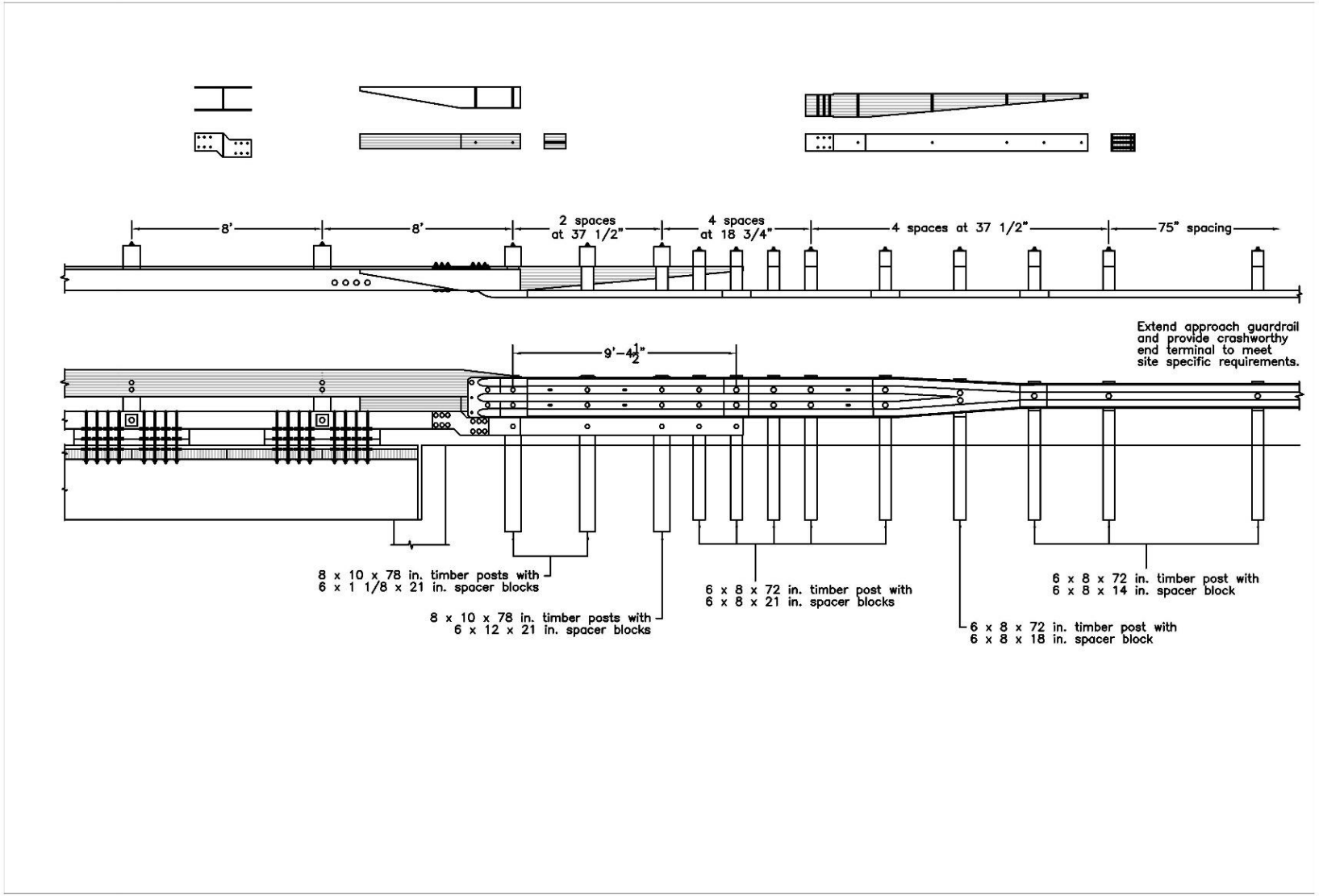

Figure K-14. Option 2.9 – Half-Post Spacing, 8-ft Gap, Shortened Thrie-Beam, No Plate, Missing Bolts, Wood Reverse Taper, Stepped Curb Taper

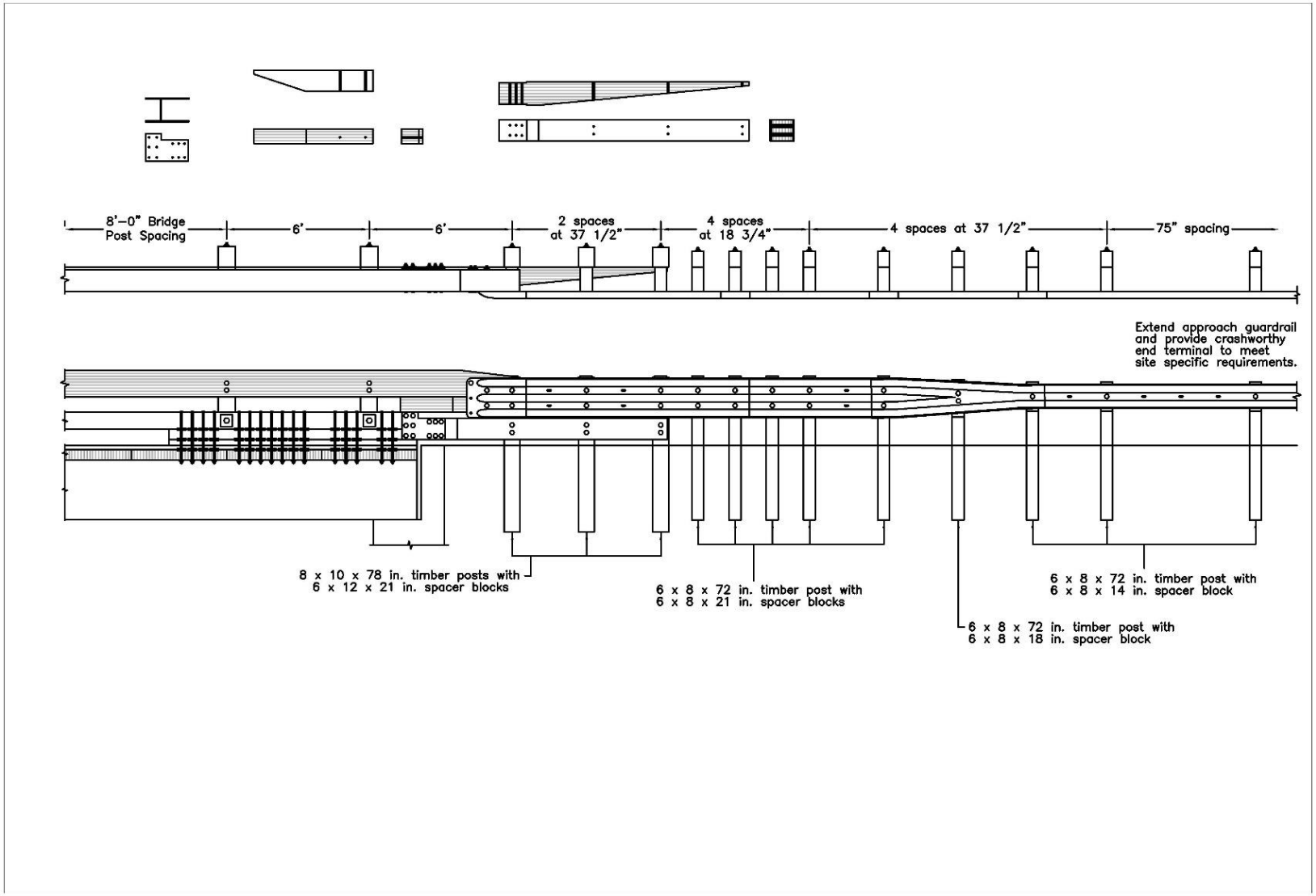

Figure K-15. Option 2.10 – Half-Post Spacing, 6-ft Gap, No Plate, Missing Bolts, Wood Reverse Taper, Stepped Thick Curb Taper

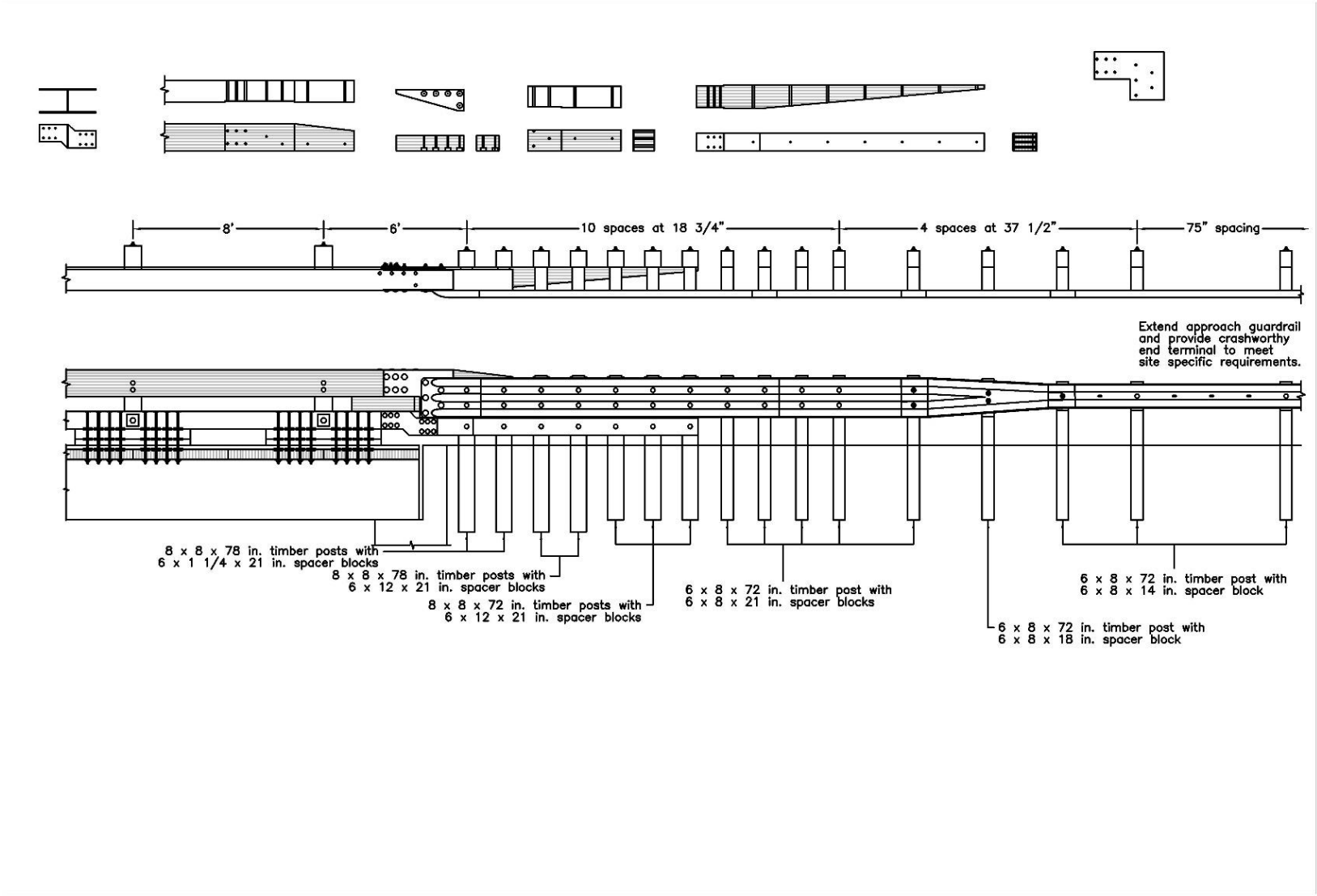

Figure K-16. Option 3.1 – Quarter-Post Spacing, 6-ft Gap L-Plate, Removed Blockouts, Wood Reverse Taper, Stepped Curb Taper

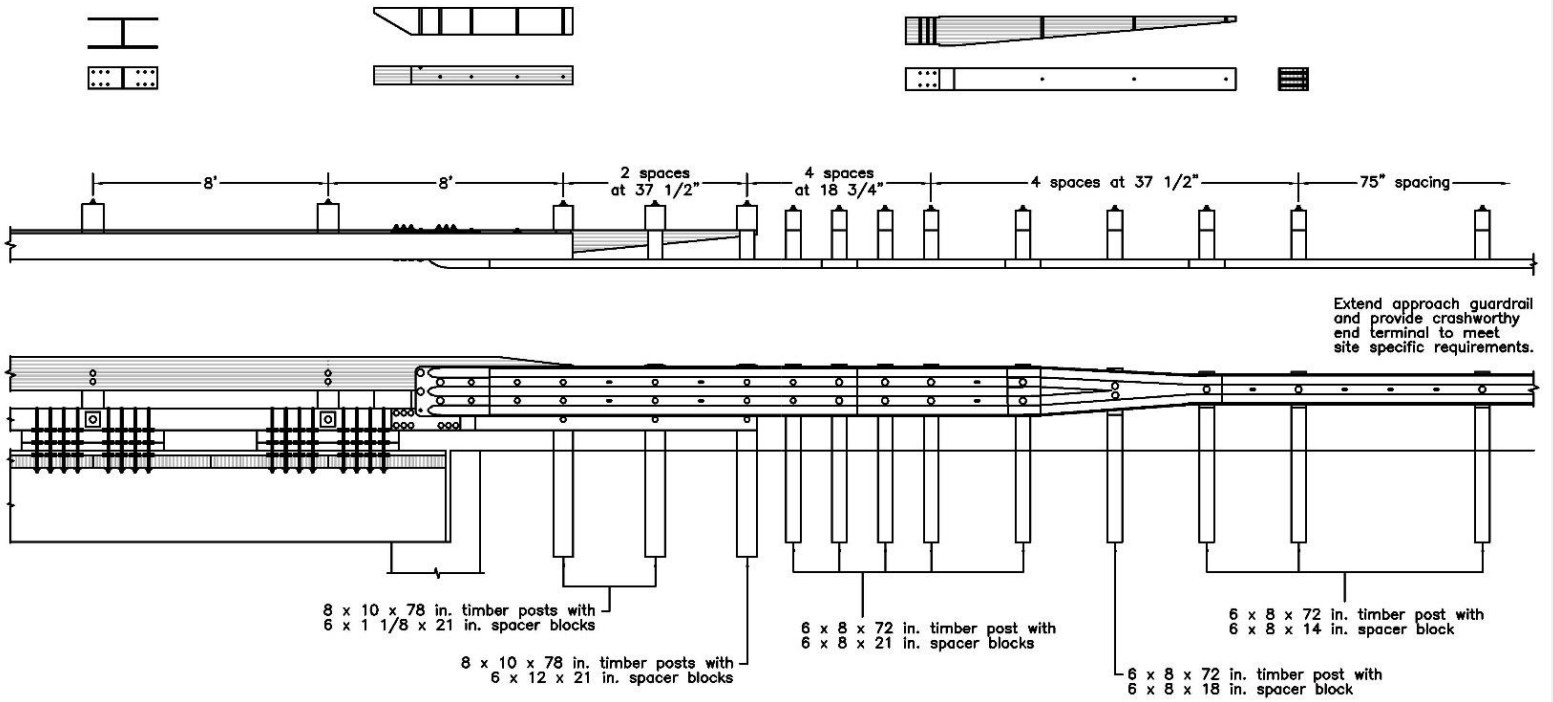

Figure K-17. Option 3.2 – Half-Post Spacing, 8-ft Gap, No Plate, Missing Bolt, Removed Blockout, Wood Reverse Taper, Curb Taper Behind Thrie-Beam

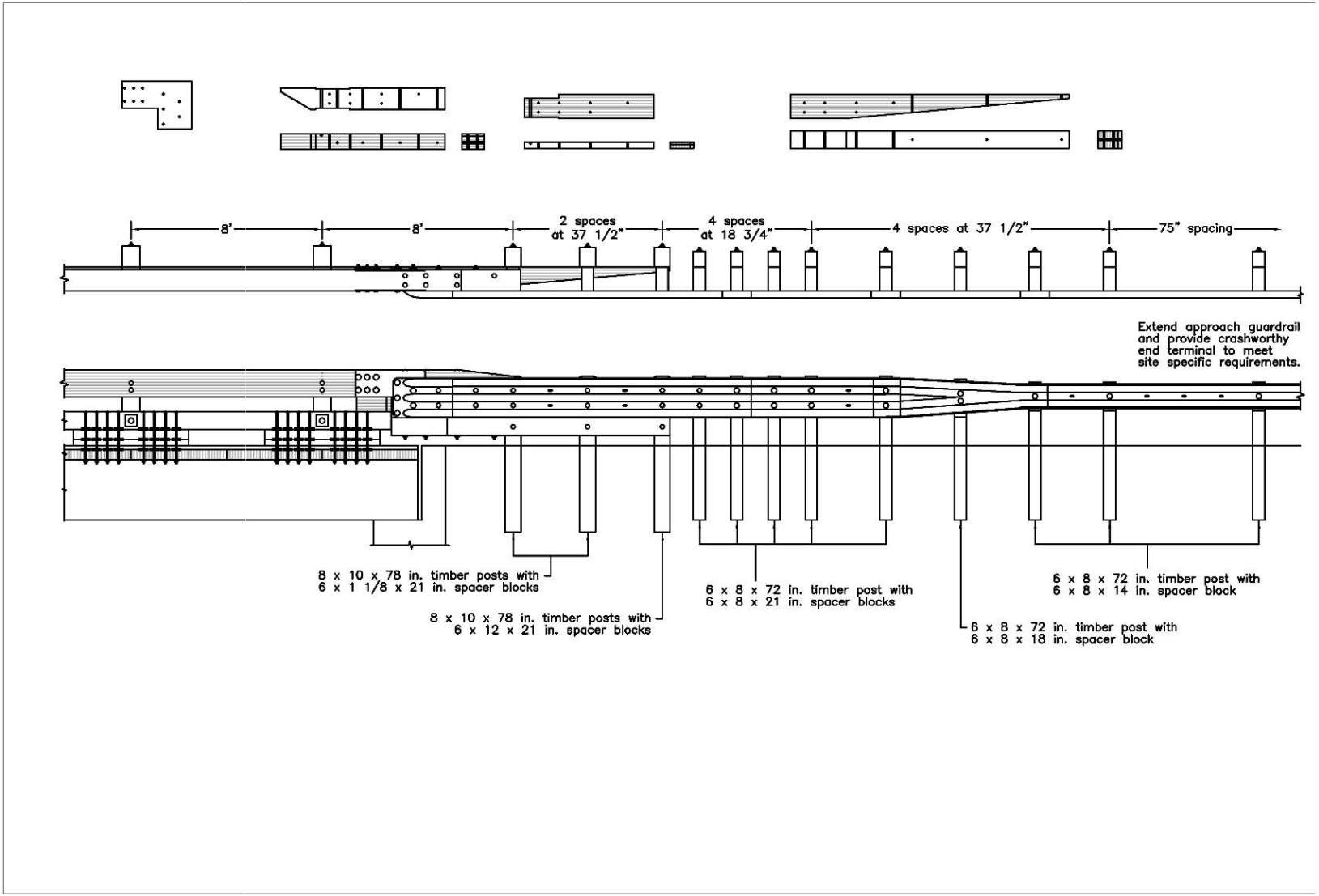

Figure K-18. Option 3.3 – Half-Post Spacing, 8-ft Gap, L-Plate, Removed Blockout, Wood Reverse Taper, Separated Stepped Curb Taper

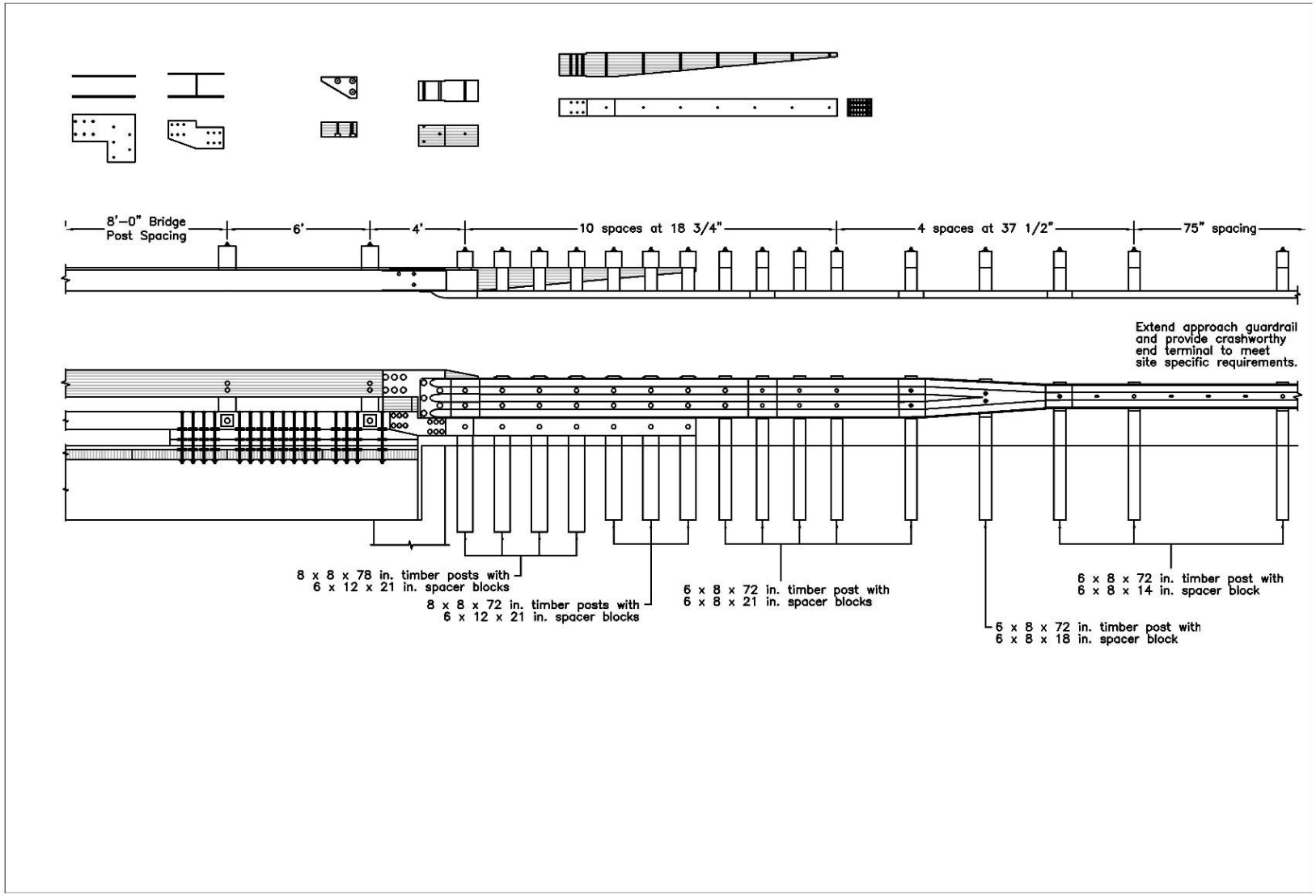

Figure K-19. Option 3.4 – Quarter-Post Spacing, 4-ft and 6-ft Gaps, L-Plate, Removed Blockout, Wood Reverse Taper, Stepped Curb Taper

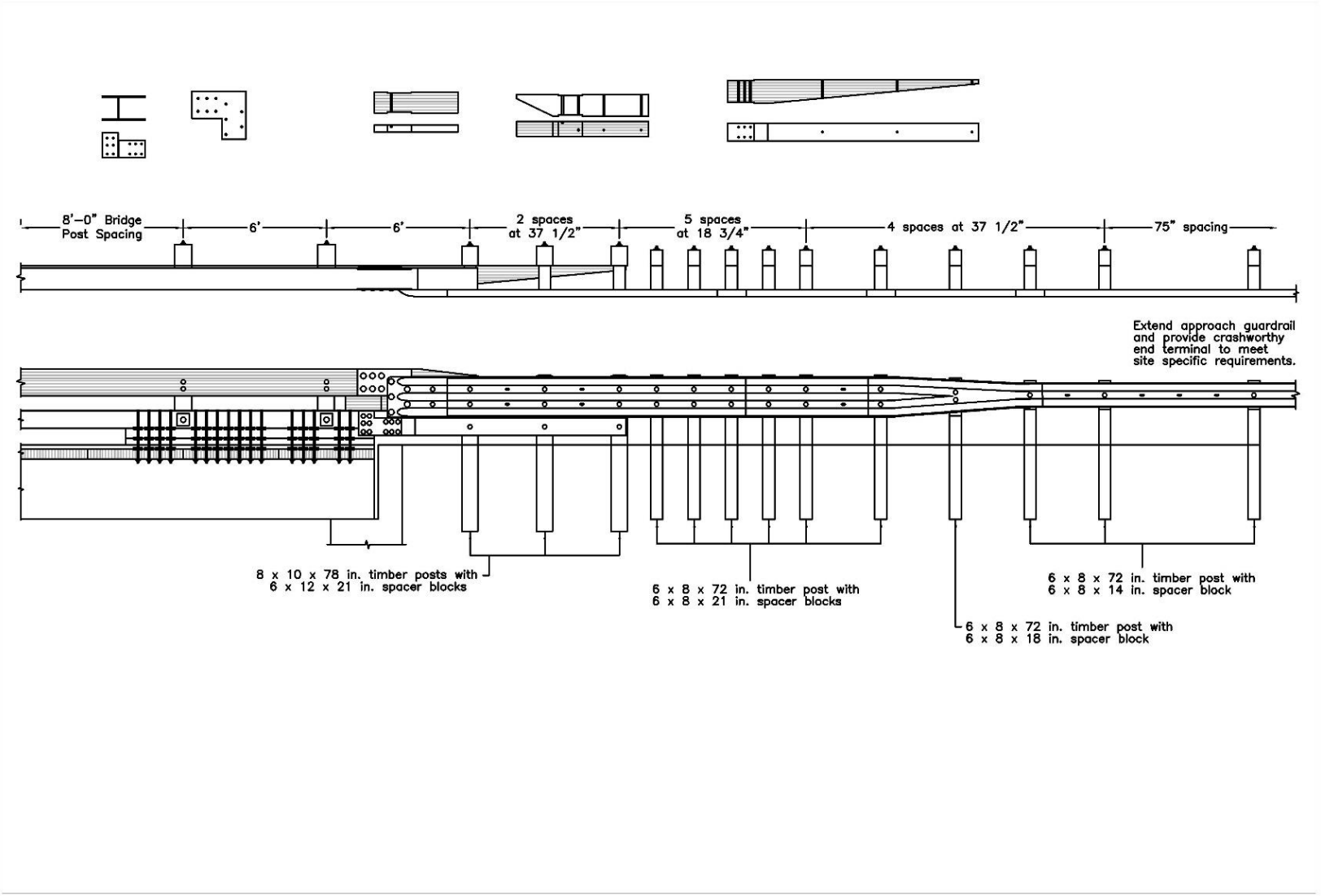

Figure K-20. Option 3.5 – Half-Post Spacing, 6-ft Gap, L-Plate, Removed Blockout, Wood Reverse Taper, Stepped Curb Taper

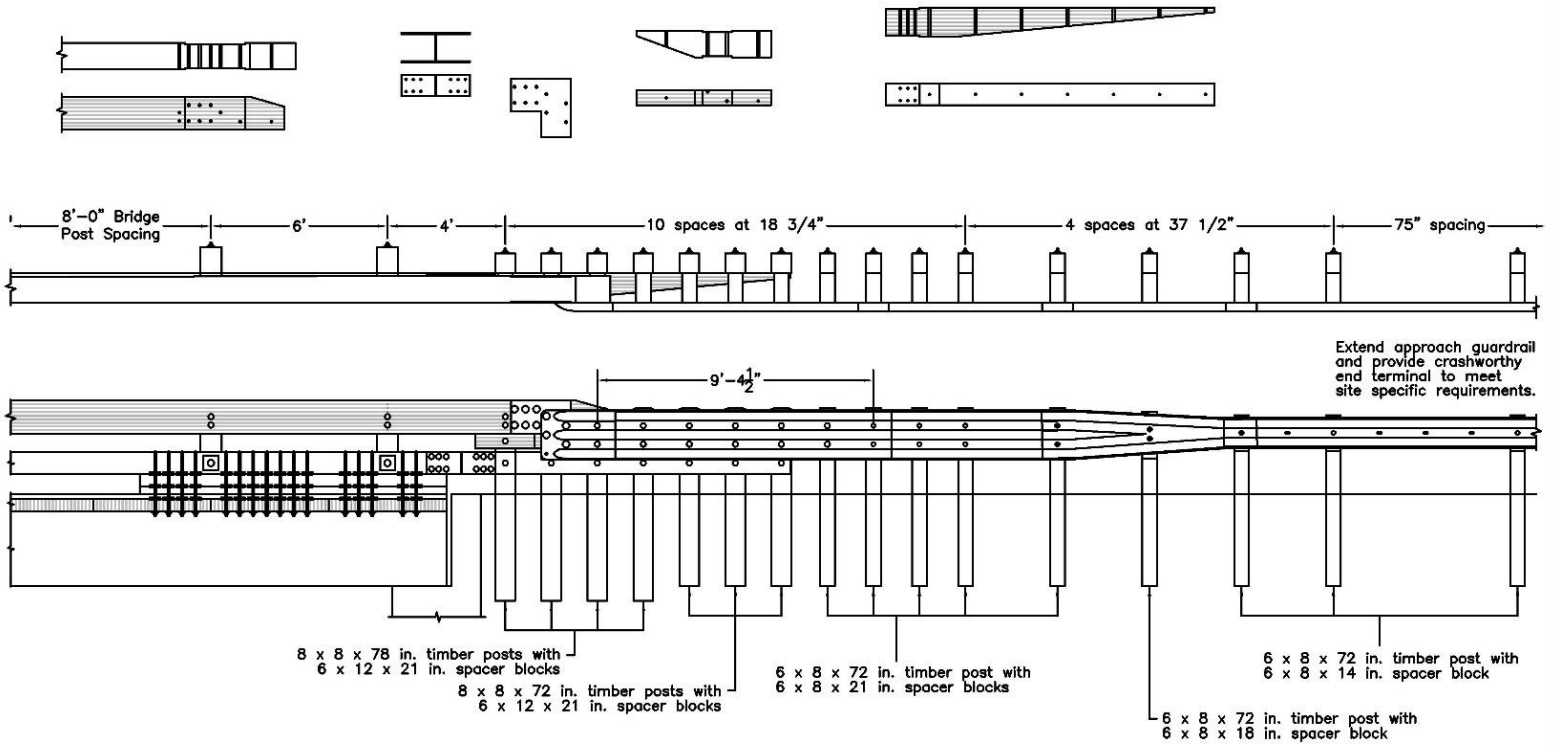

Figure K-21. Option 3.6 – Quarter-Post Spacing, 4-ft and 6-ft Gaps, L-Plate, Removed Blockouts, Missing Bolt, Wood Reverse Taper, Curb Taper Behind Thrie-Beam

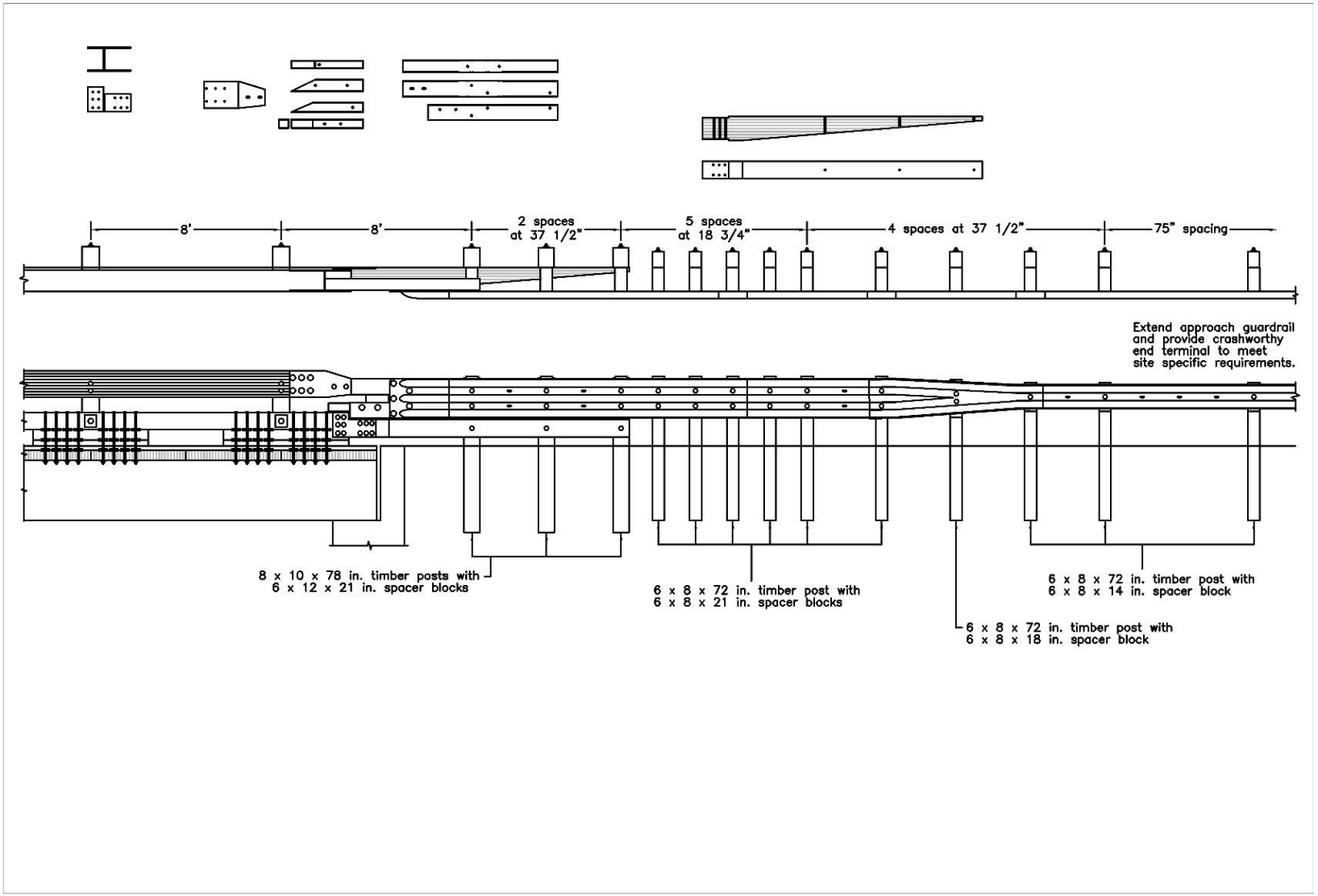

Figure K-22. Option 3.7 – Half-Post Spacing, 8-ft Gap, Steel Components, Partially Removed Blockout, Two Steel Reverse Tapers, Stepped Thick Curb Taper

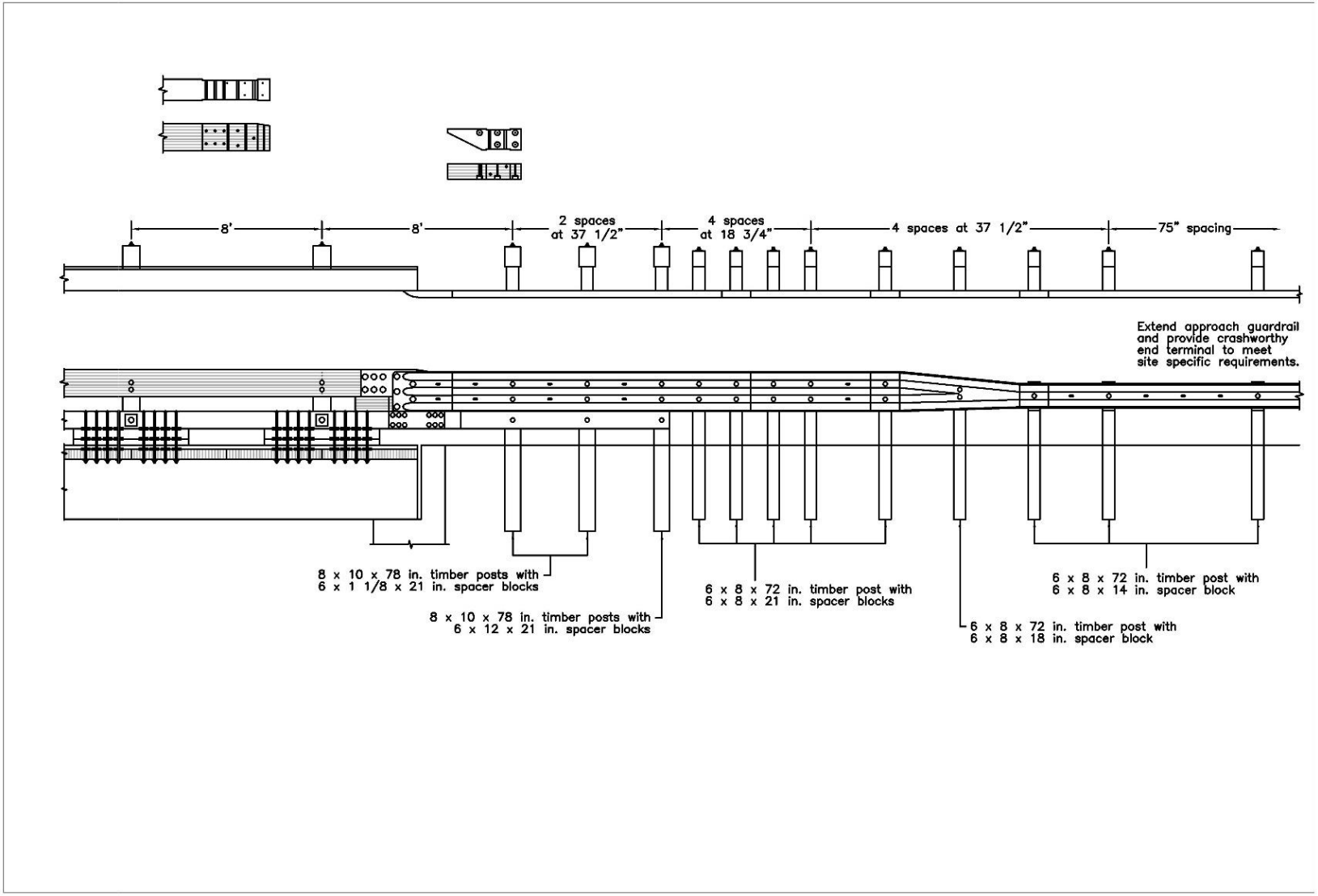

Figure K-23. Option 3.8 – Half-Post Spacing, 8-ft Gap, Custom Thrie-beam to W-beam Transition, L-Plate, Wood Reverse Taper, Curb Taper

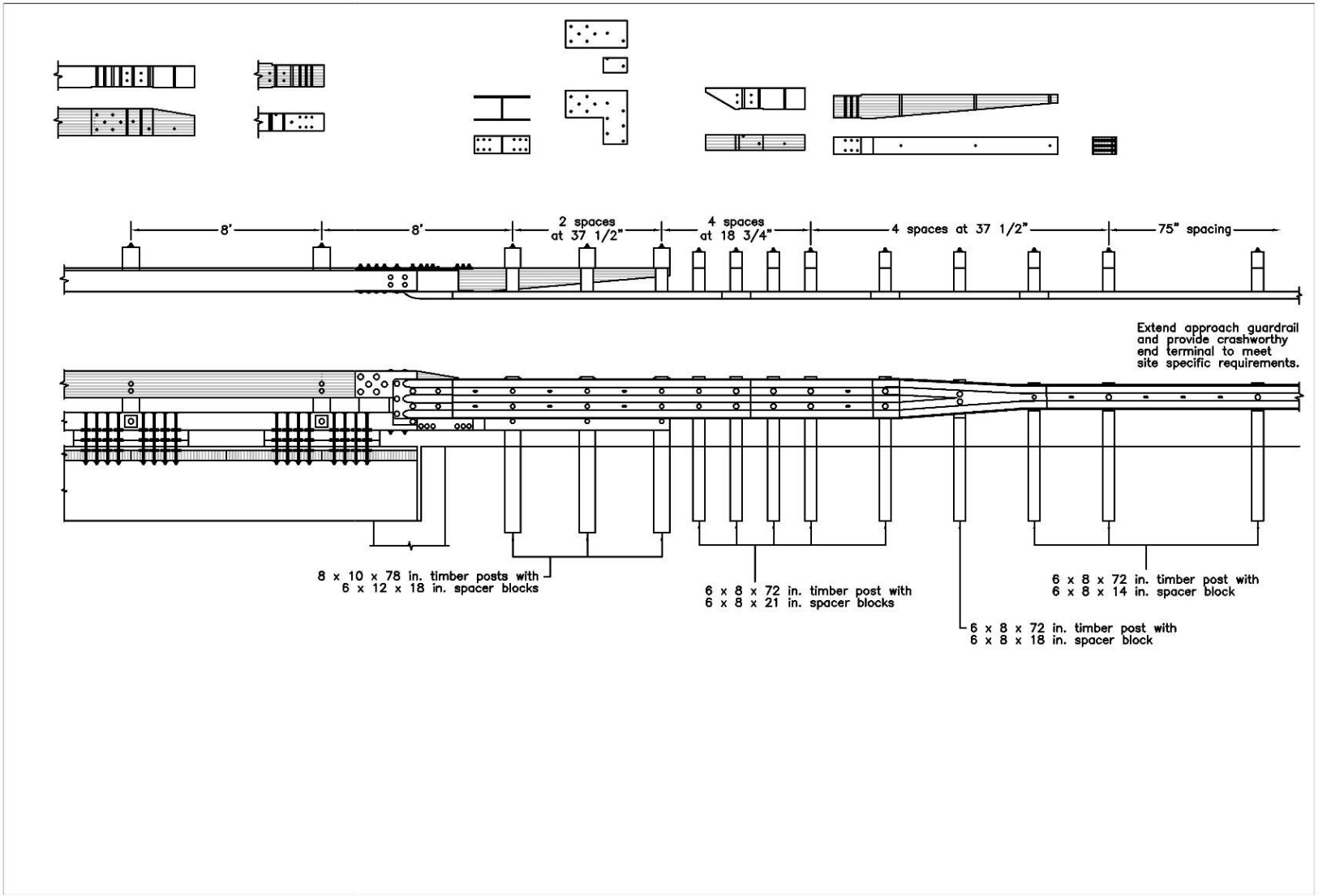

Figure K-24. Option 4.1 – Half-Post Spacing, 8-ft Gap, L-Plate, Wood Reverse Taper, Curb Taper Behind Thrie-beam

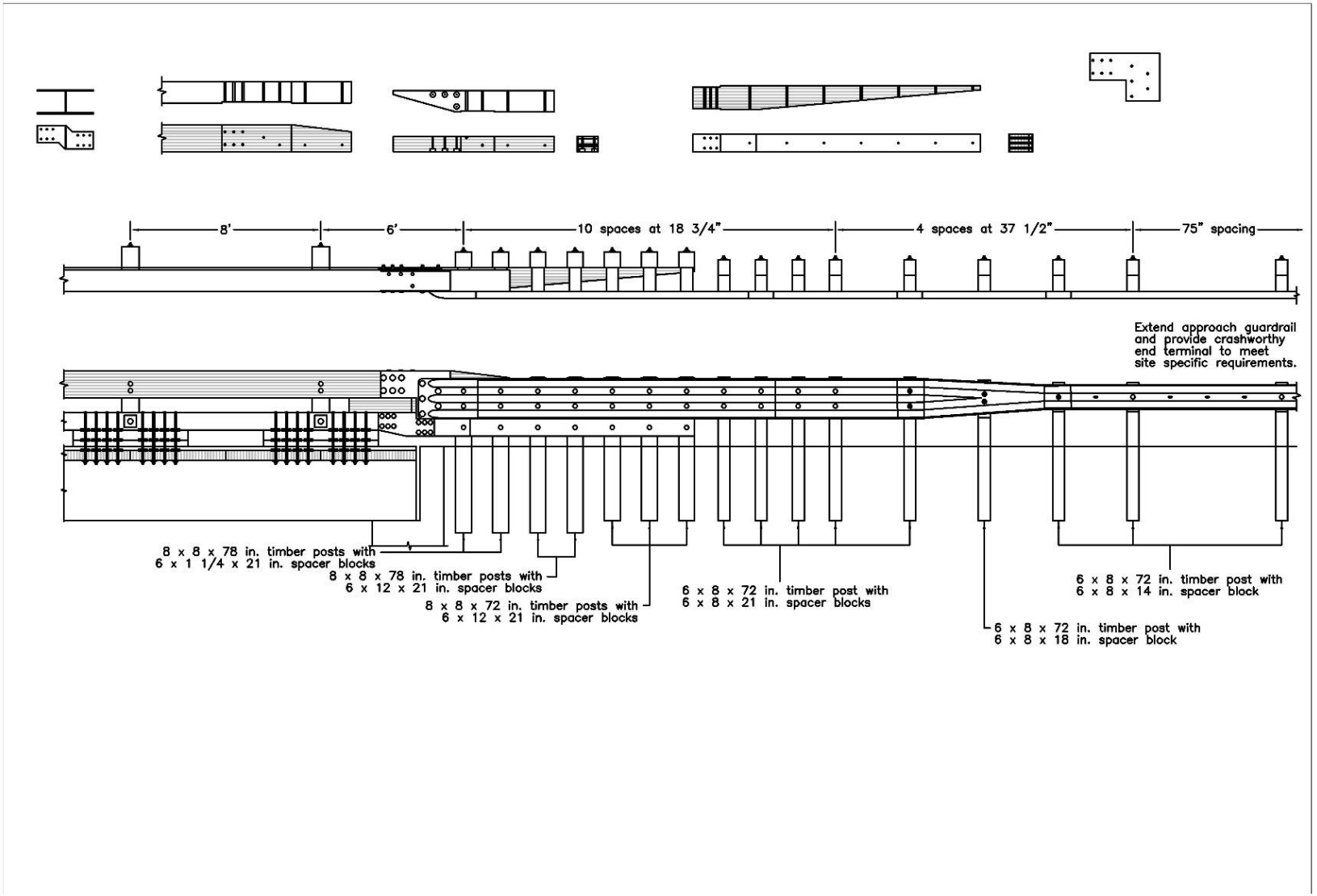

Figure K-25. Option 4.2 – Quarter-Post Spacing, 6-ft Gap, L-Plate, Removed Blockouts, Wood Reverse Taper, Stepped Curb Rail Taper

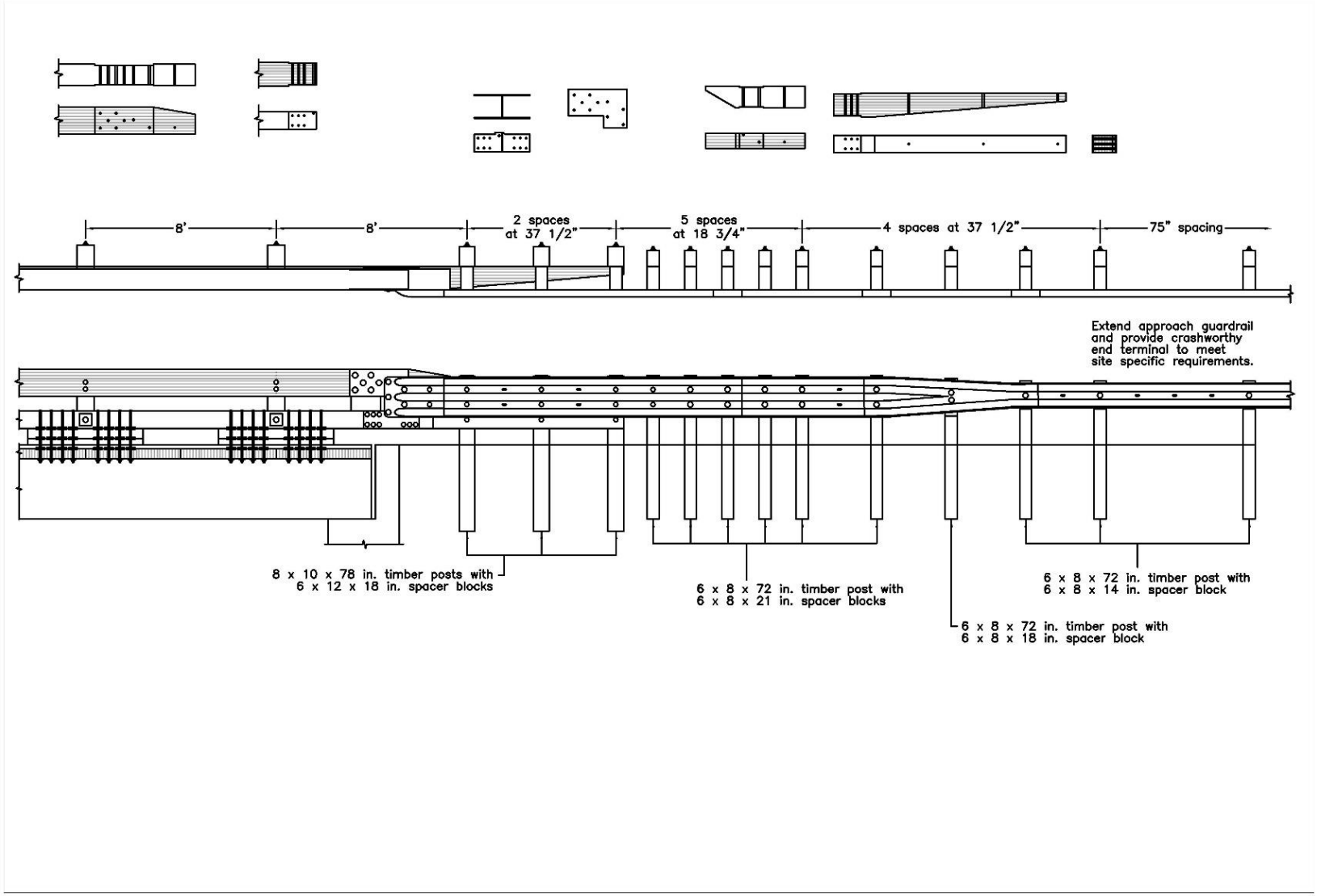

Figure K-26. Option 4.3 – Half-Post Spacing, 8-ft Gap, L-Plate, Wood Reverse Taper, Curb Taper with Bumpout Behind Thrie-Beam

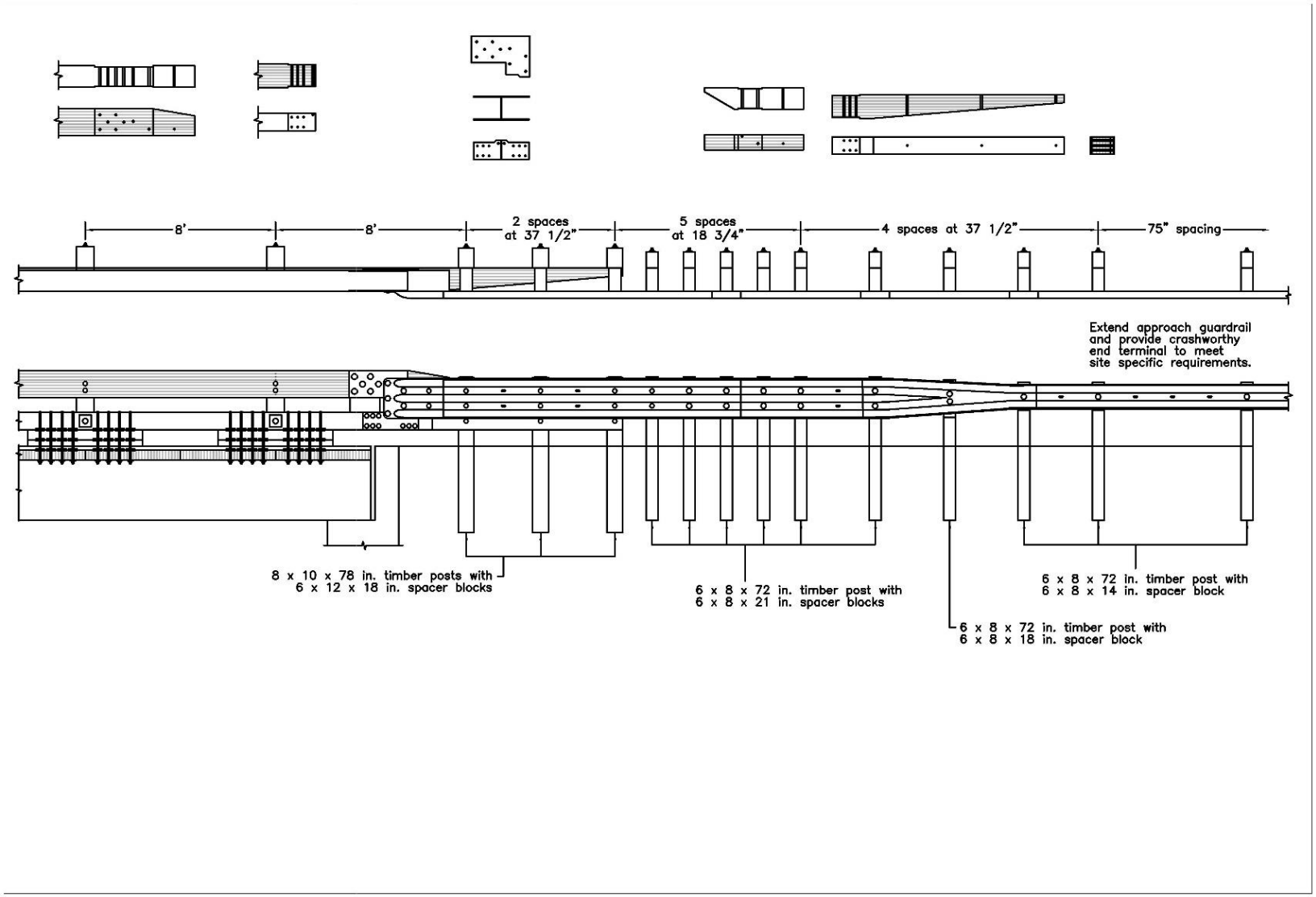

Figure K-27. Option 5.1 – Half-Post Spacing, 8-ft Gap, L-Plate, Wood Reverse Taper, Curb Taper with Bumpout Behind Thrie-beam

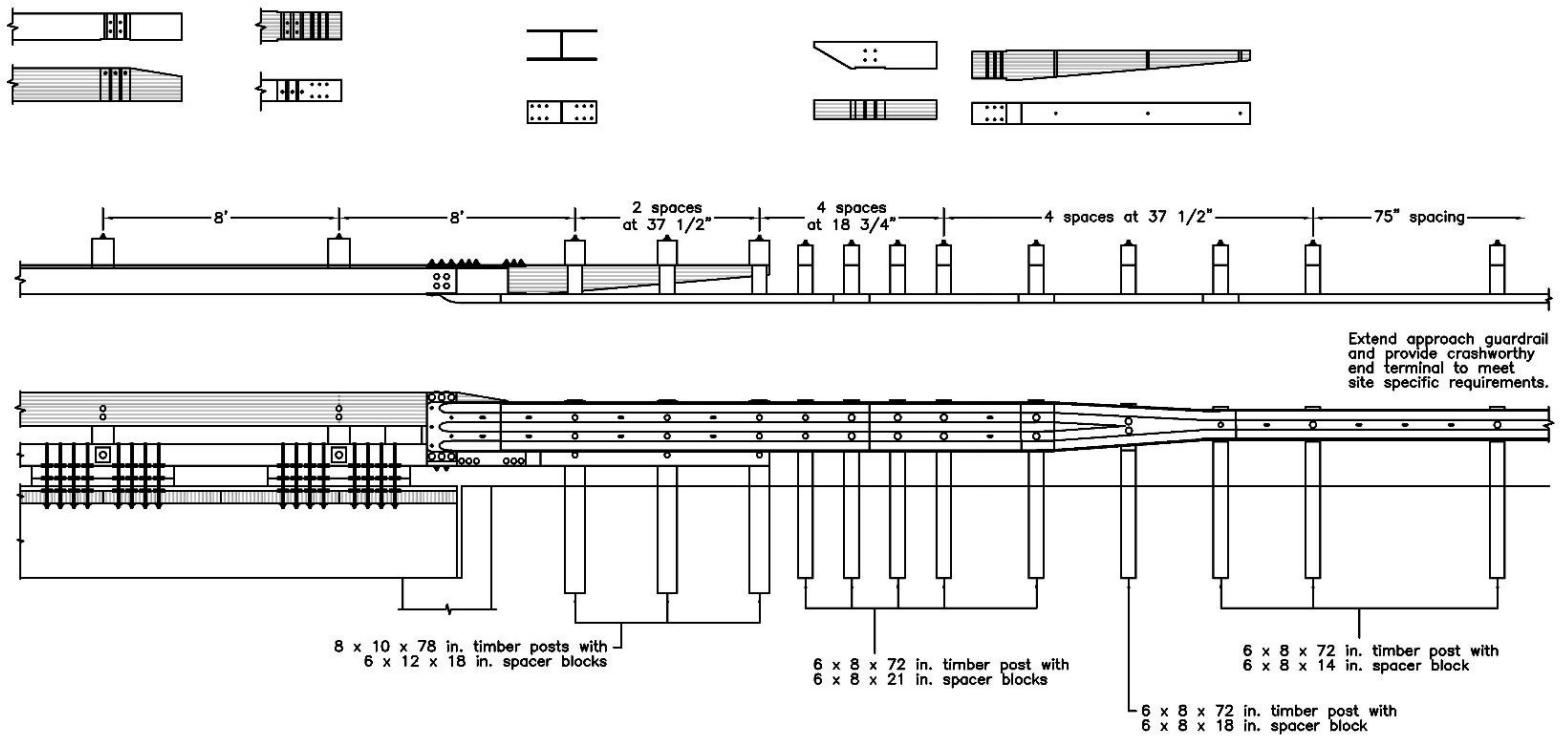

Figure K-28. Option 5.2 – Half-Post Spacing, 8-ft Gap, Welded End-Shoe, Wood Reverse Taper, Curb Taper Behind Thrie-beam

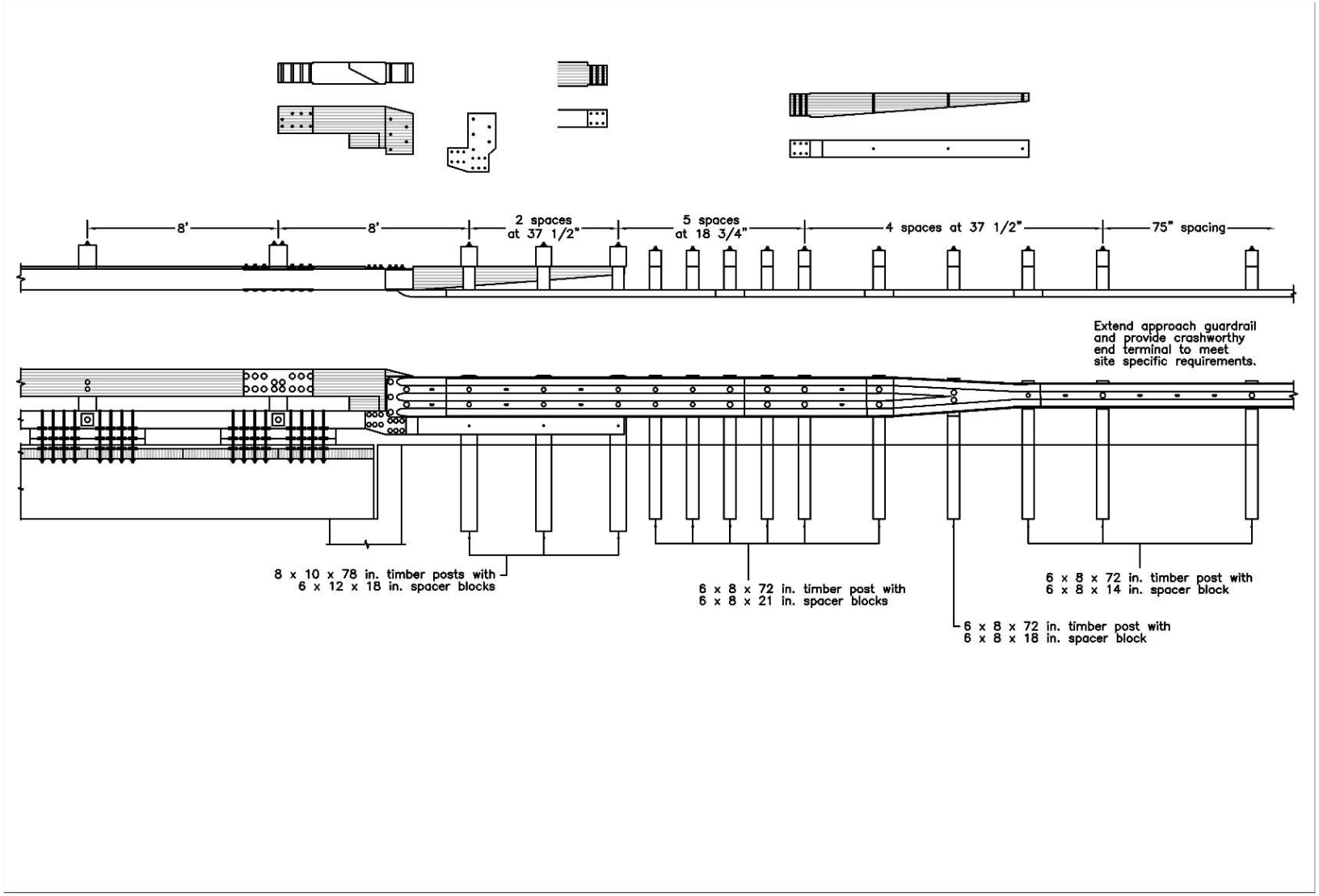

Figure K-29. Option 5.3 – Half-Post Spacing, 8-ft Gap, Custom Glulam Piece, Stepped Curb Taper

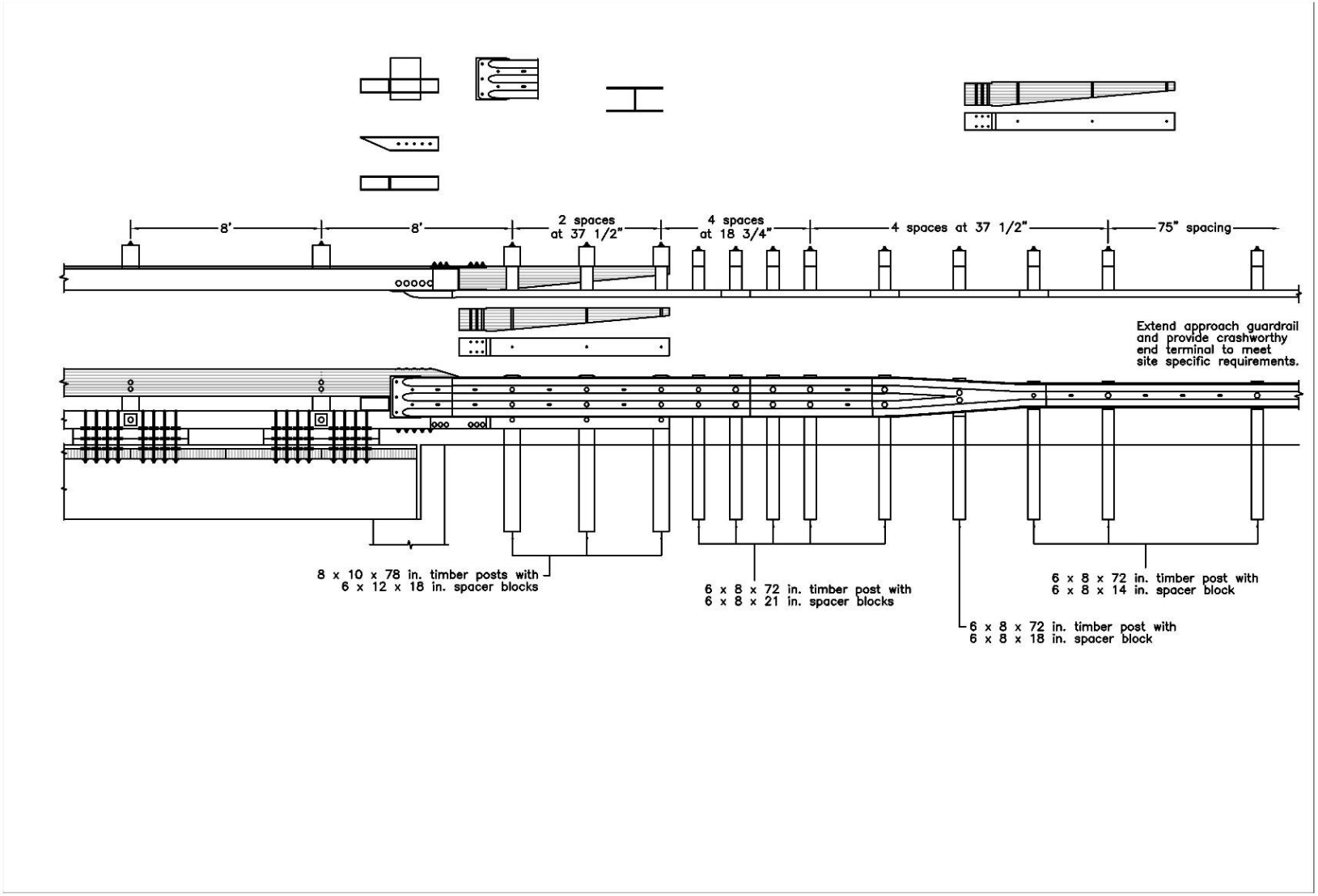

Figure K-30. Option 5.4 – Half-Post Spacing, 8-ft Gap, Welded End Shoe, Steel Reverse Taper, Curb Taper Behind Thrie-beam

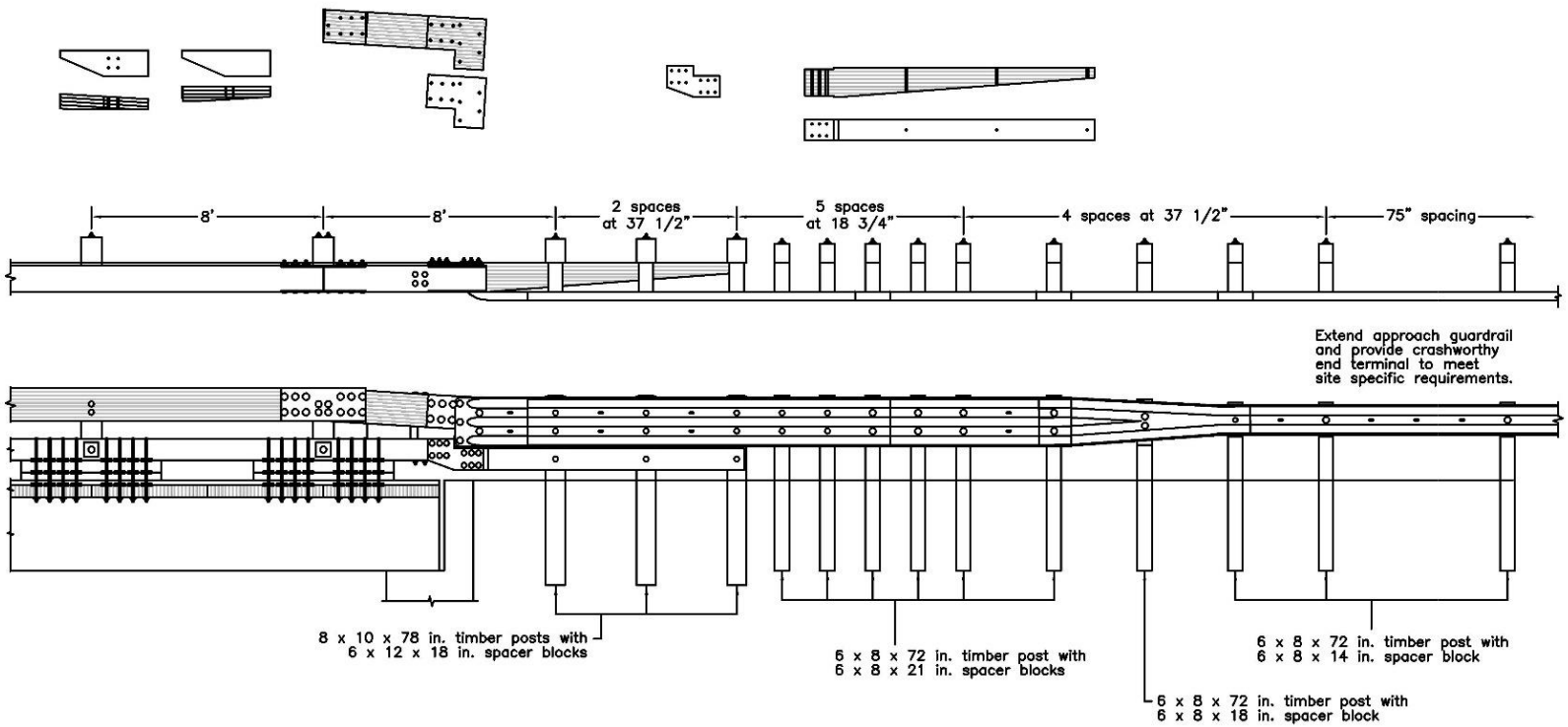

Figure K-31. Option 5.5 – Half-Post Spacing, 8-ft Gap, Rotated Custom Glulam Piece, Wood Reverse Taper, Stepped Curb Taper

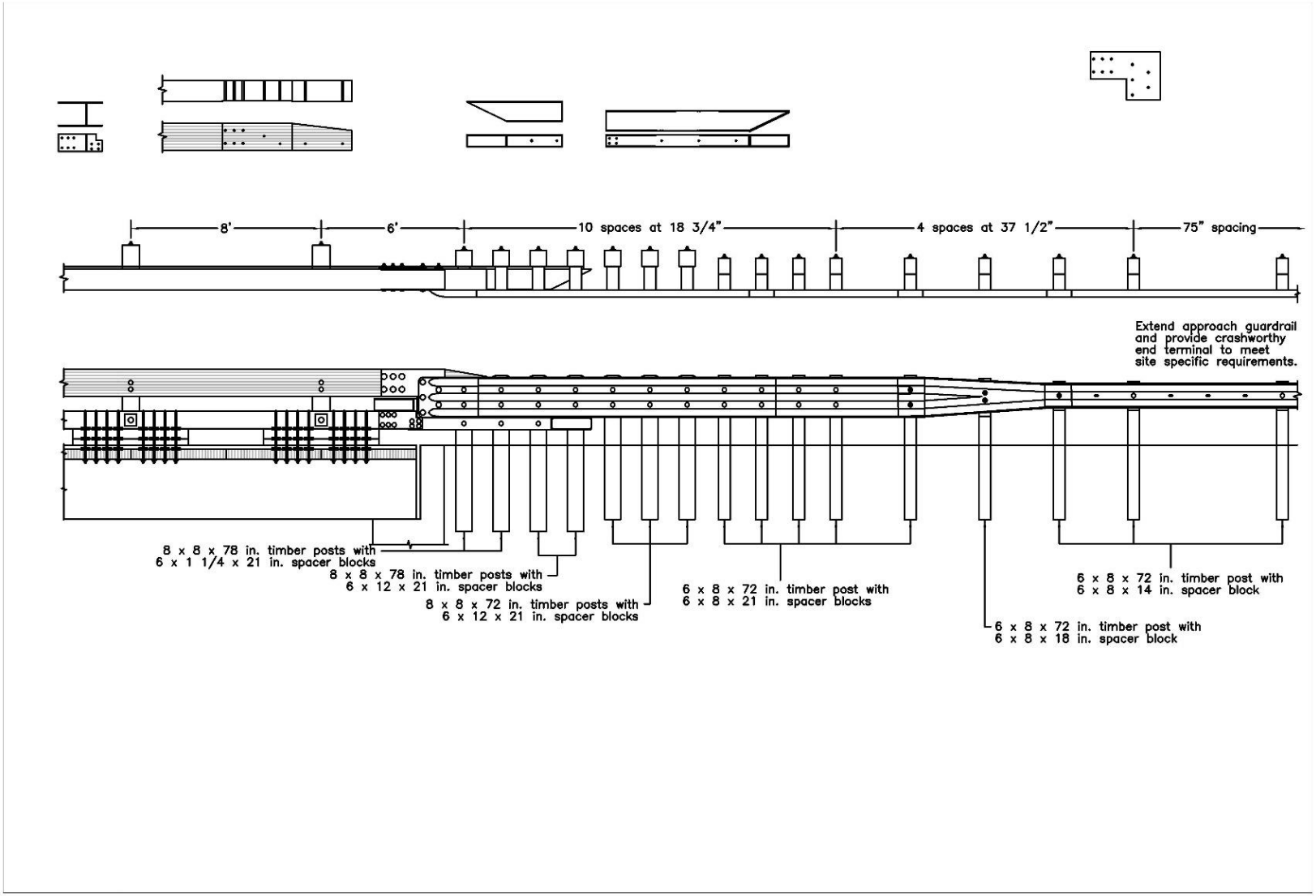

Figure K-32. Option 6.1 – Quarter-Post Spacing, 6-ft Gap, L-Plate, Removed Blockout, Steel Reverse Taper, Steel Curb Taper

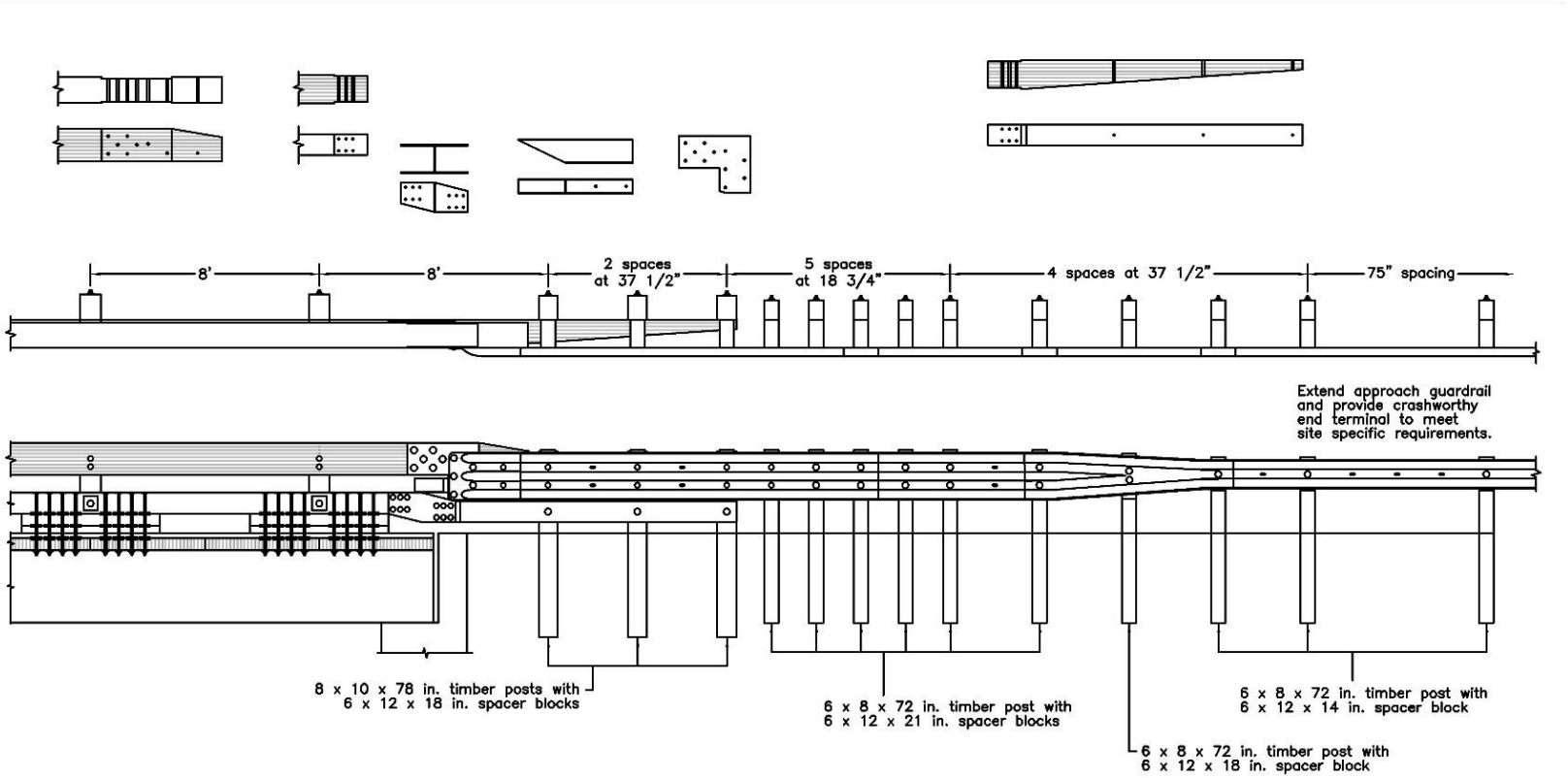

Figure K-33. Option 6.2 – Half-Post Spacing, 8-ft Gap, L-Plate, Steel Reverse Taper, Stepped Curb Taper

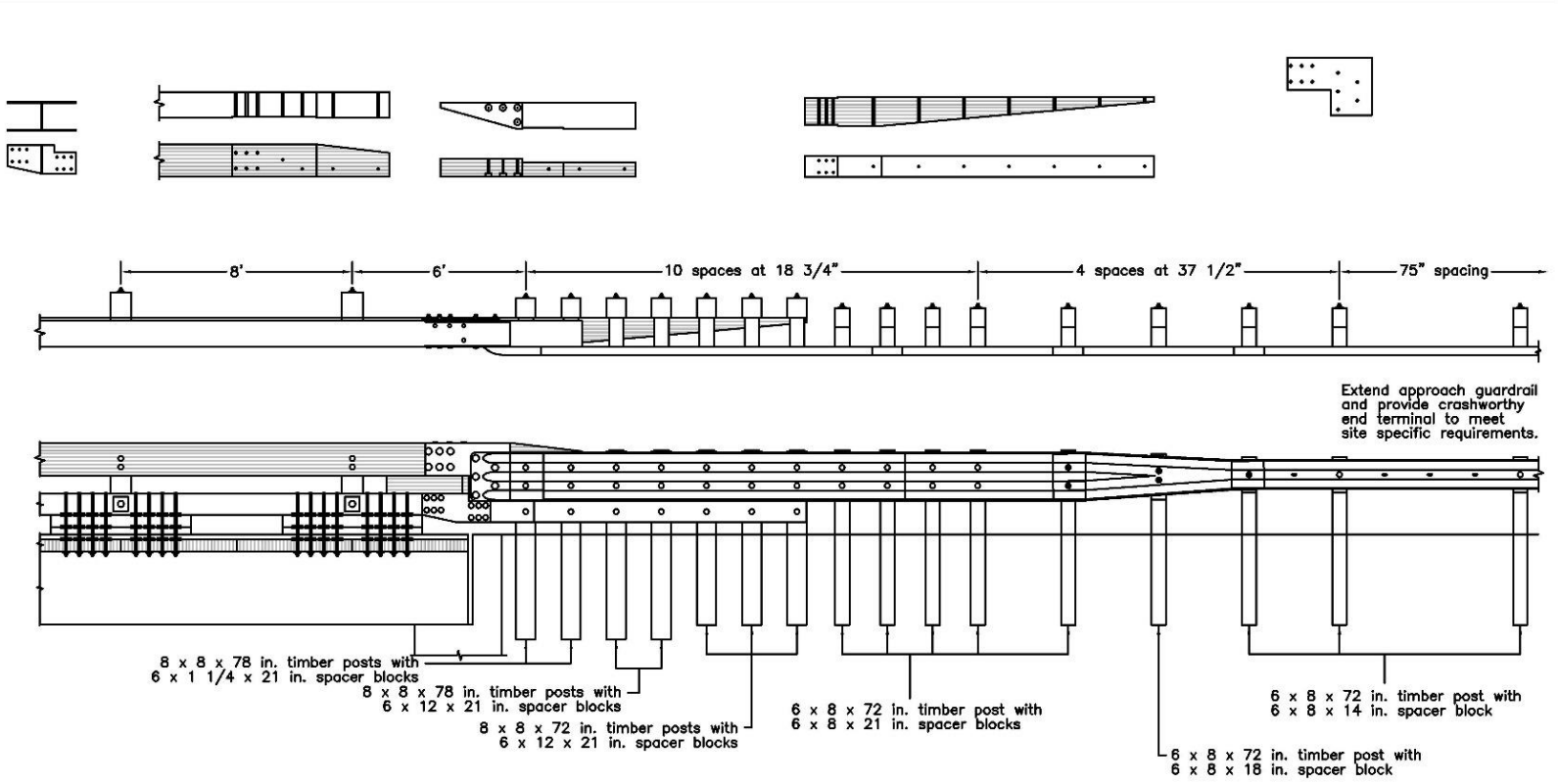

Figure K-34. Option 6.3 – Quarter-Post Spacing, 6-ft Gap, L-Plate, Removed Blockouts, Wood Reverse Taper, Stepped Curb Taper

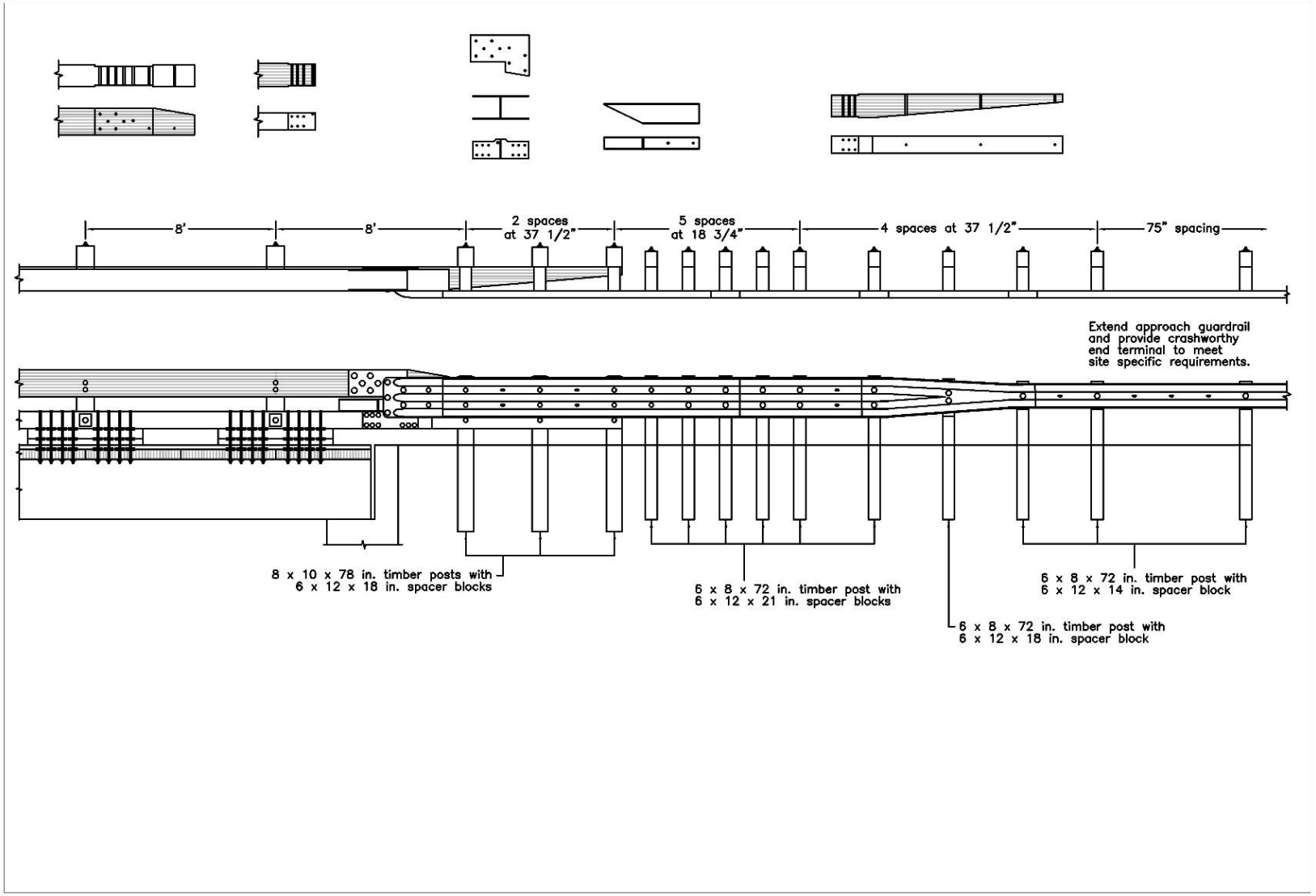

Figure K-35. Option 6.4 – Half-Post Spacing, 8-ft Gap, L-Plate, Steel Reverse Taper, Curb Taper Behind Thrie-beam

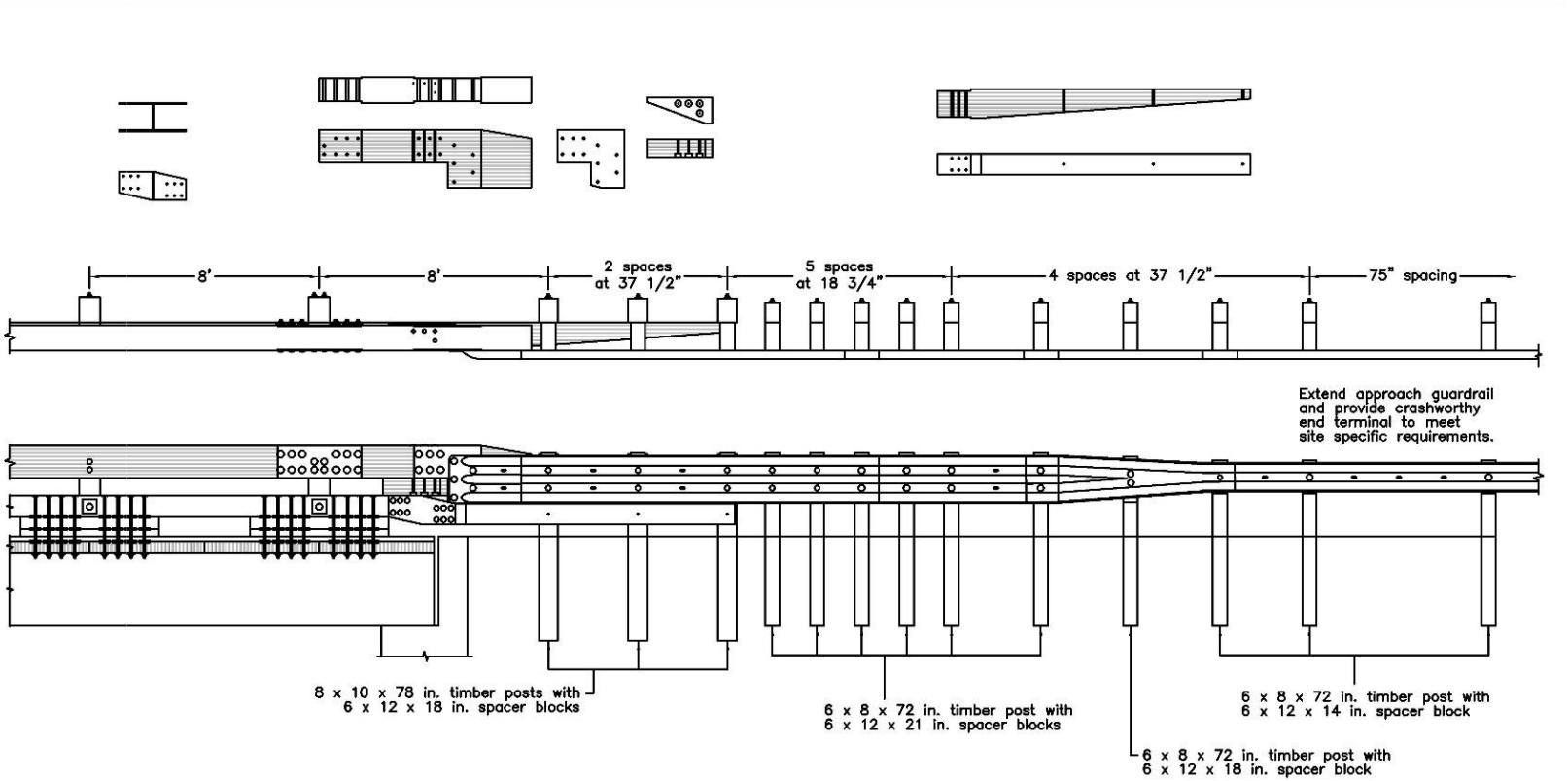

Figure K-36. Option 6.5 – Half-Post Spacing, 8-ft Gap, Notched L-Plate, Custom Glulam Piece, Wood Reverse Taper, Stepped Curb Taper

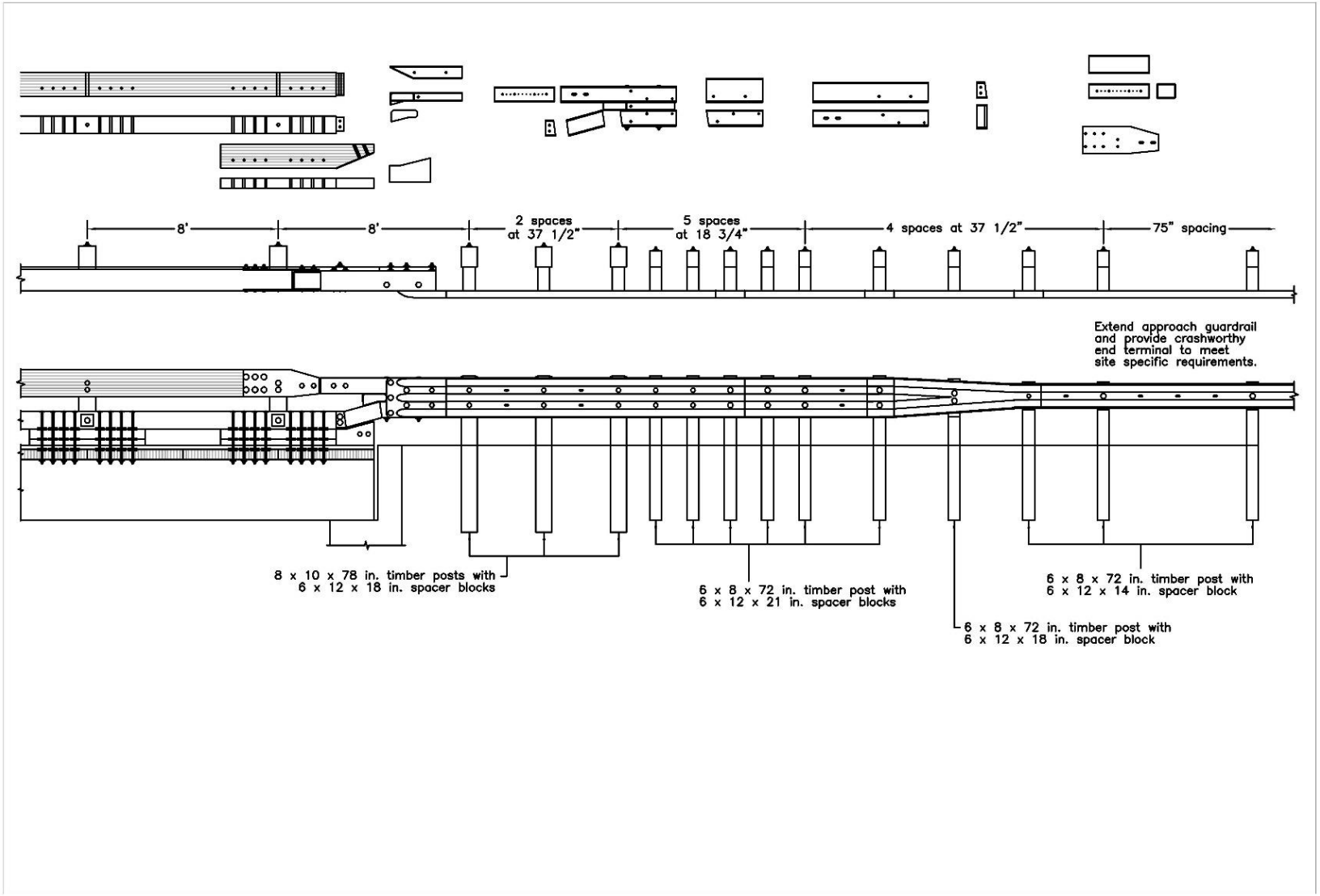

Figure K-37. Option 6.6 – Half-Post Spacing, 8-ft Gap, Steel Components, Steel Reverse Taper, Steel Flap Curb Taper

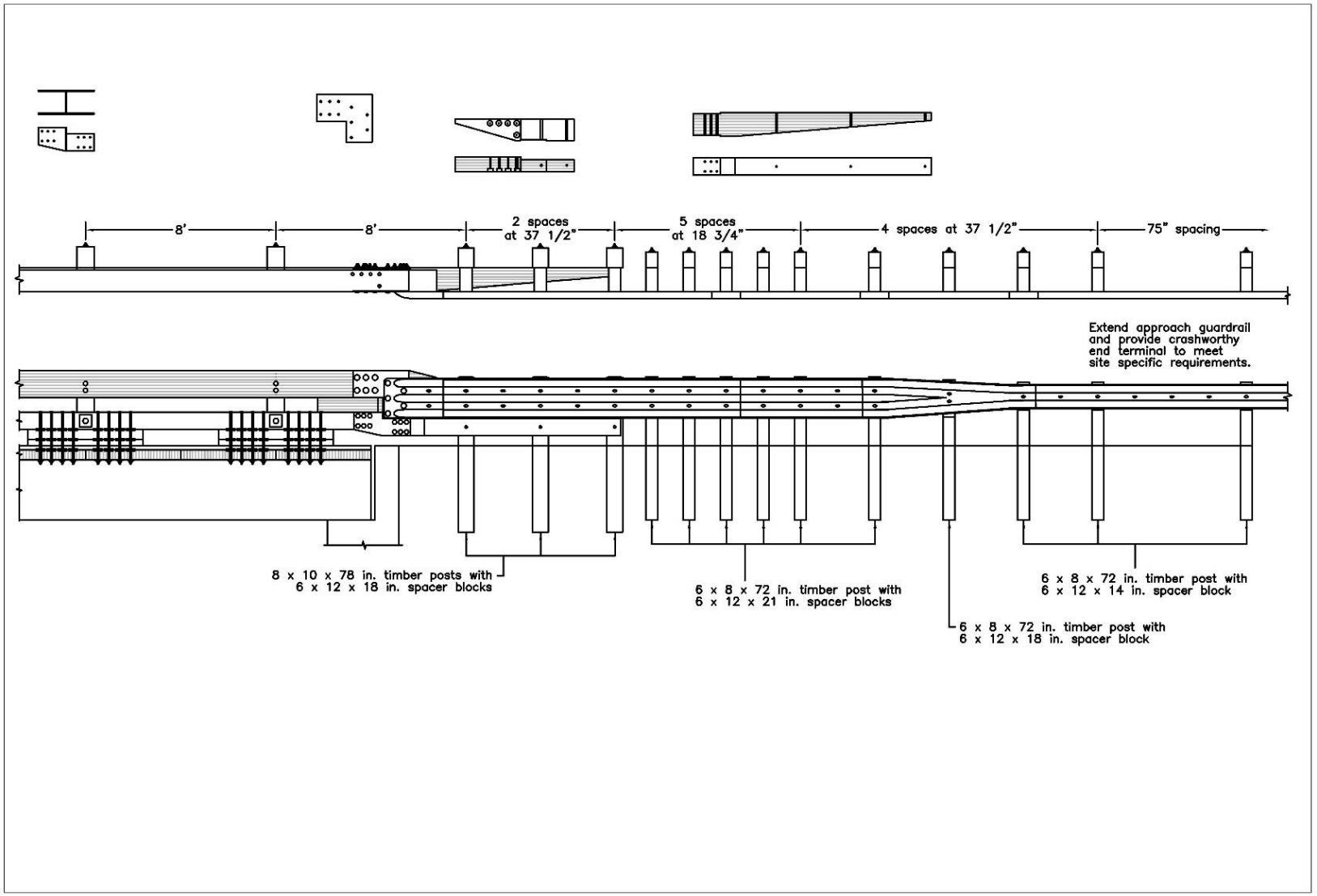

Figure K-38. Option 7.1 – Half-Post Spacing, 8-ft Gap, L-Plate, Wood Reverse Taper, Stepped Curb Taper

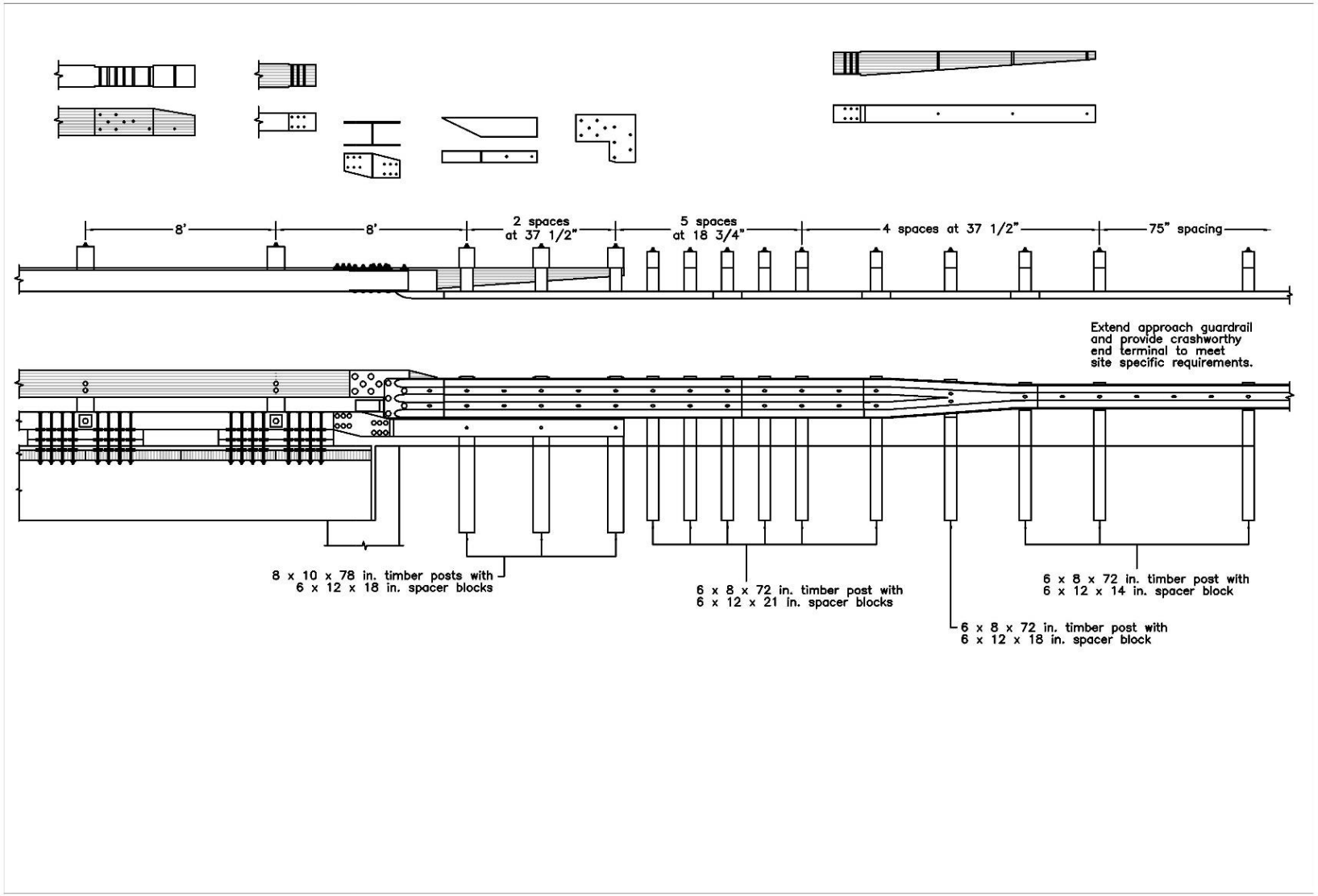

Figure K-39. Option 7.2 – Half-Post Spacing, 8-ft Gap, Notched L-Plate, Steel Reverse Taper, Stepped Curb Taper

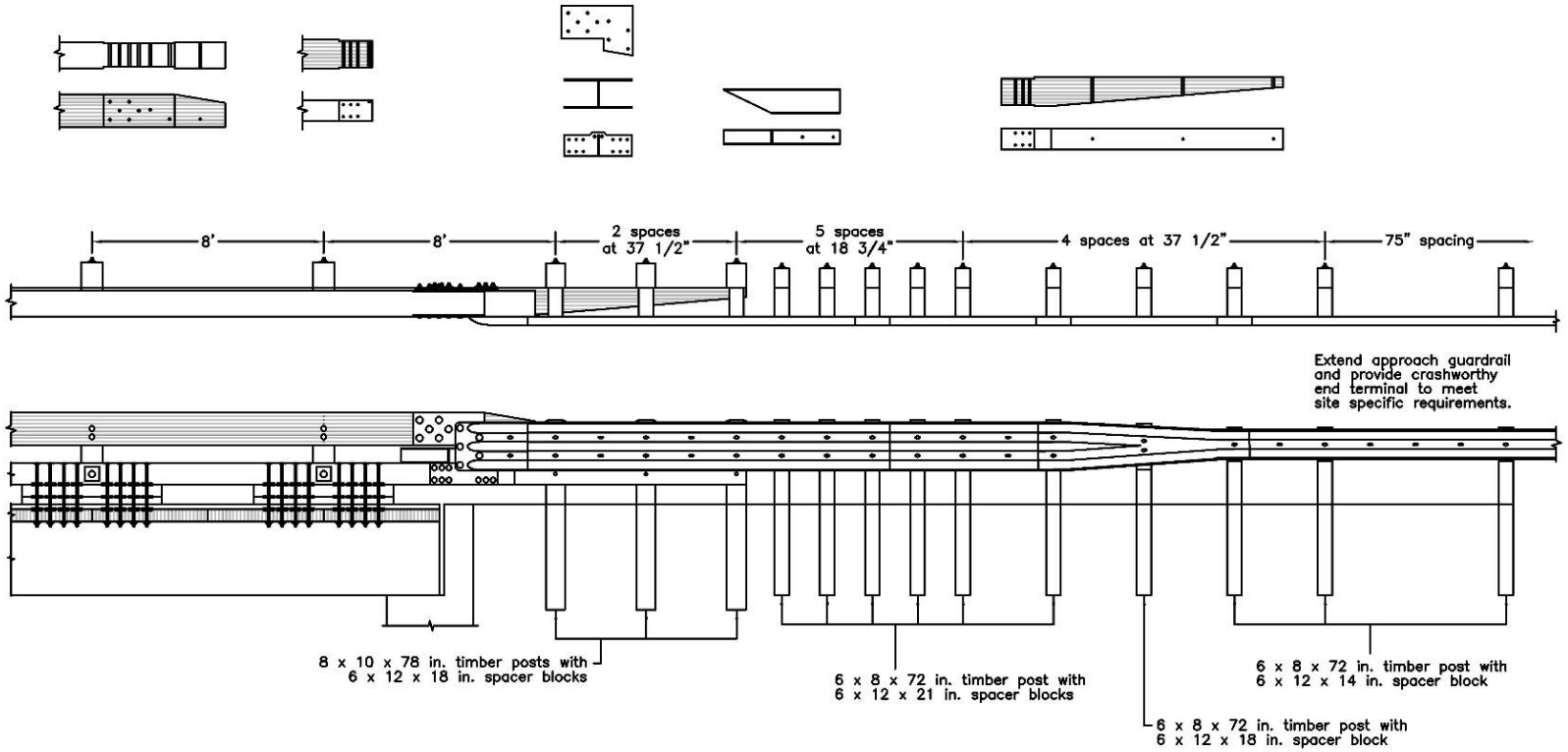

Figure K-40. Option 7.3 – Half-Post Spacing, 8-ft Gap, Cut L-Plate, Steel Reverse Taper, Curb Taper with Bumpout Behind Thrie-beam

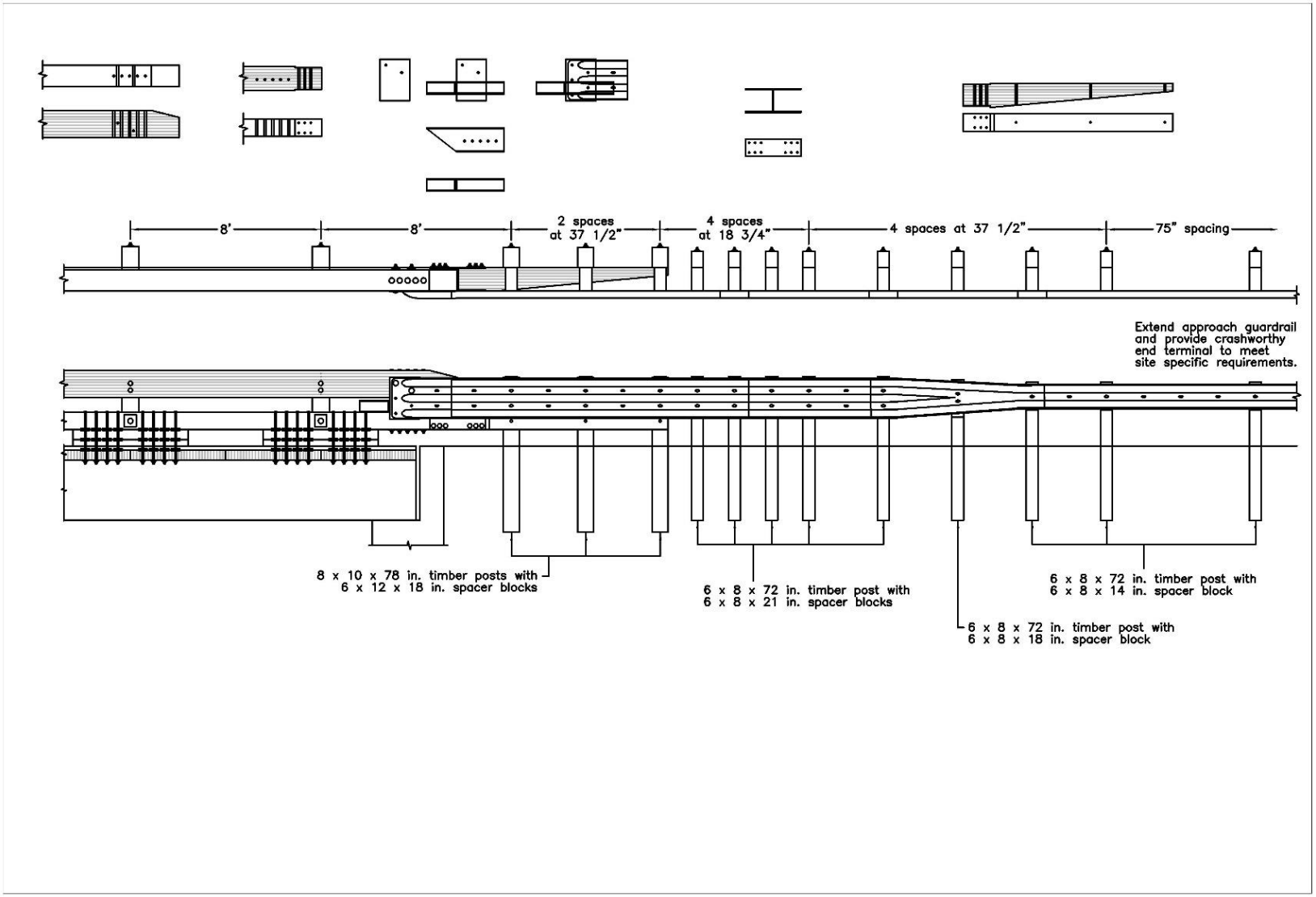

Figure K-41. Option 7.4 – Half-Post Spacing, 8-ft Gap, Welded End Shoe to Steel Reverse Taper, Curb Taper Behind Thrie-beam

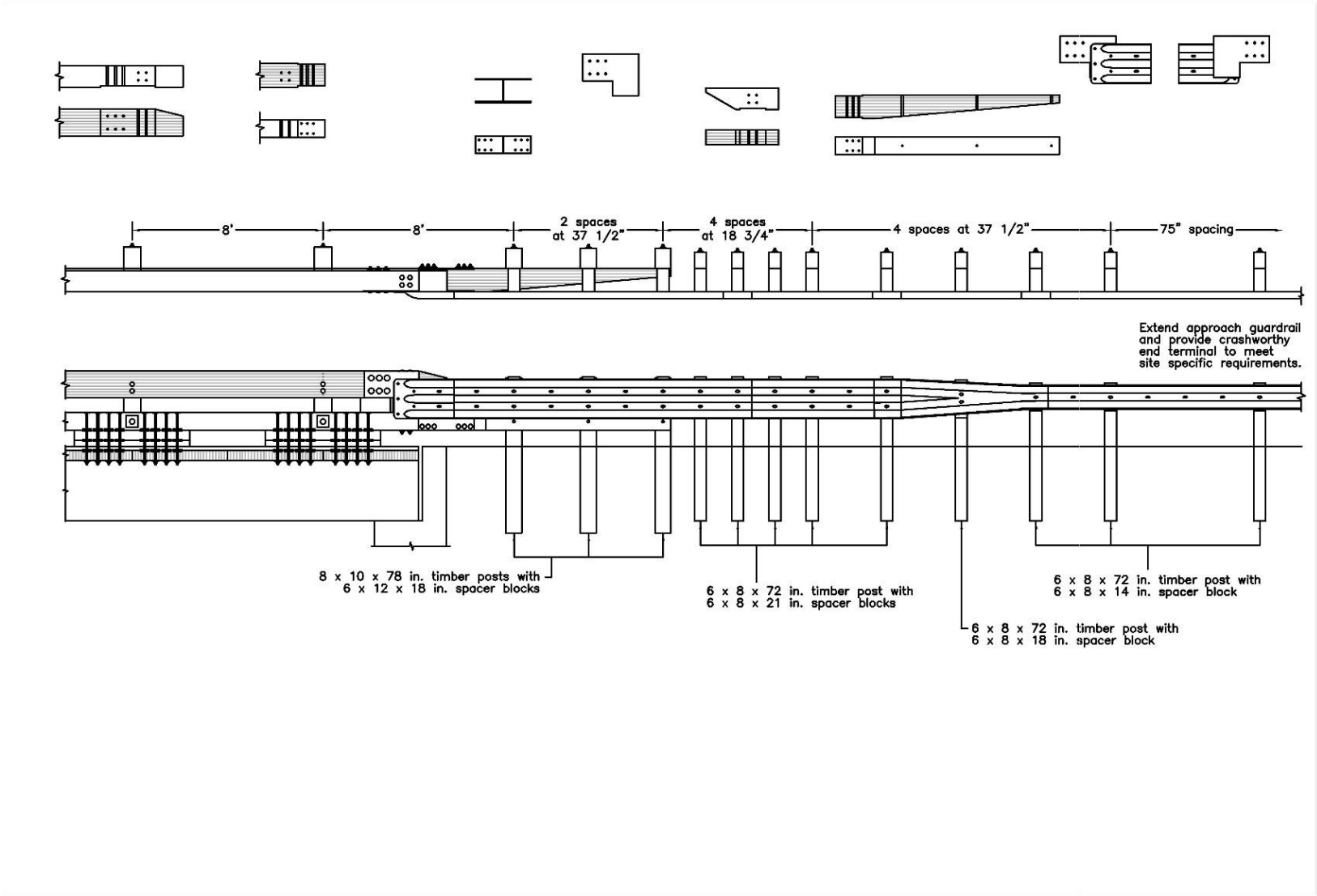

Figure K-42. Option 7.5 – Half-Post Spacing, 8-ft Gap, Welded L-Plate to End Shoe, Wood Reverse Taper, Curb Taper Behind Thrie-beam

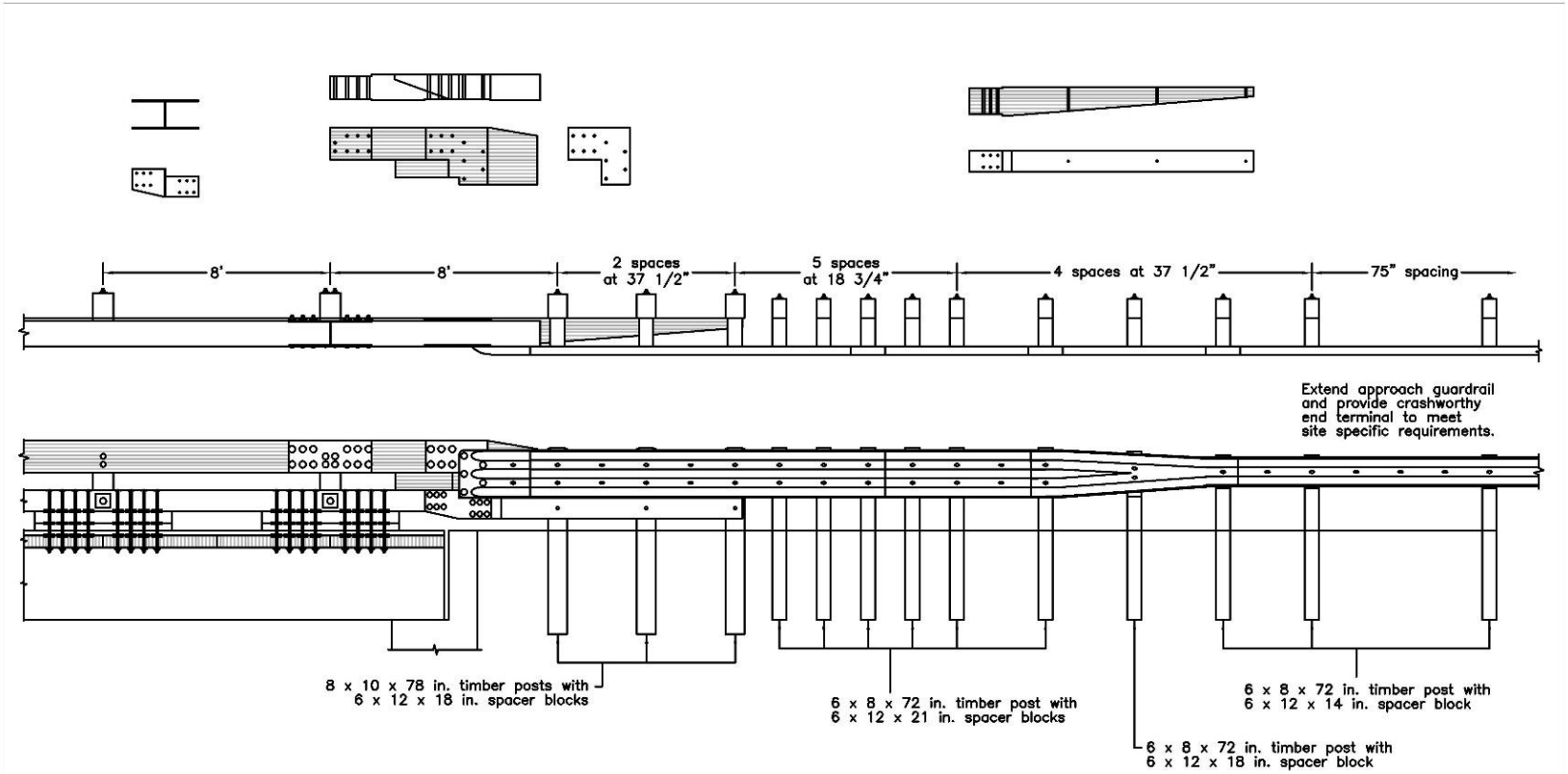

Figure K-43. Option 7.6 – Half-Post Spacing, 8-ft Gap, L-Plate, Custom Glulam Piece, Stepped Curb Taper

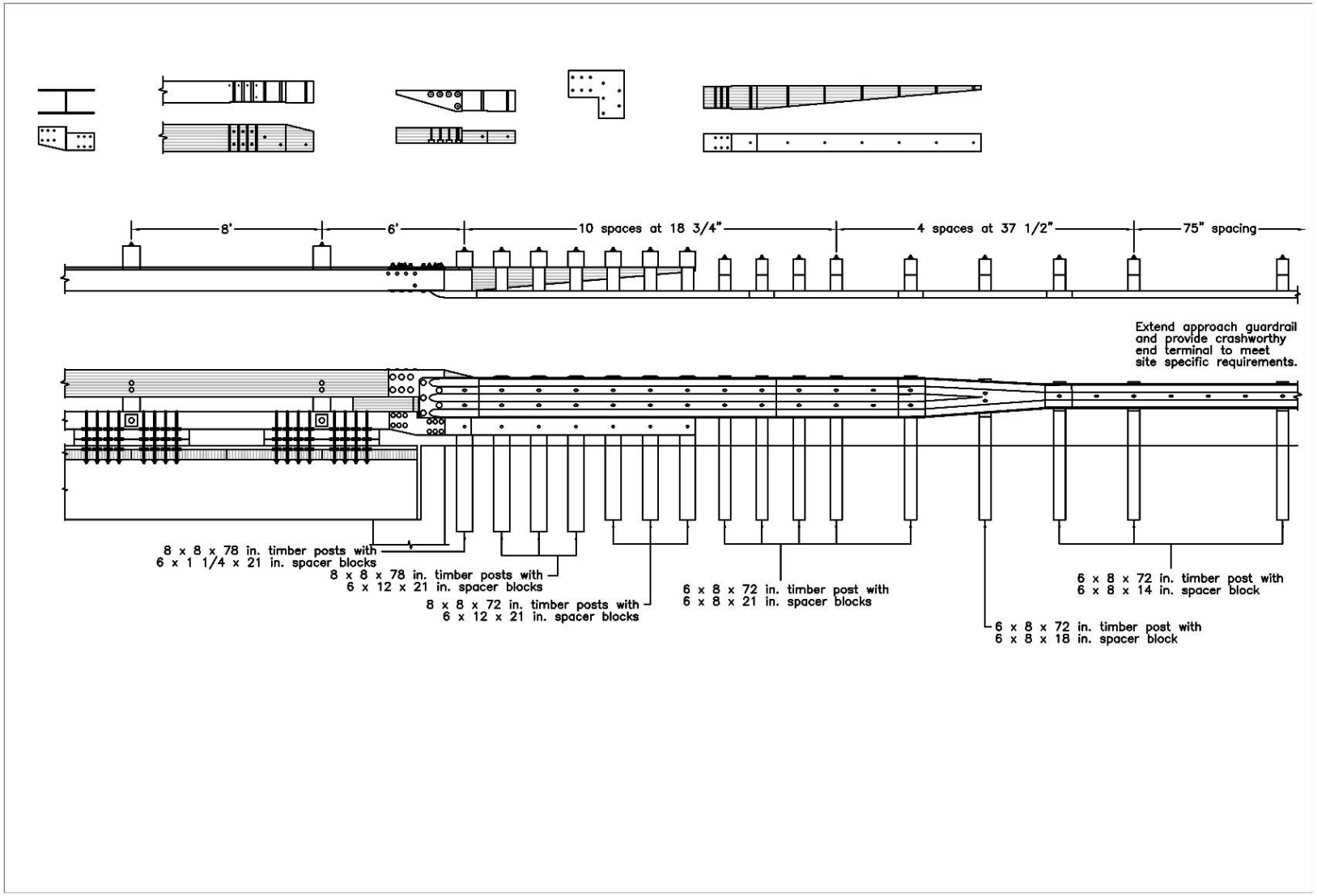

Figure K-44. Option 7.7 – Quarter-Post Spacing, 6-ft Gap, L-Plate, Wood Reverse Taper, Stepped Curb Taper

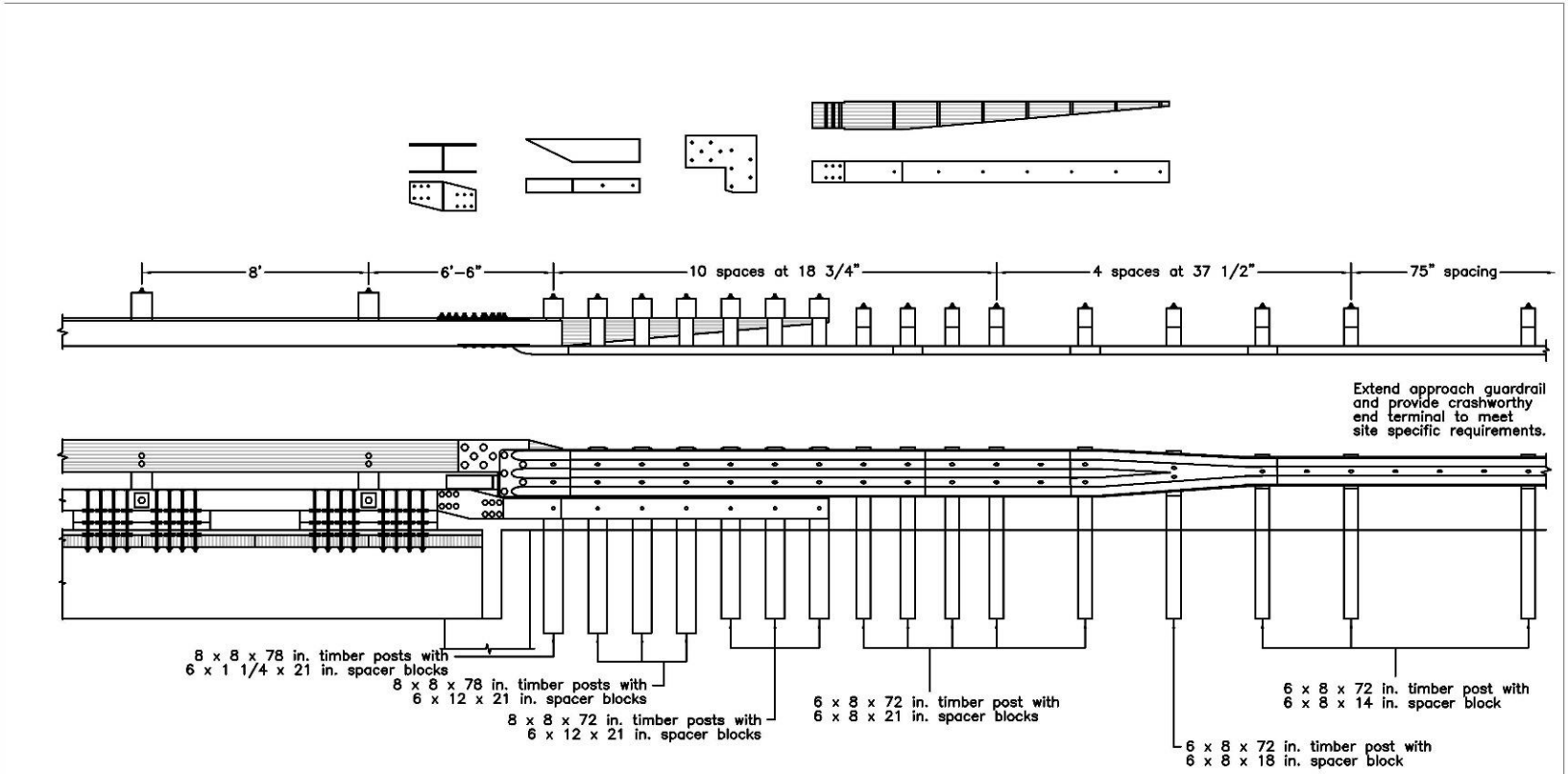

Figure K-45. Option 7.8 – Quarter-Post Spacing, 6.5-ft Gap, Notched L-Plate, Steel Reverse Taper, Stepped Curb Taper

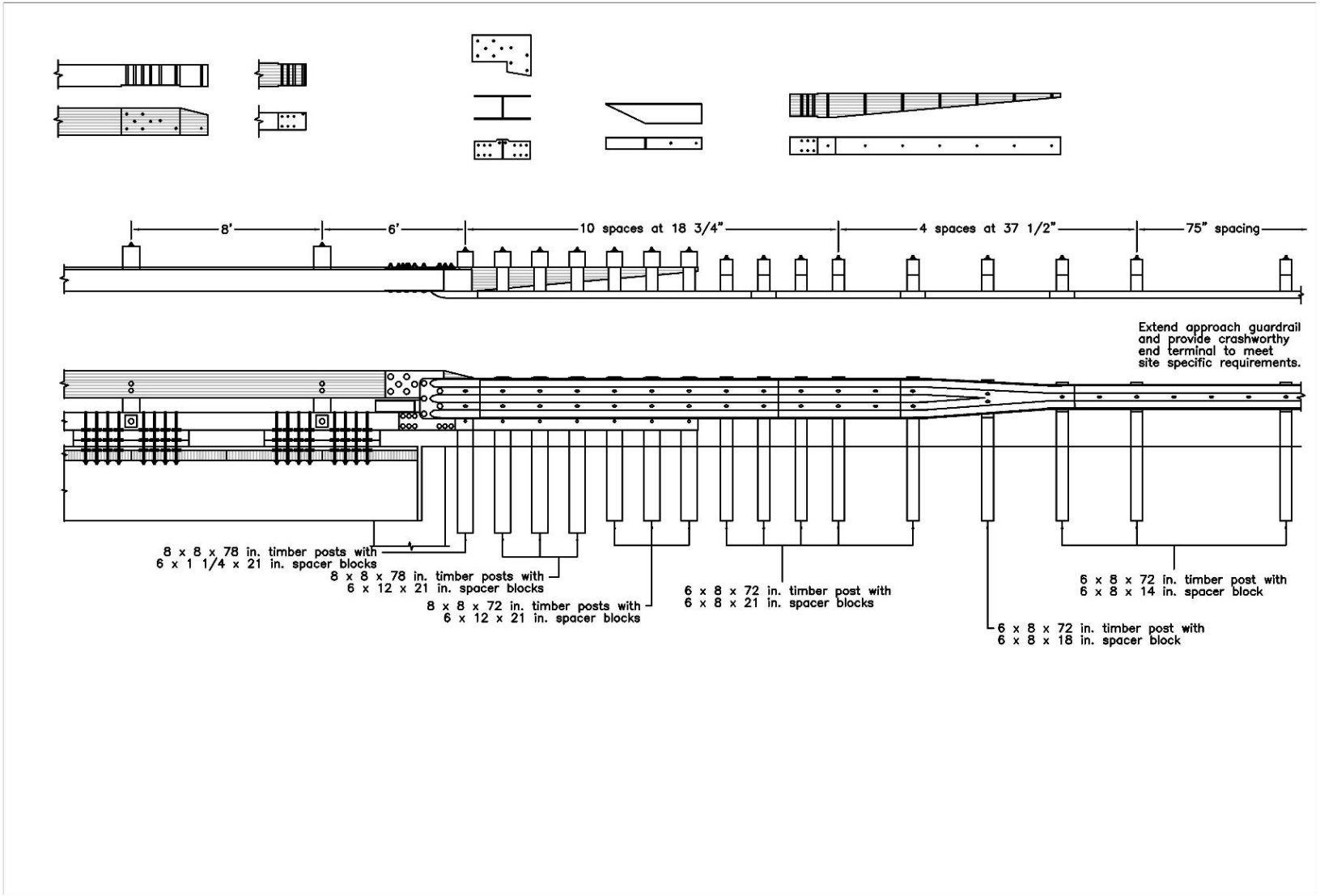

Figure K-46. Option 7.9 – Quarter-Post Spacing, 6-ft Gap, Cut L-Plate, Steel Reverse Taper, Curb Taper with Bumpout Behind Thrie-beam

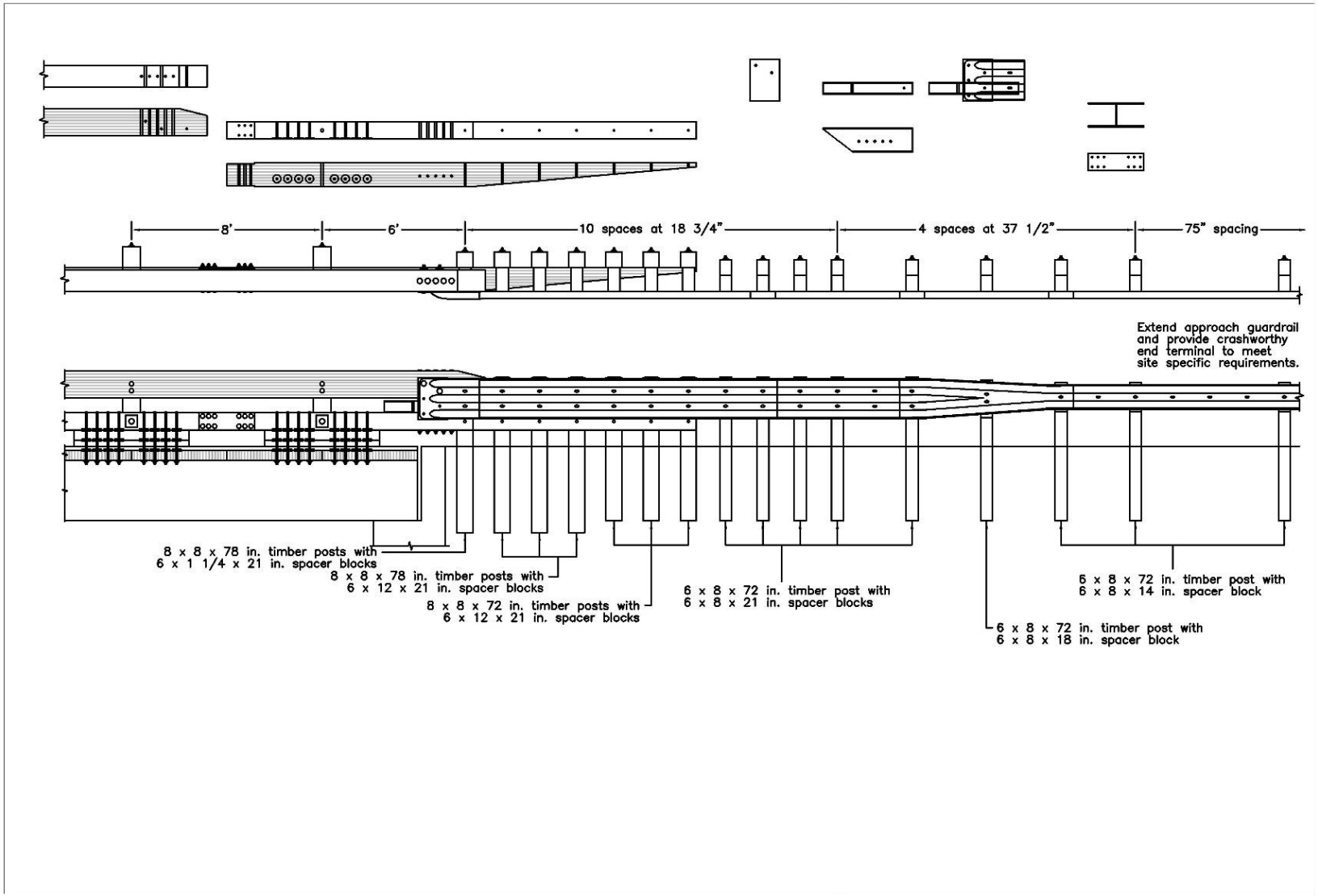

Figure K-47. Option 7.10 – Quarter-Post Spacing, 6-ft Gap, Welded End Shoe to Steel Reverse Taper, Curb Taper Behind Thrie-beam

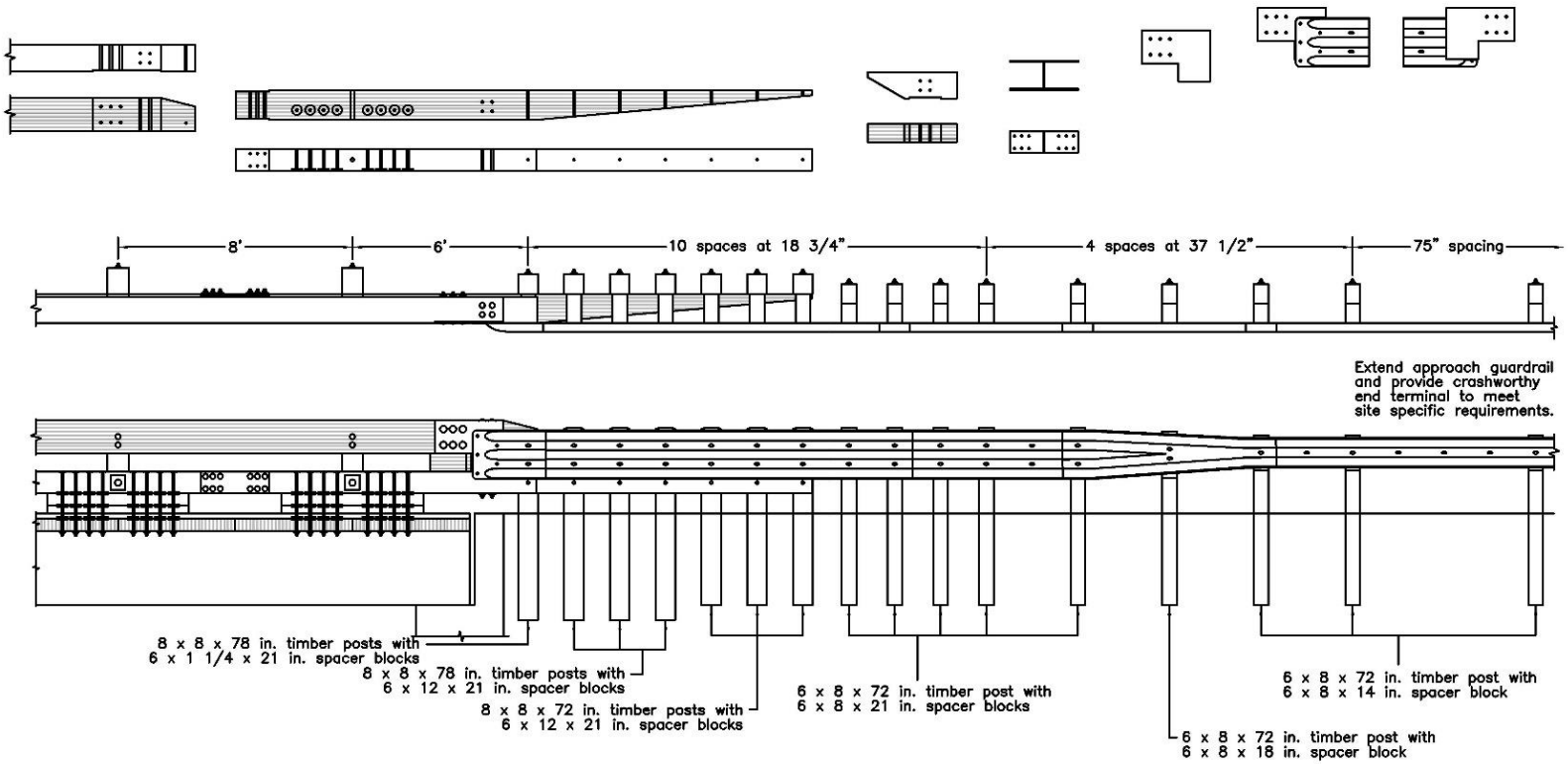

Figure K-48. Option 7.11 – Quarter-Post Spacing, 6-ft Gap, Welded L-Plate to End Shoe, Wood Reverse Taper, Curb Taper Behind Thrie-beam

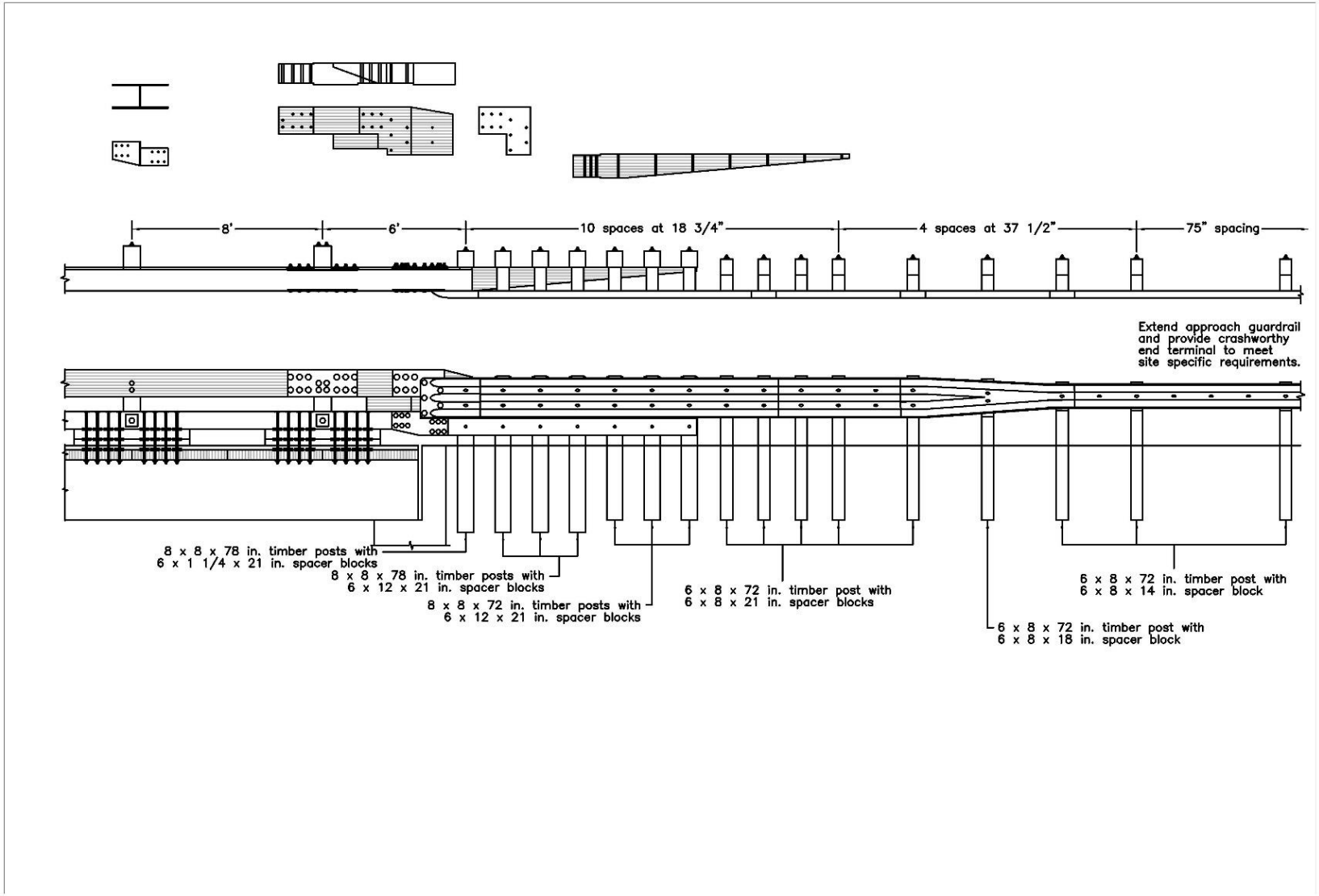

Figure K-49. Option 7.12 – Quarter-Post Spacing, 6-ft Gap, L-Plate, Custom Glulam Piece, Stepped Curb Taper

Appendix L. Post Inspection Sheets

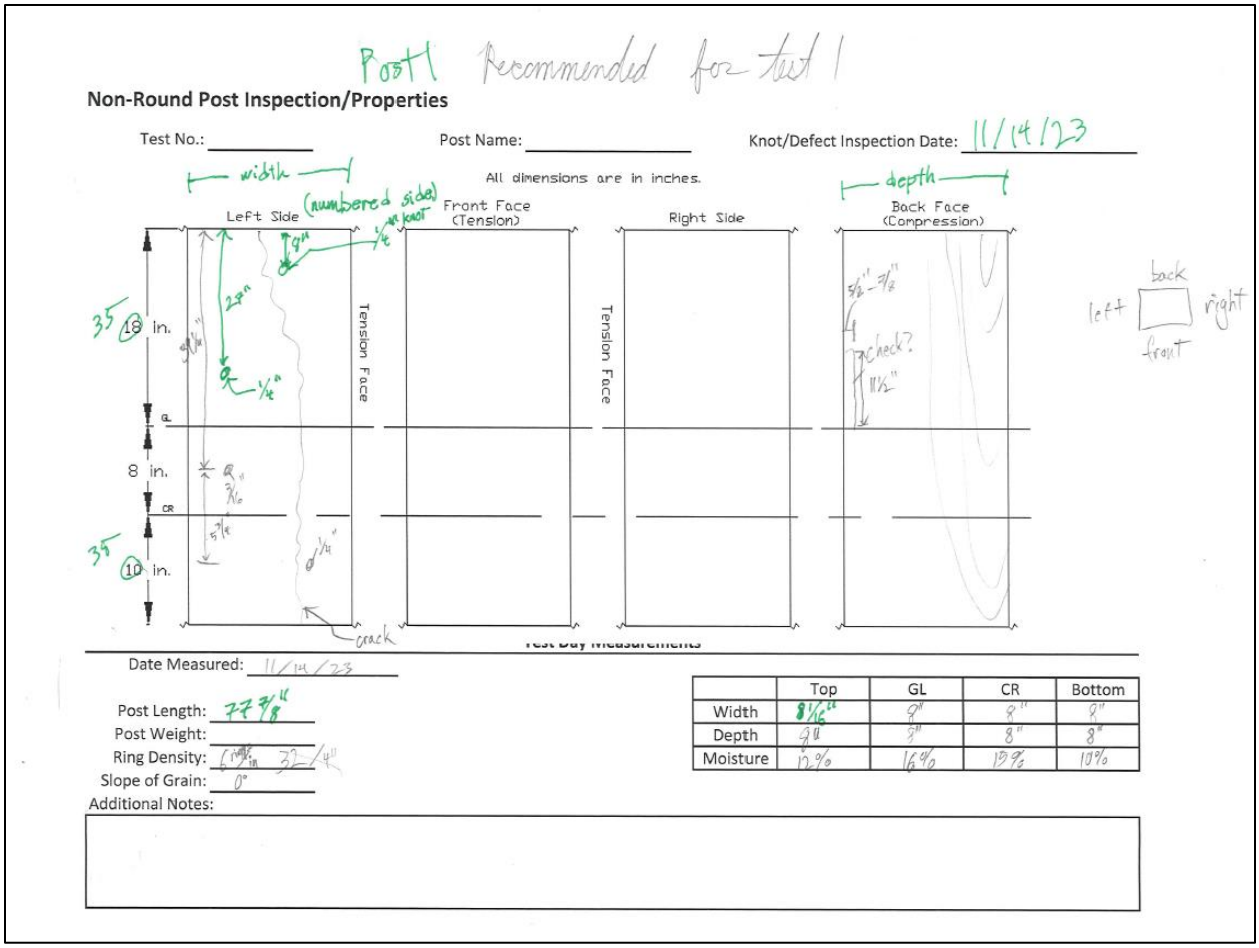

Figure L-1. Post 1 Inspection Sheet, Test No. TRAGT-1

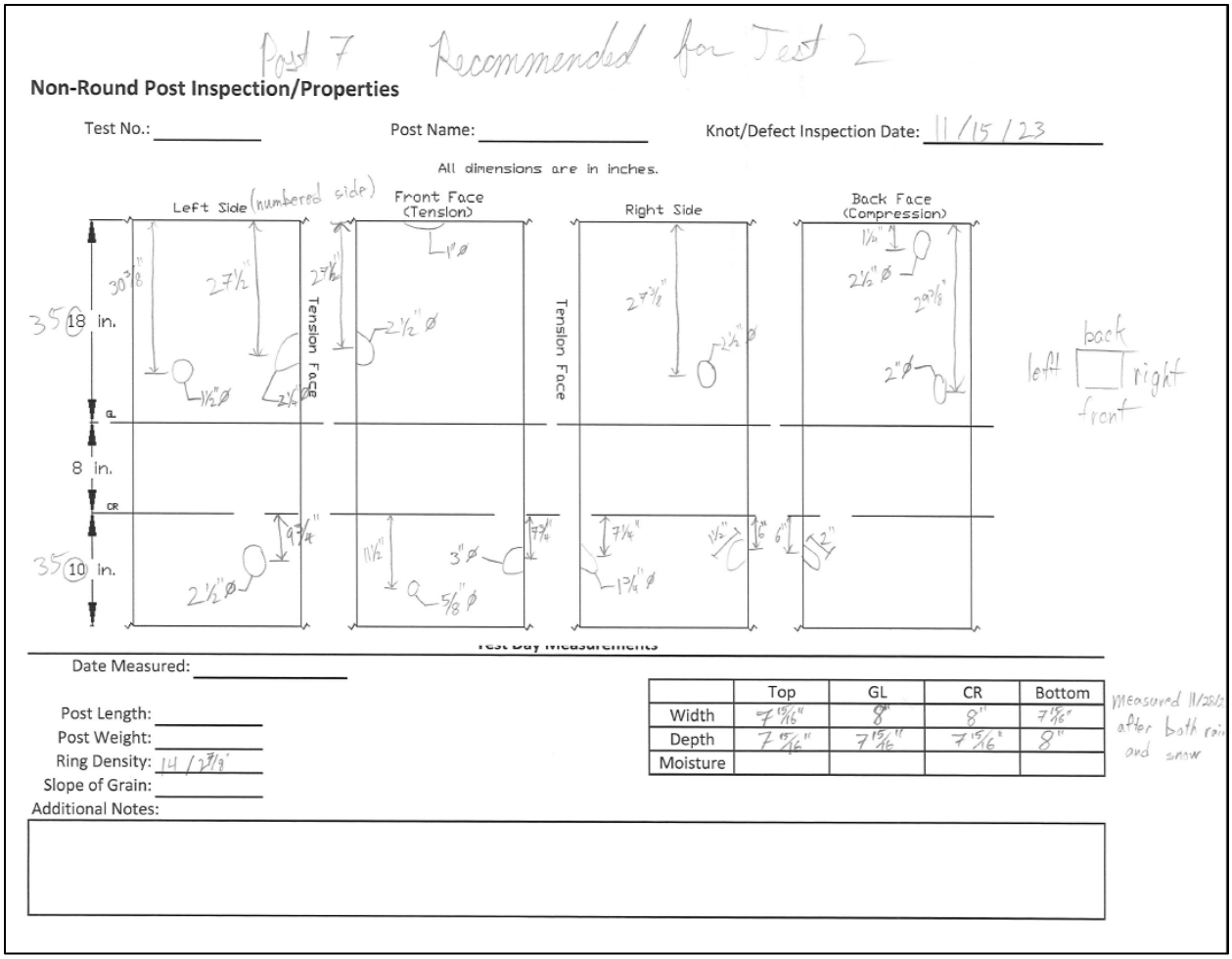

Figure L-2. Post 7 Inspection Sheet, Test No. TRAGT-2

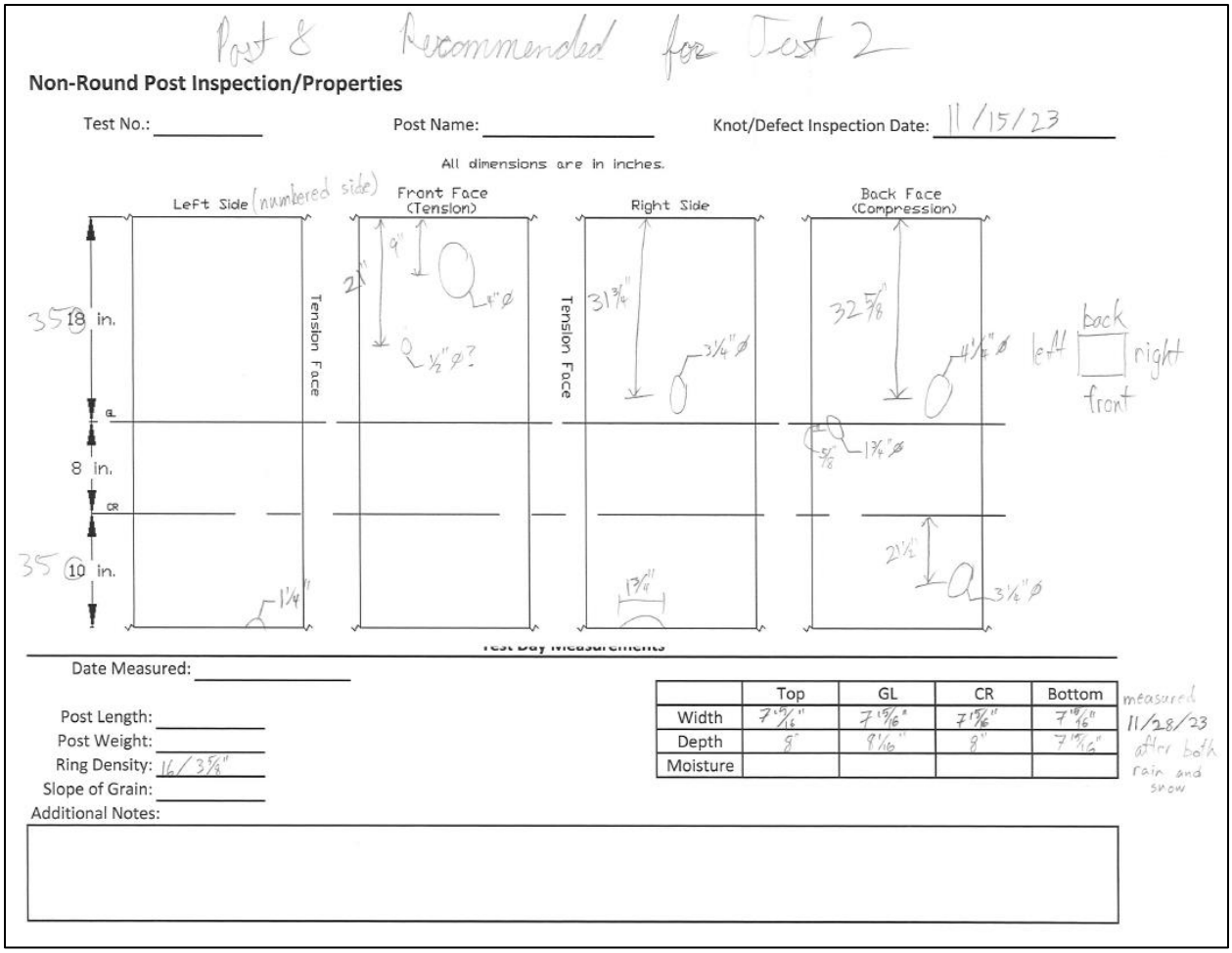

Figure L-3. Post 8 Inspection Sheet, Test No. TRAGT-2

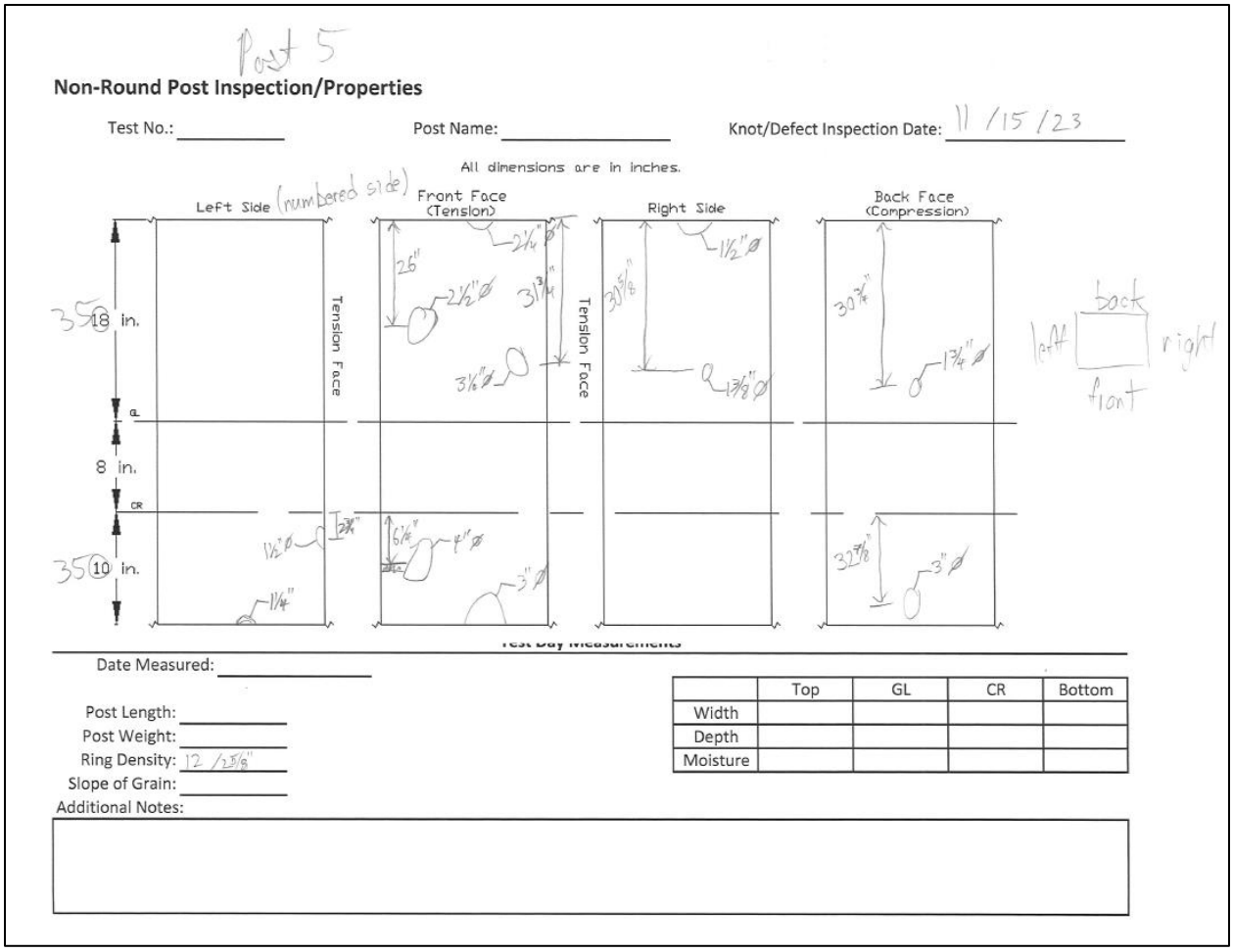

Figure L-4. Post 5 Inspection Sheet, Test No. TRAGT-3

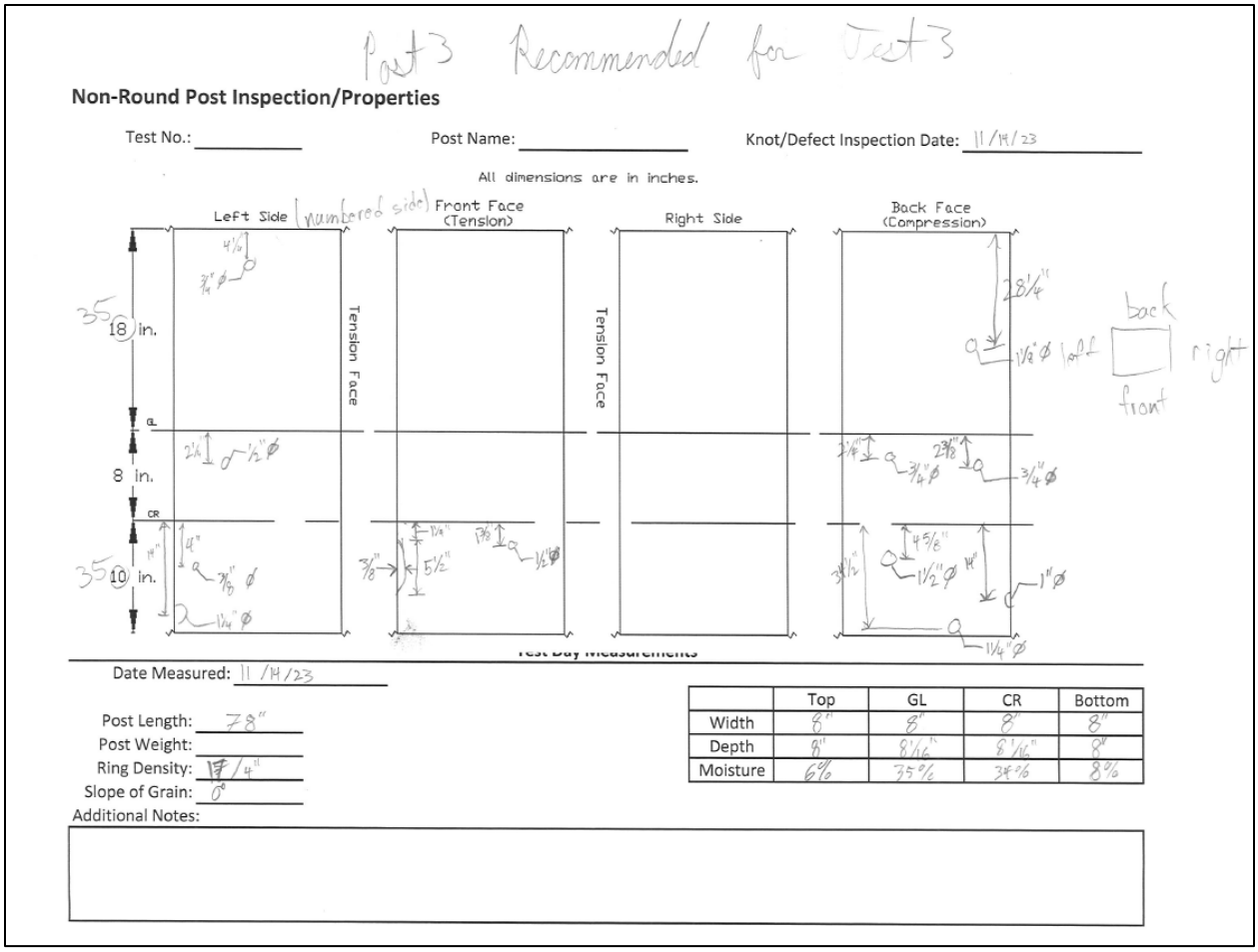

Figure L-5. Post 3 Inspection Sheet, Test No. TRAGT-3

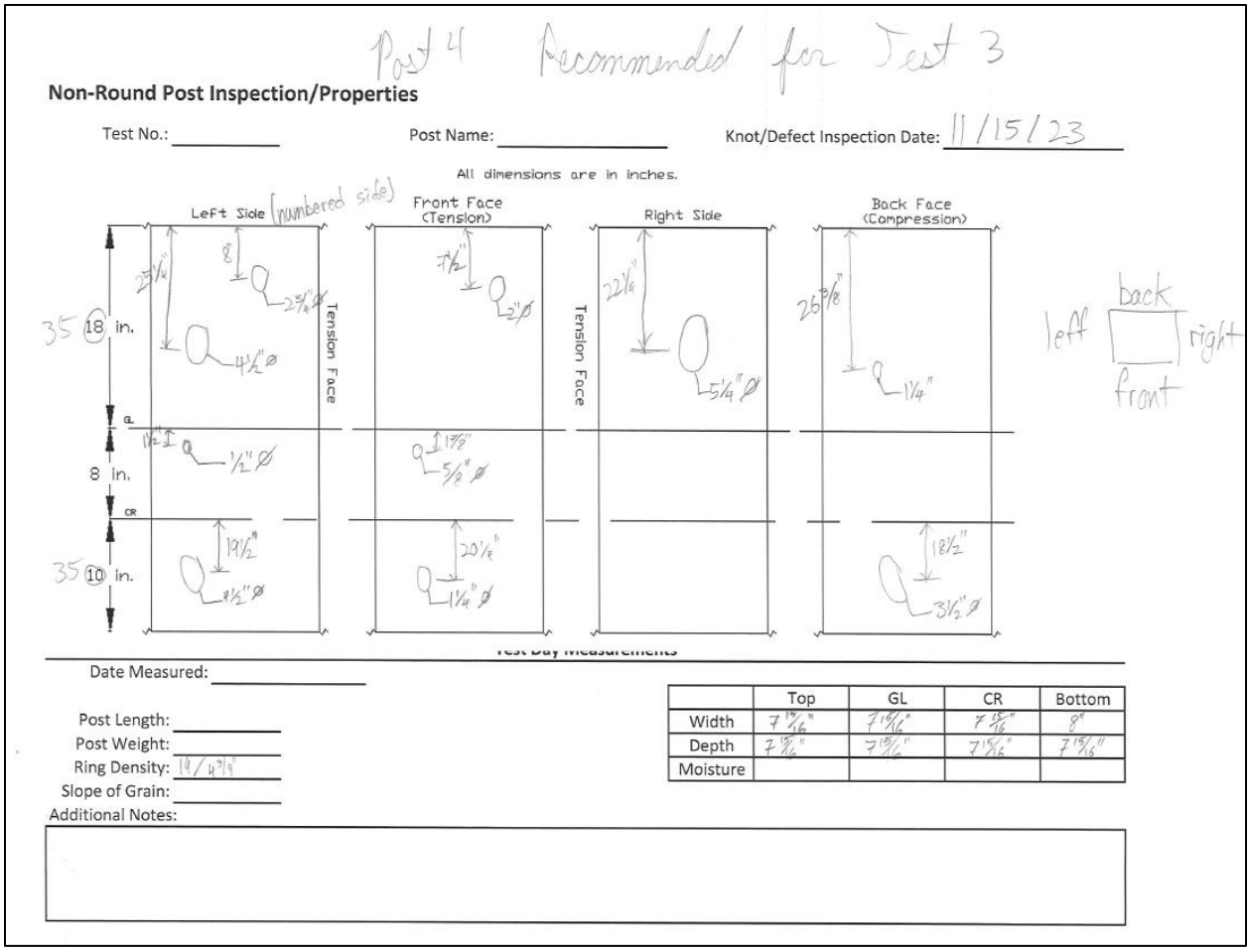

Figure L-6. Post 4 Inspection Sheet, Test No. TRAGT-3

Appendix M. Python Code for Google Colab

```
!apt-get install -y xvfb
!dpkg --add-architecture i386
!apt update
!apt install -y wine32 xvfb

import pandas as pd
import os
import shutil
import subprocess
from openpyxl import Workbook, load_workbook
from openpyxl.utils import get_column_letter
from math import atan, pi
import numpy as np
import time
import csv
import re

# Read the CSV file containing nodes and x-coordinates
csv_file = '/content/BARRIER_VII/Impact Locations.csv'
df = pd.read_csv(csv_file)
print(df.head())

##########################################################################
###### OBSERVE ########## UPDATE ######### FILE PATHWAYS ##########
##########################################################################

# Function to modify the .b7 file and move it to the appropriate directory
def modify_and_move_b7_file(node, x_coordinate):
    original_file = '/content/BARRIER_VII/n16_PUT.b7'  # Replace with the path to your
template .b7 file
    new_file = f'n{int(node)}_PUT.b7'
    directory_name =
f'/content/BARRIER_VII/half_post_CIP/impact_n{int(node)}_{x_coordinate:.4f}'

    # Create directory if it doesn't exist
    if not os.path.exists(directory_name):
        os.makedirs(directory_name)

    with open(original_file, 'r') as file:
        lines = file.readlines()

    # Modify the x-coordinate on line 131
    line_index = 130  # Line 131 in 0-indexed Python is 130
    new_x_coordinate = f"{x_coordinate:>10.4f}"
    lines[line_index] = lines[line_index][:5] + new_x_coordinate + lines[line_index][15:]

    # Write the new file in the appropriate directory
```

```
    new_file_path = os.path.join(directory_name, new_file)
    with open(new_file_path, 'w') as file:
        file.writelines(lines)

# Function to run the BARRIER VII executable
def run_barrier_vii(directory, input_file):
    barrier_executable = '/content/BARRIER_VII/BARlrg8d.exe'
    output_file1 = 'b.out'
    output_file2 = 'v.out'
    output_file3 = 's.out'

    cmd = f'xvfb-run wine {barrier_executable}'
    process = subprocess.Popen(
        cmd,
        stdin=subprocess.PIPE,
        stdout=subprocess.PIPE,
        stderr=subprocess.PIPE,
        shell=True,
        cwd=directory
    )

    input_data = f"{input_file}\n{output_file1}\n{output_file2}\n{output_file3}\n"
    stdout, stderr = process.communicate(input=input_data.encode())

    # Check for any errors
    if stderr:
        print("Error:", stderr.decode())
    else:
        print("Output:", stdout.decode())

################################################################################
######## OBSERVE ########### UPDATE #### FILE PATHWAYS #############
################################################################################

# Iterate over the DataFrame and create directories, .b7 files, and .xlsm files
for index, row in df.iterrows():
    node = row['Node']
    x_coordinate = row['X-coord']
    # Handle potential NaN values
    if pd.isna(node) or pd.isna(x_coordinate):
        #print(f"Skipping row {index} due to missing Node or X-coord value.")
        continue  # Skip to the next iteration
    directory_name =
f'/content/BARRIER_VII/half_post_CIP/impact_n{int(node)}_{x_coordinate:.4f}'

    modify_and_move_b7_file(node, x_coordinate)
```

```
    # Run the BARRIER VII executable
    input_file = f'n{int(node)}_PUT.b7'
    run_barrier_vii(directory_name, input_file)

# Function to identify and return number of nodes, members, and posts
def b7_info(input_file):
    with open(input_file, 'r') as f:
        content = f.read()
        lines = content.splitlines()

    # Extract barrier nodes
    barrier_nodes_match = re.search(r'NUMBER OF BARRIER NODES\s*=\s*(\d+)', content)
    b7_n = int(barrier_nodes_match.group(1))

    beam_header = " BEAMS, 100 SERIES"
    post_header = " POSTS, 300 SERIES"

    def count_lines_after_header(header):
        count = 0
        recording = False
        for i, line in enumerate(lines):
            if header in line:
                recording = True
                skip_lines = 4
            if recording:
                if skip_lines > 0:
                    skip_lines -= 1
                else:
                    if line.strip() == '':
                        break
                    count += 1
        return count

    num_beams = count_lines_after_header(beam_header)
    num_posts = count_lines_after_header(post_header)

    return b7_n, num_beams, num_posts

file_path = '/content/BARRIER_VII/half_post_CIP/impact_n16_450.0000/b.out'
b7_n, num_beams, num_posts = b7_info(file_path)

# Function to filter basic file for beam force outputs
def filter_beams(input_file, num_beams):
    with open(input_file, 'r') as f:
        content = f.readlines()
        b = num_beams + 3
        beam_data = []
```

```
        beam_header = " BEAMS, 100 SERIES"
        keep_lines = 0
        first = 0
        current_time = -0.001

        for line in content:
            if keep_lines > 0 and keep_lines < 2:
                keep_lines += 1
            elif keep_lines >= 2 and keep_lines < b:
                node_info = [current_time] + line.split()
                beam_data.append(node_info)
                keep_lines += 1
            elif beam_header in line:
                if first == 0:
                    first = 1
                else:
                    keep_lines = 1
                    current_time += 0.001
            else:
                keep_lines = 0

        return beam_data

# Function to filter basic file for post force outputs
def filter_posts(input_file, num_posts):
    with open(input_file, 'r') as f:
        content = f.readlines()
        b = num_posts + 2
        post_data = []
        post_header = " POSTS, 300 SERIES"
        keep_lines = 0
        first = 0
        current_time = -0.001

        for line in content:
            if keep_lines > 0 and keep_lines < 2:
                keep_lines += 1
            elif keep_lines >= 2 and keep_lines < b:
                node_info = [current_time] + line.split()
                post_data.append(node_info)
                keep_lines += 1
            elif post_header in line:
                if first == 0:
                    first = 1
                else:
                    keep_lines = 1
                    current_time += 0.001
```

```
            else:
                keep_lines = 0

        return post_data

# Function to parse railing and vehicle nodes into seperate files from structural output
def filter_s_out(input_file, num_railing_nodes):
    with open(input_file, 'r') as f:
        content = f.readlines()

    # Remove "MASH 2016 AGT..." lines and separate railing and vehicle nodes
    railing_data = []
    vehicle_data = []
    current_time = -0.005
    r_count = 0
    v_count = 0

    for line in content:
        parts = line.split()
        if len(parts) == 5:
            node_info = [current_time] + parts
            if r_count < num_railing_nodes:
                railing_data.append(node_info)
                r_count += 1
            elif v_count < 20:
                vehicle_data.append(node_info)
                v_count += 1
            else:
                railing_data.append(node_info)
                r_count = 1
                v_count = 0
        else:
            current_time += 0.005

    return railing_data, vehicle_data

# Function to create a dataframe from the vehicle and railing files and add the 'Time' column
def create_df(data, headers):
    return pd.DataFrame(data, columns=headers)

def wheel_snag(vehicle_df, railing_df, post_loc, num_steps):
    # Initialize counters for front and back tire snags
    fcnt = 0
    bcnt = 0

    ft_snag, ft_snag_loc, bt_snag, bt_snag_loc = [], [], [], []
```

```
# Ensure 'Node' column is of type integer
vehicle_df['Node'] = vehicle_df['Node'].astype(int)
railing_df['Node'] = railing_df['Node'].astype(int)

# Tolerance for comparing floating-point numbers
tolerance = 1e-6

# Ensure 'Y-Coordinate' is numeric in both DataFrames
vehicle_df['Y-Coordinate'] = vehicle_df['Y-Coordinate'].astype(float)
railing_df['Y-Coordinate'] = railing_df['Y-Coordinate'].astype(float)

# Iterate over time steps, starting at 1 to compare with the previous step
for step in range(1, num_steps):
    t1 = (step-1) * 0.005
    t2 = step * 0.005

    # Use a tolerance for comparing time values
    vehicle_t1 = vehicle_df[abs(vehicle_df['Time'] - t1) < tolerance]
    vehicle_t2 = vehicle_df[abs(vehicle_df['Time'] - t2) < tolerance]
    railing_t1 = railing_df[abs(railing_df['Time'] - t1) < tolerance]

    # Retrieve x-coordinates for front and back tires at the current and previous time steps
    xft1 = vehicle_t1[vehicle_t1['Node'] == 19]['X-Coordinate'].values[0]
    xft2 = vehicle_t2[vehicle_t2['Node'] == 19]['X-Coordinate'].values[0]
    xbt1 = vehicle_t1[vehicle_t1['Node'] == 20]['X-Coordinate'].values[0]
    xbt2 = vehicle_t2[vehicle_t2['Node'] == 20]['X-Coordinate'].values[0]

    # Iterate over all post x-coordinates
    for r in post_loc['X-Coordinate']:
        # Check for front tire snag
        if xft1 < r <= xft2:
            # Calculate the adjusted y-coordinate for the front tire
            railing_y = railing_t1[railing_t1['Node'] == 19]['Y-Coordinate'].values[0]
            #print(railing_y)
            ft_snag_y = (vehicle_t1[vehicle_t1['Node'] == 19]['Y-Coordinate'].values[0]
                         - 12 + 5.25
                         - railing_y * (40*2/3) / (40*2/3 + 24))
            #print(ft_snag_y)
            # Store the snag information
            ft_snag.append(ft_snag_y)
            ft_snag_loc.append(post_loc.loc[post_loc['X-Coordinate'] == r, 'Node'].values[0])
            fcnt += 1

            # Check for back tire snag
        if xbt1 < r <= xbt2:
            # Calculate the adjusted y-coordinate for the back tire
            railing_y = railing_t1[railing_t1['Node'] == 20]['Y-Coordinate'].values[0]
```

```
            bt_snag_y = (vehicle_t2[vehicle_t2['Node'] == 20]['Y-Coordinate'].values[0]
                    - 12 + 11.963
                    - railing_y * (40*2/3) / (40*2/3 + 24))
            # Store the snag information
            bt_snag.append(bt_snag_y)
            bt_snag_loc.append(post_loc.loc[post_loc['X-Coordinate'] == r, 'Node'].values[0])
            bcnt += 1

    return ft_snag, ft_snag_loc, bt_snag, bt_snag_loc

# pocketing analysis
def pocketing(railing_df, num_beams, num_steps):
    # Tolerance for comparing floating-point numbers
    tolerance = 1e-6

    pocket3_total, pocket3_total_loc, pocket5_total, pocket5_total_loc, pocket9_total,
pocket9_total_loc = [], [], [], [], [], []

    # Identify the unique X-Coordinates within the first num_beams entries
    unique_x_coords = railing_df.loc[:num_beams, 'X-Coordinate'].unique()

    # Filter the original railing_df to keep only the rows with these unique X-Coordinates
    filtered_railing_df = railing_df[railing_df['X-Coordinate'].isin(unique_x_coords)]

    # Keep only the first n unique X-Coordinates
    filtered_railing_df = filtered_railing_df.groupby('X-Coordinate').head(1)

    # Create the new dataframe preserving the original indices
    upper_rail_df = filtered_railing_df.loc[:, ['Node', 'X-Coordinate']]

    # Create a dictionary to map Node to its coordinates for each time step
    node_time_dict = {}
    for step in range(0,num_steps):
        t = step * 0.005
        # filter to adjust 0.000001 value issues
        node_time_dict[t] = railing_df[abs(railing_df['Time'] - t) < tolerance].set_index('Node')

    for step in range(num_steps):
        t = step * 0.005
        node_t = node_time_dict[t]

        pocketing3, pocketing3_loc, pocketing5, pocketing5_loc, pocketing9, pocketing9_loc = [],
[], [], [], [], [], []

        for r in range (len(upper_rail_df)): # 'r' represents the number of
            # upper railing nodes from the beginning to the end of the system
            node_number = upper_rail_df.iloc[r]['Node'] # the number of upper
```

```
            # railing nodes is not equal to the number of nodes because of the
            # curb railing, hence the 'number' of the upper railing node from
            # above needs to be matched to the actual upper railing node
            node_x0 = float(node_t.loc[node_number]['X-Coordinate'])
            node_y0 = float(node_t.loc[node_number]['Y-Coordinate'])
            if 17 <= r <= 75:
                node_x3 = float(node_t.loc[upper_rail_df.iloc[r-2]['Node']]['X-Coordinate'])
                node_y3 = float(node_t.loc[upper_rail_df.iloc[r-2]['Node']]['Y-Coordinate'])
                pocketing3.append(atan((node_y0 - node_y3) / (node_x0 - node_x3)) * 180 / pi) if
node_x0 != node_x3 else 0
                pocketing3_loc.append(node_number)
            if 19 <= r <= 75:
                node_x5 = float(node_t.loc[upper_rail_df.iloc[r-4]['Node']]['X-Coordinate'])
                node_y5 = float(node_t.loc[upper_rail_df.iloc[r-4]['Node']]['Y-Coordinate'])
                pocketing5.append(atan((node_y0 - node_y5) / (node_x0 - node_x5)) * 180 / pi) if
node_x0 != node_x5 else 0
                pocketing5_loc.append(node_number)
            if 23 <= r <= 75:
                node_x9 = float(node_t.loc[upper_rail_df.iloc[r-8]['Node']]['X-Coordinate'])
                node_y9 = float(node_t.loc[upper_rail_df.iloc[r-8]['Node']]['Y-Coordinate'])
                pocketing9.append(atan((node_y0 - node_y9) / (node_x0 - node_x9)) * 180 / pi) if
node_x0 != node_x9 else 0
                pocketing9_loc.append(node_number)

        # Ensure non-empty lists before finding max values
        if pocketing3:
            max_pocketing3_index = pocketing3.index(max(pocketing3))
            pocket3_total.append(pocketing3[max_pocketing3_index])
            pocket3_total_loc.append(pocketing3_loc[max_pocketing3_index])
        if pocketing5:
            max_pocketing5_index = pocketing5.index(max(pocketing5))
            pocket5_total.append(pocketing5[max_pocketing5_index])
            pocket5_total_loc.append(pocketing5_loc[max_pocketing5_index])
        if pocketing9:
            max_pocketing9_index = pocketing9.index(max(pocketing9))
            pocket9_total.append(pocketing9[max_pocketing9_index])
            pocket9_total_loc.append(pocketing9_loc[max_pocketing9_index])
    return pocket3_total, pocket3_total_loc, pocket5_total, pocket5_total_loc, pocket9_total,
pocket9_total_loc

CIP_halfpost_max_defl = []
CIP_halfpost_node_max_defl = []
CIP_halfpost_loc_max_defl = []
CIP_halfpost_time_max_defl = []
CIP_halfpost_max_force = []
CIP_halfpost_node_max_force = []
CIP_halfpost_time_max_force = []
```

```
CIP_halfpost_pocket3 = []
CIP_halfpost_pocket3_loc = []
CIP_halfpost_pocket5 = []
CIP_halfpost_pocket5_loc = []
CIP_halfpost_pocket9 = []
CIP_halfpost_pocket9_loc = []
CIP_halfpost_snagf = []
CIP_halfpost_snagf_loc = []
CIP_halfpost_snagb = []
CIP_halfpost_snagb_loc = []

for index, row in df.iterrows():
    node = row['Node']
    x_coordinate = row['X-coord']
    # Handle potential NaN values
    if pd.isna(node) or pd.isna(x_coordinate):
        #print(f"Skipping row {index} due to missing Node or X-coord value.")
        continue  # Skip to the next iteration
    directory_name =
f'/content/BARRIER_VII/half_post_CIP/impact_n{int(node)}_{x_coordinate:.4f}'

    # Input and output file paths
    b_input_file = os.path.join(directory_name, 'b.out')
    s_input_file = os.path.join(directory_name, 's.out')

    # Filter data for beams
    beam_data = filter_beams(b_input_file, num_beams)
    beam_headers = ['Time', 'Member', 'Node I', 'Node J', 'Type', 'Force', 'I-Moment', 'J-Moment',
'F-Code', 'M-Code']
    beam_df = create_df(beam_data, beam_headers)

    # Convert the necessary columns to float
    beam_df['Force'] = beam_df['Force'].astype(float) # data needs to be read as floating points in
order to be read correctly!
    beam_df['I-Moment'] = beam_df['I-Moment'].astype(float) # data needs to be read as floating
points in order to be read correctly!
    beam_df['J-Moment'] = beam_df['J-Moment'].astype(float) # data needs to be read as floating
points in order to be read correctly!

    # Filter data for posts
    post_data = filter_posts(b_input_file, num_posts)
    post_headers = ['Time', 'Member', 'Node I', 'Node J', 'Type', 'A-Shear', 'B-Shear', 'B-Moment',
'A-Moment', 'Code']
    post_df = create_df(post_data, post_headers)

    # Process s.out for railing and vehicle nodes
```

```
    railing_data, vehicle_data = filter_s_out(s_input_file, b7_n)
    railing_headers = ['Time', 'Node', 'X-Deflection', 'Y-Deflection', 'X-Coordinate', 'Y-
Coordinate']
    railing_df = create_df(railing_data, railing_headers)
    railing_df['Y-Deflection'] = railing_df['Y-Deflection'].astype(float) # data needs to be read as
floating points in order to be read correctly!
    vehicle_headers = ['Time', 'Node', 'X-Deflection', 'Y-Deflection', 'X-Coordinate', 'Y-
Coordinate']
    vehicle_df = create_df(vehicle_data, vehicle_headers)

    # Find the maximum force and the corresponding member and time
    max_force = beam_df['Force'].max()
    max_force_member = beam_df.loc[beam_df['Force'].idxmax(), 'Member']
    max_force_time = beam_df.loc[beam_df['Force'].idxmax(), 'Time']

    # Find the maximum deflection and the corresponding node, location, and time
    max_deflection = railing_df['Y-Deflection'].max()
    max_deflection_node = railing_df.loc[railing_df['Y-Deflection'].idxmax(), 'Node']
    max_deflection_loc = railing_df.loc[railing_df['Y-Deflection'].idxmax(), 'X-Coordinate']
    max_deflection_time = railing_df.loc[railing_df['Y-Deflection'].idxmax(), 'Time']

    # post locations array for wheel snag analysis
    post_loc = pd.DataFrame()
    post_loc['Node'] = post_df.loc[0:num_posts-1,'Node I']
    post_loc = pd.merge(post_loc, railing_df.loc[0:num_beams,['Node', 'X-Coordinate']],
left_on='Node', right_on='Node', how='left')

    # wheel snag analysis
    num_steps = vehicle_df['Time'].nunique()
    ft_snag, ft_snag_loc, bt_snag, bt_snag_loc =
wheel_snag(vehicle_df,railing_df,post_loc,num_steps)
    max_ft_snag = max(ft_snag)
    max_ft_snag_loc = ft_snag_loc[ft_snag.index(max_ft_snag)]
    max_bt_snag = max(bt_snag)
    max_bt_snag_loc = bt_snag_loc[bt_snag.index(max_bt_snag)]

    # pocketing analysis
    pocket3_total, pocket3_total_loc, pocket5_total, pocket5_total_loc, pocket9_total,
pocket9_total_loc = pocketing(railing_df, num_beams, num_steps)

    # Append the results to the respective lists
    CIP_halfpost_max_force.append(max_force)
    CIP_halfpost_node_max_force.append(max_force_member)
    CIP_halfpost_time_max_force.append(max_force_time)
    CIP_halfpost_max_defl.append(max_deflection)
    CIP_halfpost_node_max_defl.append(max_deflection_node)
    CIP_halfpost_loc_max_defl.append(max_deflection_loc)
```

```
    CIP_halfpost_time_max_defl.append(max_deflection_time)

    CIP_halfpost_snagf.append(max_ft_snag)
    CIP_halfpost_snagf_loc.append(max_ft_snag_loc)
    CIP_halfpost_snagb.append(max_bt_snag)
    CIP_halfpost_snagb_loc.append(max_bt_snag_loc)
    CIP_max_pocket3_index = pocket3_total.index(max(pocket3_total))
    CIP_halfpost_pocket3.append(pocket3_total[CIP_max_pocket3_index])
    CIP_halfpost_pocket3_loc.append(pocket3_total_loc[CIP_max_pocket3_index])
    CIP_max_pocket5_index = pocket5_total.index(max(pocket5_total))
    CIP_halfpost_pocket5.append(pocket5_total[CIP_max_pocket5_index])
    CIP_halfpost_pocket5_loc.append(pocket5_total_loc[CIP_max_pocket5_index])
    CIP_max_pocket9_index = pocket9_total.index(max(pocket9_total))
    CIP_halfpost_pocket9.append(pocket9_total[CIP_max_pocket9_index])
    CIP_halfpost_pocket9_loc.append(pocket9_total_loc[CIP_max_pocket9_index])

    # Save final dataframes to CSV
    final_post_df = os.path.join(directory_name, 'post_df.csv')
    final_beam_df = os.path.join(directory_name, 'beam_df.csv')
    final_railing_df = os.path.join(directory_name, 'railing_df.csv')
    final_vehicle_df = os.path.join(directory_name, 'vehicle_df.csv')
    post_df.to_csv(final_post_df, index=False)
    beam_df.to_csv(final_beam_df, index=False)
    railing_df.to_csv(final_railing_df, index=False)
    vehicle_df.to_csv(final_vehicle_df, index=False)

# Create a DataFrame

results = {
    'Max Deflection': CIP_halfpost_max_defl,
    'Node of Max Deflection': CIP_halfpost_node_max_defl,
    'Location of Max Deflection': CIP_halfpost_loc_max_defl,
    'Max Force': CIP_halfpost_max_force,
    'Node of Max Force': CIP_halfpost_node_max_force,
    'Maximum 3-Node Pocket': CIP_halfpost_pocket3,
    'Maximum 3-Node Pocket Node': CIP_halfpost_pocket3_loc,
    'Maximum 5-Node Pocket': CIP_halfpost_pocket5,
    'Maximum 5-Node Pocket Node': CIP_halfpost_pocket5_loc,
    'Maximum 9-Node Pocket': CIP_halfpost_pocket9,
    'Maximum 9-Node Pocket Node': CIP_halfpost_pocket9_loc,
    'Front Tire Snag': CIP_halfpost_snagf,
    'Front Tire Snag Node': CIP_halfpost_snagf_loc,
    'Back Tire Snag': CIP_halfpost_snagb,
    'Back Tire Snag Node': CIP_halfpost_snagb_loc
}

rdf = pd.DataFrame(results)
```

```
rdf = pd.merge(df, rdf, left_index=True, right_index=True)
# Save DataFrame to a CSV file
rdf.to_csv('/content/Results.csv', index=False)
```

Appendix N. Dynamic Component Test TRTD-3

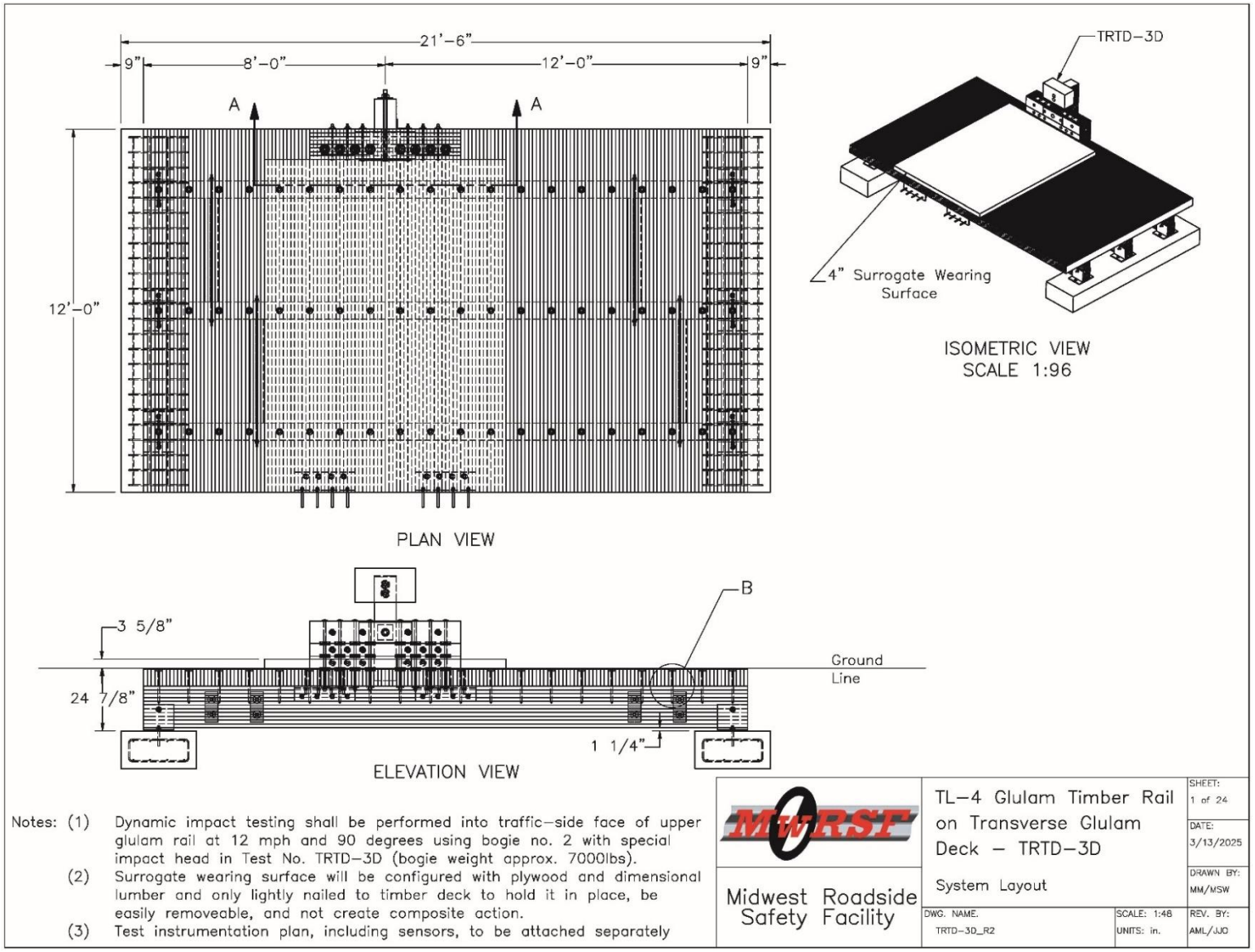

Figure N-1. Test No. TRTD-3 System Layout

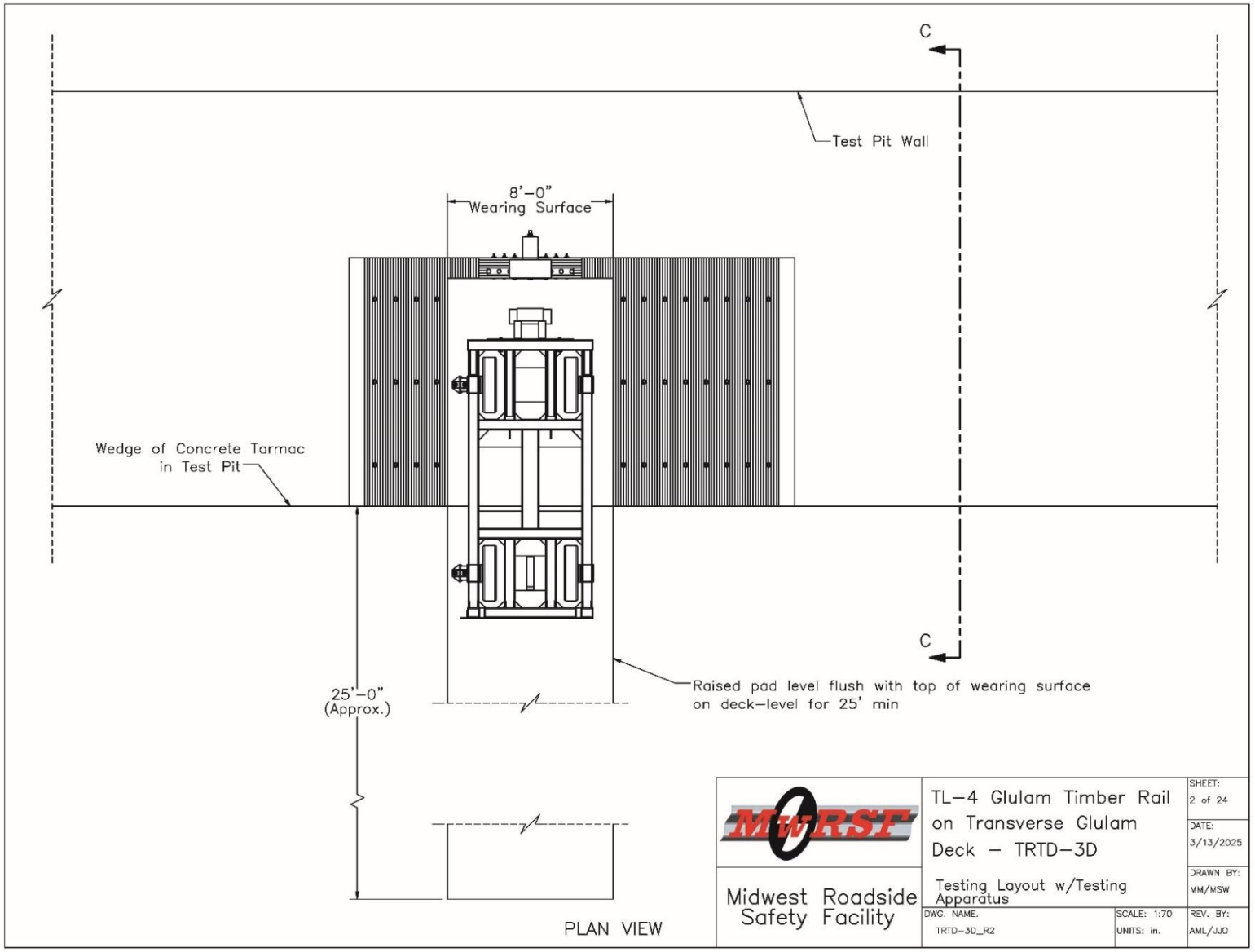

Figure N-2. Test No. TRTD-3 Layout with Bogie

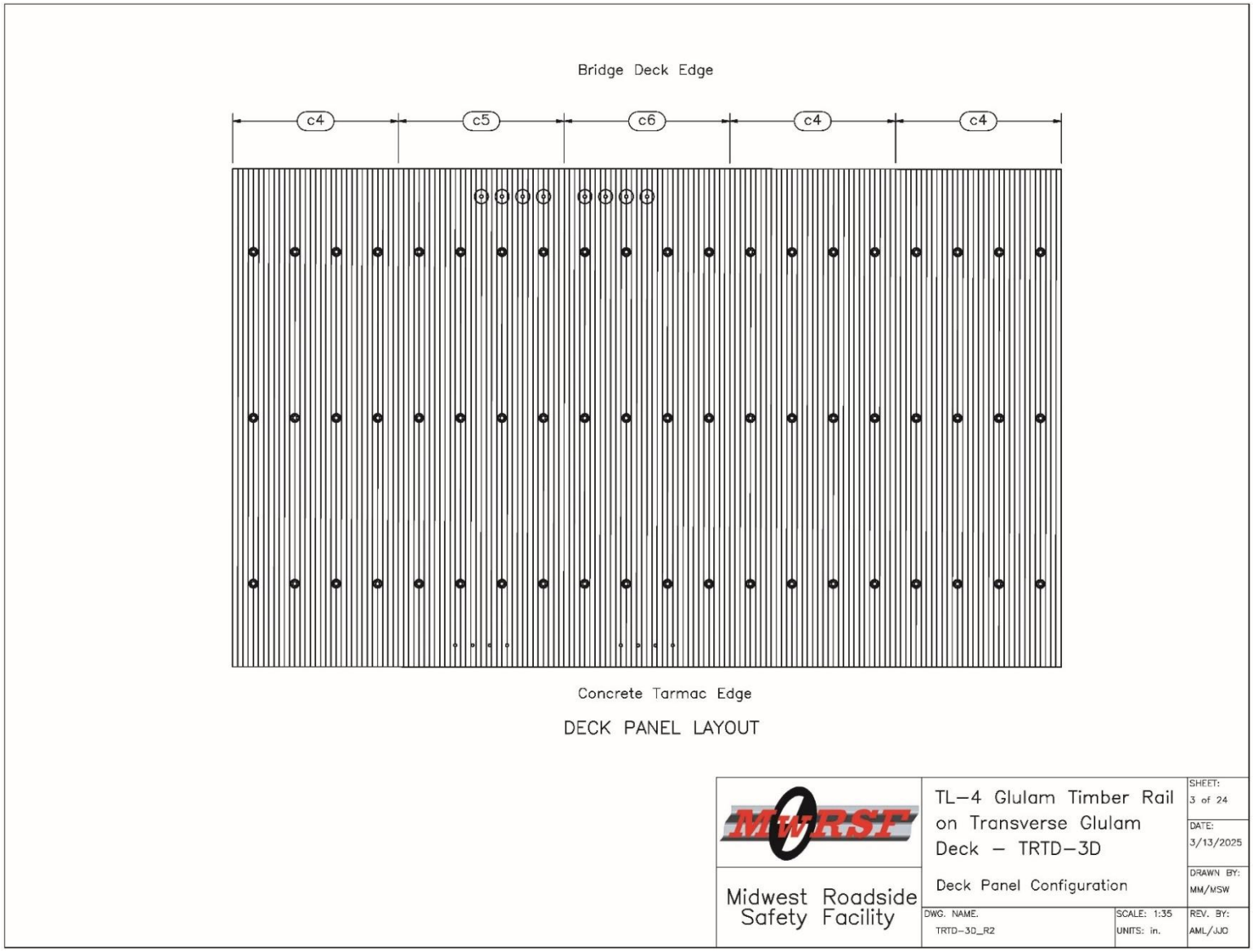

Figure N-3. Test No. TRTD-3 Deck Panel Configuration

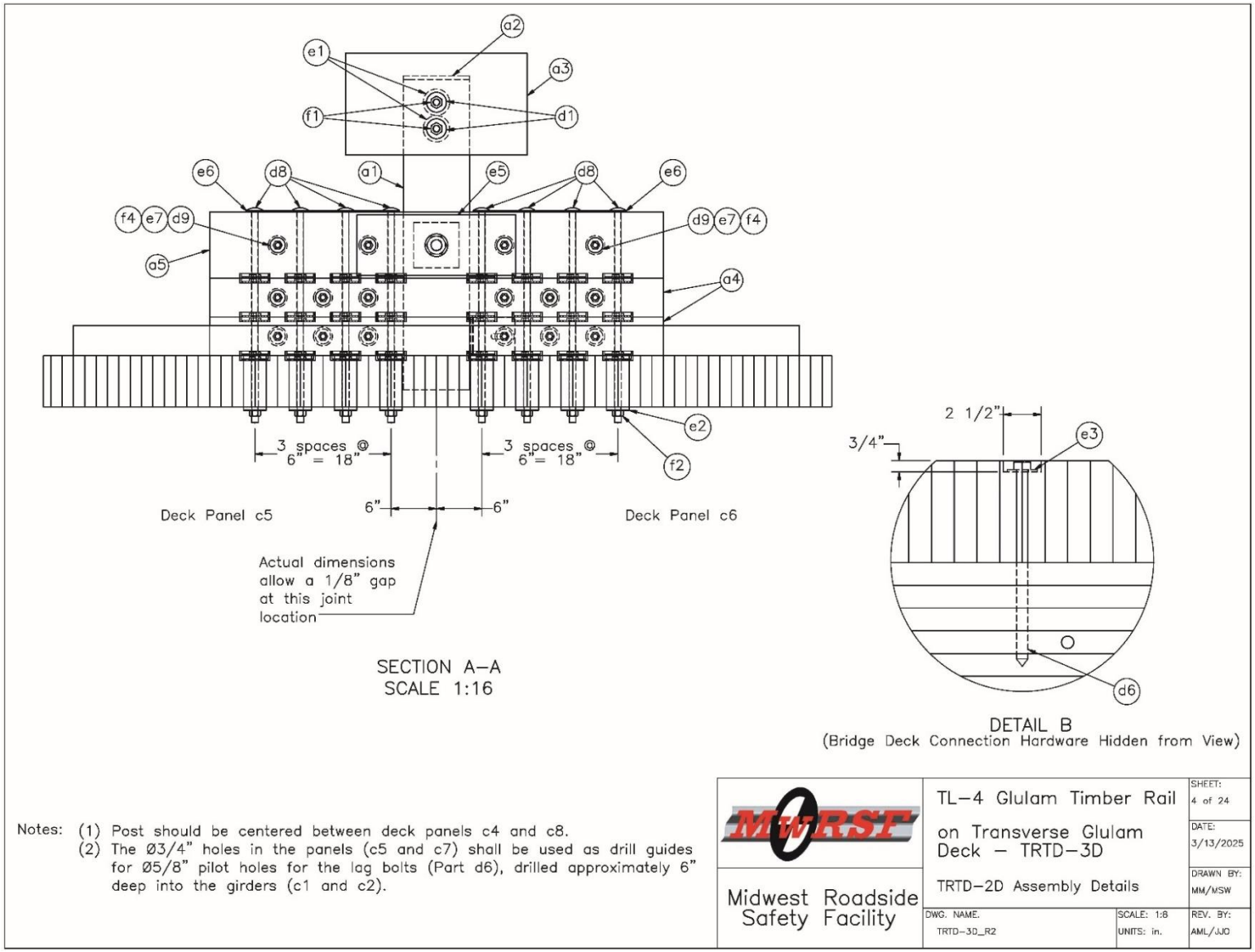

Figure N-4. Test No. TRTD-3 Post and Deck Assembly Details

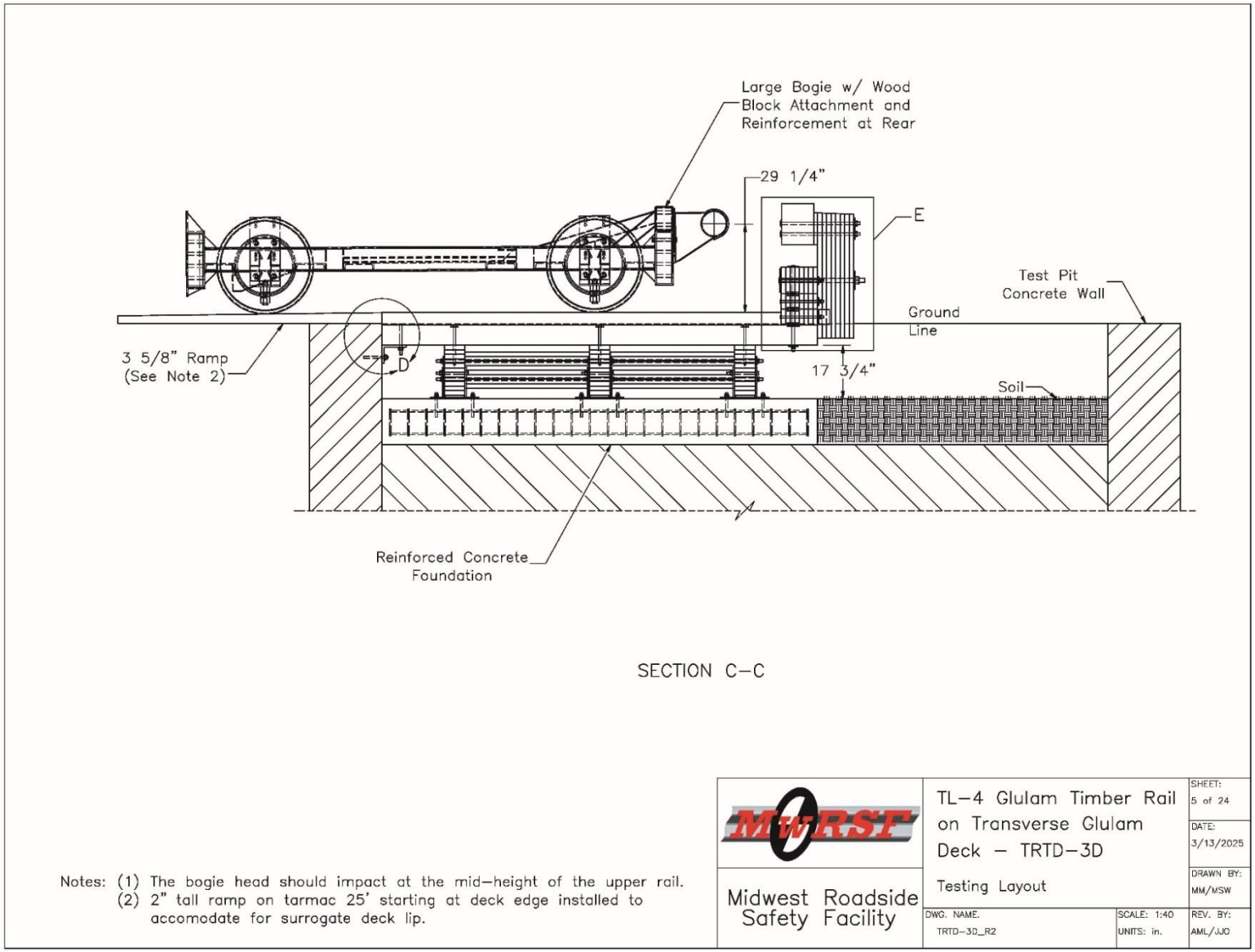

Figure N-5. Test No. TRTD-3 Layout, Elevation View

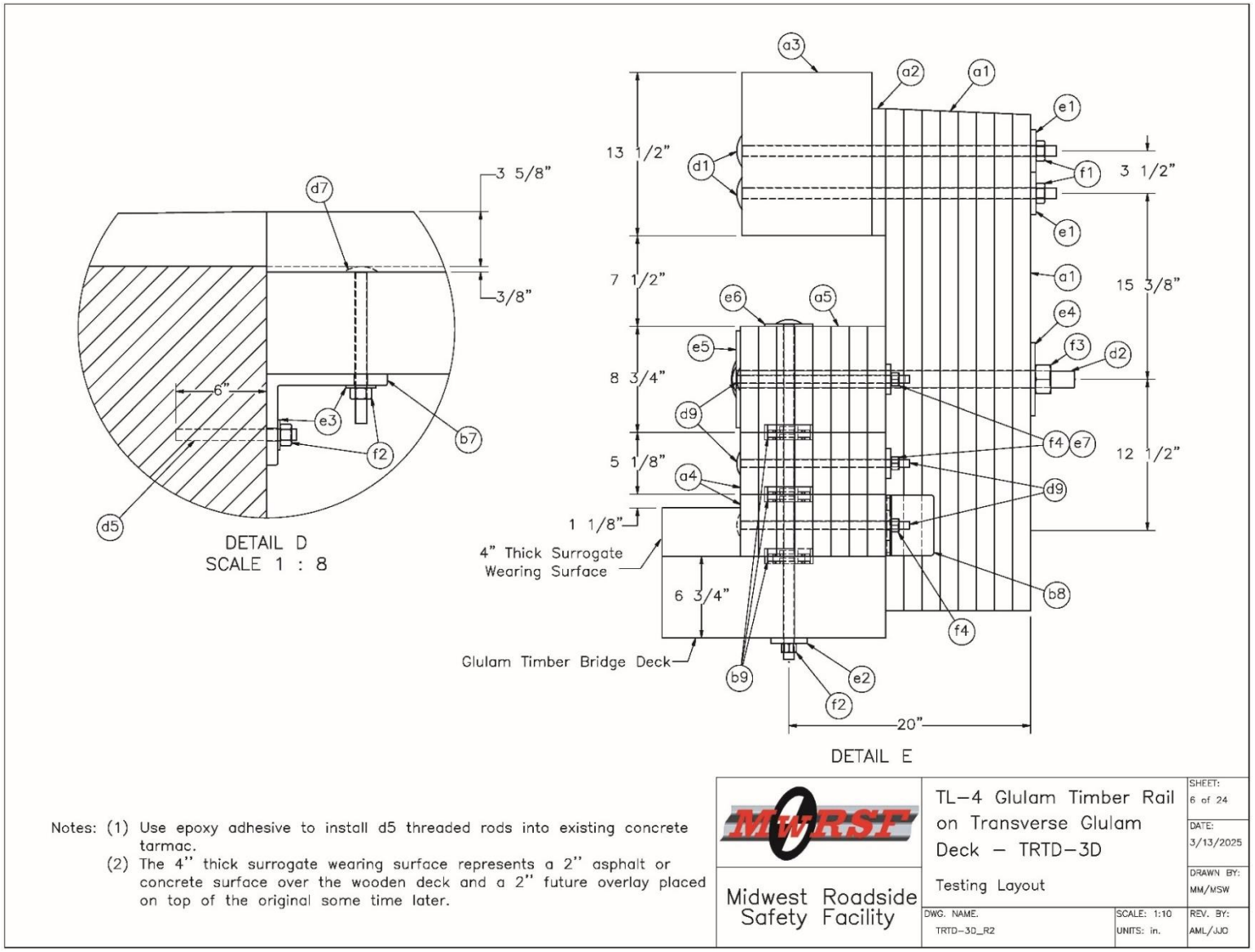

Figure N-6. Test No. TRTD-3 Post and Deck Assembly Details, Section View

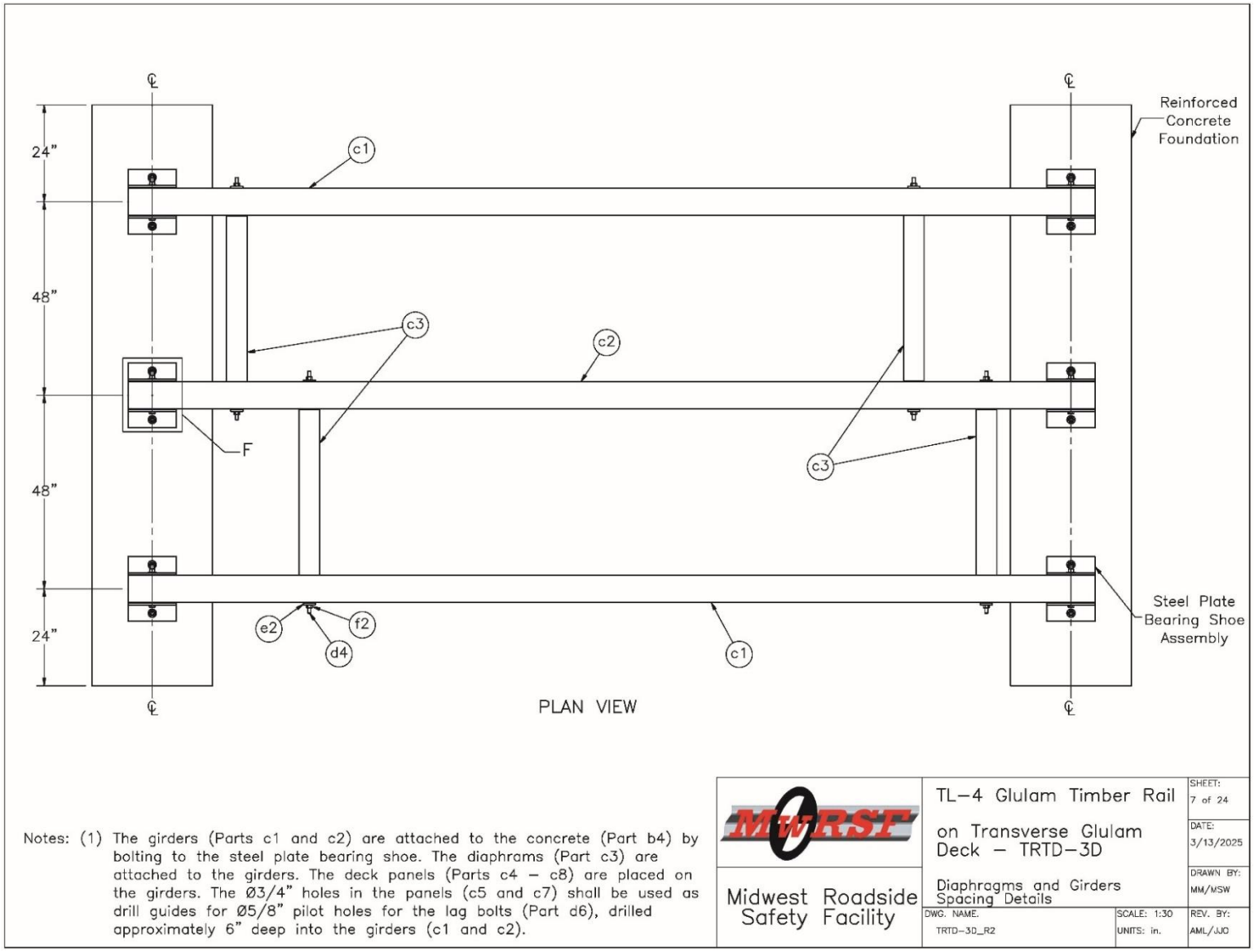

Figure N-7. Test No. TRTD-3 Diaphragms and Girders Spacing Details

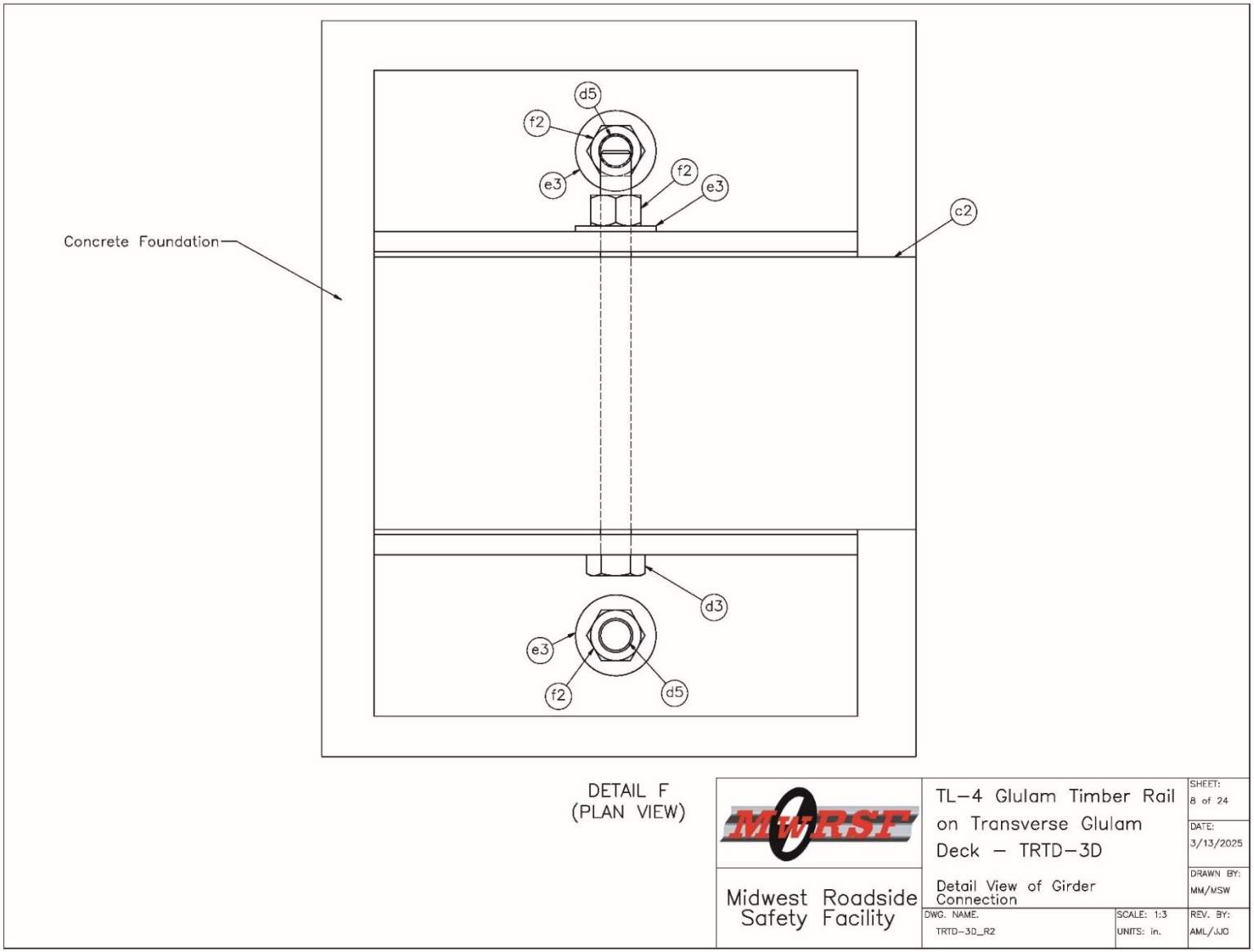

Figure N-8. Test No. TRTD-3 Girder Connection Details

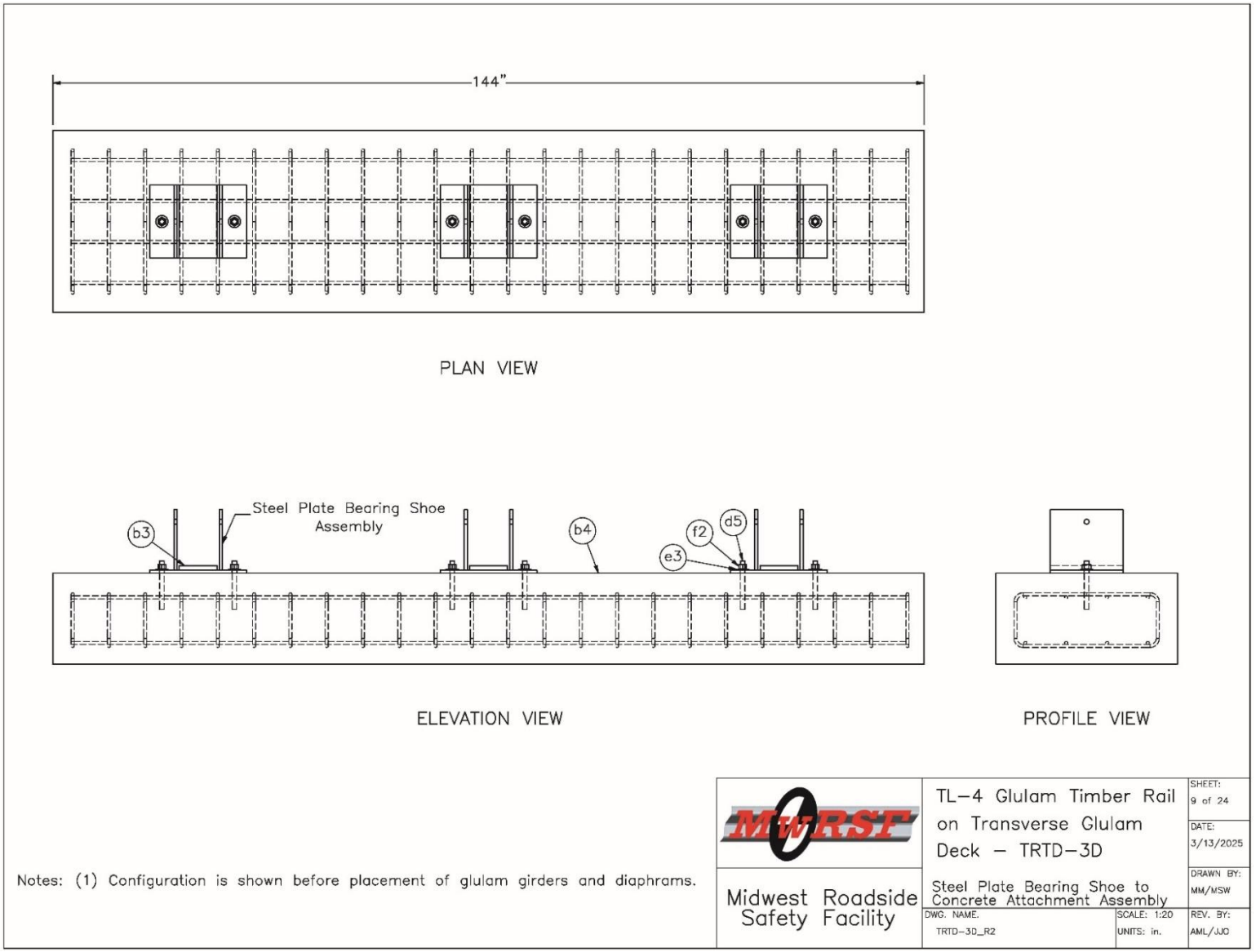

Figure N-9. Test No. TRTD-3 Concrete and Bearing Assembly Details

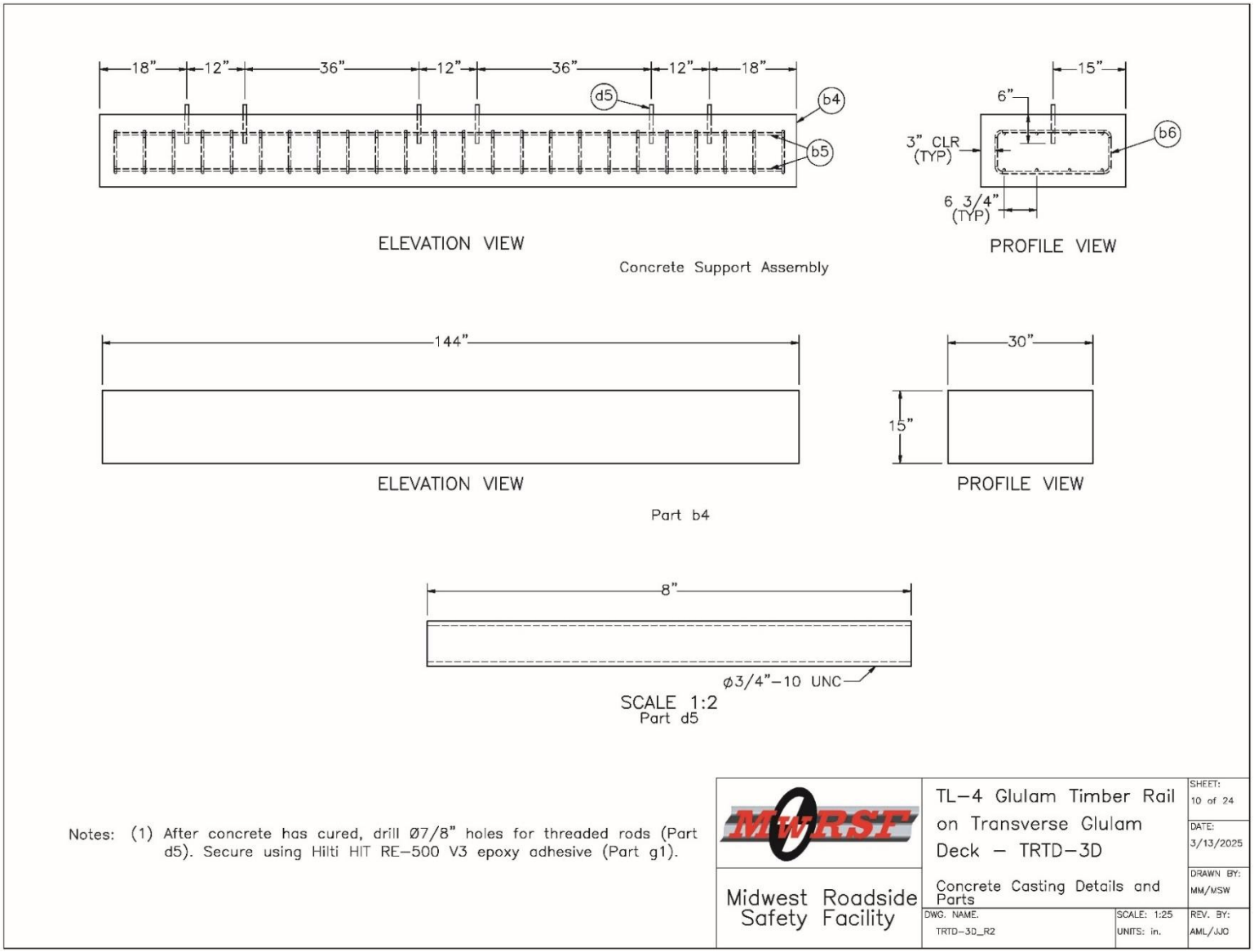

Figure N-10. Test No. TRTD-3 Concrete Casting and Embedded Rod Details

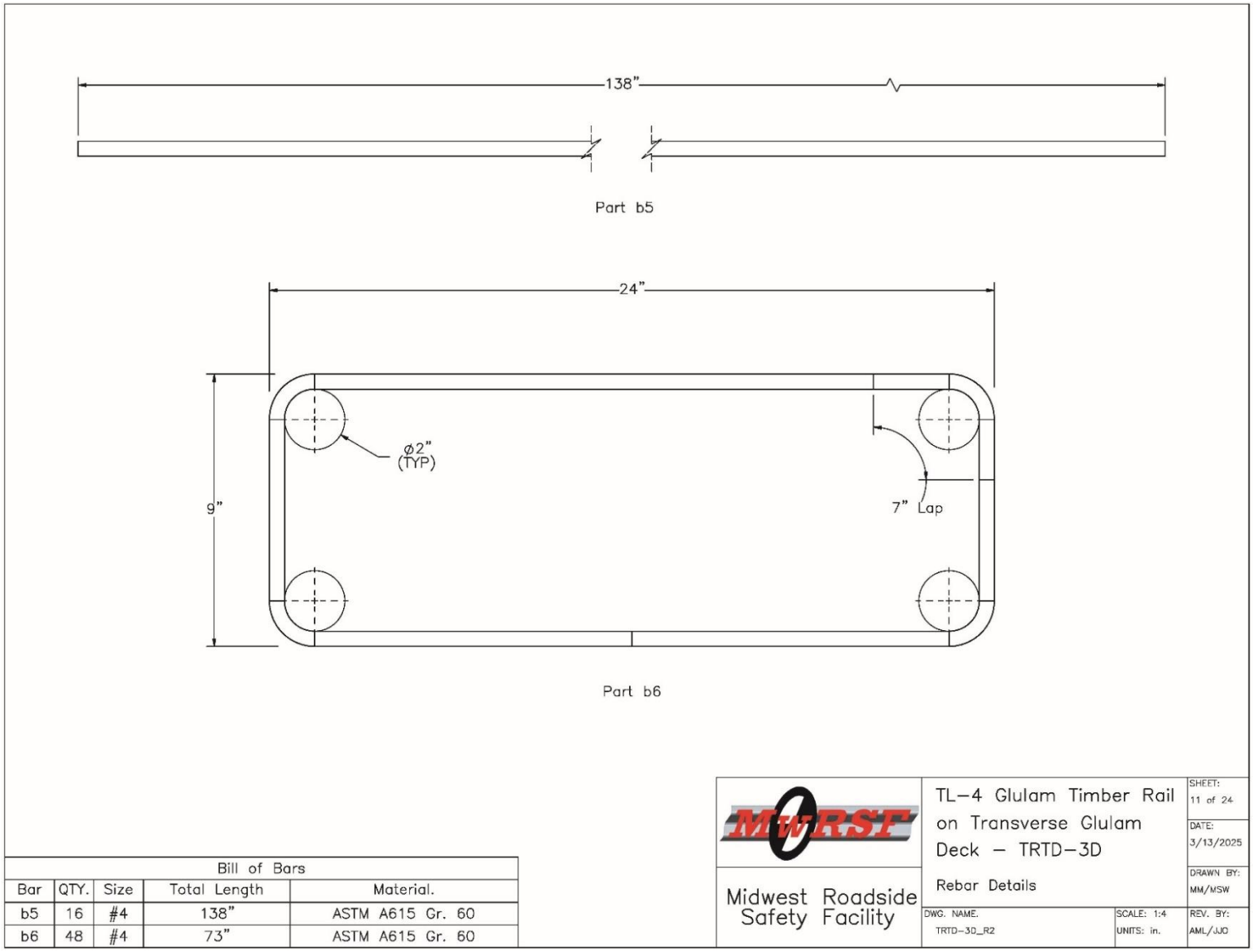

Figure N-11. Test No. TRTD-3 Rebar Details

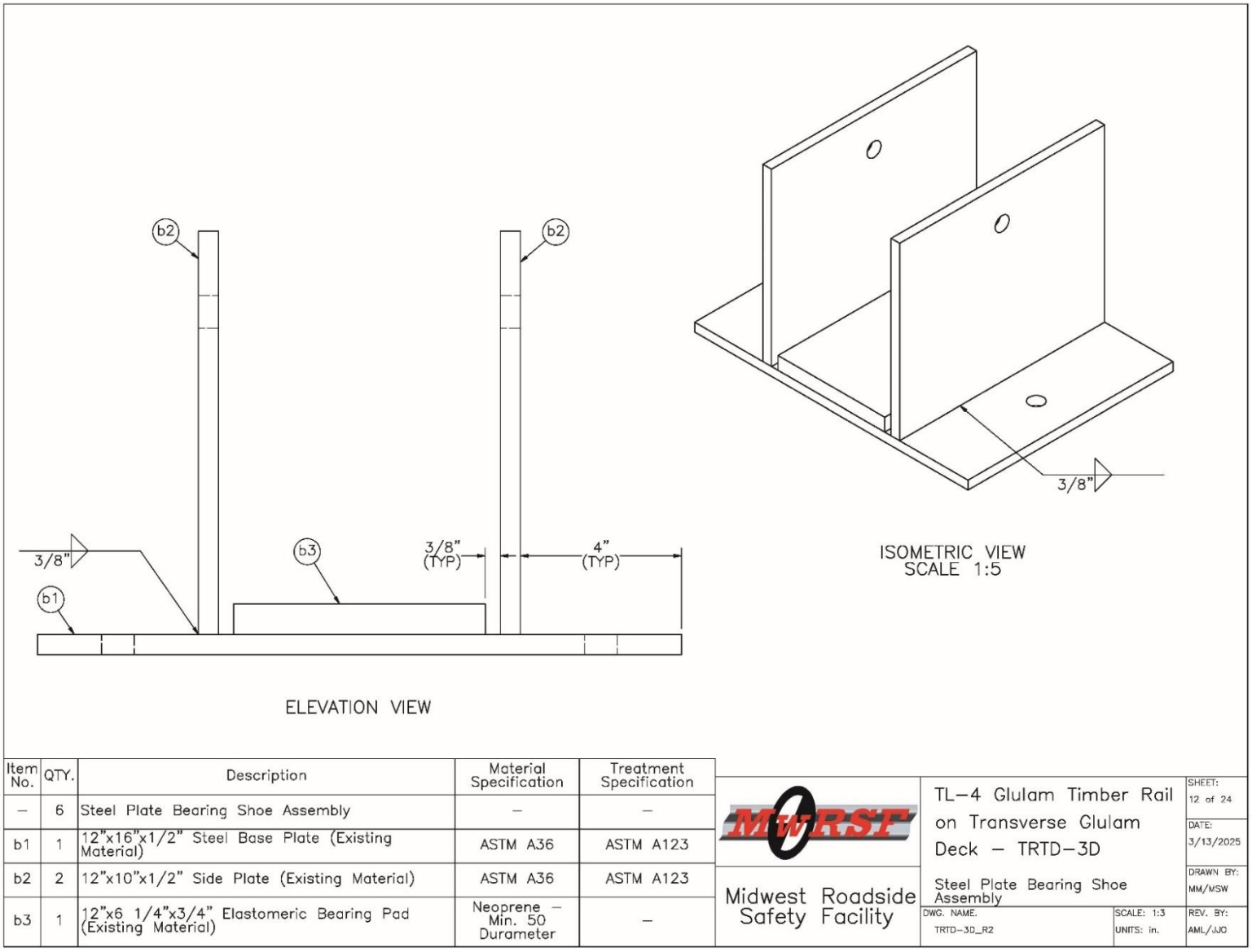

Item No.	QTY.	Description	Material Specification	Treatment Specification
–	6	Steel Plate Bearing Shoe Assembly	–	–
b1	1	12"x16"x1/2" Steel Base Plate (Existing Material)	ASTM A36	ASTM A123
b2	2	12"x10"x1/2" Side Plate (Existing Material)	ASTM A36	ASTM A123
b3	1	12"x6 1/4"x3/4" Elastomeric Bearing Pad (Existing Material)	Neoprene – Min. 50 Durameter	–

Midwest Roadside Safety Facility

TL–4 Glulam Timber Rail on Transverse Glulam Deck – TRTD–3D

Steel Plate Bearing Shoe Assembly

DWG. NAME. TRTD–3D_R2 | SCALE: 1:3 | UNITS: in.

SHEET: 12 of 24

DATE: 3/13/2025

DRAWN BY: MM/MSW

REV. BY: AML/JJO

Figure N-12. Test No. TRTD-3 Steel Plate Bearing Assembly Details

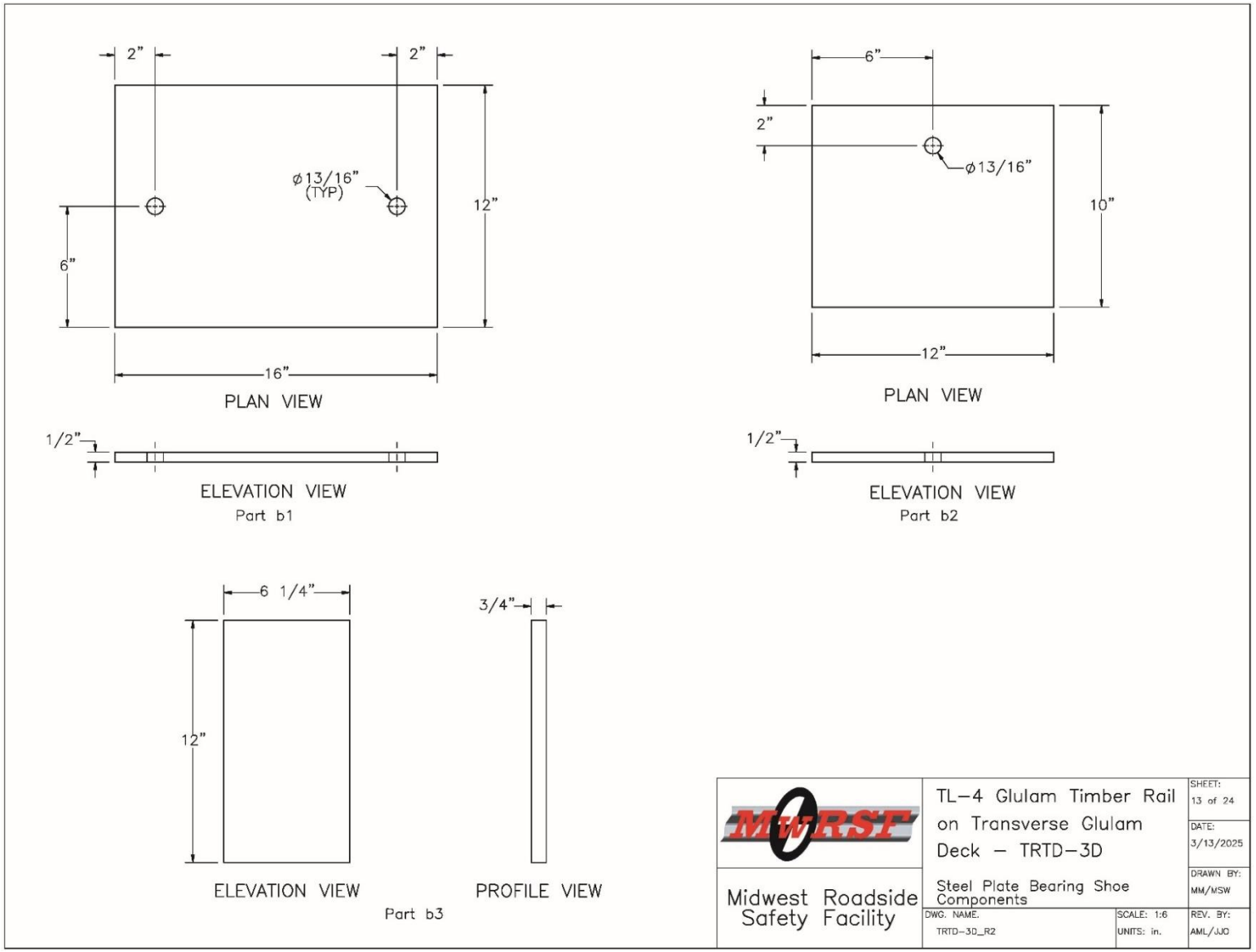

Figure N-13. Test No. TRTD-3 Steel Plate Bearing Assembly Component Details

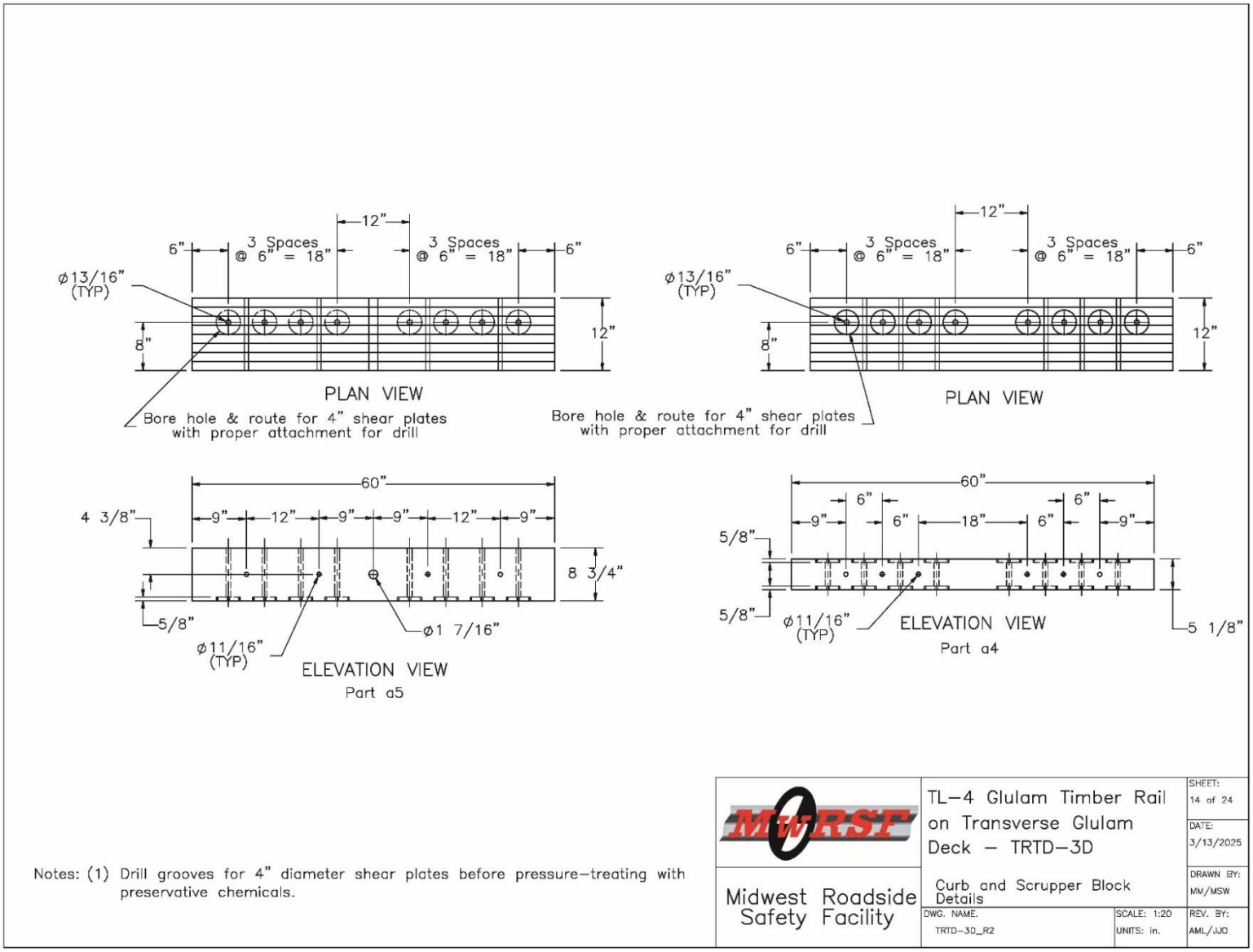

Figure N-14. Test No. TRTD-3 Scupper and Curb Rail Details

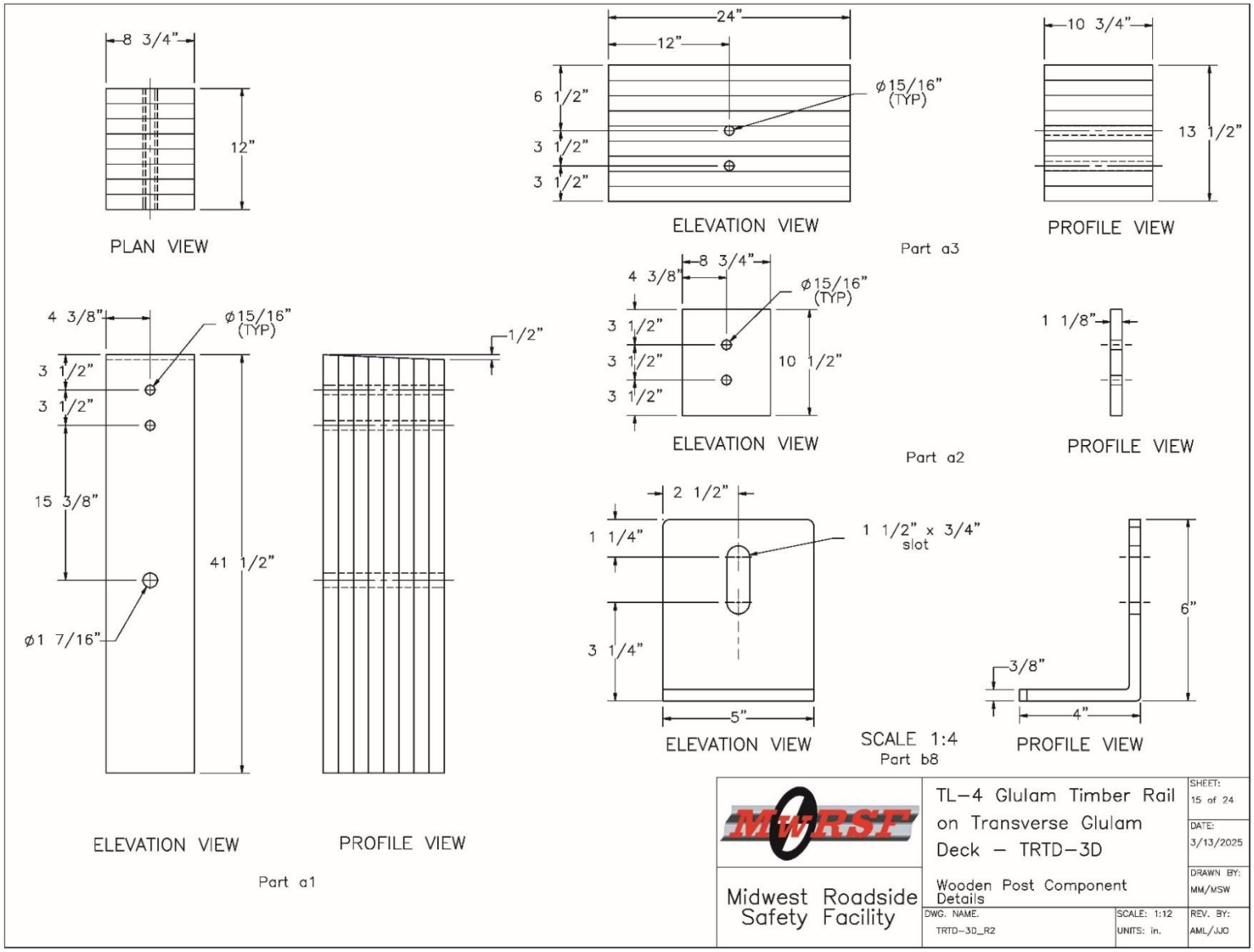

Figure N-15. Test No. TRTD-3 Vertical Post, Upper Rail, Blockout, and Angle Guide Details

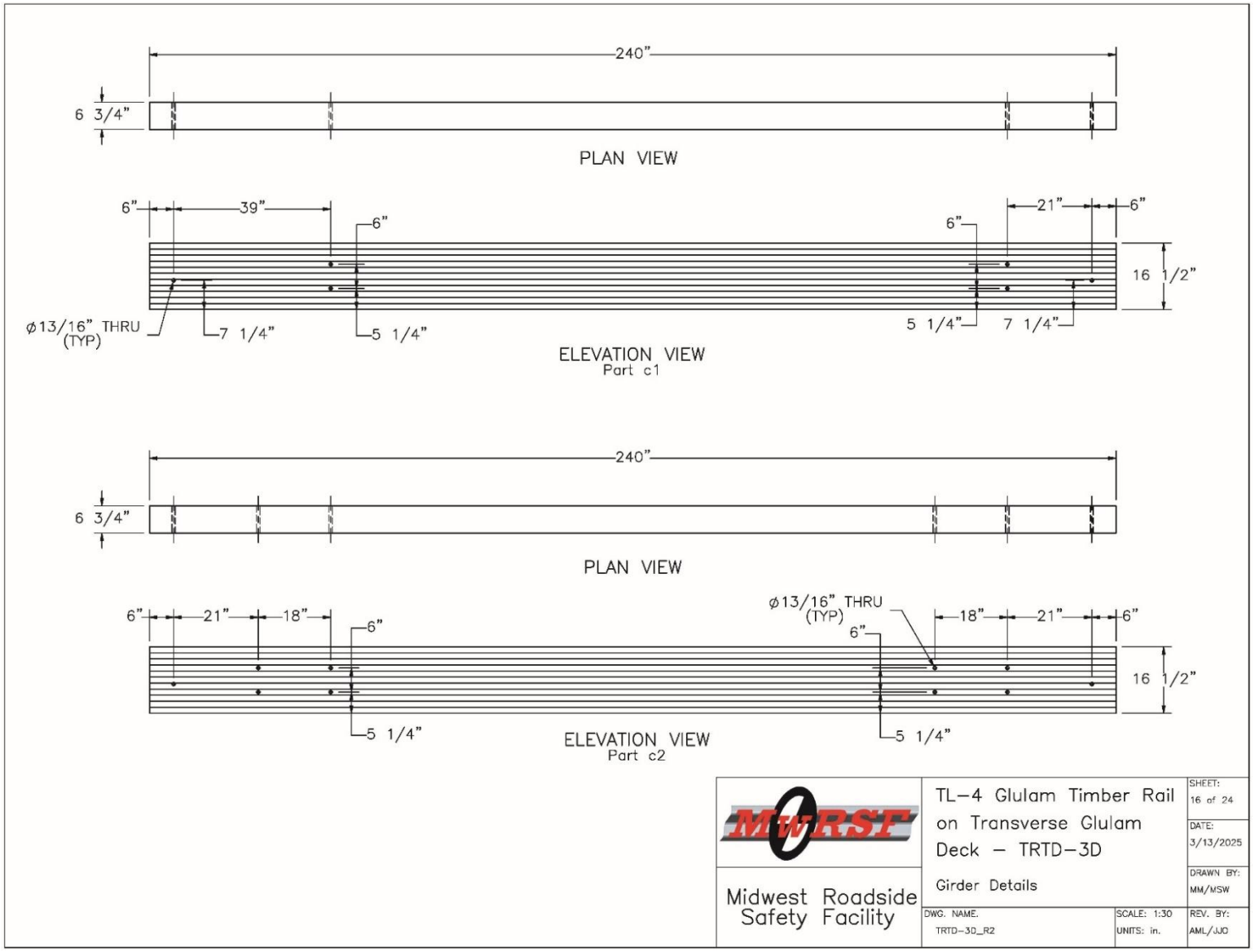

Figure N-16. Test No. TRTD-3 Girder Details

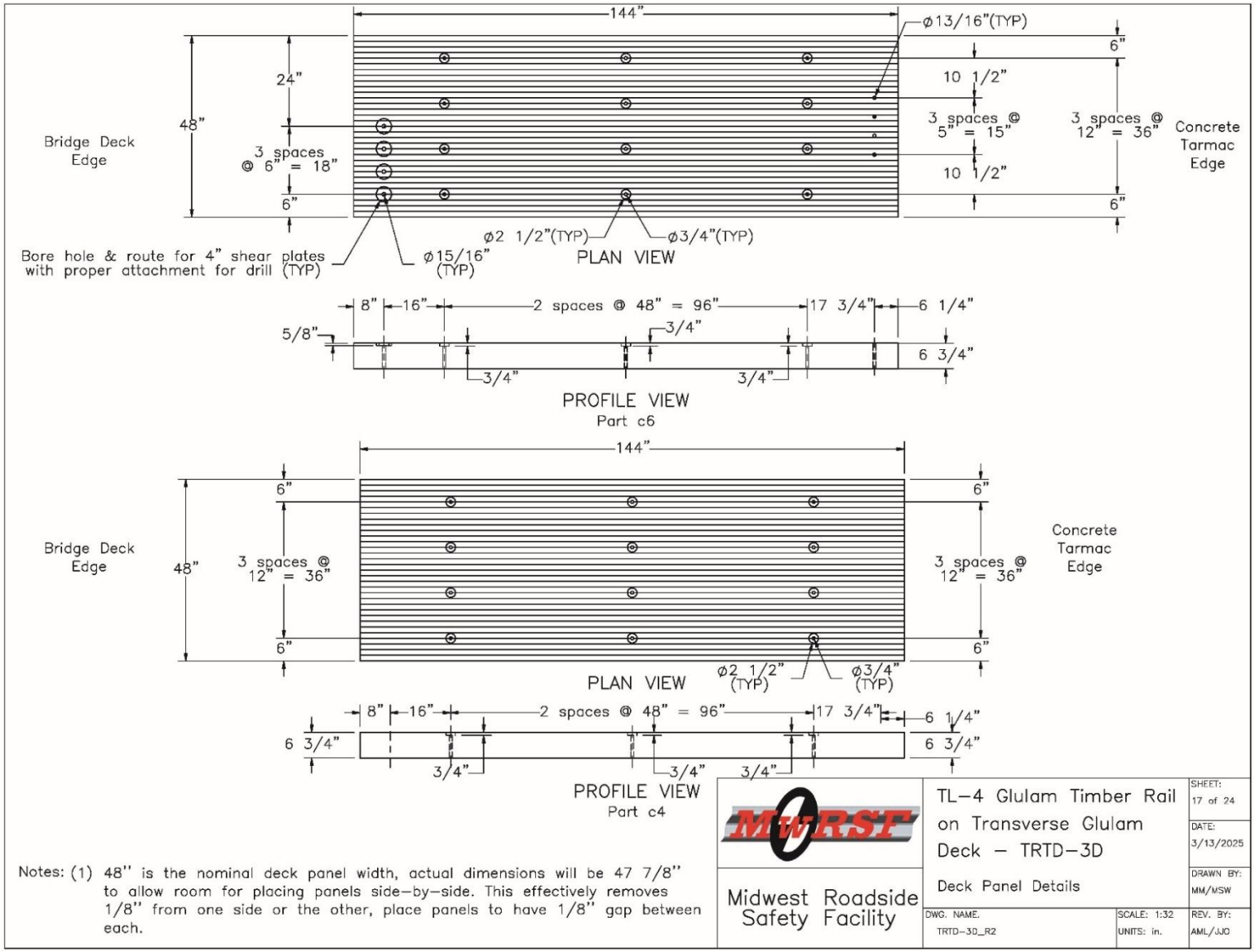

Figure 267: Test No. TRTD-3 Deck Panel Details, Page 1

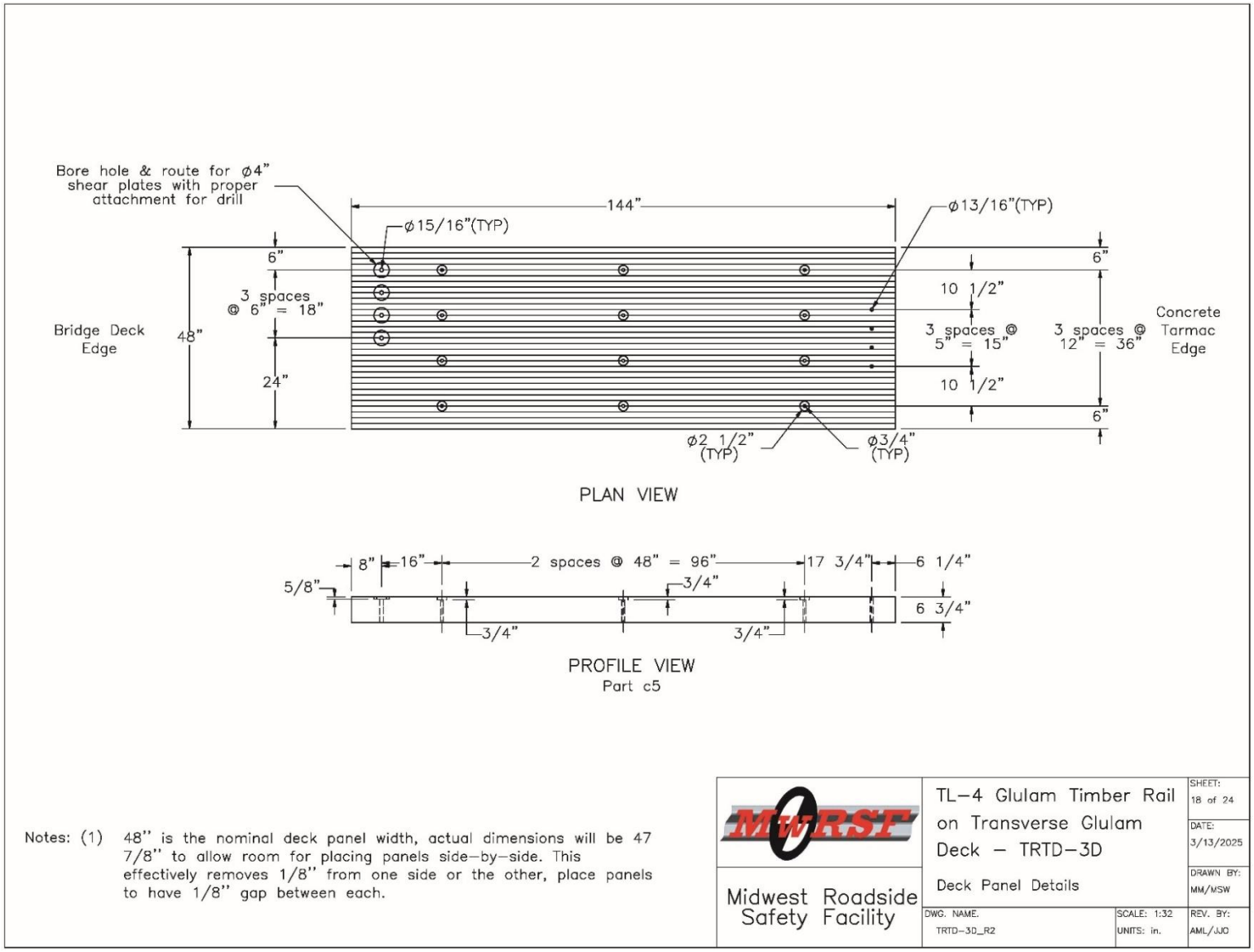

Figure 268: Test No. TRTD-3 Deck Panel Details, Page 2

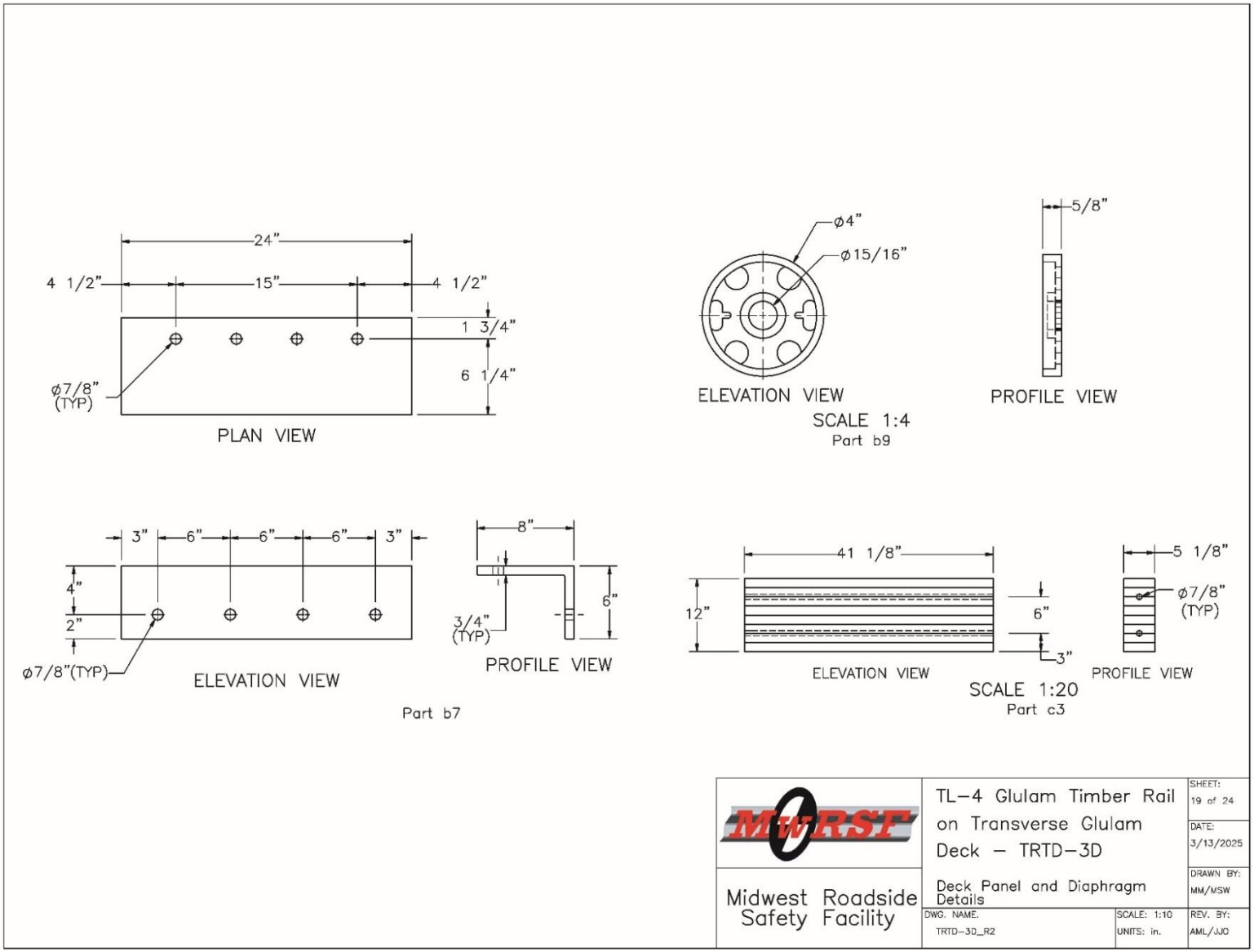

Figure 269: Test No. TRTD-3 Tarmac Angle Restraint, Diaphragm, and Shear Plate Details

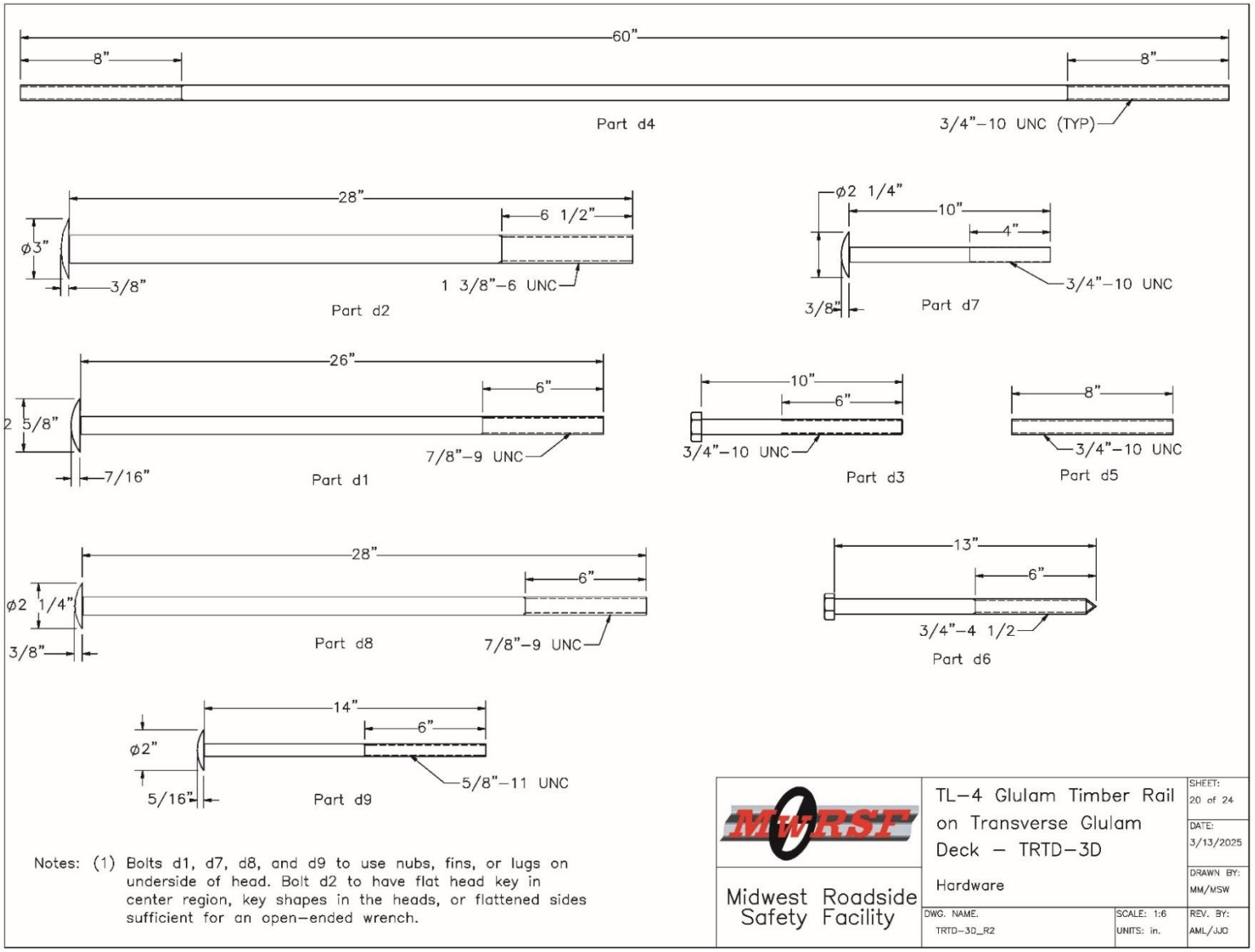

Figure 270: Test No. TRTD-3 Connection Hardware Details, Page 1

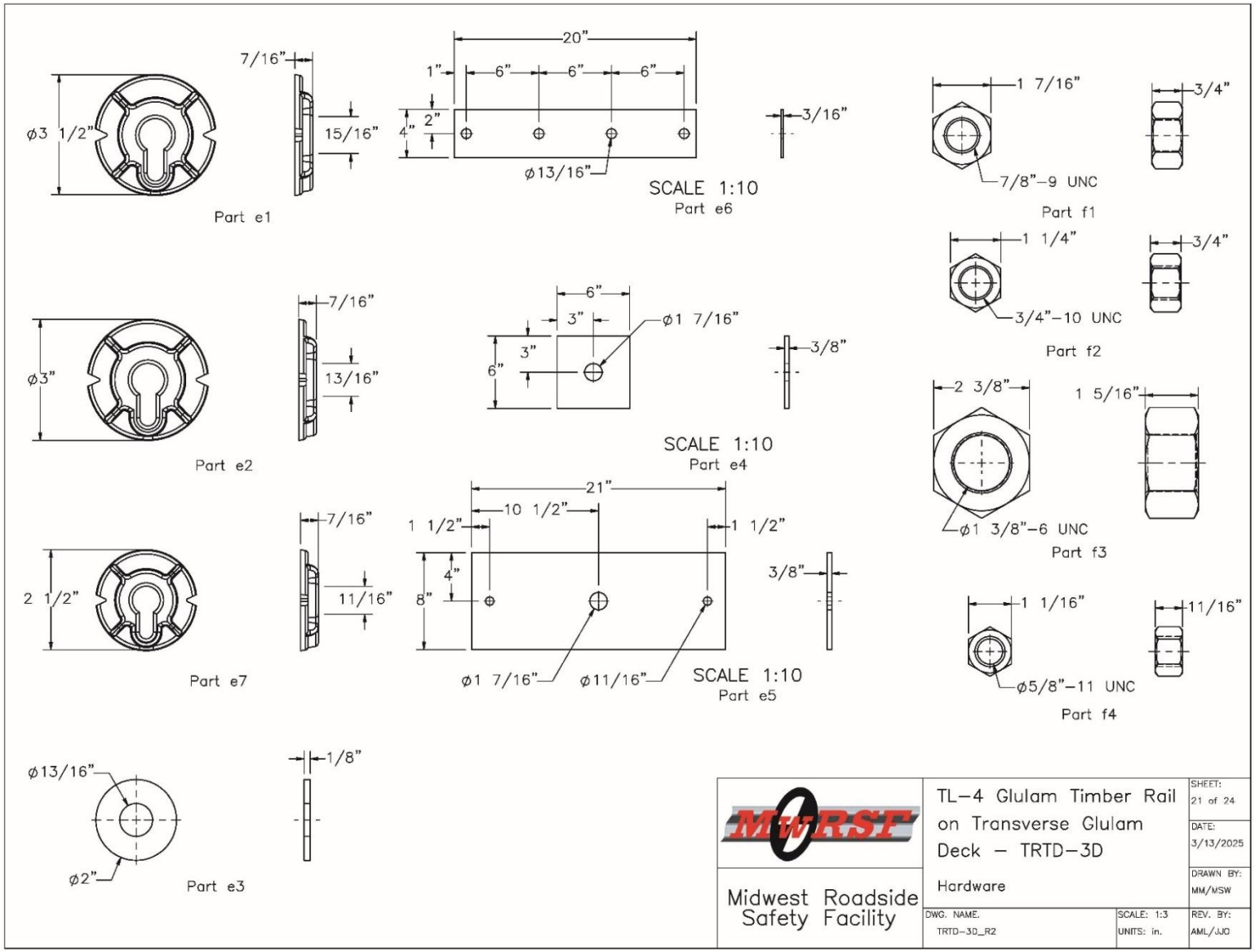

Figure 271: Test No. TRTD-3 Connection Hardware Details, Page 2

Item No.	QTY.	Description	Material Specification	Treatment Specification	Hardware Guide
–	1	4" Thick Surrogate Wearing Surface	–	–	
a1	1	41 1/2"x12"x8 3/4" Glulam Post (Existing Material)	Comb. 48 (SP) or Comb. 2 (Western Species)	See Notes 1–3	–
a2	1	1 1/4"x10 1/2"x8 3/4" Glulam Blockout (Existing Material)	Comb. 48 (SP) or Comb. 2 (Western Species)	See Notes 1–3	–
a3	1	24"x13 1/2"x10 3/4" Glulam Upper Rail (Existing Material)	Comb. 48 (SP) or Comb. 2 (Western Species)	See Notes 1–3	–
a4	2	60"x12"x5 1/8" Glulam Scupper Block (Existing Material)	Comb. 48 (SP) or Comb. 2 (Western Species)	See Notes 1–3	–
a5	1	60"x12"x8 3/4" Glulam Curb Rail (Existing Material)	Comb. 48 (SP) or Comb. 2 (Western Species)	See Notes 1–3	–
b1	6	12"x16"x1/2" Steel Base Plate (Existing Material)	ASTM A36	ASTM A123	–
b2	12	12"x10"x1/2" Side Plate (Existing Material)	ASTM A36	ASTM A123	–
b3	6	12"x6 1/4"x3/4" Elastomeric Bearing Pad (Existing Material)	Neoprene – Min. 50 Durameter	–	–
b4	2	15"x30"x12' Concrete Support (Existing Material)	Min f'c = 4,000 psi NE mix 47 BD	–	–
b5	16	#4 Rebar, 138" Long (Existing Material)	ASTM A615 Gr. 60	Epoxy Coated (ASTM A775 or A934)	–
b6	48	#4 Rebar, 73" Unbent Length (Existing Material)	ASTM A615 Gr. 60	Epoxy Coated (ASTM A775 or A934)	–
b7	2	8"x 6", 3/4" Thick 24" Long Steel Angle (Existing Material)	ASTM A36	ASTM A123	–
b8	1	6"x4", 3/8" Thick, 5" Long Steel Angle (Existing Material)	ASTM A36	ASTM A123	–
b9	48	7/8"x4"x5/8" Shear Plate	ASTM A47 Grade 32510 or ASTM D5933	Hot–Dip	12405

Notes: (1) Timber rails, posts, scuppers, and blockouts shall be treated with Copper Naphthenate (CuN) or 4,5–Dichloro–2–N–Octyl–4–Isothiazolin–3–One (DCOI) in heavy oil to a minimum retention of 0.075 lbs/cu. ft. or 0.20 lbs/cu. ft. respectively in accordance with AWPA Standard UI to the requirements. Use category 4B (UC4B).
(2) Wood shall be cut, drilled, and completely fabricated prior to treatment with preservative. Drain excess chemicals and dry all treated wood at the place of manufacture.
(3) All field cuts, bore holes, and damages shall be treated with material acceptable to the engineer prior to installation.

Midwest Roadside Safety Facility

TL–4 Glulam Timber Rail on Transverse Glulam Deck – TRTD–3D

Bill of Materials

SHEET: 22 of 24		
DATE: 3/13/2025		
DRAWN BY: MM/MSW		
DWG. NAME. TRTD–3D_R2	SCALE: None UNITS: in.	REV. BY: AML/JJO

Figure 272: Test No. TRTD-3 Bill of Material, Page 1

Item No.	QTY.	Description	Material Specification	Treatment Specification	Hardware Guide
c1	2	16 1/2"x6 3/4"x20' Long Outside Glulam Girder (Existing Material)	24F-V4 Douglas Fir	Pentachorophenal in Heavy Oil 0.6 lbs/cu. ft Retention	–
c2	1	16 1/2"x6 3/4"x20' Long Glulam Girder (Existing Material)	24F-V4 Douglas Fir	Pentachorophenal in Heavy Oil 0.6 lbs/cu. ft Retention	–
c3	4	12"x5 1/8"x41 1/8" Long Glulam Diaphragm (Existing Material)	Comb. No. 2 Douglas Fir	Pentachorophenal in Heavy Oil 0.6 lbs/cu. ft Retention	–
c4	3	6 3/4"x4'x12' Long Glulam Deck Panel	Comb. 48(SP) or Comb. 2 (Western Species)	See Notes 1-3	–
c5	1	6 3/4"x4'x12' Long Glulam Deck Panel	Comb. 48(SP) or Comb. 2 (Western Species)	See Notes 1-3	–
c6	1	6 3/4"x4'x12' Long Glulam Deck Panel	Comb. 48(SP) or Comb. 2 (Western Species)	See Notes 1-3	–
d1	2	7/8"-9 UNC x 26" Timber Bolt w/ Nubs (Existing Material)	ASTM A307A	ASTM A123	–
d2	1	1 3/8"-6 UNC x 28" Timber Bolt w/o Nubs (Existing Material)	ASTM A449	ASTM A123	–
d3	6	3/4"-10 UNC x 10" Hex Bolt (Existing Material)	ASTM A307A	ASTM A123	FBX20a
d4	8	3/4"-10 UNC x 8" on a 60" Long Tie Rod (Existing Material)	ASTM A307A or F1554 Gr. 36 or SAE J429 Gr. 2	ASTM A123	FRR28a
d5	20	3/4"-10 UNC x 8" Threaded Rod (Existing Material)	ASTM A193 Gr. B7 or SAE J429 Gr. 5	ASTM A123	FRR20a
d6	60	3/4"-4 1/2 x 13" Lag Bolt (Existing Material)	ASTM A307A	ASTM A123	FBL20
d7	8	3/4"-10 UNC x 10" Timber Bolt w/ Nubs	ASTM A307A	ASTM A123	FBB08
d8	8	7/8"-9 UNC x 28" Timber Bolt w/ Nubs	ASTM A307A	ASTM A123	FBB08
d9	16	5/8"-11 UNC x 14" Timber Bolt w/ Nubs (Existing Material)	ASTM A307A	ASTM A123	FBB08

Notes: (1) Timber rails, posts, scuppers, and blockouts shall be treated with Copper Naphthenate (CuN) or 4,5-Dichloro-2-N-Octyl-4-Isothiazolin-3-One (DCOI) in heavy oil to a minimum retention of 0.075 lbs/cu. ft. or 0.20 lbs/cu. ft. respectively in accordance with AWPA Standard U1 to the requirements. Use category 4B (UC4B).
(2) Wood shall be cut, drilled, and completely fabricated prior to treatment with preservative. Drain excess chemicals and dry all treated wood at the place of manufacture.
(3) All field cuts, bore holes, and damages shall be treated with material acceptable to the engineer prior to installation.

Midwest Roadside Safety Facility

TL-4 Glulam Timber Rail on Transverse Glulam Deck – TRTD-3D

Bill of Materials

SHEET: 23 of 24
DATE: 3/13/2025
DRAWN BY: MM/MSW
REV. BY: AML/JJO
DWG. NAME. TRTD-3D_R2
SCALE: 1:96
UNITS: in.

Figure 273: Test No. TRTD-3 Bill of Material, Page 2

Item No.	QTY.	Description	Material Specification	Treatment Specification	Hardware Guide
e1	10	7/8" Dia. Malleable Iron Washer	ASTM A47	ASTM A123	–
e2	24	3/4" Dia. Malleable Iron Washer	ASTM A47	ASTM A123	–
e3	94	3/4" Flat Washer (Existing Material)	ASTM F844	ASTM A123 or A153 or F2329	FWC20a
e4	1	6"x6"x3/8" Steel Plate Washer (existing material)	ASTM A36	ASTM A123	–
e5	1	8"x21"x3/8" Steel Plate Washer	ASTM A36	ASTM A123	–
e6	2	4"x20"x3/16" Steel Plate Washer	ASTM A36	ASTM A123	–
e7	14	5/8" Dia. Malleable Iron Washer	ASTM A47	ASTM A123	–
f1	10	7/8"–9 UNC Dia. Heavy Hex Nut	ASTM A563A	ASTM A123	FNX22b
f2	58	3/4"–10 UNC Dia. Heavy Hex Nut	ASTM A563A	ASTM A123	FNX20b
f3	1	1 3/8"–6 UNC Dia. Heavy Hex Nut	ASTM A563A	ASTM A123 or A153 or F2329	–
f4	16	5/8"–11 UNC Dia. Heavy Hex Nut	ASTM A563A	ASTM A123	FNX16b
g1	–	Epoxy Adhesive (Existing Material)	Hilti HIT RE–500 V3 or equivalent with min. bond strength 1,670 psi	–	–

Midwest Roadside Safety Facility

TL–4 Glulam Timber Rail on Transverse Glulam Deck – TRTD–3D

Bill of Materials

SHEET: 24 of 24
DATE: 3/13/2025
DRAWN BY: MM/MSW
REV. BY: AML/JJO
DWG. NAME. TRTD–3D_R2
SCALE: None
UNITS: in.

Figure 274: Test No. TRTD-3 Bill of Material, Page 3

Appendix O. Full Scale Crash Test Plans for TL-4 Bridge Railing and TL-3 AGT

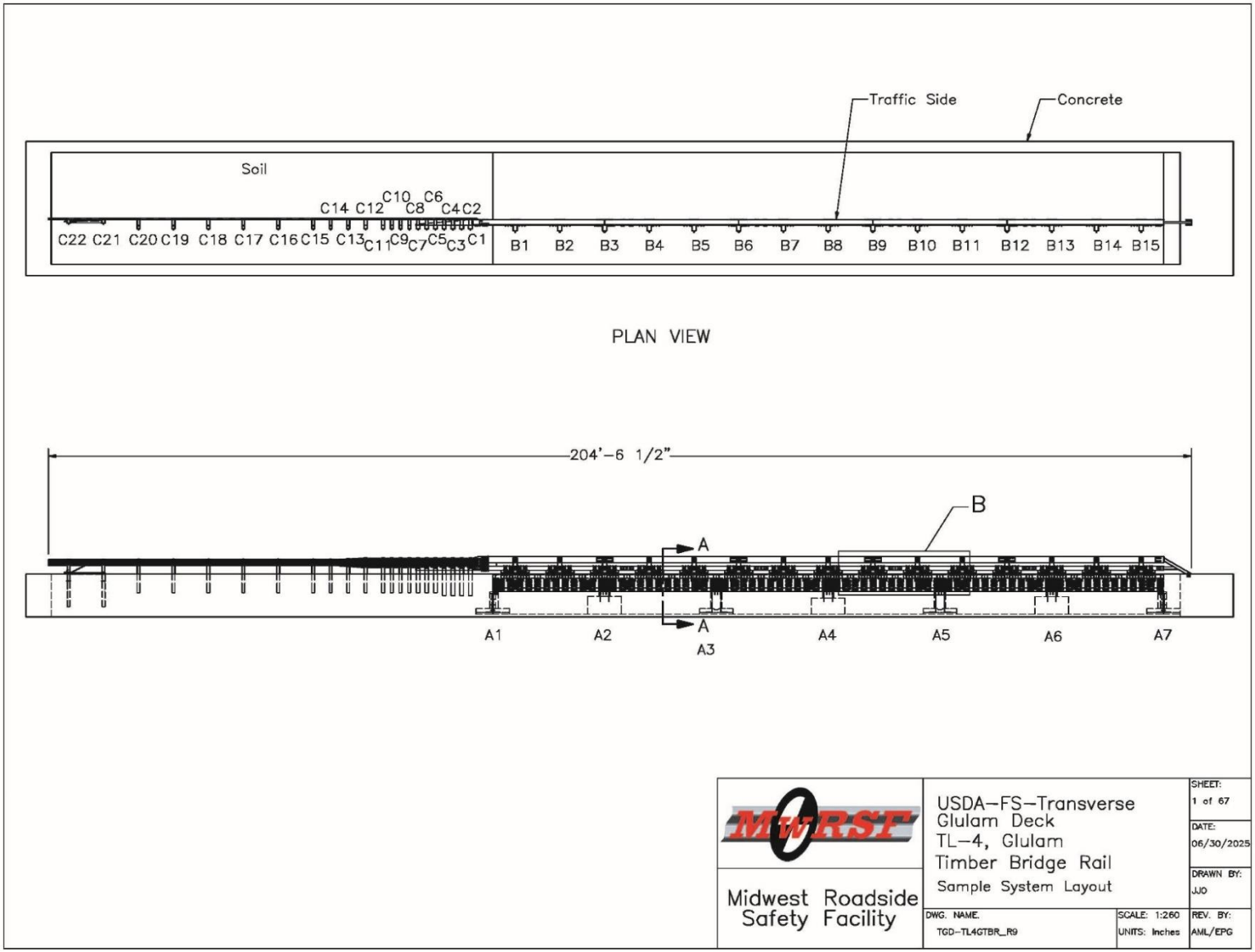

Figure O-1. Full-Scale Crash Test System Layout Plan and Elevation Views

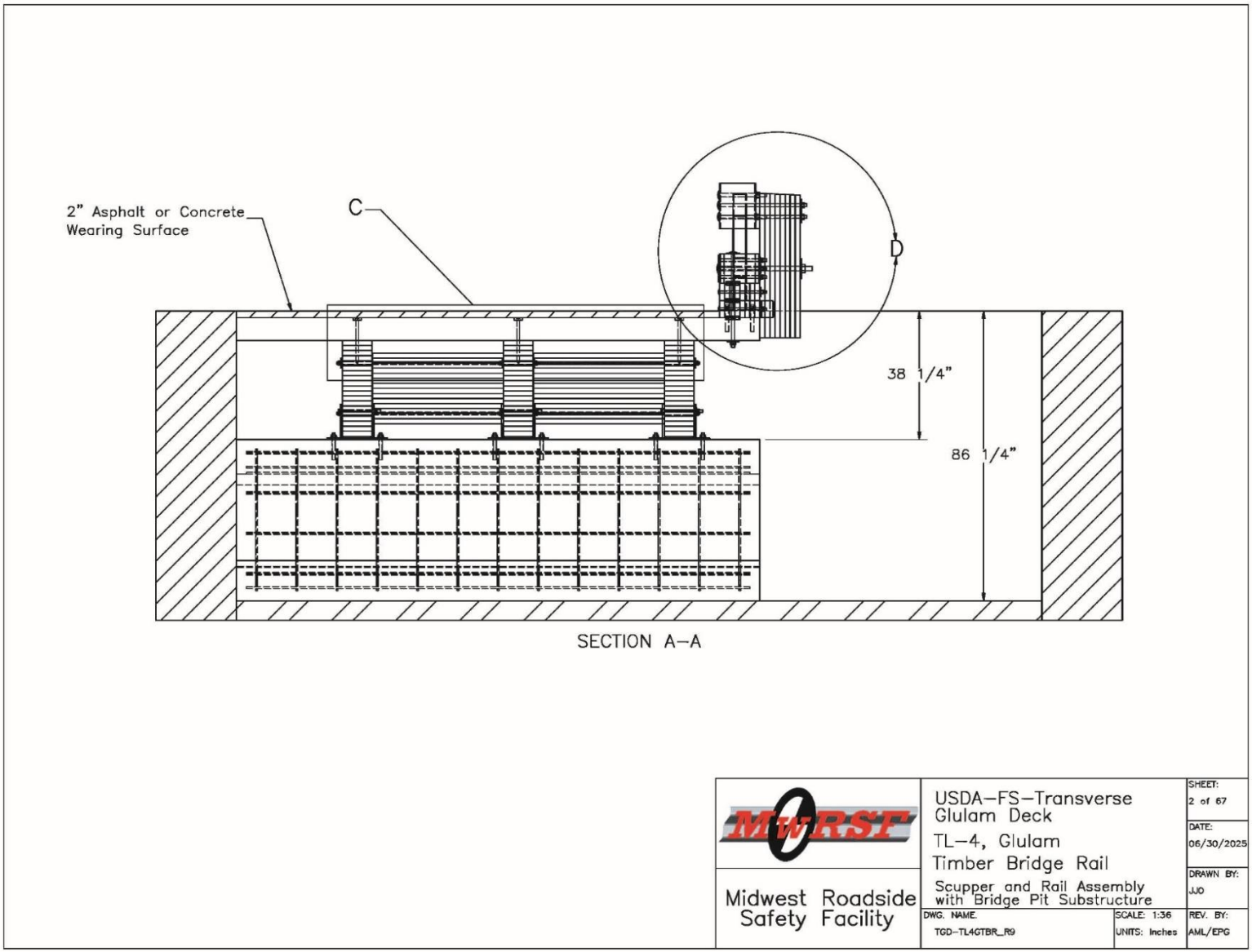

Figure O-2. Full-Scale Crash Test System Cross-Section View

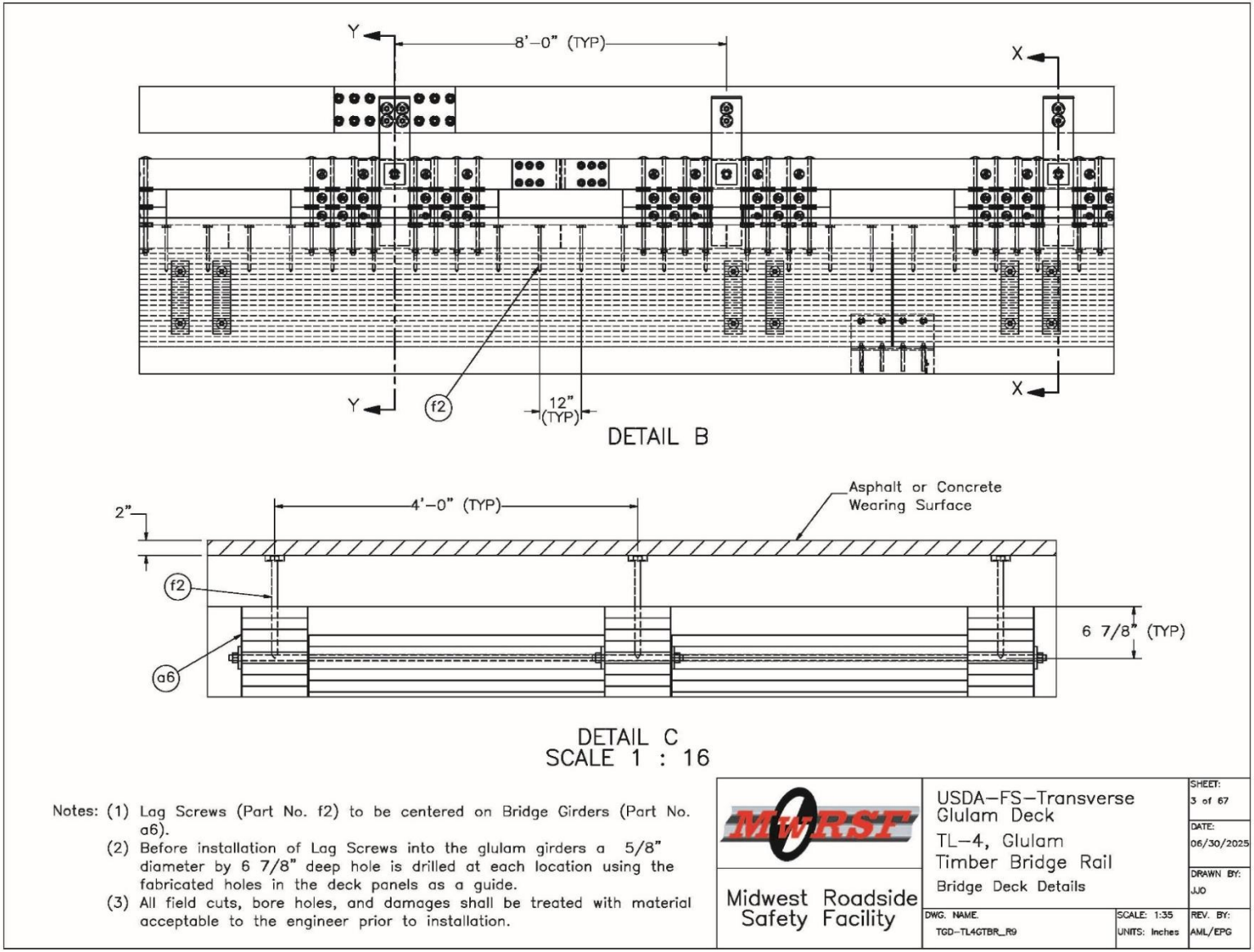

Figure O-3. Full-Scale Bridge System Superstructure Details

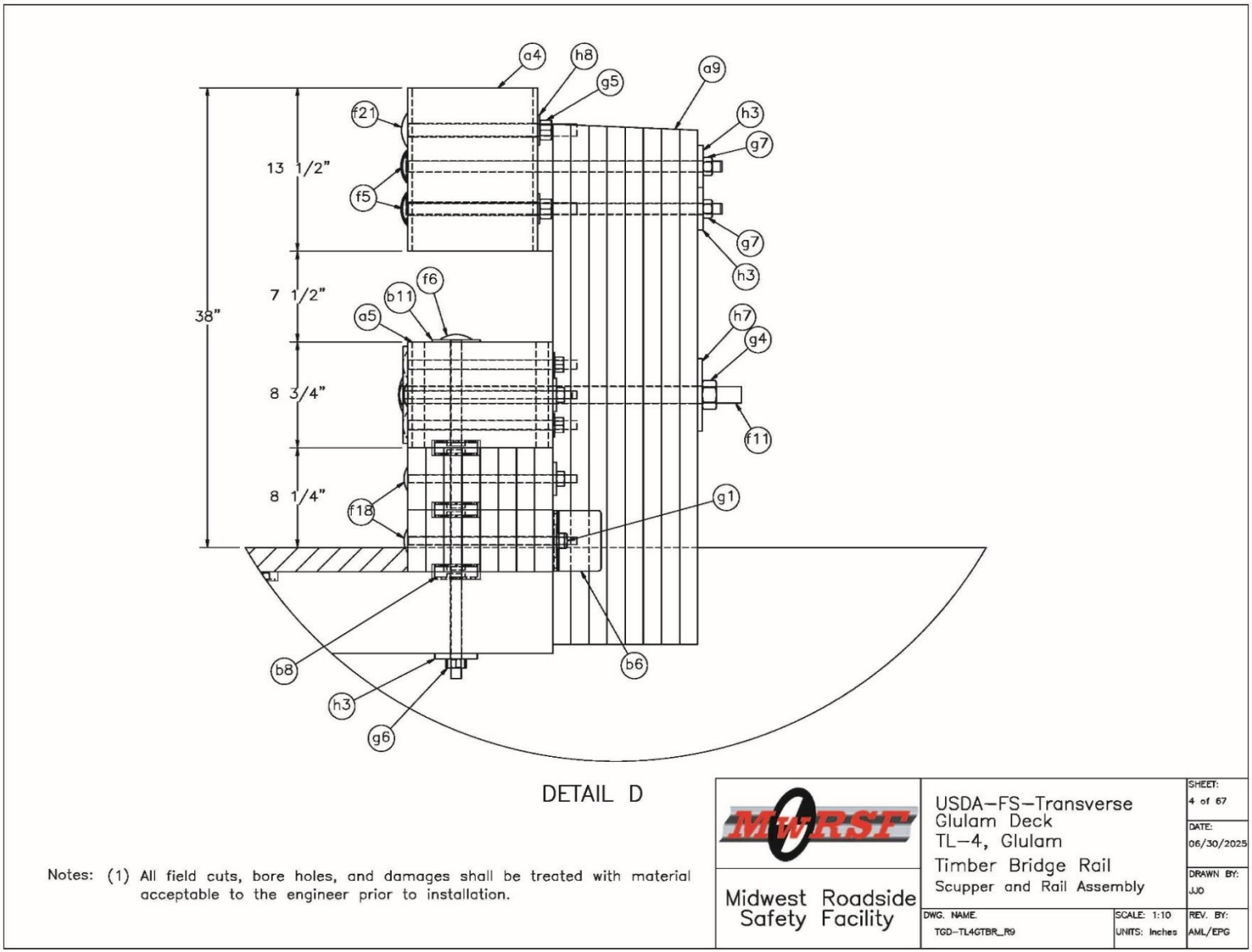

Figure O-4. Bridge Railing Assembly Cross-Section View

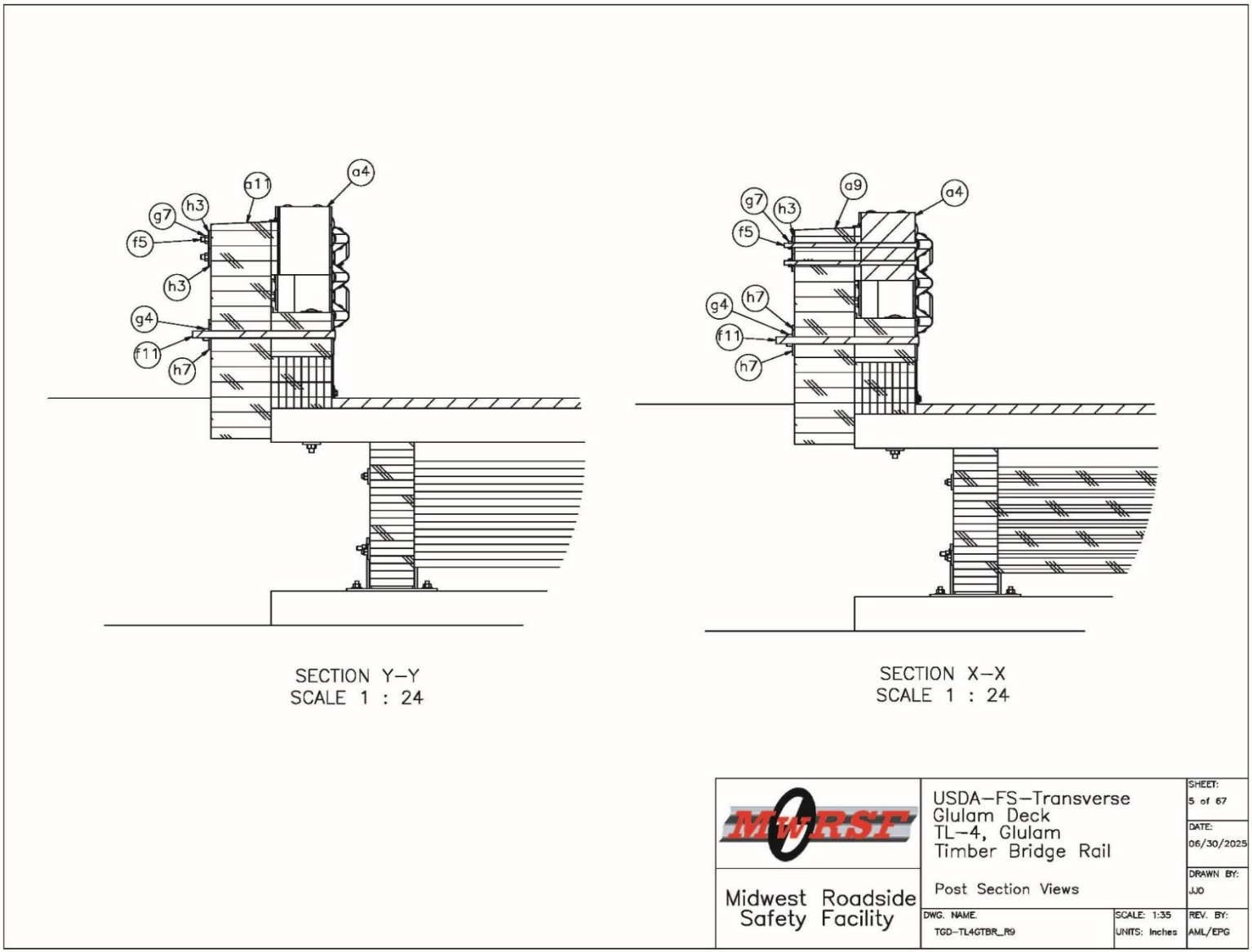

Figure O-5. Post Cross-Section View at Upper Railing Splice and at Typical Post Locations

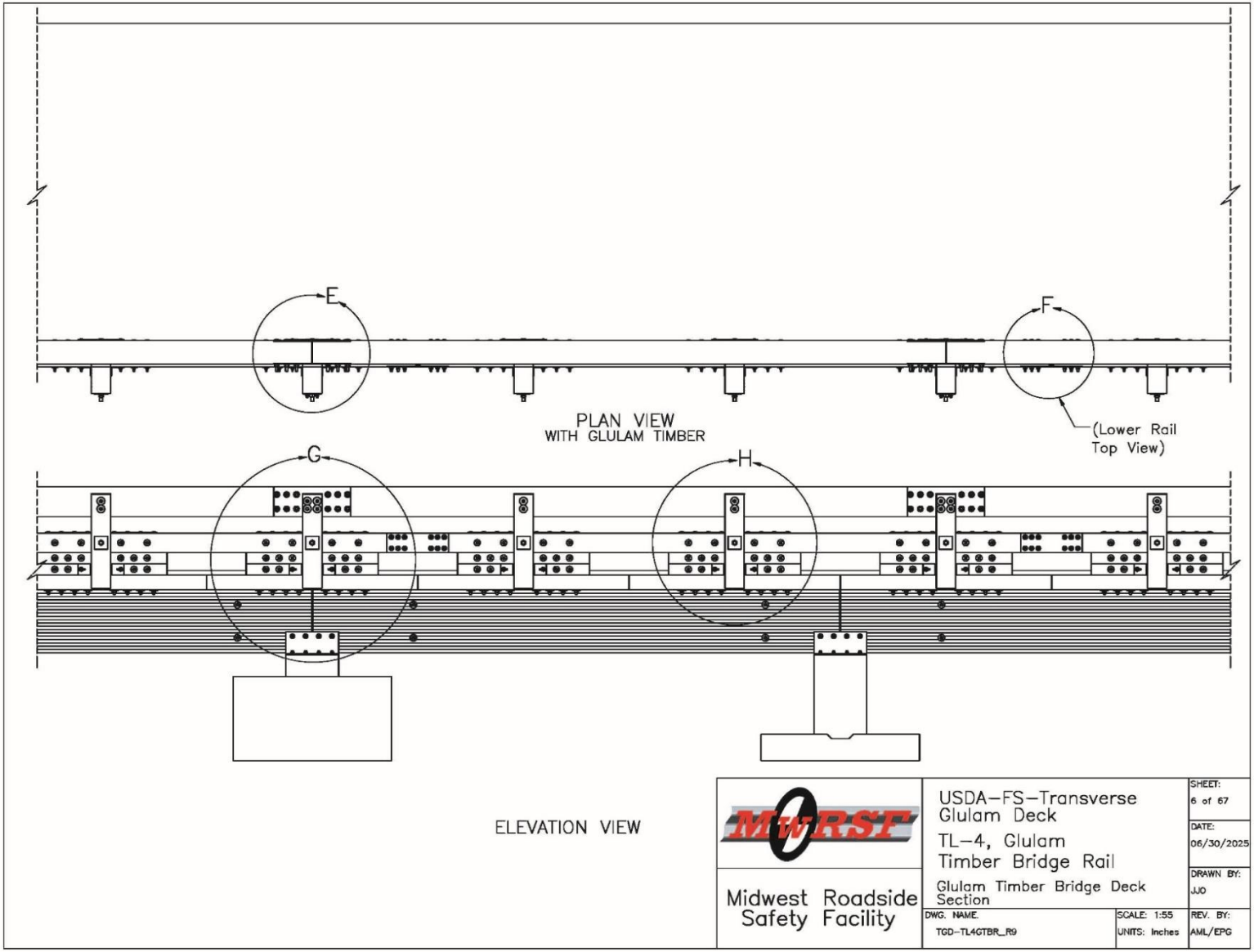

Figure O-6. System Plan and Elevation View of Upper and Curb Rail Splice Locations

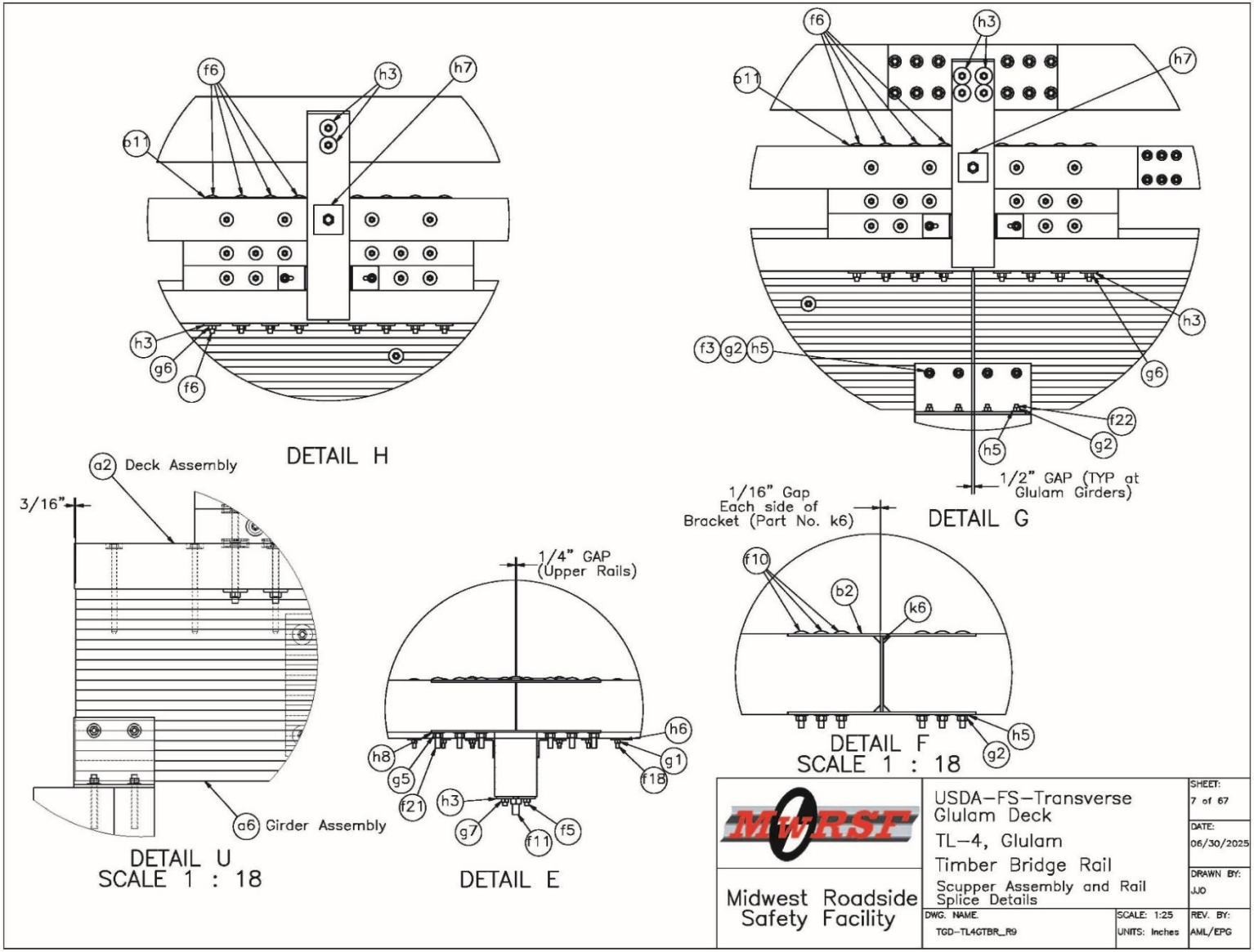

Figure O-7. System Details for Scupper and Rail Splice Assemblies

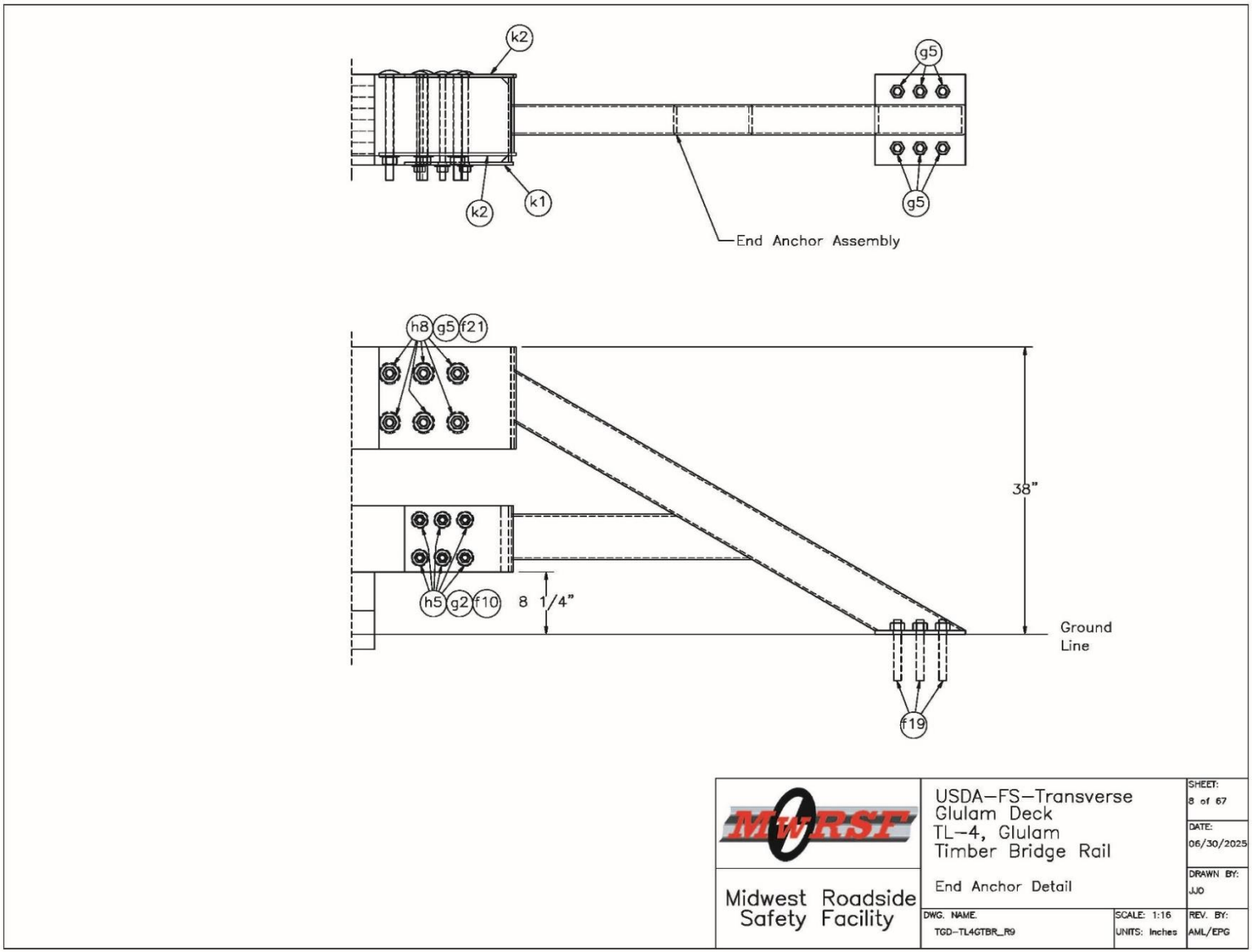

Figure O-8. Bridge Railing End Anchor Detail

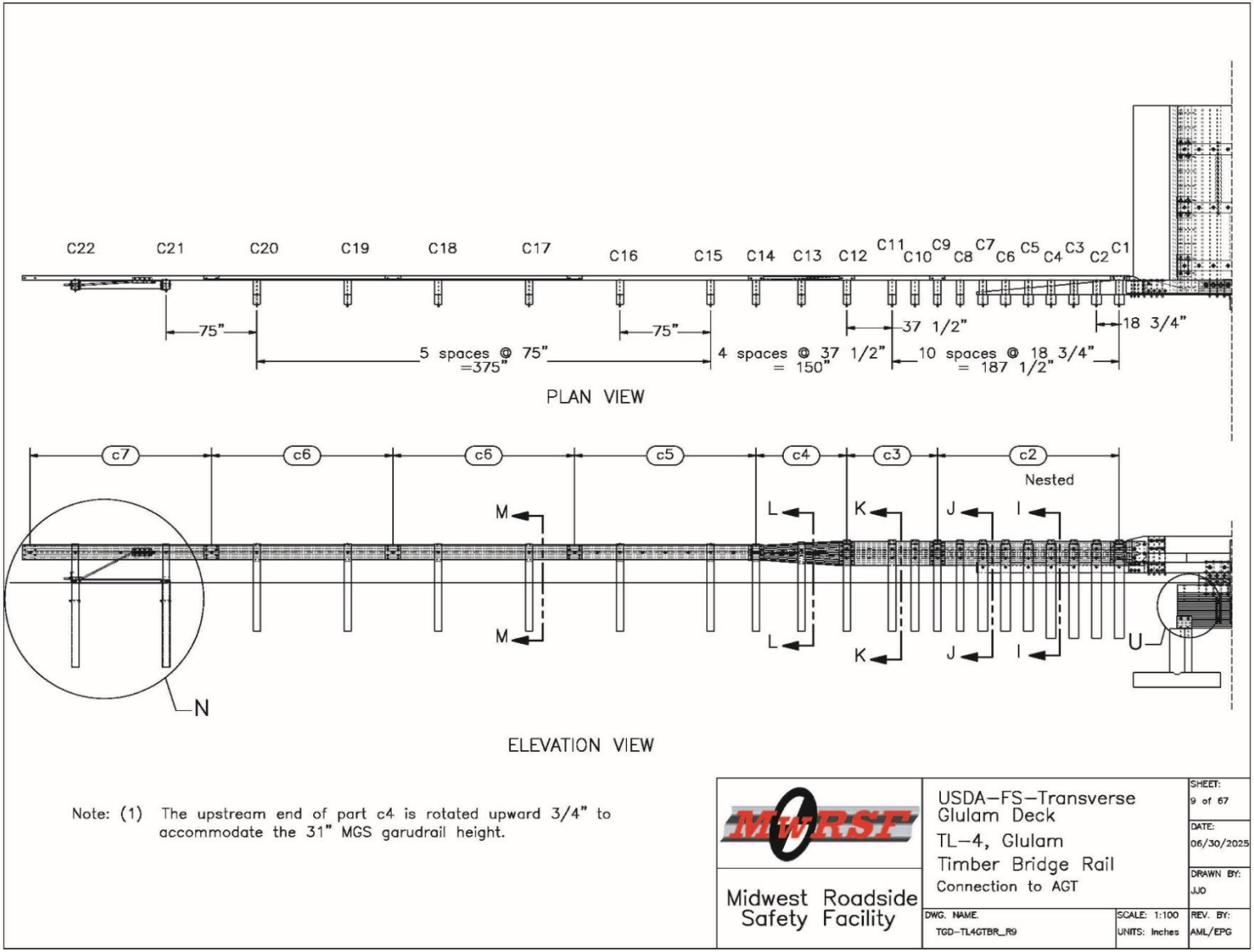

Figure O-9. Plan and Elevation View of AGT

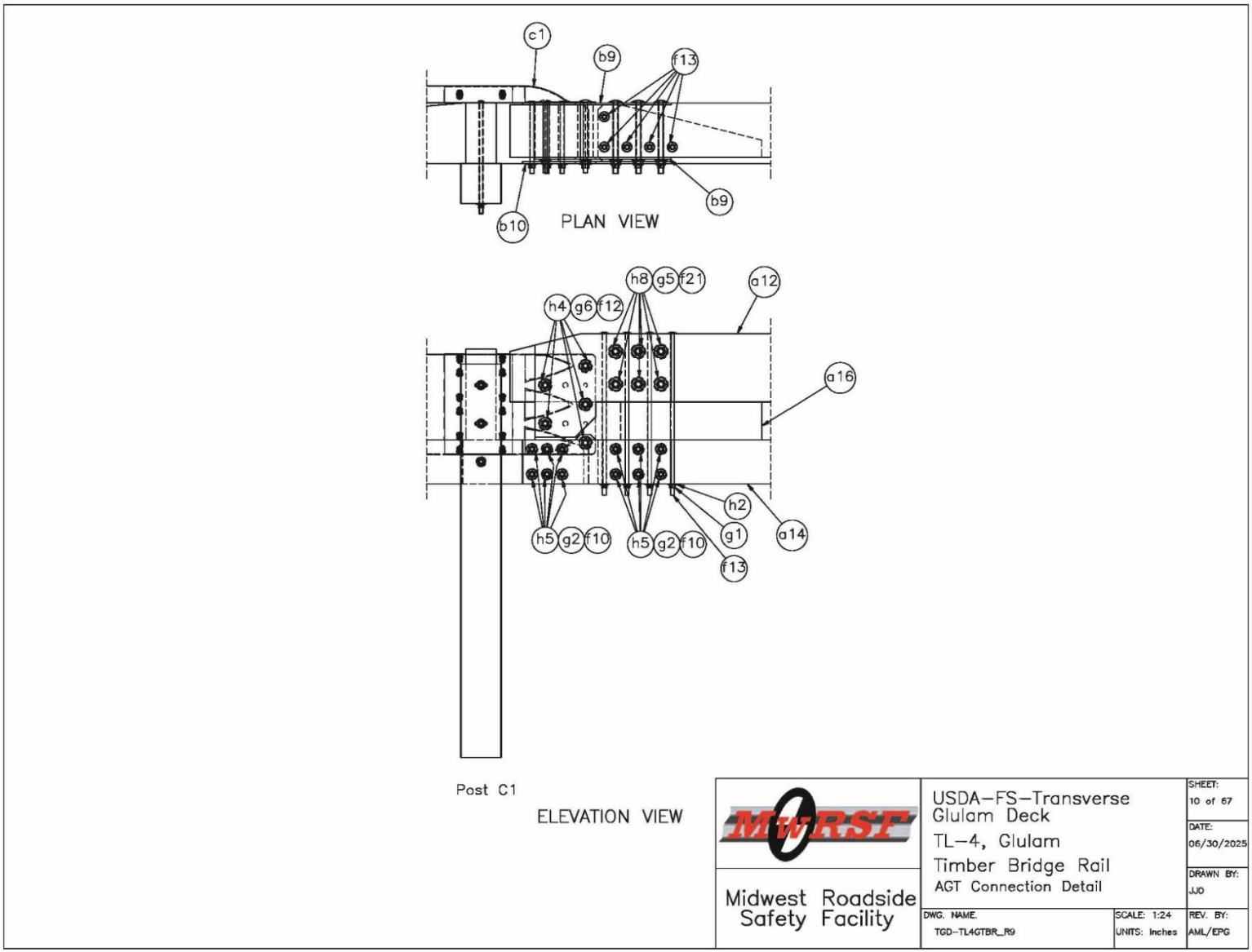

Figure O-10. AGT System Connection to Bridge Railing Detail

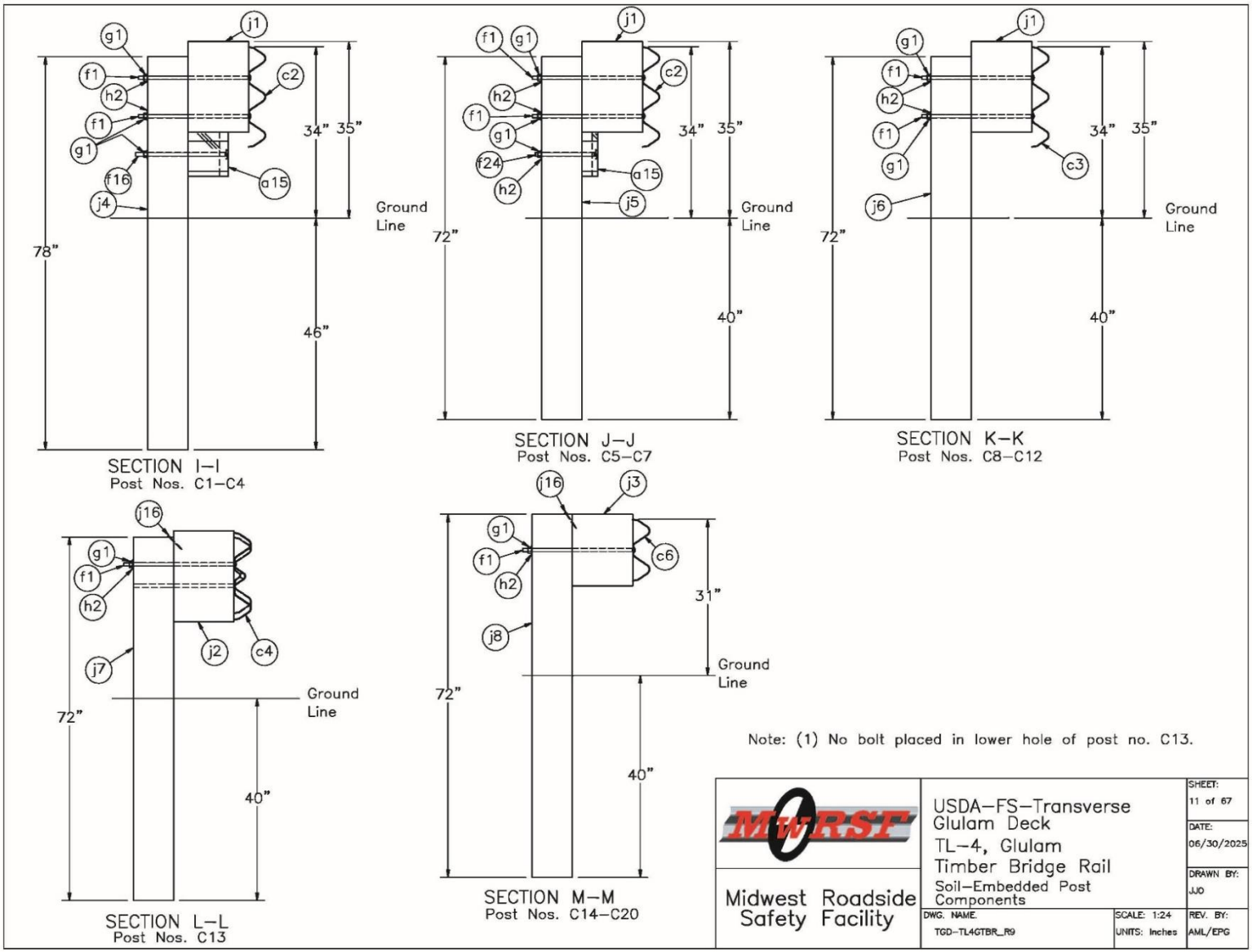

Figure O-11. AGT Post Cross-Section Views

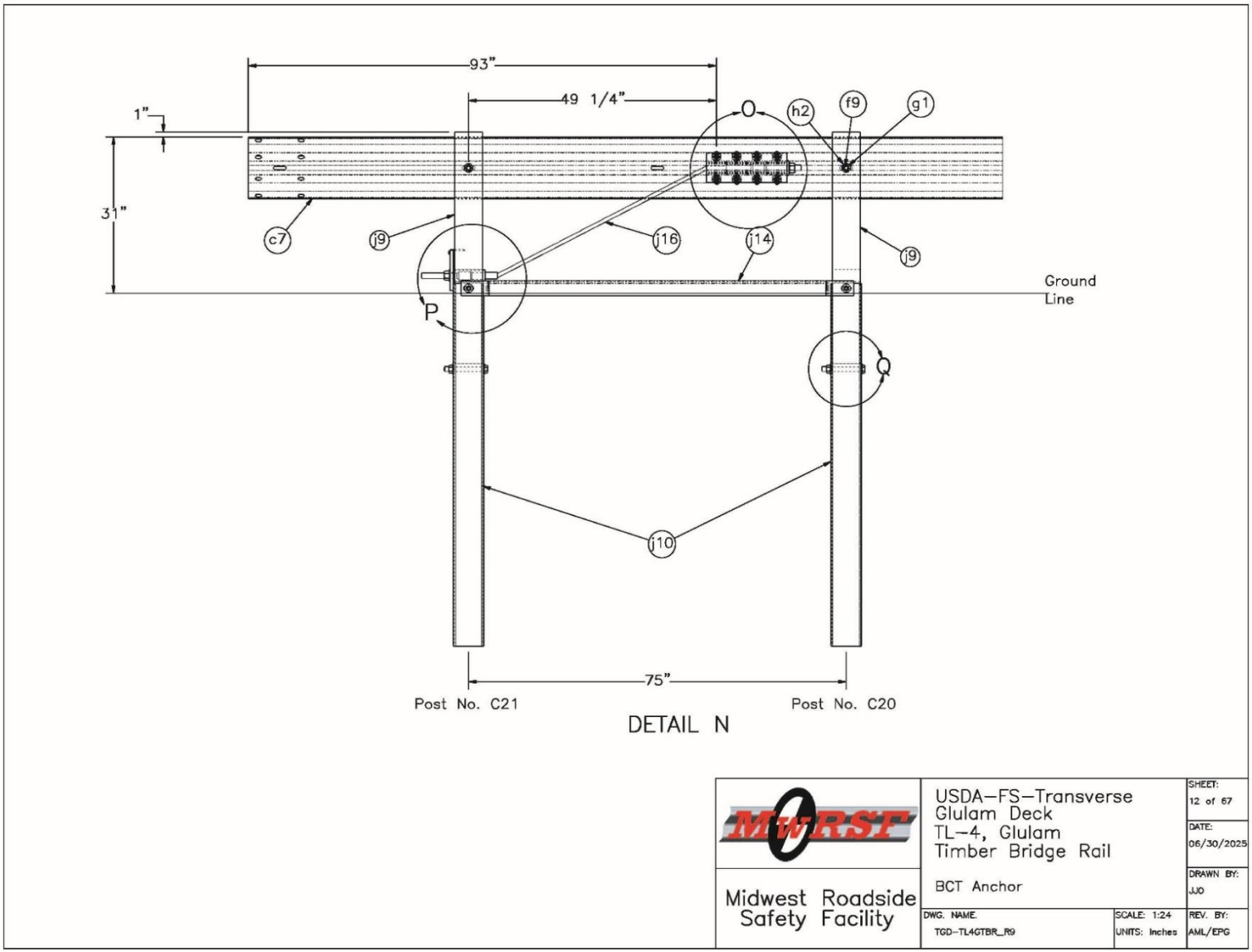

Figure O-12. AGT BCT End Anchor Elevation View

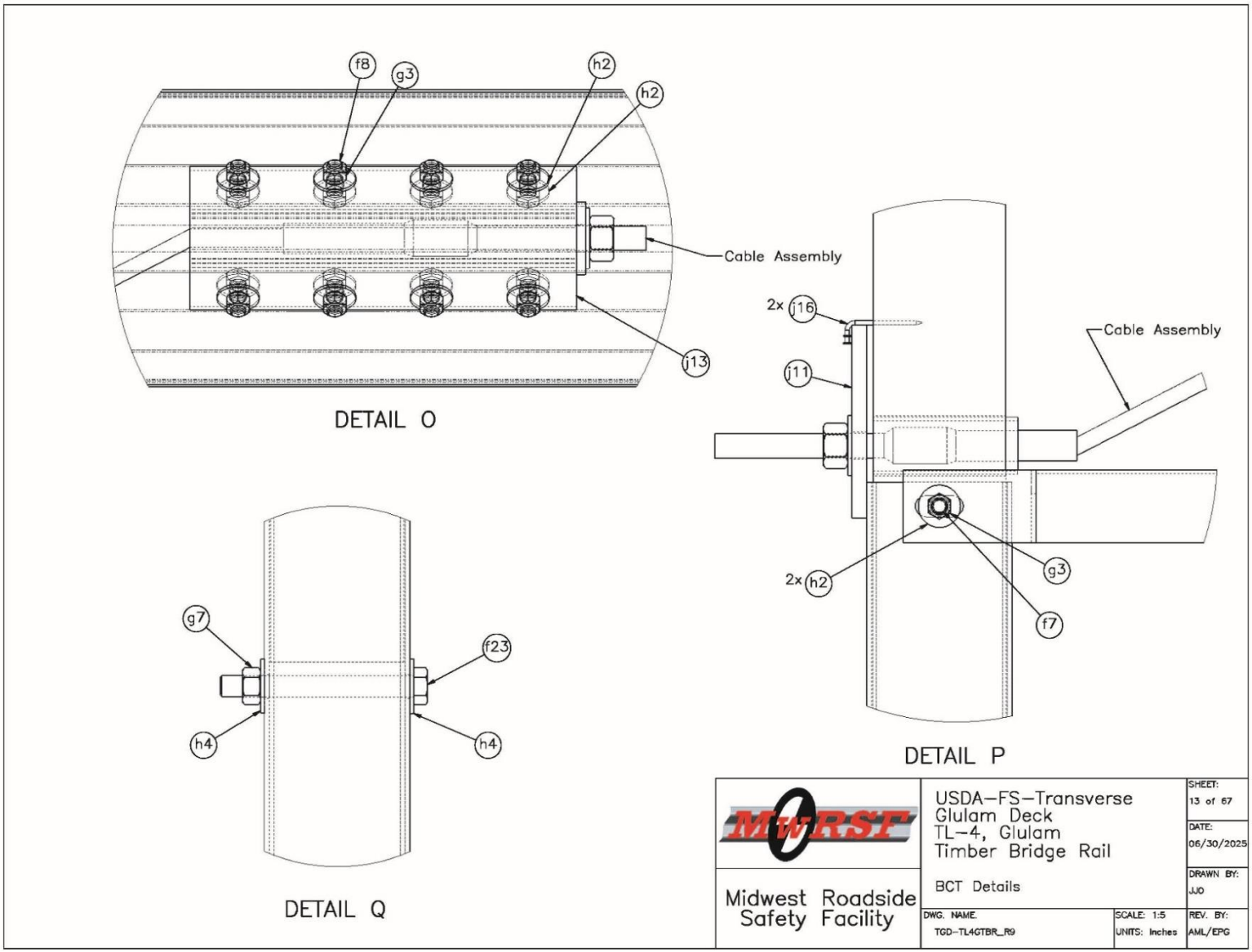

Figure O-13. AGT BCT End Anchor Component Details

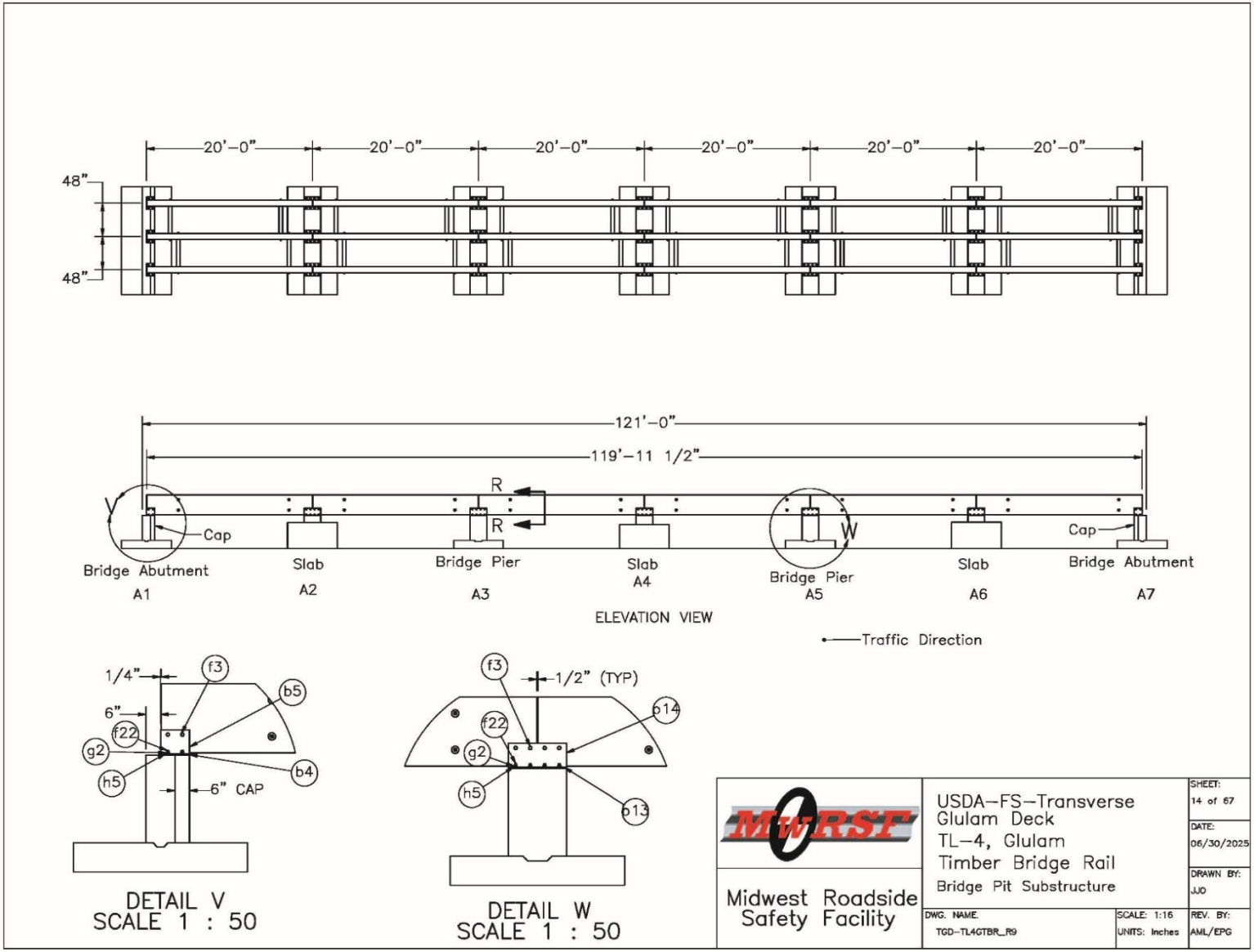

Figure O-14. Bridge Pit Substructure Plan and Elevation Views and Details

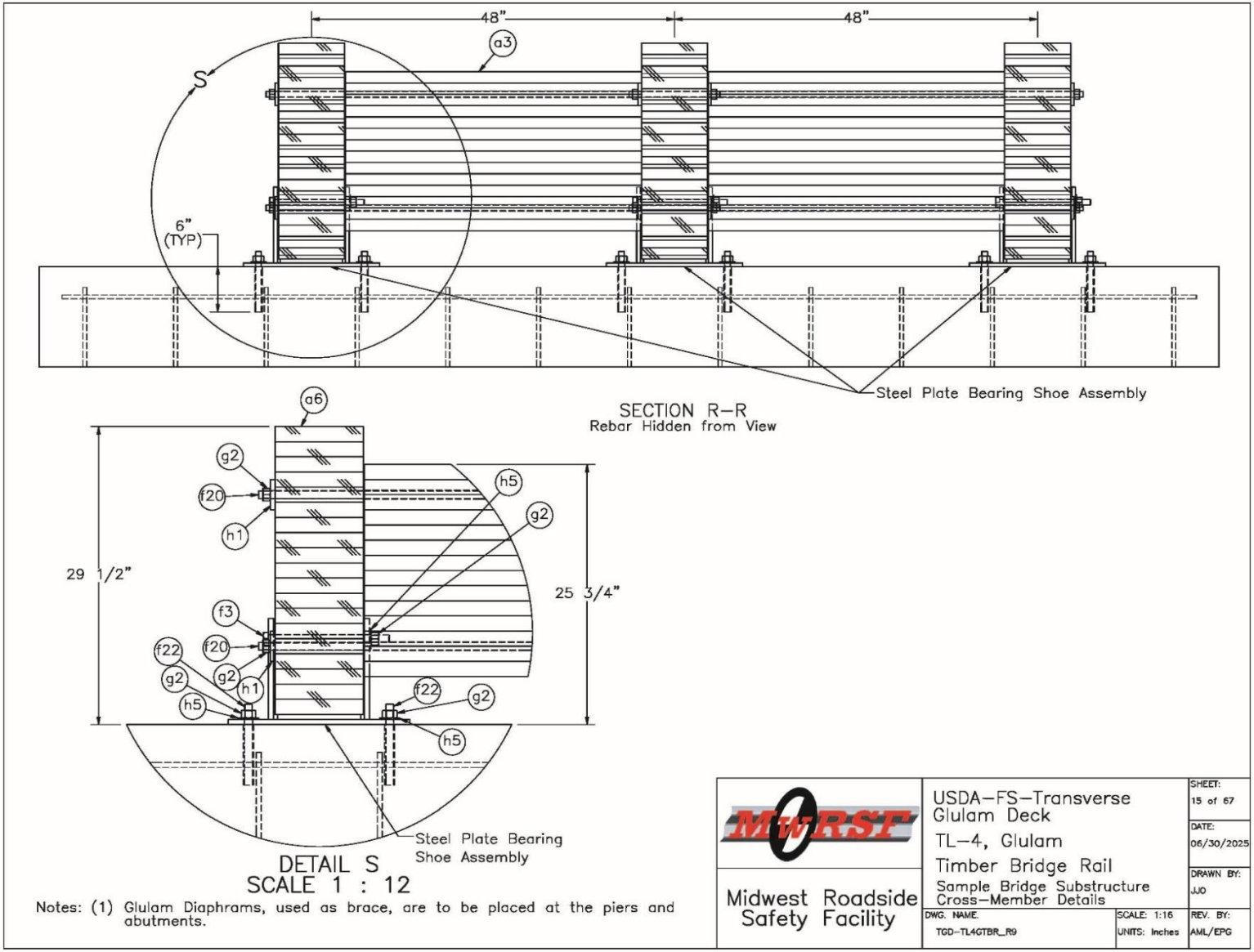

Figure O-15. Bridge Superstructure and Bearing Connection Details

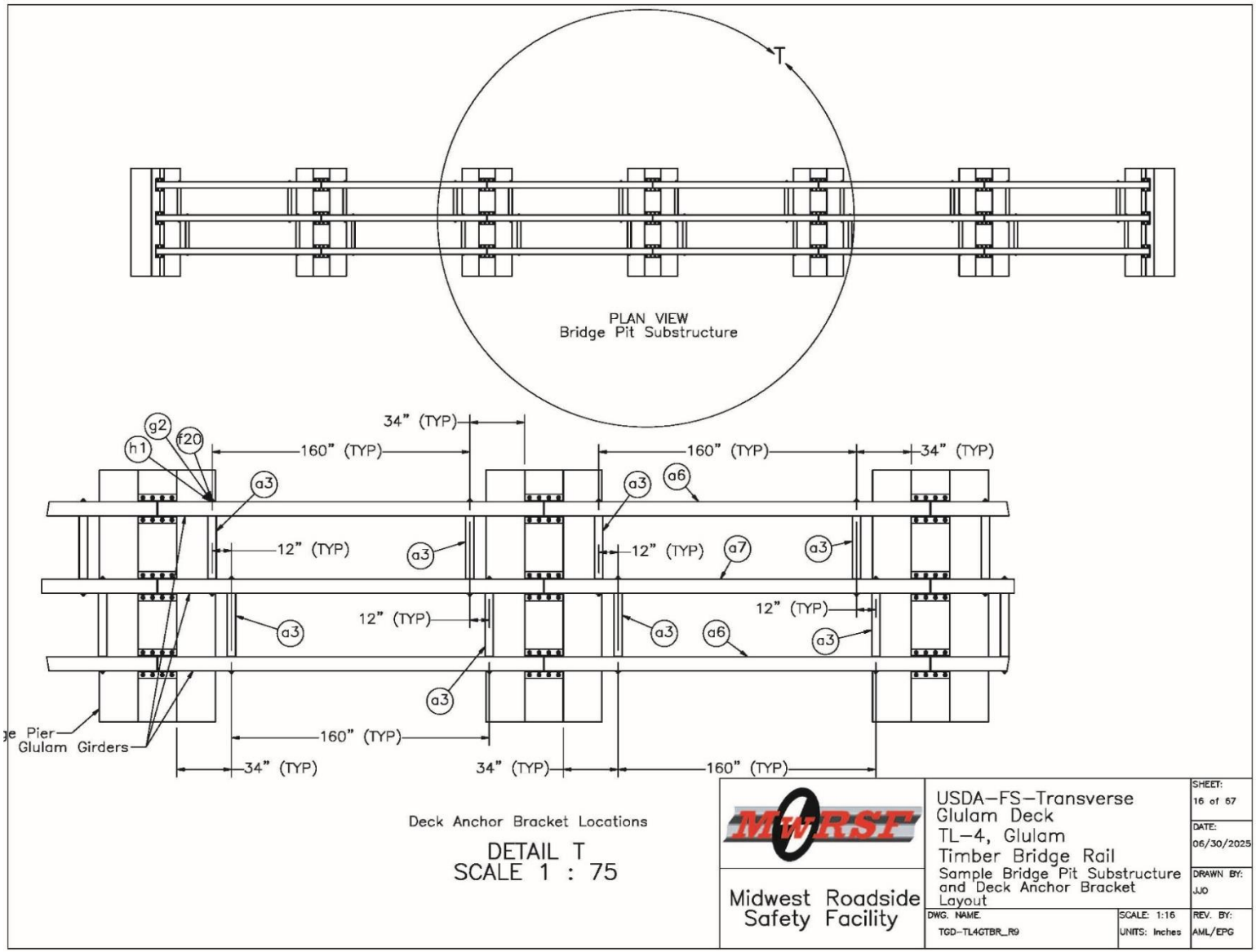

Figure O-16. Bridge Pit Typical Substructure Span Details

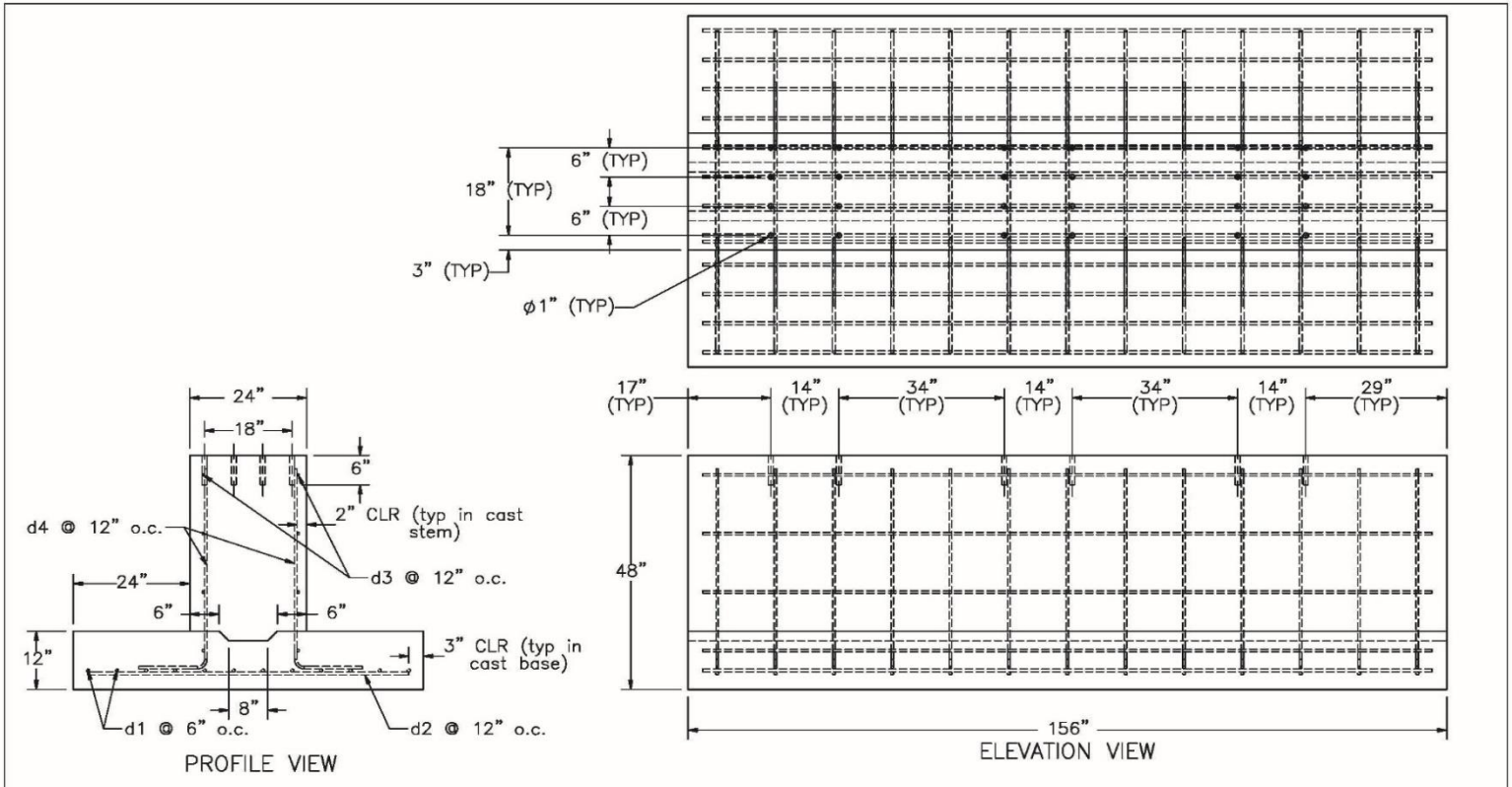

* rebar does not need to be epoxy–coated for testing purposes.

Item No.	QTY.	Description	Material Specification	Treatment Specification
–	2	Pier Assembly	–	–
d1	12	#5 Rebar, 12'–6" Total Length	ASTM A615 Gr. 60	*Epoxy Coated (ASTM A775 or A934)
d2	13	#5 Rebar, 5'–6" Total Length	ASTM A615 Gr. 60	*Epoxy Coated (ASTM A775 or A934)
d3	8	#4 Rebar, 12'–6" Total Length	ASTM A615 Gr. 60	*Epoxy Coated (ASTM A775 or A934)
d4	26	#4 Bent Rebar, 54" Total Length	ASTM A615 Gr. 60	*Epoxy Coated (ASTM A775 or A934)
e1	1	Pier Concrete	Min f'c = 4,000 psi	–

Notes: (1) Pier Concrete to be poured in two sections, base and then pillar.

Midwest Roadside Safety Facility

USDA–FS–Transverse Glulam Deck
TL–4, Glulam Timber Bridge Rail
Sample Bridge Pier Details (Laboratory Specimens Only)

DWG. NAME. TGD–TL4GTBR_R9 | SCALE: 1:50 | UNITS: Inches

SHEET: 17 of 67
DATE: 06/30/2025
DRAWN BY: JJO
REV. BY: AML/EPG

Figure O-17. Bridge Substructure Typical Pier Details

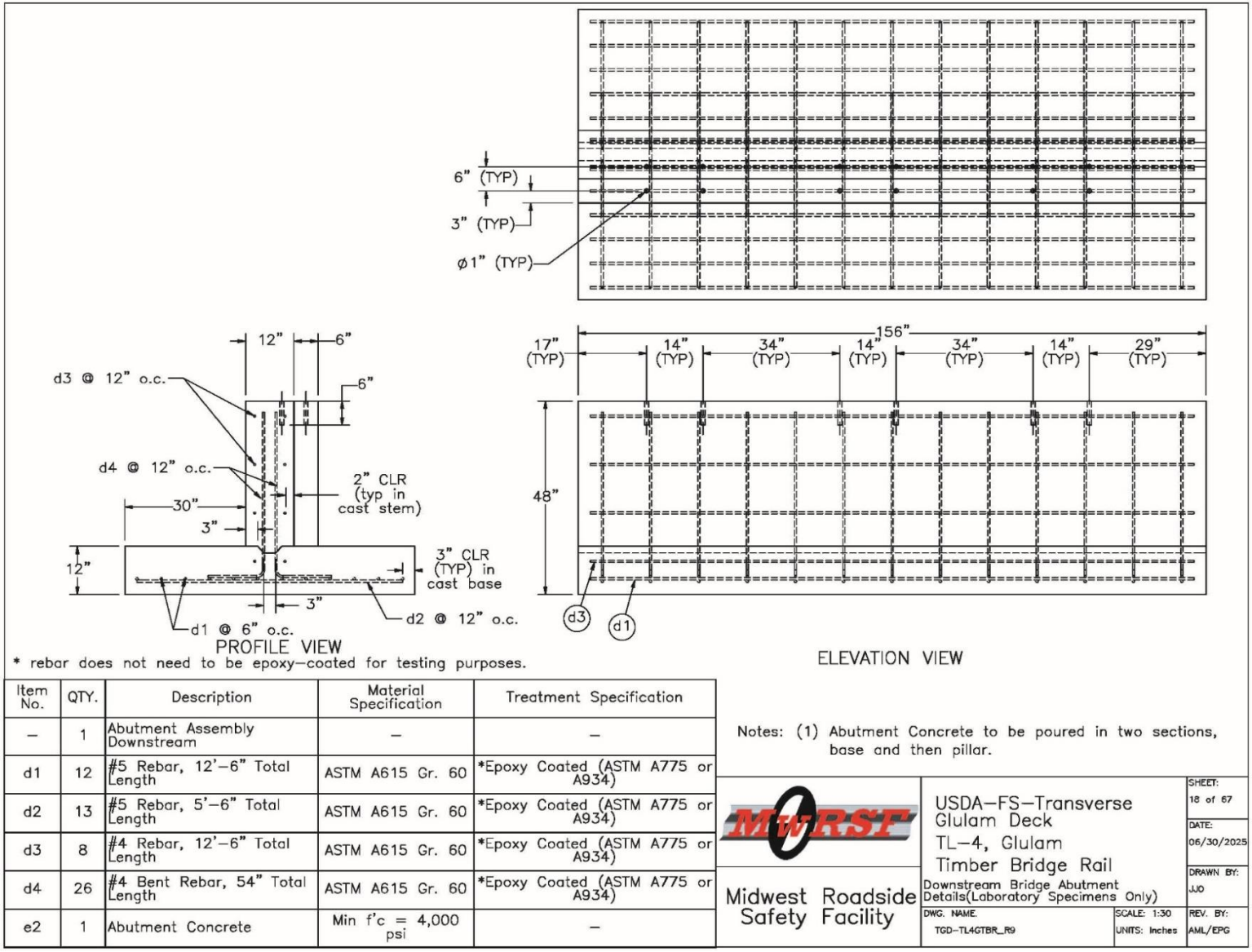

* rebar does not need to be epoxy-coated for testing purposes.

Item No.	QTY.	Description	Material Specification	Treatment Specification
–	1	Abutment Assembly Downstream	–	–
d1	12	#5 Rebar, 12'-6" Total Length	ASTM A615 Gr. 60	*Epoxy Coated (ASTM A775 or A934)
d2	13	#5 Rebar, 5'-6" Total Length	ASTM A615 Gr. 60	*Epoxy Coated (ASTM A775 or A934)
d3	8	#4 Rebar, 12'-6" Total Length	ASTM A615 Gr. 60	*Epoxy Coated (ASTM A775 or A934)
d4	26	#4 Bent Rebar, 54" Total Length	ASTM A615 Gr. 60	*Epoxy Coated (ASTM A775 or A934)
e2	1	Abutment Concrete	Min f'c = 4,000 psi	–

Notes: (1) Abutment Concrete to be poured in two sections, base and then pillar.

Midwest Roadside Safety Facility

USDA-FS-Transverse Glulam Deck
TL-4, Glulam Timber Bridge Rail
Downstream Bridge Abutment Details(Laboratory Specimens Only)

SHEET: 18 of 67
DATE: 06/30/2025
DRAWN BY: JJO
REV. BY: AML/EPG
DWG. NAME: TGD-TL4GTBR_R9
SCALE: 1:30
UNITS: Inches

Figure O-18. Bridge Substructure North Abutment Details

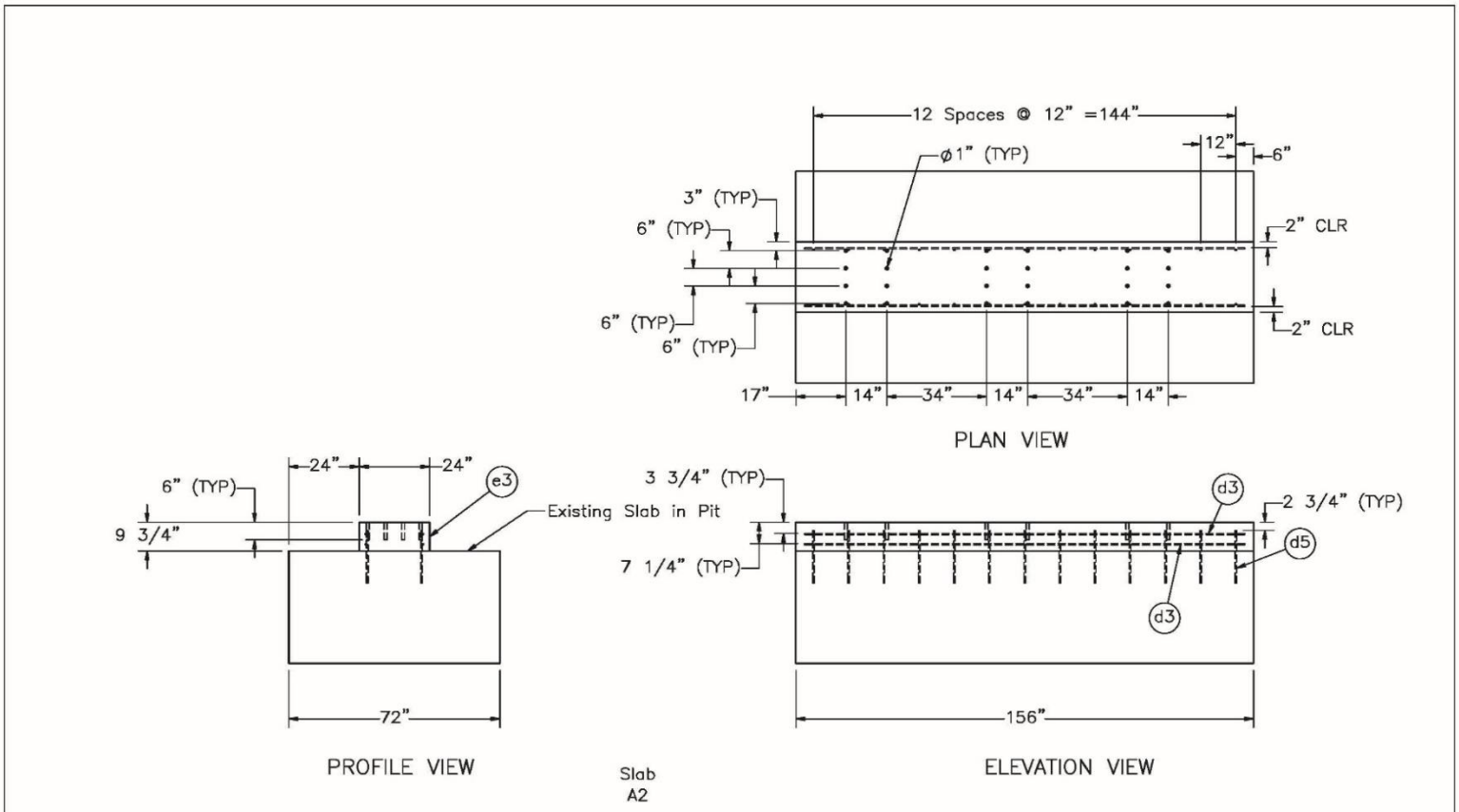

Note: Install vertical Rebar part no. d5 as shown anchored into existing slab A2 with chemical epoxy adhesive with a minimum bond strength of 1,450 psi.

Item No.	QTY.	Description	Material Specification	Treatment Specification
–	1	Slab and Cap A2	–	–
d3	4	#4 Rebar, 12'–6" Total Length	ASTM A615 Gr. 60	*Epoxy Coated (ASTM A775 or A934)
d5	26	#4 Rebar, 18" Total Length	ASTM A615 Gr. 60	*Epoxy Coated (ASTM A775 or A934)
e3	1	Cap A2 Concrete	Min f'c = 4,000 psi	–

Midwest Roadside Safety Facility

USDA–FS–Transverse Glulam Deck TL–4, Glulam Timber Bridge Rail

Slab and Cap A2

DWG. NAME. TGD–TL4GTBR_R9

SCALE: 1:48

UNITS: Inches

SHEET: 19 of 67

DATE: 06/30/2025

DRAWN BY: JJO

REV. BY: AML/EPG

Figure O-19. Bridge Substructure Intermittent Pier A2 Details

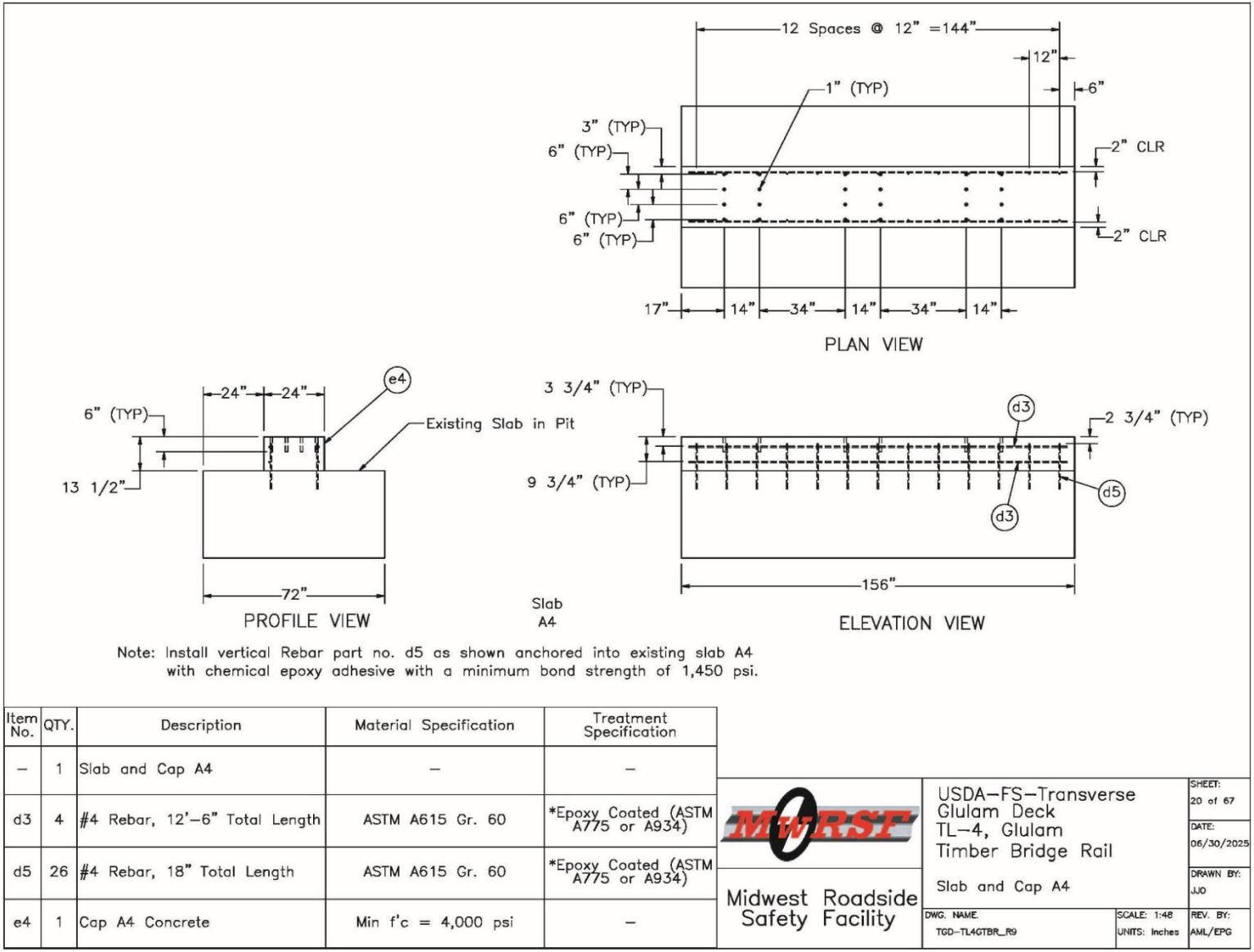

Item No.	QTY.	Description	Material Specification	Treatment Specification
–	1	Slab and Cap A4	–	–
d3	4	#4 Rebar, 12'–6" Total Length	ASTM A615 Gr. 60	*Epoxy Coated (ASTM A775 or A934)
d5	26	#4 Rebar, 18" Total Length	ASTM A615 Gr. 60	*Epoxy Coated (ASTM A775 or A934)
e4	1	Cap A4 Concrete	Min f'c = 4,000 psi	–

Midwest Roadside Safety Facility

USDA–FS–Transverse Glulam Deck TL–4, Glulam Timber Bridge Rail

Slab and Cap A4

DWG. NAME. TGD–TL4GTBR_R9 | SCALE: 1:48 | UNITS: Inches | REV. BY: AML/EPG | DRAWN BY: JJO | DATE: 06/30/2025 | SHEET: 20 of 67

Figure O-20. Bridge Substructure Intermittent Pier A4 Details

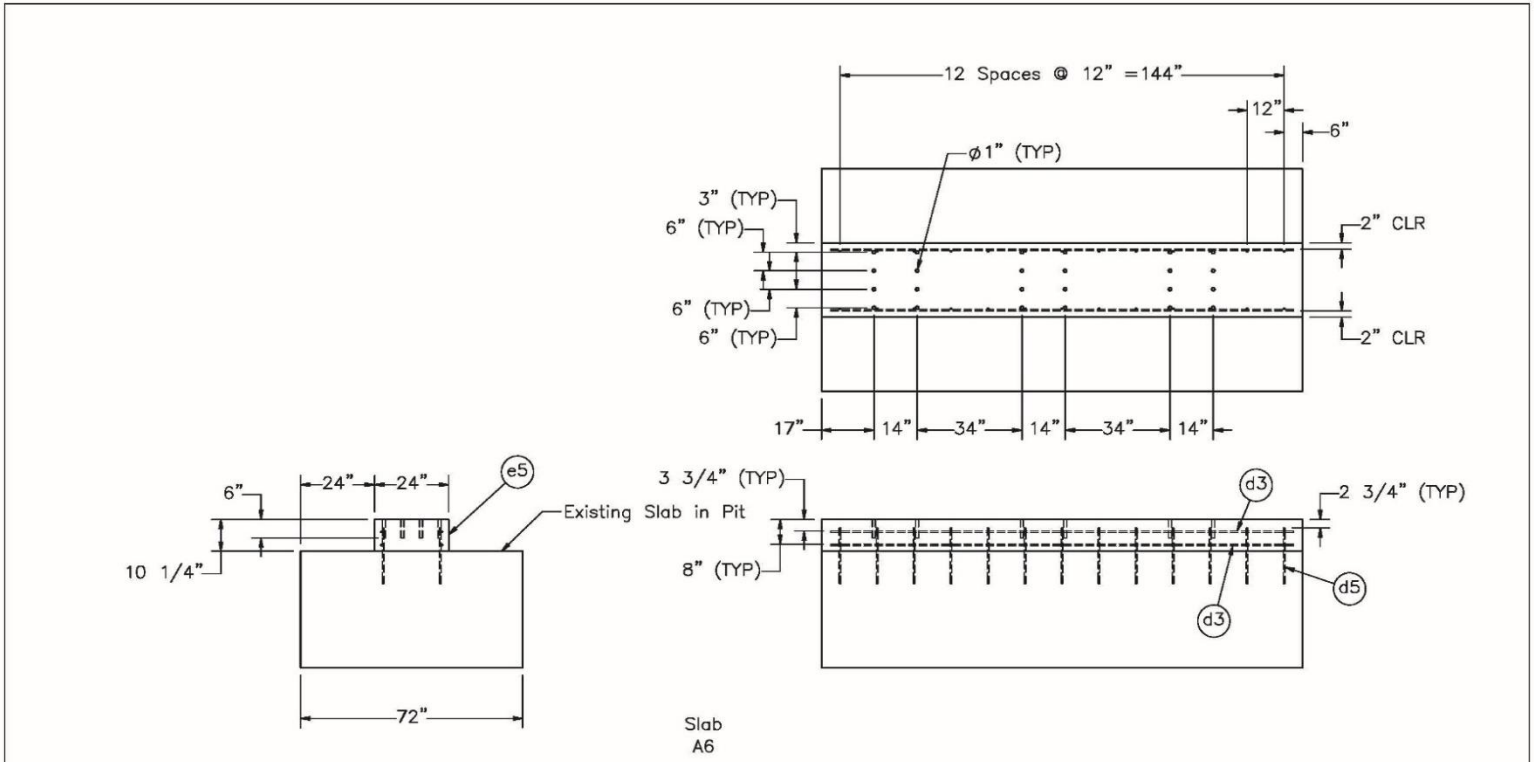

Note: Install vertical Rebar part no. d5 as shown anchored into existing slab A6 with chemical epoxy adhesive with a minimum bond strength of 1,450 psi.

Item No.	QTY.	Description	Material Specification	Treatment Specification
–	1	Slab and Cap A6	–	–
d3	4	#4 Rebar, 12'–6" Total Length	ASTM A615 Gr. 60	*Epoxy Coated (ASTM A775 or A934)
d5	26	#4 Rebar, 18" Total Length	ASTM A615 Gr. 60	*Epoxy Coated (ASTM A775 or A934)
e5	1	Cap A6 Concrete	Min f'c = 4,000 psi	–

Midwest Roadside Safety Facility

USDA–FS–Transverse Glulam Deck TL–4, Glulam Timber Bridge Rail

Slab and Cap A6

SHEET: 21 of 67
DATE: 06/30/2025
DRAWN BY: JJO
REV. BY: AML/EPG
DWG. NAME: TGD–TL4GTBR_R9
SCALE: 1:48
UNITS: Inches

Figure O-21. Bridge Substructure Intermittent Pier A6 Details

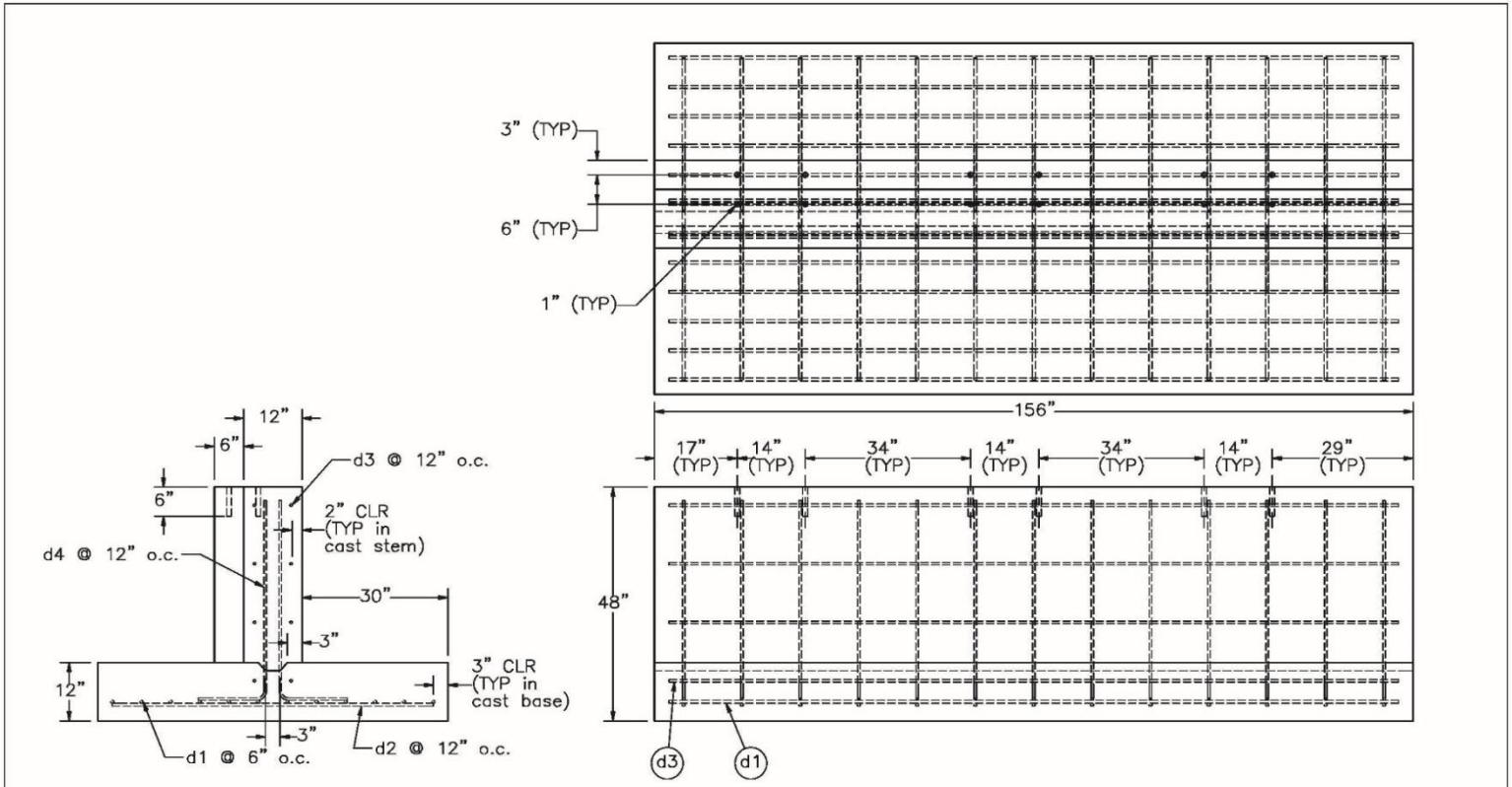

* rebar does not need to be epoxy–coated for testing purposes.

Item No.	QTY.	Description	Material Specification	Treatment Specification
–	1	Abutment Assembly Upstream	–	–
d1	12	#5 Rebar, 12'–6" Total Length	ASTM A615 Gr. 60	*Epoxy Coated (ASTM A775 or A934)
d2	13	#5 Rebar, 5'–6" Total Length	ASTM A615 Gr. 60	*Epoxy Coated (ASTM A775 or A934)
d3	8	#4 Rebar, 12'–6" Total Length	ASTM A615 Gr. 60	*Epoxy Coated (ASTM A775 or A934)
d4	26	#4 Bent Rebar, 54" Total Length	ASTM A615 Gr. 60	*Epoxy Coated (ASTM A775 or A934)
e2	1	Abutment Pillar	Min f'c = 4,000 psi	

Midwest Roadside Safety Facility

USDA–FS–Transverse Glulam Deck
TL–4, Glulam Timber Bridge Rail
Upstream Bridge Abutment Details(Laboratory Specimens Only)

DWG. NAME. TGD–TL4GTBR_R9 | SCALE: 1:30 | UNITS: Inches

SHEET: 22 of 67
DATE: 06/30/2025
DRAWN BY: JJO
REV. BY: AML/EPG

Figure O-22. Bridge Substructure South Abutment Details

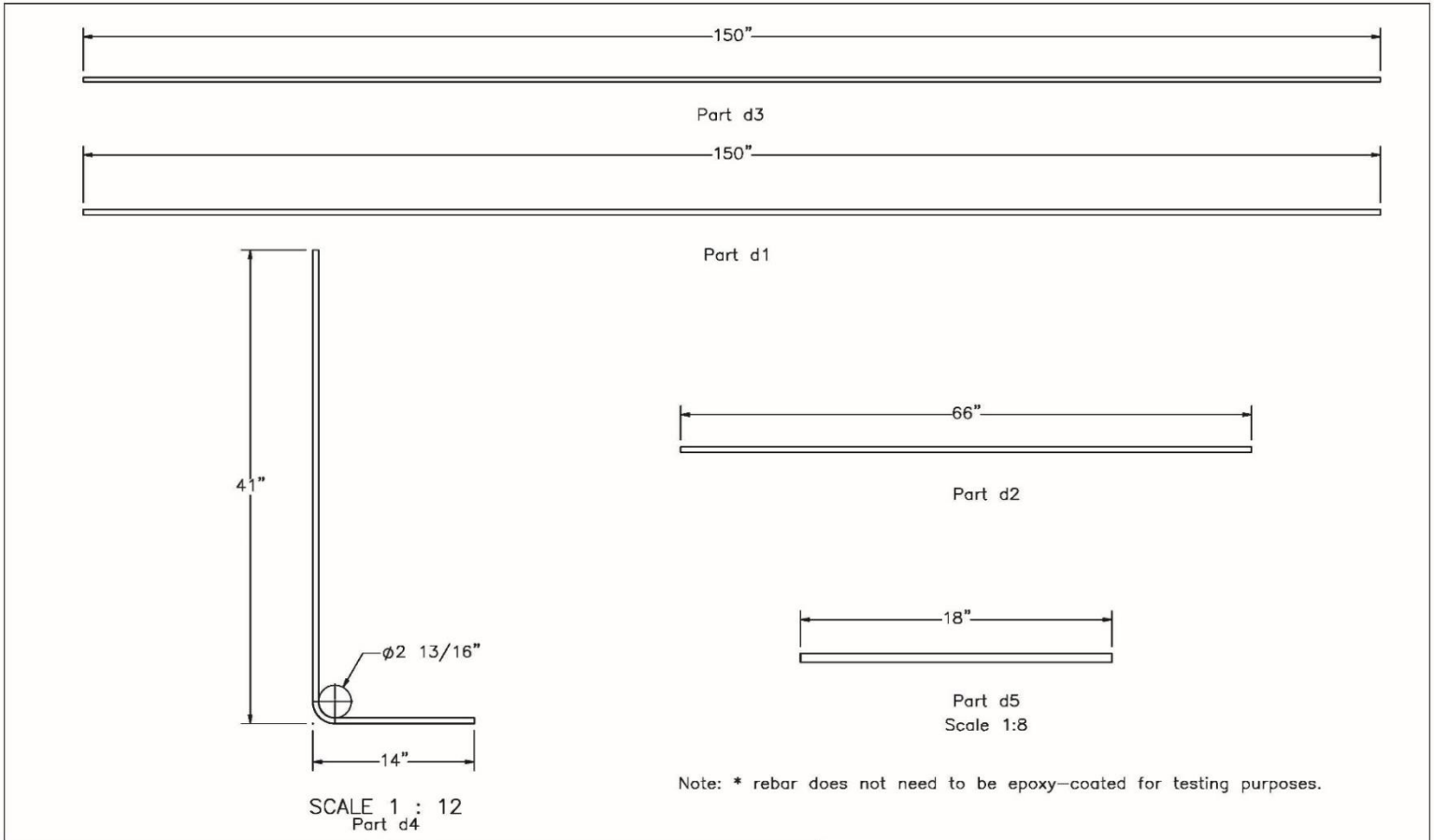

Bill of Bars

Bar	Qty.	Size	Total Length	Material Specifications	Treatment Spaecifcatons
d1	48	#5	150"	ASTM A615 Gr. 60	*Epoxy Coated (ASTM A775 or A934)
d2	52	#5	66"	ASTM A615 Gr. 60	*Epoxy Coated (ASTM A775 or A934)
d3	44	#4	150"	ASTM A615 Gr. 60	*Epoxy Coated (ASTM A775 or A934)
d4	104	#4	54"	ASTM A615 Gr. 60	*Epoxy Coated (ASTM A775 or A934)
d5	78	#4	18"	ASTM A615 Gr. 60	*Epoxy Coated (ASTM A775 or A934)

Midwest Roadside Safety Facility

USDA–FS–Transverse Glulam Deck
TL–4, Glulam
Timber Bridge Rail
Rebar Details

SHEET: 23 of 67
DATE: 06/30/2025
DRAWN BY: JJO
REV. BY: AML/EPG
DWG. NAME: TGD-TL4GTBR_R9
SCALE: 1:16
UNITS: Inches

Figure O-23. Bridge Substructure Rebar Details

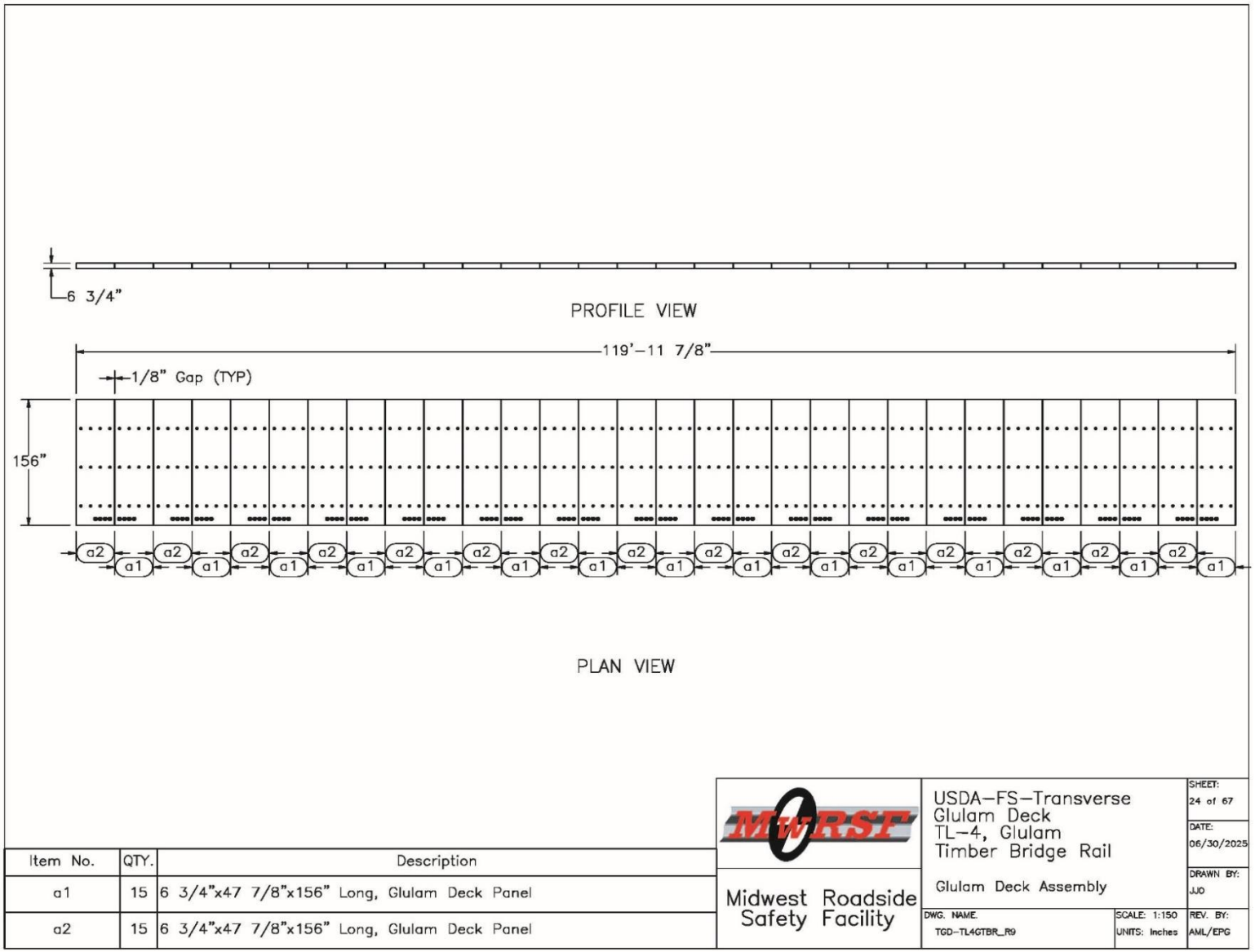

Item No.	QTY.	Description
a1	15	6 3/4"x47 7/8"x156" Long, Glulam Deck Panel
a2	15	6 3/4"x47 7/8"x156" Long, Glulam Deck Panel

Figure O-24. Bridge Superstructure Deck Panel Layout

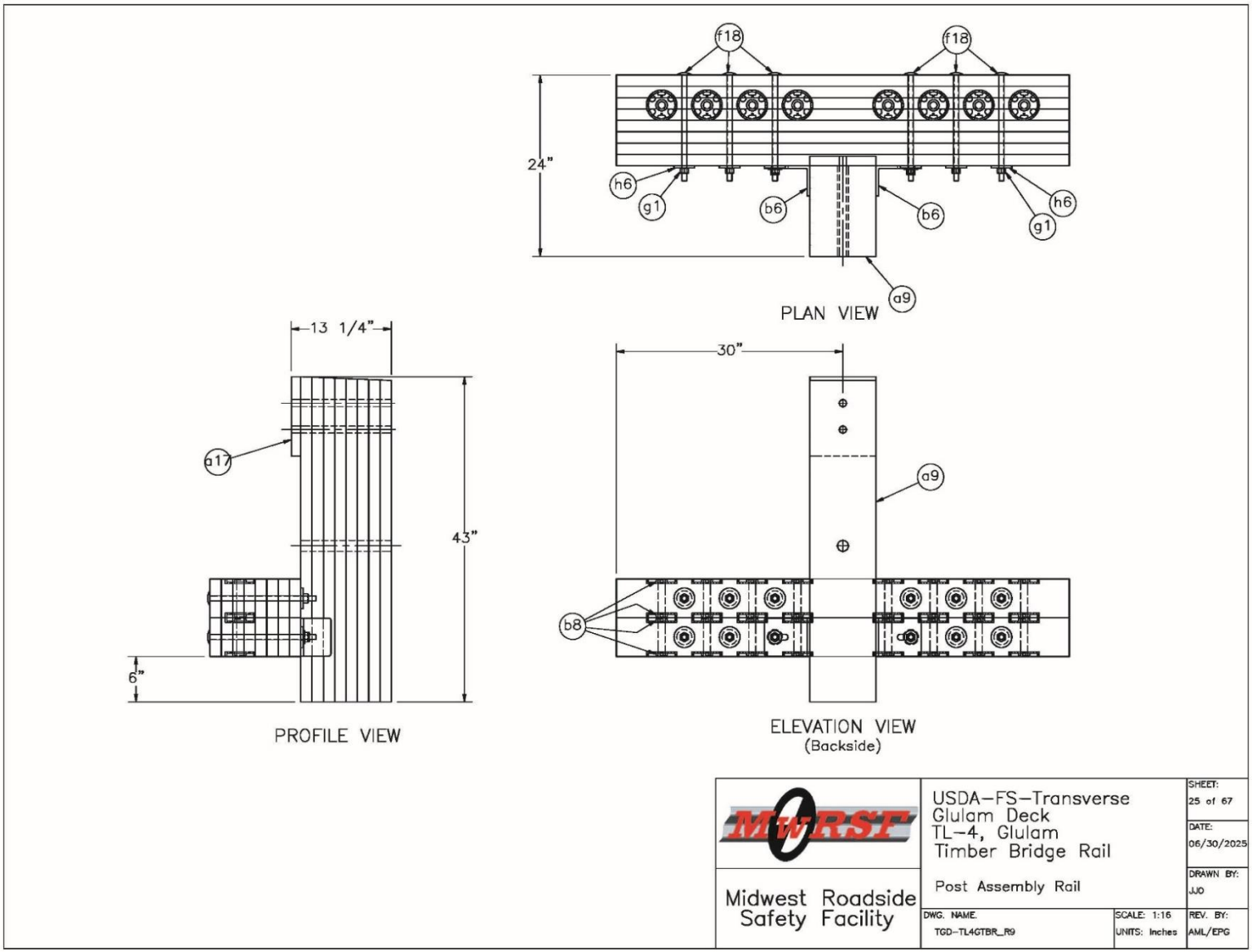

Figure O-25. Bridge Typical Post Assembly Details

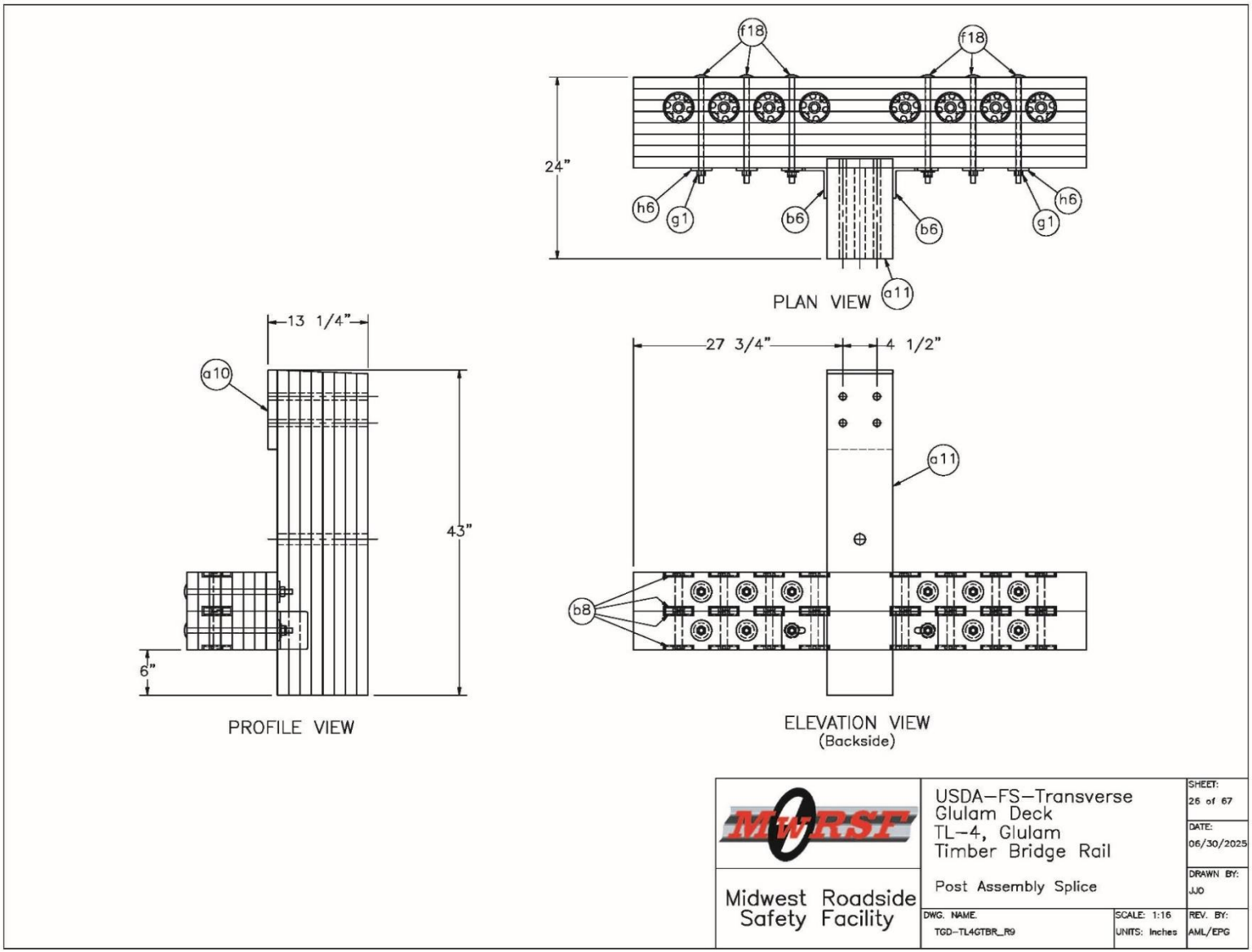

Figure O-26. Bridge Splice Post Assembly Details

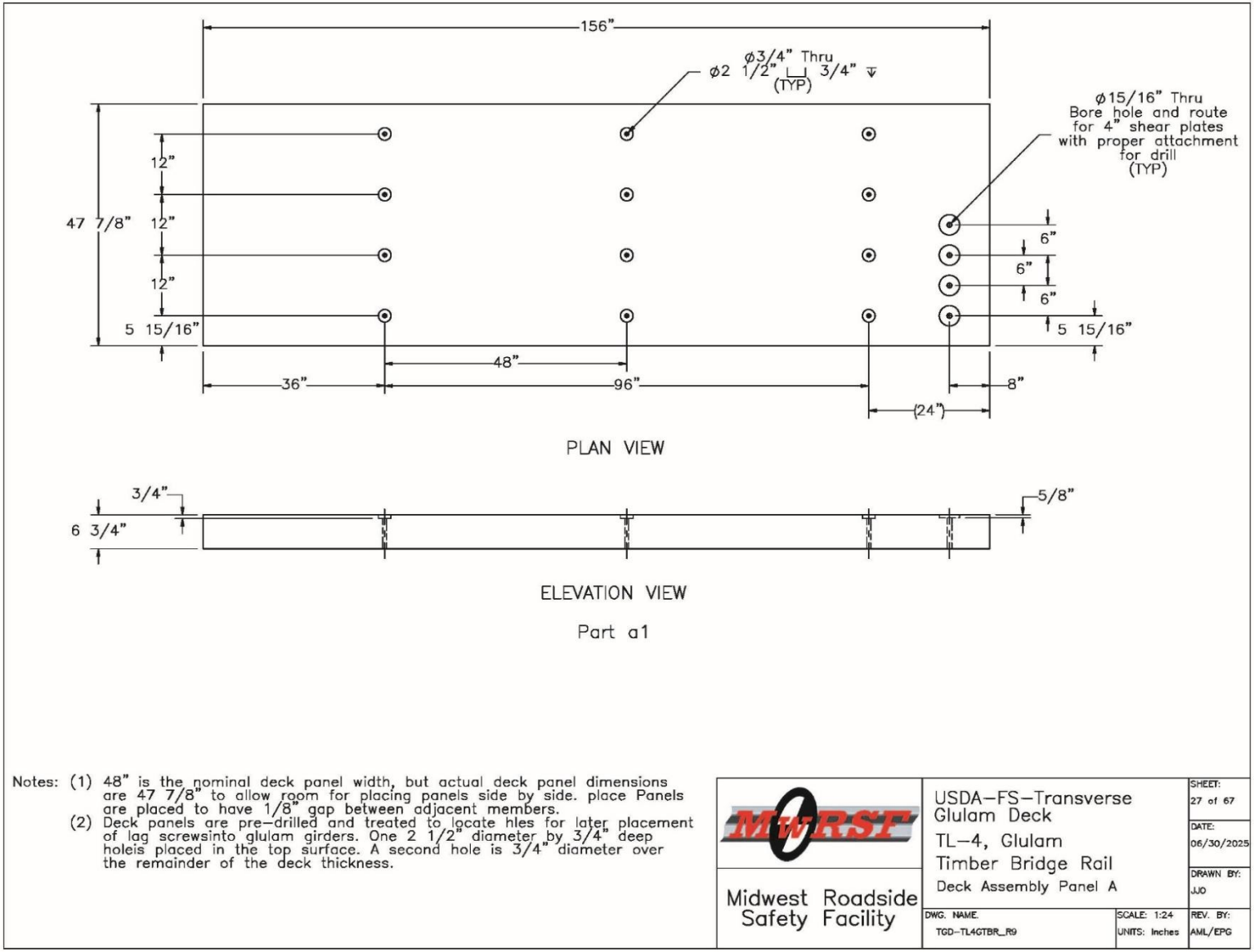

Figure O-27. Deck Assembly Panel Type A Details

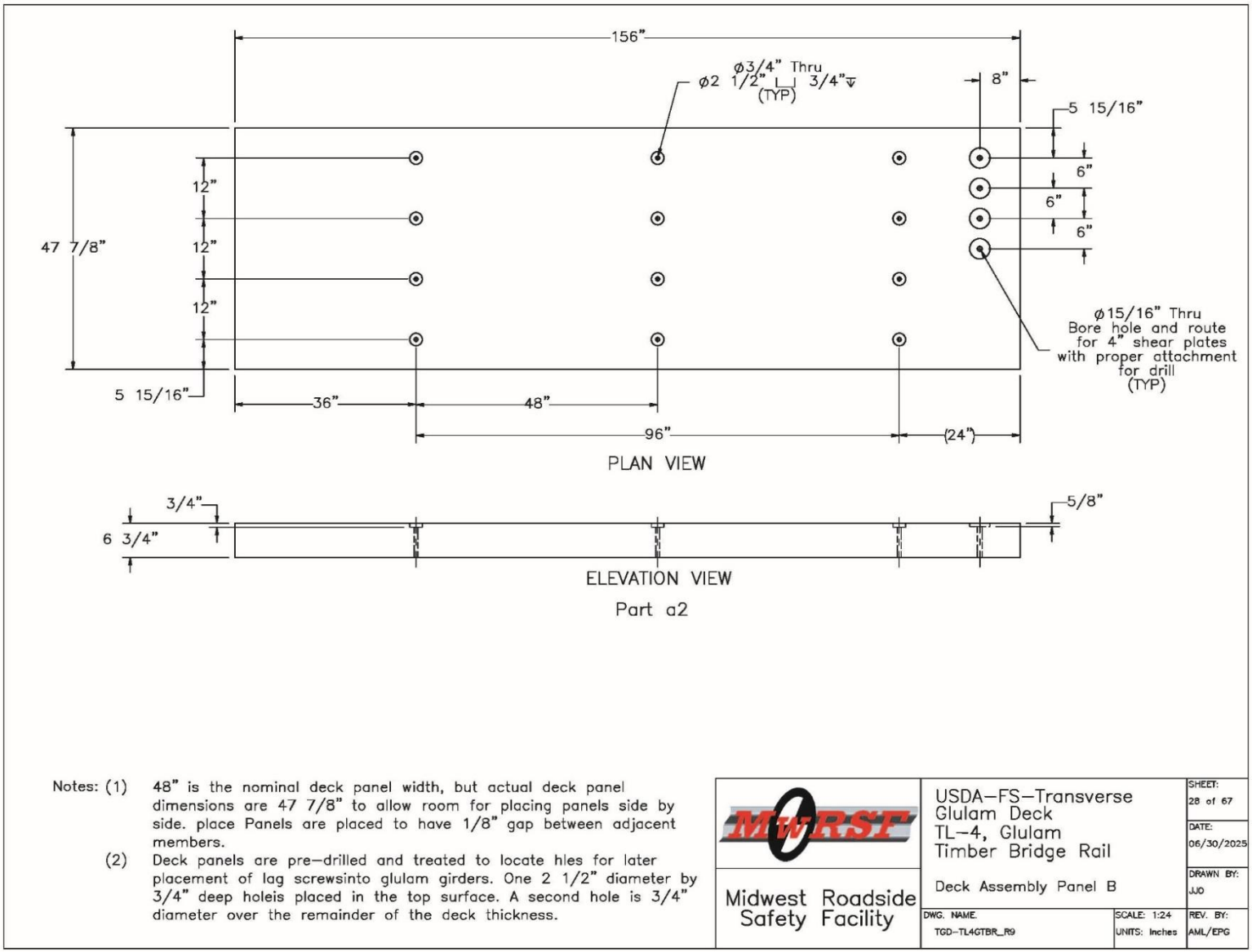

Figure O-28. Deck Assembly Panel Type B Details

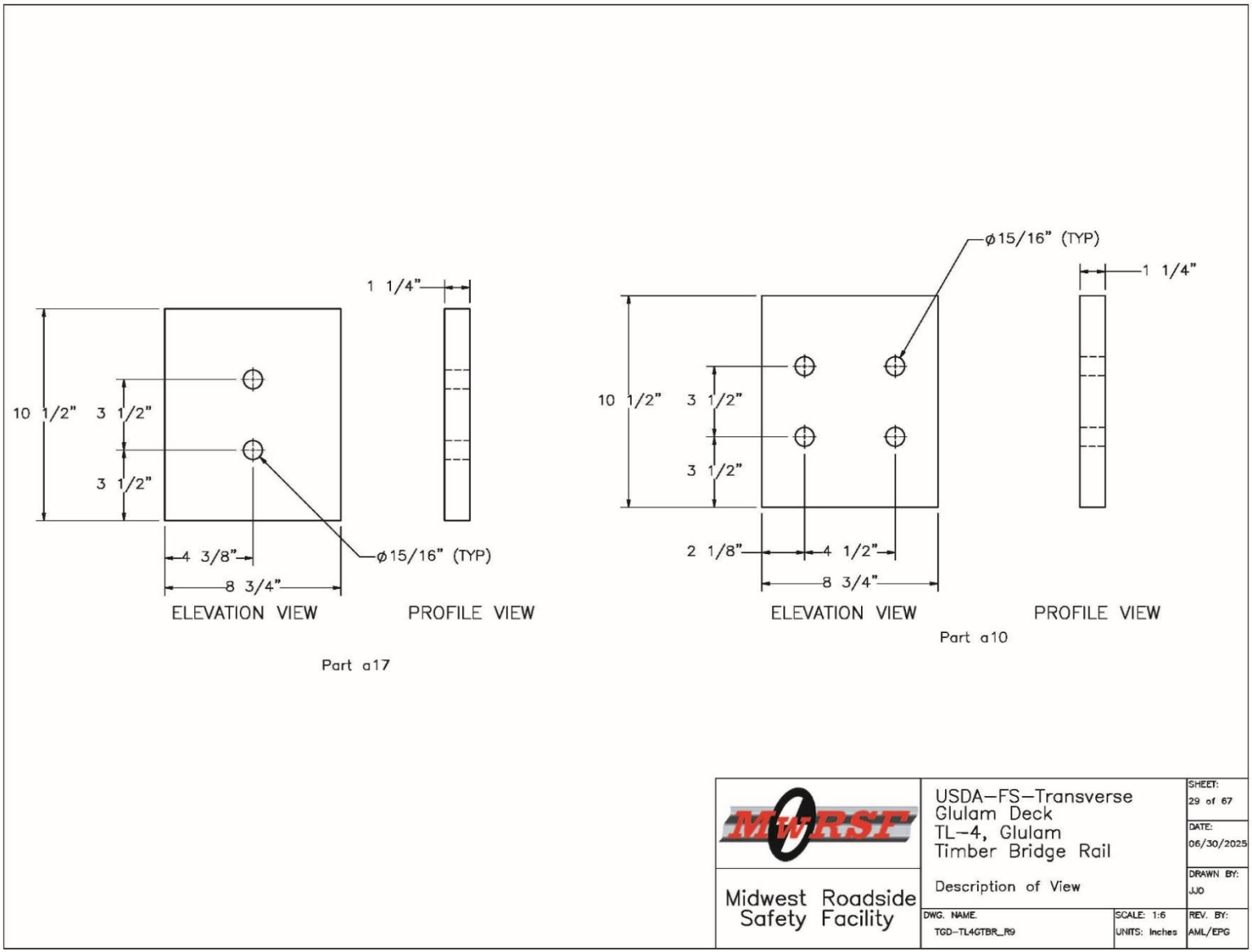

Figure O-29. Bridge Post Typical and Splice Blockout Details

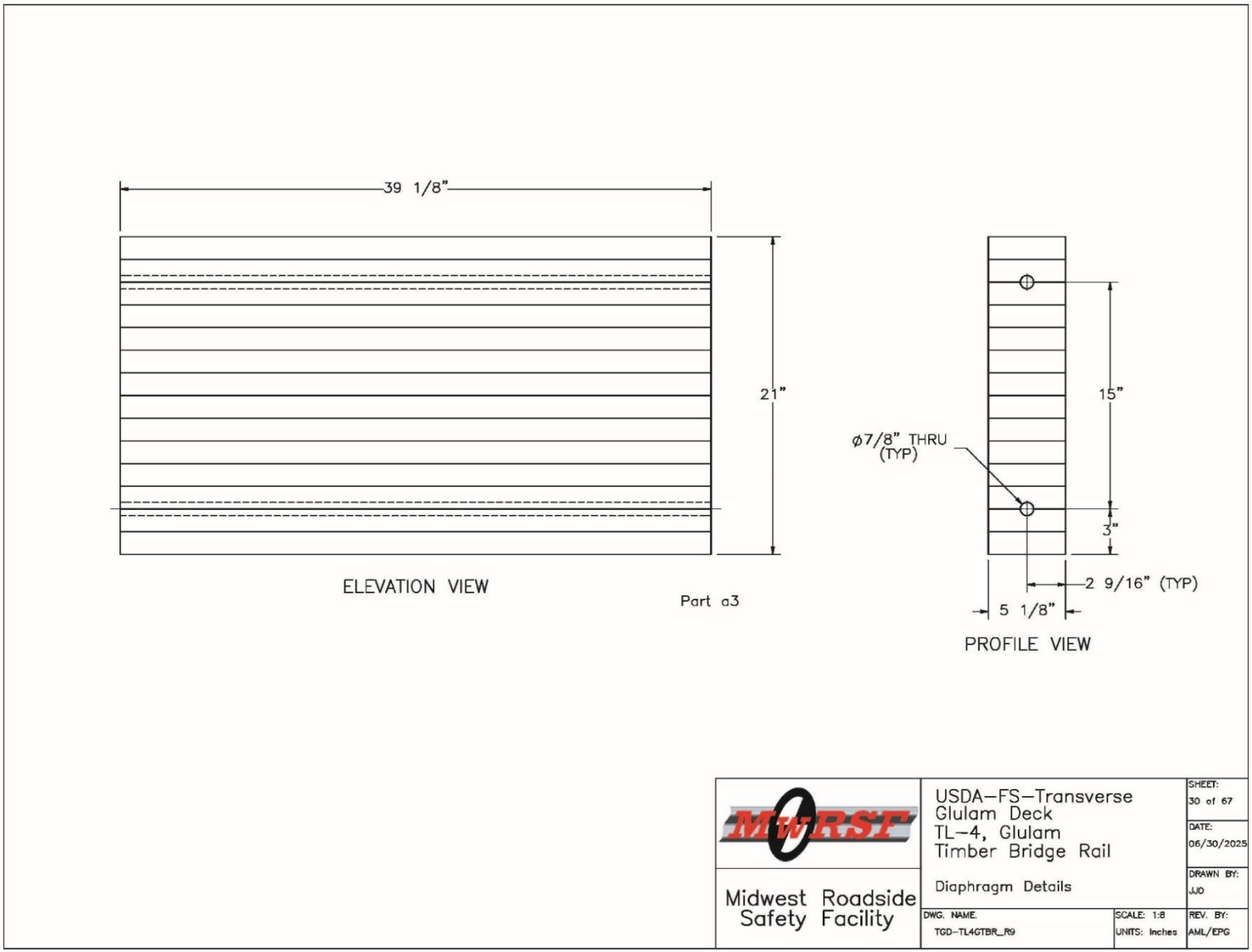

Figure O-30. Bridge Superstructure Diagram Details

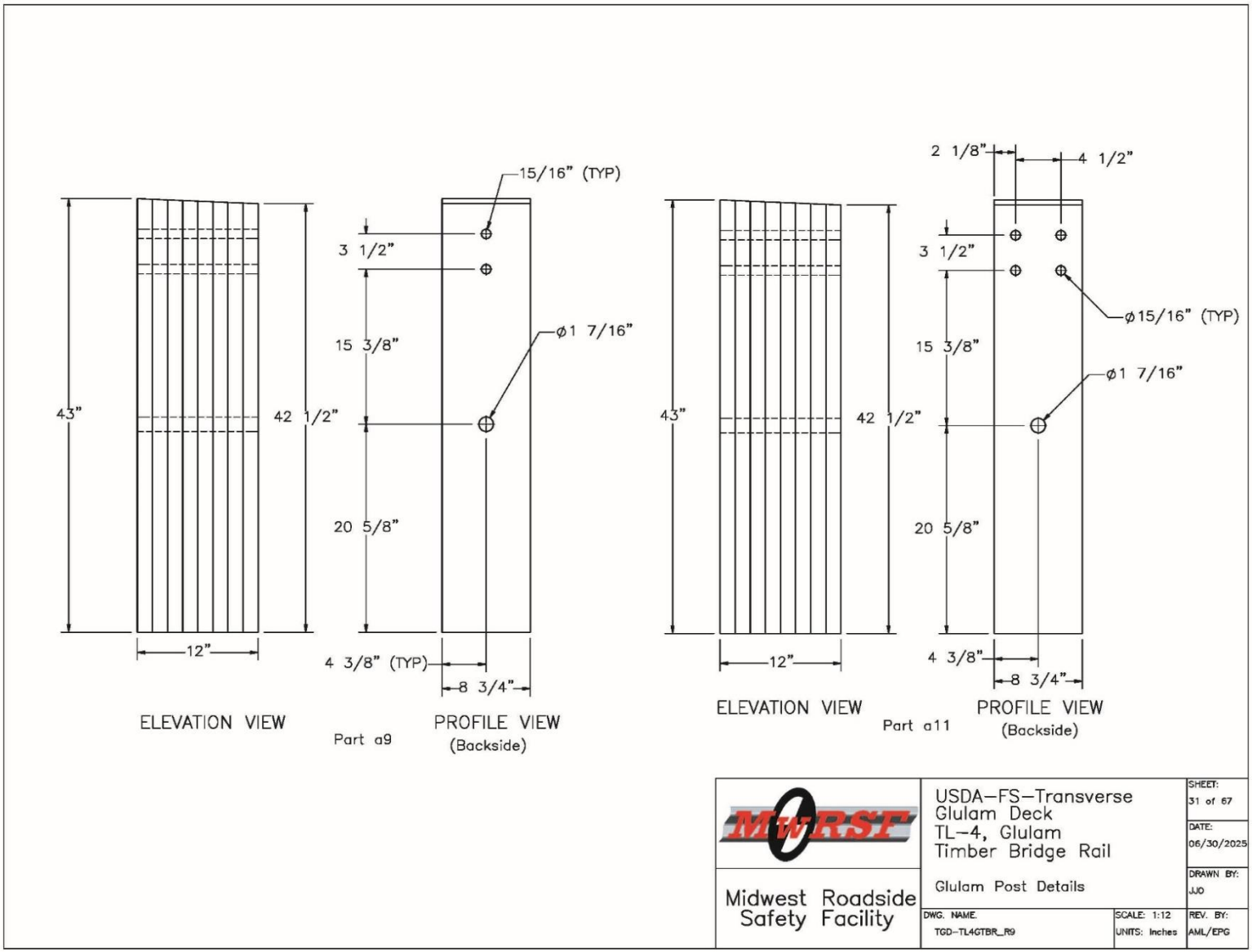

Figure O-31. Bridge Typical and Splice Vertical Post Details

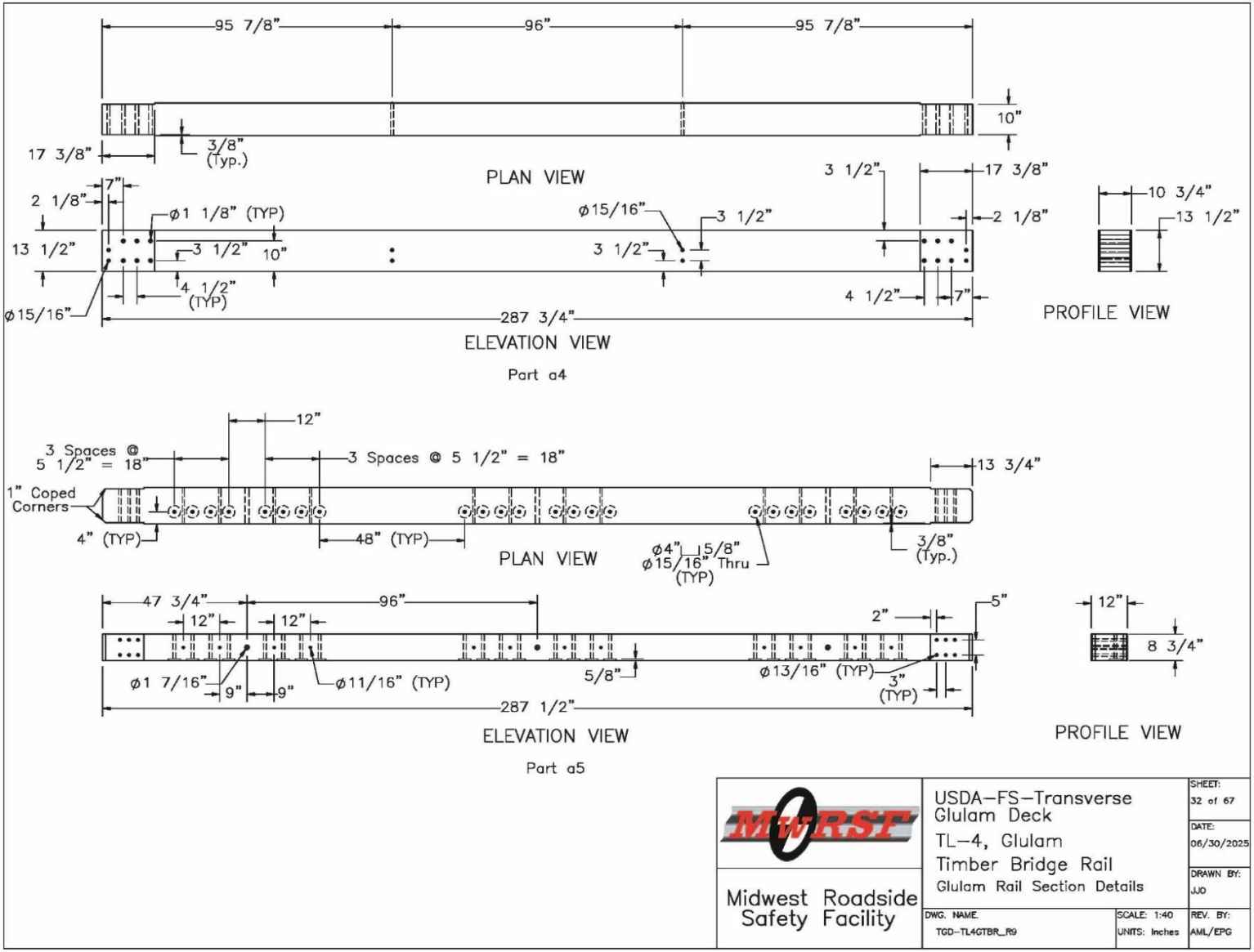

Figure O-32. Bridge Typical Upper and Curb Glulam Railing Pieces

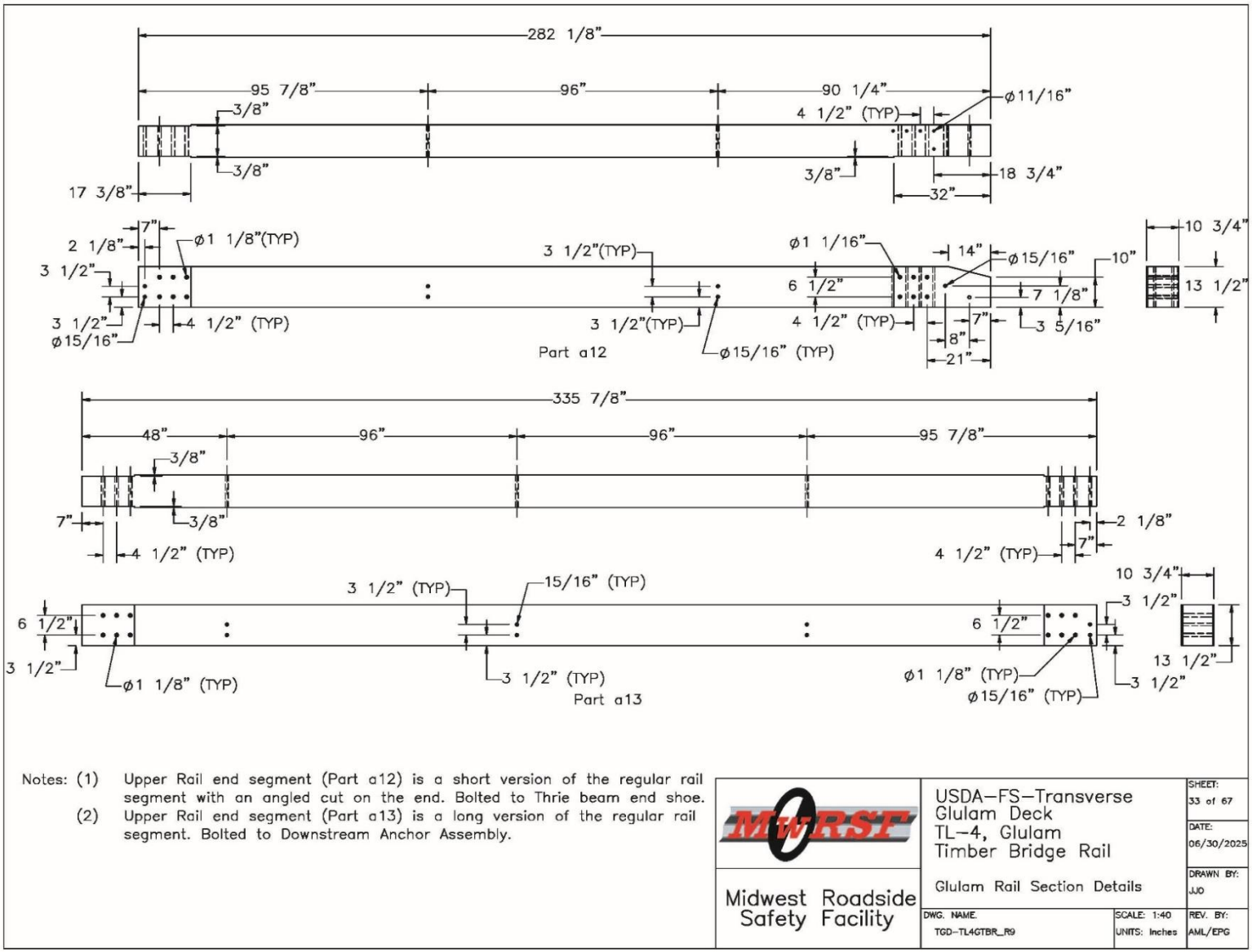

Figure O-33. Bridge Upper Glulam Railing End Pieces

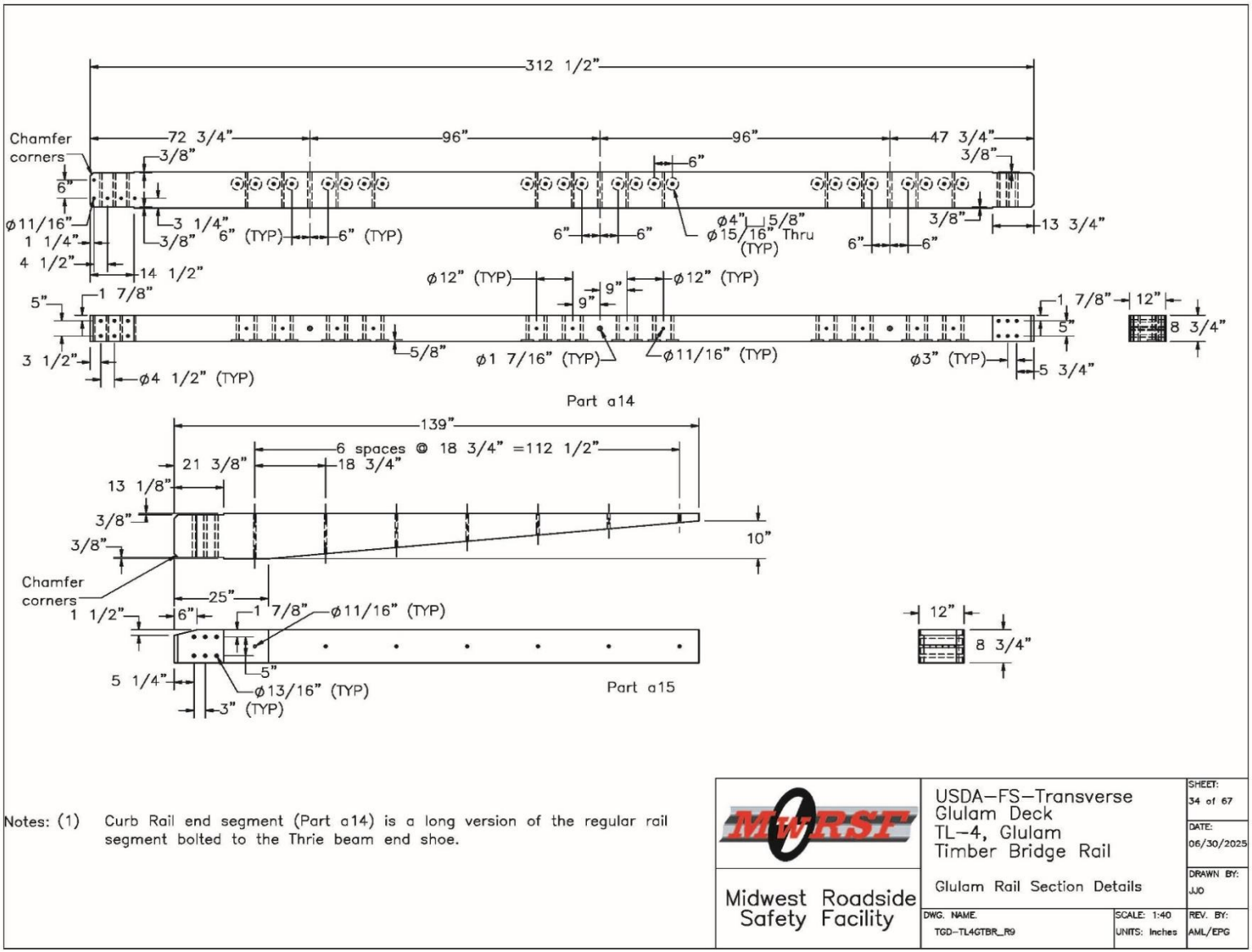

Figure O-34. Bridge Curb Glulam Railing End Pieces

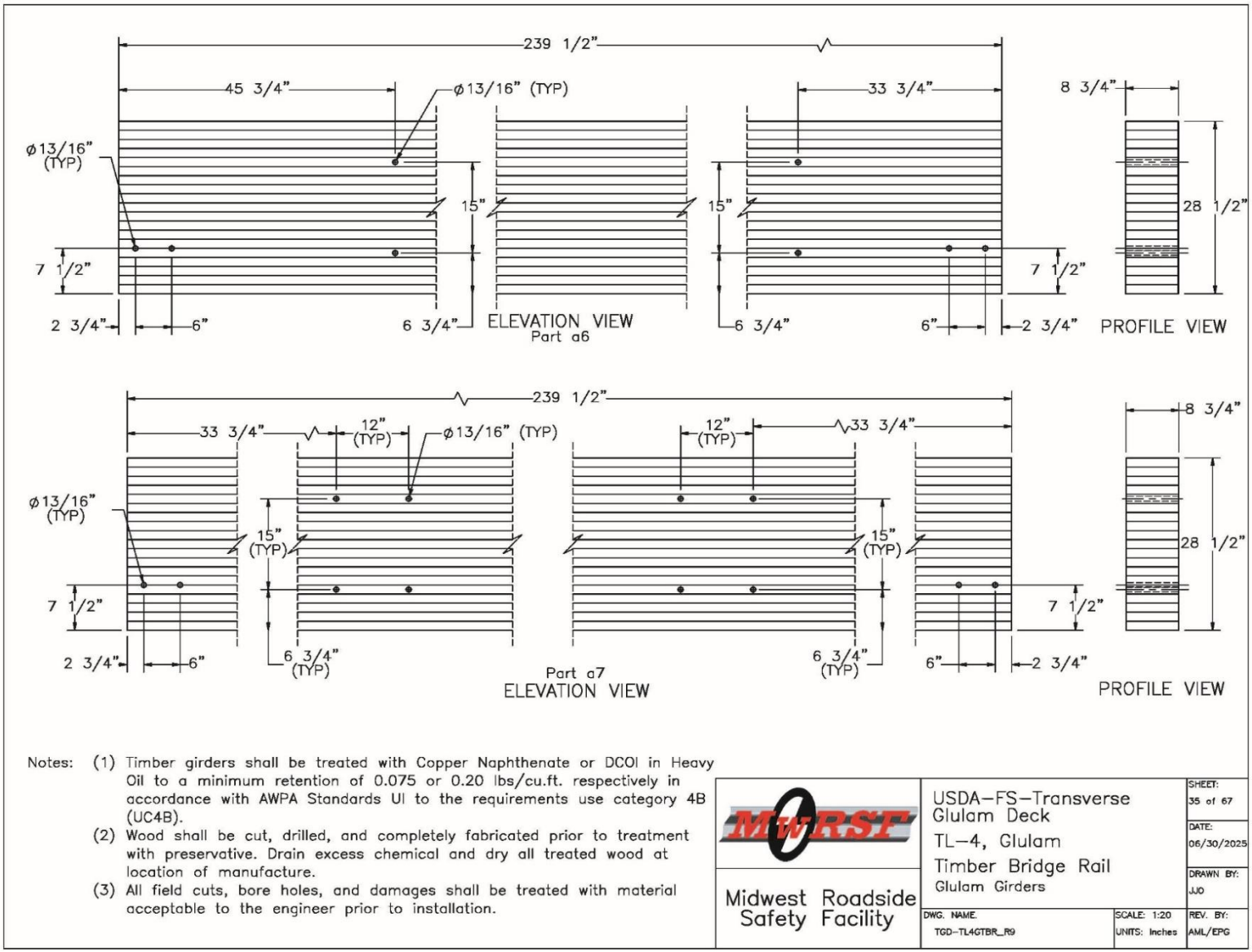

Figure O-35. Bridge Superstructure Girder Details

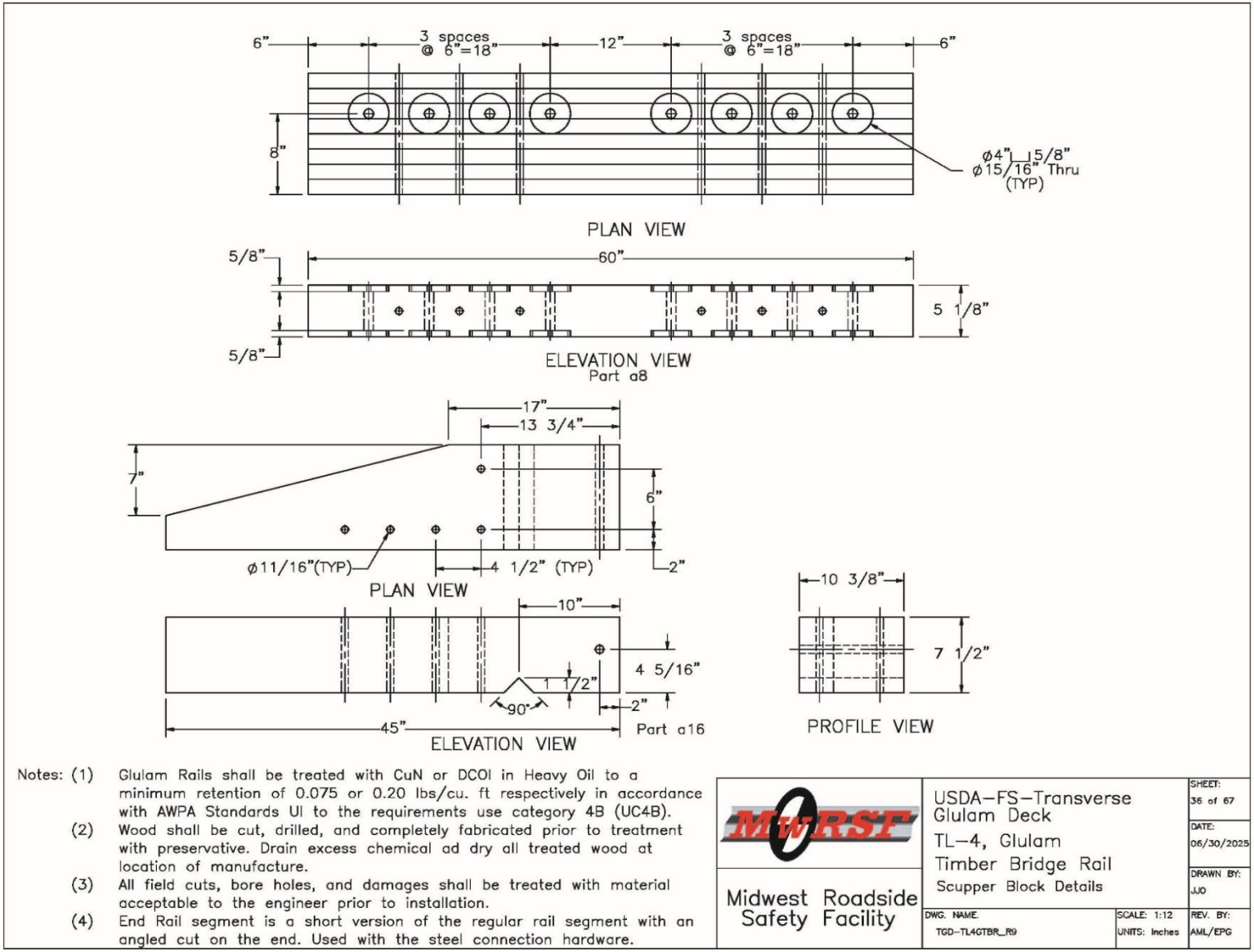

Figure O-36. Bridge Railing Reverse Taper and Scupper Details

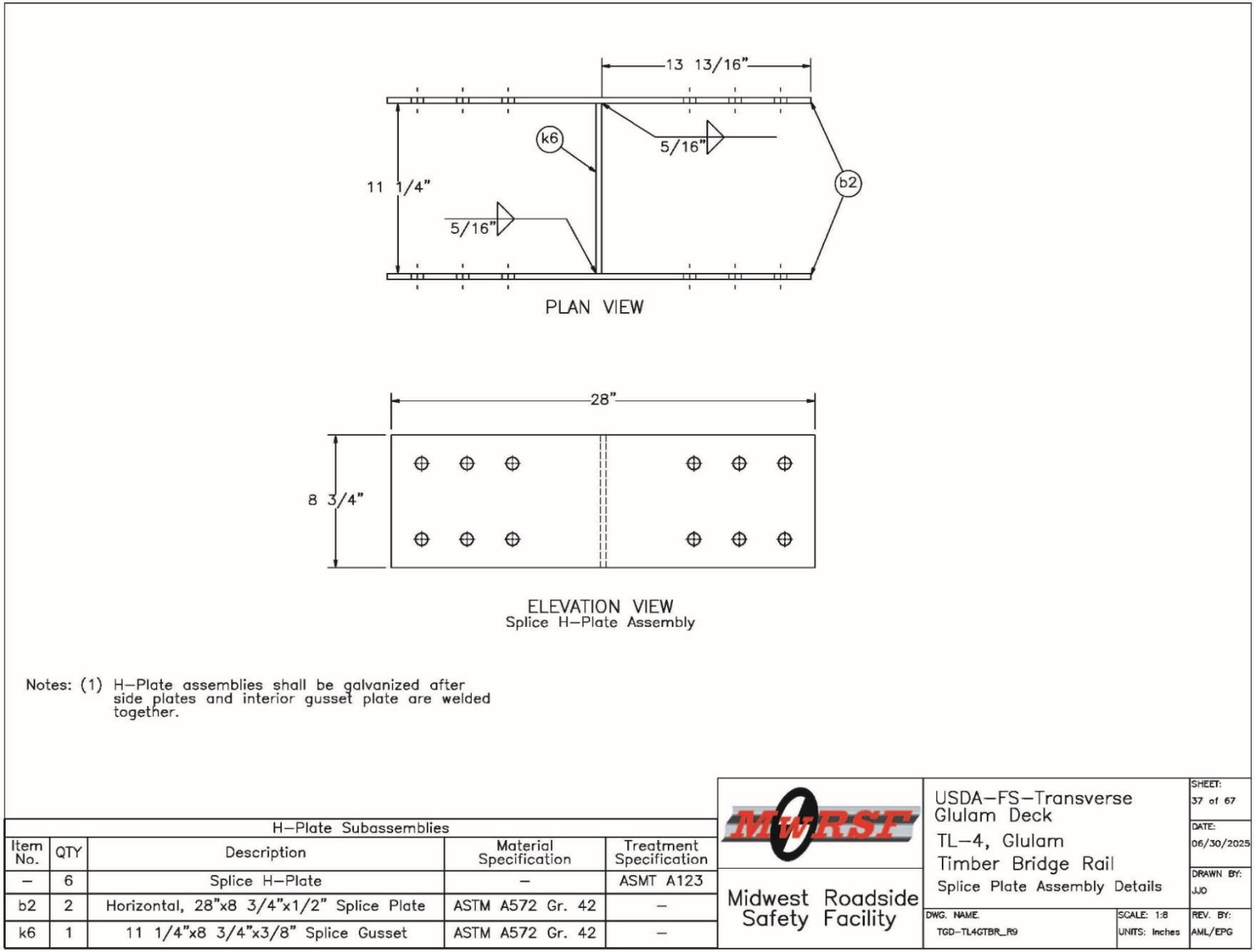

Figure O-37. Bridge Curb Railing Splice Plate Assembly Details

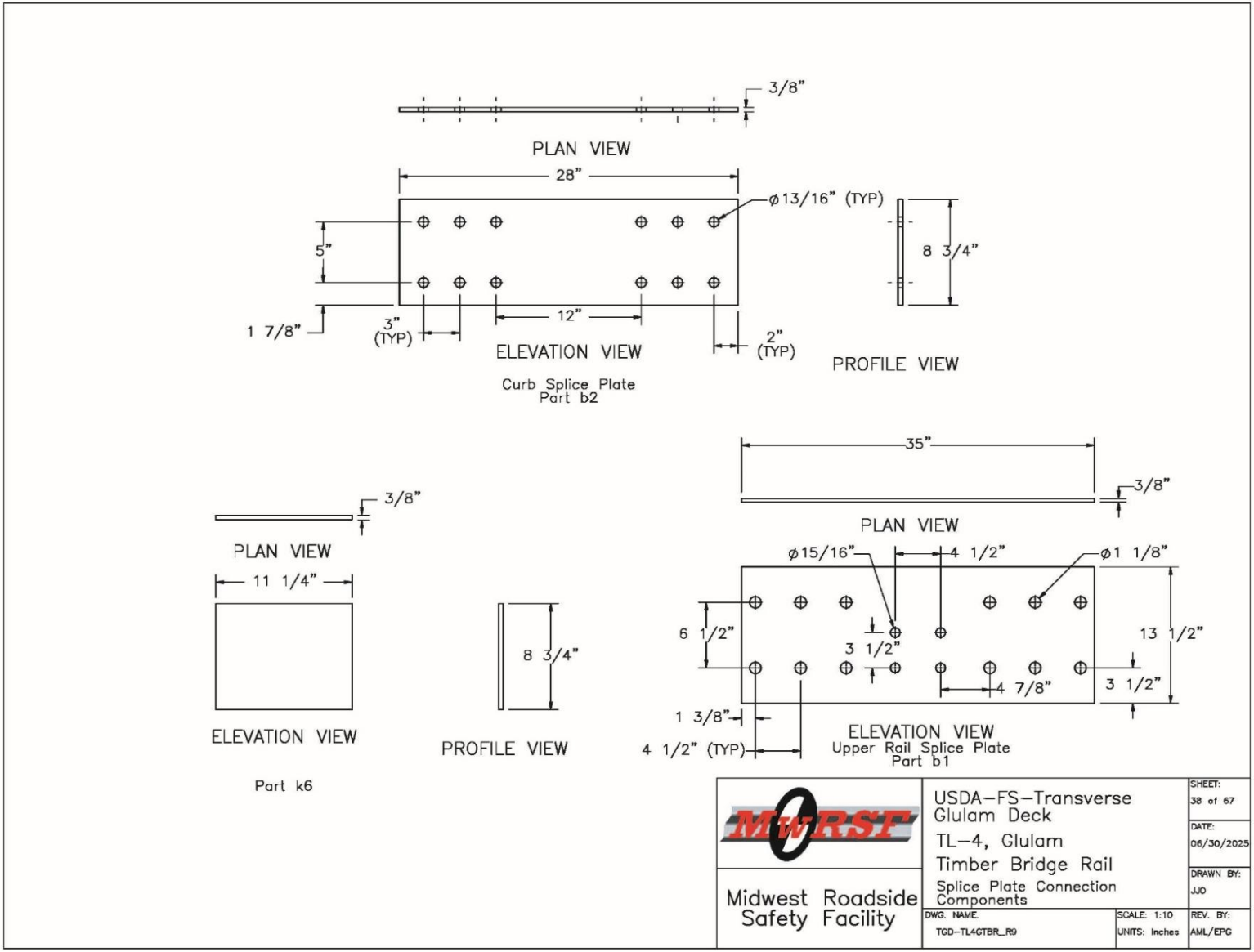

Figure O-38. Bridge Upper and Curb Railing Splice Pieces Details

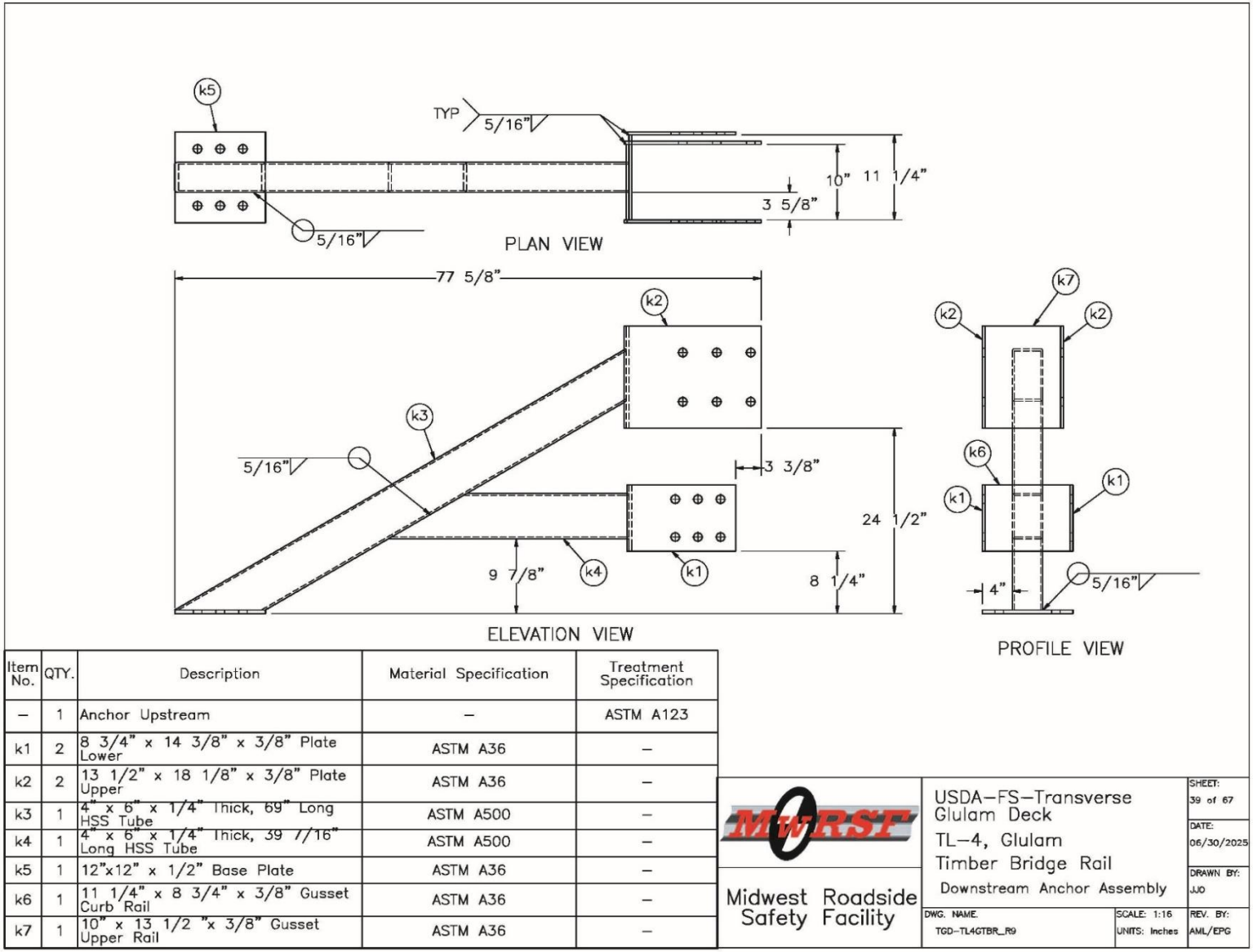

Item No.	QTY.	Description	Material Specification	Treatment Specification
–	1	Anchor Upstream	–	ASTM A123
k1	2	8 3/4" x 14 3/8" x 3/8" Plate Lower	ASTM A36	–
k2	2	13 1/2" x 18 1/8" x 3/8" Plate Upper	ASTM A36	–
k3	1	4" x 6" x 1/4" Thick, 69" Long HSS Tube	ASTM A500	–
k4	1	4" x 6" x 1/4" Thick, 39 7/16" Long HSS Tube	ASTM A500	–
k5	1	12"x12" x 1/2" Base Plate	ASTM A36	–
k6	1	11 1/4" x 8 3/4" x 3/8" Gusset Curb Rail	ASTM A36	–
k7	1	10" x 13 1/2 "x 3/8" Gusset Upper Rail	ASTM A36	–

Midwest Roadside Safety Facility

USDA–FS–Transverse Glulam Deck
TL–4, Glulam Timber Bridge Rail
Downstream Anchor Assembly

SHEET: 39 of 67
DATE: 06/30/2025
DRAWN BY: JJO
REV. BY: AML/EPG
DWG. NAME: TGD–TL4GTBR_R9
SCALE: 1:16
UNITS: Inches

Figure O-39. Bridge Railing End Anchor Component Assembly

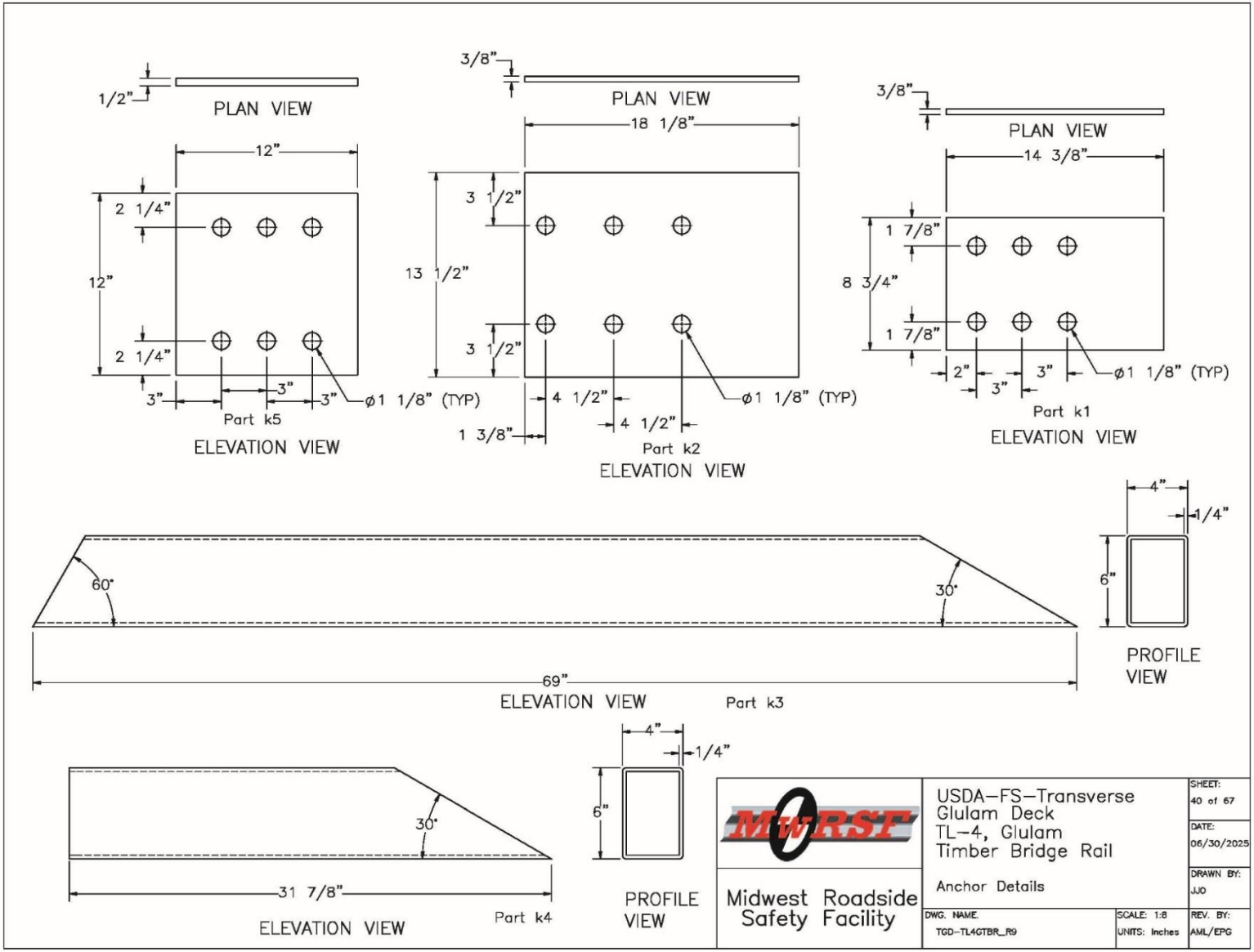

Figure O-40. Bridge Railing End Anchor Component Details

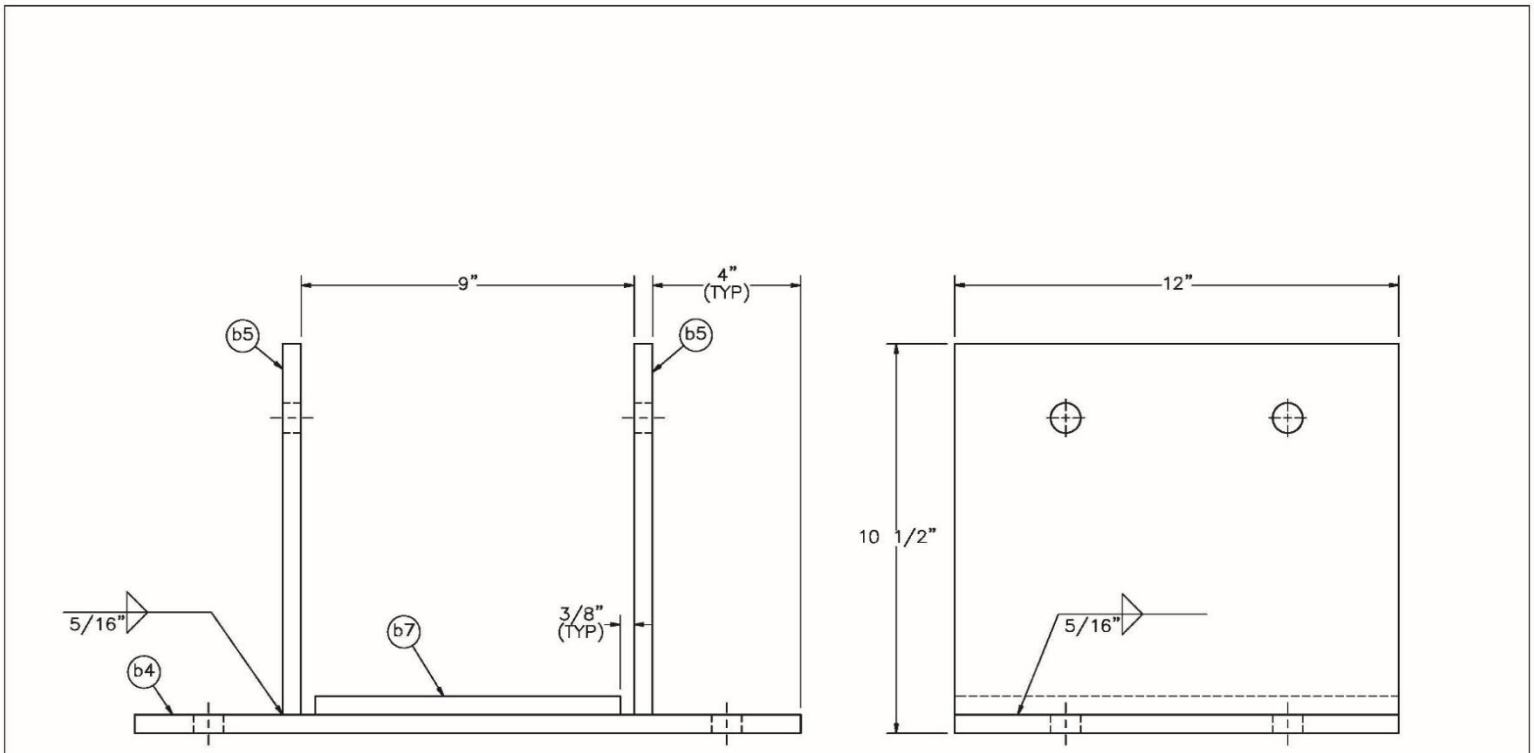

Notes: (1) Bearing Shoe assembly shall be galvanized after side plates and base plate are welded together.

Item No.	QTY.	Description	Material Specification	Treatment Specification
–	6	Steel Plate Bearing Shoe Short	–	ASTM A123
b4	1	12"x16"x1/2" Steel Base Plate	ASTM A36	–
b5	2	12"x10"x1/2" Side Plate	ASTM A36	–
b7	1	12"x8 1/4"x1/2" Elastomeric Bearing Pad	Neoprene – Min. 50 Durameter	–

Midwest Roadside Safety Facility

USDA–FS–Transverse Glulam Deck
TL–4, Glulam Timber Bridge Rail
Steel Plate Bearing Shoe Assembly Short

SHEET: 41 of 67
DATE: 06/30/2025
DRAWN BY: JJO
REV. BY: AML/EPG
DWG. NAME. TGD–TL4GTBR_R9
SCALE: 1:4
UNITS: Inches

Figure O-41. Bridge Superstructure Abutment Bearing Assembly Details

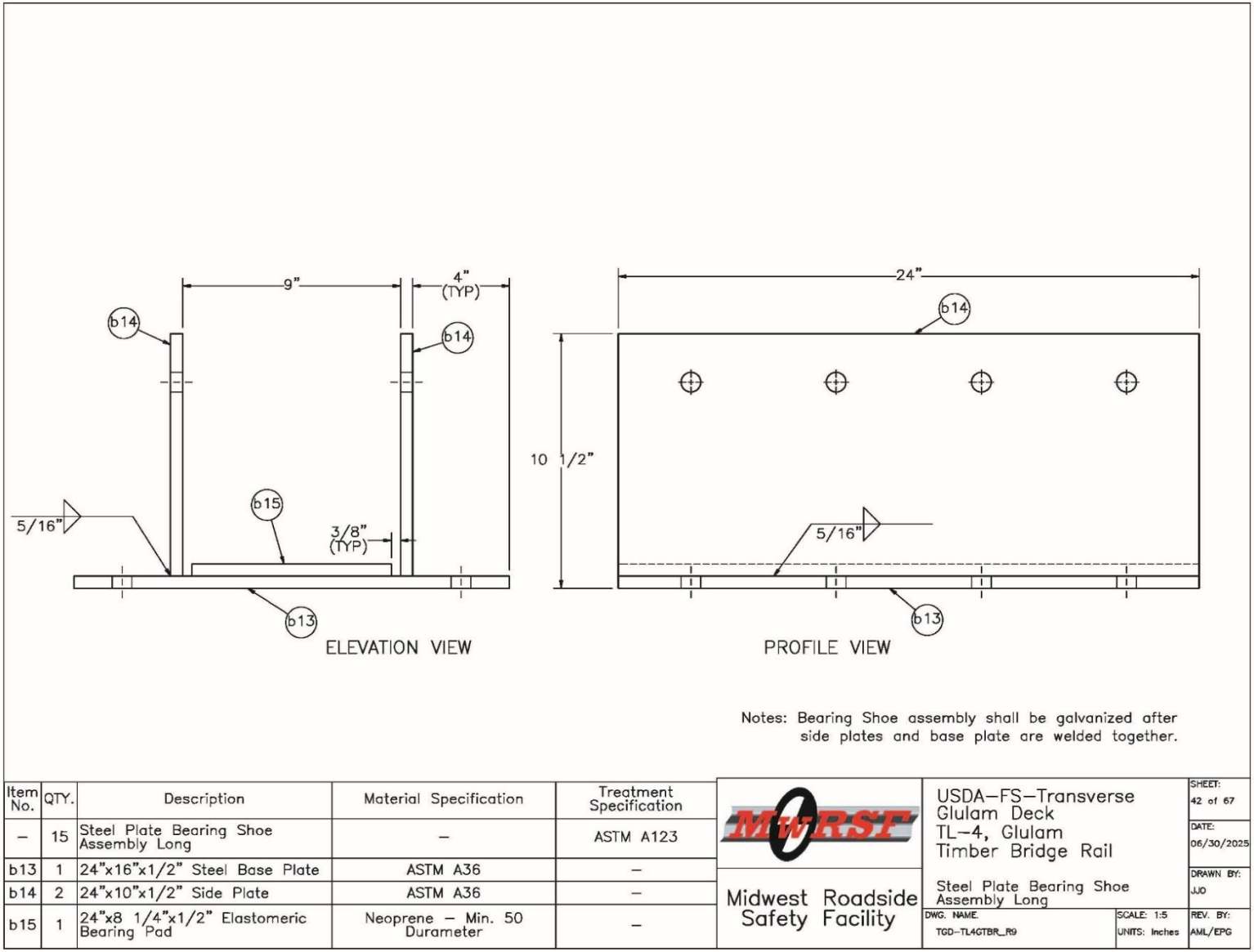

Item No.	QTY.	Description	Material Specification	Treatment Specification
–	15	Steel Plate Bearing Shoe Assembly Long	–	ASTM A123
b13	1	24"x16"x1/2" Steel Base Plate	ASTM A36	–
b14	2	24"x10"x1/2" Side Plate	ASTM A36	–
b15	1	24"x8 1/4"x1/2" Elastomeric Bearing Pad	Neoprene – Min. 50 Durameter	–

Midwest Roadside Safety Facility

USDA–FS–Transverse Glulam Deck TL–4, Glulam Timber Bridge Rail

Steel Plate Bearing Shoe Assembly Long

DWG. NAME. TGD–TL4GTBR_R9 | SCALE: 1:5 | UNITS: Inches

SHEET: 42 of 67 | DATE: 06/30/2025 | DRAWN BY: JJO | REV. BY: AML/EPG

Figure O-42. Bridge Superstructure Pier Bearing Assembly Details

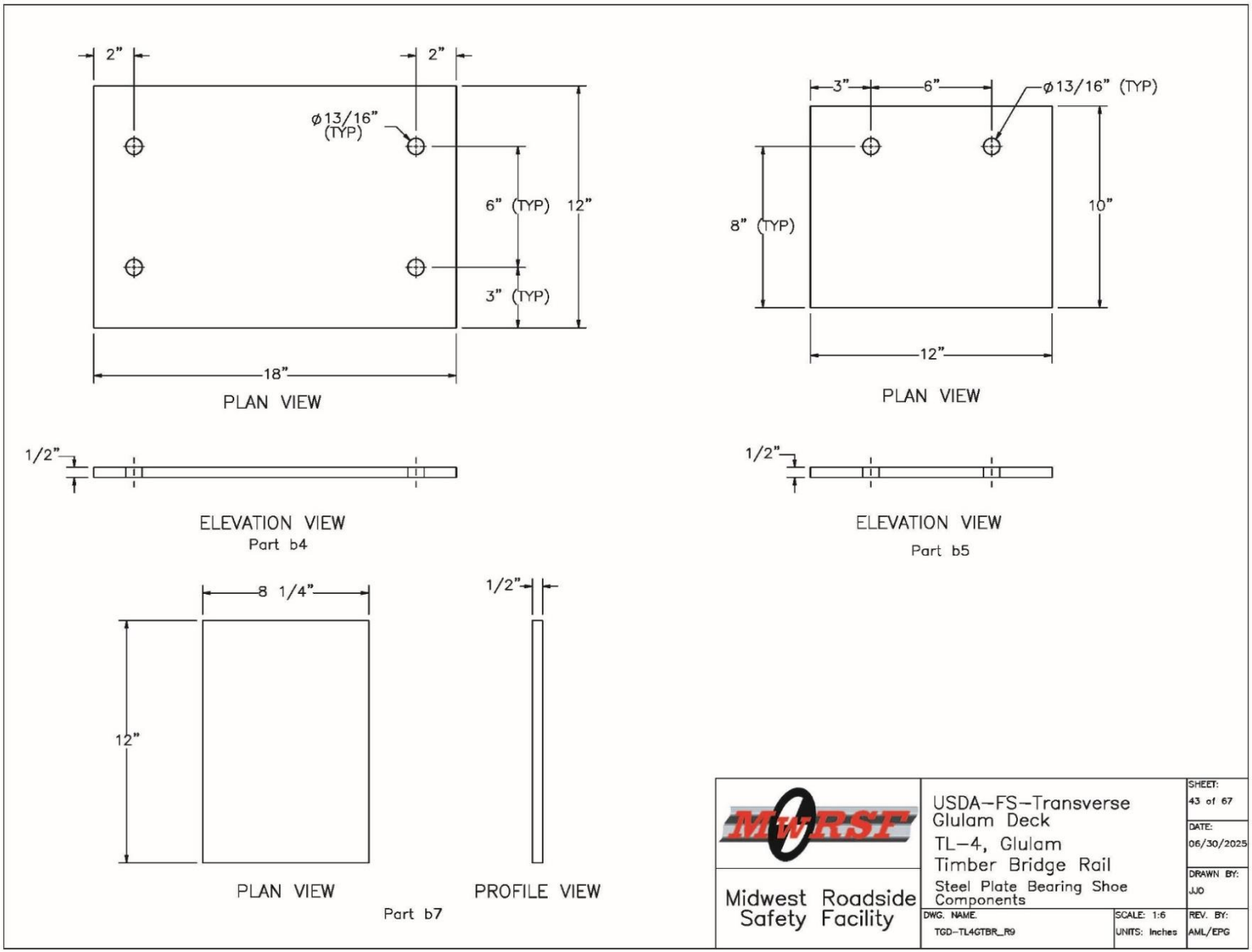

Figure O-43. Bridge Superstructure Abutment Bearing Component Details

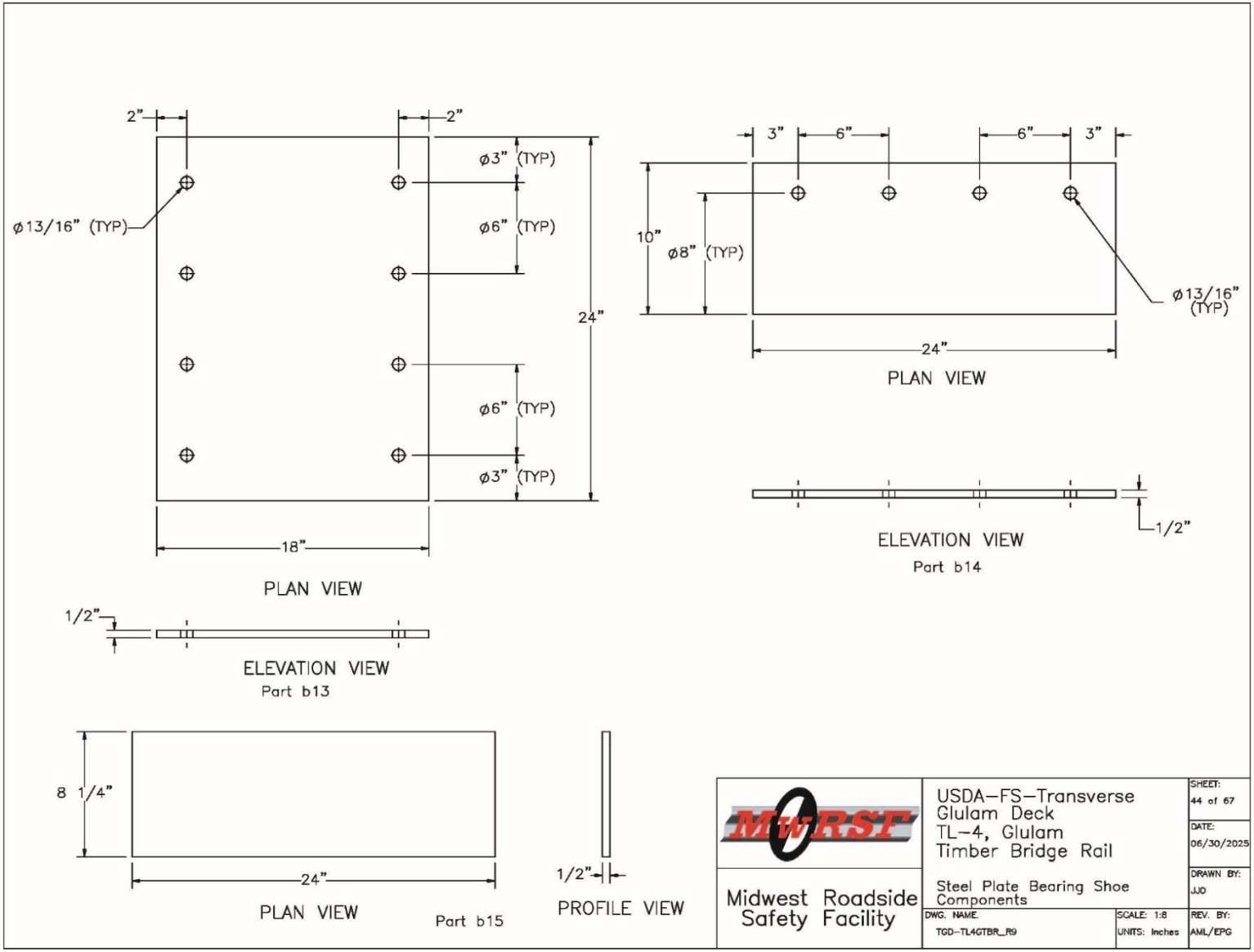

Figure O-44. Bridge Superstructure Pier Bearing Assembly Details

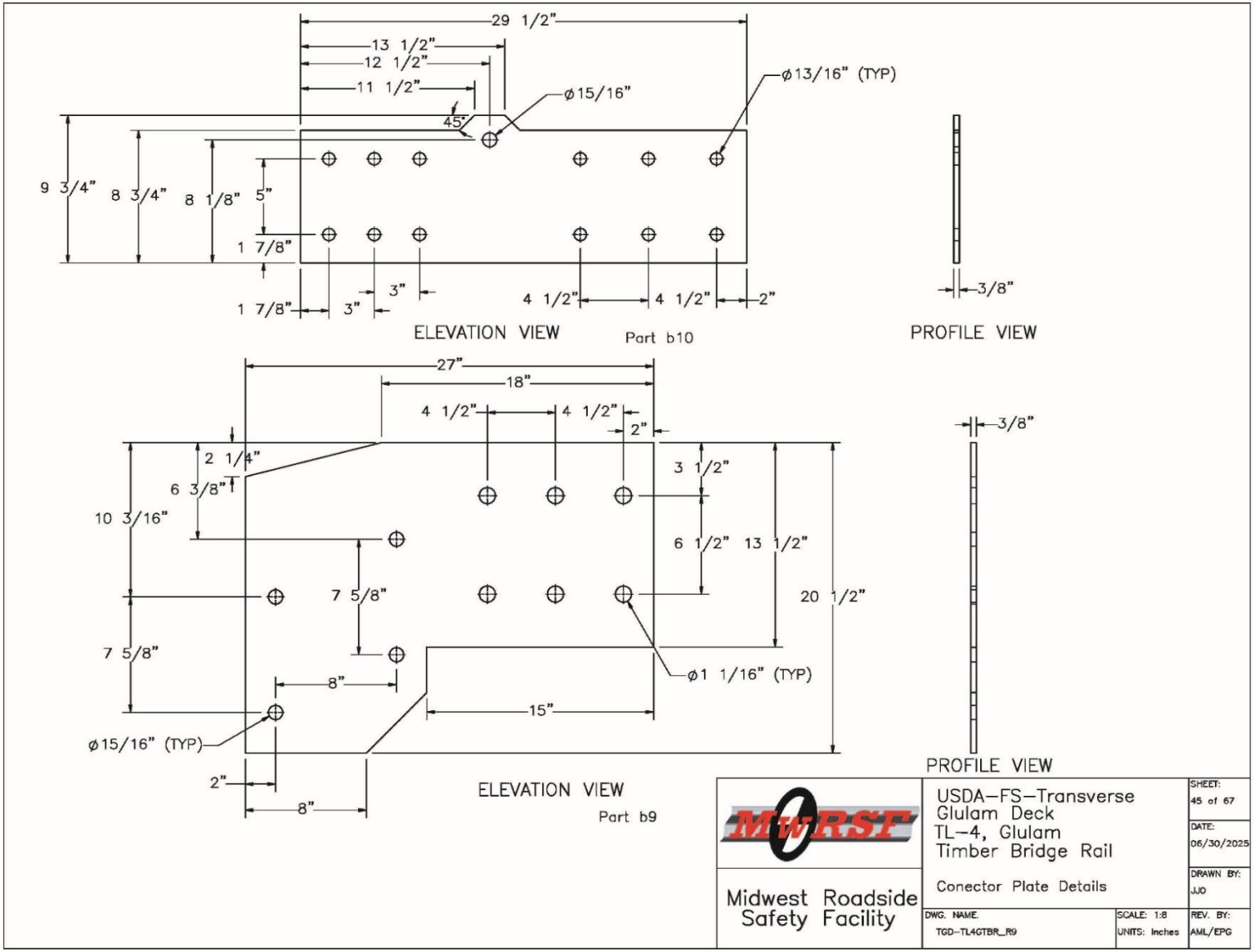

Figure O-45. Bridge Railing to AGT Steel Plate Connection Details

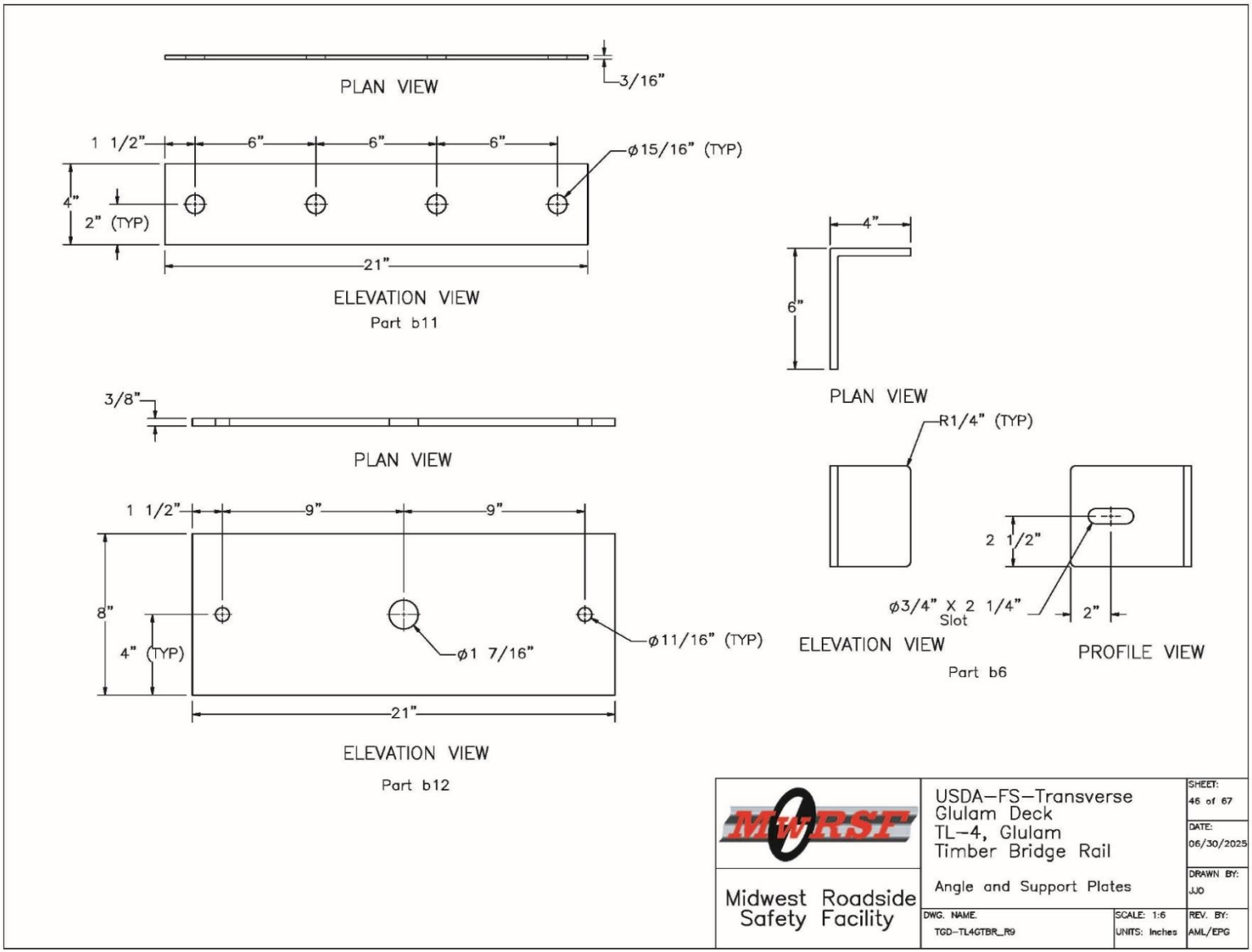

Figure O-46. Bridge Post Connection Hardware Details

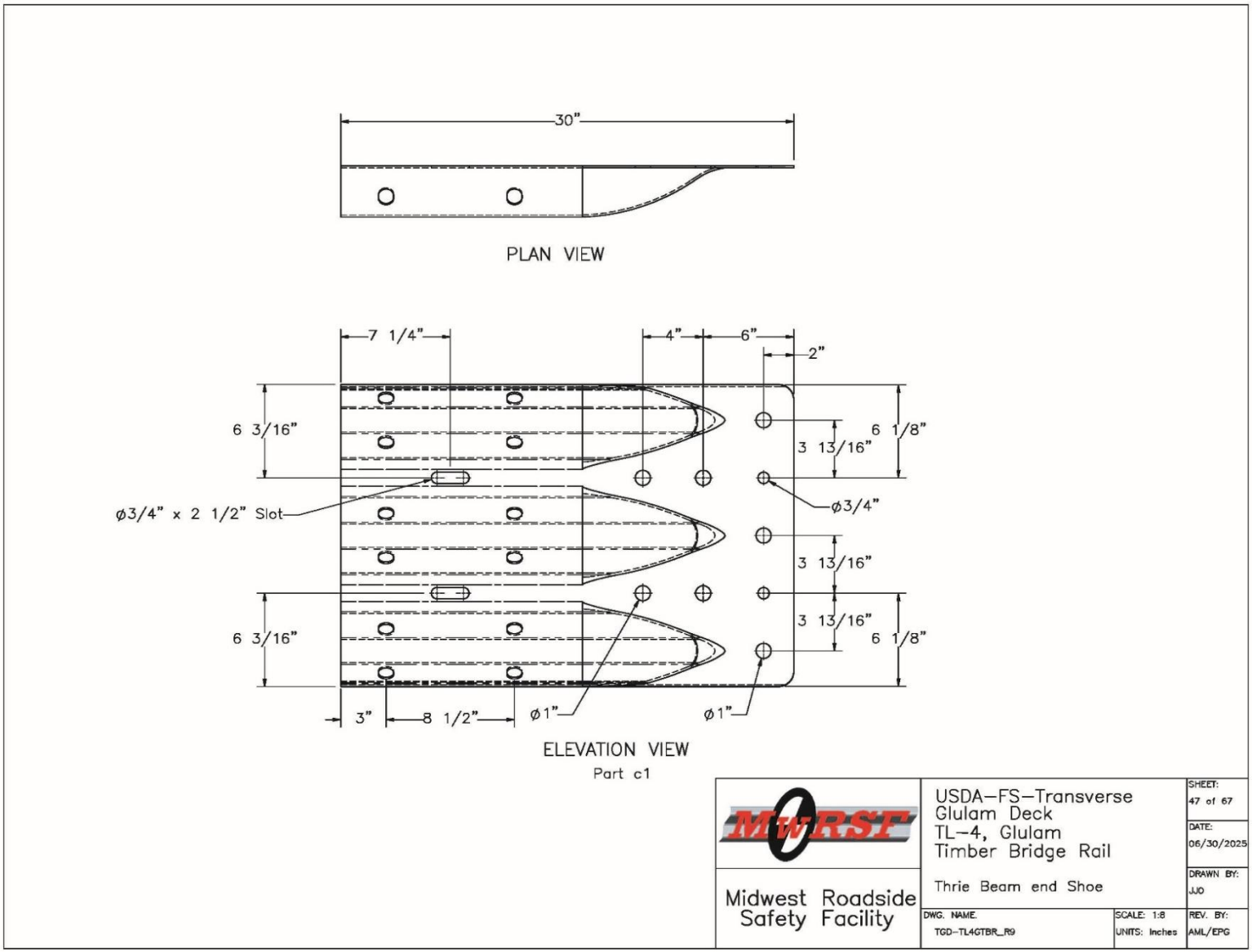

Figure O-47. Bridge AGT Thrie Beam End Shoe Details

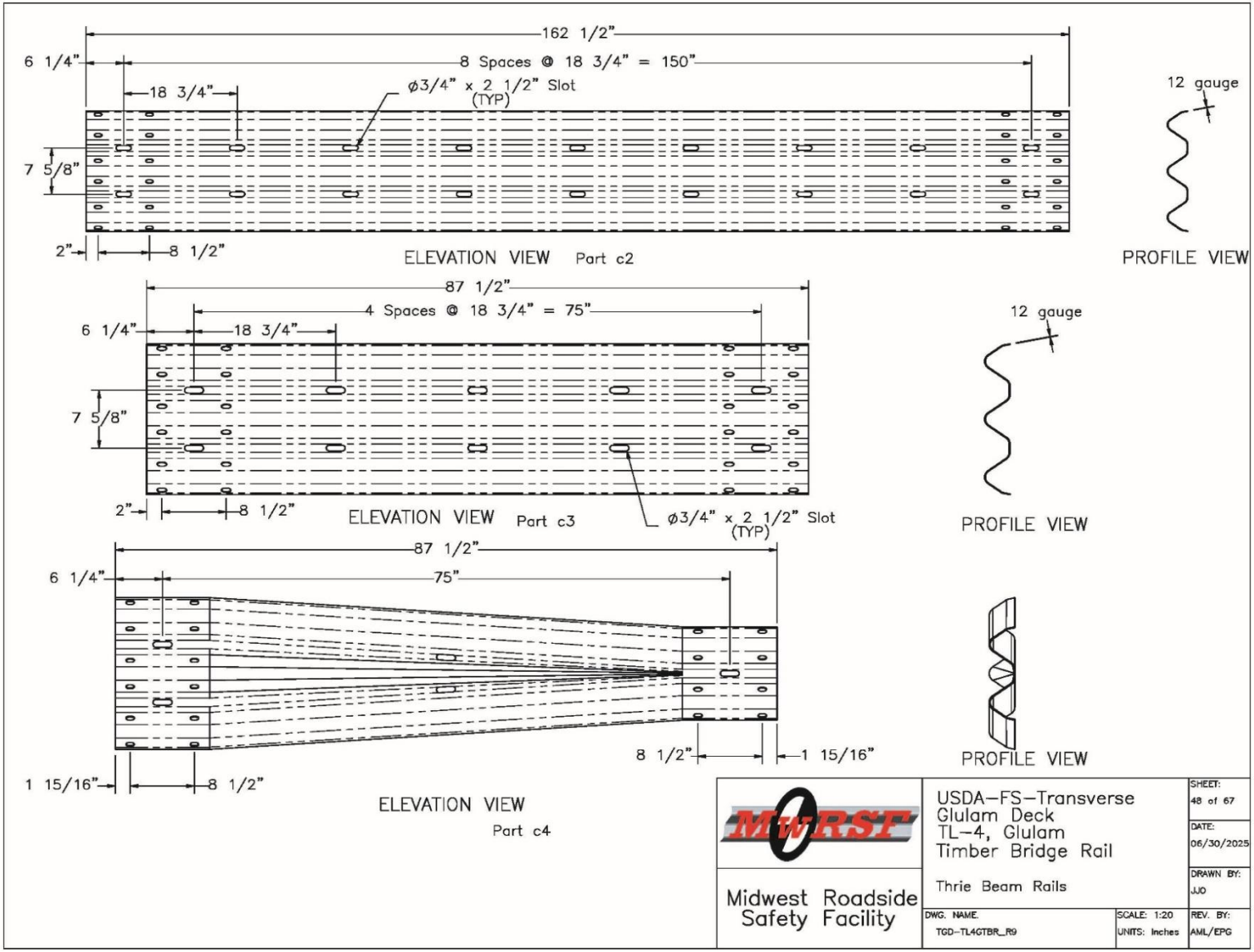

Figure O-48. Bridge AGT Thrie-Beam Rail Details

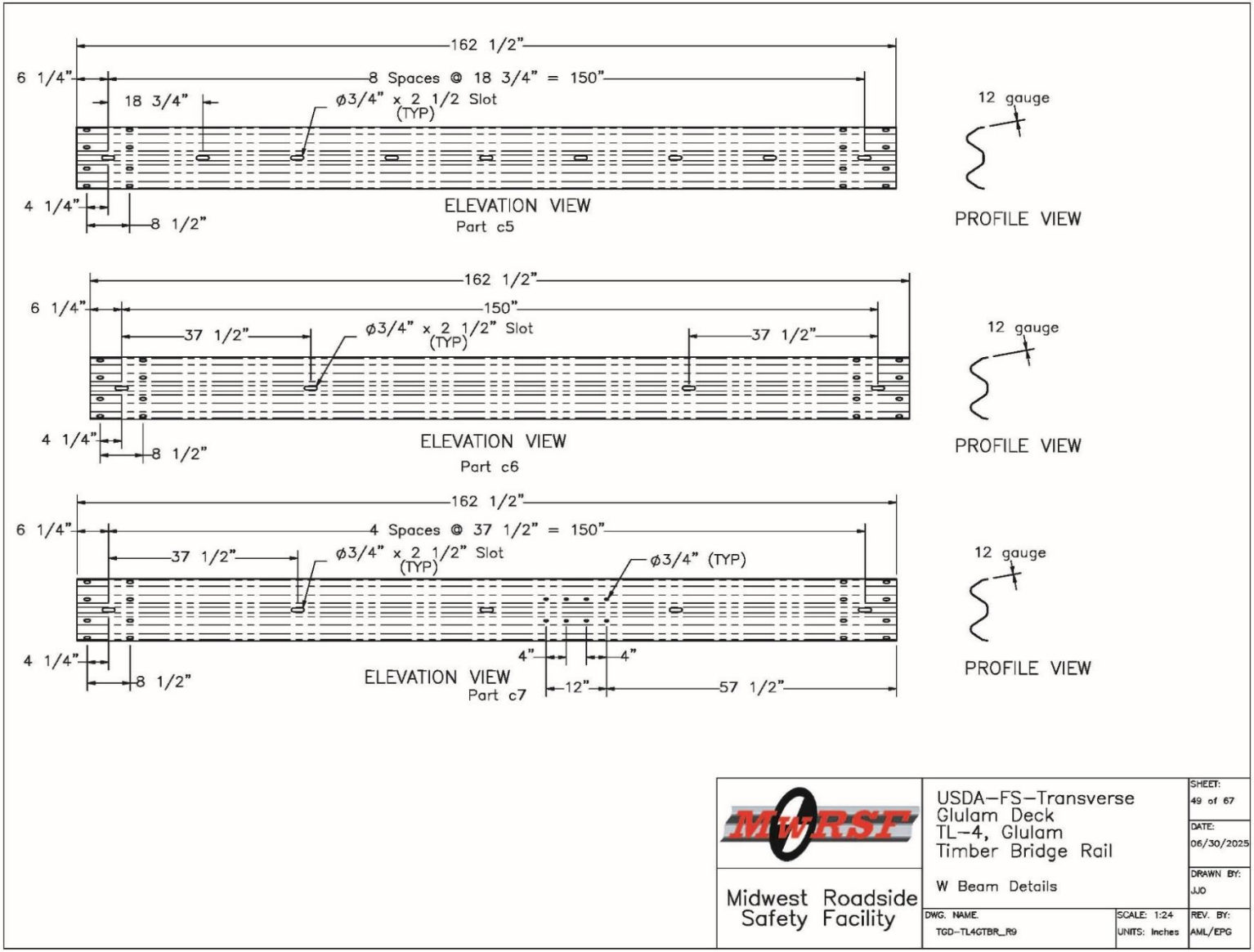

Figure O-49. Bridge AGT W-Beam Rail Details

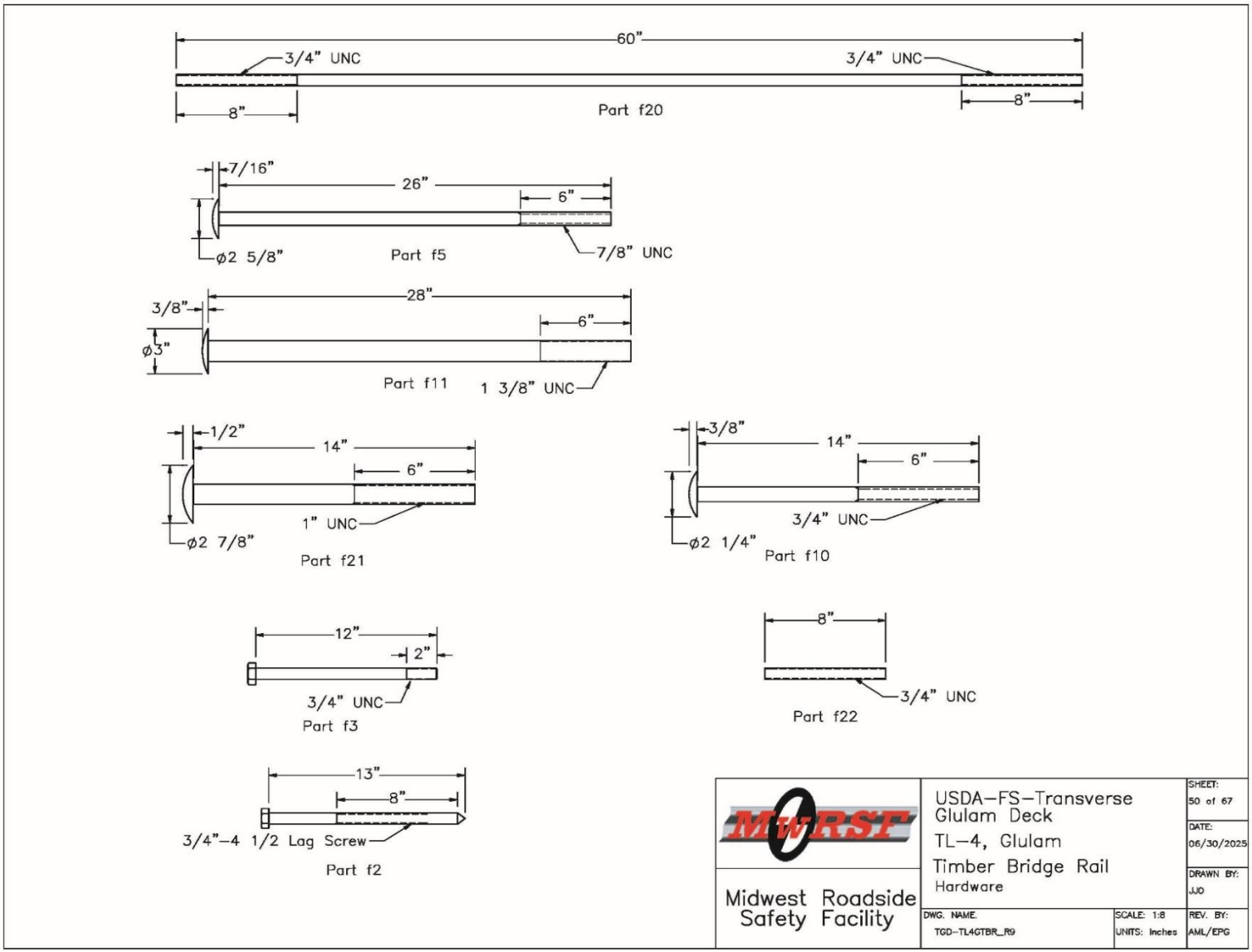

Figure O-50. Bridge Bolt Hardware Details, Page 1

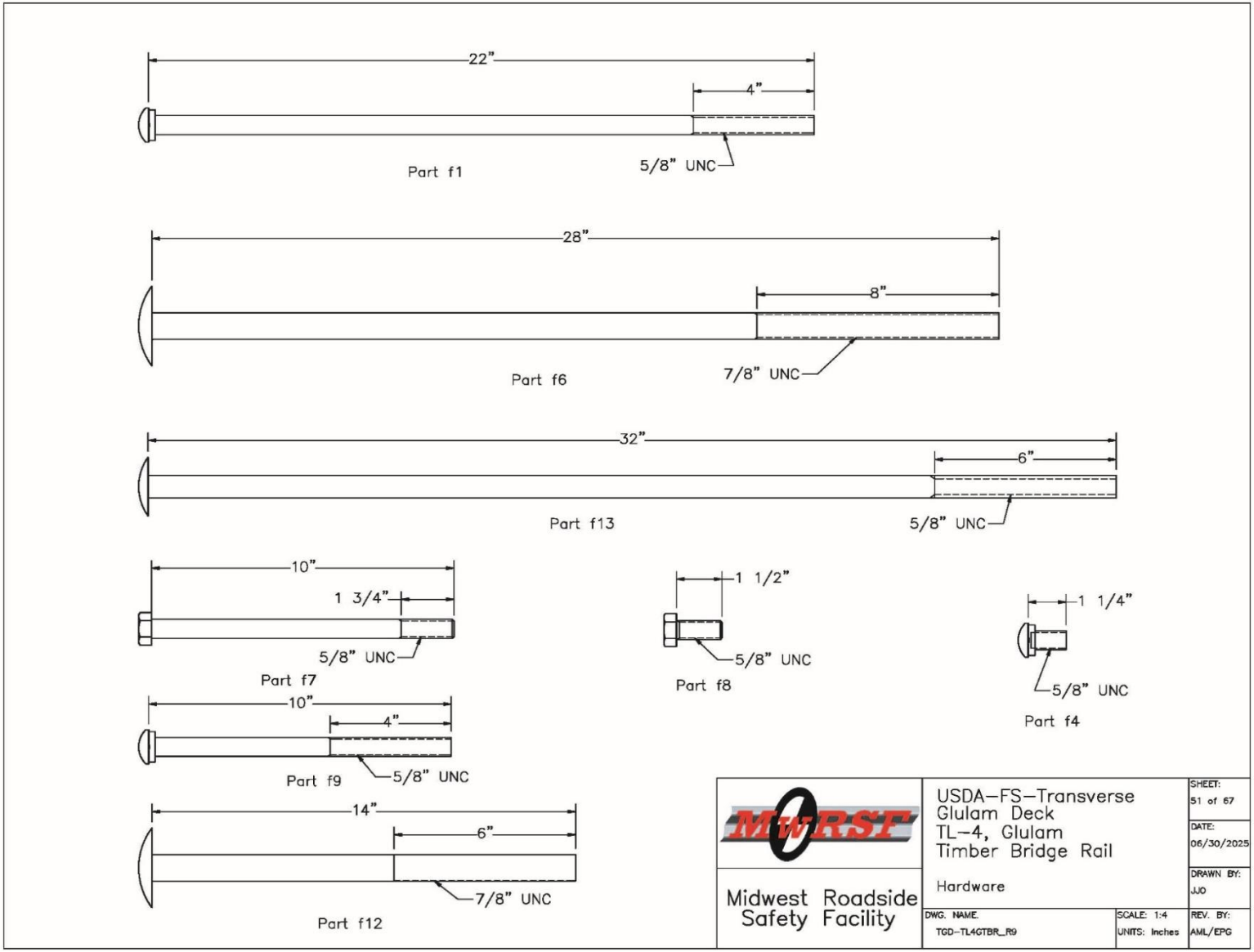

Figure O-51. Bridge Bolt Hardware Details, Page 2

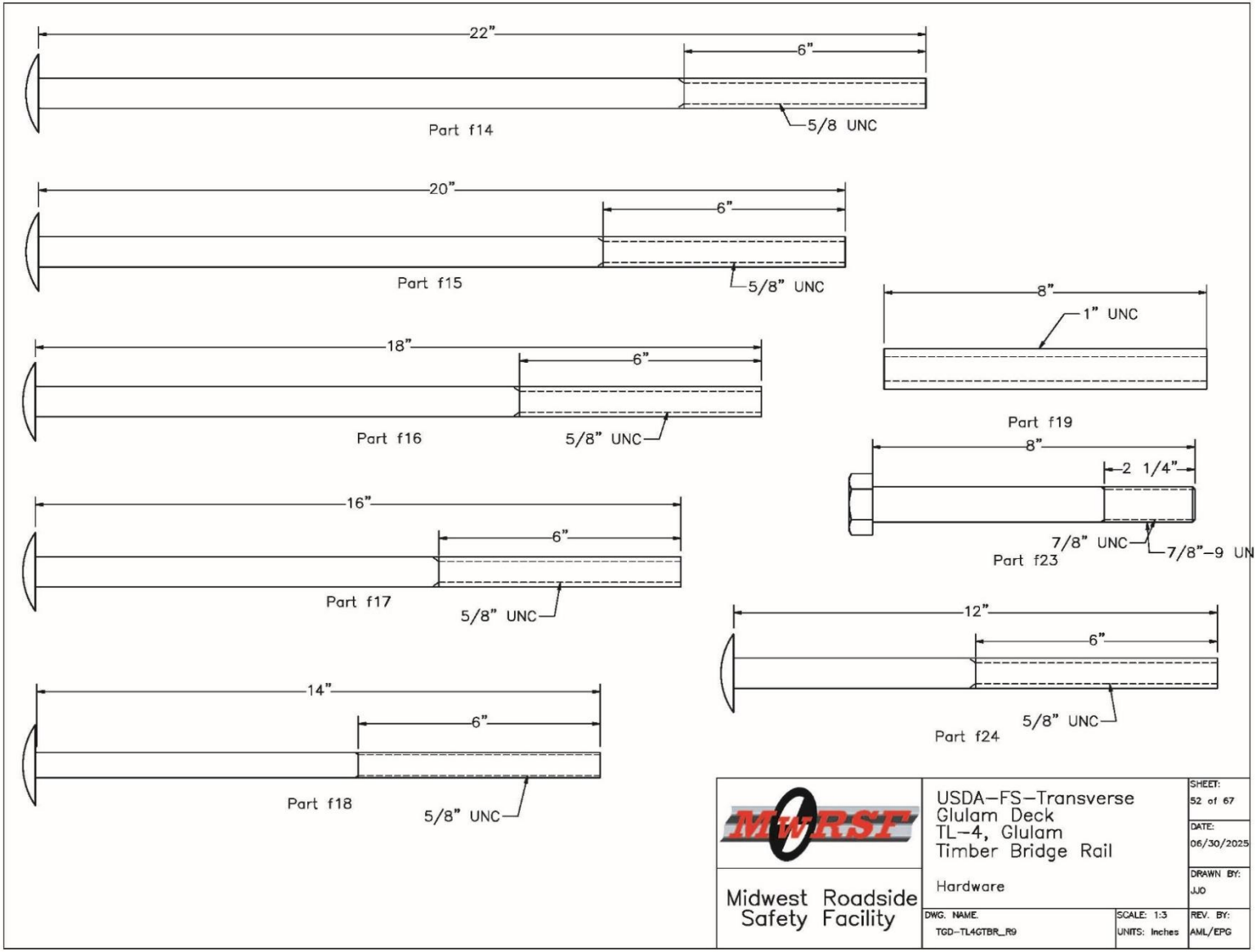

Figure O-52. Bridge Bolt Hardware Details, Page 3

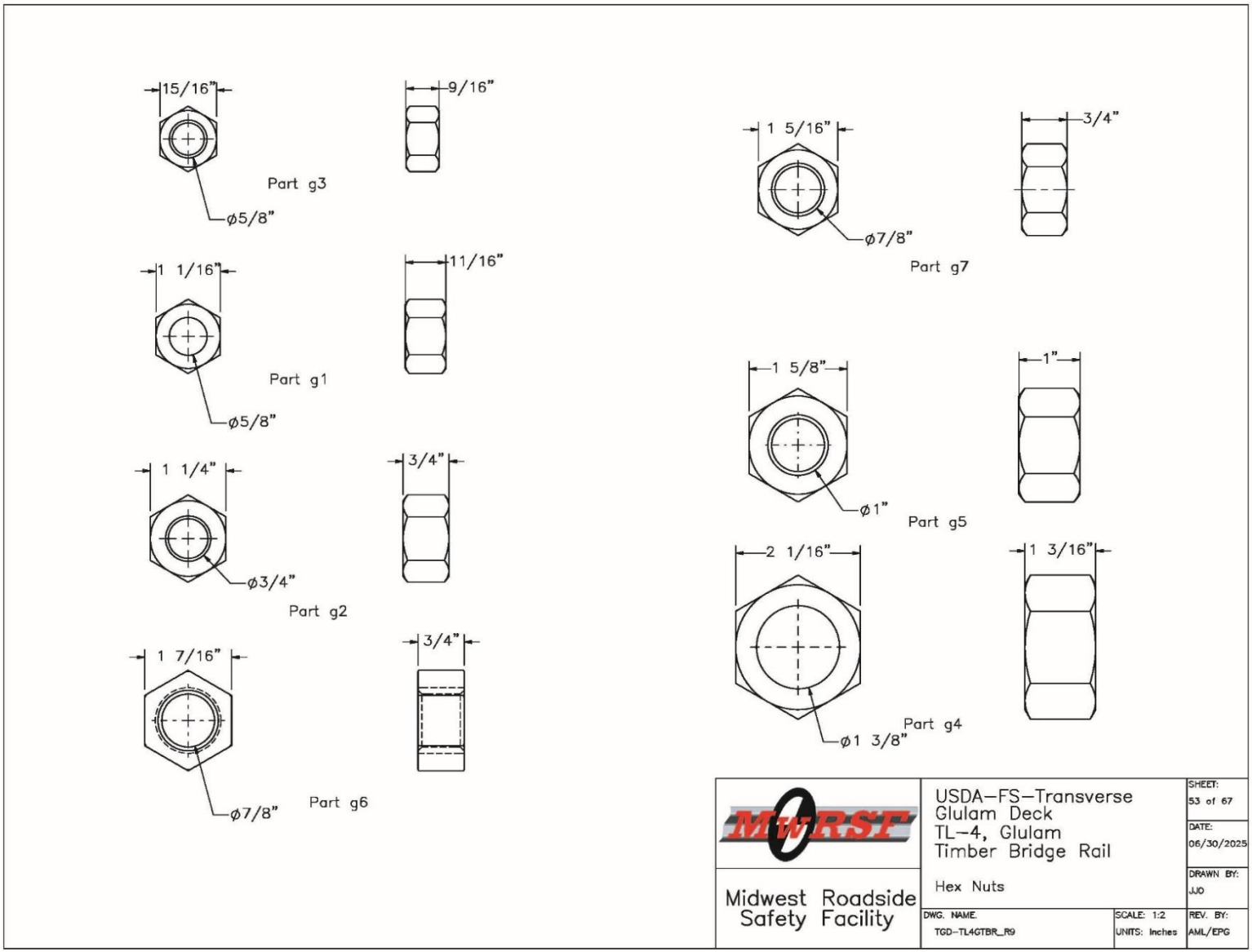

Figure O-53. Bridge Nut Hardware Details

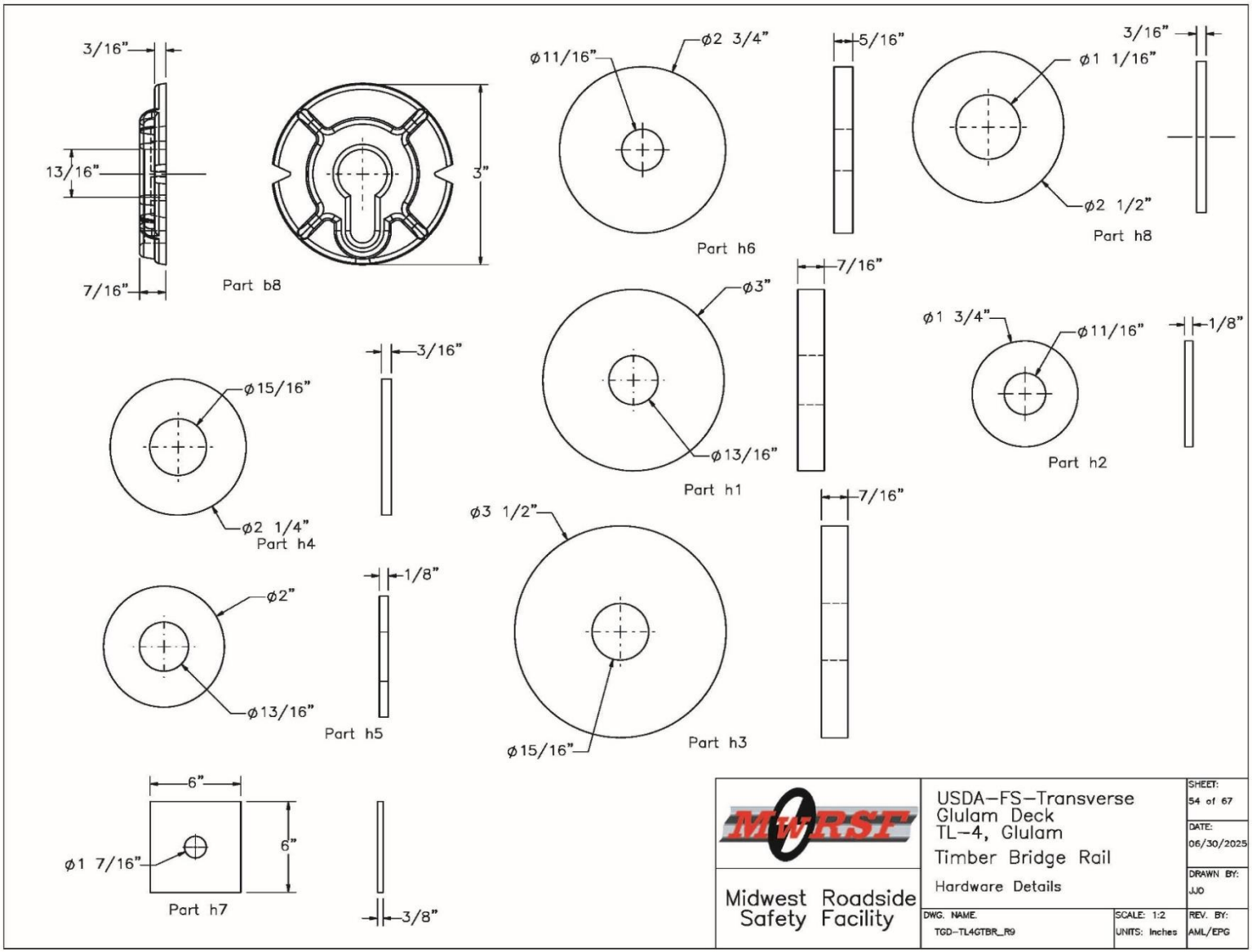

Figure O-54. Bridge Washer Hardware Details

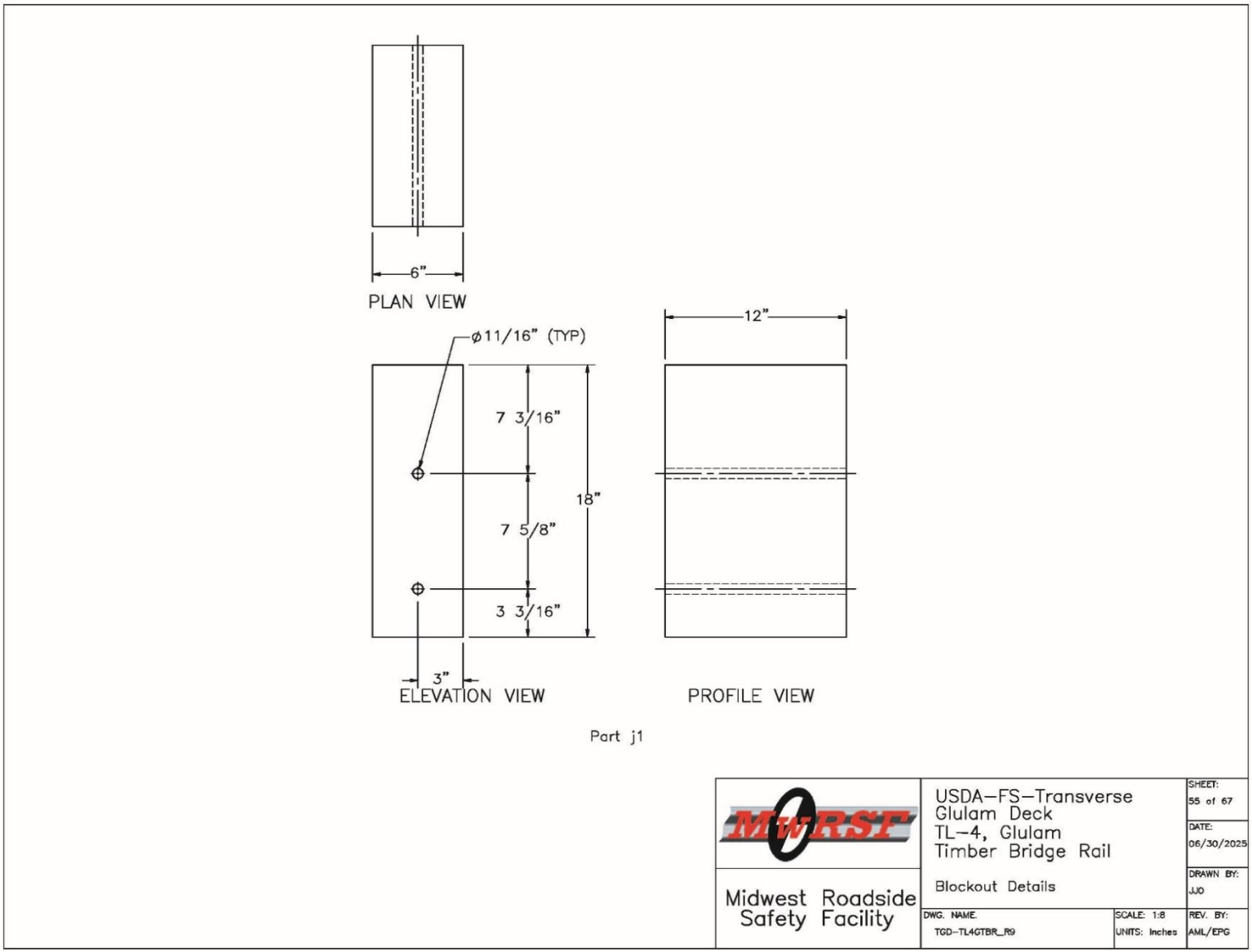

Figure O-55. Bridge AGT Blockout Details, Page 1

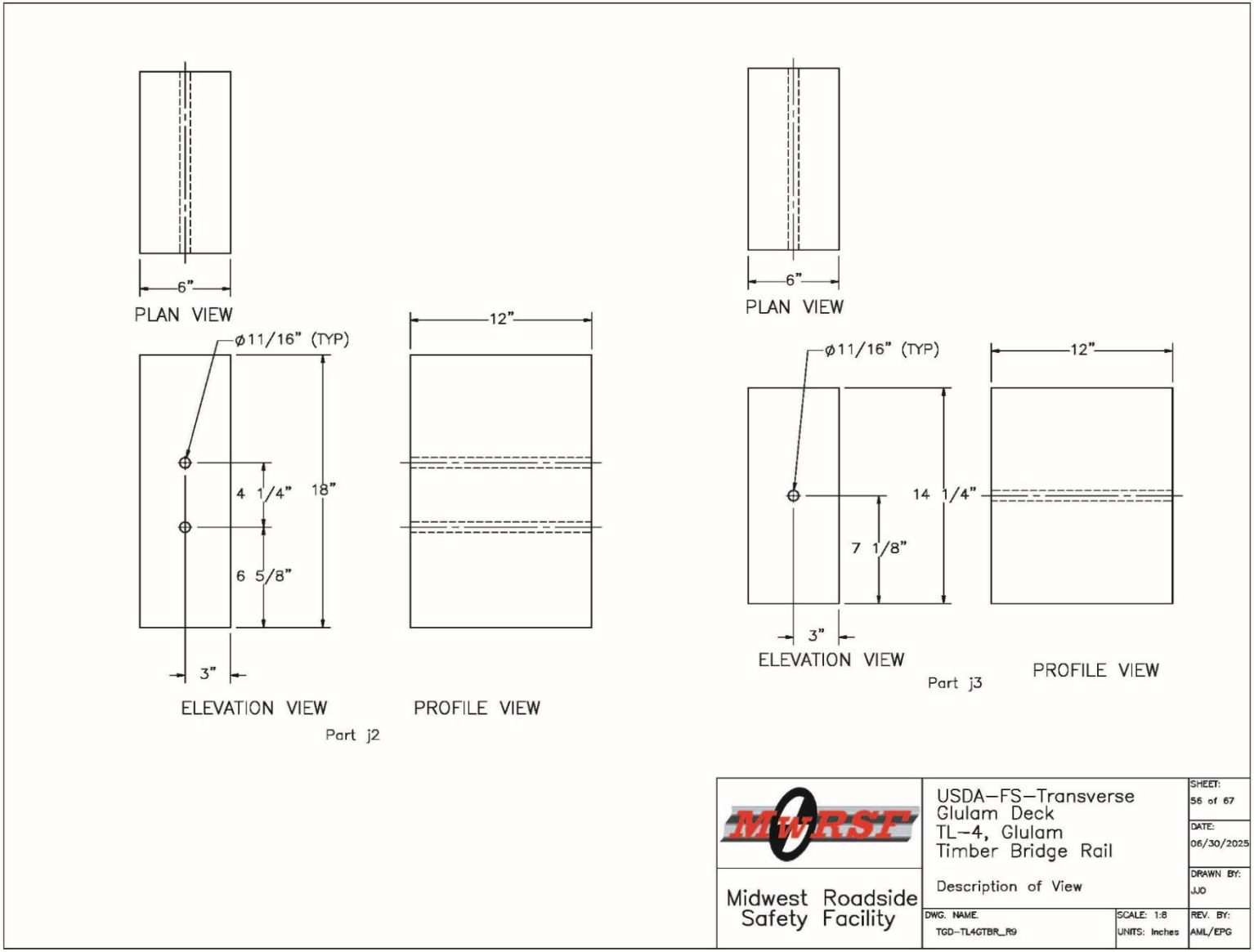

Figure O-56. Bridge AGT Blockout Details, Page 2

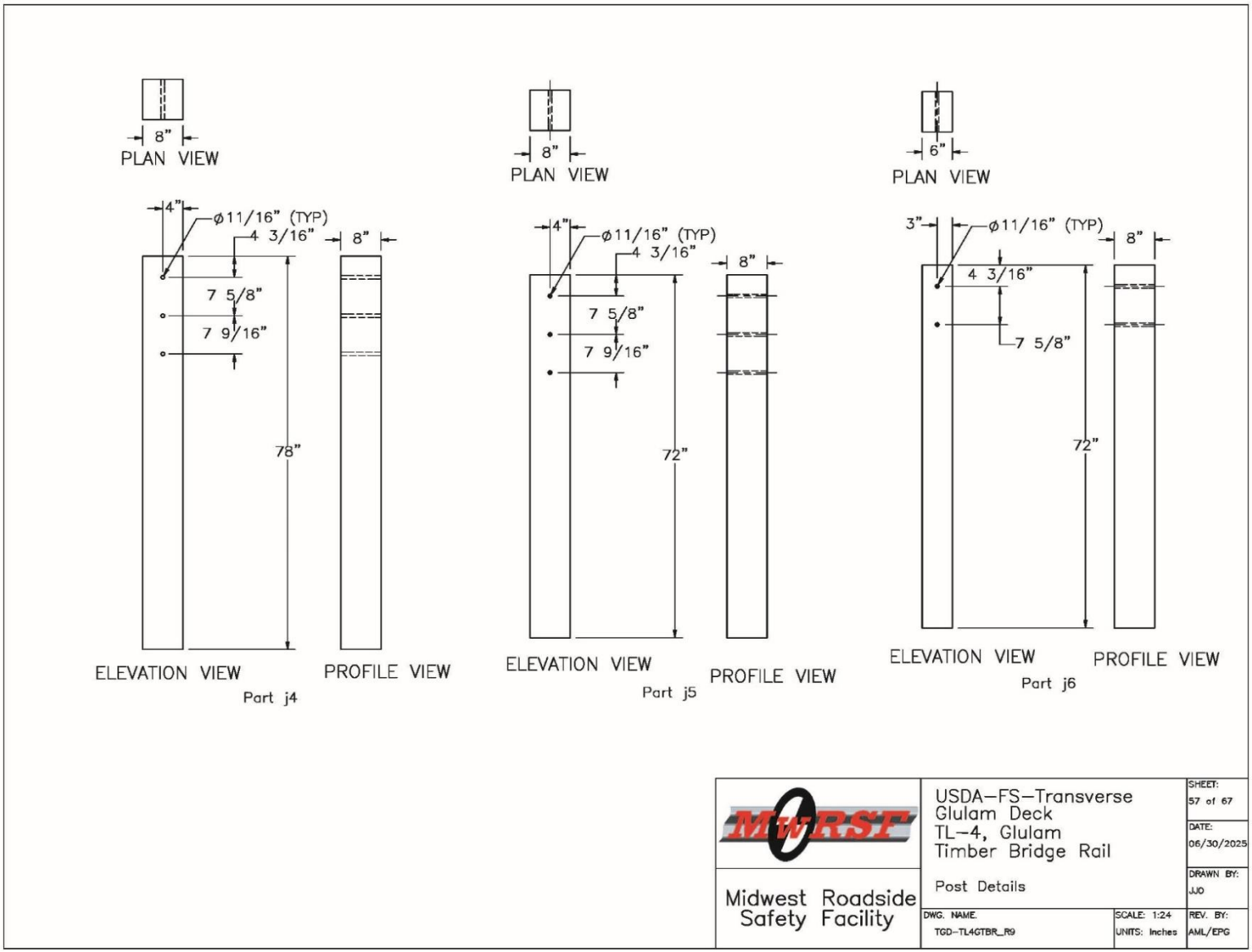

Figure O-57. Bridge AGT Post Details, Page 1

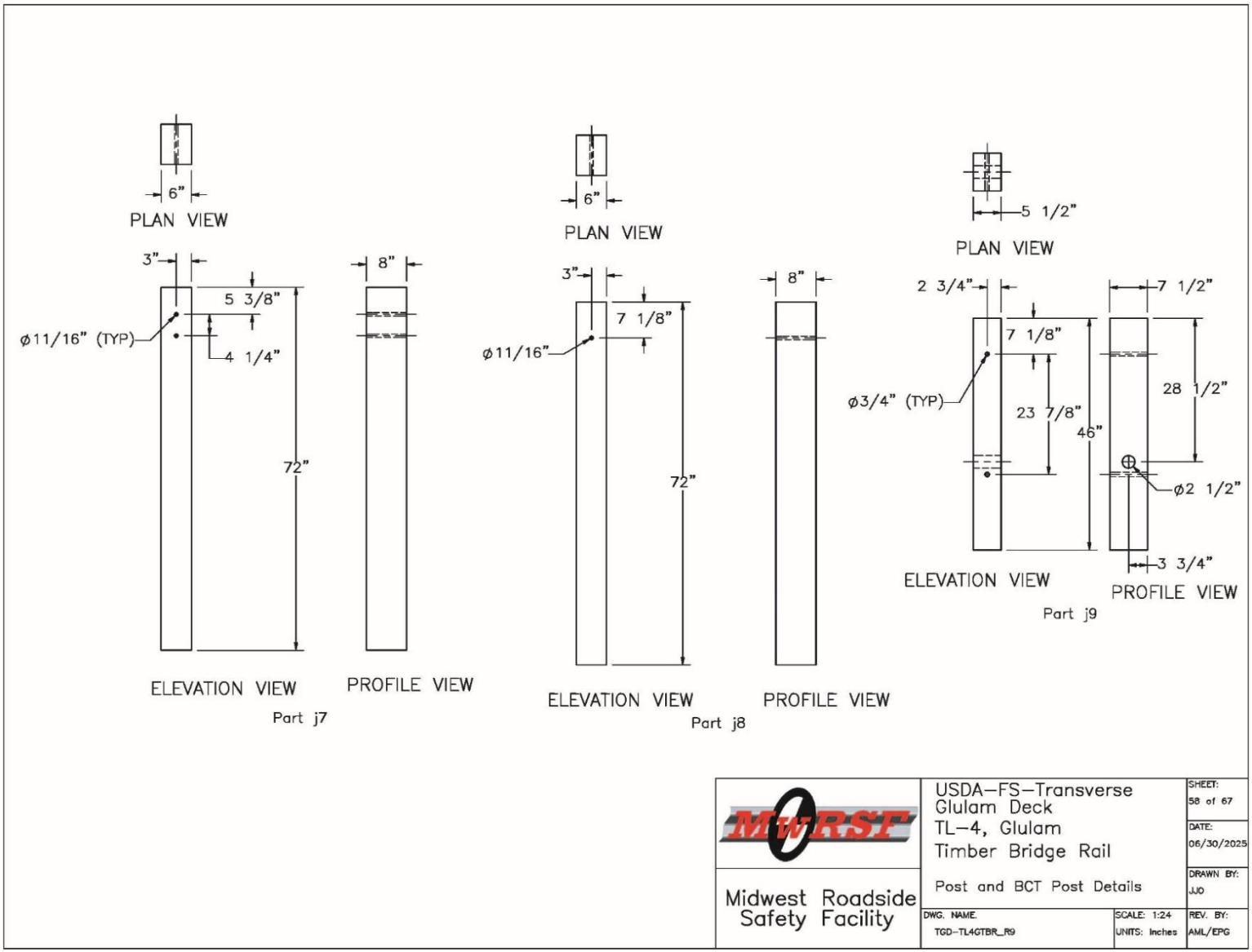

Figure O-58. Bridge AGT Post Details, Page 2

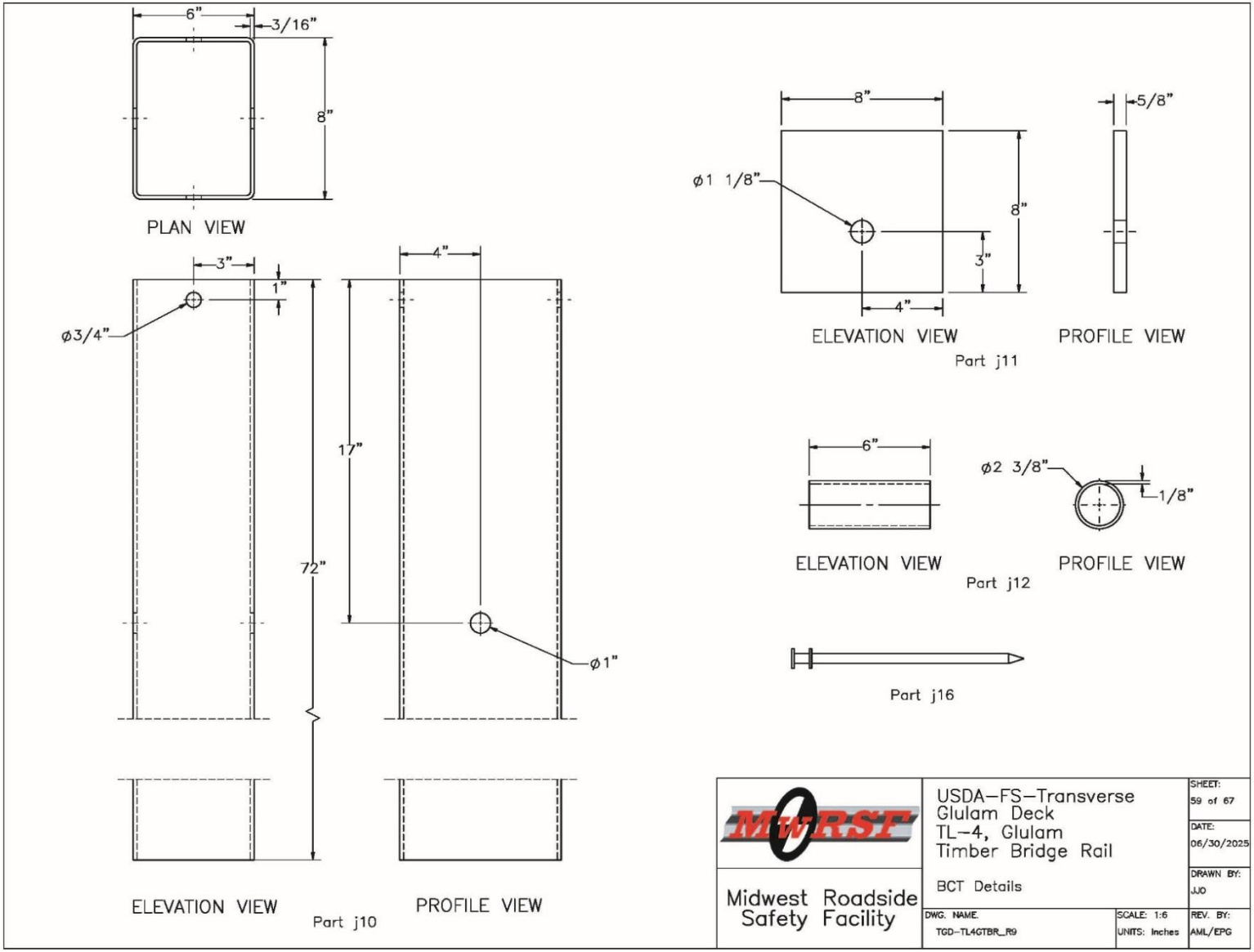

Figure O-59. Bridge AGT BCT Details, Page 1

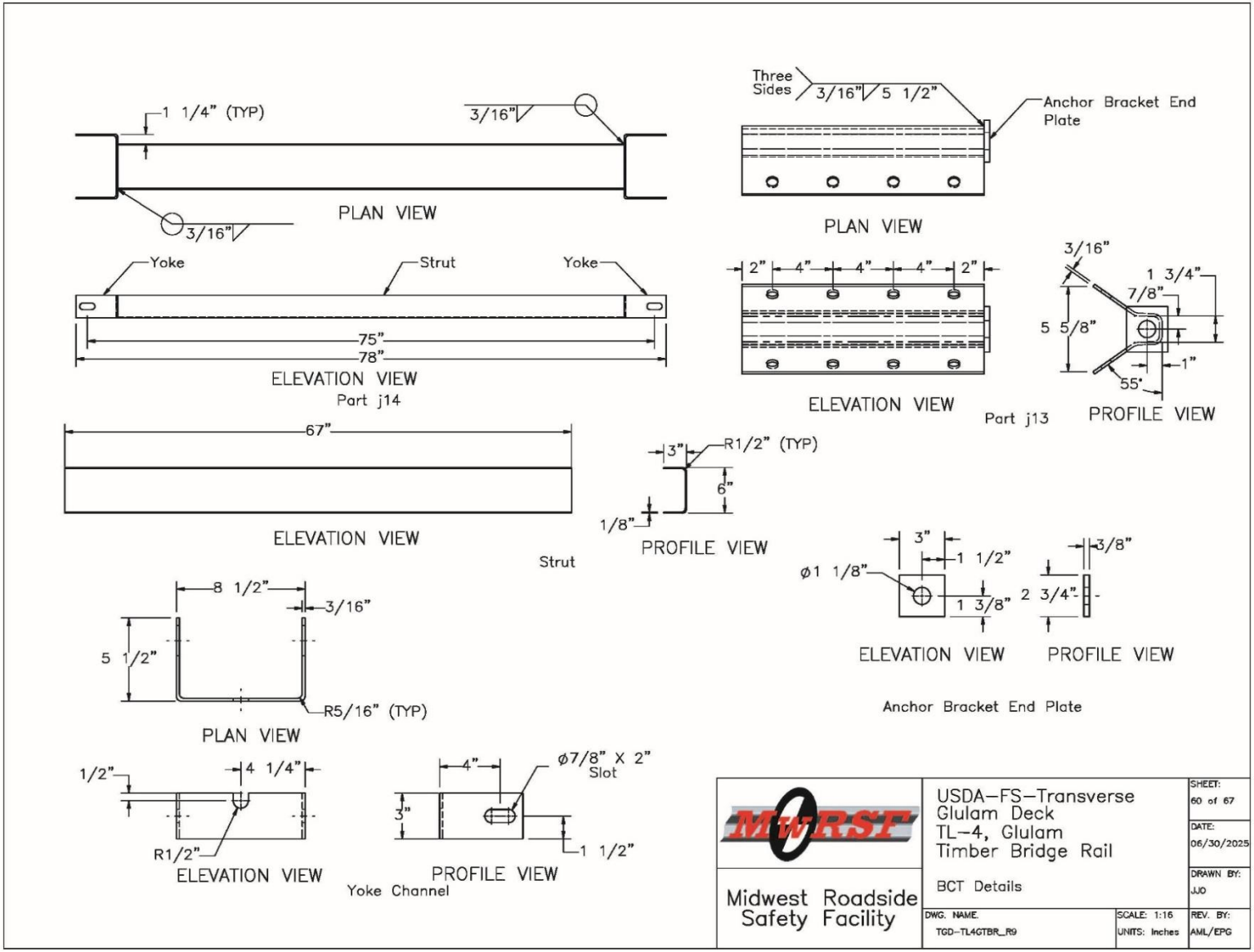

Figure O-60. Bridge AGT BCT Details, Page 2

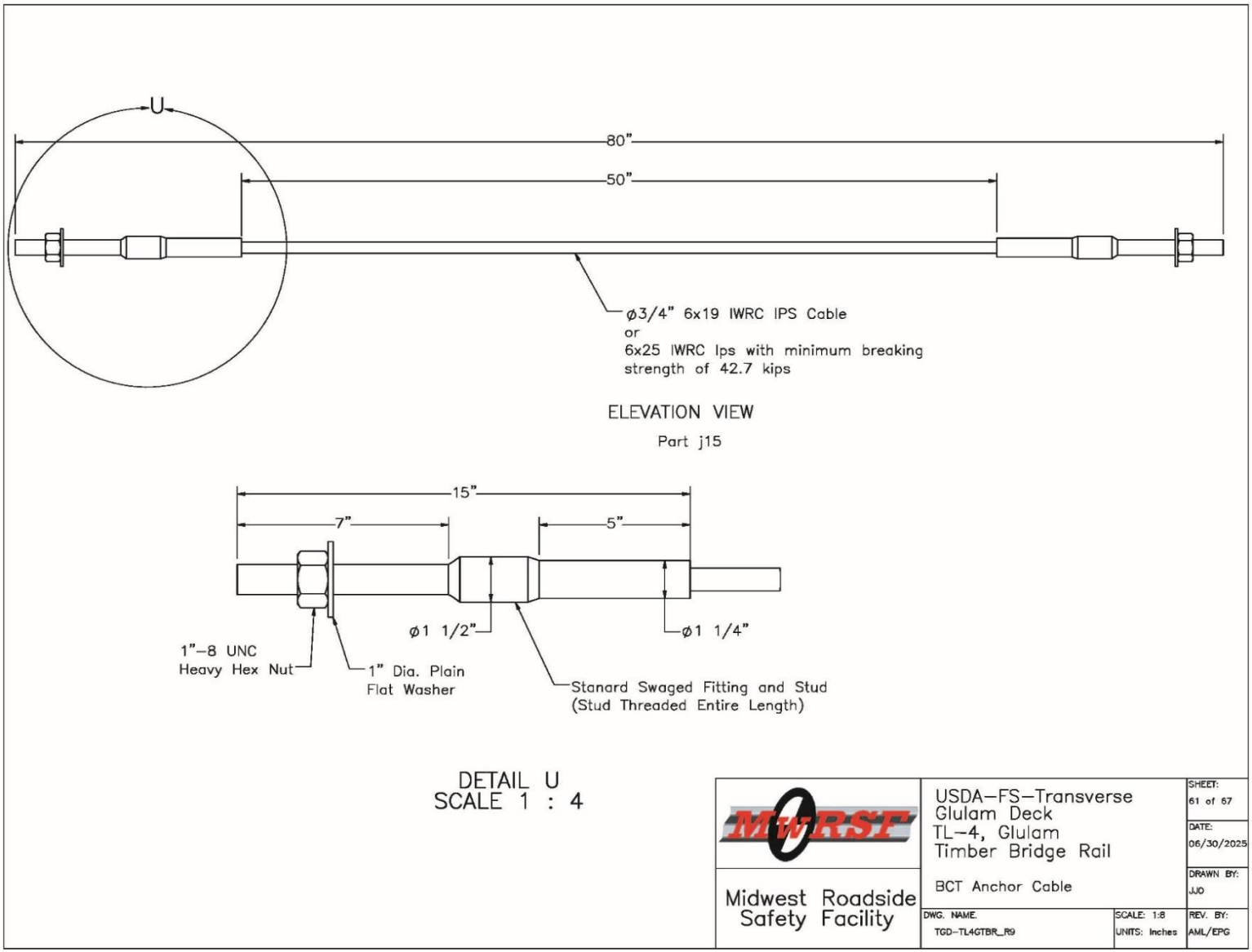

Figure O-61. Bridge AGT BCT Details, Page 3

Item No.	QTY.	Description	Material Specification	Treatment Specification	Hardware Guide
–	1	2" Thick Asphalt or Concrete Wearing Surface	–	–	–
a1	15	6 3/4"x47 7/8"x156" Long, Glulam Deck Panel	Comb. 48 (SP) or Comb. 2 (DF)	Copper Naphthenate (CuN) or 4.5–Dichloro–2–N–Octyl–4–Isothiazolin–3–One (DCOI)	–
a2	15	6 3/4"x47 7/8"x156" Long, Glulam Deck Panel	Comb. 48 (SP) or Comb. 2 (DF)	Copper Naphthenate (CuN) or 4.5–Dichloro–2–N–Octyl–4–Isothiazolin–3–One (DCOI)	–
a3	24	21"x5 1/8"x41 1/8" Long Glulam Diaphragms	Comb. 47 (SP) or Comb. 1 (DF)	Copper Naphthenate (CuN) or 4.5–Dichloro–2–N–Octyl–4–Isothiazolin–3–One (DCOI)	–
a4	3	287 3/4"x13 1/2"x10 3/4" Glulam Upper Rail Section	Comb. 48 (SP) or Comb. 2 (DF)	Copper Naphthenate (CuN) or 4.5–Dichloro–2–N–Octyl–4–Isothiazolin–3–One (DCOI)	–
a5	4	287 1/2"x12"x8 3/4" Glulam Curb Rail Section	Comb. 48 (SP) or Comb. 2 (DF)	Copper Naphthenate (CuN) or 4.5–Dichloro–2–N–Octyl–4–Isothiazolin–3–One (DCOI)	–
a6	12	28 1/2"x8 3/4"x239 1/2" Long Exterior Glulam Girder	24F–V3 (SP) or 24F–V4 (DF)	Copper Naphthenate (CuN) or 4.5–Dichloro–2–N–Octyl–4–Isothiazolin–3–One (DCOI)	–
a7	6	28 1/2"x8 3/4"x239 1/2" Long Interior Glulam Girder	24F–V3 (SP) or 24F–V4 (DF)	Copper Naphthenate (CuN) or 4.5–Dichloro–2–N–Octyl–4–Isothiazolin–3–One (DCOI)	–
a8	30	60"x12"x5 1/8" Glulam Scupper Block	Comb. 47 (SP) or Comb. 1 (DF)	Copper Naphthenate (CuN) or 4.5–Dichloro–2–N–Octyl–4–Isothiazolin–3–One (DCOI	–
a9	11	43"x12"x8 3/4" Glulam Post	Comb. 48 (SP) or Comb. 2 (DF)	Copper Naphthenate (CuN) or 4.5–Dichloro–2–N–Octyl–4–Isothiazolin–3–One (DCOI	–
a10	4	1 1/4"x10 1/2"x8 3/4" Splice Location Glulam Timber Blockout	Comb. 47 (SP) or Comb. 1 (DF)	Copper Naphthenate (CuN) or 4.5–Dichloro–2–N–Octyl–4–Isothiazolin–3–One (DCOI)	–
a11	4	43"x12"x8 3/4" Splice Location Glulam Post	Comb. 48 (SP) or Comb. 2 (DF)	Copper Naphthenate (CuN) or 4.5–Dichloro–2–N–Octyl–4–Isothiazolin–3–One (DCOI)	–
a12	1	282 1/8"x13 1/2"x10 3/4" Glulam Rail Section	Comb. 48 (SP) or Comb. 2 (DF)	Copper Naphthenate (CuN) or 4.5–Dichloro–2–N–Octyl–4–Isothiazolin–3–One (DCOI	–
a13	1	335 7/8"x13 1/2"x10 3/4" Glulam Rail Section	Comb. 48 (SP) or Comb. 2 (DF)	Copper Naphthenate (CuN) or 4.5–Dichloro–2–N–Octyl–4–Isothiazolin–3–One (DCOI)	–
a14	1	312 1/2"x12"x8 3/4" Glulam End Rail Section	Comb. 47 (SP) or Comb. 1 (DF)	Copper Naphthenate (CuN) or 4.5–Dichloro–2–N–Octyl–4–Isothiazolin–3–One (DCOI)	–
a15	1	139"x12"x8 3/4" Glulam Curb Rail Taper	Comb. 47 (SP) or Comb. 1 (DF)	Copper Naphthenate (CuN) or 4.5–Dichloro–2–N–Octyl–4–Isothiazolin–3–One (DCOI)	–
a16	1	10 3/8" x 7 1/2" x 45" Long Glulam Reverse Taper	Comb. 47 (SP) or Comb. 1 (DF)	Copper Naphthenate (CuN) or 4.5–Dichloro–2–N–Octyl–4–Isothiazolin–3–One (DCOI)	–

Notes:

(1) Quantities listed herein are for one bridge section.
(2) Timber rails shall be treated with Copper Naphthenate (CuN) or 4.5–Dichloro–2–N–Octyl–4–Isothiazolin–3–One (DCOI) in Heavy Oil to a minimum retention of 0.075 lbs/cu. ft or 0.20 lbs/cu.ft respectively, in accordance with AWPA Standards UI to the requirements use category 4B (UC4B)
(3) Wood shall be cut, drilled, and completely fabricated prior to treatment with preservative. Drain excess chemical and dry all treated wood at location of manufacture.
(4) All field cuts, bore holes, and damages shall be treated with material acceptable to the engineer prior to installation.

Midwest Roadside Safety Facility

USDA–FS–Transverse Glulam Deck
TL–4, Glulam Timber Bridge Rail
Bill of Materials

DWG. NAME. TGD–TL4GTBR_R9
SCALE: 1:50
UNITS: Inches

SHEET: 62 of 67
DATE: 06/30/2025
DRAWN BY: JJO
REV. BY: AML/EPG

Figure O-62. Bridge System Bill of Material, Page 1

Item No.	QTY.	Description	Material Specification	Treatment Specification	Hardware Guide
a17	11	1 1/4"x10 1/2"x8 3/4" Glulam Timber Blockout	Comb. 47 (SP) or Comb. 1 (DF)	Copper Naphthenate (CuN) or 4.5–Dichloro–2–N–Octyl–4–Isothiazolin–3–One (DCOI)	–
b1	8	35"x13 1/2"x3/8 Upper Rail Splice Plate	ASTM A572 Gr. 50	ASTM A123	–
b2	8	28"x8 3/4"x3/8 Curb Rail Splice Plate	ASTM A572 Gr. 50	–	–
b4	6	12"x16"x1/2" Steel Base Plate	ASTM A36	–	–
b5	12	12"x10"x1/2" Side Plate	ASTM A36	–	–
b6	30	6"x4", 3/8" Thick, 5" Long Steel Angle	ASTM A36	ASTM A123	–
b7	6	12"x8 1/4"x1/2" Elastomeric Bearing Pad	Neoprene – Min. 50 Durameter	–	–
b8	720	4" Dia, 5/8" Thick Shear Plate	ASTM A47 Grade 32510	Hot–Dip	12405
b9	2	27" x 20 1/2" x 3/8" Thick. Upper rail end plate	ASTM A572 Gr. 50	ASTM A123	
b10	2	29 1/2" x 10" x 3/8" Thick Curb rail end plate	ASTM A572 Gr. 50	ASTM A123	–
b11	30	Plate 21" x 4" x 3/16" Thick	ASTM A36	ASTM A123	–
b12	15	Plate 21" x 8" x 3/8" Thick	ASTM A36	ASTM A123	–
b13	15	24"x16"x1/2" Steel Base Plate	ASTM A36	–	–
b14	30	24"x10"x1/2" Side Plate	ASTM A36	–	–
b15	15	24"x8 1/4"x1/2" Elastomeric Bearing Pad	Neoprene – Min. 50 Durameter	–	–
c1	1	10–gauge Thrie End Shoe Section	AASHTO M180 Gr. 50 Min. yield strength = 50 ksi Min. ultimate strength = 70 ksi	ASTM A123 or A653	RTE01b
c2	2	12'–6" 12–gauge Thrie Beam Section	AASHTO M180	ASTM A123 or A653	RTM08a
c3	1	6'–3" 12–gauge Thrie Beam Section	AASHTO M180	ASTM A123 or A653	RTM19a
c4	1	10–gauge Symmetrical W–beam to Thrie Beam Transition	AASHTO M180	ASTM A123 or A653	RWT01b
c5	1	12'–6" 12–gauge W–Beam Section – 1/4 Post Spacing	AASHTO M180	ASTM A123 or A653	RWM04a
c6	2	12'–6" 12–gauge W–Beam MGS Section	AASHTO M180	ASTM A123 or A653	RWM04a

Midwest Roadside Safety Facility

USDA–FS–Transverse Glulam Deck
TL–4, Glulam Timber Bridge Rail
Bill of Materials

DWG. NAME. TGD–TL4GTBR_R9
SCALE: 1:50
UNITS: Inches

SHEET: 63 of 67
DATE: 06/30/2025
DRAWN BY: JJO
REV. BY: AML/EPG

Figure O-63. Bridge System Bill of Material, Page 2

Item No.	QTY.	Description	Material Specification	Treatment Specification	Hardware Guide
c7	1	12'–6" 12–gauge W–Beam MGS End Section	AASHTO M180	ASTM A123 or A653	RWM14a
d1	48	#5 Rebar, 12'–6" Total Length	ASTM A615 Gr. 60	*Epoxy Coated (ASTM A775 or A934)	–
d2	52	#5 Rebar, 5'–6" Total Length	ASTM A615 Gr. 60	*Epoxy Coated (ASTM A775 or A934)	–
d3	44	#4 Rebar, 12'–6" Total Length	ASTM A615 Gr. 60	*Epoxy Coated (ASTM A775 or A934)	–
d4	104	#4 Bent Rebar, 54" Total Length	ASTM A615 Gr. 60	*Epoxy Coated (ASTM A775 or A934)	–
d5	78	#4 Rebar, 18" Total Length	ASTM A615 Gr. 60	*Epoxy Coated (ASTM A775 or A934)	–
e1	2	Pier Concrete	Min f'c = 4,000 psi	–	–
e2	2	Abutment Concrete	Min f'c = 4,000 psi		–
e3	1	Cap A2 Concrete	Min f'c = 4,000 psi	–	–
e4	1	Cap A4 Concrete	Min f'c = 4,000 psi	–	–
e5	1	Cap A6 Concrete	Min f'c = 4,000 psi	–	–
f1	32	5/8"–UNC, 22" Long Guardrail Bolt	ASTM A307A	ASTM A153 or B695 Class 55 or F2329	FBB06
f2	360	3/4"–4 1/2, 13" Long Lag Bolt	ASTM A307A	ASTM A123 or A153 or F2329	FBL20
f3	84	3/4"–UNC x 12" Long Hex Bolt	ASTM A307A	ASTM A123	FBX20a
f4	68	5/8"–UNC, 1 1/4" Long Guardrail Bolt	ASTM A307A	ASTM A153 or B695 Class 55 or F2329	FBB01
f5	38	7/8"–UNC x 26" Long Timber Bolt w/ Nubs	ASTM A307A	ASTM A123	FBB08
f6	120	7/8"–UNC x 28" Long Timber Bolt w/out Nubs	ASTM A307A	ASTM A123	FBB08
f7	2	5/8"–UNC, 10" Long Hex Head Bolt	ASTM A307A	ASTM A153 or B695 Class 55 or F2329	FBX16a

Notes: * rebar does not need to be epoxy–coated for testing purposes.

Midwest Roadside Safety Facility

USDA–FS–Transverse Glulam Deck
TL–4, Glulam Timber Bridge Rail
Bill of Materials

SHEET: 64 of 67
DATE: 06/30/2025
DRAWN BY: JJO
REV. BY: AML/EPG
DWG. NAME. TGD–TL4GTBR_R9
SCALE: 1:8
UNITS: Inches

Figure O-64. Bridge System Bill of Material, Page 3

Item No.	QTY.	Description	Material Specification	Treatment Specification	Hardware Guide
f8	8	5/8"–UNC, 1 1/2" Long Hex Head Bolt	ASTM A307A	ASTM A153 or B695 Class 55 or F2329	FBX16a
f9	2	5/8"–UNC, 10" Long Guardrail Bolt	ASTM A307A	ASTM A153 or B695 Class 55 or F2329	FBB03
f10	66	3/4"–UNC, 14" Long Timber Bolt	ASTM A307A	ASTM A153 or F2329	–
f11	15	1 3/8"–UNC x 28" Long Timber Bolt w/out Nubs	ASTM A307A	ASTM A123	FBB08
f12	5	7/8"–UNC, 14" Long Timber Bolt w/out Nubs	ASTM A307A	ASTM A153 or F2329	–
f13	5	5/8"–UNC, 32" Long Timber Bolt w/ Nubs	ASTM A307A	ASTM A153 or F2329	–
f14	1	5/8"–UNC, 22" Long Timber Bolt w/ Nubs	ASTM A307A	ASTM A153 or F2329	–
f15	2	5/8"–UNC, 20" Long Timber Bolt w/ Nubs	ASTM A307A	ASTM A153 or F2329	–
f16	1	5/8"–UNC, 18" Long Timber Bolt w/ Nubs	ASTM A307A	ASTM A153 or F2329	–
f17	1	5/8"–UNC, 16" Long Timber Bolt w/ Nubs	ASTM A307A	ASTM A153 or F2329	–
f18	241	5/8"–UNC, 14" Long Timber Bolt w/out Nubs	ASTM A307A	ASTM A153 or F2329	–
f19	6	1"–UNC, 8" Long Fully Threaded Rod	ASTM A193 Gr. B7 or SAE J429 Gr. 5	ASTM A123 or A153 or F2329	FRR20a
f20	48	3/4"–UNC x 8" on a 60" Long Tie Rod	ASTM A307A or F1554 Gr. 36 or SAE J429 Gr. 2	ASTM A123	FRR28a
f21	60	1"–UNC, 14" Long Timber Bolt w/out Nubs	ASTM A307A	ASTM A153 or F2329	–
f22	168	3/4"–UNC x 8" Threaded Rod	ASTM A193 Gr. B7 or SAE J429 Gr. 5	ASTM A123	FRR20a
f23	2	7/8"–UNC, 8" Long Hex Head Bolt	ASTM A307A	ASTM A153 or B695 Class 55 or F2329	FBX22a
f24	1	5/8"–UNC, 12" Long Timber Bolt w/ Nubs	ASTM A307A	ASTM A153 or F2329	–
g1	354	5/8" –UNC Heavy Hex Nut	ASTM A563A or better	ASTM A153 or B695 Class 55 or F2329	FNX16b
g2	414	3/4"–UNC Heavy Hex Nut	ASTM A536A or better	ASTM A123	FNX20b
g3	10	5/8"–UNC Hex Nut	ASTM A563A	ASTM A153 (AASHTO M232) for Class C or ASTM B695 (AASHTO M298) for Class 50	FNX16a
g4	15	1 3/8"–UNC Hex Nut	ASTM A563A	ASTM A123 or A153 or F2329	
g5	66	1"–UNC Heavy Hex Nut	ASTM A563A or better	ASTM A123 or A153 or F2329	–

Midwest Roadside Safety Facility

USDA–FS–Transverse Glulam Deck
TL–4, Glulam Timber Bridge Rail
Bill of Materials

SHEET: 65 of 67
DATE: 06/30/2025
DRAWN BY: JJO
REV. BY: AML/EPG
DWG. NAME. TGD–TL4GTBR_R9
SCALE: 1:8
UNITS: Inches

Figure O-65. Bridge System Bill of Material, Page 4

Item No.	QTY.	Description	Material Specification	Treatment Specification	Hardware Guide
g6	125	7/8"–Heavy Hex Nut	ASTM A563A or better	ASTM A123 or A153 or F2329	–
g7	40	7/8"–UNC Dia. Hex Nut	ASTM A563A	ASTM A153 (AASHTO M232) for Class C or ASTM B695 (AASHTO M298) for Class 50	–
h1	96	3/4" Malleable Iron Washer	ASTM A47	ASTM A123 or A153 or F2329	–
h2	96	5/8" Flat Washer	ASTM F844	ASTM A123 or A153 or F2329	FWC16a
h3	158	7/8" Malleable Iron Washer	ASTM A47	ASTM A123	–
h4	9	7/8" Dia. Flat Washer	ASTM F844	ASTM A123 or A153 or F2329	FWC20a
h5	678	3/4" Flat Washer	ASTM F844	ASTM A123 or A153 or F2329	FWC20a
h6	210	5/8" Malleable Iron Washer	ASTM A47	ASTM A123 or A153 or F2329	–
h7	15	6"x6"x3/8" Steel Plate Washer	ASTM A36	ASTM A123	–
h8	60	1" Flat Washer	ASTM F844	ASTM A123 or A153 or F2329	–
j1	12	6" x 12" x 18" Long Blockout Thrie	SYP Grade No. 1 or better	–	–
j2	1	6" x 12" x 18" Long Blockout Transition	SYP Grade No. 1 or better	–	–
j3	7	6" x 12" x 14" Long Blockout W Beam	SYP Grade No. 1 or better	–	–
j4	4	8" x 8" x 78" Long Timber Post	SYP Grade No. 1D or better (No knots +/– 18" from ground on tension face)	–	PDE06
j5	3	8" x 8" x 72" Long Timber Post	SYP Grade No. 1D or better (No knots +/– 18" from ground on tension face)	–	PDE07
j6	5	6" x 8" x 72" Long Thrie Beam Timber Post	SYP Grade No. 1D or better (No knots +/– 18" from ground on tension face)	–	PDE02
j7	1	6" x 8" x 72" Long Transition Timber Post	SYP Grade No. 1D or better (No knots +/– 18" from ground on tension face)	–	PDE02
j8	7	6" x 8" x 72" Long W Beam Timber Post	SYP Grade No. 1D or better (No knots +/– 18" from ground on tension face)	–	PDE02
j9	2	BCT Timber Post – MGS Height	SYP Grade No. 1D or better (No knots +/– 18" from ground on tension face)	–	PDF01

Midwest Roadside Safety Facility

USDA–FS–Transverse Glulam Deck
TL–4, Glulam Timber Bridge Rail
Bill of Materials

SHEET: 66 of 67
DATE: 06/30/2025
DRAWN BY: JJO
REV. BY: AML/EPG
DWG. NAME: TGD–TL4GTBR_R9
SCALE: 1:8
UNITS: Inches

Figure O-66. Bridge System Bill of Material, Page 5

Item No.	QTY.	Description	Material Specification	Treatment Specification	Hardware Guide
j10	2	72" Long Foundation Tube	ASTM A500 Gr. B	ASTM A123	PTE06
j11	1	8"x8"x5/8" Anchor Bearing Plate	ASTM A36	ASTM A123	FPB01
j12	1	2 3/8" O.D. 6" Long BCT Post Sleeve	ASTM A53 Gr. B Schedule 40	ASTM A123	FMM02
j13	1	Ground Anchor Bracket Assembly	ASTM A36	ASTM A123	FPA01
j14	1	Ground Strut Assembly	ASTM A36	ASTM A123	PFP02
j15	1	BCT Anchor Cable Assembly with Heavy Hex Nuts and Washers	Fitting–ASTM A576 Gr. 1035 Stud–ASTM F568 Class C	Fitting–ASTM A153 Stud– ASTM A153 or B695, Cable, Nut and Washer	FCA01
j16	10	16D Double Head Nail	–	–	–
k1	2	8 3/4" x 14 3/8" x 3/8" Plate Lower	ASTM A36	–	–
k2	2	13 1/2" x 18 1/8" x 3/8" Plate Upper	ASTM A36	–	–
k3	1	4" x 6" x 1/4" Thick, 69" Long HSS Tube	ASTM A500	–	–
k4	1	4" x 6" x 1/4" Thick, 39 7/16" Long HSS Tube	ASTM A500	–	–
k5	1	12"x12" x 1/2" Base Plate	ASTM A36	–	–
k6	5	11 1/4" x 8 3/4" x 3/8" Gusset Curb Rail	ASTM A36	–	–
k7	1	10" x 13 1/2 "x 3/8" Gusset Upper Rail	ASTM A36	–	–
–	–	Soil	–	–	–

Midwest Roadside Safety Facility

USDA–FS–Transverse Glulam Deck TL–4, Glulam Timber Bridge Rail

Bill of Materials

SHEET: 67 of 67
DATE: 06/30/2025
DRAWN BY: JJO
REV. BY: AML/EPG
DWG. NAME. TGD–TL4GTBR_R9
SCALE: 1:8
UNITS: Inches

Figure O-67. Bridge System Bill of Material, Page 6

END OF DOCUMENT